Journal of Sensors

Information Fusion and Its Applications for Smart Sensing

Lead Guest Editor: Mu Zhou
Guest Editors: Ying-Ren Chien and Qiao Zhang

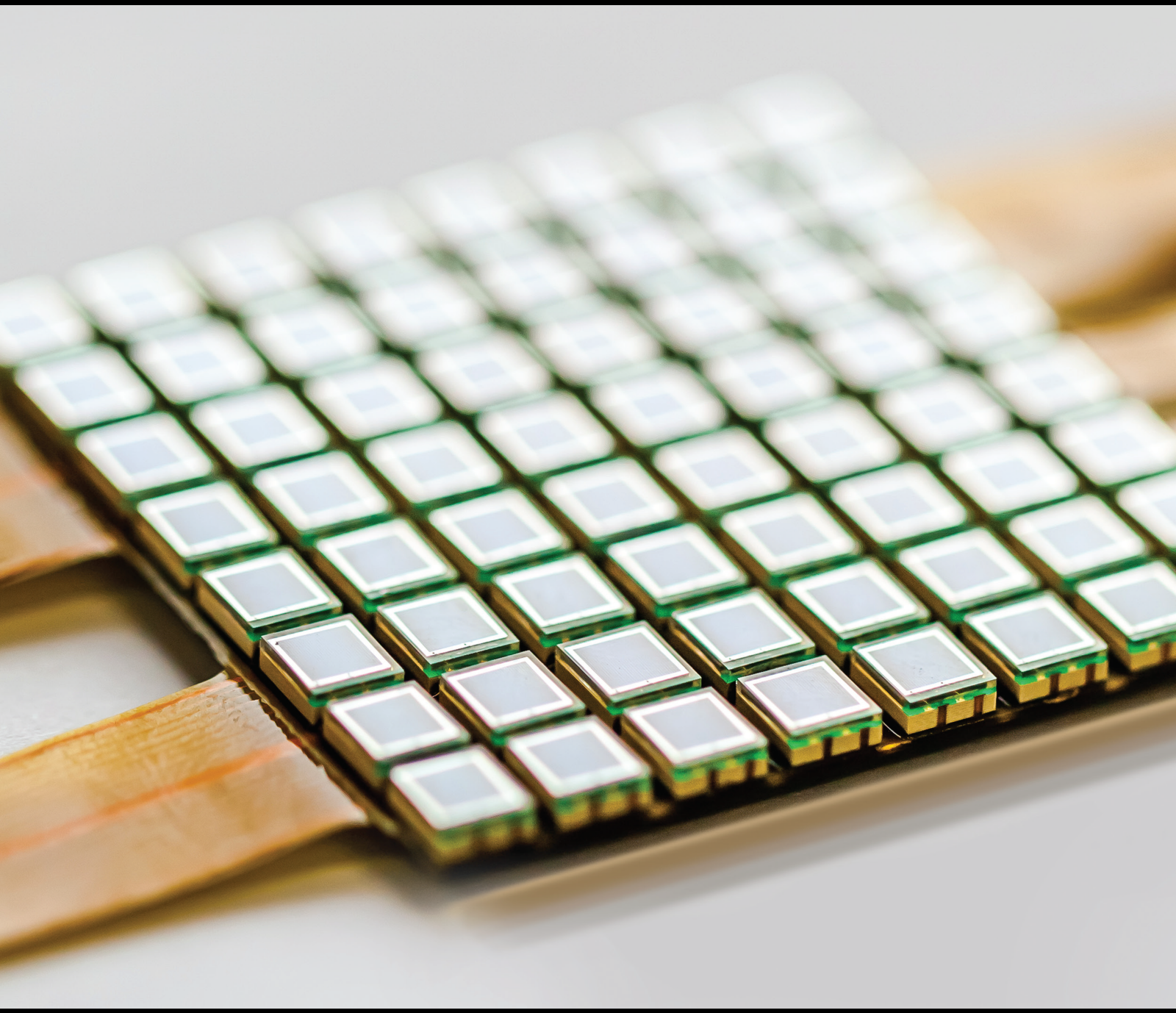

Information Fusion and Its Applications for Smart Sensing

Journal of Sensors

Information Fusion and Its Applications for Smart Sensing

Lead Guest Editor: Mu Zhou
Guest Editors: Ying-Ren Chien and Qiao Zhang

Contents

Contents

Contents

Contents

Hindawi
Journal of Sensors
Volume 2023, Article ID 9868193, 1 page
https://doi.org/10.1155/2023/9868193

Retraction

Retracted: Multimode Intelligent Control Based on Multidata Fusion Filtering in High-Speed Train Traffic Signal and Control

Journal of Sensors

Received 31 October 2023; Accepted 31 October 2023; Published 1 November 2023

This article has been retracted by Hindawi following an investigation undertaken by the publisher [1]. This investigation has uncovered evidence of one or more of the following indicators of systematic manipulation of the publication process:

(1) Discrepancies in scope
(2) Discrepancies in the description of the research reported
(3) Discrepancies between the availability of data and the research described
(4) Inappropriate citations
(5) Incoherent, meaningless and/or irrelevant content included in the article
(6) Peer-review manipulation

The presence of these indicators undermines our confidence in the integrity of the article's content and we cannot, therefore, vouch for its reliability. Please note that this notice is intended solely to alert readers that the content of this article is unreliable. We have not investigated whether authors were aware of or involved in the systematic manipulation of the publication process.

Wiley and Hindawi regrets that the usual quality checks did not identify these issues before publication and have since put additional measures in place to safeguard research integrity.

We wish to credit our own Research Integrity and Research Publishing teams and anonymous and named external researchers and research integrity experts for contributing to this investigation.

The corresponding author, as the representative of all authors, has been given the opportunity to register their agreement or disagreement to this retraction. We have kept a record of any response received.

References

[1] B. Huang and Y. Huang, "Multimode Intelligent Control Based on Multidata Fusion Filtering in High-Speed Train Traffic Signal and Control," *Journal of Sensors*, vol. 2021, Article ID 6081999, 10 pages, 2021.

Hindawi
Journal of Sensors
Volume 2023, Article ID 9896282, 1 page
https://doi.org/10.1155/2023/9896282

Retraction

Retracted: Personalized Marketing Recommendation System of New Media Short Video Based on Deep Neural Network Data Fusion

Journal of Sensors

Received 17 October 2023; Accepted 17 October 2023; Published 18 October 2023

This article has been retracted by Hindawi following an investigation undertaken by the publisher [1]. This investigation has uncovered evidence of one or more of the following indicators of systematic manipulation of the publication process:

(1) Discrepancies in scope
(2) Discrepancies in the description of the research reported
(3) Discrepancies between the availability of data and the research described
(4) Inappropriate citations
(5) Incoherent, meaningless and/or irrelevant content included in the article
(6) Peer-review manipulation

The presence of these indicators undermines our confidence in the integrity of the article's content and we cannot, therefore, vouch for its reliability. Please note that this notice is intended solely to alert readers that the content of this article is unreliable. We have not investigated whether authors were aware of or involved in the systematic manipulation of the publication process.

Wiley and Hindawi regrets that the usual quality checks did not identify these issues before publication and have since put additional measures in place to safeguard research integrity.

We wish to credit our own Research Integrity and Research Publishing teams and anonymous and named external researchers and research integrity experts for contributing to this investigation.

The corresponding author, as the representative of all authors, has been given the opportunity to register their agreement or disagreement to this retraction. We have kept a record of any response received.

References

[1] F. Huang, "Personalized Marketing Recommendation System of New Media Short Video Based on Deep Neural Network Data Fusion," *Journal of Sensors*, vol. 2021, Article ID 3638071, 10 pages, 2021.

Hindawi
Journal of Sensors
Volume 2023, Article ID 9876029, 1 page
https://doi.org/10.1155/2023/9876029

Retraction

Retracted: Facing Big Data Information Fusion and Data Mining Technology to Construct College Physical Education Teaching Evaluation System

Journal of Sensors

Received 17 October 2023; Accepted 17 October 2023; Published 18 October 2023

This article has been retracted by Hindawi following an investigation undertaken by the publisher [1]. This investigation has uncovered evidence of one or more of the following indicators of systematic manipulation of the publication process:

(1) Discrepancies in scope
(2) Discrepancies in the description of the research reported
(3) Discrepancies between the availability of data and the research described
(4) Inappropriate citations
(5) Incoherent, meaningless and/or irrelevant content included in the article
(6) Peer-review manipulation

The presence of these indicators undermines our confidence in the integrity of the article's content and we cannot, therefore, vouch for its reliability. Please note that this notice is intended solely to alert readers that the content of this article is unreliable. We have not investigated whether authors were aware of or involved in the systematic manipulation of the publication process.

In addition, our investigation has also shown that one or more of the following human-subject reporting requirements has not been met in this article: ethical approval by an Institutional Review Board (IRB) committee or equivalent, patient/participant consent to participate, and/or agreement to publish patient/participant details (where relevant).

Wiley and Hindawi regrets that the usual quality checks did not identify these issues before publication and have since put additional measures in place to safeguard research integrity.

We wish to credit our own Research Integrity and Research Publishing teams and anonymous and named external researchers and research integrity experts for contributing to this investigation.

The corresponding author, as the representative of all authors, has been given the opportunity to register their agreement or disagreement to this retraction. We have kept a record of any response received.

References

[1] Y.-t. Ma, "Facing Big Data Information Fusion and Data Mining Technology to Construct College Physical Education Teaching Evaluation System," *Journal of Sensors*, vol. 2021, Article ID 7168855, 15 pages, 2021.

Hindawi
Journal of Sensors
Volume 2023, Article ID 9842945, 1 page
https://doi.org/10.1155/2023/9842945

Retraction

Retracted: Course Ideological and Political Teaching Platform Based on the Fusion of Multiple Data and Information in an Intelligent Environment

Journal of Sensors

Received 17 October 2023; Accepted 17 October 2023; Published 18 October 2023

This article has been retracted by Hindawi following an investigation undertaken by the publisher [1]. This investigation has uncovered evidence of one or more of the following indicators of systematic manipulation of the publication process:

(1) Discrepancies in scope
(2) Discrepancies in the description of the research reported
(3) Discrepancies between the availability of data and the research described
(4) Inappropriate citations
(5) Incoherent, meaningless and/or irrelevant content included in the article
(6) Peer-review manipulation

The presence of these indicators undermines our confidence in the integrity of the article's content and we cannot, therefore, vouch for its reliability. Please note that this notice is intended solely to alert readers that the content of this article is unreliable. We have not investigated whether authors were aware of or involved in the systematic manipulation of the publication process.

In addition, our investigation has also shown that one or more of the following human-subject reporting requirements has not been met in this article: ethical approval by an Institutional Review Board (IRB) committee or equivalent, patient/participant consent to participate, and/or agreement to publish patient/participant details (where relevant).

Wiley and Hindawi regrets that the usual quality checks did not identify these issues before publication and have since put additional measures in place to safeguard research integrity.

We wish to credit our own Research Integrity and Research Publishing teams and anonymous and named external researchers and research integrity experts for contributing to this investigation.

The corresponding author, as the representative of all authors, has been given the opportunity to register their agreement or disagreement to this retraction. We have kept a record of any response received.

References

[1] J. Zhou, Z. Wei, F. Jia, and W. Li, "Course Ideological and Political Teaching Platform Based on the Fusion of Multiple Data and Information in an Intelligent Environment," *Journal of Sensors*, vol. 2021, Article ID 1558360, 10 pages, 2021.

Hindawi
Journal of Sensors
Volume 2023, Article ID 9762451, 1 page
https://doi.org/10.1155/2023/9762451

Retraction

Retracted: College English Teaching Quality Evaluation System Based on Information Fusion and Optimized RBF Neural Network Decision Algorithm

Journal of Sensors

Received 17 October 2023; Accepted 17 October 2023; Published 18 October 2023

This article has been retracted by Hindawi following an investigation undertaken by the publisher [1]. This investigation has uncovered evidence of one or more of the following indicators of systematic manipulation of the publication process:

(1) Discrepancies in scope
(2) Discrepancies in the description of the research reported
(3) Discrepancies between the availability of data and the research described
(4) Inappropriate citations
(5) Incoherent, meaningless and/or irrelevant content included in the article
(6) Peer-review manipulation

The presence of these indicators undermines our confidence in the integrity of the article's content and we cannot, therefore, vouch for its reliability. Please note that this notice is intended solely to alert readers that the content of this article is unreliable. We have not investigated whether authors were aware of or involved in the systematic manipulation of the publication process.

Wiley and Hindawi regrets that the usual quality checks did not identify these issues before publication and have since put additional measures in place to safeguard research integrity.

We wish to credit our own Research Integrity and Research Publishing teams and anonymous and named external researchers and research integrity experts for contributing to this investigation.

The corresponding author, as the representative of all authors, has been given the opportunity to register their agreement or disagreement to this retraction. We have kept a record of any response received.

References

[1] Y. Chen, "College English Teaching Quality Evaluation System Based on Information Fusion and Optimized RBF Neural Network Decision Algorithm," *Journal of Sensors*, vol. 2021, Article ID 6178569, 9 pages, 2021.

Hindawi
Journal of Sensors
Volume 2022, Article ID 1569197, 11 pages
https://doi.org/10.1155/2022/1569197

Research Article

Image Data Fusion Algorithm Based on Virtual Reality Technology and Nuke Software and Its Application

Hongchang Song[1] **and Tengfei Li**[2]

[1]*School of Arts, Xi'an International Studies University, Xi'an, 710010 Shaanxi, China*
[2]*Terminal Business Division, Zhongxing Telecom Equipment, Xi'an, 710055 Shaanxi, China*

Correspondence should be addressed to Hongchang Song; songhongchang@xisu.edu.cn

Received 10 September 2021; Revised 13 January 2022; Accepted 14 February 2022; Published 23 March 2022

Academic Editor: Mu Zhou

As an important branch of multisensor information fusion, image fusion is widely used in various fields. As a hot research technology, virtual reality technology can bring different levels of experience to image fusion. At the same time, with the development of existing image processing software, it is conducive to the further analysis and processing of images. In today's market, image processing technology still faces many problems, and with the advancement of technology, virtual technology is widely used in various fields, so combining virtual technology with images is conducive to improving image processing technology. This article mainly introduces the image fusion algorithm and its application research based on virtual reality technology and Nuke software. This paper first proposes a picture fusion model and a picture fusion system through the analysis of virtual technology and Nuke software and, on this basis, proposes a particle algorithm and a picture edge algorithm. Secondly, the optimal fusion of images is studied on Nuke software, and finally the experimental results are analyzed through image fusion algorithm. Studies have shown that the best image fusion greatly improves the security and privacy of the image, and the difficulty of cracking is as high as 80%. The data in the experimental analysis of the graphic fusion algorithm shows that the execution efficiency and time consumption of the algorithm are greatly shortened, and the time consumption is greatly reduced. The rate is reduced by about 50%, and a good image fusion effect has been achieved.

1. Introduction

1.1. Research Background and Significance. With the development of information technology, the field of development of virtual reality technology has gradually expanded. Virtual reality technology will play an important role in the development of future high-tech industries and the improvement of national technological innovation capabilities. The combination of image processing and virtual technology has become a research hotspot [1]. The use of image processing technology is often required in the medical field, and combining virtual technology with image processing can improve the hierarchy of image analysis and enable more accurate determination of the cause of disease. Among them, the rapid development of synthesis technology is based on the development of virtual reality technology. In the field of graphic image design, virtual reality technology is involved, and it is widely used, and the effect it presents has reached a very high level [2, 3]. At the same time, with the development of computer technology and the rapid development of image processing software, the Nuke software is the leader in many image processing, and its functions in image fusion, image three-dimensional integration, and film processing are extremely powerful, which further promotes image processing [4, 5]. The Nuke software provides artists with the means to create images with high-quality photo effects. Nuke requires no special hardware platform, yet provides artists with the flexibility, efficiency, economy, and full functionality to combine and manipulate

scanned photographs, video boards, and computer-generated images. Having been used in nearly a hundred films and hundreds of commercial and music TVs in the digital sector, Nuke has the advanced ability to seamlessly integrate the final visuals with the rest of the film and TV, regardless of the style or complexity of the visuals to be applied. Among them, image fusion in image processing has attracted much attention. Image fusion is to fuse images about the same target collected through different methods through different algorithms, extract the information of each image, and finally generate an image containing each image feature [6, 7]. It extracts useful information in different images, eliminates the redundancy between image information obtained in different ways, and accurately, concisely, and completely describe the target in one image, which greatly facilitates people's observation of the target and the subsequent processing of the target image [8, 9]. Since the emergence of image fusion technology, it has been applied to various occasions, and it was first applied in the use of satellites to observe ground conditions. Now it has very good applications in the detection of military field, the integration of information in the field of remote sensing, the transportation in daily life, and the diagnosis in the medical field.

1.2. Related Content. As the international standard of virtual reality, the virtual reality modeling language is developing rapidly. Sun and Zhao proposed a VRML method [10]. Through audiovisual-based virtual communication, virtual reality (VR) has played an indispensable role in dealing with this epidemic. They extended the functions of script nodes by introducing Java and script programs written in the Java script language. Make the library virtualized to meet the normal use of users. In principle, any text editing system can be used for VRML programming, but some editing systems have few related functions, so they are not suitable for large-scale VRML scene design [11]. The VRML algorithm they proposed can be applied to large buildings. The VRML algorithm they proposed is superior to traditional algorithms in terms of authenticity, interactivity, design rationality, and execution speed. Prove the practicability of the VRML algorithm. It provides assistance to people who are inconvenient to go out during the COVID-19 protection period. However, there are still limitations to its use in other periods. Allen et al. developed an open source software package [12], which is available for free on GitHub and distributed to other health systems under the Apache 2.0 open source license. They adopt the quality improvement project registry and promote it to the intended audience is an important factor in the success of the registry. To help understand the impact of improving quality project management in the hospital system, eventually reduce the time for approving quality improvement projects, increase the collaboration of the entire UF health hospital system, and reduce the redundancy and translation of quality improvement projects. They developed a registry matching algorithm based on Jaccard similarity coefficient, which uses quality project characteristics to find items of similar quality. The algorithm allows quality researchers to find existing or previous quality improvement projects to encourage collaboration and reduce duplicate projects. They also developed the QIPR approver algorithm, which can guide researchers to solve a series of problems that can enable projects of appropriate quality to be approved without manual intervention. Although it is convenient, it requires professional operation. Li et al. proposed a multifocus image fusion algorithm based on multilevel morphological decomposition and classifier [13]. The attraction of this algorithm is that it can decompose an image into several layers with different morphological components, thereby preserving more detailed information of the source image. In the algorithm they proposed, the source image is first decomposed by multilevel morphological component analysis [14, 15]. Then, feature vectors are extracted from the natural layer and classified by two well-trained support vector machines. Then, the consistency verification is used to verify the decision matrix set. Finally, the coefficients are fused based on the set of decision matrices. Their experimental results proved the superiority of this method in subjective and objective evaluation. But this algorithm has errors [16].

1.3. Main Content and Innovation. This paper is mainly based on virtual reality technology and Nuke software to carry out the research of image fusion algorithm and the research of algorithm application. It mainly uses virtual technology to build image fusion model and design graphics system model, then proposes image fusion algorithm, and conducts algorithm research and experiment on the Nuke software to get the effect and function of image fusion algorithm. The innovation of this paper is to combine virtual technology and software technology to propose an image fusion algorithm and conduct an image fusion experiment analysis to get the application and effect of the image fusion algorithm.

The first part of the article introduces the relevant background and significance of virtual reality technology and NUKE software and provides a brief overview of the relevant work involved and a brief outline of the innovations in the article.

The second part of the article focuses on the evolution of image fusion algorithms and software design and image evaluation metrics.

The third part of the article focuses on image fusion models for image edge detection and virtual techniques.

The fourth part of the article introduces the optimal image fusion and image fusion algorithms and analyzes the experimental results.

The fifth part of the article provides a brief discussion and analysis of the experiments and analysis of the article.

2. Software Overview and Image Fusion Algorithm

2.1. Overview of Nuke Software. Nuke as a picture and film synthesis software, Nuke won the Oscar Award. After more than ten years of experience, film and television professionals can now provide solutions for creating high-quality, high-precision photo-effect images [17]. Nuke does not need to define itself on the hardware platform and is very close to people. In terms of performance, it is an effective tool for artists to

combine and process scanned photos and video cards, and it can also provide flexible, effective, and practical tools. With the preservation of picture fusion processing and complete picture processing solutions, the Nuke platform is favored by most users due to its own advantages. Nuke was originally a unique secret weapon developed and used by D2. It is used in conjunction with Houdini, the world's most powerful special effects software, and mainly relies on these two powerful software. The functional practicability and speed of Nuke can be reflected in the relevant data [18, 19]. Nuke is used in many award-winning films and photography works, and many well-known artists use the software to create. Nuke has many additional components. Among them, three-dimensional film production additional program: Ocula is one of The Foundry's best works and is an additional program designed specifically for the production of three-dimensional film. Ocula can help users quickly solve various problems in the production process of stereoscopic film. Its amazing appearance and performance make it possible to save a lot of productivity in the three-dimensional film production industry and improve production efficiency. In the subsequent Hollywood stereoscopic movies, almost all are Okura characters [20, 21]. Nuke is a cross-platform comprehensive software with a powerful composite type, which has great compatibility. It can be used and used on multiple systems on the network because it has different versions for different system platforms. In this way, users do not have to worry about being unable to use the software due to system incompatibility. Nuke can independently create its own model objects, cameras and lights on its own platform, can quickly and freely switch between 3D scene mode and 2D composition mode at runtime, and can also paste composite scenes. Attach as a texture to the newly created model. Nuke can perform multicamera settings, and a combination of multiple light shows on the three-dimensional scene created by itself, including projecting between multiple objects and adjusting the depth of field effect of the camera [22]. Nuke allows you to perform color correction and comparison between different color ranges on the screen and can quickly and easily switch between different color ranges on the same screen, so that users can use it quickly and effectively. More importantly, the Nuke platform has different color grading filters for different color ranges, and users can find their own different color grading methods and corresponding filter combinations [23]. It should also be mentioned here that Nuke also integrates the famous coding plug-ins Primatte, Uimatte, and Keylight by default, which adds fun and unlimited possibilities for postcoding work. Based on the powerful image processing function of the software, this paper conducts experiments and analysis on the image fusion algorithm on the software, and in the proposed image fusion algorithm, it gives the experimental basis and provides pictures for the proposal and application research of the image fusion algorithm fusion platform [24, 25].

2.2. Particle Swarm Algorithm (PSO). Particle swarm algorithm is another new swarm intelligence algorithm after ant colony algorithm, and it has become an important branch of evolutionary algorithm [26, 27]. The particle swarm algorithm is a stochastic search algorithm based on group collaboration developed by simulating the foraging behaviour of a flock of birds. It basically combines the ideas of quantum physics to modify the "evolution" method of PSO (that is, the method of updating the position of particles). To update the position of the particles, center on the best current local position information and the best global position information of each particle. In PSO, the movement of particles is carried out in the following three types. The full name of the particle swarm algorithm is Particle Swarm Optimization, so it is abbreviated as "PSO."

$$\begin{aligned} m\text{best}(t) &= \frac{1}{M}\sum_{i=1}^{M} P(t), \\ PP(t) &= f(t+1) * P(t) + (1 - f(t+1)) * P(t), \\ X(t) &= PP(t+1) + \text{Rand}(t) \times a(t+1). \end{aligned} \tag{1}$$

The function f produces a particle evolution formula with a value range of 0-1: obey a uniformly distributed random number, and f takes -1 and 1 with a certain probability. Our method is as follows:

$$\text{Rand}(t) = \begin{cases} -1, \text{if} : \text{rand}\,() \le 0.1, \\ +1, \text{if} : \text{rand}\,() > 0.1. \end{cases} \tag{2}$$

a is the contraction and expansion coefficient of PSO, the value of a depends on the situation, it can be fixed, and it can be dynamically changed in a certain way, generally according to the following formula:

$$a(t) = m - (m - n) \times \frac{t}{\text{MaxT}}. \tag{3}$$

That is, a linearly decreases from m to n with iteration, where MaxT is the maximum number of iterations. The algorithm flow of POS is as follows: *Initialization*. Initialize the initial positions of M particles randomly, and set the current best position of each particle as follows: $P = X$, and let the global best position be

$$P(0) = \max\{x(0, x(1) \cdots x(m)\}. \tag{4}$$

Calculate the objective function value of the particle according to the calculation formula of the objective function f; update the new local optimal position p of each particle according to the following formula, assuming that we are maximizing the objective function:

$$P(t) = \begin{cases} p(t)\,; \text{if} f(P(t)) \ge f(X(t)), \\ X(t)\,; \text{if} f(P(t)) < f(X(t)). \end{cases} \tag{5}$$

Update the global optimal position P according to the following formula:

$$P_g(t) = \max\{P(t1), P(t2) \cdots P(tm)\}. \tag{6}$$

Repeat the above calculations until the general number of iterations in the algorithm reaches a certain value.

2.3. Evaluation Index of Image Fusion. After the fusion process is completed, it is not a simple matter to judge the quality of the image algorithm [28]. Images include image fidelity and image readability. Image fidelity refers to the degree of deviation of the evaluated image from the standard image; the smaller the deviation, the higher the fidelity. Readability refers to the ability of an image to provide information to a person or machine, not only in relation to the application requirements of the image system, but also often in relation to the subjective perception of the human eye. Image quality indicators include aspects such as resolution, color depth, and image distortion. The evaluation of image algorithm quality should consider the following aspects. First, the result image after fusion should contain as much of the important information of the original image as possible; second, the result image after fusion should not introduce wrong image information, so as not to mislead the result image, the observation, and subsequent processing of the image; third, in the process of acquiring the image, the image quality may be reduced due to climate or other factors, or the image quality during the preprocessing process is not very good. At this time, the result of the image fusion algorithm should not fluctuate too much; fourth, when the acquired image is mixed with noise, the algorithm should minimize the effect of noise on the result of the image fusion; fifth, the image fusion algorithm needs to be processed in real time. The occasion should be able to be easily transplanted to the hardware platform [29, 30]. The evaluation criteria for the result image after fusion can be divided into two parts, including the subjective method of direct observation by the human eye and the objective method of calculation using image parameters and related formulas. According to the subjective method of direct observation by the human eye, the viewer evaluates the image quality of the result according to the existing evaluation level and his own image evaluation experience. Sometimes, the viewer can also provide some standard images used to make comparative judgments. According to the subjective method of direct observation by the human eye, it is not easy to operate in practical applications and is easily affected by the observer's own conditions and psychological aspects. Therefore, objective methods that combine image parameters and related formula calculations are often used in practical applications. It can not only overcome subjective the shortcomings of the method but also can achieve automatic evaluation of the result image. Because the preprocessing process of the image is completed by the computer, the objective method for the later quality evaluation is effectively combined with the preprocess to improve the efficiency of the entire image processing.

Image fusion maximizes the extraction of favorable information from the respective channels and finally combines them into a high-quality image to increase the utilisation of image information, improve the accuracy and reliability of computer interpretation, enhance the spatial and spectral resolution of the original image, and facilitate monitoring.

3. Image Fusion Model of Image Edge Detection and Virtual Technology

3.1. The Detection Operator of the Image Edge. The image information contains many image features that can be cited, among which the commonly used features include the following: color features, geometric features, and texture features. The feature extraction work in this paper focuses on edge extraction. The selection of edge features is mainly based on this consideration: the edge features are invariant, and the edge of the same scene remains basically unchanged under different conditions (lighting and color). The two most useful features that effectively describe this change are the rate and direction of grayscale change. Generally, the grayscale change rate along the edge is relatively small, while the grayscale perpendicular to the edge changes more drastically. The actual digital image is represented by the magnitude and direction of the gradient vector. The neighborhood of each pixel is checked, and the gray-scale change rate is quantified, and the difference is approximated by differential differentiation. The benefits of edge algorithms include real-time technical processing, the ability to reduce the impact of broadband limitations, increased security of sensitive and private data, operational data reliability, and the versatility of application development. Figure 1 shows a specific process diagram:

(1) Roberts edge operator

The Roberts edge operator is a kind of analysis using the edge of a partial image, and the edge amplitude is calculated as follows:

$$\begin{aligned} g(x,y) &= |X| + |Y|, \\ g &= f(x,y) - f(x+1, y+1). \end{aligned} \tag{7}$$

(2) Sobel edge operator

The Sobel edge operator calculates the level value in the $3 * 3$ field, and the level value convolution formula is as follows:

$$G_x \begin{cases} -1, \\ -2, \\ 1. \end{cases} \tag{8}$$

(3) Laplace operator

The Laplacian operator is an edge detection operator. It is commonly used for edge detection. For a continuous function f, its position (x, y) is defined as follows:

$$\Delta f(x,y) = \frac{\vartheta}{\vartheta x} f(x,y). \tag{9}$$

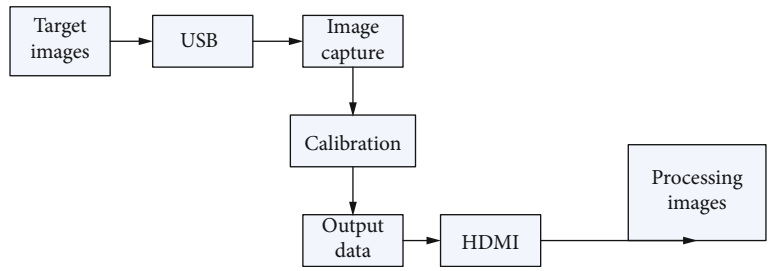

Figure 1: Flow chart of the proposed method.

Table 1: Laplacian operator template.

0	-1	0	-1	-1	1
-1	4	-1	-1	7	1
0	3	0	-1	-1	-1

Figure 2: A photo taken with a fish-eye lens (picture source http://image.baidu.com/).

Figure 3: The expanded cube panorama (picture source http://image.baidu.com/).

One of the two commonly used forms of expression using difference equations in practice is as follows:

$$\Delta f(x,y) = 4f(x,y) - [f(x+1,y) + f(x-1,y)]. \quad (10)$$

The numerical approximation method involving the diagonal field is given by the following:

$$\Delta f(x,y) = 8f(x,y) - F,$$
$$F = f(x+1,y-1) + f(x+1,y) + f(x+1,y+1). \quad (11)$$

In digital images, Laplacian operators can be implemented with the help of various templates. The two common templates are as follows:

As shown in Table 1, there are only two types of Laplacian operator templates, which have both the smoothing characteristics of Gaussian operators and the sharpening characteristics of Laplacian operators.

The Sobel operator is a discrete difference operator that is used to approximate the gradient of the image brightness function. The Laplace operator is the simplest isotropic differential operator with rotational invariance; the Roberts edge operator can be used to obtain the contours of the edges of a fixed-format document image, and the Hough algorithm can be used to extract straight lines from the contoured image.

3.2. Virtual Technology Integrated Image Model. Panorama is a technology that uses real images to create a virtual environment. A panoramic image is a representation of a continuous image created by processing discrete sample images. Panoramic images can be divided into spherical and cubic shapes according to the different shapes of the image surface. We call them spherical panoramic images or panoramic cube images.

3.2.1. Spherical Panorama. A spherical panorama is the shape of a spherical surface connected to photos taken by a normal camera. Obviously, the spherical panorama is the description of the panorama closest to the human eye model, but the spherical mapping is a nonuniform sampling representation, which will cause image distortion and distortion of the scene. The two poles are particularly serious. When storing spherical projection data, one will be lost. Project the computer data storage structure and the real plane photo on the spherical image, so that a nonlinear deformation process can occur in the image plane. A nonlinear image conversion operation must be performed, resulting in a decrease in display speed. At present, the spherical panorama is mainly obtained by a special fish-eye camera (Figure 2 shows the picture taken by the fish-eye camera), and the spherical panorama is finally obtained by restoring

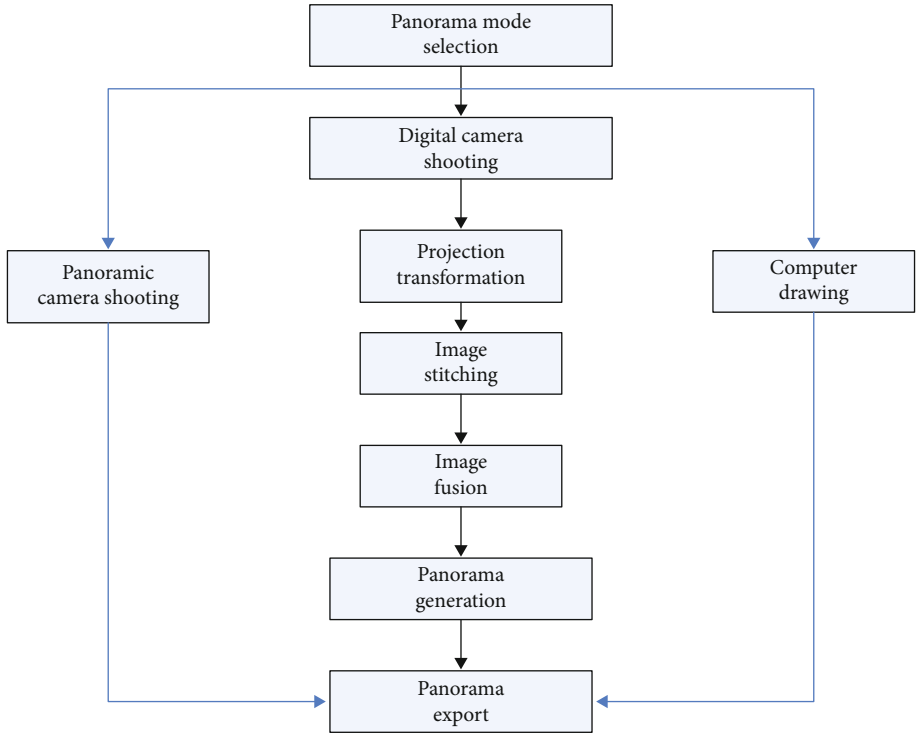

Figure 4: The process of generating a panorama.

the distortion, synthesizing the picture, and adjusting the brightness.

3.2.2. Cube Panorama. The generation of the cube panorama is to map the real image to the six surfaces of a cube. This structure pattern has good regularity and easy data storage. The expanded cube panorama is shown in Figure 3. However, at the junction of the cube surface, the image is prone to change. The camera is required to be placed very accurately when the camera is sampled. The six sides are perpendicular to each other to avoid optical distortion, and each plane image captured requires a 90° wide-angle lens, to avoid image distortion.

The spherical panorama takes the longitude and latitude coordinates of the sphere and directs them to a grid of horizontal and vertical coordinates, a grid that is approximately twice as high as it is wide. Thus, from the equator to the poles, the horizontal stretch intensifies and the north and south poles are stretched into a flattened grid across the upper and lower edges. The spherical panorama allows a realistic 360 panorama of the entire horizontal and vertical. The cube panorama is a panorama divided into six sides, front, back, left, right, top, and bottom, which when viewed are combined into a confined space to realise the entire horizontal and vertical 360 panorama.

The use of panoramas in image data fusion allows a nonlinear deformation process to take place in the image plane, performing a nonlinear image transformation operation, thus reducing the display speed and avoiding image distortion.

The method of taking photos with a normal camera and then stitching them together to form a panorama does not require scene modeling and can be viewed in real time. In the component environment, the processing time has nothing to do with the complexity of the scene, so the real world can be preserved without special hardware acceleration, powerful graphics, and real-time interactive development. Therefore, people often use this method to create panoramas. Panorama generation is a complex process, including the establishment of a panorama model, image collection, image patchwork, image synthesis, and panorama. Show and explore five stages. The process of generating a panorama is shown in Figure 4.

3.3. Image System Model Based on Virtual Reality Technology. Existing virtual reality imaging systems usually have two main modules: preprocessing and interaction. In the preprocessing module, the system completes the function of generating virtual scenes, while the interactive module mainly supplements the interactive activities between the system and participants and performs the roaming function. The programming module is responsible for finding the panorama corresponding to the current viewpoint. And set the current viewing direction. Part of the panoramic image is sent to the buffer, and the projection module is responsible for converting the cylindrical projection image in the buffer into a plane projection image and displaying it on the observation screen. Image fusion technology is an important branch of digital image processing, widely used in spatial texture detection, heritage conservation, medical images, public security forensics, virtual reality, and other fields. Due to the influence of various factors such as illumination, angle, displacement, and dithering of the captured images, image fusion is prone to distortion and deformation.

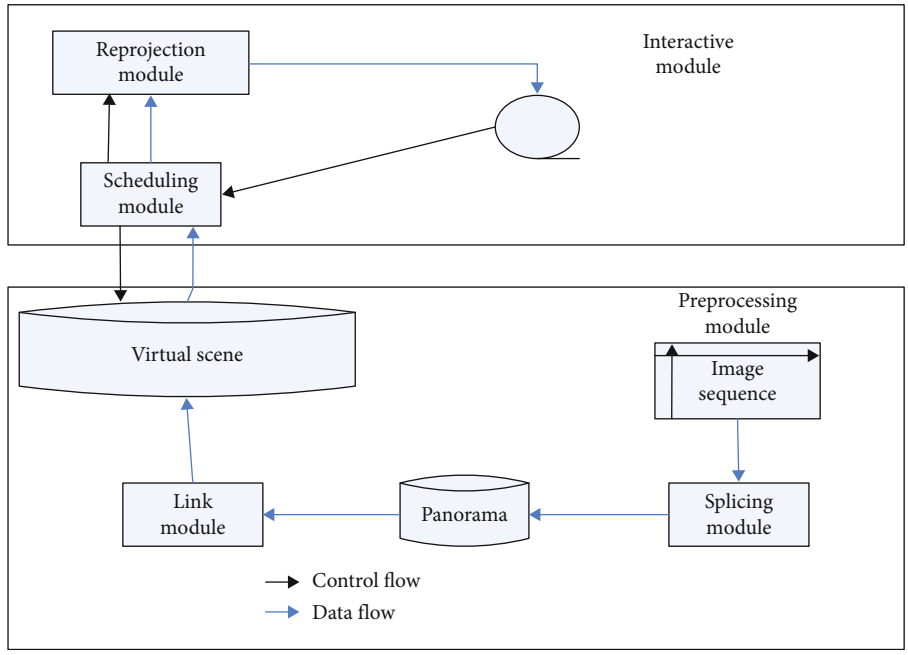

Figure 5: Image system frame model based on virtual reality technology.

Table 2: Fusion factors of different images.

Image	Actual fusion factor	Critical fusion factor
Cloud tower image	0.1	0.2
Cabin image	0.17	0.4
Gobi images	0.11	0.3
Watermark image	0.15	0.25
Lean image	0.07	0.11

The projection model and image fusion are used to study the distortion and deformation and to improve the traditional fusion techniques. In summary, the existing virtual reality image system has a frame model as shown in Figure 5.

As shown in Figure 4, the frame model of the image system based on virtual reality technology is composed of two parts. The first part is the interaction module, and the second part is the preprocessing module. These two modules are independent but related. In the preprocessing module, there is a splicing module that analyzes the image sequence into a panoramic image and then processes it into a virtual scene through the link module. Then, carry out the joint processing between the interactive module and the preprocessing module.

4. Best Image Fusion and Image Fusion Algorithm

4.1. Best Fusion of Images

4.1.1. Direct Integration in the Airspace. In this paper, software experiments are carried out on the fusion of pictures, the images in Table 2 are merged into the original images, and the corresponding critical fusion factors and actual fusion factors are calculated. The measured data are shown in Table 2.

As shown in Table 2, there is a big difference between the actual melting factor and the critical factor. The purpose of this research is to bring the actual melting factor closer to the critical melting factor to improve the ability to resist hidden images. The watermark image is fused into the lean image, and the fusion factor is 0.07. The fused image is shown in Figure 6(a), and its peak signal-to-noise ratio is 28. The extracted hidden image is shown in Figure 6(b), and the watermark is extracted. The normalized correlation coefficient of is 0.9. The higher the actual melting factor and criticality factor during the experiment, the better the peak signal-to-noise ratio of its fused image, and the better the effect of hiding the image.

To determine the robustness of the algorithm, perform various jamming attacks on the algorithm. The attack types are as follows: image cropping, JPEG compression, adding Gaussian noise, salt and pepper noise, product noise, Gaussian filtering, etc., and normalized correlation coefficients are shown in Table 3, and the extracted watermark is shown in Figures 6 and 7.

Based on Figure 8, it can be seen that the shear impact parameter is 2 with a correlation coefficient of 0.66, the Gaussian noise has a mean value of 0, a variance of 0.02, and a correlation coefficient of 0.3, and the product noise has a mean value of 2, a variance of 0.03, and a correlation coefficient of 0.2.

4.1.2. Research and Analysis of the Best Fusion Factor. By multiplying the image watermark to reduce the gray level by 0.6 and obtain the best geometric transformation, it is used to hide the image watermark, and the fusion factor is measured to be 0.15. Due to the method of reducing the gray level and the best geometric transformation, the fusion

(a) (b)

Figure 6: (a) Fused image; (b) extracted watermark image.

Table 3: Normalized correlation coefficient.

Attack type	Parameter	Correlation coefficient
Shear attack	Cut in half	0.66
JPEG compression	Quality = 50	0.5
Gaussian noise	The mean is 0, and the variance is 0.02	0.3
Salt and pepper noise	Intensity $d = 0.1$	0.7
Product noise	The mean is 2, and the variance is 0.03	0.2
Gaussian filtering	Gaussian, 0.5	0.9

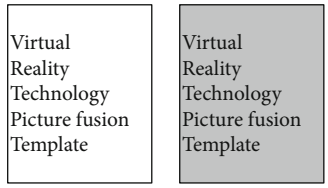

(a) (b)

Figure 7: (a) Cut in half; (b) JPEG compression.

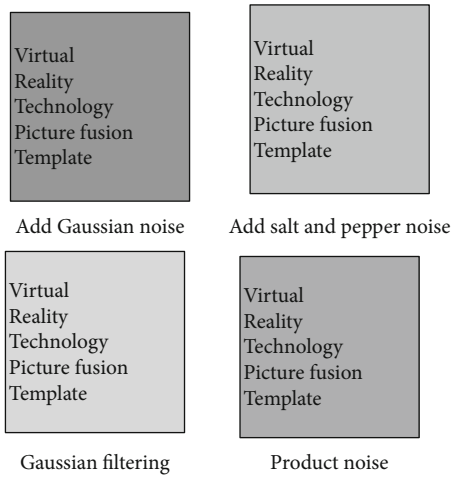

Figure 8: Each operation image.

factor is not only greater than the direct fusion factor of the image in the spatial domain, and the image is fused into the image with this fusion factor. The fused image is shown in Figure 9(a), and its peak signal-to-noise ratio is 28. The extracted hidden image is as a shown in Figure 9(b), and the normalized correlation coefficient of the extracted watermark is 0.9.

In order to determine the robustness of the algorithm, various types of attacks are performed on the algorithm as follows: image cropping, JPEG compression, adding Gaussian noise, salt and pepper noise, multiplicative noise, Gaussian filtering, etc., and the normalized correlation coefficients measured are as follows. As shown in Table 4, the extracted watermark is shown in Figures 9 and 10. The coefficients in Table 4 are calculated by normalizing the parameters of the experimental target to obtain the correlation coefficient.

As shown in Figures 10 and 11 and Table 4, it can be seen that the best fusion algorithm uses the iterative changes related to image fusion to greatly increase the fusion factor of the image and greatly improve the image's antiattack ability. Since the calculation of the fusion factor is related to two images, the matrix and number of iterations used in the fusion factor and various attacks can be used as the key to improving the security of the algorithm.

4.2. Experimental Results and Analysis of Image Fusion Algorithm. The data sets used in the experiment in this

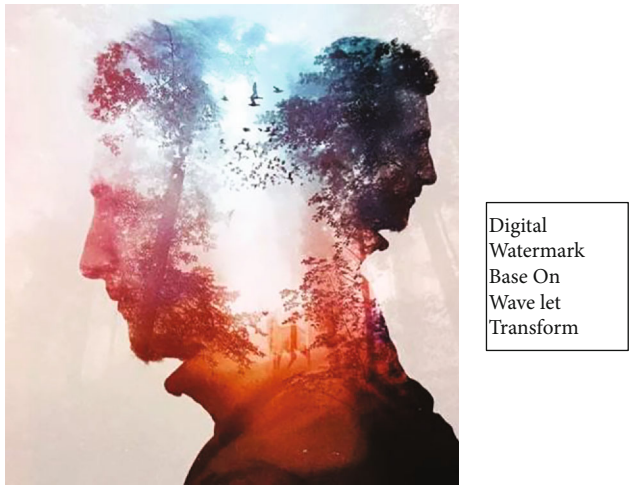

(a) (b)

Figure 9: (a) Fused image; (b) extracted watermark image.

Table 4: Normalized correlation coefficients under image processing and attack.

Attack type	Parameter	Correlation coefficient
Shear attack	Cut in half	0.68
JPEG compression	Quality = 50	0.85
Gaussian noise	The mean is 0, and the variance is 0.02	0.6
Salt and pepper noise	Intensity $d = 0.1$	0.75
Product noise	The mean is 2, and the variance is 0.03	0.9
Gaussian filtering	Gaussian, 0.5	0.88

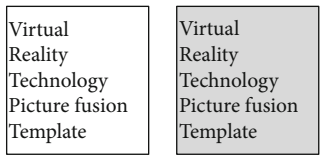

(a) (b)

Figure 10: (a) Cut in half; (b) JPEG compression.

article are collected data set and standard data set. The algorithm proposed in this article is tested. The spatial data set contains two point cloud images, including three-dimensional coordinates and intensity information. The two point clouds are collected from different angles. The laboratory data set contains four point cloud data, which also contains coordinate information and color information. In this part, the abovementioned image fusion algorithm will be tested and compared with the execution time and final fusion accuracy of conventional algorithms. During the experiment, the Nuke data set was used, and an accurate fusion algorithm was executed based on the initial fusion. The first is to reduce the resolution of the point cloud to different degrees to obtain point clouds with different resolutions. The number of iterations is calculated during the execution of the algorithm after sampling. When experimenting, the total number of iterations between the proposed algorithm and the conventional algorithm is 90.

As shown in Table 5, the sampling parameter tables of the two data sets are described, respectively, including the resolution, the number of source and target points, and the number of iterations. As the resolution of the room data set decreases, the number of source points decreases significantly; the number of target points also decreases significantly, but the number of iterations increases. The number of source and target points and the number of iterations all show a clear downward trend as the resolution of the laboratory data set gets lower. In the fusion process, the time consumed by the algorithm in this paper and the traditional algorithm under different data sets are recorded, as shown in the table below.

In the text, algorithms refer to types of data fusion, including linear programming, quadratic programming, integer programming, and hybrid programming, with and without constraints. As shown in Table 6, in the room data set, the traditional algorithm consumes 60 times, and the algorithm time in this paper is 33, which is shortened by 27 minutes and increased by about 40%. Under the lab data set, the traditional algorithm consumes 120 times, and the algorithm in this paper is 40, which shortens 80 minutes and improves about 60%. Each iteration of the process consumes a different amount of time for both the room data set and the laboratory data set, a significant improvement compared to the traditional method. It saves time consumption

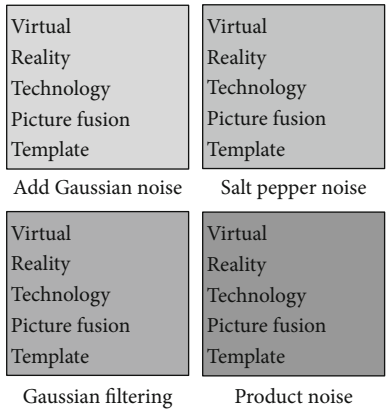

Figure 11: Various types of attack images.

Table 5: Data set downsampling parameter table.

Data set	Resolution	Number of source points	Number of target points	Number of iterations
Room data set	100%	1300	1400	10
	70%	980	1000	15
	40%	560	570	20
	20%	230	250	35
Lab data set	100%	1500	3800	5
	80%	1200	3000	15
	50%	800	1500	30
	30%	300	750	40

Table 6: Algorithm consumption time under different data sets.

Data set	Algorithm	Each iteration process consumes time	Total elapsed time
Room data set	Traditional algorithm	60	60
	Algorithm	10,10,7,6	33
Lab data set	Traditional algorithm	120	120
	Algorithm	10,11,9,10	40

to a large extent, and the efficiency is greatly improved. However, compared to the time comparison of the algorithm in the room data set and the lab data set, the time consumption under the room data set will be more, indicating that the execution efficiency of the algorithm in this data set is higher, but no matter from which data set, all the algorithms in this article are effective and beneficial.

5. Discussion

This paper uses the combined application of virtual reality technology and Nuke software to study the image fusion algorithm and the application of the algorithm, builds an image fusion model and model system through virtual reality technology, then proposes an image fusion algorithm, and then uses NUKE software to compare the algorithm. Through experiments and analysis, it is obtained that the algorithm shows sufficient protection in privacy protection, and comparing the image fusion algorithm with traditional algorithms, it is concluded that the image fusion algorithm has obvious advantages in time consumption. Image fusion can increase image spatial resolution, improve image geometric accuracy, enhance feature display capability, improve classification accuracy, provide change detection capability, replace or repair the defects of image data, etc. bring into play the advantages of different remote sensing data sources, compensate for the shortcomings of a certain kind of remote sensing data, and improve the applicability of remote sensing data.

Data Availability

No data were used to support this study.

Conflicts of Interest

All authors declare that they have no conflict of interest.

References

[1] D. Ross, "Digital twinning [information technology virtual reality]," *Engineering & Technology*, vol. 11, no. 4, pp. 44-45, 2016.

[2] L. Zeming, "Design and implementation of a Korean language teaching system based on virtual reality technology," *Agro Food Industry Hi-Tech*, vol. 28, no. 1, pp. 2156–2159, 2017.

[3] W. Mai, L. Fang, Z. Chen, X. Wang, and W. He, "Application of the somatosensory interaction technology combined with virtual reality technology on upper limbs function in cerebrovascular disease patients," *Journal of Biomedical Science and Engineering*, vol. 13, no. 5, pp. 66–73, 2020.

[4] L. Lan, Y. Fei, D. Shi, J. Shi, and Q. Jiang, "Application of virtual reality technology in clinical medicine," *American Journal of Translational Research*, vol. 9, no. 9, pp. 3867–3880, 2017.

[5] H. Chen, "Research of virtools virtual reality technology to landscape designing," *Open Construction & Building Technology Journal*, vol. 9, no. 1, pp. 164–169, 2015.

[6] D. Cao, G. Li, W. Zhu, Q. Liu, and X. Li, "Virtual reality technology applied in digitalization of cultural heritage," *Cluster Computing*, vol. 22, no. 4, pp. 1–12, 2017.

[7] P. Lai and W. Zou, "The application of virtual reality technology in medical education and training," *Global Journal of Information Technology Emerging Technologies*, vol. 8, no. 1, pp. 10–15, 2018.

[8] Z. Liang and R. Shuang, "Research on the value identification and protection of traditional village based on virtual reality technology," *Boletin Tecnico/Technical Bulletin*, vol. 55, no. 4, pp. 592–600, 2017.

[9] T. N. Chen, X. T. Yin, and X. G. Li, "Application of 3D virtual reality technology with multi-modality fusion in resection of glioma located in central sulcus region," *Zhonghua Yi Xue Za Zhi*, vol. 98, no. 17, pp. 1302–1305, 2018.

[10] W. Sun and C. Zhao, "Applications of virtual reality modeling language technology for COVID-19 pandemic," *Journal of Intelligent and Fuzzy Systems*, vol. 39, no. 6, pp. 8643–8653, 2020.

[11] S. Yong, H. Ying, Y. Dai, and F. Li, "The development of an interactive automatic tool changer system based on virtual reality technology," *International Journal of Multimedia & Ubiquitous Engineering*, vol. 11, no. 9, pp. 329–342, 2016.

[12] A. L. Allen, C. Barnes, K. S. Hanson, D. Nelson, and T. G. Akirala, "2510: QIPR: creating a quality improvement project registry," *Journal of Clinical and Translational Science*, vol. 1, no. S1, pp. 20-21, 2017.

[13] X. Li, L. Wang, J. Wang, and X. Zhang, "Multi-focus image fusion algorithm based on multilevel morphological component analysis and support vector machine," *IET Image Processing*, vol. 11, no. 10, pp. 919–926, 2017.

[14] Z. Xiaobing, Z. Wei, and S. Mengfei, "Oil exploration oriented multi-sensor image fusion algorithm," *Open Physics*, vol. 15, no. 1, pp. 188–196, 2017.

[15] G. Wang and Y. Huang, "Medical-image-fusion algorithm based on a detail-enhanced and pulse-coupled neural-network model stimulated by parallel features," *Scientia Sinica Informationis*, vol. 50, no. 2, pp. 239–260, 2020.

[16] J. Wang, C. Qin, X. Zhang, K. Yang, and P. Ren, "A multi-source image fusion algorithm based on gradient regularized convolution sparse representation," *Journal of Systems Engineering and Electronics*, vol. 31, no. 3, pp. 447–459, 2020.

[17] Y. Yuan and Q. Yang, "An image fusion algorithm based on wavelet transform and Fourier measurement matrix," *Journal of Information Hiding and Multimedia Signal Processing*, vol. 10, no. 1, pp. 30–36, 2019.

[18] Z. Cao, G. Shi, and Q. Wu, "A novel high dimensional image fusion algorithm based on smooth contourlet transformation and multi-scale model," *IPPTA: Quarterly Journal of Indian Pulp and Paper Technical Association*, vol. 30, no. 5, pp. 39–48, 2018.

[19] M. A. M, B. B. Wang, C. Q. Yan, and Q. Xue, "Image fusion algorithm-based rotating electrodes for electrical capacitance tomography," *Jiliang Xuebao/Acta Metrologica Sinica*, vol. 39, no. 1, pp. 43–46, 2018.

[20] Y. Li, Z. Zuo, G. Jin, and D. Su, "Research progresses of PET/CT image fusion algorithm based on wavelet transform," *Chinese Journal of Medical Imaging Technology*, vol. 34, no. 8, pp. 1267–1270, 2018.

[21] L. I. Jiao, Y. Yang, J. Dang, and Y. Wang, "NSST and guided filtering for multi-focus image fusion algorithm," *Journal of Harbin Institute of Technology*, 2018.

[22] K. J. Xia, J. Q. Wang, and J. Cai, "A novel adaptive PET/CT image fusion algorithm," *Current Bioinformatics*, vol. 14, no. 7, pp. 658–666, 2019.

[23] "A wavelet image fusion algorithm based on multi-resolution and multi-scale transform," *Boletin Tecnico/Technical Bulletin*, vol. 55, no. 7, pp. 35–41, 2017.

[24] H. M. Wang, Q. I. Zi-Long, S. O. Astronautics, and University, N. P, "A novel image fusion algorithm using adaptive PCNN based on artificial fish swarm optimization," *Guangdianzi Jiguang/Journal of Optoelectronics Laser*, vol. 28, no. 4, pp. 427–432, 2017.

[25] Z. Qi, "A multi sensor image fusion algorithm based on multi resolution analysis," *International Journal of simulation: systems*, vol. 17, no. 36, 2016.

[26] P. Wu, W. L. Li, D. Y. Qi, and W. L. Song, "An image fusion algorithm based on threshold-improved contourlet transform," *Journal of South China University of Technology (Natural Science Edition)*, vol. 45, no. 1, pp. 35–41, 2017.

[27] J. Qin, X. Shen, H. Chen, Y. Lv, and X. Zhang, "A fusion algorithm for medical structural and functional images based on adaptive image decomposition," *Multimedia Tools and Applications*, vol. 78, no. 22, pp. 32605–32629, 2019.

[28] C. He, J. Wang, S. Lai, and A. Ennadi, "Image fusion in remote sensing based on spectral unmixing and improved non - negative matrix factorization algorithm," *JOURNAL OF ENGINEERING SCIENCE AND TECHNOLOGY REVIEW*, vol. 11, no. 3, pp. 79–88, 2018.

[29] F. Wang, Y. Cheng, and H. Li, "Image fusion algorithm of focal region detection and TAM-SCM based on SHT domain," *Xibei Gongye Daxue Xuebao/Journal of Northwestern Polytechnical University*, vol. 37, no. 1, pp. 114–121, 2019.

[30] Z. Qu, X. Huang, K. Chen, and L. Liu, "Algorithm of multiexposure image fusion with detail enhancement and ghosting removal," *Journal of electronic imaging*, vol. 28, no. 1, 2019.

Hindawi
Journal of Sensors
Volume 2022, Article ID 9970879, 13 pages
https://doi.org/10.1155/2022/9970879

Research Article

Radar Signal Recognition and Localization Based on Multiscale Lightweight Attention Model

Weijian Si,[1,2] Jiaji Luo,[1,2] and Zhian Deng[1,2]

[1]*College of Information and Communication Engineering, Harbin Engineering University, Harbin 150001, China*
[2]*Key Laboratory of Advanced Marine Communication and Information Technology, Ministry of Industry and Information Technology, Harbin 150001, China*

Correspondence should be addressed to Zhian Deng; dengzhian@hrbeu.edu.cn

Received 3 November 2021; Accepted 25 January 2022; Published 14 February 2022

Academic Editor: Abdellah Touhafi

The recognition technology of the radar signal modulation mode plays a critical role in electronic warfare, and the algorithm based on deep learning has significantly improved the recognition accuracy of radar signals. However, the convolutional neural networks became increasingly sophisticated with the progress of deep learning, making them unsuitable for platforms with limited computing resources. ResXNet, a novel multiscale lightweight attention model, is proposed in this paper. The proposed ResXNet model has a larger receptive field and a novel grouped residual structure to improve the feature representation capacity of the model. In addition, the convolution block attention module (CBAM) is utilized to effectively aggregate channel and spatial information, enabling the convolutional neural network model to extract features more effectively. The input time-frequency image size of the proposed model is increased to 600×600, which effectively reduces the information loss of the input data. The average recognition accuracy of the proposed model achieves 91.1% at -8 dB. Furthermore, the proposed model performs better in terms of unsupervised object localization with the class activation map (CAM). The classification information and localization information of the radar signal can be fused for subsequent analysis.

1. Introduction

Radar is widely deployed on the current battlefield and has progressively become the dominant key technology in modern warfare as a result of the continuous improvement of radar technology [1–4]. Therefore, recognizing the modulation type of enemy radar signals rapidly and accurately can effectively obtain battlefield information and situation and provide decent support for subsequent decision-making. It is significantly vital in the field of electronic warfare.

Traditional radar signal recognition methods rely on handcraft features extraction [5–11]. However, these methods lack flexibility and are computationally inefficient. With the continuous development of radar technology, radar signal parameters have become more complex, and radar signals have become more concealed. In addition, the widespread application of radar equipment and the rapid increase in the number of radiation sources have made the electromagnetic environment on the battlefield more complicated. Therefore, the traditional radar signal recognition method cannot effectively recognize radar signal modulation in the complex electromagnetic environment.

Deep learning has progressed rapidly in the last few years, and it has been extensively used in a wide range of traditional applications. Radar signal recognition methods based on convolutional neural networks have surpassed traditional recognition methods based on handcraft feature extraction [2, 7, 12–14]. The convolutional neural networks automatically extract the deep features of objects through supervised learning and have significant generalization performance [15]. Besides, the convolutional neural network has a hierarchical structure, and the model structure and parameters can be adjusted arbitrarily, which significantly reduces labor costs and is more convenient to use. To achieve higher recognition accuracy, the convolutional neural network becomes larger and the model structure tends to be more complicated. On the other hand, it is also important to strike a balance between recognition speed and computational efficiency in practical

applications. Therefore, this paper proposes a new multiscale lightweight structure, ResXNet, which has the advantages of lightweight and high computational efficiency.

In addition, the convolution block attention module (CBAM) attention mechanism is utilized in the model proposed in this paper. CBAM is a lightweight general attention module that can be seamlessly integrated into any convolutional neural network structure and trained end-to-end together with the basic convolutional neural networks [16–18]. The convolutional layer can only capture local feature information, ignoring the context relationship of features outside the receptive field. The CBAM significantly improves the feature representation capability of the model by enhancing or suppressing specific features in the channel and spatial dimension. And its calculation and memory overhead can be ignored.

At the same time, this paper also investigates the application of object localization based on class activation mapping (CAM) in radar signal recognition. Class activation mapping is a weakly supervised localization algorithm that locates the object position in a single forward pass, which improves the interpretability and transparency of the model and helps researchers build trust in the deep learning models [19, 20].

Therefore, this paper proposes a multiscale ResXNet model based on grouped residual modules and further improves the recognition accuracy of the model through the CBAM attention module. The ResXNet lightweight attention network model proposed in this paper is based on grouped convolution and constructs a hierarchical connection similar to residuals within a single convolution block. ResXNet can expand the size of the receptive field and improve the multiscale feature representation ability. The grouped residual convolutional layers effectively reduce the number of parameters while also improving the generalization performance. In addition, CAM is used to obtain the localization information of the radar signal in the time-frequency image, and the classification information and localization information of the radar signal can be fused for subsequent analysis.

2. Related Work

2.1. Radar Signal Classification. Traditional radar signal recognition methods usually rely on handcrafted feature extraction, such as cumulants, distribution distance, spectral correlation analysis, wavelet transform, and time-frequency distribution features [21]. Machine learning algorithms, such as clustering algorithms [22], support vector machines [9, 23], decision trees [7], artificial neural networks [5], and graph models [24], are used to classify radar signals according to the extracted features. However, the traditional radar signal recognition method is inefficient since it relies significantly on manual feature extraction and selection. And it is affected by noise easily, and the recognition performance substantially decreases in low SNR.

Convolutional neural networks have found their way into the field of radar signal classification as the development of deep learning. The radar signal recognition based on convolutional neural networks first converts one-dimensional time-domain radar signals into two-dimensional time-frequency images through time-frequency analysis and then automatically extracts features from time-frequency images of different radar signals by training convolutional neural networks. The radar signal recognition based on the convolutional neural network significantly improves the recognition accuracy in low SNRs.

Kong et al. [3] proposed a convolutional neural network (CNN) for radar waveform recognition and a sample averaging technique to reduce the computational cost of time-frequency analysis. However, the input size of this method is small, and there is a significant loss of information. Hoang et al. [13] introduced a radar waveform recognition technique based on a single shot multibox detector and a supplementary classifier, which achieved extraordinary classification performance. However, this method requires much manual annotation, and the computational efficiency is low. Wang et al. [12] proposed a transferred deep learning waveform recognition method based on a two-channel architecture, which can significantly reduce the training time and the size of the training dataset, and multiscale convolution and time-related features are used to improve the recognition performance. On the other hand, the transfer learning method requires a large convolutional neural network as a pretraining model, which has a high computational cost and is incompatible for embedded platforms or platforms with limited computing resources.

2.2. Convolutional Neural Network. In 1995, LeNet created the history of deep convolutional neural networks. AlexNet [25], the first deep convolutional neural network structure, achieved breakthrough success in image classification and recognition applications in 2012. The VGG [26] model modularizes the convolutional neural network structure, increases the network depth, and uses 3×3 small-size convolution kernels. Experiments show that expanding the receptive field by increasing the depth of the convolutional neural network can effectively improve performance [27]. The GoogLeNet model utilizes parallel filters with varied convolution kernel sizes to increase the feature representation ability and recognition performance [15]. ResNet [28] presents a 152-layer deep convolutional neural network that incorporates the identity connection into the convolutional neural network topology, alleviating the vanishing gradient problem.

With the continuous development of deep learning, the depth of the convolutional neural network is deeper, the calculation is more sophisticated, and the requirements for hardware are higher to achieve higher accuracy. As a result, the construction of small and efficient convolutional neural networks has gained more attention. DenseNet [29] connects the output of each layer to each subsequent layer. All previous layers serve as inputs for each convolutional layer, and the output features serve as inputs for all subsequent layers. DenseNet enables the network to extract features on a larger scale and alleviate the vanishing gradient problem. MobileNet [30] employs a depthwise separable convolution to build lightweight convolutional neural networks. The advantages of MobileNet include a tiny model,

lower latency, lower computing complexity, and higher inference efficiency. It can easily match the requirements for platforms with limited computing resources and embedding applications.

Grouped convolution was first introduced in AlexNet [25] for distributing the convolutional neural network model over multiple GPU resources. ResNeXt [31] found that grouped convolution can reduce the number of parameters and simultaneously improve the accuracy. Channel-wise convolution is a special case of grouped convolution in which the number of groups is equal to the number of channels. The channel-wise convolutions are components of depth separable convolution [30].

3. Proposed Method

The overview of the proposed algorithm is depicted in Figure 1. The proposed algorithm first converts the radar signal into a time-frequency image through time-frequency analysis. The ResXNet model proposed in this paper is presented for radar signal recognition, and the CAM is utilized for signal localization in time-frequency images. The ResNet model is composed of a grouped residual module and a CBAM attention mechanism.

3.1. Radar Signal Processing. In this paper, the radar signal interfered by additive white Gaussian noise can be expressed as

$$y(t) = x(t) + N(t) = Ae^{j\theta(t)} + N(t), \tag{1}$$

where $x(t)$ signifies complex radar signal samples and $N(t)$ stands for additive Gaussian white noise (AWGN) with zero mean value and variance σ^2. A represents the nonzero constant amplitude, and $\theta(t)$ denotes the instantaneous phase of the radar signal. The inherent difference between radar signals of different modulation types is the frequency variation over time. The one-dimensional radar signal is transferred into two-dimensional time-frequency images (TFIs) through time-frequency analysis. The pattern in the time-frequency image corresponds to the frequency variation with time.

The instantaneous phase $\theta(k)$ consists of instantaneous frequency $f(k)$ and the phase function $\phi(k)$, which determine the modulation type of the radar signal. The instantaneous phase $\theta(k)$ is defined as

$$\theta(k) = 2\pi f(k)(kT_s) + \phi(k). \tag{2}$$

Eight LPI radar waveforms considered in this paper are grouped into two categories, FM (frequency modulation) and PM (phase modulation). In the FM, the instantaneous frequency $f(k)$ varies while the phase $\phi(k)$ is constant; in the PM, the phase $\phi(k)$ varies while the instantaneous frequency $f(k)$ is constant [3], as defined in Table 1.

The Choi-Williams distribution (CWD) based on the time-frequency distribution of Cohen's class has the advantages of high resolution and cross-term suppression. The resolution of the time-frequency analysis can be modified by adjusting the parameters of its exponential kernel function. The time-frequency image of radar signals based on Choi-Williams distribution is defined as

$$C(t,\omega) = \frac{1}{2\pi}\iiint_{\infty} f(\theta,\tau)x(s+\tau/2)x^*(s-\tau/2)e^{-j(\theta t+w\tau-s\theta)}dsd\tau d\theta, \tag{3}$$

where t and ω denote frequency and time axes, respectively. And $f(\theta,\tau)$ is the exponential kernel function of the Choi-Williams distribution. The kernel function is regarded as a low-pass filter that can suppress cross-terms effectively.

$$f(\theta,\tau) = \exp\left[\frac{-\theta^2\tau^2}{\sigma}\right]. \tag{4}$$

Figure 2 depicts the time-frequency images of different radar signals by Choi-Williams distribution considered in this paper. The time-frequency images visualize the frequency variation over time and thus recognize the radar signals effectively. Before feature extraction, time-frequency images are normalized to reduce the influence of the bandwidth of distinct radar signals. The time-frequency images are transformed to gray images as follows:

$$G(x,y) = \frac{I(x,y) - \min\left(I(x,y)\right)}{\max\left(I(x,y)\right) - \min\left(I(x,y)\right)}, \tag{5}$$

where $I(x,y)$ indicates the time-frequency image by Choi-Williams distribution, $G(x,y)$ is the gray images, and (x,y) denotes each pixel in the time-frequency images. The gray time-frequency images contain significant components and information of radar signals.

3.2. ResXNet Module. The traditional convolutional neural network expands the receptive field size of the model by simply stacking convolutional layers. This strategy, on the other hand, increases the size of the model and the number of parameters, making the training of the model increasingly complex. The development of advanced model structures reveals a tendency toward improving the receptive field size and multiscale learning capability of the models while maintaining lightweight.

A multiscale model based on group convolution is proposed in this paper. On the premise of keeping the model lightweight, the receptive field of each convolutional layer is increased to improve the capabilities of feature extraction and multiscale representation. The proposed model structure is a modular design, which can flexibly adjust the size and parameters of the model.

Grouped convolution significantly reduces the size of the model and the number of parameters. Grouped convolution splits the input feature maps along the channel dimension into several feature map subsets, and each branch can only use a subset of the feature map and cannot use the entire input feature map [27]. The ResXNet proposed in this paper employs channel-wise convolution to each branch, and each branch takes the complete input feature map as input. 1×1

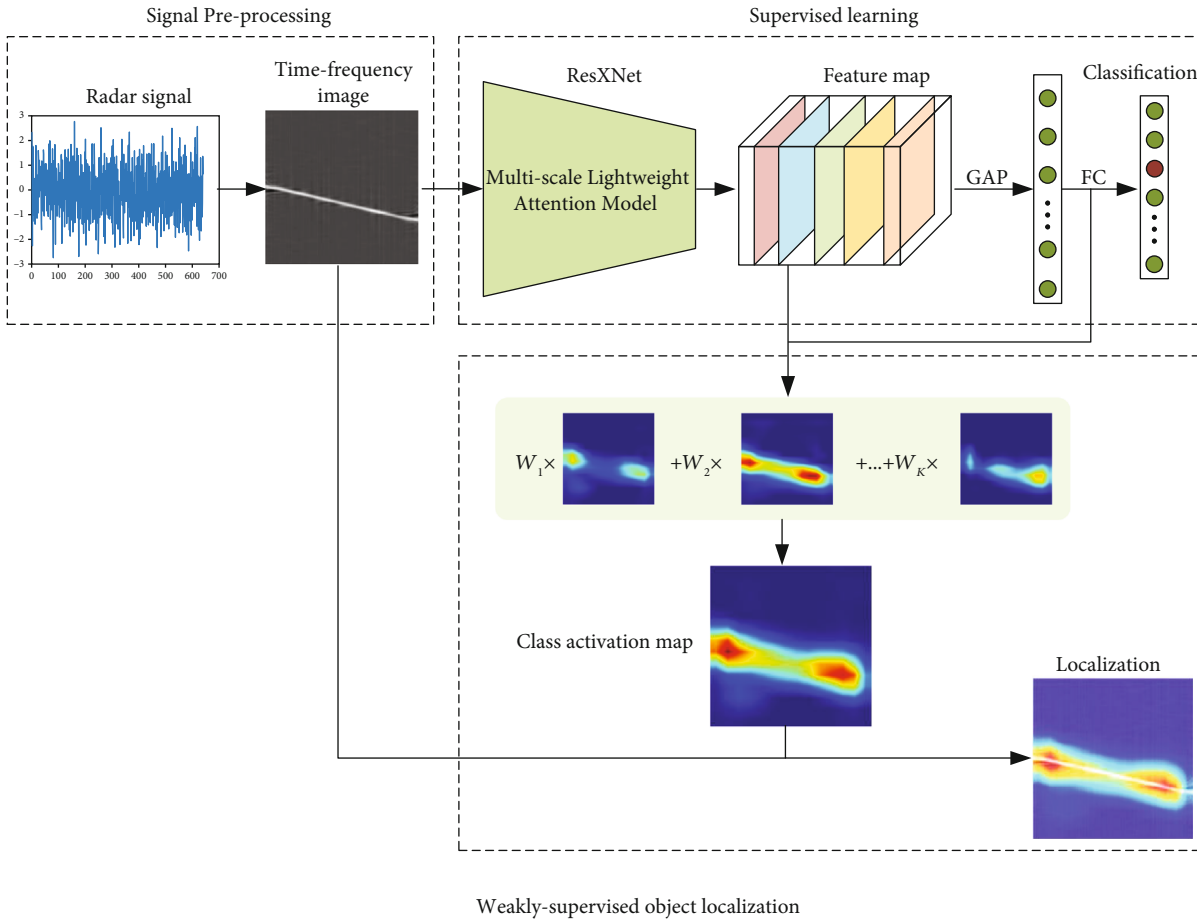

Figure 1: The overview of radar signal classification and localization based on ResXNet and CAM.

Table 1: LPI radar waveform.

Modulation type	$f(k)$	$\phi(k)$
LFM	$f_0 + (B/\tau_{pw})(kT_s)$	Constant
Costas	f_j	Constant
BPSK	Constant	0 or π
Frank	Constant	$(2\pi/M)(i-1)(j-1)$
P1	Constant	$-(\pi/M)[(M-(2j-1))][(j-1)M+(i-1)]$
P2	Constant	$-(\pi/2M)[2i-1-M][2j-1-M]$
P3	Constant	$(\pi/\rho)(i-1)^2$
P4	Constant	$(\pi/\rho)(i-1)^2-\pi(i-1)$

channel-wise convolution compresses the number of channels of the input feature map, and then a 3×3 convolution with the same number of channels is used for feature extraction. Then, the output feature maps of each branch are concatenated, and features maps of different scales are fused using channel-wise convolution.

As shown in Figure 3, the same feature map is input to each branch, and the 1×1 convolution in each branch is used to compress the number of channels of the feature map, and each branch contains a 3×3 convolutional layer for feature extraction. K_i and C_i represent 3×3 convolution operation and 1×1 channel-wise convolution, respectively. The 3×3 convolution input of the ith branch is the summation of C_i and K_{i-1}; thus, the output feature map y_i can be expressed as

$$y_i = \begin{cases} K_i(C_i(x)), & i = 1, \\ K_i(C_i(x) + y_{i-1}), & 2 \le i \le s, \end{cases} \tag{6}$$

where x is the input feature map, and the convolution operation of each branch extracts features from the input

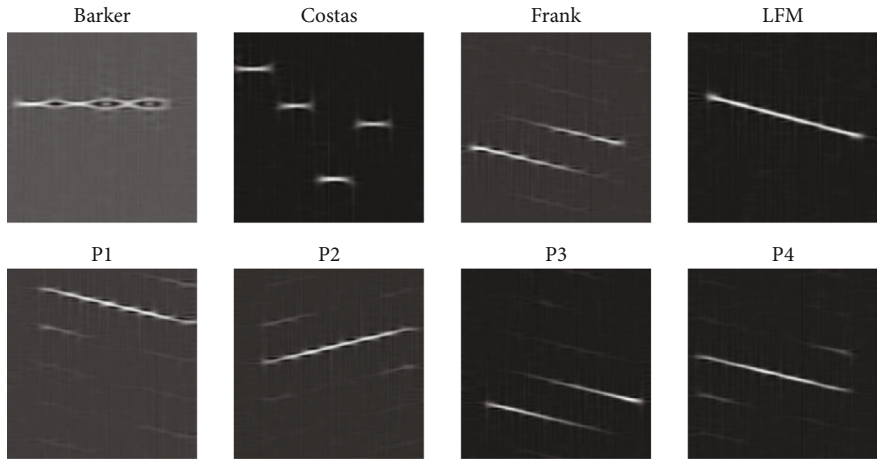

Figure 2: Time-frequency images of different radar waveforms.

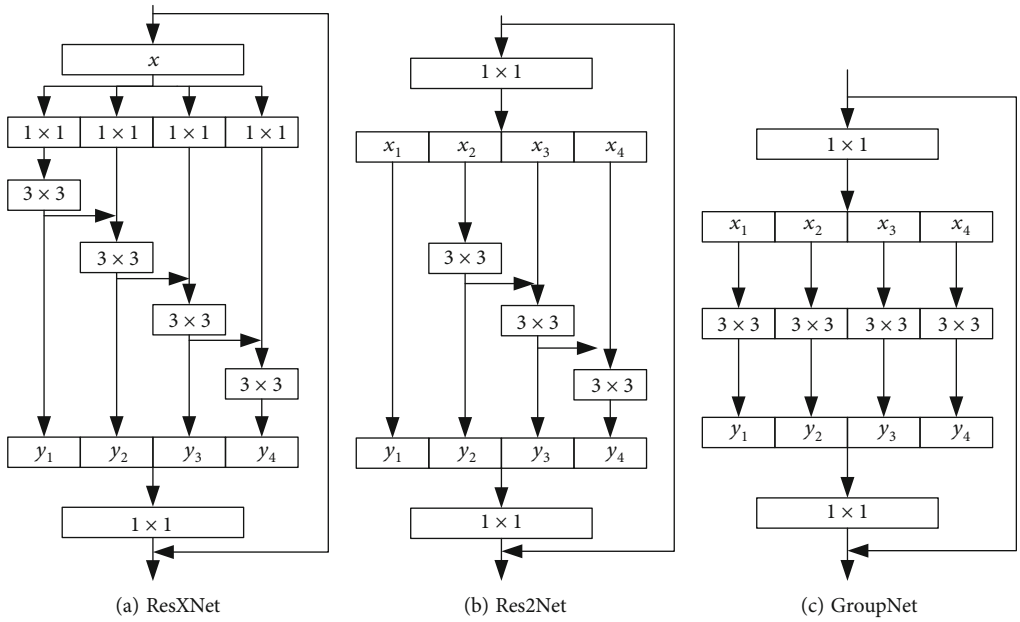

(a) ResXNet (b) Res2Net (c) GroupNet

Figure 3: Schematic representation of ResXNet modules ($S = 4$).

features and the output of the preceding branches. Therefore, the multibranch structure and the connection of different branches are beneficial to extract global and local features.

In ResXNet, S refers to the number of branches of each convolution module, larger S can learn the features of larger receptive field size, and the calculation and memory overhead introduced is negligible. ResXNet further improves the multiscale capability of convolutional neural networks and can be integrated with existing state-of-the-art methods to improve recognition accuracy and generalization performance. The proposed ResXNet model can be regarded as an improvement of Res2Net [27]. Changing the grouping convolution in the Res2Net model to several 1×1 channel-wise convolutions makes the parameters and structural design of the model more flexible.

3.3. Convolution Block Attention Module. The convolution block attention module (CBAM) is an attention module for convolutional neural networks that is simple and efficient [18]. The diagram of CBAM is depicted in Figure 4. CBAM sequentially calculates the channel and spatial attention of the feature map and then multiplies the two attention maps with the input feature map to refine the adaptive feature. CBAM is a lightweight general module that can be seamlessly inserted into any convolutional neural network architecture, with negligible computing and memory overhead, and can be trained end-to-end together with the base convolutional neural network.

The attention module allows the model to concentrate on informative features and suppress irrelevant features. CBAM applies the channel attention module and the spatial attention module sequentially to enable the model to

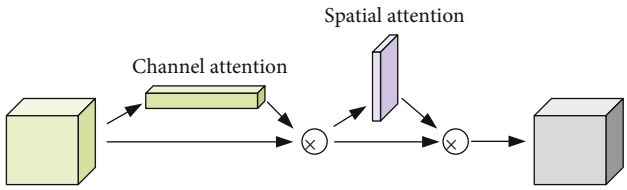

Figure 4: The convolution block attention module (CBAM).

reinforce effective features. Given the feature map $F \in \mathbb{R}^{C\times H\times W}$ as input, CBAM calculates one-dimensional channel attention map $M_c \in \mathbb{R}^{C\times 1\times 1}$ and two-dimensional spatial attention map $M_s \in \mathbb{R}^{1\times H\times W}$. The overall attention module is expressed as

$$\begin{aligned} F' &= M_c(F) \otimes F, \\ F'' &= M_c(F) \otimes F', \end{aligned} \tag{7}$$

where $\otimes$ is the element-wise multiplication and F'' denotes the feature map of the final CBAM attention module output. In the multiplication process, the attention feature is broadcasted accordingly: the channel attention value is broadcast along the spatial dimension and vice versa [18]. The specific details of channel attention and spatial attention are introduced as follows.

3.3.1. Channel Attention Module. The channel attention module (CAM) exploits the interchannel relationship of the feature maps to generate the channel attention map. Figure 5 depicts the computation process of the channel attention map. Average pooling and maximum pooling are used to aggregate spatial information, then the fully connected layer is used to compress the channel dimensions of the feature map, and the multilayer perceptron is used to generate the final attention map.

Specifically, first, we use global average pooling and global maximum pooling to aggregate the spatial context information of the feature mapping to generate two different spatial descriptors, which denote the global average pooling feature F^c_{avg} and the global maximum pooling feature F^c_{max}. Then, the two feature descriptors are forwarded into a shared network to generate channel attention map $M_c \in \mathbb{R}^{C\times 1\times 1}$. The shared network is a multilayer perceptron that contains one hidden layer. To reduce the computational overhead, the activation unit size of the hidden layer multilayer perceptron is set to $\mathbb{R}^{c/r\times 1\times 1}$, where r is the reduction rate. The shared network is applied to the different spatial descriptors, and then, the two feature descriptors are merged using an element-wise summation to obtain the final channel feature vector. Therefore, the channel attention can be written as

$$\begin{aligned} M_c(F) &= \sigma(\text{MLP}(\text{AvgPool}(F)) + \text{MLP}(\text{MaxPool}(F))) \\ &= \sigma\left(W_1\left(W_0\left(F^c_{\text{avg}}\right)\right) + W_1(W_0(F^c_{\text{max}}))\right), \end{aligned} \tag{8}$$

where σ represents the sigmoid activation function, $W_0 \in \mathbb{R}^{c/r\times c}$ and $W_1 \in \mathbb{R}^{c\times c/r}$ denote the weights of MLP, and the ReLU activation function is used in each layer.

3.3.2. Spatial Attention Module. The spatial attention module (SAM) utilizes the interspatial relationship of feature maps to generate spatial attention maps. As illustrated in Figure 6, the average pooling and maximum pooling are applied to the feature map along the channel dimension, and then, the two feature maps are concatenated to create the spatial feature descriptor. The spatial attention map highlights informative regions [18]. Finally, the spatial attention map is generated by convolution operation on the spatial feature descriptor to enhance or suppress the feature region.

Specifically, using spatial global average and max pooling to calculate the spatial information of the feature map, two 2-dimensional spatial feature maps $F^s_{\text{avg}} \in \mathbb{R}^{1\times H\times W}$ and $F^s_{\text{max}} \in \mathbb{R}^{1\times H\times W}$ are generated. Then, the 2D spatial attention map is calculated by a convolution operation. The spatial attention is computed as

$$\begin{aligned} M_s(F) &= \sigma\left(f^{7\times 7}([\text{AvgPool}(F)\,;\text{MaxPool}(F)])\right) \\ &= \sigma\left(f^{7\times 7}\left(\left[F^s_{\text{avg}}\,;F^s_{\text{max}}\right]\right)\right), \end{aligned} \tag{9}$$

where σ represents sigmoid activation function and $f^{7\times 7}$ denotes a convolution operation with the kernel size of 7×7.

The convolution block attention module (CBAM) divides attention features into the channel and spatial attention modules and achieves a significant performance improvement while keeping a small overhead. CBAM can be seamlessly integrated into any convolutional neural network architecture and trained end-to-end with the CNN model. The CBAM can prompt the network to learn and aggregate the feature information in the target area, effectively strengthen or suppress the features of a specific space or a specific channel, and guide the convolutional neural network to make good use of the feature maps [18].

3.4. Class Activation Map. The class activation map (CAM) is portable and applied to a variety of computer vision tasks for weakly supervised object localization. The CAM is trained end-to-end based on image-level annotation and localizes objects simply in a single forward pass. CAM avoids the flattening of the feature map by replacing the fully connected layer with the global average pooling, which completely preserves the spatial information of the objects in the embedded features. More importantly, CAM can make the existing state-of-the-art deep models interpretable and transparent and help researchers understand the logic of predictions hidden inside the deep learning models.

For each image I, $A = F(I)$ denotes the feature map of the last convolutional layer. Suppose that there are K feature maps in the last convolution layer. The $A_k(x, y)$ indicates the activation of the kth channel at spatial coordinate (i, j), where $k = 1, 2, \cdots, K$. Each node of the GAP (global average pooling) layer F_k is spatial average of the activation and can be computed by

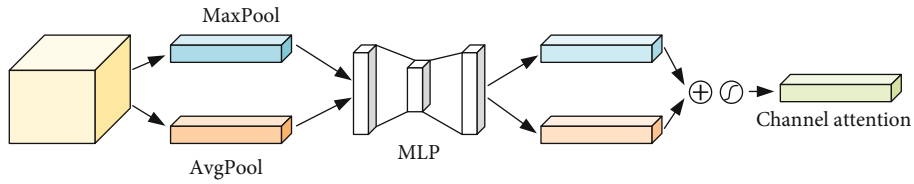

Figure 5: Channel attention module.

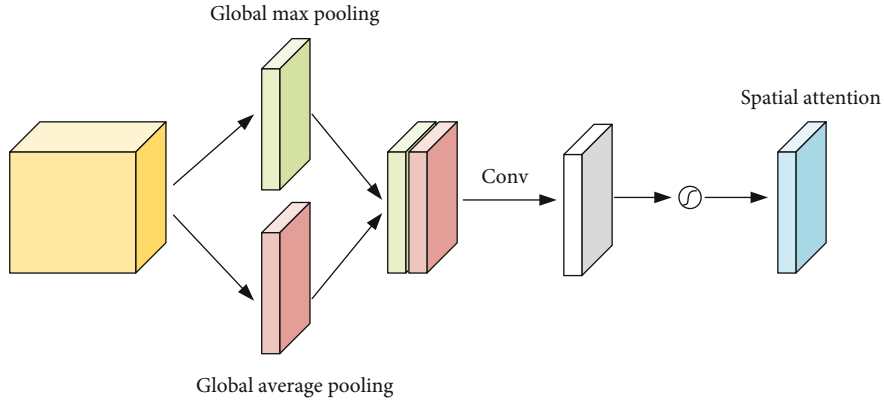

Figure 6: Spatial attention module.

$$F_k = \sum_{i,j} A_k(x, y). \tag{10}$$

The function definition of CAM is

$$M_c(x, y) = \sum_k w_k^c A_k(x, y), \tag{11}$$

where M_c is the class activation map for class c and w_k^c represents the weight corresponding to class c for unit k. $M_c(x, y)$ signifies the importance of the activation at spatial grid (x, y) for class c.

Each class activation map consists of the weighted linear sum of these visual patterns at different spatial locations, which contain a series of part saliency maps. Upsampling is applied to resize the class activation map to the size of the input time-frequency image to localize the image saliency regions most relevant to a particular class.

3.5. ResXNet Architecture. The group dimension indicates the number of groups within a convolutional layer. This dimension converts single-branch convolutional layers to multibranch, improving the capacity of multiscale representation [31]. The CBAM block adaptively recalibrates channel and spatial feature responses by explicitly modeling interdependencies among channel and spatial [18].

Table 2 shows the specification of ResXNet, including depth and width. ResXNet makes extensive use of 3×3 convolution and uses average pooling layers to reduce the feature size. The proposed models are constructed in 5 stages, and the first stage is a 7×7 conventional convolution block with stride = 2. The following 4 stages, respectively, contain [1, 2, 4] ResXNet modules to construct the proposed ResXNet model. The number of channels in each stage of the module is [32, 64, 128, 256], respectively. The global average pooling is followed by a fully connected layer as the head for the classification task. A dropout layer is inserted before the fully connected layer to prevent the model from overfitting. A CBAM attention mechanism is implemented after the output of each ResXNet module to improve the capability of global feature extraction.

Each convolutional module is composed of the convolutional layer without bias, batch normalization layer, and ReLU activation function. The input size of the proposed model is 600×600. The last convolutional layer connects the fully connected layer through global average pooling (GAP) instead of flattening the features, such that changes

Table 2: Architectural specification of ResXNet.

Stage	Output size	Channels	Modules
Input	600×600	3	—
0	300×300	32	—
1	150×150	32	2
2	75×75	64	2
3	37×37	128	4
4	18×18	256	1

Table 3: Model information.

S	Parameters	Model size
1	5.8 M	22.5 M
2	3.2 M	13.0 M
4	1.9 M	8.5 M
8	1.3 M	6.7 M

Table 4: Radar signal parameter variation.

	Parameter	Data scale
General parameters	Sampling frequency f_s	1
Linear frequency modulation	Carrier frequency f_c	$U(0, 1/4)$
	Bandwidth Δf	$U(1/12, 1/4)$
	Modulation period τ	$(600, 800)$
Binary phase codes	Carrier frequency f_c	$U(1/12, 1/4)$
	Subpulse frequency	$f_c/4$
	Modulation period	$U(350, 650)$
Costas code	Number of subpulse N	4
	Lowest frequency f_0	1/24
	Frequency hop Δf	$U(1/24, 1/12)$
	Modulation period τ	$U(400, 600)$
Polyphase codes	Carrier frequency f_c	$U(1/12, 1/4)$
	Subpluse frequency	$f_c/4$

in the input size do not affect the number of parameters. Table 3 shows the model information with different groups, including model size and the number of parameters. When $S = 1$, the ResXNet model degenerates to a normal conventional convolutional neural network.

4. Simulation and Analysis

The proposed ResNet model was evaluated and compared with the Res2Net and GroupNet on the simulation dataset to verify the effectiveness and robustness. In this section, we evaluate the performance of the proposed ResXNet model to recognize radar signals with different modulations and the ability of the class activation map (CAM) to localize radar signals in time-frequency images. We implement the proposed models using the TensorFlow 2.0 framework. Cross-entropy is used as a loss function. We trained the networks using SGD and a minibatch of 16 on NVIDIA 3090 GPU. The learning rate was initially set to 0.01 and divided by 0.1 every 10 epochs. All models, including the proposed and compared models, are trained for 30 epochs with the same training strategy.

The dataset consists of 8 types of radar signals, including Barker, Costas, Frank, LFM, P1, P2, P3, and P4. In the training dataset, the SNR of each signal category is from -18 dB to 10 dB with the step of 2 dB, and each SNR contains 500 signals, totaling 60000 signal samples in the training dataset. In the test dataset, each SNR contains 100 samples for a total of 12000 signal samples. The parameters variations of each kind of radar signal are listed in Table 4.

4.1. Recognition Accuracy of the Different Models. The first experiment is to compare the effectiveness of group dimensions on model accuracy. As shown in Table 5, the accuracy of the ResXNet improves with the increase of the number of groups. The number of parameters of the ResXNet model decreases as the increase of group; meanwhile, the training time will gradually increase. Because the convolution output of the proposed model is connected to the classification layer through the global average pooling (GAP) layer, changing the input size of the model does not change the size and the number of parameters of the model. The proposed model has the combined effect of the hierarchical residual structure, which can generate abundant multiscale features and effectively improve the recognition accuracy. Increasing the input data size of the model can significantly reduce the information loss of the input data, which is beneficial to the convolutional neural network to extract the informative features from the time-frequency images.

Table 5: Recognition accuracy for different numbers of groups.

Input size	Group dimensions	Accuracy	Train time/epoch
224	$S = 2$	88.1%	207 s
	$S = 4$	88.4%	242 s
	$S = 8$	88.6%	325 s
600	$S = 2$	88.4%	555 s
	$S = 4$	88.6%	595 s
	$S = 8$	88.9%	690 s

Table 6: Overall recognition accuracy ($S = 8$).

Model	Accuracy
ResXNet	88.9%
Res2Net	87.5%
GroupNet	86.9%

4.2. Recognition Accuracy of the Different Models. Table 6 lists the overall recognition accuracy of the proposed and compared models for radar signal modulations with the group dimension is 8. Compared with Res2Net and

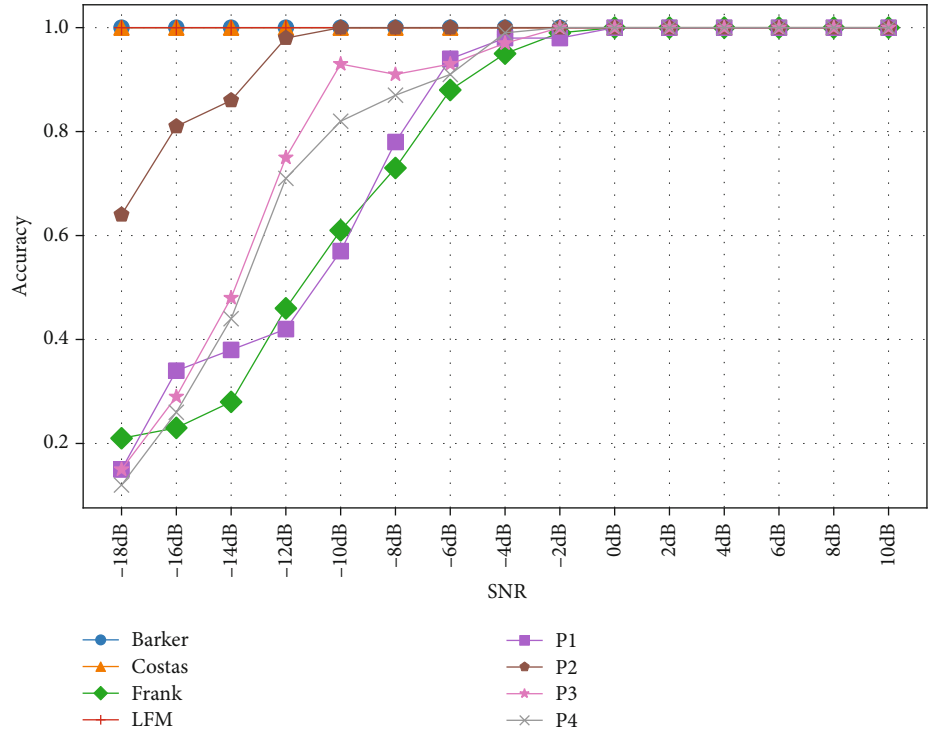

Figure 7: The performance of the proposed ResXNet models under different SNRs.

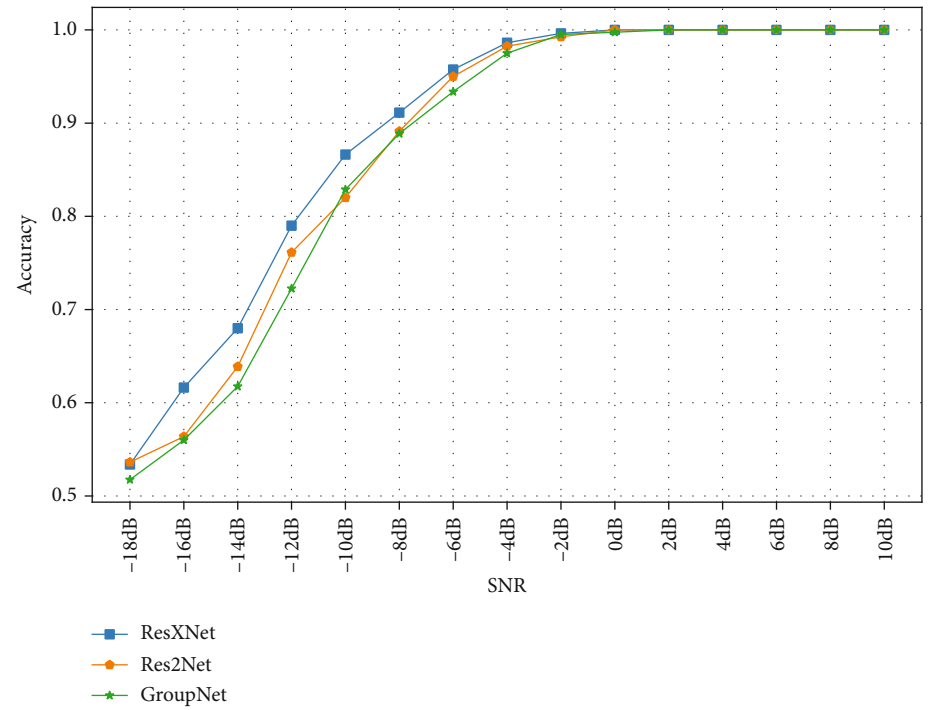

Figure 8: The average recognition accuracy of different models under different SNRs.

GroupNet, ResXNet has higher recognition accuracy. The recognition accuracy of the proposed ResXNet model can achieve 88.9%, which outperforms Res2Net by 1.4%.

Figure 7 depicts the recognition accuracy of the proposed ResXNet model for different radar signals at various SNRs. The accuracy of Barker code, Frank code, and LFM is still 100% even at -18 dB. The average recognition accuracies of all radar modulations under different SNRs for Res2Net, GroupNet, and proposed ResXNet models are presented in Figure 8. The average accuracy of all radar

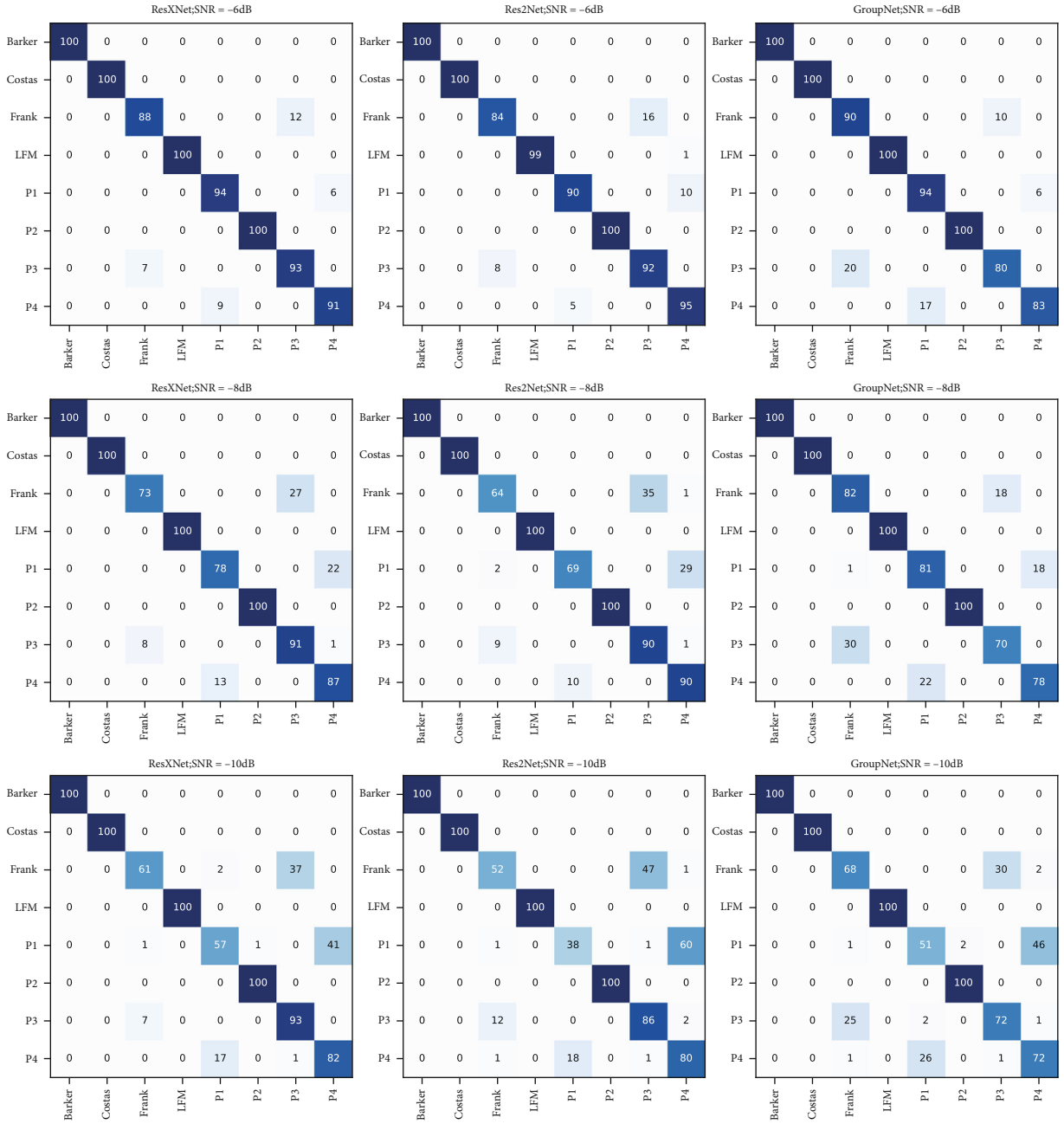

Figure 9: The confusion matrixes of different models.

modulations is still above 50% at -18 dB. The average recognition accuracy of the model is above 90% at -8 dB. The radar signals are disrupted by Gaussian white noise at low SNR, resulting in misclassifications. As the SNR increases, the features extraction becomes more distinguishable from each other.

Figure 9 illustrates the confusion matrix of different models to further analyse the recognition capability for radar modulation types. Frank code and P3 code, as well as P1 code and P4 code, are similar and easy to confuse. The recognition accuracy of the other four radar signals is 100%.

4.3. Comparison of Object Visualization. The visualization of model features can accurately explain the features learned by the model and provide reasonable explanations for the prediction results. In this paper, the predictions are visualized by the class activation mapping (CAM) [19], which is commonly used for localizing the discriminative regions in image classification. CAM generates the object saliency map by calculating the weighted sum of the feature maps of the last convolutional layer. By simply upsampling the class activation map to the size of the input time-frequency image, we can identify the image regions most relevant to the particular category [19]. CAM can reveal the decision-making process of the convolutional neural network model. CAM makes the model based on the convolutional neural network more transparent by generating visual explanations. And CAM can localize objects without additional bounding box annotations.

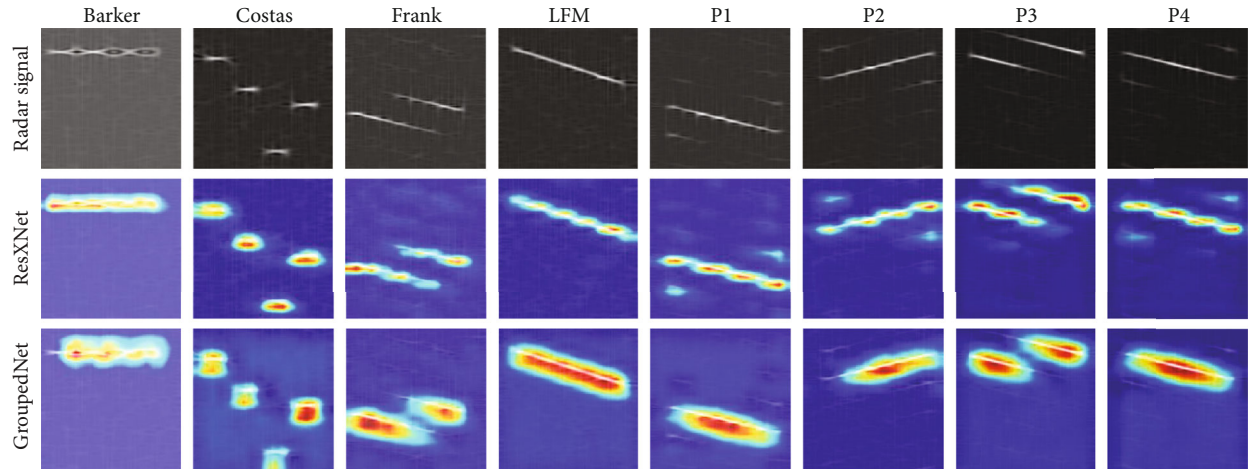

Figure 10: CAM comparison of different models.

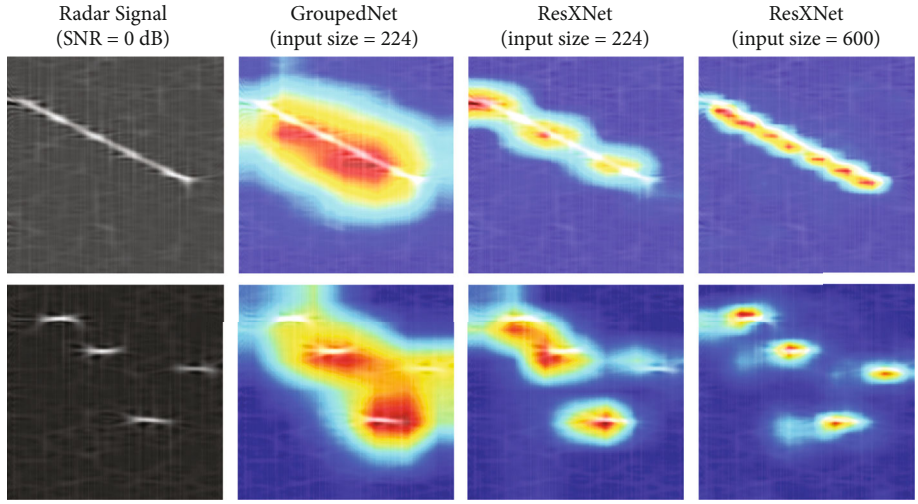

Figure 11: CAM results of different input sizes.

Figure 10 depicts the CAM visualization results of the ResXNet model and the grouped convolution model for different radar signals, with the discriminative CAM regions highlighted. Figure 10 shows that the ResXNet model outperforms GroupNet in terms of visual object localization. Compared with GroupNet, the CAM results of ResXNet have more concentrated activation maps. The ResXNet localizes the radar signal more precisely and tends to encompass the entire object in the time-frequency image due to its better multiscale capability. The ResXNet model proposed in this paper can help researchers develop confidence in artificial intelligence systems by improving the interpretability and trustworthiness of the model. This ability to precisely localize discriminative regions makes ResXNet potentially valuable for object region mining in weakly supervised localization tasks of radar signals.

4.4. Comparison of Object Visualization with Different Input Sizes. In addition, the paper also explored the impact of the input size of the proposed models on CAM visualization. Figure 11 shows the CAM visualization results with various input sizes. As demonstrated in Figure 11, the model can generate more precise CAM with a higher resolution as the input image size increases, improving the visual localization capacity of the model. Especially for the Costas signals, ResXNet can accurately localize each signal component.

Therefore, the multiscale feature extraction capability of ResXNet helps to better localize the most discriminative regions in radar time-frequency images compared to GroupNet. For the same ResXNet model, increasing the input image size of the model can obtain more precise and complete discriminative regions. As a result, the proposed ResXNet model contributes to improving the target localization capability of the model and the interpretability of the prediction.

5. Conclusions

In this paper, a radar signal recognition approach based on the ResXNet lightweight model is proposed. The proposed model substantially improves the multiscale representation

ability and recognition accuracy by grouping and cascading convolutional layers. The CBAM attention mechanism is employed to effectively aggregate the channel features and spatial features, so that the convolutional neural network model can make better use of the given feature maps.

Experiments demonstrate that the proposed model has capable multiscale representations and achieves higher recognition performance in low SNR. And the model is tiny, the number of parameters is low, and it is suitable for the embedded platform application. ResXNet adds the grouped dimension by channel-wise convolution, allowing to adjust the size and number of parameters of the model and improve the multiscale representation capability of the model. The proposed ResXNet model provides a superior capacity for object localization, and the radar signal can be localized more precisely through CAM.

For future research, more lightweight models for radar signal recognition, as well as the use of CAM in radar signal recognition and localization, will be explored.

Data Availability

The data used to support the findings of this study are available from the corresponding author upon request.

Conflicts of Interest

The authors declare that there are no conflicts of interest regarding the publication of this paper.

Acknowledgments

This work was financially supported by the National Natural Science Foundation of China (Grant Nos. 61971155 and 61801143), Natural Science Foundation of Heilongjiang Province of China (Grant No. JJ2019LH1760), Fundamental Research Funds for the Central Universities (Grant No. 3072020CF0814), and Aeronautical Science Foundation of China (Grant No. 2019010P6001).

References

[1] X. Ni, H. L. Wang, F. Meng, J. Hu, and C. K. Tong, "LPI radar waveform recognition based on multi-resolution deep feature fusion," *IEEE Access*, vol. 9, pp. 26138–26146, 2021.

[2] X. Ni, H. Wang, Y. Zhu, and F. Meng, "Multi-resolution fusion convolutional neural networks for intrapulse modulation LPI radar waveforms recognition," *IEICE Transactions on Communications*, vol. E103B, no. 12, pp. 1470–1476, 2020.

[3] S. H. Kong, M. Kim, M. Hoang, and E. Kim, "Automatic LPI radar waveform recognition using CNN," *IEEE Access*, vol. 6, pp. 4207–4219, 2018.

[4] L. T. Wan, R. Liu, L. Sun, H. S. Nie, and X. P. Wang, "UAV swarm based radar signal sorting via multi-source data fusion: a deep transfer learning framework," *Information Fusion*, vol. 78, pp. 90–101, 2022.

[5] J. Lunden and V. Koivunen, "Automatic radar waveform recognition," *IEEE Journal of Selected Topics in Signal Processing*, vol. 1, no. 1, pp. 124–136, 2007.

[6] C. C. Xu, J. Y. Zhang, Q. S. Zhou, and S. W. Chen, "Modulation classification for radar pulses in low SNR levels with graph features of ambiguity function," in *2017 IEEE 9th International Conference on Communication Software and Networks (ICCSN)*, pp. 779–783, Guangzhou, China, 2017.

[7] T. R. Kishore and K. D. Rao, "Automatic intrapulse modulation classification of advanced LPI radar waveforms," *IEEE Transactions on Aerospace and Electronic Systems*, vol. 53, no. 2, pp. 901–914, 2017.

[8] T. Wan, K. L. Jiang, Y. L. Tang, Y. Xiong, and B. Tang, "Automatic LPI radar signal sensing method using visibility graphs," *IEEE Access, Article*, vol. 8, pp. 159650–159660, 2020.

[9] G. Vanhoy, T. Schucker, and T. Bose, "Classification of LPI radar signals using spectral correlation and support vector machines," *Analog Integrated Circuits and Signal Processing*, vol. 91, no. 2, pp. 305–313, 2017.

[10] C. M. Jeong, Y. G. Jung, and S. J. Lee, "Deep belief networks based radar signal classification system," *Journal of Ambient Intelligence and Humanized Computing*, 2018.

[11] J. Li, G. Zhang, Y. Sun, E. Yang, L. Qiu, and W. Ma, "Automatic intra-pulse modulation recognition using support vector machines and genetic algorithm," in *2017 IEEE 3rd Information Technology and Mechatronics Engineering Conference (ITOEC)*, pp. 309–312, Chongqing, China, 2017.

[12] Q. Wang, P. F. Du, J. Y. Yang, G. H. Wang, J. J. Lei, and C. P. Hou, "Transferred deep learning based waveform recognition for cognitive passive radar," *Signal Processing*, vol. 155, pp. 259–267, 2019.

[13] L. M. Hoang, M. Kim, and S. H. Kong, "Automatic recognition of general LPI radar waveform using SSD and supplementary classifier," *IEEE Transactions on Signal Processing*, vol. 67, no. 13, pp. 3516–3530, 2019.

[14] C. Wang, J. Wang, and X. Zhang, "Automatic radar waveform recognition based on time-frequency analysis and convolutional neural network," in *2017 IEEE International Conference on Acoustics, Speech and Signal Processing (ICASSP)*, pp. 2437–2441, New Orleans, LA, USA, 2017.

[15] A. Khan, A. Sohail, U. Zahoora, and A. S. Qureshi, "A survey of the recent architectures of deep convolutional neural networks," *Artificial Intelligence Review*, vol. 53, no. 8, pp. 5455–5516, 2020.

[16] X. Li, W. H. Wang, X. L. Hu, J. Yang, and I. C. Soc, "Selective kernel networks," in *2019 IEEE Conference on Computer Vision and Pattern Recognition*, pp. 510–519, Long Beach, CA, 2019,.

[17] J. Hu, L. Shen, S. Albanie, G. Sun, and E. H. Wu, "Squeeze-and-excitation networks," *IEEE Transactions on Pattern Analysis and Machine Intelligence*, vol. 42, no. 8, pp. 2011–2023, 2020.

[18] S. Woo, J. Park, J.-Y. Lee, and I. S. Kweon, "CBAM: convolutional block attention module," http://arxiv.org/abs/1807.06521.

[19] B. Zhou, A. Khosla, A. Lapedriza, A. Oliva, and A. Torralba, "Learning deep features for discriminative localization," in *Proceedings of the IEEE conference on computer vision and pattern recognition*, pp. 2921–2929, Seattle, WA, 2016.

[20] K. Huang, F. Meng, H. Li, S. Chen, Q. Wu, and K. N. Ngan, "Class activation map generation by multiple level class grouping and orthogonal constraint," in *2019 Digital Image Computing: Techniques and Applications*, pp. 182–187, Perth, Australia, 2019.

[21] K. Konopko, Y. P. Grishin, and D. Janczak, "Radar signal recognition based on time-frequency representations and multi-dimensional probability density function estimator," in *2015 Signal Processing Symposium*, Debe, Poland, 2015.

[22] M. Zhu, W.-D. Jin, J.-W. Pu, and L.-Z. Hu, "Classification of radar emitter signals based on the feature of time-frequency atoms," in *2007 International Conference on Wavelet Analysis and Pattern Recognition*, pp. 1232–1237, Beijing, China, 2007.

[23] A. Pavy and B. Rigling, "SV-means: a fast SVM-based level set estimator for phase-modulated radar waveform classification," *IEEE Journal of Selected Topics in Signal Processing*, vol. 12, no. 1, pp. 191–201, 2018.

[24] C. Wang, H. Gao, and X. D. Zhang, "Radar signal classification based on auto-correlation function and directed graphical model," in *2016 IEEE International Conference on Signal Processing, Communications and Computing*, Hong Kong, 2016.

[25] A. Krizhevsky, I. Sutskever, and G. E. Hinton, "ImageNet classification with deep convolutional neural networks," *Advances in Neural Information Processing Systems*, vol. 60, no. 6, pp. 84–90, 2017.

[26] K. Simonyan and A. Zisserman, "Very deep convolutional networks for large-scale image recognition," 2014, http://arxiv.org/abs/1409.1556.

[27] S. H. Gao, M. M. Cheng, K. Zhao, X. Y. Zhang, M. H. Yang, and P. Torr, "Res2Net: a new multi-scale backbone architecture," *IEEE Transactions on Pattern Analysis and Machine Intelligence*, vol. 43, pp. 652–662, 2021.

[28] K. M. He, X. Y. Zhang, S. Q. Ren, and J. Sun, "Deep residual learning for image recognition," in *2016 IEEE Conference on Computer Vision and Pattern Recognition*, pp. 770–778, Seattle, WA, 2016.

[29] G. Huang, Z. Liu, L. van der Maaten, and K. Q. Weinberger, "Densely connected convolutional networks," in *Proceedings of the IEEE conference on computer vision and pattern recognition*, pp. 2261–2269, Honolulu, HI, 2017.

[30] A. G. Howard, M. Zhu, B. Chen et al., "MobileNets: efficient convolutional neural networks for mobile vision applications," http://arxiv.org/abs/1704.04861.

[31] S. N. Xie, R. Girshick, P. Dollar, Z. W. Tu, and K. M. He, "Aggregated residual transformations for deep neural networks," in *30th IEEE Conference on Computer Vision and Pattern Recognition*, pp. 5987–5995, Honolulu, HI, 2017.

Hindawi
Journal of Sensors
Volume 2022, Article ID 8205929, 11 pages
https://doi.org/10.1155/2022/8205929

Research Article

Multisource Heterogeneous Data Fusion Analysis of Regional Digital Construction Based on Machine Learning

Mengmeng Jiang,[1] Qiong Wu ,[1] and Xuetao Li[2]

[1]*School of Economics, Wuhan Donghu University, Wuhan, 430212 Hubei, China*
[2]*School of Economics and Management, Hubei University of Automotive Technology, Shiyan, 442000 Hubei, China*

Correspondence should be addressed to Qiong Wu; wuqiong@wdu.edu.cn

Received 13 August 2021; Revised 14 October 2021; Accepted 2 November 2021; Published 10 January 2022

Academic Editor: Mu Zhou

In modern urban construction, digitalization has become a trend, but the single source of information of traditional algorithms can not meet people's needs, so the data fusion technology needs to draw estimation and judgment from multisource data to increase the confidence of data, improve reliability, and reduce uncertainty. In order to understand the influencing factors of regional digitalization, this paper conducts multisource heterogeneous data fusion analysis based on regional digitalization of machine learning, using decision tree and artificial neural network algorithm, compares the management efficiency and satisfaction of school population under different algorithms, and understands the data fusion and construction under different algorithms. According to the results, decision-making tree and artificial neural network algorithms were more efficient than traditional methods in building regional digitization, and their magnitude was about 60% higher. More importantly, the machine learning-based methods in multisource heterogeneous data fusion have been better than traditional calculation methods both in computational efficiency and misleading rate with respect to false alarms and missed alarms. This shows that machine learning methods can play an important role in the analysis of multisource heterogeneous data fusion in regional digital construction.

1. Introduction

With the rapid development of China's urbanization process, people's demand for a better life is increasing, and the traditional urban management model can no longer meet the needs of reality. At the same time, the rapid development of modern information technology provides a new way for urban management. It applies modern information technology to city management, divides the city management area into a series of unit grids, and classifies its components and events. The platform quickly finds problems and solves them in a timely manner, improving the efficiency of urban management.

Many source data fusion is a method which deals with data from multiple sources. The estimates and judgments from the original data sources are derived in terms of conclusions attained and knowledge recognition developed to increase data confidence, improve reliability, and reduce uncertainty. It is an idea that comes from the multisensor datalink technique proposed during the 1970s to obtain more complete and successful information and to improve the robustness and accuracy of the system because the detection range and computing power as well as the accuracy of each sensor has been limited. Similarly, in combat scenarios, there are potential conflicts due to the heterogeneity of single sensor information sources, the differentiation of multiple sources of information, and the high intensity of information sources and electronic countermeasures. As a result, multisensor information fusion technology was born and began to flourish [1].

Experts at home and abroad have done a lot of research on the digital construction of districts. Ding et al. use three-dimensional (3D) laser scanning to realize the RE process. The framework also incorporates supporting technologies (virtual reality, 3D printing, and prefabrication) to better

understand design and construction and tools (work breakdown structure and model breakdown structure) to improve the quality of organization and management. The implementation of this proposed framework in a refurbished shopping center has optimized the efficiency of the renovation process by 15%, reduced design changes by 30%, and rework by 25% [2]. Rytova and Gutman propose methods to address both tasks using modern tools, including balanced exponential systems adapted to regional development. He believed that the quality of innovative activities and human capital should be increased, creating effective conditional arrangements for regional development of socioeconomic systems, and innovative creation and development of the digital economy, and the formalization of strategic objective assessment using a fuzzy set method [3]. López et al. believe that digitalization is a global phenomenon that affects all human activities. The public administration department also incorporates new information and communication technologies into its structure and public sector. Computer auditing is a tool that allows auditing of public administration departments and improving accountability. The article examines the main advantages and risks of digitization and provides a case study of a regional audit institution that implements computer audits in Spain [4]. For data fusion solutions, there are also different views on this research. Queiroz et al. established the interregional DIH created by the cooperation between entities to transform the region into a reference pole for innovation. This article is aimed at describing the innovation quality management and improvement strategies developed by this cross-regional DIH within the scope of the DISRUPTIVE project. In addition to considering the personal strategies of affiliated members, it also includes the aspect of cooperation, on the sharing of knowledge, technology, and skills, aimed at improving the quality of innovation, and the adoption of digitalization by companies in the region [5]. Bareinboim and Pearl focus on the latest technology of sensor fusion technology, which is applied to sensors embedded in mobile devices as a means to help identify the daily activities of mobile device users. Sensor data fusion technology is used to integrate data collected from multiple sensors to improve the reliability of algorithms that identify different activities [6]. Liu and Huang believe that the rapid development of sensing and computing technology has enabled multiple sensors to be embedded in a system to simultaneously monitor the degradation state of an operating unit. It is aimed at solving these two challenging problems in a unified way. Specifically, a method was developed to construct a health index by fusing multiple degradation-based sensor data [7]. Mou et al. discussed the scientific results of the 2016 Data Fusion Competition organized by the Image Analysis and Data Fusion Technical Committee of the IEEE Society of Earth Sciences and Remote Sensing. These include a pair of ultrahigh resolution panchromatic and multispectral Deimos-2 images and videos taken by the Iris camera on the International Space Station. The problems solved and the technologies proposed by the contest participants covered a wide range of topics, as well as mixed ideas and methods from remote sensing, video processing, and computer vision [8]. These methods provide a certain reference for this article, but because the amount of data in related studies is too small and the sample experiment time is short, it is difficult to reproduce the experimental conclusions.

A novel feature of this paper is the use of decision tree-based algorithms and artificial neural network algorithms which are used as generative methods to construct an algorithm for complex model discriminations. With respect to the uncertain information available in the data source, reliability of assignment of the method should be used to determine the confidence function. Finally, the production weight is determined through a reliable mathematical structure, and a weighted data fusion correction model is established to be better applied in practice. The experiment has achieved good results.

2. Regional Digital Construction Methods

2.1. Data Fusion. Change the data with new data from multiple data sources to draw the top choices. This book is superior to options made by a data source or a single decision book [9, 10]. The data model should change the breakpoint by changing the breakpoint. The data comes from a variety of information sources, which improves the final segmentation performance, thereby improving the quality of the final decision.

It reflects the many features of the information and the target, and only when the features are fully analyzed are they effectively consolidated [11]. Through the analysis of multisource heterogeneous data fusion, the characteristics of multisource heterogeneous data fusion are summarized as follows:

Heterogeneity: the data for fusion processing in a data fusion system often comes from data generated by multiple independent systems. Because different data sources were independent of each other, not only the data model is heterogeneous but also the semantics and syntax of the data. There are also different degrees of heterogeneity.

Scatterability: in multisource heterogeneous data, which is often distributed heterogeneously, interference between some data is transmitted through the network, so there are problems of network transmission reliability and security, etc. As well as the timeliness and error of data, which can be caused by various interference problems, there are some obstacles to the data conversion system.

Autonomy: since the source of data may come from some independent systems, these mutually independent systems have strong autonomy, and they are likely to change their own structure and data according to their own needs without notifying the fusion system. This poses a great challenge to the data fusion system, and the robustness of the fusion system will also be affected.

It is observed that the main expressions and manifestations of heterogeneous data in converged systems can be divided into syntactic dissimilarities and semantic dissimilarities [12]. A grammatical heterogeneity mainly represents the fact that the same objects and facts in the domain are described in different ways. The different data table structures are for example different in different databases with

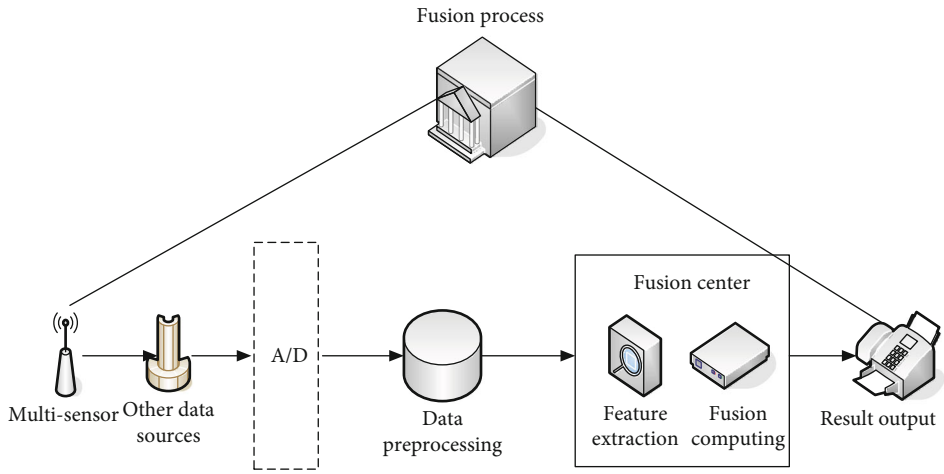

Figure 1: Multisource data fusion process.

the same data stored, due to the different naming rules and data types that are present in different databases [13]. For example, when describing parts of the system, some files use parts to describe, and some files use components to describe. Compared with the elimination of semantic heterogeneity, the elimination of grammatical heterogeneity only needs to implement the mapping relationship from field to field or record to record in specific operations and then resolve the naming and data type conflicts between these concepts. The heterogeneous data in the fusion system is shown in Figure 1:

For that reason, the syntactical heterogeneity which is easier to achieve, there is no reason to understand about the specific content and meaning of the data in the mapping process. That can be solved if we can obtain data structure in the information and complete the mapping in different data sources between the structure of the data [14]. Semantic heterogeneity is relatively more complicated than synthetic heterogeneity, because semantic heterogeneity usually destroys the personality between fields and needs to be processed immediately at the data content level.

2.2. Data Processing. An important guidance for data preprocessing operation can be found in the stream shape learning algorithm. From these analysis, this paper proposes a data preprocessing operation combining noise-removal operation and noise-cancellation operation in a streaming learning method, i.e., data preprocessing operation of the streaming learning algorithm [15, 16]. Located on a local linear was plane of the manifold structure. Each data point in the manifold structure has k neighbors.

$$Z_j = B^T\left(x_{ij} - d\right) \in R^m. \tag{1}$$

This transformation should be reversible, where Z_j is the mapping result of X_{ij}, which can also be obtained by Z_j doing the inverse transformation X_{ij}. d is the translation vector, and m is the spatial dimension after projection and satisfies the orthogonal normalization condition, namely

$$b_j^T b_k = \delta_{jk}, \tag{2}$$

where at that time, $j = k$ and $\delta_{jk} = 1$; otherwise, $\delta_{jk} = 0$.

$$X'_{ij} = d + BB^T\left(X_{ij} - d\right) = d + BZ_j. \tag{3}$$

The formula is inverse transformation. In actual operation, due to the influence of noise data or different transformation methods, there are errors between X'_{ij} and X_{ij} them, as shown below:

$$\varepsilon_j = X_{ij} - X'_{ij} = X_{ij} - d - BB^T\left(X_{ij} - d\right). \tag{4}$$

Perform objective optimization operations on B and d. The specific formula is as follows:

$$\min\left\{\sum_{j=1}^{k}\omega_j\left\|\varepsilon_j\right\|^2\right\} = \min\left\{\sum_{j=1}^{k}\omega_j\left\|X - d1^T - BZ\right\|^2\right\}, \tag{5}$$

where ω_j is the weight of the error ε_j. According to the feature decomposition, the minimum weighted mean square value of B is obtained. S is the weighted covariance matrix of neighboring points. Then, calculate the minimum mean square value of the translation vector d:

$$d = \frac{\sum_{j=1}^{k} w_j X_{ij}}{\sum_{j=1}^{k} w_j}, \tag{6}$$

$$S = \frac{1}{k}\sum_{j=1}^{k} w_j\left(X_{ij} - d\right)\left(X_{ij} - d\right)^T. \tag{7}$$

When the above formula is transformed, the size is related. The weight of the sample point reflects the possibility that the point ε is noisy data. If the error is large, it means that the point is likely to be noised; otherwise, the point is less likely to be noise. The following functional relationship is satisfied between the weight and the error:

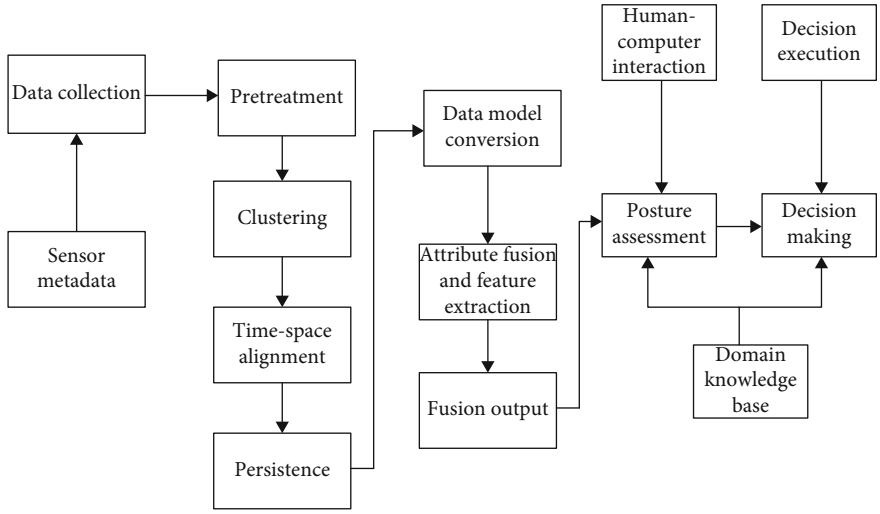

Figure 2: Multisensor data fusion model.

$$\omega(\varepsilon) = \begin{cases} 1, |\varepsilon| \le \mu, \\ \exp\left[\dfrac{(\varepsilon-\mu)^2}{2\sigma^2}\right]. \end{cases} \tag{8}$$

ε and μ defined as follows:

$$\mu = \frac{1}{n}\sum_{i=1}^{n} \varepsilon i, \tag{9}$$

$$\sigma^2 = \frac{1}{n}\sum_{i=1}^{n} (\varepsilon_i - \mu)^2. \tag{10}$$

Divide the data X_i to be classified into c fuzzy partition groups, find the cluster center under each fuzzy partition, initializing a membership $i * j$ matrix U with a random number in the range of [0, 1], and any element u_{ij} in the matrix satisfies the condition:

$$\sum_{i=1}^{c} u_{ij} = 1, \forall i = 1, 2, \cdots, n. \tag{11}$$

u_{ij} represents the degree X_i of membership of the cluster centers v_i and calculates each cluster center v_j:

$$v_j = \frac{\sum_i^n = 1 u_{ij}^m x_i}{\sum_i^n = 1 u_{ij}^m}. \tag{12}$$

Calculate the cost function. If the cost function is less than a certain threshold or the change of the cost function during two iterations is less than a certain threshold, the algorithm stops β, and the cost function is

$$J(U, v_1, \cdots, v) = \sum_{i=1}^{c} J_i = \sum_{i=1}^{n} u_{ij}^m d^2(x_i, v_j). \tag{13}$$

Update the membership matrix U, and then return to the step:

$$u_{it} = \sum_{j=1}^{c} (d_{it}/d_{it})^{-2/(m-1)}. \tag{14}$$

For the membership matrix output by the algorithm U, no human intervention is required in the algorithm implementation process. In order to avoid the possible misjudgment of this method, based on the cosine similarity, the cosine value of the angle between the point and the cluster center is used to weight the Euclidean distance. But

$$d_v(x_t, v_j) = \mathrm{sim}\left(x_t^{(j)}, v_j\right) * \sqrt{\left(x_t^{(j)} - v_j\right)^T \left(x_t^{(j)} + v_j\right)}. \tag{15}$$

Among them $t = |v_j|$, $|v_j|$ represents the number of samples in a cluster v_j that is the cluster center, and $x_t^{(j)}$ represents all sample points v_i in the cluster where the cluster center is located.

During the feature-level data fusion stage, which is the input from the structured data file output at the data-level data fusion stage, it is necessary to describe the sensor data in a unified manner, i.e., transform the data model, with a view to facilitating feature extraction and association of browser data, while at the same time sharing the sensor data with the subsequent fusion process [17, 18]. The multisensor data fusion model is shown in Figure 2:

The decision-level data fusion stage accepts situation reports from the feature-level data fusion stage. These situation reports are only a situation description of a certain aspect of the current scene. In order to obtain the overall situation in the current scene, these situation ontology fragments need to be fused and fused. After that, the situation ontology has a global situation description for the current scene, and then, the situation assessment can be carried out with the help of the global situation ontology

description. Situation assessment is a higher-level abstraction of data [19]. An eventual decision would be generated based on the current situation assessment then the decision information in the global situation ontology about the current situation by searching in the global situation ontology on the basis of the rule-based ontology reasoning [20].

2.3. Data Model Conversion in Data Fusion. The main task of the multisensor feature-level data fusion stage is to deal with the problem of information representation and correlation [21]. Feature-level data fusion needs to extract the attribute information of the fusion target, but the data description form of different sensors is different, so it is difficult to extract attributes from the data of different description forms, which requires a unified and standardized description of these data. This is the operation of data model conversion performed in the feature-level data fusion stage [22]. The data model conversion operation is aimed at shielding the obstacles to data fusion caused by the difference in data description form, so that the sensor data can be shared and fused in different fusion stages in the same representation form [23].

In the environment of multisensor data fusion, sensor data needs to be processed at different fusion levels, and different data representations and different data abstraction levels need to design corresponding data processing methods [24]. In order to better achieve multisource heterogeneous data fusion, we have drawn the data model conversion flowchart of multisource heterogeneous data fusion, as shown in Figure 3:

As this flow diagram shows, the sensor metadata at the sensor's metadata layer is captured for the data level fusion layer for organized representation, where various structured data files are formed at the data level and stored in different media [25]. When some sensor data needs to be processed at a higher level, heterogeneous data in different formats need to be processed at the data level to form structured data about the fusion target and upload it to a higher level of data processing. After the feature-level data fusion layer receives the structured data file about the fusion target input by the data-level fusion layer, in order to realize the feature extraction of the fusion target and the unified processing of heterogeneous data, these heterogeneous data need to be described uniformly [26].

Since the sensor is susceptible to various interferences from the external environment, the data obtained from the sensor is likely to be distorted, and the error registration operation is performed on these data in the preprocessing stage [27]. The data after the preprocessing stage is of higher quality than the original data, and it is also convenient for data clustering operations. Data clustering is to classify and synthesize multiple vectors describing the same attribute of the target, so that the sensor has a unified attribute description for a single attribute of the target, and then perform spatio-temporal alignment operations on these attribute descriptions. Because some data forms are not structured, it is difficult to establish an effective description of these data. In order to make inference judgments and combined decision-making for multisource heterogeneous data during fusion, the solution is to extract the semantics of multisource heterogeneous data in the feature-level data fusion stage and establish a unified data description [28].

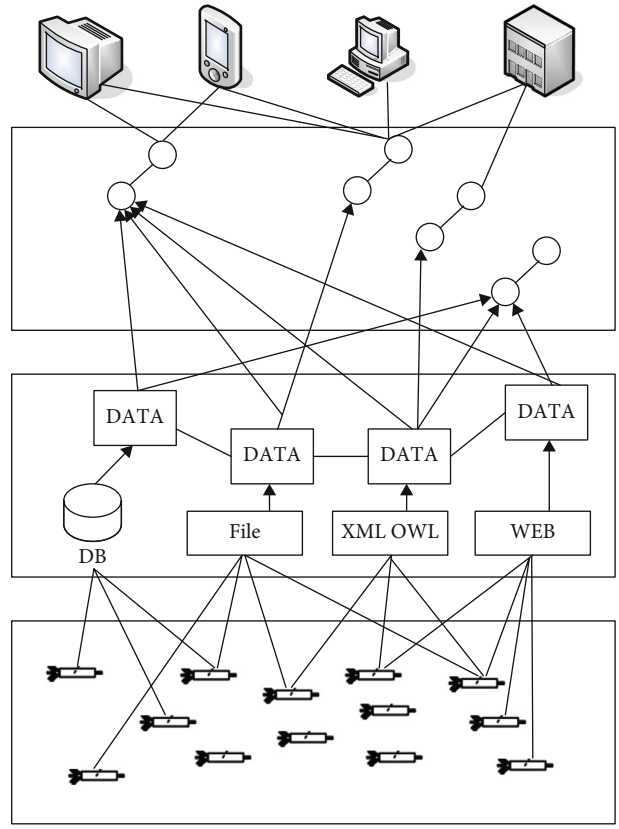

Figure 3: Data model conversion flowchart.

Table 1: Experimental equipment parameter list.

Category	Parameter
Server	Intel(R)
CPU	Core i7-7700
Main frequency	4.0 GHz
RAM	8 G
Operating system	Linux
Simulation software	MATLAB 2016
Cloud environment	Hadoop

Table 2: Basic information of the data set.

Data set	Training data set	Test data set
Total number of samples	494317	335287
Number of normal samples	95632	57482
Number of abnormal samples	245632	258037
Number of DoS samples	380334	218742
R2L sample number	1015	15078
Number of U2R samples	41	217
Probe sample number	4096	4055
Unknown number of samples	—	17601

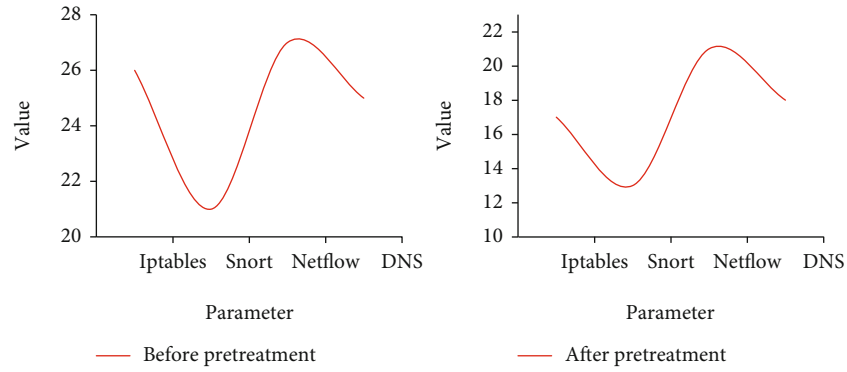

Figure 4: Data preprocessing results.

3. Regional Digital Construction Experiments and Conclusions

3.1. Regional Digital Environment. This article first builds a cloud environment to verify the machine learning algorithm proposed in the paper. We select the decision tree in machine learning and artificial neural network for comparison. According to the existing equipment in the laboratory and the preliminary scientific research work, the machine learning safe data source is selected for the experiment. The experimental equipment parameters are shown in Table 1.

The training data is shown in Table 2.

The data volume is reduced after the data source is preprocessed. In this experiment, a total of 4 GB of data was used for preprocessing, and the results of data preprocessing are shown in Figure 4.

The differences before and after data were large, as can be seen from Figure 4, where the maximum value before data processing reached 27, but the maximum value after processing was 22, with Iptables decreasing by about 20% after processing, and in the case of DNS decreasing by about 30%.

In order to comprehensively evaluate the decision tree and artificial neural network algorithm proposed by the theory, the proposed method is verified and analyzed through the existing classic data sources, and the comparison is made. We use the evaluation index of algorithm stability; it is associated with accuracy rate, mistake rate, and the missing rate. Implementation of the algorithm enhancement effect involves two stages: data preprocessing stages and security analysis. Verification metrics are determined by the classification results of the algorism. When the input sample type is malicious and the detected result type is also malicious, it is called true positive (TP). When the sample is malicious and the result is normal, it is called false negative (FN). When the sample is normal and the result is normal, it is called true negative. Among them, "1" means normally, and "0" means error. The test results are shown in Table 3.

To compare the effect of the decision tree and the artificial neural network, we compare the differences between the training set and the test set between the error report rate and the missed report rate. Figure 5 shows the training set comparison result, and Figure 6 is the test set comparison result.

Table 3: Test results.

Index	TN	FN	FP	TP
Sample type	1	0	1	0
Test result	1	1	0	1

It is evident from the comparison of the two datasets from this paper that the overall performance of the proposed machine and the improved method KNN-DST based for D-S evidence theoretical is significantly better than that of the other method KNN-DST. More specifically, in the training set, because the data are all known data of this type, the difference between the two algorithms in terms of detection accuracy, false alarm rate, and disappearance rate is not obvious.

3.2. Regional Digitization. During the time-consuming comparison of different models, this paper compares the prediction time required to handle the number of events at different sizes, with the time-consuming comparison results in seconds as shown in Figure 7.

It can be seen that the prediction model processing with different orders of magnitude, the prediction time consumption is always lower than the traditional prediction model. With the amount of data as 30,000 points, the time consumption began to grow rapidly. The traditional model has the fastest increase in time-consuming when the processing volume is less than 5,000, and the growth tends to be stable when the data volume is 5,000 to 30,000, and it grows rapidly again when the processing data level is more than 30,000. Compared with traditional models, the heterogeneous data matching algorithm based on decision tree and artificial neural network in this paper is more accurate and less time-consuming.

For regional digital construction, we take a school in this city as an example to compare the digital proportions in this area for statistics. The specific results are shown in Figure 8.

It can be seen from Figure 8 that the digital construction of this area, taking our school as an example, has not changed much in recent years. In terms of teaching mode and network capacity, the digital construction of this school is basically stable at around 2, which basically does not meet the standards of digital construction. High-speed network

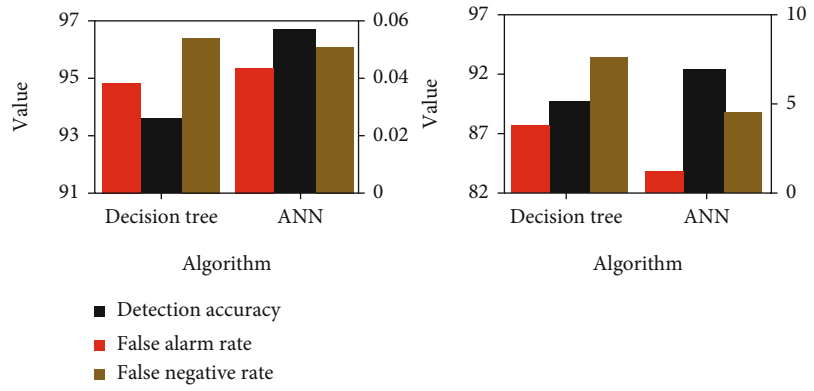

Figure 5: Training set comparison.

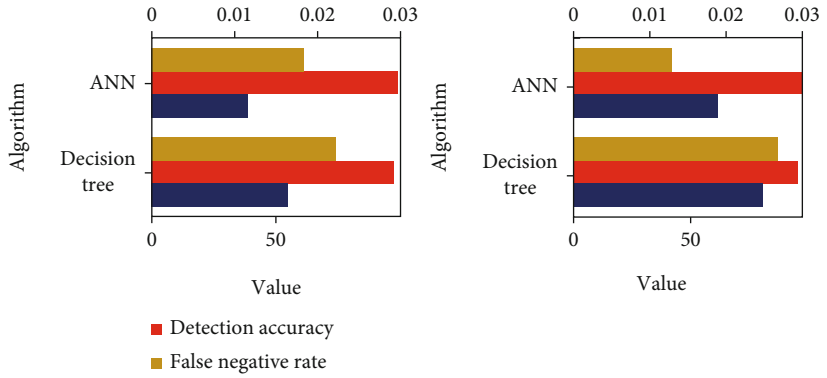

Figure 6: Test set comparison.

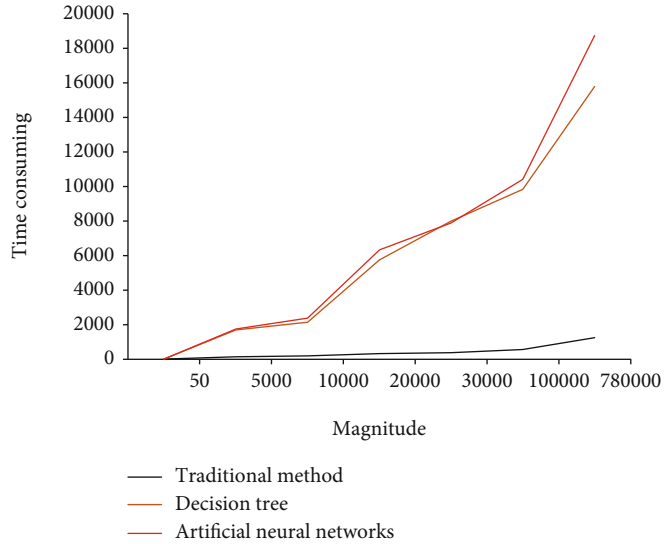

Figure 7: Model time-consuming comparison.

technology spans the distance of time and space. Teachers can teach a course at their own convenient time and place and guide students' learning without being restricted by the time and place of class. Therefore, we carried out a data fusion transformation for the digitization of the school, and the digital construction after the transformation is shown in Figure 9.

It can be seen that after the analysis of heterogeneous data fusion, the school's digital construction has shown an increasing trend. The average value of digital construction is about 3.2, which is an increase of about 1.2 compared to before the fusion, and the growth rate is about 60%. This shows that there has been a considerable increase in regional digital construction of data fusion through machine

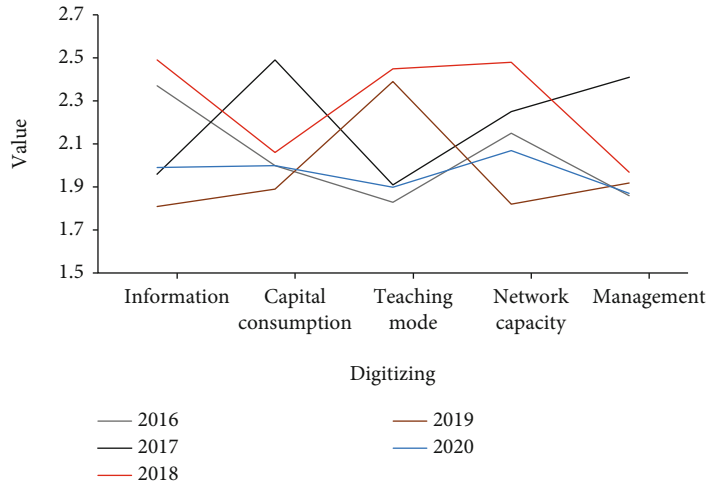

Figure 8: Digitization ratio statistics.

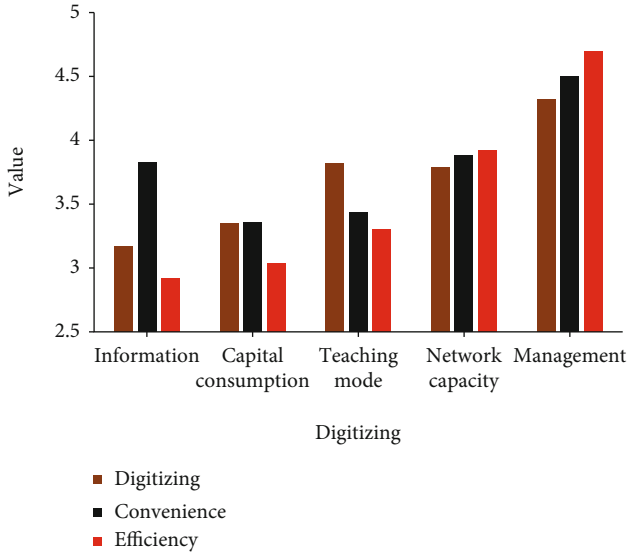

Figure 9: Digital construction parameters after integration.

learning. In order to compare the impact of digital construction in different regions on the region, we compare the management of the school before and after the integration, as shown in Figure 10.

It can be seen from Figure 10 that in the school management before data fusion, the school's management level of teachers and students is at a low level. After problems occur in learning, the feedback time is longer and cannot be handled well. But after the data fusion processing, the management of the school has been greatly improved, the average value has been increased from 2.2 to 4.5, and the feedback of the school's problems can also be dealt with in a timely manner. In order to verify the effectiveness of the data fusion, we select 10 days each to calculate the processing efficiency of different methods, and the results are shown in Figure 11.

It can be seen from Figure 11 that the efficiency of school transaction processing before and after the fusion is obvious. In the selected time, the comparison between the traditional method and the decision tree and neural network selected in this paper is obvious. The two algorithms of the machine school are more effective in transaction processing. The efficiency is significantly better than traditional methods. Of course, in management, we should not only look at the resolution of affairs but also take into account personal feelings. Therefore, we conducted random surveys at the school to compare satisfaction under different methods. The results are shown in Figure 12.

It can be seen from the figure that there is a huge difference in satisfaction under different methods. The traditional management method is rude, without skill, and cannot understand the needs of students and teachers. As a result, it is still not satisfactory after the problem is solved. Under the machine school, after data fusion analysis, problems can be solved well, and people's satisfaction can be improved.

4. Discuss

4.1. Impact of Digital Construction. With the widespread application of the Internet of Things, the fusion technology of multisource heterogeneous data has gradually become a research hotspot in the field of data processing. Due to the grammatical and semantic heterogeneity of multisource heterogeneous data, the interaction, sharing, and fusion reasoning between data are facing obstacles, and the value contained in the data is difficult to be fully utilized. By using the ontology as the description model of multisensor data, the sensor data can be described uniformly, which is convenient for the fusion system to retain the original semantics of the sensor data during the data fusion operation at different fusion levels. The interfusion reasoning provides high-quality data.

Regional digital construction can effectively improve the management efficiency in the region. This is mainly due to the new management model. According to the actual situation of urban management, a management model different from other urban areas is adopted, and the urban management coordination mechanism is rebuilt to improve the

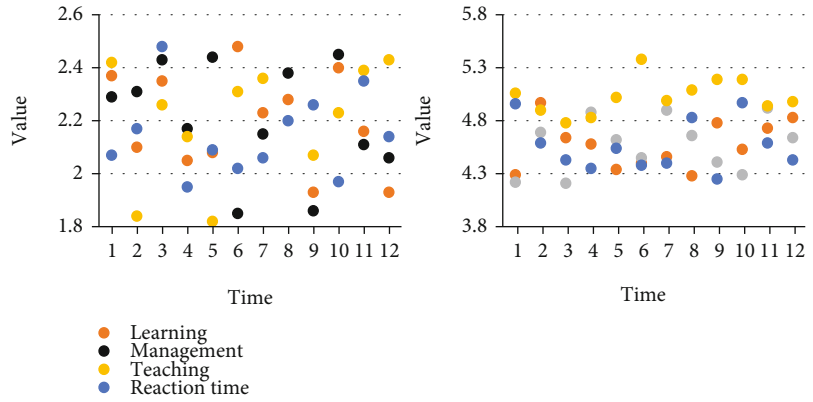

Figure 10: Postintegration learning management.

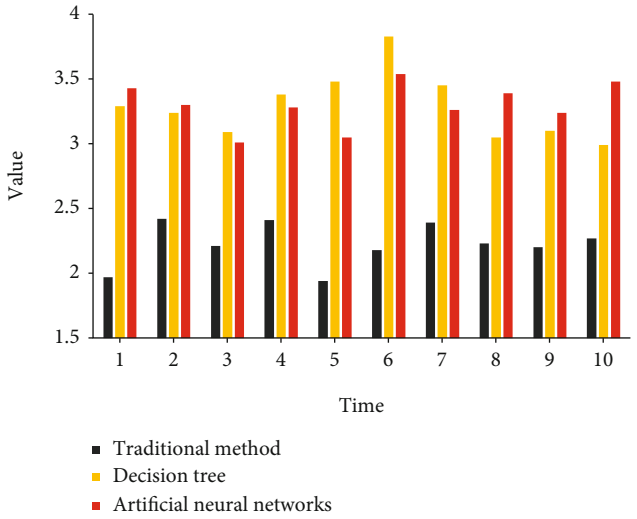

Figure 11: Efficiency comparison before and after fusion.

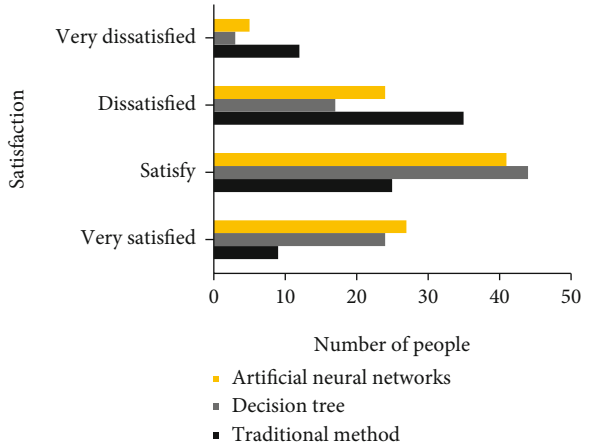

Figure 12: Satisfaction comparison survey.

urban management digital platform supervision center. With the construction of the command center, it can clarify the division of responsibilities and highlight the city management method of departmental cooperation and coordination. And it can also determine the work system of territorial management, effectively break through the traditional city management model, develop from the pyramid level structure to flattening. At the meanwhile, it can improve city management work supervision and management, communication, and coordination capabilities, to achieve an optimized model to promote efficiency improvement.

In the digital construction of city management, make full use of the existing platform construction and information resources, do a good job of horizontal resource integration while doing vertical integration, and connect the platforms of other city-level city management-related departments and the platforms of subordinate district-level departments. It can effectively avoid duplication of construction to achieve resource sharing. In the newly constructed digital platform, high-level configuration and reserved interfaces can be avoided, which can avoid the inability to expand in later construction. It can be found that by integrating the resources of the original urban management-related departments and configuring new data resources at a high level, the urban management digital system between the city-level departments and the urban two-level departments can be interconnected, resource-sharing, and step-by-step. Consistently, how to improve the processing capacity and resource was allocation of urban management digitization in the quick and efficient way.

Digitization accelerates the process of information construction in universities by promoting and deepening information production. It will impact old teaching concepts and bring about reforms in teaching methods. In traditional educational thought, teachers are the main tools of teaching. In most cases, they passively accept various knowledge impart by teachers. However, with the development of information technology, the subject of educational activities will be changed. Teachers are more drivers, encouraging students to actively acquire relevant knowledge through digital platforms and resource networks and pay more attention to self-study. It supports students' learning initiative.

4.2. Enlightenment of Digital Construction. In the regional digital construction, through digital means, the problems in urban management are quickly collected, and the collected data is professionally analyzed. Through the analysis of the causes of urban management problems by

professionals, the city can be continuously optimized. The process of management improves the quality of service and avoids the recurrence of the same problem or the inadequate handling of one problem multiple times. At the same time, it opens the handling process, increases the enthusiasm of the public to participate, and creates an atmosphere for the government, society, and the public to work together in urban management.

During the promotion of digital construction, it is necessary to pay attention to the publicity and popularization of laws and regulations, so that the public can develop a clearer understanding of the relevant requirements of urban management, while strict law enforcement is carried out under adequate publicity and training, to establish the majesty of the law, to well apply legal weapons for urban management, while increasing the public's legal awareness on the establishment of a society in accordance with the rule of law. Each department has a clear division of functions and clear responsibilities. At the same time, each department holds regular meetings to communicate while using digital means to strengthen contact with the public. Finding shortcomings and making timely improvements can greatly improve the efficiency of urban management and avoid departmental interference. Refuse each other, misplaced cognition between the department and the public, and the information communication is not smooth. Through efficient communication, more resources can be provided to better provide city management services.

5. Conclusions

With the advent of the information explosion, data from a single source can no longer meet people's needs for data richness, real-time, accuracy, and reliability. This requires data fusion technology to obtain estimates and decisions from multisource data to improve the credibility of data; this paper uses heterogeneous data aggregation technology to study the regional digital design based on machine learning methods, and from an experimental point of view, good results have been achieved. At present, the development of evidence theory is mainly related to the structure of machine learning, and computer complexity is rarely considered. The next step should be to combine the construction of fast algorithms, construct similar fast algorithms for specific application areas, and also combine corresponding improved synthesis rules to improve the fusion efficiency of algorithms in practical applications.

Data Availability

No data were used to support this study.

Conflicts of Interest

The authors declare that there is no conflict of interest with any financial organizations regarding the material reported in this manuscript.

Acknowledgments

This work was supported by the School level youth fund project of Wuhan Donghu University (No. 2019dhsk006).

References

[1] M. Zhou, X. Li, Y. Wang, S. Li, Y. Ding, and W. Nie, "6G multi-source information fusion based indoor positioning via gaussian kernel density estimation," *IEEE Internet of Things Journal*, vol. 99, pp. 1–1, 2020.

[2] Z. Ding, S. Liu, L. Liao, and L. Zhang, "A digital construction framework integrating building information modeling and reverse engineering technologies for renovation projects," *Automation in Construction*, vol. 102, pp. 45–58, 2019.

[3] E. Rytova and S. Gutman, "Assessment of regional development strategy in the context of economy digitization on the basis of fuzzy set method," *IOP Conference Series: Materials Science and Engineering*, vol. 497, no. 1, pp. 12060–12060, 2019.

[4] A. López, M. Ángeles, and G. P. Beneyto, "Information systems and the computer audit applied to a regional Audit institution: la Sindicatura de Comptes de la Comunidad Valenciana (Spain)," *Revista Gestão e Secretariado-GeSec*, vol. 11, no. 2, pp. 120–138, 2020.

[5] J. Queiroz, P. Leitão, J. Pontes, A. Chaves, J. Parra, and M. E. Perez-Pons, "A quality innovation strategy for an inter-regional digital innovation hub," *Advances in Distributed Computing and Artificial Intelligence Journal*, vol. 9, no. 4, pp. 31–45, 2020.

[6] E. Bareinboim and J. Pearl, "Causal inference and the data-fusion problem," *Proceedings of the National Academy of Sciences of the United States of America*, vol. 113, no. 27, pp. 7345–7352, 2016.

[7] K. Liu and S. Huang, "Integration of data fusion methodology and degradation modeling process to improve prognostics," *IEEE Transactions on Automation Science and Engineering*, vol. 13, no. 1, pp. 344–354, 2016.

[8] L. Mou, X. Zhu, M. Vakalopoulou et al., "Multitemporal very high resolution from space: outcome of the 2016 IEEE GRSS data fusion contest," *IEEE Journal of Selected Topics in Applied Earth Observations & Remote Sensing*, vol. 10, no. 8, pp. 3435–3447, 2017.

[9] B. García de Soto, I. Agustí-Juan, J. Hunhevicz et al., "Productivity of digital fabrication in construction: cost and time analysis of a robotically built wall," *Automation in Construction*, vol. 92, pp. 297–311, 2018.

[10] Chemical Engineering World, "Hexagon PPM partners with Skanska on HxGN SMART build collaboration accelerates strategic development of digital construction technologies," *Chemical Engineering World*, vol. 52, no. 6, pp. 16–18, 2017.

[11] E. Vinson, "Applying an established format to the Houston archives bazaar," *Microform & digitization review*, vol. 48, no. 1, pp. 46–53, 2019.

[12] A. Sudrajat, I. Sudirman, and R. Prasetyo, "Digitalization of logistics processes and comparison with several Asian countries related to logistics information systems: propositions of National Logistics System Architecture," *Solid State Technology*, vol. 63, no. 3, pp. 2824–2836, 2020.

[13] S. Maksimov, Y. Vasin, N. Valuyskov, and K. Utarov, "The digitization of criminal policy as a tool of overcoming its

unsystematicity," *Russian Journal of Criminology*, vol. 13, no. 3, pp. 395–407, 2019.

[14] I. Ahmad, R. W. Aslam, L. Li et al., "Evaluating focal mechanism of September 24, 2013 Awaran earthquake with geospatial techniques," *International Journal of Innovations in Engineering and Technology*, vol. 2, no. 3, pp. 108–124, 2021.

[15] P. B. Fenberg, A. Self, J. R. Stewart, R. J. Wilson, and S. J. Brooks, "Exploring the universal ecological responses to climate change in a univoltine butterfly," *Journal of Animal Ecology*, vol. 85, no. 3, pp. 739–748, 2016.

[16] W. Liao, X. Huang, F. Van Coillie et al., "Processing of multiresolution thermal hyperspectral and digital color data: outcome of the 2014 IEEE GRSS data fusion contest," *IEEE Journal of Selected Topics in Applied Earth Observations & Remote Sensing*, vol. 8, no. 6, pp. 2984–2996, 2015.

[17] M. Berkow, C. M. Monsere, P. Koonce, R. L. Bertini, and M. Wolfe, "Prototype for data fusion using stationary and mobile data: sources for improved arterial performance measurement," *Transportation Research Record*, vol. 2099, no. 1, pp. 102–112, 2018.

[18] A. Amamra and N. Aouf, "Real-time multiview data fusion for object tracking with RGBD sensors," *Robotica*, vol. 34, no. 8, pp. 1855–1879, 2016.

[19] N. Yokoya, C. Grohnfeldt, and J. Chanussot, "Hyperspectral and multispectral data fusion: a comparative review of the recent literature," *IEEE Geoscience & Remote Sensing Magazine*, vol. 5, no. 2, pp. 29–56, 2017.

[20] R. Cabral Farias, J. E. Cohen, and P. Comon, "Exploring multimodal data fusion through joint decompositions with flexible couplings," *IEEE Transactions on Signal Processing*, vol. 64, no. 18, pp. 4830–4844, 2016.

[21] K. M. Nunes, M. V. O. Andrade, A. M. P. Santos Filho, M. C. Lasmar, and M. M. Sena, "Detection and characterisation of frauds in bovine meat _in natura_ by non- meat ingredient additions using data fusion of chemical parameters and ATR- FTIR spectroscopy," *Food Chemistry*, vol. 205, pp. 14–22, 2016.

[22] F. Xiao, "Multi-sensor data fusion based on the belief divergence measure of evidences and the belief entropy," *Information Fusion*, vol. 46, no. 46, pp. 23–32, 2019.

[23] W. Sun, X. Zhang, Z. Zhang, and R. Zhu, "Data fusion of near-infrared and mid-infrared spectra for identification of rhubarb," *Spectrochimica Acta Part A Molecular & Biomolecular Spectroscopy*, vol. 171, pp. 72–79, 2017.

[24] A. Majumder, L. Behera, and V. K. Subramanian, "Automatic facial expression recognition system using deep network-based data fusion," *IEEE Transactions on Cybernetics*, vol. 48, no. 99, pp. 103–114, 2017.

[25] D. Zhou, K. Zhang, A. Ravey, F. Gao, and A. Miraoui, "On-line estimation of lithium polymer batteries state-of-charge using particle filter based data fusion with multi-models approach," *IEEE Transactions on Industry Applications*, vol. 52, no. 3, pp. 2582–2595, 2016.

[26] F. C. Chen, M. R. Jahanshahi, R. T. Wu, and C. Joffe, "A texture-based video processing methodology using Bayesian data fusion for autonomous crack detection on metallic surfaces," *Computer-Aided Civil and Infrastructure Engineering*, vol. 32, no. 4, pp. 271–287, 2017.

[27] Z. Tao and P. Bonnifait, "Sequential data fusion of GNSS pseudoranges and Dopplers with map-based vision systems," *IEEE Transactions on Intelligent Vehicles*, vol. 1, no. 3, pp. 254–265, 2016.

[28] M. Zhou, Y. X. Long, W. P. Zhang et al., "Adaptive genetic algorithm-aided neural network with channel state information tensor decomposition for indoor localization," *IEEE Transactions on Evolutionary Computation*, vol. 25, no. 5, pp. 913–927, 2021.

Hindawi
Journal of Sensors
Volume 2022, Article ID 9511009, 12 pages
https://doi.org/10.1155/2022/9511009

Research Article

Auxiliary Teaching of Badminton Basic Movements Based on Wireless Network Communication and Kinect

Fusheng Liang

Department of Physical Education, Northeast Forestry University, Harbin, 150040 Heilongjiang, China

Correspondence should be addressed to Fusheng Liang; liangfusheng@nefu.edu.cn

Received 11 September 2021; Revised 23 November 2021; Accepted 16 December 2021; Published 7 January 2022

Academic Editor: Mu Zhou

Badminton is a sport with relatively delicate and complicated technical movements, which is widely welcomed in China. In order to study the specific impact of the sports game teaching method and traditional teaching method on the three aspects of the badminton learning technology mastery level, interest level, and subjective experience, with the reference of the wireless network to the students and Kinect on the students, in a three-month group teaching of students without foundation in a medical school in this city, the badminton action is broken down and the doubling of the badminton action is detected by WiFi and Kinect, to compare the traditional pedagogy and the method with this paper before and the lesson and to draw out conclusions. The results of the study found that badminton-assisted teaching based on wireless network communication and Kinect can achieve good results. The learning efficiency of students is significantly higher than that of traditional teaching methods, and badminton teaching based on wireless network communication and Kinect can effectively improve students' interest in learning, 24% higher than the traditional method. This shows that wireless network communication and Kinect technology can play an important role in badminton teaching.

1. Introduction

With the continuous in-depth development of the teaching reform in my country's universities, the continuous improvement of various hardware and software conditions, and the development of networked teaching, there are more and more ways for students to acquire knowledge [1, 2]. It is also multichannel. The difficulties of the current teaching reforms are also becoming more and more common in order to improve the quality of physical education. In recent years, my country's badminton industry has developed rapidly and universities have successively opened badminton courses but the teaching effect is not very satisfactory. Badminton is a seemingly simple sport. There are many of his technical movements, and they are complex and subtle. They were very difficult to master quickly in classes for which the students had no foundation. There was also a crowded practice space for the most usual classes, a large number of a class' students, and only one class to teach per week. A shortage of teachers also contributes significantly to its teaching due to these limitations of teaching time and space. There is therefore an urgent need to improve the instruction of badminton in colleges and institutes.

Based on wireless network communication, Kinect can play an important role in badminton teaching [3, 4]. Kinect is a 3D sensor camera, which relies on the camera to record the player's movement in 3D space. Users can interact with objects in the virtual environment in a nearly natural way, so that participants can interact with the virtual environment. In recent years, wireless communication and Kinect technology have changed from a hot spot in the information field to competition among multiple disciplines. Kinect-related topics and terminology have always been the focus of attention in many fields. Kinect technology is very important for the progress and progress of educational theory. The biggest feature of Kinect is the presence of participants. Compared with traditional multimedia teaching, students are no longer just passive recipients but the two aspects of Kinect participants and the virtual environment interact as a whole, allowing students to change from passive to active, encouraging students to explore independently, and changing the traditional learning mode. "Teaching to promote

learning" means that students learn knowledge through interaction with the virtual environment.

For badminton teaching, many domestic and foreign experts have studied it. Mehmood et al. proposes an energy-saving fault-tolerant scheme to improve the reliability of WBAN. The proposed scheme adopts cooperative communication and network coding strategies to minimize channel damage and volume fading effects, thereby reducing the subsequent failure, bit error rate, and energy consumption. It can be seen from the obtained results that the proposed scheme reduces energy consumption, delay, and bit error rate, thereby improving the throughput and reliability of WBAN [5]. Mehmood et al. proposed a trust-based communication scheme to ensure the reliability and privacy of WBAN. In order to ensure reliability, a cooperative communication method is adopted, and in order to protect privacy, a cryptographic mechanism is adopted. The performance of the proposed scheme is evaluated using the MATLAB simulator. The output results show that the proposed scheme improves the service delivery rate, reliability, and trust, while reducing the average delay [6]. Kang et al. analyzed the application of multimedia simulation platform in badminton teaching. The results show that multimedia technology is only an auxiliary method and cannot replace traditional teaching methods. In order to obtain a good teaching effect, multimedia technology should be combined with traditional teaching methods [7]. For teaching methods, different researchers have different methods. Yang obtained 40 people through purposeful sampling techniques. The samples were processed 8 times, 3 times a week. The data collection technology of the badminton technical test used the data analysis technology of the t-test. The results of the research have a significant effect on the implementation of a distributed practice learning model using audiovisual media to improve the basic technical skills of badminton students [8]. In order to study the best badminton teaching, on the basis of previous research, Kamaruddin et al. introduced neural networks, connected the intelligent learning of the network, designed experimental applications, and then conducted data analysis. The results of the study show that using the smart phone mobile learning teaching method, the experimental group students' technical movements, theoretical knowledge, learning interest, and learning enthusiasm are about 20% higher than those of the control group [9]. Wang introduced the teaching experience of badminton teaching based on the critical teaching method, aiming to overcome the limitations of physical education based only on technical improvement and physical fitness in the school environment. The practice of badminton enhances the critical reflection of local sports culture, allowing students to place themselves at the center of the educational process through dialogue and realize that the problematic social background is more possible [10]. In order to identify the influence of the democratic coaching style on badminton players' game strategies, Araujo et al. evaluated the effectiveness of democratic coaching on their game strategies. The results show that the democratic coaching style based on popularity has a positive impact on players' competitive strategies in the game. Finally, it is found that the democratic coaching style has a greater impact on players' game strategies. These data will increase the settings between universities and departmental badminton projects and ultimately more successful chasing capabilities [11]. These studies have a certain guiding role for this article, but there are also certain problems in the study, such as insufficient experimental samples and time, resulting in unconvincing results.

A new point of innovation in this paper is that we have built a badminton sports action database from the wireless network communication and Kinect. With the wireless network communication and Kinect, we trap the students' badminton sports action and compare the badminton action with the standard action, with the Kinect device being noninvasive for the hard mass-oriented movement which pointed out the shortcomings of the traditional action comparison method based on direct comparison and proposed an action comparison method based on wireless network communication and Kinect [12].

2. Auxiliary Teaching Methods of Basic Badminton Movements

2.1. Wireless Network Communication. With the rapid development of network and communication technology, people's requirements for wireless communication are getting higher and higher [13, 14]. In the meantime, the longest used short-range wireless communicate technologies are Bluetooth, wireless area networks, and infrared data transmission technologies. And there are also some low-bandwidth wireless technology standards with exploit capability, such as Zigbee, high bandwidth, GPS/short-range wireless communication, and dedicated wireless and systems. Both have their own basic set of features or are in accordance with specific thrusts on transmission speed, a distance, and power consumption or focus on functional scalability, meeting or introducing differentiation of specific requirements of in some individual applications to be used in competing services [15]. The badminton movement is captured by the sensor and Kinect to ensure the movement standard. The result is shown in Figure 1:

In the transmission process of the signal from the transmitter to the receiver, it has to go through various complicated transmission paths. Due to the different terrain and the existence of obstacles, phenomena such as reflection, diffraction, and diffraction will occur. Due to the multipath effect [16], the signal received by the receiver is not a single signal but a composite signal composed of incident waves from different paths [17, 18]. In addition, the signal is also accompanied by attenuation in the propagation process. Since the arrival time of the incoming waves of different paths is different [19], the phase of the received signal is also different. Waveform amplitude of the signals follows the principle of in-phase and reverse-phase superimposed and attenuated. The appropriate modifications are made. The fading is generally of a frequency selective nature, so it will not only affect the signal amplitude but also cause frequency transconductance, thus limiting the background bandwidth of the waveform. With the change of relative position between the transmitter and acceptor, a Doppler effect is

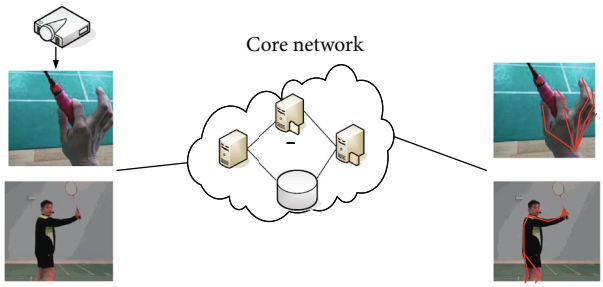

Figure 1: Badminton action to capture.

generated, which makes the signal received by the receiver different in value from the signal emitted by the transmitter. In this case, the difference exists between the receiving and receiving transmitters. The difference between the two is therefore called the Doppler shift [20].

The wireless network designed in this article adopts the Zigbee technology, so the Zigbee technology is mainly introduced and other technologies are not introduced. Zigbee comes from a swarm of bees dancing in the shape of ZigZag to inform other bees of the location of pollen and other information to achieve the purpose of mutual communication, so it is called a new generation of wireless communication technology [21, 22]. For embedded devices, those with higher values and relatively complex protocol stacks are not suitable. Compared with the Bluetooth technology, a larger main network is the advantage of using the Zigbee technology. The Bluetooth technology can only have one slave unit in the piconet at most, while the Zigbee network includes at most one network node [23]. The different technical parameters are shown in Table 1.

The Zigbee technology has the advantages of low power consumption, low cost, large network capacity, and flexible frequency bands. Although the communication rate is relatively slow, the communication data volume of badminton-assisted training is only one byte per second, which can fully meet the needs of the system. The Zigbee technology can support network operation well, but it occupies relatively few hardware resources [24, 25]. Through a comprehensive comparison with other short-range wireless communication technologies, in systems with limited resources but more sensitive to interference, such as badminton teaching, it is more appropriate to use this technology as a wireless communication method [26].

For the Zigbee chip architecture, the chip is mainly used for packet processing and it is used for receiving and processing RF signals by PHY. As the Zigbee system architecture [27], due to its low transmission rate on the simple data processing, it only requires a simple bit handler on the host side in one of the system structure, making the chip unit for a single chip, where the future Zigbee processor chip will be integrated [28]. The Zigbee chip structure is shown in Figure 2.

2.2. Kinect. Kinect is a 3D sports camera that can record sports. The current materials used to capture human motion have bid farewell to the usual traditional cameras, and a variety of home sports cameras have been developed [29, 30]. Although the current motion capture systems are diverse and use similar or completely different principles, they can all be divided into two categories: filtered motion recording systems and noninvasive motion capture systems [31].

Medical motion capture devices began as a way to capture human movements. Usually this kind of equipment is light or medium weight, it is connected to a computer through a cable, and the collected electromagnetic wave, ultrasound or traffic data is downloaded for later data calculation [32]. Mediator devices are relatively in simple principle and easy to use. By their invasive nature, however, it is more restrictive for the perforators and these devices inappropriate for a recording of complex moves [33].

The delayed appearance of nonintrusive motion capture devices is also the basic method of current motion capture. Generally speaking, performers only need to place some highly reflective signs or wear tights, so the impact on the performers is small [34]. Compared with invasive devices, noninvasive devices tend to be more expensive and inaccurate. With the development of high-precision cameras, the accuracy of noninvasive devices has been offset but such systems are relatively expensive [35].

It was initially announced by Microsoft at E3 in June 2009 as the "NatalProject," a 3D Somatic (body-aware) camera for Xbox 360 with instant motion capture, image recognition, microphone input, voice recognition, and social interactive capabilities. In addition, Natal is a 3D somatosensory camera which provides instant motion capture, image recognition, microphone input, voice awareness, and community interaction, providing computers of the ability to understand people's body language [36]. At the same time, it makes "human-computer interaction" as natural, interesting, and rich as possible and brings out the concept of "human-computer interest" more successfully.

Although the Kinect device was officially launched in November 2010, its WindowsKinectSDK for academic research and application development was only late in June 2011 but the appearance of Kinect aroused the attention of researchers and application developers [37]. In the past year, related research and development based on Kinect have sprung up like bamboo shoots after a rain. Some people even cracked Kinect's communication method to obtain more internal data. Nevertheless, Kinect has not been allowed to enter the Chinese Mainland market. Kinect has three cameras in total: the middle of the front is the RGB color camera and the left and right sides are the infrared transmitter and the infrared CMOS camera, respectively. An array microphone system is integrated at the bottom of the Kinect fuselage for voice recognition. In addition, Kinect is also equipped with the focus tracking technology and the base motor will follow the movement of the focus object. The Kinect organization is shown in Figure 3.

Kinect is able to have powerful in-depth image acquisition and motion data capture functions, mainly because of the built-in somatosensory detection device PrimeSensor developed by the Israeli PrimeSense company and sensor chip PS1080; these two hardware devices rely on light coding (LightCoding) technology to capture the depth information of the current scene. The so-called optical encoding technology

Table 1: Comparison of network communication indicators.

Attributes	IEEE802.11b	Zigbee	Bluetooth
Data rate	11 Mbps	868 MHz : 200 Kbps, 2.4 GHz : 250 Kbps	Asymmetric connection: 721Kbps, symmetrical connection: 432.6 Kbps
Communication range	Indoor ≤ 100 m, outdoor ≤ 300 m	Indoor ≤ 10 m, outdoor ≤ 75 m	Indoor ≥ 10 m
Network node	>255	255	7
Frequency band	2.4 GHz	868 MHz/2.4 GHz	2.4 GHz–2.48 GHz
Relative price	High	Medium	Medium

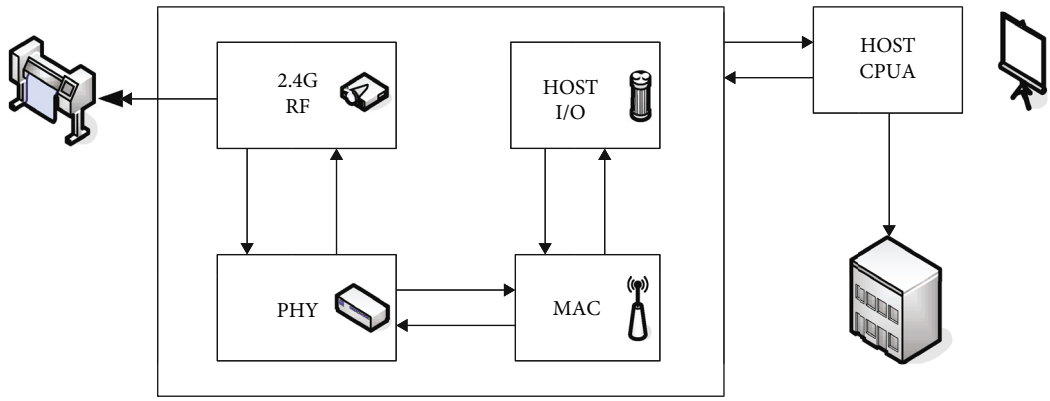

Figure 2: Zigbee system architecture diagram.

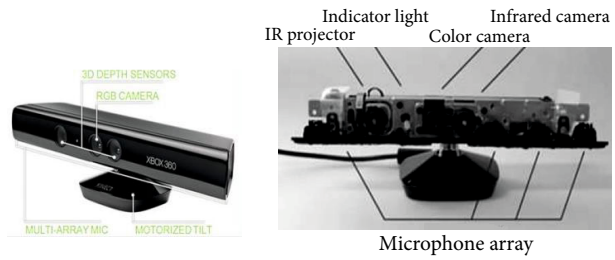

Figure 3: Kinect appearance and disassembly diagram.

refers to the use of continuous light (near infrared) to encode the measurement space, and then, the encoded light is read by the sensor and then decoded by the chip operation to generate an image with depth information.

The key to optical coding technology is laser speckle. When the laser hits rough objects or passes through ground glass, it will form random reflection points, called light spots. The stigma has a high degree of randomness, and its pattern will change with the distance. The points at any two positions in the space will have different patterns, which is equivalent to adding a point to the entire scanning space, so any object can accurately record the position of the object when it enters the space and moves in the space [38, 39]. The so-called coding of the space to be measured refers to the use of lasers to create this position. Kinect uses infrared to emit a type of laser that is invisible to the human eye. Through the grid in front of the lens, also called the diffuser, the laser is evenly distributed and projected to the measurement area, and then, each spot in the area is recorded by the infrared camera, and finally, the image information with depth is calculated by the wafer.

The platform integrates motion data collection and Kinect control functions, which are mainly implemented by the function interface provided by KinectSDK. A standard Kinect motion data collection process is shown in Figure 4.

When Kinect is turned on, the team will detect the number of Kinect devices used on the current machine and then turn over all Kinect devices and find one that is at the ready state, and after the initialization, we will enter the data recovery cycle and the kinematic data acquisition and algorithm processing stage.

2.3. Action Data Collection and Image Processing. It is a key aspect of this work to construct an intermediate representation layer for human regions. This intermediate presentation layer turns the problem into a problem that can be easily solved using effective classifier algorithms. This regions are defined in a vein map that redirects to different skin when rendering different characters. Breadth images and those of the human body area are tagged data when learned from the classifier.

In order to classify pixel x in image I, it is necessary to repeatedly calculate the expression from the root node and determine whether to take the left branch or the right branch by comparing the result with the threshold. The leaf node of each decision tree stores a learned distribution of the human body area $P_t(c|I, x)$

$$P_t(c|I, x) = \frac{1}{T}\sum_{t=1}^{T} P_t(c|I, x). \quad (1)$$

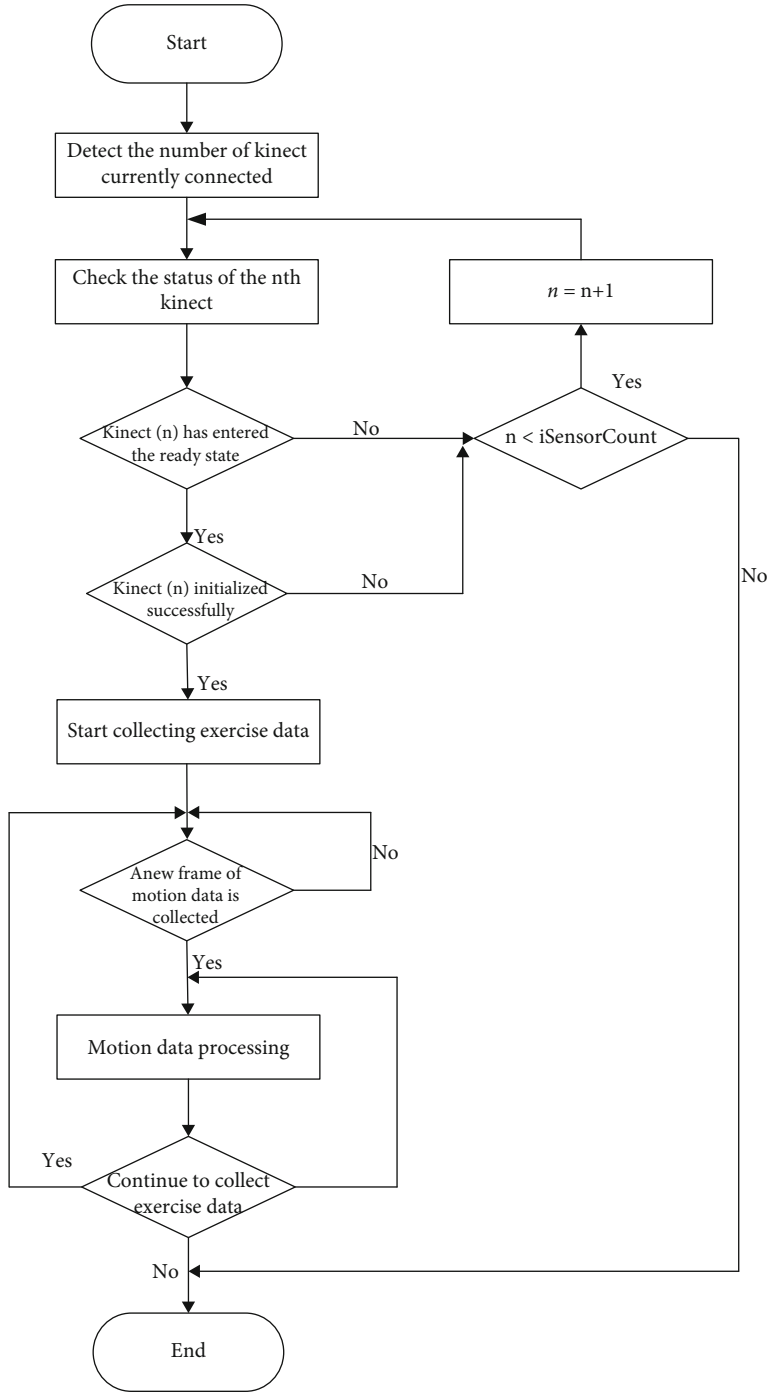

Figure 4: Kinect motion data collection process.

We define a density evaluation function for each body region:

$$f_c(\widehat{x}) \infty \sum_{i=1}^{N} \omega_{ic} \exp\left(-\left\|\frac{x\wedge - x\wedge i}{b_c}\right\|^2\right). \quad (2)$$

$\widehat{x}$ is the three-dimensional coordinates in the world coordinate system, N is the total number of pixels in the image, ω_{ic} is the weight of the pixels, and $\widehat{x}i$ is the relocation coordinate of image pixel x in the world coordinate system according to the given depth, but the width of each learning area. Pixel weight b_c is based on the possibility of the human body area in the pixel and the world surface area where the pixel ω_{ic} is located

$$\omega_{ic} = P(c|I, x_i) * d_I(x_i)^2. \quad (3)$$

In order to describe the movement of the limbs, it is necessary to record the relative posture of the limbs in each

frame of movement data. Since the movement of the limbs is basically formed by the rotation of the joints, pure displacement movement is not common. Therefore, the posture changes during the movement of the limbs can be described by the angle-axis posture description method.

Assuming that the direction vector of the right arm is $\hat{v}_2$ and the z-axis direction vector of the upper body root coordinate system $\hat{v}_1$ is $\hat{v}_2$, it is stipulated that the initial time and direction are the same; then at any time, the posture of the right arm can be expressed as

$$G = (\theta, \omega_1, \omega_2, \omega_3). \tag{4}$$

Therefore,

$$\begin{aligned} \theta &= \arccos \frac{\hat{v}_1 \hat{v}_2}{|\hat{v}_1||\hat{v}_2|}, \\ A(\omega x, \omega y, \omega z) &= \hat{v}_1 * \hat{v}_2. \end{aligned} \tag{5}$$

The general method of driving joint rotation by angular velocity is

$$\text{AngVel} = \frac{(\text{TarAng} - \text{CurAng}) * k}{\text{step}}. \tag{6}$$

Among them, TarAng is the target joint angle, CurAng is the current joint angle, k is the scale factor, step is the simulation cycle length, and AngVel is the calculated angular velocity.

In order to obtain better edge calculation, the fitness function is determined according to the idea of the maximum between-class variance method and the formula is as follows:

$$f(t) = \sigma(t)^2 = w_1(t) * w_2(t) * (u_1(t)) - u_1(t)^2. \tag{7}$$

Among them, t is the threshold, $f(x)$ is the fitness function, $w_1(t)$ is the number of nodes less than the threshold, and $w_2(t)$ is the number of nodes greater than the threshold. Generate a random number in the interval, and select the individual corresponding to the area to which the random number belongs.

Where K is the set of possible values of x and when another y is known, conditional entropy is used to measure the residual uncertainty in the discrete random variable x. It is defined as follows:

$$h(x|y) = -\sum_{x \in \kappa, y \in \kappa} p(x, y) * \log(x|y). \tag{8}$$

The algorithm is generally as follows:

$$t(s) = \exp\left(-\int_0^s \kappa(t)dt\right). \tag{9}$$

From this, we can see

$$\partial = 1 - t(s) = 1 - \exp\left(-\int_0^s \kappa(t)dt\right). \tag{10}$$

When Δs approaches zero, use the following differential equation to illustrate the change:

$$\begin{aligned} \frac{dI}{ds} &= T(s) * \rho(s) * A = T(s) * \kappa(s), \\ I(s) &= I_0 + \int_0^s g(t)dt. \end{aligned} \tag{11}$$

We generally adopt the following formula to proceed:

$$x(k+1) = Ix(k) + Jv(k), \quad k = 1, 2. \tag{12}$$

The quadratic performance indicators are as follows

$$K = \sum_{k=1}^{\infty} \left[x^i(k) J x(k) + r^i(k) c J\right]. \tag{13}$$

If two or more standard samples are given and their characteristic values are all the same and their corresponding categories are also the same, it means that two or more samples are consistent; otherwise, it means that they are inconsistent.

The customization of data is based on the premise of which distribution it conforms to, and then, training and analysis are carried out according to the hypothetical distribution model. Therefore, learning the distribution of feature data according to the energy model can solve all the above problems. Later,

$$E(v, h|\theta) = -\sum_{i=1}^{n} a_i v_i - \sum_{j=1}^{m} b_j h_j. \tag{14}$$

Among them, θ is the parameter model, a_i is the bias of the visible layer unit, b_j is the bias of the hidden layer unit, and W_{ij} is the connection weight between the visible layer and the hidden layer. The joint probability distribution that can be obtained according to the energy function is as follows:

$$Z\theta = \sum_{v,h} e^{-E(v,h|\theta)}, \tag{15}$$

Where $Z(\theta)$ represents the normalization factor in the calculation of joint probability. The likelihood function solved through specific calculations can be expressed as

$$p(v|\theta) = \frac{\sum_h e^{-E(v,h|\theta)}}{Z(\theta)}. \tag{16}$$

Table 2: Student index test before the experiment.

Index	Control group	Test group	t	P
High-flying skill evaluation	7.14 ± 0.712	7.34 ± 0.762	0.792	>0.05
High ball reaches the target	7.09 ± 0.836	6.95 ± 1.147	0.624	>0.05
Backhand technique review	7.45 ± 0.853	7.14 ± 0.821	−0.741	>0.05
Backhand goal	7.14 ± 0.981	7.45 ± 1.014	0.585	>0.05

Table 3: Comparison of forehand lob technical evaluation.

Index	Control group	Test group	t	P
Forehand lob technical review	6.97 ± 0.957	7.94 ± 0.877	1.757	<0.01
Forehand lob meets the target	7.02 ± 0.774	7.14 ± 1.542	0.356	>0.05

Table 4: Comparison of forehand statistics.

Index	Control group	Test group	t	P
Forehand technique review	6.69 ± 1.021	7.76 ± 1.053	2.486	<0.05
Forehand hit goal	7.27 ± 1.433	8.64 ± 1.327	2.596	<0.05

According to the state of the hidden layer unit, the formula for obtaining the visible layer unit in reverse is

$$P(v_i = 1|h, \theta) = \sigma\left(a_i + \sum_j W_{ij} h_j\right). \tag{17}$$

The specific solution $P(v|\theta)$ algorithm of the function is to use the contrast divergence algorithm, and the specific solution process will be described as follows in conjunction with specific applications.

3. Auxiliary Teaching Experiment and Results of Basic Badminton Movements

3.1. Student Information. Before the teaching experiment to test that the wireless network communication and Kinect-assisted effect of the method applied to the teaching of the optional general college badminton class, the forehand high stroke technique and round return technique were tested, and the effect of the independent sample t-test after is being analyzed by SPSS to indicate that the technical evaluation and conformance scores of the experimental class and the controlled group for the forehand high squad and the preselected backhand technical appreciation and conformance scores do not show significant differences. Teaching experiment ($P > 0.05$). At this time, the experimental class and the control class are comparable in indicators, laying a foundation for the next experiment and ensuring the convenience of the experiment. The student indicators before the experiment are shown in Table 2:

A forehand is a ball near the finish line of the backcourt area, and the front handle is used to pass the ball back to the opponent's frontcourt area (near the front serving line and between the net) near the corner of the sideline. The flight trajectory of the pod is suitable for the ball to fall quickly after crossing the net. Combining the high ball in the backcourt can effectively mobilize the opponent and is the main offensive technique in the backcourt.

It can be seen in Table 3 that after the experiment, the comparison between the control class and the experimental class forehand technical evaluation score $P < 0.01$, indicating that there is a significant difference between the two. And because the average score of 7.94 in the rod evaluation of the experimental class is higher than the average score of 6.97 in the forehand leaf evaluation of the control class, it shows that teaching with the help of a video tape is helpful. Improve students' forehand podium scores. Although the average score of 7.14 for the experimental class forehand is higher than the average score of 7.03 for the control class, the comparison of the experimental class and the control class forehand score $P > 0.05$, so there is no significant difference between the two, indicating that wireless communication and Kinect teaching aids have no significant effect on the performance of badminton lob hand.

A forehand shot is aimed at the opponent hitting the ball in the backcourt or midfield. Try to hit the ball as high as possible. Use the forehand to hold the ball from top to bottom on the opponent's court. The master hits the ball. The smash technique has the greatest hitting force, fastest speed, and greatest power and is an important means of offensive scoring.

It can be seen in Table 4 that after the end of the experiment, the average score of forehand in the experimental class was 7.76 greater than the average score of forehand in the control class, 6.69, and the average score of forehand in the experimental class was 8.64 greater. The average forehand score of the control class is 7.27, and the comparison of the forehand technical evaluation scores of the two classes and the comparison of the standard scores are $P < 0.05$, indicating the technical evaluation scores of the two classes of forehands and the forehand scores. There are significant

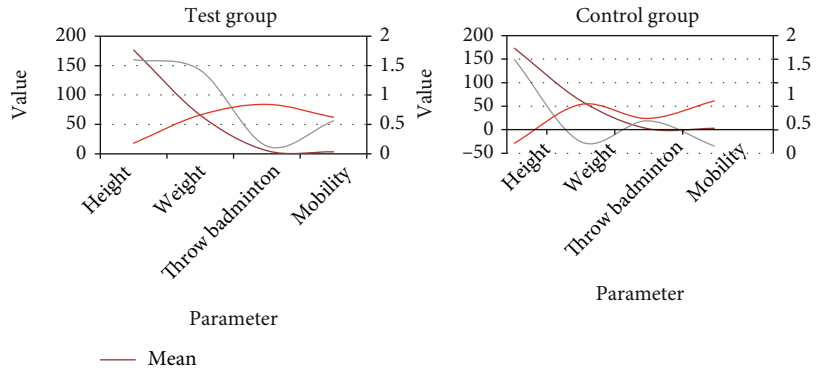

Figure 5: Basic situation of students.

Figure 6: Wireless network communication and Kinect training for students.

differences in the achievement of the standard, so wireless network communication and Kinect-assisted teaching can help improve the performance of the badminton forehand technique evaluation and the achievement of the forehand goal.

Make statistics on the basic physical conditions of students, as shown in Figure 5.

It can be seen that the students before the experiment have similar physical functions, regardless if the indicators between height, weight, and athletic ability are at a similar level, which shows that good results have been achieved in selecting students.

3.2. Training Process. We train the students in the experimental group on wireless network communication and Kinect. First, they train the learning through wireless network communication and Kinect and analyze the students' movements, as shown in Figure 6.

The training content of this experiment is mainly divided into three parts: introduction of badminton, physical fitness training of badminton, and basic technical training of badminton. Among them, wireless network communication and Kinect auxiliary training are mainly used in basic technical training of badminton and the other two training content experiments. There is no significant difference between the group and the control group.

Before the training begins, students and parents are consulted through classroom inquiry or questionnaire surveys to understand the badminton learning experience of the experimental subjects, and further observation and screening of students with learning experience are carried out to determine their existing learning level. The experience will not interfere with the experimental results, and the survey results are shown in Table 5.

It can be seen that most of the students have no badminton learning experience, which also shows that in learning groups, the two groups of learning are in line with the positioning of badminton learners and have homogeneity. Investigate students' interest in badminton, and the statistical results are shown in Figure 7.

It can be seen in Figure 7 that both the experimental group and the control group have higher enthusiasm for

Table 5: Student learning experience.

N	More than 3 months		Within 3 months		Never touched	
	Number of people	Percentage	Number of people	Percentage	Number of people	Percentage
Test group	0	0%	2	11.5%	24	88.5%
Control group	1	1.66%	3	6.54%	26	91.6%
Total	1	1.61%	5	7.49%	50	90.1%

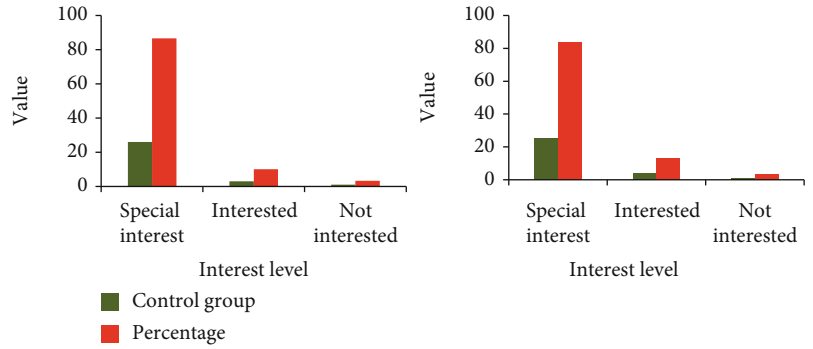

Figure 7: Preexperiment interest survey results.

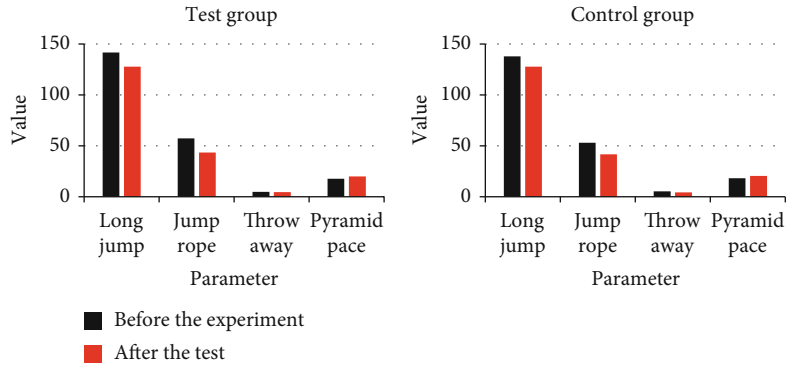

Figure 8: Training data comparison.

badminton training, and there is no forced training. There is no significant difference in badminton training interest between the experimental group and the control group.

3.3. Comparison of Experimental Results. We taught different groups of students for 3 months and then compared the differences between the badminton parameters between the two groups. The changes in the technical control group of the experimental group are shown in Figure 8.

It can be seen in Figure 8 that regardless of the experimental group and the control group, the average value of the test data before and after training has been significantly improved, the variance is generally reduced, and the statistical analysis P value is less than 0.01, so there is a significant difference between the data before and after training. It shows that the physical fitness of the trainees before and after the training has been significantly improved; whether it is the traditional training method or the training method that combines wireless network communication and Kinect, the training effect has been achieved. We statistically analyze

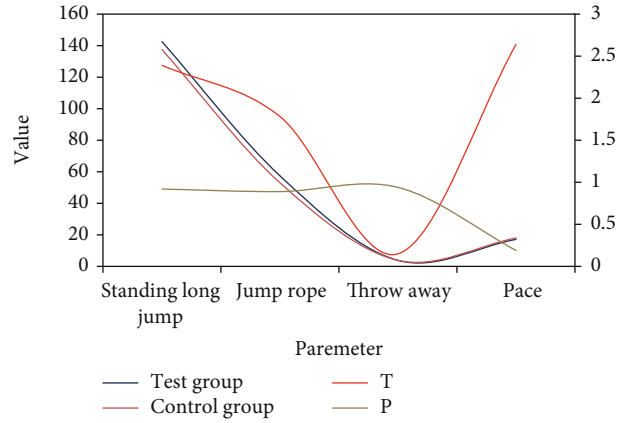

Figure 9: Physical fitness test results.

the physical fitness test data of the experimental group and the control group after the experiment, as shown in Figure 9.

After the experiment, the test data of the experimental group and the control group are slightly higher than those

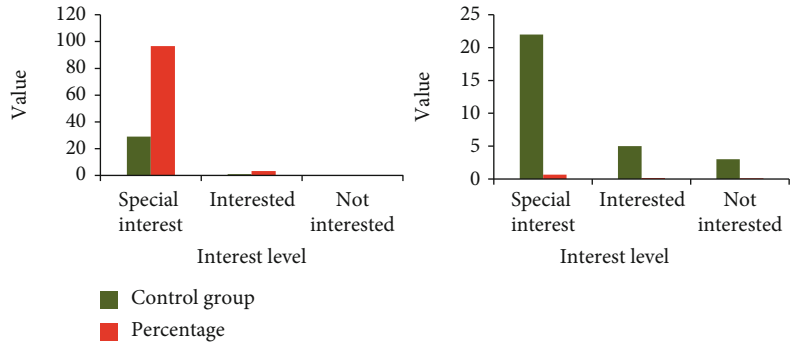

Figure 10: Preexperiment interest survey results.

of the control group but the gap is smaller (less than 5%). In the independent t-test, the P values of the four test data are all greater than 0.05, indicating that there is no significant difference between the test data of the experimental group and the control group.

We surveyed the two groups of experimental subjects about their interest in badminton after 3 months of teaching. The survey results are shown in Figure 10.

After three months of group teaching, it follows in Figure 10 that in the experimental group applying the method of this paper, the learning of a lot of interest in badminton accounts for more than 90%, and in the traditional teaching method, the students taking a lot of interest in badminton represent only about 66%, more than the method of this paper by 24 percentage points, which also shows that the teaching of badminton in wireless network communication with Kinect than the method of traditional can cause students' confidence more.

4. Discuss

The survey found that most of the trainees are positive about their interest in badminton based on wireless network communication and Kinect, the cultivation of sports confidence, and the effect of badminton training. The trainees' enthusiasm for badminton training has been greatly improved. In the sense of progress, look forward to the opportunity to train and learn in this environment in the future. Of course, the problems caused by wireless network communication and Kinect cannot be ignored. Some students cannot accept or adapt to this training method. Try to find solutions to make wireless network communication and Kinect acceptable to everyone.

With the emergence of new technologies, there are indeed certain difficulties for those who are not very skilled or have little exposure to it. It is impossible to say that there is no difficulty at all. In the wireless network with the communication and Kinect learning platform, it is not only the loading that comes with the use of new technology. As a result of the wireless network communicating with the Kinect learning environment, teachers not only need to prepare the teaching content on the classroom, their teachers also need to continue to be involved in the students' learning after the period, and they should be ready to solve the students' questions after the class, while for the students, it provides them with seamless learning opportunities from nowhere.

The emergence of a new technology is always full of controversy. The application of wireless network communication and Kinect's mobile learning to the badminton teaching classroom has been compared and analyzed through experiments. Although the new teaching method is conducive to stimulating the enthusiasm and initiative of students in learning, it has changed the traditional model of "teaching" by teachers and "learning" by students. The interaction between teachers, students, and classmates has brought closer the relationship, but it requires the cooperation and support of more people.

Although students have a certain degree of self-control ability and a certain ability to restrain themselves, sometimes, the nature to like to play is still exposed and the tasks assigned by the teacher may be forgotten. This requires the teacher to set and participate in the evaluation during the implementation process and form an evaluation to fully mobilize the participation of students.

5. Conclusions

This paper mainly studies the motion modeling method for the human motion data captured by Kinect and establishes a human skeleton model based on the Kinect motion data and uses the kinematics model and the captured motion data to drive human actions. Based on the motion model proposed in this paper, a motion evaluation method based on similarity comparison is proposed. The algorithm is introduced into the action evaluation, and the movement data of different lengths are aligned on the time axis, and then, the distance is calculated as the evaluation index of the similarity of the two groups of actions. It makes up for the shortcomings of the traditional Euclidean distance in measuring the similarity of nonequal length data and can evaluate actions more objectively. While the complexity and variability of human movements make it impractical to describe them with a common mathematical model, there are no guarantees that different people will perform the same movement data; however, the same kinds of movements will always have similar characteristics. Analyzing and categorizing the acquired human motion data and motion characteristics,

and identifying the type of exercise performed is the next research focus of this article.

Data Availability

The data that support the findings of this study are available from the corresponding author upon reasonable request.

Conflicts of Interest

The author declared no potential conflicts of interest with respect to the research, authorship, and/or publication of this article.

References

[1] S. Zhou, L. Chen, and V. Sugumaran, "Hidden two-stream collaborative learning network for action recognition," *Computers, Materials & Continua*, vol. 63, no. 3, pp. 1545–1561, 2020.

[2] Z. Lv and H. Song, "Trust mechanism of feedback trust weight in multimedia network," *ACM Transactions on Multimedia Computing, Communications, and Applications*, vol. 17, no. 4, pp. 1–26, 2021.

[3] B. Han, J. Li, J. Su, and J. Cao, "Self-supported cooperative networking for emergency services in multi-hop wireless networks," *IEEE Journal on Selected Areas in Communications*, vol. 30, no. 2, pp. 450–457, 2012.

[4] C. Li, S. Zhang, P. Liu, F. Sun, J. M. Cioffi, and L. Yang, "Overhearing protocol design exploiting Intercell interference in cooperative green networks," *IEEE Transactions on Vehicular Technology*, vol. 65, no. 1, pp. 441–446, 2016.

[5] G. Mehmood, M. Z. Khan, S. Abbas, M. Faisal, and H. U. Rahman, "An energy-efficient and cooperative fault- tolerant communication approach for wireless body area network," *IEEE Access*, vol. 8, pp. 69134–69147, 2020.

[6] G. Mehmood, M. Z. Khan, A. Waheed, M. Zareei, and E. M. Mohamed, "A trust-based energy-efficient and reliable communication scheme (trust-based ercs) for remote patient monitoring in wireless body area networks," *IEEE Access*, vol. 8, pp. 131397–131413, 2020.

[7] H.-E. Kang, I. K. Eom, and Y.-I. Kim, "Design and implementation of the badminton swing coaching system with accelerometers for badminton beginner's swing analysis," *The Journal of Korean Institute of Information Technology*, vol. 15, no. 8, pp. 1–9, 2017.

[8] H. Yang, "Application of multimedia simulation platform in badminton teaching," *Boletin Tecnico/Technical Bulletin*, vol. 55, no. 4, pp. 193–198, 2017.

[9] I. Kamaruddin, M. Nur, and S. Sufitriyono, "Distributed practice learning model using audiovisual media for teaching basic skills of badminton," *Journal of Educational Science and Technology (EST)*, vol. 6, no. 2, pp. 224–232, 2020.

[10] P. Wang, "Modeling of badminton intelligent teaching system based on neural network," *Wireless Communications and Mobile Computing*, vol. 2021, Article ID 9933285, 10 pages, 2021.

[11] S. Araujo, L. O. Rocha, M. C. Coelho, and F. Bossle, "A pedagogia crítica da educação física escolar: relatos de uma experiência docente com o badminton," *Caderno de Educação Física e Esporte*, vol. 18, no. 2, pp. 93–99, 2020.

[12] N. Zhang, N. Cheng, A. T. Gamage, K. Zhang, J. W. Mark, and X. Shen, "Cloud assisted HetNets toward 5G wireless networks," *IEEE Communications Magazine*, vol. 53, no. 6, pp. 59–65, 2015.

[13] M. H. Darya, N. A. Khaskheli, and J. A. Soomro, "Effect of democratic coaching style on the game strategy of badminton players, at region, Sukkur-Sindh," *Sir Syed Journal of Education & Social Research*, vol. 4, no. 1, pp. 398–404, 2021.

[14] S. Aryanti, S. Solahuddin, and S. Azhar, "Learning forehand service badminton using teaching games for understanding (TGFU) students," *Halaman Olahraga Nusantara (Jurnal Ilmu Keolahragaan)*, vol. 4, no. 2, pp. 305–307, 2021.

[15] Y. Chen, "Explore the reform of modern university badminton classroom teaching methods," *Advances in Higher Education*, vol. 3, no. 3, pp. 23–26, 2019.

[16] Y. Wang and G. Zhang, "Big data and data mining application in autonomous learning and badminton skill teaching," *Revista de la Facultad de Ingenieria*, vol. 32, no. 3, pp. 448–454, 2017.

[17] L. Wu, C. H. Chen, and Q. S. Zhang, "A mobile positioning method based on deep learning techniques," *Electronics*, vol. 8, no. 1, p. 59, 2019.

[18] Z. Lv, L. Qiao, Q. Wang, and F. Piccialli, "Advanced machine-learning methods for brain-computer interfacing," *IEEE/ACM Transactions on Computational Biology and Bioinformatics*, vol. 18, no. 5, pp. 1688–1698, 2020.

[19] M. W. Berhimpong, C. A. Motto, and S. Selian, "The effect of reciprocal teaching styles on the ability to hit drop shot in badminton games for SMA Negeri 1 Tahuna students," *Britain International of Linguistics Arts and Education (BIoLAE) Journal*, vol. 3, no. 1, pp. 42–56, 2021.

[20] F. S. Uzunz, G. E. Lker, Y. Arslan, and G. Demirhan, "The effect of different teaching styles on critical thinking and achievement goals of prospective teachers," *Ankara Üniversitesi Beden Eğitimi ve Spor Yüksekokulu Spormetre Beden Eğitimi ve Spor Bilimleri Dergisi*, vol. 17, no. 2, pp. 80–95, 2018.

[21] R. Zhang, P. Xie, C. Wang, G. Liu, and S. Wan, "Classifying transportation mode and speed from trajectory data via deep multi- scale learning," *Computer Networks*, vol. 162, article 106861, 2019.

[22] I. Butun, P. Österberg, and H. Song, "Security of the Internet of things: vulnerabilities, attacks, and countermeasures," *IEEE Communications Surveys & Tutorials*, vol. 22, no. 1, pp. 616–644, 2020.

[23] E. L. Dong, S. Moon, J. Y. Ahn, J. H. Kim, and J. Kim, "Epidemiology and risk factors for sports- and recreation-related eye injury: a multicenter prospective observational study," *International Journal of Ophthalmology*, vol. 14, no. 1, pp. 133–140, 2021.

[24] G. Kosiba, J. Jaworski, E. Madejski, and A. Gądek, "The knowledge of early education schoolgirls about teaching aids used in physical education classes," *Health Promotion & Physical Activity*, vol. 1, no. 1, pp. 39–46, 2017.

[25] Z. Lv, R. Lou, J. Li, A. K. Singh, and H. Song, "Big data analytics for 6g-enabled massive internet of things," *IEEE Internet of Things Journal*, vol. 8, no. 7, pp. 5350–5359, 2021.

[26] P. P. Segura and O. Oliverio, "Through a son's eyes – a tribute to dad," *Philippine Journal of Otolaryngology Head and Neck Surgery*, vol. 36, no. 1, pp. 73–75, 2021.

[27] C. C. Kao and Y. J. Luo, "The influence of low-performing students' motivation on selecting courses from the perspective of

the sport education model," *Physical Education of Students*, vol. 23, no. 6, pp. 269–278, 2019.

[28] P. Buckley, S. Noonan, C. Geary, T. Mackessy, and E. Nagle, "An empirical study of gamification frameworks," *Journal of Organizational and End User Computing*, vol. 31, no. 1, pp. 22–38, 2019.

[29] D. Du, B. Qi, M. Fei, and Z. Wang, "Quantized control of distributed event-triggered networked control systems with hybrid wired-wireless networks communication constraints," *International Journal*, vol. 380, no. C, pp. 74–91, 2017.

[30] K. C. Chang and Y. M. Seow, "Protective measures and security policy non-compliance intention," *Journal of Organizational and End User Computing*, vol. 31, no. 1, pp. 1–21, 2019.

[31] L. Tong, X. Zhu, H. M. Georges, Z. Luo, and D. Wang, "Performance analysis of co- and cross-tier device-to-device communication underlaying macro-small cell wireless networks," *KSII Transactions on Internet and Information Systems*, vol. 10, no. 4, pp. 1481–1500, 2016.

[32] J. Pedersen, A. Graell i Amat, I. Andriyanova, and F. Brannstrom, "Distributed storage in mobile wireless networks with device-to-device communication," *IEEE Transactions on Communications*, vol. 64, no. 11, pp. 4862–4878, 2016.

[33] Y. Zhou and W. Zhuang, "Performance analysis of cooperative communication in decentralized wireless networks with unsaturated traffic," *IEEE Transactions on Wireless Communications*, vol. 15, no. 5, pp. 3518–3530, 2016.

[34] T. Hong, W. Zhao, R. Liu, and M. Kadoch, "Space-air-ground iot network and related key technologies," *IEEE Wireless Communications*, vol. 27, no. 2, pp. 96–104, 2020.

[35] W. Kan, F. R. Yu, H. Li, and Z. Li, "Information-centric wireless networks with virtualization and D2D communications," *IEEE Wireless Communications*, vol. 24, no. 3, pp. 104–111, 2016.

[36] M. Li, F. R. Yu, P. Si, and Y. Zhang, "Green machine-to-machine communications with mobile edge computing and wireless network virtualization," *IEEE Communications Magazine*, vol. 56, no. 5, pp. 148–154, 2018.

[37] Z. Z. Li, G. Xu, X. B. Chen, X. Sun, and Y. X. Yang, "Multi-user quantum wireless network communication based on multi-qubit GHZ state," *IEEE Communications Letters*, vol. 20, no. 12, pp. 2470–2473, 2016.

[38] B. S. Thigale, R. K. Pandey, P. R. Gadekar, V. A. Dhotre, and A. A. Junnarkar, "Lightweight novel trust based framework for IoT enabled wireless network communications," *Periodicals of Engineering and Natural Sciences*, vol. 7, no. 3, pp. 1126–1129, 2019.

[39] S. Pierre, "Quality of experience aware multimedia communications over heterogeneous wireless networks," *IET Networks*, vol. 5, no. 2, pp. 37–43, 2016.

Hindawi
Journal of Sensors
Volume 2022, Article ID 3415055, 13 pages
https://doi.org/10.1155/2022/3415055

Research Article

Data Mining of Regional Economic Analysis Based on Mobile Sensor Network Technology

Yucong You

Department of Economy and Trade, Guangzhou College of Business and Technology, Guangzhou, 510000 Guangdong, China

Correspondence should be addressed to Yucong You; yucong_you@sohu.com

Received 10 September 2021; Revised 25 November 2021; Accepted 10 December 2021; Published 6 January 2022

Academic Editor: Mu Zhou

With the continuous development of regional economy, the difference of regional economy has also aroused the attention of all walks of life. Due to the limitations of the traditional research methods, the research results are relatively simple and unable to conduct a more comprehensive analysis. The traditional methods include the following: (1) analyze the evolution of regional logistics based on the location Gini coefficient and location quotient of GIS, and reflect the situation of industrial agglomeration from the annual change curve of the location Gini coefficient; (2) use SPSS12.0 software to perform multivariate or event factors, and analyze and calculate the factor score to sum up several principal component factors; and (3) the production function analysis method is used to measure the economies of scale and agglomeration. As an extension, the relationship between the estimated total output and the agglomeration index of the factor input to measure the uniform state of the industrial distribution department is an effective measurement method for the agglomeration economy. In order to promote the sustainable development of regional economy, this paper analyzes the regional economy comprehensively based on the emerging mobile sensor network technology and data mining technology. Firstly, this paper analyzes the location technology of mobile sensor networks based on sequential Monte Carlo, selects the *C*-means clustering method which is suitable for economic large-sample clustering analysis, and constructs a complete data mining model. Then, the model is used to analyze the economic, social, natural, and educational science and technology indicators of a certain region from 2015 to 2019. The results show that the first principal component weight of economic indicators is the highest proportion of fiscal revenue, which is 0.986. This shows that the role of fiscal revenue in economic indicators is greater. The main index of urban consumption is 72.0, which is the highest. This shows that the population growth rate and the average consumption of urban households in social indicators play a greater role. The first principal component of natural index has the highest weight of pollution emission, which is 0.47, while the second principal component has the highest weight of total energy consumption, which is 0.48. This shows that the pollution emissions and total energy consumption in the natural indicators play a greater role. In the educational science and technology index, the first principal component weight is the highest, which is 0.61. This shows that the education funds play an important role in educational science and technology indicators. Therefore, the data mining model based on mobile sensor network technology can comprehensively and accurately analyze various indicators of regional economy.

1. Introduction

1.1. Background Significance. The regional economy is closely related to the local economic revitalization, which has an important reference role for the government to make a decision. If the economic development of a certain area is good, then it means that the local government's decision is correct, and the government will maintain the original decision; but if there are signs of economic recession, it means that there is a problem with the government's decision and it will push the government to renew decision-making. Mobile sensor network technology can monitor and collect all kinds of information in real time and has superior information acquisition ability [1, 2]. Data mining technology is a collection of machine learning, artificial intelligence, and statistics-related results and is widely used in various fields [3]. The combination of mobile sensor network technology and data mining technology can improve the efficiency and

quality of data acquisition and mining and obtain effective information quickly. The application of this synthetic technology to the analysis of regional economy does not only provide a new idea for the analysis of regional economy but also can transform the research results into productivity and promote the development of regional economy.

1.2. Related Work. Wireless sensor networks have been used in many mobile applications, such as wildlife tracking and participatory urban sensing. Zhu et al. introduce the impact of industrial agglomeration on the regional economy in a simulated intelligent environment based on machine learning and propose a method to detect the industrial agglomeration index to analyze industrial agglomeration. By establishing an industrial agglomeration index system, the level of manufacturing industry integration is objectively analyzed and the impact of manufacturing industry integration is empirically tested [4]. Lu et al. solve the environmental monitoring problem by developing an event-triggered limited time control scheme for mobile sensor networks. The proposed control scheme can be executed independently by each sensor node and consists of two parts: one part is a finite-time consensus algorithm, and the other part is an event trigger rule. The consensus algorithm is used to enable the position and speed of sensor nodes to quickly track the position and speed of the virtual leader within a limited time. The event trigger rule is used to reduce the update frequency of the controller to save the computing resources of the sensor node. Under the fixed communication topology and the switched communication topology, some stability conditions are derived for the mobile sensor network using the proposed control scheme [2].

The application of data mining technology in the economic field is also a lot of research. Based on data warehouse, data mining, and OLAP technology, Min and Rui propose a modular design decision support system and describe its structure and key technologies [5]. The system test results show that data mining has a good prediction effect on economic prediction. Arends-Kuenning et al. forecast according to the industry that the change of Mexico-US tariff will lead to regional economic growth, and trade liberalization seems to benefit manufacturing industry to a large extent [6]. The increase in national tariffs leads to a decrease in external demand, which also affects prices on the international market, causing them to fall, and the increase in tariffs results in the internal market being the same as the international market after the levy, so in this case, the tariff on the levy has to be shared between internal consumers and exports over, which can affect the regional economy. Their research only analyzes the impact of trade on regional economic development, without considering other factors.

1.3. Innovative Points in This Paper. In order to have a more comprehensive and thorough understanding of the regional economy, provide data support for the relevant government work, and promote the development of regional economy, this paper conducts an in-depth study on regional economic analysis based on mobile sensor network technology and data mining technology. The innovation points of this study are as follows: (1) based on mobile sensor network positioning technology, this paper selects the appropriate C-means clustering method as the basic model of data mining and constructs a data mining model which can be used to analyze the relevant indicators of regional economy; (2) using this model, the economic, social, natural, educational, and scientific and technological indicators of a certain region are cluster analyzed; and (3) it is concluded that in the development of the regional economy, the financial revenue, the average consumption level of urban households, dye emissions, total energy consumption, and education funds play an important role. If fiscal revenue increases, then the corresponding government investment will increase, which will promote the development of the regional economy; the increase in consumption will further stimulate consumption, and consumption will stimulate regional economic growth; education is the cornerstone of the nation and will cultivate local talents. This will also boost the regional economy. Therefore, in order to promote the development of regional economy, we must start with these factors.

2. Mobile Sensor Network Technology and Data Mining Technology

2.1. Mobile Sensor Network Technology

2.1.1. Routing Protocol. Wireless sensor networks have limited computing, storage, wireless communication, and power supply capabilities. Good routing protocols can reduce energy consumption as much as possible and prolong the network lifetime. There are two functions of routing protocol. The first is to find the optimal path between the source node and the destination node efficiently and accurately. The second is to group the obtained data and forward the grouped data according to its optimized path [7, 8]. For the application scenario with a small number of nodes moving, the routing protocol can be simplified.

According to the network topology, routing protocols can be divided into two types: plane and cluster. Plane routing protocol has the advantages of simple and easy to expand, while cluster routing protocol has the advantages of low communication cost, low energy consumption, and convenient management [9]. Routing is divided into static routing and dynamic routing. Dynamic routing protocols can be divided into distance vector routing protocols and link state routing protocols. The distance vector routing protocol is based on the Bellman-Ford algorithm, mainly including RIP and IGRP; the link state routing protocol is based on the very famous Dijkstra algorithm in graph theory, that is, the shortest first path algorithm. In the distance vector routing protocol, the router transmits part or all of the routing table to its neighboring routers; in the link state routing protocol, the router transmits link state information to all routers in the same area. According to the router's position in the autonomous system, routing protocols can be divided into interior gateway protocols and exterior gateway protocols. There are two types of interdomain routing protocols: exterior gateway protocol and border gateway protocol. EGP is designed for a simple tree topology. It has

obvious shortcomings when dealing with routing cycles and setting routing strategies. It has been replaced by BGP at present. EIGRP is a proprietary protocol of Cisco, which is a hybrid protocol. It not only has the characteristics of the distance vector routing protocol but also inherits the advantages of the link state routing protocol. Various routing protocols have their own characteristics and are suitable for different types of networks. Low-power adaptive cluster layering (LEACH) protocol uses a fully distributed mechanism to generate cluster heads [10]. Each node produces a random number between [0,1]. If the number is less than the threshold $Y(n)$, then the node will not be the cluster head node for a long time. The calculation of threshold is shown in the following formula:

$$Y(n) = \begin{cases} \dfrac{r}{1 - r * t[\mathrm{mod}\ (1/r)]}, & n \in J, \\ 0, \quad \text{other}, \end{cases} \tag{1}$$

where r is the percentage of ordinary nodes becoming cluster heads in each round, t is the number of current rounds, and J is the set of nodes without selected cluster heads in the last $1/r$ round. When $t = 0$, the threshold is equal to r. When $t = 1$, the threshold is shown in the following formula:

$$Y(n) = \frac{r}{1 - r}. \tag{2}$$

The energy consumption formula in the LEACH protocol is the first-order radio mode. The calculation of energy consumption of sending and receiving 1 bit byte by sensor node is shown in formula (3) and formula (4), respectively:

$$E_{Tx}(i, l) = iE_{\mathrm{elec}} + i\varepsilon l^{\alpha}, \tag{3}$$

$$E_{Rx}(i) = iE_{\mathrm{elec}}, \tag{4}$$

where ε, α are the amplification factor and constant of the signal amplifier, respectively. E_{elec}, l is energy consumption and transmission distance.

The LEACH protocol has the advantages of low energy consumption and long network life cycle. However, the signal between multiple nodes will produce interference, which will affect the communication quality and connectivity of the whole network. In addition, the number of cluster head nodes will directly affect the network life cycle.

2.1.2. Positioning Technology. At present, wireless sensor network positioning technology can be divided into two categories: static and mobile. Static wireless sensor network positioning based on distance measurement uses the received signal strength ranging mechanism to calculate the distance between receiving and receiving nodes by using the radio signal transmission model [11, 12]. The localization technology of mobile wireless sensor network nodes is currently a major research hotspot in wireless sensor networks. In mobile wireless sensor networks, nodes are mobile, and nodes with unknown location information in the network can use a certain positioning mechanism and prediction mechanism to determine their own current and underlying coordinates. The existing wireless sensor network node's own positioning algorithm has relatively low positioning accuracy and poor positioning real-time performance, and some algorithms have high complexity, and the ranging error is greatly affected by the environment, which is not suitable for locating mobile nodes. Aiming at the abovementioned problems, this paper begins to study the positioning technology of mobile wireless sensor network nodes, as shown in the following formula:

$$P(l)[lB] = P(l_0) - 10n \lg\left(\frac{l}{l_0}\right) + R_{\sigma}, \tag{5}$$

where $P(l), P(l_0)$ are the received power at a distance of l, l_0, n is the channel attenuation factor, and R_{σ} is a Gaussian random variable. When the signal transmission time is used for ranging, as shown in the following formula:

$$l = (t - t_0) \times v, \tag{6}$$

where t, t_0 are the time of transmitting and receiving signals, respectively; v is the propagation speed of signals; and l stands for distance. When the time difference of signal arrival is used for ranging, the calculation is shown in the following formula:

$$l = [(t_2 - t) - (t_1 - t_0)]\frac{v_1 - v_2}{v_1 v_2}. \tag{7}$$

Among them, t, t_0 are the time of receiving and transmitting RF signal and t_2, t_1 are the time of receiving and transmitting ultrasonic signal, respectively. They are the propagation speed of RF signal and ultrasonic signal.

Although the accuracy of static wireless sensor network positioning without ranging is low, it does not need hardware support, so the cost and energy consumption are low.

MCL algorithm for mobile wireless sensor network localization based on sequence Monte Carlo improves the accuracy and reduces the cost of localization by using the mobility of nodes, but the storage is very limited [13]. MCB algorithm improves the sampling power and reduces the amount of calculation. The DRL algorithm of nonstatistical mobile wireless sensor network localization can reduce the information flooding between nodes and improve the positioning accuracy [14]. CDL algorithm belongs to centralized location and is easier to implement.

2.1.3. MIMO Technology. Multiple-input multiple-output (MIMO) technology can improve transmission rate and expand coverage without increasing bandwidth and transmitting power [15]. The channel capacity of the MIMO system is shown in the following formula:

$$C = [\min\ (f, r)]B \log_2\left(\frac{\varpi}{2}\right), \tag{8}$$

where f, r are the number of transmitting and receiving antennas, respectively; B, ϖ represent the signal bandwidth

and the average signal-to-noise ratio of the receiving end, respectively; and C represents channel capacity.

MIMO technology has two functional forms: diversity and multiplexing [16]. The space-time code gain is reduced by space-time coding. The transmitter of spatial multiplexing divides the data into several substreams and sends them at the same time. After the receiver extracts and recovers the signals, it merges them into the original data stream.

Cooperative virtual MIMO technology in wireless sensor networks mainly studies energy consumption characteristics and transmission strategy. The energy consumption characteristics are studied based on the point-to-point transmission model, and the transmission strategy is to explore the scenario of data collection nodes in the detection area.

2.2. Regional Economic Analysis Model

2.2.1. Regression Analysis Model. Regression analysis model uses statistical methods to analyze the causal relationship between variables. If there is only one independent variable and dependent variable in the regression analysis and the relationship is linear, then the analysis model is univariate linear regression [17]. If the independent variables are greater than or equal to two and the relationship is still linear, then the analysis model is multiple linear regression [18]. The univariate linear regression model is shown in the following formula:

$$y = ax + b + \sigma, \tag{9}$$

where a, b are regression coefficients and σ is random disturbance term, which is generally assumed to obey normal distribution. The standard equations solved by multiple linear regression model are shown in the following formula:

$$\begin{cases} \sum y = n\alpha_0 + \alpha_1 \sum x_1 + \alpha_2 \sum x_2, \\ \sum x_1 y = \alpha_0 \sum x_1 + \alpha_1 \sum {x_1}^2 + \alpha_2 \sum x_1 x_2, \\ \sum x_2 y = \alpha_0 \sum x_2 + \alpha_1 \sum {x_2}^2 + \alpha_2 \sum x_1 x_2. \end{cases} \tag{10}$$

When using the regression analysis model, it is assumed that dependent variables are affected by independent variables, and their relationship is expressed by regression mathematical model. Then, get the required data, use statistical methods to determine the relationship between dependent variables and independent variables, and finally, get the regression equation, and use the equation to predict the analyzed object. For example, if the goods on the market are within the normal fluctuation range, then the sales of the goods are also within the normal range. If the value of the goods increases, then the sales of the goods will decrease. Based on this change, a regression can be drawn to predict sales.

2.2.2. Principal Component Analysis Model. Principal component analysis will reflect the sample characteristics of multiple index variables through the clustering of principal components into a small number of comprehensive variables [19]. Because a large number of indicators will be involved in the regional economic analysis, these indicators are not completely independent but are interrelated and jointly reflect the economic development of the region [20]. A large number of related indicators will increase the workload and increase the difficulty of analysis. But simply reducing the indicators will reduce the credibility of the results.

The original indexes in the index matrix describing the comprehensive characteristics of a region are dimensionless.

$$Y_i' = \frac{Y_i - \bar{Y}}{S}, \tag{11}$$

where Y_i, $\bar{Y}$ are the ith original index and sample mean value, S is the standard deviation. Then, calculate the correlation coefficient matrix of the index, as shown in the following formula:

$$R_{zp} = \frac{1}{n} \sum_{i=1}^{n} Y_{iz} Y_{zp}. \tag{12}$$

The third step is to calculate the eigenvalue and eigenvector and solve the characteristic equation as shown in the following formula:

$$|R - \omega P| = 0. \tag{13}$$

The fourth step is to calculate the contribution rate of principal components, as shown in the following formula (14):

$$Q_p = \frac{\omega_p}{\sum_{i=1}^{p} \omega_i}. \tag{14}$$

Finally, the score of the principal component is calculated, as shown in formula (15). After calculation, the principal component is arranged in the order of score.

$$F = v_1 y_1 + v_2 y_2 + \cdots + v_n y_n, \tag{15}$$

where v_n is the common factor weight.

2.2.3. Prediction Analysis Model. The prediction analysis model can explain the relationship between the prediction object and the related factors. The main prediction and analysis model used is the grey prediction model, which analyzes the mathematical relationship between the factors themselves and the factors according to the behavior characteristic data and information of the specific gray system [21]. The grey prediction is based on the grey system theory and uses the differential equation model to predict the change of the eigenvalue of the system and estimate the occurrence time of the abnormal value of the eigenvalue [22, 23].

Sequence grey prediction predicts the eigenvalues of variables in a future period according to the existing eigenvalues. According to the occurrence time of the current abnormal value, the catastrophe grey prediction can predict the occurrence time of the future abnormal value. The grey prediction of seasonal disaster is very special, and the abnormal value of its eigenvalue often appears in a specific period

of time. Topological grey prediction can be used to predict a group of data without changing rules. However, the grey prediction of the system is different from the above-mentioned prediction methods, which is aimed at the overall prediction of the system [24].

2.3. Data Mining Technology and Process

2.3.1. Data Mining Technology. Neural network method uses a large number of neurons, which are connected into a network to achieve a large number of parallel computing [25]. The neural network algorithm needs to construct a threshold object. If the sum of a set of logical unit variables is not less than a given threshold, a value will be output [26]. Suppose that the input value is $x_1, x_2, \cdots, x_n$ and the weighted coefficient of the input value is $g_1, g_2, \cdots, g_n$, the variable summation is shown in the following formula:

$$M = \sum_{i=1}^{n} (x_i * g_i). \tag{16}$$

Naive Bayes method is also one of the common data mining methods. In order to use naive Bayes classification, the assumption of independence must be satisfied. The expression of naive Bayes classifier is shown in the following formula:

$$C = \arg \max_{C_i \in C} P(C_j) \cdot \prod_{i=1}^{n} P(t_i | C_j), \tag{17}$$

where C, C_j represent the set of categories and category j, respectively; $P(C_j)$ denotes the probability of occurrence of category j; and $P(t_i|C_j)$ represents the probability of occurrence of term t_i in category C_j.

K-nearest neighbor algorithm finds k-nearest neighbor documents which are closest to a given test document in the training set and then takes the categories of adjacent documents as candidate categories of the test documents and scores them according to the classification. The decision rule of scoring is shown in the following formula:

$$P(\bar{c}_t, l_j) = \sum_{u_j \in \mathrm{KNN}} \mathrm{sim}(\bar{c}_t, \bar{u}_j) y(\bar{u}_j, l_j) - a, \tag{18}$$

where $y(\bar{u}_j, l_j)$ is 1 or 0; $\mathrm{sim}(\bar{c}_t, \bar{u}_j)$ is the similarity between test document $\bar{c}_t$ and training document $\bar{u}_j$; and a is the threshold of binary decision.

Based on the minimum Euclidean distance, the C-means clustering method divides the point set $(x_1, x_2, \cdots, x_n)$ into m clusters, calculates the Euclidean distance between the center of the set and each point, and generates the distance set L. Find m points $(c_1, c_2, \cdots, c_m)$ in the distance set as the original center point; then, the distance from other vector points to the M original center points is shown in the following formula:

$$l(x_i, c_j) = \sqrt{\sum_{m=1}^{n} (x_{im} - c_{jm})^2}. \tag{19}$$

Then, adjust the cluster center according to the following formula:

$$c_{jm} = \frac{\sum_{x_{jm} \in c_j} x_{jm}}{N_j}. \tag{20}$$

2.3.2. The Basic Process of Data Mining. Data mining process generally includes three main stages: data preparation, data mining, and result expression and interpretation [27]. Data preparation stage can be subdivided into data integration, selection, and preprocessing. According to the specific needs of the search-related raw data, select the targeted data. Data preprocessing uses cleaning and transformation methods to process noisy and random data, which can improve the quality of data mining [28].

In the stage of data mining, it is necessary to select appropriate tools for data mining and then to determine the appropriate tools for data mining. When selecting data mining tools, we need to consider the characteristics of data and the requirements of the actual running system.

According to the final decision-making purpose, the information mined needs to be interpreted and evaluated by experts in related fields. The process of knowledge discovery in database needs to be evaluated according to the initial requirements and then optimized after analysis. Finally, the most valuable information is visualized and conveyed to decision-makers.

2.3.3. System Structure of Data Mining. The structure of data mining system usually includes data source and its server, data mining engine, pattern evaluation, graphical user interface, and knowledge base [29]. Data source mainly provides data needed by data mining, which can be database, data warehouse, or other types. The data source server can filter and clean the data in the data source according to the user requirements and integrate the required target data sets.

Data mining engine is the core of the system, which has the analysis functions of characterization, association mining, classification, and clustering. Pattern evaluation can remove useless patterns and retain interesting patterns according to interest threshold. GUI presents interesting patterns to users in a more intuitive way, that is, visualization of mining results. The role of knowledge base is embodied in storing knowledge, guiding data mining, pattern interpretation, and evaluation.

3. Experiments on Data Mining of Regional Economic Analysis

3.1. Mobile Sensor Network Localization Based on Sequential Monte Carlo

3.1.1. Prediction and Filtering. The MCL algorithm is divided into two stages: prediction and filtering, and the node motion in the prediction stage obeys the random model. The maximum velocity of node motion is $v_{\max}$. At moment e, the circle is drawn with k_{e-1} as the center and the maximum velocity as the radius.

$$p(k_e|k_{e-1}) = \begin{cases} \dfrac{1}{(\pi v^2{}_{\max})}, & \text{if } d(k_e, k_{e-1}) < v_{\max}, \\ 0, & \text{if } d(k_e, k_{e-1}) \geq v_{\max}, \end{cases} \tag{21}$$

where $d(k_e, k_{e-1})$ is the Euclidean distance between k_e, k_{e-1}. The greater the speed of the node, the larger the predicted area.

In the filtering stage, the node will filter out the sample points which do not conform to the actual situation according to the new observation value. If the number of remaining sample points after filtering is too small, it is necessary to repeat the prediction stage and the correction stage until the number meets the requirements.

3.1.2. Important Sampling. MCL algorithm uses importance sampling, assuming that all samples are obtained from the normalized important function π independent sampling. After measuring the weight of each sample, the posterior probability distribution is estimated. In order to simplify the calculation, the prior distribution is selected as the recommended distribution. The calculation of important functions is shown in the following formula:

$$\pi(k_e|q_0, q_1, \cdots, q_e) = p(k_0) \prod_{n=1}^{e} p(k_n|k_{n-1}). \tag{22}$$

3.1.3. Resampling. With the increase of the variance of important weights, the important samples will degenerate, so it is necessary to resample to eliminate the small normalized full-time sample points. In MCL algorithm, the weight is either 1 or 0, so it is necessary to keep enough effective samples to ensure that the effective sampling scale is not less than the total number of samples for repeated sampling.

In the process of resampling, the sample points collected in each round are saved to the same set until the requirements are met. In this way, the computational complexity of resampling is reduced and the robustness is avoided. In the sampling process, in order to reduce the computational difficulty, we divide the weight of the MCL into 1 or 0, compare the weight of the sample with it, classify the sample, and divide it into two sets.

3.2. Establishment of Regional Economic Data Mining Model

3.2.1. Application of C-Means Clustering Method in Regional Economy. The *C*-means clustering method is based on the minimum Euclidean distance, and its specific calculation process has been described in detail in Section 2, and will not be repeated here. *C*-means clustering method has the advantages of less calculation, stronger robustness, and faster processing speed, which is suitable for clustering analysis of economic samples.

3.2.2. Selection of Samples and Indicators. The principles of comprehensiveness, objectivity, periodicity, and independence should be followed in the selection of indicators. The cluster index of regional economy must be able to reflect the comprehensive content of sustainable development of regional economy, so it should include not only economic indicators but also social, natural, educational, and technological indicators. Sample independence means that the samples are independent of each other, and there is no pairing relationship. Both samples are required to be from a normal distribution, and the mean is required to be a descriptive statistic that is meaningful for testing, such as the comparison of the wages of boys and girls. Objectivity means that the selection conditions of these samples are fixed and cannot be regarded as transfer; periodicity means that the indicators have certain rules; the comprehensive principle means that the basic information reflected by the samples is more comprehensive.

In the economic indicators, we need to consider the per capita income and consumption, the proportion of the secondary and tertiary industries, and the proportion of fiscal revenue. In the social indicators, we need to consider the average consumption of urban and rural households, population growth, aging, and social infrastructure construction. The natural indicators include pollution emissions and treatment costs, the consumption of various types of energy, and the storage of various resources. The indicators of educational science and technology include educational funds, the number of students and teachers, scientific research funds, and the number of patent applications.

In addition, because the data in the indicators change greatly, the variables with small absolute values may not show their role, and the clustering effect will also be affected. In order to avoid this kind of situation as much as possible, each data is dimensionless, and the processing method is shown in formula (11).

3.2.3. Modeling. Based on the mobile sensor network positioning technology, this paper models the factors under the four indicators of a region from 2015 to 2019 and analyzes the impact of economy, society, nature, education, and science and technology on the regional economic development. There are two types of hierarchy-based clustering methods: (1) aggregate hierarchical clustering. Initially, each object is a cluster, and then, these atomic clusters are merged according to their similarity to each other. Most hierarchical methods fall into this category, the main difference between them being the different definitions of similarity between clusters; (2) divided hierarchical clustering, which is the opposite of the above process. The processing flow of the data mining model is as follows.

As shown in Figure 1, input all the data of each attribute index, preprocess it, and then, put it into storage. The *C*-means clustering method and association analysis are used for data mining, and the mining results are visualized and compared.

4. Discussion on Data Mining Results of Regional Economic Analysis

4.1. Cluster Analysis Results of Economic Indicators. The data of per capita income and consumption, the proportion of the secondary and tertiary industries, and the proportion of fiscal revenue in the region from 2015 to 2019 are input into

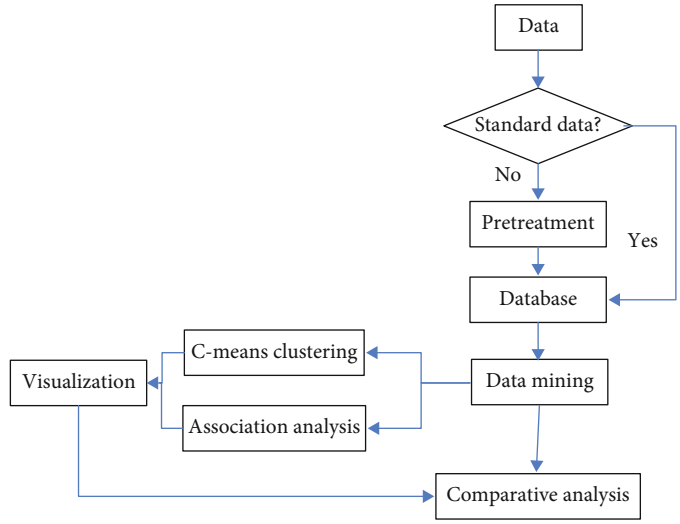

Figure 1: Processing flow chart of the data mining model.

Table 1: Economic index data.

Index	2015	2016	2017	2018	2019
Per capita income (yuan)	15936	18225	21740	23819	25084
Per capita consumption (yuan)	6798	8976	10035	11652	13447
Proportion of secondary industry (%)	42.3	47.1	50.8	53.6	55.3
Proportion of tertiary industry (%)	26.2	28.9	32.4	35.9	38.6
Proportion of fiscal revenue (%)	13.8	14.3	15.4	15.8	16.1

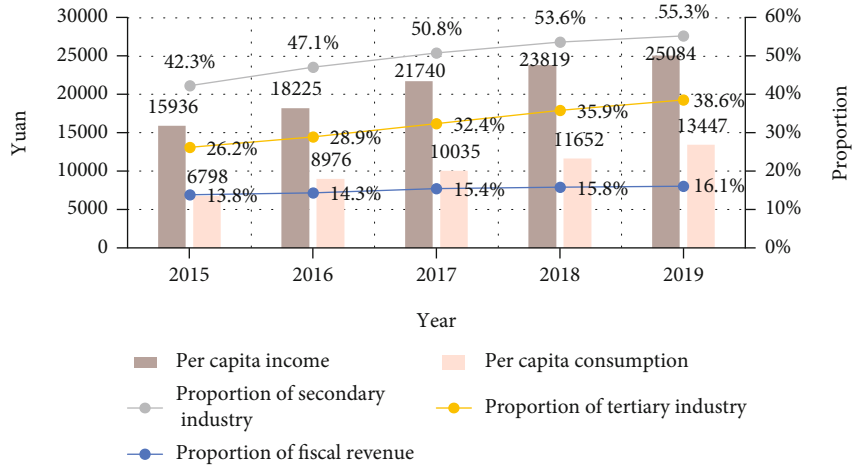

Figure 2: Changes in economic indicators.

the data mining model based on mobile sensor network positioning technology, and cluster analysis is carried out.

As shown in Table 1, the per capita income and consumption, the proportion of the secondary and tertiary industries, and the proportion of fiscal revenue in the region from 2015 to 2019 are increasing year by year.

As shown in Figure 2, the per capita consumption level in the region has increased by 97.81% and the per capita income level has increased by 57.4%. The proportion of the secondary industry increased by 30.73%, that of the tertiary industry increased by 47.33%, and the proportion of fiscal

Table 2: Calculation results of principal components of economic indicators.

Principal component	Characteristic value	Variance contribution rate (%)	Cumulative variance contribution rate (%)
1	6.387	63.872	63.872
2	2.883	28.829	92.701
3	0.539	5.394	98.095
4	0.186	1.859	99.954
5	0.005	0.046	100.000

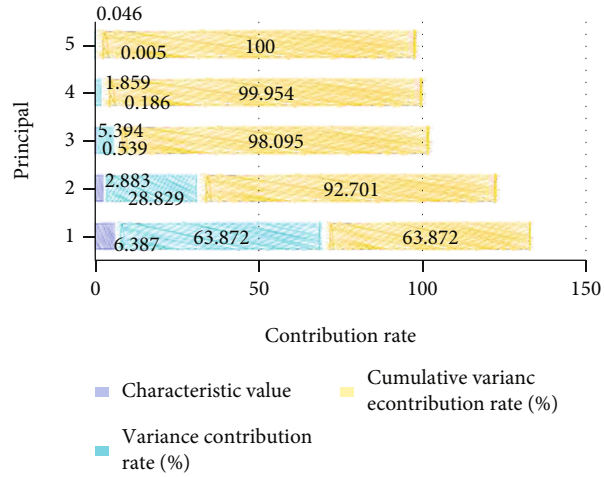

Figure 3: Contribution rate of principal component variance of economic indicators.

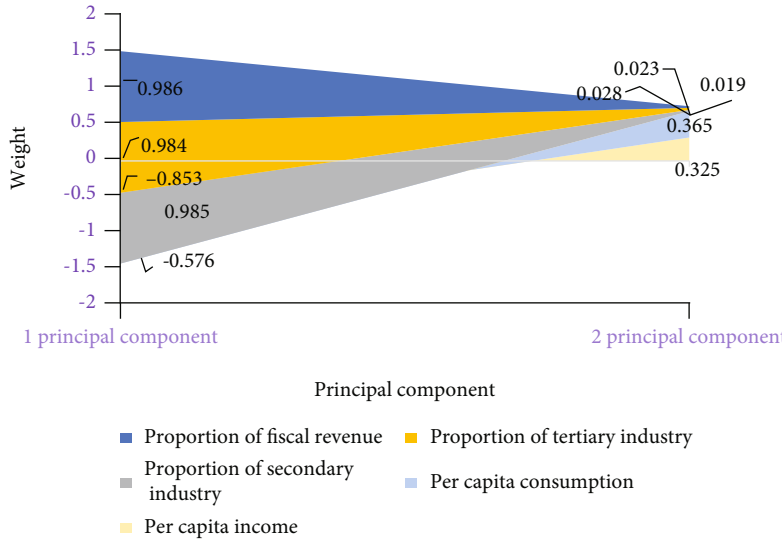

Figure 4: Weight values of main components of economic indicators.

revenue increased by 16.67%. This shows that the regional economy presents a stable and sustained growth trend.

The principal component analysis model is used to analyze the data, and the eigenvalues, variance contribution rate, and cumulative variance contribution rate of the indicators such as per capita income and consumption, the proportion of the secondary and tertiary industries, and the proportion of fiscal revenue are calculated.

As shown in Table 2, the eigenvalue of the first principal component is 6.387, and its variance contribution rate is 63.872%. The eigenvalue of the second principal component is 2.883, and its variance contribution rate is 28.829%. The eigenvalue of the third component is 0.539, and its variance contribution is 5.394; the eigenvalue of the fourth component is 0.186, and its variance contribution is 1.859; the eigenvalue of the fifth component is 0.005, and its variance contribution is 0.046.

As shown in Figure 3, the cumulative variance contribution rate of the first two principal components reaches 92.701%, which indicates that only the numerical changes of the first two principal components need to be analyzed.

As shown in Figure 4, the index with the highest weight in the first principal component is the proportion of fiscal revenue, which is 0.986. The second is the proportion of the secondary industry and the tertiary industry. In the second principal component, the index of per capita consumption with the highest weight is 0.365. This shows that the financial revenue and the proportion of the secondary and tertiary industries play a greater role in the economic indicators affecting the regional economic development.

4.2. Results of Cluster Analysis of Social Indicators. The data of average consumption of urban and rural households, social infrastructure construction projects, population growth, and aging population proportion in the region from 2015 to 2019 are input into the data mining model based on mobile sensor network positioning technology, which is created in this paper, for clustering analysis.

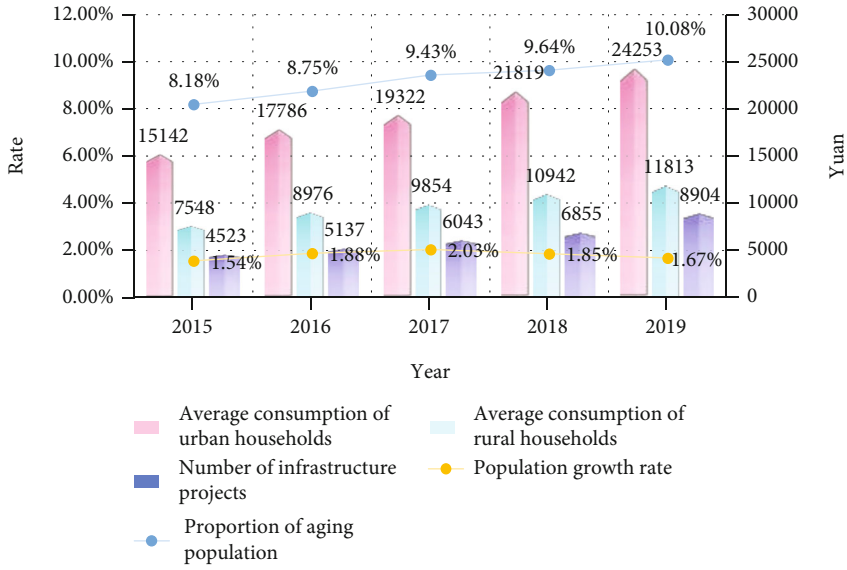

Figure 5: Changes in social indicators.

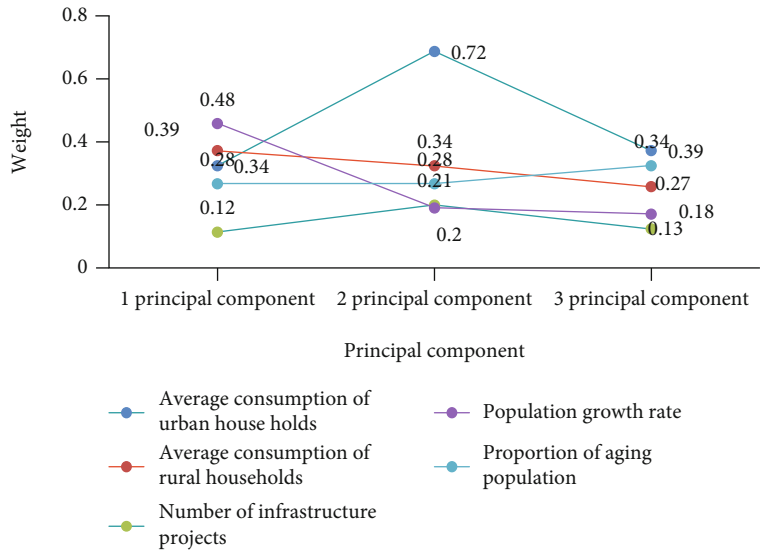

Figure 6: The weight value of main components of social indicators.

As shown in Figure 5, the average consumption of urban and rural households and the number of social infrastructure construction projects in the region are increasing year by year, with a cumulative growth of 60.17%, 56.51%, and 96.86%, respectively, in the five years. The population growth rate showed a trend of first growth and then decline, with a cumulative growth rate of 8.44% over the past five years. The proportion of the aging population shows a trend of increasing year by year, with a cumulative increase of 23.23% in the past five years.

According to the clustering results of social indicators, the weights of social indicators are calculated.

As shown in Figure 6, the population growth rate with the highest weight is 0.48 in the first principal component, 0.72 in the second principal component, and 0.39 in the third principal component. This shows that the population

Table 3: Calculation results of principal components of natural indexes.

Principal component	Characteristic value	Variance contribution rate (%)	Cumulative variance contribution rate (%)
1	3.547	35.472	35.472
2	2.381	23.809	59.281
3	1.796	17.963	77.224
4	1.056	10.563	87.807
5	0.404	4.041	91.848
6	0.311	3.112	94.960
7	0.257	2.569	97.529
8	0.114	1.142	98.671
9	0.087	0.871	99.542
10	0.046	0.458	100.000

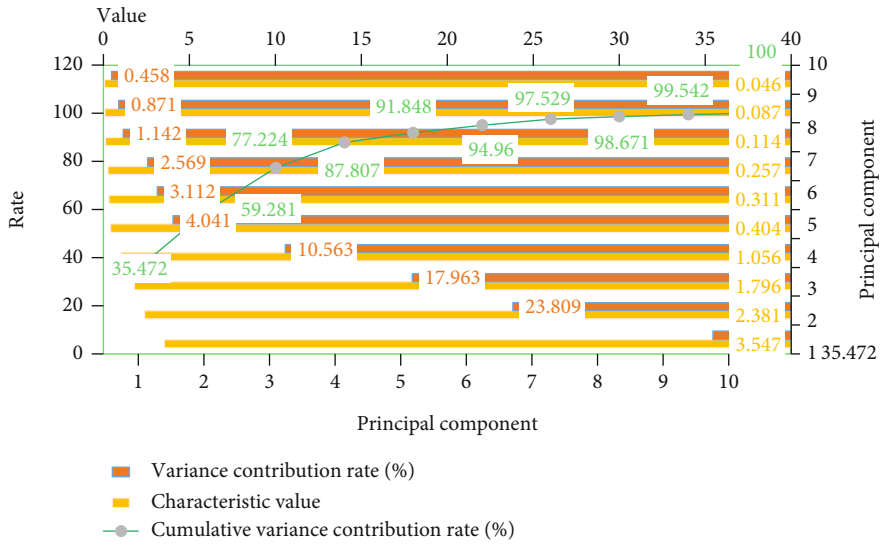

Figure 7: Contribution rate of principal component variance of natural indicators.

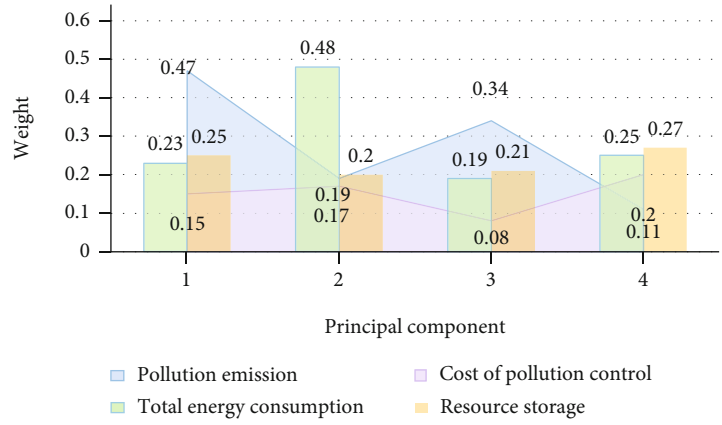

Figure 8: Weight values of main components of natural indexes.

growth rate and the average consumption of urban households play a greater role in the social indicators affecting the regional economic development.

4.3. Results of Natural Index Cluster Analysis. The data of pollution emissions and treatment costs, energy consumption, and resource storage in the region from 2015 to 2019 are input into the data mining model based on mobile sensor network positioning technology, and cluster analysis is conducted. Because there are many subindexes in natural indexes, it is necessary to reduce the dimension. The principal component analysis model is used to analyze the data and calculate the eigenvalue, variance contribution rate, and cumulative variance contribution rate.

As shown in Table 3, the eigenvalue of the first principal component is 3.547, and its variance contribution rate is 35.472%. The eigenvalue of the second principal component is 2.381, and its variance contribution rate is 23.809%. The eigenvalue of the third principal component is 1.796, and its variance contribution rate is 17.963%. The eigenvalue of the fourth principal component was 1.056, and its variance contribution rate was 10.563%.

Table 4: Calculation results of principal components of educational science and technology indicators.

Principal component	Characteristic value	Variance contribution rate (%)	Cumulative variance contribution rate (%)
1	5.045	50.453	50.453
2	2.089	20.891	71.344
3	1.800	18.003	89.347
4	0.692	6.924	96.271
5	0.373	3.729	100.000

As shown in Figure 7, the cumulative variance contribution rate of the first four principal components reaches 87.807%, which indicates that only the numerical changes of the first four principal components need to be analyzed.

As shown in Figure 8, the pollution emission with the highest weight in the first principal component is 0.47; the highest weight in the second principal component is the

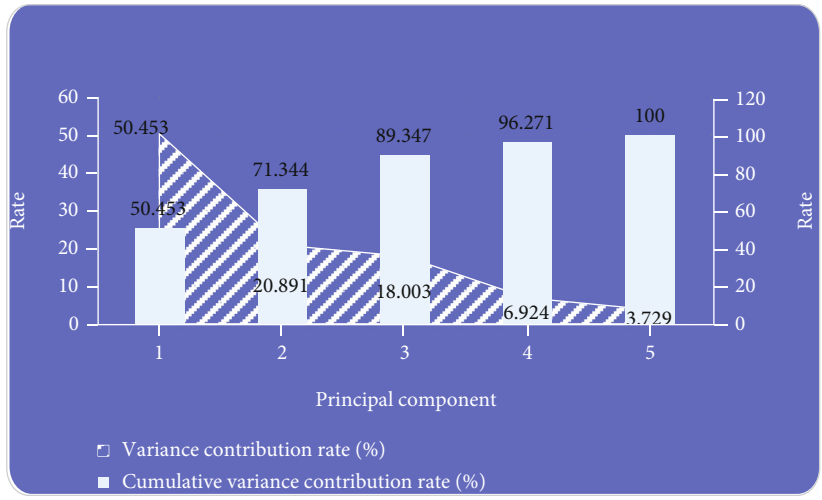

Figure 9: Contribution rate of principal component variance of educational science and technology indicators.

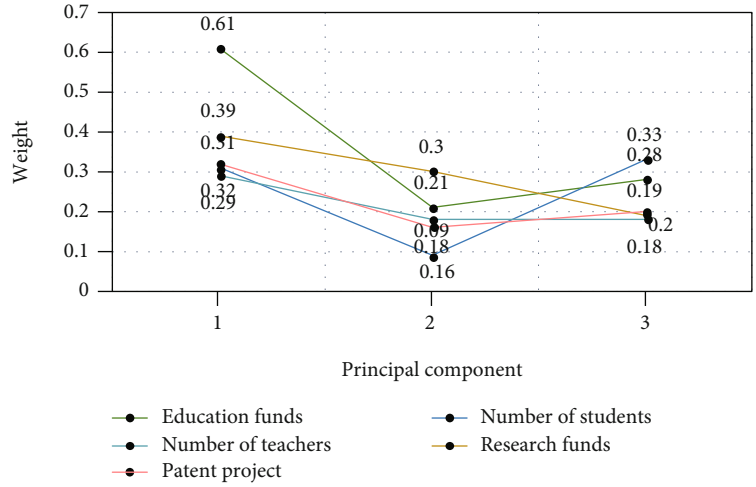

Figure 10: Main component weight values of educational science and technology indicators.

total energy consumption, which is 0.48; and the pollution emission with the highest weight in the third principal component is 0.34. In the fourth principal component, the highest weight is energy storage, which is 0.27. This shows that the two factors of pollution emission and total energy consumption play an important role in the natural indicators of regional economic development.

4.4. Cluster Analysis Results of Educational Science and Technology Indicators. The data of education funds, the number of students and teachers, scientific research funds, and patent applications in this region from 2015 to 2019 are input into the data mining model based on mobile sensor network positioning technology, and cluster analysis is conducted.

As shown in Table 4, the eigenvalue of the first principal component is 5.045, and its variance contribution rate is 50.453%. The eigenvalue of the second principal component was 2.089, and its variance contribution rate was 20.891%. The eigenvalue of the third principal component is 1.8, and its variance contribution rate is 18.003%.

As shown in Figure 9, the cumulative variance contribution rate of the first three principal components reaches 89.347%, which indicates that only the numerical changes of the first three principal components need to be analyzed.

As shown in Figure 10, in the first principal component, the highest weight is education funding, which is 0.61; in the second principal component, the highest weight is scientific research funding, which is 0.3; in the third principal component, the number of students is the highest, which is 0.33. This shows that the education funds, scientific research funds, and the number of students play an important role in the development of the regional economy.

5. Conclusions

The *C*-means clustering method has the advantages of less calculation, stronger robustness, and faster processing speed, which is suitable for clustering analysis of economic samples. Therefore, this paper combines the mobile sensor network localization technology based on sequential Monte Carlo

and *C*-means clustering method to establish the data mining model. Following the principles of comprehensiveness, objectivity, periodicity, and independence, the indicators of economy, society, nature, and education science and technology which can reflect the comprehensive content of regional economic sustainable development are selected.

Through cluster analysis and principal component analysis of the relevant index data of a certain region, we find that among many factors, financial income, average consumption level of urban households, pollution emissions, total energy consumption, and education funds are particularly important. This paper accomplishes the following: (1) a comprehensive analysis of the regional economy based on emerging mobile sensor network technology and data mining techniques; (2) production function analysis is used to measure economies of scale and agglomeration economies. The relationship between total output and the agglomeration index of factor inputs is derived as an effective measure of agglomeration economy to measure the state of unity of industry distribution sectors.

Due to the limited time and knowledge, there are still some deficiencies in this study. In the selection of sample data, only the data of nearly five years are used, but the growth of some development indicators shows a long periodicity, and the data of five years may be difficult to reflect its change law. The *C*-means clustering method is suitable for the analysis of economic samples, but its own shortcomings are ignored in this study. Therefore, in the future research work, we need to increase the selection range of sample data and improve the *C*-means clustering method to make its performance better.

Data Availability

No data were used to support this study.

Conflicts of Interest

There are no potential competing interests in this paper.

Authors' Contributions

The author has seen the manuscript and approved its submission.

Acknowledgments

This work was supported by the 2020 Guangdong Province Ordinary University Characteristic Innovation Project "Research on the Path of Guangdong Foreign Trade Enterprises' Response to the Epidemic from the Perspective of Digital Economy" (Project No. 2020WTSCX114); the 2020 Guangdong Provincial Science and Technology Projects "Guangdong Province Cold Chain Standardization," the Joint Co-construction of Engineering Technology Research Center" (Project No. 2020440121000082); and the 2020 Disciplinary Co-construction Project of the "13th Five-Year Plan" of Philosophy and Social Sciences of Guangdong Province in 2020 "Research on the Digital High-quality Development Path of Guangdong Foreign Trade Enterprises Under the Visual Threshold of Post-epidemic "(Project No. GD20XYJ23) funding.

References

[1] G. Dartmann, H. B. Song, and A. Schmeink, *Big Data Analytics for Cyber-Physical Systems: Machine Learning for the Internet of Things*, Elsevier, 2019.

[2] Q. Lu, Q. L. Han, B. Zhang, D. Liu, and S. Liu, "Cooperative control of mobile sensor networks for environmental monitoring: an event-triggered finite-time control scheme," *IEEE Transactions on Systems, Man, and Cybernetics Part B, Cybernetics*, vol. 47, no. 12, pp. 4134–4147, 2017.

[3] V. Chaurasia and S. Pal, "A novel approach for breast cancer detection using data mining techniques," *Social ence Electronic Publishing*, vol. 3297, no. 1, pp. 2320–9801, 2017.

[4] L. Zhu, Z. Yu, and H. Zhan, "Impact of industrial agglomeration on regional economy in a simulated intelligent environment based on machine learning," *Access*, vol. PP (99), pp. 1–1, 2020.

[5] Z. Min and Q. Rui, "Data mining and economic forecasting in DW-based economical decision support system," *International journal of reasoning-based intelligent systems*, vol. 11, no. 4, pp. 300–307, 2019.

[6] M. Arends-Kuenning, K. Baylis, and R. Garduno-Rivera, "The effect of NAFTA on internal migration in Mexico: a regional economic analysis," *Applied Economics*, vol. 51, no. 10, pp. 1052–1068, 2019.

[7] S. K. Singh and P. Kumar, "A load balancing virtual level routing (LBVLR) using mobile mule for large sensor networks," *Journal of Supercomputing*, vol. 75, no. 11, pp. 7426–7459, 2019.

[8] I. Butun, P. Österberg, and H. Song, "Security of the Internet of Things: vulnerabilities, attacks, and countermeasures," *IEEE Communications Surveys & Tutorials*, vol. 22, no. 1, pp. 616–644, 2020.

[9] S. Wan, "Topology hiding routing based on learning with errors," *Concurrency and Computation: Practice and Experience*, no. 6, p. e5740, 2020.

[10] N. Ganganath, C. T. Cheng, and C. K. Tse, "Distributed anti-flocking algorithms for dynamic coverage of mobile sensor networks," *IEEE Transactions on Industrial Informatics*, vol. 12, no. 5, pp. 1795–1805, 2016.

[11] S. Sharma, D. Puthal, S. K. Jena, A. Y. Zomaya, and R. Ranjan, "Rendezvous based routing protocol for wireless sensor networks with mobile sink," *The Journal of Supercomputing*, vol. 73, no. 3, pp. 1168–1188, 2017.

[12] S. Sun, M. Kadoch, L. Gong, and B. Rong, "Integrating network function virtualization with SDR and SDN for 4G/5G networks," *IEEE Network*, vol. 29, no. 3, pp. 54–59, 2015.

[13] S. H. Semnani and O. A. Basir, "Multi-target engagement in complex mobile surveillance sensor networks," *Unmanned Systems*, vol. 5, no. 1, pp. 31–43, 2017.

[14] G. Yogarajan Revathi et al., "Nature inspired discrete firefly algorithm for optimal mobile data gathering in wireless sensor networks," *Wireless Networks*, vol. 24, no. 8, pp. 2993–3007, 2018.

[15] K. Karunanithy and B. Velusamy, "CSDGP: cluster switched data gathering protocol for mobile wireless sensor networks," *IET Communications*, vol. 13, no. 18, pp. 2973–2985, 2019.

[16] D. Chen, Q. Lu, D. Peng, K. Yin, C. Zhong, and T. Shi, "Receding horizon control of mobile robots for locating unknown wireless sensor networks," *Assembly Automation*, vol. 39, no. 3, pp. 445–459, 2019.

[17] S. M. H. Tabatabaie, H. Tahami, and G. S. Murthy, "A regional life cycle assessment and economic analysis of camelina biodiesel production in the Pacific Northwestern US," *Journal of Cleaner Production*, vol. 172, part 3, pp. 2389–2400, 2018.

[18] H. T. Van and D. Ushakov, "Analysis of economic imbalances under the conditions of regional agrarian markets' integration," *E3S Web of Conferences*, vol. 175, no. 1, pp. 13034–13034, 2020.

[19] Y. Xiong, H. Wang, and X. Gao, "Evaluation of regional economic efficiency in Hubei province based on cross data envelopment analysis algorithm," *Journal of Interdisciplinary Mathematics*, vol. 20, no. 8, pp. 1715–1729, 2017.

[20] H. Kasseeah, "Investigating the impact of entrepreneurship on economic development: a regional analysis," *Journal of Small Business and Enterprise Development*, vol. 23, no. 3, pp. 896–916, 2016.

[21] T. P. Sari and F. Rahmawati, "The analysis of excellent economic sector in regional economic building in Kediri City 2012–2015," *KnE Social Sciences*, vol. 3, no. 3, pp. 91–91, 2018.

[22] B. Crane, C. Albrecht, M. K. Duffin, and C. Albrecht, "China's special economic zones: an analysis of policy to reduce regional disparities," *Regional Studies, Regional Science*, vol. 5, no. 1, pp. 98–107, 2018.

[23] I. Kavakiotis, O. Tsave, A. Salifoglou, N. Maglaveras, I. Vlahavas, and I. Chouvarda, "Machine learning and data mining methods in diabetes research," *Biotechnology Journal*, vol. 15, no. C, pp. 104–116, 2017.

[24] S. B. Tsai, Y. C. Lee, and J. J. Guo, "Using modified grey forecasting models to forecast the growth trends of green materials," *Proceedings of the Institution of Mechanical Engineers, Part B: Journal of Engineering Manufacture*, vol. 228, no. 6, pp. 931–940, 2014.

[25] A. Buczak and E. Guven, "A survey of data mining and machine learning methods for cyber security intrusion detection," *IEEE Communications Surveys & Tutorials*, vol. 18, no. 2, pp. 1153–1176, 2016.

[26] C. Helma, T. Cramer, S. Kramer, and L. De Raedt, "Data mining and machine learning techniques for the identification of mutagenicity inducing substructures and structure activity relationships of noncongeneric compounds," *Journal of Chemical Information and Computer Sciences*, vol. 35, no. 4, pp. 1402–1411, 2004.

[27] X. Zhao and J. Tang, "Crime in urban areas:," *Acm Sigkdd Explorations Newsletter*, vol. 20, no. 1, pp. 1–12, 2018.

[28] J. H. Kao, T. C. Chan, F. Lai et al., "Spatial analysis and data mining techniques for identifying risk factors of out-of-hospital cardiac arrest," *International Journal of Information Management*, vol. 37, no. 1, pp. 1528–1538, 2017.

[29] A. Hazra, S. K. Mandal, A. Gupta, A. Mukherjee, and A. Mukherjee, "Heart disease diagnosis and prediction using machine learning and data mining techniques: a review," *Advances in Computational Ences and Technology*, vol. 10, no. 7, pp. 2137–2159, 2017.

Hindawi
Journal of Sensors
Volume 2022, Article ID 5160050, 10 pages
https://doi.org/10.1155/2022/5160050

Research Article

Random Forest Feature Selection and Back Propagation Neural Network to Detect Fire Using Video

Jin-Xing Liang,[1,2,3] **Jian-Fu Zhao**,[1,2,3] **Ning Sun**,[4] **and Bao-Jun Shi**[1,2,3]

[1]*State Key Laboratory of Reliability and Intelligence of Electrical Equipment, Hebei University of Technology, Tianjin 300401, China*
[2]*Hebei Key Laboratory of Robot Sensing and Human-Robot Integration, Tianjin 300401, China*
[3]*School of Mechanical Engineering, Hebei University of Technology, Tianjin 300401, China*
[4]*School CITIC Heavy Industry Kaicheng Intelligent Equipment Co., Ltd., Tangshan 063000, China*

Correspondence should be addressed to Bao-Jun Shi; 2018029@hebut.edu.cn

Received 19 July 2021; Revised 11 October 2021; Accepted 8 December 2021; Published 5 January 2022

Academic Editor: Mu Zhou

As the most common serious disaster, fire may cause a lot of damages. Early detection and treatment of fires are of great significance to ensure public safety and to reduce losses caused by fires. However, traditional fire detectors are facing some focus issues such as low sensitivity and limited detection scenes. To overcome these problems, a video fire detection hybrid method based on random forest (RF) feature selection and back propagation (BP) neural network is proposed. The improved flame color model in RGB and HSI space and the visual background extractor (ViBe) in moving target detection algorithm are used to segment the suspected flame regions. Then, multidimensional features of flames are extracted from the suspected regions, and these extracted features are combined and selected according to the RF feature importance analysis. Finally, a BP neural network model is constructed for multifeature fusion and fire recognition. The test results on several experimental video sets show that the proposed method can effectively avoid feature interference and has an excellent recognition effect on fires in a variety of scenarios. The proposed method is applicable for fire recognition applied in video surveillance and detection robots.

1. Introduction

With the continuous improvement of social development, the possibility of fires with large losses is also increasing. The traditional fire recognition methods mainly use detectors to sample the temperature, spectrum, and smoke of a specific region to determine whether a fire has occurred [1]. However, due to the limitation of the detection range and sensitivity of the detector, it is difficult to achieve timely detection in open spaces and harsh environments.

In recent years, fire recognition based on image processing technology has become the focus of researchers' attention. By analyzing the static and dynamic features of flame, researchers can distinguish flames from other objects. The static features of flame mainly include color and texture features. Chen et al. [2] proposed a flame recognition rule in RGB and HSI color space by analyzing the chromaticity and disorder of flames. Celik and Demirel [3] proposed a flame classification model based on YCbCr color space, and this flame model can better adapt to lighting changes compared with the RGB color model. Wang and Ren [4] improved the image brightness by performing histogram equalization on the V channel in HSV color space and then combined the flame pixel distribution rules in RGB and YCbCr color space to perform image segmentation. Prema et al. [5] extracted texture features based on wavelet decomposition and then used an extreme learning classifier to classify images. Their method can effectively eliminate red interference. Sheng et al. [6] studied the color, texture, and gray-scale statistical features of flame images and constructed a deep belief network (DBN) for fire detection. Jamali et al. [7] introduced texture features based on color features to detect fires. They combined different features to improve the accuracy of the fire detection system.

The dynamic features of flame mainly include motion features and geometric change features. Barnich and Van Droogenbroeck [8] proposed a visual background extractor (ViBe) algorithm, which provides a new idea for extracting

flame motion features. To improve the overall performance of a fire detection system, Foggia et al. [9] attempted to combine the information of color, motion, and shape change to reduce the false alarm rate of the system. Gong et al. [10] proposed a flame centroid stabilization algorithm. They used color and motion features to segment suspected flame regions and further judged whether it is a flame by analyzing the changes of its area, shape, and center of mass.

The fire recognition model mainly includes machine learning classifiers and deep learning networks. Yang et al. [11] analyzed the shape features of flames and used support vector machine (SVM) to recognize fire images. Huang and Du [12] proposed a fire recognition method combining rough set (RS) theory and SVM. Their method can reduce overfitting and improve the accuracy of fire prediction. Qu et al. [13] extracted the red and blue color components and brightness component of flames in YCbCr color space and used the back propagation (BP) neural network model to detect fires. Li and Zhao [14] performed fire detection based on convolutional neural network (CNN) such as Faster-RCNN, R-FCN, SSD, and YOLO v3. Sheng et al. [15] improved the detection capabilities of flames and smokes by combining simple linear iterative clustering (SLIC), density-based spatial clustering of application with noise (DBSCAN), and CNN. Muhammad et al. [16] proposed a CNN framework for fire detection. The framework can be applied to video surveillance systems.

The above researches have enriched and developed fire recognition methods, but there are still some important problems. Firstly, region segmentation based on color features will inevitably overlap with the color space of other objects, which may result in inaccurate segmentation of suspected flame regions. Secondly, the extracted flame features are not comprehensive or have little correlation to the classification and recognition model, which makes it difficult to achieve accurate fire recognition in complex scenes. Thirdly, deep learning methods require high equipment performance, and the related model training and testing are complex.

In view of the shortcomings of the current fire recognition methods, the flame color model and the ViBe algorithm are combined to segment suspected flame regions in this paper. Then, multidimensional features are extracted on the suspected flame regions, and the random forest (RF) method is used to analyze the importance of each feature, and then, these features are combined and selected accordingly. Finally, a BP neural network model is built for fire detection. The proposed fire detection method is verified by using several experimental video sets.

This paper is organized as follows: Section 2 describes a hybrid approach adopted in this study. Section 3 presents experiments and experimental results with discussions. Section 4 concludes this paper.

2. Hybrid Method

2.1. Region Segmentation Based on Color Model and ViBe Algorithm. Region segmentation is a process to divide an image (being processed) into multiple regions with different characteristics and then to separate the target region from its background. The flame presents a special color distribution pattern and has the dynamic characteristics of spreading and diffusion. Therefore, the suspected flame region in an image can be segmented by using the color model and moving target detection method.

2.1.1. Color Model for Segmentation. In order to describe the color distribution of flame pixels, a statistical flame color model can be established. Yan et al. [17] established a color model of flames in RGB and HSI color space. The color model overcomes the cavity inside flames to a great extent, but there is still undersegmentation of the interference with high saturation. In the study of flame image saturation, Horng et al. [18] proposed an HSI color model of flames, which restricted the saturation component. Combining the characteristics of flames in RGB and HSI color space, we adopt the flame color segmentation rules as shown in

$$\begin{cases} R \geq B, G \geq B, \\ R \geq R_0, \\ S \geq S_0, \\ R \geq R_1, G \geq G_1 \text{ or } T_1 \geq Th_1, T_2 \geq Th_2, \\ T_2 + T_3 \geq Th_3, \end{cases} \tag{1}$$

where $T_1 = |R - G|$, $T_2 = |G - B|$, and $T_3 = |R - B|$. R, B, and G are the red, blue, and green color components of an image, respectively. R_0 is the threshold of the red component of an image. S_0 is the threshold of the saturation of an image. For a darker environment, $S_0 = 20$, and a brighter environment, $S_0 = 40$. R_1 and G_1 are the improved thresholds of the red and green components of an image, respectively. Th_1, Th_2, and Th_3 are the thresholds of T_1, T_2, and $T_2 + T_3$, respectively.

We use the improved color model, equation (1), to separate the region in the image that meets the constraints of the color model from the background. The images collected by Chino et al. [19] were used to test the segmentation effect. Figure 1 shows a segmentation example of a flame image using different flame color models.

From Figure 1, it can be found that compared with the method in [17], the improved color model can effectively eliminate the brown-yellow wood and the illuminated ground and achieve the accurate segmentation of the flame regions.

2.1.2. ViBe Moving Target Segmentation. It is difficult to exclude objects whose colors are highly similar to flames only by using the color model, so it is necessary to segment moving objects based on the dynamic features of flames in a video. In the process of fire recognition, the interframe difference method [20], optical flow method [21], or background subtraction method [22] are commonly used to segment moving targets. The interframe difference method has low computational complexity, but it depends too much on the moving speed of the target. The optical flow method is computationally complex and sensitive to light. The

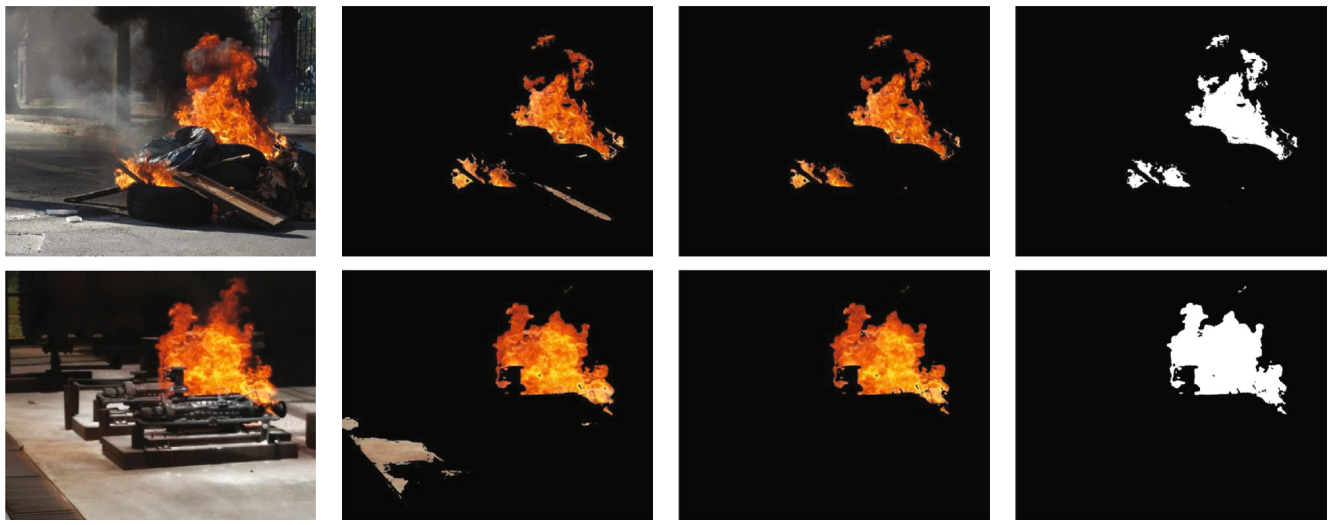

(a) (b) (c) (d)

Figure 1: Segmentation example using different flame color models: (a) original flame image; (b) segmented image with the color model in [17]; (c) segmented image with the improved color model; (d) binarized image.

background subtraction method is simple, and the extracted target is complete. The background subtraction method includes Gaussian mixture modeling (GMM) [23] and ViBe modeling methods [24] to establish the background statistical model. Compared with the GMM method, the ViBe algorithm randomly selects neighborhood pixel values to model or update the background according to the similarity between the neighboring pixels and does not need a lot of estimation or operation, so its time complexity to build a background model is lower. The followings are the calculation process of the ViBe algorithm:

(1) Background model initialization. The background model initialization is the process to fill pixel sample set for building a background model. For each pixel in an image, use $v_i(x, y)$ to represent its pixel value. Taking a certain point (x, y) as the center, N samples are randomly selected within a certain radius to build a sample set of the background model. The sample set $v(x, y)$ can be defined as follows:

$$v(x, y) = \{v_1(x, y), v_2(x, y), \cdots, v_N(x, y)\} \quad (2)$$

(2) Moving target detection. For the point (x, y) in an image to be tested, its pixel value $m(x, y)$ is compared with each sample value in the background model. If the absolute value of the difference with a certain sample point is greater than a given threshold K_0, the sample point is considered not similar to the point to be detected. If there are more than the given number K_1 of sample points that are not similar to the point to be detected, the point is considered to be the foreground (moving target). Otherwise, the detected point is the background, as shown in

$$D_n(x, y) = \begin{cases} 1, & |m(x, y) - v_n(x, y)| > K_0, \\ 0, & \text{others}, \end{cases} \quad (3)$$

$$f(x, y) = \begin{cases} 1, & \sum_{n=1}^{N} D_n(x, y) > K_1, \\ 0, & \text{others}, \end{cases} \quad (4)$$

where $D_n(x, y)$ represents the distance between the point to be detected and the n^{th} sample point. $f(x, y)$ represents the judgment result of background or foreground

(3) Background model update. The ViBe algorithm uses a random updating strategy to update the background model from time to time. After a certain period of time t, the probability $P(t, t + dt)$ that a certain sample in the sample set is still retained can be defined as follows:

$$P(t, t + dt) = \left(\frac{N - 1}{N}\right)^{(t+dt)-t} \quad (5)$$

The accuracy of region segmentation will affect feature extraction. The more accurate region segmentation is, the more extracted flame features can reflect the actual situation of flames. In the proposed hybrid method of video fire detection, color and motion features are combined for region segmentation. Based on the color distribution of flames in RGB and HSI color space, the improved color model is adopted to obtain segmented images. Meanwhile, the ViBe algorithm is adopted to obtain segmented images based on motion feature. The improved color model segmentation images and ViBe algorithm segmentation images are intersected, and the final suspected flame regions are obtained after corrosion, expansion, and region filling. Figure 2 shows some

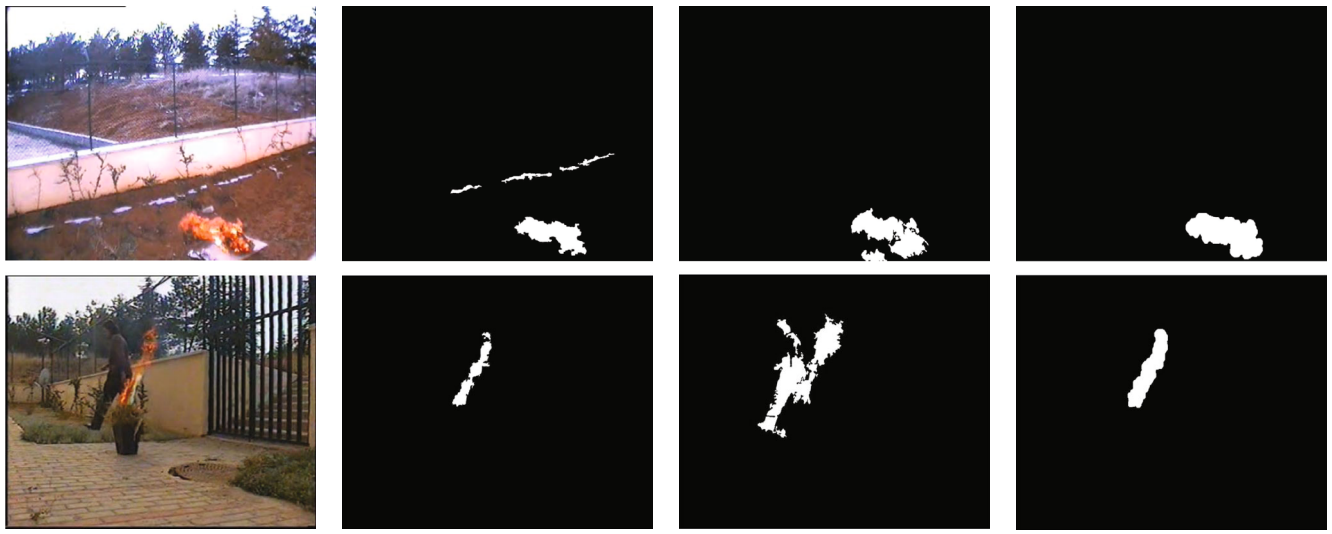

(a) (b) (c) (d)

Figure 2: Segmentation examples based on the flame color model and ViBe algorithm: (a) original flame images; (b) segmented images with the improved color model; (c) segmented images with the ViBe algorithm; (d) segmented images with the improved color model and ViBe algorithm.

segmentation examples based on the improved color model and ViBe algorithm. As shown in Figure 2, the region segmentation method combining the improved color model and ViBe algorithm can effectively exclude the land with color similar to flame and the moving pedestrians and get an accurate flame region.

2.2. Multidimensional Feature Extraction and RF Feature Selection. With the improvement of the ability of sensors to obtain information, multifeature fusion technology is widely used in the field of image recognition [25]. After region segmentation, there may still be regions that are mistakenly segmented as flames. Thus, it is necessary to extract multidimensional features such as geometry, texture, and dynamics of images and use multifeature fusion technology to achieve fire detection. However, some features are irrelevant or redundant to the recognition model, so it is necessary to select the feature subset with high discriminative ability from the multidimensional features.

2.2.1. Multidimensional Feature Extraction. The multidimensional features extracted from an image mainly include its circularity, aspect ratio, texture features, area change rate, flicker feature, and edge jitter feature. The followings are a brief introduction and related formulas for each of them:

(1) Circularity. Circularity reflects the degree to which the shape of the target region is close to a theoretical circle. The circularity C is calculated as

$$C = \frac{4\pi S}{L^2}, \tag{6}$$

where S represents the area of the flame region and L represents the perimeter of the flame region

(2) Aspect ratio. Aspect ratio reflects the stretching degree of a flame. The aspect ratio W is calculated as

$$W = \frac{E}{H}, \tag{7}$$

where E represents the width of the smallest rectangle in the flame region and H represents the length of the smallest rectangle in the flame region

(3) Texture features. In the description of the spatial relationship of image textures, the commonly used method is based on the statistical gray-level cooccurrence matrix (GLCM) [26], which is used to calculate the representative contrast, correlation, energy, and homogeneity of texture features. Specifically, the pixel offset is set to 1, and the texture feature statistics are calculated from the GLCM at four different angles of 0°, 45°, 90°, and 135°, and then, the average value of the four directions is taken as texture feature criterion for fire recognition.

The gray value of two points at a certain distance in an image is represented by (i, j). Suppose $P(i, j)$ is the probability of the gray value (i, j). The formula of its contrast f_1, correlation f_2, energy f_3, and homogeneity f_4 of the image is as follows:

$$f_1 = \sum_{i=1}^{K}\sum_{j=1}^{K}(i-j)^2 P(i,j),$$

$$f_2 = \frac{1}{\sigma_x \sigma_y}\sum_{i=1}^{K}\sum_{j=1}^{K}\left(ijP(i,j) - \mu_x \mu_y\right),$$

$$f_3 = \sum_{i=1}^{K}\sum_{j=1}^{K} P^2(i,j),$$

$$f_4 = \sum_{i=1}^{K}\sum_{j=1}^{K} \frac{P(i,j)}{1+(i-j)^2}, \tag{8}$$

where K represents the gray level of an image. μ_x and μ_y represent the mean value of $P(i,j)$ in row and column, respectively. σ_x and σ_y represent the standard deviation of $P(i,j)$ in row and column, respectively

(4) Area change rate. Area change rate represents the area change of a flame region. The area change rate ΔS is calculated as

$$\triangle S = \frac{|S_n - S_{n-1}|}{S_{n-1}}, \quad n \geq 2, \tag{9}$$

where S_n represents the area of the flame region in the current frame and S_{n-1} represents the area of the flame region in the previous frame

(5) Flicker feature. Flame flicker will cause the image pixels to change from nonflame to flame. In order to effectively reflect the flicker characteristics of a flame without increasing the complexity of the algorithm, the change amplitude of the flame foreground is used to characterize the flicker feature of the flame. The flicker feature ΔF is calculated as

$$\triangle F = \frac{|(S_n \cap S_{n-1}) \cup (S_{n-1} \cap S_n)|}{S_n}, \quad n \geq 2 \tag{10}$$

(6) Edge jitter feature. Edge jitter measures the degree of the edge change of an object in the process of deformation. The edge jitter feature ΔL is calculated as

$$\triangle L = \frac{|L_n - L_{n-1}|}{L_{n-1}}, \quad n \geq 2, \tag{11}$$

where L_n represents the perimeter of the flame region of the current frame and L_{n-1} represents the perimeter of the flame region of the previous frame

2.2.2. Random Forest Feature Selection. Random forest (RF) [27] is an integrated machine learning method that uses decision tree as the basic learner and makes decision through voting mechanism. For feature selection, the importance of a single feature variable is calculated by the RF method, and then finding the feature variables that are highly related to the dependent variable. Thus, we can select a small number of feature variables which can fully guarantee the accuracy of the prediction results.

The purpose of feature selection is to select the relevant feature subset from the existing feature set. After feature extraction on the suspected flame region, we can get a 9-dimensional feature vector [$\mathbf{C\,W\,f_1\,f_2\,f_3\,f_4\,\Delta S\,\Delta F\,\Delta L}$]. We use the RF method to select the features with a strong correlation with the actual results as the input of the BP neural network model.

Since there is no published standard dataset in the field of fire prevention and detection at present, we mainly use a series of typical databases proposed in [28–30] to build our video set. Our video set includes 30 fire videos and 10 interference videos. Fire videos mainly include different shapes of flames in indoor, highway, and forest scenes. Interference videos mainly include street lights, car lights, and red objects. The resolution of the videos is uniformly adjusted to 1280×720, and 20 consecutive frames of images are selected from each video to form a sample dataset. The sample dataset has a total of 800 images, some of which are shown in Figure 3.

In this paper, the suspected flame regions are segmented on the sample dataset and the multidimensional features of the flame are extracted. The RF feature importance is calculated based on the Scikit-learn tool in the Python machine learning library. Specifically, the number of decision trees in the RF is set to 100, and the maximum depth of the decision trees is set to unlimited. The minimum number of samples required to split an internal node is set to 2; the minimum number of samples required to be at a leaf node is set to 1. The measurement criterion of split quality is set to mean square error (MSE). The ranking of the feature importance is given in Figure 4. From Figure 4, it can be found that flicker feature has the highest ranking and edge jitter feature has the lowest ranking.

According to the ranking in Figure 4, the flame features are divided into combined features F1-F9, which, respectively, represent [$\mathbf{\Delta F}$], [$\mathbf{f_1\,\Delta F}$], [$\mathbf{C\,f_1\,\Delta F}$], [$\mathbf{C\,W\,f_1\,\Delta F}$], [$\mathbf{C\,W\,f_1\,f_3\,\Delta F}$], [$\mathbf{C\,W\,f_1\,f_3\,f_4\,\Delta F}$], [$\mathbf{C\,W\,f_1\,f_2\,f_3\,f_4\,\Delta F}$], [$\mathbf{C\,W\,f_1\,f_2\,f_3\,f_4\,\Delta S\,\Delta F}$], and [$\mathbf{C\,W\,f_1\,f_2\,f_3\,f_4\,\Delta S\,\Delta F\,\Delta L}$]. The BP neural network method is used for training and classification, and the correct classification results of each combination feature are given in Figure 5. The correct classification rate is the average of 10 prediction results.

According to the classification results of the combined features as shown in Figure 5, the correct classification rate of samples reaches a high level starting from the 5th combined feature, F5, and with the increase of features, the correct classification rate of samples tends to be stable. To avoid interference caused by excessive features and ensure the accuracy of classification results, the 5th combined feature, F5, is selected for fire recognition, which includes circularity, aspect ratio, contrast, energy, and flicker feature.

2.3. Construction of the BP Neural Network Model. The BP neural network [31] is also called error back propagation neural network. Because the weights of neurons in adjacent layers are interrelated, the network has a nonlinear mapping ability to solve complex problems. Considering the simplicity and practicability, a three-layer BP neural network with

Figure 3: Some images of the sample dataset.

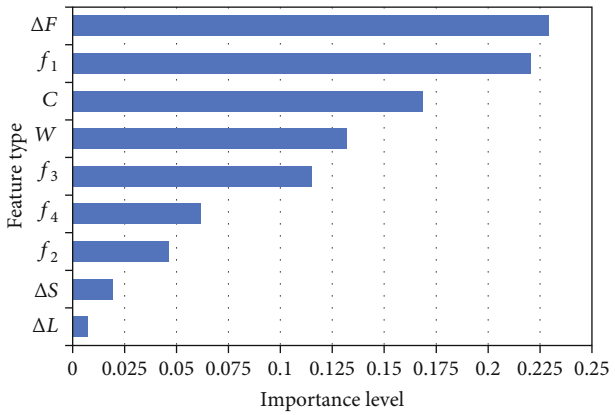

Figure 4: Feature importance ranking.

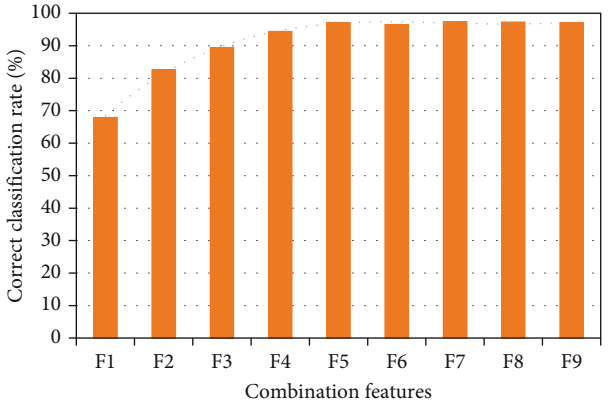

Figure 5: Combination feature classification results.

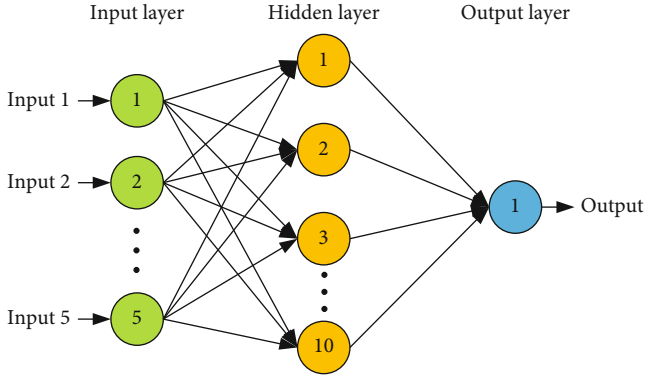

Figure 6: Structure diagram of the constructed BP neural network.

one input layer, one hidden layer, and one output layer is constructed for multifeature fusion and fire recognition.

The number of nodes in the input layer of the BP neural network depends on the dimension of the feature vector. In this paper, five features of each fire image are selected to form the feature vector $[\mathbf{C}\,\mathbf{W}\,\mathbf{f_1}\,\mathbf{f_3}\,\mathbf{\Delta F}]$, so there are 5 nodes in the input layer. The output layer outputs the recognition result, so there is 1 node. The normalized output value ranges from [0, 1], and when the output value belongs to [0, 0.5), it means nonflame. When the output value belongs to [0.5, 1], it is expressed as flame. The number of hidden layer nodes is calculated using empirical equation (12), in which, m and n represent the number of nodes in the input layer and output layer, respectively, and a is a constant between [1, 10]. Through repeated experiments, it is found that when the number of the hidden layer nodes h is 10, the neural network achieves the optimal training effect.

$$h = \sqrt{m+n} + a. \tag{12}$$

Based on above analysis, the structure of the BP neural network constructed in this paper is given in Figure 6. The BP neural network model will be used for fire recognition in the following section.

3. Experiments and Results Analysis

3.1. Experimental Environment. The experimental environment is Windows 10 operating system, 8 GB memory, Intel (R) core (TM) i5-10500 CPU @ 3.10 GHz, MATLAB 2018a platform.

3.2. Detection Process. The process of video fire detection in this paper is given in Figure 7.

3.3. Training and Experiments. The sample dataset of the training set and the test set is divided based on typical standards of 70% and 30%. The division is given in Table 1. Specifically, the maximum number of epochs is set to 2000. The Levenberg-Marquardt (LM) algorithm is selected as the learning algorithm, and the learning rate is set to 0.001. MSE is used as the loss function, and the minimum value of the loss function is set to 0.01. The neural network training performance is shown in Figure 8. From Figure 8, it can be found that the value of the loss function gradually decreases during the training process and reaches the minimum value of the set loss function at 30 epochs.

After neural network training is completed, the correct classification rate on the test sample set is 96.67%. In order to further verify the performance of the fire detection method, five videos that have not participated in the training are selected to test the trained neural network model, including three fire videos and two interference videos. The experimental video sets are shown in Figure 9. The descriptions of the experimental videos are shown in Table 2.

3.4. Results Analysis. The combined RF feature selection and BP neural network method (abbreviated as RF-BP) and the directly performed BP neural network method (abbreviated as Dir-BP) are used to do tests with several experimental videos. Furthermore, the two proposed methods are compared with the fire recognition method in [11, 13]. The accuracy, precision, recall, and F-score are used to evaluate the effect on fire recognition [32], as shown in

$$\text{Accuracy} = \frac{\text{TP} + \text{TN}}{\text{TP} + \text{TN} + \text{FP} + \text{FN}}, \tag{13}$$

$$\text{Precision} = \frac{\text{TP}}{\text{TP} + \text{FP}}, \tag{14}$$

$$\text{Recall} = \frac{\text{TP}}{\text{TP} + \text{FN}}, \tag{15}$$

$$F\text{-score} = 2 * \frac{\text{Precision} * \text{Recall}}{\text{Precision} + \text{Recall}}, \tag{16}$$

where TP represents the number of correctly classified frames of the fire videos. TN represents the number of correctly classified frames of the interference videos. FN represents the number of misclassified frames of the fire videos.

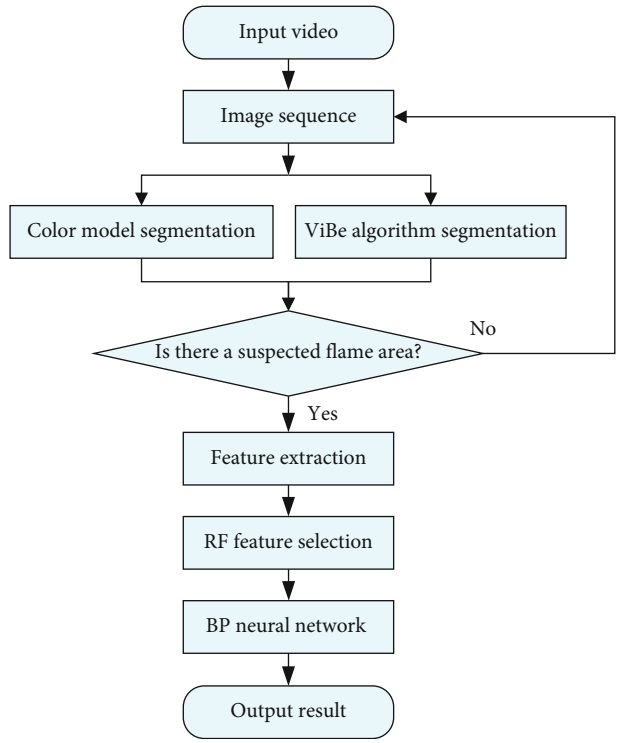

Figure 7: Video fire detection process.

Table 1: The division of sample dataset.

Class	Training samples	Test samples	Total
Flame images	420	180	600
Interfering images	140	60	200

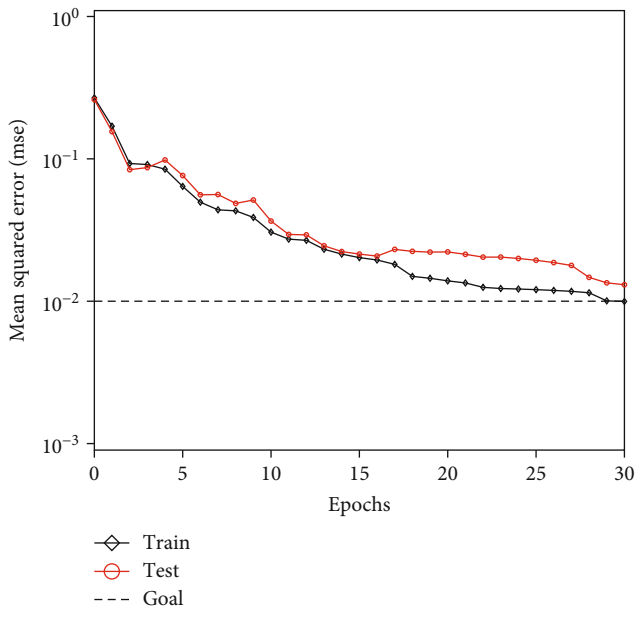

Figure 8: Neural network training performance.

Video 1 Video 2 Video 3

Video 4 Video 5

Figure 9: Experimental video sets.

Table 2: Experimental video description.

Video	Number of frames	Number of flame frames	Video description
video1	758	758	Fire video. The ground color is highly similar to a flame.
video2	352	352	Fire video. There is strong light and shaking branches.
video3	140	140	Fire video. There are two workers walking around with torches.
video4	298	0	Interference video. There are car lights interference.
video5	150	0	Interference video. There are car lights and pedestrian interference.

FP represents the number of misclassified frames of the interference videos.

The fire recognition result is determined by the output value of BP neural network. The experimental results are given in Table 3, and the recognition effect evaluation is given in Table 4.

For the scene in Figure 9, the lights and the ground illuminated by the lights may be segmented into suspected flame areas. In [11], the shape change and centroid displacement of flame are concerned, and the recognition of fire images was realized by support vector machine. Since the lights follow the movement of the vehicle in interference videos, the ground illuminated by the lights has dynamic features similar to flames. This method did not perform well in interference videos (video4 and video5) according to the results in Table 3. In [13], the recognition of fire images was realized by the fusion of Y, Cb, and Cr components in YCbCr color space. There were too many false detection frames in fire videos (video1, video2, and video3) according to the results in Table 3. This shows that using only the color features of flames as a criterion, it is difficult to distinguish the interference of objects similar to the flame color in the background. Compared with the method in [11, 13], the proposed Dir-BP method directly performs BP neural network fusion, in which the extracted features include 9-dimensional features and are not selected. Since the texture and dynamic features of the flames are considered, this method has a certain degree of improvement in accuracy,

Table 3: Experimental results.

Method	TP	TN	FN	FP
SVM [11]	1109	102	141	346
BP [13]	910	376	340	72
Dir-BP (ours)	1190	410	60	38
RF-BP (ours)	1213	421	37	27

Table 4: Evaluation of recognition effect.

Method	Accuracy	Precision	Recall	F-score
SVM [11]	0.713	0.762	0.887	0.820
BP [13]	0.757	0.927	0.728	0.815
Dir-BP (ours)	0.942	0.969	0.952	0.961
RF-BP (ours)	0.962	0.978	0.970	0.970

precision, recall, and F-score according to the results in Table 4. However, due to the features with small correlation that may interfere with the recognition results, the number of false detection frames is still large. The proposed RF-BP method with the combination of RF feature selection and BP neural network makes full use of the geometric features, texture features, and dynamic features of flames, which can effectively avoid some feature interferences and perform the best in the evaluation indexes.

4. Conclusion

In this paper, an effective video fire detection hybrid method based on RF feature selection and BP neural network is proposed. The improved color model and ViBe algorithm are used to segment the suspected flame regions, and the RF importance analysis method is used for the feature combination and selection. Multidimensional features of flames are extracted from the suspected regions, and these extracted features are combined and selected according to the RF feature importance analysis. In addition, a BP neural network model is built for multifeature fusion to determine the fire recognition result. Experimental results show that the features extracted by this RF-BP hybrid approach can effectively avoid the interference caused by the features with small correlation and can well complete the fire detection of experimental videos in different scenes.

The proposed method will be further investigated and have a possible application for fire recognition in video surveillance and detection robots. Considering that the performance of the BP neural network model is easily affected by the sample dataset, the next step is to expand the existing dataset to make the features covered by the training samples with more comprehensive information.

Data Availability

The data supporting this study are from previously reported studies and datasets, which have been cited in the article.

Conflicts of Interest

The authors declare that there is no conflict of interest regarding the publication of this paper.

Acknowledgments

This work was supported by the National Key R&D Program of China (Grant No. 2019YFB1312102), the National Natural Science Foundation of China (Grant No. U20A20201), the Key R&D Program of Hebei Province (Grant No. 20311803D), and the Natural Science Foundation of Hebei Province (Grant No. E2019202338).

References

[1] A. Molina-Pico, D. Cuesta-Frau, A. Araujo, J. Alejandre, and A. Rozas, "Forest monitoring and wildland early fire detection by a hierarchical wireless sensor network," *Journal of Sensors*, vol. 2016, Article ID 8325845, 8 pages, 2016.

[2] T. H. Chen, P. H. Wu, and Y. C. Chiou, "An early fire-detection method based on image processing," in *Proceedings of IEEE International Conference on Image Processing (ICIP)*, pp. 1707–1710, Singapore, 2004.

[3] T. Celik and H. Demirel, "Fire detection in video sequences using a generic color model," *Fire Safety Journal*, vol. 44, no. 2, pp. 147–158, 2009.

[4] Y. Wang and J. Ren, "Low-light forest flame image segmentation based on color features," *Journal of Physics: Conference Series (JPCS)*, vol. 1069, article 012165, 2018.

[5] C. Emmy Prema, S. Vinsley, and S. Suresh, "Efficient flame detection based on static and dynamic texture analysis in forest fire detection," *Fire Technology*, vol. 54, no. 1, pp. 255–288, 2018.

[6] D. Sheng, J. Deng, W. Zhang, J. Cai, W. Zhao, and J. Xiang, "A statistical image feature-based deep belief network for fire detection," *Complexity*, vol. 2021, Article ID 5554316, 12 pages, 2021.

[7] M. Jamali, N. Karimi, and S. Samavi, "Saliency based fire detection using texture and color features," in *Proceedings of 28th Iranian Conference on Electrical Engineering (ICEE)*, pp. 1–5, Iran, 2020.

[8] O. Barnich and M. Van Droogenbroeck, "ViBe: a universal background subtraction algorithm for video sequences," *IEEE Transactions on Image Processing*, vol. 20, no. 6, pp. 1709–1724, 2011.

[9] P. Foggia, A. Saggese, and M. Vento, "Real-time fire detection for video-surveillance applications using a combination of experts based on color, shape, and motion," *IEEE Transactions on Circuits and Systems for Video Technology*, vol. 25, no. 9, pp. 1545–1556, 2015.

[10] F. Gong, C. Li, W. Gong et al., "A real-time fire detection method from video with multifeature fusion," *Computational Intelligence and Neuroscience*, vol. 2019, Article ID 1939171, 17 pages, 2019.

[11] X. Yang, J. Wang, and S. He, "A SVM approach for vessel fire detection based on image processing," in *Proceedings of International Conference on Modelling, Identification and Control*, pp. 150–153, China, 2012.

[12] X. Huang and L. Du, "Fire detection and recognition optimization based on virtual reality video image," *IEEE Access*, vol. 8, pp. 77951–77961, 2020.

[13] N. Qu, J. H. Wang, and Q. H. Chen, "A flame image detection method based on YCbCr color space and BP neural network," *Journal of Shenyang University (Natural Science Edition)*, vol. 31, no. 4, pp. 298–301, 2019.

[14] P. Li and W. Zhao, "Image fire detection algorithms based on convolutional neural networks," *Case Studies in Thermal Engineering*, vol. 19, article 100625, 2020.

[15] D. Sheng, J. Deng, and J. Xiang, "Automatic smoke detection based on SLIC-DBSCAN enhanced convolutional neural network," *IEEE Access*, vol. 9, pp. 63933–63942, 2021.

[16] K. Muhammad, J. Ahmad, I. Mehmood, S. Rho, and S. W. Baik, "Convolutional neural networks based fire detection in surveillance videos," *IEEE Access*, vol. 6, pp. 18174–18183, 2018.

[17] Y. Yan, Q. Wu, and J. Du, "Video fire detection based on color and flicker frequency feature," *Journal of Frontiers of Computer Science and Technology*, vol. 8, no. 10, pp. 1271–1279, 2014.

[18] W. B. Horng, J. W. Peng, and C. Y. Chen, "A new image-based real-time flame detection method using color analysis," in

Proceedings of IEEE International Conference on Networking, Sensing and Control, pp. 100–105, USA, 2005.

[19] D. Y. T. Chino, L. P. S. Avalhais, J. F. Rodrigues, and A. J. Traina, "BoWFire: detection of fire in still images by integrating pixel color and texture analysis," in *Proceedings of 28th SIBGRAPI Conference on Graphics, Patterns and Images*, pp. 95–102, Brazil, 2015.

[20] K. Chen, Y. Cheng, H. Bai, C. Mou, and Y. Zhang, "Research on image fire detection based on support vector machine," in *Proceedings of International Conference on Fire Science and Fire Protection Engineering (ICFSFPE)*, pp. 1–7, China, 2019.

[21] M. Mueller, P. Karasev, I. Kolesov, and A. Tannenbaum, "Optical flow estimation for flame detection in videos," *IEEE Transactions on Image Processing*, vol. 22, no. 7, pp. 2786–2797, 2013.

[22] P. Gomes, P. Santana, and J. Barata, "A vision-based approach to fire detection," *International Journal of Advanced Robotic Systems*, vol. 11, no. 9, pp. 149–575, 2014.

[23] X. F. Han, J. S. Jin, M. J. Wang, W. Jiang, L. Gao, and L. P. Xiao, "Video fire detection based on gaussian mixture model and multicolor features," *Signal Image & Video Processing*, vol. 11, no. 8, pp. 1419–1425, 2017.

[24] Q. Zhang, X. Liu, and L. Huang, "Video image fire recognition based on color space and moving object detection," in *Proceedings of International Conference on Artificial Intelligence and Computer Engineering (ICAICE)*, pp. 367–371, China, 2020.

[25] Y. Wang, Y. Shu, X. Jia, M. Zhou, L. Xie, and L. Guo, "Multi-feature fusion-based hand gesture sensing and recognition system," *IEEE Geoscience and Remote Sensing Letters*, vol. 19, pp. 1–5, 2021.

[26] J. H. Jun, M. J. Kim, Y. S. Jang, and S. H. Kim, "Fire detection using multi-channel information and gray level co-occurrence matrix image features," *Journal of Information Processing Systems*, vol. 13, no. 3, pp. 590–598, 2017.

[27] R. Genuer, J. M. Poggi, and C. Tuleau-Malot, "Variable selection using random forests," *Pattern Recognition Letters*, vol. 31, no. 14, pp. 2225–2236, 2010.

[28] B. U. Toreyin, Y. Dedeoglu, and A. E. Cetin, "Contour based smoke detection in video using wavelets," in *Proceedings of 14th European Signal Processing Conference (EUSIPCO)*, pp. 1–5, Italy, 2006.

[29] B. C. Ko, K. H. Cheong, and J. Y. Nam, "Fire detection based on vision sensor and support vector machines," *Fire Safety Journal*, vol. 44, no. 3, pp. 322–329, 2009.

[30] R. Steffens, R. N. Rodrigues, and S. Botelho, "An unconstrained dataset for non-stationary video based fire detection," in *Proceedings of 12th Latin American Robotics Symposium and Third Brazilian Symposium on Robotics*, pp. 25–30, Brazil, 2015.

[31] D. Zhang, S. Han, J. Zhao et al., "Image based forest fire detection using dynamic characteristics with artificial neural networks," in *Proceedings of International Joint Conference on Artificial Intelligence (JCAI)*, pp. 290–293, Hainan, China, 2009.

[32] A. Khalil, S. U. Rahman, F. Alam, I. Ahmad, and I. Khalil, "Fire detection using multi color space and background modeling," *Fire Technology*, vol. 57, no. 3, pp. 1221–1239, 2021.

Hindawi
Journal of Sensors
Volume 2022, Article ID 2603939, 14 pages
https://doi.org/10.1155/2022/2603939

Research Article

Superresolution Reconstruction of Remote Sensing Image Based on Middle-Level Supervised Convolutional Neural Network

Xiu Zhang

School of Information Engineering, Shaanxi Xueqian Normal University, Xi'an, Shaanxi, China

Correspondence should be addressed to Xiu Zhang; zhangxiu@st.btbu.edu.cn

Received 17 September 2021; Revised 29 October 2021; Accepted 18 November 2021; Published 4 January 2022

Academic Editor: Mu Zhou

Image has become one of the important carriers of visual information because of its large amount of information, easy to spread and store, and strong sense of sense. At the same time, the quality of image is also related to the completeness and accuracy of information transmission. This research mainly discusses the superresolution reconstruction of remote sensing images based on the middle layer supervised convolutional neural network. This paper designs a convolutional neural network with middle layer supervision. There are 16 layers in total, and the seventh layer is designed as an intermediate supervision layer. At present, there are many researches on traditional superresolution reconstruction algorithms and convolutional neural networks, but there are few researches that combine the two together. Convolutional neural network can obtain the high-frequency features of the image and strengthen the detailed information; so, it is necessary to study its application in image reconstruction. This article will separately describe the current research status of image superresolution reconstruction and convolutional neural networks. The middle supervision layer defines the error function of the supervision layer, which is used to optimize the error back propagation mechanism of the convolutional neural network to improve the disappearance of the gradient of the deep convolutional neural network. The algorithm training is mainly divided into four stages: the original remote sensing image preprocessing, the remote sensing image temporal feature extraction stage, the remote sensing image spatial feature extraction stage, and the remote sensing image reconstruction output layer. The last layer of the network draws on the single-frame remote sensing image SRCNN algorithm. The output layer overlaps and adds the remote sensing images of the previous layer, averages the overlapped blocks, eliminates the block effect, and finally obtains high-resolution remote sensing images, which is also equivalent to filter operation. In order to allow users to compare the superresolution effect of remote sensing images more clearly, this paper uses the Qt5 interface library to implement the user interface of the remote sensing image superresolution software platform and uses the intermediate layer convolutional neural network and the remote sensing image superresolution reconstruction algorithm proposed in this paper. When the training epoch reaches 35 times, the network has converged. At this time, the loss function converges to 0.017, and the cumulative time is about 8 hours. This research helps to improve the visual effects of remote sensing images.

1. Introduction

Superresolution reconstruction (superresolution, SR) is the process of obtaining the highest quality image from one or more low-resolution images through signal processing and image processing methods. After the low-resolution (LR) small image is enlarged by interpolation (convolved with the interpolation function), it is enlarged to the required size and then reconstructed by the reconstruction algorithm. It can be seen that the selection of the interpolation function and the reconstruction algorithm determine the quality and efficiency of the reconstruction. Because remote sensing images are acquired by satellites at high altitude, ground targets may only occupy dozens or even a few pixels in low-resolution remote sensing images; so, it is difficult to capture some smaller targets on the ground. The image superresolution technology can provide more effective information for the detection, recognition, and understanding of small targets in remote sensing images.

The image superresolution reconstruction technology not only overcomes the limitation of the inherent resolution of imaging equipment but also considers the influence of

down sampling, blurring, noise, and other factors in the image degradation process. It improves the resolution of the image and also improves the reconstructed the quality of image. Therefore, it shows important application prospects in many fields. In satellite imagery, if the image resolution is high, you can see more detailed information or identify more objects in the same satellite remote sensing image. Compared with improving the performance of image capture equipment, using a more effective superresolution reconstruction algorithm is undoubtedly a more cost-effective choice. The use of algorithms for high and low resolution conversion has low cost and has been successfully applied to video, face recognition, medical images, and satellite images. Therefore, in the field of image processing today, superresolution reconstruction algorithms are a hot issue that has attracted widespread attention.

Over the past few years, significant efforts have been made to develop various data sets or to come up with various methods for classifying scenes from remote sensing images. Gong believed that a systematic review of the literature on data sets and scene classification methods was still lacking. He began with a comprehensive review of recent developments. He then proposed a large-scale dataset called "NWPU-ResISC45" [1]. Zhang proposes an effective nonlinear approximation scheme that uses Saito and Remy's multiharmonic local sine transform (PHLST) in conjunction with an algorithm to automatically and adaptically tile a given image based on its local smoothness and singularity. To measure this local smoothness, he introduced what is called the image local Besov index, which is based on the point-by-point modulus of image smoothness. This adaptive partitioning of the image is important for image approximations using PHLST, because PHLST stores angular and boundary information for each partition; so, it is wasteful to divide a smooth region of a given image into a set of smaller partitions. He used remote sensing images of the South Pole to demonstrate the superiority of the proposed algorithm over PHLST using uniform tiling. Due to global climate change, the analysis of these images, including their effective approximation and compression, is becoming increasingly important [2]. Alimjan believes that distance measurement and classification standards are equally important in remote sensing image classification. And the accuracy of any one will affect the classification accuracy. He believes this is based on the separability of classes using SVM and the spatial and spectral characteristics of remote sensing data. In addition, he proposed a distance formula as a metric to consider the brightness and direction of vectors. First, a SVM is trained, and a support vector (SV) is obtained for each class. In the test phase, enter a sample of the new test and use the distance formula to calculate the average distance between the test sample of each class and the SV. Finally, it was decided to classify the test samples into the category with the minimum mean distance. Repeat this process until all test samples have been classified [3]. Gong noted that while significant efforts have been made to develop a variety of remote sensing image scene classification methods, most of them rely on hand-crafted features. Extensive evaluation of publicly available remote sensing image scene classification benchmarks and comparison with the most advanced methods prove the effectiveness of the proposed BoCF method for remote sensing image scene classification [4]. Wang proposed an effective deep neural network for remote sensing image registration. Unlike the traditional method of feature extraction and feature matching, he pairs patches in the perceptual image and reference image and then directly learns the mapping between these patch pairs and their matching tags for later registration. This end-to-end architecture makes it possible to optimize the entire processing (learning mapping function) through information feedback while training the network, which is lacking in traditional methods. In addition, to alleviate the small data problem of remote sensing images for training, his proposal introduces self-learning by using the image and its transformed copy learning mapping function. In addition, his application of transfer learning to reduce the training phase of the huge computing costs. It not only speeds up our framework but also gets an additional performance boost [5]. Guo believes that the explosive availability of remote sensing images poses challenges to supervised classification algorithms such as support vector machines (SVM), because training samples are often very limited due to the expensive and laborious tasks of ground reality. Temporal correlation and spectral similarity between multitemporal images provide an opportunity to alleviate this problem. In his research, he proposed a SVM-based sequence classifier training (SCT-SVM) method for multitemporal remote sensing image classification. His method uses classifiers of previous images to reduce the number of training samples required for classifier training of input images. For each input image, the crude classifier is first predicted based on the temporal trend of a set of previous classifiers. The current training sample is then used to fine-tune the predicted classifier to a more accurate position. This method can be gradually applied to sequential image data, and only a small number of training samples are required for each image [6]. Munoz-mari sees HyperLabelMe as a network platform that allows automated benchmarking of remote sensing image classifiers. To demonstrate the attributes of the platform, he collected and coordinated large datasets of labeled multispectral and hyper spectral images with different categories, dimensions, noise sources, and levels. He suggested that registered users could download training data pairs (spectrum and land cover/usage tags) and submit predictions for the invisible test spectrum. The system then evaluates the accuracy and robustness of the classifier and reports the different scores as well as a ranking list of the best methods and users. The system he studied was modular and extensible, and the data set and classifier results were growing [7]. The goal of artificial intelligence (AI) is to design a machine that can perceive, remember, and recognize like humans. Perceptron is a machine learning algorithm that can feel and learn first, but its learning ability is limited. Later, a neural network model with multiple hidden layers appeared, which can learn more complex functions, but it is not a learning algorithm that can meet the needs of artificial intelligence. Although deep learning research has brought impressive theoretical results, learning algorithms and theoretical experiments, due to its numerous parameters, high training data and computational requirements, and prone to overfitting, the future development of algorithms still faces challenges. Convolutional neural

network is a feed-forward neural network, including convolutional layer, pooling layer, and output layer. It is an efficient pattern recognition method.

The current superresolution reconstruction based on a single image can be divided into two categories: (1) interpolation-based methods without training samples and (2) learning-based methods with training samples. Among them, the method based on interpolation only upsampling the low-resolution image, recovering the high-frequency components of the image, and finally enhancing the edge of the image, but does not fundamentally increase the amount of information contained in the image, and the reconstructed image lacks deeper details. This research mainly discusses the superresolution reconstruction of remote sensing images based on the middle layer supervised convolutional neural network. This paper designs a convolutional neural network with middle layer supervision. There are 16 layers in total, and the seventh layer is designed as an intermediate supervision layer. The middle supervision layer defines the error function of the supervision layer, which is used to optimize the error back propagation mechanism of the convolutional neural network to improve the disappearance of the gradient of the deep convolutional neural network. The algorithm training is mainly divided into four stages: the original remote sensing image preprocessing, the remote sensing image temporal feature extraction stage, the remote sensing image spatial feature extraction stage, and the remote sensing image reconstruction output layer. The current research results of superresolution reconstruction algorithms based on single images are mostly devoted to finding new features that make it easier to obtain image detail information for training, and these methods usually have high dependence on pre-defined features and calculations. The complexity is high, the robustness is not strong, and the input image needs to be a fixed size problem. The three-layer reconstruction model based on the convolutional neural network solves the problem of the lack of robustness of these methods and the need for fixed-size input images, and the network can obtain features by itself, without manual settings, and only need to set the parameters of the network to be trained in advance.

2. Methods

2.1. Image Superresolution Reconstruction. In improving the accuracy of pattern recognition, high-resolution images also play a pivotal role. Therefore, how to obtain and analyze high-resolution images under limited conditions has become a research hotspot in image processing.

In the 1970s, image sensor technology developed, and image acquisition devices based on CCD and CMOS sensors were comprehensively developed and popularized. Although these digital image devices can basically meet the various applications in people's daily life, they have higher image resolution. In order to meet people's growing demand for images, it is also a hotspot of modern research. By increasing the density of the acquisition unit and increasing the area of the sensor, better quality images can be obtained intuitively and quickly. The cost of the equipment is too expensive to be widely used. These conditions limit the improvement of the image spatial resolution from the hardware aspect. People began to study how to use software processing technology to obtain higher resolution images, and the image superresolution reconstruction technology (superresolution, SR) has thus been developed.

The current sequence image superresolution algorithm is mainly divided into two stages: motion estimation and image reconstruction. The motion estimation stage makes full use of the time-dimensional motion information between the sequence images through accurate motion estimation to obtain the registered image; the image reconstruction stage uses registration after the image is reconstructed, the image resolution is improved. It can be seen from this that motion estimation is essentially to extract the temporal motion information of the sequence image. Therefore, how to better extract the motion information has become the key content of the research of the sequence image superresolution algorithm. By designing multiple convolutional layers, the network can extract multiple different image features [8].

$$y_j = b_j + \sum_i w_{ij} \times x_i. \tag{1}$$

The feed forward operation of the convolutional neural network is based on the convolution operation, adding a bias B to each feature plane:

$$C_{\mathrm{i}}^L = F\left(A_{\mathrm{i}}^L + B_{\mathrm{i}}^L\right). \tag{2}$$

Then, the training error of the network on the entire training sample is expressed as [9]

$$E = \frac{1}{2}\left\|\mathrm{t}_n - y_n\right\|_2^2 = \frac{1}{2}\sum_{n=1}^{N}\sum_{t=1}^{n}\left\|\mathrm{t}_n - y_n\right\|_2^2. \tag{3}$$

Then, the training error of the network on a training sample can be [10]

$$E = \frac{1}{2}\left\|\mathrm{t}_n - y_n\right\|_2^2 = \frac{1}{2}\sum_{n=1}^{N}\left\|\mathrm{t}_n - y_n\right\|_2^2. \tag{4}$$

At present, the input images of many single-frame image superresolution algorithms will be processed by cubic cubic interpolation [11, 12].

$$S(\mathrm{w}) = |w|^3 - 2|w|^2 + 1, \tag{5}$$

$$S(\mathrm{w}) = -|w|^3 + 5|w|^2 - 8|w| + 4. \tag{6}$$

The interpolation value of the corresponding pixel is [13, 14]

$$G(i+u, j+v) = A \times B \times C. \tag{7}$$

Among them,

$$A = [S(1+u), S(u), S(1-u), S(2-u)]. \tag{8}$$

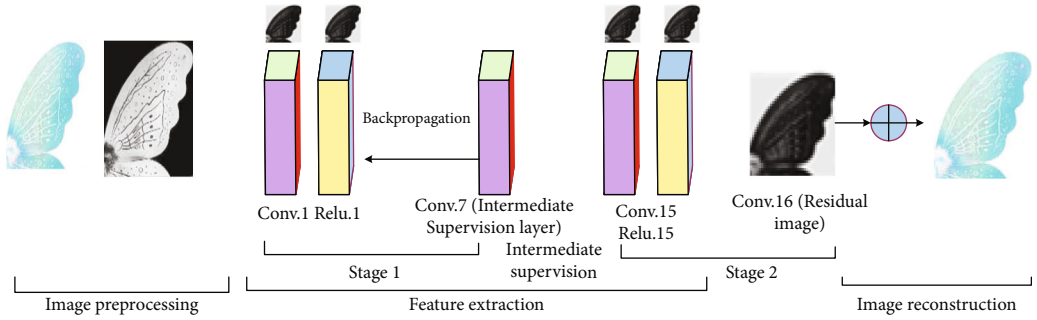

Figure 1: Convolutional neural network structure with intermediate layer supervision.

Assuming that $P(Y \mid X)$ is the maximum posterior probability of high-resolution image Y under low-resolution image X, then [15]

$$A = [S(1+u), S(u), S(1-u), S(2\text{-}u)]. \tag{9}$$

The error between the output image and the real high-resolution image is, namely, [16]

$$E = F(X_L) - X_H. \tag{10}$$

Among them, X_L is the network input [17, 18].

2.2. Intermediate Layer Supervised Convolutional Neural Network. Therefore, the method to improve the resolution of the image from the hardware point of view not only requires high cost, but also has limited room for improving the quality of the equipment. The research is difficult, the cycle is long, and it is not easy to make rapid progress in the short-term. In addition, even if the imaging device collects ultra-high-resolution images, there are new problems in image transmission. Ultra-high-resolution images take up a lot of space, and the pressure when transmitting images through the network is relatively large. Therefore, by improving the imaging equipment method of improving image resolution by quality has been greatly restricted in practical applications.

The structure of the convolutional neural network with intermediate supervision designed in this paper is shown in Figure 1. There are 16 layers, namely, Conv.1, Conv.2 … Conv.16, and the seventh layer is designed as an intermediate supervision layer. The intermediate supervision layer defines the error function of the supervision layer, which is used to optimize the error back propagation mechanism of the convolutional neural network, and realize the iterative update of the weight parameters of the network layer to improve the disappearance of the gradient of the deep convolutional neural network [19].

2.3. Residual Activation Block. In this paper, the traditional residual structure is improved, and the residual activation block RAB is proposed. By adopting a new spatial and channel attention mechanism, the network can simultaneously analyze the spatial relationship between the features at different positions in the channel in the feature map. The relationship between features located at the same position in different channels is modeled. The spatial channel attention mechanism enables the network to give higher response values to features that are rich in spatial information and are located in important channels, while suppressing features that are scarce in surrounding spatial information and are located on less important channels, so that the network can adaptively adjust features. The expression of the residual block is [20]

$$X_{l+1} = X_l + f(X_l). \tag{11}$$

In the formula, X_l is the input feature of the residual block. The ReLU function is a modified linear unit [21]:

$$\mathrm{ReLU}(x) = \max(x, 0). \tag{12}$$

The improved residual network uses the L2 norm as the loss function, and its expression is [22]

$$L_2(y, f) = \frac{1}{2N} \sum_{i,j} [y(i,j) - f(i,j)]^2. \tag{13}$$

2.4. Superresolution Steps of the Sequence Image SRCNN (Image Superresolution Reconstruction) Algorithm Based on the Intermediate Layer Supervised Convolutional Neural Network. The main goal of the algorithm is to find the mapping function F between the input and the output, so that the high-resolution images output by the network and the real high-resolution remote sensing images are as close as possible. The algorithm training is mainly divided into four stages: the original remote sensing image preprocessing, the remote sensing image temporal feature extraction stage, the remote sensing image spatial feature extraction stage, and the remote sensing image reconstruction output layer.

(1) Preprocessing the input layer: like the single-frame remote sensing image superresolution convolutional neural network algorithm, the original remote sensing image sequence X is first preprocessed and expanded into an interpolated picture of the same size as the output remote sensing image, as the input of the network remote sensing image sequence [23]

(2) Remote sensing image temporal feature extraction stage: in this stage, a two-layer network can be designed. The two layers are equivalent to the use of filters and time sliding windows for sequence remote sensing image processing, and the middle layer supervised convolutional neural network is used to perform three-frame remote sensing. Image joint convolution, first three frames of remote sensing images are separately convolved, and then the corresponding positions obtained by the separate convolution operation are "and mapped" to obtain the feature remote sensing image that is jointly matched, and the value of each pixel of the feature remote sensing image is obtained. Schematic diagram of the supervised convolutional neural network in the middle layer is described above. The feature remote sensing image extracted in this network stage contains the information of all frames of remote sensing image, thereby enhancing the detailed information of the reference frame remote sensing image, which contains more remote sensing image information than the feature remote sensing image obtained from the reference frame remote sensing image alone. Schematic diagram of the middle layer supervised convolutional neural network. The feature remote sensing image extracted in this network stage contains the information of all frames of remote sensing image, thereby enhancing the detailed information of the reference frame remote sensing image, which contains more remote sensing image information than the feature remote sensing image obtained from the reference frame remote sensing image alone

At the beginning of network training, the parameters of the middle layer supervised convolutional neural network are initialized. The result of spatiotemporal fusion feature remote sensing image may not be good, and mismatching and ghosting will occur, but after the iterative feedback of the network, error adjustment, and finally fusion feature, remote sensing image obtained at this stage will definitely contain more detailed information, which provides a good basic remote sensing image for the subsequent spatial feature extraction of remote sensing image.

(3) Remote sensing image spatial feature extraction layer: the main purpose of this stage is to extract and abstractly combine a series of feature remote sensing images through a multilayer network to obtain the features needed to reconstruct high-resolution remote sensing images, which are essentially features process of extraction and aggregation. In this layer, the feature maps of spatiotemporal feature fusion have been obtained; so, there is no need to extract the time dimension information at this time, only the spatial dimension information needs to be extracted, using a series of 2D convolution kernels, that is, selecting a series of different filters to convolve the remote sensing image, and supervising the selection and optimization of these filters through the iterative network [24]

$$F(X_{t-1}) = \max\left(0, W \times X_{t-1} + B_t\right). \tag{14}$$

Among them, X_{i-1} represents the feature remote sensing image of the previous network layer, including n_{i-1} feature planes. The input of the first layer network at this stage is the n feature remote sensing images obtained in the remote sensing image fusion stage, and the subsequent network layer input is the previous output of a layer network. W_i represents the filter bank of this layer, each layer of network contains n_i group filters, and the number of feature planes output through this layer of network is n_i. B_t is a n_i-dimensional vector, which represents the offset coefficient corresponding to each feature map of this hidden layer.

The spatial characteristics extraction stage of the remote sensing image here can set up a multilayer network to increase the ability to extract abstract features. As the number of network layers increases, the extracted features are more sufficient, providing more and better feature information for subsequent remote sensing image reconstruction. But the price that needs to be paid is that with the increase of network complexity and calculation, the efficiency of network training and remote sensing image reconstruction decreases.

(4) Remote sensing image reconstruction output layer: the last layer of the network draws on the single-frame remote sensing image SRCNN algorithm, and the output layer overlaps and adds the remote sensing images of the previous layer, performs an average operation on the overlapped blocks, eliminates the effect of blackness, and finally gets high-resolution remote sensing image that is also equivalent to a filter operation; so, the operation expression of this layer is similar to the operation expression of the previous spatial feature extraction stage

For accuracy evaluation, the result of change detection can also be regarded as a special classification result, and the detection of change can be regarded as a multiclass classification problem. We use indicators including overall accuracy (OA), producer accuracy (PA), user accuracy (UA), and kappa coefficient to evaluate change detection accuracy. Overall accuracy (OA): the number of samples that correctly detect the type of change divided by the total number of samples [25].

$$\mathrm{OA} = \frac{\sum_{i=1}^{k} N_{ii}}{N}. \tag{15}$$

Producer accuracy (PA): the ratio of the number of samples N_{ii} of the correct detection change type i and the number of samples of the change type $i(N_{+i})$ in the real data are also known as the inspection rate [26].

$$UA_i = \frac{N_{\mathrm{ii}}}{N_{i+}}. \tag{16}$$

The calculation formula of Kappa coefficient is as follows [27]:

$$\text{Kappa} = \frac{N\sum_{i=1}^{k} N_{ii} - \sum_{i=1}^{k}(N_{+i}N_{+i})}{N^2 - \sum_{i=1}^{k}(N_{+i}N_{+i})}, \tag{17}$$

where N is the total number of samples evaluated for accuracy, and k is the number of categories of the change type. The accuracy of traditional CNN model change detection is shown in Table 1.

2.5. Implementation of Qt-Based Remote Sensing Image Superresolution Software Platform. In order to allow users to compare the superresolution effect of remote sensing images more clearly, this paper uses the Qt5 interface library to implement the user interface of the remote sensing image superresolution software platform and uses the intermediate layer convolutional neural network and the remote sensing image superresolution reconstruction algorithm proposed in this paper. This software allows users to see more intuitive superresolution results, also provides a platform for learners and researchers of remote sensing image superresolution, and allows them to easily run without understanding the superresolution reconstruction algorithm. The algorithm in this paper obtains superresolution images.

2.5.1. The Functional Framework of Remote Sensing Image Superresolution Reconstruction Software. The problem of image superresolution reconstruction is an ill-conditioned inverse problem. Because multiple images with different high resolutions may correspond to the same low-resolution image, there is no unique solution to solving a high-resolution image through a low-resolution image. In the imaging process, because there are many factors that can degrade the image, such as system noise, imaging noise, motion blur, or downsampling,, the reasons for image degradation must be fully considered in the image reconstruction process to better deal with the degraded image. The main interface of the software contains the main panel, toolbar, and menu bar. The menu bar contains all the functional modules of the software, and the main panel and toolbar contain commonly used functional modules. The software is mainly divided into three modules, namely, file operation module, superresolution reconstruction module, and other functional modules. Among them, the superresolution reconstruction module implements a bicubic interpolation algorithm, an improved residual network remote sensing image superresolution algorithm, and a remote sensing image superresolution algorithm based on the middle layer supervised convolutional neural network. After the superresolution algorithm is executed, you can directly view the superresolution result image on the main panel and parameter indicators such as peak signal-to-noise ratio and structural similarity. Figure 2 is the module division diagram of this software, and the figure also contains shortcut keys for some functions.

2.5.2. Software Module. The software contains three modules:

Table 1: Change detection accuracy of the traditional CNN model.

Test	PA	UA	OA	Kappa
Unchanged	0.9692	0.8695		
Variation type 2	0.0082	0.0143		
Variation type 5	0.2330	0.2118	0.8172	0.3761
Variation type 6	0.1153	0.7426		
Variation type 7	0.3174	0.6918		

(1) File Operation Module. The function of this module includes opening the image, saving the image, and closing the software. Opening the image refers to opening the remote sensing image that needs superresolution on the disk, and saving the image refers to saving the generated superresolution image on the disk. And these three functions use shortcut keys consistent with other software.

(2) Superresolution Reconstruction Module. This module implements the improved convolutional neural network remote sensing image superresolution reconstruction algorithm in this article and also includes a faster bicubic interpolation algorithm. This module also uses the objective parameters PSNR (peak signal-to-noise ratio) and SSIM to evaluate the image quality of the superresolution reconstruction result image. The expression of peak signal-to-noise ratio (PSNR) is

$$\text{PSNR} = 10\lg\frac{L^2}{\text{MSE}} = 10\lg\frac{L^2\text{MN}}{\sum_{i=1}^{m}\sum_{j=1}^{n}[y(i,j) - f(i,j)]^2}. \tag{18}$$

In the formula, MSE is the mean square error, L is the peak signal, and the value is 255 for the 8-bit gray scale image. The larger the PSNR, the better the image quality. Natural images have a specific structure, and each pixel in the image has a strong subordination relationship, which reflects the structure in the image. The structural similarity measures this structure and is used to evaluate the quality of the image [28].

$$\text{SSIM} = \frac{\left(2\mu_x m_y + c_1\right)\left(2\sigma_{xy} + c_2\right)}{\left(\mu^2{}_x + \mu^2{}_y + c_1\right)\left(\sigma^2{}_x + \sigma^2{}_y + c_2\right)}. \tag{19}$$

In the formula, μ_x, μ_y is the mean value, σ_x, σ_y is the standard deviation, σ_{xy} is the covariance, and L is 255 for the 8-bit gray scale image. SSIM indicates the degree of similarity between the structure of the superresolution image and the actual high-resolution image, its value does not exceed 1, and the closer the SSIM is to 1, the more similar the structure and the better the reconstruction effect.

Mean pixel accuracy (MPA, mean pixel accuracy) is a simple improvement based on the PA index, which is to

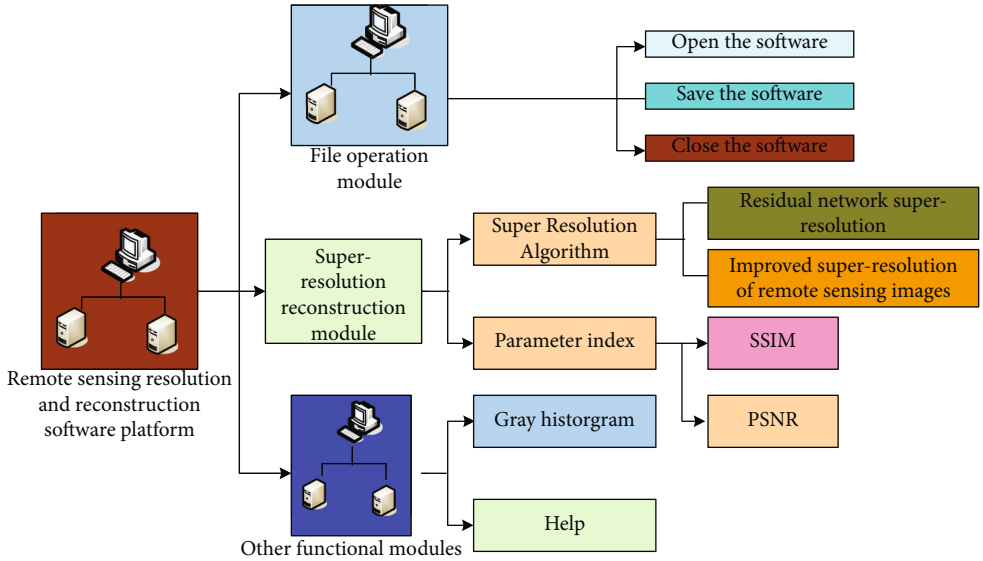

Figure 2: Module division of the software.

average the proportion of all correctly classified pixels to the total pixels. The mathematical expression is as follows:

$$\mathrm{MPA} = \frac{1}{k+1}\sum_{i=0}^{k}\frac{P_{ij}}{\sum_{j=0}^{k}P}. \tag{20}$$

The superresolution reconstruction module runs the SRR (image superresolution reconstruction) algorithm on the input image and displays the output image and various parameters after running. This software includes three algorithms for use, namely, the bicubic interpolation algorithm, the improved residual network superresolution algorithm in this article, and the improved densely connected network superresolution algorithm in this article. These three algorithms are placed in the main panel in the form of radio buttons. After selecting the buttons of different algorithms, the software will also run different superresolution algorithm programs.

(3) Other Functional Modules. This module provides users with more convenient functions, including viewing the grayscale histogram, which is opened in the toolbar in the main interface, and the shortcut keys are Ctrl+1 and Ctrl+2, which are used to view the input image and output image, respectively, histogram of grayscale. Another function of this module is the help and about of the software, displayed in the menu. The configuration used to build this software: operating system Win10 Professional Edition, and CPU is Intel-Corei7-7700 K, memory 16GB, graphics card GTX10606GB.

3. Results

After the image degradation model is established, the reconstruction-based method mainly uses multiframe low-resolution (LR) images as a consistency constraint, combined with the prior knowledge of low-resolution images for superresolution reconstruction, thereby obtaining super-resolution image. It makes full use of the information complementarity between multiple low-resolution images in the same scene and effectively fuses these complementary information to achieve the purpose of reconstructing high-resolution images.

The network performs a total of 40,000 training iterations, and the cumulative time is 40 minutes. At this time, the loss function value of the training set has converged to 1.44. A test is performed every 500 iterations, and the network with the largest PSNR in the test process is taken as the final network. The relationship between the network training loss function and the number of iterations is shown in Figure 3.

The generalization experiment results show that the superresolution effect of the network on the verification set is better than that of the network before the improvement. Here, 8 remote sensing images are selected for verification and display, as shown in Figure 4.

The advantages of the iterative back projection method are simple, intuitive, and fast calculation speed, but the selection of its back projection operator is more difficult, the solution is not unique, and it is very dependent on the initial value. This method cannot take advantage of the inherent characteristics of high-resolution images priori constraint knowledge. In the iterative process, the error of the back projection only accumulates evenly on the reconstructed image, resulting in a sawtooth effect on the edge of the reconstructed high-resolution image. The experiment chooses low-resolution images, bicubic interpolation, VDSR algorithm, and improved methods for comparison. For the rationality of the experiment comparison, the size scaling factor is 3 in the experiment. Only the comparison results of 4 groups of experiments are listed here as shown in Figure 5.

The image superresolution reconstruction algorithm based on learning is also called the image superresolution reconstruction based on example learning, and it is one of

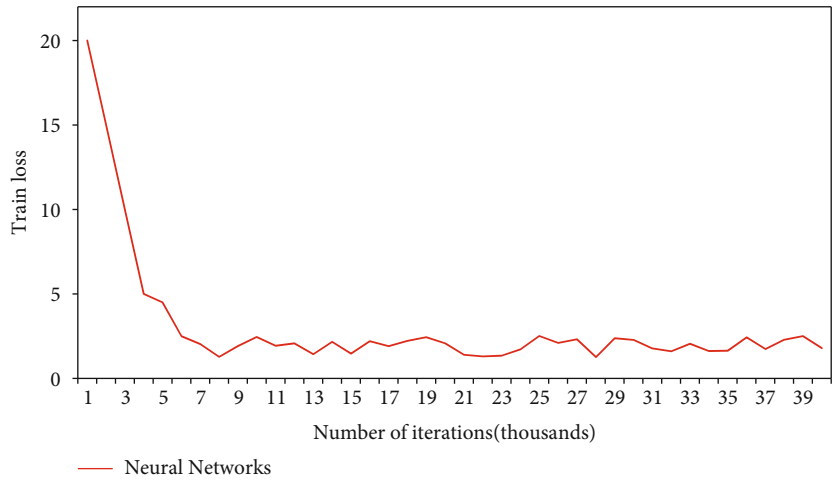

Figure 3: The relationship between the network training loss function and the number of iterations.

Figure 4: Select 8 remote sensing images for result verification.

Figure 5: Four comparison results of groups of experiments.

the main research hotspots in the image superresolution reconstruction algorithm in recent years. This method finds a mapping relationship between low-resolution images and high-resolution images by learning to construct a sample library of low-resolution images and high-resolution images in advance and finally reconstructs high-resolution images through this mapping relationship.

Through the superresolution renderings, it can be seen that the subjective visual effect of the superresolution algorithm in this chapter is better than that of the VDSR network, and it can generate higher-quality superresolution images with more detailed information about the image texture. The second set of comparison results is shown in Figure 6.

Figure 6: The second set of comparison results.

Table 2: Eight PSNR comparison of the results of the three algorithms for remote sensing images.

Image	Bicubic interpolation	VDSR	Method of this article
Group 1	20.65	21.94	22.40
Group 2	16.31	17.37	17.82
Group 3	20.98	2241	22 85
Group 4	23.99	24. 96	25.41
Group 5	24. 90	27.25	27.70
Group 6	19.85	21.95	22.40
Group 7	22.37	24.75	25.20
Group 8	22.80	23.82	24.28
Average value	21.48	23.06	23.51

Table 3: SSIM comparison.

Image	Bicubic interpolation	VDSR	Method of this article
Group 1	0.594	0.701	0.729
Group 2	0.456	0. 590	0.630
Group 3	0.649	0.735	0760
Group 4	0.654	0.738	0763
Group 5	0.775	0.858	0.872
Group 6	0.712	0.828	0.845
Group 7	0.730	0.838	0.854
Group 8	0.779	0.834	0.850
Average value	0.669	0.765	0.788

Table 2 shows the PSNR comparison of the three algorithm results of 8 remote sensing images.

Most of the reconstruction algorithms based on single-frame image superresolution basically use the characteristics of the image detail information for training, but these methods rely on the pretrained image features relatively high, and the reconstruction speed is relatively slow. In addition, there are problems such as unclear edges of the reconstructed image, the need to fill the edges of the image, and the lack of robustness. The SSIM comparison is shown in Table 3. The PSNR of 8 sets of remote sensing images under different algorithms is compared with SSIM. It can be seen that compared with the VDSR algorithm, the objective parameter PSNR of the improved algorithm is increased by about 0.45 dB, and the SSIM is increased by about 0.023.

In order to improve the superresolution effect of remote sensing images, the experimental training samples use remote sensing images provided by the cooperative unit, the image size is 2000×2000, and it is intercepted into 100×100 subimages as the data set. In order to increase the number of data sets, the previously captured subimage data sets were rotated by 90°, 180°, and 270° respectively, which increased the number of data sets by 3 times, and finally got about 25,000 100×100 small images. Then, use 80% of the data set as the training set, 10% as the test set, and 10% as the verification set. The training set is still used to train the network and update the parameter weights of the network. The test set is only used to evaluate the superresolution ability that changes with the number of network iterations, not to update the weights. The training set image itself is used as the output of the network, and the training set image (2 times under sampling) is reduced twice to 50×50, which is used as the low-resolution image of the network input. The network training performs an epoch for about 14 minutes. When the training epoch reaches 35 times, the network has converged. At this time, the loss function has converged to 0.017, and the cumulative time is about 8 hours. The relationship between the error and the number of iterations in the network training process is shown in Figure 7. The test carried out after each epoch training is close to stable at about 35 training sessions.

The four-layer convolutional network model based on multifeature map input proposed in this paper can input multiple images with different features, which provides more features of superresolution images to the greatest extent, and is more conducive to the reconstruction of superresolution images. Compared with the three-layer convolutional layer, the four-layer convolutional layer can extract more image features. This paper also discusses the influence of the number of convolution kernels and the parameters of the convolution layer on the network through experimental results. Because multiple images with different characteristics are obtained by interpolation from the same low-resolution image, the model proposed here is essentially a reconstruction model based on single-frame image superresolution. As shown in Figure 7, it can be seen that the training of

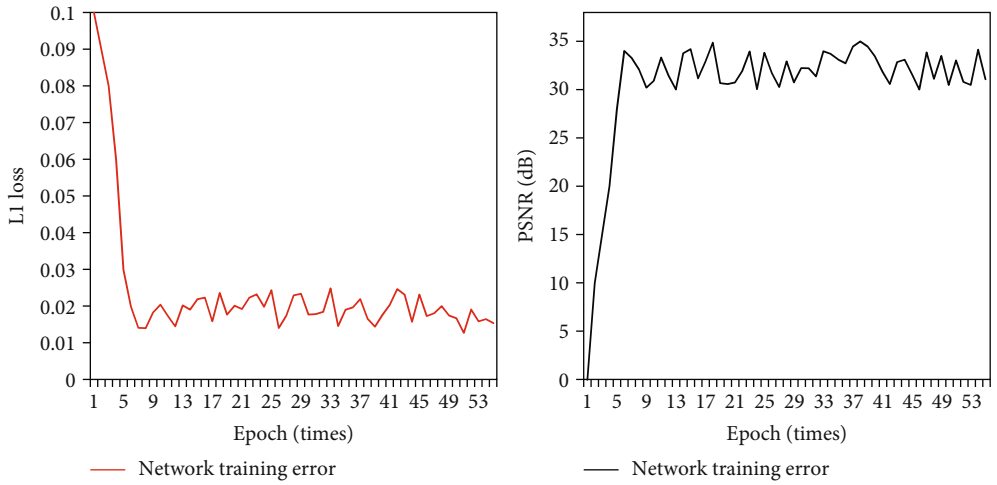

Figure 7: The relationship between the error and the number of iterations in the training process of the network.

Table 4: Accuracy evaluation of experimental area change detection results.

Model	5 × 5 neighborhood		5 × 5 neighborhood (CNN+)	
	Accuracy	Recall rate	Accuracy	Recall rate
CNN	0.8179	0.7336	0.7990	0.7518
LSTM	0.8007	0.7680	0.8597	0.7502
SRR	0.7228	0.8577	0.8256	0.8589
This research	0.8337	0.9252	0.9822	0.8981

the network has converged when the epoch reaches about 32 times, the training set error is still decreasing as the epoch increases, and the PSNR of the test set shows a slight downward trend, which is due to cause by over fitting. In order to solve the problem of network overfitting, this experiment takes the network when the network converges, and the PSNR of the test set reaches the maximum as the final network. At this time, the epoch is the 35th time.

The accuracy evaluation of the experimental area change detection results is shown in Table 4. The difference between different recurrent network models does not seem to be large. The 5 × 5 neighborhood (CNN+) input method combined with this research method achieves the highest accuracy rate (0.8337) and recall rate (0.9252).

We will divide into 5 groups according to the input method, each group contains 6 types of recurrent neural networks, we can see that the method of first facing the pixel neighborhood has higher accuracy, recall and accuracy, the input method of larger neighborhood can significantly improve the recall rate and accuracy rate, and the combination of CNN can further improve the recall rate and accuracy rate. Here, the average accuracy rate and average recall rate of the input method are in this study. It is obvious that they reach the highest level, and in this way, the accuracy of different cyclic neural networks is more different. The comparison between CNN and this research method is shown in Figure 8.

The change detection accuracy of the twin convolutional neural network model is higher, especially when the convolutional neural network model is simple and the number of layers is small, and it is more obvious, and when the convolutional neural network model is more complex and the number of layers is large, the single channel accuracy difference between the change detection of the twin convolutional neural network model and the twin convolutional neural network model will be significantly reduced. The accuracy comparison of different convolutional neural network models is shown in Figure 9.

Because mask RCNN realizes the process of detection and segmentation through a network, the change detection method based on mask RCNN has higher detection accuracy than the change detection method based on fast RCNN. After adding FPN, the change detection accuracy based on mask RCNN can be further improved. Like the change detection method based on fast RCNN, the detection effect of this research model is better than mmrcnn. Remote sensing image change detection is shown in Table 5.

It can be seen from Figure 10 that the model test MPA of the middle layer supervised convolutional neural network model reached 0.86, MIOU reached 0.82, and the training loss dropped to 0.15. From the trend of each indicator curve of the model, it can be seen that the model obtained a good convergence. The change of MIOU of the middle layer supervised convolutional neural network model is shown in Figure 10.

4. Discussion

On the one hand, the single-frame image superresolution convolutional neural network is considered from a global

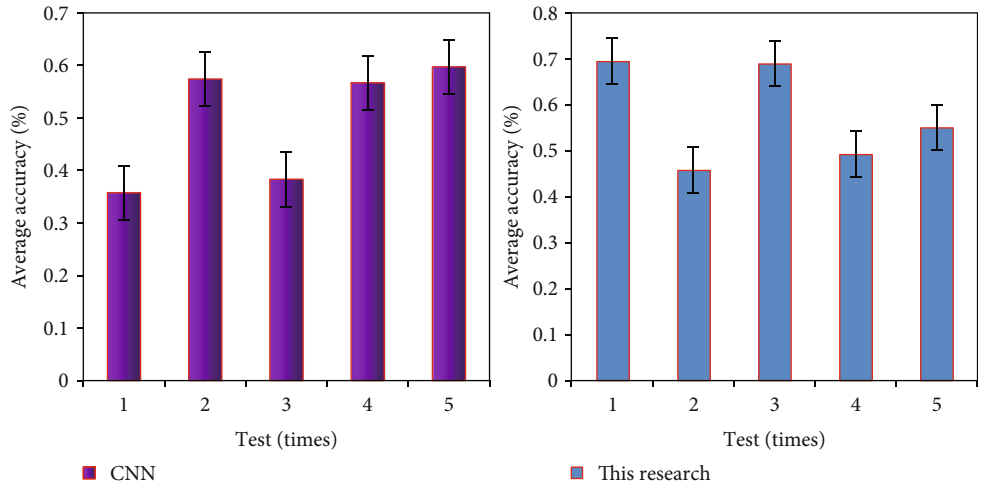

Figure 8: Comparison of CNN and this research method.

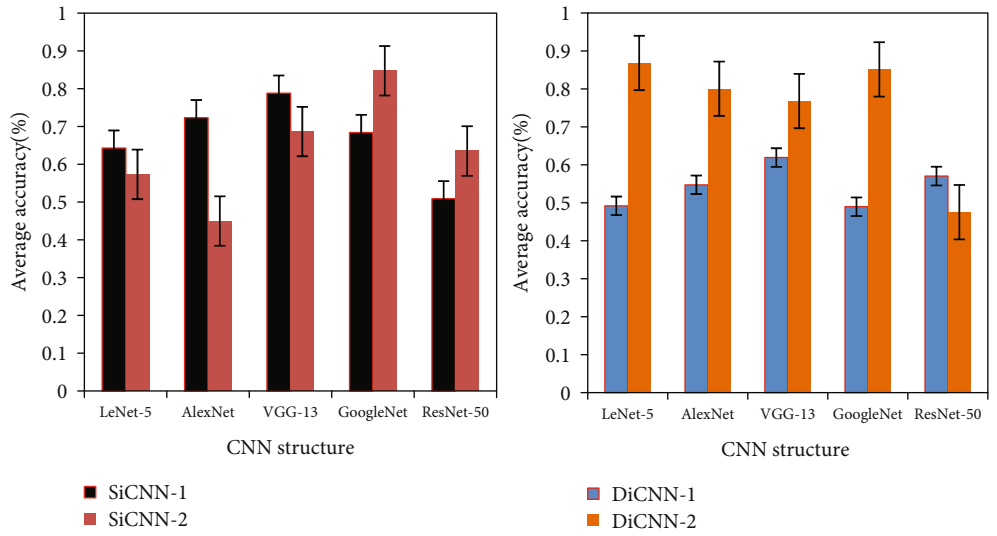

Figure 9: Accuracy comparison of different convolutional neural network models.

Table 5: Remote sensing image change detection.

Method		Variety	Unchanged	OA	Kappa
MMRCNN	PA	0.6929	0.9954	0.9885	0.7284
(NoFPN)	UA	0.7810	0.9928		
This research	PA	0.7518	0.9971	0.9914	0.7970
(NoFPN)	UA	0.8579	0.9942		
MMRCNN	PA	0.7601	0.9984	0.9929	0.8281
(FPN)	UA	0.9181	0.9944		
This research	PA	0.8354	0.9980	0.9943	0.8676
(FPN)	PA	0.9218	0.9961		

perspective. When the convolutional neural network is trained, the entire network parameters are adjusted synchronously, and finally, the optimization of the output is global. However, most of other superresolution algorithms based on learning are optimized step by step; that is, the solution of each step is the current local optimal, but the final output is not necessarily the global optimal. On the other hand, when using a single-frame image superresolution

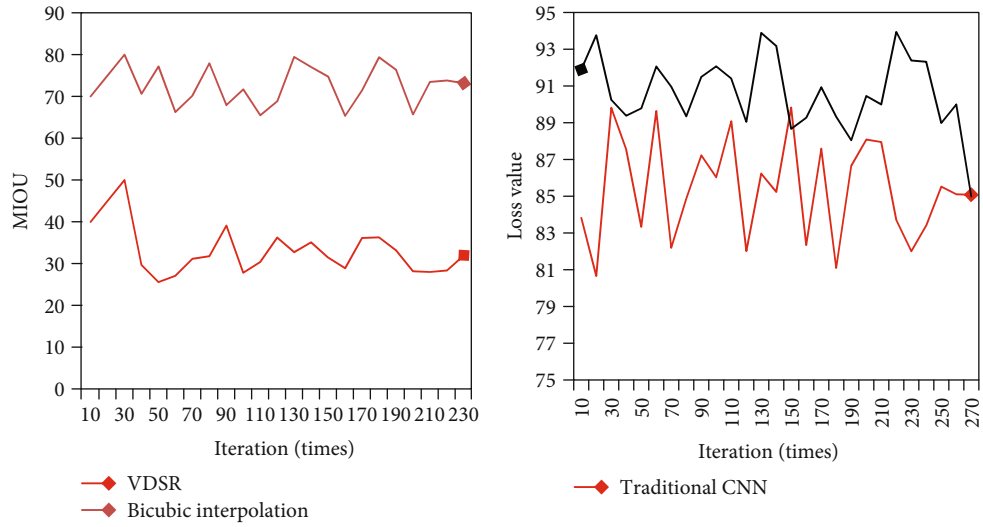

Figure 10: The change of MIOU in the middle layer supervised convolutional neural network model.

convolutional neural network to process images, the input image does not require complex preprocessing, and the hidden layer structure of the convolutional neural network is consistent, which can be distributed calculations, which greatly improves the computational efficiency, thereby improving the efficiency of the entire superresolution reconstruction. Convolutional neural networks are currently used for single-frame image superresolution processing and have achieved good results in image reconstruction efficiency and quality. However, in recent years, some people have used convolutional neural network for motion feature analysis, used the middle layer supervised neural network to extract the time characteristics of sequence images, and achieved certain results in the recognition of motion behavior. This discovery provides the possibility for convolutional neural networks to be used in the superresolution of sequence images [29].

In a convolutional layer of a convolutional neural network, it usually contains one or more feature planes composed of several neurons. All neurons on the same feature plane share weights, and the shared weights here are the convolution kernels. The convolution kernel generally generates a matrix in the form of Gaussian function for initialization and then obtains the weights in the convolution kernel through network training. The superresolution research of a single frame image is considered to be a typical ill-conditioned inverse problem. Most of its ideas are to combine some prior knowledge and use regularization methods to improve image quality. When there are more input images, that is, multiple continuous images are input, more structural similarity and information redundancy of the images are obtained. Using these additional information and previous image knowledge can better integrate and improve the image quality, so that the output image quality is better. Therefore, the research on the superresolution reconstruction algorithm of sequence images has gradually gained people's attention.

The last layer of the network is the image reconstruction layer. In traditional methods, it is often necessary to decompose the whole image into small image blocks and then restore the small image blocks, respectively. Finally, all image blocks are overlapped and fused, and the blocking effect is eliminated for the overlapped part of the image blocks. In srcnn algorithm, the operation of image reconstruction layer is to reconstruct the features extracted from the above network layer into a high-resolution image and smooth filter the image to obtain the final high-resolution image. This overlapping addition operation can also be regarded as a filtering operation in convolutional neural network, which is consistent with the previous network layer. In the stage of image superresolution reconstruction, image preprocessing is carried out first, and the image to be reconstructed is expanded by cubic convolution interpolation according to the superresolution factor. Then, the mapping coefficients are obtained, the interpolated three frame sequence images are input into the trained network, and the high and low resolution image mapping coefficients of the sampled frame images are solved through the network. Finally, the high-resolution image is solved, the mapping coefficient gray and the sampling frame interpolation input image are point multiplied, and the solution result is normalized to obtain the high-resolution output image [30].

The result of image registration directly affects the effect of subsequent image reconstruction. Only with accurate motion estimation can it be possible to accurately find the correspondence between high and low resolution subimage blocks and to obtain a better superresolution effect. However, in the case of complex motion, on the one hand, the number of images directly affects the computational efficiency of the motion estimation algorithm. To obtain accurate motion estimation, enough images are required, which will lead to a higher computational complexity of the algorithm. On the other hand, the current motion matching technology is difficult to ensure that its accuracy

requirements are met every time. If the accuracy of motion estimation is too poor, the registered image may have ghosts or mismatches, which will lead to poor subsequent superresolution reconstruction effects. It may even appear worse than the original image quality.

5. Conclusion

This research analyzes the difficult problems in the research of traditional serial remote sensing image superresolution, and realizes that the essence of motion estimation is to use the motion information between remote sensing images. Therefore, the middle layer convolutional neural network is studied, and the convolutional neural network is used to extract the sequence. The spatiotemporal characteristics of remote sensing images and the continuous optimization of parameters are improved on the basis of the superresolution convolutional neural network of single-frame remote sensing images. The superresolution algorithm of sequential remote sensing images based on the intermediate layer convolutional neural network is proposed, which avoids the traditional motion estimation problem in the superresolution algorithm of sequence remote sensing images has achieved good superresolution results. In addition, in order to improve the efficiency of the serial remote sensing image superresolution algorithm based on the intermediate layer convolutional neural network, the dictionary learning superresolution algorithm based on sparse representation is used for reference, and the convolutional neural network is used to obtain the coefficient matrix, which reduces the network scale. Improve the efficiency of superresolution calculation. There is a large amount of redundant information in the front and rear frames. If you directly use the single-frame remote sensing image superresolution processing, you may also achieve better results, but it is very wasteful, and the efficiency will not be improved. Sequence remote sensing image superresolution algorithms may be able to use redundant information and use a smaller-scale network for superresolution processing to achieve faster efficiency.

Data Availability

The data that support the findings of this study are available from the corresponding author upon reasonable request.

Conflicts of Interest

The author declared no potential conflicts of interest with respect to the research, authorship, and/or publication of this article.

Acknowledgments

The research was partially sponsored by the Scientific Research Program in Shaanxi Provincial Department of Education (Grant No. 20JK0583).

References

[1] C. Gong, J. Han, and X. Lu, "Remote sensing image scene classification: benchmark and state of the art," *Proceedings of the IEEE*, vol. 105, no. 10, pp. 1865–1883, 2017.

[2] Z. Zhang and N. Saito, "Phlst with adaptive tiling and its application to antarctic remote sensing image approximation," *Inverse Problems & Imaging*, vol. 8, no. 1, pp. 321–337, 2014.

[3] G. Alimjan, T. Sun, Y. Liang, H. Jumahun, and Y. Guan, "A new technique for remote sensing image classification based on combinatorial algorithm of SVM and KNN," *International Journal of Pattern Recognition and Artificial Intelligence*, vol. 32, no. 7, p. 1859012, 2018.

[4] G. Cheng, Z. Li, X. Yao, L. Guo, and Z. Wei, "Remote sensing image scene classification using bag of convolutional features," *IEEE Geoscience and Remote Sensing Letters*, vol. 14, no. 10, pp. 1735–1739, 2017.

[5] S. Wang, D. Quan, X. Liang, M. Ning, Y. Guo, and L. Jiao, "A deep learning framework for remote sensing image registration," *ISPRS Journal of Photogrammetry and Remote Sensing*, vol. 145, pp. 148–164, 2018.

[6] Y. Guo, X. Jia, and D. Paull, "Effective sequential classifier training for SVM-based multitemporal remote sensing image classification," *IEEE Transactions on Image Processing*, vol. 27, no. 6, pp. 3036–3048, 2017.

[7] J. Munoz-Mari, E. Izquierdo-Verdiguier, M. Campos-Taberner et al., "HyperLabelMe : a web platform for benchmarking remote-sensing image classifiers," *IEEE Geoence & Remote Sensing Magazine*, vol. 5, no. 4, pp. 79–85, 2017.

[8] M. Gohil, N. Patel, and R. D. Kamboj, "Investigation and analysis of land use/land cover (LULC) change using remote sensing image interpretation for urban area of Rajkot municipal corporation, Gujarat," *Disaster Advances*, vol. 14, no. 16, pp. 28–34, 2021.

[9] C. Yu, L. Wang, J. Zhao, L. Hao, and Y. Shen, "Remote sensing image classification based on RBF neural network based on fuzzy C-means clustering algorithm," *Journal of Intelligent Fuzzy Systems*, vol. 38, no. 4, pp. 3567–3574, 2020.

[10] F. Sun, H. Li, Z. Liu, X. Li, and Z. Wu, "Arbitrary-angle bounding box based location for object detection in remote sensing image," *European Journal of Remote Sensing*, vol. 54, no. 1, pp. 102–116, 2021.

[11] D. Hou, Z. Miao, H. Xing, and H. Wu, "Two novel benchmark datasets from ArcGIS and bing world imagery for remote sensing image retrieval," *International Journal of Remote Sensing*, vol. 42, no. 1, pp. 240–258, 2021.

[12] J. Uthayakumar, M. Elhoseny, and K. Shankar, "Highly reliable and Low-Complexity image compression scheme using neighborhood correlation sequence algorithm in WSN," *IEEE Transactions on Reliability*, vol. 69, no. 4, pp. 1398–1423, 2020.

[13] Z. Zhang, Y. Liu, T. Liu, Z. Lin, and S. Wang, "DAGN: a real-time UAV remote sensing image vehicle detection framework," *IEEE Geoscience and Remote Sensing Letters*, vol. 17, no. 11, pp. 1884–1888, 2020.

[14] H. Chen, Y. Zhang, M. K. Kalra et al., "Low-dose CT with a residual encoder-decoder convolutional neural network," *IEEE Transactions on Medical Imaging*, vol. 36, no. 12, pp. 2524–2535, 2017.

[15] C. Zhang, P. Wang, K. Chen, and J. K. Kämäräinen, "Identity-aware convolutional neural networks for facial expression

recognition," *Journal of Systems Engineering and Electronics*, vol. 28, no. 4, pp. 784–792, 2017.

[16] S. Kruthiventi, K. Ayush, and R. V. Babu, "DeepFix: a fully convolutional neural network for predicting human eye fixations," *IEEE Transactions on Image Processing*, vol. 26, no. 9, pp. 4446–4456, 2017.

[17] E. Laxmi Lydia, J. S. Raj, R. P. Selvam, M. Elhoseny, and K. Shankar, "Application of discrete transforms with selective coefficients for blind image watermarking," *Transactions on Emerging Telecommunications Technologies*, vol. 32, no. 2, article e377, 2021.

[18] W. Shen, M. Zhou, F. Yang et al., "Multi-crop convolutional neural networks for lung nodule malignancy suspiciousness classification," *Pattern Recognition*, vol. 61, no. 61, pp. 663–673, 2017.

[19] Y. Hou, Z. Li, P. Wang, and W. Li, "Skeleton optical spectra-based action recognition using convolutional neural networks," *IEEE Transactions on Circuits and Systems for Video Technology*, vol. 28, no. 3, pp. 807–811, 2018.

[20] U. R. Acharya, H. Fujita, O. S. Lih, M. Adam, J. H. Tan, and C. K. Chua, "Automated detection of coronary artery disease using different durations of ECG segments with convolutional neural network," *Knowledge-Based Systems*, vol. 132, pp. 62–71, 2017.

[21] C. Yuan, X. Li, Q. Wu, J. Li, and X. Sun, "Fingerprint liveness detection from different fingerprint materials using convolutional neural network and principal component analysis," *Computers, Materials and Continua*, vol. 53, no. 4, pp. 357–371, 2017.

[22] S. Biswas, D. Devi, and M. Chakraborty, "A hybrid case based reasoning model for classification in Internet of Things (Iot) environment," *Journal of Organizational and End User Computing*, vol. 30, no. 4, pp. 104–122, 2018.

[23] J. Zhu, S. Liao, Z. Lei, and S. Z. Li, "Multi-label convolutional neural network based pedestrian attribute classification," *Image and Vision Computing*, vol. 58, pp. 224–229, 2017.

[24] S. Poria, H. Peng, A. Hussain, N. Howard, and E. Cambria, "Ensemble application of convolutional neural networks and multiple kernel learning for multimodal sentiment analysis," *Neurocomputing*, vol. 261, pp. 217–230, 2017.

[25] Q. Liu, X. Lu, Z. He, C. Zhang, and W. S. Chen, "Deep convolutional neural networks for thermal infrared object tracking," *Knowledge-Based Systems*, vol. 134, pp. 189–198, 2017.

[26] P. Khosravi, E. Kazemi, M. Imielinski, O. Elemento, and I. Hajirasouliha, "Deep convolutional neural networks enable discrimination of heterogeneous digital pathology images," *eBioMedicine*, vol. 27, pp. 317–328, 2018.

[27] J. C. Hou, S. S. Wang, Y. H. Lai, Y. Tsao, H. W. Chang, and H. M. Wang, "Audio-visual speech enhancement using multimodal deep convolutional neural networks," *IEEE Transactions on Emerging Topics in Computational Intelligence*, vol. 2, no. 2, pp. 117–128, 2018.

[28] Y. Lu, S. Yi, N. Zeng, Y. Liu, and Y. Zhang, "Identification of Rice diseases using deep convolutional neural networks," *Neurocomputing*, vol. 267, pp. 378–384, 2017.

[29] S. Pang, Z. Yu, and M. A. Orgun, "A novel end-to-end classifier using domain transferred deep convolutional neural networks for biomedical images," *Computer Methods and Programs in Biomedicine*, vol. 140, pp. 283–293, 2017.

[30] Y. Wang, Y. Li, and Q. H. Zhao, "Region-based multiscale segmentation of panchromatic remote sensing image," *Kongzhi yu Juece/Control and Decision*, vol. 33, no. 3, pp. 535–541, 2018.

Hindawi
Journal of Sensors
Volume 2021, Article ID 1500829, 16 pages
https://doi.org/10.1155/2021/1500829

Research Article

Optimized Design of Multilines Center of Subway AFC System via Distributed File System and Bayesian Network Model

Hui Fang,[1,2] **Jiandi Jiang**,[2] **Feng Lin**,[3] **and Wei Zhang**[1]

[1]*Zhejiang University, Hangzhou, Zhejiang 310027, China*
[2]*Mechanical and Electrical Department, Ningbo Rail Transportation Group Co., Ltd., Ningbo, Zhejiang 315040, China*
[3]*Digital Information Division, UniTTEC Co., Ltd., Hangzhou, Zhejiang 310051, China*

Correspondence should be addressed to Wei Zhang; cstzhangwei@zju.edu.cn

Received 7 September 2021; Revised 26 October 2021; Accepted 9 November 2021; Published 20 December 2021

Academic Editor: Mu Zhou

Automatic fare collection system (AFCS) is a modern, automatic, networked toll collection system for rail transit ticket sales, collection, billing, charging, statistics, sorting, and management. To realize the subway transit networking operation, this paper designs the subway AFCS based on a distributed file system (DFS), namely, Gluster File System (GlusterFS). Firstly, the multiline center (MLC) in the subway AFCS is designed to analyze the status and current situation of distributed file processing in subway MLC system; secondly, the relevant technical theories are summarized, the Bayesian Network (BN) theoretical model and DFS are explored, and the principles of four DFS are comparatively analyzed; thirdly, the architecture and cluster mode of GlusterFS is expounded, and then based on GlusterFS, the architecture of subway AFCS is discussed. This paper presents several innovation points: first, the subway AFCS is designed based on GlusterFS by analyzing and aiming at the functional requirements, performance requirements, and safety requirements of the MLC subway system; second, the safety risk analysis (SRA) of AFCS is conducted from six security requirements, and a Web scanning system is designed to ensure the system data security. Finally, the design scheme is used to analyze the subway passenger flow and power consumption. The results demonstrate that the design scheme can competently adapt to three different application scenarios. Through comparison of two deployment modes of the Web scanning system, the data security Web scanning system can ensure the safe operation of the AFCS. Furthermore, the statistical analysis of subway passenger flow and power supply data shows that the proposed scheme can support the smooth operation of the subway system, which has significant practical value.

1. Introduction

As early as the 1970s, some foreign countries have already adopted the automatic fare collection system (AFCS) in urban rail transit (URT) [1]. The current social development and technological advancement have seen the formation of a more intelligent and reliable AFCS [2]. Multiple lines under the same operating entity share a multilines center (MLC) to realize rail transit networking operation through the same MLC and the AFC clearing center (ACC) interface; thus, MLC is the core of the multiline AFCS [3]. The newly built MLC system usually adopts the microservice architecture and runs on the private cloud or container cloud to ensure high availability, scalability, and operability [4]. The system itself or its internal services generally invoke each other through Remote Procedure Call Protocol (RPC), while such core data as transaction and reconciliation in the subway system is usually transmitted through the File Transfer Protocol (FTP) service in the form of files. The FTP server is essentially a long-connected and stateful service based on Transmission Control Protocol (TCP), which is usually single [5]. Additionally, new features, such as microservices, virtualization, and containerization also require the infrastructure layer to provide the function of sharing data volumes and files [6]. In the subway MLC system, there are mainly four kinds of data files [7]: (1) data interface between MLC and subordinate systems, which is stipulated by the urban subway network specification and contains messages and data files, among which the transaction data files and MLC parameter files are usually transmitted over FTP; (2)

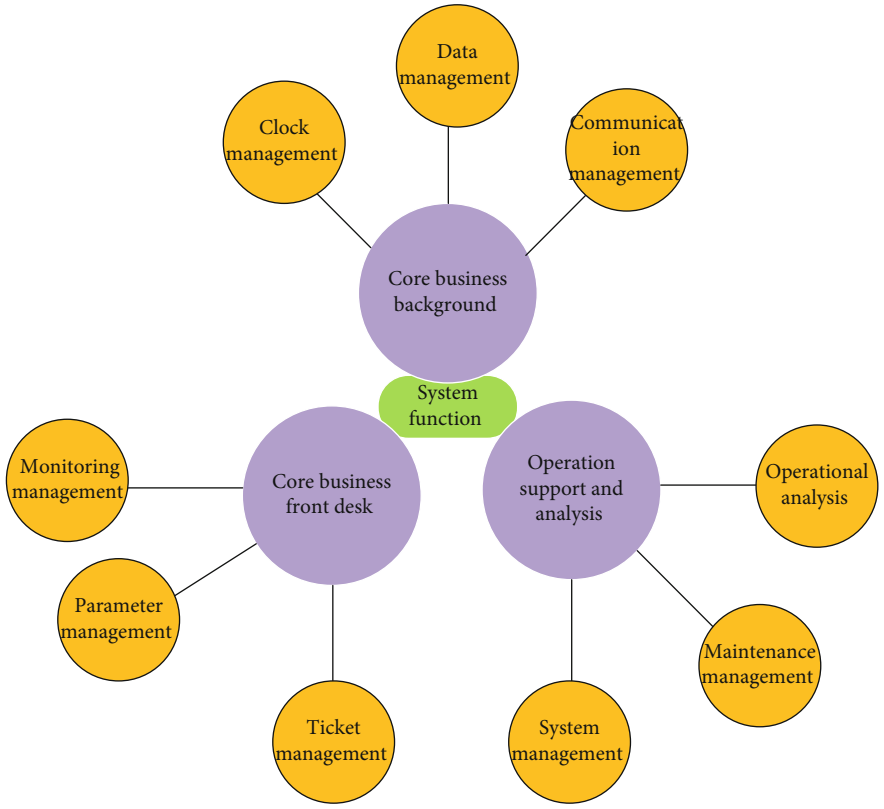

Figure 1: Functions of each systematic module.

data interface between MLC and the subway external system [8], which is jointly negotiated by the MLC system and the external system and can be presented invarious forms, such as messages, message queues, and files. The reconciliation data files are usually transmitted over FTP; (3) intertransmitting data files among subsystems within MLC. For example, the management workbench passes the generated parameter file to the communication service, and the communication service sends the file to the station over FTP [9]; and (4) backup files among primary-spare centers of MLC. Backup data of the master center and the disaster recovery center consists of database and data files [10].

To store data files, MLC usually mounts a block device of Storage Area Networking (SAN) on a computing node and then establishes a local file system (LFS) on the block device. However, the computing node that mounts a SAN volume is a single point, and SAN has some shortcomings. Typically, as a kind of dedicated device, SAN usually designates specific manufacturers for maintenance or expansion in the life cycle of the project. Therefore, the distributed file system (DFS) is taken as a solution scheme [11, 12].

Based on the above description, this paper tries to analyze and meet the functional requirements, performance requirements, and safety requirements of the MLC subway system design. First, four data cluster modes of the DFS software Gluster File System (GlusterFS) are analyzed, and the requirements of subway AFCS are discussed. Then, a subway MLC system is designed based on GlusterFS. Further, the six major risks in the MLC system are explored. Finally, the DFS-based subway security AFCS is constructed to ensure the security of system data, and the design scheme is applied to the concrete scenario. The designed MLC in AFCS cannot only meet the common functions of the subway system, such as ticket selling, checking, billing, charging, statistics, sorting, and management, but also can analyze the safety risks of the subway system and meet the six major safety requirements of the subway system.

2. Overview of Related Technologies

2.1. System Requirement Analysis (RA)

2.1.1. Functional RA. The fundamental functions of the AFCS for subway rail transit in China should include ticket management, ticket price management, data control, and urban rail transit card interface.

According to the overall planning of the system, the system can be roughly divided into three functional modules: core business background, core business foreground, and operation support and analysis. Figure 1 expatiates the functions of each module.

2.1.2. Performance RA. The performance requirements of the subway rail transit system are as follows.

(1) *Elementary Performance Indicator*. System capacity should be able to meet the line access and processing requirements of the maximum passenger flow within the jurisdiction. The system should accept and process the ticket price list and related system

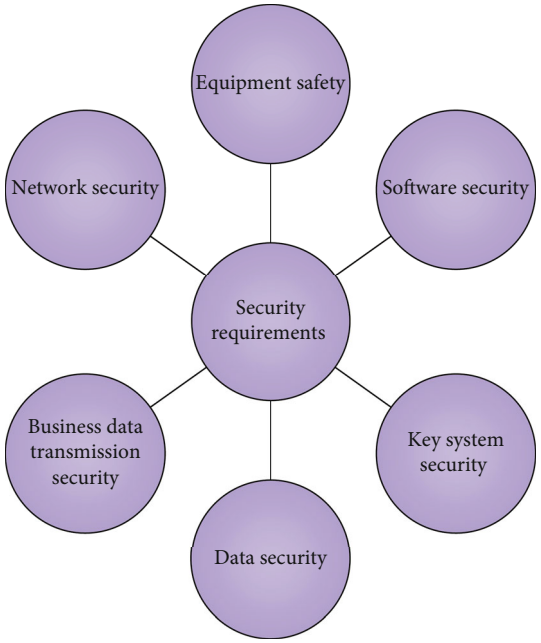

Figure 2: System security requirements.

parameters of the sorting center. In the case of normal network communication conditions, it must have the ability to receive various parameters set by ACC in real-time and issue various commands to SC devices in time

(2) *Transaction Data Processing Performance Indicator*. The system also needs to be able to handle multiple lines simultaneously

(3) *Report Generation Performance Indicator*. All operating reports in the system need to be completed within the specified time

(4) *Data Backup and Recovery Performance Indicator*. The regional center stores and manages the data collected by the station equipment and backs them up in time, so that different operators can sort, reconcile, and restore the damaged or lost data

2.1.3. Security RA. The AFCS is the center of subway rail transit, and security is crucial. Figure 2 demonstrates the security requirements.

Here is the expatiation of Figure 2.

(1) Equipment security

The AFCS needs management equipment to record the information in detail; the system data should be updated in real-time, including the system blacklist and configuration parameters.

(2) Software security

Software security in AFCS primarily refers to user identification, access restrictions, security protection, and monitoring management. Managers of the AFCS need to set the

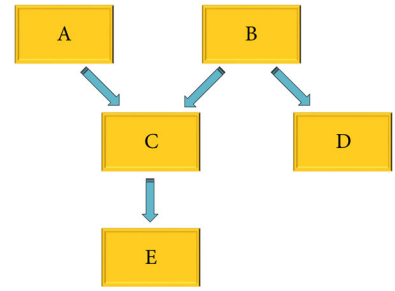

Figure 3: Directed acyclic graph.

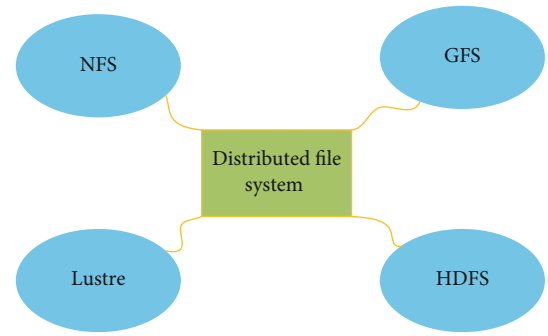

Figure 4: Classification of distributed file system.

corresponding user access accounts and passwords. Only through legal applications can access permissions be obtained. Additionally, the system must have a robust automatic data backup and recovery ability against misoperations.

(3) Key and system security

The key means the main key and sensitive data stored in the SAM card related to all offline transactions. The main key needs to set different versions and indicators to prevent them from losing.

(4) Data security

A considerable amount of transaction data will be generated in the AFCS, which are at risk of leakage, theft, tampering, and damage. Therefore, a complete AFCS must strengthen the management of data security from both hardware and software environments.

2.2. Bayesian Network (BN) Theory. BN is usually regarded as the fusion of the association graph (or directed graph) and Bayes theorem [13, 14]. The BN, or the belief network, mainly indicates the conditional probability relationship and causal relationship between variables. The conditional probability refers to the probability of an event occurring under the occurrence of another event [15], which is most commonly modeled using a directed acyclic graph (DAG). In a DAG, each node represents a variable, and the nodes are associated with each other. Generally, the relationship between nodes is represented by an arrow, illustrating the probability relationship between variables [16, 17]. Figure 3 reveals a simple DAG.

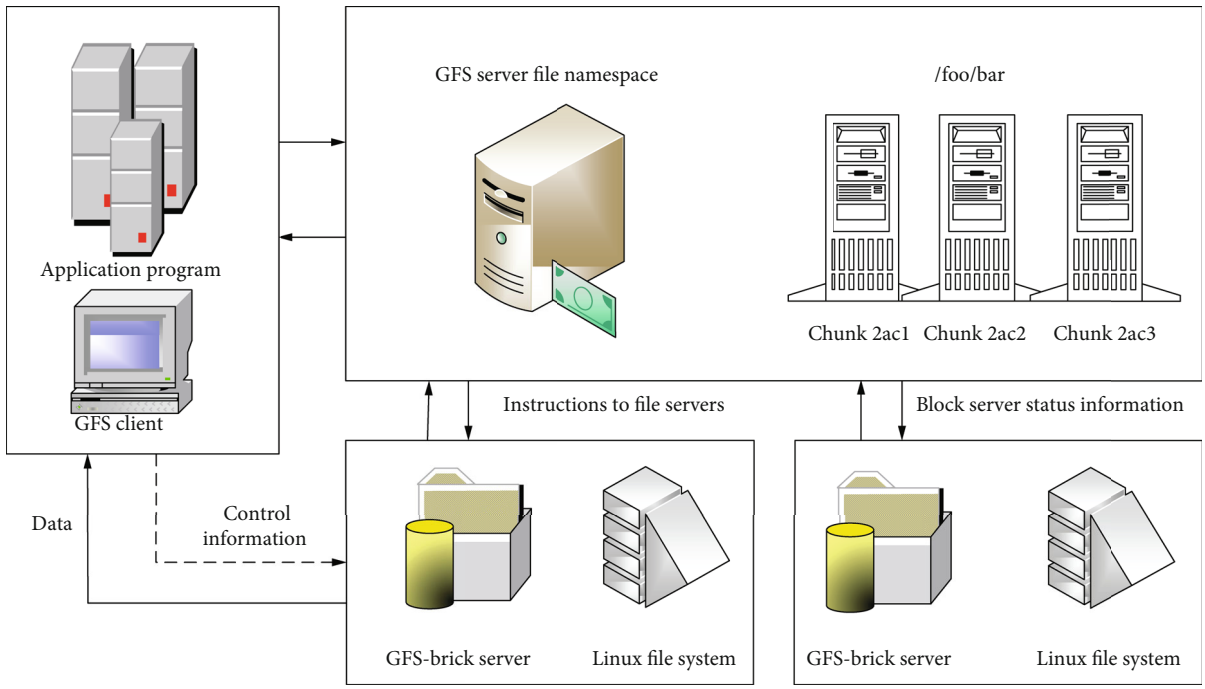

Figure 5: Google File System.

As displayed in Figure 3, the starting and ending nodes of each side are usually defined as the parent node and the child node, respectively; A is the parent node of C, and C is the child node of A; B is also a parent node, A and B are both the parent nodes of C, and C is a common child node of A and B. The node after another node is usually defined as a child node, and the node before another node is usually defined as its parent node [18]. For example, C and E are both the child node of A and B, and E is also a child node of C. In terms of node C, it can be used as either the child node of A and B or the parent node of E. In contrast, D is the unique child node of B. Obviously, the BN is an acyclic network [19, 20].

2.3. DFS

2.3.1. Brief Introduction to DFS. DFS is a storage system that can store data or information in multiple different devices [21, 22]. Its essence lies in the unified management (storage and reading) of computer network files and computer system local files by creating a large file system with a unified name. The DFS is compatible with other file systems with an ordinary file disk interface [23].

2.3.2. Typical DFS. Figure 4 illustrates the categories of DFS.

As shown in Figure 2, DFS contains the Network File System (NFS), Google File System (GFS), Lustre file system, and Hadoop Distributed File System (HDFS) [24].

(1) NFS

NFS provides users with easy and real-time access to network files anywhere through three versions: NFSv2, NFSv3, and NFSv4 by sharing data on remote servers with the local file. The NFS adopts the communication mode of RPC. When users access the network remote file, the NFS client will make a request to the server through the network. After receiving the request, the PRC finds the file access port and then passes the file to the NFS client, so that the file can be accessed normally.

(2) GFS

GFS is a DFS developed by Google, composed of a master node and multiple block servers. As shown in Figure 5, these system nodes are based on Linux machines. The block servers and clients can run simultaneously on a machine equipped with servers with better performance [25].

(3) Lustre file system

The Lustre file system is an open-source file system with high requirements for computer performance. The top ten computers in the world are equipped with the Lustre file system. In a file cluster, the Lustre file system is usually outfitted with tens of thousands of clients, which can handle tens of megabytes of storage. The architecture of the Lustre file system usually includes three parts, namely, metadata server (MDS), object storage server (OSS), and management server (MGS). MDS is mainly used for metadata storage. MDS can process 3 billion files according to statistics. OSS is primarily responsible for the actual exclusive data storage, which can provide multiple network request services for the unit storing the user file data. MGT is responsible for the registration and configuration information of the file system [26]. Figure 6 illustrates the architecture of the Lustre file system.

(4) HDFS

HDFS has strong data processing ability, able to process large data sets across computer clusters. Besides, HDFS has

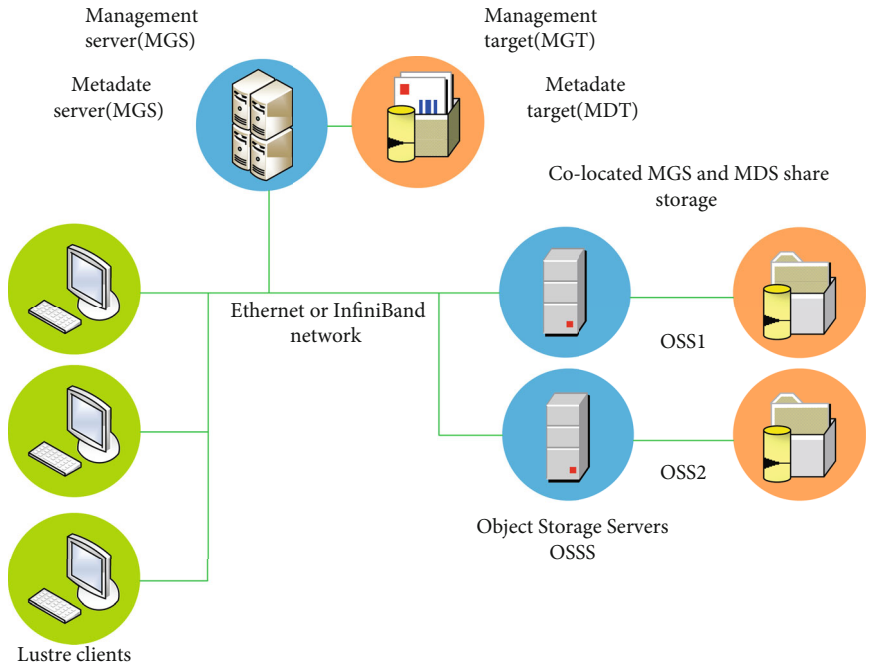

Figure 6: Architecture of the Lustre file system.

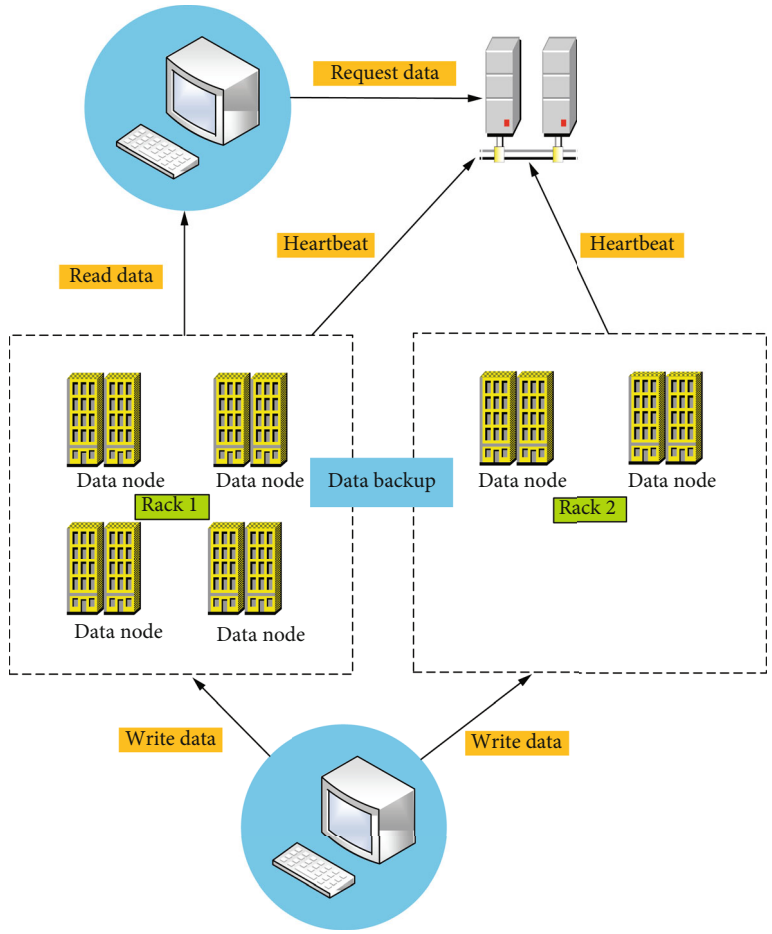

Figure 7: Architecture of Hadoop distributed file system.

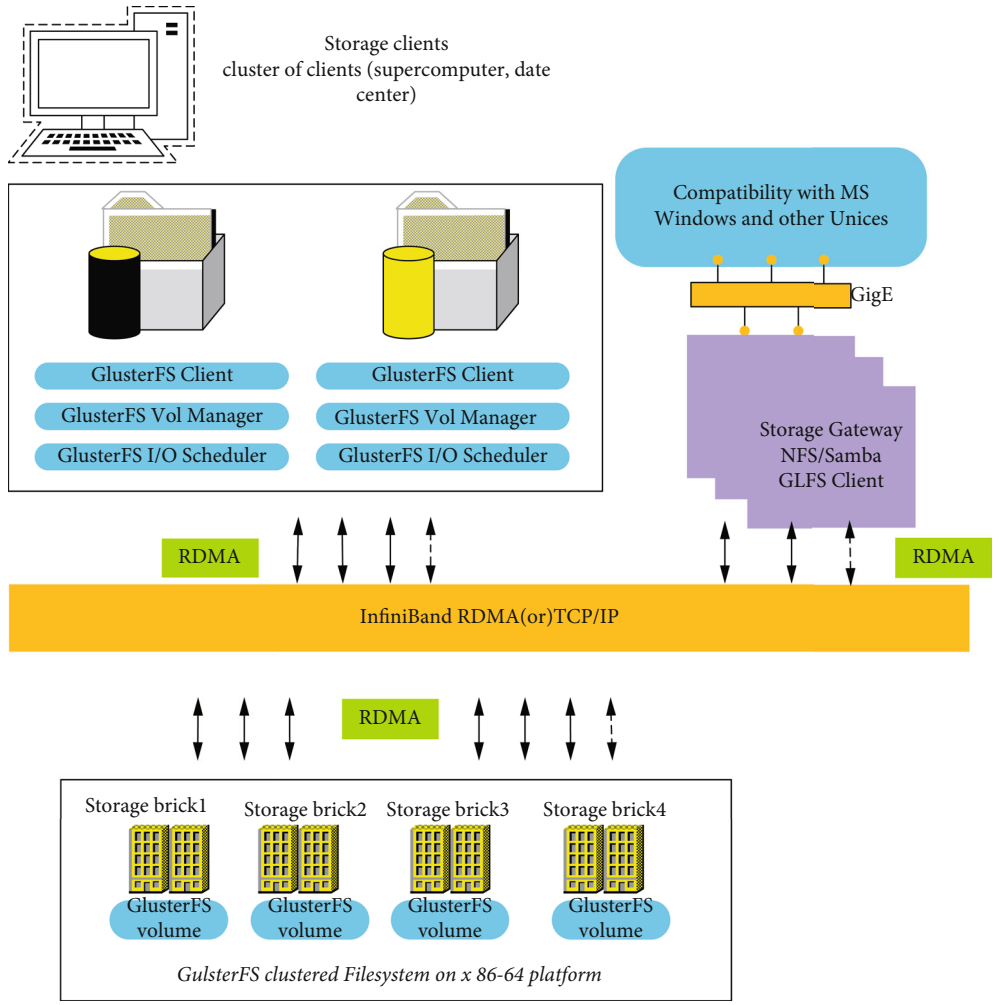

Figure 8: Architecture of Gluster File System.

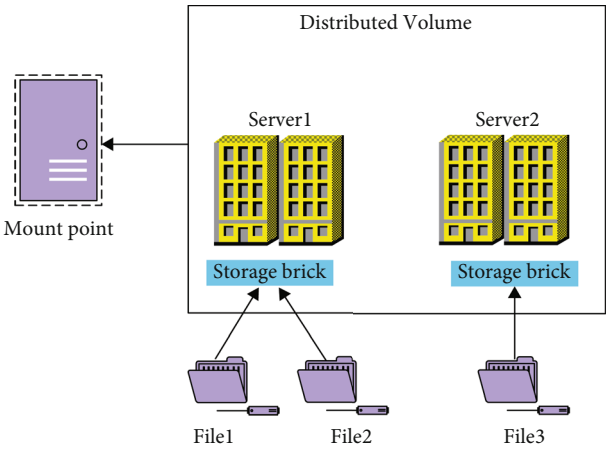

Figure 9: Framework of distributed Gluster File System volume.

low requirements for hardware, so it can run on ordinary and inexpensive hardware. HDFS is divided into metadata of the storage file system and application data. As presented in Figure 7, HDFS can store all files in the system as a series of blocks of the same size [27, 28].

2.3.3. Metadata Management. There are two main ways of metadata management. (1) Centralized metadata management. Centralized metadata only uses one metadata server, which is outstanding in data management. However, it has two inevitable problems of performance bottleneck and single point failure. (2) Distributed metadata management. The distributed metadata management disperses data in multiple servers. Each server is independent with the capability to provide independent data services. This method solves the two inevitable problems of centralized metadata management but also makes the system complicated with a performance overhead and consistency problems [29, 30].

2.4. GlusterFS

2.4.1. Architecture of GlusterFS. GlusterFS is an open-source DFS developed by Red Hat Inc. It has strong horizontal scalability and can integrate data from different servers. Figure 8 provides the architecture of GlusterFS.

Figure 8 shows that the server and client make up the GlusterFS; Remote Direct Memory Access (RDMA) or TCP is used to link the cluster server; the server can contain one or multiple nodes, and each node may contain multiple

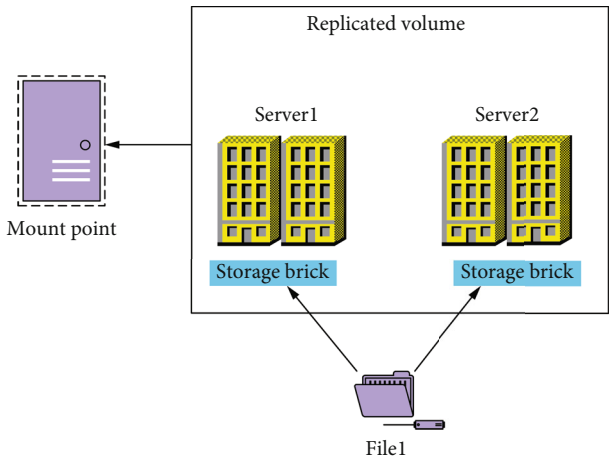

Figure 10: Framework of replicated Gluster File System volume.

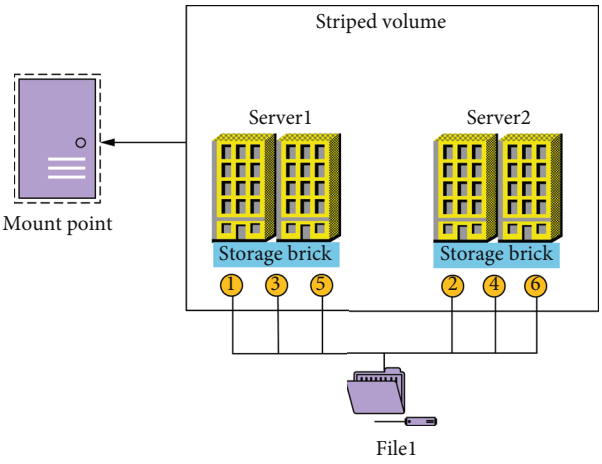

Figure 11: Framework of striped Gluster File System volume.

blocks; additionally, each block can be any directory in the LFS, and then, multiple blocks are combined to form various types of volume.

2.4.2. Cluster Modes of GlusterFS

(1) Distributed GlusterFS Volume (DGV). DGV assigns data files to block through the default algorithm and adjusts the volume capacity at a low cost. However, it cannot guarantee the data fault tolerance. The loss or damage of single block data will lead to the loss or damage of the entire file data. Figure 9 signifies the framework of two-block DGV, which utilizes the default algorithm to determine which block File 1, File 2, and File 3 belong to.

(2) Replicated GlusterFS Volume (RGV). RGV can reduce data damage or loss in DGV through the data backup mechanism of each block. The damaged data can be retrieved from the backup information of other blocks, or the RGV mechanism can be used to repair and restore data, thus greatly improving the fault tolerance. Figure 10 shows the framework of the two-block RGV.

As shown in Figure 10, the information of File 1 is stored in every block, so that the damaged File 1 information can be recovered through other blocks.

(3) Striped GlusterFS Volume (SGV). SGV divides the file into multiple blocks and then puts the file into a separate block in the way of "block packaging," thus achieving low redundancy and fault tolerance. However, SGV can improve the data reading ability. Figure 11 displays a two-block SGV.

(4) Dispersive GlusterFS Volume (DIGV). DIGV is realized based on erasure codes. The reliability can be adjusted by specifying the redundancy when creating a dispersive volume, and the redundancy determines the maximum number of deletable blocks in the volume under normal data access. Figure 12 indicates the six-block DIGV.

In Figure 12, there are six available spaces of DIGV, and the information of File 1 is stored in all six blocks. As long as any block data are normal, File 1 can be read normally. Therefore, DIGV has greater fault tolerance than RGV and SGV.

2.5. Brief Introduction to the AFCS. The AFCS is an automated system for the whole process of rail transit, including ticketing, ticket checking, billing, charging, statistics, sorting, and management, based on computer, communication, network, automatic control, etc. The AFCS of a line often includes three levels, called three subsystems, i.e., the line center system, the station system, and the station terminal equipment. In urban transit, the ACC system is often employed to share information and clear ticket between the lines. Figure 13 provides the basic structure of the AFCS in a subway rail transit project.

3. Design of the Subway MLC System

3.1. Design of Shared MLC of AFCS. First, multiple computing nodes form a DFS cluster, and each computing node mounts and manages its own disk. Meanwhile, the DFS cluster provides remote access interfaces to the external and maps all disks into one or more data volumes. Moreover, a DFS driver is set up on the business server, which connects to the DFS server, mounts remote data volumes as local volumes, and provides standard POSIX interfaces for upper applications. The upper application employs the POSIX interface to read and write local files or read and write remote files, so it needs no change here. Figure 14 represents the logical view of applying DFS in the MLC system.

As illustrated in Figure 14, DFS is the core of all systematic intertransmission files. An application on a server writes files to a remote volume, which can be read in real-time by any other server with the same data volume. Like the relational database, NoSQL, object storage, or other storage middleware, DFS, as a common mechanism for storing and exchanging data files, is the infrastructure provided by the MLC system for business applications. Therefore, MLC should deploy a separate DFS cluster to provide differentiated services to individual business systems.

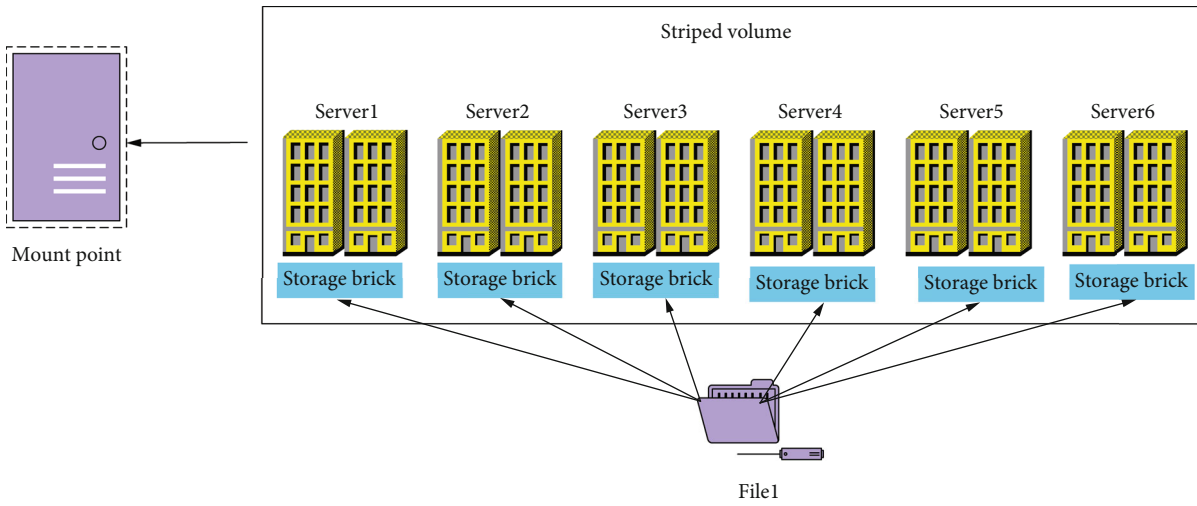

Figure 12: Framework of dispersive Gluster File System volume.

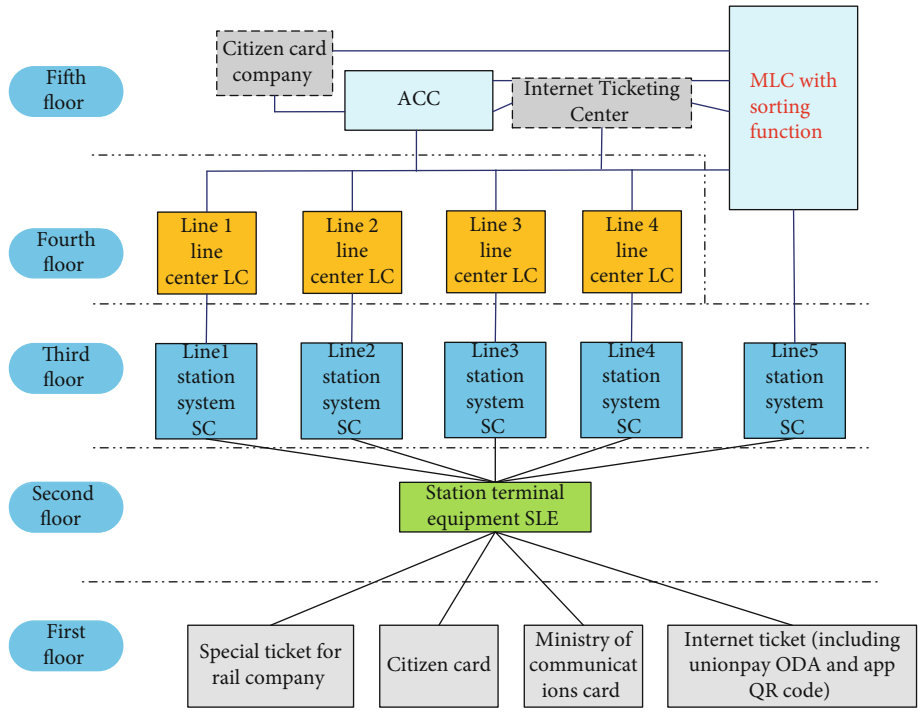

Figure 13: Systematic framework of the AFCS in a subway rail transit project.

Typically, DSF nodes mount local disks directly. DFS servers communicate with each other and automatically synchronize and backup data among nodes to ensure data security and high availability. However, according to the hardware resources of the project, DFS can also mount SAN equipment. At this time, DFS parameters can be adjusted to reduce the number of copies, and the data security is more dependent on SAN. DFS itself only ensures the high availability of computing nodes.

DFS is substantially a kind of technology with several implementation methods. After comparing CIFS, NFS, HDFS, Fast DFS, and other similar protocols or systems, the MLC system chooses GlusterFS or Ceph as the implementation of DFS. GlusterFS is relatively simple with low deployment and maintenance costs, but it is poor in low reading and writing small files. By contrast, Ceph has comprehensive functions and supports three access interfaces, namely, block device, file system, and object storage. Its access interfaces of the block device have been extensively tested in OpenStack. However, Ceph is complicated and requires high maintenance costs. In short, both Ceph and GlusterFS are mature open-source software, not subject to any technical, and Ceph has been transplanted to the domestic ARM server.

3.2. Security Design of Subway AFCS Based on GlusterFS. Figure 15 illustrates the security network architecture of the AFCS.

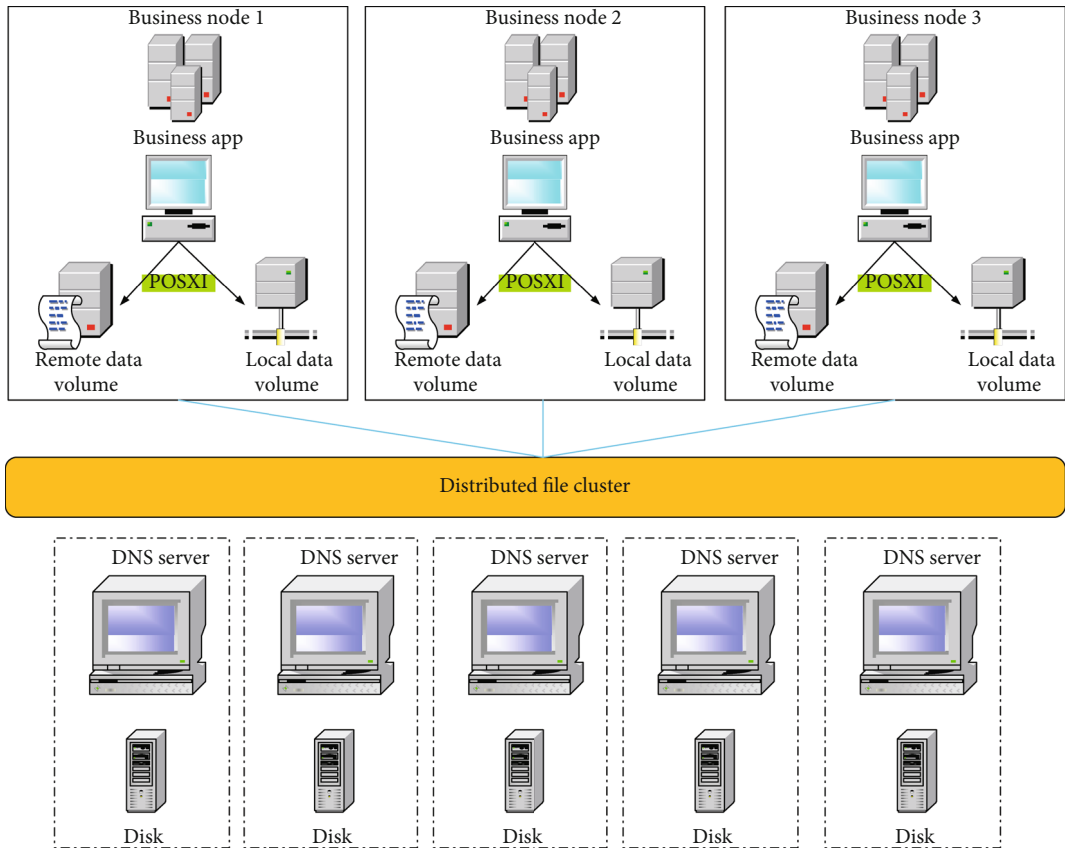

Figure 14: Logical view of applying DFS in the MLC system.

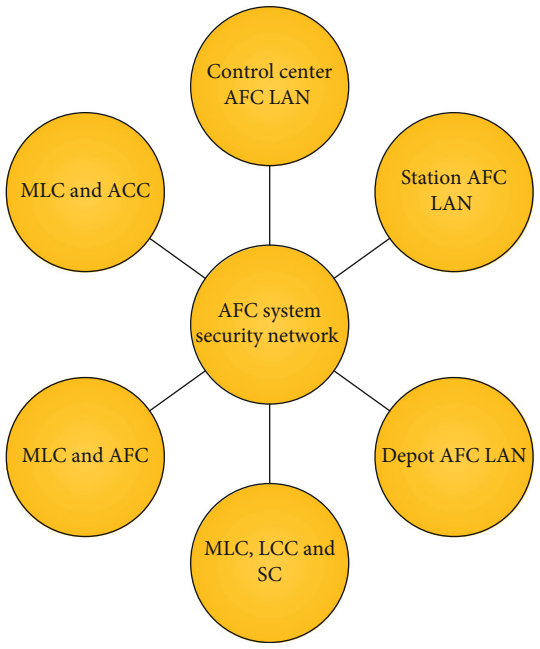

Figure 15: Security network architecture of the AFCS.

In Figure 15, the data transmission channels between the control center MLC and the depot and between MLC and the station are provided by the communication system. Additionally, the data transmission channels among the control center, depot, and the local area network (LAN) of the station AFCS are provided by the AFCS. The control center LAN is the Ethernet of 1,000 Mbps. The whole network adopts a switching-based network structure and considers necessary redundancy design. The station AFC LAN is the Ethernet with an industrial ring structure of 100 Mbps, and the recovery time of the switch ring network breakpoint is not more than 20 milliseconds.

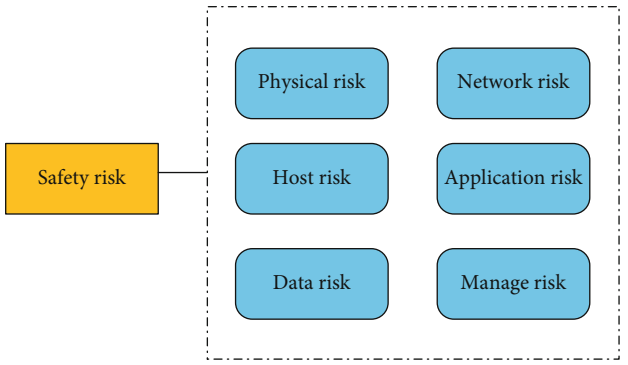

Figure 16: Security risks of the AFCS.

3.2.1. Security Risk Analysis (SRA) of the AFCS. The security risks of rail transit AFCS and network are generally reflected in the following six aspects, as shown in Figure 16.

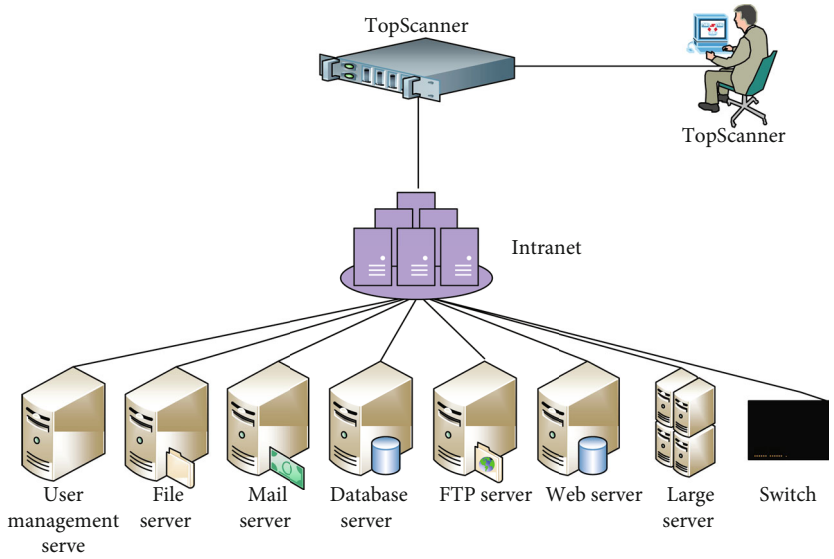

Figure 17: Independent deployment of the Web scanning system.

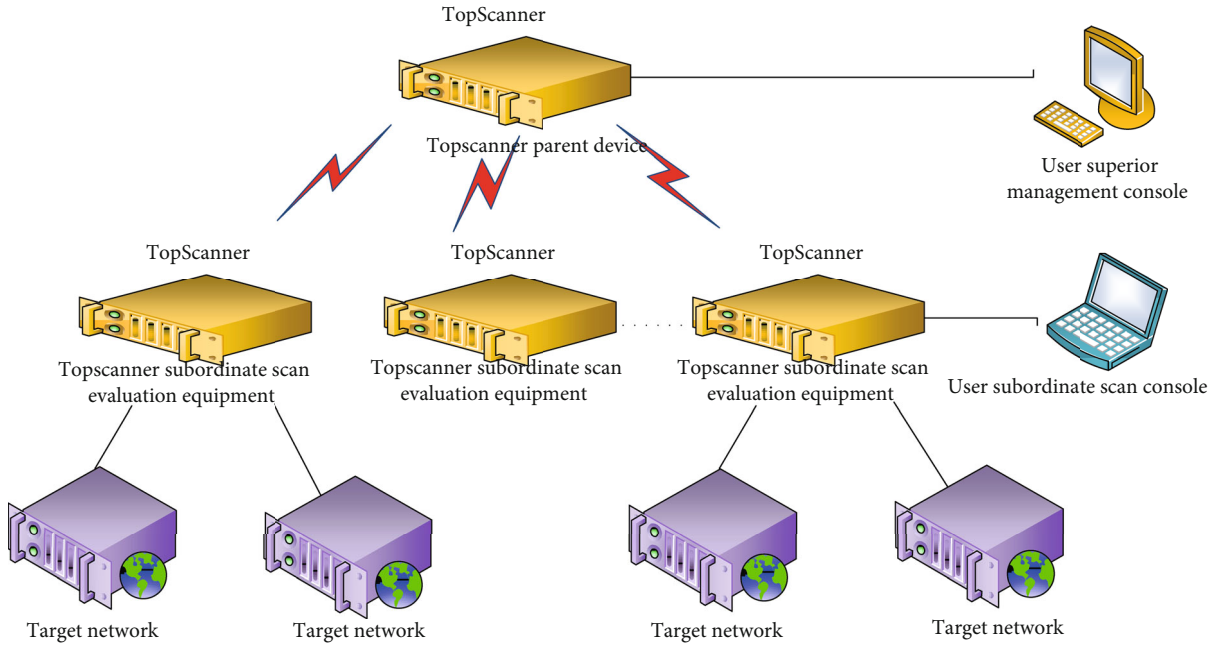

Figure 18: Distributed deployment.

Figure 16 demonstrates that there are six security risks for the AFCS. In this section, a Web scanning system is designed for data risks.

3.2.2. Web Scanning System for the Data Security of the Subway AFCS. A Web scanning system is designed to detect database vulnerabilities. The purpose is to check and evaluate the overall security of the database system, including the settings, the vulnerabilities, and the integrity of the database system. There are two kinds of deployment of the Web scanning system for application scenarios, and Figure 17 reveals an independent deployment.

Figure 17 implies that under independent deployment, only one TopScanner device is deployed in the network to connect to the network with the correct configuration, and then, it can be used normally. Its working range usually includes the entire network address of the user enterprise. The user can log in to the TopScanner system given any address and issue scanning inspection tasks. The address of the inspection task must be within the authorization range of the product and the assigned user. Figure 18 reveals the distributed deployment.

According to Figure 18, the distributed deployment employs several TopScanner systems to work jointly in the large-scale network, which can share and aggregate data among systems, facilitating users' unified management of distributed networks. TopScanner supports the two-level or multilevel distributed or layered deployment by users.

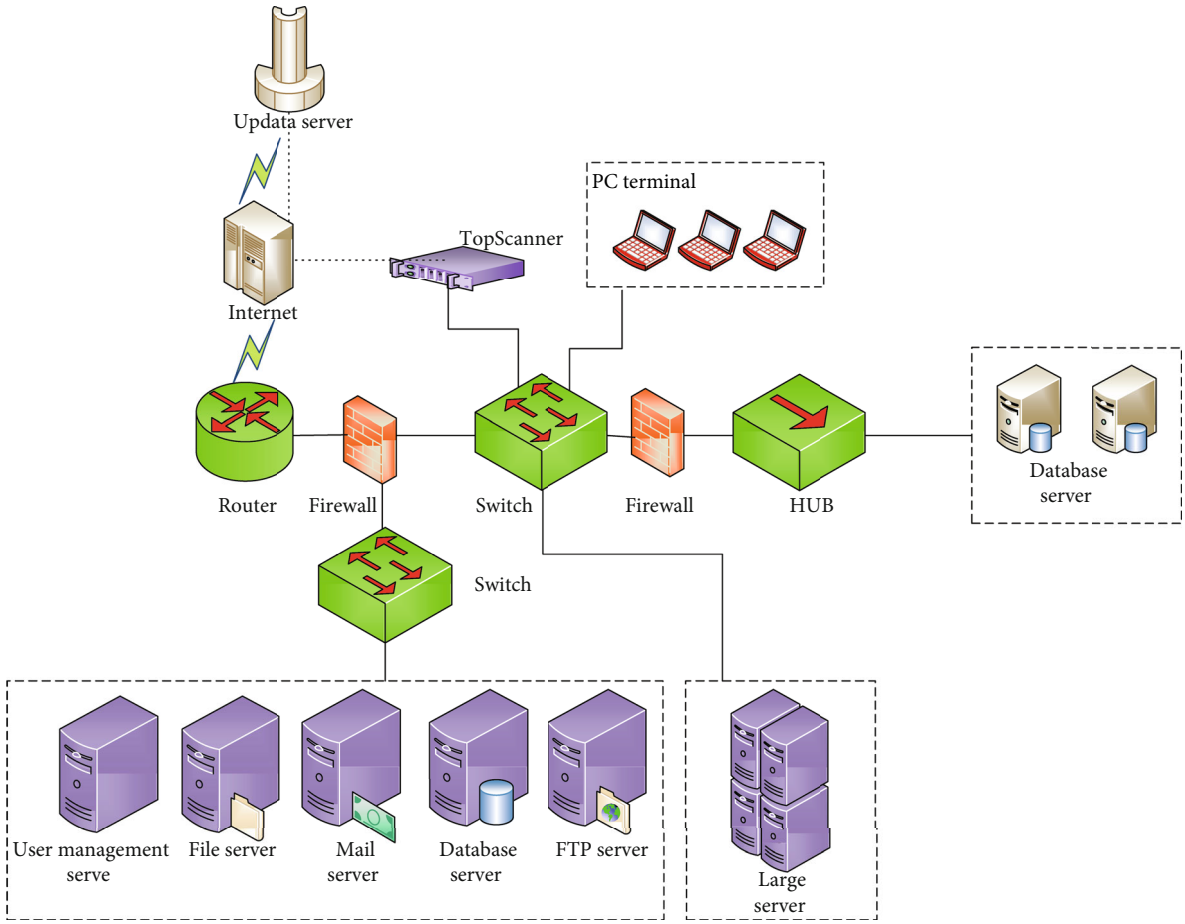

Figure 19: Web database scanning system.

Figure 19 provides the Web database scanning system designed based on the above deployment mode.

On the one hand, the Web scanning system can be deployed on the core switch for safety protection, and the system port addresses are distributed according to different networks. On the other hand, a distributed vulnerability scanning system can be configured alone in different networks to regularly detect the host in multiple different segments of the network and provide corresponding solutions. These solutions have effective protection effects.

3.3. Analysis of System Application Scenarios. The designed DFS is applied to three application scenarios of MLC, including the external data fire interface scenario, container cloud scenario, and primary-spare center data synchronization scenario.

3.3.1. External Data File Interface. Figure 20 is the logic diagram of the external data file interface scenario of MLC.

From Figure 20, the business of the external data file interface of MLC is as follows.

Business 1: MLC builds the FTP server, and the lines and stations upload transaction data, equipment audit data, and other information to the FTP server. MLC monitors the data files in the FTP server in real-time through DFS for analysis. At the same time, MLC writes the operating parameter files to the data volume mounted on the FTP server through DFS, and the station downloads the files through FTP.

Business 2: MLC builds the FTP server, and MLC regularly packs the transit card transaction as a file and stores it in the FTP server through DFS. The railway transit card company downloads the transaction file from FTP and returns the reconciliation file. MLC regularly scans the data volume mounted on FTP and obtains the reconciliation file.

In this scenario, the FTP server and MLC business server mount the same volume of DFS. The external system reads and writes volume files through the FTP interface, and the MLC system reads and writes volume files through the POSIX interface. DFS ensures data security and high availability. Moreover, the FTP server deploys multiple nodes, and multiple service nodes share the same Variable Information Processing (VIP). The FTP service nodes with VIP provide services to the outside world, and other nodes are in a standby state to ensure the high availability of the FTP server.

3.3.2. Persistent Volume (PV) of the K8S Cluster. Figure 21 displays the application scenarios of MLC in the container cloud.

MLC can also be deployed in the container cloud, which is generally managed by the K8S cluster. In the K8S cluster, each server is running on a Pod. After the Pod starts, it can be destroyed and reconstructed at any time. The

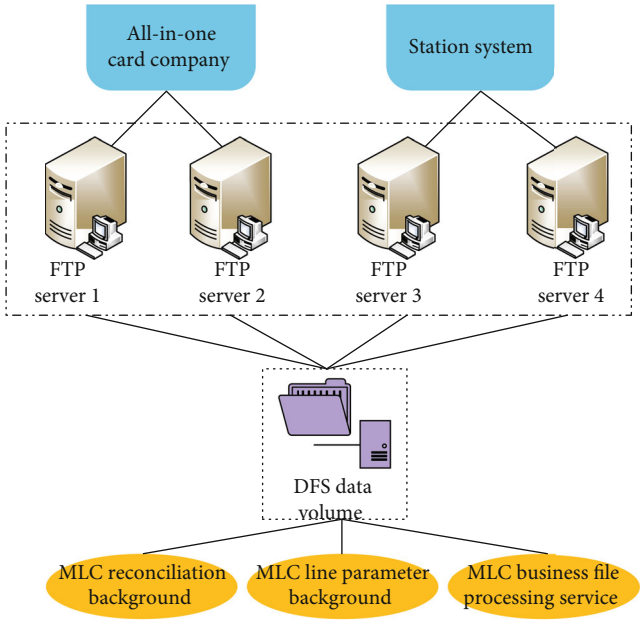

Figure 20: Architecture of the external data file interface of MLC.

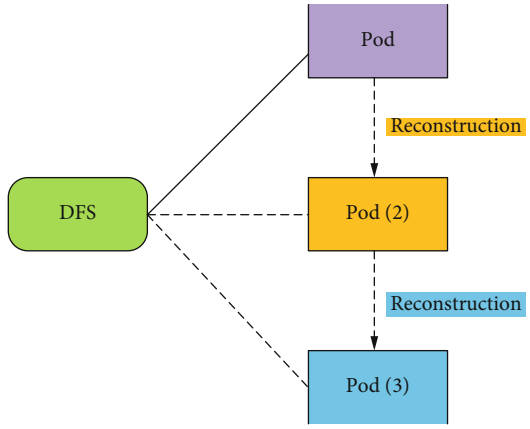

Figure 21: Application scenarios of MLC in the container cloud.

reconstructed Pod is completely new and does not save any state. However, the MLC system is developed from the existing system. In such a case, some servers are stateful, and the state is saved in files. Some middleware is also saved in local files. It is necessary to configure the PV in the K8S cluster through the shared volume service provided by DFS, to support this stateful server.

As shown in Figure 21, firstly, several volumes are allocated in advance in the DFS, and each volume has attributes, such as size. Then, all volumes and their attributes are declared in the form of PV in the K8S cluster. After each Pod is created, it applies for PV to the K8S cluster, and the K8S cluster assigns PV that meets the conditions to the Pod. The server in the Pod writes the state data into the volume corresponding to PV. Besides, the K8S cluster ensures that the allocated PV remains unchanged after the Pod is reconstructed so that the reconstructed Pod can read the previously saved data.

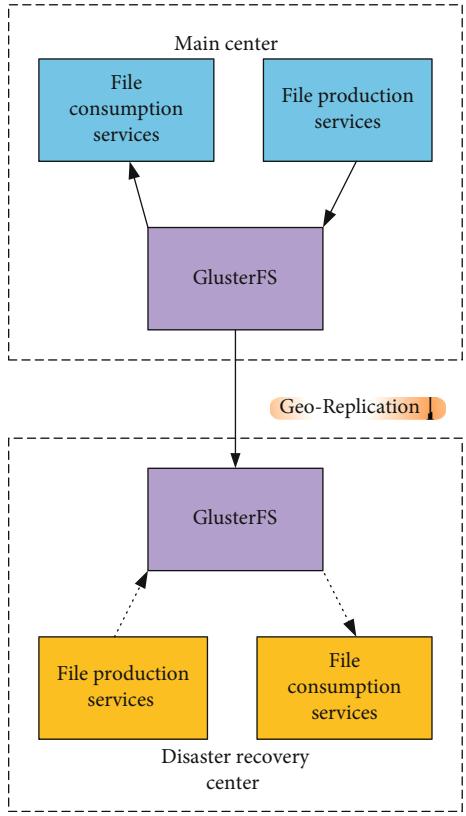

Figure 22: Geo-Replication function.

3.3.3. Primary-Spare Center Data Synchronization. The business files uploaded by the station are parsed by the MLC business processing module and moved to the local backup directory. Meanwhile, these business files are synchronized to the disaster recovery center in time to ensure that the data is not lost in extreme cases. After referring to DFS, the main center and disaster recovery center deploy their own DFS clusters. There are two methods to realize file synchronization between two centers. Figures 22 and 23 describe the main backup center data synchronization application scenarios.

Method 1: synchronizes by the file remote mirroring function of DFS, such as the Geo-Replication function of GlusterFS, as shown in Figure 22.

Method 2: the data volumes of two DFS clusters of the primary-spare center and the disaster recovery center are simultaneously mounted on the backup node of the disaster recovery center, and the folders are synchronized through the local file interface, as shown in Figure 23.

According to the above analysis, this MLC system has strong adaptability in different application scenarios, which proves that the designed scheme has high practical value.

3.3.4. Analysis of the Passenger Flow and Power Consumption of the System. This section verifies the data analysis ability of the proposed DFS-based subway AFCS from passenger flow and electric energy. Figure 24 indicates the statistical results of passenger flow.

According to statistical data in Figure 24, passenger flow increases from 8 : 00 to 20 : 00, decreases slightly at noon and afternoon, and peaks in the morning and evening. The

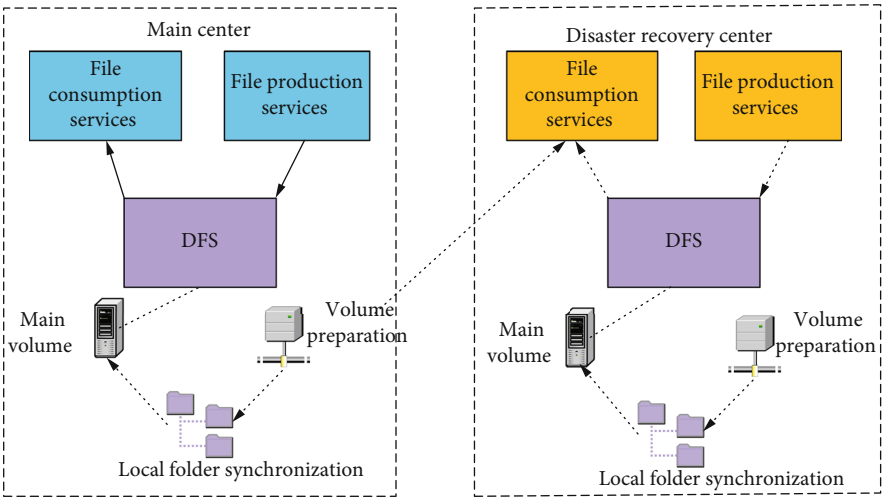

Figure 23: Data volumes in the DFS cluster.

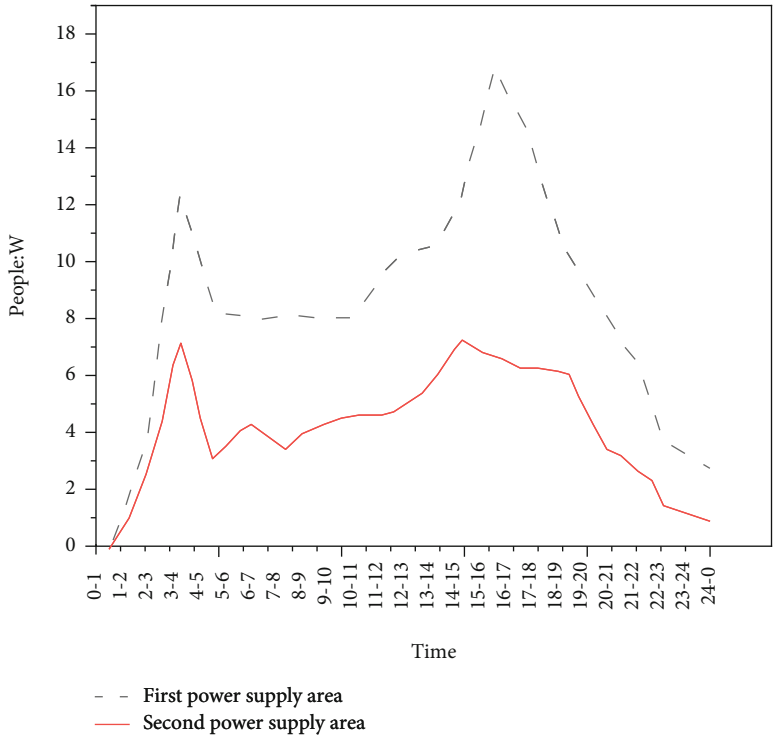

Figure 24: Statistical results of passenger flow.

passenger flow statistics results indicate that the passenger flow statistics of the proposed AFCS are in line with the actual situation, and the proposed AFCS can accurately predict the passenger flow of the first power supply area and the second power supply area. Figure 25 reveals the statistical results of power consumption.

As presented in Figure 25, the power consumption in the first power supply area is higher than that in the second power supply area. Moreover, the trend of consumption is consistent with the trend of passenger flow, and the power consumption increases sharply in the evening peak period. The comparative analysis of Figures 24 and 25 shows that the power consumption of the subway system is positively correlated with the passenger flow; besides, in the same power supply area, the time-variation of the power consumption and passenger flow of the subway system are consistent, which proves that the surge of power consumption of the subway system is caused by the change of passenger flow. The result proves that this AFCS can statistically analyze the subway data and provide accurate results, showing excellent feasibility and practicability. Table 1 displays the comparison between the actual and predicted passenger flow of the proposed subway AFCS during peak hours.

Table 1 demonstrates that the analysis forecasted errors of passenger flow in the first power supply area are 3.9%, 1.4%, and 3.4%, respectively, during three different periods.

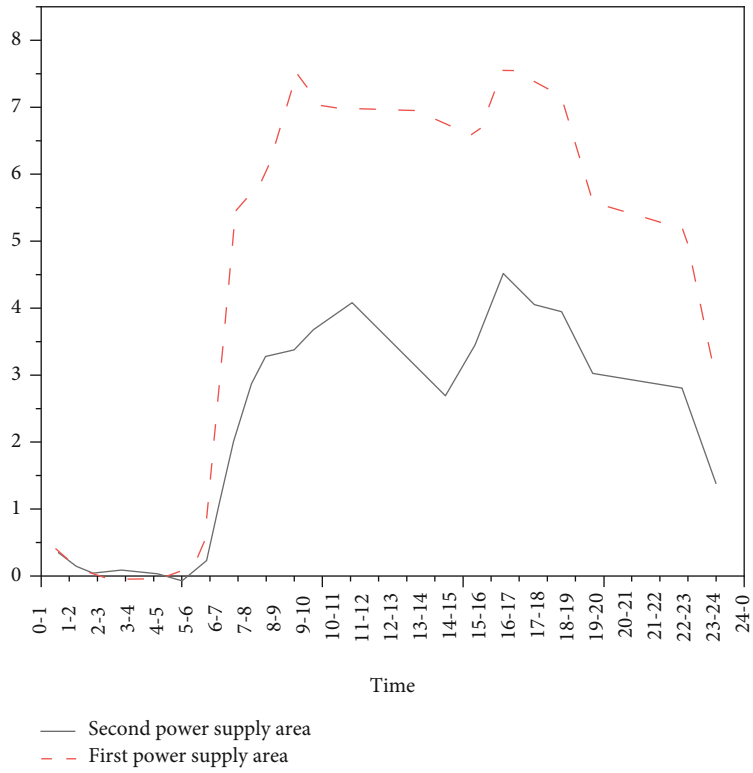

Figure 25: Statistical results of power consumption.

Table 1: Comparison between actual and predicted passenger flow of subway AFCS.

		8 : 00 AM -9 : 00 AM passenger flow (ten thousand)	11 : 00 AM-12 : 00 AM passenger flow (ten thousand)	14 : 00-15 : 00 passenger flow (ten thousand)
First power supply area	Analysis forecasted value	10.70	13.28	14.59
	Actual value	10.29	13.09	14.10
Second power supply area	Analysis forecasted value	4.61	5.38	6.91
	Actual value	4.21	5.08	6.61

The passenger flow analysis predicted errors of the second power supply area are 9.5%, 5.9%, and 4.5%, respectively, during three different periods, and the average error of the two power supply areas is 4.78%, indicating that the data analysis ability of the proposed subway AFCS is strong. Thus, the proposed AFCS can be used for subway information prediction and analysis.

4. Conclusion

Based on DFS, an MLC for subway AFCS is constructed, and a Web scanning system is designed for the data security of the subway AFCS. The conclusions are as follows.

(1) The subway AFCS based on GlusterFS can realize information management, data management, operation control, and ticket management within the jurisdiction of the subway

(2) The security system based on GlusterFS can maximally protest the whole system against attacks by the external network and prevent system data damage, which greatly improves the antirisk ability of the system

(3) The analysis results of subway passenger flow and power supply confirm the practical value of the system reported here

Data Availability

The labeled dataset used to support the findings of this study are available from the corresponding author upon request.

Conflicts of Interest

The authors declare no competing interests.

Authors' Contributions

Hui Fang designed technical route, performed the analyses, and wrote initial draft. Jiandi Jiang collected and managed the data and performed the analysis. Feng Lin reviewed and revised the manuscript. Wei Zhang provided direction selection, designed technical route, and edited manuscript.

Acknowledgments

This work was supported by the national key research and development program of China (2018yfb2101300).

References

[1] A. Salem, "Design, implementation and control of a SiC-based T5MLC induction drive system," *IEEE Access*, vol. 8, no. 99, pp. 82769–82780, 2020.

[2] P. Kurčík, M. Blatnický, J. Dižo, A. Pavlík, and J. Harušinec, "Design of a technical solution for a metro door system," *Transportation Research Procedia*, vol. 40, pp. 767–773, 2019.

[3] A. P. Rodrigues, R. Fernandes, and P. Vijaya, "Performance study on indexing and accessing of small file in Hadoop distributed file system," *Journal of Information & Knowledge Management*, vol. 20, no. 4, pp. 31–46, 2021.

[4] L. Tong, N. Liu, and S. Hu, "Study on key design parameters of subway source heat pump system with capillary exchanger," *Renewable Energy*, vol. 164, pp. 183–193, 2021.

[5] Q. Li, J. Loy-Benitez, S. K. Heo, S. Lee, H. Liu, and C. K. Yoo, "Flexible real-time ventilation design in a subway station accommodating the various outdoor PM_{10} air quality from climate change variation," *Building and Environment*, vol. 153, no. 4, pp. 77–90, 2019.

[6] J. Jiang, H. Nggar, and C. Xu, "Effect of ground motion characteristics on seismic fragility of the subway station," *Soil Dynamics and Earthquake Engineering*, vol. 143, no. 5, pp. 1169–1174, 2021.

[7] Q. J. Chen, T. Y. Zhang, N. Hong, and B. Huang, "Seismic performance of a subway station-tunnel junction structure: a shaking table investigation and numerical analysis," *KSCE Journal of Civil Engineering*, vol. 25, no. 5, pp. 1653–1669, 2021.

[8] P. A. Song, H. W. Wang, and X. X. Zhang, "An investigation on energy consumption of air conditioning system in Beijing subway stations," *Energy Procedia*, vol. 142, pp. 2568–2573, 2019.

[9] M. Méndez, "Operación Araña: reflections on how a performative intervention in Buenos Aires's subway system can help rethink feminist activism," *Estudos históricos*, vol. 33, no. 70, pp. 280–297, 2020.

[10] D. Gong and G. Li, "Research on multi-objective optimized target speed curve of subway operation based on ATO system," *International Core Journal of Engineering*, vol. 6, no. 2, pp. 133–137, 2020.

[11] A. S. Yadav, S. Agrawal, and D. S. Kushwaha, "Distributed ledger technology-based land transaction system with trusted nodes consensus mechanism," *Journal of King Saud University - Computer and Information Sciences*, 2021.

[12] H. E. Ciritoglu, T. Saber, and T. S. Buda, "Hadoop distributed file system," pp. 104–111, 2018.

[13] Y. Zhai, J. Tchaye-Kondi, and K. J. Lin, "Hadoop Perfect File: a fast and memory-efficient metadata access archive file to face small files problem in HDFS," *Computing*, vol. 156, pp. 119–130, 2021.

[14] J. Zou, A. Iyengar, and C. Jermaine, "Architecture of a distributed storage that combines file system, memory, and computation in a single layer," *The VLDB Journal*, vol. 29, no. 5, pp. 1049–1073, 2020.

[15] C. Chen, X. M. Liu, and Q. Li, "A rear-end collision risk evaluation and control scheme using a Bayesian network model," *IEEE Transactions on Intelligent Transportation Systems*, vol. 20, no. 1, pp. 264–284, 2019.

[16] C. Stokes, G. Masselink, M. Revie, T. Scott, D. Purves, and T. Walters, "Application of multiple linear regression and Bayesian belief network approaches to model life risk to beach users in the UK," *Ocean & Coastal Management*, vol. 139, no. 4, pp. 12–23, 2017.

[17] Y. Zhao, S. Hua, and X. Ren, "Relevance research of threat/error and undesired states in air traffic management based on Bayesian network model," *Journal of Air Transport Management*, vol. 60, no. 5, pp. 45–48, 2017.

[18] S. Gheisari and M. R. Meybodi, "A new reasoning and learning model for cognitive wireless sensor networks based on Bayesian networks and learning automata cooperation," *Computer Networks*, vol. 124, no. 12, pp. 11–26, 2017.

[19] L. Wu, "Student model construction of intelligent teaching system based on Bayesian network," *Personal and Ubiquitous Computing*, vol. 24, no. 3, pp. 419–428, 2020.

[20] A. Kab, B. Sl, and A. Ksp, "Detection of lung cancer by modified irregular tree structure Bayesian network model-based image segmentation," *Materials Today: Proceedings*, vol. 11, no. 3, pp. 1130–1138, 2021.

[21] V. S. Marichamy and V. Natarajan, "Big data performance analysis on a Hadoop Distributed File System based on geometric data perturbation technique," *Procedia Computer Science*, vol. 165, pp. 415–420, 2019.

[22] M. Alhowaidi, B. Ramamurthy, B. Bockelman, and D. Swanson, "Enhancing the SDTMA-NDN architecture for transferring the scientific data software using named data networking," *Computer Networks*, vol. 166, pp. 106954.1–106954.9, 2020.

[23] J. Liao, L. Li, H. Chen, and X. Liu, "Adaptive replica synchronization for distributed file systems," *IEEE Systems Journal*, vol. 9, no. 3, pp. 865–877, 2015.

[24] S. Lee, S. J. Hyun, H. Y. Kim, and Y. K. Kim, "Fair bandwidth allocating and strip-aware prefetching for concurrent read streams and striped RAIDs in distributed file systems," *Journal of Supercomputing*, vol. 74, no. 8, pp. 3904–3932, 2018.

[25] M. H. Cha, D. O. Kim, and H. Y. Kim, "Adaptive metadata rebalance in the exascale file system," *Journal of Supercomputing*, vol. 73, no. 4, pp. 1337–1359, 2020.

[26] X. Liu, Y. T. Lu, J. Yu, P. F. Wang, J. T. Wu, and Y. Lu, "ONFS: a hierarchical hybrid file system based on memory, SSD, and HDD for high performance computers," *Frontiers of Information Technology & Electronic Engineering*, vol. 18, no. 12, pp. 1940–1971, 2017.

[27] P. Bartus and E. Arzuaga, "GDedup: distributed file system level deduplication for genomic big data," in *2018 IEEE International Congress on Big Data (BigData Congress)*, vol. 7no. 10, pp. 120–127, San Francisco, CA, USA, 2020.

[28] Y. Chen, Z. Yi, and S. Taneja, "AHDFS: an erasure-coded data archival system for Hadoop clusters," *IEEE Transactions on*

Parallel & Distributed Systems, vol. 28, no. 11, pp. 3060–3073, 2019.

[29] M. W. U. Rahman, N. S. Islam, X. Lu, D. Shankar, and D. K. Panda, "MR-Advisor: a comprehensive tuning, profiling, and prediction tool for MapReduce execution frameworks on HPC clusters," *Journal of Parallel and Distributed Computing*, vol. 120, no. 10, pp. 237–250, 2018.

[30] L. Chen, S. Du, and C. Huang, "Design and implementation of teaching cloud platform based on the distributed file system," *Wireless Internet Technology*, vol. 5, no. 10, pp. 1–1, 2019.

Hindawi
Journal of Sensors
Volume 2021, Article ID 8222721, 10 pages
https://doi.org/10.1155/2021/8222721

Research Article

A Sleep Stage Classification Algorithm of Wearable System Based on Multiscale Residual Convolutional Neural Network

Qinghua Zhong[1,2] **Haibo Lei**[2] **Qianru Chen**[2] **and Guofu Zhou**[1,3,4]

[1]*Guangdong Provincial Key Laboratory of Optical Information Materials and Technology & Institute of Electronic Paper Displays, South China Academy of Advanced Optoelectronics, South China Normal University, Guangzhou 510006, China*
[2]*School of Physics and Telecommunication Engineering, South China Normal University, Guangzhou 510006, China*
[3]*Shenzhen Guohua Optoelectronics Tech. Co. Ltd., Shenzhen 518110, China*
[4]*Academy of Shenzhen Guohua Optoelectronics, Shenzhen 518110, China*

Correspondence should be addressed to Qinghua Zhong; zhongqinghua@m.scnu.edu.cn

Received 27 September 2021; Accepted 30 November 2021; Published 16 December 2021

Academic Editor: Mu Zhou

Sleep disorder is a serious public health problem. Unobtrusive home sleep quality monitoring system can better open the way of sleep disorder-related diseases screening and health monitoring. In this work, a sleep stage classification algorithm based on multiscale residual convolutional neural network (MRCNN) was proposed to detect the characteristics of electroencephalogram (EEG) signals detected by wearable systems and classify sleep stages. EEG signals were analyzed in each epoch of every 30 seconds, and then 5-class sleep stage classification, wake (W), rapid eye movement sleep (REM), and nonrapid eye movement sleep (NREM) including N1, N2, and N3 stages was outputted. Good results (accuracy rate of 92.06% and 91.13%, Cohen's kappa of 0.7360 and 0.7001) were achieved with 5-fold cross-validation and independent subject cross-validation, respectively, which performed on European Data Format (EDF) dataset containing 197 whole-night polysomnographic sleep recordings. Compared with several representative deep learning methods, this method can easily obtain sleep stage information from single-channel EEG signals without specialized feature extraction, which is closer to clinical application. Experiments based on CinC2018 dataset also proved that the method has a good performance on large dataset and can provide support for sleep disorder-related diseases screening and health surveillance based on automatic sleep staging.

1. Introduction

Sleep plays an important role in human health [1]. The sleep monitoring of human has significant implications for medical research and practice [2]. Sleep specialists usually evaluate the quality of sleep by analyzing signals from sensors connected to different parts of body in accordance with the Rechtschaffen and Kales Rules [3] or the American Academy of Sleep Medicine (AASM) sleep score manual [4]. In particular, polysomnography (PSG), which records EEGs, electrooculograms (EOG), electrocardiograph (ECG), electromyography (EMG), respiratory effort, leg movement, and blood oxygen saturation over several nights in a sleep laboratory, is considered as a gold standard for evaluating sleep status of subjects [5]. In order to improve the efficiency of sleep monitoring, several effective sleep staging methods based on EEG, ECG, and EMG signals have been proposed in recent years [6]. However, wearing too many sensors during sleep is obtrusive and uncomfortable, the silver/silver chloride electrodes with certain adhesive or conductive paste the signal acquisition are adopted mostly, and the placement of them is demanded carefully in hairy regions of scalp to minimize movement-related noise, which affects the natural sleep of subjects and is not suitable for long-term sleep monitoring in home environment.

In recent years, noninvasive [7, 8] or noncontact [9, 10] measurement of cardiac, respiratory, and body movement signals which offers the potential of low cost and easy operation for long term dynamic sleep monitoring has gradually gained the favour of researchers. But its performances badly depend on the quality of signal acquisition and complex

signal processing. EEG recordings play a crucial role in the classification of sleep stages. In order to solve the problem of wearers' comfort, classification of sleep stages based on single-channel EEG signals has been extensively investigated [11, 12], because compared to complex PSG devices, the corresponding dual-electrode device has the advantages of wearable and less interference.

Compared with frontal electrodes, EEG recordings from central, occipital, and parietal electrodes could better detect sleep spindles, vertex waveforms, and rhythms [13]. However, channel selection is important for measurement convenience. Fp1, Fp2, and Fpz electrodes below hairline are suitable for wearing and data collection, so do F3 and F4 electrodes. Researchers have tried to address this problem by extracting the same relevant information from frontal electrodes [14]. But the information which can support for W, N1, N2, and N3 stages is different from that extracted from the parietal lobe, so it can affect the credibility of staging results.

The performance of most sleep stage classification methods relies on the selection of representative features for different sleep stages. Frequency domain [15], time-domain, and time-frequency domain [16] decompositions are the common steps for processing time signals and extracting features directly, and various mathematical models have been established in the process of discovering hidden features. After feature extraction, various machine learning algorithms are used for classification [17, 18], such as linear discriminant analysis, nearest neighbour classifier, decision tree, support vector machine, random forest, and ensemble learning. It also shows the good results with combinatorial machine learning models [19]. In recent years, deep learning methods such as convolutional neural network (CNN) [20], recurrent neural network, and other deep neural networks have become common in pattern recognition in biomedical signal processing. In [21], long short-term memory (LSTM) model which takes advantage of sequential data learning to optimize classification performance was proposed for automated sleep stage. Since feature-based approaches may not be suitable for a comprehensive description of subject heterogeneity, CNNs were also applied to learn multiple filters to extract time-invariant features from raw EEG channel [22].

To solve both the subject heterogeneity and temporal pattern recognition problems, the combination of CNN and LSTM has shown a good performance for the usage of precomputed spectrograms in [23]. However, most representative deep learning models rely heavily on hyperparameter tuning, which is challenging to extend. Although some studies such as [24] consider the temporal context, training must be divided into pretraining and fine-tuning. In addition, since the learning rate is set to a very low value during fine-tuning, it takes more time to reach the optimum or may not even be optimal. Therefore, the computation cannot be performed in parallel, which also prolongs the training process.

Increasing the network layer number of CNNs can improve the extraction effect of signal features. Multiscale CNNs were also proposed to perform multiscale feature extraction and classification simultaneously [25]. However, gradient dispersion or gradient explosion is likely to occur when the depth of CNNs increases. The residual network (ResNet) proposed by He et al. [26] was aimed to solve the degeneration problem of network. The method was applied to the machine fault detection and achieved good results [27]. The sleep stage classification based on residual-based attention model was also adopted in [28], but only k-fold cross validation not subject cross-validation was performed, and in the meantime, the amount of test data was not enough.

Considering that multiscale convolutional neural network can capture the detailed signal features required for pattern classification, the idea was adopted to realize a wearable smart eye-mask in our prior study [29]. This method uses single-channel original EEG signals and omits the process of special feature extraction. It has good performance and application potential and can provide support for clinical applications such as screening and diagnosis of sleep disorders. The main contributions of this work are as follows:

(1) A deep learning architecture of ResNet with different filter sizes was developed. Time-invariant features from original single-channel EEG signals can be extracted by training learning filters, so it can save the time of features computation, while residual can be trained to encode temporal information such as sleep phase transition rules into the model

(2) A training algorithm that can effectively train the model end-to-end was developed. Single-channel EEG from forehead was adapted to reduce the patients impact and increase usability

(3) The proposed approach is evaluated on two publicly available datasets: sleep-EDF-expanded [30] and CinC2018 [31] through subject cross-validation experiment with a strong robustness performance. The results are compared with state-of-the-art results in the field of sleep stage classification to demonstrate the superiority of our method, and it solves the problem that too little data may lead to poor generalization effect of sleep stage model

2. Methods

Sleep staging is a problem of recognition or regression of time series signals. According to the sleep manual, experts divided the EEG, EOG, EMG, and other signals obtained by sensors at intervals of 30 s into W, REM, N1, N2, and N3. In this paper, the multiscale feature learning was integrated into a residual network (ResNet) to automatically learn sleep features of original physiological signals at different time scales, and classification in a parallel way from complex original physiological signals of sleep was achieved.

2.1. Residual Block. In general, the more layers in convolutional neural network, the more diverse features can be extracted. But previous experiments show that there exists a degradation problem in deep networks: when the network

depth of network increases, accuracy saturates and then degrades, and the addition of more layers can lead to an even higher training error, which is not caused by overfitting.

Although the CNN of dozens in layers can be trained by normalized initialization and batch normalization (BN), it is prone to degenerate as the number of layers increases. Theoretically, if the additional layer of a certain layer in the deep network does not learn anything, but just copies the features of last layer, it is called identity mapping, and the training error should not increase. A deep residual learning framework was proposed to solve the degradation phenomenon [26]: if an identity mapping was optimal, it would be easier to push the residual to zero than to fit an identity mapping by a stack of nonlinear layers.

For the network with an input x, the learning feature is denoted as $H(x)$, expected network learning residuals $F(x) = H(x) - x$. Because residual learning is easier than the traditional feature learning, the residual learning adopts every few stacked layers, as shown in Figure 1, a residual block is formed by neural network with shortcuts connections. It contains two kinds of mappings: one is the identity mapping, which is the shortcut curve in the graph, and the other is the residual mapping. If the residual error is not equal to 0, the network performance can still be improved by increasing the number of network layers. If the residual is 0, the current layer is just an identity mapping which neither improves nor degrades, thus, the network degradation problem can be solved.

The output y from the shortcut operation is given as the following equation.

$$y = F(x, \mathrm{W}_i) + x, \tag{1}$$

where x and y are the input and output vectors of the layer under consideration, $F(x, W_i)$ is the residual mapping function to be learned, and it can be expressed by the following equation.

$$F = \mathrm{W}_2\sigma(\mathrm{W}_1 x), \tag{2}$$

where σ is the rectified linear unit (ReLU) activation function.

2.2. MRCNN. In order to extract features from different receiving domains, we used three ResNet pathways constructed by multiple ResNet units as shown in Figure 2, and time series signal fragments were directly used as inputs of the network. Each path contained four ResNet units with two convolutional layers and a shortcut. Each convolution layer was followed by the BN and the activation function ReLU. The solid line shortcut means that it can be added data directly, dashed line shortcuts indicated that they need to be added the 1×1 convolution (Conv) to the same dimension, and the result of each path was averaged by pooling 512 features. Each ResNet block had a different convolution kernel when the core size was set to 1×3, 1×5, and 1×7.

According to the above description, the expression of ResNet unit constructed can be expressed by the following equations.

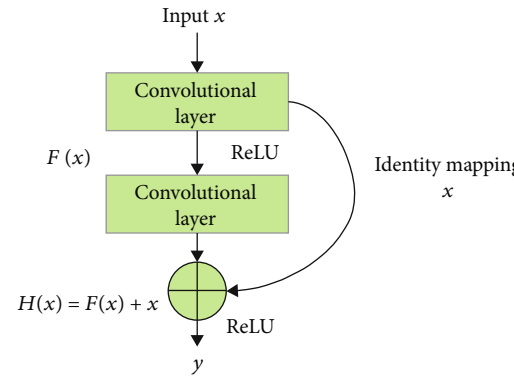

Figure 1: Schematic diagram of residual block.

$$y_1 = \mathrm{W} \otimes x + b, \tag{3}$$

$$y_2 = \mathrm{BN}(y_1), \tag{4}$$

$$y_3 = \mathrm{ReLU}(y_2), \tag{5}$$

$$y_4 = \mathrm{W} \otimes y_3 + b, \tag{6}$$

$$y_5 = \mathrm{BN}(y_4), \tag{7}$$

$$y_6 = y_5 + x, \tag{8}$$

$$y = \mathrm{ReLU}(y_6), \tag{9}$$

where $\otimes$ is convolution operator, BN is used to improve generalization capability.

CNN is a unique artificial neural network inspired by the cerebral cortex, which uses convolution method to extract signal features and compress signal size. In order to retain valid information, it reduces the amount of input data by several orders of magnitude, which can form an optimal network and reduce the risk of network overfitting. CNN contains two core layers: convolution and pooling. The purpose of convolution is to extract features at different levels from original data, and a certain number of filters are used to extract feature maps of input data. The pooling layer is periodically inserted between CNN's convolutional layers, and a subsampling operation is used to reduce the number of parameters. At the end of the algorithm, the ReLU activation function which can significantly improve the training speed is used.

In a CNN, receptor field is defined as the size of the region mapped on the input image by pixel points on the output feature map in each layer of CNN. In layman's terms, this is the area where the input feature is "seen" by the output feature point. The receptive field is calculated by the following equation.

$$\mathrm{RF}_i = (\mathrm{RF}_{i+1} - 1) \times \mathrm{stride}_i + \mathrm{kernel}_i, \tag{10}$$

where RF_i is the receptive field of the i-th convolutional layer, RF_{i+1} is the receptive field of the $(i+1)$-th layer, stride_i is the convolution step size of the i-th layer, and kernel_i is the size of the convolution kernel of i-th layer.

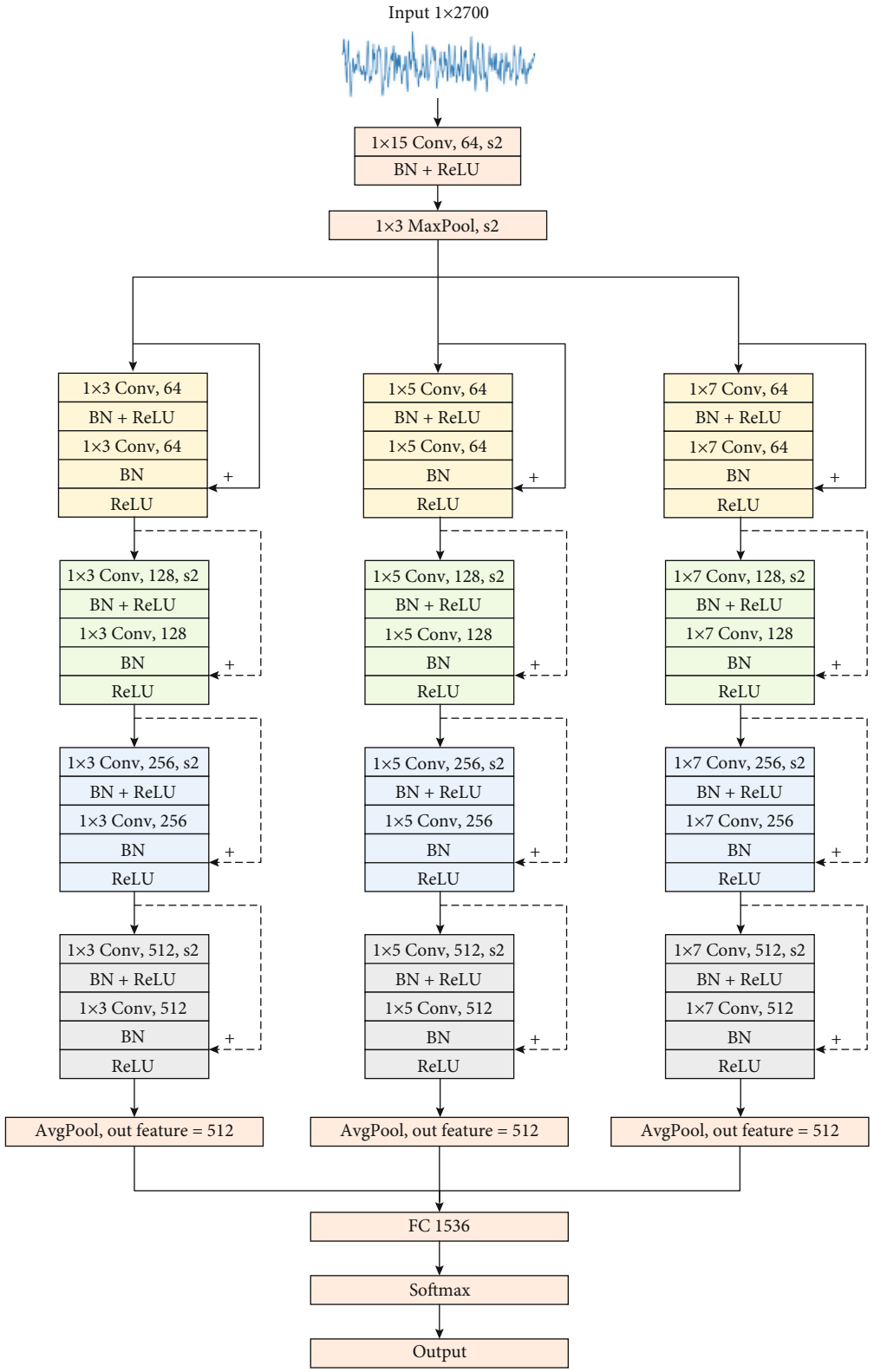

Figure 2: Flow of sleep staging method based on MRCNN.

The EEG signals input to the network are processed by the convolution layer with a convolution kernel length of 15 and transmitted to the BN and ReLU activation functions for maximum pooling. Then, the output data was sent to three channels of different sizes of the convolution kernel for calculation. Finally, the characteristics of three channels

were combined and connected to the full connection layer with 1536 neurons, and the network classification results were obtained by the softmax function.

The receptive field of each convolution layer can be calculated according to equation (1). The receptive field of the output characteristic graph of the last convolution layer in the network was 563 in the input data. EEG signals had a sampling frequency of 100 Hz, and the effective frequency resolution of 563 data points was 0.35 Hz, which can meet the frequency resolution requirements of all rhythmic waves.

2.3. Network Training. In order to realize the loss calculation of multiclassification of sleep stage, cross entropy (CE) was used as the loss function, and its definition was shown as the following equation.

$$\begin{aligned}\text{loss}(\text{input}, \text{target}) &= \text{weight}[\text{target}] \\ &\times \left(-\text{input}[\text{target}] + \log\left(\sum_j e^{\text{input}[j]}\right)\right),\end{aligned} \tag{11}$$

where input is one-dimensional array (the array consists of predicted probability values for each tag) after being processed by Softmax, target is the actual label. input$[j]$ represents the element in the input array whose ordinal number is j. weight[target] is the actual label weight. Since the classification of sleep stages is an unbalanced classification task, this paper tried to balance differences in the amount of data of each label, and weight[target] is defined as the following equation.

$$\text{weight}[\text{target}] = \ln\left(\frac{1}{p(\text{target})}\right), \tag{12}$$

where p(target) is the proportion of the label target in total label.

For the loss function, the adaptive moment estimation solver (Adam) was used for optimization. Learning rate was set to 5×10^{-4}, and all other parameters were set to default. Each time the network training was performed, the algorithm would be used to optimize all training set data for 20 times, and then the verification set would be used to obtain the system performance index results. The MRCNN was built by using PyTorch 1.0, and it was trained by using GTX950M with Ubuntu 18.04 system. Other hardware configurations include Intel Core i7-4710MQ, 12 GB RAM.

2.4. Performance Evaluation. Recall (Re_k), accuracy (Acc_k), and specificity (Sp_k) were used to evaluate the results of sleep staging. Overall recall (Re_ε), overall accuracy (Acc_ε), and overall specificity (Sp_ε) were expressed by the following equations.

$$\text{Re}_k = \frac{\text{TP}}{\text{TP} + \text{FN}}(\%), \text{Re}_\varepsilon = \frac{\sum_{k=1}^{n} \text{Re}_k}{n}(\%), \tag{13}$$

$$\text{Acc}_k = \frac{\text{TP} + \text{TN}}{\text{TP} + \text{FN} + \text{TN} + \text{FP}}(\%), \text{Acc}_\varepsilon = \frac{\sum_{k=1}^{n} \text{Acc}_k}{n}(\%), \tag{14}$$

$$\text{Sp}_k = \frac{\text{TN}}{\text{TN} + \text{FP}}(\%), \text{Sp}_\varepsilon = \frac{\sum_{k=1}^{n} \text{Sp}_k}{n}(\%), \tag{15}$$

where TP, TN, FP, FN represent the true cases, true negative cases, false positive cases, and false negative cases formed by the classifier to judge the category, respectively. In these equations, $n = 5, k = 1, 2, 3, 4, 5$ represents five different stages of sleep. At the same time, the *kappa* coefficient which could describe overall performance of the system would also be calculated as the following equation.

$$\text{err} = \frac{\sum(1 \mid Y_i \neq \text{PY}_i)}{\sum(1 \mid Y_i = Y_i)}, \text{kappa} = \frac{p_o - p_e}{1 - p_e}, p_e = \frac{\sum a_i b_i}{n^2}, \tag{16}$$

where Y_i represents the real label of the sample i, PY_i represents the predicted label of the sample i of the model, p_o presents the sum of the samples of each correct category divided by the total number of samples, $p_o = 1 - \text{err}$, a_i is the actual number of the sample i, b_i is the predicted number of the sample i, and n is the total number of samples.

3. Experiments

3.1. Datasets. In order to ensure the robustness and reproducibility of the results, two public datasets were conducted experiments. The first dataset used in the experiment was sleep-EDF-expanded and contains two different groups of subjects, named as Sleep Cassette (SC) group and Sleep Telemetry (ST) group, respectively. The annotation files included sleep stages W, REM, Stage 1 (S1), Stage 2 (S2), Stage 3 (S3), Stage 4 (S4), movement time (M), and UNKNOWN, and it consisted of a manual score by a skilled technician. Stage M and UNKNOWN were deleted for their extremely small percentage. At the same time, according to the latest AASM sleep scoring manual, S1 and S2 were corresponded to N1 and N2, respectively, and S3 and S4 were combined into N3. In this study, we cropped the SC∗ files in the dataset, and only signals in the period from 30 minutes before the beginning of sleep to 30 minutes after the end of sleep were retained, data from FPz-Cz channels was used.

The second dataset used in the experiment was provided by the CinC2018, which contains 1,985 samples. The sleep stages of each sample were labeled by Massachusetts General Hospital clinical staff and divided into six stages: W, N1, N2, N3, REM, and Undefined. For research and application consideration, data from F4-M1 channels was selected here. The data was divided into a training set ($n = 994$) and a test set ($n = 989$). We randomly selected 500 subjects from the training set as the dataset and deleted the undefined period with a small proportion. To adapt to the AASM sleep scoring manual, the EEG signals of datasets were divided into 30 s as an epoch. After processing, the sleep stage statistics of the two datasets are shown in Table 1.

Table 1: The number and proportion of epochs of various sleep stages.

Dataset	W	N1	N2	N3	REM	Total
Sleep-EDF-expanded (197 samples)	71197 (29.8%)	25169 (10.5%)	88975 (37.2%)	19454 (8.1%)	34181 (14.3%)	238976 (100%)
CinC2018 (500 samples)	82368 (17.95%)	66243 (14.4%)	197338 (43.0%)	54318 (11.835%)	58672 (12.78%)	458939 (100%)

Table 2: Subject cross-validation statistics in sleep-EDF-expanded dataset.

	Samples	W (%)	N1 (%)	N2 (%)	N3 (%)	REM (%)
Total	197	71199 (29.8%)	25174 (10.5%)	88983 (37.2%)	19454 (8.1%)	34184 (14.3%)
Train	157	53014 (27.7%)	20236 (10.6%)	73213 (38.3%)	16235 (8.5%)	28497 (14.9%)
Eval	40	18185 (38.0%)	4938 (10.3%)	15770 (33.0%)	3219 (6.7%)	5687 (11.9%)

Table 3: Subject cross-validation statistics in CinC2018 dataset.

	Samples	W (%)	N1 (%)	N2 (%)	N3 (%)	REM (%)
Total	500	82368 (18.0%)	66243 (14.4%)	197338 (43.0%)	54318 (11.8%)	58672 (12.8%)
Train	400	64477 (17.8%)	48227 (13.3%)	155927 (43.1%)	45090 (12.5%)	47942 (13.3%)
Eval	100	17891 (18.4%)	18016 (18.5%)	41411 (42.6%)	9228 (9.5%)	10730 (11.0%)

Table 4: 5-fold cross-validation confusion matrix and performance in sleep-EDF-expanded.

	W	N1	N2	N3	REM	Re_k(%)	Acc_k(%)	Sp_k(%)	Kappa
W	63232	6813	254	58	840	88.81	95.93	98.38	\
N1	1871	16228	3869	141	3060	64.48	86.91	89.55	\
N2	345	10401	68533	5401	4295	77.02	87.87	94.30	\
N3	30	93	2566	16738	27	86.04	96.51	97.44	\
REM	470	5036	1864	25	26786	78.36	93.46	95.99	\
Overall						78.94	92.06	95.13	0.7360

Table 5: Subject cross-validation confusion matrix and performance in sleep-EDF-expanded.

	W	N1	N2	N3	REM	Re_k(%)	Acc_k(%)	Sp_k(%)	Kappa
W	16097	1483	63	17	517	88.56	94.13	97.55	\
N1	532	2971	668	14	753	60.17	85.78	88.73	\
N2	78	2494	11064	1006	1141	70.10	86.83	95.07	\
N3	6	78	450	2670	16	82.92	96.67	97.67	\
REM	110	778	397	6	4399	77.31	92.22	94.24	\
Overall						75.81	91.13	94.65	0.7001

Table 6: Performance comparison of different sleep staging models based on subject cross-validation.

Method	Re_k(%)					Acc_ε(%)	Re_ε(%)	Kappa
	W	N1	N2	N3	REM			
LSTM	83	39	80	74	68	80	68.8	0.64
CNN	80	40	81	69	64	78	66.8	0.58
CNN-LSTM	84	45	82	83	82	86	75.2	0.71
ResNet18	89	49	71	81	82	91	74.4	0.70
Our MRCNN	89	60	70	83	77	91	75.8	0.70

Table 7: Subject cross-validation confusion matrix and performance in CINC2018.

	W	N1	N2	N3	REM	Re_k(%)	Acc_k(%)	Sp_k(%)	Kappa
W	14518	2442	427	62	440	81.15	92.49	95.05	\
N1	3131	8588	2670	33	3590	47.67	83.57	91.00	\
N2	582	4416	29880	4077	2454	72.16	83.75	91.62	\
N3	22	9	1469	7663	65	83.04	94.33	95.47	\
REM	193	973	537	6	9918	84.04	92.04	92.96	\
Overall						73.61	89.24	93.22	0.6224

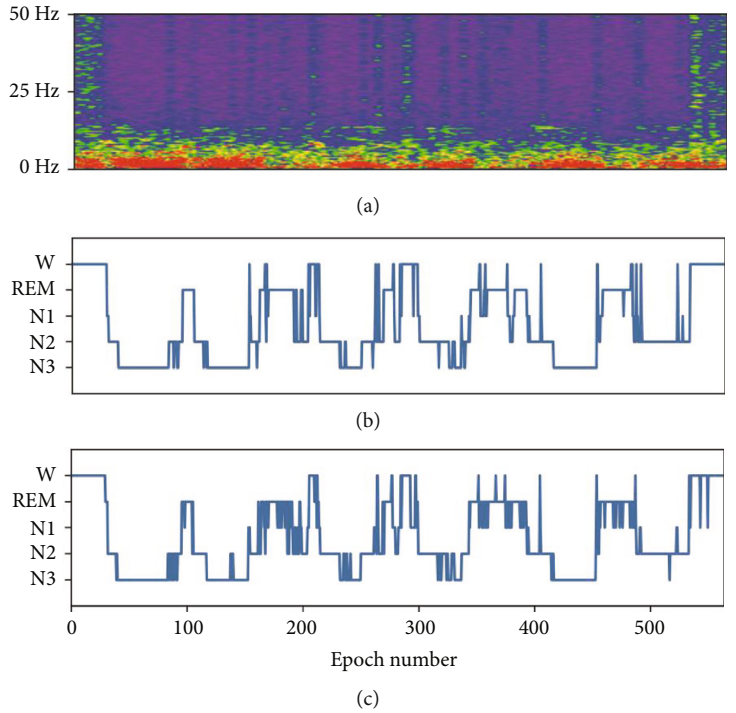

Figure 3: Comparison of effects of automatic sleep staging and expert manual staging in sleep-EDF-expanded. (a) EEG spectrum, (b) manual staging of expert, and (c) automatic staging.

3.2. Preprocessing. In order to adapt to different PSG devices and individual differences of subjects, EEG signals were normalized by using the 5-th and 95-th quantiles [32], as shown in the following equation.

$$x_{\text{norm}} = 2\frac{x - Q_{0.05}(x)}{Q_{0.95}(x) - Q_{0.05}(x)} - 1, \tag{17}$$

where x_{norm} is the result of signal normalization, x is original signal, and $Q_{0.05}(x)$ and $Q_{0.95}(x)$ are the 5% and 95% largest value of the signals.

In order to expand the dataset and improve the network generalization ability, each input data should be randomly clipped (the 3000 data points in each epoch were randomly clipped to 2700), the flip probability was 50%, and 0.01 times random noise was added. Finally, the preprocessed data were integrated, and then added batch size and channel number, and it was converted to tensor data type, as shown in the following equation.

$$x_{nct} \in R^{N\times C\times T}, \tag{18}$$

where $N = 16$, $C = 1$, $T = 2700$ represented batch size, channel number, and data points of single epoch, respectively. In order to input the sleep stages corresponding to the EEG of each Epoch into the network, sleep stages were mapped as the following equation.

$$\text{N3} \longrightarrow 0, \text{N2} \longrightarrow 1, \text{N1} \longrightarrow 2, \text{REM} \longrightarrow 3, \text{W} \longrightarrow 4. \tag{19}$$

3.3. Performance Evaluation. The cross-validation used in this paper included k-fold cross-validation and subject cross-validation. The former randomly divided the entire dataset into k subsets with epoch as the smallest unit. Each subset was taken as the verification set, and the remaining $k - 1$ subsets was taken as the training set. Experiments were performed for k times, and the results of all verification sets were weighted and summarized to get the final result.

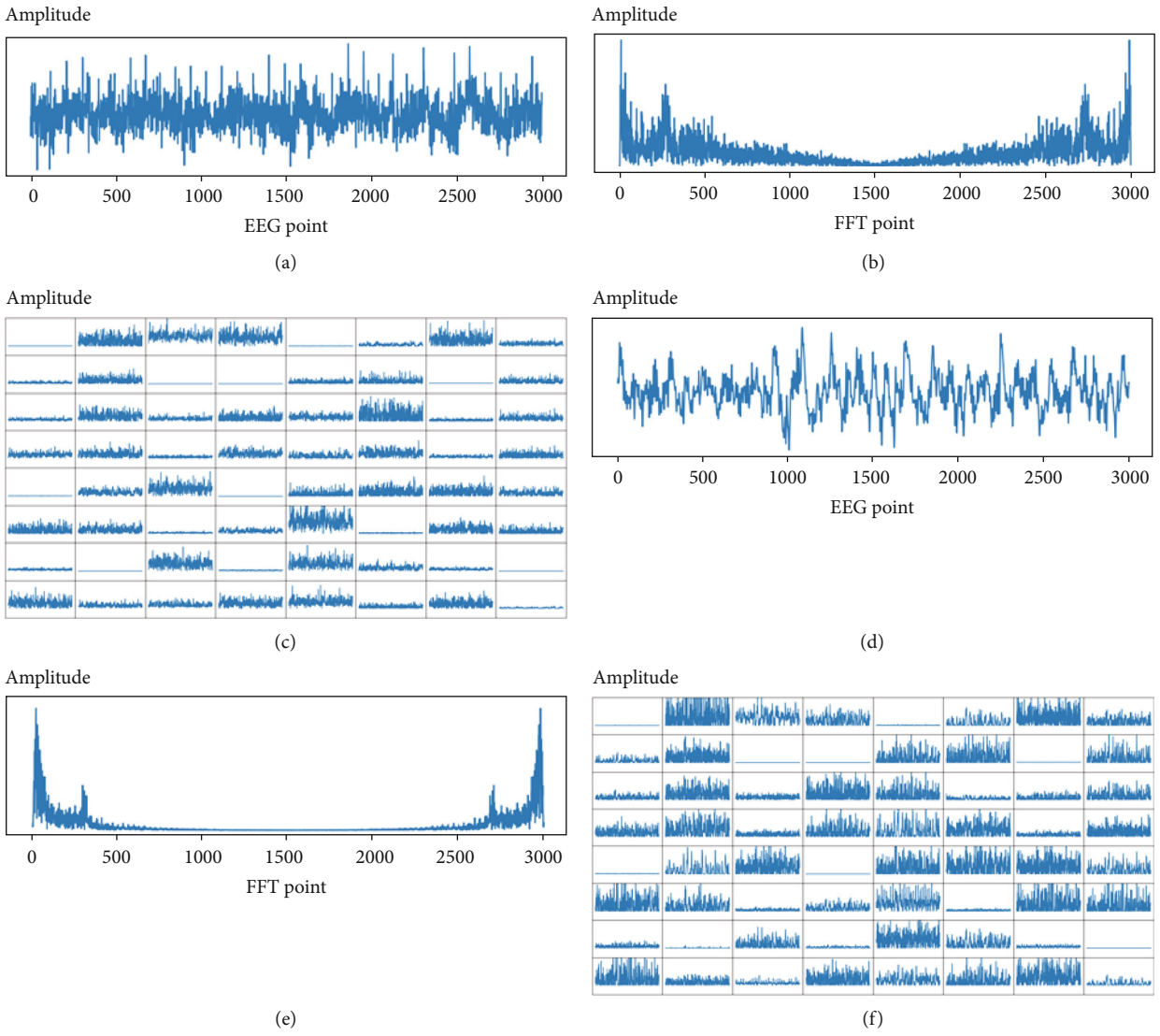

Figure 4: Output results of the first convolution layer in CinC2018 dataset. (a) primitive EEG in W stage. (b) Fast Fourier transform results of EEG in W stage. (c) Output results of the first convolution layer in W stage. (d) Primitive EEG in N3 stage. (e) Fast Fourier transform results of EEG in N3 stage. (f) Output results of the first convolution layer in N3 stage.

In order to evaluate the performance of proposed method, 5-fold cross-validation and subject cross-validation were completed on sleep-EDFx dataset, and data of 197 subjects from FPz-Cz channels was used. Subject cross-validation divided the dataset into training set and verification set with a partition ratio of 8 : 2, and statistical information is shown in Tables 2 and 3. In order to evaluate the effect in practical application, subject cross-validation was also completed on CinC2018 dataset, and the data of 500 subjects from F4-M1 channel was used.

4. Results and Discussion

4.1. Cross-Validation. The results of 5-fold cross-validation are shown in Table 4. The table contains the classification performance index of each sleep stage and the overall performance index of the original confusion matrix obtained after cross-validation. The overall recall rate, accuracy rate, specificity, and kappa coefficient are 78.94%, 92.06%, 95.13%, and 0.7360, respectively. It can be seen that the network proposed in this paper can provide good classification performance with high resolution for the period W, but poor resolution for N1. In particular, it is found by the confusion matrix that N1 is easily misjudged as N2 and REM, which is consistent with the results in [33]. This may be due to the relatively small proportion of sleep time in N1, resulting in less training data. In the meantime, N1 is a transitional period between waking state and sleep state and contains both α and β waves, which makes classification difficult.

The results of subject cross-validation on the dataset are shown in Table 5. The overall recall rate, accuracy rate, specificity, and kappa coefficient of classification are 75.81%, 91.13%, 94.65%, and 0.7001, respectively. Results compared with the existed sleep staging methods are shown in

Table 6. It can maintain better system performance for the data of invisible subjects in the case of large amount of data and reach the similar effect of CNN-LSTM [21]. This cross-validation method can effectively prove the generalization ability of the system on unknown subjects and has high practical application value. In terms of N1 resolution, the recall rate of our proposed network for N1 is 60%, which is much more than other deep learning models.

In [29], several methods based on residual network were compared by using sleep-EDF-expanded dataset, and it can be seen that our proposed MRCNN performs better than other residual networks also in terms of N1 resolution. In this paper, ResNet18 [26] and MRCNN were compared in same circumstances. In order to adapt to the input of one-dimensional data, all two-dimensional layers in the network structure of ResNet18 were modified to one-dimensional layers. It can also be seen that our proposed MRCNN performs better than ResNet18 in terms of N1 resolution. From the data shown in Table 6, it can be also seen that the proposed network can provide poor resolution for N2. In particular in Table 5, it was found by the confusion matrix that N2 was easily misjudged as N1 or N3. This may be due to N2 is a transitional period between N1 and N3 and contains both sleep spindles and *K*-complex waves, which makes classification difficult.

4.2. Performance Evaluation in Wearable Application. Especially, the channel used in the experiments is F4-M1, which is suitable for wearable application. Training set of 400 samples and test set of 100 samples from CinC2018 were used for subject cross-validation. The results of performance are shown in Table 7. Even though the performance of the system decreased a little when it applied to large amount of data, it still demonstrated the generalization ability of the system in the presence of unknown subjects.

4.3. Comparison of Automatic and Artificial Sleep Staging. Automated sleep staging was performed by using the trained model and compared with manual scoring results of expert, as shown in Figure 3, the automatic staging results are close to the manual staging results.

4.4. Automatic Extraction of EEG Features by MRCNN. The results of MRCNN's extraction of effective EEG features are shown here. EEG data in W stage and N3 stage from CinC2018 dataset were fed into the trained network model, respectively, and then the output of the first convolution layer of the model was visualized. It contains 64 convolution kernels, corresponding to the output of 64 channels, and the final results are shown in Figure 4. It can be seen from the figure that for the same input signal, different convolution kernels have different outputs. In addition, by comparing the convolution layer output results of W stage and N3 stage, it can be found that there are significant differences in the output of the same convolution kernel of different input signals, which fully demonstrates that the convolutional neural network can automatically extract the features of EEG signals.

5. Conclusions

In this paper, a new sleep staging method based on multiscale residual network was proposed. It can automatically extract useful information from original single-channel EEG signals and classify sleep stages. By the cross-validation of datasets, the system performance can be maintained for the data of invisible subjects in the case of large data volume. Compared with other deep learning methods, our method only uses a single-channel EEG, and it does not require complex data preprocessing and specialized feature extraction processes to achieve better system performance, which provides the possibility for the clinical application of automated sleep staging. In addition, the multiscale residual network could be further deepened when the computing capacity was enough, and then, a larger amount of data could be used for training, so that the model with better robustness and system performance can be obtained theoretically.

Data Availability

The data used to support the findings of this study are available from the corresponding author upon request.

Conflicts of Interest

The authors declare that there is no conflict of interest regarding the publication of this paper.

Acknowledgments

The research was supported by the Science and Technology Program of Guangzhou (2019050001), Program for Chang Jiang Scholars and Innovative Research Teams in Universities (no. IRT_17R40), Guangdong Provincial Key Laboratory of Optical Information Materials and Technology (2017B030301007), Guangzhou Key Laboratory of Electronic Paper Displays Materials and Devices (201705030007), and MOE International Laboratory for Optical Information Technologies and the 111 Project. "A multiscale residual convolutional neural network for sleep staging based on single channel electroencephalography signals" as the preliminary study has been presented as a preprint according to the following link: https://www.researchsquare.com/article/rs-554671/v1.

References

[1] L. Xie, H. Kang, Q. Xu et al., "Sleep drives metabolite clearance from the adult brain," *Science*, vol. 342, no. 6156, pp. 373–377, 2013.

[2] A. M. Bianchi, M. O. Martin, and S. Cerutti, "Processing of signals recorded through smart devices: sleep-quality assessment," *IEEE Transactions on Information Technology in Biomedicine*, vol. 14, no. 3, pp. 741–747, 2010.

[3] E. A. Wolpert, "A manual of standardized terminology, techniques and scoring system for sleep stages of human subjects," *Electroencephalography & Clinical Neurophysiology*, vol. 26, no. 2, pp. 644–644, 1969.

[4] R. B. Berry, R. Budhiraja, D. J. Gottlieb et al., "Rules for scoring respiratory events in sleep: update of the 2007 AASM manual for the scoring of sleep and associated events," *Journal of Clinical Sleep Medicine*, vol. 8, no. 5, pp. 597–619, 2012.

[5] H. T. Wu, R. Talmon, and Y. L. Lo, "Assess sleep stage by modern signal processing techniques," *IEEE Transactions on Biomedical Engineering*, vol. 62, no. 4, pp. 1159–1168, 2015.

[6] S. Khalighi, T. Sousa, G. Pires, and U. Nunes, "Automatic sleep staging: a computer assisted approach for optimal combination of features and polysomnographic channels," *Expert Systems with Applications*, vol. 40, no. 17, pp. 7046–7059, 2013.

[7] M. Takano and A. Ueno, "Noncontact in-bed measurements of physiological and behavioral signals using an integrated fabric-sheet sensing scheme," *IEEE Journal of Biomedical and Health Informatics*, vol. 23, no. 2, pp. 618–630, 2019.

[8] J. Lomaliza, H. Park, and M. Billinghurst, "Combining photoplethysmography and ballistocardiography to address voluntary head movements in heart rate monitoring," *IEEE Access*, vol. 8, pp. 226224–226239, 2020.

[9] G. Scebba, G. Poian, and W. Karlen, "Multispectral video fusion for non-contact monitoring of respiratory rate and apnea," *IEEE Transactions on Biomedical Engineering*, vol. 68, no. 1, pp. 350–359, 2021.

[10] J. Liu, Y. Chen, Y. Wang, X. Chen, J. Cheng, and J. Yang, "Monitoring vital signs and postures during sleep using WiFi signals," *IEEE Internet of Things Journal*, vol. 5, no. 3, pp. 2071–2084, 2018.

[11] S. Liang, C. Kuo, Y. Hu, Y. H. Pan, and Y. H. Wang, "Automatic stage scoring of single-channel sleep EEG by using multiscale entropy and autoregressive models," *IEEE Transactions on Instrumentation and Measurement*, vol. 61, no. 6, pp. 1649–1657, 2012.

[12] D. Jiang, Y. Lu, Y. Ma, and Y. Wang, "Robust sleep stage classification with single-channel EEG signals using multimodal decomposition and HMM-based refinement," *Expert Systems with Applications*, vol. 121, pp. 188–203, 2019.

[13] G. Zhu, Y. Li, and P. Wen, "Analysis and classification of sleep stages based on difference visibility graphs from a single-channel EEG signal," *IEEE journal of biomedical and health informatics*, vol. 18, no. 6, pp. 1813–1821, 2014.

[14] C. Huang, C. Lin, L. Ko, S. Y. Liu, T. P. Su, and T. P. Lin, "Knowledge-based identification of sleep stages based on two forehead electroencephalogram channels," *Frontiers in Neuroscience*, vol. 8, 2014.

[15] Y. Hsu, Y. Yang, J. Wang, and C. Hsu, "Automatic sleep stage recurrent neural classifier using energy features of EEG signals," *Neurocomputing*, vol. 104, no. 1, pp. 105–114, 2013.

[16] O. Tsinalis, P. M. Matthews, and Y. Guo, "Automatic sleep stage scoring using time-frequency analysis and stacked sparse autoencoders," *Annals of Biomedical Engineering*, vol. 44, no. 5, pp. 1587–1597, 2016.

[17] R. Boostani, F. Karimzadeh, and M. Nami, "A comparative review on sleep stage classification methods in patients and healthy individuals," *Computer Methods and Programs in Biomedicine*, vol. 140, pp. 77–91, 2017.

[18] T. Lajnef, S. Chaibi, P. Ruby et al., "Learning machines and sleeping brains: automatic sleep stage classification using decision-tree multi-class support vector machines," *Journal of Neuroscience Methods*, vol. 250, pp. 94–105, 2015.

[19] I. Fernandez-Varela, E. Hernandez-Pereira, D. Alvarez-Estevez, and V. Moret-Bonillo, "Combining machine learning models for the automatic detection of EEG arousals," *Neurocomputing*, vol. 268, no. 11, pp. 100–108, 2017.

[20] A. Sors, S. Bonnet, S. Mirekc, L. Vercueil, and J. Payen, "A convolutional neural network for sleep stage scoring from raw single-channel EEG," *Biomedical Signal Processing and Control*, vol. 42, pp. 107–114, 2018.

[21] N. Michielli, U. Acharya, U. Rajendra, and F. Molinari, "Cascaded LSTM recurrent neural network for automated sleep stage classification using single-channel EEG signals," *Computers in Biology and Medicine*, vol. 106, pp. 71–81, 2019.

[22] M. Sokolovsky, F. Guerrero, S. Paisarnsrisomsuk, C. Ruiz, and S. A. Alvarez, "Deep learning for automated feature discovery and classification of sleep stages," *IEEE/ACM transactions on computational biology and bioinformatics*, vol. 17, no. 6, pp. 1835–1845, 2020.

[23] A. Supratak, H. Dong, C. Wu, and Y. Guo, "DeepSleepNet: a model for automatic sleep stage scoring based on raw single-channel EEG," *IEEE Transactions on Neural Systems and Rehabilitation Engineering*, vol. 25, no. 11, pp. 1998–2008, 2017.

[24] H. Dong, A. Supratak, W. Pan, C. Wu, P. M. Matthews, and Y. Guo, "Mixed neural network approach for temporal sleep stage classification," *IEEE Transactions on Neural Systems and Rehabilitation Engineering*, vol. 26, no. 2, pp. 324–333, 2018.

[25] G. Jiang, H. He, J. Yan, and P. Xie, "Multiscale convolutional neural networks for fault diagnosis of wind turbine gearbox," *IEEE Transactions on Industrial Electronics*, vol. 66, no. 4, pp. 3196–3207, 2019.

[26] K. He, X. Zhang, S. Ren, and J. Sun, *Deep Residual Learning for Image Recognition*, CVPR, 2016.

[27] R. Liu, F. Wang, B. Yang, and S. Qin, "Multiscale kernel based residual convolutional neural network for motor fault diagnosis under nonstationary conditions," *IEEE Transactions on Industrial Informatics*, vol. 16, no. 6, pp. 3797–3806, 2020.

[28] W. Qu, Z. Wang, H. Hong et al., "A residual based attention model for EEG based sleep staging," *IEEE Journal of Biomedical and Health Informatics*, vol. 24, no. 10, pp. 2833–2843, 2020.

[29] Q. Zhong, H. Lei, Q. Chen, and G. Zhou, "A multiscale residual convolutional neural network for sleep staging based on single channel electroencephalography signals.

[30] "The sleep-EDF database [Expanded]," http://www.physionet.org/physiobank/database/sleep-edfx/.

[31] The PhysioNet Computing in Cardiology Challenge, 2018, https://www.physionet.org/content/challenge-2018/1.0.0/.

[32] A. N. Olesen, P. Jennum, P. Peppard, E. Mignot, and H. B. D. Sorensen, "Deep residual networks for automatic sleep stage classification of raw polysomnographic waveforms," in *2018 IEEE 40th Annual International Conference of the IEEE Engineering in Medicine and Biology Society (EMBC)*, 2018.

[33] P. Memar and F. Faradji, "A novel multi-class EEG-based sleep stage classification system," *IEEE Transactions on Neural Systems and Rehabilitation Engineering*, vol. 26, no. 1, pp. 84–95, 2018.

Hindawi
Journal of Sensors
Volume 2021, Article ID 6296505, 12 pages
https://doi.org/10.1155/2021/6296505

Research Article

A Revisit Histogram of Oriented Descriptor for Facial Color Image Classification Based on Fusion of Color Information

Huy Nguyen-Quoc and Vinh Truong Hoang

Faculty of Information Technology, Ho Chi Minh City Open University, 97 Vo Van Tan, District 3, Ho Chi Minh City, Vietnam

Correspondence should be addressed to Vinh Truong Hoang; vinh.th@ou.edu.vn

Received 30 August 2021; Revised 27 October 2021; Accepted 18 November 2021; Published 30 November 2021

Academic Editor: Ying-Ren Chien

Histogram of Oriented Gradient (HOG) is a robust descriptor which is widely used in many real-life applications, including human detection, face recognition, object counting, and video surveillance. In order to extract HOG descriptor from color images whose information is three times more than the grayscale images, researchers currently apply the maximum magnitude selection method. This method makes the information of the resulted image is reduced by selecting the maximum magnitudes. However, after we extract HOG using the unselected magnitudes of the maximum magnitude selection method, we observe that the performance is better than using the maximum magnitudes in several cases. Therefore, in this paper, we propose a novel approach for extracting HOG from color images such as Color Component Selection and Color Component Fusion. We also propose the extended kernels in order to improve the performance of HOG. With our new approaches in the color component analysis, the experimental results of several facial benchmark datasets are enhanced with the increment from 3 to 10% of accuracy. Specifically, a 95.92% of precision is achieved on the Face AR database and 75% on the Georgia Face database. The results are better more than 10 times compared with the original HOG approach.

1. Introduction

Nowadays, image classification is one of the most extensive fields in computer vision which attracts the attention of many researchers because of its wide range of application in real life such as human detection, facial recognition, object classification, and diagnose diseases in medical. Many local and global image descriptors have been proposed in order to handle this task [1–3]. The key step is to find a robust descriptor which can discriminate classes. A large number of descriptors have been proposed to extract feature from image, including Color Local Binary Pattern (LBP) [4], Scale Invariant Feature Transform (SIFT) [5], Histogram of Oriented Gradients (HOGs) [6], and GIST [7]. Among them, HOG is a successful descriptor with various applications in real life, including pedestrian detection, face recognition, object classification, security, and industrial inspection. For example, Ding et al. [8] fuse HOG features and global normalized histogram for human detection task by the AdaBoost classifier. Qi et al. [9] apply HOG for railway track detection by using region-growing methods. Qingbo et al. [10] combine HOG features and Discriminative Multimanifold Analysis Method (DMAM) for face recognition in few shot learning context. In this approach, facial features were extracted from image patches fusing and then applied DMAM to transform to lower dimensional space. Chowdhury et al. [11] introduced an improved version of HOG for human detection. Nabila et al. [12] present an optimized version of HOG for road car detection. This approach is based on the concatenation of shape features and motion integration. Aytac et al. [13] extract LBP and HOG features from stomach cancer images. Then, multiple reduction techniques are applied to select the most useful attributes. Hmood et al. [14] introduce an improved version of HOG by proposing an approximate windows that can cover whole object, namely, Dynamic-HOG. This method requires less processing time and achieves a higher accuracy for coin classification. Jebril et al. [15] apply HOG for

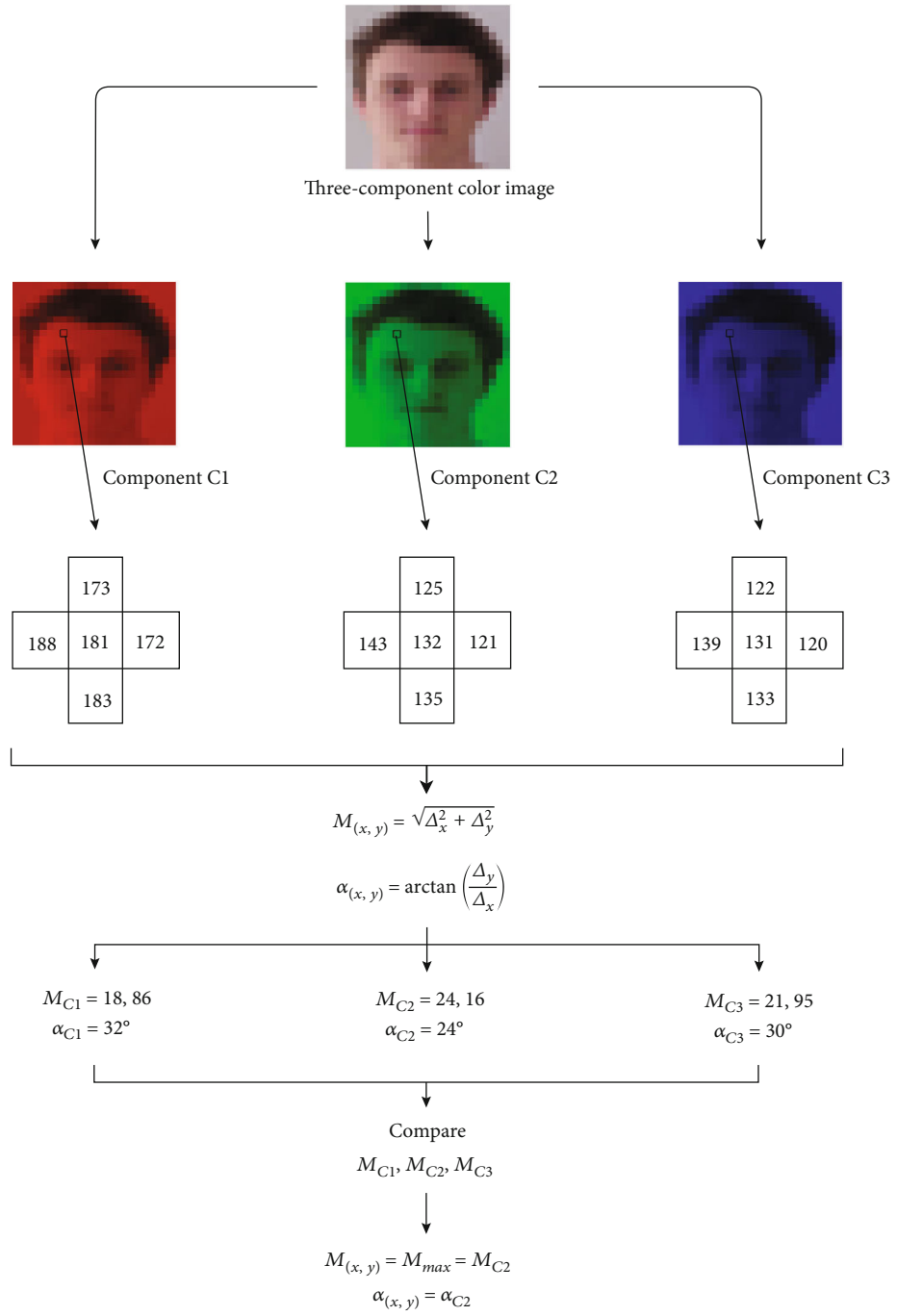

Figure 1: An illustration of maximum magnitude selection method.

handwritten character recognition from grayscale images transformed from RGB color space. The authors used both R-HOG and C-HOG with different windows. Uddin et al. create another HOG version named T20-HOG with the ability to extract the textural features from seed varieties for identification [16]. A two-stage classification process is proposed by Chandrakala and Devi in combination with HOG descriptors [17]. With the robustness of deep neural networks and the advantage of HOG, Hung created a hybrid combination of HOG and CNN named HOG-CNN approach with promising results [18].

Various advancement versions of HOG are proposed in recent years by incorporating with convolutional neural networks (CNNs). Zaffar et al. [19] present CoHOG which is based on CNN in order to extract features from ROI for visual place recognition. Xiong et al. [20] introduce a method for handling depth information of images based on HOG, namely, Histogram of Oriented Depth (HOD) features. The proposed approach is applied for pedestrian detection by combining color image edge information and HOD. Wang et al. [21] present an approach based on HOG and multiorientation computation, namely, MO-HOG. This

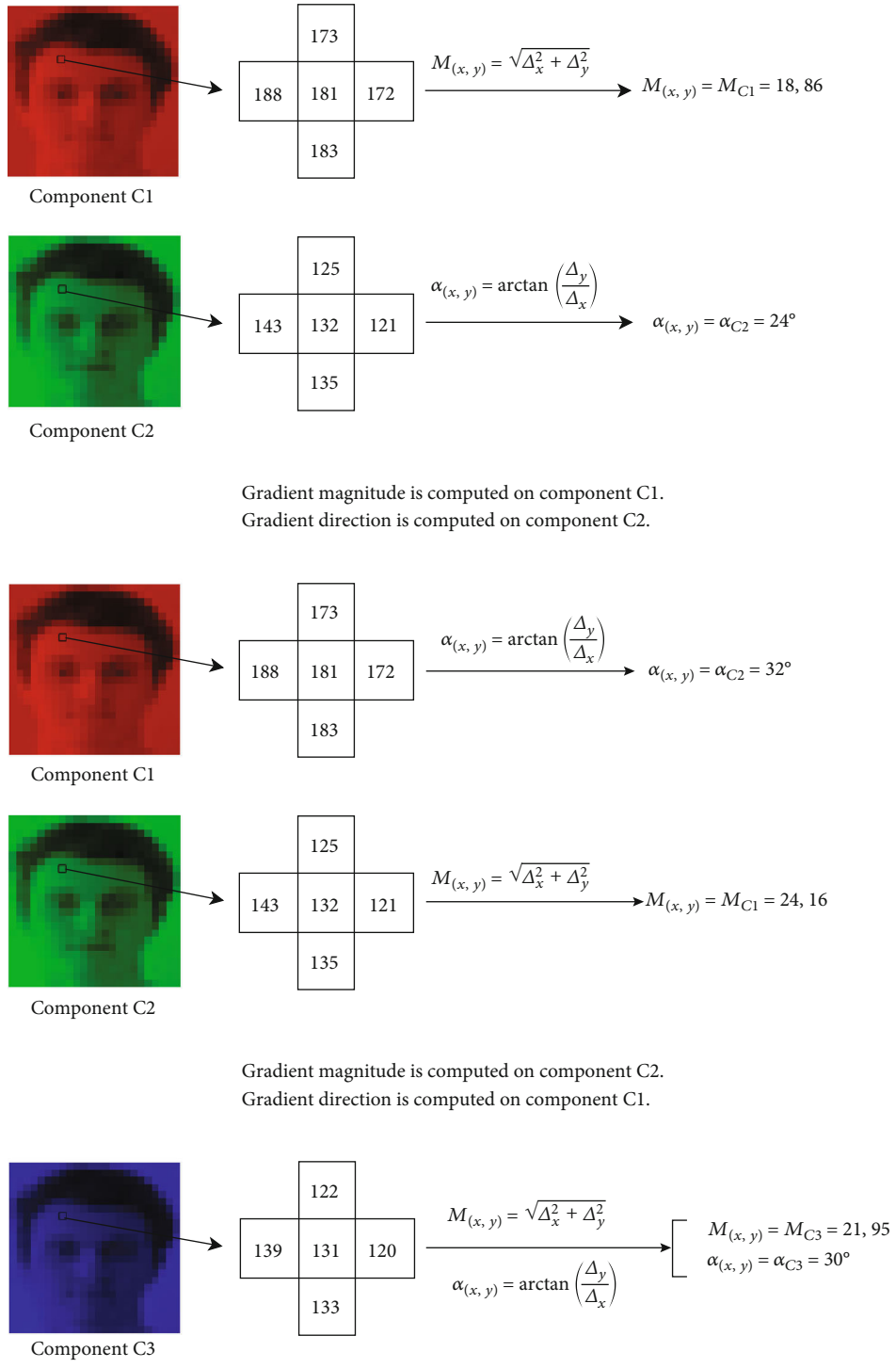

Figure 2: An illustration of the Color Component Selection method.

method combines two-part gradient information to build MO-HOG and applied for facial expression recognition. Pan [22] combines HOG and CNN for facial expression classification. In this approach, HOG features are extracted from CNN's shallow features. Joshi et al. [23] present a method for selecting optimal parameter for HOG descriptor. A multi-level HOG based on sign language image is applied for several windows size of 30×30 and 20×20. Wang et al. [24] concatenate HOD and the Zernike moment's features of SAR images for terrain matching.

Furthermore, HOG has outperformed other descriptors in the classification stage for grayscale image. However,

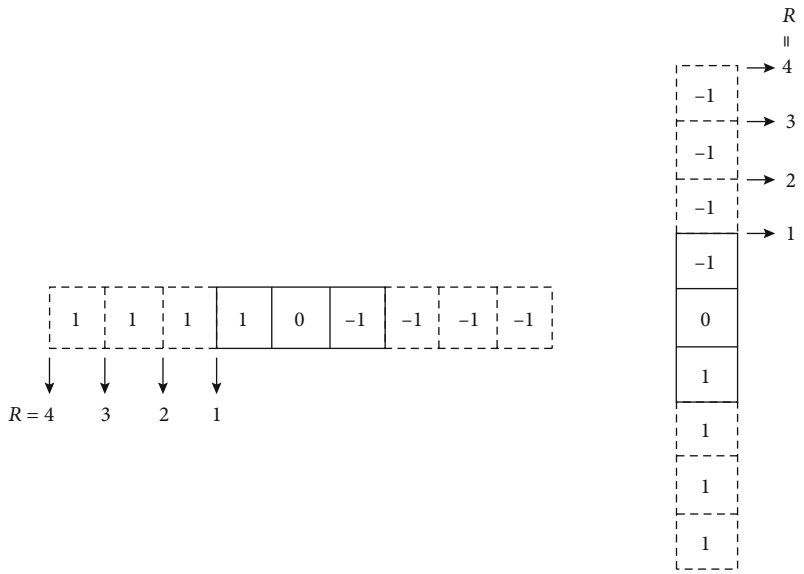

Figure 3: An illustration of original kernels and extended kernels.

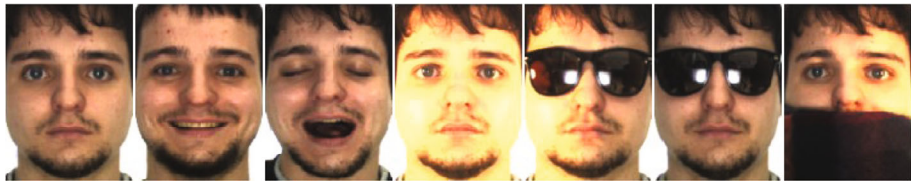

(a) AR dataset

(b) Georgia dataset

(c) CLV dataset

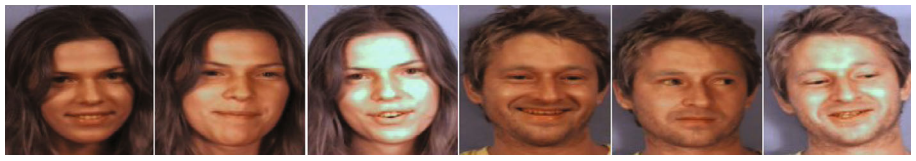

(d) MUCT dataset

Figure 4: The four datasets used to evaluate the proposed approach.

when we extract HOG from color image, the performance usually degrades seriously. The reason is because the information that the color image contains is three times more than the grayscale image does. Moreover, most descriptors are first designed to perform on grayscale images only. Therefore, color has been well investigated in recent years for extracting HOG features. For example, Hoang et al. [25] extract local image descriptors, including LBP, HOG, and GIST for an application of rice seed image recognition. In this approach, features extracted from independent color component are then fused to form final feature vector. Aslan et al. [26] compare HOG-SVM and CNN for human tracking based on video in occlusion context. Zhou et al. [27] introduce a method for extracting HOG features based on

Table 1: Description of experimental dataset.

Dataset	Image size	Class	Training set	Testing set	Total
AR	165 × 120	100	1,300	1,300	2,600
CLV	256 × 256	111	333	444	777
Georgia	128 × 128	50	350	400	750
MUCT	256 × 256	199	199	398	597

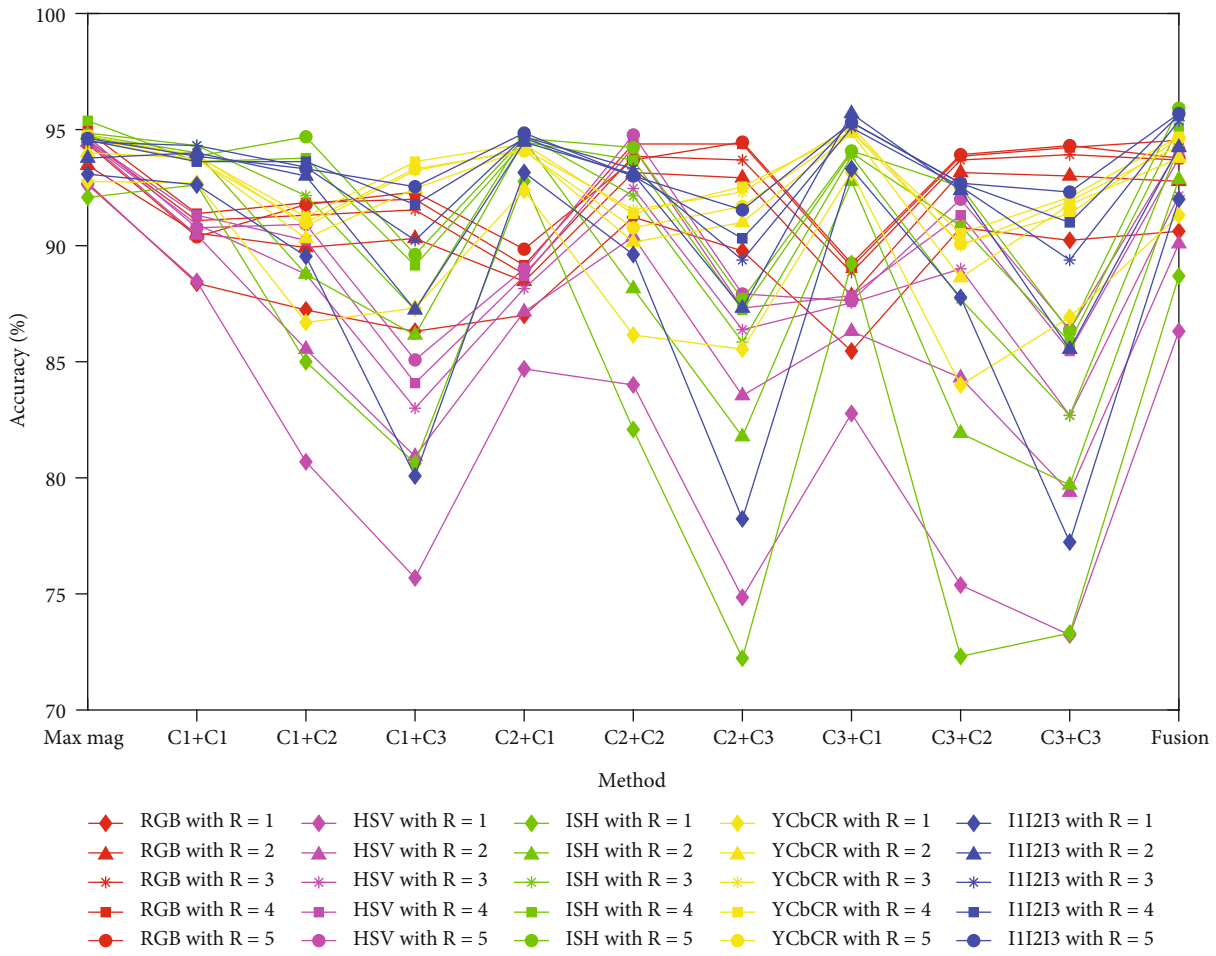

Figure 5: Different values of extended kernels for HOG by CCS and CCF on AR dataset.

a color filter array. Each Bayer pattern is then applied to convert into three component color images by downsampling operation. A new extension of bin was added to HOG and extracted in HSI color space for removing shadow region. Nhat and Hoang [28] enhance the accuracy of face recognition by the fusion of three popular features (LBP, HOG, and GIST). Duong and Hoang [29] apply to extract rice seed images based on features coded in multiple color spaces using HOG descriptor. Banerji et al. [30] enhance the HOG descriptor by subjecting the image to the Haar wavelet transform to improve the HOG descriptor for image classification. Recently, Z. Zhou and Y. Zhou [31] handle color space information for extracting features, namely, CCS-HOG. They apply a between component color space similarity, combining with HOG for extracting facial features. This approach has been shown its effectiveness in kinship verification. Van and Hoang extract HOG features for coding facial image in different color spaces [32, 33]. The final features are obtained by concatenating all features extracted from each color component. Fekri-Ershad and Tajeripour analyzed the color information of color-texture images for classification using hybrid color LBP [34]. Color-texture can also be analyzed using weighted color order of LBP for classification [35].

Although the current researchers have applied maximum magnitude selection method in order to selectively

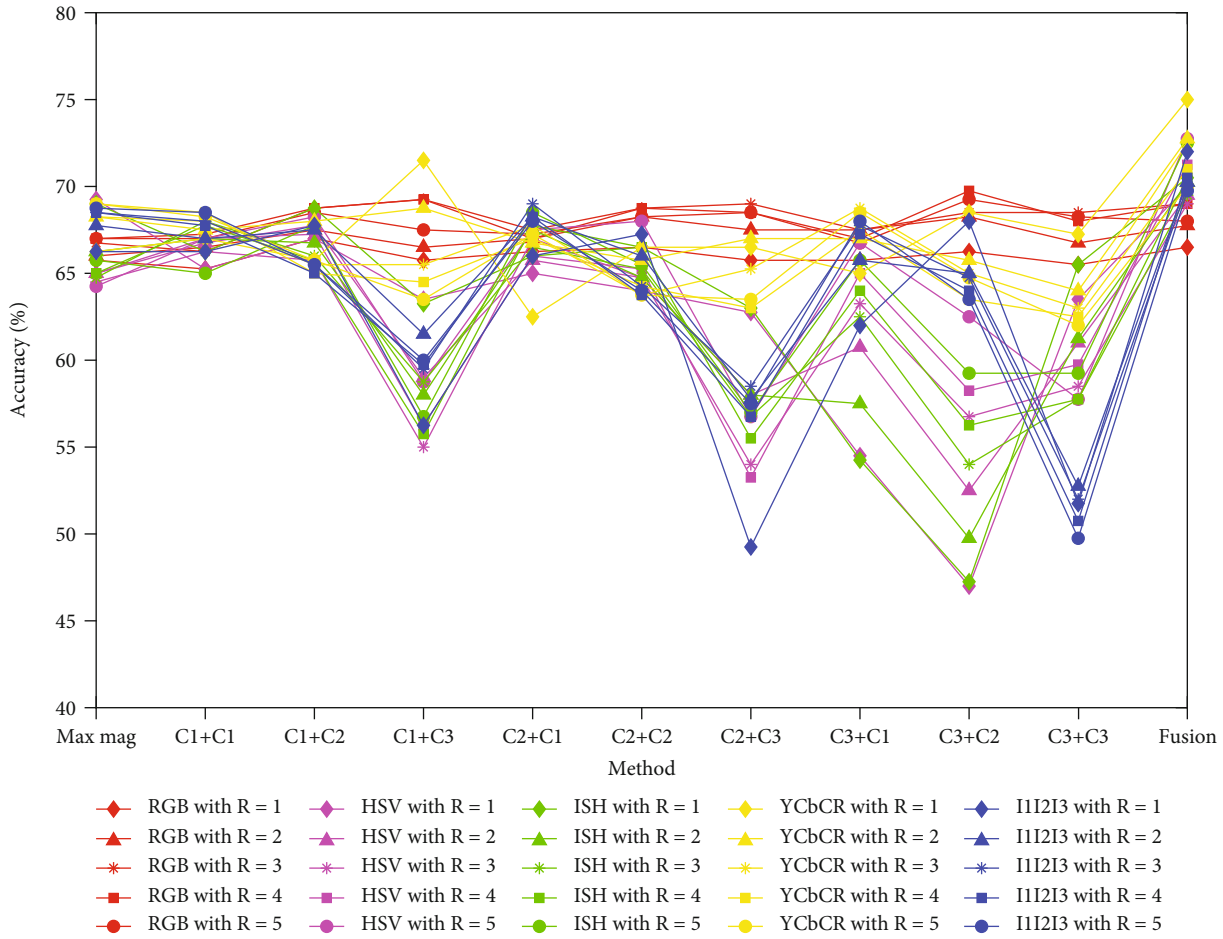

Figure 6: Different values of extended kernels for HOG by CCS and CCF on Georgia dataset.

reduce the information of color image so it can meet the requirements of the following stage of HOG extraction process, the performance is not completely optimized. The impact of color component for extracting features is first mentioned in [36] for LBP descriptors. This issue is extensively investigated to incorporate color information by various proposed method in recent years. It can be used by fusing features extracted from each color component independently or jointly [4]. Specifically, better performances are achieved when we use the unselected magnitudes of maximum magnitude selection method. Novel approaches for extracting HOG from color image are Color Component Selection and Color Component Fusion. Furthermore, we also upgrade the kernels in the gradient computation stage by extending it in horizontal and vertical dimensions. The intention is to figure out the connection between surrounding pixels and the computing pixel, whether the surrounding pixels cause any effects on the output performance.

The rest of this paper is organized as follows. Section 2.1 and Section 3 introduce HOG descriptor with Color Component Selection, Color Component Fusion, and the extended kernels. Then, experimental results are presented in Section 4. Finally, the conclusion and future works are discussed in Section 5.

2. HOG Descriptor with Color Component Selection and Color Component Fusion

This section briefly introduces HOG computation and the two proposed approaches with Color Component Selection (CCS) and Color Component Fusion (CCF) for HOG descriptor.

2.1. HOG Descriptor. Before extracting HOG feature, an image I is split into three subimages I_{C1}, I_{C2}, and I_{C3} which are three color components of I. Next, several image processing algorithms are applied on these images in order to reduce noisy for enhancing the performance. After preprocessing step, on each image, gradient magnitude and direction of each pixel are computed by using the horizontal and vertical gradients. The gradient computation of pixel located at coordinate (x, y) is defined as follows [6]:

$$\Delta_x = \left| G_{(x-1,y)} - G_{(x+1,y)} \right|, \tag{1}$$

$$\Delta_y = \left| G_{(x,y-1)} - G_{(x,y+1)} \right|, \tag{2}$$

$$M_{(x,y)} = \sqrt{\Delta_x^2 + \Delta_y^2}, \tag{3}$$

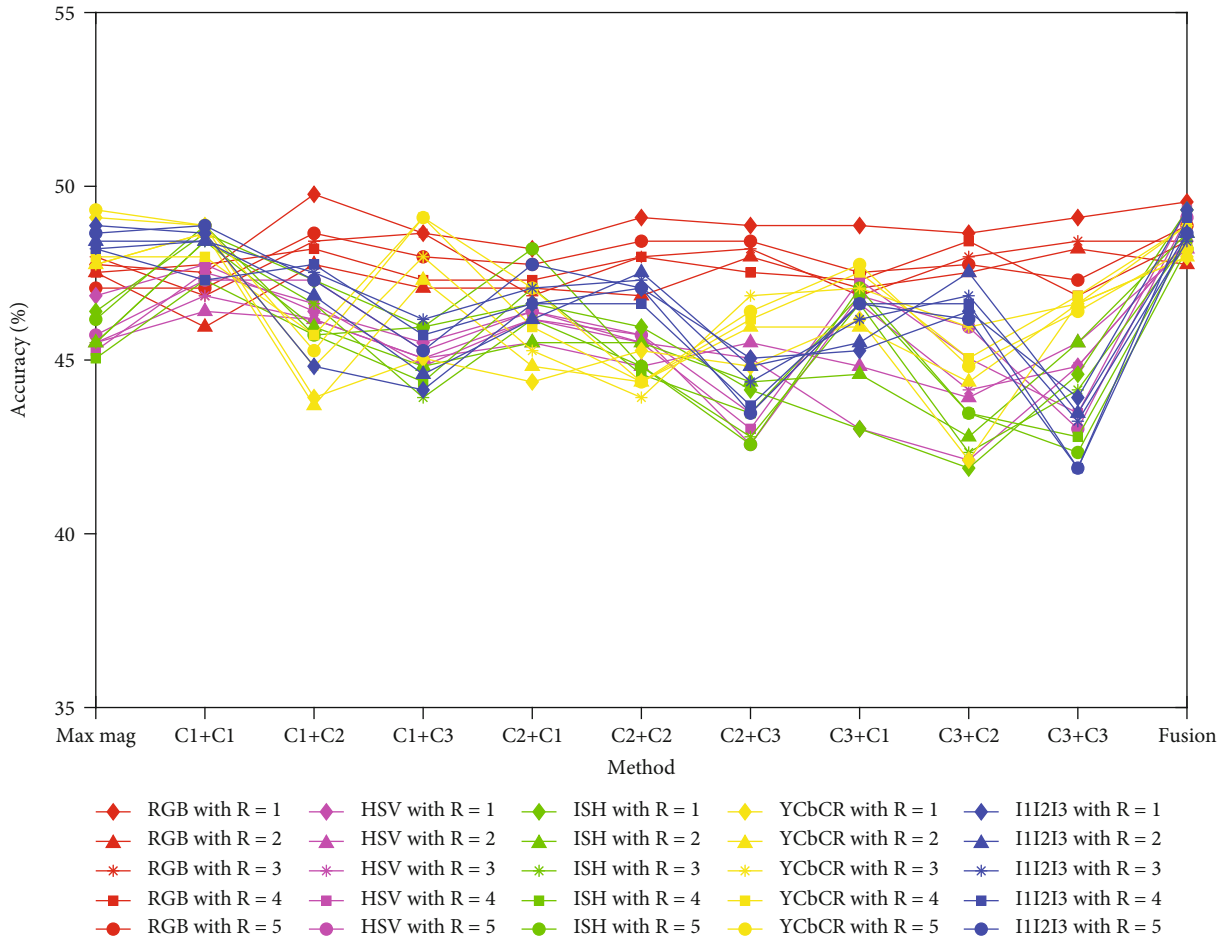

Figure 7: Different values of extended kernels for HOG by CCS and CCF on CLV dataset.

$$\alpha_{(x,y)} = \arctan\left(\frac{\Delta_y}{\Delta_x}\right), \tag{4}$$

where G is grayscale value of the computing pixel, Δ_x and Δ_y represent horizontal and vertical gradients, and $M_{(x,y)}$ and $\alpha_{(x,y)}$ sequentially define gradient magnitude and gradient direction.

2.2. Proposed Approaches. Each image then results in a pair of matrices which contains one gradient magnitude matrix and one the gradient direction matrix. So there are three achieved pairs of matrices in total which are M_{C1} and α_{C1}, M_{C2} and α_{C2}, and M_{C3} and α_{C3}. As the following step requires only one pair of matrices, the current task is to figure out which pair of matrices should be selected in order to produce an optimal feature vector. The most popular solution is maximum magnitude selection. This method compares three gradient magnitudes in each pixel. Then, the maximum is chosen for the final magnitude of this pixel. The final direction is also extracted from the same color component with the selected magnitude. The detail of maximum magnitude selection method is illustrated in Figure 1.

After selection step, two final matrices are obtained to meet the requirement of the orientation binning step. In this step, the original image is divided into cells (8×8 per cell) and a 9-bin histogram is built in each cell based on the gradient features of the inner pixels. The bins are ranged from 0 to 180 degrees for unsigned gradient (α_{unsigned}) and from 0 to 360 degrees in case of signed gradient (α_{signed}). Gradient magnitude of each pixel is added into the corresponding index number of a bin in the histogram. The index number $B_{idx(x,y)}$ is then computed by Equation (5) or (6) and used the ceiling value.

$$B_{idx(x,y)} = \left\lceil \frac{\alpha_{(x,y)}}{\left(\alpha_{\text{unsigned}}/B_{\text{num}}\right)} \right\rceil \left(\alpha_{\text{unsigned}} \in (0,180], B_{\text{num}} = 9\right), \tag{5}$$

or

$$\left\lceil \frac{\alpha_{(x,y)}}{\left(\alpha_{\text{unsigned}}/B_{\text{num}}\right)} \right\rceil \left(\alpha_{\text{signed}} \in (0,360], B_{\text{num}} = 9\right), \tag{6}$$

where B_{num} stands for the default number of orientation bins of the histogram and is usually set to 9 by default. $\alpha_{(x,y)}$ is computed above by Equation (4).

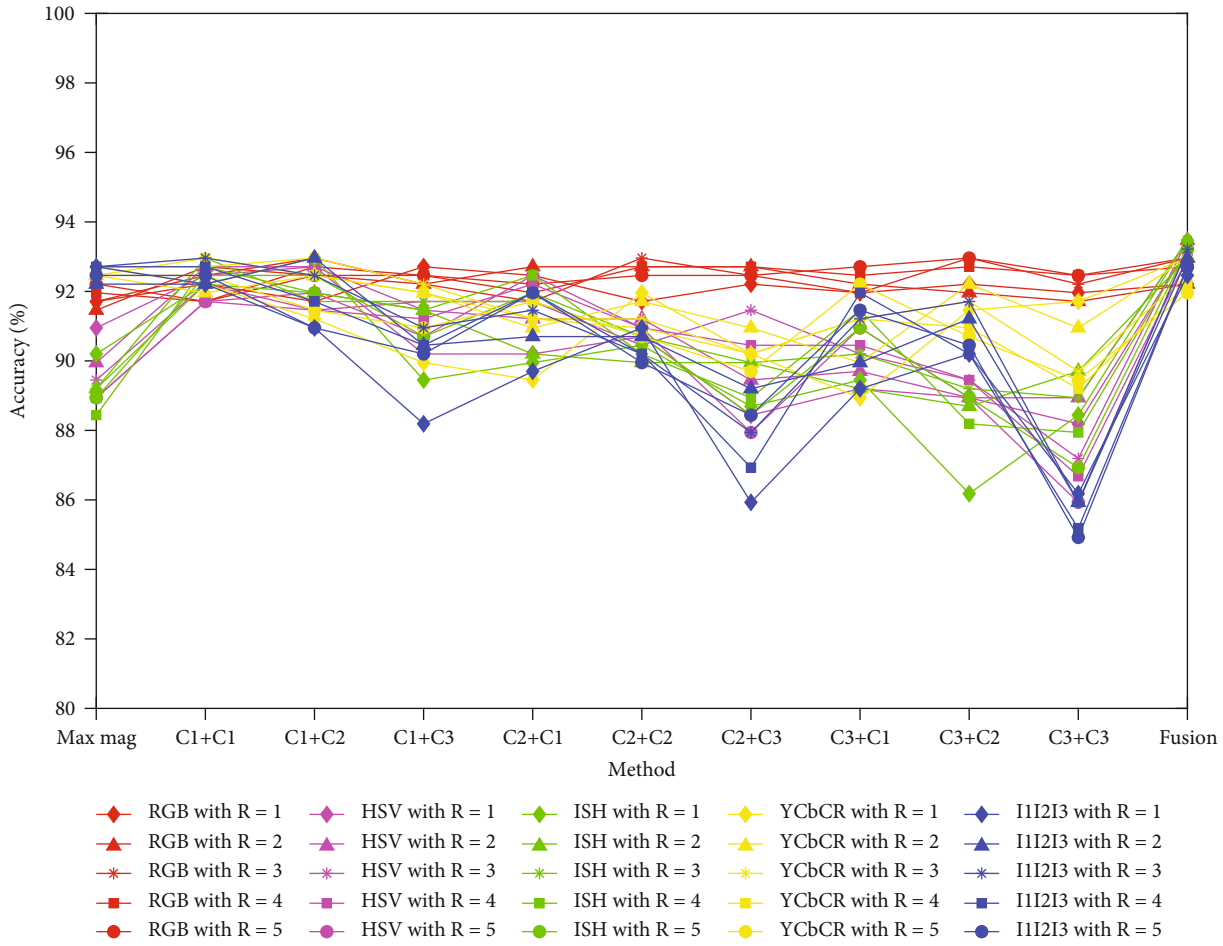

Figure 8: Different values of extended kernels for HOG by CCS and CCF on MUCT dataset.

For the normalization stage, the original image is then divided into blocks (each block contains 2×2 cells which equal to 256×256 pixels). An effective normalization is able to reduce noise and cancel the ill effects. In each block, 50% of the surrounding blocks are overlapped so each cell can be normalized more than once except the cells locate in the corner. Histograms of each block are concatenated and then normalized by using L1-norm, L2-norm, or L1-sqrt. Finally, all normalized histograms are combined together as a feature vector.

In practice, we observe that the maximum magnitude selection method is not optimal enough as it may cause information loss. When we use the unselected values of the maximum magnitude selection for HOG extraction, the achieved results are higher than use the maximum magnitude in several experiments. Therefore, we apply Color Component Selection and Color Component Fusion methods to improve the performance. For the Color Component Selection method, instead of considering which magnitude or direction should be selected for the next stage, we choose the final pair of matrices based on the color components. There are three matrices of each kind so nine different pairs of matrices are achieved in total. The orientation binning stage sequentially applies these pairs to proceed. In the end, nine feature vectors are obtained which are corresponding to nine selected pairs. These vectors are then evaluated to find out the best performance. The process of the Color Component Selection method is presented in Figure 2. The Color Component Fusion simply takes the achieved vectors and concatenates all of them into a fusion vector.

3. Extended Kernels for HOG Extraction

In order to speed the gradient computation process up, researchers used kernels which are illustrated in Figure 3. By filtering the image with these kernels, the horizontal gradient Δ_x and vertical gradient Δ_y are computed faster than calculating based on Equations (1) and (2). We define these original kernels are kernels with $R = 1$. As we sequentially extend the kernels through horizontal and vertical dimension, the parameter R also increases. Figure 3 describes specifically the kernels which parameter R in range from 1 to 4. Then, the achieved horizontal and vertical gradients are divided by parameter R.

4. Experiments

4.1. Dataset Description. The proposed approaches are evaluated on four common facial databases, including AR,

Table 2: Several experimental cases on the AR database.

Color space	R	Max magnitude	AR C2 C1	AR C2 C2	AR C2 C3	AR C3 C1	Fusion
	1	92.69	87.00	91.23	89.77	85.46	90.62
	2	93.46	88.46	93.15	92.92	87.85	92.77
RGB	3	94.54	88.77	93.85	93.69	88.85	93.69
	4	94.92	89.15	94.38	94.38	89.08	94.54
	5	94.38	89.85	93.69	94.46	89.23	93.77
	1	92.62	84.69	84.00	74.85	82.77	86.31
	2	94.46	87.15	90.38	83.54	86.31	90.08
HSV	3	94.46	88.15	92.46	86.38	87.54	92.15
	4	94.54	88.69	94.23	87.31	87.85	93.77
	5	94.69	89.00	94.77	87.92	87.62	94.15
	1	92.08	92.77	82.08	72.23	89.23	88.69
	2	94.77	94.54	88.15	81.77	92.77	92.85
ISH	3	94.85	94.77	92.15	85.85	93.85	94.23
	4	95.38	94.46	93.69	87.23	94.00	95.08
	5	94.69	94.62	94.23	87.69	94.08	**95.92**
	1	92.77	92.38	86.15	85.54	93.15	91.31
	2	94.00	94.15	90.15	91.00	94.85	93.77
YCbCr	3	94.54	94.15	91.54	92.31	95.15	94.31
	4	94.77	94.38	91.38	92.54	94.92	94.69
	5	94.54	94.08	90.77	91.69	94.92	94.62
	1	93.08	93.15	89.62	78.23	93.31	92.00
	2	93.77	94.46	93.08	87.31	95.69	94.23
I1I2I3	3	94.46	94.69	93.31	89.38	95.08	95.38
	4	94.54	94.62	93.00	90.31	95.31	95.62
	5	94.62	94.85	93.00	91.54	95.31	95.69

Table 3: Several experimental cases on the Georgia database.

Color space	R	Max magnitude	Georgia C1 C2	Georgia C1 C3	Georgia C2 C2	Georgia C3 C2	Fusion
	1	65.75	67.00	65.75	66.50	66.25	66.50
	2	66.00	67.50	66.50	68.25	68.25	67.75
RGB	3	66.75	68.75	69.25	68.75	68.50	69.00
	4	67.00	68.75	69.25	68.75	69.75	69.00
	5	67.00	68.50	67.50	68.25	69.25	68.00
	1	69.25	67.00	63.50	64.00	47.00	70.00
	2	65.00	67.75	59.00	64.75	52.50	69.50
HSV	3	64.50	65.75	55.00	64.75	56.75	69.00
	4	65.00	67.25	56.25	65.25	58.25	71.25
	5	64.25	68.25	58.75	68.00	62.50	72.75
	1	69.00	68.75	63.25	66.50	47.25	70.50
	2	66.25	66.75	58.00	64.75	49.75	70.25
ISH	3	64.75	66.00	58.75	65.25	54.00	69.50
	4	65.00	65.75	55.75	66.50	56.25	70.50
	5	65.75	67.75	56.75	65.50	59.25	72.50
	1	66.25	65.75	71.50	66.50	68.50	**75.00**
	2	68.25	68.00	68.75	65.75	65.75	72.75
YCbCr	3	68.25	65.50	65.50	63.75	65.00	72.50
	4	69.00	65.00	64.50	64.25	63.50	71.00
	5	69.00	65.75	63.50	63.75	64.75	70.00
	1	66.25	67.75	56.25	67.25	68.00	72.00
	2	67.75	67.50	61.50	66.00	65.00	70.25
I1I2I3	3	68.50	65.50	59.50	64.25	64.75	70.00
	4	68.50	65.00	59.75	63.75	64.00	70.50
	5	68.75	65.50	60.00	64.00	63.50	69.75

Georgia, CLV, and MUCT (see Figure 4). In order to experiment the proposed approaches, these databases are split into 50% of training and 50% of testing. However, databases, such as Georgia, CLV, and MUCT, have an odd number of images per class. For instance, the MUCT dataset includes 3 images in each class so we decide to randomly split one image for training and the other two for testing in order to make the training more challenging. The 1-NN classifier is employed to evaluate the classification performance, and accuracy metric is employed to measure the performance on testing set. The summary of those databases is presented in Table 1.

4.2. Experimental Setup. As our proposed approaches are designed to fit in every three-component color images, we also experiment them in several well-known color spaces, including HSV, ISH, I1I2I3, and YCbCr. These spaces are frequently applied for pattern recognition [4]. According to Section 2, each image after applying Color Component Selection results in 10 different feature vectors, including 9 different vectors and one fusion vector which is extracted by the Color Component Fusion method. These results are then deployed to a 1-NN classifier for evaluating. Moreover, we set the kernels with R from 1 to 5, respectively, for comparison. The experiments are implemented by Matlab 2017b and conducted on a PC with a configuration of a CPU I3 8100 3.60 GHz and 8 GBs of RAM.

4.3. Results. The experimental results are presented by charts in Figures 5–8. By converting in many color spaces and increasing parameter R, the performance of maximum magnitude selection method has been upgraded. Furthermore, the Color Component Selection and the Color Component Fusion have also outperformed the maximum magnitude selection method according to the charts. For the AR database, the highest achieved accuracy is 95.92% which is 0.54% more than the highest accuracy can be achieved by using the maximum magnitude selection method, and this result is obtained by the Color Component Fusion with $R = 5$ kernels, and the used color space is ISH. For the Georgia database, when we apply the Color Component Fusion method combined with $R = 1$ kernels and YCbCr color space, the achieved result is 75.00%. This is the highest accuracy in all experiments on the Georgia database. Better performance is also obtained in experiment for the MUCT database and even in experiment with the CLV database

Table 4: Several experimental cases on the CLV database.

Color space	R	CLV						
		Max magnitude	C1 C1	C1 C2	C1 C3	C3 C2	C3 C3	Fusion
RGB	1	47.75	47.52	49.77	48.65	48.65	49.10	49.55
	2	47.52	45.95	47.75	47.07	47.52	48.20	47.75
	3	47.97	46.85	48.42	48.65	47.97	48.42	48.42
	4	47.52	47.75	48.20	47.30	48.42	46.85	48.42
	5	47.07	47.07	48.65	47.97	47.75	47.30	48.87
HSV	1	46.85	47.75	46.40	45.50	42.12	44.82	48.42
	2	45.50	46.40	46.17	45.05	43.92	45.50	48.20
	3	45.50	46.85	46.17	45.05	44.14	44.82	48.42
	4	45.27	47.52	46.62	44.82	45.05	43.47	49.32
	5	45.72	47.30	47.30	45.27	45.95	43.02	49.10
ISH	1	46.40	48.65	47.30	45.95	41.89	44.59	49.32
	2	45.50	48.42	45.95	44.82	42.79	45.50	48.65
	3	45.50	48.42	46.62	43.92	42.34	44.14	48.42
	4	45.05	47.30	45.72	44.37	43.47	42.79	48.42
	5	46.17	48.87	45.72	45.95	43.47	42.34	48.20
YCbCr	1	49.10	48.87	43.92	45.05	42.12	46.62	47.97
	2	47.75	48.65	43.69	47.30	44.37	46.62	47.97
	3	47.75	48.65	44.82	47.97	45.95	46.62	48.87
	4	47.97	47.97	45.72	49.10	45.05	46.85	48.87
	5	49.32	48.87	45.27	49.10	44.82	46.40	48.20
I1I2I3	1	48.87	48.65	44.82	44.14	46.40	43.92	49.32
	2	48.42	48.42	46.85	44.59	47.52	43.47	48.65
	3	48.20	48.42	47.52	46.17	46.85	43.24	48.42
	4	48.20	47.30	47.75	45.72	46.62	41.89	49.10
	5	48.65	48.87	47.30	45.27	46.17	41.89	48.65

Table 5: Several experimental cases on the MUCT database.

Color space	R	MUCT						
		Max magnitude	C1 C1	C1 C2	C1 C3	C2 C1	C3 C2	Fusion
RGB	1	91.71	92.21	91.71	92.71	92.46	92.21	92.21
	2	91.46	92.71	92.46	92.21	92.71	91.96	92.21
	3	91.71	92.46	92.96	92.21	91.71	92.96	92.96
	4	91.96	91.71	92.71	92.46	91.96	92.71	92.96
	5	92.21	91.71	92.46	92.46	92.21	92.96	92.71
HSV	1	90.95	92.46	92.71	90.20	90.20	88.94	93.22
	2	89.95	92.71	92.71	91.46	91.21	88.94	93.47
	3	89.45	92.21	91.46	91.71	91.71	89.45	93.47
	4	88.94	91.71	91.46	91.21	92.21	89.45	92.96
	5	88.94	91.71	91.96	90.70	92.46	88.94	93.22
ISH	1	90.20	92.21	92.96	89.45	89.95	86.18	93.47
	2	89.20	92.21	91.96	91.46	90.20	88.69	92.96
	3	89.20	92.96	91.71	91.71	91.71	89.20	93.47
	4	88.44	92.71	91.96	91.46	92.46	88.19	93.22
	5	88.94	92.46	92.46	90.70	91.96	88.94	93.22
YCbCr	1	92.71	92.21	91.21	89.95	89.45	91.46	92.96
	2	92.46	91.96	92.46	91.96	90.95	92.21	92.96
	3	92.71	92.71	92.96	92.21	91.21	91.71	92.46
	4	92.46	92.96	92.46	91.96	91.21	90.95	92.21
	5	92.46	92.46	91.46	90.95	91.71	90.70	91.96
I1I2I3	1	92.71	92.21	90.95	88.19	89.70	90.20	92.46
	2	92.21	92.21	92.96	90.45	90.70	91.21	92.96
	3	92.71	92.96	92.46	90.95	91.46	91.71	93.22
	4	92.71	92.71	91.71	90.45	91.96	90.20	92.71
	5	92.46	92.46	90.95	90.20	91.96	90.45	92.71

which is the most challenging image set. Generally, we observe that the best results are mostly achieved with Fusion approach in comparing with other approaches, which can tell the promising performance of our proposed approaches.

Several of best cases are reported in Tables 2–5. In these tables, the Max magnitude abbreviation stands for maximum magnitude selection method while Fusion abbreviation stands for Color Component Fusion method. We found that the best accuracy obtained for AR dataset is 95.92% by using Fusion approach. Similarly, this approach achieves 75.00%, 49.77%, and 93.47% for Georgia, CLV, and MUCT datasets, respectively. Note that the performance of each color space is different according to the feature extraction methods. Moreover, the increment of parameter R in the extended kernels has also improved several experimental results. In most cases, the accuracy when applying R=5 kernels is higher compared to the others. However, there are also several cases where highest precision is achieved with R=1 so we cannot yet tell if the higher the parameter R of kernels, the higher accuracy we can achieve. But we believe that these results are the foundation of the advantageous effectiveness of kernel size in HOG performance, which leads us to study deeper about it in the future.

5. Conclusion

In this paper, we propose novel approaches to extract HOG descriptor from color images such as the Color Component Selection method and Color Component Fusion in order to improve the classification performance. In our observation, we recognize that the proposed methods outperform the current maximum magnitude selection method in face classification task, especially the Color Component Fusion method. The color space conversion and extended kernels also efficiently improve the accuracy of the classification. However, in several cases, the extended kernels still cause the accuracy to decrease. The Color Component Selection method requires a long time to finish the extraction from every available case, and the Color Component Fusion may cause computer memory issues due to its deep dimension. Therefore, our future work is to figure out the optimal pair of matrices without experimenting all cases to enhance the inference speed. Feature selection methods are also recommended to reduce the vector dimension. Several CNN-

related works are considered to combine with the proposed approaches for further improvement.

Data Availability

The datasets generated during and/or analyzed during the current study are available from the corresponding author on reasonable request.

Conflicts of Interest

We have no conflict of interest to declare.

References

[1] D. Huang, C. Shan, M. Ardabilian, Y. Wang, and L. Chen, "Local binary patterns and its application to facial image analysis: a survey," *IEEE Transactions on Systems, Man, and Cybernetics, Part C*, vol. 41, no. 6, pp. 765–781, 2011.

[2] A. Humeau-Heurtier, "Texture feature extraction methods: a survey," *IEEE Access*, vol. 7, pp. 8975–9000, 2019.

[3] S. Fekri-Ershad, "Gender classification in human face images for smart phone applications based on local texture information and evaluated Kullback-Leibler divergence," *Traitement du Signal*, vol. 36, no. 6, pp. 507–514, 2019.

[4] V. T. Hoang, *Multi Color Space LBP-Based Feature Selection for Texture Classification, [Ph. D thesis]*, Universit'e du Littoral Cˆote d'Opale, 2018.

[5] L. Zhang, J. Chen, L. Yue, and P. Wang, "Face recognition using scale invariant feature transform and support vector machine," in *2008 The 9th International Conference for Young Computer Scientists*, pp. 1766–1770, Hunan, China, 2008.

[6] N. Dalal and B. Triggs, "Histograms of oriented gradients for human detection," in *2005 IEEE Computer Society Conference on Computer Vision and Pattern Recognition (CVPR'05)*, vol. 1, pp. 886–893, San Diego, CA, USA, 2005.

[7] M. Douze, H. Jégou, H. Sandhawalia, L. Amsaleg, and C. Schmid, "Evaluation of gist descriptors for web-scale image search," in *Proceedings of the ACM International Conference on Image and Video Retrieval*, pp. 1–8, New York, NY, USA, 2009.

[8] J. Ding, Y. Wang, and W. Geng, "An HOG-CT human detector with histogram-based search," *Multimedia Tools and Applications*, vol. 63, no. 3, pp. 791–807, 2013.

[9] Z. Qi, Y. Tian, and Y. Shi, "Efficient railway tracks detection and turnouts recognition method using HOG features," *Neural Computing and Applications*, vol. 23, no. 1, pp. 245–254, 2013.

[10] J. Qingbo, Z. Enze, Y. Xinqi, X. Yu, and L. Yun, "Face recognition method based on HOG and DMMA from single training sample," *Multimedia Tools and Applications*, vol. 75, no. 21, pp. 13163–13177, 2016.

[11] S. A. Chowdhury, M. Mir, S. Kowsar, and K. Deb, "Human detection utilizing adaptive background mixture models and improved histogram of oriented gradients," *ICT Express*, vol. 4, no. 4, pp. 216–220, 2018.

[12] M. Nabila, B. J. Yousra, and W. Eric, "*Optimized HOG descriptor for on road cars detection*," in *Proceedings of the 10th International Conference on Distributed Smart Camera-ICDSC'16*, pp. 166–171, Paris, France, 2016.

[13] S. Aytaç Korkmaz and H. Binol, "Classification of molecular structure images by using ANN, RF, LBP, HOG, and size reduction methods for early stomach cancer detection," *Journal of Molecular Structure*, vol. 1156, pp. 255–263, 2018.

[14] A. K. Hmood, C. Y. Suen, and L. Lam, "An enhanced histogram of oriented gradient descriptor for numismatic applications," *Pattern Recognition and Image Analysis*, vol. 28, no. 4, pp. 569–587, 2018.

[15] N. A. Jebril, H. R. Al-Zoubi, and Q. A. Al-Haija, "Recognition of handwritten Arabic characters using histograms of oriented gradient (HOG)," *Pattern Recognition and Image Analysis*, vol. 28, no. 2, pp. 321–345, 2018.

[16] M. Uddin, M. A. Islam, M. Shajalal, M. A. Hossain, M. Yousuf, and S. Iftekhar, "Paddy seed variety identification using t20-hog and haralick textural features," in *Complex & Intelligent Systems*, pp. 1–15, Springer, 2021.

[17] M. Chandrakala and P. D. Devi, "Two-stage classifier for face recognition using hog features," *Materials Today: Proceedings*, vol. 47, pp. 5771–5775, 2021.

[18] B. T. Hung, "Face recognition using hybrid HOGCNN approach," *Research in Intelligent and Computing in Engineering: Select Proceedings of RICE 2020*, , pp. 715–723, Springer, 2021.

[19] M. Zaffar, S. Ehsan, M. Milford, and K. McDonald-Maier, "CoHOG: a light-weight, compute-efficient, and training-free visual place recognition technique for changing environments," *IEEE Robotics and Automation Letters*, vol. 5, no. 2, pp. 1835–1842, 2020.

[20] X. Zhang, H. Shangguan, A. Ning, A. Wang, J. Zhang, and S. Peng, "Pedestrian detection with EDGE features of color image and HOG on depth images," *Automatic Control and Computer Sciences*, vol. 54, no. 2, pp. 168–178, 2020.

[21] H. Wang, S. Wei, and B. Fang, "Facial expression recognition using iterative fusion of MO-HOG and deep features," *The Journal of Supercomputing*, vol. 76, no. 5, pp. 3211–3221, 2020.

[22] X. Pan, "Fusing HOG and convolutional neural network spatial–temporal features for video-based facial expression recognition," *IET Image Processing*, vol. 14, no. 1, pp. 176–182, 2020.

[23] G. Joshi, S. Singh, and R. Vig, "Taguchi-TOPSIS based HOG parameter selection for complex background sign language recognition," *Journal of Visual Communication and Image Representation*, vol. 71, 2020.

[24] K. Wang, H. Wang, and J. Wang, "Terrain matching by fusing HOG with Zernike moments," *IEEE Transactions on Aerospace and Electronic Systems*, vol. 56, no. 2, pp. 1290–1300, 2020.

[25] V. T. Hoang, D. P. van Hoai, T. Surinwarangkoon, H.-T. Duong, and K. Meethongjan, "A comparative study of rice variety classification based on deep learning and hand-crafted features," *ECTI Transactions on Computer and Information Technology (ECTI-CIT)*, vol. 14, no. 1, pp. 1–10, 2020.

[26] M. F. Aslan, A. Durdu, K. Sabanci, and M. A. Mutluer, "CNN and HOG based comparison study for complete occlusion handling in human tracking," *Measurement*, vol. 158, 2020.

[27] W. Zhou, S. Gao, L. Zhang, and X. Lou, "Histogram of oriented gradients feature extraction from raw Bayer pattern images," *IEEE Transactions on Circuits and Systems II: Express Briefs*, vol. 67, no. 5, pp. 946–950, 2020.

[28] H. T. M. Nhat and V. T. Hoang, "Feature fusion by using LBP, HOG, GIST descriptors and Canonical Correlation Analysis for face recognition," in *2019 26th International Conference on Telecommunications (ICT)*, pp. 371–375, Hanoi, Vietnam, 2019.

[29] H.-T. Duong and V. T. Hoang, "Dimensionality reduction based on feature selection for rice varieties recognition," in *2019 4th International Conference on Information Technology (InCIT)*, pp. 199–202, Bangkok, Thailand, 2019.

[30] S. Banerji, A. Sinha, and C. Liu, "Haarhog: Improving the hog descriptor for image classification," in *2013 IEEE International Conference on Systems, Man, and Cybernetics*, pp. 4276–4281, Manchester, UK, 2013.

[31] Z. Zhou and Y. Zhou, "Cross-channel similarity based histograms of oriented gradients for color images," in *2019 IEEE International Conference on Systems, Man and Cybernetics (SMC)*, pp. 1621–1625, Bari, Italy, 2019.

[32] T. N. Van and V. T. Hoang, "Early and late features fusion for kinship verification based on constraint selection," in *2019 25th Asia-Pacific Conference on Communications (APCC)*, pp. 116–121, Ho Chi Minh City, Vietnam, 2019.

[33] T. N. Van and V. T. Hoang, "Kinship verification based on local binary pattern features coding in different color space," in *2019 26th International Conference on Telecommunications (ICT)*,, pp. 376–380, Hanoi, Vietnam, 2019.

[34] S. Fekri-Ershad and F. Tajeripour, "Impulse-noise resistant color-texture classification approach using hybrid color local binary patterns and Kullback–Leibler divergence," *The Computer Journal*, vol. 60, no. 11, pp. 1633–1648, 2017.

[35] T. Song, J. Feng, S. Wang, and Y. Xie, "Spatially weighted order binary pattern for color texture classification," *Expert Systems with Applications*, vol. 147, 2020.

[36] T. Mäenpää and M. Pietikäinen, "Classification with color and texture: jointly or separately?," *Pattern Recognition*, vol. 37, no. 8, pp. 1629–1640, 2004.

Hindawi
Journal of Sensors
Volume 2021, Article ID 8103183, 7 pages
https://doi.org/10.1155/2021/8103183

Research Article

Automatic Recognition and Correction of Volleyball Players' Release Angle Based on Feature Statistics

Rui Fang

School of Physical Education, Xinyang Vocational and Technical College, Xinyang, Henan 464000, China

Correspondence should be addressed to Rui Fang; fangrui0213@xyvtc.edu.cn

Received 10 September 2021; Revised 11 October 2021; Accepted 26 October 2021; Published 27 November 2021

Academic Editor: Mu Zhou

The constant reform of the competition rules has promoted the innovation of volleyball techniques and tactics. In order to improve the training efficiency and competitive level of volleyball players, this study designed a volleyball player shooting angle automatic recognition and correction method based on the process of feature statistics. Firstly, the basic structure of the information acquisition system is analyzed, and the acquisition process is determined. Then, grayscale and binarization operations are carried out for color-moving images to separate their foreground and background, and a median filtering algorithm is used to remove the image noise. Then, the image pyramid of different sizes is generated by the filter. Based on setting the datum direction, the feature of volleyball shooting is extracted by using the line formula. On this basis, we construct a support vector machine (SVM) classifier to statistically classify the features, use the histogram additive kernel support vector machine method to obtain the lens angle recognition results, and correct the lens angle through feature point matching. Simulation experiments show that this method can effectively remove image noise and make the image signal-to-noise ratio higher, and it can effectively identify whether volleyball players' release Angle is correct, to achieve the purpose of timely correction.

1. Introduction

Volleyball is a sport that makes the Chinese people proud, especially the Chinese women's national volleyball team, which has achieved impressive results in the past and has become a spirit of the times, inspiring the Chinese people to strive for self-improvement [1]. As the rules of the volleyball game system continue to change, it imposes higher demands on the physical quality and skill level of the players. Most of the traditional training methods rely on the coaches' observation and analysis of the angles of the players' shots through their own experience to find out the deficiencies and give training suggestions and instructions. The training in this way relies more on the coaches' own quality and is somewhat subjective.

In recent years, for various reasons, the development of volleyball in China has slowed down, which has caused widespread concern among enthusiasts. Modern sports involve high technology from players' equipment to training methods [2]. Therefore, the development of technology in volleyball training has become the goal of future development. Moreover, having information related to the angle of the athlete's shot is the first step to improve the technique [3].

In this study, the image acquisition system is used to collect the information of the shot angle of players, and the feature statistics are input into the Support Vector Machine (SVM) classifier to complete the shot angle recognition, and then the feature matching is performed on the collected information combined with the sample inventory in the information acquisition system. If it matches with the sample information, the shot angle meets the requirements; if not, it is corrected.

The reason for the use of feature statistics is that, in the use of mathematical statistics to study overall features, the focus is not on individuals in a population, but on the distribution of related features among different individuals in a population.

This paper adopts this method to realize angle recognition, which reduces the complexity of recognition process and improves the accuracy of recognition.

2. Information Acquisition and Processing of Shot Angle

2.1. Information Acquisition System Structure and Acquisition Process. The motion information acquisition system, also known as the motion capture system, can realize the measurement, tracking, and recording of the target, which mainly includes the results of master controller, RF transceiver unit, network communication unit, and serial communication unit. The structure of shooting angle information collection system is shown in Figure 1.

2.1.1. Master Controller. The core part of the master controller is the master chip, and the selected microprocessor varies for different application scenarios. The microprocessor required in this study needs not to be portable and handheld. Therefore, in order to save resources, this study selects the embedded microcontroller as the system processor. In addition, the reader and the RFID both need to feature low-power consumption, so this study uses the ultra-low-power sixteen-bit industrial-grade microcontroller introduced by TI as the master chip.

2.1.2. RF Transceiver Unit. Generally, the acquisition system utilizes the acquisition method based on the signal reception strength, so the signal acquisition capability of the RF transceiver chip should be strong [4, 5]. Based on a comprehensive analysis of the system requirements and functions, the 2.4 GHz CC2500 is selected as the RF transceiver chip in this study because of its advantages of small size, low power consumption, and user-friendly design.

2.1.3. Network Communication Unit. This unit mainly refers to the Ethernet communication part, and the ENC28J60 from Microchip is selected in this study because it has only twenty-eight pins and has the advantages of low computational complexity and low cost [6].

2.1.4. Serial Communication Unit. The serial communication unit in this system uses MAX232, a level logic conversion chip to interconnect the UART port of the master controller with the PC to achieve communication.

Combining the structure of the above-mentioned information collection system, the construction of a volleyball information collection program is shown in Figure 2.

2.2. Image Information Preprocessing. The acquired volleyball motion images are preprocessed. Usually, the information contained in the image is complex, and the useful information generally accounts for only a small portion. In addition, there is also a certain amount of noisy information in the image due to the effect of illumination. The purpose of preprocessing is to improve the image quality and thus fundamentally improve the recognition effect. Image preprocessing in this study mainly includes grayscale, binarization, and filtering and denoising.

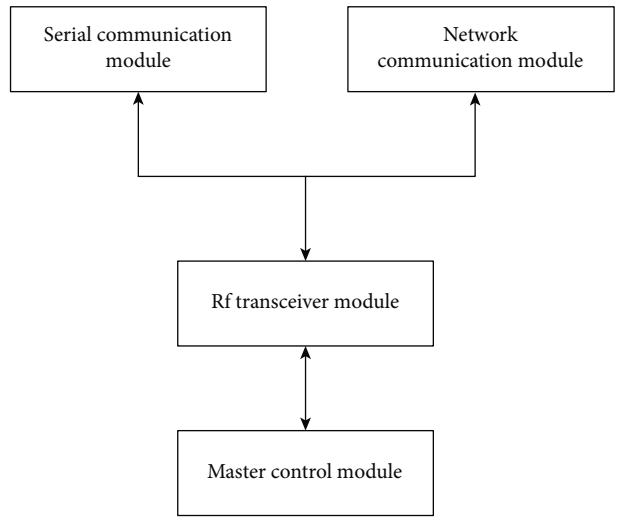

Figure 1: Schematic diagram of the structure of shooting angle information collection system.

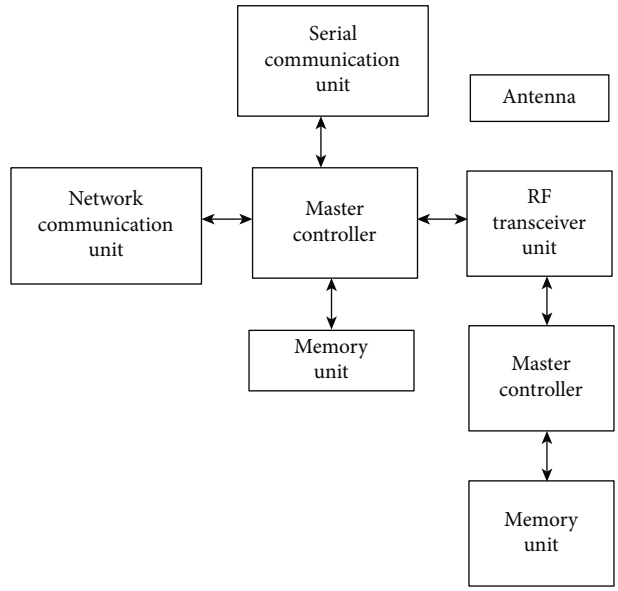

Figure 2: Volleyball information collection program.

2.2.1. Image Grayscale. Since the images acquired by the system are color images, the essence of image grayscale is to take the same values for the red component R, green component G, and blue component B. The processed color image realizes less postprocessing calculation and occupies less memory space. Grayscale image is an image with only one sampling color on any pixel. It is usually displayed as grayscale from the brightest black to white.

The component value interval of R, G, and B is generally [0, 255], the grayscale is 256, and grayscale images can represent 256 colors. The grayscale values are represented by Gray. In this paper, the weighted average method is used to realize the grayscale of color images.

Combining the three values R, G, and B, their respective weights are defined and a weighted average of them is calculated as follows:

$$R = G = B = \text{Gray} = \frac{\alpha R + \beta G + \gamma B}{3}. \quad (1)$$

In equation (1), α, β, and γ represent the weights of R, G, and B, respectively. Since green produces the strongest stimulus effect on human eyes, followed by red and blue, grayscale images are obtained with higher quality when $\beta > \alpha > \gamma$. Combined with experience, it is known that the best grayscale images are obtained when $\alpha = 0.299$, $\beta = 0.587$, and $\gamma = 0.114$ [7, 8]. The expression for grayscale of color images is as follows:

$$f(i,j) = 0.299R(i,j) + 0.587G(i,j) + 0.114B(i,j). \quad (2)$$

In equation (2), (i,j) represents the point within the image, $f(i,j)$ represents the grayscale value after grayscale transformation, and the three values of this point in the initial color graphics R, G, and B are described as $R(i,j)$, $G(i,j)$, and $B(i,j)$, respectively.

2.2.2. Image Binarization. The essence of grayscale image binarization is to separate the foreground and background of the image [9]. Firstly, a threshold T is set to divide the image into two parts, and the part above T is called the foreground image and the part less than T the background image. Assuming that the input and output images are represented as $f(x,y)$ and $g(x,y)$, respectively, the following equation is applied:

$$g(x,y) = \begin{cases} 1, & f(x,y) \geq T, \\ 0, & f(x,y) < T. \end{cases} \quad (3)$$

If the target grayscale values are distributed in several nonadjacent regions, the following equation is applied:

$$g(x,y) = \begin{cases} 1, & f(x,y) \in \Phi, \\ 0, & \text{other}. \end{cases} \quad (4)$$

In equation (4), Φ represents the set of different grayscale value intervals of the foreground target.

2.2.3. Filtering and Denoising Processing. In the process, the median filter algorithm is used to remove image noise. The median filter algorithm mainly applies the sorting statistics theory. The core of this algorithm is the sorting statistical theory, which belongs to a nonlinear smooth filtering image processing technique [10]. The filtering expression in the two-dimensional filtering window W is as follows:

$$g_{\text{median}}(x,y) = [f(s,t)]. \quad (5)$$

In equation (5), $f(s,t)$ represents the grayscale value of the pixel in the neighborhood.

Through the above-mentioned implementation of image graying, binarization, filtering, and denoising processing operations on volleyball moving images, not only can the foreground information and background information in the picture be effectively separated but also the noise information in the image can be effectively removed, thereby improving the image information. Furthermore, the noise ratio lays the foundation for the subsequent volleyball shot feature extraction process.

3. Automatic Recognition and Correction of Shot Angle Based on Feature Statistics

3.1. Feature Extraction. Upon completion of image preprocessing, direct detection of feature points enables to avoid image segmentation, which is easier to implement. For this reason, this study implements feature point detection using approximate Hessian matrix based on Speeded-Up Robust Features (SURF). Assume that the Hessian matrix of the point $I(x', y')$ in the scale space that is σ is represented as

$$H = \begin{bmatrix} L_{x'x'}(x', \sigma) & L_{x'y'}(x', \sigma) \\ L_{x'y'}(x', \sigma) & L_{y'y'}(x', \sigma) \end{bmatrix} \quad (6)$$

In equation (6), $L_{x'x'}(x', \sigma)$, $L_{x'y'}(x', \sigma)$, and $L_{y'y'}(x', \sigma)$ are the results obtained from the second-order partial derivatives of the Gaussian function at $I(x', y')$ [11] and the convolution of the image $I(x', y')$.

On this basis, the image pyramid is constructed. In this process, the image needs to be resampled and then convoluted with Gaussian functions of different scales. A surf operator approximates the second-order Gaussian function through a box filter to improve the calculation speed. The image pyramids of different sizes can be generated in the image depending only on the filter size, and the convolution acceleration of the image is achieved using integral images [12, 13], and thus, the determinant of Hessian matrix is obtained as follows:

$$\Delta H = D_{x'x'} D_{x'y'}(x') - \left(0.9 D_{y'y'}(x)\right)^2 \quad (7)$$

In equation (7), Δ indicates the response value of the box filter in the region near the point $I(x', y')$ [14], and $D_{x'x'}$, $D_{x'y'}$, and $D_{y'y'}$ represents the prefiltering image line, the filter convolution line, and the postfiltering image line, respectively. The value of the matrix determinant is used to judge the feature point, and if the value is positive and the two feature values are different, the point is defined as an extreme point.

Based on this, some among the extreme points are selected as candidate feature points. The selection method is to do the nonmaximum suppression in the $3 \times 3 \times 3$ regions centered on the extreme points and compare the adjacent scales with the 26 neighborhood values near the scale, and only the points that are larger or smaller than the neighborhood values can be identified as feature points.

To ensure the rotational invariance of the descriptors and give the reference direction for feature point assignment, a neighborhood with the feature point as the center of the circle and 6s (s refers to the scale value where the feature point is located) as the radius is established firstly, and the Harr wavelet responses in different directions are computed in this

region, while weights are attached to these response values to ensure that the weights of the adjacent feature points are larger; its rotation is performed in a circle by a sector template with a circular angle of sixty degrees to obtain the vector consisting of the cumulative sums of the Harr responses in all sliding windows, and the direction corresponding to the highest cumulative sum is set to be the reference direction of this feature point [15].

After determining the reference direction, construct a square with a side length of 20 cm along the direction centered on the feature point, and divide the window neighborhood into 4×4 subareas. In any subregion, the Harr wavelet response values of the sampling points are calculated for the reference direction x' and y', which are recorded as $d_{x'}$ and $d_{y'}$ and weighted, and the statistical results of different subregion response values are expressed as $\Sigma_{d^{x'}}, \Sigma_{d^{y'}}, |\Sigma_{d^{x'}}|, |\Sigma_{d^{y'}}|$; then, a four-dimensional vector $V = [\Sigma_{d^{x'}}, \Sigma_{d^{y'}}, |\Sigma_{d^{x'}}|, |\Sigma_{d^{y'}}|]$ is obtained, which is the feature descriptor of this subregion.

3.2. Feature Statistical Classification Based on Support Vector Machine Classifier. The feature extraction of volleyball players' shot angle has been completed above, and the next step is to classify and recognize the extracted features.

The greatest advantage of SVM is its excellent learning and generalization ability [16]. The main idea of SVM is to construct the plane by mapping the initial nonlinear data into a high-dimensional space and to maximize the distance from all sample sets to this plane [17]. For this purpose, this study uses the linear support vector machine in a linearly separable case to obtain the optimal classification hyperplane.

Assume that the training set is represented as

$$T' = \{(x_1^*, y_1^*), (x_2^*, y_2^*), \cdots, (x_i^*, y_i^*), \cdots, (x_N^*, y_N^*)\}. \quad (8)$$

In equation (8), the sample type $(x_i^*, y_i^*) \in \{0, 1\}$, and N represents the number of samples. Then, linear separability means that a certain classification plane is capable of correctly classifying all the data in the set, and the hyperplane is expressed as

$$\omega \cdot x^* + b = 0. \quad (9)$$

In equation (9), ω represents the Euclidean space dimension, x^* represents the data set, and b represents the flat subset. The classification decision function relative to the hyperplane is as follows [18]:

$$f(x) = \text{sign}\ (\omega \cdot x^* + b). \quad (10)$$

The distance margin between two planes is referred to as the classification interval between two sets of classified samples [19], and a larger value indicates a higher classification accuracy. Its expression is as follows:

$$\text{margin} = \frac{2}{|\omega|}. \quad (11)$$

In the case that all the two types of classified samples are correct, the classification interval is maximized when ω has the minimum value. Then, the optimal classification of linear separability can be expressed by the following equation:

$$\begin{cases} \min\limits_{\omega,b} \quad \frac{1}{2}|\omega|^2, \\ y_i(\omega \cdot x_i^* + b) - 1 \geq 0. \end{cases} \quad (12)$$

Using the Lagrangian function to calculate equation (12), assume that the function is expressed as

$$L'(\omega, b, a) = \frac{1}{2}\omega^T\omega - \sum_{i=1}^{l} a_i\left\{y_i\left[\omega \cdot x_i' + b\right] - 1\right\}. \quad (13)$$

In equation (13), $a_i (i = 1, 2, \cdots, l)$ represents the Lagrangian operator.

Then, the first-order partial differentiation is performed on b and ω so that it is equal to 0:

$$\begin{cases} \dfrac{\partial L'}{\partial b} = \sum\limits_{i=1}^{l} y_i^* a_i = 0, \\ \dfrac{\partial L'}{\partial \omega} = \omega - \sum\limits_{i=1}^{l} y_i^* a_i x_i^* = 0. \end{cases} \quad (14)$$

Equation (14) is substituted into equation (13) to obtain the dual optimization problem as follows:

$$\max_{\alpha} -\frac{1}{2}\sum_{i=1}^{N}\sum_{j=1}^{N} a_i a_j x_i^* y_j^* \left(x_i^* \cdot x_j^*\right) - \sum_{i=1}^{N} a_i. \quad (15)$$

Then, the optimal classification function can be expressed as follows:

$$\begin{aligned} f(x) &= \min\ \frac{1}{2}\sum_{i=1}^{N}\sum_{j=1}^{N} a_i a_j x_i^* y_j^* \left(x_i^* \cdot x_j^*\right) - \sum_{i=1}^{N} a_i, \\ s \cdot t \cdot &\sum_{i=1}^{N} x_i^* y_i^* = 0, \quad a_i \geq 0,\ i = 1, 2, \cdots, N. \end{aligned} \quad (16)$$

In summary, the statistical classification of players' shot angle features can be achieved by using the optimal classification function.

3.3. Feature Recognition and Correction. In the process of lens angle recognition, this research realizes the final recognition combined with data features. For each acquired image, a q_{word}-dimensional statistical histogram is obtained after the description of the key frame feature library, and the shot angle recognition is performed by using the histogram intersection kernel support vector machine. The expression of the histogram intersection kernel is as follows:

$$K_{hi}(u, v) = \sum_{i=1}^{m}\{u_i, v_i\}. \quad (17)$$

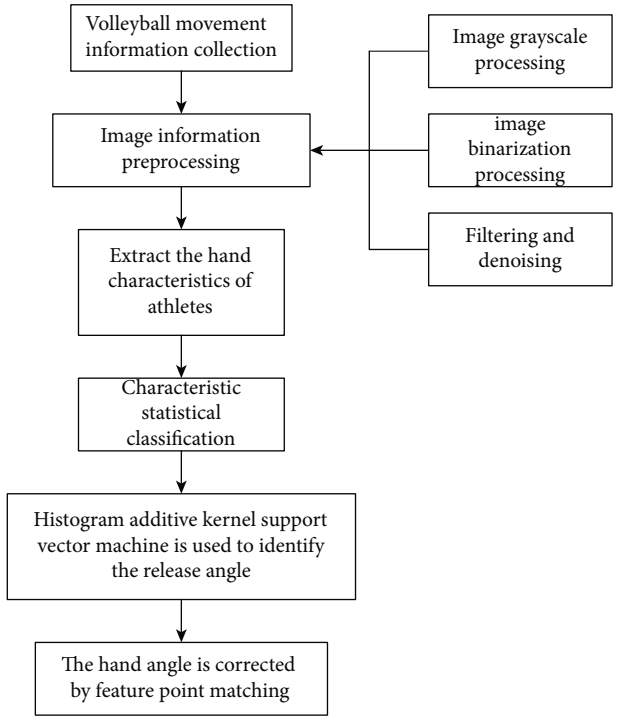

Figure 3: The realization process of the automatic recognition and correction method of volleyball players' shooting angle based on feature statistics.

In equation (17), $u = (u_1, u_2, \cdots, u_i, \cdots, u_m)$ and $v = (v_1, v_2, \cdots, v_i, \cdots, v_m)$ represent the statistical histograms of m species, respectively.

The image features are then described to obtain a statistical histogram, and with intersection kernel SVM, a linear combination is made between the probabilities of occurrence of different angles, and the highest probability value after the combination is taken as the recognition result [20], and the algorithmic procedure is shown in

$$P^{(o)} = p_1^{(o)}, p_2^{(o)}, \cdots, p_{\text{action}}^{(o)}, \tag{18}$$

$$M = \text{index}\left(\max\left(\sum_{o=1}^{2} \partial_o P^{(o)}\right)\right). \tag{19}$$

In the above equations, action represents the number of different shot angles, o represents the extracted species features, $P^{(o)}$ represents the probability combination of occurrence of tested images, and ∂_o represents the decision coefficient.

Feature point matching is performed for the recognition results and the feature library images in the acquisition system to derive the difference between the players' shot angle and the standard angle, so that the wrong shot angle can be corrected more accurately. For this purpose, this paper uses the paradigm of the ratio of nearest neighbor and second nearest neighbor for bidirectional matching. The equation is as follows:

Table 1: Simulation environment settings.

Name	Configuration
Operating system	Windows 10, 32
CPU	Intel(R) Core(TM) i5-3230M@2.6GHZ
RAM	8GB
Development tools	Visual Studio 2019, OpenCV 2.3.8
Optical camera model	L5163MX140-4

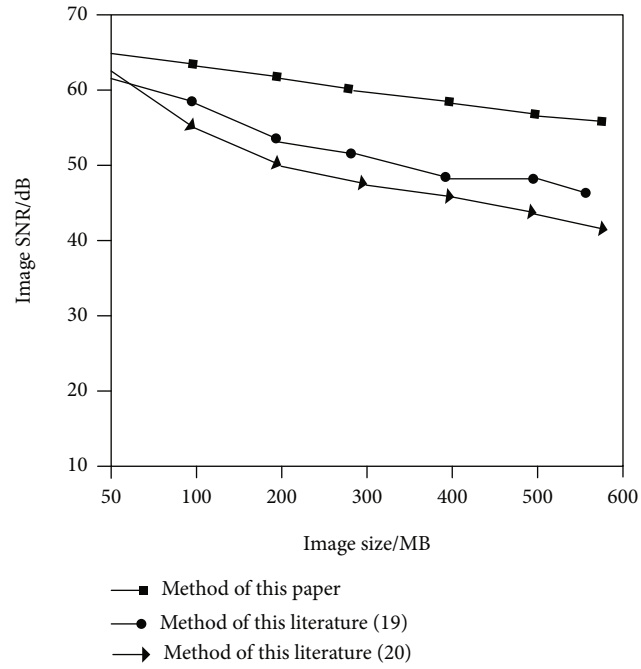

Figure 4: Comparison of image signal-to-noise ratio of different methods.

$$D' = \sqrt{\left(\varsigma_1 - \varsigma_1'\right)^2 + \left(\varsigma_2 - \varsigma_2'\right)^2 + \cdots \left(\varsigma_\eta - \varsigma_\eta'\right)^2}. \tag{20}$$

In equation (20), $(\varsigma_1, \varsigma_2, \cdots, \varsigma_\eta)$ and $(\varsigma_1', \varsigma_2', \cdots, \varsigma_\eta')$ represent the eigenvectors of the two feature points.

In summary, the design of the automatic recognition and correction method of volleyball players' shooting angle based on feature statistics is completed, and the realization process is shown in Figure 3.

4. Simulation Experimental Data Analysis and Research

In order to verify the feasibility of the automatic recognition and correction method of volleyball players' shot angle based on feature statistics designed above, the following simulation experiment is set up. The simulation environment is shown in Table 1.

In the experiment, volleyball spike is taken as an example. Assume that the ball speed is 80 km/h and the height of the hitting point is about 3.2 m. Firstly, 10 images of players' spike

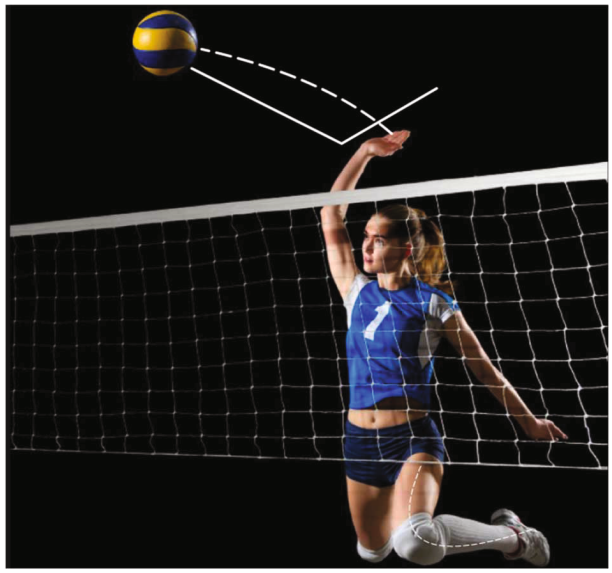

Figure 5: Elbow and hand shot angle.

Figure 6: Leg angle change.

shot angles are acquired using Gabor filter and feature extraction is performed using an 8×8 grid. Before feature extraction, image denoising is performed using the method in this paper, 3D shear domain image denoising in the literature [19], and convolutional neural network-based denoising method in the literature [20]. The final image signal-to-noise ratio obtained is shown in Figure 4.

It can be seen from Figure 4 that with the increase of image size, the image signal-to-noise ratio decreases after denoising by the three methods. The decreasing trend of the image signal-to-noise ratio is not obvious after applying the method in this paper, and it always remains high. This indicates that the median filtering algorithm in this study can effectively denoise images, which lays a good foundation for the subsequent feature statistics.

After the image processing mentioned above, the shot angle is recognized using the recognition algorithm in this paper. A variety of features such as players' legs, elbows, and hands are counted in the experiment to more accurately recognize whether the shot angle is correct. The recognition results are shown in Figures 5 and 6.

As shown in Figures 5 and 6, through the statistics of multiple image frame features, this study recognizes that the angle between the arm and the right angle of the volleyball is greater than 90 degrees and the knee bending is closer to 90 degrees during the spike action in Figure 5. This kind of shot angle is conducive to release force, thus improving the spike effect, while in Figure 6, the player's arm and knee bending degree is smaller and the body weight falls on the feet, which affects the jump, thus reducing the spike strength.

5. Conclusion

In this study, a volleyball sports information acquisition system is designed to acquire images of the players' shot angles, and after a series of processing, the images are obtained with high signal-to-noise ratio, while feature extraction is completed based on the key features of each frame, and the feature statistics are accomplished through a support vector machine classifier to achieve the recognition of the shot angles, which helps coaches to correct nonstandard movements. The method features strong image processing capability and can accurately complete image recognition, which will play an important supporting role in sports training.

In the future research, a variety of positioning measurement technologies such as computer vision, machine vision, and ultrasonic positioning can be introduced, and the advantages of different methods can be used to obtain a more ideal image acquisition effect and make volleyball training more scientific.

Data Availability

The labeled dataset used to support the findings of this study are available from the corresponding author upon request.

Conflicts of Interest

The author declares no competing interests.

References

[1] C. A. DiCesare, A. Montalvo, K. D. B. Foss et al., "Sport specialization and coordination differences in multisport adolescent female basketball, soccer, and volleyball athletes," *Journal of Athletic Training*, vol. 54, no. 10, pp. 1105–1114, 2019.

[2] H. M. Yin, P. Sun, G. U. Song et al., "The specific physical ability basic feature of volleyball players during the game," *Journal*

of Beijing University of Physical Education, vol. 9, pp. 15–23, 2019.

[3] P. Iodice, P. Ripari, and G. Pezzulo, "Local high-frequency vibration therapy following eccentric exercises reduces muscle soreness perception and posture alterations in elite athletes," *European Journal of Applied Physiology*, vol. 119, no. 2, pp. 539–549, 2019.

[4] H. Zhi, T. Ma, D. Pei et al., "Magnetic target recognition and localization method unaffected by attitude," *EPL (Europhysics Letters)*, vol. 129, no. 4, pp. 49–55, 2020.

[5] X. Zheng, X. Chen, and X. Lu, "A joint relationship aware neural network for single-image 3D human pose estimation," *IEEE Transactions on Image Processing*, vol. 29, pp. 4747–4758, 2020.

[6] J. Nye, L. Zingaretti, and M. Perez-Enciso, "224 automatic image feature extraction for genetic analysis in cattle," *Journal of Animal Science*, vol. 97, Supplement_3, pp. 47–47, 2019.

[7] B. Kumar, O. Dikshit, A. Gupta, and M. K. Singh, "Feature extraction for hyperspectral image classification: a review," *International Journal of Remote Sensing*, vol. 41, no. 16, pp. 6248–6287, 2020.

[8] K. Ichiyama, "Image processing apparatus, image pickup apparatus and image processing method," *Journal of Oral Rehabilitation*, vol. 8, no. 3, pp. 203–208, 2018.

[9] M. Rezaei Abkenar, H. Sadreazami, and M. O. Ahmad, "Salient region detection using feature extraction in the nonsubsampled contourlet domain," *IET Image Processing*, vol. 12, no. 12, pp. 2275–2282, 2018.

[10] T. Santos, S. Schrunner, B. C. Geiger et al., "Feature extraction from analog Wafermaps: a comparison of classical image processing and a deep generative model," *IEEE Transactions on Semiconductor Manufacturing*, vol. 32, no. 2, pp. 190–198, 2019.

[11] S. Echegaray, S. Bakr, D. L. Rubin, and S. Napel, "Quantitative Image Feature Engine (QIFE): an open-source, modular engine for 3D quantitative feature extraction from volumetric medical images," *Journal of Digital Imaging*, vol. 31, no. 4, pp. 403–414, 2018.

[12] R. B. Shang, R. Archibald, A. Gelb, and G. P. Luke, "Sparsity-based photoacoustic image reconstruction with a linear array transducer and direct measurement of the forward model (erratum)," *Journal of Biomedical Optics*, vol. 24, no. 8, pp. 1–9, 2019.

[13] Y. Zhang, S. S. Zhu, J. Lin, and P. Jin, "High-quality panchromatic image acquisition method for snapshot hyperspectral imaging Fourier transform spectrometer," *Optics Express*, vol. 27, no. 20, pp. 28915–28928, 2019.

[14] S. Bazeille, Y. Maillot, F. Cordier, C. Riou, and C. Cudel, "Light-field image acquisition from a conventional camera: design of a four minilens ring device," *Optical Engineering*, vol. 58, no. 1, pp. 1–9, 2019.

[15] S. Routray, A. K. Ray, C. Mishra, and G. Palai, "Efficient hybrid image denoising scheme based on SVM classification," *Optik*, vol. 157, pp. 503–511, 2018.

[16] S. Javed, A. Mahmood, S. al-Maadeed, T. Bouwmans, and S. K. Jung, "Moving object detection in complex scene using spatiotemporal structured-sparse RPCA," *IEEE Transactions on Image Processing*, vol. 28, no. 2, pp. 1007–1022, 2019.

[17] X. Liu, Y. Tang, and Y. Yang, "Primal-dual algorithm to solve the constrained second-order total generalized variational model for image denoising," *Journal of Electronic Imaging*, vol. 28, no. 4, pp. 1–15, 2019.

[18] S. Seo, "Image denoising and refinement based on an iteratively reweighted least squares filter," *KSCE Journal of Civil Engineering*, vol. 24, no. 3, pp. 943–953, 2020.

[19] S. Zhang, L. Wang, C. Chang, C. Liu, L. Zhang, and H. Cui, "An image denoising method based on BM4D and GAN in 3D shearlet domain," *Mathematical Problems in Engineering*, vol. 2020, Article ID 1730321, 11 pages, 2020.

[20] C. Shan, X. Guo, and J. Ou, "Residual learning of deep convolutional neural networks for image denoising," *Journal of Intelligent & Fuzzy Systems*, vol. 37, no. 2, pp. 2809–2818, 2019.

Hindawi
Journal of Sensors
Volume 2021, Article ID 9699110, 7 pages
https://doi.org/10.1155/2021/9699110

Research Article

Application of Image Style Transfer Technology in Interior Decoration Design Based on Ecological Environment

Shan Liu,[1] **Yun Bo**,[1] **and Lingling Huang**[2]

[1]*Design Art College, Xijing University, Xi'an Shaanxi 710123, China*
[2]*Public Art Department, Xi'an Academy of Fine Arts, Xi'an Shaanxi 710065, China*

Correspondence should be addressed to Shan Liu; 249838340@qq.com

Received 11 September 2021; Revised 9 October 2021; Accepted 26 October 2021; Published 25 November 2021

Academic Editor: Mu Zhou

With the further development of the social economy, people pay more attention to spiritual and cultural needs. As the main place of people's daily life, the family is very important to the creation of its cultural atmosphere. In fact, China has fully entered the era of interior decoration, and people are paying more and more attention to decorative effects and the comfort and individual characteristics of decoration. Therefore, it is of practical significance to develop the application of decorative art in interior space design. However, the transfer effect of current interior decoration art design tends to be artistic, which leads to image distortion, and image content transfer errors are easy to occur in the process of transfer. The application of image style transfer in interior decoration art can effectively solve such problems. This paper analyzes the basic theory of image style transfer through image style transfer technology, Gram matrix, and Poisson image editing technology and designs images from several aspects such as image segmentation, content loss, enhanced style loss, and Poisson image editing constrained image spatial gradient. The application process of style transfer in interior decoration art realizes the application of image style transfer in interior decoration art. The experimental results show that the application of image style transmission in interior decoration art design can effectively avoid the contents of the interior decoration errors and distortions and has a good style transfer effect.

1. Introduction

The purpose of interior decoration is to meet the needs of contemporary people for social activities and the urgent needs of daily life and to create a beautiful, comfortable, and convenient indoor living environment, which has gradually become a kind of comprehensive art in modern society [1]. The interior decoration industry has now become a rising and popular industry, which has also produced many interior decoration design companies. Contemporary interior decoration design has evolved from product design to culture, environment, and atmosphere design. Regarding the interior decoration art design, there are also many studies at home and abroad, including the original and simple table and chair layout, the ancient magnificent architectural interior layout, and the current home style design [2].

Nowadays, a single household style can not meet the needs of people's life and, people began to pursue higher quality, more free household style design. Therefore, it is very necessary to apply image style transfer technology to modern interior decoration art design [3]. Using two different styles of image migration to complete the interior decoration migration effect map, people can more intuitively understand the aesthetics of interior decoration art and then choose the interior decoration art design that suits them and satisfies their needs. The soul of the traditional art of ethnic minorities in China is fully reflected in the decoration of traditional buildings [4]. Although time has changed, traditional architectural art still has the value of eternal inheritance, and it will have a great influence on the interior and exterior decorative arts of current buildings as the role of inspiration and reference. As China gradually enters the postindustrial era, in essence, the material foundation has reached a certain level, characterized by the acceleration and strength of the service economy. Therefore, people's appreciation standards for architectural art are also getting

higher and higher. The single modern decorative art with modernism as the main source of ideas has long been unable to meet people's increasingly diversified indoor and outdoor decorative needs, so it is necessary to inherit the traditional architectural decorative art context of ethnic minorities and save the shortcomings of the development of modern decorative art. The method is to combine the traditional architectural decoration art of ethnic minorities with the innovative integration of modern indoor and outdoor decoration culture. With the visual and artistic characteristics of decorative materials, the visual expression methods of decorative materials and their role in interior design are specified [5]. Combined with the theories of indoor space artistic conception and artistic creation, the application of decorative materials is innovated. We take it as the material basis of interior design, propose several methods of decoration material innovation, use graphic combinations to create different layers, enhance the visual depth of space, and use texture conversion to create unexpected visual design effects. These methods are used to further enhance the innovation of interior design in artistic expression.

2. Materials and Methods

2.1. Image Style Transfer Technology. Different image styles are used to express the semantic content of images, and the way to complete the processing of images is the transfer of image styles [6]. The simple explanation is to display an ordinary image in another image style while preserving the central content and structure of the original image. For example, there are two images: one is a style image and the other is a content image [7]. Firstly, we must retain the content and structure images of all content, extract the main feature style of the image, then use the extracted features to complete the image reorganization of the original content, and finally transform the style image and content image into an image output image. Its structure is shown in Figure 1.

2.2. Gram Matrix. Image style transfer requires a content image to be converted and a style image. The correlation between the two image features is calculated through the Gram matrix, and the amount of each feature in the image is found to grasp the whole style of the image [8]. The mathematical form of Gram matrix calculation is

$$G(x) = A \times A^{\mathrm{T}}. \tag{1}$$

In practical application, Gram matrix is the inner product operation of matrix and can also be regarded as the eccentric covariance matrix between image features. In the interior decoration art feature image, each number represents the strength of a feature, and the elements on the diagonal of the Gram matrix precisely reflect the amount of each feature in the interior decoration art image, which helps better grasp the general style of interior decoration art. By using the difference between Gram matrices, we measure the difference between interior decoration art design images and realize the style transfer of interior decoration art design images [9].

2.3. Poisson Image Editing Technology. The image used for image style transfer is generally blurred. Logically speaking, a blurred image is an image with inconspicuous contours of the object and insufficient grayscale changes in the contour edges, resulting in a weak sense of hierarchy. If we want to generate a clear image, we need to calculate the rate of change of the image gray level and then obtain a clearer style transfer image. When completing the interior decoration art design, we must also pay special attention to not let the entire decoration look fuzzy. We need to find the "change rate of image grayscale" and then complete the pixel fusion of the source image and the target image. The schematic diagram of image pixel construction in the fusion area is shown in Figure 2.

In Figure 2, V represents the source image gradient field, u represents the interior decoration source image, $\partial\Omega$ represents the boundary of the image, f^* represents the merged result of images other than Ω, Ω represents the area covered by the image, and f represents the images within Ω.

2.4. Research on Image Style Transfer in Interior Decoration Art. Because the style migration of interior decoration art design images has authenticity and complexity in content, it is necessary to maintain the consistency of the content and images during the migration process, and the style should also be consistent, so that no interior will be generated. Errors or distortions occur in the image content of decorative art design during the migration, which makes the effects of interior decorative art real and effective [10]. The realization process of style transfer is shown in Figure 3.

2.4.1. Image Segmentation. Due to the different styles of the interior decoration art design, the design styles are not consistent, so in the process of calculating the style loss of the entire interior decoration art image, the content of the art image will not be considered [11]. The texture of the interior decoration art design image will be mapped to an area that does not correspond to the texture semantics, and the image content could be different. The interior decoration art design style is directed to other parts of the image, the content of the style content image appears inconsistent with the style on the style image, and the content of the interior decoration art image and the content of the migration change do not match [12].

The image semantic segmentation method can be applied to complete the style transmission of similar semantic content in interior decoration art design images. First, it is divided into the input content image and style image, and then, the same type of interior decoration art design image is marked with the same mask color. Different colors are used for different categories of interior decoration art design images, which highlight the difference in style of each semantic category without causing losses. Then, the style image and content image are used as input images to substitute into the VGG-19 [13] network of the fully connected layer, and the basic features of each image at different levels are extracted to complete the migration between semantically equivalent subregions; thus, the mapping on each subregion can be unified [14].

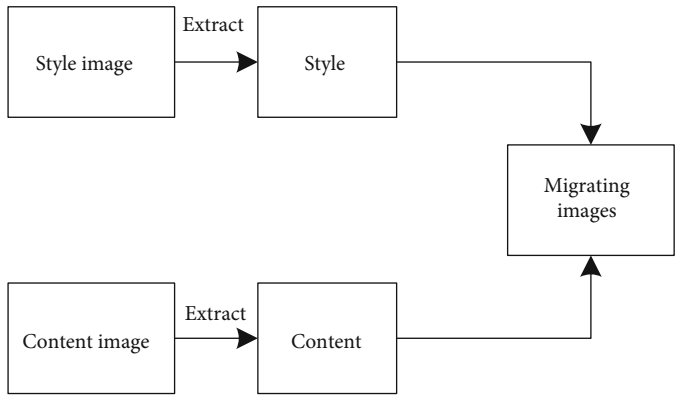

Figure 1: Image style transfer flow chart.

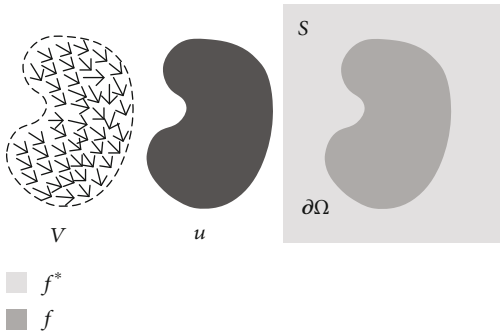

Figure 2: Schematic diagram of image pixel construction in the fusion area.

2.4.2. Content Loss. For interior decoration art, we define its style image as s, content image as c and white noise image, input them into the VGG-19 network, and extract the style of interior decoration art image through low-level response. Responding to extract the content of the interior decoration art design image, the random white noise map is used as the initial input [15]. In this way, we can make up the content defect of the content feature map and the white noise feature map and get many feature maps under the action of the convolution layer and take conv3_2 and conv 4_2 layers as the content image of interior decoration art design. Images in interior decorative art design, similar to content image C [16] in content design, were generated. The average loss function is translated into the calculation of content loss; the calculation formula is

$$L_{\text{coabut}}(c, g, l) = \frac{1}{2}\sum \|K_l(g) - K_l(c)\|^2. \tag{2}$$

Among them, l represents the convolutional layer, and K_l represents the feature matrix of the image in the interior decoration art design.

Using the related theory of error direction propagation, the gradient value of the generated image in the interior decoration art design is calculated, and it is updated as the input image, so that the initial random image keeps changing until the content image appears the same response in the interior decoration art design network c.

2.4.3. Enhanced Style Loss. The style of the image is expressed by the correlation between the features. The image style is the texture information, which refers to the calculation of the relationship between the features through the Gram matrix, thereby capturing the texture information of the interior decoration art design image. The conv2_1, conv1_1, conv4_1, conv3_1, and conv5_1 are used as image styles, and the white noise image gradient descent mode is used to match images similar to the image style [17]. Also, we mark the segmented image in another channel and use it as the input mode to form a style loss for each semantic category [18]. We use the segmentation channel to enhance the algorithm of the convolutional neural network and form the output image g and loss of style between images s through the calculation of the function:

$$L_{\text{style}}(s, g, l, c) = \sum_{c=1}^{c} \frac{1}{2}\sum \left\| G_{c,l}(g) - G_{c,l}(s) \right\|^2. \tag{3}$$

Among them, $G_{c,l}$ represents the calculation method of the Gram matrix, that is, the inner product between interior decoration art design drawings, and c represents the number of semantic segmentation mask categories in the interior decoration art design.

The loss function of the interior decoration art design image is

$$L_{\text{total}} = \alpha L_{\text{content}} + \beta L_{\text{style}}. \tag{4}$$

The loss function is minimized and the stylized image of interior decoration art design is obtained.

2.4.4. Poisson Image Editing Constrains Image Spatial Gradient. In order to generate a clear style transfer effect map in the interior decoration art design, the interior decoration art design image after stylization is used as input; then, the gradient field of the content image can be expressed as

$$g(x, y) = \nabla c(x, y). \tag{5}$$

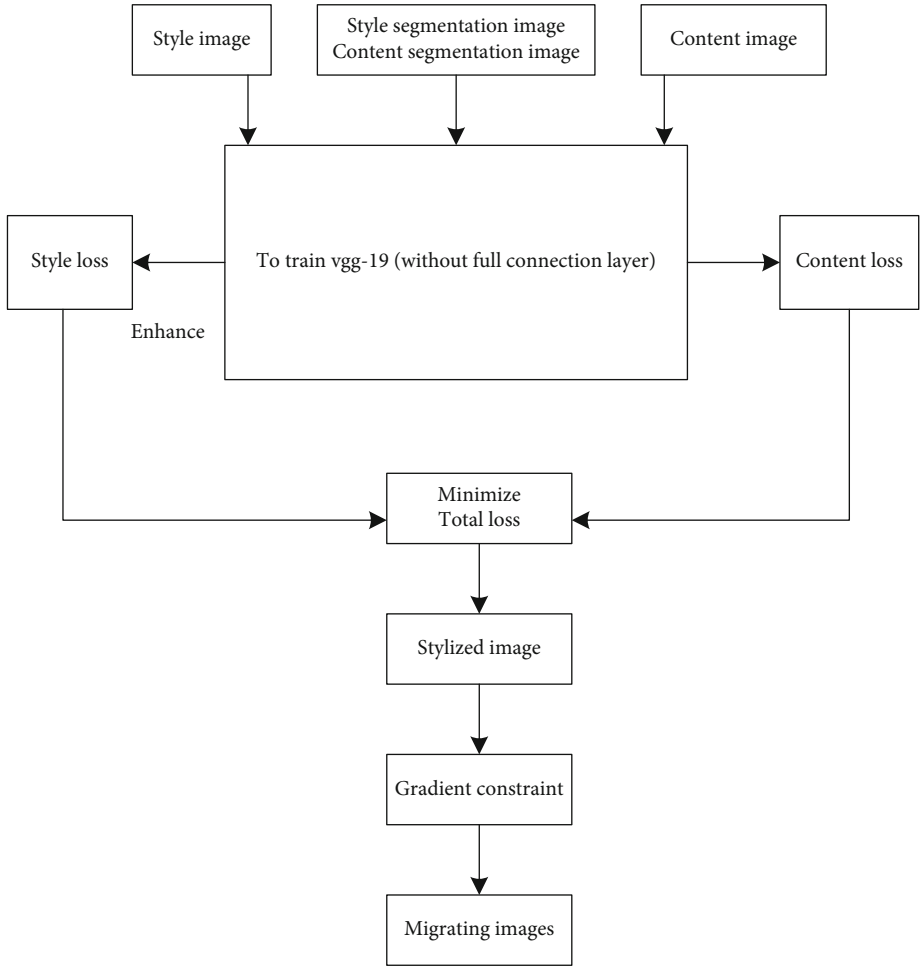

Figure 3: The application process of image style transfer in interior decoration art.

While completing the constraints on the image spatial gradient, it also needs to meet

$$L^* = \min \iint_{\Omega} \|\nabla F - g\|^2 + (F - C_s)^2 dF dg. \quad (6)$$

Based on the objective function of the spatial gradient constraint, the Poisson equation is established, which is expressed as

$$F\left(1 - \lambda \nabla^2\right) = C_s - \lambda \nabla g. \quad (7)$$

Among them, λ represents the relative weight between the control content image and the style image.

3. Results and Analysis

3.1. Experimental Dataset. For the application experiment of image style transfer in interior decoration art, we select the indoor scene dataset. The original dataset included a total of 22 million indoor scenes. The design style is the same as the modern interior scene.

This article studies the image style migration in the interior decoration art design. Therefore, we randomly select 10,000 indoor scenes of different styles from the 2200 indoor scenes as the pretraining dataset, pretrain the VGG-19 network model, obtain the model parameters, and construct a network model suitable for interior decoration art design scenes, saving model training time [19].

3.2. Analysis of Experimental Results. In the experiment process, using different types and scenes of interior decoration art design style images, through calculation, it can be obtained that the image style transfer effect is the best as $\alpha = 1$, $\beta = 100$, and $\lambda = 20$. In order to obtain a more satisfactory migration effect of the interior decoration art design style image, the experimental test needs to complete two rounds of iterations; each iteration number is 2000 times. Before the experimental test starts, we reextract the interior decoration art design image style so as to minimize the objective function [20].

In the process of precise segmentation of the semantic content of the interior decoration art design image, different color marks are generally used, and the mask operation method is used [21]. Masking refers to a baffle layer on the original layer. Through the change of the gray color value, the gray color value with a different transparency is formed and projected to different layers, so that the transparency of different parts of the layer can occur. The

(a) Kitchens of different styles

(b) Kitchens of the same style

(c) Living room

(d) Restaurant

(e) Bedroom

Figure 4: The effect of image style migration of interior decoration art design.

corresponding changes form the protection of the original picture content [22].

The specific steps are as follows: We import the style image in Photoshop, create a new blank layer in the Layers panel, fill it with a full color, make the background image consistent with the image style, select the Style image in the Layers panel, click the Add Layer Mask button, and change the selected mask's foreground color and background color to black and white. Then, we select the brush tool to complete the drawing of the image of the same area in the style image, adjust the size of the brush, and modify the front and back background colors to draw the semantic content of the image. After the segmentation is performed, we mark the color that it is filled and finally fill the background layer with different colors repeatedly, until all the style content is marked with different colors and the segmentation is implemented, and the content image is also operated in the same way. The steps of style migration for interior decorative art design images are as follows.

Step 1. We input the interior decoration art design style image, interior decoration art design content image, and the segmented images of the two together into the trained VGG-19 network, complete the initialization of the white noise map of the image pixels, and input them into VGG-19 together in the network.

Step 2. In the conv3_2and conv4-2 layers of the VGG-19 network, we extract the content feature matrix of the interior decoration art design content image and calculate the content loss value between the image pixel white noise map and the content map.

Step 3. In the conv1_1 layer, conv2-1 layer, conv3_1 layer, conv4-1 layer, and conv5-1 layer in the VGG-19 network, we extract the style feature matrix of the interior decoration art design style image and divide the color-coded segmented image as another channel of image style transfer. After connecting all the segmentation channels, we calculate the enhanced style loss value of the image pixel white noise map and the style image.

Step 4. We calculate the total loss function of the interior decoration art design image used for training in terms of content loss and style loss.

Step 5. By training the interior decoration art design image, the white noise gradient of the image pixels can be reduced, thereby minimizing the total loss function. After multiple iterations of calculation, the total loss function is adjusted to obtain the stylized image of the interior decoration art [23]. Poisson image editing technology completes the gradient constraint on the programmed image and obtains the image style of interior decoration art design style and the image content migration effect of interior decoration art design content [24].

It can be seen from the migration results in Figure 4 that the content image corresponding to the kitchen art design scene (Figure 4(a)) belongs to the American style, the corresponding style image belongs to the modern minimalist

style, and a good migration effect can be produced between the content image and the style image. The kitchen art design scene (Figure 4(b)) is to test the style conversion effect of interior decoration art design images with the same style and different content. The corresponding style images and content images are American styles, but they can still produce a good migration effect.

The content image corresponding to the living room art design scene belongs to the modern style, and the corresponding style image belongs to the minimalist style. In this decorative art, the pictures on the wall can also complete the image style transfer, but the effect of the transfer depends on the interior decoration art design Image segmentation mark map. Restaurant art design scene corresponding content image belongs to European style, corresponding style image belongs to industrial style. After the image style is transferred, the color changes to fusion color. The content image corresponding to the bedroom art design scene belongs to the new Chinese style; the corresponding style image belongs to the retro style. Overall, the image style transfer effect is good, especially on the left wall of the bedroom art design scene, which achieves a very reliable image style transfer.

4. Conclusion

(1) This article proposes to introduce the image style transfer technology into the field of modern home style images for interior decoration design. The semantic content of modern interior decoration style design images is complex, the color is varied, and the layout is exquisite. In the field, a good image style transfer effect can be achieved, and the content of the content image and the style image can be effectively prevented from causing the migration overflow phenomenon

(2) Image style transfer technology can effectively specify whether a semantic content needs to be transferred and maintain the authenticity of the image. Using Poisson image editing method to constrain the gradient of the image, we can obtain a clear migration image that meets the needs of modern home style design

(3) The result of image transfer proves the effectiveness of image style transfer in interior decoration art. It shows that the image style transfer technology is very robust and can realize various art design scenes and various types of image style transfer in interior decoration. The application of image style transfer to interior decoration art can not only achieve a better transfer effect but also will not cause distortion of interior decoration art design images, showing good application prospect

Data Availability

The labeled dataset used to support the findings of this study is available from the corresponding author upon request.

Conflicts of Interest

The authors declare no competing interests.

Acknowledgments

This study is supported by the General Special Scientific Research Project of Shaanxi Provincial Department of Education: Research on the Innovative Application of Northern Shaanxi's Folk Cloth and Pasting Art Elements in Modern Fiber Art under the Background of Traditional Cultural Renaissance (21JK0415).

References

[1] R. M. Mcelhaney, "Algorithms for graphics and image processing," *Proceedings of the IEEE*, vol. 71, no. 9, pp. 1116-1117, 1982.

[2] M. van Heel, G. Harauz, E. V. Orlova, R. Schmidt, and M. Schatz, "A new generation of the IMAGIC image processing system," *Journal of Structural Biology*, vol. 116, no. 1, pp. 17–24, 1996.

[3] L. Alvarez, F. Guichard, P. L. Lions, and J. M. Morel, "Axioms and fundamental equations of image processing," *Archive for Rational Mechanics & Analysis*, vol. 123, no. 3, pp. 199–257, 1993.

[4] G. A. Mckinley, "An introduction to digital image processing," *Clinical Microbiology Newsletter*, vol. 12, no. 12, pp. 89–92, 1990.

[5] T. Gorji, E. Sertel, and A. Tanik, "Recent satellite technologies for soil salinity assessment with special focus on Mediterranean countries," *Fresenius Environmental Bulletin*, vol. 26, no. 1, pp. 196–203, 2017.

[6] R. P. Roesser, "A discrete state-space model for linear image processing," *IEEE Transactions on Automatic Control*, vol. 20, no. 1, pp. 1–10, 1975.

[7] N. C. Andreasen, G. W. Cohen, G. Harris, T. Cizadlo, and V. W. Swayze, "Image processing for the study of brain structure and function: problems and programs," *Journal of Neuropsychiatry*, vol. 4, no. 2, pp. 125–133, 1992.

[8] K. S. Kwan, A. C. Evans, and G. B. Pike, "MRI simulation-based evaluation of image-processing and classification methods," *IEEE Transactions on Medical Imaging.*, vol. 18, no. 11, pp. 1085–1097, 1999.

[9] P. Salembier and L. Garrido, "Binary partition tree as an efficient representation for image processing, segmentation, and information retrieval," *IEEE Transactions on Image Processing*, vol. 9, no. 4, pp. 561–576, 2000.

[10] J. B. Heymann and D. M. Belnap, "Bsoft: image processing and molecular modeling for electron microscopy," *Journal of Structural Biology.*, vol. 157, no. 1, pp. 3–18, 2007.

[11] A. C. Davies, H. Y. Jia, and S. A. Velastin, "Crowd monitoring using image processing," *Electronics & Communication Engineering Journal*, vol. 7, no. 1, pp. 37–47, 1995.

[12] M. Reuter and B. Fischl, "Avoiding asymmetry-induced bias in longitudinal image processing," *NeuroImage*, vol. 57, no. 1, pp. 19–21, 2011.

[13] S. Zhang, L. Yao, A. Sun, and Y. Tay, "Deep learning based recommender System," *ACM Computing Surveys*, vol. 52, no. 1, pp. 1–38, 2019.

[14] A. K. Jain, "Advances in mathematical models for image processing," *Proceedings of the IEEE.*, vol. 69, no. 5, pp. 502–528, 1981.

[15] U. Veit and H. Moser, "Ecotoxicological test assays with macrophytes," *Fresenius Environmental Bulletin*, vol. 12, no. 6, pp. 545–549, 2003.

[16] I. Bloch, "Fuzzy spatial relationships for image processing and interpretation: a review," *Image & Vision Computing*, vol. 23, no. 2, pp. 89–110, 2005.

[17] A. Asher, W. A. Segal, S. A. Baccus, L. P. Yaroslavsky, and D. V. Palanker, "Image processing for a high-resolution optoelectronic retinal prosthesis," *IEEE Transactions on Biomedical Engineering*, vol. 54, no. 6, pp. 993–1004, 2007.

[18] W. Huber, "Ebimage—an R package for image processing with applications to cellular phenotypes," *Bioinformatics*, vol. 26, no. 7, pp. 979–981, 2010.

[19] U. Handmann, T. Kalinke, C. Tzomakas, M. Werner, and W. V. Seelen, "An image processing system for driver assistance," *Image & Vision Computing*, vol. 18, no. 5, pp. 367–376, 2000.

[20] P. C. Cosman, K. L. Oehler, E. A. Riskin, and R. M. Gray, "Using vector quantization for image processing," *Proceedings of the IEEE*, vol. 81, no. 9, pp. 1326–1341, 2014.

[21] J. Yang, J. H. Kim, K. Abdel-Malek, T. Marler, S. Beck, and G. R. Kopp, "A new digital human environment and assessment of vehicle interior design," *Computer-Aided Design*, vol. 39, no. 7, pp. 548–558, 2007.

[22] K. I. Lantitsou and G. D. Panagiotakis, "Thermal analysis of residencies based on solar design principles - a case study in Thessaloniki," *Greece. Fresenius Environmental Bulletin*, vol. 26, no. 2, pp. 1254–1262, 2017.

[23] C. L. Ruff and M. A. Olson, "The attitudes of interior design students towards sustainability," *International Journal of Technology & Design Education*, vol. 19, no. 1, pp. 67–77, 2009.

[24] C. Goksel, D. E. Mercan, S. Kabdasli, F. Bektas, and D. Z. Seker, "Definition of sensitive areas in a lakeshore by using remote sensing and GIS," *Fresenius Environmental Bulletin*, vol. 13, no. 9, pp. 860–864, 2004.

Hindawi
Journal of Sensors
Volume 2021, Article ID 2505119, 10 pages
https://doi.org/10.1155/2021/2505119

Research Article

Application of Virtual Reality Human-Computer Interaction Technology Based on the Sensor in English Teaching

Shuai Jiang,[1] Lei Wang,[1] and Yuanyuan Dong[2]

[1]*Department of Foreign Languages, Cangzhou Normal University, Cangzhou 061001, China*
[2]*School of Foreign Languages, Xi'an Shiyou University, Xi'an 710016, China*

Correspondence should be addressed to Yuanyuan Dong; dongyuanyuan0125@xsyu.edu.cn

Received 13 August 2021; Revised 16 September 2021; Accepted 5 October 2021; Published 19 November 2021

Academic Editor: Mu Zhou

In order to improve the online English teaching effect, the paper applies the sensor and human-computer interaction into the English teaching. The paper improves the sensor information by applying Kalman Filter, combines sensor positioning algorithm to trace the students in the English teaching online, and turns the kernels by the skeleton algorithm into corresponding coordinates of space rectangular coordinate system taking the waist as a coordinate origin to get a human-computer interaction skeleton model in the virtual reality. According to the actual needs of English teaching human-computer interaction, the paper builds a new English teaching system based on the sensor and the human-computer interaction and tests its performance. The experiments suggest that the smart system in the paper can effectively improve English teaching effects.

1. Introduction

The traditional English teaching mode has already been unable to fulfill the need of English teaching in the information age, especially in the period of the COVID-19. Online tutoring has already become a new trending. Therefore, it is necessary to conduct a revolution in the English teaching through information technology and smart technology [1]. With the extensive application of the computer, the users have been gradually increased, which are not just the early computer professionals. Generally speaking, the users have different needs and opinions toward the data, kinds of ways to solve the problems as well; and for the same user, he could present changes in different periods [2]. The traditional fixed user interface designed is not to the point, which cannot satisfy the specific need of the user and even the needs in different periods; the traditional Human-computer interaction system is just a system without any "flexibility," and the users have to follow the interaction way and operate [3]. Sometimes, the user just needs a simple operation, which is obviously with a purpose especially understanding the user on the basis of previous operations, but the system is unable to know the real intention and just treats it as a normal operation. So this cannot cause a smooth information exchange between the system and the user. The user cannot freely interact with the computer, and the computer cannot deal with the requests from the user just like humans understand their friends. The user-centered human-computer interaction technology is the best effective way to solve the foresaid problems. The human-computer interaction system, to a certain degree, can allow the users to freely talk to the computer in their own familiar way; the computer has a certain ability of understanding and can understand the users to a certain degree or can smartly give the users a specific feedback although the intension is not clear enough [4].

A current research focus of human-computer interaction is to improve the performance of user interaction when users use computers to complete tasks. The improvement of user interaction performance includes a variety of human-computer interaction interface components, such as display media, display content, interface structure and style, and various input mechanisms. These human-computer interaction elements are closely related to user's perception, perception, processing, and reaction to the computer. To get the best user interaction performance, the interactive system must be built on the basis of a full understanding of users.

The first thing to study is how people conduct daily communication in real life, including the way of expressing intentions, the way of receiving outside information, and the way people express their intentions to people in the outside world and people's response models when asking questions. These expression models and response models are related to the types of users, users' experience, abilities, skills, and preferences in the field. At the same time, different users have different computer knowledge, comprehensive capabilities, and various factors that affect their interactions. It is necessary to understand the characteristics of all aspects of user behavior (from behavior to primary perception), establish the corresponding user model, then establish the user model of the corresponding application field, and improve the efficiency of interaction by improving system's understanding of people.

Based on above studies, the paper applies the sensor and virtual reality into the English teaching and builds a smart system so as to improve the English teaching effect.

2. Related Work

The ITS (intelligent tutoring system) is a multidisciplinary field of traditional CAI (computer aided instruction), AI (artificial intelligent), and cognitive science; ITS has internationally become a larger research mode and achieved convincing results [5]. Especially in recent 10 years, ITS grows fast abroad and turns into the commercial stage from research stage [6]. ITS can be established and maintain the student model; on one hand, the system can simulate the teaching decision-making and provide real-time tailored tutor to the students; on the other, the system can automatically analyze the historical data of a set of students in the student model and help teachers objectively understand the overall condition of students so that the teachers can timely adjust their own teaching plans and contents. The student model can tell the knowledge level, learning ability, and cognitive feature of the students; it is essentially a programme based on the algorithm that solves the actual problems in the way that students do [7].

Human-computer interactive learning systems using multimedia ingenuity are widely used at home and abroad. Human-computer interaction learning can provide students with a safe, predictable, repeatable, relaxed, and lively interactive learning environment. The system follows the basic principles of human-computer interaction and scientifically designs learning goals based on related theories and establishes corresponding human-computer interaction learning activities [8]. At the same time, the human-computer interactive learning environment pays attention to the design of interactive experience, is committed to letting students participate in interactive operations in an entertaining way, and focuses on the friendliness and fun of the game interface. The color matching and screen display design can attract students for different student groups. Attention is a system that mobilizes students' interest in learning and guides students to learn actively [9]. Literature [10] designed and implemented a three-dimensional drawing model tool, which can outline and model the Lanwei model. Users can interact with gestures and pens. Although its accuracy is not as good as professional modeling software, it can satisfy students and nonbasic professional needs. Literature [11] uses an infrared camera to obtain the facial feature data of children, uses a pressure seat to obtain the child's body posture, and combines the learning behavior on child's computer to identify child's rational state. Literature [12] uses computer vision technology to study joint attention (that is, to follow and guide others' attention). The experiment uses a web camera to detect learner's head posture in real time to estimate learner's attention. Literature [13] establishes a multichannel learning environment by using video and audio fusion technology. In this learning environment, the video signal of the lips is obtained through the camera and merged with the voice signal obtained by the microphone. The speech recognition result and the handwriting recognition result are combined for human-computer interaction.

The rapid development of multimedia technology has also greatly promoted the progress of the T human-machine interface. The human-computer interaction gradually uses multimedia input and output devices such as microphones and cameras [14]. With the rise and development of emerging disciplines such as cognition, science, artificial intelligence, graphics, and image processing, multimedia-based multichannel human-computer interaction has gradually become a research hotspot. Virtual reality technology is a computer system that can create and experience a virtual world. It uses computer technology to generate a realistic virtual environment with multiple perceptions such as sight, hearing, and touch. The user uses various interactive devices to be the same as the virtual environment. The interactive visual simulation and information exchange that produce immersive feelings in the interaction between the entities in the world is an advanced digital human-computer interface technology, and its appearance will change the way of life of human beings [15]. For the research of virtual reality technology, literature [16] searched the WPI database and counted the country/regional distribution of related patents. From the perspective of the development of human-computer interaction, it can be found that the overall trend is towards naturalization and intelligent development. It is believed that the future human-computer interaction design will bring people a more relaxed and comfortable life [17].

3. Sensor Intelligent Fusion Algorithm

Extended Kalman filter (extended Kalman filter, EKF) is suboptimal that performs Kalman filtering after linearizing a nonlinear system.

Assuming that the system equation is represented by a discrete equation that remains constant under stochastic nonlinear conditions, the equation of state described above and the sensor measurement equation of the moving student can be expressed as follows [18]:

$$\begin{aligned} x(k+1) &= f(k, x(k)) + w(k), \\ z(k) &= h(x(k)) + v(k), \end{aligned} \tag{1}$$

in which $w(k) \sim (N, Q(k))$ and $v(k) \sim (0, R(k))$ represent the Gaussian white noise sequence.

And $f(x) = [f_1(x), f_2(x), \cdots, f_m(x)]^T$, and $h(x) = [h_1(x), h_2(x), \cdots, h_p(x)]^T$, assuming that f, h can be expressed as the Taylor formula as followed.

$$f(x(k)) = f(\hat{x}(k)) + J_f(\hat{x}(k))[x(k) - \hat{x}(k)] + \cdots. \quad (2)$$

$J_f(x)$ is the Jacobi matrix of function f on $\hat{x}(k)$, then [19]:

$$J_f(x) = \left.\frac{\partial f}{\partial x}\right|_{x=\hat{x}(k)} = \begin{pmatrix} \frac{\partial f_1}{\partial x_1} & \frac{\partial f_1}{\partial x_2} & \cdots & \frac{\partial f_1}{\partial x_m} \\ \frac{\partial f_2}{\partial x_1} & \frac{\partial f_2}{\partial x_2} & \cdots & \frac{\partial f_2}{\partial x_m} \\ \vdots & \vdots & \vdots & \vdots \\ \frac{\partial f_m}{\partial x_1} & \frac{\partial f_m}{\partial x_2} & \cdots & \frac{\partial f_m}{\partial x_m} \end{pmatrix}. \quad (3)$$

Similarly,

$$h(x(k)) = h(\hat{x}(k)) + J_h[x(k) - \hat{x}(k)] + \cdots. \quad (4)$$

If the Kalman filter incorporates several readings of the above ranging sensors, then $H(x(k))$ can be expressed as $H(x(k)) = d_i^j$

$$d_i^j = \frac{(ax_i + by_i + c)}{\sqrt{a^2 + b^2}}, \quad (5)$$

in which $P(k =)$ is the distance from moving student sensor i to a point on the j wall in the environment; thus, the line segment characteristics of the global coordinates in the environment can be expressed as [20]:

$$ax_i + by_i + c = 0. \quad (6)$$

The Kalman algorithm is

(1) Testing phase

$$\hat{x}\left(\frac{k+1}{k}\right) = f\left(\hat{x}\left(\frac{k}{k}\right)\right), \quad (7)$$

$$P\left(\frac{k+1}{k}\right) = F(k) * P\left(\frac{k}{k}\right) * F(h)^T + Q(k). \quad (8)$$

In the above formula, P is the variance matrix of X, and F is the Jacobian matrix of f.

$$f(x(k)) = \begin{bmatrix} x(k) + T * v(k) * \cos\theta(k) \\ y(k) + T * v(k) * \sin\theta(k) \\ \theta(k) + T * (v(k)) * \sin\alpha(k)/l \end{bmatrix}, \quad (9)$$

$$F(k) = \nabla f(k) = \begin{bmatrix} 1 & 0 & -T * v(k) * \sin\theta(k) \\ 0 & 1 & T * v(k) * \cos\theta(k) \\ 0 & 0 & 1 \end{bmatrix}. \quad (10)$$

(2) Observation phase

From formula (7) and formula (10), the predicted measurement equation can be obtained:

$$\hat{z}(k+1) = h\left(\hat{x}\left(\frac{k+1}{k}\right)\right). \quad (11)$$

We use the predicted error of the sensor measurements to correct the predicted equation of state $\hat{x}(k+1)$, and we can obtain the predicted error of the measurements $\gamma(k+1)$, which can be expressed as

$$\gamma(k+1) = z(k+1) - \hat{z}(k+1). \quad (12)$$

The measurement error variance is

$$S(k+1) = H(k)P(k+1)H(k)^T + R(k). \quad (13)$$

H is the Jacobian matrix of $h(x(k))$ in the measurement Equation (7) [21]:

$$H(k) = \nabla h(k) = \frac{\partial h}{\partial x_{x=\hat{x}(k)}} = \begin{pmatrix} \frac{\partial h_1}{\partial x_1} & \frac{\partial h_1}{\partial x_2} & \cdots & \frac{\partial h_1}{\partial x_m} \\ \frac{\partial h_2}{\partial x_1} & \frac{\partial h_2}{\partial x_2} & \cdots & \frac{\partial h_2}{\partial x_m} \\ \vdots & \vdots & \vdots & \vdots \\ \frac{\partial h_m}{\partial x_1} & \frac{\partial h_m}{\partial x_2} & \cdots & \frac{\partial h_m}{\partial x_m} \end{pmatrix}. \quad (14)$$

(3) Estimation phase

It is seen from the above two steps that $\hat{x}(k+1)$ is the predicted value of the state that is realized by extending the Kalman filter to obtain the prediction error information based on the measured value. Among them, the measured variance $S(k)$ represents the corrected weight factor.

If the extended Kalman filter gain matrix is K, state is estimated as x, and its covariance matrix is P, and the

estimation value can be expressed in the following formula:

$$K(k+1) = P\left(\frac{k+1}{k}\right) H(k)^T S^{-1}(k+1),$$
$$\hat{x}\left(\frac{k+1}{k+1}\right) = \hat{x}\left(\frac{k+1}{k}\right) + w(k+1)\gamma(k+1), \quad (15)$$
$$P\left(\frac{k+1}{k+1}\right) = (I - K(k+1) * H(k)) * P\left(\frac{k+1}{k}\right).$$

In conclusion, the recursive formula of EKF includes the test, observation, and estimation phase. To obtain the optimal estimation value for the system, we can assume that some parameters are not related to the system, including the initial input noise $w(k)$ of the system and the measurement noise $v(k)$ generated during the measurement in the process, then we can handle the system by the irrelevant Gaussian white noise.

The sources of error in information fusion are summarized as follows:

(1) Milodometer system

An odometer is a sensor that uses data obtained from the mobile sensor to estimate the change of the object position over time, usually installed in the internal body position of the moving student. Its working principle is first use the pattern information or coding information on the code plate to obtain the rotation radian information of students' left and right wheel, and the forward direction and speed changes of the students can be calculated through these radian information.

According to the statements above, the odometer can represent the line speed and angular speed of the moving student; thus, odometer movement model can be represented as shown in Figure 1. We take the student as a mobile robot. Based on which, assuming that the student radius of movement is r, photocode disk is p line/turn, in a cycle time ΔT, the movement distance of the left wheel is Δs_l, the moving distance of the right wheel is Δs_r, and the moving distance of the car body Δs, the output pulses of student's photoelectric code disk is M, and the movement distance of the car body is

$$\Delta s = \left[\frac{2M}{p}\right] \cdot \pi r. \quad (16)$$

By the nonlinear regression analysis, it can be assumed that in a sampling cycle time ΔT, the movement track of the moving student is almost a straight line. If the distance between the left and right wheels is a, and then, the moving student is moved from the position $X(k-1) = (x_{k-1}, y_{k-1}, \theta_{k-1})$ to the position $X(k) = (x_k, y_k, \theta_k)$, the distance that the moving student moved is $\Delta s = (\Delta s_l + \Delta s_r)/2$, the angle information that the moving student rotated is $\Delta\theta = (\Delta s_l + \Delta s_r)/a$, and the odometer model input is $\mu(k)$ in the formula $\mu(k) = (\Delta D_k, \Delta\theta_k)^T$ obtained by the control command (v, w). During a sampling cycle ΔT, the motion path of the moving e student is $\Delta D_k = v \times \Delta T$, and the pose relative angle is $\Delta D_k = v \times \Delta T$.

The odometer has two models: circular arc and straight lines. Since the linear model is simplified from the arc model, the arc mode is generally used in practice, which is more accurate.

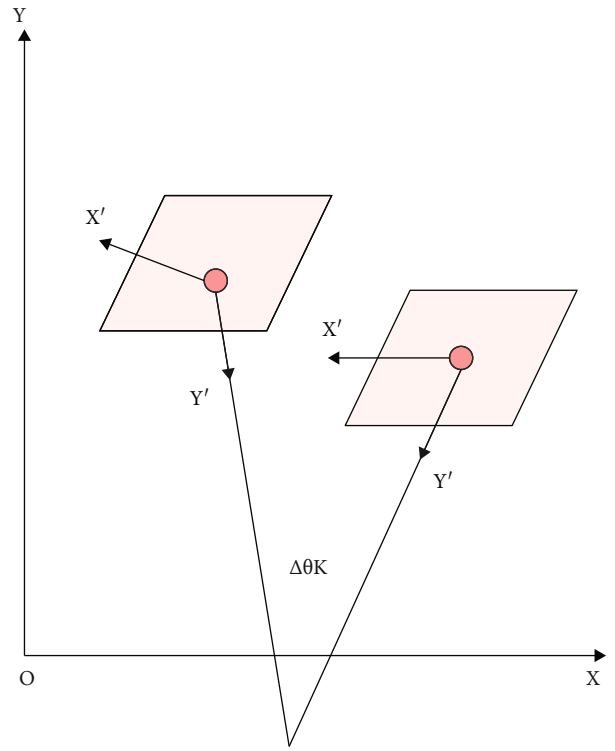

Figure 1: Mileometer motion system.

(2) Arc model

$$x(k) = f(x(k-1), u(k)) = \begin{bmatrix} x_{k-1} - \frac{\Delta D_k}{\Delta\theta_k}(\cos(\theta_{k-1} + \Delta\theta_k) - \cos\theta_{k-1}) \\ y_{k-1} + \frac{\Delta D_k}{\Delta\theta_k}(\sin(\theta_{k-1} + \Delta\theta_k) - \sin\theta_{k-1}) \\ \theta_k = \theta_{k-1} + \theta_k \end{bmatrix}. \quad (17)$$

$\Delta\theta_k$ in formula (17) indicates the rotation angle difference between the end point and the beginning point of the moving student, in which ΔD_k is the movement displacement of the moving student during the sampling period AT time.

(3) Line model

Assuming that the moving students makes a small displacement in a very small period of time, the extremal method of nonlinear regression analysis method can be used for processing, and the model dealing with the problem becomes a linear model, which can be represented by simplified lines, namely, $|\triangle 0 = 0$, then the model equation can be expressed as

$$x(k) = f(x(k-1), u(k)) = \begin{bmatrix} x_k + \Delta D_k \sin\theta_k \\ y_k + \Delta D_k \cos\theta_k \\ \theta_k + \Delta\theta_k \end{bmatrix}. \quad (18)$$

To calculate the position of moving students, in this paper, linear model and arc model are used. The specific implementation method is the displacement calculation adapts a straight line model, and the arc model is used to calculate the change difference of direction angle. Then, the two models are represented as

$$x(k+1 \mid k) = f(x(k \mid k), u(k)) = \begin{bmatrix} x_k + \Delta D_k \sin\theta_k \\ y_k + \Delta D_k \cos\theta_k \\ \theta_k + \Delta\theta_k \end{bmatrix}. \tag{19}$$

At the k moment, if line speed and angular speed values of the moving student are known, formula (19) can be transformed as

$$x(k+1 \mid k) = f(x(k \mid k), u(k)) = \begin{bmatrix} x_{k+1} \\ y_{k+1} \\ \theta_{k+1} \end{bmatrix} = \begin{bmatrix} x_k + v \times \Delta T \sin\theta_k \\ y_k + v \times \Delta T \cos\theta_k \\ \theta_k + W \times \Delta T \end{bmatrix}. \tag{20}$$

The errors of the moving student odometer include two types, namely, nonsystematic error and systematic errors (as shown in Figure 2). Its systematic error accumulation is always existed, while the nonsystematic error accumulation is random and indeterminable.

(4) Sonar calculation method

Generally, most of the sonar applications adapts very cheap Polaroid6500 sonar modules. Among them, the environmental road sign characteristic is used for the sonar sensor to scan the environmental information, extract useful environmental feature information, and correctly calculate the specific location of the environmental characteristics. Assuming that the coordinate position of the line segment in the local coordinate system is (x_l, y_l), the predicted coordinate position (x_w, y_w) for observation can be estimated and obtained. Among them, the width of the sonar beam and the reflection of the sonar signal are the important factors affecting the sonar sensor. Figure 3 shows the coordinate system transformation diagram.

In Figure 3, the point O' is the origin in this local coordinate system that represents the moving student, the point P represents the wall in the moving student walking area, a is the sonar sensor, and O represents the offset angle of the on-board coordinate relative to the coordinate OXY. The degree of the sonar is represented by the point S, and the distance to the point P is d, and the relative position of each of the sonar is fixed.

Figure 4 shows the interrelationship between the global and local coordinate systems for moving students. The width of the sonar beam and the reflection of the sonar signal are two factors affecting the principle of the sonar sensor.

Assuming that in the moving student environment, the reflected wall is represented by P, the distance from the origin O to the plane and the distance between the plane and

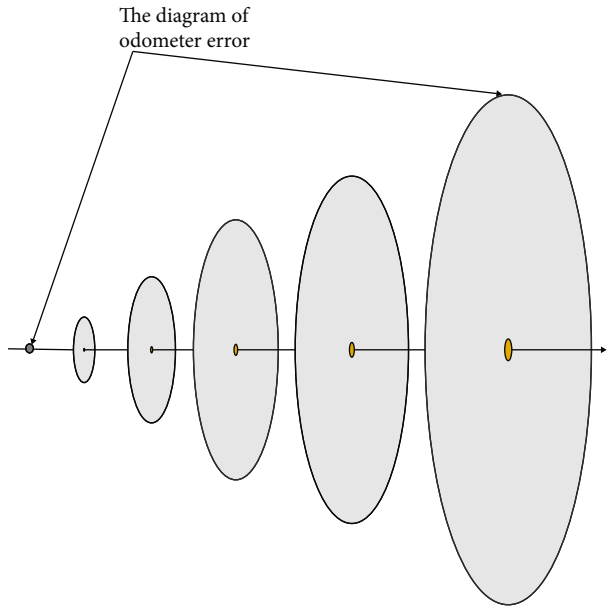

Figure 2: The diagram of odometer error.

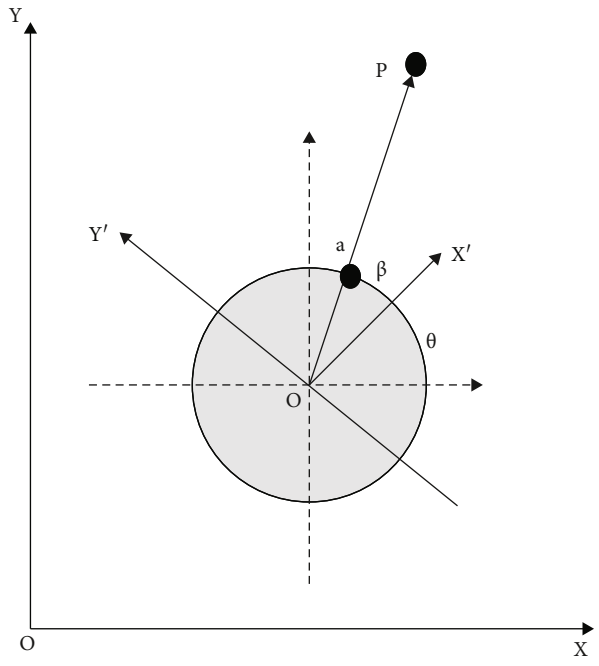

Figure 3: The coordinate system transformation of sonar data.

the sonar sensor in the environment are represented by P_r^j, P_n^j, P_r^j. Since the relative position information of the sonar in the local coordinate system is known, which can be represented by (x_i, y_i, θ_i), formula (22) and formula (23) can be used to calculate and coordinate position of d_i^j and P point on the wall in the environment.

In the figure above, j is the number of planes, $d_i^j(k)$ is the number of sonar sensors, and the distance from the obstacle

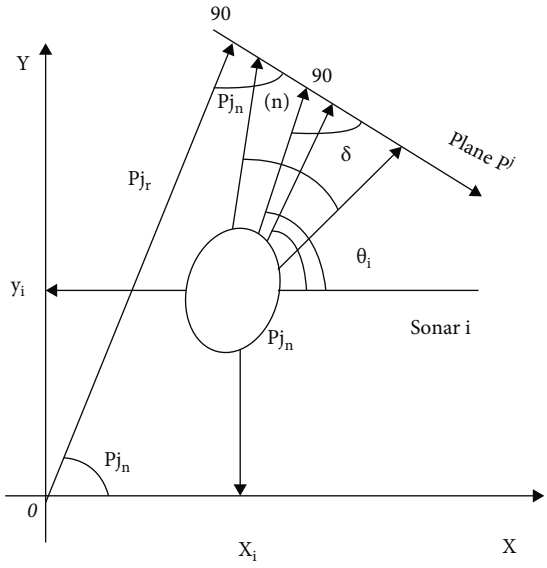

Figure 4: The position of sonar in the global coordinate system.

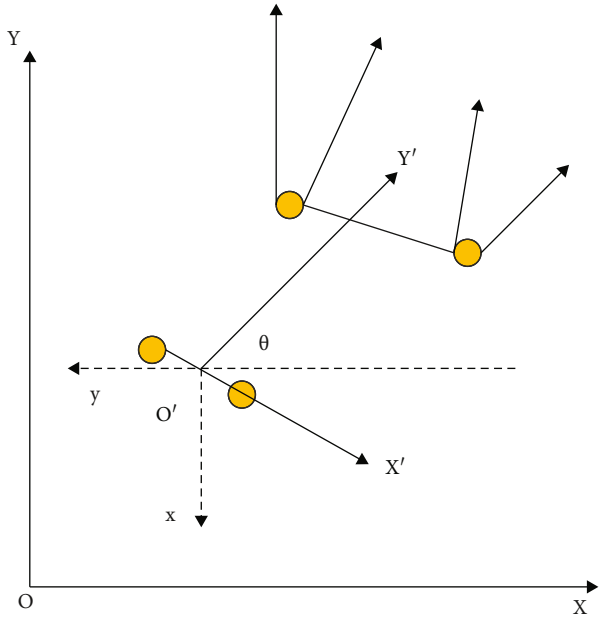

Figure 5: Odometer and coordinates.

plane p^i to the sonar i at the k moment is $d_i^j(k)$, which can be simplified as

$$d_i^j(k) = P_r^j - x_i(k)\cos\left(P_n^j\right) - y_i(k)\sin\left(P_n^j\right). \tag{21}$$

Set $P_n^j = \theta_l$, $P_r^j = D$, in $P_n^j \in [\theta_i(n) - \delta/2, \theta_i(n) + \sigma/2]$, δ is the sonar beam width, and $d_i^j(k)$ may be represented based on formula (21) above as

$$d_i^j(k) = D - x_i(k)\cos(\theta_l) - y_i(k)\sin(\theta_l) = \frac{ax_i + by_j + c}{\sqrt{a^2 + b^2}}. \tag{22}$$

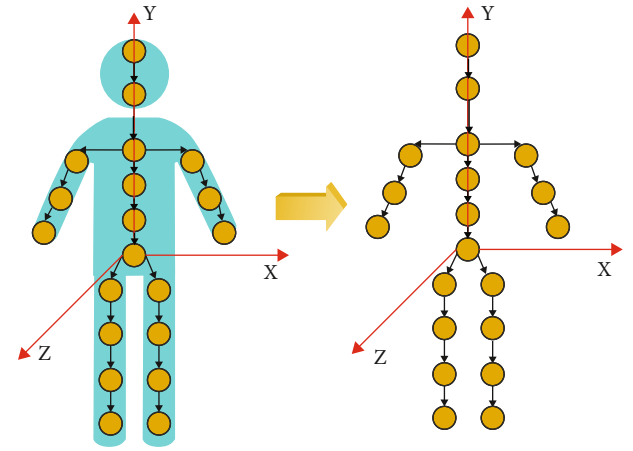

Figure 6: Coordinate system of English human-computer interaction.

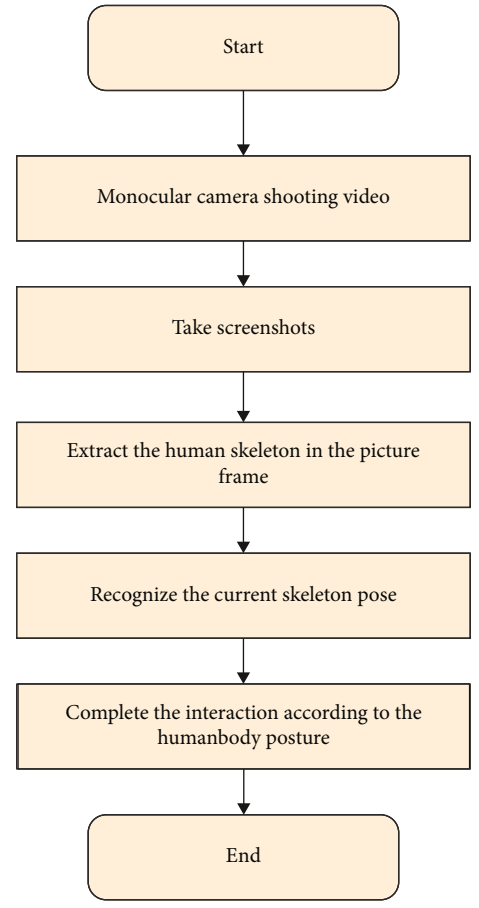

Figure 7: Process of human-computer interaction in English teaching.

According to the view of Figure 5 above, assuming we are sampling at the k time, the position of the moving student is $X(k) = (x(k), y(k), \theta(k))$. After a rotating coordinate transformation, we can convert the coordinate numbers (x'_i, y'_i, θ'_i) of i in OX 'Y' system to (x_i, y_i, θ_i) in the OXY

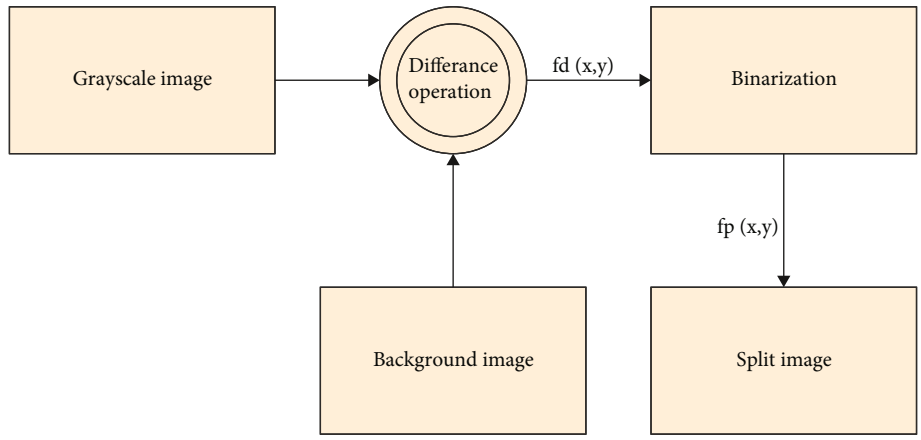

Figure 8: Principle process of background subtraction.

Table 1: Performance appraisal of English teaching system based on sensor and human-computer interaction technology.

Number	Sensor performance	Human-computer interaction effect	Number	Sensor performance	Human-computer interaction effect
1	88.66	91.65	25	92.27	93.08
2	94.53	93.03	26	96.85	80.75
3	87.85	80.98	27	86.34	93.00
4	87.70	94.24	28	95.74	81.96
5	94.49	86.22	29	89.47	86.43
6	90.02	79.25	30	95.93	90.59
7	91.49	84.28	31	96.30	88.78
8	96.77	91.27	32	91.53	91.93
9	96.69	93.75	33	86.41	89.75
10	96.10	84.68	34	95.50	86.21
11	89.65	94.55	35	86.79	87.97
12	94.61	88.78	36	91.01	79.27
13	94.37	81.09	37	93.39	85.66
14	86.32	82.13	38	87.51	93.74
15	89.84	89.90	39	96.28	87.71
16	92.45	90.37	40	88.11	91.88
17	88.14	83.13	41	87.76	79.93
18	87.21	81.10	42	91.21	85.00
19	94.42	79.82	43	94.64	85.07
20	86.71	87.15	44	94.73	82.44
21	96.06	90.64	45	88.49	81.41
22	94.55	91.73	46	96.01	94.98
23	94.37	93.82	47	89.35	85.58
24	92.06	93.69	48	95.78	82.30

coordinate system, then the model of the sonar sensor is expressed as the following formula:

$$\begin{cases} x_i(k) = x(k) - x_i'(k)\sin(\theta(k)) + y_i'(k)\cos(\theta(k)), \\ y_i(k) = y(k) - x_i'(\cos(k)) + y_i'\sin(\theta(k)), \\ \theta_i(k) = \theta(k) + \theta_i. \end{cases} \tag{23}$$

As the P point on the wall in the sonar coordinate system in Figure 5, the point P, a, O' is on the same line, and the position detected by moving the student odometer and the sonar sensor can be represented as

$$\begin{aligned} X_p &= x_0 + x_p = x_0 + x_l \times \cos(\theta) - y_i \times \sin(\theta) + d_i^j \times \cos(\theta), \\ Y_p &= y_0 + y_p = y_0 + x_l \times \sin(\theta) - y_i \times \sin(\theta) + d_i^j \times \sin(\alpha + \theta). \end{aligned} \tag{24}$$

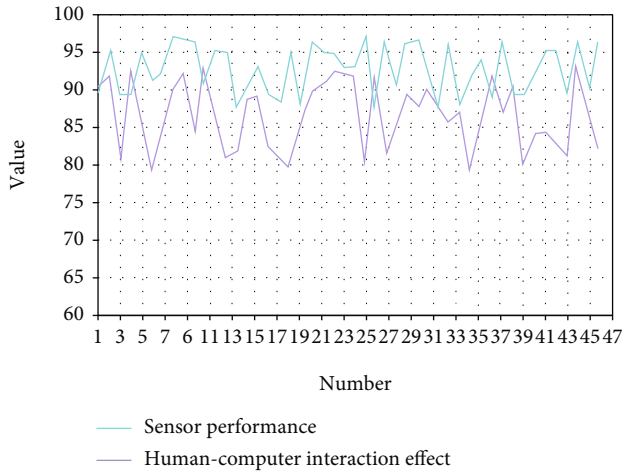

Figure 9: Statistics of English teaching system performance based on sensor and human-computer interaction.

Mobile students must rely on the collected external environment information to achieve more accurate navigation and positioning. However, in the real environment, there are various uncertainties and intertwined complexity in the environment itself, which leads to the absence of theoretically reliable environmental information. In addition, the data measured by the mobile student's own sensors will also be disturbed by the environment. As a result, the measured environmental information is not our ideal information, and there are often extremely complex uncertain factors. In order to reduce or even eliminate these interferences in the observation information of mobile student sensors, we can establish a reliable noise simulation system to express the uncertain factors described above. However, this is only our ideal state. In fact, due to the nonlinear and incomplete constraint system of moving students, it is not easy to establish an efficient and accurate mathematical model. In this case, we use a model (also called an error model) that introduces noise that obeys the Gaussian function model to approximate it.

In this paper, the sonar sensor is used to detect the road signs of environmental information. Due to the characteristics of the sonar sensor, if an observation point cannot be selected correctly in the process of selecting an observation point, it will lead to the environment corresponding to it. It is impossible for the feature information to perform correct data association, which will cause the divergence of the filter. The divergence of the filter will cause all the predicted observations to be wrong. In order to make the road sign data scanned by the sonar sensor match correctly, a data association model can be introduced to solve this problem.

The analysis shows that the position estimation inferred by the mobile student through the odometer and sonar sensor is inaccurate, so the correct position estimation of the mobile student cannot be obtained. In this paper, a two-dimensional vector road sign is selected as the observation in the position of the global coordinate system. Since the environment in the space is variable and complex, but there is a certain correlation between the environmental characteristics, it can be estimated; how to eliminate the interference of the correlation between these variables is the problem we want to solve. A large number of studies have verified that Mahalanobis distance can well eliminate these interferences, so Mahalanobis distance is selected as the measure of data association in this article. In addition, it should be noted that the correlation gate used in this article is an elliptical correlation gate.

Mahalanobis (Mars distance) is defined as $d_k^2(x) = (x - m_k)s_k^{-1}(x - m_k)$, $d_k^2(x)$ represents the mean distance of the measured value within group k, the vector m in the formula represents the mean of the variable in group k, x represents the value of the variable in the environment observed by the sensor model, and s represents the covariance matrix within the group.

4. English Teaching System Based on the Sensor and Human-Computer Interaction

The kernels of the skeleton extracting algorithm are universally turned into corresponding coordinates of space rectangular coordinate system taking the waist as a coordinate origin. The right part of the body is x-axis, the vertical upper part is y-axis, the front of vertical to the body is z-axis, which is shown in Figure 6.

The paper proposes human-computer interaction method based on monocular camera. First extract the physical skeleton from the video taken by monocular camera and complete the interaction with virtual environment through the human body pose. The process is shown in Figure 7.

After cutting out the current frame, first of all, pretreat the picture. That is because the profiles in the video are of sizes, if the body in the frame takes up smaller, which can greatly reduce the precision of the later kernels. At the same time, much irrelative information in the frame could cause too much useless information in the network training process and affect the precision of identification result. Therefore, we need to find out the boundary of human profile and get it out from the frame to identify aiming to improve the precision in the following stages. There are many ways to extract from the RGB images. As the video in the paper is shot by a fixed camera and there is only one person in the frame, our background is fixed, and we use background subtraction to extract the human profile from the video; the principle is shown in Figure 8.

The paper builds English teaching system based on the sensor and human-computer interaction technology and tests the performance. According to actual needs, the paper conducts a test on the basis of the real-time information transmission in English teaching by the sensor and human-computer interaction. The simulation experiment is used to test the performance of the system, transmission effect of sensor, and human-computer interaction (by the way of experts' appraisal); the statistics is shown in Table 1 and Figure 9.

From above experiment, the English teaching system in the paper based on sensor and human-computer can effectively improve the English teaching effect and have some positive influence on the following English teaching revolution.

5. Conclusion

In the teachers-centered link, teachers play roles of traditional instructor, teaching monitor, after-school tutor, homework assigner and corrector, and document provider. With further development of teaching-related theory and interaction design theory, the human-computer interaction between teachers and students has attracted more and more attention among people, from the feasibility of human-computer interaction in English teaching in the light of theory and study, to the theory foundation of creating learning environment. In order to improve the effect of human-computer interaction in English teaching, the paper studies the sensor technology and puts a Kalman Filter Algorithm which stresses the precision to solve the problems from the human-computer interaction information by the positioning in sensor information. The virtual reality is used to build in English teaching online interaction system. The system goes through the performance test, and the study suggests that the system in the paper has certain effects.

Data Availability

The labeled dataset used to support the findings of this study are available from the corresponding author upon request.

Conflicts of Interest

The authors declare no competing interests.

Authors' Contributions

Yuanyuan Dong completed the analysis and thesis writing as the main writer. Shuai Jiang and Lei Wang completed the collection and sorting of experimental data and jointly participated in the revision, polishing, and typesetting of the article, so I decided to add them to the list of authors of the article. Shuai Jiang and Lei Wang assisted in the analysis through constructive discussions based on their professional expertise.

Acknowledgments

This study is sponsored by "The 2020 year project of 13th Five- year plan of Educational Science in Shaaxi Province, China (grant no. SGH20Y1131)".

References

[1] L. Delgaty, "Twelve tips for academic role and institutional change in distance learning," *Medical Teacher*, vol. 37, no. 1, pp. 41–46, 2015.

[2] M. Stefanovic, D. Tadic, S. Nestic, and A. Djordjevic, "An assessment of distance learning laboratory objectives for control engineering education," *Computer Applications in Engineering Education*, vol. 23, no. 2, pp. 191–202, 2015.

[3] B. P. Remesh, "Developing open and distance learning programme in labour and development: results of a needs assessment study," *Journal of natural history*, vol. 196, no. 29, pp. 265–291, 2015.

[4] P. Wu, S. P. Low, J. Y. Liu, J. Pienaar, and B. Xia, "Critical success factors in distance learning construction programs at Central Queensland University: students' perspective," *Journal of Professional Issues in Engineering Education and Practice*, vol. 141, no. 1, 2015.

[5] E. A. Willis, A. N. Szabo-Reed, L. T. Ptomey et al., "Distance learning strategies for weight management utilizing social media: a comparison of phone conference call versus social media platform. Rationale and design for a randomized study," *Contemporary Clinical Trials*, vol. 47, no. 6, pp. 282–288, 2016.

[6] H. J. Ye, D. C. Zhan, and Y. Jiang, "Fast generalization rates for distance metric learning," *Machine Learning*, vol. 108, no. 2, pp. 267–295, 2019.

[7] Y. Luo, Y. Wen, T. Liu, and D. Tao, "Transferring knowledge fragments for learning distance metric from a heterogeneous domain," *IEEE Transactions on Pattern Analysis and Machine Intelligence*, vol. 41, no. 4, pp. 1013–1026, 2019.

[8] T. Chuk, A. B. Chan, and J. H. Hsiao, "Understanding eye movements in face recognition using hidden Markov models," *Journal of Vision*, vol. 14, no. 11, pp. 8–8, 2014.

[9] H. Bouchech, "Selection of optimal narrowband multispectral images for face recognition," *Monthly notices of the royal astronomical society*, vol. 402, no. 4, pp. 2140–2186, 2015.

[10] R. Ramachandra and C. Busch, "Presentation attack detection methods for face recognition systems," *ACM Computing Surveys*, vol. 50, no. 1, pp. 1–37, 2017.

[11] Z. Huang, S. Shan, R. Wang et al., "A benchmark and comparative study of video-based face recognition on COX face database," *IEEE Transactions on Image Processing*, vol. 24, no. 12, pp. 5967–5981, 2015.

[12] C. P. Wei and Y. C. F. Wang, "Undersampled face recognition via robust auxiliary dictionary learning," *Image Processing IEEE Transactions*, vol. 24, no. 6, pp. 1722–1734, 2015.

[13] N. L. Ajit Krisshna, V. K. Deepak, K. Manikantan, and S. Ramachandran, "Face recognition using transform domain feature extraction and PSO-based feature selection," *Applied Soft Computing*, vol. 22, pp. 141–161, 2014.

[14] R. Weng, J. Lu, and Y. P. Tan, "Robust point set matching for partial face recognition," *Image Processing IEEE Transactions*, vol. 25, no. 3, pp. 1163–1176, 2016.

[15] Z. Cui, H. Chang, S. Shan, B. Ma, and X. Chen, "Joint sparse representation for video-based face recognition," *Neurocomputing*, vol. 135, pp. 306–312, 2014.

[16] P. J. Phillips and A. J. Otoole, "Comparison of human and computer performance across face recognition experiments," *Image and Vision Computing*, vol. 32, no. 1, pp. 74–85, 2014.

[17] D. Tang, N. Zhu, F. Yu, W. Chen, and T. Tang, "A novel sparse representation method based on virtual samples for face recognition," *Neural Computing & Applications*, vol. 24, no. 3-4, pp. 513–519, 2014.

[18] R. Mehta, J. Yuan, and K. Egiazarian, "Face recognition using scale-adaptive directional and textural features," *Pattern Recognition*, vol. 47, no. 5, pp. 1846–1858, 2014.

[19] M. Pinxten, C. V. Soom, C. M. Peeters, T. De Laet, and G. Langie, "At-risk at the gate: prediction of study success of first-year science and engineering students in an open-admission university in Flanders—any incremental validity of study strategies?," *European journal of psychology of education*, vol. 34, no. 1, pp. 45–66, 2019.

[20] M. Brehm, S. A. Imberman, and M. F. Lovenheim, "Achievement effects of individual performance incentives in a teacher merit pay tournament," *Labour Economics*, vol. 44, no. 5, pp. 133–150, 2017.

[21] R. J. Mcgill and A. R. Spurgin, "Assessing the incremental value of KABC-II Luria model scores in predicting achievement: what do they tell us beyond the MPI?," *Psychology in the Schools*, vol. 53, no. 7, pp. 677–689, 2016.

Hindawi
Journal of Sensors
Volume 2021, Article ID 4183881, 12 pages
https://doi.org/10.1155/2021/4183881

Research Article

Water Dragon Boat Training Monitoring System Based on Multisensor Data Fusion Technology

Heng Shen

School of Physical Education, Huazhong University of Science and Technology, Wuhan, 430074 Hubei, China

Correspondence should be addressed to Heng Shen; 2017210210@hust.edu.cn

Received 13 August 2021; Revised 8 October 2021; Accepted 26 October 2021; Published 18 November 2021

Academic Editor: Mu Zhou

With the development of science and technology, a variety of electronic devices have entered our lives, making our lives more intelligent and making our work more effective. This article is aimed at studying the application of multisensor data fusion technology to the water dragon boat training monitoring system. In that case, we can analyze the various physical indicators of dragon boat athletes based on the data reflected by these sensors, when they can reach their physical limits and can perform in the best state to obtain the best results. The sensor is used to decompose the relevant data of each part of the athlete's limbs. This step is based on the image and understands the maximum value of the data to adjust the training goal. This article proposes some data fusion algorithms, using Kalman filter method, Bayesian estimation method, and DS evidence theory algorithm to compare data fusion systems, through the comparison to find the best fusion accuracy, and then get the most suitable method is then applied to this water dragon boat monitoring system to enhance the training efficiency of dragon boat athletes. The experimental results in this paper show that when the value of the parameter increases from 0.97 to 2.5, the average classification accuracy of the k-NN classifier decreases from 0.97 to 0.4, and the accuracy of the fusion results of the three fusion rules is also reduced correspondingly, but in this paper proposed, RP fusion rule still has better performance than the other two fusion rules. When the classifier is k-NN, the three fusion rules increase with the number of sensors, and the accuracy of the fusion results is correspondingly improved. However, the final fusion accuracy obtained by the RP fusion rule proposed in this paper is always better than NB integration rules, and WMV integration rules are higher. Through these analyses, a training program that is most suitable for dragon boat athletes can be worked out, so that the athletes will not be useless. Multisensor data fusion technology brings great convenience to water dragon boat training and can provide more reasonable and accurate data to explore a practical way on the basis of ensuring the safety of personnel.

1. Introduction

1.1. Background. Competitive water boat sports are a traditional sport that perfectly combines entertainment and competition. With the development of science and technology, the stimulation of economic interests, and the drive of national culture, competitive sports have developed rapidly. In the modern competitive sports arena, competition has become more intense, which places higher demands on athletes' physical fitness. The water dragon boat started in the Spring and Autumn Period and the Warring States Period and has a history of more than 2,000 years. The water dragon boat activity is easy to hold in the south because it is more suitable for natural conditions. The natural environment in the north is limited, and the vast waters are lacking; so, the dragon boat dance in the dry land came into being. Although it does not have the surging momentum of the water, it also gives people a refreshing feeling, making the North Dragon Boat Festival atmosphere stronger. In recent years, multisensor data fusion technology has been widely used in both military and civil fields. Multisensor fusion technology has become a concern in many aspects such as military, industrial, and high-tech

development [1]. With the rapid development of electronic information technology, various large-scale electronic systems continue to emerge, and their application backgrounds continue to become more complicated. The realization of their functions requires the support of various multisensor data systems. Therefore, it is necessary to support various sensors and different information source for more effective integration. At the same time, with the development of modern warfare, the role of multisensor data fusion technology in the military has become more prominent. It combines the characteristics of a variety of different sensors to obtain different types of target information from multiple directions and angles and improve the system in all dimensions. The coverage of the above improves the detection and recognition capabilities of the target. After years of development, multisensor data fusion technology has made considerable progress. In terms of fusion level, three levels are formed: data-level fusion, feature-level fusion, and decision-level fusion. In terms of system structure, centralized, decentralized, distributed, and hybrid structures are proposed; in terms of fusion algorithms, algorithms such as weighted average method, neural network method, Kalman filtering method, Bayesian estimation method, and D-S evidence theory are formed. In terms of application, multisensor data fusion has been widely used in military and civilian fields and has achieved remarkable results.

1.2. Significance. For wireless sensor networks, collaboration and real-time monitoring can be achieved, and the collected information can be processed and transmitted to users. It can be realized through information technology based on our real world cognition, thus effectively changing the way of information interaction between human beings and nature. We are fully able to use wireless sensor-based network technology to recognize things in the world, as far as possible to expand the existing network functions and human cognition of the world. With the continuous and rapid development of sensor technology, wireless communication technology, and computer technology, the use of sensor networks in environmental monitoring has also become a reality. Most of today's environmental monitoring systems use wired monitoring methods. Therefore, this kind of system generally has two problems: one is that the wired monitoring system is more dependent on the line; so, the layout of the system will inevitably be affected by the wiring [2]. The second is that the distribution of wired nodes is relatively fixed. Once some of the nodes have problems, it will inevitably lead to the loss of the monitoring function in a local area. This article uses a wireless sensor network to collect ambient temperature and humidity and transmits the collected information to the monitoring center in time. Compared with traditional monitoring methods, the use of wireless sensors has the following obvious advantages: (1) the network nodes have a higher distribution density, and each node involved can monitor the information in the local environment and transmit it to the data center; so, it has the characteristics of large amount of data collection and high precision. (2) The sensor node has a small volume, and the entire network only needs to be deployed once. (3) The wireless sensor node itself should have good computing capabilities, storage capability, and wireless communication capabilities and be able to perform more complex monitoring.

1.3. Related Work. After reading a lot of related literature, I found that multisensor data fusion technology is applied in many fields. With technological breakthroughs, we have more extensive applications. In Zhang's research, their team proposed a method to use redundant information to fuse spatial data and multimedia information in a multimedia sensor network. Experimental results show that their proposed method can reduce the energy consumption of spatial data and multimedia information fusion in multimedia sensor networks, and the fusion accuracy is high. Although their application prospects are very good, there are still certain technical barriers [3]. In Wu research, a path design method based on ant colony optimization (ACO) algorithm is proposed, which can improve the accuracy and effectiveness of data. However, it was not considered comprehensively in the experiment, and some factors were not taken into account. Aiming at the problem of PID controller parameter optimization design, the results of ant colony algorithm design and genetic algorithm design were compared. Numerical simulation results show that the ant colony algorithm has the effectiveness and application value of a new simulation evolution optimization method. However, this is just the emergence of simple rules [4]. In Zhang's research, artificial intelligence immune agents are proposed and applied to solve the problems of low data accuracy and delay caused by dynamic environmental changes. The experimental results show that the proposed method can improve the performance of the system by using this method. However, in this study, the results of the study were not so accurate. When he conducted the experiment, many environmental factors were not taken into consideration, which led to the lack of rigor of the results [5]. In Ma's research, a mileage pile positioning technology based on multisensor information fusion is proposed. This can avoid the cumulative error per kilometer using GPS and road environment video. The gyroscope is used as a substitute when the GPS signal is lost and is also used to correct wobble errors. The practical value of his experiment is very high, but there are still certain technical barriers [6]. In Xu's research, his research results show that the clustering fitting effect is as high as 99.83%, which proves that the multiattribute DBSCAN algorithm and clustering analysis algorithm have higher reliability and provide better theoretical guidance for the analysis of abnormal ship behavior. Although the research prospects are perfect due to technical defects, the current results are still not so perfect [7]. In Zhang's research, a cooking production safety monitoring and early warning system based on information fusion was proposed. To achieve the goal of accurate monitoring of safety conditions and reliable early warning of dangerous situations, the security information of the monitoring and early warning area is collected through a sensor network such as combustible gas sensors, dust sensors, temperature sensors, pressure sensors, flow meter, and IP cameras, to establish security monitoring and early warning information fusion The model is then used to fuse various safety information through BP neural network and DS evidence theory algorithms. This research is of great practical value, but there are certain limitations [8]. In Cui's research, their team proposed a new program based on Hilbert-Huang transformation and deep learning for network attack detection in direct current (DC), microgrid (MG), and distributed power

generation (DG) attack detection unit and its sensors. A deep learning method for advanced elective group using krill swarm optimization (KHO) algorithm is proposed. Due to the incompleteness of science and technology, there are still some differences in the results [9].

1.4. Innovation. As the current training and monitoring of water dragon boats no longer use manual operations in many fields, the methods usually used tend to be realized by network automatic communication technology, which will make the operating cost relatively high, which is completely unsuitable for the entire water dragon boat training. For the future development of monitoring, it also severely restricts the development of monitoring and monitoring of water dragon boat training. On this basis, a water environment monitoring based on wireless sensor network technology is proposed, which can efficiently and quickly collect all kinds of athletes for dragon boat training. This article is aimed at establishing a hybrid water dragon boat training and monitoring transmission mode by using terminal nodes, cluster head nodes, convergence nodes, and monitoring centers. The water dragon boat training monitoring system designed in this paper has many characteristics: low cost, good scalability, strong reliability, etc., can be used not only in outdoor environments, but also in small monitoring fields such as small homes, and has a very broad application prospect. The entire sensor equipment can monitor the water environment in real time and transmit the collected data to the remote wireless back-end and perform certain analysis and processing at the back-end, which can predict the changing trend of the water body relatively quickly. It can prevent the pollution of the water environment and reduce certain economic losses. Therefore, the main purpose is to comprehensively monitor various parameters in the water dragon boat training monitoring in real time, such as pressure and temperature, to achieve remote monitoring and management. The composition of the wireless sensor network includes many wireless sensor network nodes, and the nodes choose tiny embedded systems. This article is aimed at establishing a hybrid water dragon boat training and monitoring transmission mode by using terminal nodes, cluster head nodes, convergence nodes, and monitoring centers. The data monitored by this system will be more accurate and fast and greatly reduce labor costs, which has application prospects and practical value. This technology has also improved the level of monitoring while providing strong support and provides dragon boat athletes with more scientific and effective data support, allowing them to use more reasonable training methods to strengthen themselves.

2. Methods and Related Concepts

2.1. Wireless Sensor Network. The wireless sensor network generally consists of the following three parts: sensor nodes, sink nodes, and task management nodes, as shown in Figure 1.

Use a sufficient number of sensor nodes to be deployed in the area to be monitored (sensor field), to use self-organization to promote it into a complete network system. In this process, the collected monitoring data can be transmitted along other nodes. The whole process is processed by many nodes and then reaches the sink node after multiple hops and then uses the network to transmit to the management node. Users can use the installed host computer software to manage the entire sensor network in a unified manner. It has weak capabilities in data processing, storage, and wireless communication. Generally speaking, some batteries with limited energy are used to power the system. In addition, any node has a certain routing function in addition to the original node terminal function. Nowadays, the software and hardware design of sensor nodes is a very critical link in sensor network technology. The only difference is that the sink node has relatively high requirements for data processing, storage, and wireless communication. Due to the need to connect to an external network, it can realize the communication conversion between two different protocols, and according to the actual instructions given by the user, each node is assigned a different monitoring task, and the information collected by the node is sent to the designated location. Therefore, the convergent sensor node is not only an enhanced function relative to the sensor node but also a management node with computing capabilities; it is also a network device that can communicate, as shown in Figure 2.

The main task is to gather the data and send it to the corresponding PC. Because the existing research does certain data preprocessing at the sink node, such as data deduplication and compression, it cannot be counted as a simple relay. The main function of the sensor module is to collect data and information in the coverage area of the node and to digitize the collected analog data; the function of the processor module is to control the normal operation of the entire wireless node and to perform the data collected by the sensor module. Processing: the main function of the wireless communication module is to realize wireless communication with other nodes, exchange existing control information, and send and receive data; the function of the energy supply module is to provide power.

With the continuous development of sensor networks, the protocol stack of the sensor node is also in the process of continuous improvement. A typical protocol stack model is shown in Figure 3. The model mainly covers five parts: the physical layer, the data link layer, the routing layer, the transmission control layer, and the upper application, which correspond to the five layers in the OSI seven-layer model [10].

The steps of this experiment and the previous experiment are similar, such as the training of the classifier and the calculation of the decision-making reliability; so, the detailed description will not be given. However, it is important to note that because the training sample set is already given, and the classification accuracy of the same type of classifier is fixed. In this experiment, the number of hidden neurons in the k-NN classification network is set to 50. The water training monitoring system is divided into two parts: hardware and software. The hardware is an embedded data acquisition module, which includes acceleration sensor module, heart rate belt, GPRS module, Bluetooth module, and microprocessor [11]. In the software, SOCKET is programmed with TCP/IP protocol to realize data communication, the acceleration sensor and GPS module on the experiment board are programmed to realize data collection, and multiple heart rate measurement nodes are networked and programmed to realize heart rate collection. Data analysis system: the schematic diagram is shown in Figure 4.

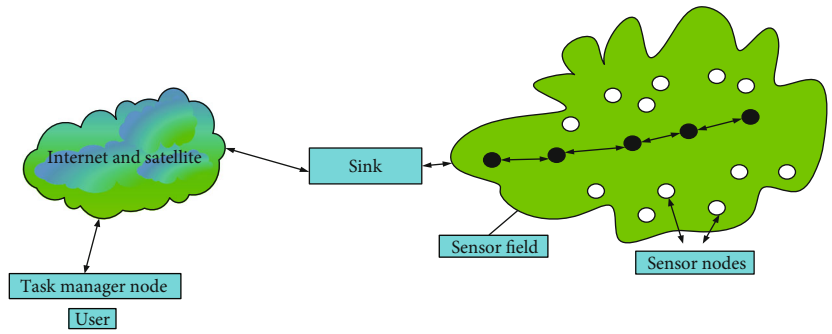

Figure 1: Wireless network structure.

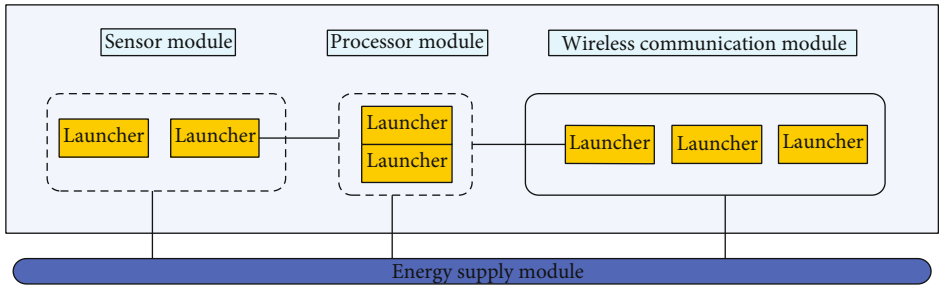

Figure 2: Block diagram of wireless sensor nodes.

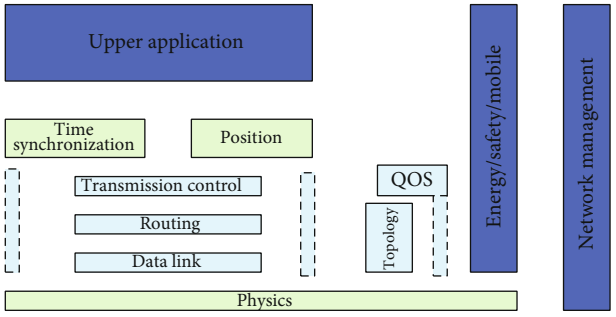

Figure 3: Protocol stack model.

Dragon boat training on the water is a symbol that reflects our national culture and represents the strength and stability of our people, and multiple heart rate belts are, respectively, connected to the Bluetooth host module of the SCM minimal system via Bluetooth. The SCM minimal system controls the Bluetooth host module, acceleration sensor, and GPS module and transmits the processed data to the GPRS module through the serial port, and the GPRS module then transmits the data to the remote computer. Because the data is transmitted through the GPRS network, there is no distance limit when the system is working [12]. The hardware system framework is shown as in Figure 5.

Make full use of the multisensor data resources of different time and spaces, use computer technology to analyze, synthesize, control, and use the multisensor observation data obtained in time series under certain criteria to obtain a consistent interpretation and description of the measured object, then realize the corresponding decision-making and estimation, and make the system obtain more sufficient information than its various components. The system mainly consists of two parts: a data collection subsystem placed in the water and a remote receipt collection subsystem. After that, the data parameters are monitored through the processing, analysis, and storage of the background software. The remote can use the WEB page to query the water dragon boat training parameter index measurement data [13]. Collect the data in the target water area in real time through the data platform, perform real-time statistical analysis, and use big data to push the real-time analysis result data to the analysis department. After the analysis department receives the data, it uses different methods to analyze the indicators, to develop training programs for athletes to help athletes get better results in the competition, as shown in Figure 6.

2.2. Kalman Filter Method. Kalman filter is an algorithm that uses linear system state equations to optimally estimate the system state through system input and output observation data. Since the observation data includes the influence of noise and interference in the system, the optimal estimation can also be regarded as a filtering process. Kalman method includes the state space method and projection method. Kalman added a concept to the method the state of the system and introduced two mathematical models state and observation, that is, the classical state equation and observation equation. The true value is inaccessible, and it can only be based on the minimum mean square error to make the

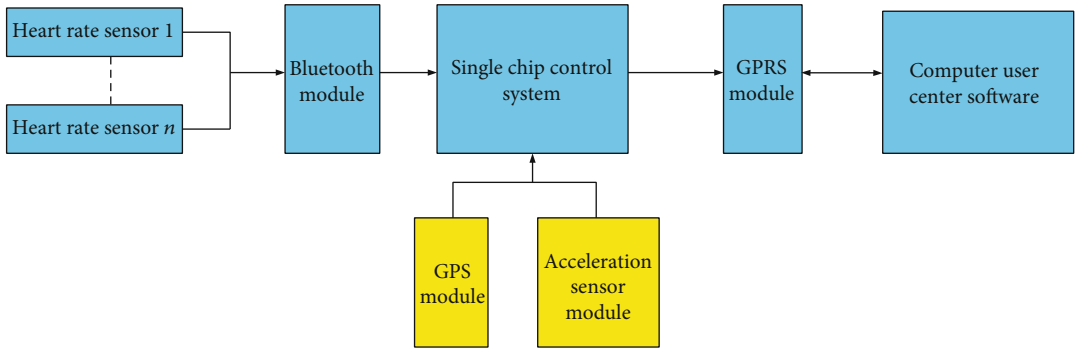

Figure 4: Schematic diagram of water training monitoring.

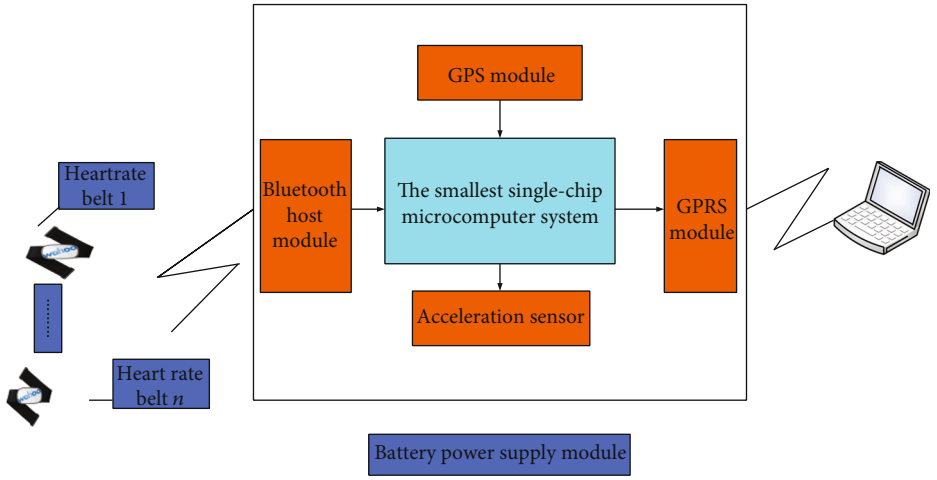

Figure 5: Hardware system framework diagram.

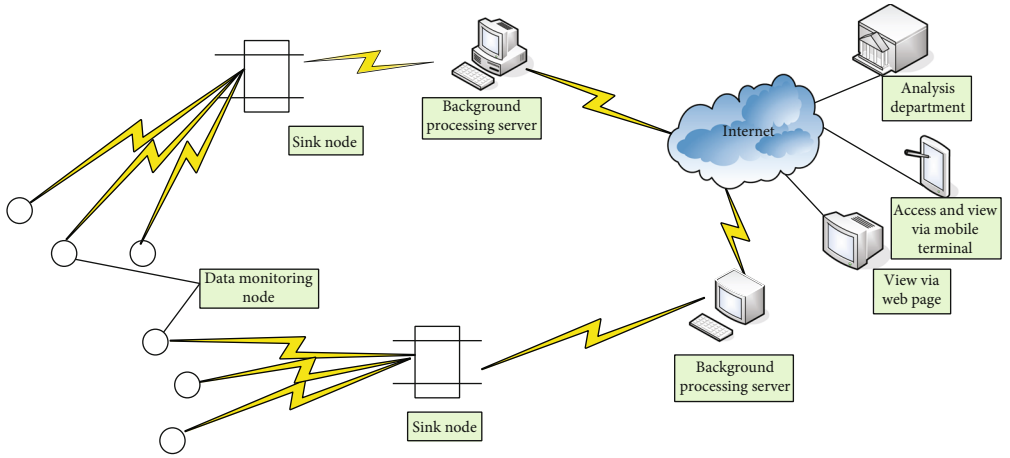

Figure 6: Data analysis system.

estimated value as close to the true value as possible, through the input and output observation data of the system, the algorithm for optimal estimation of the system state. Since the observation data includes the influence of noise and interference in the system, the optimal estimation can also be regarded as a filtering process. On this basis, he used the projection method to propose the optimal and Kalman filter equations [14]. The biggest advantage of Kalman filtering is that filtering is a state-space method in the time domain, which has obvious intuitive meaning. At the same

time, the Kalman filter method is a recursive method, so that the fusion system does not need to store large data and perform complex calculations and can be conveniently used in real time on a computer [15]. Kalman filtering is suitable for filtering problems in stationary or nonstationary random processes, as well as filtering problems in time-varying systems and multivariable systems.

The specific equation of Kalman filter is as follows:

$$x(t+1) = b(t)x(t) + g(t)u(t) + w(t). \tag{1}$$

In the above formula, we can see that $X(k)$ represents an n-dimensional vector, which represents the target state at time t, which is called the state equation; $\beta(t)$ is the $n \times n$ order state transition matrix at time t, $U(t)$ is the m-dimensional input vector, $G(t)$ is the $n \times m$-order input matrix, and $W(t)$ is the n-dimensional process noise, which conforms to the Gaussian white noise distribution, and $E[W(\mathrm{t})] = 0, E[W(\mathrm{t})W^T(J)] = Q(K)\eta_{TJ}$.

Among them, they satisfy

$$h_{tj} = \begin{cases} 0, t^{i} j \\ 1, t = j \end{cases}. \tag{2}$$

The sensor observation equation used for target tracking is

$$z(t) = h(t)x(t) + v(t). \tag{3}$$

$Z(t)$ is a p-dimensional vector, which represents the measurement vector at time t, $H(t)$ is a $p \times n$-order measurement matrix, $V(t)$ represents p-dimensional measurement noise, which conforms to the Gauss white noise distribution, and have

$$\begin{cases} E[V(\mathrm{t})] = 0, \\ E[V(\mathrm{t})]V^T(J) = R(\mathrm{t})\eta_{\mathrm{ij}}. \end{cases} \tag{4}$$

If the filtered value $x^U(t/t)$ and the covariance $P(t/t)$ of the target observation state $X(t)$ at time t are known, then the Kalman filter method can be used to obtain the state prediction value of the moving target at time $t+1$:

$$\overset{U}{x}(t+1/t) = j(t)\overset{U}{x}(t/t) + g(t)u(t). \tag{5}$$

Forecast covariance matrix is as follows:

$$p(t+1/t) = j(t)p(t/t)j^t + q(t). \tag{6}$$

Innovation covariance matrix is as follows:

$$s(t+1) = h(t+1)p(t+1/t)h^t(t+1) + r(t+1). \tag{7}$$

Gain matrix is as follows:

$$k(t+1) = P(t+1/t)h^t(t+1)s^{-1}(t+1). \tag{8}$$

State filter value is as follows:

$$\overset{U}{x}(t+1/t+1) = \overset{U}{x}(t+1/t) + k(t+1)\left[z(t+1)\overset{U}{z}(t+1/t)\right]. \tag{9}$$

The filter covariance matrix is

$$p(t+1/t+1) = p(t+1/t) - k(t+1)s(t+1)k^t(k+1). \tag{10}$$

Two of the more significant problems are as follows: first, when the combined data of multiple sensors is redundant, the amount of calculation will increase drastically by the geometric exponent of the filter dimension, which will make the real-time performance difficult to meet; the second is the number of sensors. Increasing generally increases the possibility of failure. When a sensor fails and the system is not found in time, the failure will affect the entire system and reduce the reliability of the system.

2.3. Bayesian Estimation Method. The installation position of the multisensor is also one of the important indicators that affect the data. How to combine the multisensor to play the best value of each part has great guiding significance for the results of the experiment. Bayesian estimation is a main method to fuse low-level multisensor data in static environments. This method is to recombine multisensor data according to probability and use conditional probability to express the measurement uncertainty. If the observation coordinates of each sensor are the same, and then the measurement data obtained from the sensors can be fused by the direct method [16]. However, most of the time, the measurement data of different sensors come from different coordinate systems. At this time, we should use indirect methods to perform Bayesian estimation and fusion of the measurement data of different sensors. Assuming that $p(x_i|x)$ is the conditional probability that the measurement is x_i under the condition that the true value is X, it is a known quantity. When the received measurement data is x_i, the posterior probability of the true value, X is calculated by the Bayes formula as

$$p(x|x_i) = \sum_{y}^{p(x_i|x)p(x)} p(x_i|y)p(y) \tag{11}$$

Assuming that the estimated value of the unknown θ is $\theta^{\wedge}$, a commonly used estimation method is to take the mean of the posterior distribution, that is to say

$$\overset{U}{q} = \overset{U}{q}(x_1, x_2, \cdots, x_n) = E(q|x_1, x_2, \cdots, x_n). \tag{12}$$

It can be seen from the above definition that the posterior distribution depends on the sample; so, the estimation of the unknown parameter must be related to the sample selection. In this estimation method, the estimated value of $\theta^{\wedge}$ is generally the average of the parameters of the posterior distribution. Another method that can be used to calculate the estimated value is the method with the smallest deviation, when he meets

$$E\left((\theta-\alpha)^2|X_1, X_2, \cdots, X_N\right). \tag{13}$$

If the minimum value of the above formula is, that is, the deviation of each parameter is the smallest. To minimize the deviation, the following formula can be derived, namely,

$$\P a\, e\left((\theta\text{-}\alpha)^2|x_1, x_2, \cdots, x_n\right) = 2e(\theta||x_1, x_2, \cdots, x_n)\text{-}2\alpha = 0. \tag{14}$$

Assuming that B1, B2, ... are several possible premises of a certain process, then $P(\mathrm{Bi})$ is the people's estimate of the probability of each premise condition in advance, which is called the prior probability. If this process yields a result A, then the Bayesian formula provides a way for us to make a new evaluation of the preconditions based on the appearance of A. The above transformation can be obtained:

$$\alpha = \theta = e(\theta|x_1, x_2, \cdots, x_n). \tag{15}$$

Bayesian decision-making is to estimate part of the unknown state with subjective probability under incomplete intelligence, then use Bayesian formula to correct the probability of occurrence, and finally use the expected value and revised probability to make the optimal decision.

2.4. D-S Evidence Reasoning Method. The Dempster-Shafer (D-S) method of evidence reasoning was first proposed by Dempster and developed by Shafer.

The method belonging to the theory of imprecise reasoning can be regarded as an extension of the Bayesian method. Compared with Bayesian estimation, which requires a priori probability, D-S evidence reasoning can solve the uncertainty caused by ignorance. In a data fusion system composed of multiple sensors, each sensor can give a set of data (or a set of evidence or propositions), so that the corresponding mass distribution function can be established [17]. Here, each data source can be regarded as a recommendation degree. Under the same conditions, after combining different evidence bodies by the Dempster combination rule, a brand-new recommendation degree is calculated, and then the credibility of this recommendation degree is calculated, and then through a certain screening rule, the final result is shown in Figure 7.

The D-S evidence reasoning method uses a recognition framework to represent the collection that needs to be fused, and it gives such a function:

$$m(\Theta) = 0, \sum_{a\subset\Theta} m(a) = 1. \tag{16}$$

For any set, D-S, evidence reasoning gives a concept of credibility function:

$$\mathrm{bel}(a) = \sum_{b\subset a} m(b). \tag{17}$$

However, it is still not enough to express the credibility of each set A with only one credibility function, because Bel (A) does not reflect the degree of suspicion for this set A [18]. Based on this, if we want to describe the credibility of a set A more comprehensively, we need to add a quantity that can reflect the degree of suspicion A. Then, this definition can be given:

$$\begin{aligned} \mathrm{pl}(a) &= 1\text{-}\mathrm{bel}(a), \\ \mathrm{dou}(a) &= \mathrm{bel}(a). \end{aligned} \tag{18}$$

We can clearly derive the fusion formula of multiple credibility; first, the following hypothesis needs to be given: $m_1, m_2, \cdots, m_n$ is used to represent the credibility distribution function of n data, and these n data are independent of each other; then, the credibility function after fusion can be written in the following form:

$$m(a) = m_1 \mathring{A} m_2 \mathring{A} \cdots \mathring{A} m_n = 1 - \sum_{a_i C b_i = Q}^{\sum_{a_i C b_i = a} m_1(a_i) m_2(b_i)} m_1(a_i) m_2(b_i). \tag{19}$$

3. Comparative Analysis Experiment

3.1. Experimental Design. The experiment was carried out in the lake where water dragon boat competitions have been held over the years. Related experimental equipment was arranged on the shore. Video monitors and sensors were installed on the dragon boat page and some parts of the athletes. Multisensor data fusion is an emerging research field, which is a research on data processing aimed at the specific problem of using multiple sensors in a system. Multisensor data fusion technology is a practical application technology developed in recent years. It is a new technology that intersects multiple disciplines. It involves signal processing, probability and statistics, information theory, pattern recognition, artificial intelligence, fuzzy mathematics, and other theories. In this experiment, the main purpose is to verify the performance of the three fusion methods proposed in this paper, RP fusion and NB and WMV fusion rules, under the conditions of different numbers of classifiers and different classification accuracy. Because in the actual classification application, the performance of the local classifier is fixed; so, the use of variable data sets can better study the impact of the accuracy of different classifiers on the performance of the fusion algorithm. In this experiment, we use the Gaussian function to randomly generate a data set. The number of target category labels is set to 5. Each sample data consists of two randomly generated attributes that conform to different Gaussian distributions, and the two attributes are independent of each other. As shown in Table 1, the standard deviation of the two attributes of the sensor can be changed by the variable α. The larger the parameter α, the larger the standard deviation of the two attributes. For example, the following two probability density functions $x_1|\omega_3 \sim n(30, 4\alpha)$, $x_2|\omega_3 \sim n(10, 4\alpha)$, respectively, represent the distribution of the two attributes of the category label ω_3. Obviously, the classification performance of the classifier is determined by α. The larger the α, the less concentrated the data distribution of each category, and the overlapping range will increase accordingly; so, the classification accuracy of the sensor will be smaller. Therefore, the

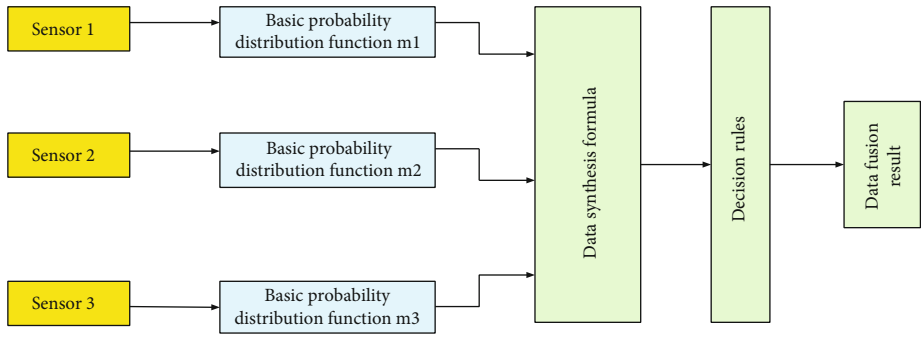

Figure 7: Flow chart of multisensor data fusion.

Table 1: Randomly generated data.

Category	$\mu 1$	$\mu 2$	β
w1	20	10	3α
w2	10	20	5α
w3	15	30	10α
w4	15	30	9α
w5	20	20	7α

classification performance of the sensor can be adjusted by the parameter α as shown in Table 1.

From the data in the above table, it can be found that the data set is mainly concentrated in the interval of 10-20, and the overlapping range can be established by using the Gaussian function. Gaussian function is widely used in statistics to describe the normal distribution.

As shown in Figure 8, it represents a data set randomly generated by the Gaussian function when α is equal to 1, and the sample data is equal to 100. In the actual experiment, the number of samples used to train the sensor is set to 300. At the same time, to prevent the one-sidedness of the simulation results, in each round of experiments, a new data set will be randomly generated. Considering the reliability of the experimental results, the experiment was repeated 20 times, and the classification decision result was obtained each time. The average classification decision result of 20 times was calculated to obtain the average classification accuracy. To obtain the classification performance of each sensor, 1500 training sample sets and 500 test sample sets were randomly generated in each experiment. And the number of training samples and test samples of each category in each experiment is the same, that is, 300 and 100, respectively. After the classifier is trained, another 1000 observations are generated, and the corresponding number of each category is about 200. Then, using the trained classifier to classify and make decisions on these data to obtain local decisions, and at the same time obtain the reliability of the classifier's decision, the fusion center then conducts decision fusion based on the local decision and decision reliability [19].

3.2. Experimental Method. Aiming at the problem of slow paddle frequency in the start and sprint phases that cannot keep up with the rhythm, the training method is mainly short-stroke training, which is high-frequency rapid strokes of 10 paddles, 20 paddles, and 30 paddles; supplemented by

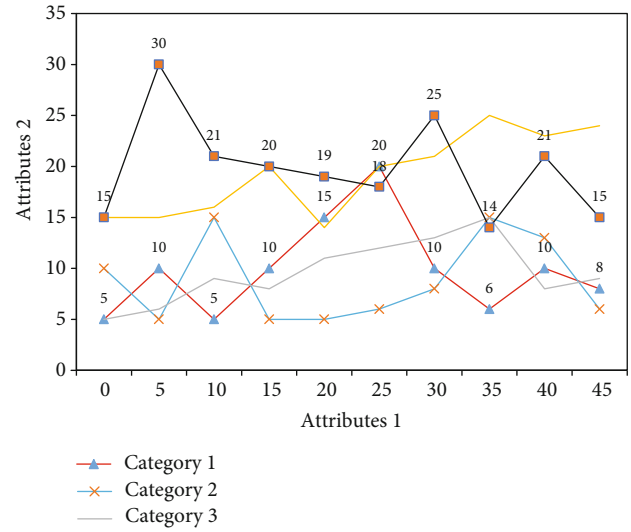

Figure 8: Example of generating sample data.

functional training, vibration rods, and power ropes, barbells and other equipment can be used for upper limb speed endurance training. This experiment will use the actual dragon boat recognition data set collected during the monitoring of the water dragon boat training project for simulation. In the monitored project, a total of 23 sensor nodes are arranged on the roadside to collect data on dragon boats and athletes [20]. When a dragon boat passes by, the sensor will collect three types of data: infrared, earthquake, and sound of the dragon boat. Perform segmentation and feature extraction on the collected data. In the actual experiment, 11 sensor-node pairs will be selected for classification. The experiment used sound and seismic signals. After fast Fourier transform, the characteristics of each signal are proposed. Each has 297 characteristics, and the length of each characteristic is 50 values between 0 and 1. The data obtained were measured using a logistic regression model, considering the different data of each individual of each athlete, and combining these variables for data screening.

4. Analysis of Experimental Results

4.1. Comparative Analysis. The experimental results obtained are shown in the following figure. The classification accuracy of the fusion result is defined as the proportion of correctly identified targets in each classification. The RP fusion rule

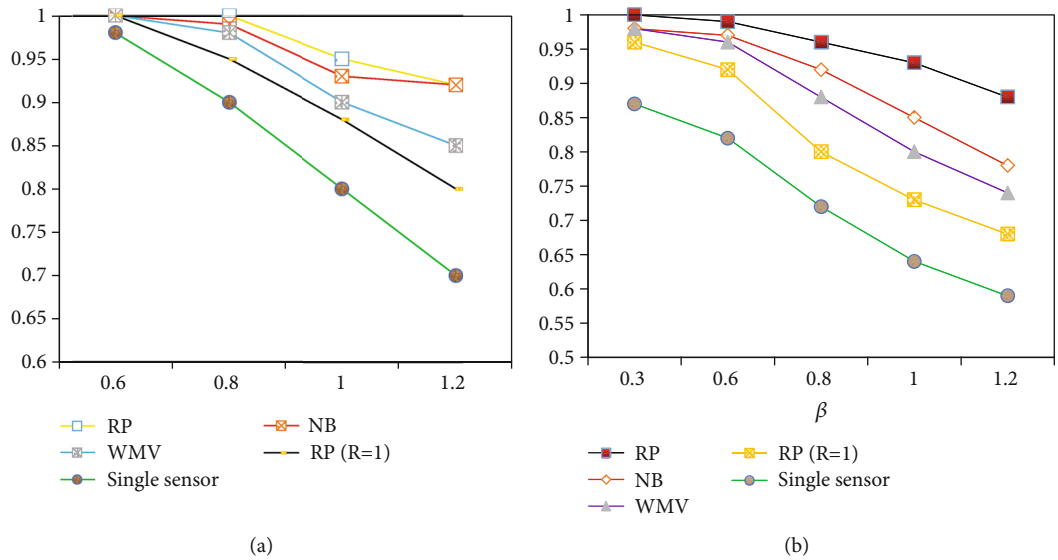

FIGURE 9: (a) When the local classifier is k-NN, the accuracy of the fusion results of each fusion rule varies β. (b) When the local classifier is ELM, the accuracy of the fusion results of each fusion rule varies β.

proposed in this paper is compared with the naive Bayes fusion rule and the fusion performance of WMV Considering the local classification decision in k-NN and ELM neural network, and the average classification accuracy of the fusion results of these three fusion methods (plus and minus one standard deviation) varies with the parameter β and the classifier number of changes, as shown in Figure 9 below.

The changes are shown in Figure 9. Figures 9(a) and 9(b), respectively, show that when the number of sensors is fixed at 5, the fusion accuracy of each fusion rule changes with β when the classifier is k-NN and ELM neural network case. It can be seen from Figure 9(a) that when the value of the parameter increases from 0.97 to 2.5, the average classification accuracy of the k-NN classifier decreases from 0.97 to 0.4, and the accuracy of the fusion results of the three fusion rules is also correspondingly, but the RP fusion rule proposed in this paper is still better than the other two fusion rules. In the simulation diagram (b), as the parameter β increases, the classification performance of the local classifier decreases accordingly, and the accuracy of the fusion results of each fusion rule changes with β to be roughly the same as the diagram (a). However, it can be seen from Figures 9(a) and 9(b) that the performance of the k-NN classifier is better than the ELM classifier, especially when the value of β is in the interval [0-1.4]. Therefore, the accuracy of the final fusion result obtained by using the k-NN classifier for local classification decision is higher than the case of using the ELM classifier [21]. Clearly, from the simulation results, it can be verified that the reliability-probability fusion rule proposed in this paper can more effectively improve the classification accuracy, and the performance is always better than the NB fusion rule and WMV fusion rule, especially when the local classifier classification performance when it is poor, the RP fusion rule proposed in this paper to fuse the classification decision results of multiple classifiers with poor classification performance, and the accuracy of the final fusion result can be greatly improved.

4.2. The Accuracy of the Fusion Result Varies with the Number of Sensors. The changes are shown in Figure 10. Figures 10(a) and 10(b) show how the accuracy of the fusion result varies with the number of sensors when the local classifiers are$k$ -NN and ELM, respectively. At this time,$\beta = 1.5$is fixed during the simulation process. Like the conclusions drawn in Figures 9(a) and 9(b), the experimental results still prove that the final fusion result obtained by the RP fusion rule proposed in this paper is more accurate than the NB fusion rule and WMV fusion rule. At the same time, the analysis shows that when the number of sensors is increased from 1 to 7, and the accuracy of the fusion result increases quickly compared with a single sensor. However, when the number of sensors is greater than 7, the accuracy of the final fusion result is the effect of increasing degree gradually decreases. In actual target classification applications, when a certain fusion accuracy is achieved, the number of sensors involved in monitoring should be minimized to reduce costs. Finally, it can be seen that the fusion rule proposed in this paper is very similar to the NB fusion rule, but the decision-making performance of the two is different. From the above simulation results, it can be concluded that when the decision reliability $R = 1$ is set, the performance of the RP fusion rule is much lower than the other two types of fusion algorithms [22]. This shows that the calculation method of decision-making reliability is a key factor that affects the accuracy of RP-based fusion. Therefore, in practical applications, it is necessary to design a reasonable reliability calculation method for different application scenarios, and it will be possible to obtain better fusion performance [23].

4.3. When the Classifier Is ELM, the Fusion Accuracy Varies with the Number of Sensors. The change is shown in Figure 11. From Figure 11(a), it can also be concluded that when the classifier is k-NN, the three fusion rules increase with the number of sensors, and the accuracy of the fusion result is also improved accordingly. Before the improvement, the highest value of a

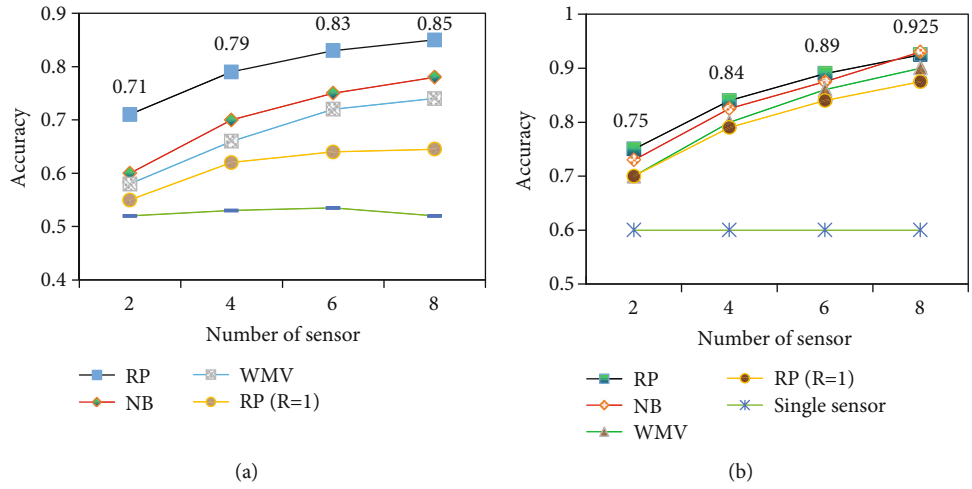

Figure 10: (a) When the local classifier is k-NN, the accuracy of the fusion results of each fusion rule varies with the number of sensors. (b) When the local classifier is ELM, the accuracy of the fusion results of each fusion rule varies with the number of sensors.

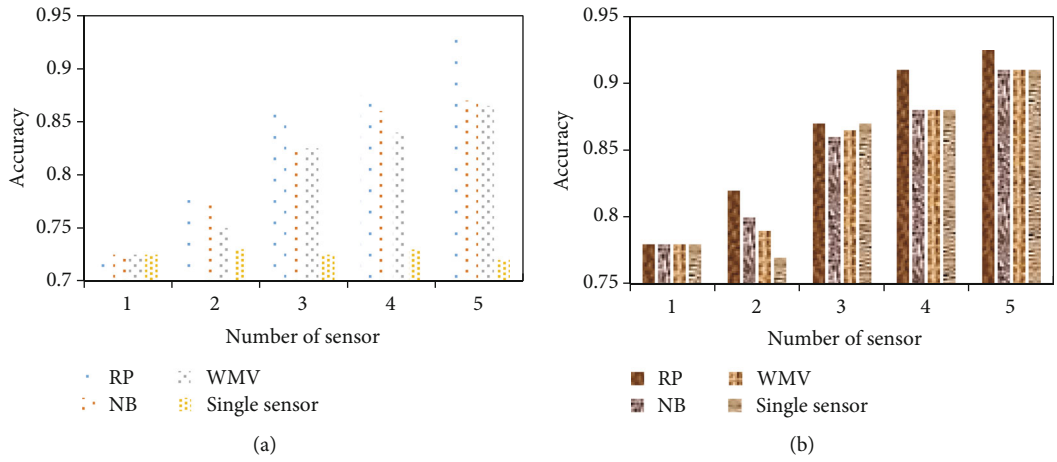

Figure 11: (a) When the classifier is k-NN, the accuracy of the fusion results of each fusion rule varies with the number of sensors. (b) When the classifier is ELM, the accuracy of the fusion results of each fusion rule varies with the number of sensors.

single sensor is 0.73; after the improvement, the highest value of a single sensor can reach 0.91; and the accuracy rates of RP, NB, and WMV have been greatly improved. However, the final fusion accuracy obtained by the RP fusion rules proposed in this paper is always higher than that of the NB fusion rule and WMV fusion rule [24]. The simulation result of analysis diagram (b) can still be obtained. When the classifier is ELM, the classification accuracy of the decision results of multiple classifiers through the fusion processing of the three fusion rules is clearly more accurate than that of a single sensor. However, the RP fusion rule performance is still better than the other two commonly used fusion rules; so, the simulation results prove that the RP fusion rule proposed in this paper has superior performance, and the decision fusion accuracy is higher than that of the NB and WMV fusion rules. From the simulation results, it can also be found that, different from the previous experimental results, the final decision accuracy of the NB fusion algorithm and WMV fusion algorithm at this time is not much different, indicating that the stability is poor due to the limitation of the application scenario, and in this article, the proposed decision fusion algorithm is more stable in improving the classification accuracy.

5. Conclusions

Bayesian estimation provides a means for data fusion and is a common method for fusing high-level information from multiple sensors in a static environment. It enables sensor information to be combined according to the principle of probability, and the measurement uncertainty is expressed in conditional probability. Based on the sports training theory and combined with the special characteristics of the competitive dragon boat event, a series of comparative analysis of different training methods and methods aimed at improving the special endurance training of the upper limbs of competitive dragon boat athletes. Indepth study of the current status of the special endurance training of the upper limbs of Chinese competitive dragon boat athletes determines the existing

problems and analyzes them. The water training monitoring system based on multisensor data fusion technology has the characteristics of high sampling frequency and strong processing ability. It can convert the collected heart rate, speed, acceleration, and other data into images for real-time display and monitor and analyze training effects. The system uses modern science and technology such as GPRS network transmission, paddle frequency calculation, embedded system, and GPS, without affecting the training of athletes, collects sports information and instantly generates monitoring process diagrams of sports training parameters, enabling coaches and athletes clearly understand the real-time kinematic parameter information in the training process, provides a scientific basis for coaches to diagnose training effects in real time, improves the efficiency of athletes' special training, and conducts targeted training. Under various methods of fusing data, we have performed a certain analysis on the data transmitted by this sensor, including the heart rate of dragon boat athletes, and what the speed of the dragon boat is at what heart rate. Understand that with our help, athletes can make their training more effective. Since the athlete's physical fitness and other factors have not been fully investigated when selecting the samples, the experimental data will still be a little biased. Weather factors and other factors will affect the parameters of the game, so the content involved in this research is too much. Monotonous, more detailed research will be carried out next.

Data Availability

Data sharing not applicable to this article as no datasets were generated or analyzed during the current study.

Conflicts of Interest

There is no potential conflict of interest in our paper.

Authors' Contributions

The author has seen the manuscript and approved to submit to your journal.

Acknowledgments

This work was supported by Huazhong University of Science and Technology Independent Innovation Research Fund (Humanities Social Sciences) (2019WKYXQN003).

References

[1] F. Xiao, "Multi-sensor data fusion based on the belief divergence measure of evidences and the belief entropy," *Information Fusion*, vol. 46, pp. 23–32, 2018.

[2] M. Elhoseny, "Multi-object detection and tracking (MODT) machine learning model for real-time video surveillance systems," *Circuits, Systems, and Signal Processing*, vol. 39, no. 2, pp. 611–630, 2020.

[3] J. Zhang and L. Du, "Research on industrial internet of things system based on multisensor data fusion," *Boletin Tecnico/Technical Bulletin*, vol. 55, no. 16, pp. 457–462, 2017.

[4] F. Wu, X. Liu, and Y. Wang, "Research on software design of intelligent sensor robot system based on multidata fusion," *Journal of Sensors*, vol. 2021, no. 20, p. 10, 2021.

[5] Z. Zhang and L. I. Fang, "Research on the water pollution monitoring and rapid decision-making system based on artificial intelligence agent.," *Journal of Environmental Protection and Ecology*, vol. 20, no. 3, pp. 1565–1573, 2019.

[6] R. G. Ma, Z. H. Ma, and Y. X. Wang, "Study on positioning technology of ,mileage piles based on multi-sensor information fusion," *Journal of Highway & Transportation Research & Development*, vol. 10, no. 4, pp. 7–12, 2016.

[7] X. Xu, D. Cui, Y. Li, and Y. Xiao, "Research on ship trajectory extraction based on multi-attribute DBSCAN optimisation algorithm," *Polish Maritime Research*, vol. 28, no. 1, pp. 136–148, 2021.

[8] N. Zhang and F. Li, "Research on safety monitoring and warning system based on information fusion for coking production," *International Journal of Hybrid Information Technology*, vol. 9, no. 8, pp. 303–314, 2016.

[9] H. Cui, X. Dong, H. Deng, M. Dehghani, K. Alsubhi, and H. M. Aljahdali, "Cyber attack detection process in sensor of DC micro-grids under electric vehicle based on Hilbert–Huang transform and deep learning," *IEEE Sensors Journal*, vol. 21, no. 14, pp. 1–1, 2021.

[10] H. S. Zhai, Z. Y. Wen, and H. P. Yu, "New method of multisensor data fusion based on multiscale analysis and UKF," *International Journal of Control & Automation*, vol. 9, no. 2, pp. 329–342, 2016.

[11] S. Ji, Z. Y. Chen, P. Guo et al., "Bayesian approach for multisensor data fusion based on compressed sensing for wireless structural damage signal," *Journal of Internet Technology*, vol. 17, no. 7, pp. 1363–1371, 2016.

[12] X. Ouyang, W. He, W. Lu, and Z. Bian, "Study on 3D border surveillance system and multi-sensor information fusion technology," *Bandaoti Guangdian/Semiconductor Optoelectronics*, vol. 39, no. 2, pp. 298–304, 2018.

[13] X. H. Wu and S. M. Song, "Covariance intersection-based fusion algorithm for asynchronous multirate multisensor system with cross-correlation," *Iet Science Measurement & Technology*, vol. 11, no. 7, pp. 878–885, 2017.

[14] S. Kumar and V. K. Chaurasiya, "A multisensor data fusion strategy for path selection in internet-of-things oriented wireless sensor network (WSN)," *Concurrency and Computation: Practice and Experience*, vol. 30, no. 18, pp. e4477.1–e4477.14, 2018.

[15] C. Yang, J. Guo, L. Zhang, and Q. Chen, "Multi-sensor fault-tolerant fusion algorithm using unscented information filter," *Journal of Nanjing University of ence and Technology*, vol. 41, no. 3, pp. 269–277, 2017.

[16] C. Bachmann, B. Abdulhai, M. J. Roorda, and B. Moshiri, "Multisensor data integration and fusion in traffic operations and management," *Transportation Research Record*, vol. 2308, no. 1, pp. 27–36, 2018.

[17] P. Braca, R. Goldhahn, G. Ferri, and K. D. LePage, "Distributed information fusion in multistatic sensor networks for underwater surveillance," *IEEE Sensors Journal*, vol. 16, no. 11, pp. 4003–4014, 2016.

[18] H. K. Lee, S. G. Shin, and D. S. Kwon, "Design of emergency braking algorithm for pedestrian protection based on multisensor fusion," *International Journal of Automotive Technology*, vol. 18, no. 6, pp. 1067–1076, 2017.

[19] Z. Yu, L. Chang, and B. Qian, "A belief-rule-based model for information fusion with insufficient multi-sensor data and domain knowledge using evolutionary algorithms with operator recommendations," *Soft Computing*, vol. 23, no. 13, pp. 5129–5142, 2019.

[20] J. W. Hu, B. Y. Zheng, C. Wang et al., "A survey on multi-sensor fusion based obstacle detection for intelligent ground vehicles in off-road environments," *Frontiers of Information Technology & Electronic Engineering*, vol. 21, no. 5, pp. 675–692, 2020.

[21] K. Da, T. Li, Y. Zhu, H. Fan, and Q. Fu, "Recent advances in multisensor multitarget tracking using random finite set," *Frontiers of Information Technology & Electronic Engineering*, vol. 22, no. 1, pp. 5–24, 2021.

[22] M. Mosalanejad and M. M. Arefi, "UKF-based soft sensor design for joint estimation of chemical processes with multi-sensor information fusion and infrequent measurements," *Science, Measurement & Technology, IET*, vol. 12, no. 6, pp. 755–763, 2018.

[23] A. Rubaiyat, Y. Fallah, X. Li, G. Bansal, and T. Infotechnology, "Multi-sensor data fusion for vehicle detection in autonomous vehicle applications," *Electronic Imaging*, vol. 2018, no. 17, pp. 257-1–257-6, 2018.

[24] L. Wang, L. Liang, D. Ma, H. Wang, and X. Liu, "Localization method of biped robot based on multi-sensor information fusion," *Zhongguo Guanxing Jishu Xuebao/Journal of Chinese Inertial Technology*, vol. 26, no. 5, pp. 629–634, 2018.

Hindawi
Journal of Sensors
Volume 2021, Article ID 4214413, 11 pages
https://doi.org/10.1155/2021/4214413

Research Article

Analysis of the Fluctuation of Bank Interest Rate Based on Computer Statistical Model and Machine Learning

Jiangning Cao [1,2]

[1]*School of Business Administration, Zhongnan University of Economics and Law (ZUEL), Wuhan 430000, China*
[2]*Business College, Xinyang Normal University (XYNU), Xinyang 464000, China*

Correspondence should be addressed to Jiangning Cao; doudou@xynu.edu.cn

Received 10 September 2021; Revised 23 October 2021; Accepted 5 November 2021; Published 18 November 2021

Academic Editor: Mu Zhou

In order to improve the effect of bank interest rate volatility analysis, this article combines actual conditions and machine learning algorithms to construct a fluctuation analysis model of bank interest rate based on computer statistical model and machine learning. For the data with system transformation, the data contains stationary and nonstationary processes; so, the power of the standard unit root test is low. This paper therefore proposes a new unit root test method. From demand analysis, system design to system implementation, and testing, advanced software engineering-related ideas are adopted, and the bank's interest rate management system is designed and implemented in strict accordance with software development-related processes. This paper adopts the modular design idea, classifies the functions to be realized according to their content, and conducts structural verification and performance analysis of the functional modules. Through experimental analysis, we can see that the system model constructed in this paper has certain effects in the analysis of interest rate fluctuations.

1. Introduction

With the continuous improvement of China's financial market mechanism and the continuous enrichment of market levels, the interest rate sensitivity of microentities has been greatly improved. Moreover, the development of China's economy has gradually shifted from extensive development to sustainable development based on structural optimization, and the shortcomings of quantitative monetary policies have gradually become apparent. In order to cope with this change in the development mode, the monetary and credit policy is changing from "overflow irrigation" to "precision drip irrigation." Therefore, it is very important to establish a price-guided financial market operation mechanism and a monetary policy guidance mechanism [1].

To implement a financial market operation mechanism based on price guidance, first of all, it is necessary to cultivate the sensitivity of microentities to prices. In addition to a complete market mechanism, it also requires the stable and orderly operation of the financial market. The central bank's monetary policy is predictable, and the central bank's monetary policy toolbox contains a wealth of tools to deal with different financial shocks [2]. Therefore, on the one hand, the financial market needs to build a stable market-based benchmark interest rate. The benchmark interest rate is determined by a market-based mechanism and can accurately reflect the liquidity fundamentals of the financial market. In addition, it is necessary to ensure the smooth operation of the benchmark interest rate of the money market and the ability to dilute liquidity shocks and ensure the smooth transmission of monetary policy guidance from the short-term money market to the long-end capital market and then to the real economy. On the other hand, the central bank has a strong ability to guide the benchmark interest rate. Based on this, the reform of interest rate marketization is imperative. Therefore, studying the characteristics of currency market interest rate fluctuations and how effective influencing factors affect money market interest rate volatility is of great significance for the central bank to gradually improve its ability to guide money market interest rates and improve the predictability of money market liquidity shocks, thereby improving participants' resilience. Judging

from the development of benchmark interest rates in my country's currency market at this stage, the current benchmark interest rates in the financial market consist of interbank lending rates, banker pledged repo rates, and money market interest rate systems such as SHIBOR that our country is vigorously fostering [3]. Judging from its volatility characteristics, the interest rate volatility of the Chinese currency market is much higher than that of other countries. As the People's Bank of China implements a liquidity management framework with structural liquidity shortage, when liquidity is relatively short, the preventive liquidity demand of commercial banks will rise sharply, which will lead to substantial fluctuations in interbank money market interest rates. However, after the Central Bank began to focus on building an interest rate corridor mechanism that stabilizes the liquidity expectations of commercial banks, the fluctuation of interest rates in the interbank money market has dropped significantly. In recent years, on the one hand, the central bank has focused on building a currency market benchmark interest rate with global representative capabilities, ensuring that its fluctuations can represent the actual situation of currency market liquidity shocks and controlling its fluctuations within a certain range. On the other hand, the government has built a rich monetary policy tool system, stabilized the liquidity impact expectations of commercial banks, improved the predictability of monetary policy, strengthened the central bank's ability to guide the money market benchmark interest rate, and reduced the friction of monetary policy in the money market-credit market-real economic transmission channel.

Based on the above analysis, this article analyzes the fluctuation of bank interest rates based on computer statistical models and machine learning models.

2. Related Work

The literature [4] constructed a stochastic model specifically used for commercial banks to describe changes in their deposit reserve requirements under different circumstances and studied the related issues of commercial banks' reserve requirements in more detail and indepth. The literature [5] analyzed the specific operation process of the interest rate corridor monetary policy control framework. The research shows that even under the zero reserve policy, the central bank's monetary policy can be very effective. Because the primary goal of commercial banks is to maximize their own profits, the central bank adjusts the width of the interest rate corridor by changing the upper and lower limits of the interest rate corridor. Without the need for open market operations, the lending rate of commercial banks will be controlled near the target interest rate expected by the central bank. The literature [6] used the method of establishing a geometric model to study and elaborate the basic and operating principles of the interest rate corridor in detail. It is believed that if the settlement balance of commercial banks at the end of each trading day can be controlled at zero, then through the control of interest rate corridors, the basic interest rate of the money market can be stabilized near the central bank's target interest rate. The research in the literature [7] is based on the commercial bank reserve requirement model. Moreover, it pointed out that if the central bank's policy target interest rate can be higher than the midpoint of the interest rate corridor, then the central bank's level of short-term market interest rate regulation will not be affected by the interest rate corridor range and the size of the policy target interest rate. The research of the literature [8] is from the perspective of social welfare. It is believed that the interest rate in the corridor should be set to a width greater than zero, so as to optimize the effect of monetary policy. The literature [9] believes that the policy control effect of the interest rate corridor is far superior to the traditional open market operation, but it believes that if only the interest rate corridor is used as a control method, it will reduce the efficiency of cash distribution. Therefore, the optimal method of monetary control policy should be a combination of interest rate corridors and open market operations. The literature [10] analyzed the new form of "floor-style" interest rate corridors that emerged after the financial crisis. It is believed that once the width of the interest rate corridor is set by the central bank, if the overall mobile interest rate corridor model does not change its width, the final control effect of the interest rate corridor on market interest rates will not be affected. The literature [11] believes that the core of the interest rate corridor, the monetary policy control framework, is the width of the interest rate corridor. The literature [12] pointed out in the research that the Fed's rediscount window is an emergency funding aid, not a regular loan facility; so, commercial banks will only apply for special circumstances. In addition, interest on deposit reserves is not available to all commercial banks. Sometimes, market segmentation occurs in the federal funds market, which will cause market interest rates to fall below the lower limit of the interest rate corridor and cause market interest rates to deviate for a long time. The literature [13] elaborated on the specific practice of adopting zero reserve system and interest rate corridor in some countries in the world. The literature [14] summarized the actual experience of China's open market operations, in which the upper limit interest rate of the interest rate corridor is selected as the overnight automatic pledge financing interest rate, and the lower limit interest rate of the interest rate corridor is selected as the reserve interest rate. The literature [15] elaborated on the origin, development, and mechanism of the interest rate corridor and explored the optimal width of the interest rate corridor and the influence of the benchmark interest rate of the money market on the interest rate corridor. The literature [16] compared the monetary policy framework of interest rate corridor with traditional open market operations and believed that our national central bank should adopt both interest rate corridor and open market operations to achieve the best regulatory effect. The literature [17] selected several typical countries and regions that have implemented interest rate corridors to prove that in the same period, the short-term market interest rate fluctuations of countries that have implemented interest rate corridors are lower than those of countries that have not implemented interest rate corridors. Moreover, the narrower the interest rate corridor, the less volatility of short-term

market interest rates. The literature [18] analyzed the regulation mechanism and regulation characteristics of the interest rate corridor, a monetary policy framework. The literature [19] believes that China's implementation of the interest rate corridor monetary policy framework is a positive response to the reform of interest rate marketization, which reduces social financing costs, improves market efficiency, and has played a strong role in promoting the pricing basis of China's marketized interest rates. The literature [20] elaborated and analyzed the operation of the interest rate corridor and analyzed the advantages and disadvantages, which can help the construction of the interest rate corridor.

3. Interest Rate Fluctuation Analysis Algorithm

We set s_t as a random variable, which can be assumed to take only an integer value $\{1, 2, \cdots, N\}$.

$$P\{s_t = j | s_{t-1} = i, s_{t-2} = k, \cdots\} = P\{s_t = j | s_{t-1} = i\} = P_{ij}. \quad (1)$$

Such a process is called an N-state Markov chain with transition probability $\{P_{ij}\}_{i,j=1,\cdots,N}$.

$$P_{i1} + P_{i2} + \cdots + P_{iN} = 1. \quad (2)$$

It is often convenient to list the transition probabilities as an $(N \times N)$ matrix P [21].

$$P = \begin{bmatrix} P_{11} & P_{21} & \cdots & P_{N1} \\ P_{12} & P_{22} & \cdots & P_{N2} \\ \cdots & \cdots & \cdots & \cdots \\ P_{1N} & P_{2N} & \cdots & P_{NN} \end{bmatrix}. \quad (3)$$

The element in the j-th row and the i-th column of P is the transition probabilityP_{ij} .

Generally, when an N-state Markov chain is reducible, if there is a way to indicate each state, the transition matrix can be written as follows:

$$P = \begin{bmatrix} B & C \\ 0 & D \end{bmatrix}. \quad (4)$$

Among them, B represents $(K \times K)$ matrix, $1 \le K < N$. If a Markov chain is not reducible, it is called irreducible.

An N-state irreducible Markov chain with a transition matrix of P is investigated. If one eigenvalue of P is assumed to be l and the remaining eigenvalues of P all fall within the unit circle, the Markov chain is called traversal. The $(N \times 1)$ vector of the traversal probability of a traversal chain is denoted as π. This vector π is defined as the feature vector h corresponding to the unit feature root of P; that is, the traversal probability vector π satisfies [22]:

$$P\pi = \pi. \quad (5)$$

The feature vector π is a normalized vector; so, the sum of its elements is l. It can be proved that if P is the transition matrix traversing the Markov chain, then

$$\lim_{m \longrightarrow \infty} P^m = \pi * 1'. \quad (6)$$

The traversal probability vector π can be interpreted as an unconditional probability vector.

The following describes how to calculate the traversal probability of an N-state Markov chain.

For a general process of traversing N states, the unconditional probability vector represents a vector π, and π has properties $P\pi = \pi$ and $1'\pi = 1$, where 1 represents an $(N \times 1)$ vector that each element is l.

We therefore look for a π that satisfies the following formula [23]:

$$A\pi = e_{N+1}. \quad (7)$$

Among them, e_{N+1} represents the $(N+1)$-th column of I_{N+1}, and

$$\underset{(N+1)\times N}{A} = \begin{bmatrix} I_N - P \\ 1' \end{bmatrix}. \quad (8)$$

Such a solution can be obtained by multiplying the front of formula (7) by $(A'A)^{-1}A'$:

$$\pi = \left(A'A\right)^{-1} A' e_{N+1}. \quad (9)$$

That is, π is the $(N+1)$-th column of matrix $(A'A)^{-1}A'$.

3.1. Parameter Estimation of Markov System Transformation Model. The Markov system transformation model is mainly used to model data containing system changes. The general model studied in this paper is as follows. We set y_t as an observed endogenous variable $(n \times 1)$ vector and x_t as an observed exogenous variable $(k \times 1)$ vector. If the process is controlled by the system $s_t = j$ in period t, the conditional density of y_t is assumed to be

$$f\{y_t | s_t = j, x_t, Y_{t-1}; \alpha\}. \quad (10)$$

Among them, α is a parameter vector that characterizes the conditional density. If there are N different systems, then there are N different densities represented by the above formula, $j = 1, 2, \cdots, N$. These densities will be listed as an $(N \times 1)$ vector, denoted as η_t.

For a first-order autoregressive, its constant term and autoregressive coefficient can be different on different subsamples:

$$y_t = c_{s_t} + \Phi_{s_t} y_{t-1} + \varepsilon_t. \quad (11)$$

Among them, $\varepsilon_t \sim i.i.d.N(0, \sigma^2)$. System s_t is regarded as the unobserved consequence of the N-state Markov chain to model. s_t is independent of ε_t for all t and τ.

Thus, for the example described in the above formula, y_t is a quantity $(n = 1)$, and the exogenous variable only contains a constant term $(x_t = 1)$. The unknown parameters in α include $c_1, \cdots, c_N, \Phi_1, \cdots, \Phi_N$ and σ^2. In system $N = 2$, the two densities represented by the above formula are

$$\eta_t = \begin{bmatrix} f\{y_t|s_t = 1, y_{t-1}; \alpha\} \\ f\{y_t|s_t = 2, y_{t-1}; \alpha\} \end{bmatrix} = \begin{bmatrix} \frac{1}{\sqrt{2\pi}\sigma} \exp\left\{\frac{-(y_t - c_1 - \Phi_1 y_{t-1})^2}{2\sigma^2}\right\} \\ \frac{1}{\sqrt{2\pi}\sigma} \exp\left\{\frac{-(y_t - c_2 - \Phi_2 y_{t-1})^2}{2\sigma^2}\right\} \end{bmatrix}. \tag{12}$$

We assume that the conditional density depends only on the current system s_t and not on the past system:

$$f\{y_t|x_t, Y_{t-1}, s_t = j; \alpha\} = f\{y_t|x_t, Y_{t-1}, s_t = j, s_{t-1} = i, s_{t-1} = \kappa, \cdots, \alpha\}. \tag{13}$$

We assume that s_t evolves according to a Markov chain, and it is independent of the past observations of y_t or the current and past observations of x_t:

$$P\{s_t = j|s_{t-1} = i, s_{t-1} = \kappa, \cdots, x_t, Y_{t-1}\} = P\{s_t = j|s_{t-1} = i\} = p_{ij}. \tag{14}$$

These parameters are listed as a vector θ. An important goal is to estimate the value of θ based on the observed value of Y_T. We assume that the value of θ is certain to the analyst. However, even if we know the value of θ, we do not know in which system the process is located in each period in the sample. What we can do is to form a probabilistic inference as a generalization of the following formula.

$$P\{s_t = j|y_t; \theta\} = \frac{P\{y_t, s_t = j; \theta\}}{f(y_t; \theta)} = \frac{\pi_j \cdot f\{y_t|s_t = j; \theta\}}{f(y_t; \theta)}. \tag{15}$$

Among them,

$$\pi_j = P(s_t = j; \theta), j = 1, \cdots, N \tag{16}$$

The above formula is the unconditional probability of the value j of s_t.

This inference takes the form of conditional probability, and the analyst can arrange this probability so that the t-th observation value is listed as a $(N \times 1)$ vector $\widehat{\xi}_{t|t}$ by system j.

These predictions are listed as a $(N \times 1)$ vector $\widehat{\xi}_{t+1|t}$, and its j-th element represents $P\{s_{t+1} = j|y_t; \theta\}$.

The optimal inference and prediction for each period t in the sample can be obtained by iterating the following equation:

$$\widehat{\xi}_{t|t} = \frac{\left(\widehat{\xi}_{t|t-1} \odot \eta_t\right)}{1'\left(\widehat{\xi}_{t|t-1} \odot \eta_t\right)}. \tag{17}$$

$$\widehat{\xi}_{t+1|t} = P \cdot \widehat{\xi}_{t|t}.$$

η_t represents the $(N \times 1)$ vector, the j-th element is the conditional density, P represents the transition probability matrix, 1 represents the $(N \times 1)$ vector with each element being 1, and $\odot$ represents the element-to-element multiplication. After the initial value $\widehat{\xi}_{1|0}$ and the assumed value θ of the overall parameter n are given, the above formula can be iterated at $t = 1, 2, \cdots, T$ to calculate the $\widehat{\xi}_{t|t}$ and $\widehat{\xi}_{t+1|t}$ values for each period t in the sample. The value of the log-likelihood function $\ell(\theta)$ for the observed data Y_T at θ used to form the iteration can be obtained as a by-product of this algorithm, which is

$$\ell(\theta) = \sum_{t=1}^{T} \log f(y_t|x_t, Y_{t-1}; \theta). \tag{18}$$

Among them,

$$f(y_t|x_t, Y_{t-1}; \theta) = 1'\left(\widehat{\xi}_{t|t-1} \odot \eta_t\right) \tag{19}$$

An initial value $\widehat{\xi}_{1|0}$ is given to calculate $\widehat{\xi}_{t|t}$ for any t. There are several options for selecting initial values. One way is to make $\widehat{\xi}_{1|0}$ equal to the unconditional probability vector, which is denoted as π. Another option is to make

$$\widehat{\xi}_{1|0} = \rho. \tag{20}$$

Among them, ρ is a fixed $(N \times 1)$ vector of nonnegative constants whose elements are 1, such as $\rho = N^{-1} \cdot 1$. In addition, ρ can be estimated by the maximum likelihood function, and its restriction is $1'\rho = 1$ and for $j = 1, \cdots, N, \rho_j \geq 0$.

$\widehat{\xi}_{t|t}$ represents the $(N \times 1)$ vector whose j-th element is $P\{s_t = j|Y_\tau; \theta\}$.When $t > \tau$, this represents the prediction of the system in a certain period in the future.

When we take the available information in period t as the condition, and use $\widehat{\xi}_{t+m}$ to represent the forward m period forecast based on period t, we can get

$$\widehat{\xi}_{t+m|t} = p^m \cdot \widehat{\xi}_{t|t}. \tag{21}$$

Smooth inference can be calculated using the algorithm established by [24]. In vector form, this algorithm can be written as

$$\widehat{\xi}_{t|T_m} \widehat{\xi}_{t|t} \odot \left\{p^t \cdot \left[\widehat{\xi}_{t+1|T}(\div)\widehat{\xi}_{t+1|t}\right]\right\}. \tag{22}$$

Among them, the symbol $(\div)$ represents element-by-element division. The above formula is about $t = T - 1, T$

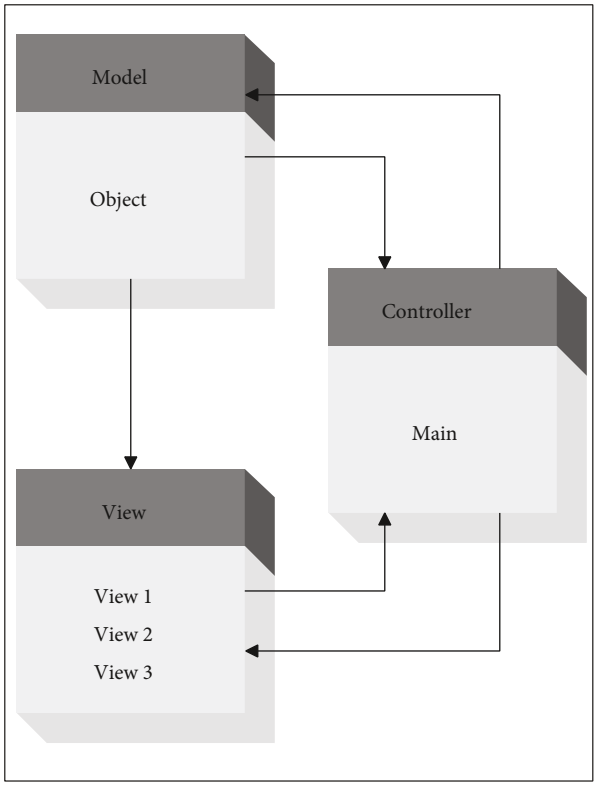

Figure 1: MVC model structure.

$-2, \cdots, 1$ backward iteration to get the smoothing probability $\widehat{\xi}_{t|T}$. The iteration starts from $\widehat{\xi}_{T|T}$ at $t = T$, and the algorithm is effective only when s_t obeys a first-order Markov chain. When the conditional density depends on $s_t, s_{t-1}, \cdots$, only through the current state s_t, and when the lag value of the explanatory variable vector x_t instead of y_t is strictly exogenous, x_t is independent of s_t for all t and τ.

The parameter vector θ is taken as a fixed known vector. For a given fixed θ, once the iteration is completed for $t = 1, 2, \cdots, T$, the log likelihood value implied by the value of θ can be known according to the formula. The value of θ that maximizes the log likelihood can be obtained by the BFGS algorithm.

4. Bank Interest Rate Analysis Model Based on Computer Statistical Model and Machine Learning

With the support of the above interest rate algorithm, the bank's interest rate fluctuation analysis model is constructed.

In actual development, the MVC development structure is the main development structure, which mainly refers to the unified operation of the display layer, control layer, and data layer to JSP or JavaBean for processing. The following is the structure diagram of the MVC development structure, as shown in Figure 1:

To implement the MVC mode in the JavaEE development environment, the most critical part is to use the RequestDispatcher interface, because the content is saved

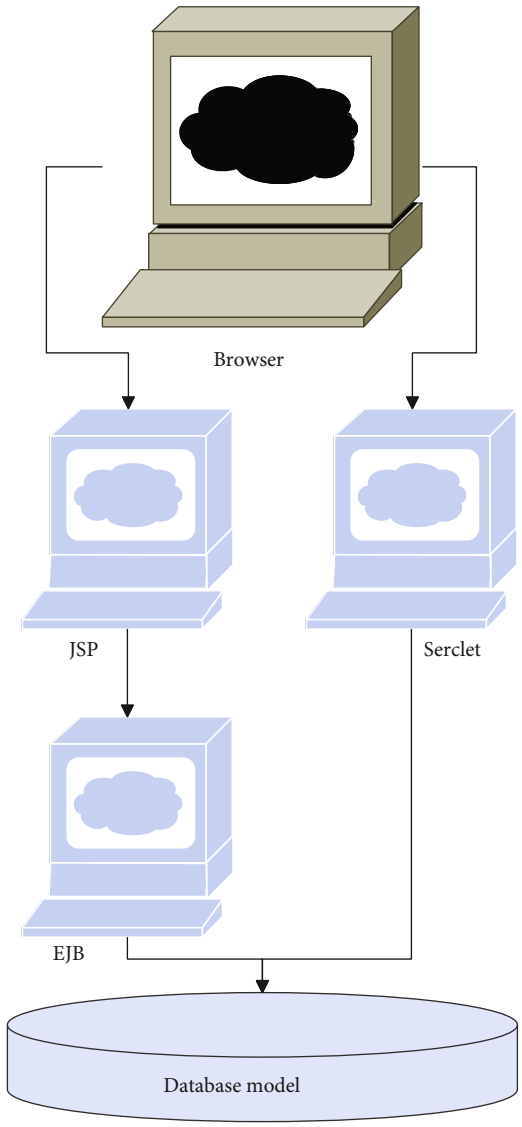

Figure 2: The architecture of the MVC pattern in J2EE.

to the JSP page for display through this interface. When a user submits a request, it will be handed over to the Servlet for processing, and then the Servlet calls the JavaBean, and the operation result of the JavaBean is passed to the JSP page through the RequestDispatcher interface. Since the content to be displayed is only valid in a request response, in the MVC design mode, all attribute transfers will be passed using the Request attribute range, which can improve the operational performance of the code, as shown in Figure 2.

The B/S structure and MVC structure adopted by this system are shown in Figure 3, and the operating structure of the application system based on the B/S structure is shown in Figure 3. The model process is client-server database.

The MVC development structure diagram of this system is divided into three layers according to the MVC model, and the technology used each time is realized by the JavaEE development environment. The following is the architecture diagram of statistical system of bank interest rate, as shown in Figure 4.

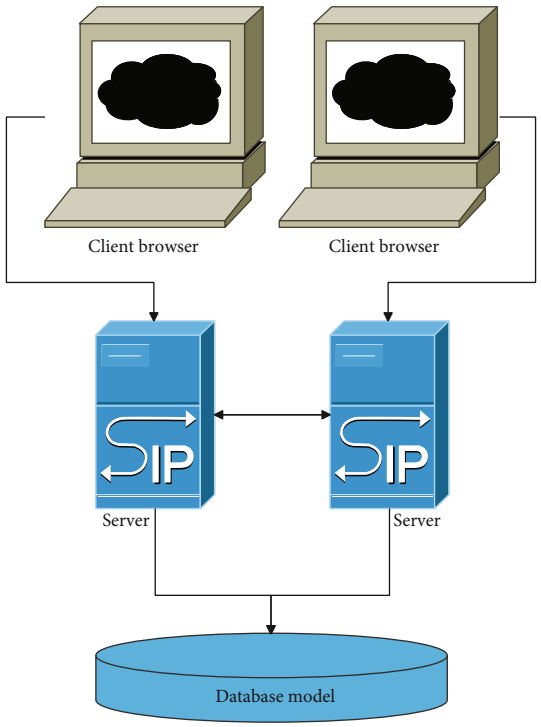

Figure 3: Three-tier structure of the system B/S model.

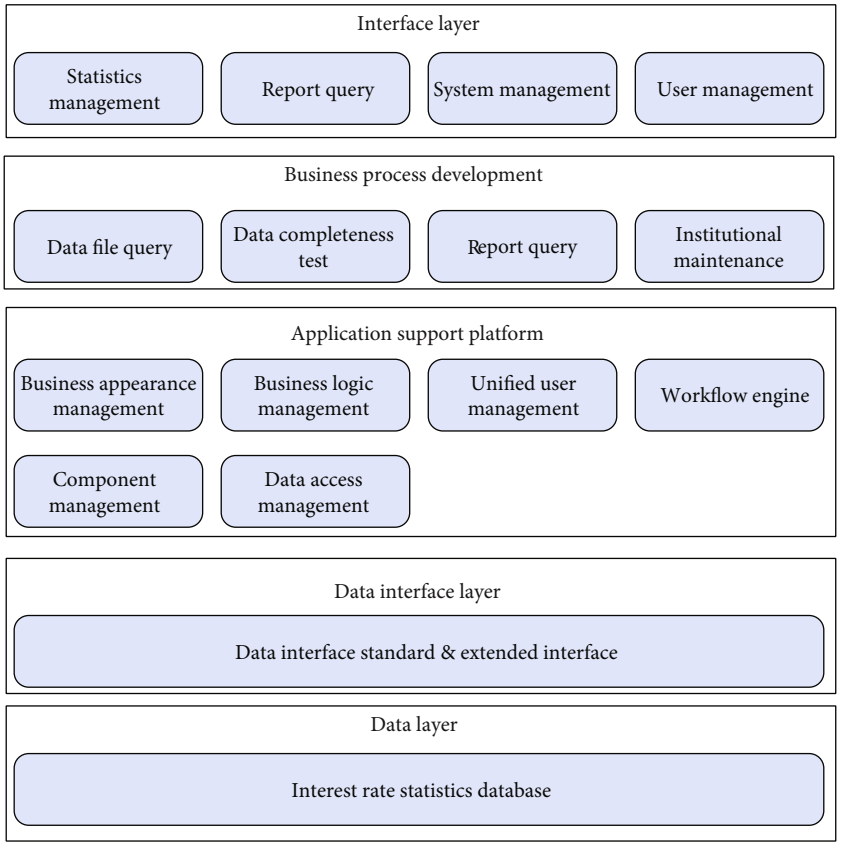

Figure 4: System structure of statistical system of bank interest rate.

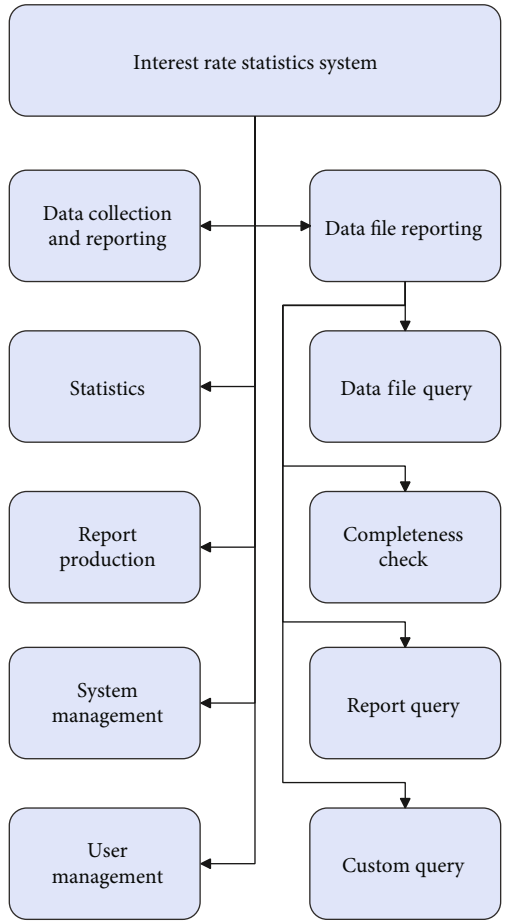

Figure 5: The modular structure of the statistical system of bank interest rates.

From the architecture diagram in the above figure, we can see that the client level is the interface between the user and the system, which is mainly implemented by JSP pages. In the corresponding layers, JSP, JavaBean, and Servlet have a clear division of labor. In the MVC framework, we use the more mature Struts framework and use the Action layer in the Struts framework to call the Javabeans in the business layer to complete various business functions. In the implementation technology of the database layer, JDBC technology is used to realize the access of other layers to the database, including database update and storage. What needs to be explained here is that Struts is just an implementation of MVC; after all, it is still an MVC development structure.

The modular design of the system comes from the needs of various financial institutions, mainly commercial banks and financial regulatory agencies, the demand specifications formed by the research, and the business needs and expected goals of each unit in the interest rate statistics work. The bank interest rate statistical analysis system is divided into five modules: data collection and reporting, data statistics, report generation, user management, system maintenance, and management. The module structure diagram is shown in Figure 5.

The data collection module is mainly composed of three modules: data upload, data verification, and data integrity check. Data upload includes data file reporting, data file query after the report is completed, data integrity check after the query is correct, and the integrity check passes after the data verification; the data reading status will be displayed after the data verification. You can check whether the data is read successfully or not. At the same time, you can query the number of data records after the data verification to prepare for missing or wrong reports. Afterwards, a data integrity report can be generated. The data integrity report is a prerequisite for data statistics and also a prerequisite for the data statistics module.

The functional structure diagram of the data collection and reporting module is shown in Figure 6.

After confirming that all the basic interest rate information tables are correctly entered into the database, the system performs summary calculations. In summary calculations, each statistical template is subjected to background summary calculation according to the specific calculation formula of each report. After the calculation is completed, the summary results are saved in the database. Due to the large amount of calculation data and the long waiting time for users to generate report calculations, it is not feasible to dynamically generate reports when querying. In order to solve this problem, the system adopts the following schemes for data aggregation: (1) the server performs centralized back-end summary in a certain period of time, generates intermediate results, and stores them in the

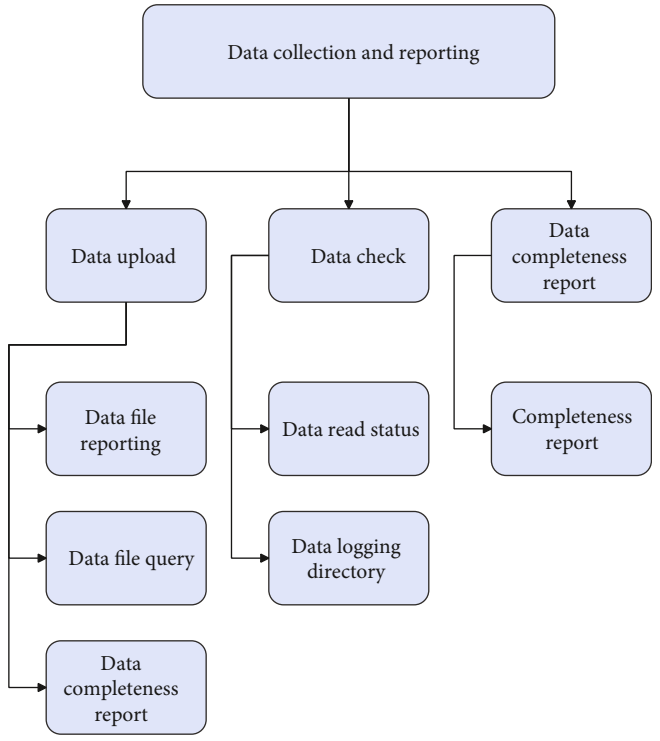

Figure 6: The structure diagram of the data collection and reporting module.

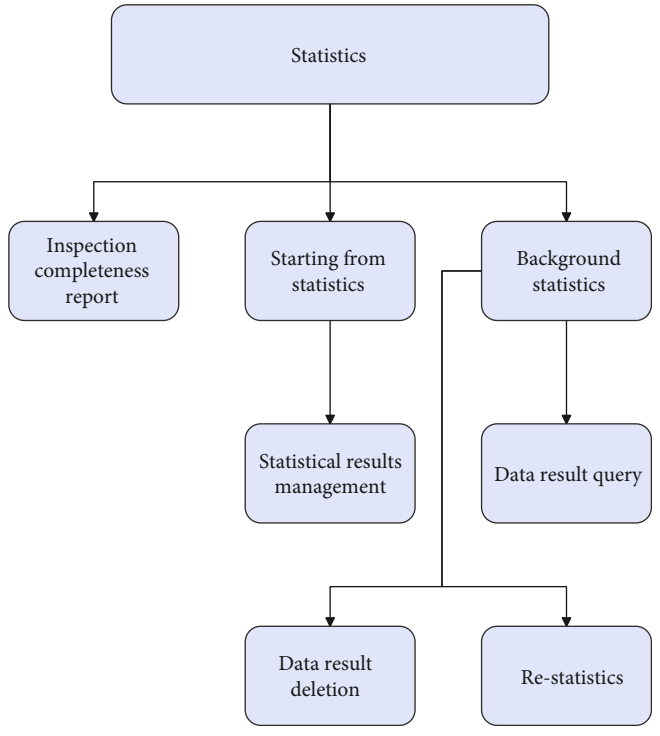

Figure 7: Structure diagram of data statistic module.

database. When users generate reports, they directly extract data from the intermediate results. (2) The function of summary calculation is triggered by the statisticians of the branches of the People's Bank of China to calculate all the data of the whole province, and the statisticians of each central branch will no longer perform the operation of summary calculation. (3) The administrator can trigger data aggregation when off-duty, and use off-duty time for

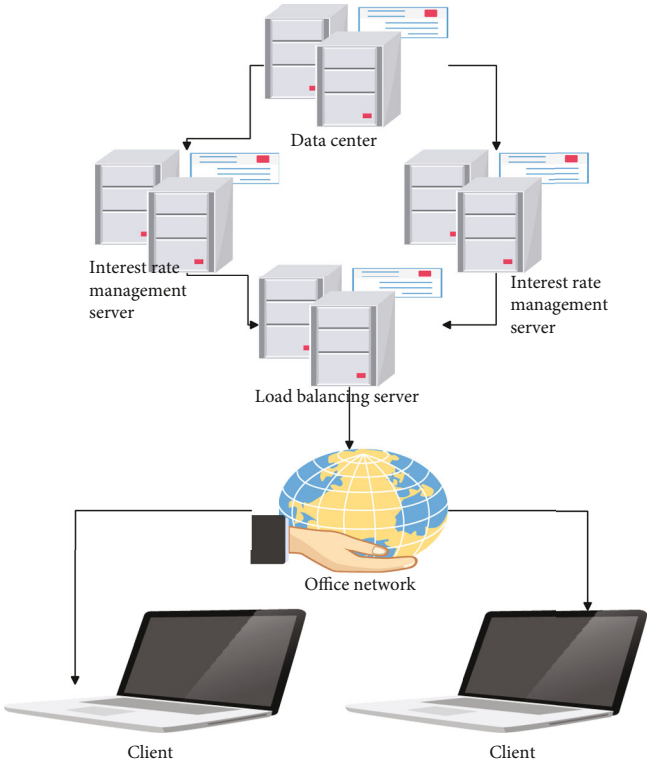

Figure 8: Schematic diagram of system physical deployment.

aggregation to reduce server pressure. The data summary statistics module is composed of three parts: completeness test report, data statistics trigger, and data statistics result management, as shown in Figure 7:

The interest rate management system is based on the B/S architecture and is developed and implemented using the JAVA programming language. The overall architecture is mainly composed of the browser side and the server side. The browser side is the entrance to access and use the system, and the server side is the business processing service provider and data processing and storage part of the entire system. The physical deployment diagram of the system is shown in Figure 8.

In order to ensure the stable and efficient operation of the system at the hardware level, the relevant parameters of current hardware manufacturers are fully studied. In terms of hardware selection, it is necessary to consider the needs of the system itself and also consider the development possibilities and trends of the bank's future deposits and loans.

5. Performance Verification of Bank Interest Rate Analysis System

After constructing the bank interest rate fluctuation model based on computer statistics and machine learning, in order to verify the effectiveness of the system in this paper, the system model is verified and analyzed. First of all, this article analyzes the stability of the system. The system constructed in this article requires a large amount of data processing. Therefore, it is necessary to ensure that the interest rate

Table 1: Statistical table of system stability.

Number	Data running speed (ms)	Number	Data running speed (ms)	Number	Data running speed (ms)
1	115.1	29	131.3	57	148.0
2	120.4	30	134.1	58	122.2
3	129.5	31	114.2	59	120.3
4	139.0	32	100.8	60	142.7
5	143.4	33	130.2	61	136.9
6	124.5	34	124.4	62	127.1
7	132.1	35	126.3	63	123.4
8	145.3	36	141.0	64	121.4
9	113.6	37	141.7	65	100.4
10	127.0	38	106.0	66	109.8
11	113.6	39	142.2	67	145.7
12	120.1	40	116.0	68	142.8
13	100.6	41	115.1	69	107.6
14	126.8	42	101.9	70	149.3
15	140.5	43	121.2	71	113.0
16	110.8	44	138.3	72	143.7
17	100.2	45	140.1	73	125.0
18	138.7	46	141.2	74	105.3
19	124.0	47	131.3	75	132.9
20	133.7	48	135.1	76	130.2
21	100.6	49	107.3	77	147.6
22	102.5	50	139.4	78	104.0
23	131.8	51	102.0	79	134.1
24	107.7	52	146.1	80	119.3
25	139.6	53	129.9	81	119.2
26	113.6	54	134.8	82	123.9
27	128.9	55	130.4	83	128.7
28	122.3	56	130.6	84	120.5

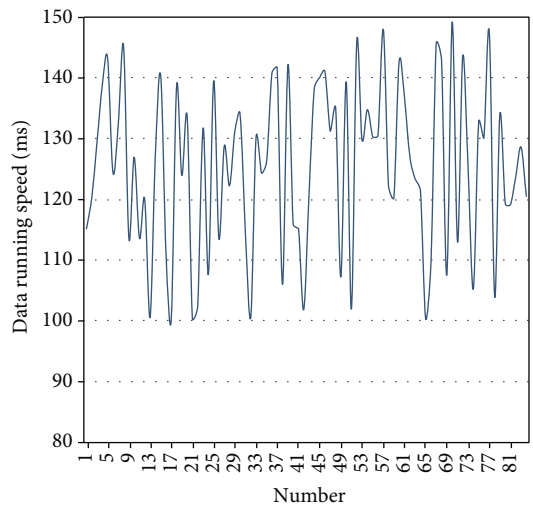

Figure 9: Statistical diagram of system stability.

Table 2: Statistical table of the bank interest rate analysis effect.

Number	Interest rate analysis effect	Number	Interest rate analysis effect	Number	Interest rate analysis effect
1	97.6	29	96.9	57	93.2
2	93.5	30	97.5	58	80.5
3	78.7	31	82.9	59	82.7
4	92.2	32	79.8	60	80.3
5	97.0	33	94.3	61	75.5
6	91.5	34	78.9	62	83.5
7	83.8	35	77.9	63	76.6
8	82.1	36	79.5	64	75.6
9	75.7	37	76.7	65	76.9
10	75.6	38	85.4	66	80.2
11	87.0	39	85.6	67	77.2
12	78.2	40	85.1	68	95.4
13	97.6	41	75.9	69	90.3
14	88.2	42	79.9	70	96.8
15	97.0	43	96.0	71	91.2
16	85.1	44	78.0	72	87.6
17	77.8	45	75.8	73	76.7
18	80.8	46	79.1	74	86.1
19	83.5	47	89.8	75	76.1
20	93.5	48	81.0	76	89.7
21	97.6	49	92.5	77	97.4
22	90.0	50	88.8	78	89.0
23	93.8	51	94.8	79	92.9
24	88.4	52	77.3	80	89.6
25	76.0	53	91.3	81	77.1
26	84.4	54	78.5	82	94.4
27	96.1	55	93.4	83	76.3
28	78.0	56	79.9	84	78.8

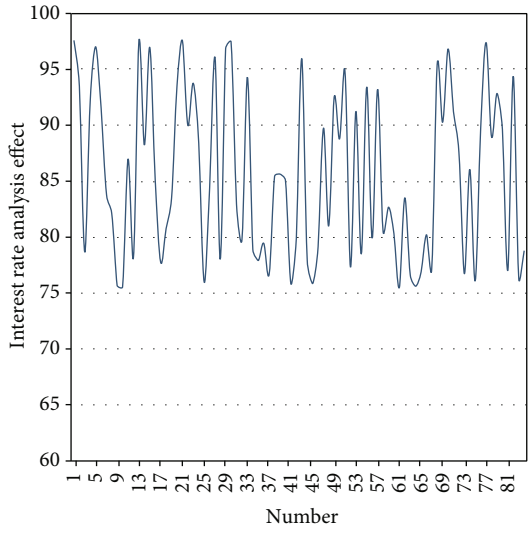

Figure 10: Statistical table of the bank interest rate analysis effect.

analysis model itself has a certain degree of stability and has the ability to continue working after processing a large amount of data. Finally, this paper uses a large amount of random financial data to train and detects the running speed of the model in this paper. The results are shown in Table 1 and Figure 9.

From the above analysis results, we can see that the bank interest rate fluctuation analysis model constructed in this paper has always performed well in the data processing process. On this basis, the bank interest rate analysis effect is evaluated, and the results are shown in Table 2 and Figure 10.

It can be seen that the bank interest rate fluctuation model based on computer statistical model and machine learning constructed in this paper has good results.

6. Conclusion

With the steady progress of financial institution reform and interest rate marketization, in the context of the People's Bank of China continuing to expand the autonomy of interest rate pricing of financial institutions, it is necessary to summarize the loan interest rates of financial institutions, grasp the actual interest rate level, and continuously optimize interest rate policies. The development of the bank's interest rate statistical analysis system has realized the unification, standardization, and efficiency of the reporting and statistics of interest rate data of various financial institutions and has provided important data references for decision-making departments. The organization structure of this article is based on the needs of the various business requirements departments. Moreover, this article designs each functional module of the system in detail, designs each part of the system process and system examples, and determines the technical route of framework development using MVC + JDBC. In addition, this article combines requirements to construct a bank interest rate fluctuation analysis model based on statistical models and machine learning and analyzes and verifies through experiments. From the research results, it can be seen that the system constructed in this paper has a significant effect.

Data Availability

The labeled dataset used to support the findings of this study are available from the corresponding author upon request.

Conflicts of Interest

The author declares no competing interests.

Acknowledgments

This study is sponsored by the Key R&D and Promotion Project (soft science research) in Henan Province (No. 212400410097) and Project of Philosophy and Social Science Planning of Henan Province (No. 2020JC31).

References

[1] J. Fichtner, E. M. Heemskerk, and J. Garcia-Bernardo, "Hidden power of the big three?," *Passive Index Funds*, vol. 19, no. 2, pp. 298–326, 2017.

[2] C. Cueva, R. E. Roberts, T. Spencer et al., "Cortisol and testosterone increase financial risk taking and may destabilize markets," *Scientific Reports*, vol. 5, no. 1, pp. 1–16, 2015.

[3] C. J. Lee and E. B. Andrade, "Fear, excitement, and financial risk-taking," *Cognition and Emotion*, vol. 29, no. 1, pp. 178–187, 2015.

[4] S. M. Bartram, G. W. Brown, and W. Waller, "How important is financial risk?," *Journal of Financial and Quantitative Analysis*, vol. 50, no. 4, pp. 801–824, 2015.

[5] W. W. Cooper, A. T. Kingyens, and J. C. Paradi, "Two-stage financial risk tolerance assessment using data envelopment analysis," *European Journal of Operational Research*, vol. 233, no. 1, pp. 273–280, 2014.

[6] W. Montford and R. E. Goldsmith, "How gender and financial self-efficacy influence investment risk taking," *International Journal of Consumer Studies*, vol. 40, no. 1, pp. 101–106, 2016.

[7] S. M. Wanjohi, J. G. Wanjohi, and J. M. Ndambiri, "The effect of financial risk management on the financial performance of commercial banks in Kenya," *International Journal of Finance and Banking Research*, vol. 3, no. 5, pp. 70–81, 2017.

[8] J. Magendans, J. M. Gutteling, and S. Zebel, "Psychological determinants of financial buffer saving: the influence of financial risk tolerance and regulatory focus," *Journal of risk research*, vol. 20, no. 8, pp. 1076–1093, 2017.

[9] E. S. Cole, D. Walker, A. Mora, and M. L. Diana, "Identifying hospitals that may be at most financial risk from Medicaid disproportionate-share hospital payment cuts," *Health Affairs*, vol. 33, no. 11, pp. 2025–2033, 2014.

[10] A. Zalik, "Resource sterilization: reserve replacement, financial risk, and environmental review in Canada's tar sands," *Environment and Planning A*, vol. 47, no. 12, pp. 2446–2464, 2015.

[11] C. Lucarelli, P. Uberti, and G. Brighetti, "Misclassifications in financial risk tolerance," *Journal of Risk Research*, vol. 18, no. 4, pp. 467–482, 2015.

[12] E. Y. Chan, "Physically-attractive males increase men's financial risk-taking," *Evolution and Human Behavior*, vol. 36, no. 5, pp. 407–413, 2015.

[13] T. West and A. C. Worthington, "Macroeconomic conditions and Australian financial risk attitudes, 2001–2010," *Journal of Family and Economic Issues*, vol. 35, no. 2, pp. 263–277, 2014.

[14] T. Tanimura, E. Jaramillo, D. Weil, M. Raviglione, and K. Lonnroth, "Financial burden for tuberculosis patients in low- and middle-income countries: a systematic review," *European Respiratory Journal*, vol. 43, no. 6, pp. 1763–1775, 2014.

[15] T. K. Scharding, "Imprudence and immorality: a Kantian approach to the ethics of financial risk," *Business Ethics Quarterly*, vol. 25, no. 2, pp. 243–265, 2015.

[16] J. Su and E. Furman, "A form of multivariate Pareto distribution with applications to financial risk measurement," *ASTIN Bulletin*, vol. 47, no. 1, pp. 331–357, 2017.

[17] G. W. Y. Wang, S. H. Woo, and J. Mileski, "The relative efficiency and financial risk assessment of shipping companies," *Maritime Policy & Management*, vol. 41, no. 7, pp. 651–666, 2014.

[18] J. Linarelli, "Luck, justice and systemic financial risk," *Journal of Applied Philosophy*, vol. 34, no. 3, pp. 331–352, 2017.

[19] P. Allen and C. Petsoulas, "Pricing in the English NHS quasi market: a national study of the allocation of financial risk through contracts," *Public Money & Management*, vol. 36, no. 5, pp. 341–348, 2016.

[20] J. Thomä and H. Chenet, "Transition risks and market failure: a theoretical discourse on why financial models and economic agents may misprice risk related to the transition to a low-carbon economy," *Journal of Sustainable Finance & Investment*, vol. 7, no. 1, pp. 82–98, 2017.

[21] O. Sosnovska and M. Zhytar, "Financial architecture as the base of the financial safety of the enterprise," *Baltic Journal of Economic Studies*, vol. 4, no. 4, pp. 334–340, 2018.

[22] D. Acemoglu, A. Ozdaglar, and A. Tahbaz-Salehi, "Systemic risk and stability in financial networks," *American Economic Review*, vol. 105, no. 2, pp. 564–608, 2015.

[23] R. Castellano, R. Cerqueti, and G. Rotundo, "Exploring the financial risk of a temperature index: a fractional integrated approach," *Annals of Operations Research*, vol. 284, no. 1, pp. 225–242, 2020.

[24] C. J. Kim, "Unobserved-component time series models with Markov-switching heteroscedasticity: Changes in regime and the link between inflation rates and inflation uncertainty," *Annals of Operations Research*, vol. 11, no. 3, pp. 341–349, 1993.

Hindawi
Journal of Sensors
Volume 2023, Article ID 9896282, 1 page
https://doi.org/10.1155/2023/9896282

Retraction

Retracted: Personalized Marketing Recommendation System of New Media Short Video Based on Deep Neural Network Data Fusion

Journal of Sensors

Received 17 October 2023; Accepted 17 October 2023; Published 18 October 2023

This article has been retracted by Hindawi following an investigation undertaken by the publisher [1]. This investigation has uncovered evidence of one or more of the following indicators of systematic manipulation of the publication process:

(1) Discrepancies in scope
(2) Discrepancies in the description of the research reported
(3) Discrepancies between the availability of data and the research described
(4) Inappropriate citations
(5) Incoherent, meaningless and/or irrelevant content included in the article
(6) Peer-review manipulation

The presence of these indicators undermines our confidence in the integrity of the article's content and we cannot, therefore, vouch for its reliability. Please note that this notice is intended solely to alert readers that the content of this article is unreliable. We have not investigated whether authors were aware of or involved in the systematic manipulation of the publication process.

Wiley and Hindawi regrets that the usual quality checks did not identify these issues before publication and have since put additional measures in place to safeguard research integrity.

We wish to credit our own Research Integrity and Research Publishing teams and anonymous and named external researchers and research integrity experts for contributing to this investigation.

The corresponding author, as the representative of all authors, has been given the opportunity to register their agreement or disagreement to this retraction. We have kept a record of any response received.

References

[1] F. Huang, "Personalized Marketing Recommendation System of New Media Short Video Based on Deep Neural Network Data Fusion," *Journal of Sensors*, vol. 2021, Article ID 3638071, 10 pages, 2021.

Hindawi
Journal of Sensors
Volume 2021, Article ID 3638071, 10 pages
https://doi.org/10.1155/2021/3638071

Research Article

Personalized Marketing Recommendation System of New Media Short Video Based on Deep Neural Network Data Fusion

Feifeng Huang

College of Business Administration, Guangzhou Huashang Vocational College, Zengcheng, 511300 Guangdong, China

Correspondence should be addressed to Feifeng Huang; sci-tech@gzhsvc.edu.cn

Received 8 June 2021; Revised 6 July 2021; Accepted 3 August 2021; Published 16 November 2021

Academic Editor: Mu Zhou

With the rapid development of mobile Internet, short video has become another darling after traditional webcast in recent years. How to make full use of short video for effective marketing has become a hot issue that academia and industry are paying close attention to. This article is mainly aimed at exploring practical new media through in-depth research and exploration of the specific implementation methods and strategies of short video marketing in social media, based on the advantages and characteristic models of short video marketing in social media. The strategy of short video marketing in social media, and the use of highly in-depth neural network analysis technology for the personalized marketing recommendation system of new media short videos, so as to better promote the use of social media short videos by enterprises or individuals. We have to learn from marketing activities. The experimental results of this article show that when the data volume reaches 80%, the performance of the VRBCH algorithm steadily improves, so the performance of the main F of the VRBCH algorithm is still relatively ideal when the data volume changes. Due to the high dilution of the experimental data set, the amount of data in the VRBCH algorithm has increased sharply by 30% to 35%, but the purchase rate of the marketing recommendation system is as high as 98%. Therefore, the system has high feasibility.

1. Introduction

1.1. Background. With the development of modern information technology, personalized marketing transaction costs have been greatly reduced, and at the same time, real-time interaction between enterprises and customers has become possible, so personalized marketing has begun to become a competitive marketing method. In 2009, the release of the Vine short video application in the United States was the starting point for large-scale social software to release short video functions. With the advent of the 4G era, the numbers of domestic short video users, such as Meipai, Miaopai, Watermelon, Kuaishou, and Pear Video, have exploded due to the acceleration of the Internet and the reduction of prices. In this case, many companies and individuals have begun to use short videos for marketing, and short videos have become the "standard configuration" of mobile Internet marketing. The process of making short films is simpler, and the barriers to participating in production are lower, which can attract more users to use and share social networks. Short videos are still part of the program but are very useful for communication and dialogue. The basic communication function of short videos is the best among many marketing methods. As the application of short video marketing on social media becomes more and more common, issues related to short video marketing on social media will also be worth discussing. As a new method system, the artificial neural network has the characteristics of distributed parallel processing, nonlinear mapping, adaptive learning, strong robustness, and fault tolerance, which makes it effective in pattern recognition, control optimization, intelligent information processing, and faults. Diagnosis and other aspects have a wide range of applications.

1.2. Significance. In today's new era of fast mobile Internet technology, discussing simple video marketing strategies based on the ideas of mobile Internet is not only a development and supplement to existing marketing theories but also a company's personal practice, which can also stimulate marketing. Therefore, this article has theoretical and practical guidance. In theory, short video marketing, as a new form

of marketing that emerged this year with the development of the mobile Internet, has attracted a lot of attention in academia, but researchers have seen short video marketing and short videos on social media. The internal research on marketing has just begun, and a systematic theoretical system has not yet been formed. Basically, related research is still in its infancy. Data fusion plays an indispensable role in the deep neural network data fusion new media short video personalized marketing recommendation system Therefore, as an exploratory research, this article will enhance the existing theory to a certain extent. From a practical point of view, the advent of the mobile Internet era will affect the traditional business marketing model of enterprises. Challenges were raised. Short film marketing is a new method of mobile Internet marketing, but it is a necessary step in the formation of corporate and personal marketing strategies. Therefore, more and more marketers have begun to carry out short film marketing activities on social media, and the theory of short film marketing research is necessary. A neural network is a highly complex nonlinear dynamic system composed of a large number of processing units with very simple structures and functions, that is, neurons are widely interconnected [1]. Based on the theory of an artificial neural network and using a single hidden layer neural network structure algorithm, a neural network model for marketing mix decision-making is established.

1.3. Related Work. In the era of new media, with the rapid development of the Internet, mobile phones have replaced PCs (personal computers) as the main tool for obtaining information. Xu et al.'s research found that short videos are unique in social networks, and their advantage is that the information release mode is concise and clear. And put forward the advantages of college students using new media to develop short video marketing [2]. However, because the experimental environment is not closed, there is a certain deviation in the experimental results. The field of marketing research is very important for the sale of goods. Soria Morillo et al. applied a new method to the field of marketing research. He recognized how the brain activity responds to the visualization of short video ads using discrete classification technology. Through low-cost electroencephalography equipment (EEG), the activation level of some brain regions was studied, and advertisements were displayed to users. You may want to know which is the use of neuroscience knowledge in marketing or can provide neuroscience to the marketing department, or why this method can improve accuracy and end-user acceptance compared to other works. Soria Morillo et al. used discretization technology on the EEG frequency band of the generated data set. C4.5, ANN, and a new recognition system based on discretization algorithm Ameva are applied to obtain the score of each TV ad by the topic. The proposed technique allows an accuracy of more than 75% to be achieved, that is, an excellent result considering the type of EEG sensor used in this work [3]. Although it was in line with expectations in most directions, it did not mention EEG factors due to external environmental factors. In some parts of the forecast, there are errors. In order to study the intrinsic link between the perceived value of mobile short videos and customers' purchase intentions, Xu et al. explored the potential key variables between the two. And based on the mediating role of user participation and attitudes, it is an early attempt to propose a conceptual framework to understand the impact of perceived value on Chinese consumers' purchasing intentions. This research uses a quantitative design to collect data from 622 users of China mobile's short video social application who have experience in mobile short video-related social applications through the snowball sampling method by developing an online questionnaire. In addition, in this study, user participation behavior has a positive impact on consumer attitudes [2]. Although the research perspective is forward-looking, there are still many unachievable parts of the technology.

1.4. Innovation. The innovations of this paper are as follows: (1) In order to solve the problem of the low proportion of users watching short video lists after sorting, considering that the convolutional neural network has the function of extracting local features, it can extract key information from sentences, such as N-gram. This feature can also be used. It is transplanted to the feature extraction of the text information of the video. (2) Although the traditional proposition theory focuses on the innovation of the algorithm level of the proposition, this paper not only focuses on the innovation of the algorithm level but also explores the architecture design of the proposition platform and proposes an early stage of the platform, proposed corresponding solutions.

2. Short Video Personalized Marketing Recommendation Algorithm-Related Technologies

2.1. User-Based Collaborative Filtering Algorithm. Through the user's preference for items, the user's neighbors in preference are calculated, and then, the user's preferences can be inferred and recommended according to the preferences of the neighbors [4, 5]. The flow of the user-based collaborative filtering algorithm is shown in Figure 1.

Specifically, the algorithm includes three main steps [6]: (1) create a user object evaluation form, (2) calculate the user proximity set, and (3) create related statements. The application is as follows:

(1) Create user data evaluation table: form users and n projects, obtain user setting functions based on the historical information of existing users and objects, and create an $m * n$ evaluation board [7]

(2) Calculate the user proximity set: based on the project-based user scoreboard, calculate the similarity between the target user and other users and use it as the basis for suggesting related projects [8]. The methods of calculating similarity mainly include cosine similarity, Pearson similarity, and Minkowski distance similarity [9]

The formula of cosine similarity is as follows:

$$\cos(u, v) = \frac{\sum_{i=1}^{k} u * v}{\sqrt{\sum_{i=1}^{k} v^2} * \sqrt{\sum_{i=1}^{k} u^2}}. \quad (1)$$

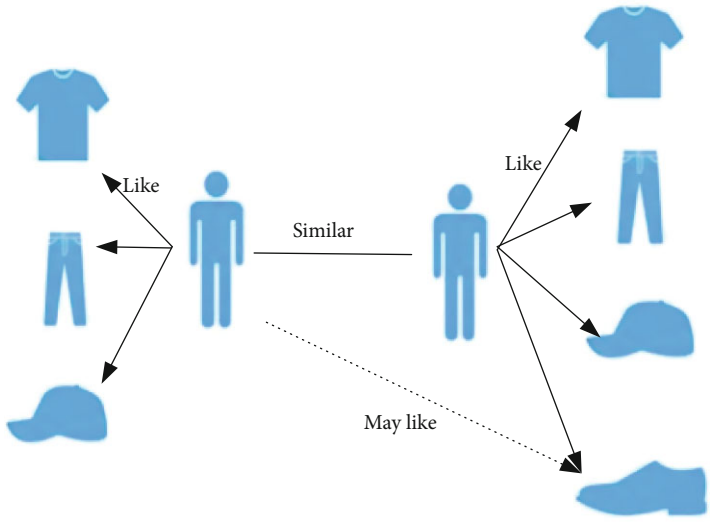

Figure 1: User-based collaborative filtering algorithm.

Pearson measures relevance on the basis of users' common ratings, and its specific formula is as follows:

$$\text{Pearson}(u,v) = \frac{\sum_{i=1}^{k}(u_i-\bar{u})(v_i-\bar{v})}{\sqrt{\sum_{i=1}^{k}(u_i-\bar{u})^2} * \sqrt{\sum_{i=1}^{k}(v_i-\bar{v})^2}}. \quad (2)$$

Minkowski distance is a common Euclidean distance. The formula for norm distance when $p = 2$ is as follows:

$$\text{dist}(u,v) = \left(\sum_{i=0}^{k}|u_i-v_i|^p\right)^{1/p}. \quad (3)$$

(3) Generate related recommendations: after calculating users who are similar to the target user, recommend items that similar users like and that the target user does not find to the target user, so as to generate a list of related recommendations [10, 11]

2.2. Item-Based Collaborative Filtering Algorithm. An item-based collaborative filtering algorithm does not use the content attributes of items to calculate the similarity between items but uses user behavior data to calculate the similarity between items [12, 13]. It is proposed that there is a greater similarity between item A and item B, because most users who like item A also like item B [14, 15]. Figure 2 is an item-based specific collaborative filtering suggestion process.

In terms of specific steps, the ItemCF process is also mainly divided into three steps: first, establish a user-item scoring matrix; then, use the scoring matrix to calculate the set of user neighboring items; finally, generate related recommendations and similarity of items based on the results.

The general algorithm for calculating the similarity of items is as follows:

$$W_{uv} = \frac{|N(u)\cap N(v)|}{\sqrt{|N(u)|\cap|N(v)|}}. \quad (4)$$

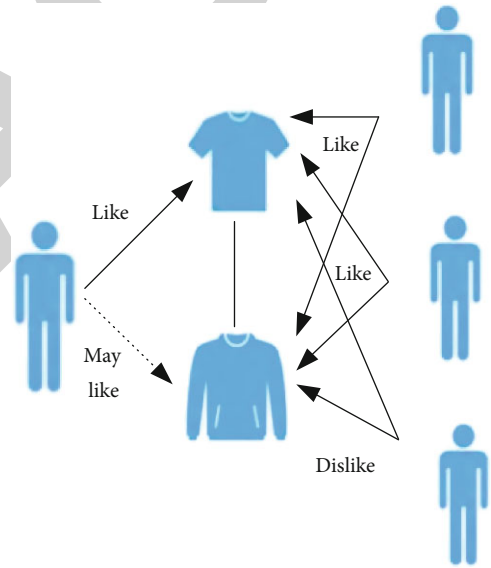

Figure 2: Collaborative filtering based on items.

In these videos, $N(u)$ and $N(v)$ are the collections of videos liked by user u and user v, respectively [16]. ItemCF is more suitable for recommendation scenarios where user interests are relatively stable, such as book purchase websites. But for the recommendation scenarios where new things often appear and items are updated and iterated quickly, such as news recommendation, it is not suitable for item-based collaborative filtering [17].

2.3. Recommendation Algorithm Based on Implicit Semantic Model. Suppose there is already a rating matrix $R_{m,n}$, which contains the ratings of n items by user m [18]. The scoring matrix should be large and sparse, because it is impossible for every user to evaluate all the data. $r_{u,i}$ represent the user evaluation u of object i. The matrix decomposition method

allows matrix $R_{m,n}$ to be decomposed into matrix P and matrix Q, as shown in the following:

$$R_{m,n} = P_{m,F} * Q_{F,n}. \tag{5}$$

Among them, F is the number of hidden factors, each row in matrix P represents the preference of each user for different hidden factors, and each column in matrix Q represents the possibility of assigning each element to different hidden factors [19, 20]. For each rating item, the corresponding predicted value can be decomposed from the matrix to obtain

$$\hat{r}_{u,i} = \sum_{f=1}^{F} P_{uf} \cdot Q_{fi}. \tag{6}$$

The goal of prediction is to make the predicted score as close to the real score as possible, so the objective function of the solution is as follows.

The purpose of prediction is to make the prediction as close to the actual as possible, so the objective function of the solution is

$$\min : \text{Loss} = \sum_{r_{u,j} \neq 0} (\hat{r}_{u,i} - r_{u,i})^2. \tag{7}$$

At the same time, in order to prevent overfitting, a regular term is added:

$$\min : \text{Loss} = \sum_{r_{u,j} \neq 0} (\hat{r}_{u,i} - r_{u,i})^2 + \gamma \left(\sum P_{uf}^2 + \sum Q_{fi}^2 \right) = f(P, Q). \tag{8}$$

Next, we need to solve the loss function. Gradient descent is usually used to solve this problem. The values of P and Q in iteration $t + 1$ are

$$P^{(t+1)} = P^{(t0} - \alpha \frac{\partial \text{Loss}}{\partial P^{(t)}}. \tag{9}$$

After obtaining P and Q using the gradient descent method, the final predicted item score is

$$\hat{r}_{u,i} = P_u^T Q_m = \sum_{k=1}^{k} P_{uk} Q_{mk}. \tag{10}$$

Compared with the two collaborative filtering algorithms introduced above, the principle of the recommendation algorithm based on the implicit semantic model is very good [21]. By adjusting the objective function, the objective function can be continuously optimized through logic optimization techniques. Essentially, this is a machine learning problem, and collaborative neighborhood filtering is more like a statistical method that does not involve the learning process [22].

2.4. Evaluation Indicators for Personalized Marketing Recommendations of Short Videos. For short video marketing recommendation systems, corresponding indicators are also needed to evaluate the quality of these algorithms. The following introduces various indicators based on offline solutions and online suggestions.

(1) Offline evaluation index

Generally, there are two types of indicators that can be used to predict scores: baseline square error (RMSE) and mean absolute error (MAE) [23]. $r_{u,i}$ shows the user u's rating of item i, and the predicted value corresponding to its recommendation algorithm. The type of RMSE is

$$\text{RMSE} = \frac{\sqrt{\sum_{u,i \in T} (\hat{r}_{u,i} - r_{u,i})^2}}{|T|}. \tag{11}$$

MAE uses the absolute value to predict the error, and its formula is

$$\text{MAE} = \frac{\sum_{u,i \in T} |\hat{r}_{u,i} - r_{u,i}|}{|T|}, \tag{12}$$

where T is the number of records rated by the user.

(2) Online evaluation indicators

The online prediction and evaluation indicators should be followed based on the actual proposed plan. For example, in a video recommendation system, a list of videos is recommended to users and click to watch user comments that they can only receive as a recommendation system [24, 25]. At present, consider entering the click-through rate as an online indicator. The calculation types are

$$\text{CTR} = \frac{N_{\text{click}}}{N}. \tag{13}$$

Among them is the number of times the user clicked on the video, and N is the total number of video impressions.

For all the videos that are clicked or watched, the time the user watches is, which means the time the user u watches the video i, and the total time of each video i is

$$\tau_{ui} = \frac{t_{ui}}{T_i}. \tag{14}$$

The CTR indicator calculation formula at this time is

$$\text{CTR} = \frac{\sum_{\tau_{ui} > \tau_0}^{k} N_i}{N}. \tag{15}$$

3. Model Building and Experimental Design

3.1. Data Acquisition and Preprocessing. Data fusion is the process of real-time and complete evaluation of the situation and threats and their importance. Add it to better understand the article. The data of this experiment comes from the video data in a short video app. It is taken from the user video click,

watch log, and user and video information table in the HDFS (Hadoop Distributed File System) of the Hadoop platform. All fields have been completed, desensitization treatment.

The experimental environment of this article is based on the Linux16.04 system, using Python 3.6 and TensorFlow 1.2 for data processing and model training. Python is an interpreted language, which is widely used because of its object-oriented programming, dynamic data types, and a large number of third-party library support. This article is based on the Python 3.6 version and is mainly used for the preliminary data preprocessing. TensorFlow is Google's second-generation open-source artificial intelligence learning system. It is a built-in framework learning software library used to implement neural networks. This article is based on TensorFlow1.2 to process the embedded features, the video title is based on TextCNN for feature extraction, and TensorFlow1.2 is used to build the network structure of the model training stage.

Before using these data to construct a recommendation model, the data needs to be preprocessed first. The data preprocessing of this part mainly includes the following 3 aspects:

(1) Classification data type conversion. For the fields in the user information table, one-hot encoding is performed for categorical variables, including gender, age category, province and city location, and other categorical variables

(2) Word segmentation of video title content. Word segmentation is the process of recombining consecutive word sequences into word sequences according to certain specifications. Due to the long content of the title, it needs to be segmented first, and then, the subsequent text vectorization process

(3) Sampling of positive and negative samples. Since the click-to-view of the video is easily affected by the title party, it is included in the field that considers the viewing time ratio. Only when the user's viewing time ratio exceeds 35% will be included in the positive sample, and the list of recommendations for each user the unwatched video in the video is negatively sampled, and the sampling ratio of positive and negative samples is 1 : 4

3.2. Embedded Feature Mapping. For categorical features of IDs such as video ID and user ID, if feature conversion is also performed through one-hot encoding, since the number of users and videos is very large, the features will eventually become high-dimensional sparse feature sequences. Therefore, here, for the ID features, this article adopts the embedded feature processing method to deal with ID features. The specific processing method is as follows. First, change the characteristics of the ID type to a numeric type. For example, after the user "U102983434" is converted, it becomes "102983434," and the string type is converted to a numeric type. Since the ID of each user is unique, the converted value can be used as a unique index to generate a matrix with dimensions (N, 128), where N is the total number of IDs and 128 is the number of columns in the matrix. Then, use this matrix as the initialization data of the input layer of the neural network.

Table 1: Video basic information table.

Parameter	Parameter value
Epoch	200
Batchy_size	256
Learning_rate	0.01
Dropout_keep	0.5

3.3. Dnn Network Construction and Model Training. After obtaining user embedded features, video embedded features, and video title features, we started to build network architecture for video recommendation score prediction.

For video features, we embed the ID and tag of the video into the feature vector: splicing it with the feature vector of the text of the video, and output a 128-dimensional vector through the fully connected layer. For some user features, directly import the user's embedded feature vector into the fully connected layer, which also outputs a 128-dimensional vector.

When using the fully connected layer to calculate the above video and user feature vectors, the activation function used is RELU. Among them, the RELU function is an activation function commonly used in artificial neural networks, which lays a solid foundation for deep neural network data fusion, and the optimization algorithm is dam. The Adam algorithm is the adaptive moment estimation method (Adaptive Moment Estimation), which can calculate the adaptive learning rate of each parameter.

The relevant model parameter configuration is shown in Table 1.

Epoch is the number of times to train a complete training set sample, batch_size is the sample size of each batch of data, dropout_keep is the probability of the dropout mechanism, and learning_rate is the learning rate, used to control the step size of each gradient, and the final convergence. The results are closely related.

After designing the network structure, it is necessary to perform score prediction on the final user features and video features. The calculation method for score prediction here is vector multiplication. A prediction value is obtained by multiplying two 128-dimensional vectors, and this value is obtained. To do regression fitting with the real value, the loss function used is the mean square error with L regularity that has been introduced in the previous chapter:

$$L(y, f(x)) = (y - f(x))^2 + \frac{\gamma}{2}\|w\|^2. \tag{16}$$

The architecture of the entire network is shown in Figure 3.

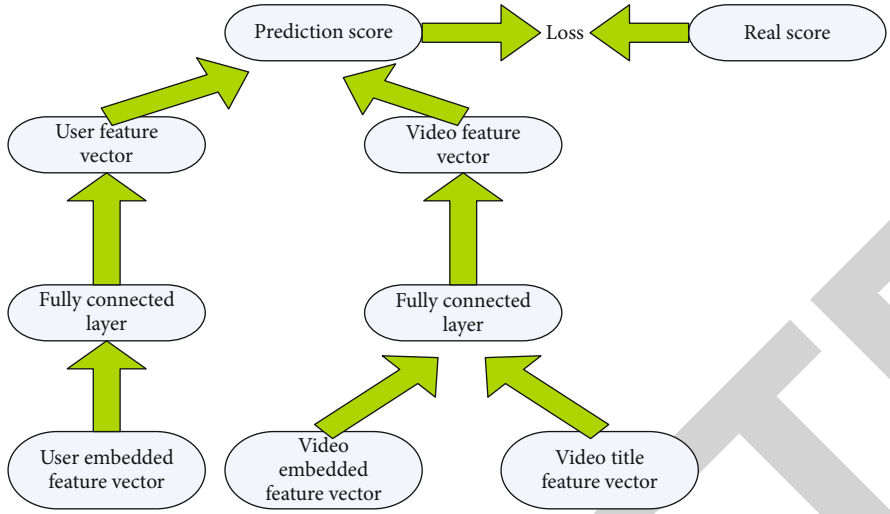

Figure 3: The architecture of the entire network.

Table 2: Descriptive statistical analysis of samples.

		Frequency	Percentage	Cumulative percentage
Age	Under 25	208	77.6	77.6
	25-30	51	19	96.6
	31-40	6	2.2	98.9
	Above 40	3	1.1	100
Education	Junior high school	2	0.7	0.7
	High school	13	4.9	5.6
	Undergraduate	130	48.5	54.1
	Master's degree or above	123	45.9	100
Monthly income	Below 2000	112	41.8	41.8
	2001-3000	57	21.3	63.1
	Above 3001	99	36.9	100
Total		268	100	

4. Result Data Analysis and Discussion

In this chapter, Spss24.0, Amos, and other tools will be used to process and analyze the collected big data samples, complete statistical analysis, factor analysis, reliability and validity testing, and variable correlation, as well as analysis, hypothesis testing, etc. Draw conclusions and discuss the theoretical assumptions of the results.

4.1. Descriptive Statistical Analysis. The questionnaire in this article is for people who have shopping experience after watching short video marketing content. This time, the online questionnaire survey tool was used to distribute the questionnaire. A total of 340 questionnaires were distributed, and the number of questionnaires returned was 290. Incomplete and other invalid data, the final number of valid questionnaires was 268, reaching an effective recovery rate of 79%. This questionnaire is issued to collect statistics on the basic information of the respondent's gender, age, educational background, per capita monthly income, etc. At the same time, in order to ensure the accuracy and authenticity of the survey data, the introductory part of the questionnaire promises to be used only for academic inquiry and can be completely based on individual actual conditions. Fill in, the answer is right or wrong. See details in Table 2.

The proportion of boys in the survey group is 32.5%, and the proportion of female surnames is 67.5%. This is more in line with the actual situation that women tend to shop online. The age of the survey group is concentrated under 30 years old, and the overall population of this age group is younger highly active online, good at accepting new things. In terms of academic qualifications, the interviewees are mostly undergraduates and postgraduates, accounting for 48.5% and 43.3%, respectively. Such groups generally have a relatively high level of education and can understand the questionnaire items more accurately, answering academic questionnaires earnestly, and guaranteeing a certain degree the reliability and validity of the questionnaire collected in

Table 3: KMO and Bartlett test.

Sampling adequacy of KMO metrics		0.865
Bartlett sphericity test	Approximate chi-square	1736.512
	Degree of freedom	55
	Significance	0.000

Table 4: Factor loading after rotation.

Gn1	Ingredient 1	Ingredient 2	Ingredient 3
Gn2	0.872		
Gn3	0.840		
Gn4	0.880		
Yl1	0.827		
Yl2		0.848	
Yl3		0.823	
Yl4		0.838	
Sj1		0.840	
Sj2			0.842
Sj3			0.859

the questionnaire. In terms of disposable monthly income, the highest tax rate of 2000 yuan and below is 39.8%, and 59.8% of the surveyed's cumulative monthly disposable income is less than 3000 yuan. Both 2000-3000 yuan and 4000 yuan people are more than 20%. It can be seen that the interviewees generally have certain spending power and space.

4.2. Exploratory Factor Analysis

4.2.1. Exploratory Factor Analysis of Content Marketing. First, perform Bartlett's sphericity test on the 11 items involved in content marketing. The Bartlett sphere test method is based on the correlation coefficient matrix. Its null hypothesis is that the correlation coefficient matrix is a unit matrix, that is, all the diagonal elements of the correlation coefficient matrix are 1, and all the elements on the off-diagonal line are the statistic of the Bartlett sphere test method which is obtained according to the determinant of the correlation coefficient matrix. From Table 3, it can be seen that the KMO value of the scale is 0.865, and the corresponding P value is lower than the significant level, indicating that the test can be used as a factor analysis. The content marketing factors were extracted by the principal component analysis method, and a total of 3 factors were extracted. The analysis results are shown in Table 4. The load value of each factor is greater than 0.5, indicating that the content marketing is effective.

4.2.2. Exploratory Factor Analysis of Psychological Distance. Exploratory factor analysis of psychological distance, as can be seen from Table 5, the KM0 value of the scale is 0.938, and the corresponding P value is lower than the significant level, indicating that the test has passed and factor analysis

Table 5: KMO and Bartlett test.

Sampling adequacy of KMO metrics		0.938
Bartlett sphericity test	Approximate chi-square	1781.512
	Degree of freedom	16
	Significance	0.000

Table 6: Factor loading after rotation.

	Ingredient 1
gm1	0.924
gm2	0.912
gm3	0.931
gm4	0.902
gm5	0.931
gm6	0.905

can be done. Principal component analysis was used to extract the psychological distance factor, and one factor was extracted. The analysis results are shown in Table 6. The factor loading values are all greater than 0.5, indicating that the psychological distance validity is good.

4.2.3. Exploratory Factor Analysis of Product Involvement. Exploratory factor analysis of product involvement is carried out, and the result of the data set is shown in Figure 4.

It can be seen from Figure 4 that the KM0 value of the scale is 0.793, and the corresponding P value is lower than the significant level, indicating that the test is passed and factor analysis can be done. The product involvement factor was extracted by the principal component analysis method, and one factor was extracted. The analysis results are shown in Table 6. The factor loading values are all greater than 0.5, indicating that the crystal production has good involvement degree validity.

4.3. Comparison of Experimental Results of Marketing Recommendation Algorithm. Through the VRBCH algorithm, people can be aware of dense and sparse areas and discover global distribution patterns and interesting interrelationships between data attributes. In order to better evaluate the performance of the proposed VRBCH algorithm, this paper chooses sequential matrix factorization (SequentialMF), which is based on sequential matrix factorization (UserCF) and collaborative filtering algorithm with uncertain neighbors (UNCF). In the time series matrix decomposition, the parameters will affect the relationship. If the data is less than 99%, a user network will be created based on the time the user watches the video, and the relationship will be created using the network diagram and the probability table. It will be calculated, and the suggested video search is calculated using this model. The algorithm divides the data set into a set of test and training sets, calculates the similarity of users $K = 10$ through the training set, and obtains the similarity of the user matrix, which is then similar to 10 videos in the

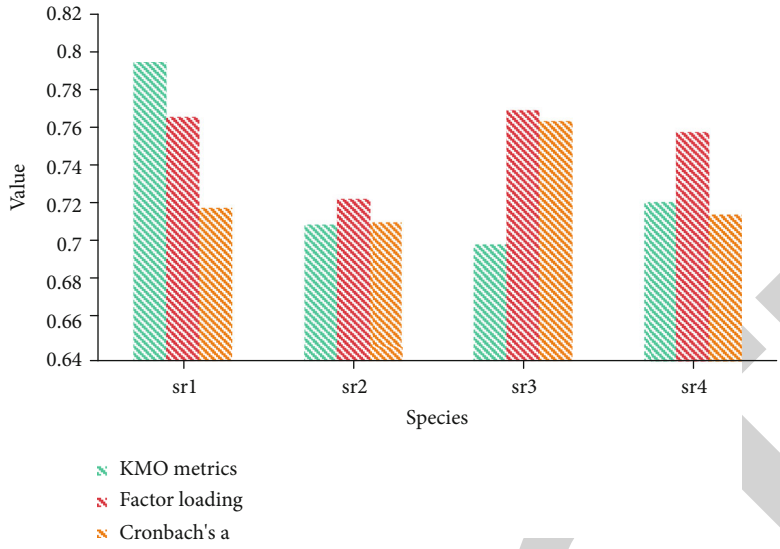

Figure 4: Exploratory factor of product involvement.

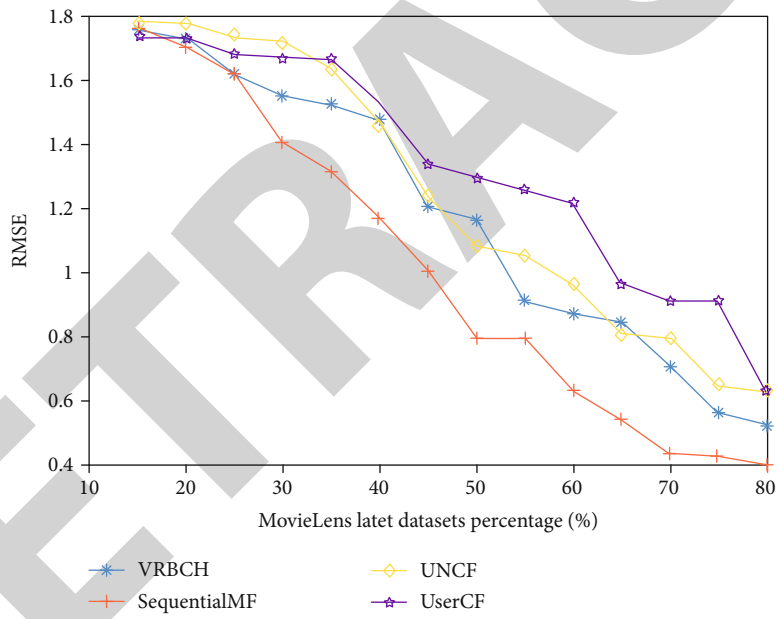

Figure 5: MovieLens Latest Datasets data set.

video. Calculate user similarity through a total of 10 interesting videos, and recommend 20 videos to users. The collaborative filtering algorithm uses video or user similarity to calculate the neighborhood factor. If the adjustment parameter is 20, the prediction factor is calculated and recommendations are made based on the proximity factor. Use RMSE scoring index and F to divide the experiment into two parts. Run the experiment using percentages from different data sets, and run the percentage values continuously at certain intervals. The first part of the experiment compares the performance of each recommendation algorithm under the MovieLens Latest Datasets data set, as shown in Figure 5.

As shown in Figure 5, the RESE performance of the VRBCH algorithm and time series matrix decomposition, time series matrix decomposition, and coordinated uncertain adjacency filtering algorithm are quite different in the early stage, but the final result is relatively ideal. If the amount of data is too small, the error will be large. Experiments show that as the percentage of data continues to increase, the trend shows a downward trend. After reaching 50%, the downward trend is slow. When the RESE performance reaches 80%, it remains almost unchanged.

The second part of the experiment compares the performance of each recommendation algorithm under the YouTube data set, as shown in Figure 6.

Figure 6 shows that due to the relatively large weakness of the YouTube data set, the VRBCH algorithm initially outperformed other algorithms. As the F table of the VRBCH

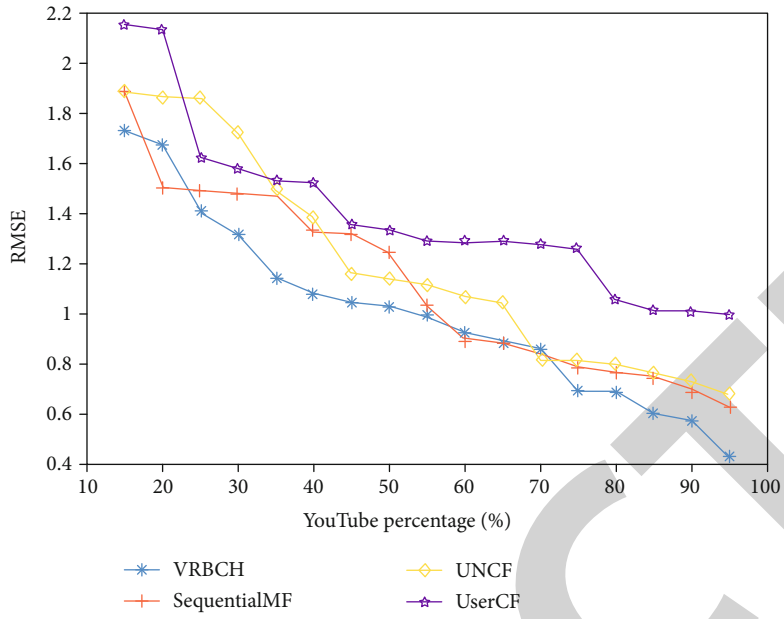

Figure 6: YouTube data set.

algorithm performs best, the performance of the algorithm will increase as the percentage of the data set increases. When the data volume reaches 80%, the performance of the VRBCH algorithm is steadily improved. Due to the high dilution of the experimental data set, the amount of data in the VRBCH algorithm has increased dramatically by 30% to 35%. Compared with other algorithms, it is not based on user evaluation. The *F*-meter performance is lower than the VRBCH performance, because there are few SequentialMF, UserCF, and UNCF algorithms that have high requirements for data failure.

5. Conclusions

The recommendation system uses special information filtering technology to recommend different items or content to users who may be interested in them. The empirical results show that the entertainment performance of short videos is generally higher than that of other e-commerce platforms. Short videos include text, images, and music. The image of the product is more three-dimensional and intuitive, and the display form can stimulate consumers, cause emotional reactions, and purchase enthusiasm. The combination of humor and exaggeration, the irony of the plot upside down, and modern language is easy to be accepted and imitated, which caused the market to promote. Embedding ads in such videos can make it easier to attract consumers and participate in the experience. The more innovative and entertaining the video content is, the more diverse it can stimulate the curiosity and psychology of consumers seeking excitement, thereby having a positive impact on consumers' emotional enjoyment and awakening. In the context of mobile short video marketing, consumer psychological emotions have a positive effect on impulsive purchases, and there is a mediating effect in the influence of stimulus variables on impulsive purchases. Emotional changes are an important internal driving factor for consumers to make impulsive purchases. Both pleasure and arousal affect consumers' impulse to purchase products. When the user's attitude towards short video marketing is positive and open, the effect of advertising marketing will be more significant, and the user will have a high acceptance of the marketing form, and it will be easier to try recommended products. The dynamic content of short video is usually short, concise, and vivid. It is more attractive than static pictures and texts. When combined with emotional background music, substituting intonation and direct copywriting content, it is usually good for consumers. Emotions have a great impact and build emotional bonds. Everyone is reluctant to watch naked advertisements but rarely refuses to listen to an infectious story. Therefore, implant marketing that is imperceptible in the output of feelings is easier to be accepted by people. Emotion is an abstract feeling, which needs to be conveyed with the help of external concrete expressions. Therefore, in marketing activities, the emotional performance characteristics can be sorted out and then used. For example, when it is found that consumers are showing pleasant emotions and aroused emotions are stimulated, adding introductory discourse or marketing temptation can enhance consumers' desire to buy and stimulate impulsive purchases. The amount of calculation is the problem of clustering. This article only clusters a small amount of low-dimensional data. In the big data environment, it is necessary to introduce a distributed computing method. This article intends to perform clustering attempts under the Spark platform as the next step. In the ranking model, the processing of historical data is rough, which reduces the recommendation accuracy and user experience.

Hindawi
Journal of Sensors
Volume 2023, Article ID 9876029, 1 page
https://doi.org/10.1155/2023/9876029

Retraction

Retracted: Facing Big Data Information Fusion and Data Mining Technology to Construct College Physical Education Teaching Evaluation System

Journal of Sensors

Received 17 October 2023; Accepted 17 October 2023; Published 18 October 2023

This article has been retracted by Hindawi following an investigation undertaken by the publisher [1]. This investigation has uncovered evidence of one or more of the following indicators of systematic manipulation of the publication process:

(1) Discrepancies in scope
(2) Discrepancies in the description of the research reported
(3) Discrepancies between the availability of data and the research described
(4) Inappropriate citations
(5) Incoherent, meaningless and/or irrelevant content included in the article
(6) Peer-review manipulation

The presence of these indicators undermines our confidence in the integrity of the article's content and we cannot, therefore, vouch for its reliability. Please note that this notice is intended solely to alert readers that the content of this article is unreliable. We have not investigated whether authors were aware of or involved in the systematic manipulation of the publication process.

In addition, our investigation has also shown that one or more of the following human-subject reporting requirements has not been met in this article: ethical approval by an Institutional Review Board (IRB) committee or equivalent, patient/participant consent to participate, and/or agreement to publish patient/participant details (where relevant).

Wiley and Hindawi regrets that the usual quality checks did not identify these issues before publication and have since put additional measures in place to safeguard research integrity.

We wish to credit our own Research Integrity and Research Publishing teams and anonymous and named external researchers and research integrity experts for contributing to this investigation.

The corresponding author, as the representative of all authors, has been given the opportunity to register their agreement or disagreement to this retraction. We have kept a record of any response received.

References

[1] Y.-t. Ma, "Facing Big Data Information Fusion and Data Mining Technology to Construct College Physical Education Teaching Evaluation System," *Journal of Sensors*, vol. 2021, Article ID 7168855, 15 pages, 2021.

Hindawi
Journal of Sensors
Volume 2021, Article ID 7168855, 15 pages
https://doi.org/10.1155/2021/7168855

Research Article

Facing Big Data Information Fusion and Data Mining Technology to Construct College Physical Education Teaching Evaluation System

Yong-tong Ma

School of Physical Education & Health, HeZe University, Heze, ShanDong 274015, China

Correspondence should be addressed to Yong-tong Ma; mayongtong@hezeu.edu.cn

Received 26 August 2021; Revised 9 October 2021; Accepted 26 October 2021; Published 16 November 2021

Academic Editor: Mu Zhou

The purpose is to enrich the evaluation system of physical education (PE) teaching in colleges and universities and to improve PE teaching methods and improve teaching quality. Based on big data information fusion and data mining technology, firstly, the related theories of teaching evaluation are analyzed and expounded, as well as the characteristics and principles of the construction of college PE teaching evaluation system. Secondly, from the perspective of evaluation index system of sports teachers' teaching and students' sports teaching, the content and evaluation index of college sports teaching evaluation are analyzed under the background of big data information fusion and data mining by questionnaire survey. Combined with model test, the results show that traditional college sports teacher pays more attention to the design and teaching methods of PE and ignore the learning process of students. The evaluation process of PE ignores the individual differences of students, the feedback method lacks openness, and the evaluation process is isolated. Based on the big data technology and teaching evaluation theory, the evaluation index is designed for PE teaching in colleges and universities. The average value of the first layer indexes is above 4, and the coefficient of variation is less than 0.2, which can basically reflect the content of PE teaching evaluation and provide some reference for the research of PE teaching evaluation.

1. Introduction

Physical education (PE) teaching evaluation is an important part of the PE teaching process. The evaluation method, evaluation executant, and evaluation object directly affect the improvement of the PE teaching quality and the development and progress of teachers and students in PE classes in colleges and universities. At present, the evaluation of college PE teaching is mainly based on students' evaluation of online teaching at the end of the semester [1]. Students are scored according to the classroom situation of PE teachers and the teaching evaluation elements formulated by the school. Finally, PE teachers have made achievements in PE this semester. This model has serious deviation, which is a significant obstacle to the model for education at all levels and PE in China. In addition, the training of PE talents and the quality of education in the index system are one of the key elements to measure the overall quality of students. To adapt to the requirements of the development of the times, school education and teaching reform are constantly being processed to ensure that students' professional knowledge level, physical level, and mental state can meet the social expectations of innovation level and personnel training objectives [2]. Colleges and universities are the last implementation stage of PE teaching in junior high school and university. They not only involve the all-around improvement of students' physical quality and spirit, and the comprehensive promotion of quality education, but also take charge of the implementation of national activities of physical conditioning and higher education personnel training [3]. However, due to many historical and social factors, college PE teaching is far from universally recognized. Therefore, in addition to increasing support in PE teaching and talent team construction, it is necessary to carry out

the essential investigation on the teaching process and assessment results, explore the existing problems, and find the direction for improvement.

With the rise of large-scale application, automatic evaluation becomes possible for college PE teaching. A large amount of data can be provided to evaluate PE teaching, making the evaluation of PE teaching more scientific and fairer. Based on information fusion of big data and data mining technology, PE teaching evaluation can provide more timely feedback on the evaluation results of PE teaching [4]. Appearing of information fusion of big data and data mining technology rises a doubt on the current technology, system and system of PE evaluation system, and other aspects. Therefore, it is necessary to explore and establish a peer PE teaching evaluation system to meet the era of big data, which is reliable and operable and really conducive to the development of students and PE teachers [5]. In the traditional PE teaching, the final examination results are the only standard to measure and evaluate students, which is not conducive to the all-round development of students. The application of big data enables schools to evaluate all aspects of students and teachers, rather than just one aspect of students or teachers [6]. For example, when evaluating students' PE, students' physical ability, physical ability, theoretical knowledge, learning attitude, and progress should be all put into consideration. In the evaluation of teachers, both students' achievements and teachers' classroom effect, record work should all be given attention [7].

Based on this, a college in Shaanxi Province is taken as the research object. A systematically study is made on the construction of college PE teaching evaluation system. And the components of the evaluation system are analyzed. The innovation is the combination of big data information fusion and data mining technology and the research of PE teaching evaluation system. The purpose is to provide reference information for PE teaching and the comprehensive quality training of talents in colleges.

2. Construction Theory of College PE Teaching Evaluation System under the Background of Big Data

2.1. Big Data and Data Mining. Big data is a set of data with large capacity, multitype, fast access, and high application value. It is rapidly developing into a new generation of information technology and services to collect, store, and analyze large amounts of data from different sources and of various formats and to discover new knowledge, create new values, and improve new capabilities [8]. Continuous assessment methods and evaluation of subjects of PE teaching are beneficial to the healthy development of the fair evaluation system, which can promote PE teaching and improve the teaching level of college PE [9]. Therefore, the advantage of big data should be utilized to ensure the integrity of the evaluation means and topics, through online, offline, and comprehensive evaluation means. Moreover, the evaluation subjects should be diversified, including the evaluation from subordinates, students, and teachers to superiors, and the evaluation from students and peer teachers to teachers, to ensure the fairness and objectivity of the evaluation. In this way, the attention of teachers and schools can be attracted to PE teaching, to ultimately promote the healthy development of school PE teaching [10]. In the era of big data, new technologies have become the mainstream. In such an environment and situation, it is also the development trend and a smart popularization to promote peer education by virtue of these new technologies which accelerate people's pace of life and improve people's work efficiency [11]. On the evaluation of college PE teaching, the traditional manual statistics and evaluation methods not only need lots of manpower and material resources but also are prone to errors. In contrast, intelligent evaluation methods can not only reduce unnecessary consumption but also ensure the speed and accuracy of evaluation, which is consistent with the development trend of the new era [12]. According to the traditional evaluation method of PE teaching in colleges and universities, the evaluation of students and teachers is generally manual [13]. There are likely to be calculation mistakes in this evaluation process which requires a lot of human and material resources and cannot achieve ideal effects efficiently [14]. However, the application of artificial intelligence (AI) to PE teaching evaluation system can achieve practical and fast results with few errors [15]. The AI technology can quickly collect, count, classify, and analyze students' indexes and data for the college PE evaluation system, save considerable time, and reduce errors with the same workload through intelligent processing [16].

Data mining is a process of extracting valuable information and knowledge from large, incomplete, noisy, unclean, and random data. The main methods of data mining include decision tree, association rules, clustering analysis, neural network, and rough set. Association rule exploration is a search process, which allows user to find some association rules between a set of data elements in the database. The design principle is to find frequent attribute sets in the database and then use frequent attribute sets to find strong association rules. Apriori algorithm is the most commonly used association rules. It finds all the common element sets after scanning the database many times. Mining association rule algorithm is the basic relationship between the information cited in the process of reasonable evaluation, so as to find out the design of education teachers and teaching effect, which is the premise and the research and development of reference teaching evaluation method.

2.2. Digital Information Fusion. With the advent of the era of big data and the rapid development of science and technology, the ability of digital information processing and large-scale collection has been greatly improved. The explosive growth of data leads to complex information structure, various forms, and scattered distribution, which is why electronic information is effectively collected and merged. The integration of digital information resources is an important process to explore the relationship between digital information resources from different perspectives by using a variety of technologies. The integration of digital information resources is an extension and development of

the integration of digital information resources. The integration of digital information resources is mainly the seamless connection between heterogeneous numbers on the same platform. This is the process of combining data information resources into an organic whole.

In big data environment, data fusion, service fusion, and platform fusion are three basic levels of digital information resource fusion. Among them, data fusion is the basis of digital information resource fusion, service fusion is the purpose of digital information fusion, and platform fusion is the key to digital information resource fusion. The integration of digital information resources and the establishment of service platform provide a new impetus for the harmonious development of information services and greatly improve the competitiveness of information institutions in the market. The merging data are mainly merging, and the atomic electronic information integrates all the digital information to connect with each other, including time, region, industry, theme, and topic, and establishes a database. Platform interoperability is a number of technologies for merging data and information in different formats and then integrated into a unified cloud platform or preconstructed integrated platform. On the basis of platform integration and data integration, the goal of service integration is to dynamically optimize service elements and realize the integration of service content, form, and function.

2.3. Teaching Evaluation and PE Teaching Evaluation. The teaching evaluation refers to a series of judgments on the achievements and values of education through information collection and processing. In the articles about modern teaching theory and PE, some experts think that "teaching evaluation is the process of measuring, analyzing and judging teaching work." Some researchers stressed that "teaching evaluation is a value judgment of the teaching process and teaching results" [17]. In a new book on curriculum, some experts state that teaching evaluation is a process of measuring and judging the evaluation objects in teaching activities according to certain standards. On the basis of objective teaching practice, here, the concept of teaching evaluation is defined as the process of judging the value of teaching work with scientific and reasonable methods [18].

In modern education theory, the evaluation of PE teaching is to judge the teaching process using certain methods based on the purpose of PE teaching [19]. Some experts believe that PE teaching evaluation is a process of measurement, analysis, and judgment in accordance with relevant standards. In summary, PE teaching evaluation is a concept of education evaluation at a lower level. Here, the concept of PE evaluation is defined as a process of value judgment on the process and results of PE teaching activities by scientific evaluation methods on the basis of PE teaching [20].

2.4. Principle of Constructing the PE Teaching Evaluation System of Colleges and Universities. The design of PE teaching evaluation system for colleges and universities should rely on big data technology and consider all aspects of PE teaching process, mainly to follow the principles in Figure 1.

(1) *Scientific and Objectivity*. Combined with the background and characteristics of the era of big data, on the basis of objective laws and practice, construction of college PE teaching evaluation should be made scientifically and objectively. For example, the selection of evaluation indicators should be based on the data collected and surveyed to ensure the scientific and objectivity of evaluation indicators [21]

(2) *Integrity and Comprehensiveness*. Namely, when constructing the evaluation system of PE teaching in colleges and universities, the selection of evaluation indexes should be comprehensive, clear, and widely representative but not repeated, which can basically reflect the whole process of PE teaching [22]

(3) *Feasibility and Measurability*. Feasibility refers to the way of PE teaching evaluation has practical operability. Testability refers to the evaluation of the evaluation index has a testable quantitative standard, such as the selection of indicators must be easy to understand and test, and there is no ambiguous index [23]

(4) *Combining Generality and Individuality*. Students in different disciplines have different learning purposes and characteristics. Teachers in different disciplines also have different teaching methods and styles. Therefore, different disciplines and students should be given different standards to evaluate. In the evaluation of PE teaching, the individuality of different subjects and students should be respected on the basis of the commonness of PE teachers and students [24]

(5) *Openness and Timeliness*. Openness is to open to the public when constructing the evaluation system of PE teaching in colleges, so that students and teachers can better understand the evaluation of PE teaching, and better supervise and evaluate that. Timeliness refers to the evaluation; analysis and feedback should be timely, especially the college PE teaching evaluation system in the feedback of this piece to have enough openness and timeliness [25]

2.5. Characteristics of the Construction of PE Teaching Evaluation System for Colleges and Universities. With the advent of the era of big data, it is possible to reconstruct the PE teaching evaluation system in colleges and universities by using big data technology. Based on the characteristics of big data, the following characteristics of the PE teaching evaluation system of colleges and universities are analyzed to obtain the applicable scope of big data. The first characteristic is the evaluation mode from the subjective experience evaluation to the objective data support [26]. In the previous PE teaching evaluation, students' physical performance is the main way of evaluation, and individual subjective image is as the main way of evaluation of PE teachers, so the evaluation is incomplete and objective. However, with the help of big data technology, the evaluation of PE class status can be recorded accurately. The second characteristic is the evaluation method from summary evaluation

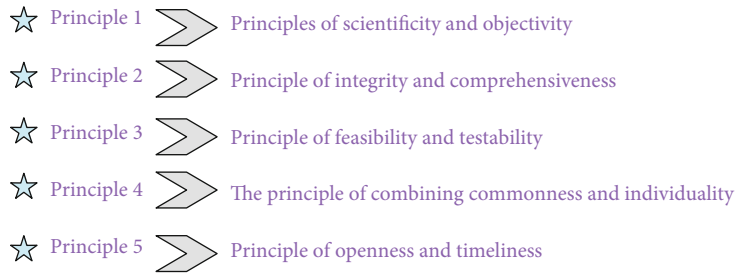

Figure 1: Principles PE education needs to follow.

Table 1: Key questions of the questionnaire.

Content	No.	Question
Teaching	Q1	What evaluation subjects are contained in the current evaluation of the PE teaching by teachers?
	Q2	How does the school evaluate the teaching of PE teachers at present?
	Q3	What evaluation contents are contained in the current evaluation of the PE teaching by teachers?
	Q4	Is there any feedback after the evaluation of PE teachers?
	Q5	What basic contents of the feedback are the PE teaching evaluation of teachers at present?
	Q6	When does the school give feedback to the PE teacher after the evaluation?
	Q7	What are the current ways for schools to give feedback after evaluating PE teachers?
Student	Q8	What are the subjects of PE teaching evaluation for students?
	Q9	What are the modes of PE teaching evaluation for students?
	Q10	What are the contents of PE teaching evaluation for students?
	Q11	According to the time of teaching evaluation, what are the methods used by schools to evaluate the PE teaching?
	Q12	Is there feedback after the student is evaluated?
	Q13	What are the ways to give feedback after evaluating students?
	Q14	When does the school usually give feedback after evaluating students?
Individual	Q15	Do you think the current evaluation of PE teaching is reasonable?
	Q16	Do you think it is reasonable to implement PE teaching evaluation?
	Q17	What problems do you think exist in the school's PE teaching? What are your suggestions on the evaluation of PE teaching in the school?
	Q18	How many times has the school conducted teaching evaluation of PE teachers?
	Q19	What are the main contents of the teaching evaluation?
	Q20	When does the school generally evaluate your PE teaching?
	Q21	What are the models of PE teaching evaluation of the school currently for you?
	Q22	How important do you think the PE teaching evaluation is in teaching evaluation?

to concurrent evaluation, to enable teachers and students to evaluate the teaching more comprehensively and objectively [27]. At present, the evaluation of college PE teaching cannot reflect the situation of students and teachers at all stages of PE teaching, because it is mainly a summary evaluation. Meanwhile, the evaluation is the combination of summative evaluation and process evaluation, so the evaluation system of equal attention to the results and process is adopted to timely record students' learning state and teachers' teaching state. The third characteristic is the evaluation content from the uniqueness to diversity. That is, the content of evaluation is diversified. For example, the PE teaching evaluation for students involves not only theoretical knowledge, education and sports, sports skills, physical condition, learning attitude, and learning ability but also the progress of sports skills and other aspects [28]. The fourth characteristic is the evaluation method from artificial evaluation to intelligent evaluation. The manual evaluation method is not only time-consuming and laborious but also prone to errors, while intelligent evaluation is fast and accurate. Therefore, the evaluation method of PE teaching in colleges and universities should be translated from the traditional manual collection, statistics and analysis to the intelligent acquisition, processing, and analysis of massive data. The fifth characteristic is the evaluation feedback from closed evaluation to open evaluation [29]. The collection, processing, and analysis of evaluation data are designed by big data technology, which will be open to

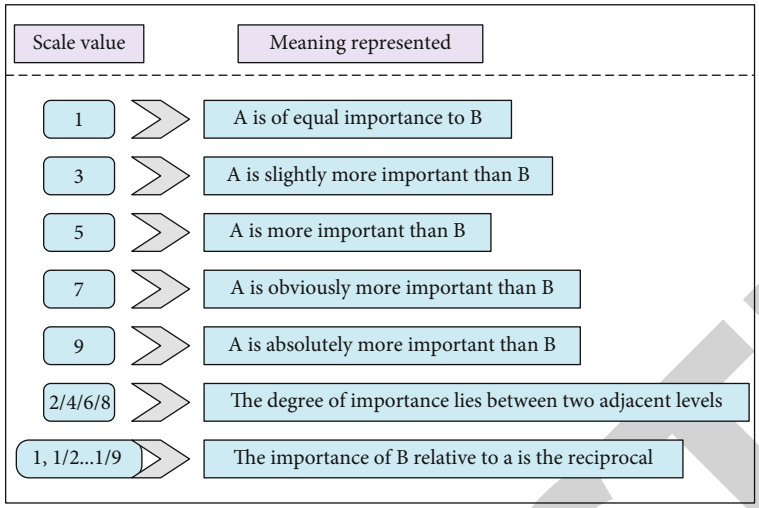

Figure 2: Scale value method.

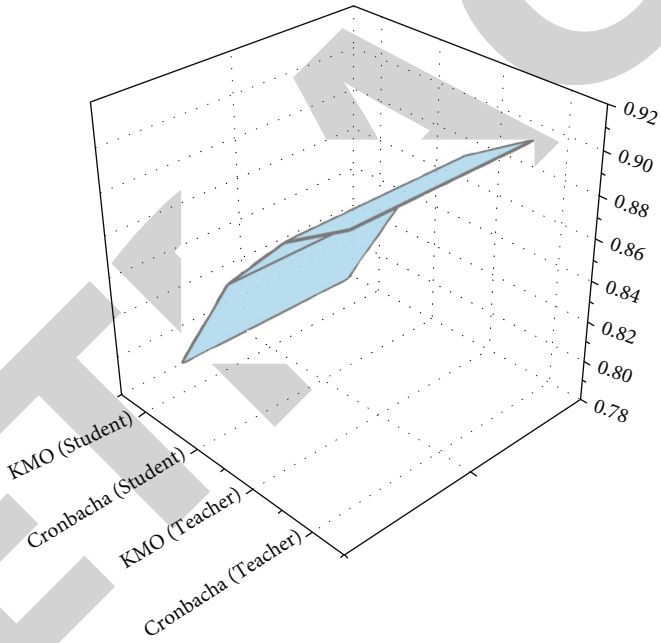

Figure 3: Reliability analysis of questionnaire survey results.

teachers and students, so that teachers and students can better understand their supervisory role in the classroom and at the same time better implement education evaluation in colleges and universities [30].

3. Research Methods of Constructing Evaluation System of College PE Teaching under the Background of Big Data

3.1. Design of Questionnaire. The research subjects of the construction of college PE teaching evaluation system based on big data technology mainly include the evaluation of PE teachers from school administrators, students, and PE teachers themselves. The evaluation methods contain evaluating by school administrators on PE teachers, evaluating between PE teachers, evaluating by students on PE teachers, and self-evaluation. Besides, an online questionnaire survey is conducted, and the issuance of the questionnaires is mainly completed through the Wenjuanxing platform. A total of 250 questionnaires are issued, with 230 valid questionnaires back, among which 30 questionnaires are for PE teachers. For the recovered questionnaires, the SPSS 25.0 software is used for reliability and validity analysis, which

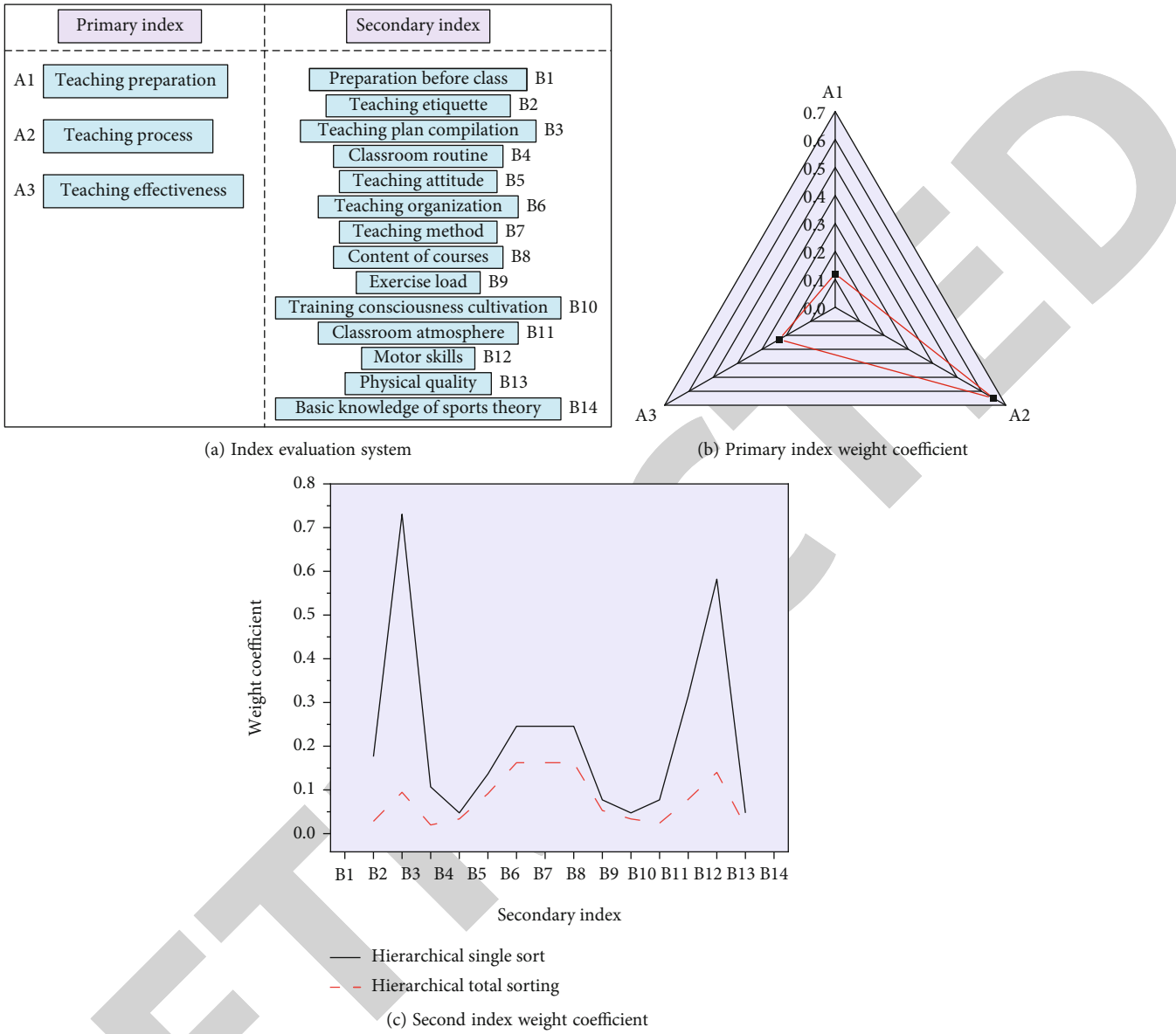

Figure 4: The weight of PE teachers' teaching evaluation index system.

indicates that the designed questionnaire has good reliability and validity. The purpose of this questionnaire survey is mainly to analyze the overall situation of the construction of college PE teaching evaluation system based on big data technology. Table 1 signifies the key problems involved in the questionnaire.

Compared with variance analysis, the advantage of coefficient of variation is that the average of reference data is not required. Coefficient of variation is a dimensionless parameter. When comparing two groups of data with different dimensions or mean values, coefficient of variation rather than standard deviation should be used as a reference for comparison. Therefore, the coefficient of variation is selected to analyze the data difference.

The coefficient of variation refers to the coordination degree, which are in a negative correlation. If the coefficient of variation is less than 0.25, the coordination degree is considered high [31]. The coefficient of variation is calculated according to:

$$W_i = \frac{A_i}{B_i},$$
$$C_i = \frac{1}{n}\sum_{i=1}^{n} X, \quad (1)$$
$$D_i = \sqrt{\frac{1}{n-1}\sum_{i=1}^{n}(X_I - C_i)}.$$

Among the above equations, W_i represents the coefficient of variation, C_i denotes the mean value, and D_i refers to the standard deviation.

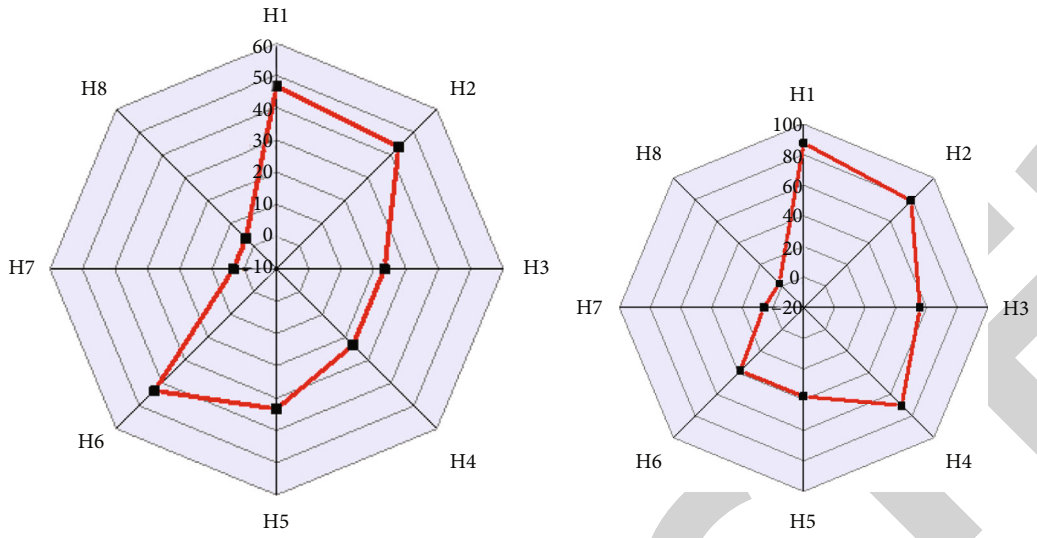

(a) Evaluation by teachers (b) Evaluation by students

Figure 5: Evaluation results.

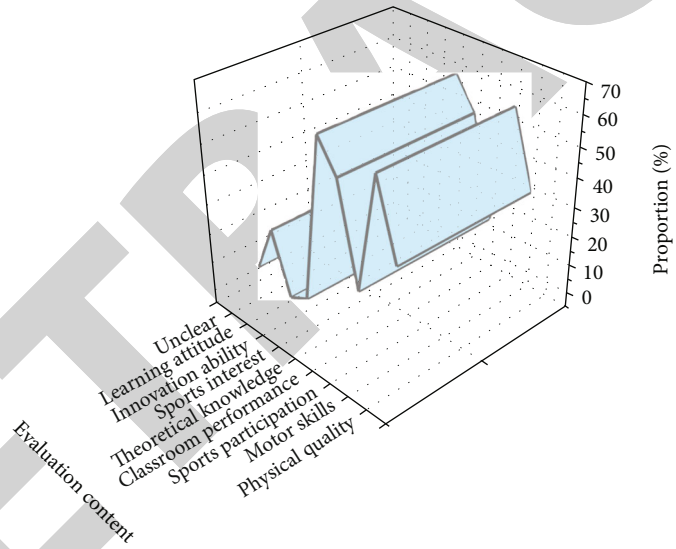

Figure 6: Evaluation results of PE teaching for students.

3.2. Calculation Method of the Weight of Indicators. Analytic hierarchy process (AHP) is used to calculate and determine the weight coefficient of evaluation indicators. AHP makes pairwise comparison on the correlation between the evaluation indexes, quantifies the final results, and finally obtains the weight coefficient of each layer of indicators. The AHP method is used to determine the weight of indicator, which ensures the rationality and scientific of the weight determination of indicator.

The steps of AHP method are as follows: First, build evaluation system. Second, establish a hierarchical structure model. Relevant indicators are divided into different levels from top to bottom according to different attributes and importance. Third, construct the corresponding judgment matrix. The judgment matrix is formed by pairwise comparison of all evaluation indexes at the same level. 1-9 scaling method of Satty is generally applied, and A and B two indicators are compared, as Figure 2.

Equation (2) displays the judging matrix.

$$A = \begin{bmatrix} a_1 & a_2 & \cdots & a_n \\ a_{11} & a_{12} & \cdots & a_{1n} \\ \cdots & \cdots & \cdots & \cdots \\ a_{n1} & a_{n2} & \cdots & a_{nm} \end{bmatrix}. \quad (2)$$

The weight vectors are calculated, and consistency check is made. The maximum eigenvalue of the matrix is $\lambda_{\max}$, and Equations (3)–(5) are the specific calculations.

$$\lambda_{\max} = \frac{1}{n}\sum_{i}\frac{(Aw)i}{wi}, \tag{3}$$

$$CI = \lambda_{\max} - \frac{n}{n-1}, \tag{4}$$

$$\mathrm{CR} = \frac{\mathrm{CI}}{\mathrm{RI}}. \tag{5}$$

CR represents consistency ratio, CI refers to consistency index, and AW is the product of judgment matrix and feature vector. RI stands for the average random consistency index.

3.3. Reliability Analysis of the Results of Questionnaire. The questionnaire survey results are tested from aspects of reliability and validity. Reliability means that when the research method does not change, the same event is analyzed, and the results do not change, which indicates that the survey results have high reliability, so it can be called reliability analysis. The commonly used reliability measurement index is the Cronbach's. Equation (6) shows its calculation.

$$\alpha = \frac{K}{K-1}\left(1 - \frac{\sum_{i=1}^{K}\sigma_{Y^i}^2}{\sigma_X^2}\right). \tag{6}$$

K is total number of questions in the questionnaire. $\sigma^2 X$ refers to variance of the total sample. $\sigma^2 Yi$ stands for the variance of the sample. SPSS25.0 is used to analyze the data obtained from the questionnaire survey. The value of Cronbach's α is in the range of 0–1, if Cronbach's $\alpha > 1$, it indicates that the survey results have high credibility. If $0.8 < \text{Cronbach's } \alpha < 0.9$, it means that the findings can be used for research analysis. If $0.7 < \text{Cronbach's } \alpha < 0.8$, it shows that the reliability of the survey results is low; it needs to be modified accordingly.

Validity characterizes how valid the research results are. Researchers can use relevant measurement tools and means to express the degree of the survey content. If the survey content can be consistent with the results, it indicates that the survey results have high validity. Kaiser-Meyer-Olkin (KMO) value is usually used to express the validity of the survey results. The simple correlation coefficient and partial correlation coefficient of variables are two relatively important variables in KMO. The sum of squares of partial correlation coefficients of all variables is calculated. If the value is far less than the sum of squares of simple correlation coefficients, the KMO value will be closer to 1, indicating that there is a strong correlation between variables.

The sample (Xi, Yi) $(i = 1, 2, 3, \cdots, N)$ is extracted from the total sample, and its partial correlation coefficient square sum R and simple correlation coefficient square sum P are calculated. Equations (9)–(12) display the specific calculation.

$$\begin{cases} r_{xy,z_1} = \dfrac{r_{xy} - r_{xz_1}r_{yz_1}}{\sqrt{\left(1 - r_{xz_1}^2\right)\left(1 - r_{yz_1}^2\right)}}, (h = 1), \\ r_{xy,z_1z_2z_3\cdots z_h} = \dfrac{r_{xy,z_1z_2z_3\cdots z_{h-1}} - r_{xz,z_1z_2z_3\cdots z_{h-1}}r_{yz,z_1z_2z_3\cdots z_{h-1}}}{\sqrt{\left(1 - r_{xz,z_1z_2z_3\cdots z_{h-1}}^2\right)\left(1 - r_{yz,z_1z_2z_3\cdots z_{h-1}}^2\right)}} (h \geq 2), \end{cases}$$

$$\rho = \frac{\sum_{i=1}^{n}\left(X_i - \widehat{X}\right)\left(Y_i - \widehat{Y}\right)}{\sqrt{\sum_{i=1}^{n}\left(X_i - \bar{X}\right)}\sqrt{\sum_{i=1}^{n}\left(Y_i - \bar{Y}\right)^2}},$$

$$\bar{X} = \frac{1}{n}\sum_{i=1}^{n}X_i,$$

$$\bar{Y} = \frac{1}{n}\sum_{i=1}^{n}Y_i. \tag{7}$$

Equation (8) is the calculation of KMO.

$$M = \frac{P}{P+R}. \tag{8}$$

The calculated KMO value is closer to 1, indicating that the validity of the survey results is higher, the correlation between variables is stronger, and it is more suitable for factor analysis.

4. Construction of College PE Teaching Evaluation System Based on Big Data

4.1. Reliability Analysis of Results of Questionnaire Survey. Based on the reliability analysis of questionnaire survey results, SPSS25.0 is used to analyze. Figure 3 presents the results.

Figure 3 shows that the Cronbach's α and KMO value of the teachers' and students' papers are at a satisfactory level, indicating that the questionnaire survey results can be used for PE teachers' teaching evaluation analysis.

4.2. Evaluation Analysis of PE Teachers Teaching. Before analyzing the teaching evaluation of PE teachers, it is necessary to calculate the weight coefficient of the teaching evaluation index of PE teachers in advance. First of all, the teaching evaluation index system of PE teachers is implemented at all levels of judgment moment, and then according to the judgment, matrix data are calculated within the trip, n square, weight value W, $\lambda_{\max}$, CI, and CR. Figure 4 shows the final weight of PE teachers' teaching evaluation index system.

From the overall survey results, 50% of the PE teachers and 44.2% of the students think that the current evaluation system of PE teaching is unreasonable, and only 16.67% of the PE teachers and 24.2% of the students think that it is reasonable, but 90% of the PE teachers and 90.4% of the students think that the evaluation of school PE teaching is important. In the meanwhile, 63.33% of the PE teachers think that the current evaluation system of college PE

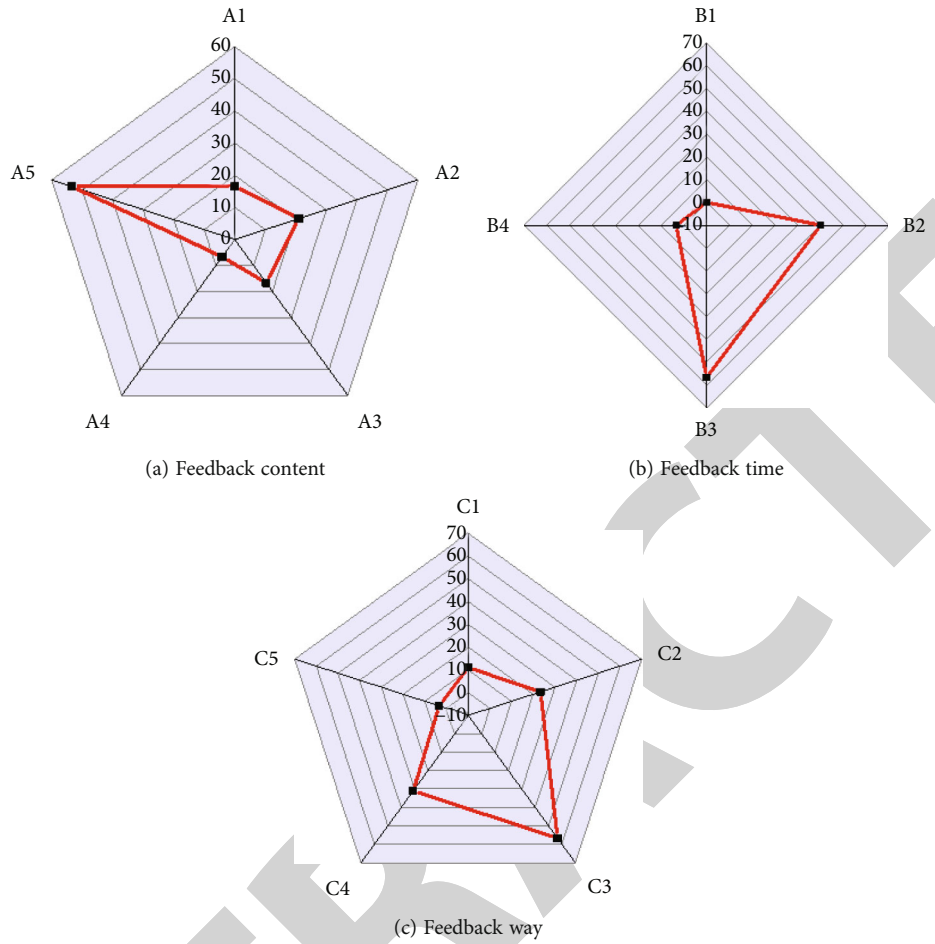

(a) Feedback content

(b) Feedback time

(c) Feedback way

Figure 7: Evaluation feedback.

teaching is poor and lack of security system. Therefore, the current implementation of PE teaching evaluation in colleges and universities is analyzed from the two subjects of physical education teachers and students.

4.3. Analysis of the Teaching Evaluation of PE Teachers. The teaching evaluation of PE teachers primarily considers teaching methods, teaching attitude, teaching effect, teaching ability, innovation ability, classroom atmosphere, moral level, and student participation. The evaluation is performed by teachers and students, and Figure 5 reveals the evaluation results.

H1-H18 in Figure 6 represent teaching attitude, teaching methods, teaching effectiveness, teachers' own ability, creativity, moral level, classroom atmosphere, and students' participation, respectively. From Figure 5, the evaluation of PE teachers is mainly based on the teaching ability, teaching methods, teaching effect, and moral level of teachers. Specifically, every index, respectively, occupies 23.34%, 43.34%, 43.34%, and 43.34% in the evolution result by teachers, while 70.3%, 78.9%, 55.7%, and 38.3% in the evolution result by students. This demonstrates that PE teachers usually ignore the degree of students' participation in the classroom and the classroom atmosphere, and the evaluation content ignores the innovation ability of PE teachers. It can be concluded that college PE teacher pays more attention to the design and teaching methods of PE but ignore the substantive content, i.e., students' learning state and learning effects.

Figure 7 shows the feedback after the content evaluation.

A1-A5 in Figure 7 refer to classroom performance, advantages and disadvantages, improvement suggestions, expectations and encouragement, and unclear. B1-B4 represent immediate feedback, time-varying feedback, new term feedback, and unclear. C1-C5, respectively, stand for network feedback, writing feedback, communication feedback, bulletin board feedback, and unclear. The survey results of PE teachers show that the evaluation results are conveyed after the evaluation. As for the feedback content, 53.34% of the PE teachers do not know the specific content of the feedback. This indicates that more than half of the teachers do not know the result feedback, evaluation and feedback content is relatively simple, and the feedback perspective is single. The feedback to teachers at the beginning of the new semester accounts for 56.68%, while the feedback given to the teachers over a period of time accounts for 40%. In general, the evaluation feedback is not timely, so most PE teachers do not consider the feedback of the results.

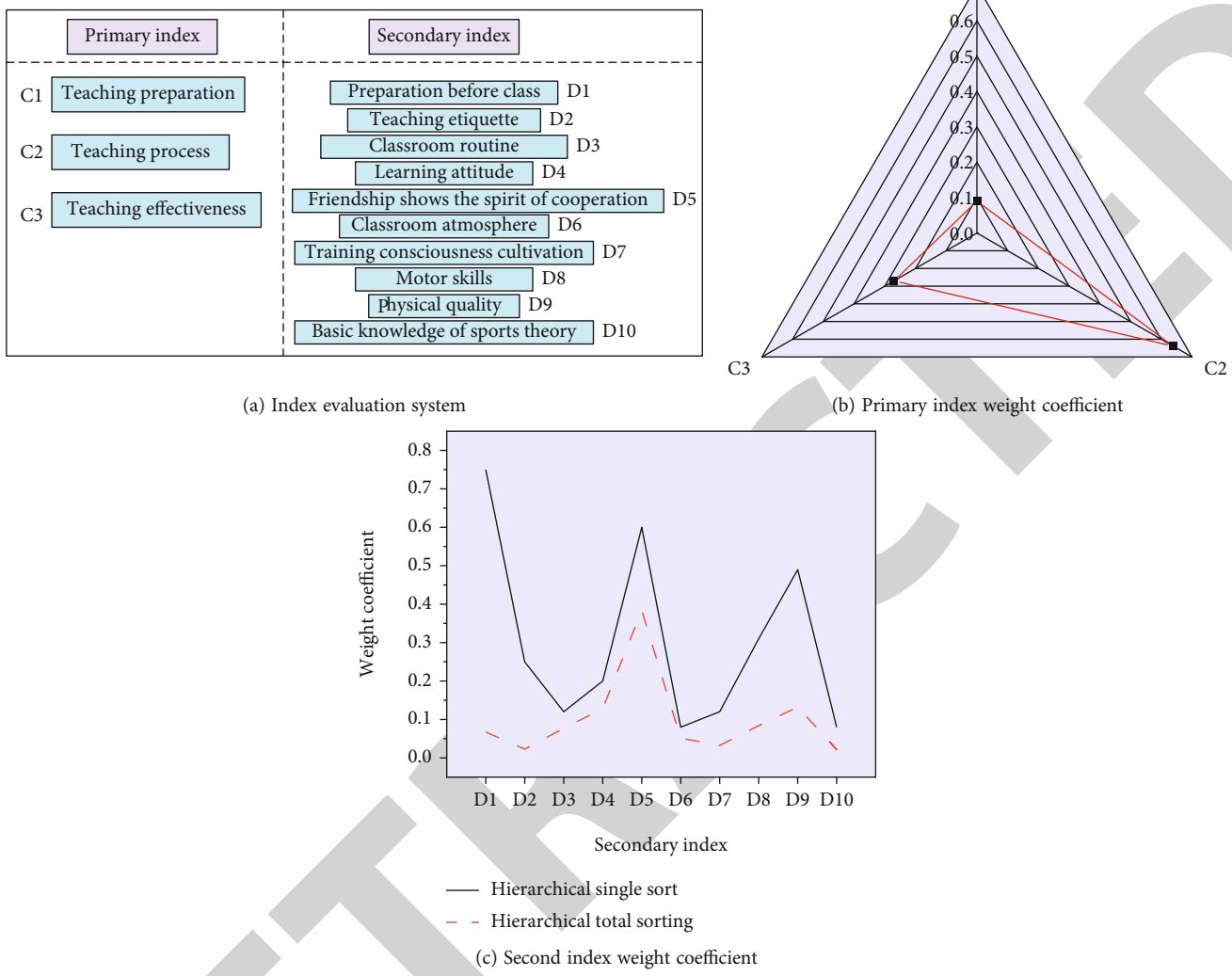

(a) Index evaluation system

(b) Primary index weight coefficient

(c) Second index weight coefficient

Figure 8: Weight of evaluation index system for students' PE.

The main methods of feedback are private conversation, accounting for 56.68%, followed by the bulletin display and written feedback. This result proves that the feedback method is outdated and lacks openness. Therefore, the method of feedback should be updated over time, such as feedback on the Internet, and feedback should be more open, so that PE teachers can notice the results of feedback.

4.4. Analysis of the Teaching Evaluation of Students. The above method is applied to calculate the weight coefficient of students' PE teaching evaluation index. Figure 8 shows the results.

Figure 6 provides the evaluation results of PE teaching for students.

According to Figure 6, the PE teaching evaluation for students mainly focuses on theoretical knowledge, sports ability, classroom performance, and physical quality, accounting for 63.34%, 61%, 53.34%, and 36.68%, respectively. The evaluation ignores students' innovative ability, sports interest, and other aspects, paying too much attention to some common content but ignoring the individual differences of students.

Figure 9 signifies the evaluation methods of PE teaching for students.

According to Figure 9, the evaluation method of PE teaching extremely highlights the summary evaluation with the proportion of 73.34%, while ignoring the progress of everyone at each stage of learning. Moreover, it emphasizes quantitative evaluation, accounting for 66.8%, while ignoring qualitative evaluation. Therefore, the evaluation process is very closed, static, lack of dynamic, and achieving limited promotion effects on student development.

Figure 10 displays the feedback on students' PE teaching evaluation.

The survey results in Figure 10 show that after the PE teaching evaluation for students, the school commented on the evaluation results. The feedback content is mainly for students' sports performance, including physical fitness tests, skill tests, theoretical knowledge tests, and normal classroom performance. Therefore, the feedback content is

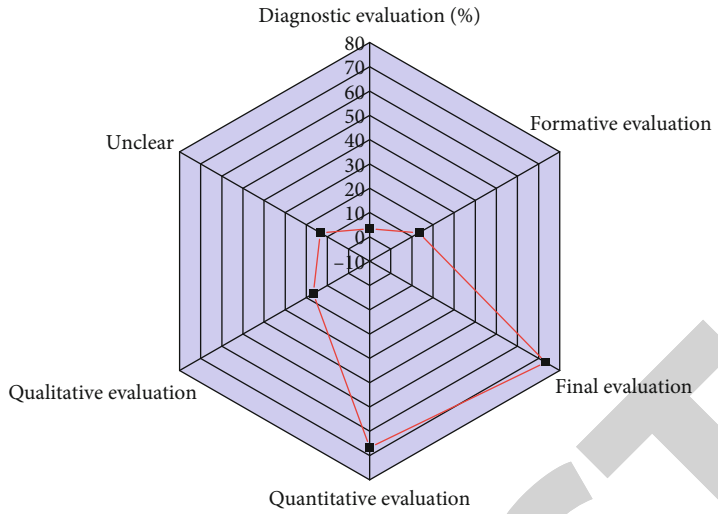

Figure 9: Evaluation method.

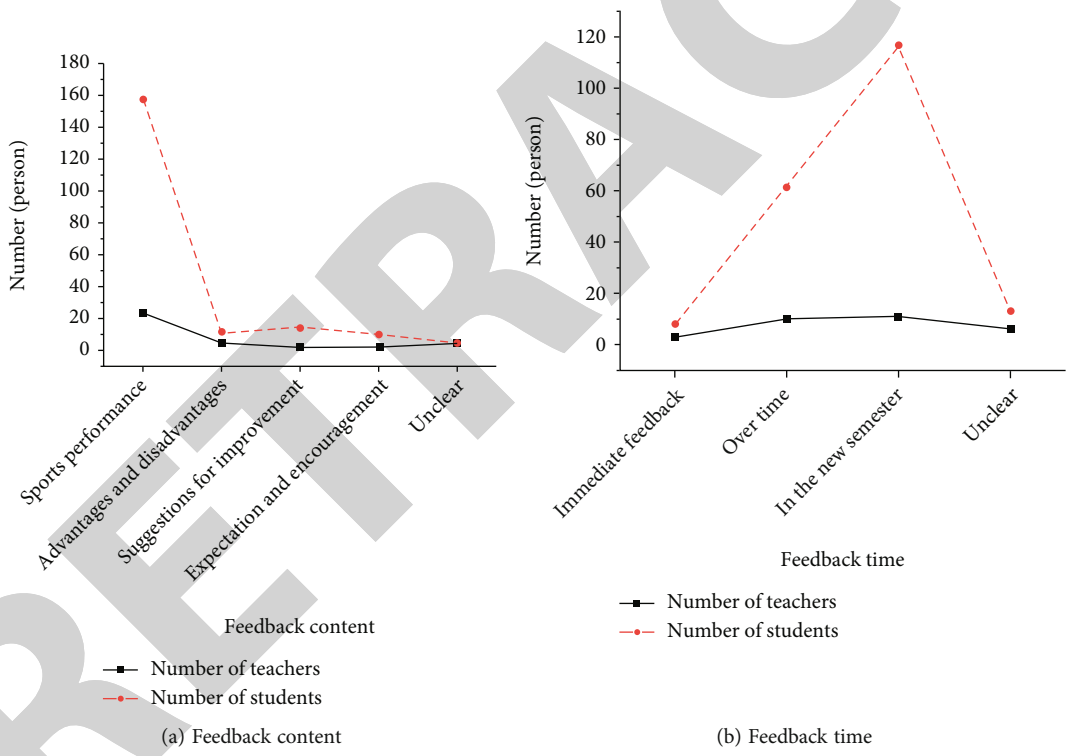

Figure 10: Feedback.

relatively simple, so it is difficult to define their advantages and disadvantages in the feedback of students, and students only focus on their own results. From the perspective of feedback time, the feedback is mainly conveyed to students after a long period of time or at the beginning of the new semester, so the feedback is not timely. Furthermore, students mainly obtain the feedback of the evaluation results of PE teaching through network.

4.5. Construction of Evaluation System of College PE. In the activities of evaluating students' PE teaching, PE teachers are the subject of evaluation, and students are the object of evaluation. The evaluation of students by PE teachers is the most real, direct, and persuasive. PE teachers are the most vocal on the situation of students' PE learning. So, when evaluating students' PE teaching, the evaluation of PE teachers is the main part. PE teachers can login the teacher system to evaluate the PE teaching of students in the class.

According to the analysis of the current situation of college PE teaching evaluation and the principle of evaluation system design, combined with the characteristics of

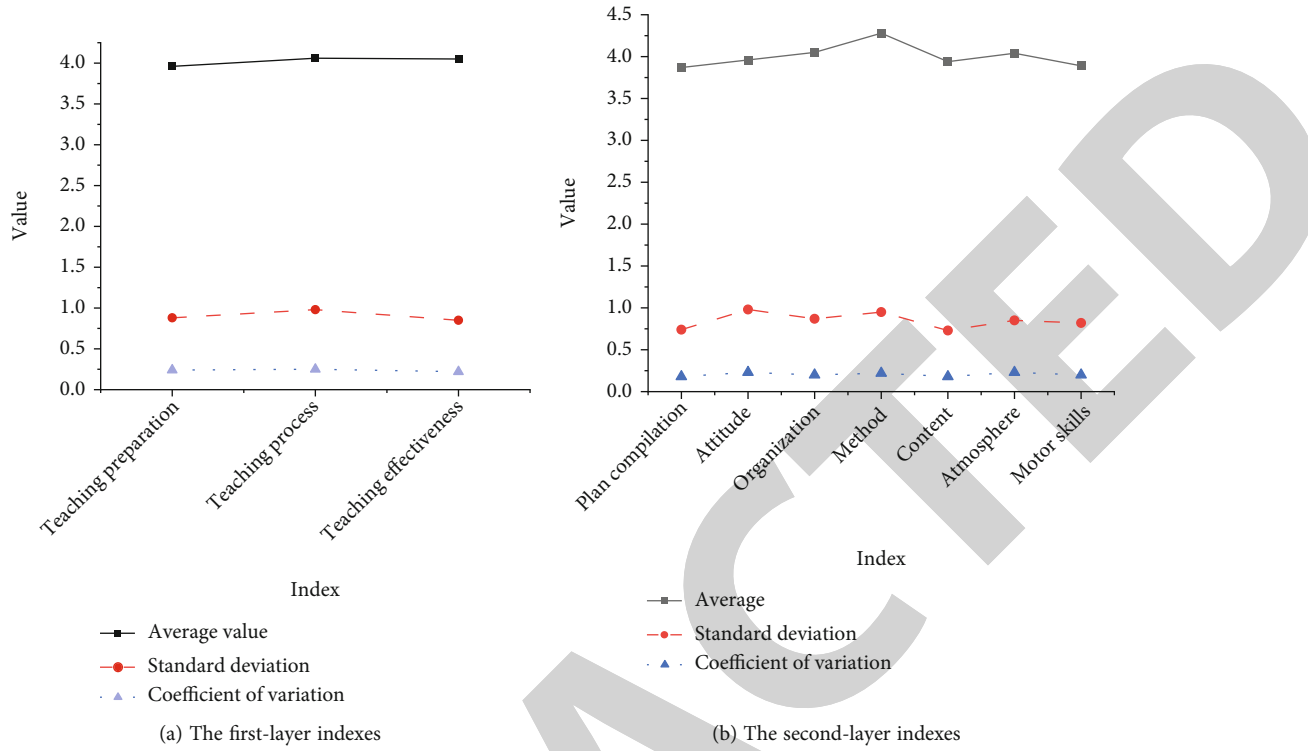

(a) The first-layer indexes (b) The second-layer indexes

Figure 11: The first-round analysis of the PE teaching evaluation indexes for PE teachers.

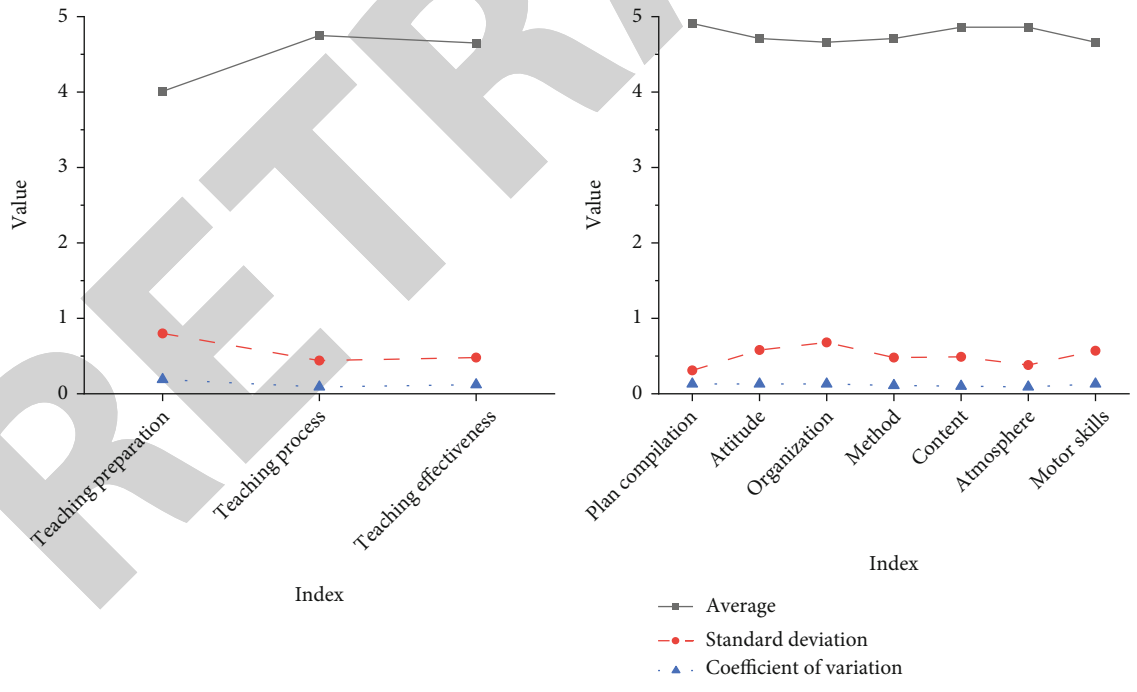

(a) The first-layer indexes (b) The second-layer indexes

Figure 12: The second-round analysis of the PE teaching evaluation indexes for PE teachers.

big data information fusion and data mining technology, the evaluation index system of students' PE teaching and PE teachers' teaching evaluation index system are designed. The evaluation index system includes two parts, the first layer index and the second layer index. The specific indicators are as follows. Firstly, Figure 11 displays the first round of analysis on the teaching evaluation index of sports teachers.

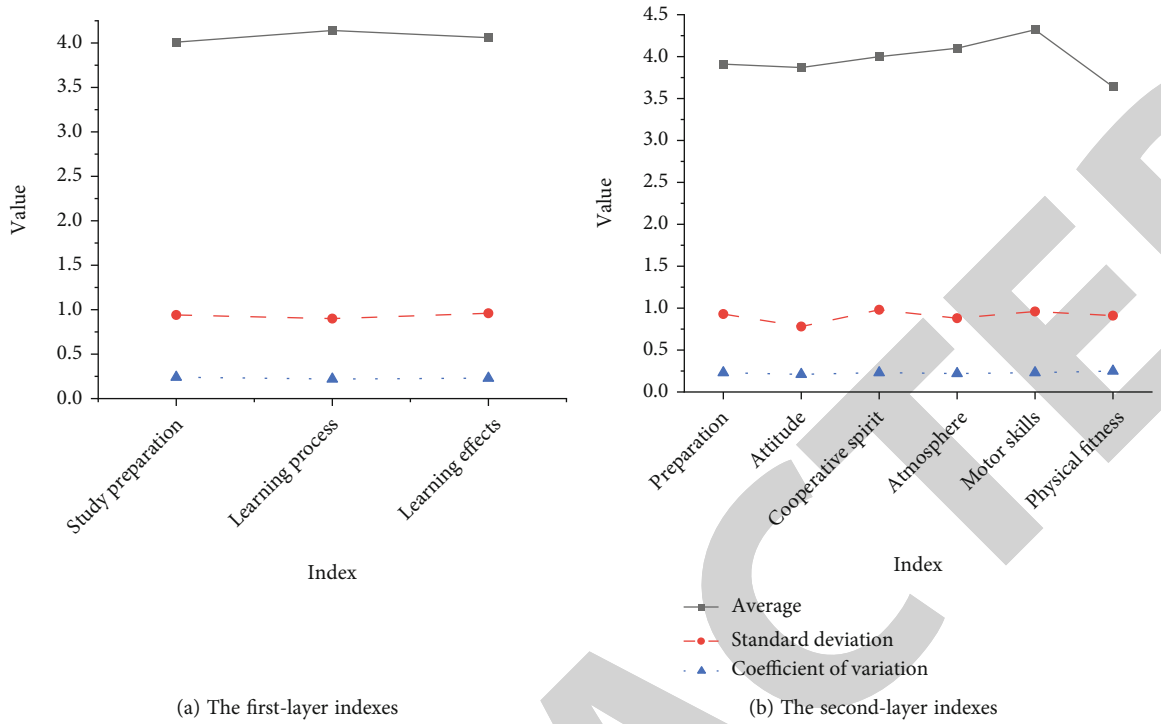

(a) The first-layer indexes (b) The second-layer indexes

Figure 13: The first-round analysis of the PE teaching evaluation indexes for students.

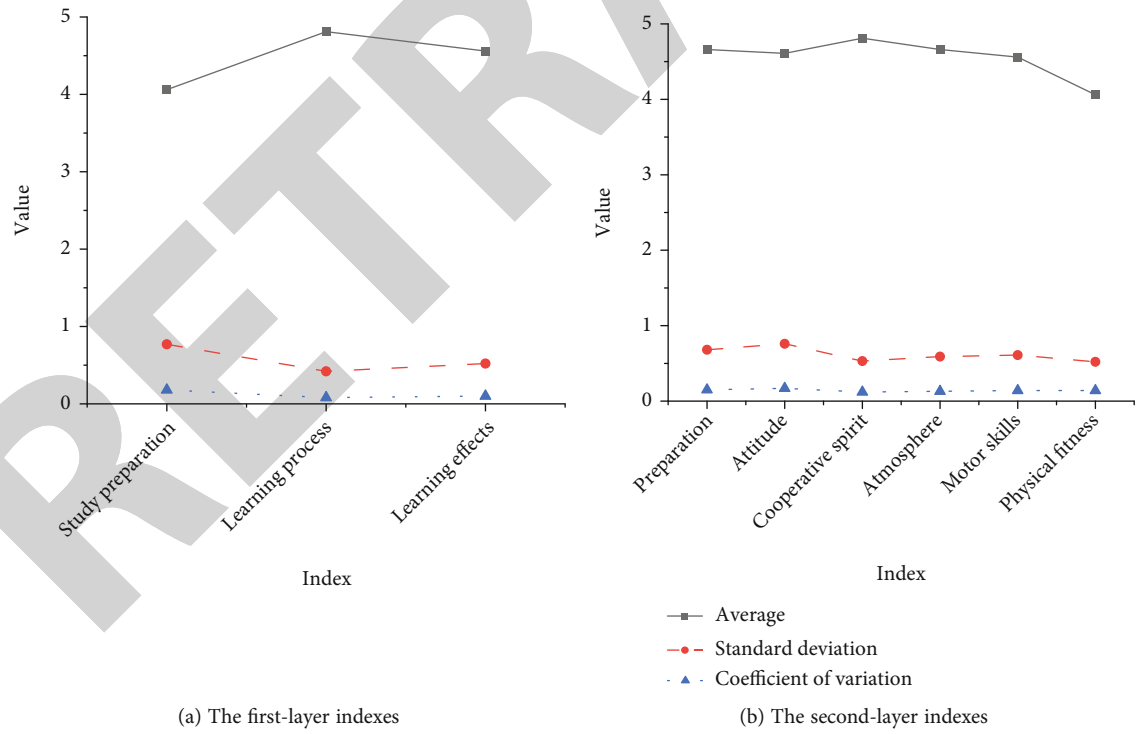

(a) The first-layer indexes (b) The second-layer indexes

Figure 14: The second-round analysis of the PE teaching evaluation indexes for students.

According to Figure 11, the coefficients of variation of three first-layer indexes are all below 0.25, and the average is above 3.9, so it is reasonable. In addition, the average score of teaching preparation is the smallest, and the coefficient of variation of teaching process is the largest, indicating that corresponding improvements should be made in teaching preparation and teaching process. The mean value of the second-layer indexes is greater than 3.8, and the coefficient

of variation is less than 0.25, demonstrating that the second-layer index setting is reasonable. The second-round analysis of the PE teaching evaluation indexes is obtained by adjusting the teaching preparation and teaching process, as Figure 12 shows.

Figure 12 shows that compared with the first round, the indexes of the second round have changed significantly. The mean value of the first-layer indexes is greater than 4, and the coefficient of variation is close to 0.2, which again verifies that the indexes of the second layer are set reasonably. Therefore, the first-layer indexes of the college PE teaching evaluation system for teachers based on big data technology are ultimately determined as teaching preparation, teaching process, and teaching results. Besides, the second-layer indexes include the preparation before class, teaching attitude, teaching organization, teaching methods, teaching content, classroom atmosphere, and sports ability of PE teachers.

Figure 13 presents the first-round analysis of the PE teaching evaluation indexes for student.

Figure 13 concludes that the coefficient of variation of the three first-layer indexes is less than 0.25, and the mean value is more than 4, so the first-layer indexes of the PE teaching evaluation for students are reasonable. Among the second-layer indexes, the mean value of physical quality is smaller than evaluation indexes, which requires reasonable adjustment. Moreover, the coefficient of variation of physical quality is equal to 0.25. Experts pointed out that physical fitness index includes physical quality, so these two items should not exist in parallel. In summary, the physical quality of the second-layer indexes needs to be improved. Figure 14 signifies the second-round analysis of the PE teaching evaluation indexes for students after adjustment.

According to Figure 14, compared with the first round, the indexes of the second round have changed significantly. The mean value of the first-layer indexes is greater than 4, and the coefficient of variation changes smaller, which again verifies the reasonable setting of the first-layer indexes. Therefore, the first-layer indexes of the PE teaching evaluation system for college students based on big data technology are finally defined as learning preparation, learning process, and learning effects. Meanwhile, the second-layer evaluation index system includes preparation before class, learning attitude, classroom atmosphere, sports ability, and physical quality.

5. Conclusion

Under the background of big data information fusion and data mining technology, the definition of sports evaluation index is put forward by analyzing the principles and characteristics of the construction of sports teaching evaluation system in colleges and universities. Based on the questionnaire survey, analyzation is made the evaluation content and evaluation system of college PE. Big data information fusion and data mining knowledge are combined to determine the evaluation index, which essentially reflects the various elements of PE teaching process. The distribution of index weight is more scientific and reasonable, and the evaluation system of PE teaching in colleges and universities is constructed. Colleges and universities are more objective and scientific than the existing system. The application of big data information fusion and data mining in college PE teaching evaluation is proved to be possible. The evaluation process includes data collection, data analysis, result generation, and feedback. The evaluation results should be accurate, and the feedback on the evaluation results should be timely and open. Each section in the whole process is an indispensable part. The results show that the average values of the first-level indicators are above 4, and the coefficient of variation is less than 0.2, which can basically reflect the content of PE teaching evaluation and provide some reference for the research of PE teaching evaluation. Due to the influence of the actual experimental conditions, the selected research samples are limited and not enough to cover the subject comprehensively. In the later study, the samples will continue to be expanded and analyzed, and more factors will be considered in the follow-up.

Data Availability

The labeled datasets used to support the findings of this study are available from the corresponding author upon request.

Conflicts of Interest

The author declares that there are no competing interests.

References

[1] T. Xia, "Based on big data college physical education teaching evaluation system research," *Journal of Physics Conference Series*, vol. 2021, no. 3, article 032010, 2021.

[2] W. Xie, "Based on big datacollege physical education teaching evaluation system research," *Journal of Physics: Conference Series*, vol. 1744, no. 3, article 032008, 2021.

[3] W. Hu and L. Ye, "Impact of big data technology on the diversity of physical education teaching methods," *Journal of Physics: Conference Series*, vol. 1744, no. 4, article 042205, 2021.

[4] J. Shao and X. Cheng, "Sea level height based on big data of internet of things and aerobics teaching in coastal areas," *Arabian Journal of Geosciences*, vol. 14, no. 15, pp. 1–15, 2021.

[5] F. Liu, "The reform of college physical education teaching methods under the background of big data," *Journal of Physics Conference Series*, vol. 1744, no. 3, article 032005, 2021.

[6] L. Wang and M. Wang, "Application of MOOC in physical education teaching mode under the background of big data," *Journal of Physics: Conference Series*, vol. 1744, no. 4, article 042233, 2021.

[7] J. Zhang, "Reform and innovation of artificial intelligence technology for information service in university physical education," *Journal of Intelligent and Fuzzy Systems*, vol. 40, no. 1, pp. 1–11, 2017.

[8] X. Zhao and C. Zheng, "Fuzzy evaluation of physical education teaching quality in colleges based on analytic hierarchy process," *International Journal of Emerging Technologies in Learning*, vol. 16, no. 6, p. 217, 2021.

Hindawi
Journal of Sensors
Volume 2021, Article ID 7889380, 13 pages
https://doi.org/10.1155/2021/7889380

Research Article

Aerobics Movement Decomposition Action Teaching System Based on Intelligent Vision Sensor

Liwei Sun

Sports Department, Xi'an Aeronautical University, Xi'an, 710077 Shaanxi, China

Correspondence should be addressed to Liwei Sun; 201007008@xaau.edu.cn

Received 27 August 2021; Revised 14 October 2021; Accepted 26 October 2021; Published 13 November 2021

Academic Editor: Mu Zhou

With the development of the times, teaching has not only stayed between people, but also gradually developed into the teaching interaction between man and machine. In the past, the teaching form was relatively single and old. Based on the intelligent visual sensor, this paper develops an auxiliary teaching system for the decomposition of aerobics action and reasonably uses the Internet and algorithms to catalog a series of aerobics action systems into the system. The DTW dynamic motion matching algorithm of the system will recognize human actions more accurately. The system will feed back human actions to the system in real time based on human feature recognition. Then, after comparison, the system will display the standard posture of this action and the aerobics posture in the next step. Therefore, this system develops teaching not only in class, but everywhere. The system not only improves the teaching quality of aerobics, but also strengthens the physical quality of teenagers. It has a new understanding of the standardization of aerobics teaching. After the function of the system is complete, the system will be distributed to aerobics learners. In many feedback information, the average use satisfaction has reached about 80%, which is a good performance index for the performance of the system itself.

1. Introduction

The physical health of students has gradually become the focus of public attention, and the concept of putting health first is thoroughly implemented. Effectively strengthen school physical education and encourage students to actively participate in sports activities. The National Standards for Student Physical Fitness and Health issued by the country clearly requires universities to conduct physical fitness tests on students every year. The "health quality and standards" of students at all levels improves people's living standards and raises health awareness, which is essential to promote the development of physical fitness testing systems. After meeting the needs of people's lives, people will pay more attention to physical fitness. With the rapid development of technologies such as networks, computers, and digital communications, other countries have entered the intelligent stage in the field of physical fitness testing. Start slowly to test the physical fitness test data, ignoring the complexity and the difficulty difference between the two in the data collection test process.

Computer-aided instruction (CAI) is a method and technology for discussing teaching content, the teaching process, and teaching of training students in a computer-assisted conversation mode. CAI covers a wide range of computer technologies such as artificial intelligence, multimedia, and databases. It makes up for the shortcomings of traditional one-sided and one-sided teaching methods and provides students with a good personal learning environment. The use of CAI can effectively improve teaching quality, reduce learning time, improve the efficiency of teaching and learning in these two fields, and achieve the most appropriate educational goals. In the current teaching of aerobics, there is a problem that students cannot have an intuitive impression of the teaching content of movement, rhythm, music, difficulty, coordination, etc., and specific analysis of the structure of the movement process, as well as the overall perceptual understanding of the complete set of movements. CAI and intelligent vision sensors the combination can be effectively solved. The intelligent image sensor clearly displays the difficult points and key points of healthy gymnastics teaching from multiple

angles. This makes aerobics education more vivid and effective, which helps to cultivate students' attention and enthusiasm for exercises. The design and development of CAI aerobics education project not only involves the transformation of aerobics teaching methods and teaching methods, but also affects the development of aerobics teaching style and teaching theory.

The research on the recognition of aerobics movements based on visual sensors is still in the theoretical stage of the laboratory, and we still need to make a certain amount of reference to other people's theories. Vision-Sensoren builds a high-speed intelligent vision sensor that integrates image acquisition and processing. The use of FPGA makes the image processing hardware, which greatly improves the speed of image acquisition and processing. The use of DSP enables the sensor to have its own CPU and perform some complex calculations. However, due to its greater flexibility, it is not suitable for general conditions [1]. Kettering realized the high-precision measurement of car body, continuously improved the level of visual inspection technology, studied the core part of the visual sensor, and analyzed the key technology of intelligent digital visual sensor, but the research did not enter a deeper theoretical discussion [2]. Zidek et al. use FPGA to implement the underlying image processing algorithm, which significantly speeds up the image processing speed and enhances the sensor performance. This design realizes the intelligentization and networking of the visual sensor and has great application value. However, because this design has developed too much quality and did not pay attention to the speed of transmission, the theory still needs to be studied [3]. Poornima et al. have carried out research on the related technology of intelligent digital vision sensor. The sensor uses fast template matching algorithm as the core and integrates the functions of image acquisition, feature coarse positioning, control decision-making, and digital information transmission to promote the detection system from analog. For signal transmission, the centralized processing mode of the central computer is converted to the digital signal transmission and the distributed processing mode of each node, which further improves the stability, real-time performance, and measurement accuracy of the system, but this theory is difficult to put into practice [4]. Shanthi studied the design of ODVS, embedded Linux ODVS system structure, ODVS video server, and ODVS application system software development, and elaborated on the specific application of the ODVS-based multi-target automatic tracking system, but the application cost is too high. There is no actual development value [5]. Suh et al. use linear scanning technology to obtain the scanning information of the object and cluster it into laser images according to the structural characteristics of the scanning information. The color vector of the laser image is extracted according to the storage arrangement method, and the edge structure of the object to be recognized is obtained through the nonlinear convolution operation to realize the edge detection of the laser image. Finally, the machine vision and laser image information point matching method is discussed. Based on the symmetry feature detection principle, the matched false information points are eliminated, and the remaining information points are output as the recognition result, but the final detection result does not reach the expected theoretical effect [6]. Harfmann proposed the use of MB-LBP texture features combined with radial basis functions as the kernel function SVM for face recognition and conducted a number of comparative experiments on the common Yale and ORL data sets. The experimental results show that the algorithm can be very good. Complete face recognition of intelligent robot vision. For face images with large illumination changes, reducing the number of iterations reduces the time complexity of face recognition, but it reduces the accuracy of the algorithm [7].

The design of this system is aimed at the shortcomings of actual aerobics teaching courseware and has developed functional modules including online courseware learning, online courseware arrangement, exchange forums, in-station message exchange, and content search. In the design of the system, this article describes and recognizes the movement characteristics of the human body and feeds the information back to the system, so that the system can provide real-time guidance and teaching for aerobics learners. The system's DTW dynamic action matching algorithm more accurately recognizes human actions. The system is based on human body feature recognition and feeds the human actions back to the system in real time. Then, the system will display the standard posture of this action after comparison and will perform the next step of bodybuilding. The posture will also appear, and the system has achieved a breakthrough in remote and man-machine teaching.

2. Introduction to the Aerobics Movement Recognition Theory Method

2.1. Theories of Body Movement Recognition Methods in Aerobics. Through training and learning to recognize aerobics movements, the computer can understand the meaning of a person's movements in a specific scene in the video. Figure 1 shows several basic processes of aerobics movement recognition, including information acquisition, preprocessing, representation, and description, and the two most important parts of classification and recognition are feature extraction and description and classification and perception. Both of these processes convert complex video data types into attributes in the form of arrays, vectors, and values containing motion data and then use classifiers to identify and classify these attributes [8–10].

The characterization and modeling of human motion is an important step in the process of perceiving human motion. The source video data consists of a series of continuous images, and each image contains a point of RGB value. Only by correctly mapping the source data can the granularity, and sensitive attributes contained in the data be produced. The current behavior methods can be divided into human body structure models, from the perspective of the structure and characteristics of motion, according to the human body model and behavior of motion.

Smart vision sensor is a highly integrated microminiature machine vision system. It is the fastest growing new technology in the field of machine vision in recent years. It

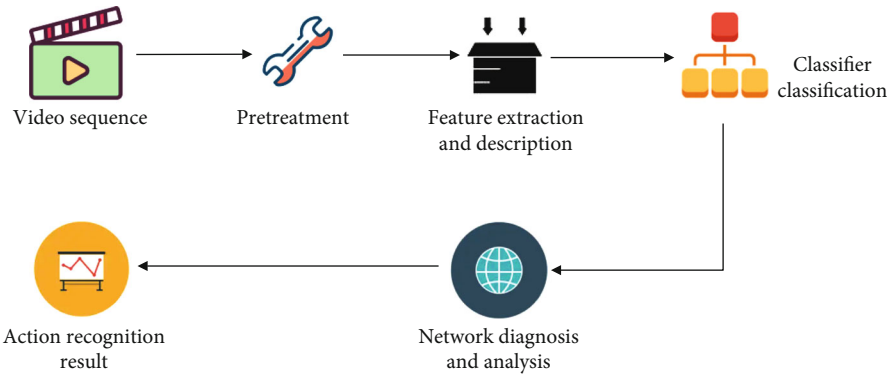

Figure 1: The basic process of human action recognition.

integrates image acquisition, processing, and communication functions into a single camera, thereby providing a machine vision solution that is multifunctional, modular, highly reliable, and easy to implement [11].

Pattern matching is one of the most common basic pattern recognition algorithms, refers to the alignment of two images. Image matching technology for the same target (or multiple images) in space is widely used in navigation, aerospace technology, and other industries and fields. Common gray-scale image matching methods such as target recognition and scene intrusion include gray-scale matching methods and feature-based matching methods. Gray matching method is generally point-to-point matching, so the relative accuracy is relatively high, and it is very sensitive to changes in interference [12, 13]. When the external light changes, the detection result will be affected. At the same time, it is very complicated from a computational point of view, and rotation, deformation, and occlusion are all subtle. The selected attributes include points, lines, borders, and textures. Resist external light changes by isolating certain characteristics. Scale changes and rotation changes then use these features to match methods to make it stable. In the coordinate distribution in the image, first preset the exposure of a coordinate point (x, y) in the image at time $t\, I(x, y, t)$ so that $u(x, y)$ and $v(x, y)$ can be regarded as points (x, y) when the motion decomposition vectors in the x and y axis directions are decomposed, respectively. In a very short time differential dt, the point (x, y) is shifted to the pixel coordinate $(x + dx, y + dy)$, and $dx = udt, dy = vdt$, which represents the relationship between the spatial gray scale of the image and the optical flow velocity [14]. Table 1 is a list of parameters taken under different video sensors under the matching method.

In the optical flow constraint equation, both u and v are unknown. And there is only one constraint equation, so the luminous flux cannot be uniquely determined. Other constraints must be added to define u and v. The introduction of different constraints will lead to different methods of calculating luminous flux [15]. The most classic is the gradient optical flow algorithm, also known as the differentiation method. Most of them are based on the gradient function of the gray image to get the motion vector of each pixel in the image. In the process of image template matching, due to some perspective distortions between the image to be matched and the template image, there are some partial and complete nonmatching phenomena. How to filter out these situations and how to measure the difference between the image to be detected and the template similarity of the distance matrix D are as follows:

$$Q = q_1, q_2 \cdots\cdots, q_n, \tag{1}$$

$$C = c_1, c_2, \cdots\cdots c_n, \tag{2}$$

$$D = \begin{matrix} d(q_1, c_1) & d(q_1, c_2) \cdots\cdots & d(q_1, c_n), \\ d(q_2, c_1) & d(q_2, c_2) \cdots\cdots & d(q_2, c_n), \\ d(q_n, c_1) & d(q_n, c_2) \cdots\cdots & d(q_n, c_n). \end{matrix} \tag{3}$$

The path of the curve is defined as follows: at two distances of different time series D, the path of curve W is defined as a series of continuous matrix elements with different relationships between time series:

$$W = \{w_1, w_2, \cdots\cdots w_n\}. \tag{4}$$

The curved path satisfies the following constraints:

(1) Boundedness

$$\text{Max}\,(m, n) \le k \le m + n - 1 \tag{5}$$

(2) Boundary conditions

$$w_1 = D(1, 1), w_k = D(n, m) \tag{6}$$

(3) Continuity

$$w_1 = D(i, j), w_{k-1} = D(O, P), I - O \le 1, J - P \le 1 \tag{7}$$

(4) Monotonicity

It is not allowed to appear at the same time.

$$I - O \le 1, J - P \le 1. \tag{8}$$

Table 1: Comparison of detection at different width thresholds.

Width threshold	Fixed threshold (5 pixels)	Template width of 1/3	Template width of 1/2	Template width 2/3
Foreign body (≤2 cm)	6589	5489	5784	5995
Foreign body (2~8 cm)	1520	1621	1425	1236
Foreign body (>8 cm)	1868	1896	1758	1851

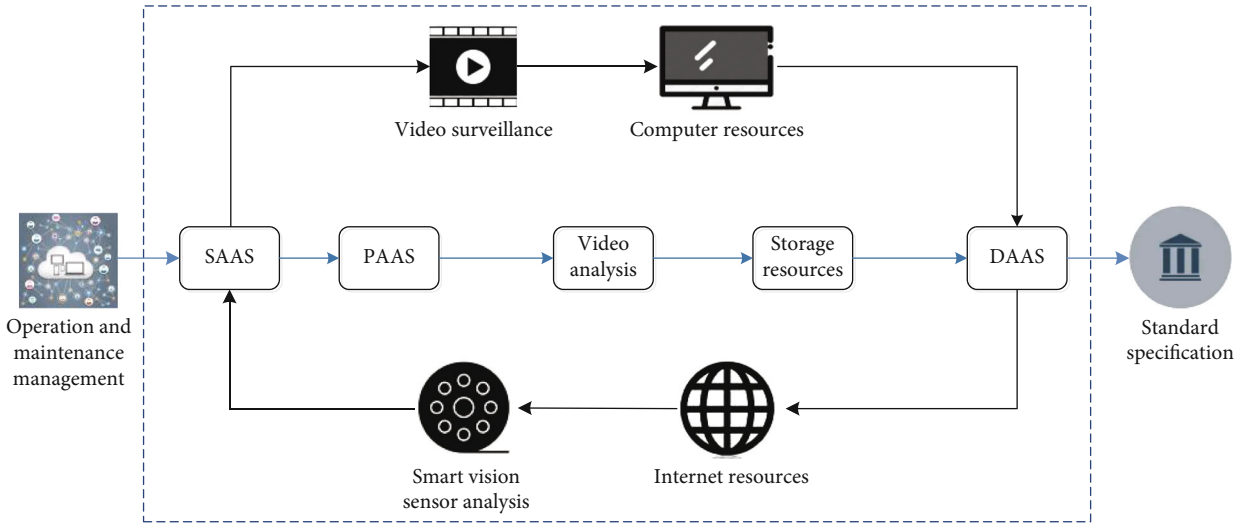

Figure 2: Framework diagram of the action collection system.

Therefore, after the above definition, find the iterative formula of the optimal path.

The motion recognition of aerobics is developed on the basis of intelligent visual sensors, using the combination of network real-time monitoring and visual sensors. The framework diagram designed is shown in Figure 2.

As an aerobics framework system, there are three main users in the aerobics teaching system: student users, teacher users, and management users. Among them, the main purpose of student users is to complete the study and review of the courseware; feedback the corresponding information to the teacher according to the mastery of the courseware; communicate with classmates and teachers. Learning experience or problems encountered in the study.

2.2. Body Movement Characteristics of Aerobics. Human body characteristics are the description of the appearance of human motion. Usually, the region of the moving human body should be identified in some key frames in the image sequence, individual textures, borders, contours, and other information [16, 17]. It is a feature model that calculates behavioral features and attributes to be measured. Pattern spacing is used to identify human behavior. This method can combine most of the image sequence data shown in Figure 3 for aerobics contour sequence. In order to describe the motion of the human body as a whole, Bobick and his colleagues superimposed the contours of the human body area to create a motion energy image (MEID) that can show the effect of motion and use dynamic functions to create motion to reflect the execution of the human body. The historical image of time (MHI) shows the generalization of recognition of human behavior. This method has a certain degree of durability as the shooting angle changes. Similarly, Huang Feiyue and others also perceive behaviors that have nothing to do with vision. It also uses cameras with different perspectives to capture the shape of the human body and calculate the "containment form."

There are six scientific methods to improve your body: weight-bearing exercise, interval training, repetitive exercise, continuous exercise conversion training, and comprehensive training. Choosing a comprehensive training method is a good way to develop a balanced body. This kind of aerobics exercise uses a comprehensive training method. Combine repetition and continuous exercises to organize student exercises. The overall content of the training is shown in Table 2.

The main content of the exercise program is self-made aerobics combined with strength exercises and flexibility exercises, and self-made aerobics uses low-impact actions and high-impact actions to be mixed and edited. The ten-week training is divided into three stages, the first stage, the second stage, and the third stage. In the three stages, the exercise load intensity will gradually increase, and the training will be carried out comprehensively, and the result is shown in Figure 3 [18].

The appearance of human body characteristics includes all the processes of human movement, which can provide complete information for action recognition, and the calculation process is relatively simple. However, the appearance of the human body depends on the image processing, such as precise background removal effect, too much positioning

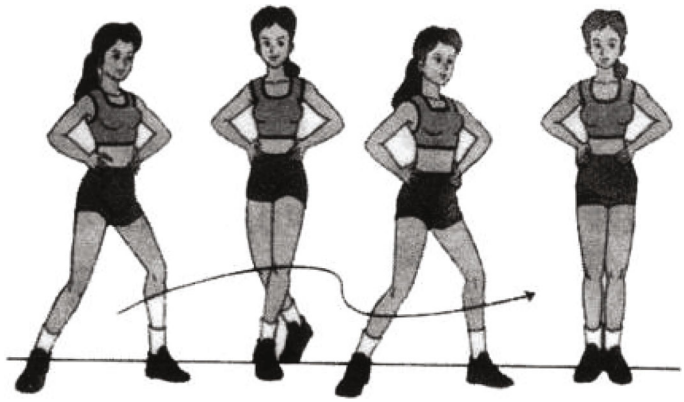

Figure 3: Schematic diagram of aerobics.

Table 2: The overall content and schedule of training.

Stage	First stage	Second stage	Third stage
Main activity content	1. Warm up 2. Slow-paced aerobics contact 3. Quality exercises	1. Warm up 2. Midrhythm aerobics contact 3. Quality exercises	1. Warm up 2. Fast-paced aerobics contact 3. Quality exercises
Time	3 weeks, 3 lessons per week. 45 minutes per class	3 weeks, 3 lessons per week. 45 minutes per class	4 weeks, 3 lessons per week. 45 minutes per class

and tracking of moving targets. When the background environment is complicated, the viewing angle will change, which in turn affects the description of the action [19, 20]. In order to implement a more systematic and reasonable teaching method and in order to verify the effectiveness of visual representation training in the early stage of aerobics skill learning, this article adds visual representation to the learning of aerobics skills.

2.3. DTW Dynamic Matching Action Recognition Algorithm. Whether the stereo matching algorithm can achieve better results mainly depends on three factors, including matching primitives, matching criteria, and matching algorithms. Among them, the stereo matching algorithm is a crucial part. The stereo matching algorithm is actually a process of finding the optimal solution, which determines the parallax of the pixel by solving the extreme value of an energy cost function. The stereo matching algorithm can realize different classifications according to different standards. Classification based on matching primitives can generally be divided into local-based stereo matching, global-based stereo matching, and feature-based stereo matching. Based on the size of the optimization range, stereo matching algorithms can be divided into local stereo matching and global stereo matching. Based on the density of the generated disparity map, it can be divided into sparse disparity matching and dense disparity matching. This article introduces several commonly used stereo matching algorithms, including the following: feature-based stereo matching, local stereo matching, and global stereo matching [21]. The factors affect the matching algorithm, from a large perspective, and the selected language has a great impact on the efficiency of the algorithm. Generally speaking, more time and space were required to use the higher-level language. In addition, the quality of the code produced by different compilers is different, which will also have an impact on the efficiency of the algorithm.

The feature-based stereo matching algorithm refers to the disparity obtained by matching some features in the image. The features in an image usually involve points, lines, and geometric regions. The point feature is the most important feature. When using feature point matching, the feature point needs to be extracted before matching, and the extracted feature point must be clearly distinguishable from other pixels, so as to ensure the accuracy of parallax. This matching method is simple to implement, fast in matching speed, and has good real-time performance. However, since the matching effect is mostly dependent on the selection of feature points, the requirements for feature point selection are very high, and the effect is not ideal in some areas with slow gray-scale changes or weak texture areas. Since the number of feature points is small, the disparity map obtained is a sparse disparity map, so after this kind of matching, an interpolation algorithm is often needed to obtain a denser disparity map [22].

This system uses the DTW algorithm to locate and describe the human body features. The system's positioning is compared with the actual human body features, and then, the system will make corrections to give the correct self-contained algorithm.

$$T = \{T(1),\cdots,T(m),\cdots,T(M)\}, \tag{9}$$

$$R = \{R(1),\cdots,R(n),\cdots,R(N)\}. \tag{10}$$

It can be expressed as follows:

$$T(M) = \{\theta_{t1}, \theta_{t2}, \cdots, \theta_{tx}\}, \tag{11}$$

$$R(N) = \{\theta_{r1}, \theta_{r2}, \cdots, \theta_{rx}\}. \tag{12}$$

According to formula (12), perform TFS code conversion on these 100 peak responses, where r represents the address number, ri is the peak response of the i-th address number, ti is the input time of the i-th address number of the neural network, and T is the expectation time of the last neuron input. In the feature sequence, the algorithm of the system is as follows:

$$P = (k_i, l_i), i = 1, j = 1, \cdots, M, \tag{13}$$

$$k_1 = l_1 = 1, \tag{14}$$

$$k_M = l_M = M, k_i < k_{i+1}, l_i < l_{i+1}. \tag{15}$$

From this, it can be deduced that the distance difference between the human body feature and the system algorithm is shown in the following formula:

$$d\left[T\left(l_j\right), R(k_i)\right] = \sum_{n=1}^{x} k_n \left\| \theta_{rn,l_j}, \theta_{tn,k_j} \right\|, \tag{16}$$

$$D[T, R] = \sum_{k_i, j_i \epsilon P} d\left[T\left(l_j\right), R(K_i)\right], \tag{17}$$

$$\mathrm{DTW}[T, R] = \min D[T, R], \tag{18}$$

$$\overrightarrow{ES} = \left(S_X - e_x, s_y - e_y\right), \tag{19}$$

$$\overrightarrow{EH} = \left(h_X - e_x, h_y - e_y\right). \tag{20}$$

The DTW algorithm is used to optimize the recognition response of the algorithm in recognizing human body aerobics actions. When the human body makes a series of exercise cycles, the simplified diagram of the optimal path of the system's feedback algorithm is shown in Figure 4.

Among them, the abscissa is the time series of the characteristic matrix. The name is the standard bone data timeline. The dotted line represents the optimal matching path, that is, the path with the greatest similarity. The weighted Euclidean distance is used to calculate the appropriate route in the area to calculate the similarity of the nodes in the graph. According to the formula, find the most similar time the sequence coordinates are compared to find the most suitable path as shown in the figure above [23].

3. Aerobics Teaching Assistant System and Simulation

3.1. Teaching System Framework. The technical architecture of the system can be divided into five layers. The Kinect data acquisition layer uses the Kinect smart camera to collect the depth images of the human body, human bone images, and human color images and transmits these data to the layout algorithm processing layer as video stream data. The algorithm processing layer filters this data. For DTW data and model matching, the processed bone node data is matched to the motion perception layer, and the results and results of the motion detection are displayed on the application layer. The frame structure of the system test system is shown in Figure 5.

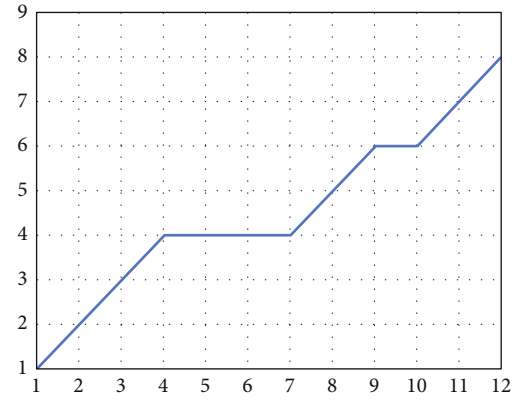

Figure 4: DTW shortest path diagram.

Action recognition is a process of judging continuous events. In actual applications, in order to achieve the purpose of recognition and improve the efficiency of the task, it is necessary to constrain the execution point and execution interval of the judgment to avoid purposeless and repetitive recognition. At the same time, an important prerequisite for action recognition in practical applications is real-time detection of human action areas. In addition, in view of the importance of the action feature extraction step in the current action recognition process, visually presenting the action features extracted by different feature extraction algorithms for action recognition as a reference is also an important aspect in the application of action recognition [24, 25]. Based on the above observations, the action recognition application based on the service robot platform selects three starting points: exploring the effects of related action feature extraction algorithms, detecting human movements in real time, and recognizing human movements in a certain time interval. In order to accomplish the above goals, this chapter will design the software interface module, video control module, feature extraction module, and feature analysis module of the motion recognition application system to realize the experiment of motion recognition application; at the same time, use the motion recognition application software system to select applications experiment with scenes to analyze related algorithms.

As a CAI system, aerobics teaching system has three users: student users, teacher users, and management users. The main purposes of student users are as follows: to complete the learning and review of courseware, to give feedback corresponding information to teachers according to the learning and mastery of courseware, and to exchange learning experience or problems encountered in learning with classmates and teachers. The main purposes of teacher users are as follows: compiling new courseware content, improving the content of courseware through students' feedback information, answering questions to students, and

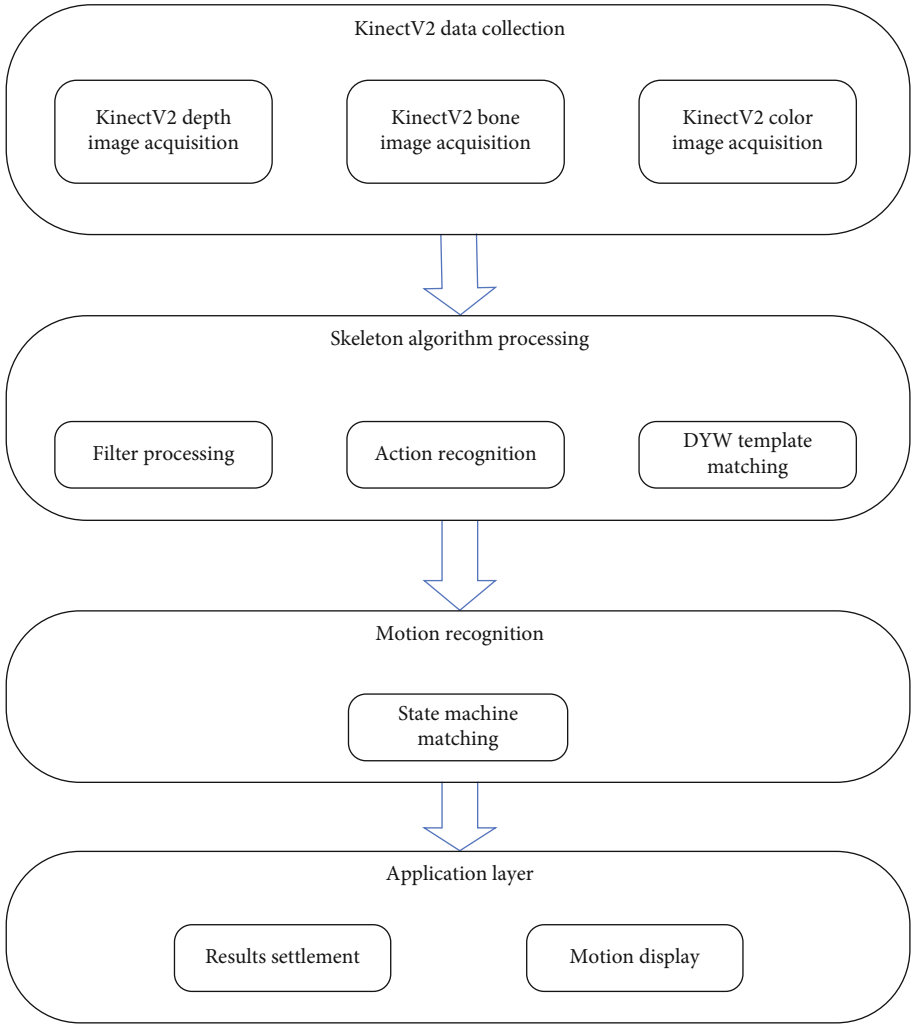

Figure 5: The frame structure of the physique test system.

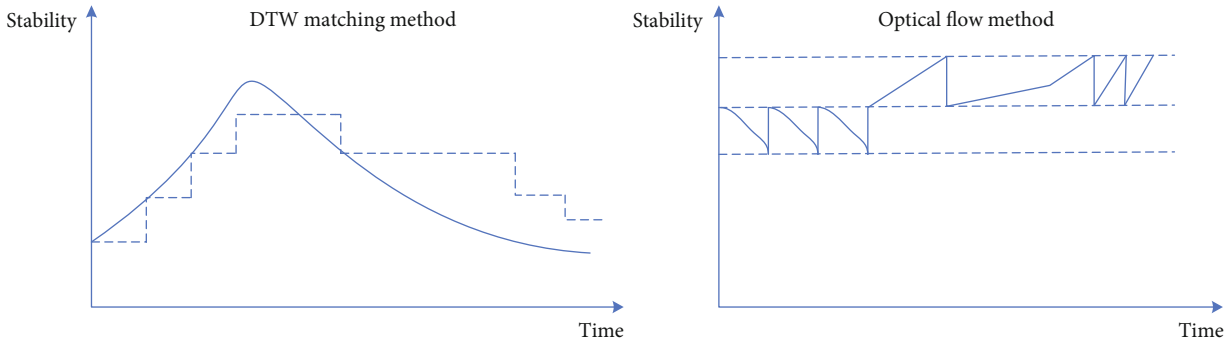

Figure 6: System stability comparison chart.

exchanging teaching experience with each other. The main purpose of managing users is to maintain system parameters and manage system users. The following systems use different methods for simulation experiments. The stability comparison of the simulation system is shown in Figure 6.

3.2. Calisthenics Action Recognition Experiment. In the algorithm based on feature point matching, the extraction of feature points is the foundation work. In order to realize the purpose of analyzing human motion, the extracted feature points must be pixels that can characterize human motion. According to the theory of topological vision, early human vision starts from a wide range of properties, and topological structure can be used as a description of this property. Among them, the human skeleton is of great significance for describing the three-dimensional information

and topological structure of the human body, so this paper selects the human skeleton points as the matching feature points [26, 27]. First, extract the skeleton of the binarized image of the target detection. The main idea of skeleton extraction is to set the refinement conditions in advance and traverse the pixels in the input binarized image in turn to determine whether each point meets the setting. If the conditions are met, then mark. After the entire image is traversed, all the marked points are finally deleted. The first pixel stripping is completed, and then, the above process is repeated until the entire image no longer changes. What is obtained at this time is the target skeleton diagram. The algorithm maintains the topological structure of the target area, while reducing the complexity of subsequent processing. Tensor Flow is a second-generation artificial intelligence learning system developed by Google for machine learning and deep neural network research. Its name comes from its operating principle, that is, by constructing a data flow graph, data of tensor type is constructed. Transfer calculations in the flow graph.

When performing action recognition, this paper uses a support vector machine classifier to classify the gradient feature transformation characterization operator based on decoding. Among them, the decoding algorithm uses the interface function provided by the VLFeat library, and the support vector machine uses the interface function provided by the LibSVM library. Decoding algorithm is a process of using a specific method to restore the digital to the content it represents or to convert electrical pulse signals, optical signals, radio waves, etc. into the information, data, etc. it represents. Decoding is the process by which the receiver restores the received symbols or codes to information, which corresponds to the encoding process. Although the gradient feature can only accurately segment the relatively fixed action of the visual scene, in order to verify its temporal and spatial representation characteristics of the action, in addition to the KTH and Weizmann databases, the experiment also selected the UCF sports database with a certain change in the scene perspective as a benchmark [28].

For the three distinct movements of squatting, opening and closing, and standing, the recognition rate has reached more than 98%; for the two similar actions of standing and opening and closing, the recognition rates are only 88.1% and 85.5%. Squat is partly similar to one-knee squat and small jump, and the recognition rate is 90.2%. The average recognition rate of algorithms based on gradient transformation features in the KTH database is 94.37%. Table 3 compares the average recognition rates of different methods.

From the effect of action recognition, compared with other popular methods, the algorithm in this paper has strong competitiveness in recognition rate. One of the important reasons is that the algorithm efficiently extracts the spatial features of the gradient and deeply explores the temporal and spatial relationships of the spatial features of the gradient. At the same time, the settings of the default parameters have also been verified by many experiments [29].

This chapter conducts experiments on the matching algorithm network model constructed on the DTW data set. Figure 7 shows the matching algorithm model constructed in this paper under the DTW data set, using only the original gray data and adding the frame difference channel to the human body action recognition accuracy curve in the figure, the solid line represents the matching algorithm model constructed in this paper without the frame difference channel, and the dotted line represents the matching algorithm model with the frame difference channel added. After adding the frame difference channel, the network reached a high accuracy rate in the first few iterations of training, the error dropped quickly, and it soon began to converge. Under the action of the frame difference channel, the network quickly captured the human behavior characteristics, while the network that did not use the frame difference channel had to find the available features in the original image by itself and gradually learned the human behavior characteristics after dozens of rounds of training [30]. Introducing a visual attention mechanism into the DTW algorithm can improve the accuracy of human behavior recognition.

Table 3: Comparison of average recognition results on KTH using different methods.

Method	Average recognition rate (%)
Derpanis etc.	88.96
Cao etc.	91.25
Laptev etc.	90.16
Le etc.	90.47
The algorithm of this paper	93.58

3.3. Aerobics Experiment Simulation. The test subjects were tested before the experiment, and the subjects were divided into intervention groups and control groups according to natural classes when there were no significant differences in the indicators of the subjects. The intervention group performed the training specified in the system exercise program of this article within ten weeks, and the control group did not do any intervention training except for physical education classes in accordance with the school syllabus. After the experiment was completed, all the experimental subjects were tested again, and the indicators of different groups were compared and analyzed, and a conclusion was reached [31].

The main content of the exercise program is self-made aerobics combined with strength exercises and flexibility exercises, and self-made aerobics uses low-impact movements and high-impact movements for mixed creation. The ten-week training is divided into three stages, the first stage, the second stage, and the third stage. The exercise load intensity of the three stages will gradually increase. Comprehensive training: the main content of this program is self-compiled aerobics with a total of 10×8 movements. The rhythm is controlled by system music or passwords. The movements are novel, but simple and easy to learn. Specific action content: all students stand in four horizontal rows. The first 8 beats are in situ running motions, with the arms swinging naturally; the second 8 beats are foot-to-ground motions with the arms extended to the side; the third 8 beats are a "one" step, and the arms are forward and natural,

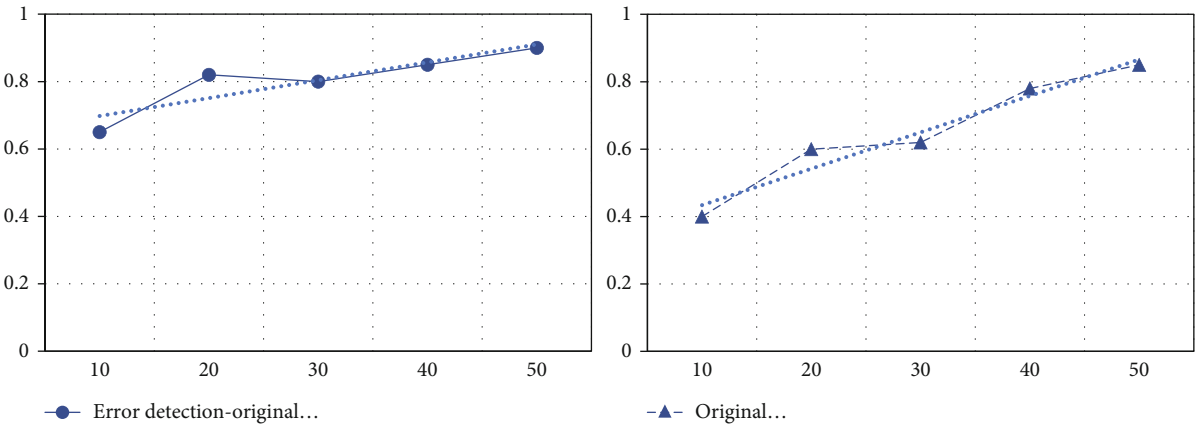

Figure 7: Recognition accuracy curve of dual-channel 3D convolutional neural network model.

respectively. Put down the action; the fourth 8th beat is a side step, and the arms are opened and closed according to the beat; the fifth 8th is a "V" step, and the arms follow the feet to make a pose; the sixth eight beats up step knee and leg movements; the seventh eight beats for kicks; the eighth eight beats for knees and legs jumps; the ninth eight beats for pony jumps; the tenth eight beats for running and jumping. This set of self-programming can jump continuously, and the system arranges the jump mode. The system uses passwords and music speed to control the exercise intensity [32].

According to the requirements of the syllabus and aerobics assessment and evaluation standards, the golden aerobics scoring standard is adopted. Due to the needs of this experimental study, the technical assessment is carried out by the way that the students do actions by calling out the password. The scoring content mainly includes six aspects: basic posture, movement proficiency, movement accuracy, movement range and strength, movement coordination, and movement rhythm and expressiveness. According to the grading rules, three professional teachers with aerobics first-level referee certificate will score the three classes under the same conditions and take the middle value of the three teachers as the final score. Use Polar meter to track and monitor students' exercise intensity during exercise, and record students' subjective movement feelings. The fourth stage: after the experiment is completed, the staff who organizes the pretest test will perform the postexperiment test of the various indicators on the experimental object.

The key to the exercise of sit-ups is the state action of sit-ups. The ratio of the scores between the supine state and the sit-up state is b1 : b2. Take a sit-up test cycle as an example. The full score of each sit-up exercise cycle is m. In actual conditions, m is 100 points. Assuming that the tester has completed n squats, the standing state similarity is g, and the sit-up state similarity is k, and the final score S is obtained according to the formula.

These three experimental classes are composed of three groups: experimental group, interference group, and control group. The experimental group is arranged for the usual aerobics training through the aerobics movement decomposition teaching system designed in this article, while the other two groups are composed of coaches and self-

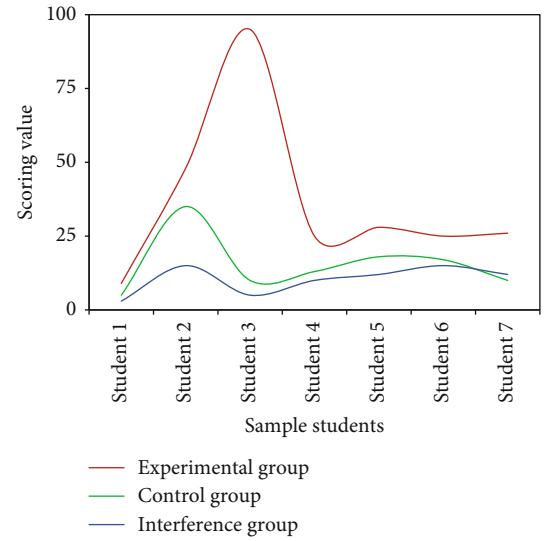

Figure 8: The scores of students' aerobics in different experimental groups.

learning. There are two ways to learn aerobics to learn aerobics movements. Figure 8 shows the scores of the above three groups.

Because aerobics can significantly increase the strength of the respiratory muscles, improve the elasticity of the lungs, increase and deepen the depth of breathing, and improve the efficiency and function of lung breathing. In the process of aerobic exercise, a lot of breathing air is required to breathe in. During exercise, the muscle contraction ifi surgery requires a lot of oxygen. The demand for oxygen increases, the number of breaths is more than normal, and the lungs contract more. Long-term exercise enhances the functioning capacity of the lungs.

The scheme is designed to monitor during training, and the combination of the two methods is used. It can be seen from Table 4 above that the exercise intensity gradually increases from the first stage to the third stage in the whole training process of the scheme. The data heart rate value in Table 4 shows that the exercise load of the scheme is medium, and the exercise sensation level of the athlete is

Table 4: Comparative analysis of the final assessment results of students in the three experimental classes learning new technical movements.

	Average	Standard deviation	t value	p value
Experiment 1	7.598	0.365	4.021	$0 < (0.05)$
Experiment 2	8.598	0.289	4.215	$0 < (0.05)$
Experiment 3	7.145	0.314	4.587	$0 < (0.05)$

between 12 and15, indicating that the load intensity is reasonable, so the exercise scheme is reasonable. This size also shows that the exercise intensity is medium, and the relative intensity is about 40%-60%. Relevant studies have shown that aerobics is a low-intensity and long-term exercise, the exercise intensity is medium or above, the heart rate range is 60%-85% of my maximum heart rate, the maximum heart rate = 200 – self age, and the ages of junior two students are between 13 and 15 years old. Therefore, this sports program is fully in line with the characteristics of aerobics. This kind of training can enhance people's cardiopulmonary endurance, improve people's cardiovascular function, enhance people's vital capacity and heart function, and lose weight and fat.

4. Experimental Results and Analysis

4.1. Stability Analysis of Aerobics Teaching Action Decomposition System. System testing is the last stage studied in this subject, and it is also the most critical link to ensure the quality of system design. It requires the use of various testing methods to detect the completeness of system functions and the efficiency of system execution. Here, the system is inspected mainly through function test, performance test, and example test. The main purpose of functional testing is to judge whether the various modules and functions designed in the system analysis process can work normally and to find and solve the problems encountered in the process of coding and design. For the functional test of the system, the main focus is on the following aspects:

(1) *User Login Function*. Verify whether the user's login function is normal, whether the user can be redirected to the specified user interface, and whether illegal user login can be rejected.

(2) *Courseware Learning and Feedback Function*. Verify whether student users can browse courseware types normally and whether various contents provided by regular learning courseware can be fed back to teacher users normally.

(3) *Courseware Layout Function and Feedback Query*. Verify whether teacher users can normally edit courseware containing text, images, sound, and video content and whether the layout function of the courseware is perfect: verify whether the feedback information of student users on the courseware can be checked normally.

(4) *User Management Function Verification*. Verify whether the administrator user can normally add, delete, and modify various user categories and user information.

(5) *Verification of the Communication Function*. Verify whether the messages in the station can be sent and received normally, and verify whether the exchange forum can normally post and reply normally.

In accordance with the above test requirements, the login, use, communication, and management functions of the system were carefully tested one by one, and the problems that appeared in the test were corrected and improved to ensure the reliability of the system's operation. Figure 9 below is a comparison diagram of the system response time for the predicted stability and actual stability of the system.

Obviously, it can be seen from Figure 9 that in the comparison, the reaction time of the system in this article is not much different from the expected response time, which shows that the reaction time of the system still meets the expected requirements and expectations when the actual system is used. Generally speaking, due to the complexity of human movements, the accuracy of training-based motion detection methods is greatly affected by training samples, and the algorithm efficiency is low, but the detection accuracy is not affected by background changes. Motion detection based on gradient transformation projection has better reliability in practical application scenarios where the background changes little, but it has a poorer detection effect for motion video with large background changes.

4.2. Analysis of the Aerobics Teaching System in Actual Use. The aerobics teaching system of this article will be distributed to 100 aerobics learners, and 100 aerobics learners will learn aerobics by themselves or by multimedia. After one stage of learning feedback, Figure 10 shows the feedback of the above 100 users.

From a physiological point of view, these data change, students participate in a certain period of planned exercise training, and after a long period of exercise, the coordination ability of the receptors will gradually increase; therefore, the balance ability will increase; training makes the cerebral cortex excited during exercise state, and the neural connection speed of the cerebral cortex will become rapid and accurate, so the agility will be improved. However, in the aerobics exercise program, there is no systematic training content designed for balance quality and reaction speed, so there is no significant difference in the changes of related indicators. This system is only aimed at the systematic teaching of the decomposition teaching of aerobics movements. According to the satisfactory responses of the teaching experimenters, most users still have a relatively good evaluation of the system, with a satisfaction rate of about 80%. It makes users more interested in aerobics training and more confident in their own learning ability. The purpose of adolescent fitness exercise is to promote the growth and development of the body and enhance the quality and health of the body. According to the law of growth and development of

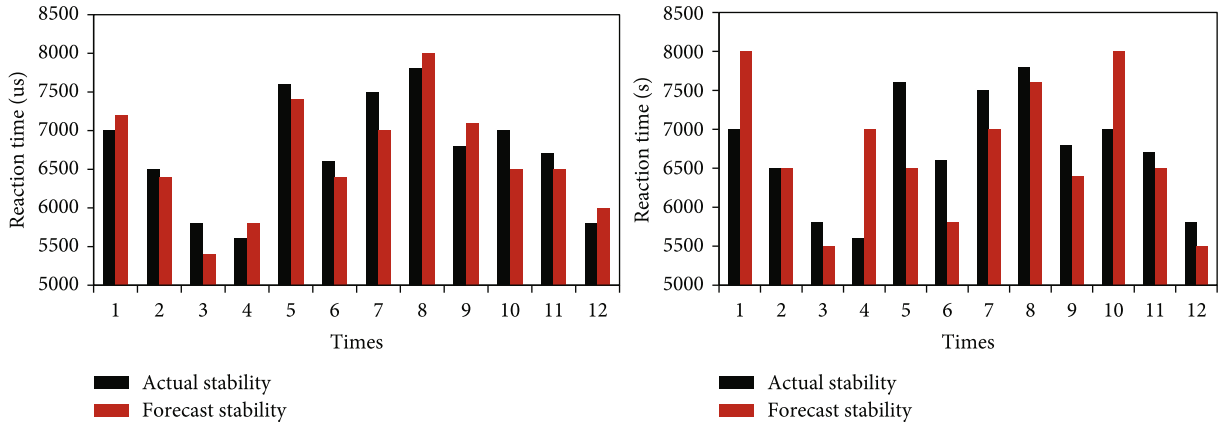

Figure 9: System response time comparison chart.

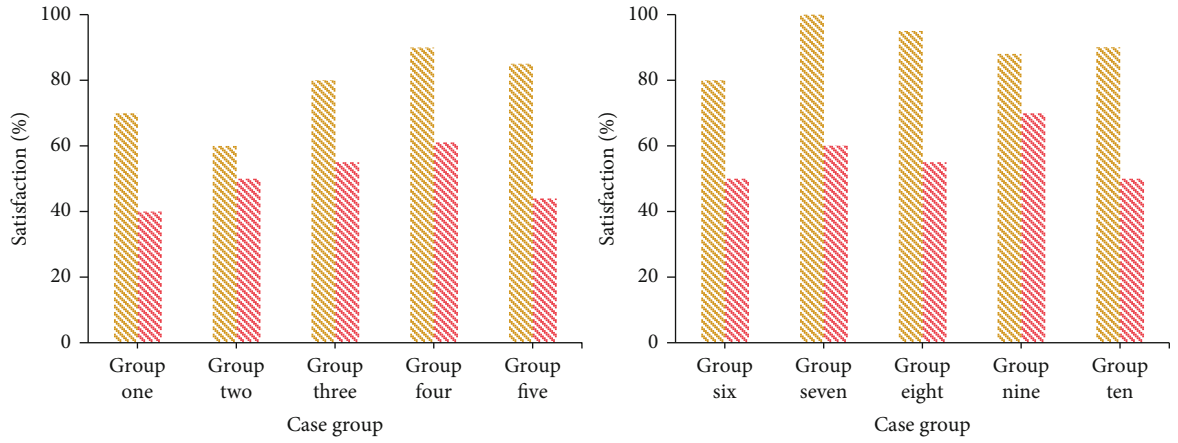

Figure 10: Use satisfaction survey.

adolescents, the main indicators that can effectively reflect the fitness effect are body shape, physical function, physical fitness, and other indicators. Therefore, the aerobics teaching system in this article effectively solves the social embarrassment of young people facing people before teaching. It is a good idea to reach an agreement between the interaction between man and machine and teaching.

5. Conclusion

Based on intelligent vision, this paper develops an auxiliary teaching system for the decomposition of aerobics movements. The aerobics teaching system based on the B/S structure has basically been designed and can be put into use. The design of this system is aimed at the shortcomings of actual aerobics teaching courseware and has developed functional modules including online courseware learning, online courseware arrangement, exchange forums, in-station message exchange, and content search. The algorithm of the aerobics system is designed through the DTW matching algorithm, so that the fluency of the system meets the basic requirements in normal operation. In the design of the system, this article describes and recognizes the movement characteristics of the human body and feeds the information back to the system, so that the system can provide real-time guidance and teaching for the aerobics learners. After a later simulation of the system and a survey on crowd use, the average satisfaction of the system reached 80%, and the level of aerobics learners has been greatly improved, indicating that the feedback on the use of the system is still relatively to a certain extent OK. Although this system has realized the functions necessary for basic aerobics teaching, it still has a certain distance compared with a perfect CAI system. Moreover, the development of domestic aerobics teaching CAI has just started, and there will be some in the future. More and more excellent development ideas and development methods appear. To get a fully functional aerobics CAI system, more manpower and material resources need to be invested.

Data Availability

No data were used to support this study.

Conflicts of Interest

There are no potential competing interests in our paper.

Authors' Contributions

The author has seen the manuscript and approved to submit to your journal.

Acknowledgments

This work was supported by the Project of Social Science Foundation of Shaanxi Province in 2020: "Research on the development path of aerobics dance in Shaanxi Province from the perspective of Healthy China" (No. 2020Q003).

References

[1] Bernd and Eckenfels, "Vision-Sensoren vereinfachen die einrichtung von pick-and-place-anwendungen: direkte kommunikation mit dem roboter," *Elektro-Automation: Elektrotechnik + Elektronik Inder Industrie*, vol. 71, no. 6, pp. 70-71, 2018.

[2] S. Lee, G. Tewolde, J. Lim, and J. Kwon, "Vision based localization for multiple mobile robots using low-cost vision sensor," *International Journal of Handheld Computing Research*, vol. 7, no. 1, pp. 12–25, 2016.

[3] K. Zidek, V. Vasek, J. Pitel, and A. Hosovsky, "Auxiliary device for accurate measurement by the smart vision system," *MM Science Journal*, vol. 2018, no. 1, pp. 2136–2139, 2018.

[4] J. Poornima, J. Vishnupriyan, G. K. Vijayadhasan, and M. Ettappan, "Voice assisted smart vision stick for visually impaired," *International Journal of Control and Automation*, vol. 13, no. 2, pp. 512–519, 2020.

[5] K. G. Shanthi, "Smart vision using machine learning for blind," *International Journal of Advanced Science and Technology*, vol. 29, no. 5, pp. 12458–12463, 2020.

[6] J. Suh, S. You, S. Choi, and S. Oh, "Vision-based coordinated localization for mobile sensor networks," *IEEE transactions on automation science and engineering*, vol. 13, no. 2, pp. 611–620, 2016.

[7] B. Harfmann, "Ensuring safety through sensor solutions," *Beverage Industry*, vol. 107, no. 7, pp. 42-43, 2016.

[8] N. Rossol, I. Cheng, and A. Basu, "A multisensor technique for gesture recognition through intelligent skeletal pose analysis," *IEEE Transactions on Human-Machine Systems*, vol. 46, no. 3, pp. 350–359, 2016.

[9] M. Zhou, Y. X. Long, W. P. Zhang et al., "Adaptive genetic algorithm-aided neural network with channel state information tensor decomposition for indoor localization," *IEEE Transactions on Evolutionary Computation*, vol. 25, no. 5, pp. 913–927, 2021.

[10] G. I. Lee, C. M. Kang, S. H. Lee, and C. C. Chung, "Sensor fusion based on the particle filter and multi-rate Kalman filter," *Journal of Institute of Control*, vol. 23, no. 11, pp. 969–980, 2017.

[11] M. Zhou, Y. M. Wang, Z. S. Tian, Y. Lian, Y. Wang, and B. Wang, "Calibrated data simplification for energy-efficient location sensing in Internet of Things," *IEEE Internet of Things Journal*, vol. 6, no. 4, pp. 6125–6133, 2019.

[12] M. Weigel, H. Fiedler, and T. Schildknecht, "Scoring sensor observations to facilitate the exchange of space surveillance data," *Advances in Space Research*, vol. 60, no. 3, pp. 531–542, 2017.

[13] J. W. Kim, Y. D. Jung, D. S. Lee, and D. H. Shim, "Landing control on a mobile platform for multi-copters using an omnidirectional image sensor," *Journal of Intelligent & Robotic Systems*, vol. 84, no. 1-4, pp. 529–541, 2016.

[14] A. Kuzdeuov, M. Rubagotti, and H. A. Varol, "Neural network augmented sensor fusion for pose estimation of tensegrity manipulators," *IEEE Sensors Journal*, vol. 20, no. 7, pp. 3655–3666, 2020.

[15] E. Joshi, D. S. Sasode, N. Singh, and N. Chouhan, "Wireless sensor network application for precision agriculture," *Research Today*, vol. 2, no. 5, pp. 125–128, 2020.

[16] R. Verma and K. Srivastava, "Middleware, operating system and wireless sensor networks for Internet of Things," *International Journal of Computer Applications*, vol. 167, no. 11, pp. 11–17, 2017.

[17] X. Sun, A. Basu, and I. Cheng, "Multi-sensor motion fusion using deep neural network learning," *International Journal of Multimedia Data Engineering and Management*, vol. 8, no. 4, pp. 1–18, 2017.

[18] S. Hensel, "Machine vision als integraler bestandteil der automation," *Elektrotechnische Zeitschrift*, vol. 138, no. s5, pp. 48–51, 2017.

[19] J. A. Lenero-Bardallo, P. Hafliger, R. Carmona-Galan, and A. Rodriguez-Vazquez, "A bio-inspired vision sensor with dual operation and readout modes," *IEEE Sensors Journal*, vol. 16, no. 2, pp. 317–330, 2016.

[20] L. Wang, W. Song, Y. Lan et al., "A smart droplet detection approach with vision sensing technique for agricultural aviation application," *IEEE Sensors Journal*, vol. 99, 2021.

[21] L. Chermak, N. Aouf, M. Richardson, and G. Visentin, "Real-time smart and standalone vision/IMU navigation sensor," *Journal of Real-Time Image Processing*, vol. 16, no. 4, pp. 1–17, 2016.

[22] F. Ortega-Zamorano, M. A. Molina-Cabello, E. López-Rubio, and E. J. Palomo, "Smart motion detection sensor based on video processing using self-organizing maps," *Expert Systems with Application*, vol. 64, no. Dec., pp. 476–489, 2016.

[23] Y. Wu, Y. Wang, W. Hu, and G. Cao, "SmartPhoto: a resource-aware crowdsourcing approach for image sensing with smartphones," *IEEE Transactions on Mobile Computing*, vol. 15, no. 5, pp. 1249–1263, 2016.

[24] B. G. Lee and M. L. Su, "Smart wearable hand device for sign language interpretation system with sensors fusion," *IEEE Sensors Journal*, vol. 18, no. 3, pp. 1224–1232, 2018.

[25] M. Behrens, K. Müller, J. I. Kilb et al., "Modified step aerobics training and neuromuscular function in osteoporotic patients: a randomized controlled pilot study," *Archives of Orthopaedic and Trauma Surgery*, vol. 137, no. 2, pp. 195–207, 2017.

[26] W. Zheng, "Experimental study on aerobics teaching model based on cognitive flexibility theory," *Aerobics & Fitness*, vol. 1, no. 1, pp. 1–5, 2016.

[27] Y. Ma, "Cultivation of the ability of creating and arranging aerobics in physical education majors," *World Scientific Research Journal*, vol. 5, no. 9, pp. 88–93, 2019.

[28] S. Tonstad, P. Herring, J. Lee, and J. D. Johnson, "Two physical activity measures: Paffenbarger physical activity questionnaire versus aerobics center longitudinal study as predictors of adult-onset type 2 diabetes in a follow-up study," *American journal of health promotion*, vol. 32, no. 4, pp. 1070–1077, 2018.

[29] M. Ebrahimi, T. N. Guilan-Nejad, and A. F. Pordanjani, "Effect of yoga and aerobics exercise on sleep quality in women with

type 2 diabetes: a randomized controlled trial," *Sleep Science*, vol. 10, no. 2, pp. 68–72, 2017.

[30] G. Ali Sholi, M. Ghanbarzadeh, A. Habibi, and R. Ranjbar, "The effects of combined exercises intensity (aerobics-resistance) on plasma cortisol and testosterone levels in active males," *International Journal of Basic Science in Medicine*, vol. 1, no. 1, pp. 18–24, 2016.

[31] W. Bei, "Research on body language in aerobics choreography and physical education based on network questionnaire," *International Journal of Future Generation Communication and Networking*, vol. 9, no. 4, pp. 207–218, 2016.

[32] N. Garrido, J. D. Silva, J. S. Novaes, M. S. Cirilo-Sousa, and G. R. Neto, "Effect of water aerobics on the quality of life, satisfaction, and perception of body image among elderly women," *Journal of Exercise Physiology Online*, vol. 19, no. 5, pp. 30–37, 2016.

Hindawi
Journal of Sensors
Volume 2021, Article ID 2000879, 10 pages
https://doi.org/10.1155/2021/2000879

Research Article

Reliability Analysis of Intelligent Electric Energy Meter under Fusion Model Illness Analysis Algorithm

Wenwang Xie,[1] Leping Zhang,[1] Bensong Zhang,[1] Wei Zhang,[1] Pingping Wang,[2] and Shuya Qiao[2]

[1]*Digital Grid Research Institute, CSG, Guangzhou 510700, China*
[2]*Zhejiang Chint Instrument & Meter Co., Ltd., Hangzhou 310052, China*

Correspondence should be addressed to Shuya Qiao; shuyaqiao@126.com

Received 13 August 2021; Revised 14 September 2021; Accepted 4 October 2021; Published 13 November 2021

Academic Editor: Mu Zhou

This work is aimed at solving the morbidity problem of the smart meter fusion model and improve the measurement accuracy and reliability of the smart meter. Starting with the topology of the smart meter, the reason for the serious morbidity of the smart meter model is discussed. First, the basic process of power system state estimation of smart meters is introduced, and the concept of error analysis of smart meters is clarified. Then, the causes and mechanisms of the ill-conditioned problems of the smart meter model are analyzed, and methods to reduce the morbidity of the smart meter calculation model are analyzed. Finally, a data optimization algorithm based on a greedy strategy and an improved Tikhonov regularization method is proposed. The model data is processed and optimized to reduce the morbidity of the smart meter measurement model. The results show that the analysis algorithm for reducing the morbidity error of the smart meter proposed in this study can effectively interfere with the morbidity of the smart meter calculation model. The processing effect shows that it can reduce the measurement error of the smart meter to about 5%, which is an order of magnitude lower than the error before processing, and the processing effect of the least square method is improved by more than 70%. From the perspective of processing speed, when the user number is between 50 and 100, the running time of the algorithm ranges between 1.5 and 3.5 s, which can be fully adapted to the actual situation and has strong practicability. In short, this study is helpful in improving the accuracy and reliability of smart meter calculations and provides a certain reference for related research.

1. Introduction

The smart meter is one of the basic equipment for data collection in the smart grid, and it plays a very important role in the entire smart grid. It is responsible for collecting, measuring, and transmitting raw electric energy data, and for information synthesis, analysis, optimization, and display [1, 2]. In addition to conventional electric meters' basic electric energy measurement functions, smart meters also have two-way multirate metering functions, user-side control functions, and two-way data communication functions [3]. As a powerful sensor terminal, the smart meter plays an essential role in the identification layer of the smart grid. It needs to perform detailed calculations and metering of electric energy for charging. In addition to supplementing energy billing based on smart meter measurement data, it can also enable and support advanced applications, such as energy consumption behavior analysis, demand response strategy design, and electricity market pricing. The normal operation of the smart grid is guaranteed through the comprehensive operation of these functions [4, 5]. Therefore, whether the smart meter measures electric energy is directly related to the normal operation of the functions as mentioned above. It is also closely related to the vital interests of each user who participates in the use of electricity. Once the smart meter fails, it may affect the transmission and distribution of electric energy, bring troubles to people's lives, and even cause serious losses. Due to the massive and scattered distribution of smart meters, it is very difficult to determine the status of each meter in operation to find and

replace expired or faulty individuals. However, if it is not ruled out and replaced directly in a large area, it will cause a lot of waste of human resources and materials [6, 7].

At present, the common method used to check the status of electric energy meters is sampling verification. The International Organization for Metrology (OIML) established the TC3/SC4 working group to create relevant documents to measure whether private electricity meters can still be used. However, the faults of smart meters are diverse, and it is difficult for sampling verification methods to ensure that all types of faulty meters are tested without omission, which will inevitably cause losses to residents [8, 9]. Some scholars tried to analyze the statistical data of smart meters to find the faults and operating errors of the energy meters. This method of identifying faults in smart meters through data can theoretically realize "full-range state monitoring of energy meters." However, after it is put into practical application, many errors will be caused due to the influence of the external complex environment and technical means. There are still many technical issues that need to be further studied and resolved. It is mainly reflected in difficulty in obtaining the loss calculation parameters of the station area as well as the poor model conditions, which lead to calculation errors and the inability to form sufficient reference values [10].

Based on the above analysis, the cause and mechanism of the serious morbidity model of the actual smart meter circuit measurement error analysis are analyzed, and methods to weaken the morbidity are discussed. A regularization method based on data preprocessing and improvement is proposed to intervene in the morbidity of the model. In addition, the least square method is introduced as a control group to carry out a simulation experiment to verify the effectiveness of the data preprocessing method, hoping to improve the error calculation accuracy of the electric energy meter.

The remainder of this paper is organized as follows. Section 2 presents some related theories and methods about smart meters. Section 3 considers algorithm verification results and the discussion. Finally, Section 4 provides some concluding.

2. Related Theories and Methods for the Study of Morbidity Models of Smart Meters

2.1. Analysis of Topological Structure Model of Electric Energy Error. The origin of power system state estimation research is traced back to 1970. With the maturity of electronic technology and the development of computer communication technology, power system measurement technology has also been further developed and improved. The related research and application of state estimation have become common, which has become an indispensable part of the power system [11]. It is responsible for helping transmission network operators to obtain real-time status information of the power system, while providing corresponding services for power users. At this stage, estimating the state of the power system is also one of the research hotspots of power energy management systems. It involves functions such as state estimation, data error management, and information prediction. The specific process is illustrated in Figure 1 [12, 13]. In addition, the state estimation of the power system also includes a reliability analysis and static safety analysis. Today, with the rapid development of network communication technology, the Internet of Everything has become a normal state. Moreover, data has also become a silent language. In 2019, Shen et al. [14] conducted bilingual text mining and analyzed the trend of *Online to Offline* business from the perspective of social media. The results of bilingual text mining were compared according to company, region, service app, and operating mode. The research provides important insights from crowd intelligence and reveals an analysis of recent trends in the development of *Online to Offline* in different language regions. Many needed information can be obtained through data analysis and mining. Therefore, the security control of network power data and the network has become more important. The general electrical topology is illustrated in Figure 1.

With the rapid development of computer technology and communication technology, the concepts of "smart city" and "smart transportation" have emerged one after another. In addition, in terms of power detection and management, new concepts such as smart meters and smart management systems have also emerged [15]. Remote online verification of smart meters in low-voltage stations is essential for maintaining the power grid. It can ensure the stable operation of users' rights and interests and reduce operating costs and power consumption [16, 17]. However, due to the serious morbidity of the fusion model, the calculation result of the smart meter has a large error, and there are still many uncertain data. The existence of these problems greatly reduces the accuracy of smart meters [18]. The focus of this research is on the serious ill-posed problems of the error analysis model of smart meters. Therefore, the causes and mechanisms of error in mathematical models and ill-conditioned models are analyzed to explore a method to reduce the ill conditions of computational models. The research mainly focuses on smart meters, and the electrical topology of smart meters is illustrated in Figure 2.

In Figure 2, the high-precision energy metering smart meter is used as a total meter to accurately measure the entire system's electrical energy and power consumption. Smart meters are installed on the user side of each residence [19, 20]. In the actual energy consumption information collection system, the measured value of the total table is defined as the energy consumption of the total station, which is because the accuracy of the total meter in the station area is higher than the accuracy of the counter-supported meter. It is assumed that there is no measurement error in the entire meter, and it is also assumed that the weighted average of the relative errors remains stable within several consecutive measurement periods [21, 22]. In addition, determining the correct relationship between household changes is a basic requirement for theoretical calculations. Suppose the collected power data is insufficient and the optimal amount of data is greater than the number of a single meter. In that case, this problem can be solved by deleting all meter data in the period.

2.2. Error Analysis of Smart Meter. In the topology diagram of the smart meter layout illustrated in Figure 2, it is

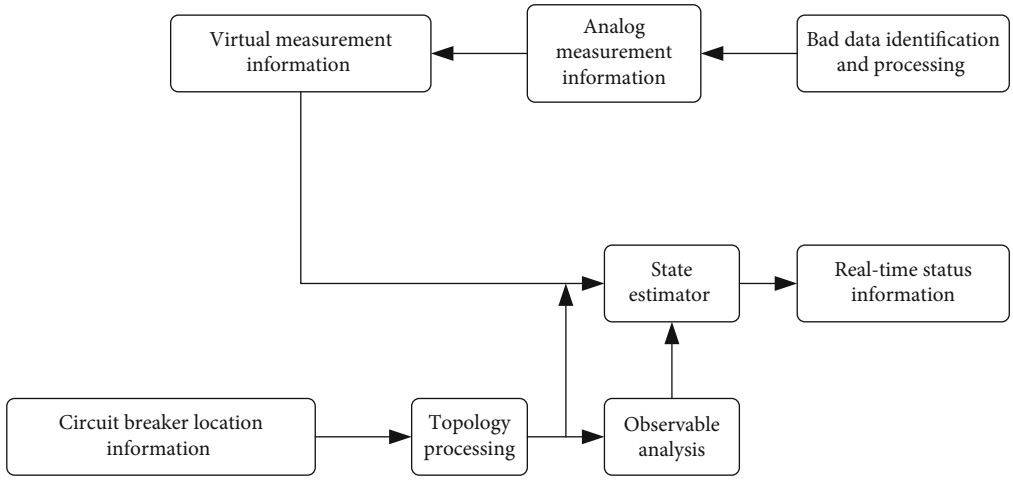

Figure 1: Basic process of power system state estimation.

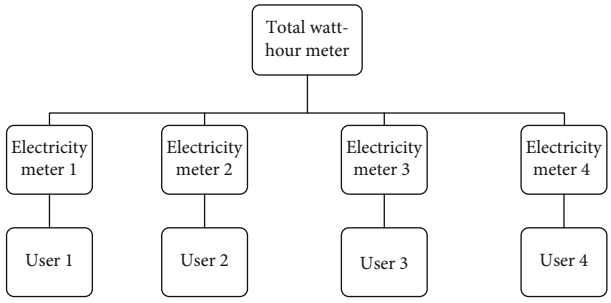

Figure 2: Smart meter electrical topology.

assumed that the measurement period of the total meter is a, and c_a is the power consumption of the period a. The number of users in this area is n, the actual power consumption of a user is m, the actual measured power of the smart meter is $a_{x,y}$, and the actual power consumption during the power consumption process is z [23, 24]. Then, in the case that there is no error in the measured value of the total meter, the relationship between the actual power consumption of the user during a certain period of time and the actual power loss during the power process is shown as follows:

$$c_a = z_a = \sum m_{x,y}. \tag{1}$$

It is assumed that the relative error of the electric energy meter is ξ, and the relative error calculation equation is shown as follows:

$$\xi = \frac{a_{x,y} - m_{x,y}}{m_{x,y}} \times 100\%. \tag{2}$$

The real power consumption at this time is expressed as follows:

$$m_{x,y} = \frac{1}{1+\xi} c_{x,y}. \tag{3}$$

The operation error of the smart meter is obtained by transforming and solving the above equations simultaneously. On this basis, the measurement error involved in the study is not the measurement error at a certain instant, but the overall error level analyzed by the instrument over a period of time.

2.3. Model Ill-Condition Analysis. The measurement error analysis model of the smart meter is represented by a linear equation set, which is shown as follows:

$$Fx = y - m = n. \tag{4}$$

In equation (4), F is the coefficient matrix, x is the measurement error analysis solution vector, y is the total power list of the smart meter, m is the power loss vector of the user's power consumption area, and n is the constant vector measured by the smart meter [25, 26]. In equation (4), the constant vector on the right side of the equal sign of the equation system contains two elements, including the total power of the meter and the power consumption of the user. In general, when the measurement error of a smart meter is calculated theoretically under ideal conditions, the total meter error and the loss in the electricity use process can be ignored. In practical applications, however, many issues need to be considered [27, 28]. The total counter is generally a high-precision counter, and the measurement accuracy is higher than that of the submeter, but there is still no guarantee that there will be no measurement errors. Moreover, the energy loss in the actual electricity use process cannot be completely accurately calculated. The occurrence of these errors and uncertain factors will cause the constant vector value on the right side of the model to be disturbed and become inaccurate. The perturbation of the constant vector-matrix n is amplified in the calculation and solution process of equation (4), which greatly influences the solution of the equation. The specific expression is shown as follows:

$$\frac{\|\omega x\|}{\|x\|} \le \|F\| \left\|F^{-1}\right\| \frac{\|\omega n\|}{\|n\|} = \operatorname{cond}(F) \frac{\|\omega n\|}{\|n\|}. \tag{5}$$

In equation (5), the notation $\|\bullet\|$ denotes the norm. ωx is the perturbation of the vector x, and $\mathrm{cond}(F)$ represents the condition number of the vector matrix. From the above mathematical relationship, the perturbation of the equation system to the vector-matrix will be magnified $\mathrm{cond}(F)$ times, and when it is solved, it will affect the stability of the solution process. The fluctuation of stability is one of the important indicators for judging the morbidity of the model. Generally speaking, when the value of $\mathrm{cond}(F)$ is greater than 103, it will be regarded as a pathological model [29, 30]. IF $\mathrm{cond}(F)$ exceeds the rated value, then it indicates that the model is very ill conditioned. The solution (counter error) obtained by the error analysis model of the smart meter is very sensitive to input interference. Even if the solution is completed, the real error value of each subcounter obtained is very large, causing the smart meter to have small fluctuations or large loss errors. Therefore, to calculate the smart meter's operating error, it is necessary to study the ill-conditioned problem of the model and propose a solution algorithm. In addition, it is necessary to reduce the influence of pathological conditions on measurement errors and improve the measurement accuracy of smart meters.

2.4. Discussion on Methods of Reducing Illness of Smart Meter. When the smart meter shows the ill condition of the error calculation model, the two algorithms can eliminate the difficulty in solving the model caused by the poor model condition. These two algorithms are the preprocessing of the measurement data and the regularization of the measurement data.

The preprocessing methods of the measurement data includes two parts of the data optimization algorithm based on the greedy strategy and the row-by-row difference method.

A greedy algorithm means that when a problem is being solved, it always makes the best choice in the current view. Without considering the overall optimality, the algorithm obtains a locally optimal solution in a sense. In this research, the greedy algorithm is applied to intervene in the morbid problems of the smart meter system. The energy consumption information collection system of smart meters can provide measurement data that exceeds the requirements of typical modeling. Choosing different data from these measurement data to build different models will change the morbidity of building models. Therefore, the optimization technique is applied to select the best performing data set from the data pool to make the smart meter error model ill conditioned. The linear equation is solved, and the result shows that when the number of users in the power consumption area is n, n periods of data are needed to represent it. It is assumed that the measurement system provides the measurement data of the m period. There are C_m^n ways to select the data [31]. In this case, a strictly exhaustive method is adopted to calculate the number of conditions in each data set, one at a time, and the amount of calculation and load will become quite large. Based on the above analysis, a data optimization algorithm based on a greedy strategy is proposed to quickly select the most useful data set to solve the model. The solution process is illustrated in Figure 3.

As illustrated in the flow chart of Figure 3, data is deleted from the selected data set in sequence, and the condition number of the matrix obtained after deletion of the corresponding data is saved. The data that meets the minimum number of conditions is found and deleted from the candidate data set, which means that the data is successfully deleted from the candidate data set. The above steps are repeated. Data is deleted until the amount of data in the data set drops to the specified value, then the data set is the output. After the best data set is obtained, the linear equation is optimized by providing a row-by-row finite difference method, which further reduces the number of conditions in the equation coefficient matrix and reduces the ill condition of the solution model. First, the column with the highest cumulative total is found in the coefficient matrix. All rows are sorted in descending order in this column. Then, the two adjacent equations are subtracted one by one to obtain the processed linear equation. Regularization is a concept in linear algebra, which refers to how a complex ill-posed problem is usually defined as a set of linear algebraic equations in linear algebra theory. This set of equations is usually derived from an inverse problem corresponding to an ill-posed problem condition. The use of massive conditions means that rounding errors and other errors will seriously affect the outcome of the problem. The regularization matrix is a diagonal matrix, and the diagonal elements can apply different resistance stresses according to different solutions. Given that different smart meters have different levels of measurement accuracy, the accuracy level of the energy meter is set as the constraint parameter of the corresponding solution.

The regularization method of measurement data is as follows. In this research, an improved Tikhonov regularization method is adopted to further reduce the mathematical model's morbidity. Data preprocessing is carried out to reduce the incidence of the model. The classic Tikhonov regularization method is used to solve the ill-conditioned problem of unfavorable conditions. Due to the prior information of the solution based on two least-squares residual norm constraints, new constraints are added to improve the stability of the solution. A suitable solution x is found, such that $Mx = N$ holds for the linear model, and the regularization parameter equation is shown as follows:

$$\min_{x} \varphi(x) = \|Mx - N\|_2^2 + \alpha \|P_a x\|_2^2. \tag{6}$$

In equation (6), the value of α is positive, which represents the regularization parameter. P_a represents a normalized matrix, $\|P_a x\|_2^2$ is a norm, and the norm vector is two. x indicates the solution corresponding to the minimum objective function $\varphi(x)$. Although Tikhonov's classic regularization method can eliminate the variability in the solution, it does not provide the option of specifying a range before the resolution. It cannot be directly applied to the solution of the problem in this research. Therefore, the corresponding improvement is needed, and the improved regularization parameter equation is shown as follows:

$$\min_{x} \varphi(x) = \|Mx - N\|_2^2 + \alpha \|P_a (x - L)\|_2^2. \tag{7}$$

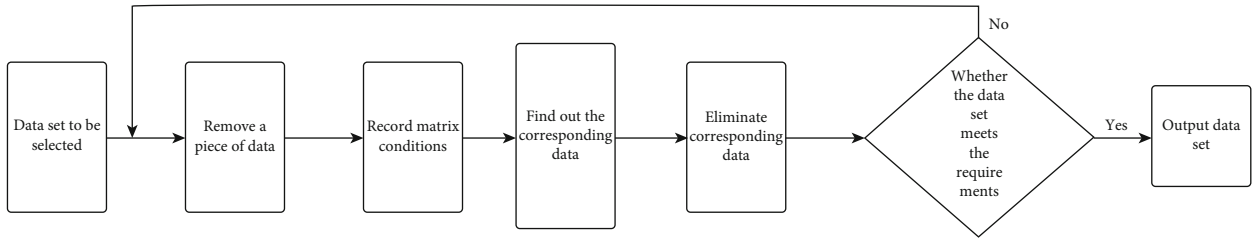

Figure 3: Data optimization algorithm flow based on the greedy strategy.

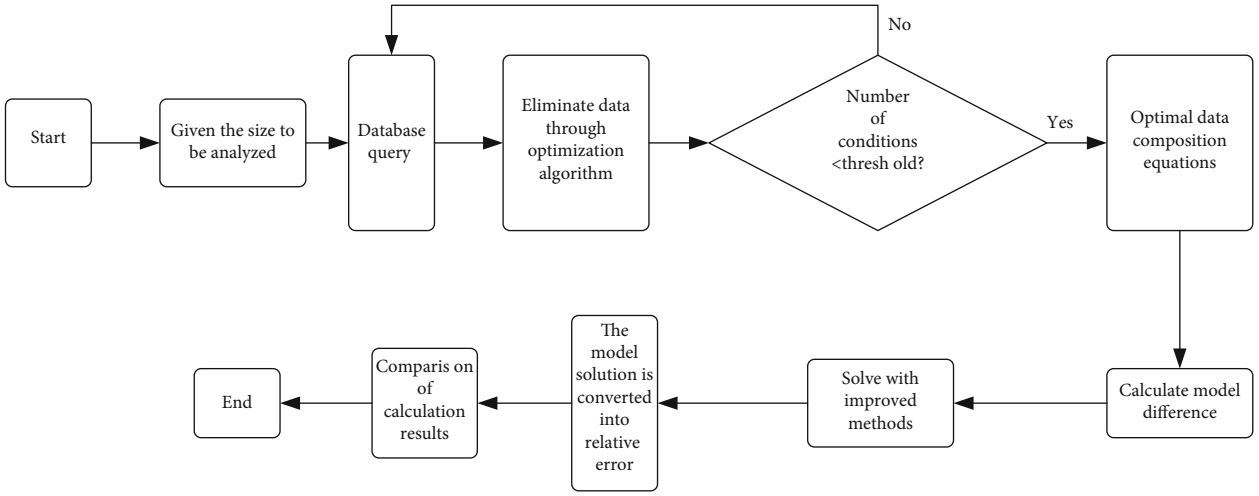

Figure 4: Analysis algorithm flow of smart meter to reduce ill-conditioned error.

In equation (7), column vector L is introduced to make the model distributed near the column vector. The value of α is positive, which indicates the regularization parameter. P_a represents a normalized matrix, and x represents the solution corresponding to the minimum objective function $\varphi(x)$. Equation (7) is solved to obtain the following:

$$x = \left(MM^T + \alpha P_a\right)^{-1}\left(M^T N + \alpha P_a L\right). \tag{8}$$

In equation (8). The value of α is positive, which indicates the regularization parameter. P_a represents a normalized matrix, and x represents the solution of equation (7). In summary, the analysis algorithm flow of the smart meter to reduce ill-conditioned errors is illustrated in Figure 4.

2.5. Performance Evaluation of Smart Meter Operation Error Analysis Algorithm. In this subsection, the effectiveness of the algorithm is verified by experiments. The data used come from the electric energy metering data of a low-voltage station in a city grid, and the universality of the experimental data is considered. The high-rise residential, isolated small residential, old residential, rural radio stations, and laboratory analog radio stations are selected and numbered as 1-5. Each type has data for 365 days a year from 10 such stations. First, all types of station data undergo preprocessing and line-by-line differential data selection. Then, the data

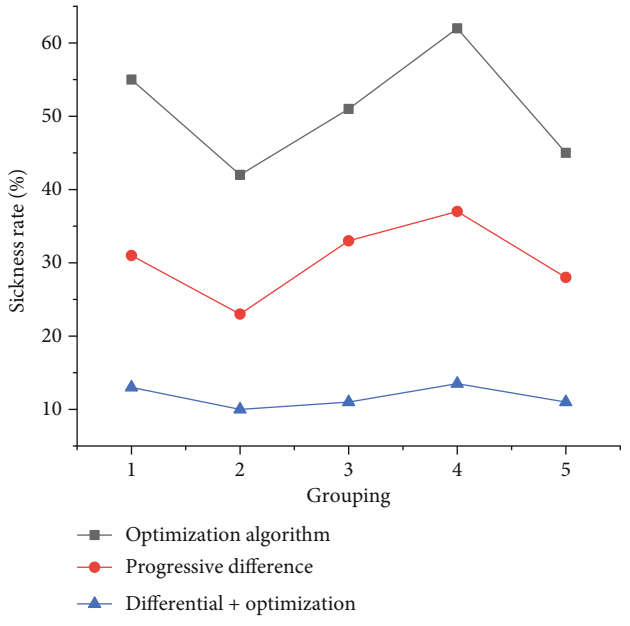

Figure 5: The effect of reducing morbidity rate of different treatment methods.

preprocessing strategy is combined with Tikhonov's improvement. The regularization method is adopted to find the measurement error and calculate it by the least square

Table 1: The relationship between user scale and running time.

User scale/user number	10	20	30	40	50	60	70	80	90	100
Running time (s)	0.45	0.63	0.92	1.27	1.59	2.01	2.43	2.87	3.35	3.86

method. The actual error of the meter is compared to determine the power of different algorithms to verify the accuracy of the meter error. The test index equation for the effect of pathological reduction is shown as follows:

$$r = \frac{a_o}{a_u} \times 100\%. \tag{9}$$

In equation (9), a_o/a_u is the ratio of the condition number of the original data to the condition number of the processed data.

3. Algorithm Verification Results and Discussion

3.1. Data Preprocessing to Test the Effect of Morbidity Reduction. To test the morbidity reduction effect of the data preprocessing method, three preprocessing methods of row-by-row difference, data optimization, and data optimization after row-by-row difference are applied to test the morbidity reduction effect of different data. The results are illustrated in Figure 5.

Figure 5 shows the effect of the coefficient matrix of the optimization algorithm, the row-by-row difference algorithm, and the combination of the two on the treatment strategy of the ill-conditioned rate. According to the comparison results of three sets of different strategies, the number of conditions in the coefficient matrix after data optimization is reduced to 42%-60% of the number of initial conditions. After the row-by-row differential data processing, the matrix condition number is reduced to 22%-35% of the original condition number. The two methods are combined, and differencing is performed after data optimization. It is found that the morbidity rate drops to about 9%-14%, which is an order of magnitude lower than the original morbidity rate. In summary, all the proposed data preprocessing strategies can effectively reduce the number of conditions in the coefficient matrix for different types of low-voltage substations, thereby reducing the morbidity rate of the model.

After previous discussions, it is found that the user size can also affect the performance of the algorithm. The larger the number of users around the site, the more data is needed, and the demand for data provided by the optimization algorithm will increase, leading to an increase in time-consuming algorithm manipulation. Therefore, it is necessary to calculate the time-consuming algorithm under different user scales, and the calculation results are shown in Table 1.

Table 1 shows the relationship between the user scale and the time required for the algorithm to run, and the selected user scale range is 10-100 households. As the scale of user usage increases, the data optimization differential algorithm's running time gradually increases and maintains a linear trend. In practical applications, however, the number of users served in a complete low-voltage zone system is roughly in the range of 50-100. When the user number is between 50 and 100, the running time range of the algorithm is between 1.5 and 3.5 s. Due to the linear growth relationship between the two, even if the number of users in the station area increases to about 110, the algorithm's running time will remain below 4 s. In summary, the data preprocessing algorithm proposed in this research can be put into practical application.

3.2. Smart Meter Error and Accuracy Calculation Results. To study the interference effect of the method proposed in this research on the measurement error and accuracy of the smart meter, the error of the smart meter of the users in the low-voltage station area is calculated, and the least square method is introduced as the control group to verify the effectiveness of the algorithm. The comparison result is illustrated in Figure 6.

Figure 6 shows the comparison of the interference error of the least square method and the method proposed on the smart meter. To further reflect the interference effect of data preprocessing on the error of the smart meter, the experimental results of data preprocessing combined with the least square method are also added as a comparison. If the least-squares method is used directly, the ill conditioning of the model will have a great impact on the measurement results of the smart meter, and the error in some nodes may even reach more than 80%, which results in a huge error. If the data is preprocessed first, and then the least square method is applied, it is clear that the relative error of the smart meter is reduced by as much as 60% and maintained at about 20%. From the comparison between the error of the algorithm processing result and the actual error, the data is optimized first, and the relative error value of the result obtained after processing by the difference method is very small, which is close to the true value of the error. Therefore, the data preprocessing method proposed has a significant effect on the morbidity reduction of the model, which can greatly reduce the relative error of the smart meter.

Further analysis of the deviation results of the three different processing methods is performed, and the deviation distribution of the three other methods is obtained. Finally, the specific results are illustrated in Figure 7.

In Figure 7, the deviation results of the three different processing methods are further statistically analyzed. The deviation results of the large and small extremes and the quartile points are selected for display to discuss the interference effect of the method in this paper proposed on the error

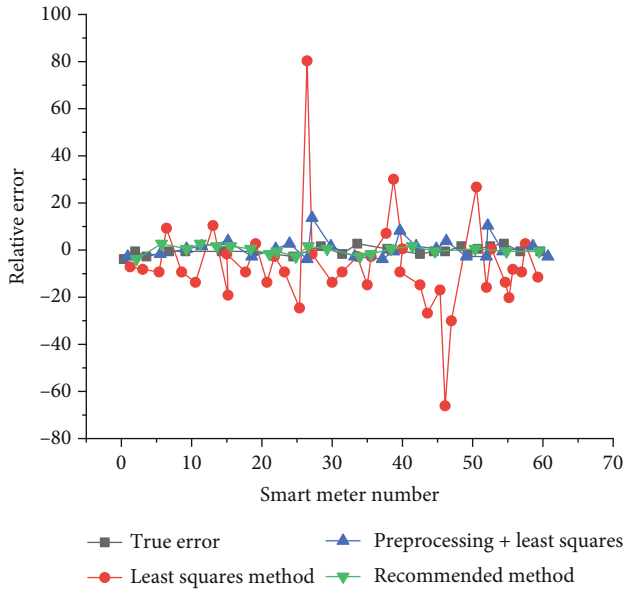

Figure 6: Error comparison of different calculation methods.

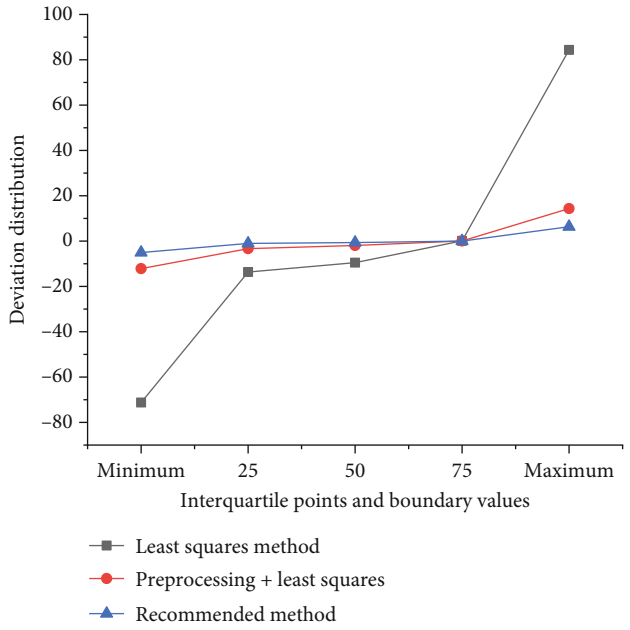

Figure 7: Deviation distribution of different calculation results.

of the smart meter. When only the least-squares method is used for processing, the maximum deviation of the smart meter calculation results is 84.53%, and the minimum deviation is -72.14%. After data preprocessing, the least-squares method is used. It turns out that the maximum deviation of the calculation result of the smart meter is 14.43%, and the minimum variation is -12.21%. Then, the proposed method is adopted, and the optimal selection of data is performed first. It is found that the maximum deviation of the calculation result obtained after the regularization processing is 6.26%, and the minimum deviation is -5.03%. Through the comparison of the above results, the calculation results of the algorithm proposed in this article have smaller errors and more accurate results. Compared with no ill-conditioned treatment method, the algorithm proposed can improve the calculation accuracy of smart meters.

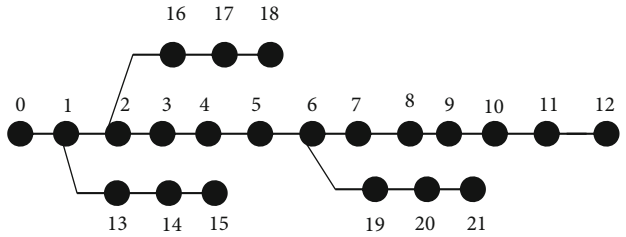

Figure 8: Experimental single-line node system.

The above results show the overall interference effect of the method proposed on the error of the smart meter. To further explore the effect of the algorithm in this research on each node, seven nodes are randomly selected from the node system illustrated in Figure 8, and the voltage and current at different nodes are measured. The resulting error and phase distribution are illustrated in Figure 9.

In Figure 9, the average voltage amplitude error of the node voltage phase error is 0.0468 V, and the node voltage phase error is 0.000215 rad before the ill-conditioned treatment method is applied. The error of the nodal branch current is 14.49%, and the phase error of the branch current is 0.1328 rad. After the ill-conditioned treatment, the average amplitude error of the node voltage is 0.0015 V, and the error of the node phase voltage is 0.000067 rad. The error of the branch current of the node is 0.2613%, and the phase error of the branch current is 0.004 rad. Thus, after the ill-conditioned processing method is applied, the calculation error of each node is greatly reduced, especially in the current error.

In summary, the analysis algorithm for reducing the ill-conditioned errors of smart meters proposed in this study can effectively interfere with the ill condition of the smart meter calculation model. The processing effect shows that it can reduce the measurement error of the smart meter to about 5%, which is an order of magnitude lower than the error before processing, and the processing effect of the least square method is improved by more than 70%. From the perspective of processing speed, when the user range is between 50 and 100, the algorithm's running time ranges between 1.5 and 3.5 s, which can be fully adapted to the actual situation and has strong practicability. In addition, the data measurement of each node also plays a role in reducing errors. The proposed smart meter reduces the ill-conditioned error analysis algorithm, which can reduce the interference of the morbidity of the fusion model on the measurement accuracy of the smart meter, and the smart meter can accurately reflect the true error level of the electric energy meter.

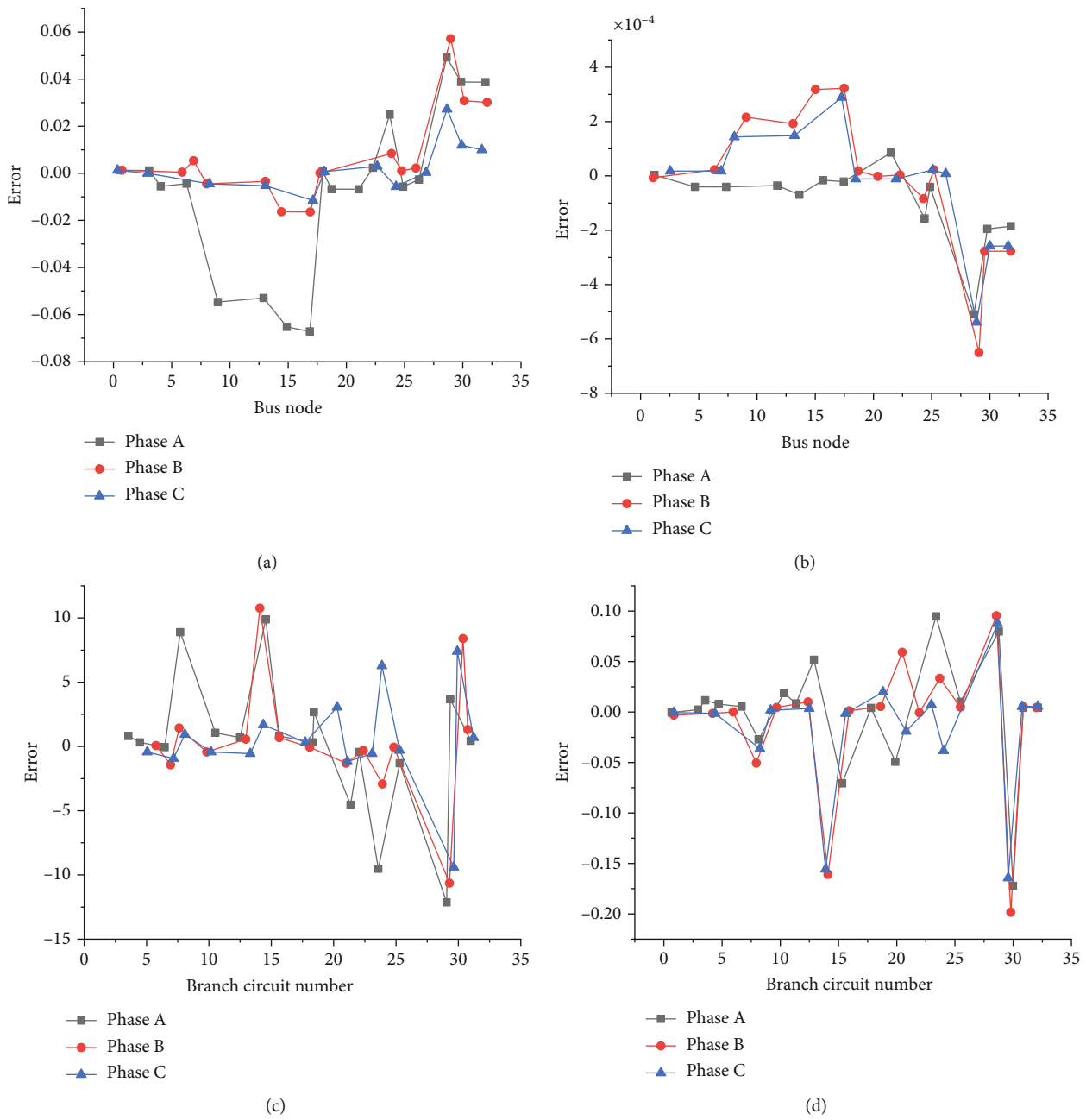

Figure 9: Node error and phase distribution of each branch ((a) represents the node voltage amplitude error, (b) represents the node voltage phase error, (c) represents the branch power amplitude error, (d) represents the branch current phase error)).

4. Conclusion

To effectively solve the problem of serious morbidity in the smart meter fusion model, data preprocessing and regularization algorithms are used to solve the bad model of the smart meter running error-checking algorithm and improve the actual situation of low calculation accuracy of the smart meter. The results show that the proposed method can effectively solve the difficult problems caused by the ill-conditioned model and remove the verification errors and calculation failures caused by the ill-conditioned model itself due to its nature. For serious problems, it can be used to verify power measurement and provide operations and deployment operations, providing certain reliable data protection. Although certain research results are harvested in this work, there are still many deficiencies in the research process due to the limitations of the research methods and some objective conditions, which are summarized as follows. First, the ill-conditioned interference method for the smart meter fusion model is only demonstrated in the ideal state, which needs further adjustment and improvement if it is to be put into practical application. Second, the impact of objective problems on the precision of smart meters caused by the environment and service life of smart meters and various

components of the circuit is not taken into account. Third, few control groups are selected in the experiment; therefore, there is no improvement in the method proposed in the research. In future studies, the above three points will be improved, more comprehensive factors will be taken into account, and more control algorithms and experiments will be set up to make the research results more convincing.

Data Availability

The labeled dataset used to support the findings of this study are available from the corresponding author upon request.

Conflicts of Interest

The authors declare no competing interests.

Acknowledgments

This work was supported in part by the Research Project of China Southern Power Grid Co., Ltd. (No. 670000KK52200011).

References

[1] I. Marzola, S. Alvisi, and M. Franchini, "Analysis of MNF and FAVAD model for leakage characterization by exploiting smart-metered data: the case of the Gorino Ferrarese (FE-Italy) district," *Water*, vol. 13, no. 5, p. 643, 2021.

[2] W. Wei, Q. Ke, J. Nowak, M. Korytkowski, R. Scherer, and M. Woźniak, "Accurate and fast URL phishing detector: a convolutional neural network approach," *Computer Networks*, vol. 178, article 107275, 2020.

[3] G. Xie, X. Zheng, D. Zhuang et al., "Research on the combination technology of smart meter status evaluation and acquisition function based on Big Data Technology," *IOP Conference Series Earth and Environmental Science*, vol. 558, article 052075, 2020.

[4] A. Cominola, M. Giuliani, A. Castelletti et al., "Long-term water conservation is fostered by smart meter-based feedback and digital user engagement," *npj Clean Water*, vol. 4, no. 1, pp. 1–10, 2021.

[5] B. Völker, A. Reinhardt, A. Faustine, and L. Pereira, "Watt's up at home? Smart meter data analytics from a consumer-centric perspective," *Energies*, vol. 14, no. 3, p. 719, 2021.

[6] K. Vortanz, "Smart meter rollout: mehrwertdienste als chance für stadtwerke, um kunden zu gewinnen und zu binden," *GWF*, vol. 160, no. 1, pp. 605–612, 2019.

[7] M. J. Booysen, M. Visser, and R. Burger, "Smart meter data," *Water Research*, vol. 149, pp. 414–420, 2019.

[8] F. Nal, A. Almalaq, and S. Ekici, "A novel load forecasting approach based on smart meter data using advance preprocessing and hybrid deep learning," *Applied Sciences*, vol. 11, no. 6, p. 2742, 2021.

[9] O. Valgaev, F. Kupzog, and H. Schmeck, "Adequacy of neural networks for wide-scale day-ahead load forecasts on buildings and distribution systems using smart meter data," *Energy Informatics*, vol. 3, no. 1, pp. 1–17, 2020.

[10] P. Kiedrowski, "Selection of the optimal smart meter to act as a data concentrator with the use of graph theory," *Entropy*, vol. 23, no. 6, p. 658, 2021.

[11] M. A. Khan and B. Hayes, "Smart meter based two-layer distribution system state estimation in unbalanced MV/LV networks," *IEEE Transactions on Industrial Informatics*, 2021.

[12] N. Kroener, K. Förderer, M. Lösch, and H. Schmeck, "State-of-the-art integration of decentralized energy management systems into the German smart meter gateway infrastructure," *Applied Sciences*, vol. 10, no. 11, p. 3665, 2020.

[13] F. Farokhi, "A fundamental bound on performance of non-intrusive load monitoring algorithms with application to smart-meter privacy," *IFAC-PapersOnLine*, vol. 53, no. 2, pp. 2280–2285, 2020.

[14] C. Shen, C. Min, and C. Wang, "Analyzing the trend of O2O commerce by bilingual text mining on social media," *Computers in Human Behavior*, vol. 101, pp. 474–483, 2019.

[15] D. Fiorillo, G. Galuppini, E. Creaco, F. de Paola, and M. Giugni, "Identification of influential user locations for smart meter installation to reconstruct the urban demand pattern," *Journal of Water Resources Planning and Management*, vol. 146, no. 8, article 04020070, 2020.

[16] M. E. Shafiee, A. Rasekh, L. Sela, and A. Preis, "Streaming smart meter data integration to enable dynamic demand assignment for real-time hydraulic simulation," *Journal of Water Resources Planning and Management*, vol. 146, no. 6, article 06020008, 2020.

[17] W. Ingram and F. A. Memon, "Rural water collection patterns: combining smart meter data with user experiences in Tanzania," *Water*, vol. 12, no. 4, p. 1164, 2020.

[18] F. N. Adhiatma, D. Perdana, N. M. Adriansyah, and R. H. Raharjo, "IEEE 802.11ah network planning for IoT smart meter application: case study in Bandung Area," *Journal Pekommas*, vol. 5, no. 1, pp. 11–22, 2020.

[19] R. Ramdani, W. Lgpww, and A. Zubaidi, "Rancang bangun smart meter system untuk penggunaan air pada rumah tangga berbasis internet of things," *Journal of Computer Science and Informatics Engineering (J-Cosine)*, vol. 4, no. 2, pp. 149–160, 2020.

[20] G. M. Jasim and K. K. Abdalla, "Single phase energy smart meter system design and implementation using RFID and based on IoT," *IOP Conference Series: Materials Science and Engineering*, vol. 1090, no. 1, article 012093, 2021.

[21] A. M. Pirbazari, M. Farmanbar, A. Chakravorty, and C. Rong, "Short-term load forecasting using smart meter data: a generalization analysis," *Processes*, vol. 8, no. 4, p. 484, 2020.

[22] M. Plenz, C. Dong, F. Grumm et al., "Framework integrating lossy compression and perturbation for the case of smart meter privacy," *Electronics*, vol. 9, no. 3, p. 465, 2020.

[23] F. Pilo, G. Pisano, S. Ruggeri, and M. Troncia, "Data analytics for profiling low-voltage customers with smart meter readings," *Applied Sciences*, vol. 11, no. 2, p. 500, 2021.

[24] Y. You, Z. Li, and T. J. Oechtering, "Energy management strategy for smart meter privacy and cost saving," *IEEE Transactions on Information Forensics and Security*, vol. 16, pp. 1522–1537, 2020.

[25] X. Kong, X. Zhang, and L. Bai, "A remote estimation method of smart meter errors based on NNF and GDRLS," *IEEE Transactions on Industrial Informatics*, 2021.

[26] F. Farokhi, "Review of results on smart-meter privacy by data manipulation, demand shaping, and load scheduling," *IET Smart Grid*, vol. 3, no. 5, pp. 605–613, 2020.

[27] J. Crawley, E. McKenna, V. Gori, and T. Oreszczyn, "Creating domestic building thermal performance ratings using smart meter data," *Buildings and Cities*, vol. 1, no. 1, pp. 1–13, 2020.

[28] R. Wang, Q. Gong, K. Zhen, X. Z. Hou, M. He, and L. Y. Wang, "Research on RFID security evaluation method in smart meter," *IOP Conference Series Earth and Environmental Science*, vol. 645, article 012081, 2021.

[29] N. S. Yusoff, Zeittey Karmilla Kaman, Abdul Rahman Zahari, Wan Hafiizhah Wan Mohamad Norafi, and Azlina Bte Abdullah, "Examining smart meter users' experience on continuance intention in adopting smart meter in Malaysia—result from a pilot study," *Asia Proceedings of Social Sciences*, vol. 7, no. 2, pp. 110–113, 2021.

[30] S. R. M. Nasir, A. Ibrahim, R. Hassan et al., "Awareness and acceptance in using smart meter by energy customers in Malaysia," *Environment-Behaviour Proceedings Journal*, vol. 5, no. SI2, pp. 35–41, 2020.

[31] Z. A. Khan, M. Adil, N. Javaid, M. N. Saqib, M. Shafiq, and J.-G. Choi, "Electricity theft detection using supervised learning techniques on smart meter data," *Sustainability*, vol. 12, no. 8023, p. 8023, 2020.

Hindawi
Journal of Sensors
Volume 2021, Article ID 4867222, 11 pages
https://doi.org/10.1155/2021/4867222

Research Article

e-Commerce Online Intelligent Customer Service System Based on Fuzzy Control

Dongmei Wei

School of Computer and Software Engineering, Xihua University, Chengdu 610039, China

Correspondence should be addressed to Dongmei Wei; wdm@mail.xhu.edu.cn

Received 12 August 2021; Revised 23 September 2021; Accepted 29 October 2021; Published 13 November 2021

Academic Editor: Mu Zhou

In order to improve the intelligence of the e-commerce online intelligent customer service system, this paper proposes a deep rejection recognition algorithm based on the maximum interval squared hinge loss and combines the actual needs of the e-commerce online customer service system to build an intelligent customer service system with the support of the fuzzy control system. Moreover, this article chooses to build a domain ontology library for structured storage of domain knowledge needed by customer service chatbots. In addition, this article analyzes the dialogue structure based on the speech act model and combines the semantic vector model of the question sentence on the basis of the dialogue structure to understand the question sentence, which helps to improve the accuracy of the answer feedback of the Internet shopping customer service robot. Finally, this article designs experiments to verify the performance of the online customer service system constructed in this article and analyzes the experimental results through statistical methods. The experimental results show that the online intelligent customer service system constructed in this paper has certain practical effects.

1. Introduction

With the rapid development of Internet e-commerce, people's lifestyles are becoming more and more convenient, and people are accustomed to shopping online [1]. The new behavior and habits gave birth to a new position-customer service. In online shopping, customers often inquire about products, place orders, logistics, after-sales, refunds, and other information, which require customer service to answer and deal with. The customer service work is arduous, boring, and highly repetitive. In reality, manual customer service often fails to deal with customer problems in a timely manner, which leads to reduced customer satisfaction, loss of customers, and impact on sales performance. Therefore, artificial intelligence-oriented customer service robot products for e-commerce came into being. The e-commerce customer service robot frees customer service from a large number of repetitive mechanical answer questions and handles complex problems in a timely manner. Moreover, it can improve customer satisfaction while also reducing business operating costs. According to the analysis of the company's actual situation, a project was established to build a customer service robot system oriented to the e-commerce field. Customers have priority access to the customer service robot system, which can automatically answer customer questions, recommend customer products based on the related products inquired, and recommend questions that customers may ask in advance. The e-commerce customer service robot is not like a mecha robot in a science fiction film but an intelligent question-and-answer system for the e-commerce field [2]. Moreover, it can understand and analyze the user's intention based on the analysis of the customer's intention and then call the corresponding matching rule system to deal with the problem and then answer the question better and accurately. Technically, customer service robots are mainly based on natural language analysis- and machine learning-related algorithms to automatically answer. The knowledge base of the customer service robot uses collected and organized conversations between human customer service and customer chats. This system can effectively help corporate customer service departments to provide 24-hour service for uncomplicated customer problems. Moreover, the service is stable, and users will not be aware of the difference in service

due to the quality of customer service. In the future, it can also analyze purchase behaviors based on purchase records and flexibly provide users with personalized recommendations and fashion advice pushes. In addition, it saves manual customer service from simple and boring answering questions, so that manual customer service can give priority to serving customers with complex problems, and it can manage user satisfaction and allow users to continue to consume. Finally, it can achieve the purpose of reducing the operating cost of enterprise customer service and improving user experience [3].

On the basis of the above analysis, based on fuzzy control technology, this article combines the actual needs of e-commerce customer service to construct an e-commerce online intelligent customer service system based on fuzzy control and analyzes the performance of the system.

2. Related Work

With the continuous huge amount of Internet data and the development of computer linguistics, question-answering systems have begun a new life. It has broken away from traditional information retrieval and developed into an independent research direction. Under the promotion of TREC, the development of automatic question answering technology has been greatly promoted. The question answering system of this period mainly obtained the answers to the user extraction questions from a large number of free text collections [4]. The language handled by TREC is English, so many technologies cannot be used in languages of Eastern countries [5]. Fact-based problems are the best type of problem solved so far and have achieved good results, but the research on other types of problems has been slow [6]. Corresponding to TREC is the evaluation task CLEF for European languages, which also joins the QA branch [7]. In addition to the question answering system based on free text, some people have proposed a question answering system based on network links or metadata results in recent years [8].

In recent years, with the development of online communities, a community question answering system with common question answering pairs as the knowledge base has emerged [9]. With the increase in interactive requirements in the question answering process, interactive question answering has appeared in recent years. Interactive question answering is a research field between the traditional question answering system and the dialogue system [10]. Interactive question answering inherits the characteristics of traditional question answering, and it allows users to ask questions of the system in natural language and gives answers in natural language or in a way that users can understand [11]. Different from traditional question answering technology, it allows users to conduct multiple rounds or further questions when they are not satisfied with the answer. The interactive question answering system based on traditional question answering adds interactive functions to the traditional question answering system, such as adding continuous question processing and contextual information processing. Although for question answering systems, allowing users to interact with the system through natural language for multiple consecutive rounds is a very important improvement; for dialogue systems, such continuous multiple rounds of human-computer interaction have existed for a long time [12]. Essentially, any dialogue system with the purpose of information consultation can be called an interactive question answering system [13].

Customer service staff often have to face a large number of customers consulting the same problem, which not only causes a waste of labor but also reduces work efficiency. As a result, the e-commerce assistant of information came into being; IBM's chat dialogue system NLA assistant [14] can help customers find the products they want through dialogue with customers and customer feedback. In each conversation, NLA provides incremental feedback to customers to feedback their understanding of customer needs and to show customer products that meet their needs. The B2C e-commerce question answering robot developed in the literature [15] can answer questions in the field of digital cameras and can be extended to multiple dedicated fields. The context-sensitive sales assistant developed in the literature [16] can intelligently communicate with customers and help customers complete the purchase of goods.

Compared with the difference in knowledge, service attitude, and style of manual customer service personnel, the intelligent customer service system can provide uninterrupted, consistent, and efficient customer consulting services. This can not only increase the satisfaction of customer consulting services in the case of a large number of customers and insufficient customer service staff but also greatly reduce the labor cost of the enterprise.

3. Intelligent Machine Semantic Analysis Function Based on Fuzzy Control

The feedforward neural network can be regarded as a series of nonlinear activation input and the function transformation of its linear combination. To solve this series of parameters, a loss function needs to be defined, and the training of the network is realized by minimizing this loss function. The simplest method is to minimize the sum of square error. The input $\{(x_n, t_n)_{n=1}^N\}$ is given, and t_n is the label corresponding to x_n.

$$y_n = f(x_n, w). \tag{1}$$

The above formula is the output of the neural network, and the minimized error function is

$$E(w) = \frac{1}{2}\sum_{n=1}^{N} \|y_n - t_n\|^2. \tag{2}$$

The following results can be obtained by seeking the partial derivative of the k-th term:

$$\frac{\partial E}{\partial y_k} = y_k - t_k. \tag{3}$$

This is the error between the output and the true value,

and the network training is performed by backpropagating this error update parameter.

If the output of the network is a probability estimate of t_n, the parameters of the neural network can be determined by the maximum likelihood framework. We set $X = \{x_1, \cdots, x_n\}$ and $t = \{t_1, \cdots, t_N\}$ and construct the likelihood function:

$$p(t|X, w) = \prod_{n=1}^{N} p(t_n|x_n, w). \tag{4}$$

It is not difficult to understand that the smallest error means the largest probability of outputting t_n. Therefore, minimizing the sum of square error is equivalent to maximizing the likelihood function. The specific two categories are as follows. The output y_n of the network is the probability estimate of $t_n = 1$, t_n obeys the Bernoulli distribution $p(t_n = 1|x_n, w)$, and the probability corresponding to $t_n = 0$ is $p(t_n = 0|x_n, w) = 1 - y_n$. Then, the probability distribution of t_n can be written as

$$p(t_n|x_n, w) = p(t_n|y_n) = y_n{}^{t_n}(1 - y_n)^{1-t_n}. \tag{5}$$

Taking the negative logarithm of the likelihood function, the following results can be obtained:

$$\begin{aligned} -\log\left(p(t|X, w)\right) &= -\sum_{n=1}^{N} \log(p(t_n|x_n, w)) \\ &= -\sum_{n=1}^{N} \{t_n \log\left(y_n\right) + (1 - t_n) \log\left(1 - y_n\right)\}. \end{aligned} \tag{6}$$

This produces an error function in the form of cross-entropy. Similarly, the cross-entropy form of the K classification problem is

$$E(w) = -\sum_{n=1}^{N} \sum_{k=1}^{K} t_{nk} I n y_{nk}. \tag{7}$$

The outlier detection algorithms of most deep learning frameworks are hybrid models, which perform feature extraction through neural networks and input "nondeep" outlier detection algorithms. Some recent works try to introduce the loss function in outlier detection into the neural network to realize an end-to-end model.

The objective function of SVDD is used to replace the cross-entropy loss, which minimizes the volume of the hypersphere surrounding the feature vector while training the neural network. Minimizing the volume of the hypersphere can closely map the data point to the center of the sphere:

$$\min_{R,W} R^2 + \frac{1}{\nu n} \sum_{i=1}^{n} \max\left\{0, \|\phi(x_i; W) - c\|^2 - R^2\right\} + \frac{\lambda}{2} \sum_{l=1}^{L} \left\| W^l \right\|_F^2. \tag{8}$$

Among them, $F \subseteq \mathbb{R}^p$ is the p-dimensional feature space and $\phi(x; W)$: $X \longrightarrow F$ represents the neural network with the L-layer weight parameter set as $W = \{W^1, \cdots, W^L\}$. R is the volume of the hypersphere, and $c \in F$ is the center of the hypersphere. The hyperparameter $\nu \in (0, 1)$ controls the trade-off between the volume of the hypersphere and the error point, that is, the ratio of outlier points. When $\lambda > 0$, the regularization term is adjusted. The algorithm uses stochastic gradient descent or its variants (such as Adam) for parameter optimization. However, since W and R exist in different dimensional spaces, these two parameters need to be optimized alternately during the iterative process, which is equivalent to continuously solving two optimization problems.

The application of a single-class support vector machine loss function in deep networks is expanded:

$$\min_{w,V,\rho} \frac{1}{2}\|w\|_2^2 + \frac{1}{2}\|V\|_F^2 + \frac{1}{\nu}\frac{1}{N}\sum_{n=1}^{N} \max(0, \rho - \langle w, g(VX_n)\rangle) - \rho. \tag{9}$$

Among them, w is the scalar output obtained from the hidden layer to the output layer, that is, the unactivated output of the entire network; V is the weight matrix; and ρ is the offset of the classification hyperplane. Compared with the loss function of OC-SVM, the key method of the above formula is to replace the dot product $\langle w, \phi(X_n)\rangle$ with the dot product $\langle w, g(VX_n)\rangle$, that is, using the output of the penultimate layer to calculate the loss function. This allows feature learning to be implemented in a neural network, and the last layer of the network is used to perfect the outlier detection function. However, after the change, the objective function becomes a nonconvex function, so the algorithm for optimizing model parameters will not lead to global optimization. The OC-SVM loss function has more parameters. Similarly, this algorithm also needs to alternate iteratively for parameter optimization.

When training a neural network, the choice of loss function is closely related to the choice of output unit. For example, how the most commonly used cross-entropy loss function represents the output determines the form of the cross-entropy function (two-class or multiclass).

For binary classification problems, the target variable is $t_n \in \{0, 1\}$. When $t_n = 0$, it means belonging to category c_0, and when $t_n = 1$, it means belonging to category c_1. We set a neural network with one output unit and set the input to x_n and the hidden layer output to $a = w^T x_n$. Using the sigmoid function as its activation function is mainly to compress the value range of the hidden layer output to $(0, 1)$ to represent the probability. The input x_n belongs to category c_1.

$$p(c_1|x_n) = \sigma(a) = \frac{1}{1 + \exp\left(-a\right)}. \tag{10}$$

At this time, the posterior probability of category c_0 is

$$p(c_0|x) = 1 - p(c_1|x). \tag{11}$$

Similarly, we set a standard multiclass neural network, and each input is divided into K mutually exclusive categories $\{c_1, c_2, \cdots, c_K\}$. In the output layer, the form of "1-of-K" is used to represent the category: the output unit of the corresponding category is 1 and the output unit of the other categories is 0. Softmax is used as the output unit activation function to predict the probability that x_n belongs to category c_k. We set the input as x_n and the output of the hidden layer as $a_k = w_k^T x_n$. Then, the conditional probability that x_n belongs to category c_k is

$$p_k = p(y = c_k | x_n) = \text{soft max}\,(a_k) = \frac{\exp\,(a_k)}{\sum_{k=1}^{K} \exp(a_k)}. \tag{12}$$

In this way, we can convert the K scalar outputs $\{a_1, a_2, \cdots, a_K\}$ of the hidden layer into a probability distribution.

$$\sum_{k=1}^{K} p_k = 1, \quad \forall k, p_k \in (0, 1). \tag{13}$$

The predicted result is

$$y_n = \arg\max_k p_k = \arg\max_k a_k. \tag{14}$$

For the k-th output unit, which is also a prediction unit of category c_k, the neural network uses data with label c_k as positive samples during training and the remaining label data as negative samples. When forecasting, we introduce a probability threshold λ to realize rejection recognition. For the k-th output unit, we check whether the probability $p_k = \text{sigmoid}(a_k)$ predicted by the k-th sigmoid function is less than the threshold λ_k of category c_k. If the predicted probabilities on all output units of an input sample are less than their corresponding threshold, the input is refused. Otherwise, the input is predicted to be the class with the highest probability value:

$$y = \begin{cases} \text{Refuse}, & \max_k p_k < \lambda_k, \\ \arg\max_k p_k < \lambda_k, & \text{otherwise}. \end{cases} \tag{15}$$

In the second classification, 0.5 is a general probability threshold.

Cross-entropy is an important concept in Shannon's information theory, which is mainly used to measure the difference information between two probability distributions. The purpose of using cross-entropy loss via the network is to reduce the error between the true distribution of the training data and the predicted distribution of the model. In addition to faster training speed and better generalization ability, another advantage of using cross-entropy lies in its versatility, which eliminates the need to design a special cost function for each model. However, for specific tasks, a customized cost function is obviously more useful.

The data in the rejection scenario is an open set, so the distribution of training samples cannot provide a reference for the true distribution of the overall data. The reason is that the unseen category causes the true sample distribution to be unpredictable. Therefore, reducing the difference between the distribution of training samples and the distribution of model predictions through cross-entropy has a limited effect on the estimation of real samples. The binary classification sigmoid function can be used to replace the softmax function. For the output of the current class, only two cases of belonging and not belonging to are considered. While the current class is known during training, the cross-entropy loss function becomes

$$E(w) = -\sum_{i=1}^{n} \sum_{k=1}^{K} \{t_{ik} I n y_{ik} + (1 - t_{ik}) \text{In}(1 - y_{ik})\}. \tag{16}$$

Among them, $y_{ik} = y_k(x_i)$.

The objective function of SVM is called L1-SVM with standard hinge loss. Since L1-SVM is not continuously differentiable, it is not a good choice for neural network training. Therefore, we use its squared variant L2-SVM as the loss function of the rejection neural network, that is, the maximum interval squared hinge loss:

$$\min_{w,b} \frac{1}{2} \|w\|^2 + C \cdot \sum_{i=1}^{n} \max\left(0, 1 - y_i \left(w^T x_i + b\right)\right)^2. \tag{17}$$

Using sigmoid activation in the output layer means that for the k-th output unit of the neural network, the data with label c_k is used as a positive sample during training, and the rest of the label data is used as a negative sample. With the help of the maximum interval squared hinge loss, the classification hyperplane with the largest separation between the two types of data can be found. The data imbalance problem caused by the OVR strategy just makes the classification boundary deviate to the "positive sample" side and obtains a compact boundary effect similar to the OC-SVM objective function, reducing the risk of the open area surrounding the classification boundary of the positive sample. Compared with DOC, the loss function of the entire network not only avoids the probability model but also affects the data representation in the hidden layer through error back propagation and obtains the sentence vector customized according to the rejection task. Janocha et al. proved through a large number of experiments that the squared hinge loss is a better choice than cross-entropy in deep neural networks for classification. Moreover, it is the best choice among the 12 experimental loss functions (including the square sum error), because it converges faster and is more robust to noise in the training data. In this article, we will only use the maximum interval squared hinge loss of the linear kernel to learn the parameters of the lower layer of the model by backpropagating the gradient from the loss function of the last layer. For this, we need to derive the loss function according to the activation value h_i of the penultimate layer.

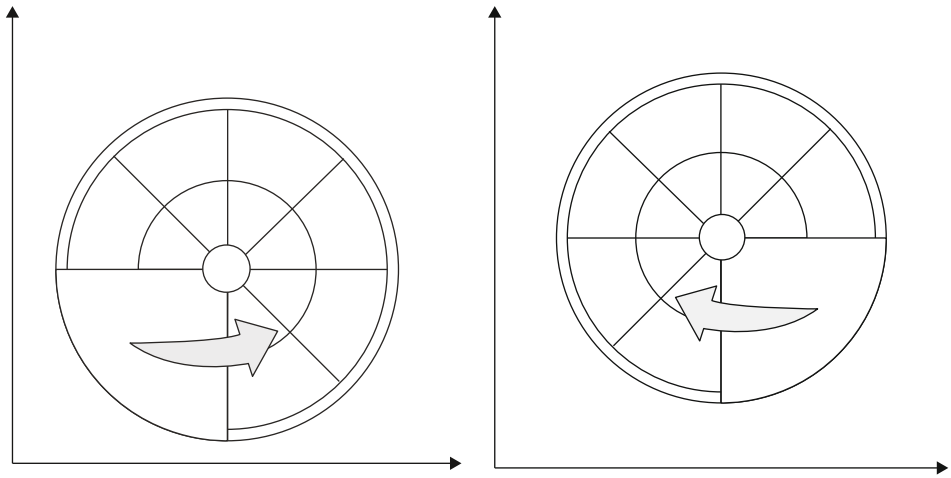

(a) L1-SVM loss (b) L2-SVM loss

Figure 1: Classification effect of two types of hinge loss.

The input of the above formula is replaced with h_i.

$$L(w) = \frac{1}{2}w^T w + C \cdot \sum_{i=1}^{n} \max\left(0, 1 - w^T h_i y_i\right). \tag{18}$$

For the loss function of L1-SVM,

$$\frac{\partial L(w)}{\partial h_i} = -C \cdot w^T y_i \cdot I\left\{w^T h_i y_i < 1\right\}. \tag{19}$$

Among them, $I(\cdot)$ is an indicator function. If $\cdot$ is true, the function value is 1; otherwise, the function value is 0. The partial derivative of L2-SVM for the activation value of the hidden layer is

$$\frac{\partial L(w)}{\partial h_i} = -2C \cdot y_i \cdot w\left(\max\left(0, 1 - w^T h_i y_i\right)\right). \tag{20}$$

We found that L2-SVM is slightly better than L1-SVM in most cases, as shown in Figure 1. In the feature space, L2-SVM produces a more clear classification boundary than L1-SVM, so we will use L2-SVM in the experimental part.

We use the adaptive gradient descent (AdaGrad) algorithm and its variants (such as Adam) to optimize the parameter W of the neural network, and the training is carried out until it converges to the local minimum. At the same time, we use AdaGrad to solve the model parameters, so that the deep OVR-SVM network can be well extended to large datasets, because its computational complexity increases linearly in the number of training batches, and each batch can be processed in parallel (for example, each batch can be processed on multiple GPUs).

Compared with OC-SVM and SVDD loss function, OVR-SVM is more convenient in parameter solving. The reason is that in addition to the parameter W, OC-SVM has an additional parameter ρ, and SVDD has the parameter radius r of the hypersphere. Both of these algorithms need to alternately optimize two parameters in the iterative process, while our algorithm only needs to pay attention to one parameter C. When OVR-SVM is used as a decision machine, each decision function $f(x) = (w_k^T x) = (a_k)$ has only two results, +1 and −1; when $K > 2$, the prediction results of multiple support vector machines will conflict. Therefore, we use the calculated probability obtained by the sigmoid function to make predictions:

$$y = \arg\max_k p_k = \arg\max_k (\text{sigmoid}(a_k))4. \tag{21}$$

For the binary classification problem, 0.5 is a natural choice as the probability threshold for classification, but this threshold does not consider the potential open-set space risk from unseen classes. Therefore, we can reduce the risk of open space by increasing the threshold.

In order to get a better threshold λ, we introduce a statistical model to select the outlier threshold. Normal distribution is one of the most important distributions in probability theory and mathematical statistics. It is Gauss's first use to describe the distribution of errors when studying error theory, so it is also called the Gaussian distribution. The central limit theorem shows that if a random variable is the result of the superposition of a large number of small and independent random factors, then this variable can generally be considered to obey a normal distribution. Therefore, many random variables can be described by normal distribution or approximate description, such as measurement error, product weight, and annual rainfall, which can be described by normal distribution.

If the density function of the random variable X is

$$p(x) = \frac{1}{\sqrt{2\pi}\sigma} \exp\left(-\frac{(x-\mu)^2}{2\sigma^2}\right), \quad -\infty < x < \infty, \tag{22}$$

then it is said that X obeys a normal distribution, denoted as $X \sim N(\mu, \sigma^2)$, where $-\infty < \mu < \infty, \sigma > 0$. $p(x)$ is a bell-shaped curve, left and right are symmetrical with respect to μ, the

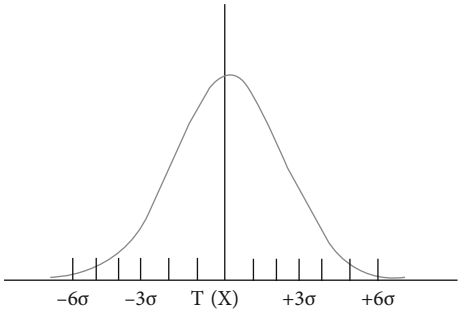

Figure 2: The 3σ rule of the normal distribution.

probability of taking a value near $x = \mu$ is the largest, and the probability of taking a value on both sides is the smallest. $\mu \pm \sigma$ is the inflection point of the curve.

The 3σ rule (three-sigma rule of thumb) means that "almost all" values are within the range of plus or minus three standard deviations of the mean, as shown in Figure 2. Specifically, if the random variable is $X \sim N(\mu, \sigma^2)$, then

$$p(|X - \mu| < k\sigma) = \begin{cases} 0.6826k = 1, \\ 0.9545k = 2, \\ 0.9973k = 3. \end{cases} \quad (23)$$

It can be seen from the above formula that although the value range of the normal variable is $(-\infty, +\infty)$, 99.73% of its value falls within $(\mu - 3\sigma, \mu + 3\sigma)$. This property is called the "3σ rule" of the normal distribution. This is very useful in practical work. For example, industrial production control charts and some product quality indexes are all formulated according to the "3σ rule." Therefore, we can set the rejection threshold according to the "3σ rule."

For each output unit, the expected probability value of the positive sample is 1, but the probability value generated by the sigmoid transformation is always less than 1, which cannot satisfy the symmetry of the Gaussian distribution. Therefore, we assume that the predicted probability of each type of training data obeys a half-Gaussian distribution of mean $\mu = 1$ and then artificially construct the other half of the data. For the probability $p(c_k|x_i)$ of the point x_i, we construct a mirror point to make its probability $2 - p(c_k|x_i)$ satisfy the mean value of 1. The reason is that this mirror point is not a probability. The probability of each type of positive sample and the corresponding mirror point are used to fit a Gaussian distribution to the output of each type to obtain the standard deviation σ_k. According to need, the threshold of rejection probability is

$$\lambda_k = \max(0.5, 1 - \alpha\sigma_k), \quad \alpha = \{1, 2, 3\}, \quad (24)$$

because each class is fitted with the Gaussian distribution and each class has its own threshold.

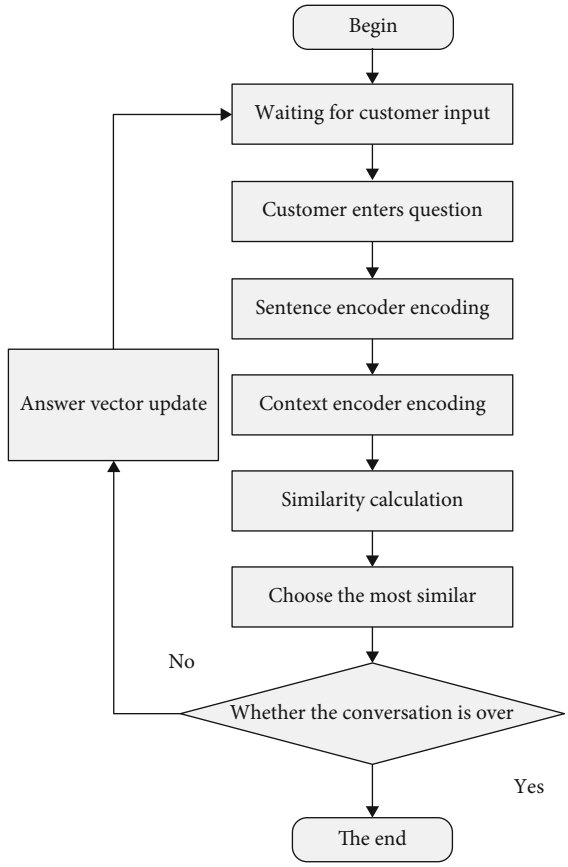

Figure 3: Flow chart of the model dialogue.

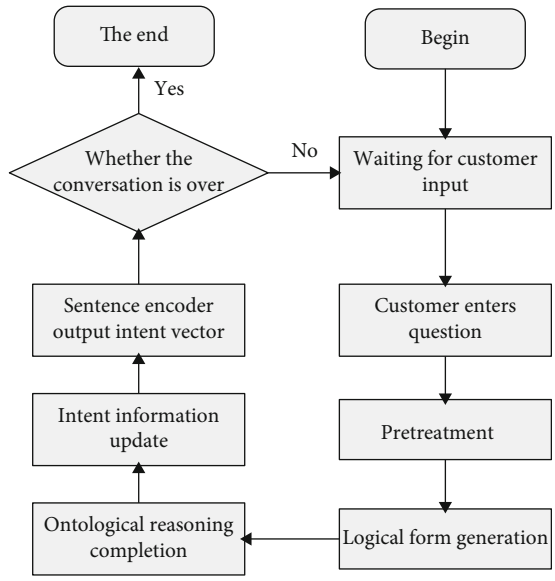

Figure 4: Flow chart of the constructing intention vector.

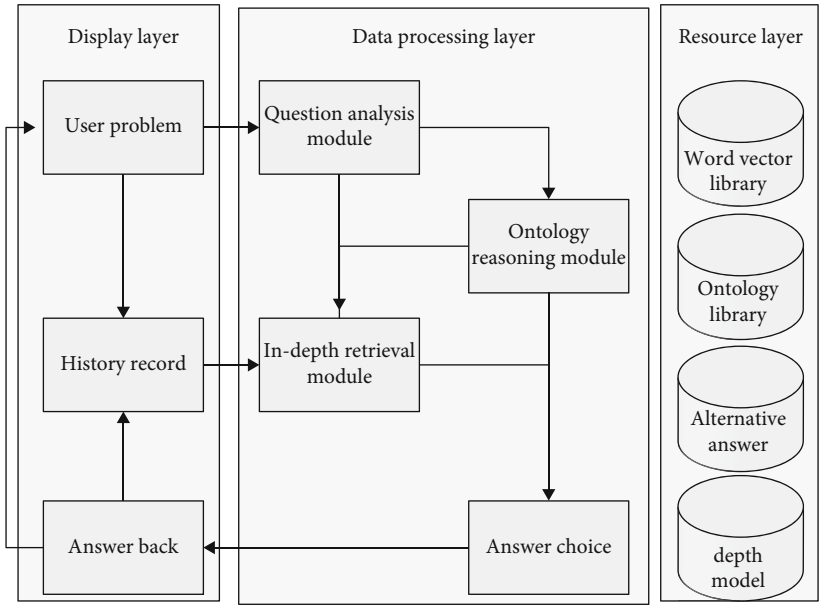

Figure 5: The overall architecture of the system.

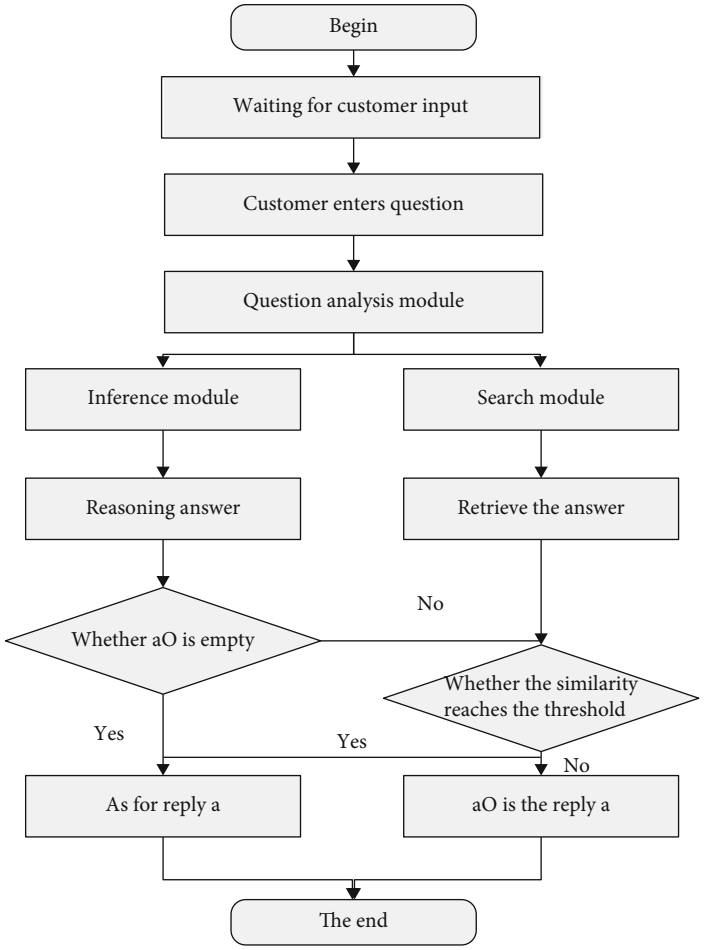

Figure 6: Flow chart of the dialogue.

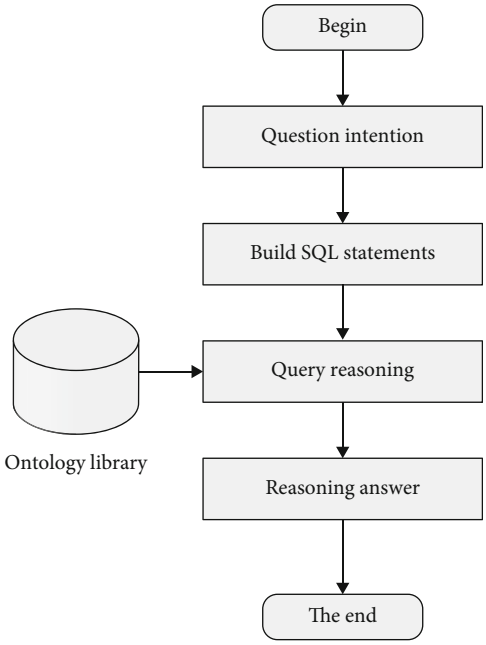

Figure 7: Flow chart of the deep retrieval module.

4. Construction of the e-Commerce Online Intelligent Customer Service System Based on Fuzzy Control

This paper chooses a retrieval model to construct a customer service chat robot, preprocesses the original manual customer service history, and deals with several problems in the original corpus. The question answering library constructed in this article has the characteristics of alternating customer speeches and manual customer service speeches. Moreover, the question answering pairs in the question answering library are in the form of customer questions and customer service answers. In the subsequent model construction, this article will select the question answering library as the training corpus and extract all the customer service answers from the question answering library.

This paper uses the structure of the contextual deep retrieval model of the hierarchical network, and the process of processing customer service dialogue is shown in Figure 3. In the following content of this article, the sentence encoder and the context encoder will be constructed separately.

The construction process of the intention vector in the dialogue is shown in Figure 4.

In the customer service chat robot system, firstly, the user's consultation intention expressed by the ontology is obtained through the semantic understanding of the customer's question. After that, the system applies the inquiry intent to the ontology library query and reasoning to generate corresponding answers and obtains the answers from the query and reasoning and the customer service answers retrieved from the human customer service history dialogue records. Finally, the system selects the answer back to the user based on the similarity of the retrieved answers. The customer service chat robot is a system that can respond to the questions raised by the customer based on the knowledge learned in advance. The overall architecture diagram of the customer service chat robot system is shown in Figure 5.

Table 1: Statistical table of data retrieval performance evaluation of the intelligent customer service system.

No.	Data retrieval performance	No.	Data retrieval performance	No.	Data retrieval performance
1	96.6	28	93.3	55	96.7
2	94.4	29	96.0	56	94.1
3	94.1	30	93.4	57	93.9
4	97.9	31	96.5	58	96.3
5	95.8	32	96.2	59	93.7
6	97.6	33	97.7	60	94.3
7	95.2	34	94.1	61	96.9
8	93.5	35	97.9	62	96.7
9	96.8	36	93.2	63	97.5
10	97.5	37	97.3	64	97.5
11	93.3	38	97.3	65	94.2
12	97.4	39	94.2	66	95.6
13	96.3	40	96.6	67	96.9
14	93.6	41	95.4	68	97.0
15	95.3	42	98.0	69	94.0
16	93.3	43	94.1	70	97.0
17	97.7	44	96.2	71	94.0
18	95.7	45	95.9	72	95.3
19	95.3	46	93.8	73	93.1
20	93.8	47	95.6	74	94.8
21	94.3	48	95.0	75	93.2
22	93.4	49	95.2	76	96.6
23	97.2	50	94.8	77	96.3
24	97.5	51	97.7	78	95.7
25	96.2	52	94.7	79	97.2
26	95.2	53	94.0	80	93.7
27	94.4	54	97.4	81	94.9

In the customer service chat robot system, the intelligent reply function is the core of the entire system. The system accepts the question raised by the user and returns an appropriate response based on the question. The processing process of the system after the customer raises a question is shown in Figure 6. In the process of answering a user, the system uses ontology library query and reasoning and question answering database retrieval to obtain answers and determines the returned answer by judging whether the similarity of the answers obtained by the retrieval exceeds a threshold.

Figure 7 shows the process of calling the ontology library query and reasoning module. The process of calling the ontology library for query and reasoning is relatively simple. After the SPARQL statement is constructed by the user's intention, Jena API can be directly called to query the ontology library to obtain the query and reasoning answer aO. Generally, if the semantics of the question is correctly

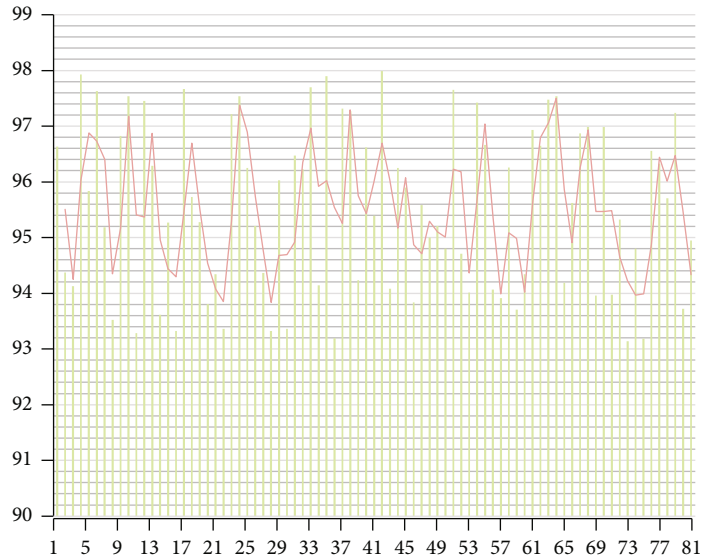

Figure 8: Statistical diagram of data retrieval performance evaluation of the intelligent customer service system.

Table 2: Statistical table of product recommendation performance evaluation of the intelligent customer service system.

No.	Product recommendation performance	No.	Product recommendation performance	No.	Product recommendation performance
1	74.4	28	82.6	55	79.8
2	71.7	29	71.7	56	76.4
3	80.0	30	80.6	57	79.5
4	79.1	31	78.0	58	77.0
5	79.1	32	75.2	59	74.9
6	81.4	33	76.0	60	77.3
7	72.5	34	78.3	61	73.6
8	84.5	35	78.6	62	72.5
9	73.4	36	81.7	63	83.1
10	72.3	37	81.2	64	73.3
11	75.3	38	73.6	65	78.7
12	78.9	39	79.1	66	81.6
13	79.6	40	81.6	67	83.1
14	83.7	41	81.5	68	82.8
15	82.7	42	83.6	69	78.8
16	71.9	43	77.6	70	71.7
17	78.9	44	79.7	71	79.1
18	76.0	45	83.2	72	81.9
19	75.2	46	81.9	73	77.7
20	79.0	47	79.0	74	74.0
21	79.2	48	75.5	75	82.7
22	78.8	49	72.3	76	83.1
23	76.2	50	73.2	77	79.8
24	83.5	51	83.9	78	77.0
25	71.1	52	84.0	79	79.6
26	71.8	53	74.5	80	83.2
27	77.5	54	79.1	81	80.1

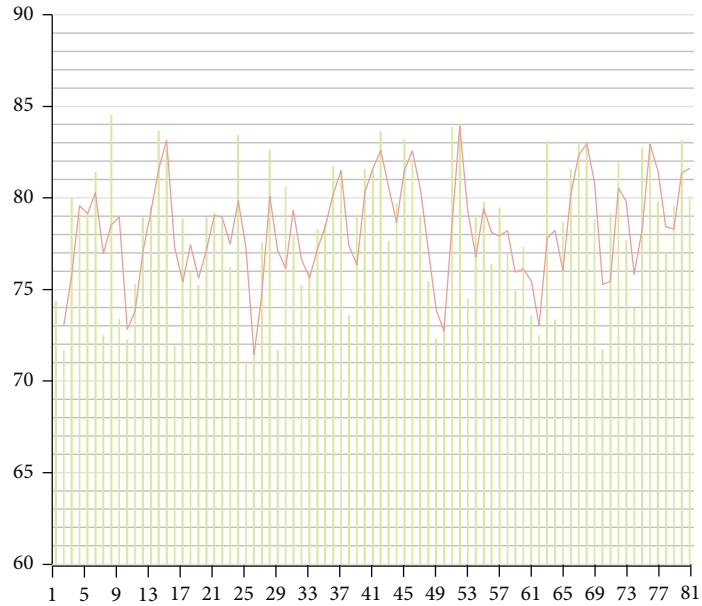

Figure 9: Statistical diagram of product recommendation performance evaluation of the intelligent customer service system.

understood, the answer can accurately return the target answer of the user's inquiry. However, when the customer input is not standard or the input content is relatively empty, such as greetings, the ontology library query and reasoning module will return empty.

5. Performance Analysis of the e-Commerce Online Intelligent Customer Service System Based on Fuzzy Control

The e-commerce online intelligent customer service system based on fuzzy control constructed in this paper can answer customers' questions in e-commerce. Therefore, when constructing the e-commerce online intelligent customer service system, this article first answers common questions through the keyword search database, which has certain requirements for the data retrieval of the online customer service system. Secondly, the intelligent customer service system of this article can also recommend the products that users need. Therefore, in the experimental research, this article firstly tests the data retrieval function of the online intelligent customer service system. This article analyzes 81 groups of simulated conversations, and the results are shown in Table 1 and Figure 8.

From the test results, it can be seen that the system constructed in this paper has a good performance in data retrieval. Next, the recommendation function of the e-commerce online intelligent customer service system is tested and analyzed. The results of the test are shown in Table 2 and Figure 9.

Through experimental analysis, it can be known that the e-commerce online intelligent customer service system based on fuzzy control constructed in this article can basically meet the actual needs, so the system constructed in this article can be used in subsequent practice to expand services.

6. Conclusion

With the rapid development of Internet commerce, more and more merchants provide online shopping services, which also bring a lot of online customer service work. At the same time, it has become the choice of more and more merchants to replace manual customer service with customer service chat robots. How to improve the work quality of customer service chatbots has become an issue of ardent concern for merchants. After analyzing the characteristics of customer service domain knowledge, this paper chooses to construct a domain ontology library for structured storage of domain knowledge required by customer service chat robots. Moreover, this article combines the ontology to construct an e-commerce online intelligent customer service system based on the fuzzy control model. In addition, this article starts with sentence vector encoding and proposes an outlier detection algorithm based on the maximum interval squared hinge loss for rejection recognition. Compared with the current baseline method, the system proposed in this paper has achieved performance improvement on the experimental dataset. It can be seen from the experimental results that the intelligent customer service system constructed in this paper has a certain effect.

Data Availability

The labeled dataset used to support the findings of this study are available from the corresponding author upon request.

Conflicts of Interest

The author declares no competing interests.

Acknowledgments

This study is sponsored by the Education Department of Sichuan Province (Research on online monitoring and processing system of spectrum occupancy for massive data, No. 18ZB0562).

References

[1] A. A. al-Musawi, A. A. H. Alwanas, S. Q. Salih, Z. H. Ali, M. T. Tran, and Z. M. Yaseen, "Shear strength of SFRCB without stirrups simulation: implementation of hybrid artificial intelligence model," *Engineering with Computers*, vol. 36, no. 1, pp. 1–11, 2020.

[2] H. Lu, Y. Li, M. Chen, H. Kim, and S. Serikawa, "Brain intelligence: go beyond artificial intelligence," *Mobile Networks and Applications*, vol. 23, no. 2, pp. 368–375, 2018.

[3] R. Ferrari, C. Mancini-Terracciano, C. Voena et al., "MR-based artificial intelligence model to assess response to therapy in locally advanced rectal cancer," *European Journal of Radiology*, vol. 118, no. 4, pp. 1–9, 2019.

[4] X. Sun, J. Young, J. H. Liu, and D. Newman, "Prediction of pork loin quality using online computer vision system and artificial intelligence model," *Meat Science*, vol. 140, no. 7, pp. 72–77, 2018.

[5] V. Nourani, A. Hosseini Baghanam, J. Adamowski, and O. Kisi, "Applications of hybrid wavelet-artificial intelligence models in hydrology: a review," *Journal of Hydrology*, vol. 514, no. 9, pp. 358–377, 2014.

[6] X. N. Bui, H. Nguyen, Y. Choi, T. Nguyen-Thoi, J. Zhou, and J. Dou, "Prediction of slope failure in open-pit mines using a novel hybrid artificial intelligence model based on decision tree and evolution algorithm," *Scientific Reports*, vol. 10, no. 1, pp. 1–17, 2020.

[7] Z. M. Yaseen, A. el-shafie, O. Jaafar, H. A. Afan, and K. N. Sayl, "Artificial intelligence based models for stream-flow forecasting: 2000-2015," *Journal of Hydrology*, vol. 530, no. 7, pp. 829–844, 2015.

[8] J. E. Laird, C. Lebiere, and P. S. Rosenbloom, "A standard model of the mind: toward a common computational framework across artificial intelligence, cognitive science, neuroscience, and robotics," *AI Magazine*, vol. 38, no. 4, pp. 13–26, 2017.

[9] K. Chapi, V. P. Singh, A. Shirzadi et al., "A novel hybrid artificial intelligence approach for flood susceptibility assessment," *Environmental Modelling & Software*, vol. 95, no. 1, pp. 229–245, 2017.

[10] M. R. Hashemi, M. L. Spaulding, A. Shaw, H. Farhadi, and M. Lewis, "An efficient artificial intelligence model for prediction of tropical storm surge," *Natural Hazards*, vol. 82, no. 1, pp. 471–491, 2016.

[11] T. Sustrova, "A suitable artificial intelligence model for inventory level optimization," *Trends Economics and Management*, vol. 10, no. 25, pp. 48–55, 2016.

[12] B. T. Pham, M. D. Nguyen, D. Van Dao et al., "Development of artificial intelligence models for the prediction of compression coefficient of soil: an application of Monte Carlo sensitivity analysis," *Science of the Total Environment*, vol. 679, no. 8, pp. 172–184, 2019.

[13] A. Enshaei, C. N. Robson, and R. J. Edmondson, "Artificial intelligence systems as prognostic and predictive tools in ovarian cancer," *Annals of Surgical Oncology*, vol. 22, no. 12, pp. 3970–3975, 2015.

[14] J. S. Chou and D. K. Bui, "Modeling heating and cooling loads by artificial intelligence for energy-efficient building design," *Energy and Buildings*, vol. 82, no. 6, pp. 437–446, 2014.

[15] Z. Ghahramani, "Probabilistic machine learning and artificial intelligence," *Nature*, vol. 521, no. 7553, pp. 452–459, 2015.

[16] A. Zappone, M. di Renzo, M. Debbah, T. T. Lam, and X. Qian, "Model-aided wireless artificial intelligence: embedding expert knowledge in deep neural networks for wireless system optimization," *IEEE Vehicular Technology Magazine*, vol. 14, no. 3, pp. 60–69, 2019.

Hindawi
Journal of Sensors
Volume 2021, Article ID 8135942, 12 pages
https://doi.org/10.1155/2021/8135942

Research Article

Recognition of Psychological Characteristics of Students' Behavior Based on Improved Machine Learning

Mingchao Li

School of Marxism Studies, Zhuhai College of Science and Technology, Zhuhai 519000, China

Correspondence should be addressed to Mingchao Li; limingchao@jluzh.edu.cn

Received 26 August 2021; Revised 6 October 2021; Accepted 23 October 2021; Published 9 November 2021

Academic Editor: Mu Zhou

Contemporary classroom teaching requires the combination of students' classroom behavior and their psychological activities and appropriately changes the teaching mode according to students' psychological characteristics. This paper analyzes the traditional characteristic recognition algorithm, and after improving its deficiencies, an improved characteristic extraction algorithm is proposed, based on the actual situation of classroom learning. This new algorithm can effectively improve the students' psychological feature prediction; with the support of this algorithm, a comprehensive analysis model with classroom behavior recognition and psychological feature recognition is constructed; also, the functional structure of the system is built up. Through experimental research, the model proposed in this paper is analyzed, and the experimental data has approved that the systemic model could play an important role in classroom teaching.

1. Introduction

Effective mental health education has become the top priority of every school's education work. In many research results, there is a common point of view that everyone recognizes, which is to take the mental activity course as an important or primary way to implement mental health education. Regardless of the form, effect, and degree of popularity among students, the actual effect of the mental activity course is obvious. The implementation of the course must be achieved through standardized teaching. In order to make the mental activity course really play its role in group tutoring, it is very necessary to do an in-depth study on the teaching design of the mental activity course. In reviewing previous studies, we found that there are many studies on the goals, functions, principles, historical development, and approaches of the mental activity course. However, there are obviously fewer studies on the age-specific mental activity course of high school students, and there are very few researches on how to design a mental activity course teaching model suitable for student development according to the features of high school students. Therefore, combining the author's own daily education practice and analyzing the design of high school mental activity course from a microperspective are the research purpose of this paper [1].

How the level of teaching design of mental activity course will directly affect the tutoring effect of the class. Moreover, effective and successful teaching design is an important prerequisite and guarantee for successful teaching. Therefore, to carry out related research on the teaching design of mental activity course has very important theoretical and practical significance for improving the teaching effect and tutoring effect of mental activity course. How to develop a mental activity course from a more detailed perspective, such as the analysis of activity concepts, the positioning of activity goals, and the design of activity links, are all related content that a good instructional design should involve. As far as psychological counseling teachers are concerned, only with a well-designed teaching design can they better manage the entire class from a big idea. Therefore, for a successful mental activity course, the teacher first calms down and makes meticulous instructional design is an important first step. Effective classroom management is an important guarantee for a good lesson. Only by controlling and managing the classroom can the effectiveness of a lesson be guaranteed. This is true for classes in other

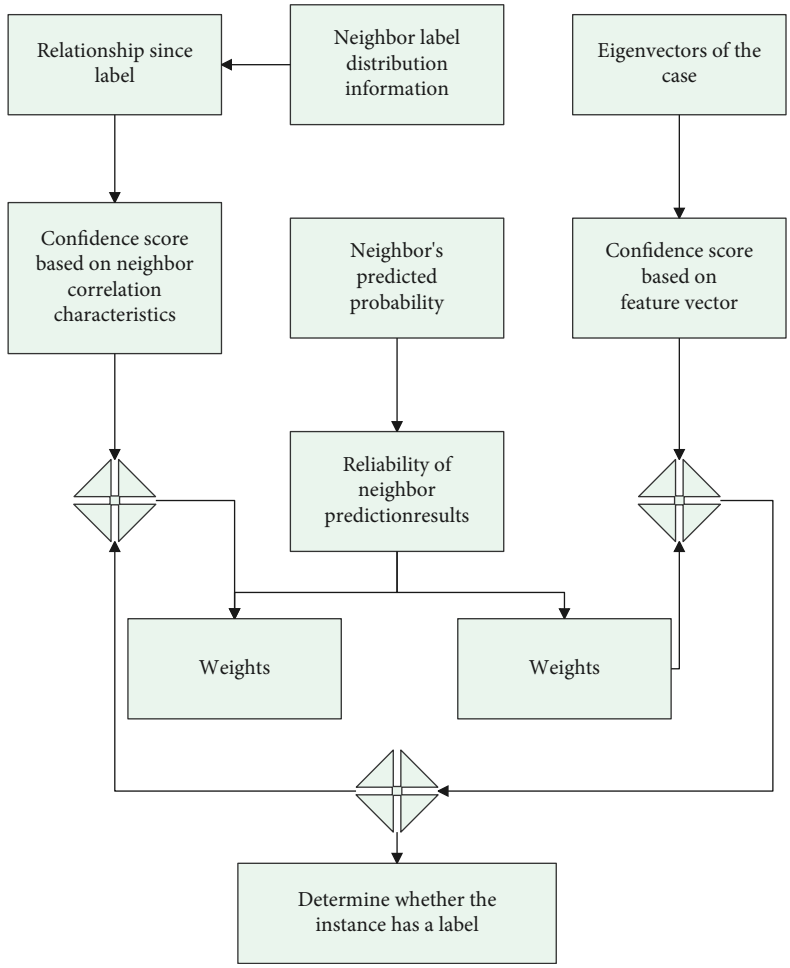

Figure 1: Design of MLNB algorithm.

subjects, especially for mental activity courses. Teachers in mental activity classrooms must be aware of classroom management. In view of the excessiveness of each link, the feedback of students answering questions, the construction of classroom group motivation, etc., all these require the teachers of the mental activity classroom to do well [2]. In classroom activities, different stages of teaching activities constitute the entire classroom. A mental activity course can be divided into a group warm-up phase, a group conversion phase, a group work phase, and a group end phase. Moreover, each stage has its tasks and requirements. At the same time, only when the activities of several stages are thoroughly developed and excavated can a section of mental activity course that is effective and touches students' hearts can be formed [3].

According to the actual needs of current teaching, based on machine learning algorithms, this paper combines the needs of teaching mental activity analysis to link mental activities and students' classroom behaviors to construct a research model of the correlation between students' classroom behaviors and mental activities based on improved machine learning and explores the correlation between students' classroom behaviors and mental activities.

2. Related Work

This paper uses improved machine learning as the basic algorithm to analyze the correlation between students' classroom behaviors and mental activities. There are many related researches on machine learning in factor correlation analysis, and these literatures are analyzed below.

The literature [4] aggregated user characteristic information from Flickr, Twitter, and Coca Cola to prove that its crossdomain user modeling strategy has a great impact on the recommendation quality in a cold start environment. This is one of the earliest studies to integrate user data from multiple fields to improve recommendation performance. Due to the heterogeneity of user preferences in different fields, literature [5] unified the social labels and semantic concepts of users in different systems. The literature [6] constructed a user relationship network and then used a random walk to identify the neighbor users of the target user in the source field, which is used for collaborative filtering recommendation in the target field. The literature [7] mapped labels to emotional categories and then used traditional content-based recommendation methods to make crossdomain recommendations. The literature [8] aggregated the

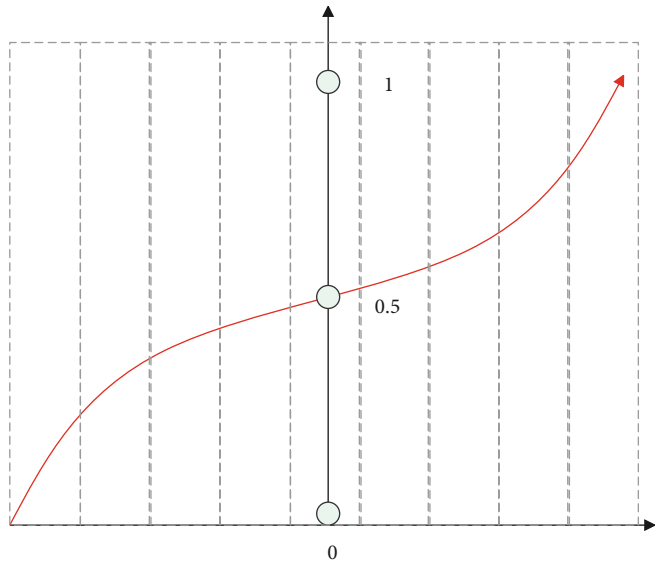

Figure 2: The process of sigmoid-fitting real value being mapped to probability.

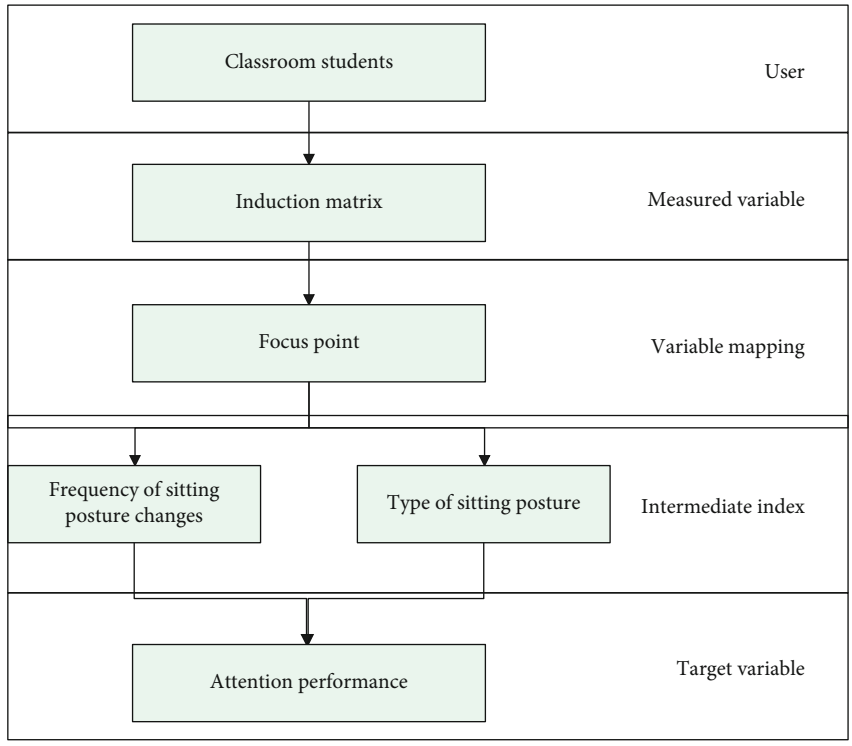

Figure 3: Evaluation model of mental activity behavior.

K-nearest neighbors of the target user in each field by weighting, which is used for collaborative filtering recommendation in the target field.

The literature [9] proposed the "Code Book Transfer (CBT)" method to achieve crossdomain collaborative filtering. Moreover, by compressing the cluster-level user item matrix scoring mode into a compact form, it obtained knowledge from the evaluation matrix of the auxiliary domain. In addition, it reconstructed the sparse matrix of the target field by extending the codebook and applied it to the real-world data set and proved that the recommendation effect of the "codebook migration method" has obvious advantages. The literature [10] proposed a three-factor factorization model based on joint nonnegative matrix. The model uses an effective alternate minimization algorithm to enhance the crossdomain recommendation effect, and it can not only learn the scoring mode shared between domains but also flexibly control the sharing level. The experimental results obtained on real-world data sets show that the proposed model outperforms many existing

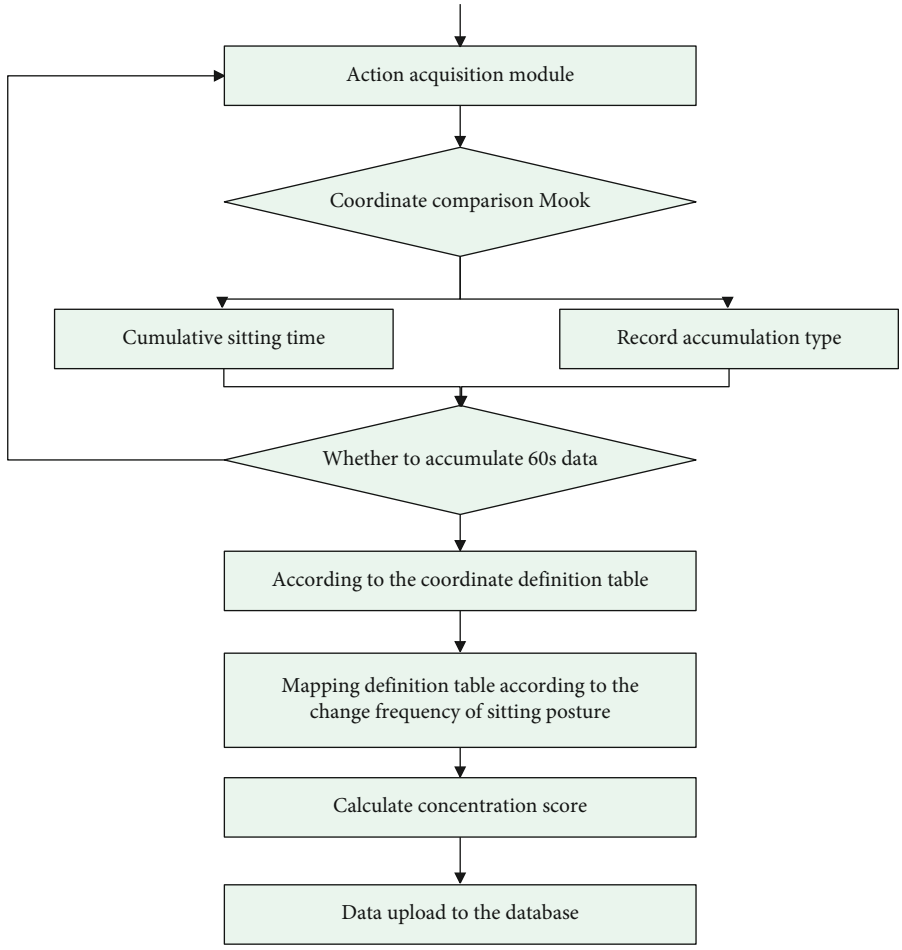

Figure 4: Flow chart of calculation algorithm for individual mental activity level of students.

methods in crossrecommendation tasks. The literature [11] proposed a crossdomain model that uses Factorization Machine (FM) to obtain additional knowledge from auxiliary domains. The model has the ability to encode domain-specific knowledge with real-valued feature vectors and can make better use of the interactive mode in the auxiliary domain, and its result is more advantageous than the existing crossdomain recommendation methods. Aiming at the crossdomain recommendation problem between users and item overlapping systems, literature [12] proposed a matrix factorization method to learn the potential feature vectors of users and items. This method assumes that there is potential consistency between systems; for example, the potential vectors in different systems all obey the same Gaussian distribution. The experimental results obtained on the rating data sets of movies, books, and electronic products show that the results obtained by this method are better than those obtained by the previous algorithms.

The literature [13] proposed a universal Crossdomain Triadic Factorization (CDTF) model based on the "user-product-domain" triad, which can better capture the relationship between user factors and project factors in a specific field. Moreover, it has designed two algorithms to take advantage of users' explicit and implicit feedback and at the same time introduces genetic algorithms to optimize the influence relationship between domains. The experimental results obtained on two real data sets verify the performance of the proposed CDTF model. The literature [14] proposed a universal crossdomain recommendation framework that combines social network information with cross-domain data. This framework uses the combination of tensor factorization and social relationship regularization to form a clustering hierarchical tensor of multiple domains. The results of experiments conducted on real-world data sets show that the proposed framework is better than previous methods. The literature [15] proposed a general framework for content-based crossdomain recommendation, which is an effective feature enhancement method. It uses the user's metadata features to achieve domain adaptation and conducts experiments on the LinkedIn data set to give users work suggestions. In 2016, literature [16] proposed an adaptive model based on transfer learning to predict user behavior in different fields. Moreover, experiments were conducted on tweets in four different fields of IMDB, YouTube, Goodreads, and Pandora to find actively participated tweets. The results show that transfer learning can improve performance.

In real-world data sets, the basic challenge of multilabel classification is the effective use of label correlation. Labels often appear in pairs, and from the perspective of learning

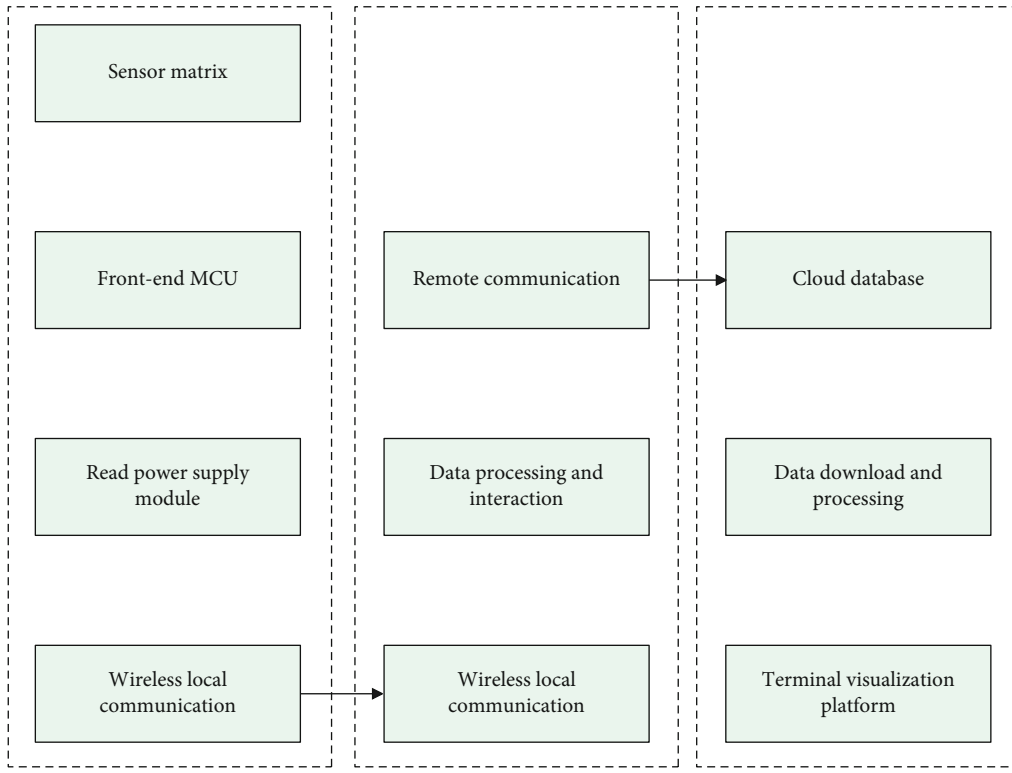

Figure 5: Overall framework of the system.

and prediction, their correlation provides useful information other than basic information for the sample. Therefore, considering the correlation of labels is beneficial to the accuracy of the algorithm and improves the hit rate of prediction. Literature [17] proposed that label correlation can improve the accuracy of multilabel classifiers. The more relevant the labels considered, the higher the complexity of the model. If only part of the label correlation is considered, the true dependency relationship cannot be captured. If all the correlations are considered, the complex relationship of the labels is more difficult to deal with.

3. Comprehensive Label Correlation Features and Sample Features of Student Mental Activities and Classroom Behavior

The two conversion strategies for multiple labels are as follows: (1) LP method: it changes the multilabel problem into the multiclass problem, regards the different label sets as the new category, converts the data into the multiclass set, and uses the multiclass classification to solve the problem; (2) BR method: it transforms multiple labels into binary classification problem solving for each single label. For each label, the instance associated with the label is placed in one class and the rest in another class. Since the binary classification algorithm can be processed in parallel when the high-order label correlation is added, which is beneficial to improve the computational efficiency, the strategy of adding correlation to the binary classification prediction results is adopted. BR method can select different algorithms, such as decision tree, random forest, SVM, and neural network.

If the intersection of similar samples is relatively small, then the similarity is not reliable. In order to improve the reliability of the prediction results, it is necessary to reduce the impact of the unreliable results. Therefore, this paper adds weight to the neighbor prediction results.

The MLNB-BR multilabel classification algorithm is proposed in this paper, and the high-order label correlation is added to the feature-based binary classification method. The overall design of the algorithm is shown in Figure 1. The BR method is used to classify the feature data set. First, the method predicts the probability p_f of the existence of label l_k based on the feature vector and reasonably adds the label correlation information to the result of feature vector prediction to improve the classification accuracy. Due to the different reliability of neighbor prediction results, the classification results based on neighbor correlation features are dynamically adjusted, and the neighbor label dependency features are added to the features to modify the classification results [18].

When the classification based on neighbor features is unreliable, the uncertainty of the neighbor prediction result is calculated, and the uncertainty probability of the neighbor prediction is used to correct the classification result of the neighbor instance. For different labels and different samples, the weights based on the original features and the weights based on the neighbor features are dynamically adjusted. If the reliability of classification based on neighbor features is high, choosing a larger value for the prediction result weight

ω_1 of neighbor features can help preserve good neighbor label relationships p_r [1]. At the same time, the result p_f is adjusted based on the original feature. If the reliability of classification based on neighbor features is low, the prediction result weight ω_2 of the feature vector can increase the influence of the original feature and help correct the error of the neighbor feature. Therefore, the correlation of neighbor labels can be integrated with the classification results based on features to improve classification performance.

$$\begin{aligned} p &= \omega_1 \cdot p_r + \omega_2 \cdot p_f, \\ \omega_1 &+ \omega_2 = 1. \end{aligned} \tag{1}$$

The greater the probability that the neighbor predicts the occurrence or nonoccurrence of the label l_k, the less the uncertainty of the result of the neighbor classification, the greater the probability that the label is correctly predicted, and the more reliable the result based on the neighbor classification. On the contrary, the smaller the probability of occurrence or nonoccurrence of the neighbor prediction label l_k, the greater the uncertainty of the result of the neighbor classification, the lower the probability that the label is correctly predicted, and the lower the reliability of the classification result based on the neighbor. For each sample, the neighbor information can be counted according to the principle of maximum posterior probability, and the probability of occurrence of label l_k can be obtained. For each sample x and each label l_k, the reliability of neighbor information is calculated according to the probability of the occurrence and nonoccurrence of the neighbor's predicted label l_k. The uncertainty of event occurrence can be measured by information entropy. The calculation formula of information entropy is

$$H(x) = -\sum_{x \in X} p(x) \log p(x). \tag{2}$$

The tests on a large number of data sets show the validity of the maximum posterior probability. The formulas for calculating the probability of occurrence and nonoccurrence of tags are, respectively [19]

$$\begin{aligned} p_1(x) &= p\left(H_1^l\right) p\left(E^l_{\vec{c}_t(l)} \middle| H_1^l\right), \\ p_0(x) &= p\left(H_0^l\right) p\left(E^l_{\vec{c}_t(l)} \middle| H_0^l\right). \end{aligned} \tag{3}$$

MLKNN algorithm that combines the traditional KNN method and Bayesian method to deal with multilabel classification problem is proposed. The MLKNN method mainly extracts label information from neighbors to predict sample labels and counts the accuracy of neighbor prediction to evaluate the probability of label occurrence and nonoccurrence. The main idea of this method is to get the label information of unknown instance K-nearest neighbor samples by using the KNN method and to get the label information of unknown instance K-nearest neighbor samples by counting the label distribution information according to the neighbor label set. After that, it counts the label distribution information based on the neighboring label sets and uses the probability of occurrence and nonoccurrence of each label l_k in the neighboring samples as the basis for classification. This paper considers that the MLKNN algorithm can only reflect the distribution features of neighbor samples, and it can be regarded as an attribute of neighbor samples. In this paper, the maximum a posteriori probability is used to count the probability of occurrence and nonoccurrence of neighbor prediction label, and the uncertainty of neighbor information is obtained through information entropy.

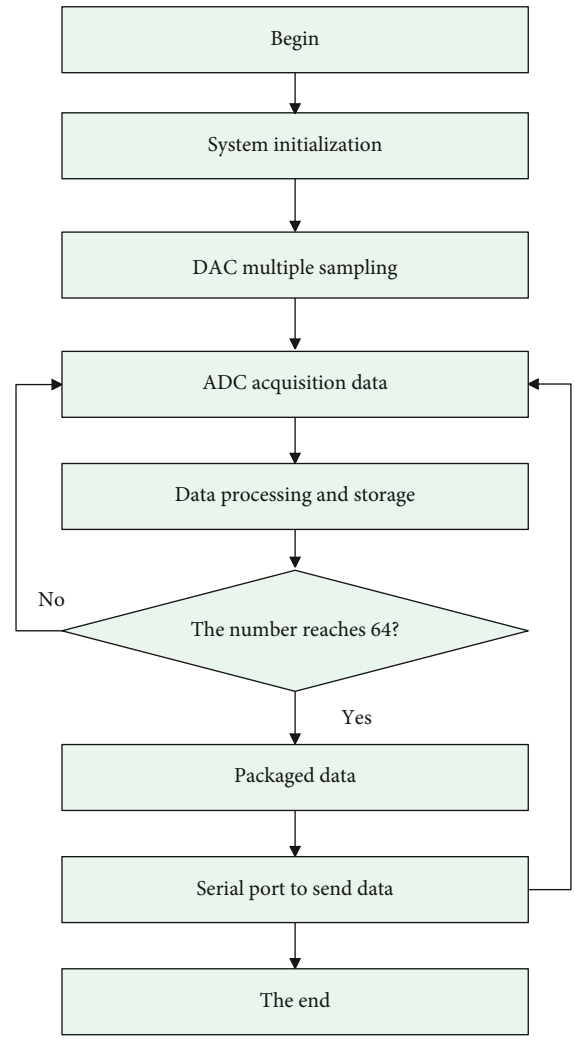

Figure 6: The working flow chart of the master single-chip microcomputer.

The modeling process of MLKNN is as follows: we give an instance X and its corresponding label set $Y_x \in Y$, Y is the set of all labels, and the total number of labels is defined as n. If there is a label l_k in Y_x, then $Y_x(l) = 1$, otherwise, $Y_x(l) = 0$. $N(x)$ is the set of K-nearest neighbors of instance X. For instance X, there are $\vec{c}_x(l)$ nearest neighbors of K with label l_k. The calculation formula is

$$\vec{c}_x(l) = \sum_{a \in N(x)} \vec{y}_a(l), \quad l \in Y. \tag{4}$$

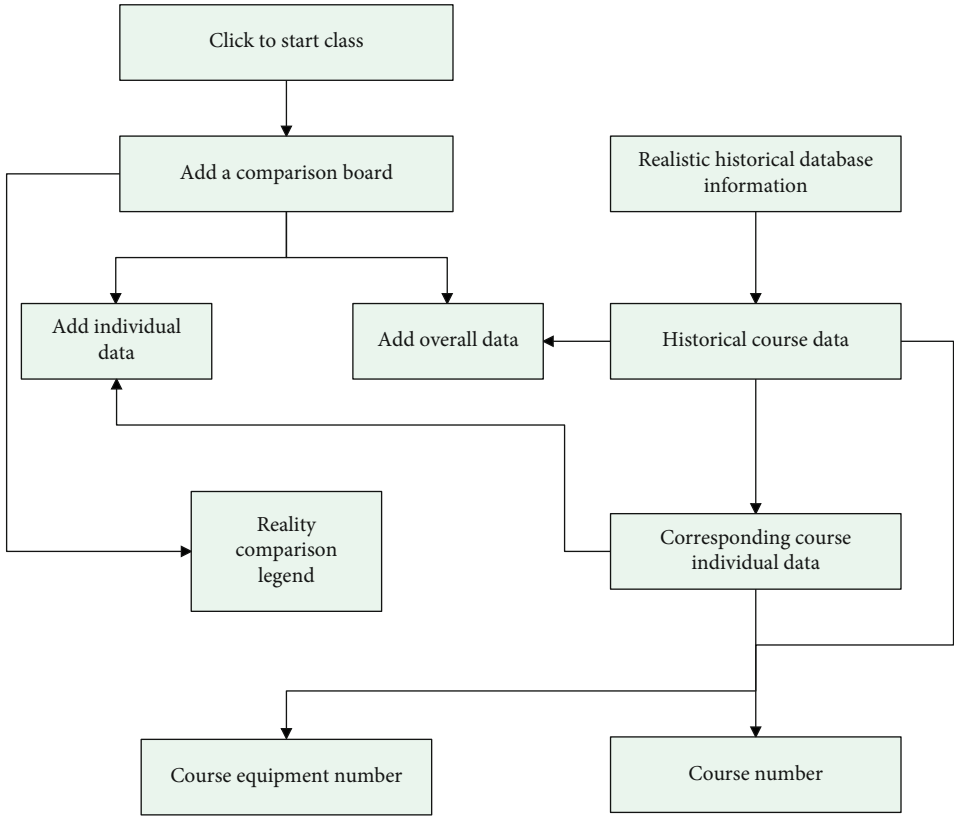

Figure 7: Flow chart of historical data module.

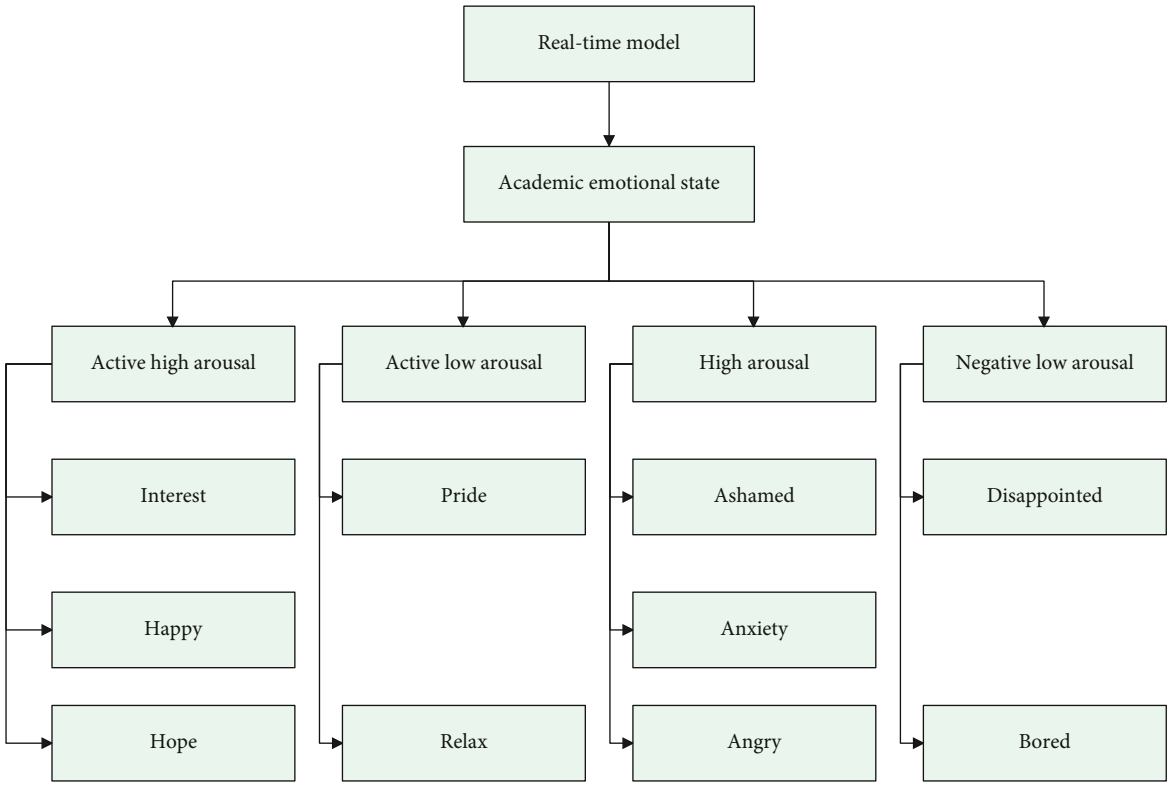

Figure 8: Real-time learner model.

Table 1: Statistical table of students' classroom behavior feature recognition and mental activity feature recognition.

No.	Behavioral feature recognition	Mental feature recognition	No.	Behavioral feature recognition	Mental feature recognition	No.	Behavioral feature recognition	Mental feature recognition
1	76.8	80.5	29	86.3	75.9	57	87.5	73.6
2	75.7	74.9	30	81.5	70.9	58	82.8	81.5
3	73.4	81.8	31	76.7	74.2	59	77.4	78.1
4	79.6	70.8	32	71.6	81.6	60	78.2	80.8
5	77.9	78.4	33	85.6	75.4	61	73.4	74.0
6	74.5	80.3	34	81.8	73.5	62	76.8	72.5
7	85.8	78.5	35	84.6	73.9	63	87.1	71.9
8	85.3	78.9	36	83.2	79.0	64	77.9	77.4
9	72.1	70.1	37	80.6	79.1	65	74.2	79.6
10	80.1	70.3	38	77.3	71.9	66	84.3	72.7
11	71.8	78.9	39	86.2	70.5	67	76.1	73.7
12	83.7	74.8	40	85.8	80.7	68	75.3	75.6
13	87.7	80.4	41	77.3	71.6	69	87.1	72.4
14	71.0	74.5	42	72.9	70.1	70	78.3	75.8
15	79.9	76.5	43	88.6	73.0	71	88.6	79.6
16	77.1	78.5	44	84.3	78.1	72	80.7	78.8
17	84.6	80.7	45	75.8	74.8	73	87.1	78.0
18	83.3	78.3	46	84.8	78.2	74	74.2	75.7
19	81.1	79.1	47	87.9	69.3	75	77.4	76.6
20	72.8	76.3	48	74.1	78.3	76	82.6	70.4
21	84.1	70.4	49	81.4	70.8	77	73.0	78.3
22	74.5	71.4	50	74.1	72.1	78	80.2	75.5
23	73.8	80.2	51	86.3	70.6	79	86.9	71.7
24	71.0	81.9	52	72.3	72.7	80	80.4	79.4
25	83.3	75.6	53	84.1	75.6	81	71.4	76.3
26	82.3	71.7	54	78.2	77.4	82	73.1	81.6
27	81.2	75.9	55	76.4	70.5	83	85.8	80.3
28	78.8	75.0	56	73.3	70.3	84	77.5	75.7

For the test instance t, the K-nearest neighbor set $N(t)$ is first obtained. For the label l_k, if there is a label l_k in the instance t, it is recorded as H_1^l, and if there is no label l_k in the instance t, it is recorded as H_0^l. We define E_j^l as j samples that contain label l in K neighbors. Based on the vector $\vec{c}_x$, the formula for obtaining whether the instance t has a label l_k through the maximum posterior probability criterion and the Bayes criterion is

$$\vec{y}_t(l) = \arg\ \max_{b\in\{0,1\}} p\left(H_b^l \middle| E^l_{\vec{c}_t(l)}\right), \quad l \in Y. \tag{5}$$

After using the Bayesian formula to transform, we get

$$\begin{aligned}\vec{y}_t(l) &= \arg\max \frac{p\left(H_b^l\right)p\left(E^l_{\vec{c}_t(l)} \middle| H_b^l\right)}{p\left(E^l_{\vec{c}_t(l)}\right)} \\ &= \arg\ \max_{b\in\{0,1\}} p\left(H_b^l\right)p\left(E^l_{\vec{c}_t(l)} \middle| H_b^l\right).\end{aligned} \tag{6}$$

Among them, $p(H_b^l)$ represents the prior probability of whether the instance t has a label l_k. When $b = 1$, $p(H_1^l)$ is equal to the number of samples with label l_k divided by the total number of samples.

$$p\left(H_1^l\right) = \frac{\sum_{i=1}^m \vec{y}_{x_i}(l)}{m}. \tag{7}$$

When $b = 0$, $p(H_0^l)$ is equal to the number of samples without label l_k divided by the total number of samples.

$$p\left(H_0^l\right) = 1 - p\left(H_1^l\right). \tag{8}$$

The posterior probability is calculated as follows:

$$p\left(E^l_{\vec{c}_t(l)} \middle| H_1^l\right) = \frac{c[j]}{\sum_{p=0}^k c[p]}. \tag{9}$$

First, for each label l, we count the number $c^{[j]}(j = 1, 2, 3, \cdots)$ of j neighbors with label l_k on the entire data set and

Figure 9: Statistical diagram of students' classroom behavior feature recognition and mental activity feature recognition.

the sample also with label l_k. If there are j neighbors in k neighbors with label l_k, then $c[j] = c[j] + 1$. Then, we count the proportion of j neighbors with label l_k and their own have label l_k in the overall sample.

Since it is necessary to synthesize neighbor correlation features and sample features and convert the output result of the classifier into a probability, different confidence scores can be synthesized according to the weight. This paper uses Platt's sigmoid-fitting method to map the real-valued output to the $[0, 1]$ probability space. The method of sigmoid-fitting real-valued output into probability is as follows Figure 2:

The function that maps real values to the range of $[0, 1]$ is

$$p = \frac{1}{1 + e^{(Af+B)}}. \tag{10}$$

Parameters A and B are the parameters to be fitted, used to adjust the size of the output value, and f is the SVM output value. On the training set, the maximum likelihood estimation is used to fit the parameters A and B in the formula, and the probability value on the training set is defined as

$$t_i = \frac{y_i + 1}{2}. \tag{11}$$

After smoothing, N_+ represents the number of positive samples, and N_- represents the number of negative samples:

$$t_i = \begin{cases} \dfrac{N_+ + 1}{N_- + 2} & \text{if } y_i = +1, \\ \dfrac{1}{N_- + 2} & \text{if } y_i = -1. \end{cases} \tag{12}$$

By minimizing the negative log likelihood function, A and B are solved to obtain the mapping function:

$$\min - \sum_i t_i \log(p_i) + (1 - t_i) \log(1 - p_i). \tag{13}$$

The prediction results of SVM based on feature vector and SVM based on label correlation are

$$\begin{aligned} p_r &= \omega_l^T \cdot x + b_l, \\ p_f &= w * x + b^*. \end{aligned} \tag{14}$$

According to the probability output function corresponding to the SVM, the standard SVM output value p_f is converted into p_f, and p_r is converted into p_r. The weight of neighbor feature classification is calculated as

$$\begin{aligned} \omega_1 &= -(p_1(x) \log p_1(x) \mp (x) \log p_0(x)), \\ \omega_2 &= 1 - \omega_1. \end{aligned} \tag{15}$$

Among them,

$$p_1(x) = p\left(H_1^l\right) p\left(E^l_{\vec{c}_t(l)} \middle| H_1^l\right),$$
$$p_0(x) = p\left(H_0^l\right) p\left(E^l_{\vec{c}_t(l)} \middle| H_0^l\right). \tag{16}$$

In the original feature classification result, the neighbor label correlation is added to obtain the final comprehensive score:

$$p_x = \omega_1 \cdot p_f + \omega_2 \cdot p_r. \tag{17}$$

According to the comprehensive score, it is judged whether there is a label l_k.

$$y_l = \begin{cases} +1 & \text{if} p_x \geq \frac{1}{2}, \\ -1 & \text{if} p_x < \frac{1}{2}. \end{cases} \tag{18}$$

4. Analysis Model of the Correlation between Students' Classroom Behaviors and Mental Activities Based on Improved Machine Learning

Attention, as an important measure of student classroom effectiveness, is what the classroom behavior analysis designed for this paper expects to capture, quantify, and apply to group studies. Using the research method of this paper to monitor and quantify the students' attention level in class not only solves the cost of manpower and material cost of traditional attention measurement methods but also helps to record and quantify the attention data in the classroom in real time. Embodied cognition theory points out the interaction between body posture and cognitive state; that is, physiological indicators of body behavior can represent different cognitive levels. At present, many studies at home and abroad are exploring the use of different behavioral indicators as intermediate variables to characterize the level of attention. Based on the previous research background and related theories, this study uses two indicators of sitting posture type and sitting posture change frequency to represent attention performance. The evaluation model is shown in Figure 3.

The mapping calculation algorithm of the attention level of this research is detailed in flow Figure 4.

Based on the previous design of classroom behavior analysis, the specific implementation process of the system is described in detail. The implementation part of the technology includes the general description of the development environment and tools, the overall architecture of the system, the specific implementation scheme of each module of the system, and the corresponding user use process for the system application in the next chapter. The overall framework of the system is shown in Figure 5.

The work flow chart of the master single-chip microcomputer is shown in Figure 6.

Table 2: Statistical table of correlation between students' classroom behaviors and mental activities.

No.	Correlation	No.	Correlation	No.	Correlation
1	72.1	29	71.4	57	66.4
2	69.1	30	70.6	58	66.7
3	67.0	31	71.7	59	70.1
4	72.6	32	68.0	60	72.3
5	74.4	33	69.6	61	73.9
6	72.1	34	65.5	62	63.5
7	71.0	35	71.1	63	72.4
8	67.1	36	65.7	64	69.4
9	74.3	37	67.9	65	68.0
10	63.4	38	64.6	66	67.0
11	69.7	39	71.5	67	74.0
12	66.1	40	70.7	68	66.7
13	67.3	41	70.7	69	74.8
14	69.2	42	71.0	70	63.4
15	72.6	43	68.1	71	73.7
16	71.2	44	70.5	72	65.2
17	67.4	45	68.5	73	69.6
18	67.8	46	71.8	74	72.2
19	70.6	47	72.7	75	70.0
20	72.2	48	72.1	76	67.8
21	71.6	49	72.8	77	66.3
22	72.0	50	67.9	78	74.5
23	72.7	51	63.4	79	70.0
24	68.8	52	74.6	80	63.1
25	68.1	53	68.9	81	71.2
26	71.7	54	65.7	82	65.8
27	74.2	55	69.9	83	71.8
28	74.5	56	71.1	84	70.2

According to the work flow chart 6 of stm32l433cbt6, when the individual action collection module starts to work, the system is initialized first, and then, the analog signal is amplified by OPAMP operational amplifier in the MCU. At the same time, by cooperating with the DAC peripheral multichannel sampling, the dynamic adjustment of the level is realized. Then, it uses ADC to collect data and transfers the data from RX data register to memory through USART DMA transceiver driver. In the data acquisition process of ADC, the data of 64 pressure points is taken as a cycle. When the data amount reaches, it is packaged according to the MQTT gateway protocol and sent to the local field processing module through the serial port, and the next ADC data acquisition is carried out, and the operation is reciprocating.

Users can also view the historical data of all recorded courses through the terminal software platform, including the overall data of the classroom and the corresponding individual data, and get the visual legend by adding comparison, so as to conduct in-depth comparative analysis of the classroom situation. The process is shown in Figure 7.

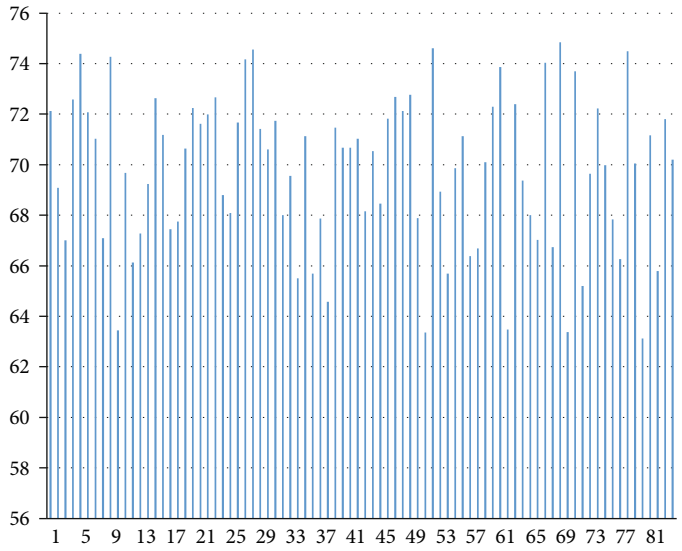

Figure 10: Statistical diagram of correlation between students' classroom behaviors and mental activities.

The real-time behavior data of learners are processed by using academic emotion theory, and the real-time learner model is constructed. Academic emotional state is mainly divided into positive and negative states. The positive state includes positive high arousal and positive low arousal, and the negative state includes negative high arousal and negative low arousal, as shown in Figure 8.

5. Correlation Analysis between Students' Classroom Behaviors and Mental Activities Based on Improved Machine Learning

After constructing the correlation analysis system between students' classroom behaviors and mental activities based on improved machine learning, this paper verifies the performance of the system and analyzes whether there is correlation between students' mental activities and their behaviors. In this paper, students' behavior features are identified and recorded, and then, students' mental activities are recorded through the system constructed in this paper. Firstly, the data collection performance of the system is evaluated, and the results are shown in Table 1 and Figure 9.

Through the above analysis, we can see that the correlation analysis system of students' classroom behaviors and mental activities based on improved machine learning constructed in this paper has high accuracy in data collection of students' classroom behavior features and students' mental activity features. On this basis, this paper studies the correlation between students' classroom behaviors and mental activities, and the results are shown in Table 2 and Figure 10.

From the above analysis results, we can see that there is a significant correlation between students' classroom behaviors and their 2-dimensional activities. Therefore, teachers can judge students' mental activities according to students' classroom behaviors, which is convenient for timely adjustment of teaching strategies and maximum improvement of classroom teaching effect.

6. Conclusion

In this paper, we improve the traditional feature recognition algorithm and show how to extract the label correlation features of neighboring instances and view the neighboring instance label distribution information as neighboring features and then use the neighboring features to calculate the label correlation. Moreover, this paper proposes a method that integrates label relevance features and sample features. The method obtains the reliability of the neighbor information by the magnitude of the probability of occurrence or nonoccurrence of the neighbor prediction labels and corrects the results of the neighbor features.

This study designs and implements analysis system of the correlation between students' classroom behaviors and mental activity based on improved machine learning, which consists of multiple smart hardware devices, a LAN off device, and a terminal visualization and analysis software. Moreover, the system can collect real-time data on classroom behavioral changes of multiple individuals in classroom teaching, transform them into group attention levels through calculation, and visualize them through terminal software. In addition, the system can be used as a real-time supplemental monitoring tool for instructors on classroom conditions, as well as a long-term digital record of classroom instruction and behavior analysis for educators and schools.

Data Availability

The labeled data set used to support the findings of this study are available from the corresponding author upon request.

Conflicts of Interest

The author declares no competing interests.

Acknowledgments

This study is sponsored by Research on the Issue of National Identity Education in Guangdong Colleges and Universities Promoting the Return of Young Students in Hong Kong Under the Perspective of Branding Vision, Research Project of Party Building in Study Conference of Party Building in Guangdong Colleges and Universities in 2019 (project No. 2020MB015), and Analysis on the Brand Development Strategy of Independent Colleges Guided by Party Construction, Key Research Topics of Party Building and Ideological and Political Education of Zhuhai College of Jilin University in 2019 (project No. 2019JZDJ001).

References

[1] G. Wang, J. Sun, J. Ma, K. Xu, and J. Gu, "Sentiment classification: the contribution of ensemble learning," *Decision Support Systems*, vol. 57, pp. 77–93, 2014.

[2] S. Vishwakarma and S. Kumar, "A lexical approach for tweets sentiment classification," *Journal of Applied Physics*, vol. 76, no. 3, pp. 1980–1982, 2015.

[3] L. Dong, F. Wei, S. Liu, M. Zhou, and K. Xu, "A statistical parsing framework for sentiment classification," *Computational Linguistics*, vol. 41, no. 2, pp. 293–336, 2015.

[4] F. Fang, K. Dutta, and A. Datta, "Domain adaptation for sentiment classification in light of multiple sources," *INFORMS Journal on Computing*, vol. 26, no. 3, pp. 586–598, 2014.

[5] S. Zhou, Q. Chen, and X. Wang, "Fuzzy deep belief networks for semi-supervised sentiment classification," *Neurocomputing*, vol. 131, pp. 312–322, 2014.

[6] S. M. Liu and J. H. Chen, "A multi-label classification based approach for sentiment classification," *Expert Systems with Applications*, vol. 42, no. 3, pp. 1083–1093, 2015.

[7] L. Shang, Z. Zhou, and X. Liu, "Particle swarm optimization-based feature selection in sentiment classification," *Soft Computing*, vol. 20, no. 10, pp. 3821–3834, 2016.

[8] A. Moreo Fernández, A. Esuli, and F. Sebastiani, "Distributional correspondence indexing for cross-lingual and cross-domain sentiment classification," *Journal of Artificial Intelligence Research*, vol. 55, pp. 131–163, 2016.

[9] S. Harer and S. Kadam, "Sentiment classification and feature based summarization of movie reviews in mobile environment," *International Journal of Computer Applications*, vol. 100, no. 1, pp. 30–35, 2014.

[10] Z. Zhang, Z. Wang, C. Gan, and P. Zhang, "A double auction scheme of resource allocation with social ties and sentiment classification for device-to-device communications," *Computer networks*, vol. 155, pp. 62–71, 2019.

[11] Y. Li, J. Wang, S. Wang, J. Liang, and J. Li, "Local dense mixed region cutting + global rebalancing: a method for imbalanced text sentiment classification," *International Journal of Machine Learning and Cybernetics*, vol. 10, no. 7, pp. 1805–1820, 2019.

[12] V. N. Phu, N. D. Dat, V. T. Ngoc Tran, V. T. Ngoc Chau, and T. A. Nguyen, "Fuzzy C-means for English sentiment classification in a distributed system," *Applied Intelligence*, vol. 46, no. 3, pp. 717–738, 2017.

[13] M. Huang, Q. Qian, and X. Zhu, "Encoding syntactic knowledge in neural networks for sentiment classification," *ACM Transactions on Information Systems*, vol. 35, no. 3, pp. 1–27, 2017.

[14] Y. Liu, J. W. Bi, and Z. P. Fan, "Multi-class sentiment classification: the experimental comparisons of feature selection and machine learning algorithms," *Expert Systems with Applications*, vol. 80, pp. 323–339, 2017.

[15] M. Iqbal, A. Karim, and F. Kamiran, "Balancing prediction errors for robust sentiment classification," *ACM Transactions on Knowledge Discovery from Data*, vol. 13, no. 3, pp. 1–21, 2019.

[16] M. E. Basiri, A. Kabiri, M. Abdar, W. K. Mashwani, N. Y. Yen, and J. C. Hung, "The effect of aggregation methods on sentiment classification in Persian reviews," *Enterprise Information Systems*, vol. 14, no. 9-10, pp. 1394–1421, 2020.

[17] D. Wang, B. Jing, C. Lu et al., "Coarse alignment of topic and sentiment: a unified model for cross-lingual sentiment classification," *IEEE Transactions on Neural Networks and Learning Systems*, vol. 32, no. 2, pp. 736–747, 2021.

[18] G. Rao, W. Huang, Z. Feng, and Q. Cong, "LSTM with sentence representations for document-level sentiment classification," *Neurocomputing*, vol. 308, pp. 49–57, 2018.

[19] G. Lee, J. Jeong, S. Seo, C. Y. Kim, and P. Kang, "Sentiment classification with word localization based on weakly supervised learning with a convolutional neural network," *Knowledge-Based Systems*, vol. 152, pp. 70–82, 2018.

Hindawi
Journal of Sensors
Volume 2021, Article ID 2251530, 17 pages
https://doi.org/10.1155/2021/2251530

Research Article

Multisource Data Fusion Diagnosis Method of Rolling Bearings Based on Improved Multiscale CNN

Yulin Jin, Changzheng Chen, and Siyu Zhao

School of Mechanical Engineering, Shenyang University of Technology, Shenyang 110000, China

Correspondence should be addressed to Changzheng Chen; czchen@sut.edu.cn

Received 24 August 2021; Accepted 15 October 2021; Published 9 November 2021

Academic Editor: Ying-Ren Chien

Intelligent diagnosis applies deep learning algorithms to mechanical fault diagnosis, which can classify the fault forms of machines or parts efficiently. At present, the intelligent diagnosis of rolling bearings mostly adopts a single-sensor signal, and multisensor information can provide more comprehensive fault features for the deep learning model to improve the generalization ability. In order to apply multisensor information more effectively, this paper proposes a multiscale convolutional neural network model based on global average pooling. The diagnostic model introduces a multiscale convolution kernel in the feature extraction process, which improves the robustness of the model. Meanwhile, its parallel structure also makes up for the shortcomings of the multichannel input fusion method. In the multiscale fusion process, the global average pooling method is used to replace the way to reshape the feature maps into a one-dimensional feature vector in the traditional convolutional neural network, which effectively retains the spatial structure of the feature maps. The model proposed in this paper has been verified by the bearing fault data collected by the experimental platform. The experimental results show that the algorithm proposed in this paper can fuse multisensor data effectively. Compared with other data fusion algorithms, the multiscale convolutional neural network model based on global average pooling has shorter training epochs and better fault diagnosis results.

1. Introduction

A rolling bearing is an indispensable part of industry. In the application process, in order to improve the safety and reliability of machine operation, the state of rolling bearings must be evaluated regularly [1–4]. The traditional fault diagnosis method is to process and analyze the fault signal in the time and frequency domains by the signal processing method and rely on certain expert experience to achieve the purpose of fault diagnosis [5–7]. However, in the actual diagnosis process, this fault diagnosis method is more complicated. In recent years, with the development of machine learning, some machine learning algorithms, such as ANN [8], SVM [9–11], and KNN [12, 13], have been applied to fault diagnosis. These machine learning algorithms have been proved to solve classification problems. However, these algorithms need to extract input features manually. In the mechanical fault signal, especially in the early stage of faults or in the presence of noise interference, it is difficult to extract sensitive fault features effectively.

In recent years, deep learning based on the deep neural network has developed rapidly and has been successfully applied to computer vision [14, 15], natural language processing [16], speech processing [17], sleep-arousal detection [18], and other fields. Deep learning introduces the convolution kernel with variable weight into the deep network to extract features adaptively, which simplifies the complex work of feature extraction and avoids the inaccuracy of manual feature extraction. The advantage makes deep learning algorithms such as convolutional neural networks (CNN) [19] and deep belief networks (DBN) [20] widely used in the field of fault diagnosis. Fault diagnosis is expected to become more intelligent and more suitable for modern industrial trends. At present, signal preprocessing methods based on CNN can be roughly divided into fault diagnosis methods based on one-dimensional (1D) CNN and fault diagnosis methods based on two-dimensional (2D) CNN. The fault diagnosis method based on 1D CNN is to take the collected 1D time-domain signal as the input of the network directly. Ince et al. used a one-dimensional

convolutional neural network model with adaptive feature extraction for fault diagnosis [21]. Liu et al. constructed a multitask one-dimensional convolutional neural network to solve the problem of fault diagnosis [22]. Liu et al. combined a denoising convolutional autoencoder with a one-dimensional convolutional neural network for fault diagnosis in the noisy environment [23]. The fault diagnosis method based on 2D CNN is to transform the one-dimensional time-domain signal into a two-dimensional form and inputs it into the network. Transforming the one-dimensional time-domain signals into two-dimensional time-frequency diagrams is a common method [24–26]. Meanwhile, some researchers have also used ingenious ways to transform the time-domain signal in dimensionality [27–29]. In terms of model improvement, researchers have also adopted a variety of ways to improve the diagnostic ability of the model. Wang et al. improved the calculation speed and stability of the network by adding a batch normalization layer [30]. Jiang et al. constructed a 1D multiscale model for fault diagnosis [31]. Wang et al. constructed a joint attention module (JAM) and added it to the diagnosis model, which effectively improved the diagnosis performance of the model [32].

The above fault diagnosis problems are dealt with by the fault signal measured by a single sensor. In practice, unilateral information is often one-sided, and the information of a single sensor may not fully reflect the fault features due to the installation location, installation direction, and other factors. Using more comprehensive multisensor signals can further improve the diagnostic capability of the deep learning model. At present, researchers have adopted a variety of methods to diagnose faults with multisource data. Wang et al. constructed time-domain multisensor signals at different locations into a two-dimensional matrix and used improved two-dimensional CNN for diagnosis and classification [33]. Xu et al. proposed an integration model based on multisensor information fusion [34]. Shan et al. fused the extracted feature factors of multiple sensor signals and used CNN for fault classification [35]. Wang et al. converted multisensor data into color images and constructed an improved CNN based on LeNet-5 for classification [36]. Xia et al. input multisensor data into the CNN model through multiple channels to solve the composite diagnosis problem [37]. Gu et al. proposed a multisensor fault diagnosis model based on discrete wavelet transform (DWT) and long short-term memory (LSTM) [38]. Kou et al. fused the monitoring information of multisensors after normalization and classified it by CNN [39]. Li et al. proposed a fault diagnosis method based on multiscale permutation entropy (MPE) and multichannel fusion convolutional neural network (MCFCNN) [40]. Peng et al. extracted features from multisensor information through short-time Fourier transform (STFT) and input the fused features into the depth residual neural network to solve the problem of fault diagnosis [41].

The above method combines multisensor information to provide more comprehensive signal features for the deep learning model to improve the representation capability.

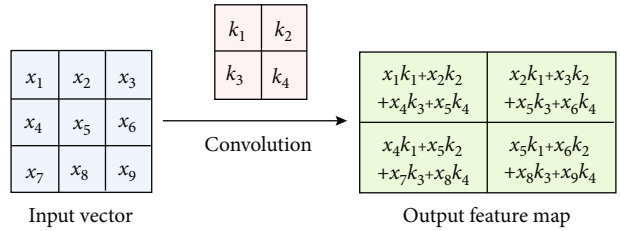

Figure 1: Schematic diagram of the convolution process.

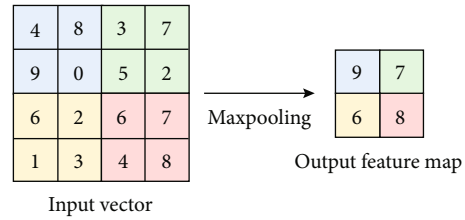

Figure 2: Schematic diagram of the maximum pooling process.

However, in the actual signal acquisition process, there is often noise interference, which will reduce the significance of fault features to a certain extent, weaken the feature differences between various fault categories, and make the training process of the deep learning model more difficult. When a certain sensor data is greatly affected by noise, adding it to the training sample will reduce the quality of the input sample. In this case, only the multisensor data is fused, but the model is not improved in a targeted manner, which will reduce the performance of the overall model.

In order to solve the problem mentioned above, this paper proposes a multiscale CNN model based on global average pooling (MSCNN-GAP). First, a data preprocessing method without expert experience is used to transform the one-dimensional time-domain signal into a two-dimensional form. Then, the processed data is input into the model. In this model, multiscale convolution kernels are introduced to extract sample features in diversity. Multifeature extraction makes the deep learning model more suitable for fault diagnosis with noise. The parallel feature extraction method in the multiscale structure is also better adapted to data fusion. In the fusion part of the network, in order to maintain the feature space of each branch channel, the global average pooling (GAP) layer is used to replace the traditional fully connected layer in the dimensionality reduction method, which further improves the performance of the network. Finally, the effectiveness of MSCNN-GAP is verified by data comparison.

The innovations and main contributions of this article are described as follows:

(1) For the multisensor fusion model, the influence of noise factors that may exist in the process of signal acquisition on the performance of the model is further considered

(2) In order to improve the adaptability of the model to noise, an MSCNN-GAP model with a parallel structure is established

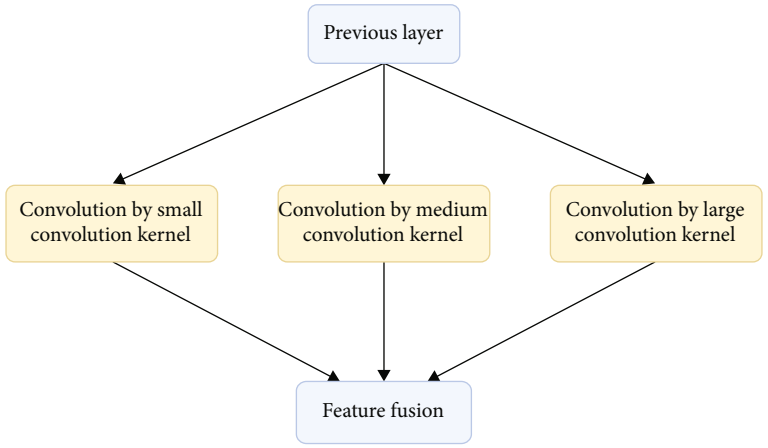

Figure 3: Schematic diagram of the multiscale CNN structure.

(3) In the feature fusion process, the GAP layer is used. The GAP layer reduces the number of network parameters and preserves the spatial structure of each feature during feature fusion to further improve the performance of the model

(4) A comprehensive experiment is designed and executed to verify the effectiveness and robustness of the proposed MSCNN-GAP comprehensively

This article is organized as follows. Section 2 introduces the basic theory of multiscale CNN and global average pooling. Section 3 introduces the diagnosis method of MSCNN-GAP. In Section 4, the experimental verification is carried out, and the experimental results are discussed. Finally, the conclusion is given in Section 5.

2. Basic Theory

2.1. Multiscale Convolutional Neural Network. CNN is a common network form in deep learning. It was first proposed by Lecun et al. and applied to classify handwritten digits [42, 43]. The basic CNN consists of three parts: convolution, activation, and pooling [44]. Convolution is the most basic and essential operation in CNN. The convolution operation adopts a fixed-size convolution kernel to slide on its input to extract the input features. The schematic diagram of the convolution operation is shown in Figure 1. The output result of the n-th feature map of the m-th layer can be expressed as

$$X_n^m = \sum_{k=1}^{K} x_k^{m-1} \cdot \omega_k + b_n^m, \tag{1}$$

where x_k^{m-1} represents the k-th output feature map of the previous layer, ω_k represents the weight of the convolution kernel corresponding to the k-th feature map, b_n^m represents the bias term, and K represents the total number of channels in the previous layer.

After the convolution operation, the activation function will process the convolution output nonlinearly. Adding a nonlinear activation layer can make the model nonlinear so that the network can be used to solve more complex nonlinear problems. The common nonlinear activation functions include the sigmoid function, tanh function, ReLU function [45], and PReLU function [46]. The output result after nonlinear activation can be expressed as

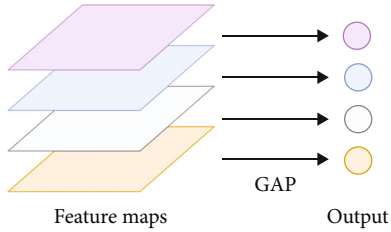

Figure 4: Schematic diagram of the GAP process.

$$z = h(X_n^m), \tag{2}$$

where $h(\cdot)$ represents the nonlinear activation function, X_n^m represents the output of the previous convolution layer, and z represents the output term.

Pooling is a way of downsampling. Adding a pooling layer after the activation function can reduce the number of parameters and extract the key features. The schematic diagram of the maximum pooling process is shown in Figure 2. Meanwhile, the pooling operation can also be used as a nonlinear operation to improve the representation capability of the model.

With the development of deep learning, CNN is used to deal with more complex problems. In the face of these problems, stacking deeper neural networks is a common solution. However, due to the excessive number of parameters of the deep neural network, the problem of gradient instability is prone to occur in the training process, which makes training more difficult. To solve this problem, the Google team first proposed a multiscale structure [47]. The multiscale structure uses multiple parallel CNN structures to replace the deep network and finally merges the feature extraction results of each branch. Multiscale CNN can also use diverse

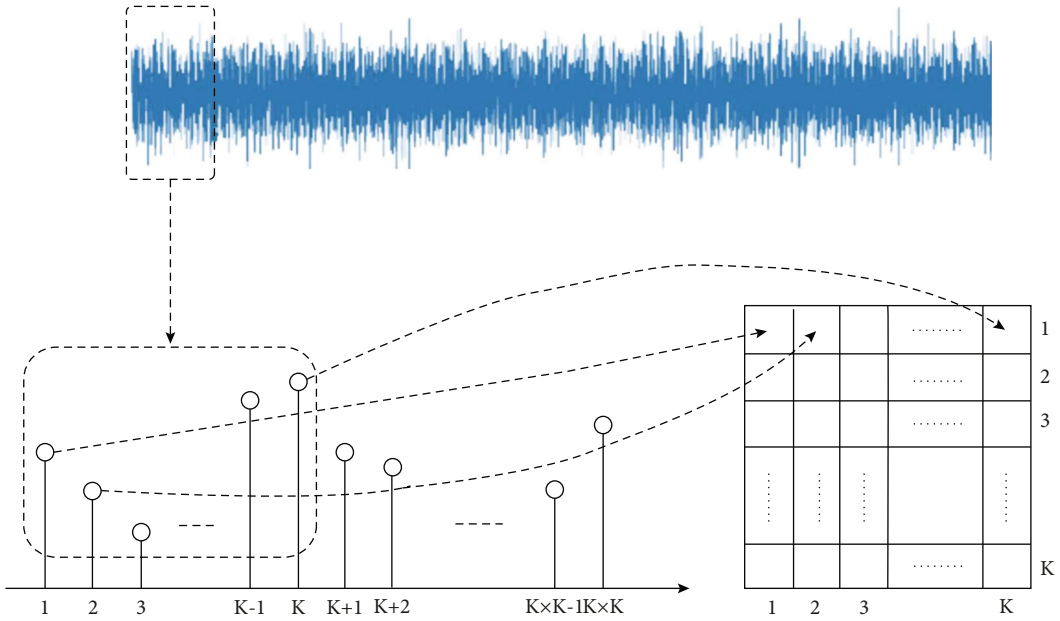

Figure 5: Data conversion process.

Table 1: Network parameters.

Layer	Input	Output	Batch normalization
C1	1 × 64 × 64	16 × 64 × 64	Yes
P1	16 × 64 × 64	16 × 32 × 32	—
C2	16 × 32 × 32	32 × 32 × 32	Yes
P2	32 × 32 × 32	32 × 16 × 16	—
C3	32 × 16 × 16	64 × 16 × 16	Yes
P3	64 × 16 × 16	64 × 8 × 8	—
C4	64 × 8 × 8	128 × 8 × 8	Yes
P4	128 × 8 × 8	128 × 4 × 4	—
GAP	128 × 4 × 4	128 × 1 × 1	—

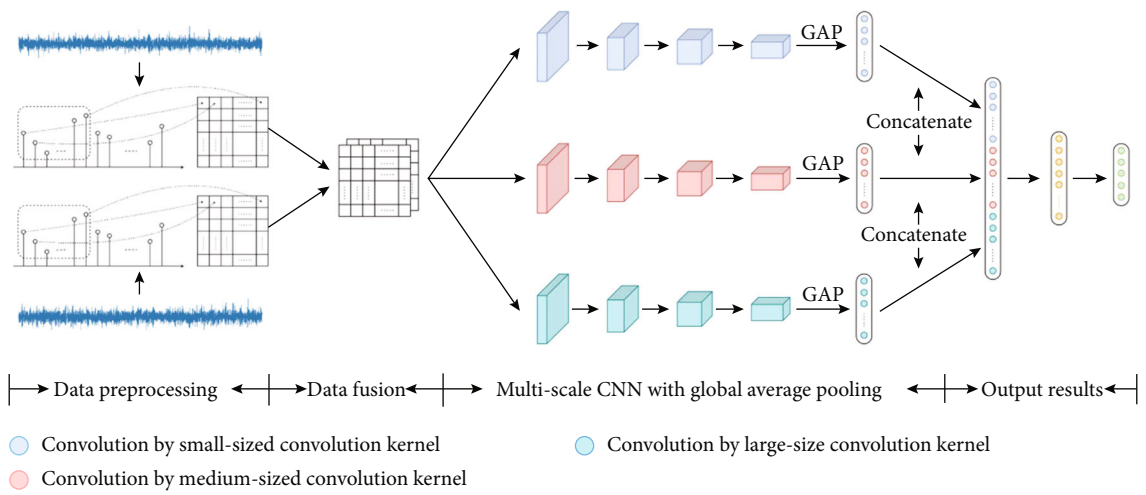

Figure 6: Fault diagnosis method based on MSCNN-GAP.

convolution kernels to extract input features at the same time, which further improves the performance of CNN. The schematic diagram of the multiscale structure is shown in Figure 3. For the multiscale structure of three branches, the fusion process can be expressed as

$$x = \text{Concatenate}(\sigma_1, \sigma_2, \sigma_3), \tag{3}$$

where σ_1, σ_2, and σ_3 represent the feature vectors extracted from each scale and Concatenate $(\cdot)$ represents the fusion process of one-dimensional vectors.

2.2. Global Average Pooling. Normally, CNN will reshape the feature maps into a set of one-dimensional feature vectors after the feature extraction and output the final classification results by using several fully connected layers. In the case of a large number of channels, there will be more parameters in the fully connected layer, and the model will be more complicated. In the reshaping process, the fully connected layer will also lose the spatial position information of the feature maps between the channels. GAP replaces the feature maps of each channel with a feature number. The GAP layer can reduce the amount of data in the model significantly, lower the risk of overfitting in the fully connected layer, and retain the spatial position information of each channel effectively. The global average pooling with c channels can be expressed as

$$x_c = \text{Avgpool}(y_c) = \frac{1}{P \times Q} \sum_{i=1}^{P} \sum_{j=1}^{Q} y_c(i, j), \tag{4}$$

where x is the output of GAP, y is the input of GAP, and P and Q are the width and height of the channel feature maps. The schematic diagram of GAP is shown in Figure 4.

3. Intelligent Diagnosis Method of MSCNN-GAP

3.1. Data Preprocessing. Data preprocessing is an essential part of the fault diagnosis process. An excellent preprocessing method can show the fault features better to improve the performance of the deep learning model. The most common preprocessing method is to transform time-domain signals into time-frequency graphs. However, this processing method is more complicated and requires a certain amount of expert experience. In this paper, one-dimensional time-domain data is transformed into two-dimensional matrices by dimension transformation [25]. The conversion diagram is shown in Figure 5. For a one-dimensional signal, $K \times K$ sampling points are taken as a sample, and each K sample point are taken as a row and arranged in columns in turn to form a two-dimensional matrix of $K \times K$. This preprocessing method does not require expert experience. Furthermore, it reduces the complexity of preprocessing.

3.2. Fault Diagnosis Method Based on MSCNN-GAP. In order to reflect the fault features more comprehensively, this paper uses multisensor data for fault diagnosis. The multisensor data will be input to the network model as multichannels. When the signal sample collection process is disturbed by noise factors, the fault features will be covered by the noise information, which will greatly impact the feature extraction process and reduce the diagnostic capability of the model. In order to weaken this influence and improve the robustness of the model, this paper constructs an MSCNN-GAP model. Compared with the single convolution kernel CNN, the multiscale CNN can select the convolution kernel size more flexibly to extract input features, thereby improving the noise tolerance of the model. Meanwhile, the multiscale CNN is a parallel structure. When facing training sample sets with noise, the multiscale structure can update the parameters of each branch more flexibly to better adapt to the multisource fusion dataset. In traditional CNN, the extracted feature maps will be reshaped into a set of one-dimensional feature vectors, and the final classification result will be output through the fully connected layer. This reshaping method will change the spatial structure of the feature maps. In the multiscale fusion process, maintaining the spatial structure of the feature maps of each branch is more helpful for training the network model. Therefore, the global average pooling is selected at the end of each branch instead of the traditional method of reshaping the

Figure 7: Experimental facility.

Table 2: Description of the bearing health condition.

	Condition description	Fault degree
NO	Normal condition	None
REF	Rolling element fault	Obvious
ORF	Outer ring fault	Obvious
IRF1	Inner ring faults	Obvious
IRF2	Inner ring faults	Serious

Table 3: Description of the fault diagnosis task.

Group	Vertical SNR	Horizontal SNR	Training sample	Test samples
A	0	0	500	500
B	-3	0	1000	500
C	-5	0	1000	500
D	0	-3	1000	500
E	0	-5	1000	500
F	-3	-3	1500	500
G	-5	-5	1500	500

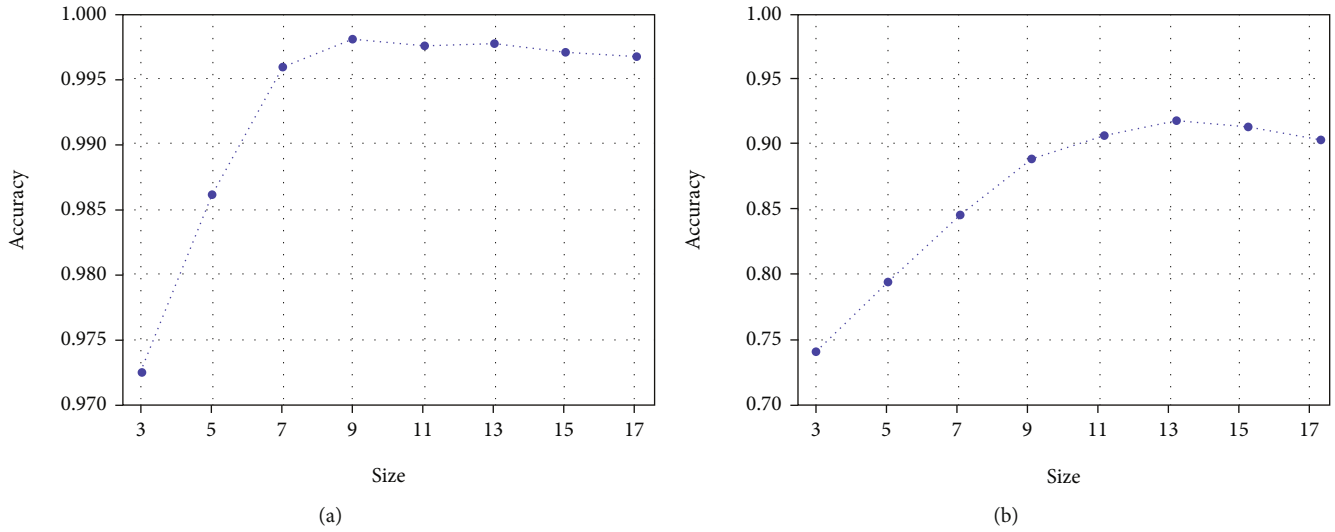

Figure 8: The influence of different sizes of convolution kernels on the model.

convolution layer into a one-dimensional vector. This makes the output results maintain the spatial structure of the feature maps in the fusion process and better adapt to the multiscale fusion process.

In order to contain as many signal features as possible, 4096 sampling points are selected as a group of signal samples. In the convolution process, three different sizes of convolution kernels are used to extract input features from the diversity. After each convolution and pooling calculation, nonlinear activation is performed by the ReLU function, and the batch normalization layer is added to improve the calculation speed. Finally, a hidden layer with 100 neurons is used to reduce the dimensionality of the fused one-dimensional vector, and the final classification result is output through the output layer. Table 1 shows the specific parameters of the convolution process of each branch. Figure 6 shows the structure diagram of the overall diagnosis model.

4. Experimental Verification

4.1. Experimental Dataset. In this paper, the fault data measured by the bearing fault experimental platform is used to verify the effectiveness of the algorithm. The experimental platform is shown in Figure 7. The platform is mainly composed of an AC motor, support bearing, base, rotating shaft, test bearing, and loading system. The model of the faulty bearing is SKFNU205. The fault types of the faulty bearing are shown in Table 2.

During the signal acquisition process, the loading system exerts a certain radial force on the faulty bearing. A horizontal sensor and a vertical sensor are used to collect signals in different directions, respectively. The sampling frequency of the signal is 16384 Hz, and the speed of the motor is 1487 r/min. In order to better verify the capability of the model to extract features, the collected fault signals are normalized in amplitude, which weakens the feature gap between the categories and further improves the difficulty of classification.

Table 4: Comparison of results of different algorithms.

Number	Algorithm	Accuracy (%)	Standard deviation
1	CNN (vertical)	99.08	0.858836
2	CNN (horizontal)	97.62	1.157411
3	MCCNN (combination)	98.6	0.758947
4	MSCNN (combination)	99.14	0.732393
5	MSCNN-GAP (combination)	99.93	0.149071

In order to better simulate the signal data in the case of noise, white noise with different signal-to-noise ratios (SNR) is added to the signals collected in different directions. The SNR can be defined as

$$\mathrm{SNR} = 10 \log_{10}\left(\frac{P_{\mathrm{signal}}}{P_{\mathrm{noise}}}\right), \tag{5}$$

where P_{signal} and P_{noise} are the power of the signal and noise.

Every 4096 sampling points of signal data are taken as a sample, and several groups of sample sets for training and testing are constructed by resampling. Among them, Group A has a relatively simple sample because there is no noise factor, and 500 training samples will be used to train the model. Group B, Group C, Group D, and Group E have certain noise factors, and 1000 training samples will be used. Group F and Group G are most affected by noise, and 1500 training samples are used for training. The specific parameters of several sample sets are shown in Table 3.

4.2. Selection of the Convolution Kernel. The size of the convolution kernel is one of the important hyperparameters in CNN. Convolution kernels of different sizes are adapted to different types of datasets. In order to maximize the

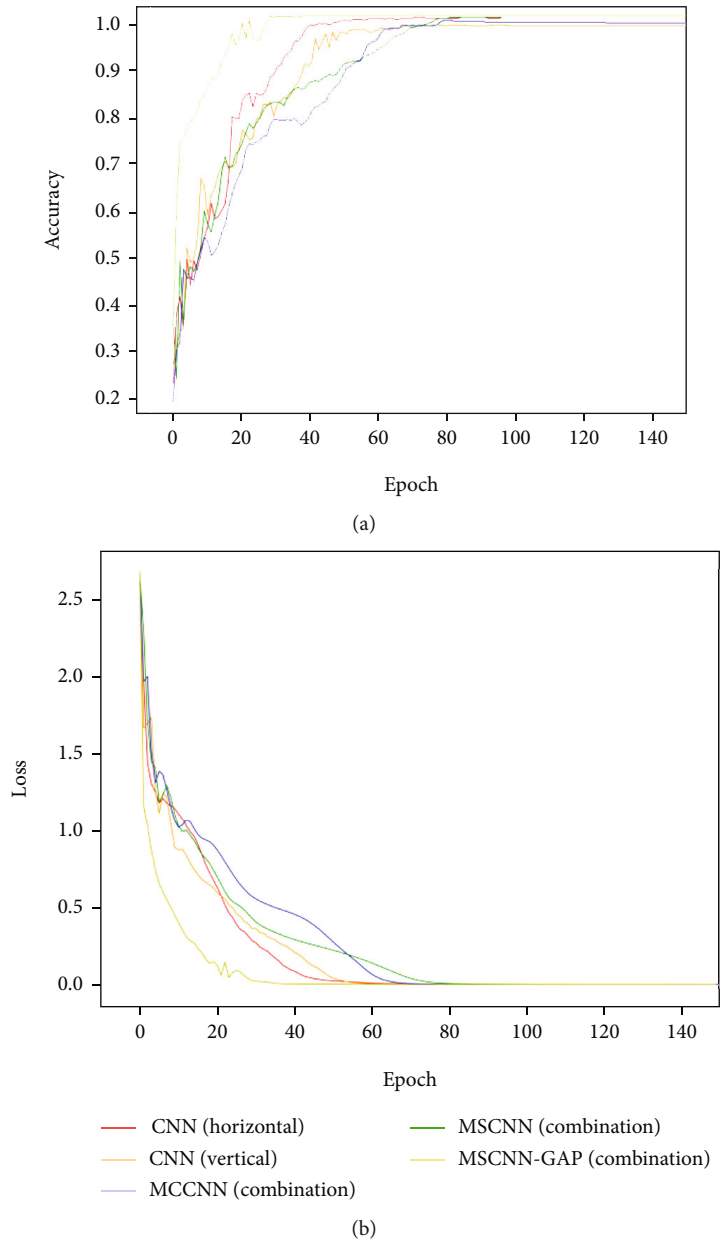

Figure 9: Model loss and classification accuracy for different algorithms.

diagnostic performance of CNN, this paper first tested the effect of different sizes of convolution kernels on the results. The signal data collected in the vertical direction is selected as the experimental sample. MSCNN-GAP with single-sensor information was chosen as the experimental algorithm. The experimental results are shown in Figure 8. The training set of Figure 8(a) uses 500 training samples. The training set in Figure 8(b) uses 1500 samples with SNR-5.

The results show that the smaller convolution kernel has a poor feature extraction effect due to the smaller receptive field for this dataset. To a certain extent, the performance of CNN is enhanced with the widening of the convolution kernel size. The convolution kernel with the size of 9 is the best when the sample has no noise interference. In the case of noise interference, the convolution kernel with the size of 13 has the best effect. After reaching the optimal value, with the gradual widening of the convolution kernel size, the diagnostic ability of CNN has a downward trend. The reason is that a large convolution kernel size is weak for local feature extraction. The comparison results of the two groups of data show that when the signal is disturbed by noise, the local features of the sample are weakened, and the larger convolution kernel that can better extract global features is more suitable for noisy datasets.

4.3. Comparative Analysis of Algorithms. In this section, we will verify the computational complexity of the proposed algorithm and its performance in multidata fusion. In order to better reflect the superiority of MSCNN-GAP, three other different algorithms are compared:

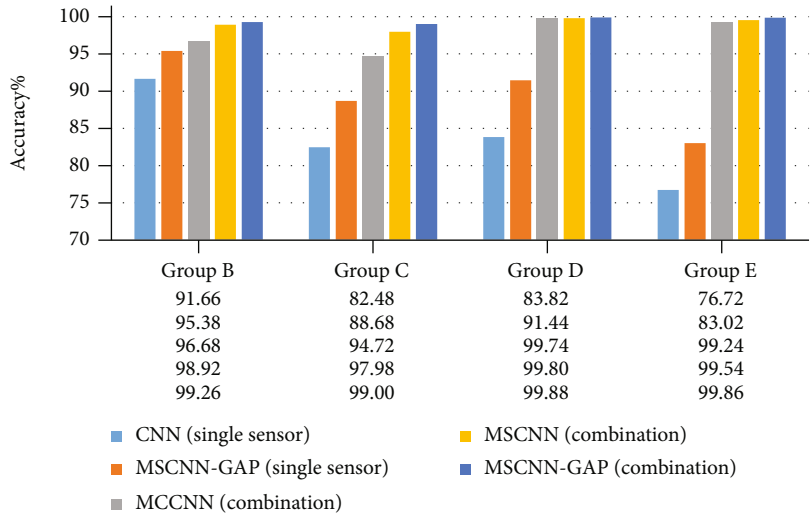

Figure 10: Comparison of results of different algorithms.

CNN (single sensor). This model uses a single-sensor signal as the input of CNN. The CNN model consists of four convolution modules and two fully connected layers. Each group of convolution modules is composed of a convolution layer, a pooling layer, and a normalization layer. At the end of convolution, the feature map is reshaped into a one-dimensional vector, and the dimension is reduced by a fully connected layer. Finally, the classification results of CNN are output [25].

Multichannel CNN (MCCNN). In order to apply multisensor information, multisensor data is input to MCCNN in the form of multichannel input. The specific structure of the MCCNN model is the same as the CNN model in algorithm 1 [34].

Multiscale CNN (MSCNN). Based on multichannel input in algorithm 2, in order to further improve the performance of CNN, this algorithm uses multiscale convolution kernel diversity to extract the features of the input. After the convolution operation of each branch, the feature map will be reshaped into a one-dimensional vector and reduced by the fully connected layer. Then, the one-dimensional vectors of each branch are merged and reduced again by the fully connected layer. Finally, the fully connected layer is used to output the final classification results [29].

MSCNN-GAP. The algorithm proposed in this paper uses multisensor data for fault diagnosis. Multisensor data will be input into the model as multiple channels. Based on CNN, a multiscale parallel structure is adopted to reduce the impact of noisy data on the model and improve the robustness of the model. After the convolution operation of each branch, the feature map of each branch will be reduced through the global average pooling layer, and the reduced feature vectors will be fused. GAP not only reduces the parameters of the model but also retains the spatial structure of the feature map before fusion. The fused feature vector will be reduced through a fully connected layer, and finally, the classification results will be output through a fully connected layer.

Computational complexity is a problem that must be considered in the deep learning model. The smaller the computational complexity, the shorter the computational time, and the higher the computational efficiency. This paper verifies the complexity of the proposed model from two aspects: time complexity and model parameters. For a convolutional neural network, its time complexity can be expressed as

$$\textbf{Time} \sim O\left(M^2 \cdot K^2 \cdot C_{\text{in}} \cdot C_{\text{out}}\right), \tag{6}$$

where M is the size of the output feature map, K is the size of the convolution kernel, C_{in} is the number of input channels of the convolution layer, and C_{out} is the number of output channels of the convolution layer [48].

Thus, the time complexity of the fully connected layer and the global average pooling layer can be deduced as follows:

$$\begin{aligned} \textbf{Time} &\sim O\left(1^2 \cdot X^2 \cdot C_{\text{in}} \cdot C_{\text{out}}\right), \\ \textbf{Time} &\sim O\left(C_{\text{in}} \cdot C_{\text{out}}\right), \end{aligned} \tag{7}$$

where X is the number of neurons in the fully connected layer.

The algorithm proposed in this paper uses the global average pooling layer to replace the traditional fully connected layer at the end of the convolution operation. We input the network parameters of the fully connected layer and the global average pooling layer into the time complexity calculation formula. The time complexity involved is

$$128^2 \cdot 4^2 \cdot 4^2 \Rightarrow 128^2. \tag{8}$$

The former represents the time complexity of traditional multiscale CNN. The latter represents the time complexity of MSCNN-GAP. The result shows that the proposed algorithm is superior to the traditional multiscale CNN model in time complexity. From the point of view of the parameters

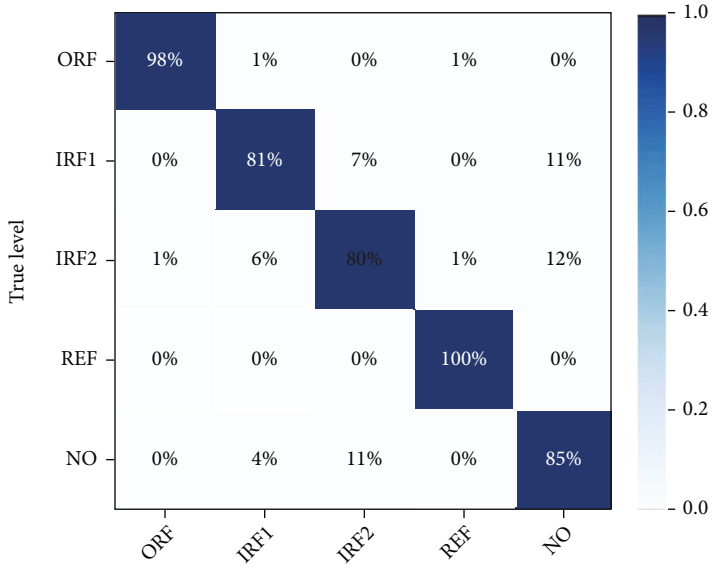

(a) MSCNN-GAP (single sensor)

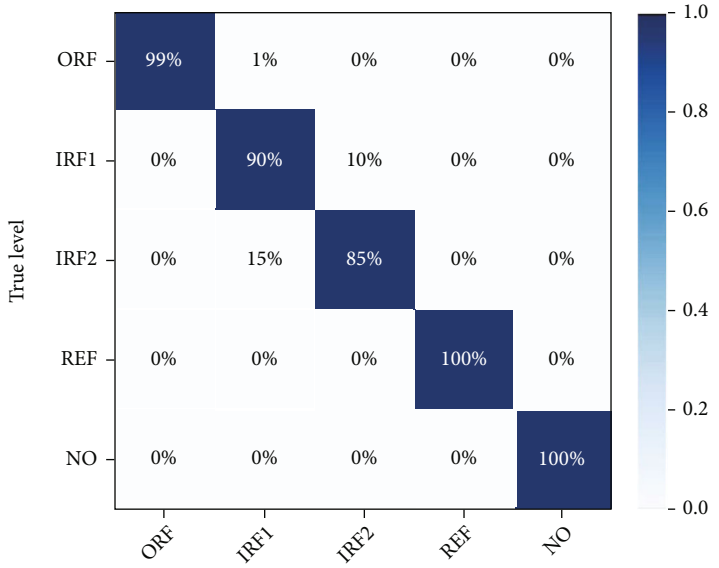

(b) MCCNN (combination)

Figure 11: Continued.

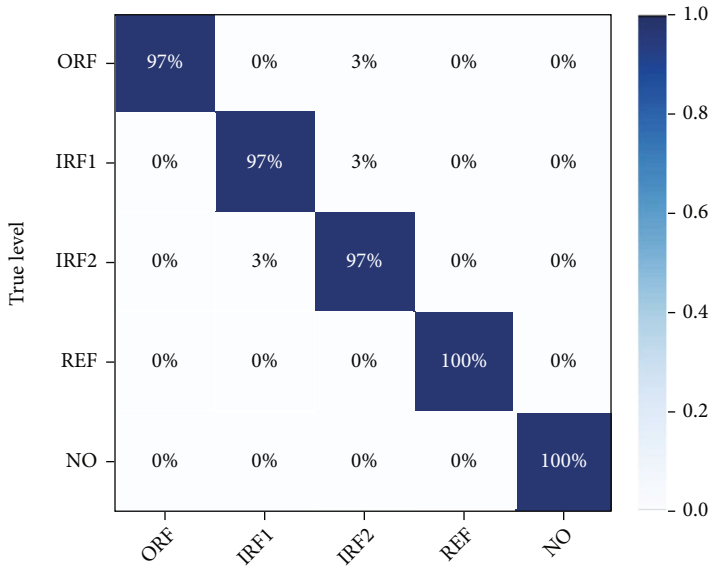

(c) MSCNN (combination)

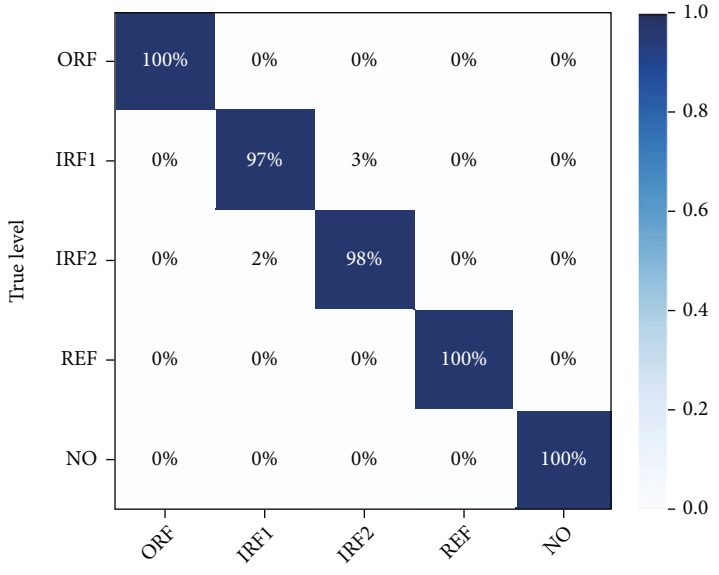

(d) MSCNN-GAP (combination)

Figure 11: Confusion matrix results of each algorithm.

of the model, K variable weights are needed to calculate the final output for the fully connected layer containing K neurons. The global average pooling layer outputs the final result by obtaining the average value of its feature map and does not need other parameters to participate in the calculation. Therefore, the algorithm proposed in this paper has fewer parameters. In conclusion, the computational complexity of the proposed algorithm is less than that of the traditional multiscale CNN model.

The performance of the algorithm will be verified below. According to the results of the previous section, we use a convolution kernel of size 9 as the feature extractor of CNN to extract the input features of noiseless samples. For noisy samples, we use a convolution kernel of size 13. For the multiscale model, the best convolution kernel size and its adjacent convolution kernel size are used for feature extraction.

In order to avoid contingency, each model is cross-validated ten times, and the average of the final results is obtained. The results are shown in Table 4.

The results show that the diagnostic ability based on the CNN algorithm can reach a high level in the absence of noise, which proves the feasibility of the CNN algorithm in fault diagnosis. In this experiment, because the

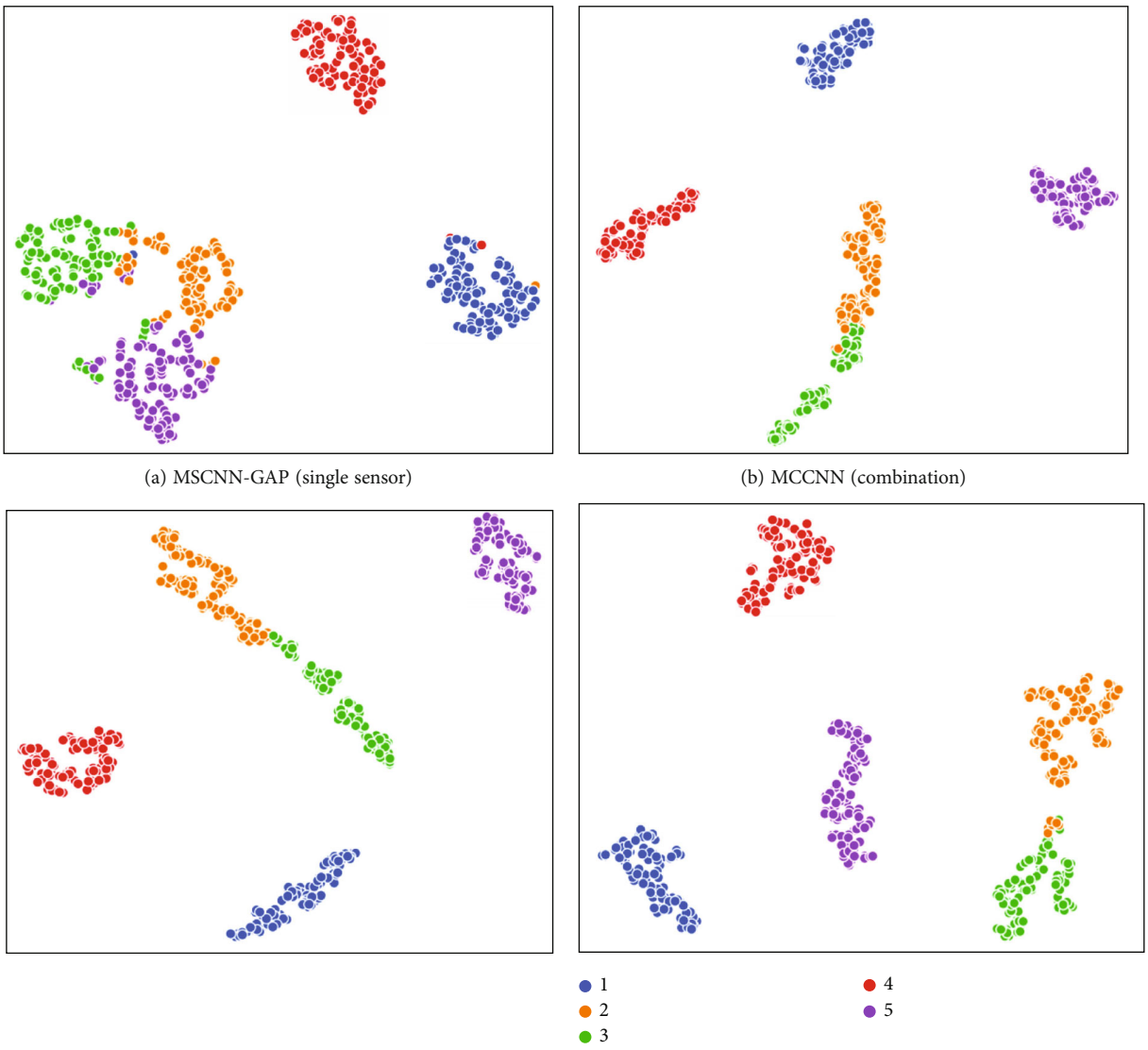

(a) MSCNN-GAP (single sensor)

(b) MCCNN (combination)

(c) MSCNN (combination)

(d) MSCNN-GAP (combination)

Figure 12: The t-SNE results of each algorithm.

surrounding noise interference is weak when the signal is collected, the fault features of each category are more obvious, and the results' gap between the algorithms is relatively small. Under the influence of different fault forms, fault locations, load directions, and other conditions, the significant degree of signal features collected by each direction sensor is different. In this experiment, since the load is applied in the vertical direction, compared with the horizontal direction, the signal features in the vertical direction will be more obvious. Therefore, the model trained by the signal collected by the vertical sensor has better results. In order to fuse multisensor data, only using multisensor information as multichannel input will make the result higher than the lower value trained by the single-sensor information and lower than the higher value. The reason is that for training samples with obvious features, the addition of samples with insufficient features causes a certain amount of noise interference and reduces the quality of the training set, which leads to the difficulty of feature extraction and reduces the performance of the model. In order to weaken the influence of this factor, a multiscale feature extraction method is introduced to effectively solve the problem of feature extraction difficulty and improve the accuracy of diagnosis. On this basis, the multiscale fusion method of global average pooling is introduced, which effectively retains the feature space structure while fusing so that the model achieves higher performance and more stable results.

Figure 9 shows the image of the accuracy and loss of each algorithm varying with the training epoch. The results show that CNN, MCCNN, and MSCNN all need more convergence epochs to achieve convergence. The convergence epoch of the MSCNN-GAP is greatly reduced. Meanwhile, the loss of the algorithm proposed in this paper decreases

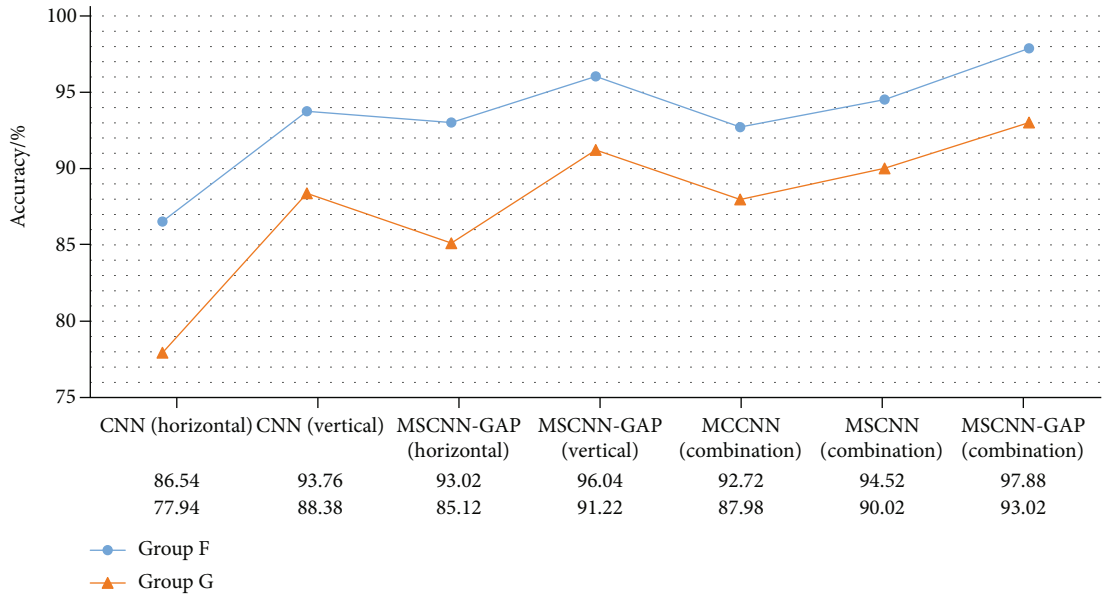

Figure 13: Comparison of diagnosis results of different algorithms.

faster, and the convergence process is more stable than other algorithms.

4.4. Comparative Analysis of Robustness. In the process of fault signal acquisition, it is often interfered with by the machine noise and surrounding noise. When there is much noise in the fault signal, the fault features will be covered by the noise information, which increases the difficulty of extracting effective features from the model. Noise will affect the quality of the dataset to a certain extent, thereby affecting the training process and the performance of the model. Therefore, the diagnostic model needs to have better robustness.

In this section, Groups B, C, D, and E will be used for comparative verification. The samples with noise factors are used as the training set for the algorithm using single-sensor data. Similarly, each algorithm is run ten times, and the average values are counted. The results are shown in Figure 10.

The results show that the diagnostic accuracy of the CNN model with single-sensor data is lower than 95% when the noise is weak. When the noise is serious, the diagnostic accuracy is lower than 85%. It also shows that the performance of the CNN model will be greatly affected by noise. The multiscale structure can extract more features and improve the diagnostic ability of the model. However, due to the interference of noise factors, the fault features are not obvious enough, and the diagnostic accuracy is relatively low. Combined with multisensor data, this problem can be alleviated effectively. In signal acquisition, due to the load in the vertical direction, the fault features of the signal collected in the vertical direction are more obvious. The feature extraction process will be more difficult when this group of signals is affected by the noise factors. This also makes the overall accuracy of Group D and Group E higher than Group B and Group C in the multisensor fusion algorithm. By adding multiscale information and using the global pooling method to save the feature space, the algorithm proposed in this paper better adapts to the samples with difficult feature extraction. It improves the diagnosis ability of the model.

Figure 11 shows the confusion matrix of each algorithm. The results show that the two categories of inner ring faults are most likely to be confused due to the same fault form. After adding the noise, this category of NO also has a certain degree of misjudgment. The diagnostic capability of CNN has declined to a certain extent. Multisource data can improve the representation capability of the network. However, it is difficult to extract features between similar fault categories, and there is still a large degree of confusion between the two inner ring faults. The multiscale model can extract features better and reduce the confusion between the two categories. The results show that this paper further improves the performance of the model by the multiscale fusion method using global average pooling.

In order to intuitively show the effectiveness of the proposed algorithm, we use the t-SNE algorithm to reduce the dimensionality and visualize the result of feature extraction. Figure 12 shows the t-SNE visualization results of the four algorithms. Among them, 1-5 represent the five fault categories of ORF, IRF1, IRF2, REF, and NO. The results show that with the continuous optimization of the algorithm, the classification effect of each algorithm is gradually improved, which corresponds to the results of the confusion matrix. The proposed algorithm shows better clustering performance. There is more excellent separability between features of different categories. It further proves the effectiveness of the algorithm proposed in this paper.

In extreme cases, multisensor signals may have noise interference at the same time, which further improves the difficulty of feature extraction. In order to further verify

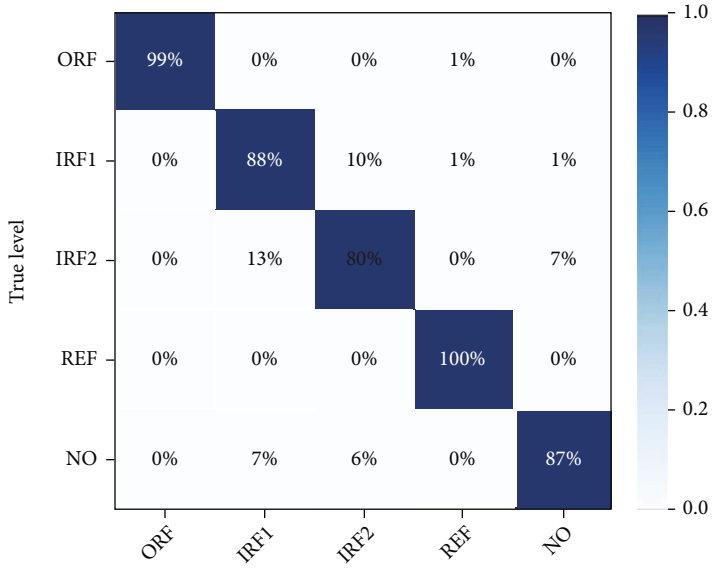

(a) MSCNN-GAP (vertical)

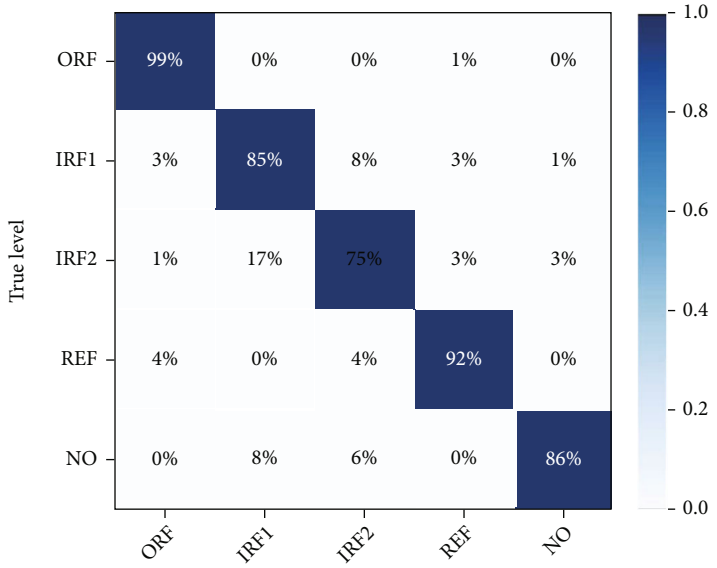

(b) MCCNN (combination)

Figure 14: Continued.

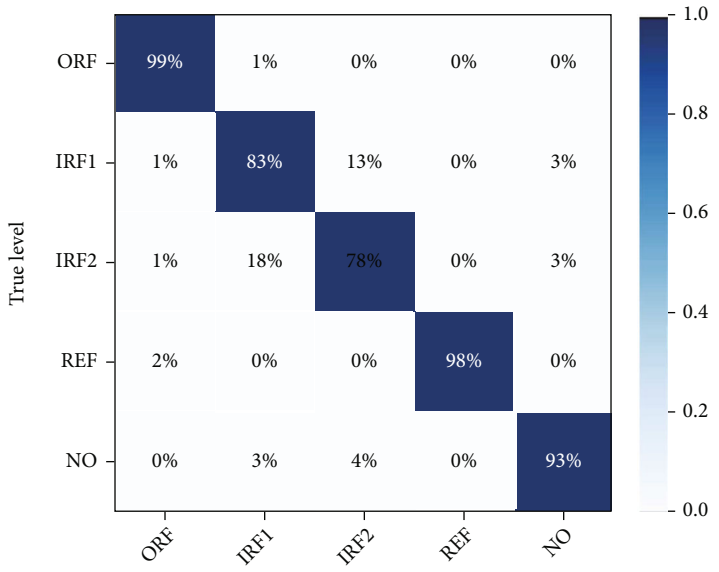

(c) MSCNN (combination)

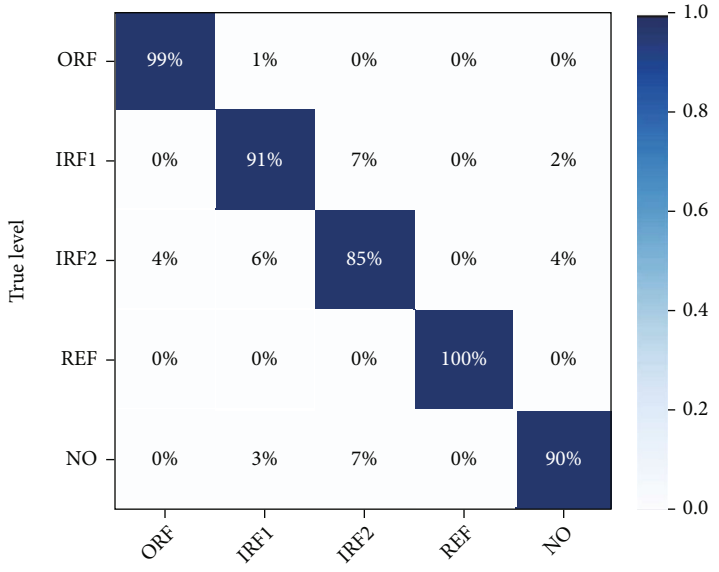

(d) MSCNN-GAP (combination)

Figure 14: Confusion matrix results of each algorithm.

the robustness of the algorithm, Group F and Group G are used to compare and verify the algorithms. Each algorithm is run ten times, and the average values are counted. The comparison results are shown in Figure 13.

The results show that under the influence of noise factors, the diagnostic accuracy of each algorithm is affected to a certain extent. Among the algorithms that use single-sensor data, MSCNN-GAP has a better classification effect than traditional CNN. In terms of the data fusion algorithm, the result of data fusion using multichannel input is slightly lower than that of the model using the vertical signal. The data fusion algorithm proposed in this paper can obtain better results than MSCNN-GAP using single-sensor data. Therefore, MSCNN-GAP can apply multisource data more efficiently. The reason is that the multiscale model is a parallel structure, and the parameters of multiple branches can be adjusted to each other. Compared with the traditional CNN algorithm, MSCNN-GAP is more flexible. Therefore, the MSCNN-GAP has better robustness and can better adapt to the fault diagnosis of multisource data under noise factors.

Similarly, Figures 14 and 15 show the confusion matrix and t-SNE visualization results of each algorithm. The results show that under the influence of noise

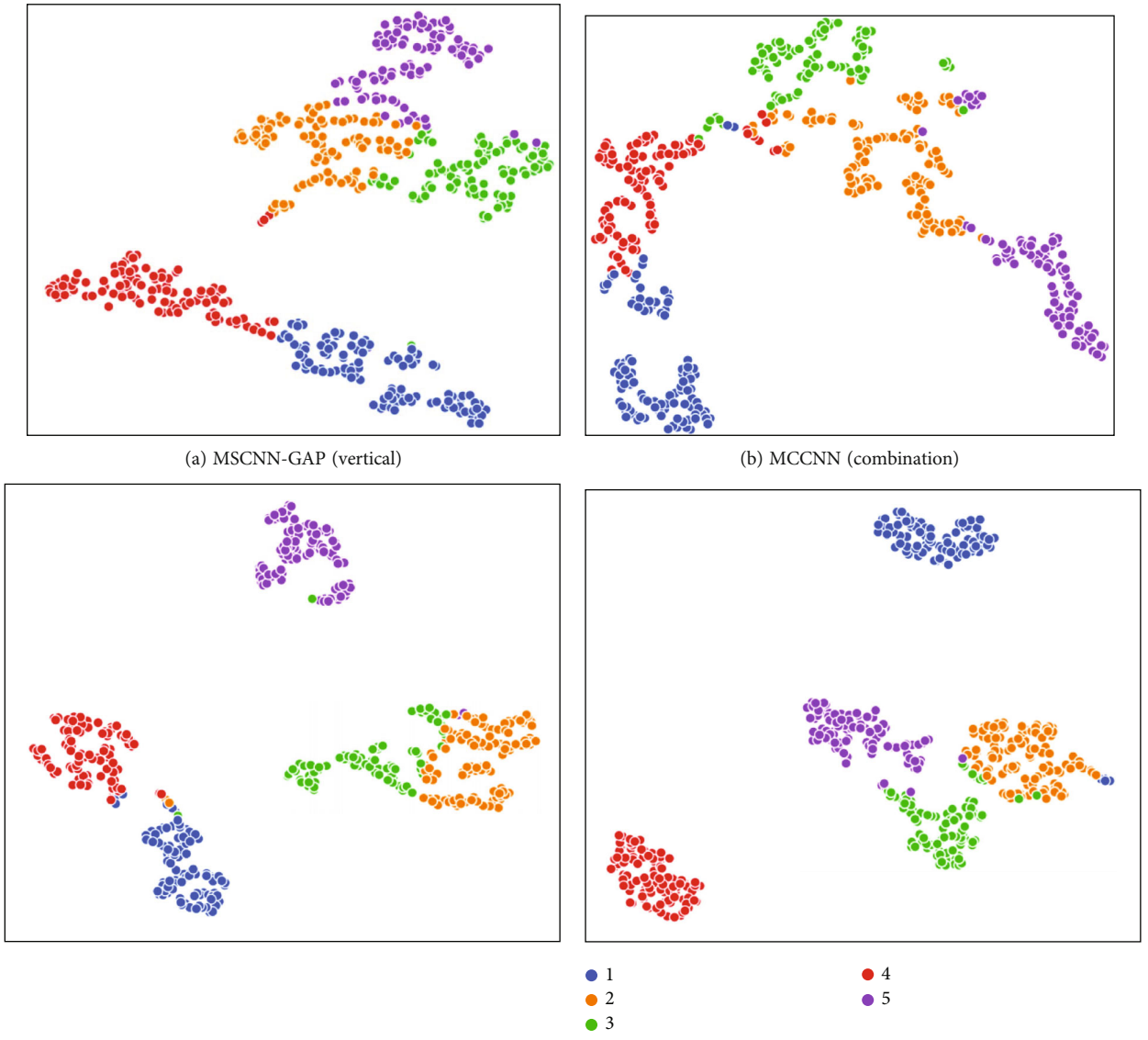

(a) MSCNN-GAP (vertical)

(b) MCCNN (combination)

(c) MSCNN (combination)

(d) MSCNN-GAP (combination)

Figure 15: The t-SNE results of each algorithm.

factors, the result of the data fusion algorithm with only multichannel input is confusing relatively. Meanwhile, the visualization shows that the boundaries between categories are also blurred. The MSCNN-GAP model can distinguish the confusing categories better, and the boundaries between the categories are more obvious than other algorithms.

5. Conclusion

In order to use multisensor data more efficiently, this paper proposes an MSCNN-GAP model. MSCNN-GAP uses multiscale convolution kernels to extract more diverse features, which alleviates the problem of poor robustness of the CNN model under noise factors effectively. The parallel structure of the multiscale model is better adapted to the data fusion process. In the fusion process, instead of reshaping the feature maps into a one-dimensional vector, the global average pooling method is adopted, which effectively retains the spatial structure and position of the feature maps in the fusion process. The proposed model is verified by the bearing fault data collected from the experimental platform. Experimental results show that, compared with other data fusion methods, the algorithm proposed in this paper makes more effective use of multisensor information and obtains a higher diagnostic accuracy and a shorter convergence period. The proposed algorithm has stronger robustness and better classification results when the signal samples are affected by noise factors.

Data Availability

The labeled datasets used to support the findings of this study are available from the corresponding author upon request.

Conflicts of Interest

The authors declare that they have no competing interests.

Acknowledgments

This work was supported in part by the Natural Science Foundation of China under grant 51675350.

References

[1] Z. Liu and L. Zhang, "A review of failure modes, condition monitoring and fault diagnosis methods for large-scale wind turbine bearings," *Measurement*, vol. 149, no. 107002, 2020.

[2] Y. Lei, B. Yang, X. Jiang, F. Jia, N. Li, and A. K. Nandi, "Applications of machine learning to machine fault diagnosis: a review and roadmap," *Mechanical Systems and Signal Processing*, vol. 138, no. 106587, 2020.

[3] M. Cerrada, R. V. Sánchez, C. Li et al., "A review on data-driven fault severity assessment in rolling bearings," *Mechanical Systems and Signal Processing*, vol. 99, pp. 169–196, 2018.

[4] H. Zhao, H. Liu, Y. Jin, X. Dang, and W. Deng, "Feature extraction for data-driven remaining useful life prediction of rolling bearings," *IEEE Transactions on Instrumentation and Measurement*, vol. 70, no. 3511910, 2021.

[5] Y. Lei, J. Lin, Z. He, and M. J. Zuo, "A review on empirical mode decomposition in fault diagnosis of rotating machinery," *Mechanical Systems and Signal Processing*, vol. 35, no. 1-2, pp. 108–126, 2013.

[6] Z. Li, Y. Jiang, Q. Guo, C. Hu, and Z. Peng, "Multi-dimensional variational mode decomposition for bearing-crack detection in wind turbines with large driving-speed variations," *Renewable Energy*, vol. 116, no. B, pp. 55–73, 2018.

[7] H. Cao, F. Fan, K. Zhou, and Z. He, "Wheel-bearing fault diagnosis of trains using empirical wavelet transform," *Measurement*, vol. 82, pp. 439–449, 2016.

[8] J. Ben Ali, N. Fnaiech, L. Saidi, B. Chebel-Morello, and F. Fnaiech, "Application of empirical mode decomposition and artificial neural network for automatic bearing fault diagnosis based on vibration signals," *Applied Acoustics*, vol. 89, pp. 16–27, 2015.

[9] X. Yan and M. Jia, "A novel optimized SVM classification algorithm with multi-domain feature and its application to fault diagnosis of rolling bearing," *Neurocomputing*, vol. 313, pp. 47–64, 2018.

[10] K. Zhu, X. Song, and D. Xue, "A roller bearing fault diagnosis method based on hierarchical entropy and support vector machine with particle swarm optimization algorithm," *Measurement*, vol. 47, pp. 669–675, 2014.

[11] M. Kang, J. Kim, J. Kim, A. C. C. Tan, E. Y. Kim, and B. Choi, "Reliable fault diagnosis for low-speed bearings using individually trained support vector machines with kernel discriminative feature analysis," *IEEE Transactions on Power Electronics*, vol. 30, pp. 2786–2797, 2015.

[12] J. Tian, C. Morillo, M. H. Azarian, and M. Pecht, "Motor bearing fault detection using spectral kurtosis-based feature extraction coupled with K-nearest neighbor distance analysis," *IEEE Transactions on Industrial Electronics*, vol. 63, no. 3, pp. 1793–1803, 2016.

[13] D. He, R. Li, and J. Zhu, "Plastic bearing fault diagnosis based on a two-step data mining approach," *IEEE Transactions on Industrial Electronics*, vol. 60, no. 8, pp. 3429–3440, 2013.

[14] Z. Zhao, P. Zheng, S. Xu, and X. Wu, "Object detection with deep learning: a review," *IEEE Transactions on Neural Networks and Learning Systems*, vol. 30, no. 11, pp. 3212–3232, 2019.

[15] E. Moen, D. Bannon, T. Kudo, W. Graf, M. Covert, and D. Van Valen, "Deep learning for cellular image analysis," *Nature Methods*, vol. 16, no. 12, pp. 1233–1246, 2019.

[16] G. Liu and J. Guo, "Bidirectional LSTM with attention mechanism and convolutional layer for text classification," *Neurocomputing*, vol. 337, pp. 325–338, 2019.

[17] D. Wang and J. Chen, "Supervised speech separation based on deep learning: an overview," *IEEE-ACM Transactions on Audio Speech and Language Processing*, vol. 26, no. 10, pp. 1702–1726, 2018.

[18] Y. Chien, C. Wu, and H. Tsao, "Automatic sleep-arousal detection with single-lead EEG using stacking ensemble learning," *Sensors*, vol. 21, no. 18, p. 6049, 2021.

[19] J. Jiao, M. Zhao, J. Lin, and K. Liang, "A comprehensive review on convolutional neural network in machine fault diagnosis," *Neurocomputing*, vol. 417, pp. 36–63, 2020.

[20] S. Xing, Y. Lei, S. Wang, and F. Jia, "Distribution-invariant deep belief network for intelligent fault diagnosis of machines under new working conditions," *IEEE Transactions on Industrial Electronics*, vol. 68, no. 3, pp. 2617–2625, 2021.

[21] T. Ince, S. Kiranyaz, L. Eren, M. Askar, and M. Gabbouj, "Real-time motor fault detection by 1-D convolutional neural networks," *IEEE Transactions on Industrial Electronics*, vol. 63, no. 11, pp. 7067–7075, 2016.

[22] Z. Liu, H. Wang, J. Liu, Y. Qin, and D. Peng, "Multitask learning based on lightweight 1DCNN for fault diagnosis of wheelset bearings," *IEEE Transactions on Instrumentation and Measurement*, vol. 70, no. 3501711, 2021.

[23] X. Liu, Q. Zhou, J. Zhao, H. Shen, and X. Xiong, "Fault diagnosis of rotating machinery under noisy environment conditions based on a 1-D convolutional autoencoder and 1-D convolutional neural network," *Sensors*, vol. 19, no. 9724, 2019.

[24] Y. Xu, Z. Li, S. Wang, W. Li, T. Sarkodie-Gyan, and S. Feng, "A hybrid deep-learning model for fault diagnosis of rolling bearings," *Measurement*, vol. 169, no. 108502, 2021.

[25] Q. Zhou, Y. Li, Y. Tian, and L. Jiang, "A novel method based on non-linear auto-regression neural network and convolutional neural network for imbalanced fault diagnosis of rotating machinery," *Measurement*, vol. 161, no. 107880, 2020.

[26] P. Liang, C. Deng, J. Wu, and Z. Yang, "Intelligent fault diagnosis of rotating machinery via wavelet transform, generative adversarial nets and convolutional neural network," *Measurement*, vol. 159, no. 107768, 2020.

[27] L. Wen, X. Li, L. Gao, and Y. Zhang, "A new convolutional neural network-based data-driven fault diagnosis method," *IEEE Transactions on Industrial Electronics*, vol. 65, no. 7, pp. 5990–5998, 2018.

[28] Z. Chen, A. Mauricio, W. Li, and K. Gryllias, "A deep learning method for bearing fault diagnosis based on cyclic spectral coherence and convolutional neural networks," *Mechanical Systems and Signal Processing*, vol. 140, no. 106683, 2020.

[29] R. Liu, G. Meng, B. Yang, C. Sun, and X. Chen, "Dislocated time series convolutional neural architecture: an intelligent fault diagnosis approach for electric machine," *IEEE Transactions on Industrial Informatics*, vol. 13, no. 3, pp. 1310–1320, 2017.

[30] J. Wang, S. Li, B. Han et al., "Construction of a batch-normalized autoencoder network and its application in mechanical intelligent fault diagnosis," *Measurement Science and Technology*, vol. 30, no. 1, p. 015106, 2019.

[31] G. Jiang, H. He, J. Yan, and P. Xie, "Multiscale convolutional neural networks for fault diagnosis of wind turbine gearbox," *IEEE Transactions on Industrial Electronics*, vol. 66, no. 4, pp. 3196–3207, 2019.

[32] H. Wang, Z. Liu, D. Peng, and Y. Qin, "Understanding and learning discriminant features based on multiattention 1DCNN for wheelset bearing fault diagnosis," *IEEE Transactions on Industrial Informatics*, vol. 16, no. 9, pp. 5735–5745, 2020.

[33] J. Wang, D. Wang, S. Wang, W. Li, and K. Song, "Fault diagnosis of bearings based on multi-sensor information fusion and 2D convolutional neural network," *IEEE Access*, vol. 9, pp. 23717–23725, 2021.

[34] X. Xu, Z. Tao, W. Ming, Q. An, and M. Chen, "Intelligent monitoring and diagnostics using a novel integrated model based on deep learning and multi-sensor feature fusion," *Measurement*, vol. 165, no. 108086, 2020.

[35] P. Shan, H. Lv, L. Yu, H. Ge, Y. Li, and L. Gu, "A multisensor data fusion method for ball screw fault diagnosis based on convolutional neural network with selected channels," *IEEE Sensors Journal*, vol. 20, no. 14, pp. 7896–7905, 2020.

[36] H. Wang, S. Li, L. Song, L. Cui, and P. Wang, "An enhanced intelligent diagnosis method based on multi-sensor image fusion via improved deep learning network," *IEEE Transactions on Instrumentation and Measurement*, vol. 69, no. 6, pp. 2648–2657, 2020.

[37] M. Xia, Z. Mao, R. Zhang, B. Jiang, and M. Wei, "A new compound fault diagnosis method for gearbox based on convolutional neural network," in *Proceedings of 2020 IEEE 9th Data Driven Control and Learning Systems Conference (DDCLS'20)*, pp. 1077–1083, Liuzhou, China, 2020.

[38] K. Gu, Y. Zhang, X. Liu, H. Li, and M. Ren, "DWT-LSTM-based fault diagnosis of rolling bearings with multi-sensors," *Electronics*, vol. 10, no. 207617, 2021.

[39] L. Kou, Y. Qin, X. Zhao, and X. Chen, "A multi-dimension end-to-end CNN model for rotating devices fault diagnosis on high-speed train bogie," *IEEE Transactions on Vehicular Technology*, vol. 69, no. 3, pp. 2513–2524, 2020.

[40] H. Li, J. Huang, X. Yang, J. Luo, L. Zhang, and Y. Pang, "Fault diagnosis for rotating machinery using multiscale permutation entropy and convolutional neural networks," *Entropy*, vol. 22, no. 8518, 2020.

[41] B. Peng, H. Xia, X. Lv et al., "An intelligent fault diagnosis method for rotating machinery based on data fusion and deep residual neural network," *Applied Intelligence*, pp. 1–15, 2021.

[42] Y. Lecun, B. Boser, J. Denker et al., "Backpropagation applied to handwritten zip code recognition," *Neural Computation*, vol. 1, no. 4, pp. 541–551, 1989.

[43] Y. Lecun and L. Bottou, "Gradient-based learning applied to document recognition," *Proceedings of the IEEE*, vol. 86, no. 11, pp. 2278–2324, 1998.

[44] A. Krizhevsky, I. Sutskever, and G. E. Hinton, "ImageNet classification with deep convolutional neural networks," *Communications of the ACM*, vol. 60, no. 6, pp. 84–90, 2017.

[45] V. Nair and G. E. Hinton, "Rectified linear units improve restricted Boltzmann machines," in *International Conference on International Conference on Machine Learning*, Haifa, Israel, 2010.

[46] K. M. He, X. Y. Zhang, S. Q. Ren, and J. Sun, "Delving deep into rectifiers: surpassing human-level performance on ImageNet classification," in *IEEE International Conference on Computer Vision*, pp. 1026–1034, New York, 2015.

[47] C. Szegedy, W. Liu, Y. Jia et al., "Going deeper with convolutions," in *IEEE Conference on Computer Vision and Pattern Recognition*, pp. 1–9, New York, 2015.

[48] K. He and J. Sun, "Convolutional neural networks at constrained time cost," in *2015 IEEE Conference on Computer Vision and Pattern Recognition (CVPR)*, pp. 5353–5360, Boston, America, 2015.

Hindawi
Journal of Sensors
Volume 2021, Article ID 8244582, 10 pages
https://doi.org/10.1155/2021/8244582

Research Article

Building Structure Simulation System Based on BIM and Computer Model

Bao Zhu and Huan Feng

School of Civil Engineering, Chuzhou Vocational and Technical College, Chuzhou 239000, China

Correspondence should be addressed to Huan Feng; fenghuan@chzc.edu.cn

Received 14 July 2021; Revised 14 August 2021; Accepted 20 October 2021; Published 8 November 2021

Academic Editor: Mu Zhou

This paper does some research and discussion on the finite element analysis of a building structure, especially the computer graphics simulation method in building structure simulation. Moreover, with the support of BIM technology and computer finite element simulation technology, this paper constructs a building structure simulation system and analyzes the building structure simulation system based on actual conditions such as building structure and stress load. In addition, this paper improves the traditional structural analysis algorithm and designs experiments to evaluate the effect of the method proposed in this paper and analyze the data in the form of simulation to compare the validity of the test results. Finally, an experiment is designed to evaluate the data processing capability of the test system in this paper. The experimental analysis results verify the effectiveness of the method in this paper, which can provide relevant theoretical references for subsequent building structure simulation.

1. Introduction

With the development of urbanization in my country, the cost management objectives of construction projects have shifted to a deeper level. Construction engineering refers to the engineering entity formed through the construction of various types of houses and their ancillary facilities and the installation of supporting lines, pipelines, and equipment. In this process, if relevant optimization theories can be used to systematically study the project, the goal of optimizing resource allocation and reducing construction costs can be achieved. China has gone through decades of experience in modern construction engineering and the process of exploring the optimal allocation of construction resources. It has formed a complete set of systems for construction projects, from cost decision-making and design budgets to construction engineering supervision and management. However, due to the inadequate use of the rapid development of modern information technology, the cost control and management methods of Chinese construction companies are relatively backward, and many projects still remain in manual manipulation [1]. As the country's requirements for construction companies increase and the factors that affect the cost control of construction companies continue to increase, the simple manual control method in the past can no longer meet the business growth needs of construction companies. To improve the current cost control system of construction enterprises, a large-scale information system must be established to conduct detailed analysis of various data to determine the most optimized construction plan. In the process of market economy development, construction companies are facing fiercer market competition. The key to whether an enterprise can be invincible in the market competition is whether it can provide the society with high-quality, short-term, and low-cost construction products. Therefore, cost management has become the core content of project construction management [2]. The cost of construction projects refers to a form of currency measurement by which construction companies use the project as the object of cost accounting to measure the transfer value of the production materials consumed in the construction process and the value created by the necessary labor of the laborers. The cost of construction projects is also called engineering cost, which is the main product cost of construction enterprises. On the premise of ensuring the quality of construction, one of the ways to reduce the cost of construction

projects is to establish a project cost management information system, which is also the most feasible and efficient management method currently. The implementation of computer-assisted informatization can not only shorten the processing time of relevant data but also facilitate the management of various comprehensive cost data. At the same time, it enables project managers to grasp complete and correct information in a timely manner through organized information circulation, thereby providing strong information support for project cost management. It can be seen that to truly realize the "dynamic, full-process, and all-round" of the project cost management system, it is necessary to realize the integrated development of cost information and establish a dynamic management system [3].

In order to meet people's increasingly abundant activity needs, a large number of buildings with unique appearances, rich functions, and reasonable structures have emerged. At the same time, in order to better realize the architect's design concept and show a more perfect design form, many buildings need to seek a breakthrough from the traditional reinforced concrete model. With the application of new materials such as high strength and light weight, many new space systems have been realized, such as space string beam structure, opening and closing space structure, cable dome structure, and other systems. In order to improve the structural efficiency of the space structure, prestressing technology is introduced, and a new type of prestressed steel structure system is formed by reasonably changing the stress state of different structures, so as to realize the designer's expected plan effect. The prestressed steel structure has attracted the attention of engineers and researchers because of its good mechanical properties and broad application prospects. Meanwhile, it has become a hot spot and cutting-edge science that conforms to the development requirements of the times, and it is also one of the main trends in the development of space structures in recent years. Compared with traditional concrete structures, a prestressed steel structure has many advantages in structural systems and materials, such as lighter weight, short construction period, and simple structure. Therefore, it is widely used in large-span spatial structures.

Based on BIM and computer models, this article simulates building structures.

2. Related Work

By analyzing the relevant construction codes and standards of American concrete structure engineering, literature [4] pointed out that there is no clear foundation for the load value of the formwork design at present and then proposed the necessity of load investigation during the construction period. Literature [5] conducted on-site surveys of the live load on the floor before and after the concrete pouring of the cast-in-place reinforced concrete structure under construction. Moreover, it used the floor live load survey method during the construction period to obtain the field measured data and used the analysis method to obtain the statistical parameters of the live load during the construction period. Literature [6] proposed a test method for construction live load, which can truly record the change process of construction live load, and can be used to study the law of more complicated construction live load such as impact load. Literature [7] analyzed and studied the dynamic load model of the floor formwork during concrete pouring and constructed a probability model according to the relevant factors that affect the dynamic load of the floor formwork. Literature [8] conducted field survey and research on live load of cast-in-situ reinforced concrete structure and discussed and summarized the law and distribution characteristics of floor live load during the construction of cast-in-situ reinforced concrete structure. Literature [9] studied the impact of the impact load caused by pouring concrete during the construction process on the temporary load-bearing system composed of the partially resistive concrete structure and the formwork and its support and proposed a method for calculating the dynamic influence of the impact load generated during concrete pouring on the "time-varying structure." Literature [10] studied the impact of the dynamic load on the temporary load-bearing system caused by a small mobile dump truck that transports concrete when driving on a newly poured concrete floor. After conducting a large-scale field survey and statistical analysis, literature [11] summarized the law of construction live load and carried out quantitative analysis on it.

Literature [12] conducted field tests on flat-slab apartments, analyzed the applicability of the simplified hand calculation method of computer simulation, and believed that the simplified method underestimated the maximum load of the floor. Literature [13] analyzed the influence of floor stiffness and unequal deflection of floor slab on load transfer and compared the theoretical and measured values of supporting load and floor load. Literature [14] carried out on-site measurements for a shear wall structure to try to analyze the load transfer data during construction. However, it obtained some data by measuring the support of the floor slab and the embedded steel bars in the floor slab, but some of the data is not logical. The subsequent testing work focused on the force analysis of the template and support. Through a series of investigations and field tests, literature [15] pointed out the possibility of obtaining data on-site and pointed out that the load on the support, the data during the curing period of the concrete slab, and the information of the multilayer support can all be obtained through the test. Literature [16] conducted field tests on low-rise concrete structures under construction. Through the measurement of the support load of the formwork during construction, it analyzed the applicability of the design load recommended by ACI, compared the order of magnitude of the lateral support and the vertical support load, and pointed out that the removal of the formwork support will cause a large change in the distribution of the floor and support load. Literature [17] measured the influence of different loading paths, different load sizes, and other factors on the load effect of scaffolding. Literature [18] conducted continuous observation experiments on cast-in-place frame structures and obtained important data. The test found that with the passage of time, the load was redistributed among the various floors, which was prominently manifested in the fact that the newly poured concrete floor slabs began to not bear the load to gradually bear part of the load. Literature [19] provided a useful discussion on the analysis of reinforced concrete structures

during the construction period considering load redistribution. However, the calculation of the load redistribution amount in the model as a fixed proportion of the weight of the floor does not conform to the time-varying structural characteristics, so it may sometimes cause a large error that is dangerous.

3. Selection of Model Element Type

The element library of the LS-DYNA program includes solid elements, shell elements, beam elements, rod elements, inertia and mass elements, and spring damping elements. The common feature of these elements is that they all use low-order elements with linear displacement interpolation functions, and the default algorithm is a reduced integration algorithm. The experience of calculation and analysis shows that these explicit dynamic elements of linear displacement interpolation function and single-point integration algorithm can be well used for the analysis of various large deformation and material nonlinear problems.

For the upper building structure, the 3D solid unit SOLID164 is used, as shown in Figure 1. Its basic characteristics are as follows [20]:

(1) There are 8 nodes. For each node, its displacement degree of freedom has practical significance

(2) It adopts a single-point integration algorithm by default

(3) It can adopt Lagrange form or ALE form

(4) It can be degenerated into degenerate units such as prisms and pyramids

(5) When applying pressure to the surface of the unit, it is necessary to pay special attention to the numbering of the surface

(6) It supports most of LS-DYNA material algorithms

(7) The volume cannot be zero

(8) SOLID164 element must be defined by 8 nodes

The thin shell element is selected to simulate the earth plane, namely, SHELL163, as shown in Figure 2. Its basic characteristics are as follows:

(1) This element is a 4-node spatial thin shell element. For each node, the displacement and rotation of the node need to be considered

(2) The default algorithm adopts the shell element algorithm of Belytschko-Tsay single point integration

(3) For various shell element algorithms, the number of integration points along the thickness direction can be selected

(4) The thickness of the shell is defined by real parameters and cannot be zero

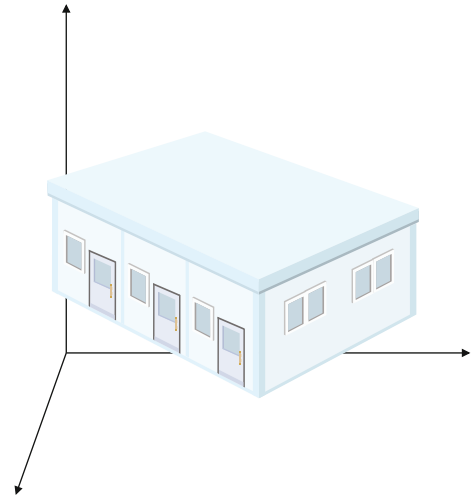

Figure 1: SOLID164 unit.

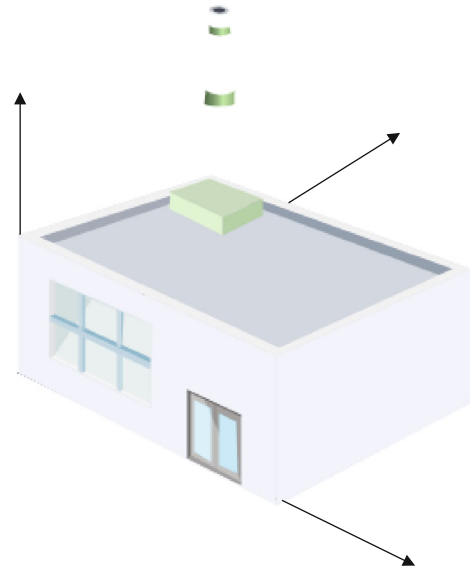

Figure 2: SHELL163 unit.

(5) The area of the SHELL163 element cannot be zero, and the degenerate element can be defined by the same node appearing twice

(6) SHELL163 element supports most material model algorithms

3.1. Basic Explicit Algorithm for 3D SOLID Elements. This paper takes three-dimensional 8-node solid elements as an example to introduce the explicit integration algorithm of LS-DYNA.

The main algorithm of LS-DYNA adopts the Lagrangian incremental method that tracks the trajectory of the particle. For the particle at the initial moment of space point $(\alpha_1, \alpha_2, \alpha_3)$, the trajectory equation is [21]

$$x_i = x_i(\alpha, t). \tag{1}$$

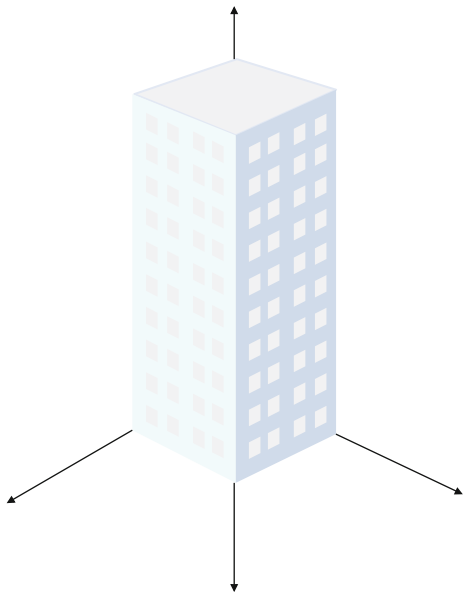

Figure 3: Schematic diagram of 8-node entity isoparametric unit.

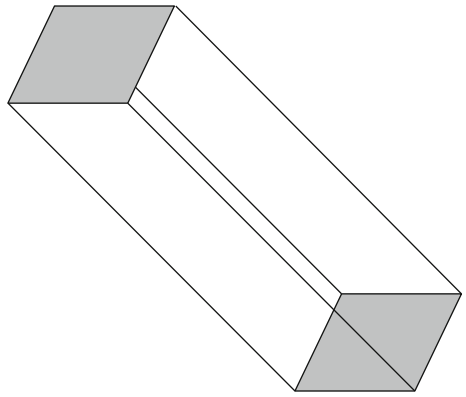

Figure 4: Spatial model of columns with central reinforcement.

Among them, α represents the initial position $(\alpha_1, \alpha_2, \alpha_3)$ of the material point, and the initial conditions of movement are

$$\begin{aligned} x_i(\alpha, 0) &= \alpha_i, \\ \dot{x}_i(\alpha, 0) &= v_i(\alpha). \end{aligned} \tag{2}$$

In addition, the differential equation of motion for the elastodynamic space problem is

$$\sum_{j=1}^{3} \frac{\partial \sigma_{ij}}{\partial x_j} + f_i = \rho \ddot{u}_i. \tag{3}$$

It satisfies the following boundary conditions:

(1) The displacement boundary condition is

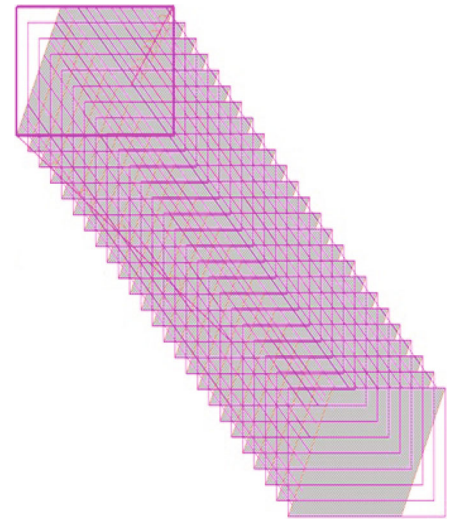

Figure 5: Rebar mesh model of columns with central reinforcement.

$$u_i = \bar{u}_i, \tag{4}$$

on the displacement boundary ∂b_1

(2) The stress boundary condition is

$$\sum_{j=1}^{3} \sigma_{ij} n_j = \bar{T}_i, \tag{5}$$

on the stress boundary ∂b_2

(3) The jumping conditions at the discontinuity of the sliding contact surface displacement are

$$\sum_{j=1}^{3} \left(\sigma_{ij}^{+} - \sigma_{ij}^{-} \right) n_j = 0 \tag{6}$$

(4) When $x_i^{+} = x_i^{-}$, contact occurs along the inner contact boundary

The integral form of the differential equation of motion is (the principle of minimum potential energy)

$$\delta \prod = \int_v \sum_{i=1}^{3} (\rho \ddot{x}_i - f_i) \delta u_i dV + \int_v \sum_{i=1}^{3} \sum_{j=3}^{3} \sigma_{ij} \delta \varepsilon_{ij} dV - \int_{\partial b_2} \sum_{i=1}^{3} \bar{T}_i \delta u_i ds = 0. \tag{7}$$

Among them, δu is the virtual displacement field that satisfies the displacement boundary condition and $\delta \varepsilon$ is the virtual strain field corresponding to δu.

If the entire structure is a series of finite discretized units, the total potential energy variation of the structure can be approximately expressed as the sum of the potential energy variation of each unit, and the basic equation of the finite

Table 1: Model parameters.

Model	Model1	Model2	Model3	Model4
Concrete strength grade	C60	C60	C60	C60
Stirrups in the core area	Æ10@50	Æ10@100	Æ10@150	Æ10@200
Core area volume matching rate	0.80%	0.40%	0.26%	0.20%
Design axial compression ratio	0.75	0.75	0.75	0.75

Table 2: Statistical table of ultimate load and displacement of each model.

Model	Model1	Model2	Model3	Model4
Core area volume matching rate	0.80%	0.40%	0.26%	0.20%
Ultimate load (kN)	5655.68	5377.89	5257.56	5108.60
Limit displacement (mm)	37.94	33.41	31.07	28.77

element for the dynamic problem can be obtained. Taking a three-dimensional 8-node solid element as an example, the structural finite element discretization can be expressed as follows [22].

Within each unit, the coordinates of any point can be obtained by interpolation of the node coordinate values, namely,

$$x_i(\xi, \eta, \varsigma, t) = \sum_{j=1}^{8} \phi_j(\xi, \eta, \varsigma) x_i^j(t). \tag{8}$$

In the formula, ξ, η, ς is the unit coordinate, as shown in Figure 3.

In the formula, the interpolation function (shape function) is

$$\phi_j(\xi, \eta, \varsigma) = \frac{1}{8}\left(1 + \xi_j\xi\right)\left(1 + \eta_j\eta\right)\left(1 + \varsigma_j\varsigma\right). \tag{9}$$

Among them, $(\xi_j, \eta_j, \varsigma_j)$ is the coordinate of the jth node of the element, and the above formula can be expressed in matrix form [23]:

$$X(\xi, \eta, \varsigma, t) = N \cdot X^e. \tag{10}$$

Among them, $X(\xi, \eta, \varsigma, t)$ is the position coordinate of any point in the unit (including three components), X^e is the position coordinate array of each node of the unit at time t, and $X(\xi, \eta, \varsigma, t) = N \cdot X^e$ is the interpolation function matrix, which can be written in the following form:

$$N(\xi, \eta, \varsigma) = [N_1, \cdots, N_8]. \tag{11}$$

In the formula, the jth subblock is $N_j = \phi_j I_{3\times 3}$.

When the whole structure is a series of discrete elements, it can be obtained from the principle of virtual displacement:

$$\delta \prod = \sum_e \delta \prod_m = \sum_e \delta X^{eT} \left[\int_{v_e} \rho N^T N dV \ddot{X}^e + \int_{v_e} B^T \sigma dV - \int_{v_e} N^T f dV - \int_{\partial b_{2e}} N^T \bar{T} dS \right] = 0. \tag{12}$$

Among them, the Cauchy stress vector is

$$\sigma = \left[\sigma_x, \sigma_y, \sigma_z, \sigma_{xy}, \sigma_{yz}, \sigma_{zx}\right]^T. \tag{13}$$

The strain matrix is

$$B = LN. \tag{14}$$

L is the differential operator matrix, and its specific elements are

$$L^T = \begin{bmatrix} \partial_x & 0 & 0 & \partial_y & 0 & \partial_z \\ 0 & \partial_y & 0 & \partial_x & \partial_z & 0 \\ 0 & 0 & \partial_z & 0 & \partial_y & \partial_x \end{bmatrix}. \tag{15}$$

In LS-DYNA, since the elements of the same row in the uniform unit mass matrix $m^e = \int_{v_e} \rho N^T N dV$ are merged into the diagonal elements to form a concentrated mass matrix and then integrated into the overall diagonal mass matrix M, the above formula can be rewritten as

$$M\ddot{X} = P(t) - F. \tag{16}$$

The above formula is the discretized equation of motion, where M is the overall mass matrix and F is formed by the collection of element stress divergence vectors, which can be obtained by the following formula:

$$F = \sum_e \int_{v_e} B^T \sigma dV. \tag{17}$$

p is the overall nodal load vector, which is formed by concentrated nodal force, surface force, physical force, etc. The formula is as follows:

$$P = \sum_e \left(\int_{v_e} N^T f dV + \int_{\partial b_{2e}} N^T \bar{T} dS \right). \tag{18}$$

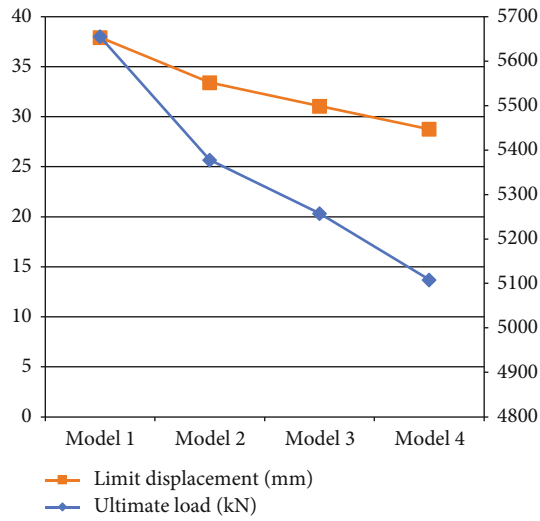

Figure 6: Statistical diagrams of ultimate load and displacement of each model.

The discretized structure motion equation of LS-DYNA3D considering the influence of damping is

$$M\ddot{X} = P - F + H - C\dot{X}. \tag{19}$$

The time integral adopts the principle of explicit central difference, and the format is as follows:

$$\begin{aligned} \ddot{X} &= M^{-1}\left[P(t_n) - F(t_n) + H(t_n) - C\dot{X}(t_{n-1/2})\right], \\ \dot{X}(t_{n+1/2}) &= \dot{X}(t_{n-1/2}) + \ddot{X}(t_n)\frac{(\Delta t_{n-1} + \Delta t_n)}{2}, \\ X(t_{n+1/2}) &= X(t_n) + \dot{X}(t_{n+1/2})\Delta t_n. \end{aligned} \tag{20}$$

Among them, $t_{n-1/2} = (t_n + t_{n-1})/2$, $t_{n+1/2} = (t_n + t_{n-1})/2$, $\Delta t_{n-1} = (t_n - t_{n-1})$, $\Delta t_n = (t_{n+1} - t_n)$, $\ddot{X}(t_n)$, $\dot{X}(t_{n+1/2})$, and $X(t_{n+1})$ are the node acceleration vector at time t_n, the node velocity vector at time $t_{n+1/2}$, the node position coordinate vector at time t_{n+1}, and so on.

Its characteristics are the following:

(1) Calculation cost is saved. For each incremental step of the nonlinear analysis, the stiffness matrix is changing, and the explicit method does not form the overall stiffness matrix. The elastic term is placed in the internal force, avoiding the inversion of the stiffness matrix. This avoids the computational cost of repeatedly updating the stiffness matrix and solving the linear equations, which is meaningful for nonlinear analysis

(2) Higher computational efficiency can be obtained. When the mass matrix of the system is a diagonal matrix, when using the above recursive formula to solve the equation of motion, it is only necessary to use the matrix multiplication to obtain the equivalent load vector at the right end, and there is no need to invert the mass matrix, so the calculation efficiency is quite high

(3) The method is conditionally stable. The stable condition is that a relatively small time step is required. If this step is exceeded, the calculation will be unstable and the displacement tends to be infinite

In order to ensure convergence, LS-DYNA3D adopts the variable step integration method. The integration step used must be less than a certain critical value; otherwise, the algorithm will be unstable. The smallest unit in the grid will determine the time step selection, namely,

$$\Delta t = \min\left\{\Delta t_{e1}, \cdots, \Delta t_{eN}\right\}. \tag{21}$$

Among them, Δt_{ei} is the limit time step length of the ith unit and N is the total number of units.

In LS-DYNA3D, the limit time step length of each type of element can be unified into the following form:

$$\Delta t_e = \alpha\left(\frac{L}{c}\right). \tag{22}$$

Among them, α is a time step factor less than 1, which is defaulted to 0.9 by the program, L is the characteristic scale of the element, and c is the sound velocity of the material. The calculation formulas for the corresponding L and c of the solid element are

$$\begin{aligned} L &= \frac{V_e}{A_{e\max}}, \\ c &= \sqrt{\frac{E(1-\mu)}{(1-\mu^2)\rho}}. \end{aligned} \tag{23}$$

4. Building Structure Simulation System Based on BIM and Computer Model

Because the material properties and performance of steel bars and concrete are quite different, it is not enough to simulate reinforced concrete structures with simple linear elastic methods. Therefore, this paper uses a nonlinear analysis method for this composite material. However, the commonly used finite element analysis software cannot accurately describe complex composite building structures, such as the variable cross-section and hollow structure of the frame-core tube structure.

In the structure, the column, as an important force-bearing member, not only bears the vertical force but also bears the role of horizontal force. In a large number of earthquake disasters, the shear damage of the structure accounts for a relatively large proportion. In order to achieve the "three-level" seismic target and ensure that the overall structure does not suffer serious damage, the study of the shear capacity of the column is particularly important. Since the 21st century, the finite element analysis method has been applied more and more widely in structural calculations. It can not only simulate the development of cracks in the structure and the failure process of the

Table 3: Longitudinal reinforcement ratio models of different core areas.

Model	Model1	Model2	Model3	Model4	Model5	Model6
Concrete strength grade	C60	C60	C60	C60	C60	C60
Column core longitudinal rib	28Φ14	28Φ18	28Φ22	28Φ28	28Φ32	28Φ36
Longitudinal reinforcement ratio of core area	0.68%	1.13%	1.68%	2.73%	3.56%	4.49%
Stirrups in the core area	Æ10@100	Æ10@100	Æ10@100	Æ10@100	Æ10@100	Æ10@100
Design axial compression ratio	0.75	0.75	0.75	0.75	0.75	0.75

structure as a whole but also calculate the weak parts and ultimate bearing capacity of the structure.

The load-displacement curves of reinforced concrete frame columns under monotonic loads, the shear capacity and failure mechanism of reinforced concrete frame columns under oblique horizontal loads, and the joints of high-strength concrete column-beam frame joints were analyzed using finite element software and theory, respectively. The hysteresis performance and the strength of the reinforced concrete frame short column under monotonic load are calculated and analyzed. The calculation results of the finite element software and the experimental results are compared to the two, indicating that the data obtained by the finite element software and the theory have a high reference value.

This paper takes the columns with central reinforcement as the research object and uses the VFEAP finite element software for analysis and research. Moreover, by considering influencing factors such as stirrup reinforcement ratio, longitudinal reinforcement ratio, concrete strength, and axial compression ratio, this paper establishes a series of comparative models to analyze the ultimate bearing capacity, stiffness degradation, and ductility performance changes of core columns under different influencing factors. The structural model is shown in Figure 4, and the simulation model based on BIM and computer is shown in Figure 5.

In order to specifically evaluate the role of stirrups in the core area of columns with central reinforcement, four columns with central reinforcement models with different stirrup spacings were established. In this paper, other parameters are kept unchanged, and the load-displacement curve and the stiffness degradation curve are used to study the influence of the spacing between the steel bars in the core area on the columns with central reinforcement. The model parameters are shown in Table 1.

The ultimate load and displacement of each model are shown in Table 2 and Figure 6.

The arrangement of longitudinal reinforcement in the core area of the column is the core of the columns with central reinforcement. Even if the outer concrete fails and exits work, the longitudinal reinforcement and stirrups in the core area can restrain the concrete in the core area to maintain good working performance. Therefore, the longitudinal reinforcement ratio of the core area is an important influencing factor for columns with central reinforcement. In this paper, the ratio of longitudinal reinforcement is changed by changing the diameter of the longitudinal reinforcement in the core area. A total of 6 models have been established. The diameter of the longitudinal reinforcement is 14 mm-36 mm. The parameters are shown in Table 3.

Table 4: Statistical table of ultimate load and displacement of each model.

Model	Longitudinal reinforcement ratio of core area	Ultimate load (kN)	Limit displacement (mm)
Model1	0.68%	5105.944	29.0678
Model2	1.13%	5247.071	30.8959
Model3	1.68%	5283.229	31.3201
Model4	2.73%	5322.831	32.6028
Model5	3.56%	5377.886	33.4108
Model6	4.49%	5547.162	36.2085

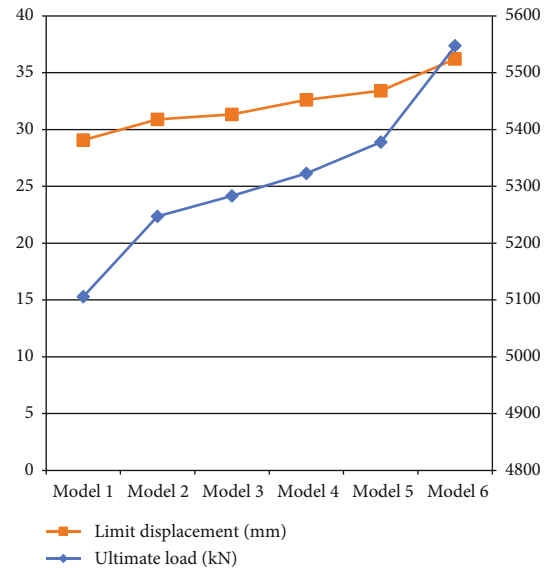

Figure 7: Statistical diagram of ultimate load and displacement of each model.

Among the longitudinal reinforcement ratios of 0.68%-4.46% in the core area, the ultimate load and ultimate displacement have a clear upward trend with the increase of the reinforcement ratio. The above shows that the longitudinal reinforcement in the core area plays the role of bearing the load in the middle and later stages of the component loading. With the increase of the reinforcement ratio of the longitudinal reinforcement in the core area, the lateral resistance gradually increases, and the failure of the component is delayed.

Table 5: Statistical table of structural simulation effect evaluation of building structure simulation system based on BIM and computer model.

Num	Simulation effect evaluation	Num	Simulation effect evaluation	Num	Simulation effect evaluation
1	89.23	25	91.77	49	90.60
2	93.15	26	92.41	50	88.10
3	91.81	27	88.50	51	79.38
4	81.07	28	79.55	52	84.02
5	85.87	29	91.15	53	92.93
6	88.62	30	90.15	54	92.72
7	89.06	31	82.89	55	82.35
8	92.88	32	87.04	56	85.23
9	83.73	33	79.34	57	90.05
10	80.57	34	82.85	58	84.31
11	80.87	35	80.95	59	85.37
12	90.91	36	87.89	60	82.08
13	81.90	37	89.87	61	86.42
14	92.57	38	81.83	62	87.92
15	87.21	39	84.90	63	89.85
16	90.98	40	93.33	64	88.14
17	83.70	41	91.28	65	92.10
18	84.27	42	93.51	66	92.48
19	88.06	43	82.46	67	92.71
20	86.41	44	84.18	68	81.00
21	83.19	45	91.03	69	91.56
22	79.52	46	88.18	70	83.75
23	83.89	47	93.59	71	87.06
24	83.24	48	87.79	72	90.70

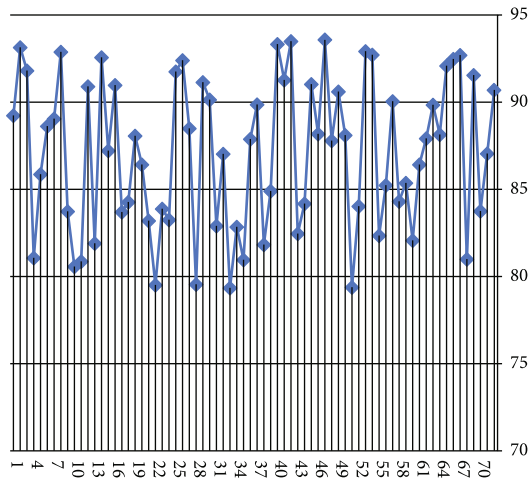

Figure 8: Statistical table of structural simulation effect evaluation of building structure simulation system based on BIM and computer model.

Table 6: Statistical table of system dynamic simulation effect evaluation.

Num	Dynamic simulation effect	Num	Dynamic simulation effect	Num	Dynamic simulation effect
1	78.1	25	81.9	49	74.5
2	74.5	26	67.8	50	82.9
3	74.8	27	71.5	51	85.1
4	74.0	28	80.8	52	83.8
5	83.7	29	81.4	53	79.2
6	86.2	30	83.6	54	67.9
7	67.6	31	79.6	55	78.2
8	73.4	32	88.3	56	81.0
9	73.2	33	89.6	57	72.2
10	79.8	34	83.0	58	73.7
11	83.6	35	90.5	59	82.2
12	88.9	36	80.7	60	73.0
13	79.3	37	78.3	61	82.0
14	74.8	38	76.7	62	70.2
15	75.0	39	80.6	63	70.4
16	78.9	40	83.7	64	90.1
17	84.3	41	87.2	65	78.7
18	90.2	42	80.3	66	68.8
19	80.4	43	74.3	67	88.1
20	77.9	44	88.0	68	74.5
21	74.8	45	72.2	69	70.8
22	80.3	46	84.5	70	73.2
23	76.7	47	79.5	71	74.7
24	73.1	48	84.1	72	85.1

The ultimate load and displacement of each model are shown in Table 4 and Figure 7.

The outer concrete cracked, and the stiffness suddenly dropped. When the component reaches the ultimate load, the higher the longitudinal reinforcement ratio, the slower the rate of stiffness degradation and the more complete the stiffness degradation. The longitudinal reinforcement in the core area can effectively alleviate the stiffness degradation of the component, thereby improving its lateral resistance.

Through the above analysis, it can be known that the system constructed in this paper has certain effects, which are basically consistent with the actual situation. On this basis, this article simulates multiple building structures through a computer simulation model and statistically simulates the data processing effect of the model. A total of 72 sets of data are simulated through the simulation of the building of a certain commercial center, and the results of the statistical simulation are shown in Table 5 and Figure 8.

From the above analysis results, the building structure simulation system based on BIM and computer model constructed in this paper performs well in structural simulation. Next, the effect of the dynamic simulation of the system is evaluated, and the results are shown in Table 6 and Figure 9.

From the above simulation results, the dynamic simulation effect of the system constructed in this paper is better,

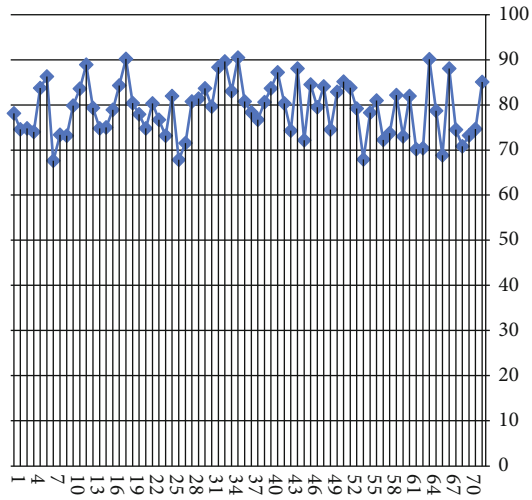

Figure 9: Statistical diagram of system dynamic simulation effect evaluation.

so the system constructed in this paper can be used for simulation analysis in subsequent building structure simulation.

5. Conclusion

Computer graphics simulation is a comprehensive computer technology involving multiple disciplines, and building structure simulation is a major and difficult subject in the engineering field. This paper does some research and discussion on the finite element analysis of a building structure, especially the computer graphics simulation method in building structure distribution. Because building structure simulation is a complex and huge research topic, the damage mechanism of structures under various loads is still under constant research and exploration. Therefore, this paper builds a building structure simulation system with the support of BIM and finite element technology and combines the actual building to simulate the physical structure of the building and evaluates the effect of this system. The research results show that the building structure simulation system constructed in this paper has a certain effect.

Data Availability

The data used to support the findings of this study are available from the corresponding author upon request.

Conflicts of Interest

The authors declare no competing interests.

Acknowledgments

This study is sponsored by the Key projects of natural science research in Anhui Colleges and Universities "The application research on reconstruction of historic building BIM model based on 3D scanning and UAV tilt photography" (KJ2020A1000), Key projects of natural science research in Anhui Colleges and Universities "Test and Simulation Analysis on steering device of externally prestressed box girder bridge with corrugated steel webs" (KJ2019A1134), High level professional group of provincial quality engineering in Colleges and universities (Higher Vocational Education) (2020zyq61), and Anhui teaching team project (2020jxtd186).

References

[1] X. Feng, D. Yan, and C. Wang, "On the simulation repetition and temporal discretization of stochastic occupant behaviour models in building performance simulation," *Journal of Building Performance Simulation*, vol. 10, no. 5-6, pp. 612–624, 2017.

[2] B. Mou, B. J. He, D. X. Zhao, and K. W. Chau, "Numerical simulation of the effects of building dimensional variation on wind pressure distribution," *Engineering Applications of Computational Fluid Mechanics*, vol. 11, no. 1, pp. 293–309, 2017.

[3] D. Chakraborty and H. Elzarka, "Advanced machine learning techniques for building performance simulation: a comparative analysis," *Journal of Building Performance Simulation*, vol. 12, no. 2, pp. 193–207, 2019.

[4] O. Guerra-Santin and S. Silvester, "Development of Dutch occupancy and heating profiles for building simulation," *Building Research & Information*, vol. 45, no. 4, pp. 396–413, 2017.

[5] T. Dodd, C. Yan, and I. Ivanov, "Simulation-based methods for model building and refinement in cryoelectron microscopy," *Journal of Chemical Information and Modeling*, vol. 60, no. 5, pp. 2470–2483, 2020.

[6] T. Abuimara, W. O'Brien, B. Gunay, and J. S. Carrizo, "Towards occupant-centric simulation-aided building design: a case study," *Building Research & Information*, vol. 47, no. 8, pp. 866–882, 2019.

[7] P. Remmen, M. Lauster, M. Mans, M. Fuchs, T. Osterhage, and D. Müller, "TEASER: an open tool for urban energy modelling of building stocks," *Journal of Building Performance Simulation*, vol. 11, no. 1, pp. 84–98, 2018.

[8] N. Endo, E. Shimoda, K. Goshome, T. Yamane, T. Nozu, and T. Maeda, "Simulation of design and operation of hydrogen energy utilization system for a zero emission building," *International Journal of Hydrogen Energy*, vol. 44, no. 14, pp. 7118–7124, 2019.

[9] I. Beausoleil-Morrison, "Learning the fundamentals of building performance simulation through an experiential teaching approach," *Journal of Building Performance Simulation*, vol. 12, no. 3, pp. 308–325, 2019.

[10] C. Xiong, J. Huang, and X. Lu, "Framework for city-scale building seismic resilience simulation and repair scheduling with labor constraints driven by time–history analysis," *Computer-Aided Civil and Infrastructure Engineering*, vol. 35, no. 4, pp. 322–341, 2020.

[11] A. D. Black, "Wor (l) d-building: simulation and metaphor at the Mars Desert Research Station," *Journal of Linguistic Anthropology*, vol. 28, no. 2, pp. 137–155, 2018.

[12] K. Hanson, L. Hernandez, and J. A. Banaski Jr., "Building simulation exercise capacity in Latin America to manage public health emergencies," *Health Security*, vol. 16, no. S1, pp. S-98–S-102, 2018.

[13] E. K. Wati and N. Widiansyah, "Design of learning media: modeling & simulation of building thermal comfort optimization system in building physics course," *Jurnal Pendidikan IPA Indonesia*, vol. 9, no. 2, pp. 257–266, 2020.

[14] C. W. Lee and S. J. Cho, "The development of converting program from sealed geological model to Gmsh, COMSOL for building simulation grid," *Journal of the Korean Earth Science Society*, vol. 38, no. 1, pp. 80–90, 2017.

[15] C. Miller, D. Thomas, J. Kämpf, and A. Schlueter, "Urban and building multiscale co-simulation: case study implementations on two university campuses," *Journal of Building Performance Simulation*, vol. 11, no. 3, pp. 309–321, 2018.

[16] X. Xie and Z. Gou, "Building performance simulation as an early intervention or late verification in architectural design: same performance outcome but different design solutions," *Journal of Green Building*, vol. 12, no. 1, pp. 45–61, 2017.

[17] A. I. Adilkhodjayev, I. M. Mahamataliev, and S. S. Shaumarov, "Theoretical aspects of structural and simulation modeling of the macrostructure of composite building materials," *Journal of Tashkent Institute of Railway Engineers*, vol. 14, no. 2, pp. 3–14, 2019.

[18] S. Imam, D. A. Coley, and I. Walker, "The building performance gap: are modellers literate?," *Building Services Engineering Research and Technology*, vol. 38, no. 3, pp. 351–375, 2017.

[19] J. S. Pei, B. Carboni, and W. Lacarbonara, "Mem-models as building blocks for simulation and identification of hysteretic systems," *Nonlinear Dynamics*, vol. 100, no. 2, pp. 973–998, 2020.

[20] A. Brunelli, F. de Silva, A. Piro et al., "Numerical simulation of the seismic response and soil–structure interaction for a monitored masonry school building damaged by the 2016 Central Italy earthquake," *Bulletin of Earthquake Engineering*, vol. 19, no. 2, pp. 1181–1211, 2021.

[21] P. Andrio, A. Hospital, J. Conejero et al., "BioExcel Building Blocks, a software library for interoperable biomolecular simulation workflows," *Scientific data*, vol. 6, no. 1, pp. 1–8, 2019.

[22] G. Petrou, A. Mavrogianni, P. Symonds et al., "Can the choice of building performance simulation tool significantly alter the level of predicted indoor overheating risk in London flats?," *Building Services Engineering Research and Technology*, vol. 40, no. 1, pp. 30–46, 2019.

[23] S. Gibeaux, C. Thomachot-Schneider, S. Eyssautier-Chuine, B. Marin, and P. Vazquez, "Simulation of acid weathering on natural and artificial building stones according to the current atmospheric SO 2/NO x rate," *Environmental Earth Sciences*, vol. 77, no. 9, pp. 1–19, 2018.

Hindawi
Journal of Sensors
Volume 2021, Article ID 6252425, 14 pages
https://doi.org/10.1155/2021/6252425

Research Article

Evolution and Quality Analysis Algorithm of Consumer Online Reviews Based on Data Fusion and Multiobjective Optimization

Hu Wang,[1] Tianbao Liang,[1,2] and Yanxia Cheng[1]

[1]*School of Management, Wuhan University of Technology, Wuhan, 430070 Hubei, China*
[2]*School of Management, Zhongkai University of Agriculture and Engineering, Guangzhou, 510225 Guangdong, China*

Correspondence should be addressed to Tianbao Liang; liangtb803@zhku.edu.cn

Received 10 August 2021; Revised 17 September 2021; Accepted 15 October 2021; Published 2 November 2021

Academic Editor: Mu Zhou

With the rise of network strategies, various businesses using the Internet as a platform have been vigorously developed, among which the scale of e-commerce transactions has increased on a large scale. In order to deeply explore the role and advantages of data fusion and multiobjective optimization technology in consumer online reviews, this paper uses the new and old evaluation model comparison method, algorithm design method, and multiobject research method to collect samples, analyze the technical model, and streamline the algorithm. And it will create an analysis algorithm model that can improve and optimize the consumer's current online reviews. First, we choose the electricity supplier on the platform of a total of four mobile phones grabbed 32,145 comments. Based on this research on the number of online comment fields of consumers, the results show that 78% of the comments are less than 55 words, indicating that most of the online comments left by consumers are short comments; at the same time, a small number of consumers have left detailed comments. Description, the longest of is reached 612 words. On this basis, further study the efficiency and function analysis of the algorithm proposed in this paper, and we can see that DCDG-MOMA is used in 14-7 and 28-7 use cases as 1 and 2, respectively, which is the least, and at 40-7 and 50-7, the time used is 15 and 20 which is close to PBI, but it is also much less time than the MOMAD algorithm. This further shows that the algorithm really plays an effective role in the actual decision-making process. It has basically realized a more efficient algorithm for consumer online reviews under the background of applying data fusion and multiobjective optimization technology.

1. Introduction

In the past few decades, due to the rapid development of computer technology, each network platform to get a good leveraging some of scalable online business also has a corresponding increase. Among them, online shopping has become an important driving force for the development of e-commerce in our country. Online purchasing platform is where all is not well, that is, the problem undetected online purchasing presence. Based on this, this approach to reduce the information asymmetry mechanism of both parties to the transaction has become the first choice of major e-commerce platforms, and online reviews are currently widely adopted by various online shopping platforms. Online comment is one that can be evaluated for their customers to buy the product after shopping on the web electronic business platform and buy the product for consumers to purchase the follow-up to provide reference. However, with the rapid development of the Internet, this approach has also exposed its own bottlenecks, requiring the integration of new technologies for optimization.

Multiobjective optimization, as a research direction in multicriteria decision-making, refers to a multiobjective optimization problem in which the number of objects to be optimized is more than one, and the optimization should be carried out at the same time. When the variable domain of the problem is a finite set, we call this type of problem a multiobjective combinatorial optimization problem. Multiobjective optimization problems exist in a large number in the real world and have important research significance. How to design corresponding algorithms to solve such problems has also attracted more and more attention from

scholars. This paper further proposes a multimodal sensor data fusion algorithm based on adaptive feedback adjustment. This method has good generalization ability, can more accurately estimate the mobile phone displacement, and dynamically adjust the screen display position, so that the mobile phone screen content is displayed smoothly and reduces frequent focus of the eyes, to achieve the effect of soothing visual fatigue. At the same time, it has great significance for online reviews and quality analysis.

Consumers have also been greatly facilitated in the development of science and technology, especially the combination of online reviews with data fusion and multiobjective optimization technology has made this advantage more obvious. Many scholars have done research here. In 2020, Jain and Vaidya reviewed most of the works reported by various authors about the use of social media during terrorist attacks in the past 10 years, how to conduct postattack social media analysis, and how to use social media analysis to detect terrorism, unrest, and hate behavior. For this goal, they used this review as a future antiterrorism research. However, this research path did not use technology [1]. In 2021, Lee and Hong used an online survey to collect data on 560 Amazon Mechanical Turk users. The results show that both perceived time pressure and perceived purchase uncertainty are positively correlated with the heuristic processing of online reviews, but negatively correlated with the systematic processing of online reviews. Their research finally discussed practical and academic significance, as well as future research directions. Although the research is complete, it lacks data support [2]. In 2016, Balakrishnan et al. conducted a bibliometric analysis based on more than 20,000 articles from Web of Science to study how knowledge about the two important multienergy systems of microgrids and smart grids has developed. Their findings identify areas that have been underresearched so far, provide a method for data fusion between different multienergy systems, and provide practical guidance for the implementation of multienergy system data fusion. Practicality is guaranteed, but the theory is somewhat inadequate [3]. In 2020, Park et al. introduced the publication of the second edition of Integrated Hierarchical Classification (ILC2), a free-side knowledge organization system (KOS), and reviewed the main changes introduced compared to the first edition (ILC1). The changes introduced in ILC2 include the following: the names and order of some major categories and the development of subcategories of various phenomena. The system can be accessed online for free via a PHP browser and SKOS format. However, there are deviations in the research process [4]. In 2019, Arora proposed that Industry 4.0 is the fourth industrial evolution: "The interconnection of the value creation process transcends the boundaries of a single company." To achieve this, there must be strong Internet access. Integration should not stay at the company boundary, but should also involve customers and serve as a digital business partner in Industry 4.0. It is a pity that it can only act on the industrial field and limit its development [5]. In 2016, Brill focused on theoretical issues, current developments, and emerging trends in all areas of the field, including detailed reviews of relevant recent literature. The editorial board and advisory board are composed of scholars and practitioners in the fields of public international law and European law to ensure that the review fully reflects the interrelationship between current developments and the continued development of this important legal theory and practice field. But based on this research, he did not understand [6]. In 2016, Meza et al. proposed a multiobjective optimization strategy based on particle swarm behavior with rotation and linear motion. The combination of exploration-utilization led to the proposed cognitive algorithm, which was tested by multiple multiobjective optimization functions. Through statistical analysis, the proposed algorithm is compared with the standard particle swarm optimization multiobjective algorithm. Although the research process is quite inspiring, it is a pity that there is no conclusion [7].

The innovations of this article are as follows: (1) this research provides new research methods and ideas for exploring the impact of online reviews and also helps companies refine the impact of online reviews, so as to take targeted marketing measures; (2) how the price (favorable and bad comments) of online comments integrated by the new method acts on the evolution of consumer attitude is closer to reality and has stronger application value; (3) in terms of basic data acquisition, this article uses online comments serve as sample data. Compared with the traditional method, the analysis conclusion will be more scientific and effective. Through the above work, the application of theories based on data fusion and multiobjective optimization is more reasonable, and the model designed from this can better have a nationwide guiding application for consumer online reviews and quality analysis.

2. Implementation Method of Online Comment and Analysis Algorithm Research Based on Data Fusion and Multiobjective Optimization

2.1. Consumer Online Reviews. With the rise of the Internet, the spread of word-of-mouth is no longer limited to the real world but extends to the virtual Internet world. Virtual reality technology is a brand-new practical technology developed in the 20th century. Virtual reality technology includes computers, electronic information, and simulation technology, and its basic realization is that a computer simulates a virtual environment to give people a sense of environmental immersion. For example, foreign shopping platforms such as Amazon and e-Bay have launched product review functions as early as the 1990s, which has also aroused scholars' attention to the impact of online word-of-mouth. Online reviews, also known as online consumer reviews, are just one of the main manifestations of Internet word-of-mouth [8].

As a kind of online word-of-mouth, online reviews are not only related to but different from traditional offline word-of-mouth. From the perspective of connotation definition, online reviews and traditional offline word-of-mouth are both informal and noncommercial evaluation information about products or services [9], but they are not just simple common concepts. The connections and differences

between the two are discussed below. The four common characteristics of online reviews and traditional offline word-of-mouth are as follows [10]:

(1) High reliability

Traditional offline word-of-mouth communication is generally carried out between relatives and friends, so recipients generally trust the source of information; online reviews are reviews left by consumers about products, because reviewers have no direct economic relationship with the merchants. The introduction of merchants is more objective and credible [11].

(2) Two-way communication

Different from one-way publicity methods such as advertising, word-of-mouth communication is two-way, and further interactive communication can be carried out between the communicator and the receiver, which can also be achieved by online reviews [12].

(3) Less interference

Compared with other communication methods, word-of-mouth information is less interfered by external factors due to word of mouth; online comments are generally kept on the Internet for more than one year, and the degree of interference is less [13].

(4) Uncontrollable

Online reviews are the same as traditional offline word-of-mouth communication. They are both intangible and intangible. Therefore, it is difficult for companies to control their communication. Moreover, in different industries, consumers have different dissemination intentions, which will affect potential consumer growth rate.

The difference between online reviews and traditional offline word-of-mouth is also very obvious. There are three differences:

(1) Anonymity

Because online comments publish information on the Internet, they can express their opinions in the most truthful manner without violating the law without worrying about any stakes [14].

(2) Not limited by time and space

Different from traditional word-of-mouth, online reviews can exist on shopping platforms for a long time and can be seen by anyone at any place and at any time, thus breaking the time and space limitations of word-of-mouth communication [15].

(3) Content format

Traditional offline word-of-mouth communication is mainly spread through language, facial expressions, body movements, etc., while online reviews are mainly spread through digital information such as text, pictures, and ratings [16].

Digital information dissemination technology includes theories, methods, technologies, and systems related to the acquisition, processing, storage, dissemination, management, security, and output of digital media information. It includes various information technologies such as computer technology, communication technology, and information processing technology. Comprehensive application technology, online comment is a process of information dissemination from initiator to receiver, as shown in Figure 1. The initiator of the comment publishes the content of the comment on the Internet and is searched or received by the receiver who needs the information. This is the communication process of online comments.

As can be seen from Figure 1, the initiator of online reviews directly determines the origin of online reviews and is also the basis for the spread of online reviews, which will also directly affect subsequent consumers' perceptions and behaviors of products [17]. Intelligent perception technology can be divided into four categories according to different objects and goals: perception technology based on human body analysis, perception technology based on vehicle analysis, perception technology based on behavior analysis, and perception technology based on image analysis. At the same time, theoretical combing is also critical. In view of the existing analysis, this article summarizes the relevant research on online reviews, as shown in Figure 2.

Judging from Figure 2, this paper analyzes several elements of online review research, the initiator (motivation, professionalism, etc.), the recipient (professionalism, network experience, etc.), the information processing process (ELM and HSM), and the dimensions of online comments themselves (quantity, valence, etc.) [18].

2.2. Data Fusion and Multiobjective Optimization Technology. Multimodal data fusion refers to the comprehensive use of computer technology to process multimodal data, so as to more accurately perceive information such as the state of the objective object and the environment in which it is located. Data fusion technology refers to information processing technology that uses computers to automatically analyze and synthesize several observation information obtained in time series under certain criteria to complete the required decision-making and evaluation tasks. Data fusion technology includes the collection, transmission, synthesis, filtering, correlation, and synthesis of useful information from various information sources to assist people in situation/environmental judgment, planning, detection, verification, and diagnosis. The focus of multimodal data fusion research includes various modal data feature extraction methods and multimodal data fusion algorithms. The focus of the fusion algorithm is to coordinate and complement different modal data and improve the accuracy of decision-making for uncertain data. The data fusion center fuses information from multiple sensors and can also fuse information from multiple sensors and the observation facts of the human-machine interface (this fusion is usually a decision-level fusion).

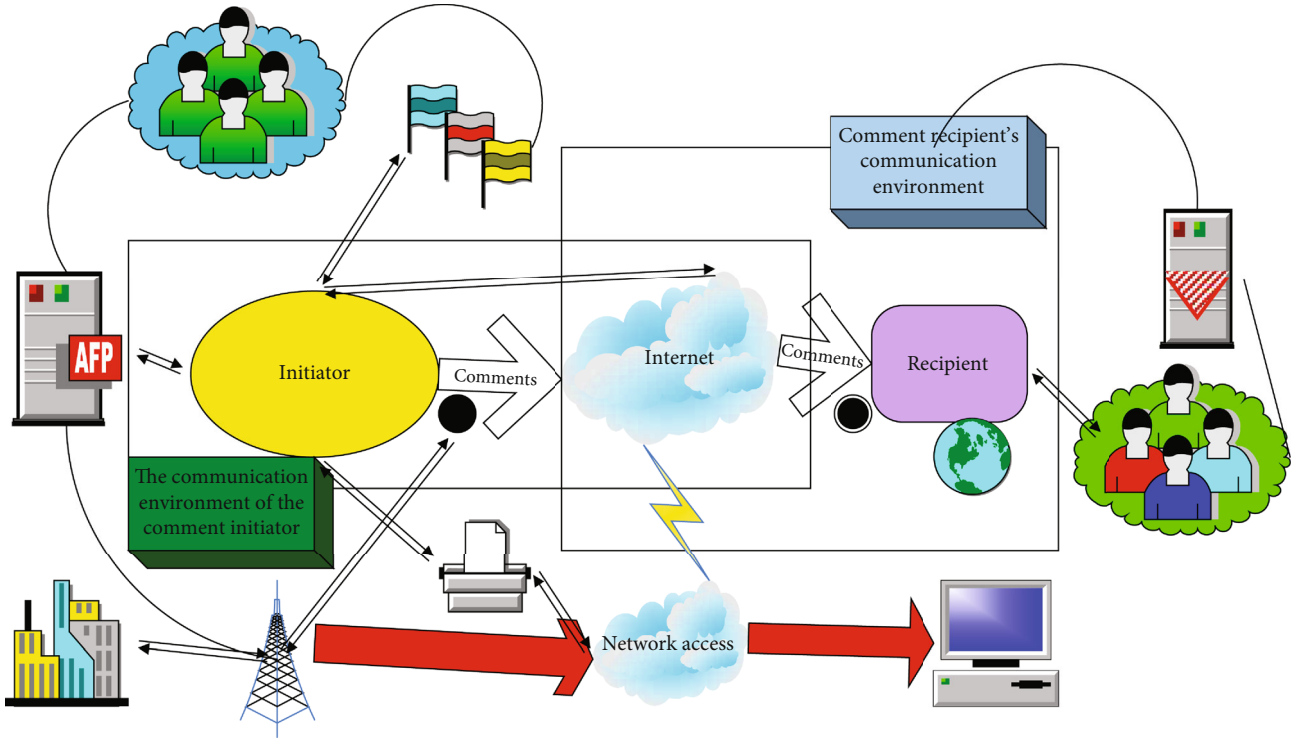

Figure 1: Online comment exchange process.

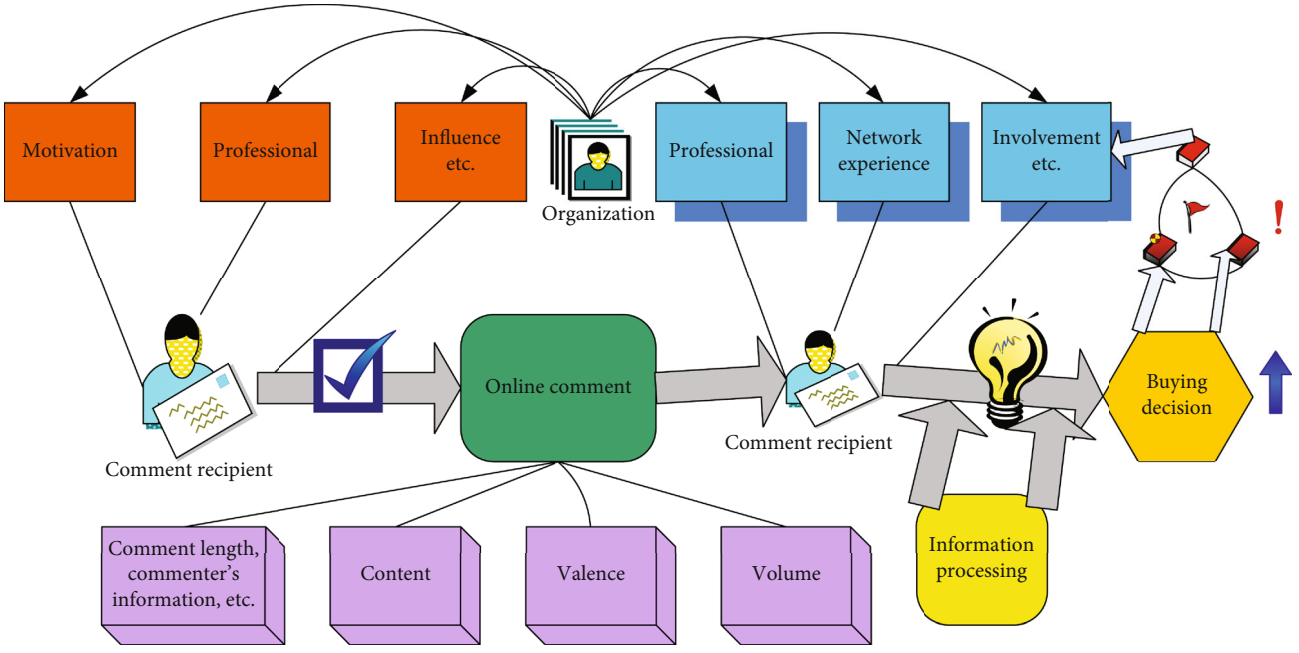

Figure 2: Theoretical research on online reviews.

Extract the symptom information, under the action of the inference engine. Match the symptoms with the knowledge in the knowledge base, make fault diagnosis decisions, and provide them to users. Compared with single mode, multimode system has the following advantages:

(1) Improve system stability

(2) Improve the continuity of information

Nowadays, multiobjective optimization problems are more and more widely used, involving many fields. In daily life and engineering, more than one index is often required to be optimized, and multiple indexes are often required to be optimized at the same time. A large number of problems

can be attributed to a category of achieving multiple goals at the same time under certain constraints.

Multisensor data fusion is shown in Figure 3 according to the level of fusion: according to the different levels of fusion, it is divided into data layer fusion, feature layer fusion, and decision layer fusion [19].

As shown in Figure 3, multisensor data fusion can be divided into the following:

(1) *Data Layer Fusion*. The data detected by all sensors are fused, and the next step is performed from the fused data. This fusion method requires the sensors to detect the same type of data without losing the original data. The accuracy is high [20].

(2) *Feature Layer Fusion*. The data detected by each sensor is extracted separately, and then, these features are fused. This method compresses the original data to a certain extent, reduces the time required for subsequent processing, and improves the system's performance real-time.

(3) *Decision-Making Layer Fusion*. After each sensor detects the data, it performs feature extraction and target recognition and then fuses each recognition result. This method is the most inaccurate, because the information of each sensor is a high degree of concentration.

"Video networking" technology is the current advanced real-time high-definition video exchange technology, which can realize large-scale, high-quality, real-time, two-way, and symmetrical high-definition video full exchange. At present, there is no universal fusion method for multisensor data fusion, and it generally needs to be determined according to the specific application background. Weighted average method and neural network method are two classic data fusion methods based on measurement signals [21].

The weighted average method is the simplest and most intuitive method for processing information and data fusion. The basic process is as follows:

Assuming that o sensors are used to measure a certain physical quantity, the output data of the u-th sensor is $a_u(u = 1, 2, \cdots o)$ and the weighting coefficient is d_u, and then, the output value of each sensor is weighted and averaged, and the weighted average fusion result is obtained as follows:

$$\bar{a} = \sum_{u=1}^{o} d_u a_u + \sum_{u=2}^{k} d a_c. \tag{1}$$

The weighted average method is the weighted average of the redundant information from each sensor, and the result is used as the fusion value. When applying this method, the system and the sensors used must be analyzed in detail to obtain the correct weights $\bar{a}$.

The biggest difference between the multiobjective optimization algorithm and the single-objective evolutionary algorithm in the calculation process is the individual fitness evaluation strategy. The use of a good individual fitness evaluation strategy and selection strategy has a great effect on the performance of the evolutionary algorithm [22].

As an improvement of the NSGA algorithm, NSGAII uses a fast nondominated sorting strategy to establish a nondominated set. The method of constructing the nondominated set is as follows: first, set two parameter variables t_q and o_q for all individuals in the group q, and put the set t_m in the individuals of $o_m - u = 0$ are stored in the m set. When $l_u = \partial$, the above operations are performed in sequence until all individuals are stratified and assigned a grade number [23].

Use a mathematical formula to describe the crowdedness of the environment in which individuals in the group are located. Suppose the crowded distance of the individual u is w_u, and the crowded distance of the nonboundary individual u is calculated as follows:

$$w_u = \frac{\sum_{k=1}^{n} |l_k(u-1) - l_k(u+1)| / l_k^{\min} - l_k^{\max}}{n}. \tag{2}$$

Among them, $l_k(u-1)$ and $l_k(u+1)$ are the objective function values of $u-1$ and $u+1$ near the individual u on the k-th target, $l_k^{\min}$ and $l_k^{\max}$ are the maximum and minimum values of the k-th objective function, and n is the number of objective functions. Number, the k-th gene of the next generation was obtained by simulating binary crossover [24].

$$\begin{aligned} b_1'(k) &= 0.5\left[(1-\tau_m(k))a_i'(k) + (1+\tau_m(k))a_1'(k)\right], \\ b_2'(k) &= 0.5\left[(1-\tau_m(k))a_i'(k) + (1+\tau_m(k))a_2'(k)\right], \\ \tau_m(k) &= \begin{cases} (2\rho(k))^{1/o_z+1} & \pi(k) < 0.5, \\ \left(\dfrac{1}{2(1-\pi(k))}\right)^{1/o_z+1} & \text{anyother.} \end{cases} \pi(k) \in [0.1], \end{aligned} \tag{3}$$

Polynomial transformation node can prevent the population due to conversion into a building partially optimized mode. Let $a_u^s(k)$ be the k-th gene of the u-th generation of individuals, and $a_u^o(k)$ and $a_u'(k)$ are the next and next generations of $a_1^i(k)$. Individual $a_u^s(k)$ mutates to produce offspring $b_u^i(k)$. Among them, ρ_n is a custom parameter, adjusted according to the actual situation, called the variation distribution index [25].

$$\begin{aligned} b_u^s(k) &= a_u'(k) + \left(a_i^o(k) - a_i'(k)\right)\overline{\tau_m}(k), \\ \overline{\tau_m}(k) &= \begin{cases} 2\bar{\pi}(k)^{1/\pi_n - 1} & \bar{\pi}(k) < 0.5, \\ 1 - [2(1-\bar{\pi}(k))]^{1/\pi_n - 1} & \text{another.} \end{cases} \bar{\pi}(k) < 0.5, \end{aligned} \tag{4}$$

Among them, $\overline{\tau_m}(k)$ is the exponential growth value, and $\bar{\pi}(k) < 0.5$ is the discrimination criterion.

The performance evaluation of multiobjective optimization algorithm mainly adopts two aspects: convergence of

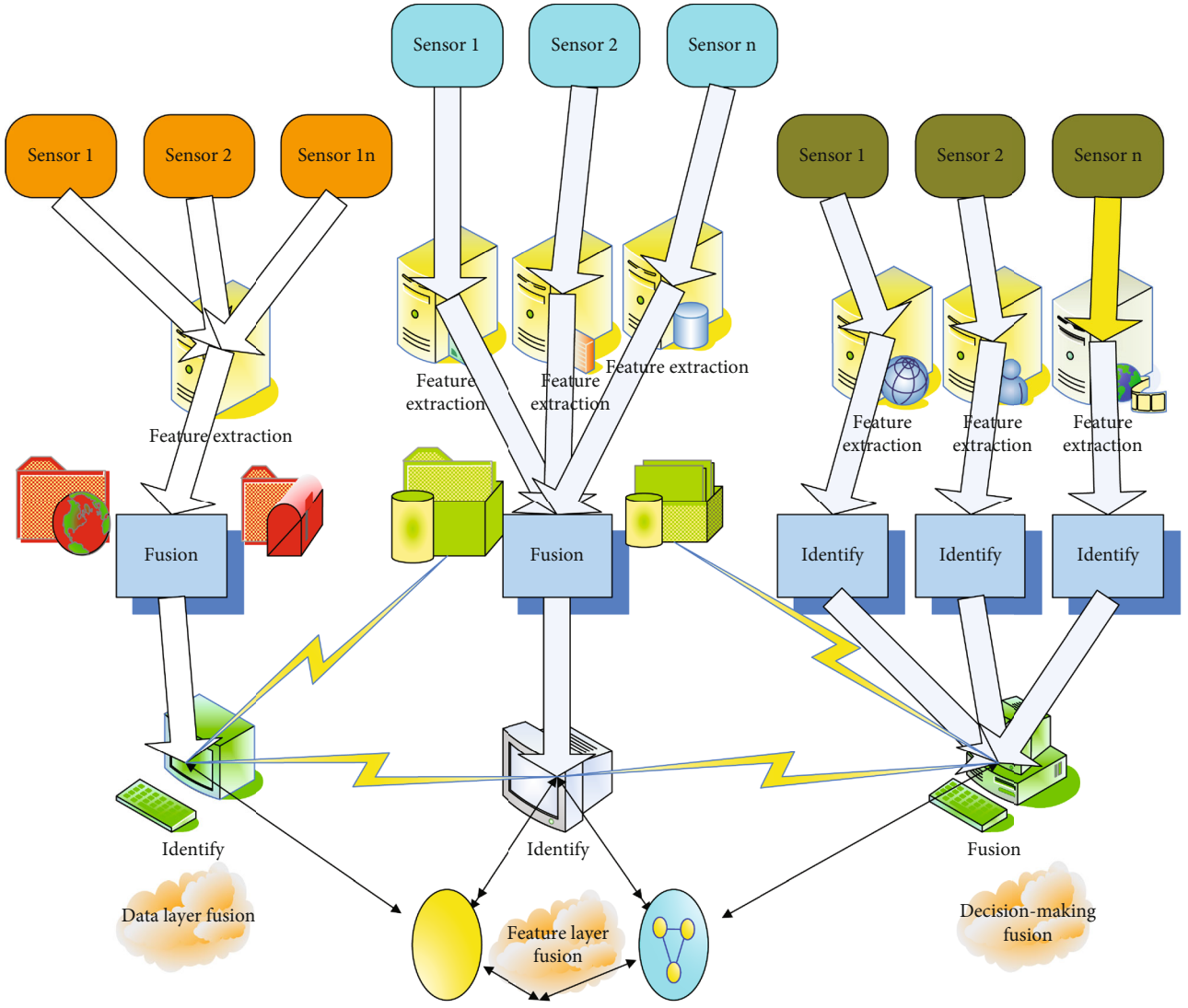

Figure 3: Schematic diagram of data fusion classification.

solution set and distribution breadth of solution set. In order to truly reflect the performance of the evolutionary algorithm, the following three evaluation indexes are mainly used in this paper, where the generation distance (GD) measures the algorithm convergence effect; the spatial distribution (SP) mainly evaluates the uniformity of the nondominant solution set distribution results, and the maximum spread cloth (MS) mainly analyzes the distribution universality of the nondominant solution set [26].

GD is used to evaluate the distance between the Pareto optimal front (PF) and the nondominated solution set front (PF) obtained by the algorithm in the ideal state of uniform distribution. The value is defined as follows:

$$\mathrm{GD} = \sum_{uc}^{\exp} h_k + \frac{1}{o}\left(\sum_{u=1}^{o} w_u^2\right)^{1/2}. \tag{5}$$

For a specific optimization problem, o is the number of individuals in PF, and w_u is the Euclidean distance between the u-th point in PF and the nearest point in PF in the target space. The uniformity of SP's main evaluation algorithm result set distribution is defined as follows:

$$\mathrm{SP} = \frac{1}{\overline{w^s}}\left[\frac{1}{o}\sum_{u=1}^{o}\left(w' - \bar{w}'\right)^2\right]^{1/2}, \overline{w'} = \frac{1}{o}\sum_{u=1}^{o} w_u^s. \tag{6}$$

Among them, w' represents the Euclidean distance between the u-th individual in PF and its nearest, and o is the number of individuals in PF [27]. MS is mainly used to measure the breadth of the distribution of nondominated solution sets obtained by evolutionary algorithms and is defined as follows:

$$\mathrm{MS} = \sqrt{\frac{1}{n}\sum_{u=1}^{n}\left\{\frac{\max\left\{l_u^{\min}, l_u^{\min}\right\} - \min\left\{l_u^{\max}, l_u^{\max}\right\}}{l_u^{\min} - l_u^{\max}}\right\}}. \tag{7}$$

Among them, n represents the number of targets, $l_u^{\min}$ and $l_u^{\max}$, respectively, represent the maximum and minimum values of the u-th dimension objective function in the PF, and $l_u^{\min}$ and $l_u^{\max}$, respectively, represent the maximum and minimum values of the i-dimensional objective function in the PF.

2.3. Algorithm

2.3.1. Time Series Prediction Technology. Time series is a set of data points arranged in chronological order. Time series are very common in daily life. For example, the weekly average temperature of a certain place, the number of people dining in a week in a restaurant, and the stock price of a certain stock in one year can all be abstracted into time series for analysis. Time series forecasting technology is actually a regression forecasting method, which belongs to quantitative forecasting. Its basic principle is as follows: On the one hand, it recognizes the continuity of the development of things, uses past time series data for statistical analysis, and infers the development trend of things.

2.3.2. LSTM. LSTM is a variation of the cyclic neural network. Traditional RNN has the problem of disappearing gradients in terms of long-term dependence, which means that it will forget information that is far away from the time series. And LSTM gains the ability to learn long-term dependence by introducing three kinds of thresholds (forgetting threshold, input threshold, and output threshold) and has the ability to learn time series distance information. A simple LSTM network structure is shown in Figure 4.

As shown in Figure 4, the input is A, the output is G, and the information of the neural network will be passed to the next state through the cyclic structure X. On this basis, Figure 5 describes the internal principles of LSTM in detail.

As shown in Figure 5, in the figure, u represents the sigmoid activation function, with a value range of 0 to 1. Now let us introduce the forgetting gate of LSTM. The forgetting gate receives the output g_{s-1} at the previous moment and the current input a_s and then passes through a sigmoid layer to choose to forget some information. If the sigmoid output is 0, it will be completely forgotten; if the output is 1, it will be completely reserved [28].

$$l_s = \sigma(d_l * [g_{s-1}, a_s] + y_l). \tag{8}$$

LSTM input gate: first, the last output g_{s-1} and the current input a_s will pass through the sigmoid layer and output u_s. u_s represents the probability of updating the state. Then, the last output g_{s-1} and the current input a_s will pass through the tanh layer to output the candidate new state $\widetilde{z_s}$.

$$\begin{aligned} u_s &= \sigma(d_u * [g_{s-1}, a_s] + y_u), \\ \widetilde{z_s} &= \cos g(d_z * [g_{s-1}, a_s] + y_z). \end{aligned} \tag{9}$$

Subsequently, a new state z_s needs to be generated, which is calculated from the output l_s of the forget gate, the candidate new state $\widetilde{z_s}$ of the input gate, and the update probability u_s.

$$z_s = l_s * z_{s-1} + u_s * z_s + \sqrt[d]{\breve{z_d^s}}. \tag{10}$$

Output gate: the last output g_{s-1} and the current input a_s will pass through the sigmoid layer, output p_s, and determine which new state information will be output. Then, the new state z_s is processed and multiplied by p_s to determine the information g_s output by the new state.

$$\begin{aligned} p_s &= \sigma\left(d_p * [g_{s-1}, a_s] + y_p\right) + \left(d_p * [g_{s-1}, a_s] + y_p\right), \\ g_s &= p_s * \sin g\left(z_s + \coprod_{z}^{u=1}(dc + on)\right). \end{aligned} \tag{11}$$

2.3.3. Linear Regression. Regression is a predictive modeling technique in which the estimated target variable is continuous [29]. The main forecasting technology models are linear regression model, moving average model, exponential smoothing model, trend extrapolation model, ARIMA forecasting model, Markov forecasting model, input-output forecasting model, grey forecasting model, artificial neural network forecasting model, etc. In reality, there are many applications of regression technology, such as forecasting stock market index, forecasting rainfall, road traffic, etc. Linear regression is divided into simple linear regression and multiple linear regressions. A variable to estimate the target variable is a simple linear regression (one-variable linear regression). For example, a data set $w = \{(a_u, b_u)/u = 1, 2, 3 \cdots o\}$ of N observation data is collected, and a linear model is used to fit the observation data.

$$l(a) = d_1 a + d_o + \prod_{g=1}^{0} x_g. \tag{12}$$

Among them, $l(a)$ is the data observation value, such that

$$\max \sum_{u=1}^{o} [b_u - l(a)] b^2. \tag{13}$$

Among them, d_1 and d_o are the regression coefficients of simple linear regression. This method is also called the least square method. It tries to minimize the error between the estimated target variable and the real target variable through the appropriate regression coefficients d_1 and d_o.

Finding the regression coefficient $d_0, d_1, \cdots d_h$ makes the following:

$$\begin{aligned} \widehat{b} &= d_0 + d_1 a_1 + d_2 a_2 + \cdots + d_h a_h, \\ \max \sum_{u=1}^{o} \left[b_u - \widehat{b}\right] &+ \begin{pmatrix} a & c \\ b & d \end{pmatrix} = uk. \end{aligned} \tag{14}$$

Among them, $b_u - \widehat{b}$ is an equation from the beginning to the end, and the above algorithm is established.

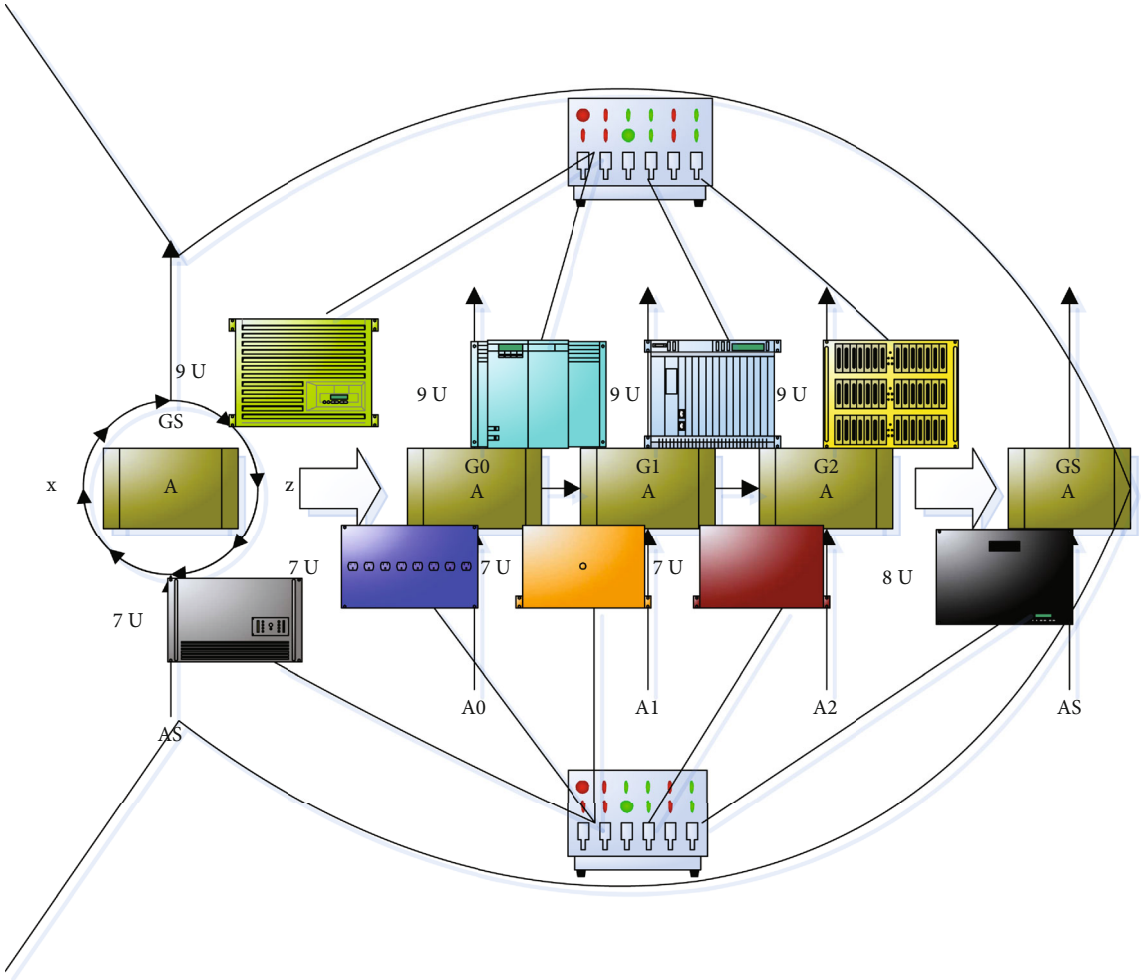

Figure 4: Schematic diagram of recurrent neural network LSTM.

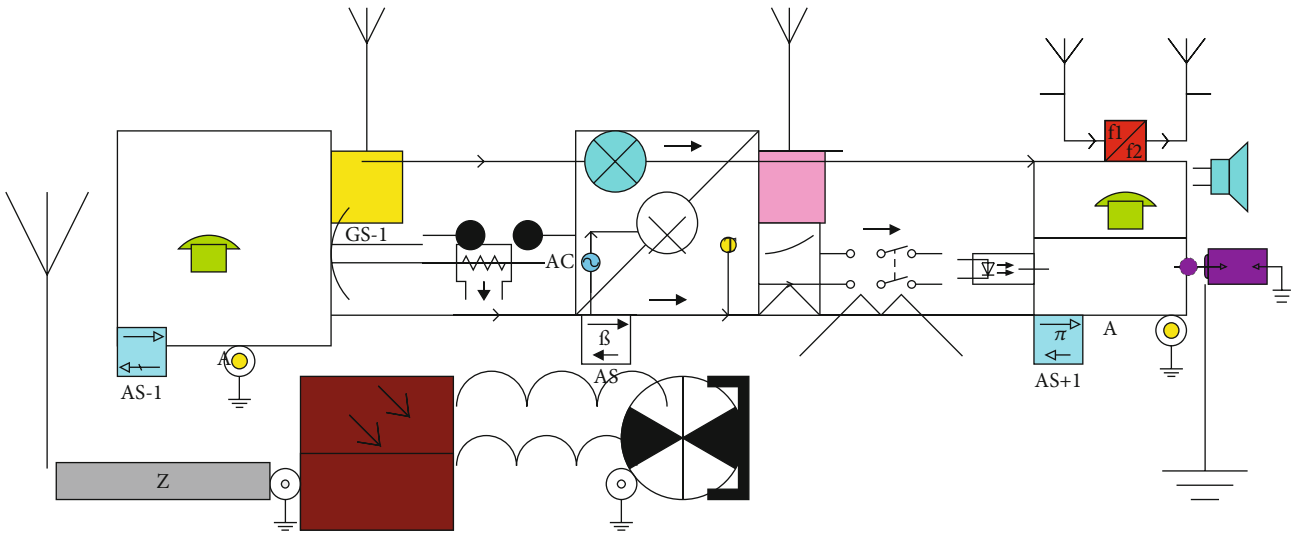

Figure 5: Schematic diagram of the LSTM structure of the recurrent neural network.

3. Based on Data Fusion and Multiobjective Optimization of Online Reviews and Analysis Algorithm Research Design and Implementation Method Experiments and Conclusions

3.1. Experimental Setup. In order to verify the effectiveness of the algorithm MSIMOPSO proposed in this paper, three multiobjective optimization algorithms will be used as the comparison algorithm for this simulation experiment. These are the multiobjective evolutionary algorithm (MOEA/D) based on decomposition idea and the genetic algorithm based on fast nondominated sorting, NSGAII, and multistrategy improved multiobjective particle swarm optimization (MIMOPSO). And it adopts ZDT, DTLZ, and some UF test functions which are set as test functions. The parameter settings of each comparison algorithm and the corresponding population size and evaluation times of each test function are set as shown in Table 1.

Table 2 shows the setting method of the test function:

The above algorithms are run 30 times independently on the i5 processor, 8 G RAM, and MATLAB2014a platform.

3.2. Model Simulation. In order to determine the value of each parameter in the model, this article obtained a series of data on a well-known domestic e-commerce website. According to the refined processing model (ELM), when consumers do not have time to carefully consider each piece of review information, their decision-making is usually quick and simple. This method usually only needs to extract the hidden meaning of the information to quickly make a choice, and the detailed description can be seen in the experiment, and the analysis can be seen below. Research shows that the number of reviews is one of the bases for many consumers to make quick decisions. In order to explore the influence of the number of reviews on consumer decision-making, this article collected reviews of these two categories of products from the mall using "laptop" and "flat-panel TV" as keywords, mainly including the number of reviews and praise rate.

This article first takes "laptop" as an example. A total of 785 products have been searched in the mall, of which 728 products have online reviews. Therefore, this article has collected a total of 258,473 online reviews of 728 products. Because some products under the same brand, although the models are different, there is little difference in configuration, and some products have less than 5 reviews, so the products can be reclassified. In order to calculate the information intensity of each product, this article classifies the 728 products collected by 30 brands, that is, each brand represents a product, and calculates the information intensity of each product based on this. Of course, the information intensity of each commodity can also be calculated separately, and the result does not affect the actual meaning of the information intensity calculation method. In the simulation of this article, each brand is regarded as a product, and reviews of products under the same brand are included in the reviews of that brand. The data is shown in Figure 6.

Table 1: Comparison algorithm parameter settings.

Algorithm name	Parameter settings	Group name	Possibility
MSI	$W1 = 0.3$, $W2 = 0.8$, $Z1 = Z2 = 3$	A	95.2%
NSG	PC = 0.8, PN = O	B	96.4%
MOE	$T = 0.1N$, ZE = 0.9	C	91.8%
MIM	$W = 0.108$, $Z1 = Z2 = 1.88$	D	93.5%

Table 2: Test function settings.

Function name	Population size	External archive size	Evaluation times
ZDT	90	90	30000
DTLZ	140	140	100000
UF	190	190	300000

It can be seen from Figure 6 that under the support of the data parameters in the figure, the information intensity of each brand product is calculated by the calculation formula, and the results are shown in Table 3.

In order to determine the influence of information intensity on consumer acceptance-acceptance probability, this paper selected 3 products from 30 products for simulation, namely, THINK, $n = 0.24$; Samsung, $n = 0.054$; and Jumper, $n = 0.00024$. The information intensity of these three commodities, respectively, represents the high information intensity, medium information intensity, and low information intensity of the online review information of these products.

3.3. Data Collection. This article uses the GooSeeker web crawler software developed based on Python to obtain online comment data on the four popular smartphones of domestic A mobile phone, domestic B mobile phone, foreign A mobile phone, and foreign B mobile phone on the online shopping platform. This article crawls the user name, user rating, evaluation time, number of likes, number of replies, and details of the comment text of the comment. The comment interface and comment data acquisition methods of the other three mobile phones are similar, so I will not repeat them here.

As shown in Table 4, there are a total of 32,145 comments on the four mobile phones crawled in this paper: domestic A mobile phone, domestic B mobile phone, foreign A mobile phone, and foreign B mobile phone. Among them, 15,487 comments were obtained from the x platform and 16,658 comments were obtained from the y platform. The number of comments on each mobile phone was basically the same, and the number of comments on foreign mobile phones was slightly larger. The time span of the comment is nearly 6 months, which is basically consistent with the current life cycle of mobile phones.

Then, study the number of words used in their comments, as shown in Figure 7.

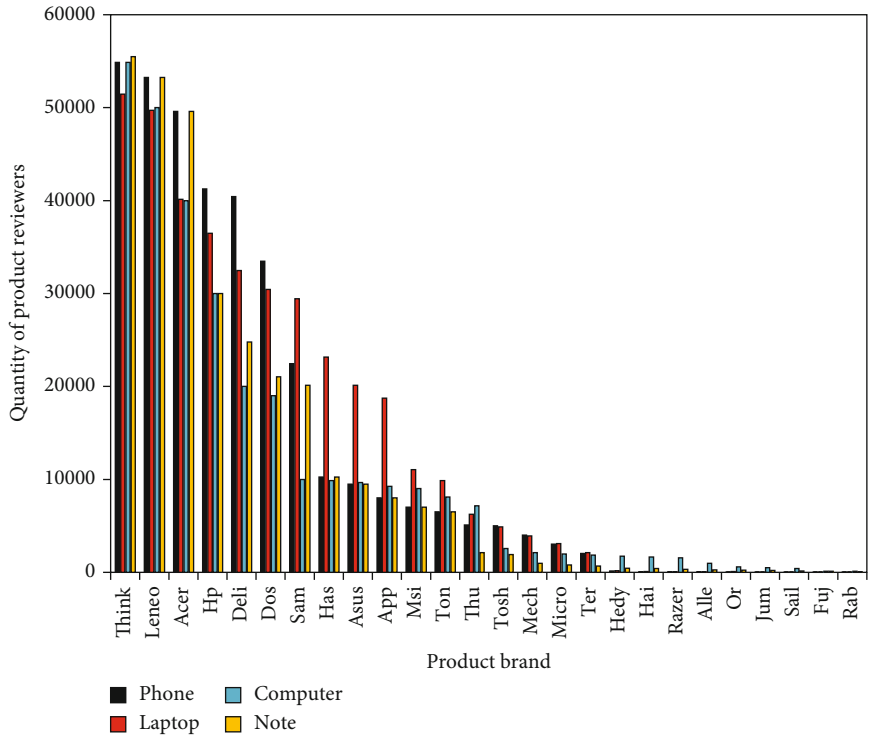

Figure 6: Number of reviews of each brand product.

Table 3: Information intensity of laptops of various brands.

Brand	Information intensity	Brand	Information intensity
THINK	0.24	ME	0.005
LENEO	0.18	MICRO	0.005
ACER	0.08	TER	0.008
HP	0.07	HEDY	0.015
DELI	0.05	HAI	0.0015
DOS	0.04	RAZER	0.0014
SAM	0.054	ALL	0.00133

It can be seen from Figure 7 that it is a word frequency chart based on the word count of each comment. This figure shows that 78% of reviews are less than 55 words, indicating that most of the online reviews left by consumers on shopping platforms are short reviews; at the same time, a small number of consumers have left a detailed description of their shopping experience. The longest comment has reached 612 words.

3.4. Survey Samples and Analysis. For all the algorithms, we compared the final results of the experiment. From these table data, we can clearly observe that RLG-PLS is superior to other algorithms in all MOKP and MOTSP test cases. This conclusion also shows that RLG-PLS has good convergence performance. The neighbor structure in the local search process is defined as follows: for a solution, one of its neighbors can be removed by removing the two hardware devices that have been placed, and then, the two hardware devices are randomly selected under the premise that all constraints are met. Choose two locations for placement, and a feasible configuration solution obtained after placement is a new neighbor. In this article, all algorithms use this neighbor structure definition method.

We can see from Table 5 that the value of DCDG-MOMA on the c-metric index is significantly better than algorithms such as MOEA/D-LS and MOMAD. Therefore, we can get that the convergence performance of DCDG-MOMA is better than these compared algorithms.

In order to further verify the pros and cons of the algorithms, we also calculated the hypervolume index of the solutions obtained by these algorithms, as shown in Figure 8.

As shown in Figure 8, the results of DCDG-MOMA on IH are better than the compared algorithms. According to the values of c-metric and IH, it can be seen that DCDG is significantly better than the compared algorithms, which conforms to the shortcomings of the decomposition methods analyzed in the article in maintaining diversity. To further study the time it takes for the algorithm to run, please see Figure 9.

It can be seen from Figure 9 the calculation time spent by all algorithms in running different DAP test cases. From these data, we can see that DCDG-MOMA uses 1 and 2 for 14-7 and 28-7 use cases, respectively. For the least, the time used on 40-7 and 50-7 is 15 and 20 is close to PBI, but it is also much less time than MOMAD algorithm.

3.5. Effect Analysis. For the device allocation problem in DIMA, the solution obtained by DCDG-MOMA and other algorithms is a solution set. In practice, decision makers

Table 4: Statistical description.

Mobile phone brands	Time to market	x platform	y platform	Total	Comment time
Domestic A mobile phone	2016.3.1	3000	3600	6600	2015.9-2016.10
Domestic B mobile phone	2015.12.9	2000	2400	4400	
Foreign A mobile phone	2015.9.9	5487	6658	12145	
Foreign B mobile phone	2016.8.3	5000	4000	9000	
Number of comments		15,487	16,658	32,145	

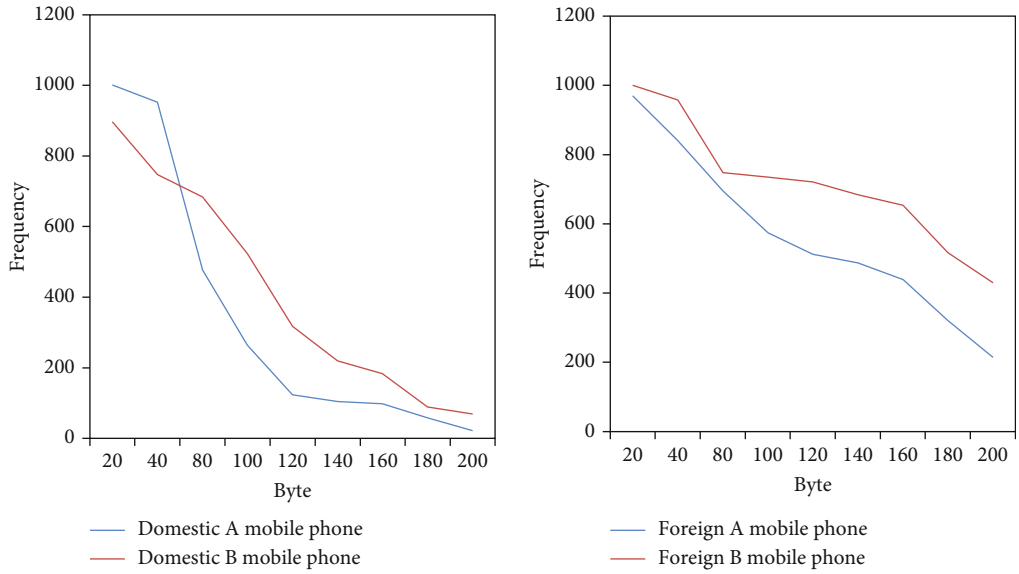

Figure 7: Frequency statistics of online comments.

Table 5: c-metric (%) of DCDG-MOMA, MOEA/D-LS, and MOMAD on DAP.

Test case	MOEA/D		WS		MOEA/D		TCH		MOEA/D		PBI		MOMAD	
	$Z(X,Y)$		$Z(Y,X)$		$Z(X,Y)$		$Z(Y,X)$		$Z(X,Y)$		$Z(Y,X)$		$Z(X,Y)$	$Z(Y,X)$
13-7	70.1		0.28		67.89		2.98		69.8		0.11		77.58	3.11
22-7	6.12		4.3		18.56		3.98		28.56		3.6		99	4.11
42-7	17.25		18.8		44.85		40.21		48.25		18.25		44.12	20.15
48-7	44.25		9.96		44.36		9.58		55.36		9.9		22.14	11.54

often choose one of these solutions as the final implementation plan without any preference. In this article, EMU will be used to determine the solution of interest, and the selected solution will be compared with the solution generated by the greedy strategy, and the practical application of DCDG-MOMA will be analyzed. As shown in Figure 10, for the two use cases 14-7 and 28-7, 25 independent runs, the IH is the median solution using EMU.

As shown in Figure 10, the target value (mass, OIC) corresponding to the selected solution and the target value corresponding to the three solutions generated by the greedy strategy are displayed. According to these target values, the solution obtained by DCDG-MOMA is much better than the solution generated by the greedy random method, especially in the 28-7 example, which further shows that DCDG-MOMA does play a role in the actual decision-making process.

4. Discussion

By using a number of comments in the above survey of online reviews, we discuss the key factors influencing changes in consumer experience a sense of online reviews. I am here with two complete description of direct review. The research results show that the information intensity of online reviews has a very important impact on consumers' receiving experience. Specifically, they are less affected by online reviews. In terms of experience changes, they have a higher probability of receiving review information, but a lower probability of accepting the information. This has

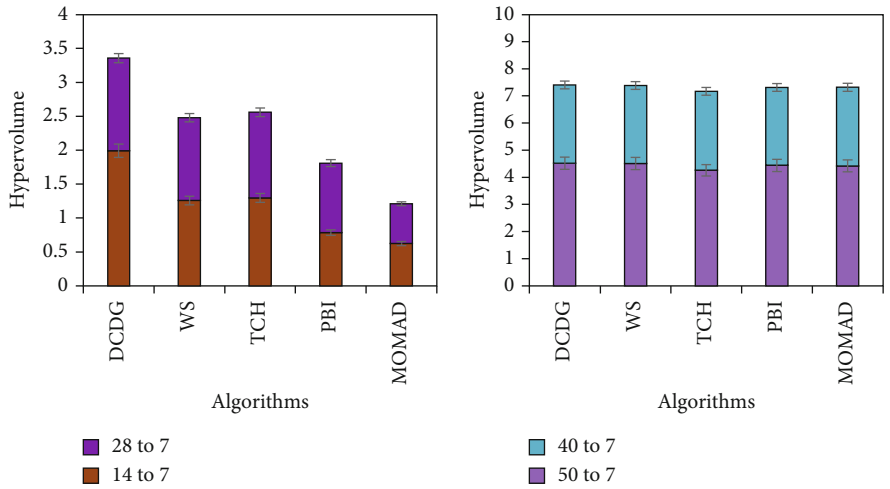

Figure 8: DCDG-MOMA, MOEA/D-LS, and MOMAD overvolume index results of 20 runs on all test cases.

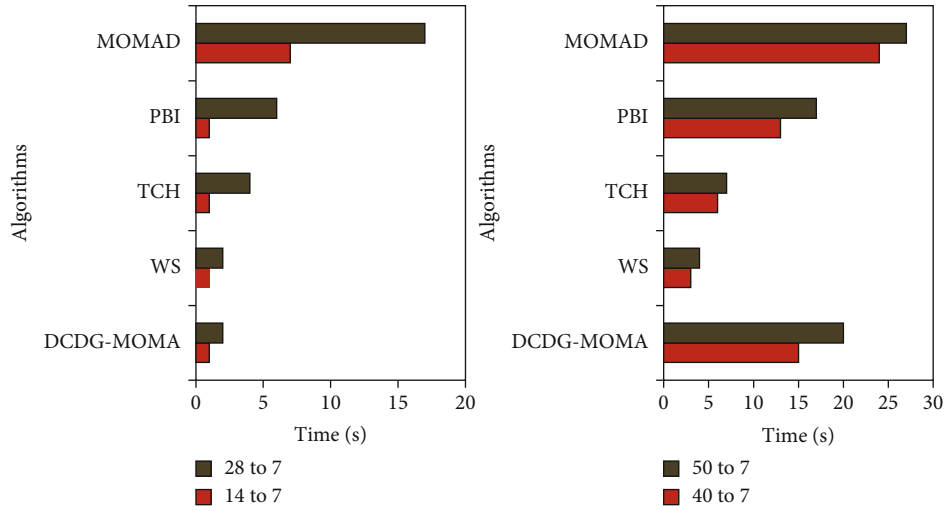

Figure 9: Running time of DCDG-MOMA, MOEA/D-LS, and MOMAD on different test cases.

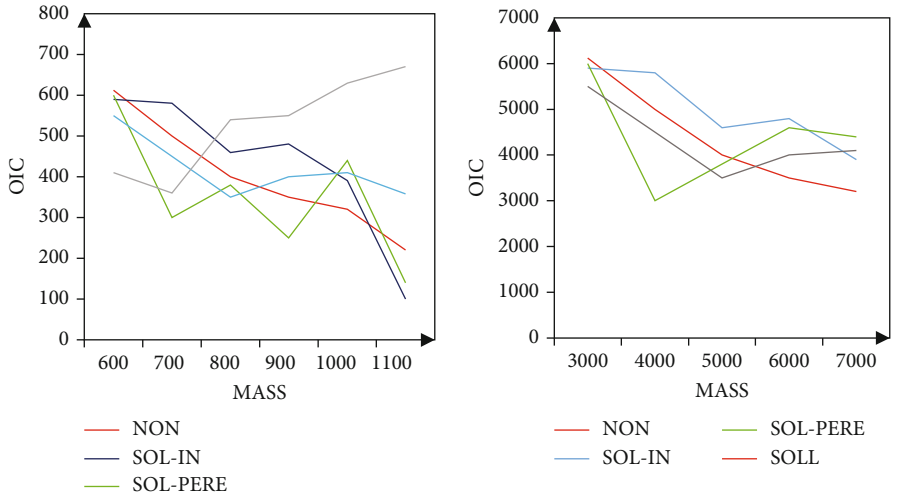

Figure 10: Diagram of the solution obtained by EMUr.

similar conclusions to the previous study by Park et al. It can be seen that consumers are more inclined to use marginal information processing methods to process review information, that is, to grasp the key points of review information and make decisions quickly. It can be seen from the research results of this article that the number of online reviews is an important factor influencing consumer decision-making. At the same time, previous studies have found that consumers are more likely to form a corresponding impression of the product in the early stage and are basically no longer affected by online reviews in the later stage. The research results of this article found that individual consumers are more likely to receive relevant information but are basically unaffected during the acceptance stage, which further reflects the independence of their comments.

First of all, in view of the impact of online reviews on consumer attitudes, companies should take measures to vigorously promote the increase in the number of reviews, because a product with a large number of reviews will increase consumers' acceptance of review information, prompting them to pay more attention to the product. Only when the product attracts the attention of consumers can it further encourage consumers to have certain existing tendencies and encourage them to further accept the product. Second, enhance the guiding nature of online reviews. Consumers who use the new algorithm have a higher probability of receiving and accepting review information, which enhances the guidance of reviews, while presenting products, such as under the product picture, some product praises are displayed, so that consumers can closely compare reviews and products. Combining them will further deepen consumers' impression of the product and increase their likelihood of accepting the product.

5. Conclusions

With the rise of e-commerce, online communities, etc., online reviews have become an important area for academics and companies to discuss consumer behavior. This article uses a variety of scientific methods, such as parameter comparison method, data fusion method, and algorithm optimization method; the purpose is to collect data and design a reasonable algorithm model. The algorithm proposed in this paper has good efficiency and ability to serve consumers. The shortcomings of this article are as follows: first, the algorithm has excellent performance in solving two goals, but as the number of goals increases, the effectiveness of the solution selection part will be weakened even when the three goals are reached. Secondly, this algorithm works well in relatively regular network scenarios, but it is not obvious in other irregular scenarios, with insufficient generalization ability and insufficient flexibility. Therefore, in the next step of research, we need to increase the algorithm's segment points to make the algorithm more universal, to accept a wider range of goals, and to enhance its stability, and its efficiency will not change with environmental changes. In the end, realizing the algorithm model proposed in this paper can have wider applications.

Data Availability

The data that support the findings of this study are available from the corresponding author upon reasonable request.

Conflicts of Interest

The authors declared no potential conflicts of interest with respect to the research, authorship, and/or publication of this article.

Acknowledgments

This work was supported by the National Social Science Foundation of China (16BGL089).

References

[1] P. Jain and A. S. Vaidya, "Analysis of social media based on terrorism — a review," *Vietnam Journal of Computer Science*, vol. 8, no. 1, pp. 1–21, 2020.

[2] J. Lee and I. B. Hong, "The influence of situational constraints on consumers' evaluation and use of online reviews: a heuristic-systematic model perspective," *Journal of Theoretical and Applied Electronic Commerce Research*, vol. 16, no. 5, pp. 1517–1536, 2021.

[3] D. Balakrishnan, A. B. Haney, and J. Meuer, "What a MES(s)! A bibliometric analysis of the evolution of research on multi-energy systems," *Electrical Engineering*, vol. 98, no. 4, pp. 1–6, 2016.

[4] Z. Park, C. Gnoli, and D. P. Morelli, "The second edition of the integrative levels classification: evolution of a KOS," *Journal of Data and Information Science*, vol. 5, no. 1, pp. 39–50, 2020.

[5] C. Arora, "Digital business leadership: digital transformation, business model innovation, agile organization, change management," *Computing Reviews*, vol. 60, no. 4, pp. 162–162, 2019.

[6] Brill, "Austrian review of international and European law," *Austrian Review of International & European Law Online*, vol. 1, no. 1, pp. 121–143, 2016.

[7] J. Meza, H. Espitia, C. Montenegro, and R. G. Crespo, "Statistical analysis of a multi-objective optimization algorithm based on a model of particles with vorticity behavior," *Soft Computing*, vol. 20, no. 9, pp. 3521–3536, 2016.

[8] S. Otto, "Religion in science fiction: the evolution of an idea and the extinction of a genre, Steven Hrotic, Bloomsbury, 2014 (ISBN 978-1-4725-3355-5), ix + 225 pp., hb £65," *Reviews in Religion & Theology*, vol. 23, no. 3, pp. 323–326, 2016.

[9] M. Zhou, Y. X. Long, W. P. Zhang et al., "Adaptive genetic algorithm-aided neural network with channel state information tensor decomposition for indoor localization," *IEEE Transactions on Evolutionary Computation*, vol. 25, 2021.

[10] H. Kaneko, Y. Otsuka, Y. Kubota, and G. Wakabayashi, "Evolution and revolution of laparoscopic liver resection in Japan," *Annals of Gastroenterological Surgery*, vol. 1, no. 1, pp. 33–43, 2017.

[11] G. C. Nunez-Mir, B. V. Iannone III, B. C. Pijanowski, N. Kong, and S. Fei, "Automated content analysis: addressing the big literature challenge in ecology and evolution," *Methods in Ecology & Evolution*, vol. 7, no. 11, pp. 1262–1272, 2016.

[12] D. Guido, H. B. Song, and S. Anke, *Big Data Analytics for Cyber-Physical Systems: Machine Learning for the Internet of Things*, Elsevier, 2019.

[13] B. T. P. Chern and F. B. S. Ahmad, "Supply chain evolution. A study of opportunities and challenges of virtual kitchens in Malaysia," *Journal of Critical Reviews*, vol. 7, no. 16, pp. 361–368, 2020.

[14] F. Vigneron and P. V. Ca, "Evolution in the chemical making of gold oxidation catalysts," *ChemInform*, vol. 47, no. 19, pp. 192–198, 2016.

[15] M. Zhou, Y. M. Wang, Z. S. Tian, Y. H. Lian, Y. Wang, and B. Wang, "Calibrated data simplification for energy-efficient location sensing in internet of things," *IEEE Internet of Things Journal*, vol. 6, no. 4, pp. 6125–6133, 2019.

[16] D. C. Adams and M. L. Collyer, "Phylogenetic comparative methods and the evolution of multivariate phenotypes," *Annual Review of Ecology Evolution and Systematics*, vol. 50, no. 1, pp. 1–21, 2019.

[17] S. K. Kamalakarababu, A. Sam, and S. Varghese, "Clinical profile and short-term outcome of acute nephritic syndrome in children," *Journal of Evolution of Medical and Dental Sciences*, vol. 6, no. 88, pp. 6157–6160, 2017.

[18] Y. Hu, C. Hu, S. Fu et al., "Survey on popularity evolution analysis and prediction," *Journal of Electronics & Information Technology*, vol. 39, no. 4, pp. 805–816, 2017.

[19] H. Fan, H. Zhan, S. Cheng, and B. Mi, "Research and application of multi-objective particle swarm optimization algorithm based on α-stable distribution," *Xibei Gongye Daxue Xuebao/-Journal of Northwestern Polytechnical University*, vol. 37, no. 2, pp. 232–241, 2019.

[20] Q. Zhou, C. Zhang, S. X. Zhao, and B. Chen, "Measuring book impact based on the multi-granularity online review mining," *Scientometrics*, vol. 107, no. 3, pp. 1435–1455, 2016.

[21] Y. Guo, P. Yan, D. Wu, H. Zhou, Y. Shi, and R. Yi, "Analysis method for factors influencing gear hobbing quality based on density peak clustering and improved multi-objective differential evolution algorithm," *International Journal of Computer Integrated Manufacturing*, vol. 34, no. 4, pp. 1–22, 2021.

[22] Y. Hou, H. G. Han, and J. Qiao, "Adaptive multi-objective differential evolution algorithm based on the dynamic parameters adjustment," *Control and Decision*, vol. 32, no. 11, pp. 1985–1990, 2017.

[23] M. Zhou, Y. X. Lin, N. Zhao, Q. Jiang, X. L. Yang, and Z. S. Tian, "Indoor WLAN intelligent target intrusion sensing using ray-aided generative adversarial network," *IEEE Transactions on Emerging Topics in Computational Intelligence*, vol. 4, no. 1, pp. 61–73, 2020.

[24] L. N. Deng and X. F. Yao, "Research on the fusion algorithm of infrared and visible images based on non-subsampled shearlet transform," *Tien Tzu Hsueh Pao/Acta Electronica Sinica*, vol. 45, no. 12, pp. 2965–2970, 2017.

[25] Z. Hao, Z. Lou, and Y. Fan, "Study on the evolution mechanism of subsurface defects in nickel-based single crystal alloy during atomic and close-to-atomic scale cutting," *Journal of Manufacturing Processes*, vol. 68, no. 3, pp. 14–33, 2021.

[26] H. Xie, "Research and case analysis of apriori algorithm based on mining frequent item-sets," *Open Journal of Social Sciences*, vol. 9, no. 4, pp. 458–468, 2021.

[27] X. Xu, D. Cui, Y. Li, and Y. Xiao, "Research on ship trajectory extraction based on multi-attribute DBSCAN optimisation algorithm," *Polish Maritime Research*, vol. 28, no. 1, pp. 136–148, 2021.

[28] C. You, Q. Li, W. Li, and B. Xu, "Research on healthy evolution and driving mechanism of cultivated land utilization system in Chongqing based on PSR-TOPSIS model," *Advance in Agriculture Science*, vol. 2, no. 4, pp. 149–165, 2020.

[29] H. Jia, Z. Wei, X. He, and M. Li, "A research on lane marking detection algorithm based on neural network and least squares method," *Qiche Gongcheng/Automotive Engineering*, vol. 40, no. 3, pp. 363–368, 2018.

Hindawi
Journal of Sensors
Volume 2021, Article ID 9330438, 9 pages
https://doi.org/10.1155/2021/9330438

Research Article

Sports Event Level Measurement Indicator System Using Multisensor Information Fusion

Weiwei Yu[1,2] **and Jinming Xing**[3]

[1]*School of Economics and Management, Dalian University of Technology, Dalian 116024, China*
[2]*Suan Sunan Rajabhat University, Bangkok 10300, Thailand*
[3]*School of Physical Education, Northeast Normal University, Changchun 130024, China*

Correspondence should be addressed to Jinming Xing; xingjm100@nenu.edu.cn

Received 11 August 2021; Revised 21 September 2021; Accepted 13 October 2021; Published 1 November 2021

Academic Editor: Mu Zhou

In view of the imperfection of the measurement index of the level of sports events, the coverage rate of the measurement index is low and the stability is poor. Therefore, this paper puts forward a sports event level measurement index system based on multisensor information fusion. First, the simulated annealing algorithm is used to cluster the grouped sensors and fuse the optimal Bayesian estimation of compatible sensors. Second, the relative entropy measure method is used to expand the compatibility measure of the sensor information in the group, and the optimal Bayesian estimation value of the consistent measure test is obtained. The outliers are eliminated, the optimal fusion value is obtained by the overall weighted statistical fusion, and the alternative measure index system is constructed. Finally, analytic hierarchy process (AHP) is used to calculate the weight of each alternative index, so as to achieve the final measurement index. The results show that the standard deviation of clustering average energy consumption is low, and the energy loss is small. The system can effectively construct the measurement index, and the index coverage rate is as high as 95%.

1. Introduction

Sporting Event is a hotspot in physical education and sports policy researches. Sporting Event promotes the development of physical education [1]. As a major part of the school work, it represents the progress of a school's physical education [2]. Development of Sporting Event Promoting School National Fitness Movement can improve students' understanding and quantity of sports skills. Also, it helps to create an excellent product of the integrity of the collective honor. Therefore, it has good teaching significance. At present, the Sporting Event level measurement indicators have a small scope of application, and there is a certain defect in terms of indicator coverage. Sporting Event itself has a strong linkage effect [3]. Therefore, Sporting Event can not only bring a lot of people and promote direct consumption but also lead the development of sports industry, thus, promoting the development of other industries. On this basis, the collaborative development of regional Sporting Event is bound to lead the development of regional sports industry and the development of regional economy.

The establishment of any index system must first have a basic framework on which specific indicators depend. This basic framework is actually an interpretation system corresponding to specific objects, also known as theoretical framework or theoretical model. According to the existing research results, the general evaluation index system models include "structure function" model, "input-output" model, and "condition result" model. The basic framework is the soul of the index system. Without the base wood framework, it cannot be called "system." The design of the basic theoretical framework of the index system is the most critical link in the construction of the index system. For sports modernization, the sports modernization index system should not only reflect the comprehensiveness of the sports system structure but also reflect the basic characteristics of modern sports development and the three basic cognitive representations of modernization. Therefore, it is difficult to reflect the face

of sports modernization according to a specific model. It can be seen that the synergy of Beijing-Tianjin-Hebei Sporting Event has an important impact on the development of the Beijing-Tianjin-Hebei Sports industry and the development of Beijing-Tianjin. Most of the risk management research in various fields has explored the risk indicator system varying degrees. However, there are very few literatures built in detail the risk identification and risk indicator system for two work sections. Obviously, the result of this is more conducive to the study of the context, which facilitates follow-up theoretical analysis. The risk factors that trust problems in Sporting Event will be initially identified by real-world research, consulting related experts, checking literature, and historical information. Then, according to the Sporting Event, trust risk is from the event participation in the main body itself, the event system, the event system, the overall operation environment, etc.; this paper is initially recognized in the trust risk of Sporting Event. Then, according to the trust risk of sports events, this paper preliminarily identifies the trust risk of sports events from the aspects of the event participants themselves, the event system, the event system, and the overall operation environment of the event.

In this regard, this paper proposes a study of Sporting Event level measurement indicators based on multisensor information fusion. Its innovation is to calculate the weight of each alternative indicator by hierarchical analysis and determine the final measurement index. The best fusion output value is obtained using the Bayesian estimation method. The multisensor fusion method is used to fuse the multiangle information. Compared with the information collected by the single sensor, the Sporting Event level measurement index system based on multisensor information fuses is studied, and more comprehensive measurement indicators are constructed.

(1) This paper proposes a research on the Sporting Event level measurement indicator system based on multisensor information fusion. The optimal Bayesian methods estimate with compatibility sensors is fused by simulating an annex algorithm clustering group sensor

(2) The weight of each alternative indicator is calculated by hierarchical analysis, and the final measurement indicator is determined. By calculating the score of the optional indicator, the range of values is obtained

(3) The priority distribution is obtained by utilizing great likelihood estimation, and the best fusion output value is obtained by using the Bayesian estimation method. Finally, the experimental results of different data sets show the effectiveness of the methods of this paper

2. Related Work

Literature [4] proposes a large span spatial structure stress recognition method based on multitype sensor information fusion. It is proposed to solve the acquisition method of large span spatial structural stress distribution and reduce the number of strain sensors in the strain sensor by using the measured information and information fusion methods of multiple types of sensors. But the method is not so stable. Literature [5] method proposes a new DEMS method to solve data loss problems in the mobile sensor network. DEMS method uses a virtual static sensor to solve the problem of sensitive sensor packets. At the same time, the mobile sensor network is also solved, and when the sensor position changes, the problem is lacking or loses history. However, the method has incomplete index. Literature [6] proposed a hierarchical weight decision analysis method. In the case where the indicator is initially determined, a hierarchical analysis method is used to assign the weight of each indicator. Finally, through the method of seeking a geometric average, the relative weights of each indicator in the modernization index system of the capital are obtained. However, the energy loss of this method is large. The literature [7] method proposes the theoretical model of public service of large sports venues and obtains the required data of the verification model through the questionnaire survey method. In addition, the structural equation model is used to verify the previously proposed influencing factors. Finally, based on the influencing factors, the propulsion strategy of the public service of large sports venues is proposed, but the prediction accuracy of this method is low. Literature [8] proposes a method of solving a sequential parameter based on gray correlation degree and attribute. The gray correlation between the state parameters and decision variables is used as a reference and basis for judging state parameters. Through the calculation of gray correlation, the preliminary screening of state parameters can be performed, the state parameters with high correlation with the decision parameters are sequentially parameters, and the professional sports club value chain system synergies are further evaluated in sequence parameters. However, the horizontal measurement error of this method is large.

Therefore, this paper proposes a research on sports event level measurement index system based on multisensor information fusion. The weight of each alternative index is calculated by analytic hierarchy process to determine the final measurement index. The risk function is obtained by constructing the risk function. Through the largest consistent sensor group, the largest associated group sensor is obtained, the total fusion group information is combed, and the total fusion output is obtained.

3. Multisensor Information Fusion Method

The Sporting Event Horizontal Measurement indicator System Based on Multisensor Information Fusion mainly includes information fusion. This paper establishes measurable indicator system and identifies metric weights and determinations [9]. Further, the Sporting Event information collected by the sensor is fused by multisensor information fusion method. The Sporting Event Horizontal Preparation Surveying Indicator System is constructed according to this information; the weight of each alternative indicator is calculated by hierarchical analysis, and the final measurement indicator is determined.

3.1. Multisensor Clustering Group Based on Simulation Annealing Algorithm. Simulation Annealing Algorithm has the advantages of failing with the overall optimal solution relative to other intelligent algorithms in solving problems and can find global optimal solutions. Therefore, this article details the mathematical model of Simulation Annealing Algorithm and its optimistic method [10]. This proves Simulation Annealing Algorithm to find the global optimal solution. Further, this paper uses analog degenerative algorithm to deploy a polymerization grouping group, and the specific steps are as follows:

Step 1. Select the lead node.

Step 2. Start the external cycle, broadcast the Hello message in the sensor network. An additional cluster is selected according to the node other than the receiving signal, and each node can only select one cluster. Set the initial cluster as $H_0(H_1, H_2, \cdots, H_N)$. When it is an initial solution, set the initial temperature T_0, and the iteration times k of each T.

Step 3. Start the internal cycle, order the current granary α $H_\alpha = H_0$, the current temperature $T_\alpha = T_0$.

Step 4. Select several nodes to readd clustering, formation of βH_β. Get the solution of H_α and H_β, and then get $\Delta h = h(H_\beta) - h(H_\alpha)$. If $h \le 0$, then $H_\alpha = H_\beta$. Conversely, in accordance with Monte Carlo accept criteria storage H_α. According to this guideline, the transfer probability definitions H_α and H_β are

$$Q\left(H_\alpha \longrightarrow H_\beta\right) = \Delta h \le 0, \tag{1}$$

where Δh is the measure function of sports event level.

Step 5. When the number of iterations is greater than or equal to t, terminate the inner loop [11–13]. When T_α decreases, it is necessary to determine whether the external circulation is terminated. If not, return to step 3 and continue the internal circulation.

Step 6. If the outer loop condition is met, terminate the algorithm and obtain the approximate optimal clustering group H_α.

3.2. Multisensor Information Fusion Based on Optimal Bayesian Estimation. After clustering and grouping, the relative entropy measurement method is used to expand the compatibility measure of the sensor information in the group to accurately present the compatibility between sensors [14, 15]. All information needs to be standardized between the compatibility measures. Assuming that the number of sensors in a group is m, if the length of each sensor data sequence is n, the information processing formula is as follows:

$$y'_{ij} = \left|\frac{y_{ij} - \bar{y}_i}{\delta_i}\right|, i = 1, \tag{2}$$

where expectation is $\bar{y}_i$; the variance is δ_i; the original information is y_{ij}. Standardized information is y'_{ij}. After arranging y'_{ij} from large to small, the compatibility between sensors is measured by relative entropy measure, so that the relative information of i and j is as follows:

$$E_{ij} = \left|\sum_{k=1}^{n}\left[1 - \frac{y_{ij}}{\sum_{k=1}^{n}\bar{y}_i}\right]\right| = 1, 2, \cdots, m, \tag{3}$$

where E_{ij} represents the data fusion coefficient. m represents the network node of the sensor, $E_{ij} \ne E_{ji}$. E_{ji} is the relative compatibility between sensors. The formula for accurately depicting the compatibility of the sensor is as follows:

$$\rho_{ij} = \frac{\min\left(E_{ij}, E_{ji}\right)}{\max\left(E_{ij}, E_{ji}\right)}, i, j = 1, 2, \cdots, m, \tag{4}$$

where in the case of $\rho_{ij} = 0$, it means that i and j are incompatible, that is, there is a contradiction between information and information fusion cannot be carried out.

When $\rho_{ij} = 1$, it means that i and j are compatible, that is, there is redundant information and information fusion can be carried out.

In the case of $0 < \rho_{ij} < 1$, it represents that i and j are partially compatible, that is, the information is complementary, and it needs to be analyzed to judge whether they can be fused [16].

The compatibility measure matrix is $R_c = \lfloor c_{ij} \rfloor$ and the compatibility degree is c_{ij}.

After $\varepsilon_c (0 < \varepsilon_c < 1)$ determines c_{ij}, follow the Zodiac Normal Statistical Strategy, shaping the consistent measurement operator as follows

$$c_{ij} = \begin{cases} 1, \text{if} \rho_{ij} \ge \varepsilon_c, \\ 0, \text{if} \rho_{ij} < \varepsilon_c. \end{cases} \tag{5}$$

where c_{ij} indicates compatibility ε_c represents the information fusion output value of the sensor. After completing the compatibility measure, the prior distribution is obtained by maximum likelihood estimation, and then the best fusion output value is obtained by the Bayesian estimation method [17]. The sensor model is represented by Gaussian distribution. Assuming that the number of sensors is L, the model of sensor i is

$$P_i(x) = c_{ij}\left(-\frac{1}{2}\left(\frac{y - \bar{y}_i}{\delta_i}\right)\right), i = 1, 2, \cdots, j, \tag{6}$$

where $P_i(x)$ represents the characteristic quantity δ_i indicates system suitability. Use the model of formula (6) to fuse information. The formula is as follows:

$$p(\theta|y_1, y_2, \cdots, y_L) = \prod_{i=1}^{N_L}[p(\theta|y_i)] = \frac{\prod_{i=1}^{N_L}[p(y_i|\theta)\cdot p(\theta)]}{\int p(|y_1, y_2, \cdots, y_L|\theta)\cdot p(\theta)}, \tag{7}$$

where the optimal fusion output is θ; according to Bayesian estimation theory, the optimal estimation value is $\widehat{\theta} = \int_{\Theta}\theta \cdot p(\theta|y_1, y_2, \cdots, y_L)$. The value parameter space of θ is Θ. According to the theory of maximum likelihood estimation, we know the distribution of θ is $N(u_0, \delta_0^2)$.

$$u_0 = \frac{\sum_{i=1}^{L}\left(1/\delta_i^2 \cdot \bar{y}_i\right)}{\sum_{i=1}^{L}\left(1/\delta_i^2\right)}. \tag{8}$$

$$\delta_0^2 = \frac{1}{N}\sum_{i=1}^{L}\left[\frac{1}{\delta_i^2}\right]. \tag{9}$$

Build a risk function to get $\widehat{\theta}$, and the risk function is as follows:

$$\lambda\left(\theta, \widehat{\theta}\right) = (\theta - \theta\wedge)^2 = \left(\theta - \int_{\Theta}\theta \cdot p(\theta|y_1, y_2, \cdots, y_L)\right)^2. \tag{10}$$

Let $\partial e(\theta)/\partial\theta|_{\theta=\widehat{\theta}} = 0$. To calculate $\widehat{\theta}$, the formula is as follows:

$$\widehat{\theta} = \frac{b + \sqrt{b^2 + 4a}}{2a}, \tag{11}$$

where b is parameter model of cluster sensor, and a is the combination parameters of cluster sensors. This method is used to process the N group sensor to obtain the best Bayesian estimation of each group of sensors $\widehat{y}_i$, $i = 1, 2, \cdots, N$ [18].

3.3. Multisensor Distribution Integration Based on Uniform Measurement. After the clustering processing sensor, each set of sensor information has dispersion. Before the information is integrated, it is necessary to conduct a consistency measurement, and the fusion output value of the N group sensor is $\widehat{y}_i$, the variance is $\widehat{\delta}_i^2$. Follow the Zodiac Normal Statistical Strategy, shaping the consistent measurement operator as follows:

$$d_{ij}\begin{cases} 1 - \dfrac{\left|\widehat{y}_i - \widehat{y}_j\right|}{3\widehat{\delta}_i}, & \text{if} \quad \widehat{y}_i \neq \widehat{y}_j, \text{ and } \left|\widehat{y}_i - \widehat{y}_j\right| < 3\widehat{\delta}_i, \\ 1 - \dfrac{\left|\widehat{\delta}_i - \widehat{\delta}_j\right|}{3\widehat{\delta}_i}, & \text{if} \quad \widehat{y}_i = \widehat{y}_j, \quad \text{and} \quad \left|\widehat{y}_i - \widehat{y}_j\right| < 3\widehat{\delta}_i, \\ 0, & \text{else.} \end{cases} \tag{12}$$

Depict the support of i to j via d_{ij}. $d_{ij} = 1$ means that the measured value of i and j is basically the same, and i strongly supports j [11, 19]; $d_{ij} \neq 0$ means the support of i to j is weak. At the same time, the variance is inversely proportional [20]; $d_{ij} = 0$ means i and j have no consistent measurement. According to d_{ij}, calculate the corresponding uniform association array $R_r = [\tau_{ij}]$, and the consistent correlation is τ_{ij}.

$$\tau_{ij} = \begin{cases} 1, \text{if} d_{ij} \geq \varepsilon_c. \\ 0, \text{if} d_{ij} < \varepsilon_c. \end{cases} \tag{13}$$

where d_{ij} represents characteristic parameter. The maximum consistent sensor group is obtained by R_r, which makes the maximum number of associated group sensors are $l(0 < l < N)$. Integrate this group of information [21, 22], get the total fusion output $\widehat{X}$.

The integration steps are as follows:

Step 1. Cluster sensor, get N group sensor. $\bar{s} = \{\bar{s}_i | i = 1, 2, \cdots, N; 1 \leq N \leq M\}$.

Step 2. Compatibility measurement test N group sensor, go to the wild point [23, 24], combine the optimal Bayesian estimate $\widehat{y}_i$.

Step 3. The overall consistent measurement test of $\widehat{y}_i$ will continue to go to the wild point, and the overall weighted statistical fusion acquisition is the optimal fusion value $\widehat{y}$.

Step 4. Get an optional measurement indicator system via $\widehat{y}$.

3.4. Determine the Measurement Indicators. The hierarchical analysis is used to calculate the weight of the measurement indicator. Determine the final measurement indicator system according to the size of the score [25, 26]. Shaping judgment matrix for subsequent indicator of the same superior indicators q_{uv}, make the number of options ς, normalize items in q_{uv}

$$\underline{q}_{uv} = \frac{q_{uv}}{\sum_1^{\varsigma} q_{uv}}, u, v = 1, 2, \cdots, a. \tag{14}$$

To process $\underline{q}_{uv}$ in a row-addition manner, the formula is as follows:

$$\underline{W}_u = \sum_1^{\varsigma}\underline{q}_{uv}. \tag{15}$$

Normalization vector $\underline{W} = (\underline{W}_1, \underline{W}_2, \cdots, \underline{W}_{\varsigma})^t$, get the weight of the lower-level indicator of the lower-level indicator:

$$W_u = \frac{\underline{W}_u}{\sum_1^{\varsigma}\underline{W}_v}. \tag{16}$$

W_v is the basis. By calculating the score of the optional indicator, the score of the score is [0, 1], according to the score of alternative indicators [27–29], select the first 15 score to be

high as the final measurement indicator. The specific structure is shown in Figure 1.

4. Experimental Analysis and Results

4.1. Experimental Environment and Data Set. This experiment uses two disclosed data sets for testing, sparse marking data set (1FPs) represented by AVA. Due to the sparse labeling, there is no clear action boundary, and the existing methods are more like an initiation level action identification, weakened timing positioning; at the same time, the operating category is daily atomic action, slow motion, small shape, low tracking difficulty, classification does not require complex people, and the model and environment modeling and reasoning. Densely labeled data set (25FPS) is represented by JHMDB. This type of data set has only one action for each video. Most of the video is that single people are doing some semantic simple repetitive actions, and the action category is related to the background height. The data set used in this paper contains 150 sequences with a resolution of 720×480. This data set represents the natural action pool in various scenes and viewpoints. By publishing data sets, we hope to encourage further research on this kind of sports action recognition in an unconstrained environment. It is shown in Table 1.

4.2. Experimental Indicators

(1) *Clustering Average Load Criteria.* The higher the standard, the higher the stability, based on the clustering average load criteria under several different methods, the stronger the stability

(2) *Energy Loss.* According to the comparison of the relationship between the monitoring area and the number of rounds (the first node death), the lowest number of times is small

$$p = W_u \leq \left(x_L^i - x_S^i\right), \tag{17}$$

where x_L^i represents the detection area, and x_S^i represents the number of rounds.

(3) *Measurement Indicator Coverage.* According to the measurement indicator coverage rate under several different methods, the higher the coverage, the more accurate the prediction accuracy

(4) *Measurement Indicator Error Rate.* According to the measurement indicator error rate under several different methods, the lower the error rate, the lower prediction effect is stronger

$$\bar{x} = p - (X_n, Y_{n-\tau}), \tag{18}$$

where X_n is the coupling coefficient of the measurement error index. $Y_{n-\tau}$ is the sequence function of measuring error index.

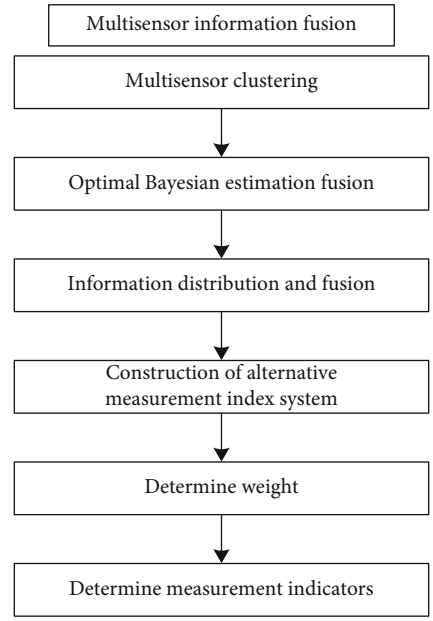

Figure 1: Structure diagram of sports event level measurement index system.

(5) *Data Transmission Security.* According to data transmission security under several different methods, the higher the security, the better the practicality

4.3. Results and Discussion. Taking a body school as an experimental object, the system of this paper is established to establish a measure indicator for the school Sporting Event level and verify the effectiveness of the system.

To test the relationship between the network extension and cluster average energy consumption standard difference, this paper tests the clustering mean load standard deviation (CMLSD) of six systems in different nodes. It is shown in Figure 2.

According to Figure 2, the number of nodes is increasing, that is, the size of the network increases, the larger the network size, and the six-series CMLSD presents an upward trend. The degree of CMLSD growth in this paper is not obvious, the fluctuation is small, the remaining five systems have a large growth, the fluctuations are large, and the stability is poor. Experiments have shown that the CMLSD is minimal and stable in the cluster of the system herein.

This paper tests the number of wheels that appear in different network monitoring area and checks the performance of 6 systems in the extension of network lifecycle. It is shown in Figure 3.

According to Figure 3, as the monitoring area increases, the number of rounds of the first node of six systems has gradually declined. The number of rounds of the first node death in this paper is significantly lower than the remaining five systems. When the monitoring area reaches $400\,m^2$, the number of wheels in the first node in six systems tends to stabilize, and the number of rounds after the system is significantly lower than the remaining five systems. Experiments prove that the number of rounds of the first node death in

Table 1: Related parameter distribution.

Variable	Mean value	Standard value	Minimum value	Average value
Physical quality	0.135	0.167	0.633	3.644
Behavior feature	0.358	0.546	0.477	2.588
Spatial planning	0.535	0.366	0.435	2.577
Joint statistical analysis value	0.267	0.454	0.155	4.655
Regression analysis value	0.534	0.356	0.143	3.577

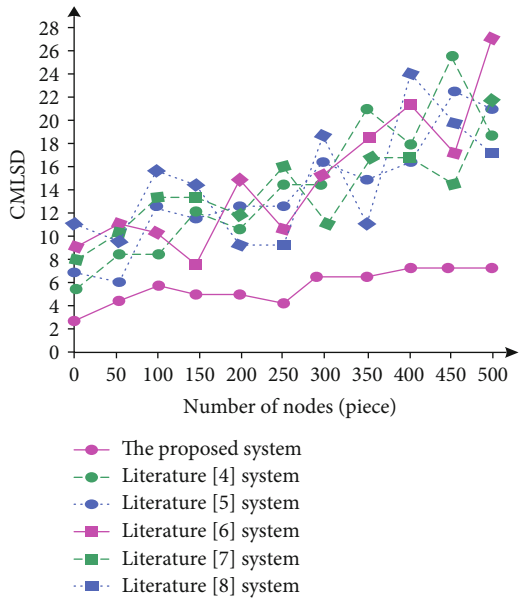

Figure 2: Standard deviation of average load of network nodes and clusters.

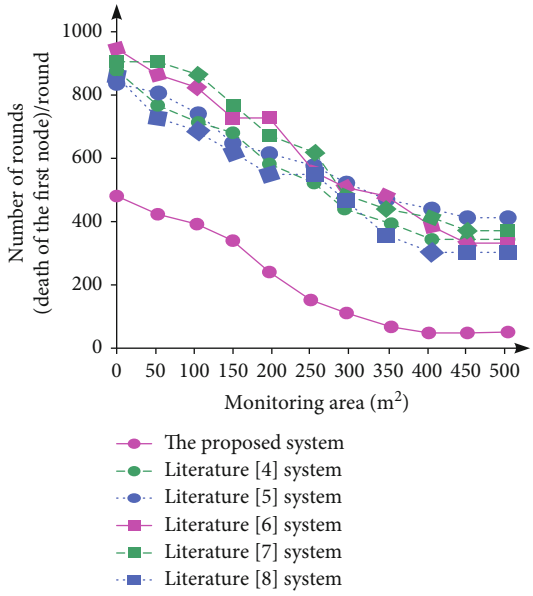

Figure 3: Relationship between monitoring area and number of rounds.

this paper has a minimum, indicating that the energy loss in the cluster is small.

After completing the information cluster, the system of this paper gets the Sporting Event level preparation selection indicator. To continue to use this article to calculate the weight of each preparation measurement indicator and calculate the corresponding indicator score, the first 15 indicators in the order of the score are selected as the final measure indicator, alternative metric weights, and score calculation results. It is shown in Table 2.

According to Table 2, the system in this paper can effectively calculate the weight of the optional measurement indicator and solve the score of each indicator. According to the score from large to small sort score, select the first 15 indicators as the final measurement indicator, in turn is the event insurance, sports slogan and logo, fair competition, funding budget, athlete sports spirit, result statistics and announcements, athletes medical examination, safety and security work, athlete code, staff satisfaction, sports equipment standardization, site facilities, event assessment, event management system, and medical security. Experiments prove that the system of this paper can effectively construct the Sporting Event level measurement indicator.

This paper uses the literature [4] to the literature [8] system to build a Sporting Event horizontal measurement indicator for the school and test the coverage of the measurement indicators of six systems, as shown in Figure 4.

According to Figure 4, the index coverage of literature [4] method is 38%, the index coverage of literature [5] method is 59%, the index coverage of literature [6] method is 46%, the index coverage of literature [7] method is 66%, the index coverage of literature [8] method is 49%, and the index coverage of this method is as high as 97%. It can be seen from this that the coverage rate coverage of this system constructed is significantly higher than the remaining five systems. This shows that the indicator of this article covers a broader field, better service, and predictions such as evaluation and prediction. Excellent measure indicators are applied to assessment and forecasting, etc., which can effectively improve the accuracy of the assessment and forecasting of these methods and lay a solid foundation for the promotion of the Sporting Event level.

According to Figure 5, the index error rate of literature [4] method is 9%, the index error rate of literature [5] method is 9.9%, the index error rate of literature [6] method is 11%, the index error rate of literature [7] method is 13%, the index error rate of literature [8] method is 13.9%, and the index error rate of this method is 4%. It can be seen from this that compared with the systems in other five literature,

Table 2: Calculation results of weights and scores of alternative measurement indicators.

Primary indicators (weight)	Secondary indicators (weight)	Tertiary indicators (weight)	Score
Basic conditions of the event (0.43)	Event funds (0.63)	Budget (0.51)	0.91
		Source of funds (0.49)	0.65
	Venue facilities (0.55)	Standardization degree of sports equipment (0.44)	0.84
		Safety of site facilities (0.56)	0.84
	Logistic service (0.45)	Medical security (0.53)	0.81
		Security work (0.47)	0.87
Event organization and management (0.32)	Precompetition preparation stage (0.34)	Composition of organization and operation organization (0.21)	0.80
		Set event scheme (0.24)	0.80
		Event insurance (0.19)	1.00
		Site layout (0.19)	0.80
		Propaganda work (0.17)	0.77
	Event stage (0.32)	Coach, team leader, and referee meeting (0.26)	0.17
		Physical examination of athletes (0.25)	0.87
		Performance statistics and announcement (0.23)	0.89
		Risk prevention (0.26)	0.77
	Event closing stage (0.19)	Event evaluation (0. 51)	0.83
		Event file storage (0.49)	0.75
Sports culture (0.25)	Competition level (0.15)	Number of participants (0.33)	0.78
		Record breaking situation (0.31)	0.23
		Participant satisfaction (0.36)	0.84
	Sports system culture (0.47)	Event management system (0.35)	0.81
		Traditional sports events (0.26)	0.67
		Athlete code (0.25)	0.86
	Sports spiritual culture (0.53)	Sports slogan and logo (0.15)	1.00
		Concept of sports events (0.17)	0.80
		Sports ethics (0.21)	0.75
		Sportsmanship of athletes (0.23)	0.90
		Spirit of fair competition (0.24)	0.92

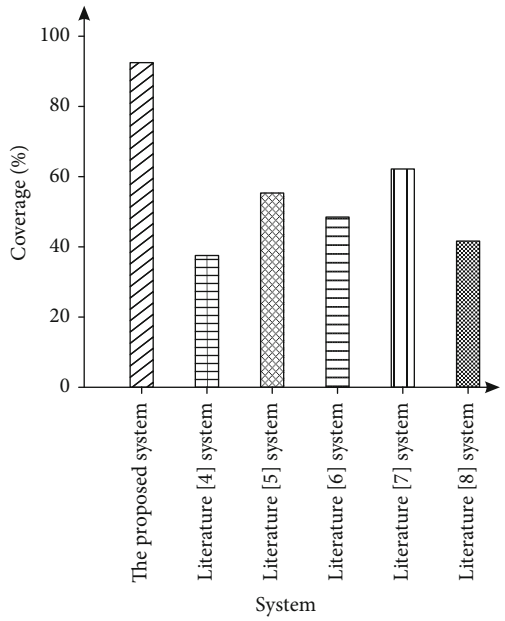

Figure 4: Indicators correlation test results.

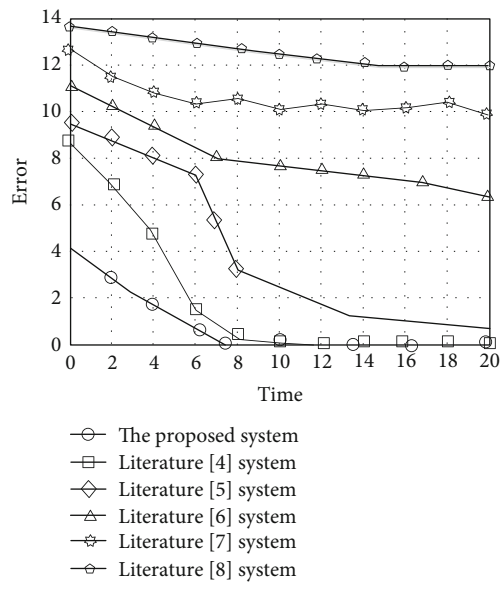

Figure 5: Comparison of measurement index errors.

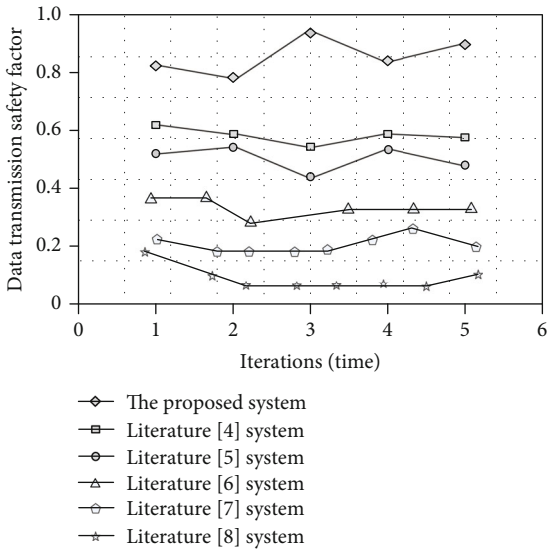

Figure 6: Safety factor of data transmission.

and the Sporting Event measurement indicator error of this paper is lower, indicating that the evaluation prediction of this paper is better and more practical.

According to Figure 6, the transmission safety factor of the method in literature [4] is 0.65%, the transmission safety factor of the method in literature [5] is 0.52%, the transmission safety factor of the method in literature [6] is 0.38%, the transmission safety factor of the method in literature [7] is 0.23%, the transmission safety factor of the method in literature [8] is 0.2%, and the transmission safety factor of the method in this paper is as high as 0.83%. Compared with several other systems, the one in this paper is significantly higher than other systems. It can be seen that the higher the index of using this system to measure the level of sports events, the better the effect of use.

5. Conclusions

The imperfection of the Sporting Event level measurement indicator causes problems such as low-conditioned coverage and poor stability. This paper obtains a priori distribution through maximum likelihood estimation and then uses Bayesian estimation to obtain an optimal fusion output value. In addition, this paper uses a hierarchical analysis to calculate the weight of the measurement indicator. Sports policies have been continuously improved, and all regions have significantly improved the organization of sporting events. To enhance the Sporting Event level, this paper studies the Sporting Event level measurement indicator system based on multisensor fusion and reasonably constructs measurement indicators. This can improve the coverage of the indicator and better serve the evaluation and forecasting methods, providing scientific basis for improving the Sporting Event level.

Data Availability

The data used to support the findings of this study are included within the article. Readers can access the data supporting the conclusions of the study from UCF101-24 and JHMDB data set.

Conflicts of Interest

The authors declare that there is no conflict of interest with any financial organizations regarding the material reported in this manuscript.

Acknowledgments

This work was supported by National Social Science Fund (20FTYB002), Key projects of Jilin Social Science Fund (2020A10), and Social science research project of Jilin Provincial Department of Education (JJKH20211320SK).

References

[1] H. Liang, Y. Yandong, and H. Xue, "Sports event risk early warning model based on BP neural network," *Statistics and decision making*, vol. 34, no. 16, pp. 85–88, 2018.

[2] L. Lu, L. Gang, and H. Haiyan, "Construction and demonstration of evaluation index system for the development of global urban sports industry," *Journal of Shanghai Institute of physical education*, vol. 43, no. 3, pp. 39–45, 2019.

[3] Y. Kim and A. Bruland, "Analysis and evaluation of tunnel contour quality index," *Automation in Construction*, vol. 99, pp. 223–237, 2019.

[4] Q. Yan and Q. Wang, "Construction of smart city development level measurement index system," *Statistics and decision making*, vol. 34, no. 11, pp. 33–36, 2018.

[5] Z. Ghaderi, M. Rajabi, and M. Walker, "Psychic income benefits of small-scale sports events: host community perspectives," *European Sport Management Quarterly*, vol. 3, pp. 1–21, 2021.

[6] L. Jian, "Analysis on the development of sports event communication under the new media environment," *Sports fashion*, vol. 396, no. 12, pp. 218-219, 2020.

[7] M. Yang, H. Junya, and R. Luo, "Evolution path and trend analysis of foreign sports event tourism research," *Journal of Xi'an Institute of physical education*, vol. 37, no. 1, pp. 78–85, 2020.

[8] Q. Tan, B. Jingshan, and C. Chaoyu, "Calibration method of design response spectrum based on simulated annealing algorithm," *Earthquake Engineering and Engineering Vibration*, vol. 40, no. 1, pp. 158–164, 2020.

[9] Z. Youhao and Y. Zheng, "Multisensor information fusion technology based on projection pursuit simulated annealing," *Sensor technology and application*, vol. 8, no. 2, p. 12, 2020.

[10] B. Pueo, J. J. Lopez, and J. M. Jimenez-Olmedo, "Audio-based system for automatic measurement of jump height in sports science," *Sensors*, vol. 19, no. 11, p. 2543, 2019.

[11] B. A. Ahmed, "The relation of the motive sport achievement and self-confidence with the level of achievement of throwing events in athletics," *International Journal of Psychosocial Rehabilitation*, vol. 24, no. 4, pp. 6919–6931, 2020.

[12] T. Eski, "Examining winter sports awareness level of university students receiving sports education," *Cypriot Journal of Educational Sciences*, vol. 14, no. 4, pp. 630–640, 2019.

[13] M. Moital, A. Bain, and H. Thomas, "Summary of cognitive, affective, and behavioural outcomes of consuming prestigious

sports events," *Sport Management Review*, vol. 22, no. 5, pp. 652–666, 2019.

[14] K. H. Lee, J. S. Lee, B. C. Lee, and E. H. Cho, "Relative weights of physical strength factors in sports events: focused on similarity sports events group according to the sports physiological view," *Applied Sciences*, vol. 10, no. 24, p. 9131, 2020.

[15] M. Gunduz and H. Laitinen, "Observation based safety performance indexing method for construction industry - validation with SMEs," *KSCE Journal of Civil Engineering*, vol. 22, no. 2, pp. 440–446, 2018.

[16] R. Socha and B. Winiewski, "Safety of mass sports events," *ASEJ Scientific Journal of Bielsko-Biala School of Finance and Law*, vol. 23, no. 1, pp. 42–44, 2019.

[17] M. Wunderlich, "Innovative approaches in sports science-lexicon-based sentiment analysis as a tool to analyze sports-related twitter communication," *Applied Sciences*, vol. 10, no. 2, p. 431, 2020.

[18] W. H. Finch and B. F. French, "A simulation investigation of the performance of invariance assessment using equivalence testing procedures," *Structural Equation Modeling*, vol. 25, no. 5-6, pp. 673–686, 2018.

[19] A. V. Iglin, "International legal basis of using sports for development and peace," *Moscow Journal of International Law*, vol. 2, pp. 102–109, 2020.

[20] A. Yefanov, "Politicization of sports through media: syncretism of social institutions," *Theoretical and Practical Issues of Journalism*, vol. 10, no. 1, pp. 130–140, 2021.

[21] C. O. Sereati, A. Sumari, T. Adiono, and A. S. Ahmad, "Architecture design for a multi-sensor information fusion processor," *TELKOMNIKA Indonesian Journal of Electrical Engineering*, vol. 17, no. 1, pp. 362–369, 2019.

[22] L. Demyanova, I. Usova, A. Tashchiyan, N. Ryzhkin, and S. Demyanov, "Role of sports tourism in the school children health improvement," *InE3S Web of Conferences*, vol. 273, p. 09037, 2021.

[23] R. Nagovitsyn, A. Osipov, M. Kudryavtsev, O. Antamoshkin, and L. Glinchikova, "The increase of physical activity in persons using sports grounds for physical training," *Human Sport Medicine*, vol. 20, no. 1, pp. 100–105, 2020.

[24] C. O. Jang and B. J. Kim, "Relationship between non-verbal communication of middle school sports club instructors and the commitment and impact on class satisfaction," *Journal of Korean Society for the Study of Physical Education*, vol. 25, no. 3, pp. 257–271, 2020.

[25] R. Wilson and C. B. Mayhorn, "On the field: examining differences in video format in sports media viewing," *Proceedings of the Human Factors and Ergonomics Society Annual Meeting*, vol. 64, no. 1, pp. 781–785, 2020.

[26] M. Karayol and M. Taze, "Investigation of entrepreneurship levels and employability perception of undergraduate students studying sports sciences," *International Education Studies*, vol. 13, no. 5, pp. 35-36, 2020.

[27] B. Liang, L. Wei, and L. Junfeng, "Study on the construction of ecological risk assessment system for urban hosting large-scale sports events," *Journal of Chengdu Institute of physical education*, vol. 46, no. 2, pp. 34–41, 2020.

[28] D. Yi and D. Jian, "Index dimension analysis and enlightenment of building London into a world-famous Sports City," *Journal of Shanghai Institute of physical education*, vol. 43, no. 1, pp. 65–71, 2019.

[29] Y. Huili, "Research on coupling time series evolution and influencing factors of sports events and host city development," *China Sports Science and technology*, vol. 55, no. 3, pp. 53–60, 2019.

Hindawi
Journal of Sensors
Volume 2021, Article ID 3859351, 7 pages
https://doi.org/10.1155/2021/3859351

Research Article

Construction of College Students' Physical Health Data Sharing System Based on Django Framework

Hui-chao Li and Shun-fa Shen

Department of Physical Education, Civil Aviation University of China, Tianjin 300300, China

Correspondence should be addressed to Shun-fa Shen; laoliu329@163.com

Received 29 July 2021; Revised 13 September 2021; Accepted 4 October 2021; Published 1 November 2021

Academic Editor: Mu Zhou

In view of the current situation of college students' physical health affected by the learning environment and living environment, which leads to the low level of students' physical health and the lack of understanding of students' physical health, this paper puts forward the construction of college students' physical health data sharing system based on Django framework. By analyzing the feasibility of constructing the data sharing system of college students' physical health, this paper constructs the organizational framework of the data sharing system of college students' physical health and constructs the data sharing system of college students' physical health according to the implementation process of the data sharing system of college students' physical health management service. Through the student's physical health test on education intervention and exercise intervention, it is concluded that college students' physical health data sharing system based on the Django framework can cultivate students' interest in sports and improve their athletic ability and physical fitness.

1. Introduction

With the rapid development of China's economy and the continuous improvement of people's living standards, health problems have gradually become a common social problem in China [1]. College students play an important role in China's future construction and development, and their health problems are getting higher attention from schools, society, and families. At present, the health level of college students in China tends to decline overall. Therefore, it is necessary to improve the health level of college students [2]. The cultivation of students' sports consciousness, exercise habits, and abilities has been paid less attention to in colleges and universities of China, which makes students attach little importance to sports and less want to participate in physical exercise, presenting no help in improving students' physical quality [3]. In these cases, it is therefore necessary to establish a physical health data sharing system of college students to enhance students' sports participation and interest and to lead students to have good sports habits to lay the foundation for the lifelong sports concept of college students.

Wang [4] analyzed the process of online health information sharing, proposed that creditworthiness is the foundation for realizing online health information sharing from the aspect of individual perception, and constructed the credit file system based on the social credit system theory. The system consists of the credit files of enterprises, government, and individuals, which focuses on the target system and exchange system, defines main tasks including transmission, collection, and evaluation of credit data, and identifies the guarantee methods of the online health sharing system in terms of content, technology, and system. Following the national big data policies, Ruhua and Fangfang [5] proposed that China's government data be kept shared and open, and further clarified the relevant system using techniques such as inquiry policies. The results prove that China's government data opening and sharing policies have three levels: infrastructure level, government governance level, and data management level, which provide a policy framework for the further development of government data and clarify the direction. Guo and Wu [6] considered seven subordinate colleges in Wuhan City, for instance, made a profound investigation into the sharing system and supposed that it

is exceptionally fundamental and plausible to fabricate a sharing component for actual well-being observing help of college understudies. What is more, the best area of the stage was the Wuhan University of Technology. The object was to give practical reference to the adapt, informatization, intellectualized, and effective development administration of college students' body well-being checking in China. van Panhuis et al. [7] led a deliberate systematic review of possible obstructions to general well-being information sharing. Reports that depicted boundaries to sharing regularly gathered general well-being information were qualified for consideration and investigated freely by a group of specialists. Zheng et al. [8] meant to build up a well-being-related information sharing framework by coordinating IoT to empower secure, charge less, alter safe, profoundly versatile, and granularly controllable well-being information trade, just as assemble a model and lead trials to confirm the attainability of the proposed arrangement. Bell et al. [9] talked with 70 solid volunteers to comprehend their decisions about how the data in their well-being record ought to be shared for research. Twenty-eight review addresses caught the individual inclinations of solid volunteers. The outcomes showed that respondents felt open to taking an interest in research in the event that they were given decisions about what parts of their clinical information would be shared and with whom that information would be shared. The outcomes recommend that straightforwardness during the time spent sharing is a significant factor in the choice to share clinical information for research. Tang et al. [10] planned an upgraded property-based encryption technique through the blend of an individual access strategy on patients and an expert access strategy on the haze hub for viable clinical benefit arrangement. Besides, a critical encryption utilization decrease was accomplished for patients by offloading a bit of the calculation and capacity trouble from patients to the haze hub. Execution assessments showed cost-proficient encryption calculation, stockpiling, and energy utilization. Conducting well-being experts' impression of granular information is concentrated by Grando et al. [11]. Semiorganized face-to-face meetings of 20 well-being experts were directed at two distinct locales. The subjective and quantitative examination was performed. This examination educates the conversation on creating innovation that helps balance supplier and patient information sharing and access needs. Maughan and Combe [12] provided a useful illustration of how a school area properly shares information with outside accomplices. It is a commonsense illustration of how to apply the standards found in the article on information sharing.

Based on the above research background, this paper applies the Django framework to the construction of college students' physical health data sharing system to promote the understanding of students' physical health status in schools and improve their physical health level.

The remainder of this paper is organized as follows. Section 2 presents the construction of college students' physical health data sharing system. Section 3 provides the analysis of the experiment. Section 4 concludes this paper with several remarks.

2. Construction of College Students' Physical Health Data Sharing System

2.1. Feasibility Analysis of the Construction of College Students' Physical Health Data Sharing System. The college students' physical health data sharing system is designed to promote the physical and mental health of college students. The data sharing system of college students' physical health mainly relies on colleges and universities' existing resources and platforms to manage and serve students' physical health [13]. At present, the school level hospital, the mental health center, and the physique test center are responsible for the management of students' physical health in colleges and universities in China. The college students' physical health data sharing system integrates these superior resources and platforms into a resource sharing platform for students. The college students' physical health data sharing system is developed to ensure better the physical fitness of college students [14]. The exercise intervention and health education intervention in the health intervention help students to establish a correct concept of health and sports, and require students to master a good scientific and reasonable physical exercise method and cultivate good exercise habits, enabling students to achieve healthy physical and mental development.

The construction of college students' physical health data sharing system has the following advantages.

(1) There is a good foundation for college students' physical health management [15]. The academic atmosphere and cultural environment of colleges and universities are conducive to promoting and constructing the college students' physical health data sharing system

(2) College students can easily accept new things [16]

(3) College students have certain cultural qualities, which makes it convenient for effective integration of sports and medical resources in colleges and universities to achieve complementary advantages

(4) The college students' physical health data sharing system can take advantage of physical education in universities [17]. Especially, improve the quality of education and train healthy students for teachers

In the college students' physical health data sharing system, the establishment of students' physical health files can rely on the existing database of college students' personal information in China. Each student has their file and physical health information database and can access personal academic information on the school website. Colleges and universities can provide assistance and support for the construction of students' personal physical health management files [18]. Students' health information including physique test results, mental health test results, and physical examination forms are entered into the database to form students' personal physical health management files. It is feasible for colleges and universities to establish students' personal physical health management files.

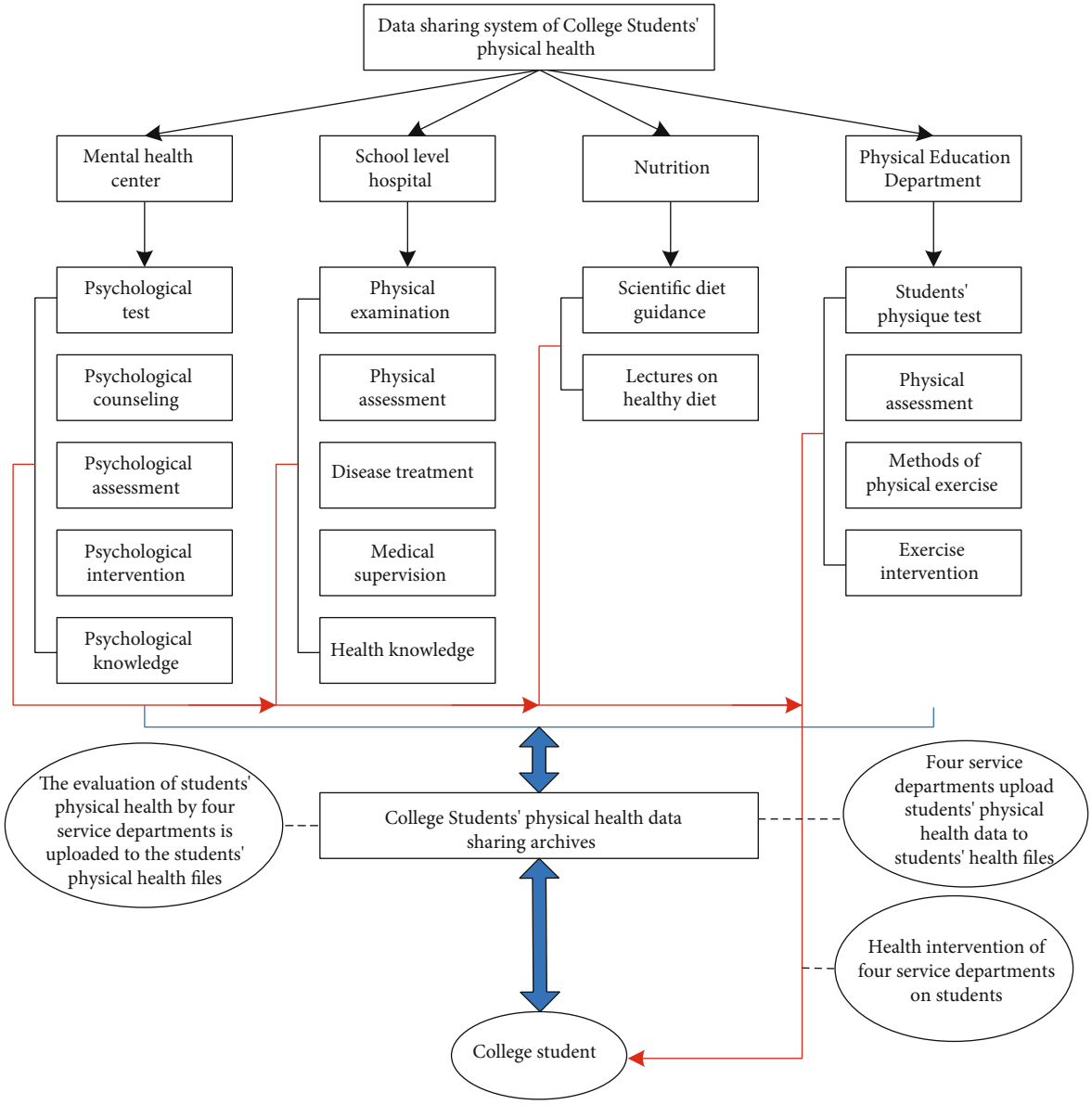

Figure 1: Organizational framework of students' physical health data sharing system.

In the college students' physical health data sharing system, the physical education department, school level hospital, and mental health center can analyze the physical health status of college students and discuss and make interventions. For example, the physical education department analyzes and evaluates students' physique test results and proposes different solutions for different students to intervene in their physique health according to their individual needs. Based on students' physical examination reports, the school level hospital diagnoses and treats students' physical diseases and provides targeted guidance for their rehabilitation [19]. The mental health center assesses the psychological status of students through psychological tests and intervenes and provides guidance on psychological disorders, including mental health lectures on common psychological disorders among students for prevention in advance. Nutrition involves instruction and publicity about a healthy diet to help students develop healthy eating habits.

2.2. Construction Model of College Students' Physical Health Data Sharing System. The college students' physical health data sharing system connects departments associated with students' physical health in colleges and universities [20] and draws on the strengths of each department to achieve the sharing of students' physical health data. The construction of college students' physical health data sharing system requires the unified leadership of departments, such as the mental health center, the school level hospital, the physical education department, and the nutrition in colleges and universities, to strengthen the ability of each department to cooperate with each other. In this paper, by reviewing literature and books related to students' physical health,

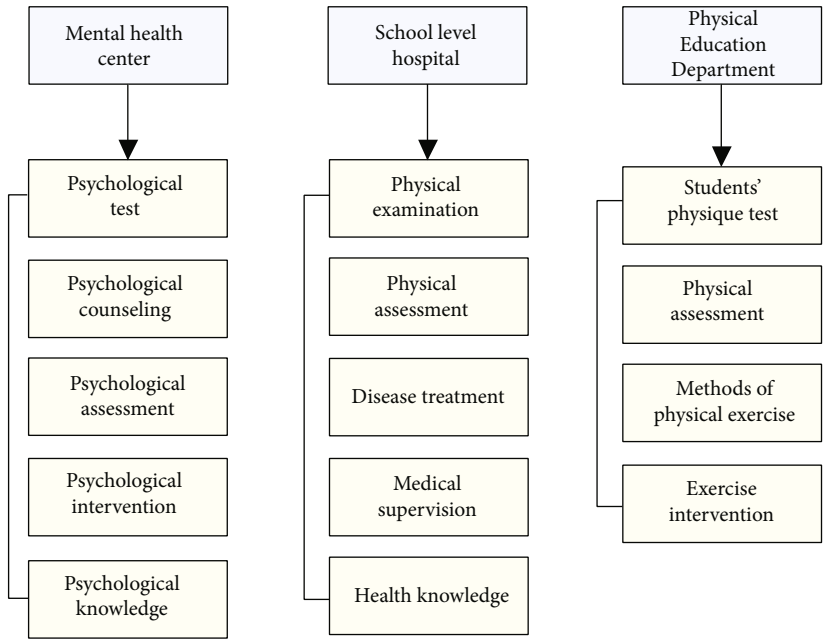

Figure 2: Test college students' physical health status.

Table 1: 50 m sprint scale.

Grade	Schoolboy		Girl student	
	Freshmen to sophomores	Junior to senior	Freshmen to sophomores	Junior to senior
Excellent	≤6.7 s	≤6.6 s	≤7.5 s	≤7.4 s
Good	(6.7 s, 7.1 s]	(6.6 s, 7.0 s]	(7.5 s, 8.0 s]	(7.4 s, 8.4 s]
Pass	(7.1 s, 9.3 s]	(7.0 s, 9.2 s]	(8.0 s, 10.5 s]	(8.4 s, 10.4 s]
Fail	>9.3 s	>9.2 s	>10.5 s	>10.4 s

combined with the Django framework and the actual situation of colleges and universities [21], the organizational framework of students' physical health data sharing system is constructed as shown in Figure 1.

The college students' physical health data sharing system should provide physical health management services for students from freshmen. The specific steps are as follows.

Step 1: Test college students' physical health status.

After freshmen enrollment, as shown in Figure 2, students' mental health data, physical health data, and physique data should first collect for the mental health center, the school level hospital, and the physical education department, which lays the foundation for students' physical health data sharing [22].

Step 2: Collect and summarize students' physical health data.

Establish the personal physical health management files for each newly enrolled student, then summarize students' physical health information from the mental health center, the school level hospital, and the physical education department, and enter the information into the newly established student personal physical health management files.

Step 3: Analyze and evaluate college students' physical health data.

The mental health center, the school level hospital, and the physical education department in the data sharing system upload the results of analysis and scientific assessments on the detected students' personal physical health data by the professionals to the students' personal physical health management files.

Step 4: Conduct students' physical health guidance and intervention.

Develop approaches to students' physical health interventions based on the assessment results of each student's physical health data [23], to help students develop a healthy lifestyle and good physical exercise habits, improving the overall level of college students' physical health.

Improving students' physical health services by the college students' physical health data sharing system is a gradual process. After the above steps, it is necessary to test the students' physical health data again, update the students' personal physical health management files promptly, evaluate the completed updated student physical health files, and provide interventions and guidance to the students' physical health based on the evaluation results [24]. Through the testing and evaluation of college students' physical health data and the physical health intervention process, encourage students to establish the correct concept of health and improve their awareness and level of physical health.

3. Experiment and Analysis

3.1. Students' Physical Health Education Intervention. Through the social education activities in students' physical health education, students take behaviors and lifestyles that are beneficial to their physical health and eliminate risk factors that affect their physical health, which not only prevents diseases in advance but also promotes their physical health

Table 2: 800 m race and 1000 m race scale.

Grade	Schoolboy		Girl student	
	Freshmen to sophomores	Junior to senior	Freshmen to sophomores	Junior to senior
Excellent	$\leq 3'27''$	$\leq 3'25''$	$\leq 3'45''$	$\leq 3'40''$
Good	$\left(3'27'', 3'42''\right]$	$\left(3'27'', 3'40''\right]$	$\left(3'45'', 4'00''\right]$	$\left(3'40'', 3'55''\right]$
Pass	$\left(3'42'', 4'32''\right]$	$\left(3'40'', 4'10''\right]$	$\left(4'30'', 5'30''\right.$	$\left(3'55'', 5'20''\right]$
Fail	$>4'32''$	$>4'10''$	$>5'30''$	$>5'20''$

Table 3: Standing long jump scale.

Grade	Schoolboy		Girl student	
	Freshmen to sophomores	Junior to senior	Freshmen to sophomores	Junior to senior
Excellent	≧2.63 m	≧2.65 m	≧1.95 m	≧1.96 m
Good	[2.48 m, 2.63 m)	[2.40 m, 2.65 m)	[1.81 m, 1.95 m)	[1.82 m, 1.96 m)
Pass	[2.08 m, 2.48 m)	[2.10 m, 2.40 m)	[1.51 m, 1.81 m)	[1.55 m, 1.82 m)
Fail	<2.08 m	<2.10 m	<1.51 m	<1.55 m

and improves their quality of life [25]. The core of students' physical health education is to help students develop an active awareness of physical health, change poor behaviors and lifestyles, understand behaviors that can affect their physical health, and consciously choose behaviors and lifestyles that are beneficial to their physical health.

3.2. Sports Intervention. As an important part of students' physical health intervention, sports intervention is realized by guiding students to perform physical exercise. Introducing the college students' physical health data sharing system to colleges and universities to realize students' physical health data sharing helps the implementation of sports intervention, improves the effect of sports intervention, and plays an important role in students' physical health intervention.

3.2.1. Students' Speed Quality Exercise. Students' speed quality refers to the ability of the human body to move quickly, which can reflect the ability of movement acceleration and a maximum speed of the human body [26]. The test programs of speed quality are mainly reflected in the 50 m sprint, and the test scale is shown in Table 1.

From Table 1, a sports program with strong explosive power and high speediness is suitable to train students' speed quality. In college students' physical health management training, the intensity, duration, and interval should be controlled according to the actual situation of the students, and stretching exercises should be done after the training to help students recover.

3.2.2. Students' Endurance Quality Exercise. Endurance quality refers to the ability of the human body to maintain a specific movement quality and intensity load for a certain period of time [27]. It is often tested in the 800-meter race and 1000 m race and is associated with the lung capacity of students. Therefore, students' middle-distance race training can improve their cardiorespiratory fitness. The 800-meter race and 1000 m race scale is shown in Table 2.

From Table 2, students' endurance quality intervention and guidance should consider student s' interest and hobbies in sports and choose a program that will help students aerobically exercise. Improving students' endurance quality requires constant accumulation in physical exercise activities, including students' active participation in physical exercise and persistence.

3.2.3. Students' Strength Quality Exercise. Strength quality refers to the ability of the human body to overcome internal and external resistance when working [28]. It is mainly tested in the standing long jump, boys pull up and girls sit up. The standing long jump can test students' lower limb strength and core strength, pull up can test students' upper limb strength, and sit up can test students' core strength of the waist and abdomen. The test scales for the three programs are shown in Tables 3 and 4.

The standing long jump training should focus on improving students' lower limb strength and core strength and teach students the correct method of standing long jump, including deep squat and frog jump. The boys pull up should combine with swimming, basketball, volleyball, and other upper limb loading programs to improve students' upper limb strength. The girls sit up focuses on a flat support, which improves students' waist and abdominal strength for physical health intervention.

In the strength training of students, the intensity and amount need to be adjusted according to the physical quality of each student to ensure the proper amount of student training and to achieve the best strength training results.

3.2.4. Students' Flexible Quality Exercise. Flexible quality refers to the range of motion of the human body's joints and the ability to stretch the soft tissues [29]. It is mainly tested in the sit and reach program, which requires students to sit in front of a tester, straighten their legs, and push the

Table 4: Pull up and sit up scale (times).

Grade	Boys pull up		Girls sit ups	
	Freshmen to sophomores	Junior to senior	Freshmen to sophomores	Junior to senior
Excellent	≧17	≧18	≧52	≧53
Good	[15, 17)	[16, 18)	[46, 52)	[47, 53)
Pass	[9, 15)	[10, 16)	[26, 46)	[26, 47)
Fail	<9	<10	<25	<26

Table 5: Sit and reach scale.

Grade	Schoolboy		Girl student	
	Freshmen to sophomores	Junior to senior	Freshmen to sophomores	Junior to senior
Excellent	≧21.3	≧21.5	≧22.2	≧22.4
Good	≧17.7	≧18.2	≧19.0	≧19.5
Pass	≧3.7	≧4.2	≧6.0	≧6.5
Fail	≦3.6	≦4.1	≦5.9	≦6.5

Table 6: Weight of single indexes in students' physical health test.

Entry name	Proportion	Entry name	Proportion
Body mass index	15%	Standing long jump	10%
Vital capacity	15%	Pull up/sit ups	10%
50-meter race	20%	1000 m/800 m	20%
Sit and lie forward	10%		

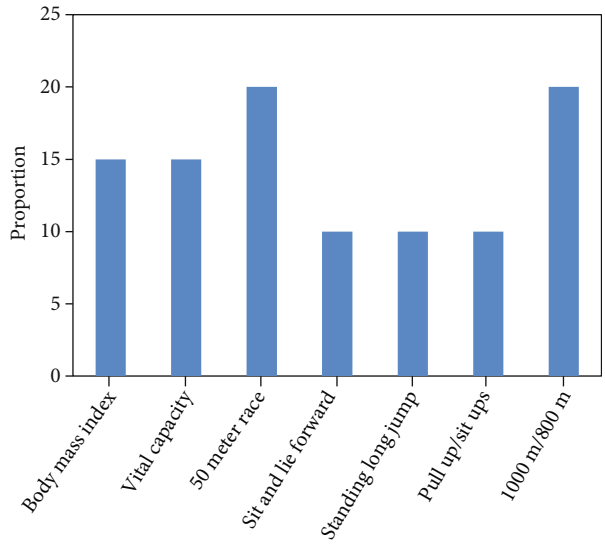

Figure 3: Weights of single indexes.

instrument with both arms to obtain the test results. The sit and reach scale is shown in Table 5.

Students' flexible quality exercise should combine with other sports programs such as yoga to enhance the whole body's flexibility by stretching. This program requires a long period of continuous stretching exercise, combined with speed, endurance, and strength training, to improve students' physical health.

3.3. Results and Analysis

3.3.1. Experiment Results. Forty-six students participated in the students' physical health training, 23 in the experiment group, and 23 in the intervention group, and the number of effective training in the experiment group was 22, with one invalid.

The number of physical exercise instruction hours during the experiment was 18, and the specific time was based on the students' spare time. Only one student was absent from the 18-hour physical exercise instruction due to physical reasons, and all other students completed all the training programs. This shows that students are highly motivated to physical health training and pay great attention to their physical health.

3.3.2. Analysis on the Comparative Results of the Individual Program Scores in Students' Physical Health Test. The weight of each single program score in students' physical health test is shown in Table 6.

From the results in Table 6, it can be seen that students attach more importance to speed quality and endurance quality training, and there is a correlation between lung capacity and speed quality training, which obviously shows the importance of endurance quality. The results are also shown in Figure 3 for a better comparison.

According to Figure 3, more programs in endurance should be arranged in the training as much as possible to improve students' physique test performance while raising students' physical health quality in other aspects.

4. Conclusion

This paper puts forward the construction of the physical health data sharing system based on the Django framework. By analyzing the feasibility of constructing the data sharing system of college students' physical health, this paper constructs the data sharing system. The results show that the data sharing system of college students' physical health based on Django framework can improve students' physical health.

Data Availability

The labeled datasets used to support the findings of this study are available from the corresponding author upon request.

Conflicts of Interest

The authors declare no competing interests.

Acknowledgments

This study was supported by the 2018 Tianjin Philosophy and Social Science Planning Funding Project: Construction

of University Sports Health Management System and Funding for Sports (TJTY18-018).

References

[1] M. Yang and Y. Yang, "An efficient hybrid peer-to-peer system for distributed data sharing," *IEEE Transactions on Computers*, vol. 59, no. 9, pp. 1158–1171, 2010.

[2] J. Sun, H. Xiong, S. Zhang, X. Liu, J. Yuan, and R. H. Deng, "A secure flexible and tampering-resistant data sharing system for vehicular social networks," *IEEE Transactions on Vehicular Technology*, vol. 69, no. 11, pp. 12938–12950, 2020.

[3] E. M. Godfrey, I. I. West, J. Holmes, G. A. Keppel, and L. M. Baldwin, "Use of an electronic health record data sharing system for identifying current contraceptive use within the WWAMI region practice and research network," *Contraception*, vol. 98, no. 6, pp. 476–481, 2018.

[4] W. Wang, "Research on the construction of credit file system based on online health information sharing," *In Chinese, Journal of Modern Information*, vol. 38, no. 12, pp. 111–115, 2018.

[5] H. Ruhua and W. Fangfang, "The policy framework and content of my country's government data open sharing: content analysis of policy texts at the national level," *In Chinese, Library and Information Work*, no. 9, pp. 5–13, 2018.

[6] M. Guo and Y. Wu, "Construct sharing mechanism of college students' physical health monitoring service based on geographic information system," *In International Conference on Machine Learning and Big Data Analytics for IoT Security and Privacy*, 2020, pp. 772–778, Springer, Cham, 2020.

[7] W. G. van Panhuis, P. Paul, C. Emerson et al., "A systematic review of barriers to data sharing in public health," *BMC Public Health*, vol. 14, no. 1, pp. 1–9, 2014.

[8] X. Zheng, S. Sun, R. R. Mukkamala, R. Vatrapu, and J. Ordieres-Meré, "Accelerating health data sharing: a solution based on the Internet of Things and distributed ledger technologies," *Journal of Medical Internet Research*, vol. 21, no. 6, article e13583, 2019.

[9] E. A. Bell, L. Ohno-Machado, and M. A. Grando, "Sharing my health data: a survey of data sharing preferences of healthy individuals," *AMIA Annual Symposium Proceedings*, vol. 2014, p. 1699, 2014.

[10] W. Tang, J. Ren, K. Zhang, D. Zhang, Y. Zhang, and X. S. Shen, "Efficient and privacy-preserving fog-assisted health data sharing scheme," *ACM Transactions on Intelligent Systems and Technology (TIST)*, vol. 10, no. 6, pp. 1–23, 2019.

[11] A. Grando, J. Ivanova, M. Hiestand et al., "Mental health professional perspectives on health data sharing: mixed methods study," *Health Informatics Journal*, vol. 26, no. 3, pp. 2067–2082, 2020.

[12] E. D. Maughan and L. G. Combe, "Data sharing: partnering with others to advance student health," *NASN School Nurse*, vol. 34, no. 4, pp. 214-215, 2019.

[13] A. J. Holmgren and E. W. Ford, "Assessing the impact of health system organizational structure on hospital electronic data sharing," *Journal of the American Medical Informatics Association*, vol. 25, no. 1, p. 10628, 2018.

[14] C. Park, "Parameter estimation from load-sharing system data using the expectation–maximization algorithm," *IIE Transactions*, vol. 45, no. 2, pp. 147–163, 2013.

[15] R. Larsen, T. Holmern, S. D. Prager, H. Maliti, and E. Røskaft, "Using the extended quarter degree grid cell system to unify mapping and sharing of biodiversity data," *African Journal of Ecology*, vol. 46, no. 3, pp. 382–392, 2009.

[16] M. Cocca, D. Giordano, M. Mellia, and L. Vassio, "Free floating electric car sharing: a data driven approach for system design," *IEEE Transactions on Intelligent Transportation Systems*, vol. 20, no. 12, pp. 4691–4703, 2019.

[17] F. Khazalah, Z. Malik, and A. Rezgui, "Automated conflict resolution in collaborative data sharing systems using community feedbacks," *Information Sciences*, vol. 298, pp. 407–424, 2015.

[18] Z. Pervez, A. M. Khattak, S. Lee, and Y. K. Lee, "SAPDS: self-healing attribute-based privacy aware data sharing in cloud," *Journal of Supercomputing*, vol. 62, no. 1, pp. 431–460, 2012.

[19] J. R. Vest and L. M. Issel, "Factors related to public health data sharing between local and state health departments," *Health Services Research*, vol. 49, pp. 373–391, 2014.

[20] D. E. Conroy, J. P. Maher, S. Elavsky, A. L. Hyde, and S. E. Doerksen, "Sedentary behavior as a daily process regulated by habits and intentions," *Health Psychology*, vol. 32, no. 11, p. 1149, 2013.

[21] P. Zarcone, D. Nordenberg, M. Meigs, U. Merrick, D. Jernigan, and S. H. Hinrichs, "Community-driven standards-based electronic laboratory data-sharing networks," *Public Health Reports*, vol. 125, no. 2, pp. 47–56, 2010.

[22] S. Rosenbaum, "Data governance and stewardship: designing data stewardship entities and advancing data access," *Health Services Research*, vol. 45, no. 5, pp. 1442–1455, 2010.

[23] Y. Lyu, V. C. S. Lee, K. Y. Ng, B. Y. Lim, K. Liu, and C. Chen, "Flexi-sharing: a flexible and personalized taxi-sharing system," *IEEE Transactions on Vehicular Technology*, vol. 68, no. 10, pp. 9399–9413, 2019.

[24] Y. Hu, Y. Zhang, D. Lamb, M. Zhang, and P. Jia, "Examining and optimizing the BCycle bike-sharing system - a pilot study in Colorado, US," *Applied Energy*, vol. 247, pp. 1–12, 2019.

[25] K. N. Genikomsakis, I. A. Gutierrez, D. Thomas, and C. S. Ioakimidis, "Simulation and design of fast charging infrastructure for a university-based e-carsharing system," *IEEE Transactions on Intelligent Transportation Systems*, vol. 19, no. 9, pp. 2923–2932, 2018.

[26] L. Lin, H. Ma, and Z. Bai, "An improved proportional load-sharing strategy for meshed parallel inverters system with complex impedances," *IEEE Transactions on Power Electronics*, vol. 32, no. 9, pp. 7338–7351, 2017.

[27] X. Qiu and J. S. L. Lam, "The value of sharing inland transportation services in a dry port system," *Transportation Science*, vol. 52, no. 4, pp. 835–849, 2018.

[28] S. C. Oh and J. Shin, "A semantic e-Kanban system for network-centric manufacturing: technology, scale-free convergence, value and cost-sharing considerations," *International Journal of Production Research*, vol. 50, no. 19, pp. 5292–5316, 2012.

[29] J. H. Lin and S. H. Cheng, "The impact of a medication record sharing program among diabetes patients under a single-payer system: the role of inquiry rate," *International Journal of Medical Informatics*, vol. 116, pp. 18–23, 2018.

Hindawi
Journal of Sensors
Volume 2021, Article ID 2119993, 7 pages
https://doi.org/10.1155/2021/2119993

Research Article

An Adaptive Deployment Algorithm for IaaS Cloud Virtual Machines Based on Q Learning Mechanism

Shuguang Chen

Department of Information Engineering, Liuzhou City Vocational College, Liuzhou, 545002 Guangxi, China

Correspondence should be addressed to Shuguang Chen; cjxub5030062@163.com

Received 5 August 2021; Revised 6 September 2021; Accepted 23 September 2021; Published 31 October 2021

Academic Editor: Mu Zhou

When deploying infrastructure as a service (IaaS) cloud virtual machines using the existing algorithms, the deployment process cannot be simplified, and the algorithm is difficult to be applied. This leads to the problems of high energy consumption, high number of migrations, and high average service-level agreement (SLA) violation rate. In order to solve the above problems, an adaptive deployment algorithm for IaaS cloud virtual machines based on Q learning mechanism is proposed in this research. Based on the deployment principle, the deployment characteristics of the IaaS cloud virtual machines are analyzed. The virtual machine scheduling problem is replaced with the Markov process. The multistep Q learning algorithm is used to schedule the virtual machines based on the Q learning mechanism to complete the adaptive deployment of the IaaS cloud virtual machines. Experimental results show that the proposed algorithm has low energy consumption, small number of migrations, and low average SLA violation rate.

1. Introduction

In recent years, the development scale of service computing model has gradually expanded and has been widely used in various fields. The rapid progress of distributed computing, virtualization, and parallel computing technology has promoted the development of cloud technology [1, 2]. At the service model level, cloud computing is usually divided into software as a service (SaaS), platform as a service (PaaS), and IaaS. IaaS belongs to the basic level in cloud computing services and can provide resources and storage resources in the network. Therefore, it is of great significance to study the algorithm of deploying IaaS cloud virtual machines [3].

Lei and Wang [4] combined the best adaptation algorithm and hierarchical clustering algorithm to optimize the efficiency. On this basis, the local search algorithm was used to optimize the deployment of the virtual machines' locations. The deployment process of the algorithm was relatively cumbersome, leading to the high energy consumption of the algorithm. Liao et al. [5] combined dynamic programming method and Markov models to predict the price of virtual machines and deployed virtual machines in a cloud environment according to the execution time limit of the workflow. However, this algorithm could not simplify the virtual machine deployment process. The number of migrations of virtual machines was relatively high. Jiliang et al. [6] established a multiservice-desk queuing model. The system energy saving rate and the average stay time of cloud user requests were obtained through the matrix geometry method and virtual birth and death process. The virtual machines were scheduled to realize deployment. The average SLA violation rate of this method was high, and the effectiveness of the algorithm was poor.

In order to solve the problems in the above algorithms, an adaptive IaaS cloud virtual machine deployment algorithm based on the Q learning mechanism is proposed.

The rest of this paper is organized as follows. Section 2 gives the basic issues of virtual machine deployment and an adaptive deployment algorithm for IaaS cloud virtual machines. The experiment is provided in Section 3 to illustrate the effectiveness of the proposed method. Finally, Section 4 concludes this paper.

2. Related Works

2.1. Basic Issues of Virtual Machine Deployment. The problem of the self-adaptive deployment of IaaS cloud virtual machines can be described as follows. n virtual machines constitute a virtual machine set [7, 8], which is denoted as $V = \{v_1, v_2, \cdots, v_n\}$, where $v_i = \{p_i, Q_i, r_i\}$ is a virtual machine. p_i is a virtual machine type; $Q_i = \{c_i, m_i, s_i, b_i\}$ is a virtual machine configuration. c_i is the number of CPUs in the virtual machine, m_i is the memory of the virtual machine, b_i represents the expected bandwidth, and s_i represents the hard disk space; r_i represents the amount of data required to build the virtual machines [9]. A host machine set is composed of m host machines, denoted as $H = \{h_1, h_2, \cdots, h_m\}$, where $h_j = \{p_j, Q_j, d_j\}$ represents a host machine. p_j is a virtualization platform existing in the host machine, $Q_j = \{C_j, M_j, S_j\}$ means the hardware configuration of the host machine, C_j means the number of CPUs in the host machine, S_j means the hard disk space of the host machine, and M_j means the memory of the host machine. A mapping $f : V \longrightarrow H$ is constructed, where $f : v_i \longrightarrow h_j$ is the deployment of the virtual machine v_i in the host machine h_j.

2.1.1. Deployment Principles. The virtual machines run on the basis of the host's hardware resources. The main hardware resources include hard disk, memory, and CPU.

After fully testing the applications existing in the virtual machines, the resource usage can be set. However, it is usually difficult to predict the behaviors of IaaS users. In order to improve the quality of service, the deployment of IaaS cloud virtual machines needs to be implemented on the basis of the following principles [10, 11]:

(a) The number of CPU cores in the host machine for all virtual machines should be lower than the number of cores in the actual host machine for CPU

(b) The memory of the host machines should be lower than the virtual memory of the virtual machines in the host machines

2.1.2. Deployment Characteristics. Regarding the deployment of virtual machines as an independent issue, its deployment has the following characteristics:

(a) Resources are limited during task execution. When the traditional method is to schedule independent tasks, any number of tasks can be allocated in a certain resource, but when deploying virtual machines, it is necessary to provide sufficient resources for the host machines [12, 13]

(b) When the task is scheduled to the resource, the task can be expanded and processed

2.1.3. Problem Description. In the virtual machine deployment algorithm, suitable host machines h_j should be found for all virtual machines v_i to optimize the target. Task scheduling goals can generally be divided into the following two categories:

(a) Optimize the period of tasks by considering the interests of resource users

(b) Optimize the specific conditions of the resources in the use process by considering the interests of resource providers

Introducing virtualization technology into the server can improve resource utilization. The main task of the IaaS cloud virtual machine deployment algorithm is to use the least host machines to complete the deployment of the virtual machines, regardless of deployment time, bandwidth, and hard disk space. There is a clear corresponding relationship between the type of virtual machines and the manager of the virtual machine of the hosts [14, 15], so the IaaS cloud virtual machine deployment problem can be simplified as follows.

For the virtual machine set $V = \{v_1, v_2, \cdots, v_n\}$, $v_i = \{c_i, m_i\}$, and the host machine set $H = \{h_1, h_2, \cdots, h_m\}$, $h_j = \{C_j, M_j\}$, we obtain a subset $H' = \{h'_1, h'_2, \cdots, h'_{|H|'}\} \subset H$, $h'_j = \{C'_j, M'_j\}$, of the host machine set H and establish a mapping $f : V \longrightarrow H'$ that satisfies

$$\begin{cases} f : V \longrightarrow H' \\ \text{s.t.} \quad \sum\limits_{v_j \longrightarrow h'_j} c_i \le C'_j \\ \quad\quad \sum\limits_{v_j \longrightarrow h'_j} m_i \le M'_j, \end{cases} \tag{1}$$

where C'_j represents the number of CPUs in the host machine after the mapping process and M'_j represents the memory of the host machine after the mapping process.

2.2. An Adaptive Deployment Algorithm for IaaS Cloud Virtual Machines. According to the above analysis of the deployment problem of IaaS cloud virtual machines, the adaptive deployment algorithm for IaaS cloud virtual machines based on the Q learning mechanism uses the Markov decision process to describe the deployment problem of IaaS cloud virtual machines. The essence of IaaS cloud virtual machine deployment is to schedule virtual machines in the cloud environment to achieve adaptive deployment.

2.2.1. Q Learning Method. The Q learning algorithm can solve the Markov decision process, which belongs to the reinforcement learning algorithm [16, 17]. The Markov model can be described with five tuples $<S, A, R, P, V>$, where S is the state set, A represents the action set, R is return function, P represents the state transition probability matrix, and V is the model function value.

Markov's strategy can be described by the mapping of the probability distribution in the action space and the state space [18, 19], expressed as $\pi : S \longrightarrow \prod(A)$, where $\prod(A)$ is the probability distribution corresponding to the action set A.

In the state-action space, the value function in the strategy can be calculated by

$$Q^{\pi}(x,a) = R_x(a) + \sum_{y \in S} p_{xy}^{a} \times V^{\pi}(y), \tag{2}$$

where $R_x(a)$ represents the return obtained when the action a is transited under the state x, p_{xy}^{a} represents the corresponding probability when the action a transits from state x to state y, and $V^{\pi}(y)$ represents the expected total discounted return corresponding to state y under the strategy π.

Using the optimal Q value to obtain the optimal strategy π^* is the principle of the Q learning mechanism, and $Q^*(x, a)$ is used to describe the optimal Q value. If $a^* = \arg\max_a Q^*(x,a)$, the optimal strategy at this time can be described by $\pi^*(x) = a^*$.

The Q learning process is usually composed of two parts, namely, plot and step. The plot is a sequence of steps between the target state and the starting state; the step is the return acquisition and action execution in the determined state.

It is supposed that x_t represents the state corresponding to the agent at the time t, and a_t represents the execution of the action. We observe the return r_t and the next state x_{t+1} during the learning process and update the value function:

$$Q_{t+1}(x,a) = \begin{cases} (1-\alpha_t)Q_t(x,a) + \alpha_t[r_t + V_t(x_{t+1})], & x = x_t, \\ & a = a_t, \\ Q_t(x,a), & \text{other}, \end{cases} \tag{3}$$

where the parameter $V_t(x_{t+1}) = \max_b \{Q_t(x_{t+1}, b)\}$ and α_t represents the learning rate.

2.2.2. Markov Description of Task Scheduling. When using reinforcement learning to solve the virtual machine scheduling problem, it is necessary to use the Markov model to replace the virtual machine scheduling problem. Markov elements can be selected according to the following principles:

(a) The state at the next moment is not affected by the historical state and is only related to the current state. The selected state needs to reflect Markov properties [20, 21]

(b) When choosing an action, it is necessary to ensure that there is a law of state transition, all states can be reached, and the goal of the agent is completed by performing a series of actions

(c) The selected return function requires the least decision-making steps to make the agent reach the target state

The Markov process is described on the basis of the above principles:

(a) The unit-task matching matrix is used to describe the Markov state. In the virtual machine scheduling process, the state of the matrix is the scheduling's feasible solution, and there is a state transition of reinforcement learning in the feasible solution space [22, 23]

(b) In all states, there are n tasks and n actions. The jth $(1 < j \le n)$ task can be transited to the next design unit through the jth action. At this time, the result obtained by executing the jth action can be expressed by $d_{kj} = 1$, and the parameter k can be calculated by

$$k = \begin{cases} i+1, & i < m, \\ 1, & i = m. \end{cases} \tag{4}$$

(c) Determine the return value through $r(x, a, x') = 1/t$ (x') in the reinforcement learning

2.2.3. Multistep Q Learning Algorithm. In the Q learning process, the value function $Q(x_t, a_t)$ is updated through $r_t + \gamma V_t(x_{t+1})$, and the return r_t is determined by

$$r_t^{(n)} = r_t + \gamma r_{t+1} + \cdots + \gamma^{n-1} r_{t+n-1} + \gamma^n V_{t+n-1}(x_{t+n}), \tag{5}$$

where n represents the number of iterations, γ represents the learning coefficient, and $r_t^{(n)}$ represents the truncated return corresponding to the correction step n at a time t.

The weighted average of the truncated return $r_t^{(n)}$ is used to update, and the learning steps are simplified. The weighted average $r_r^{\lambda,k}$ of truncated return $r_t^{(n)}$ can be calculated by k step time difference TD(λ).

$$r_r^{\lambda,k} = (1-\lambda) \sum_{i=1}^{k-1} \lambda^{i-1} r_t^{(i)} + \lambda^{k-1} r_t^{(k)}, \tag{6}$$

where λ represents the time difference.

$r_t^{(n)}$ is substituted in the weighted average $r_r^{\lambda,k}$ to simplify the processing:

$$r_r^{\lambda,k} = r_t + \gamma V_t(x_{t+1}) + \sum_{i=1}^{k-1} (\lambda\gamma)^i [r_{t+1} + \gamma V_{t+i}(x_{t+i+1}) - V_{t+i-1}(x_{t+i})]. \tag{7}$$

Equation (7) is converted to

$$r_r^{\lambda,k} = r_t + \gamma V_t(x_{t+1}) + \sum_{i=1}^{k-1} (\lambda\gamma)^i [r_{t+1} + \gamma V_{t+i}(x_{t+i+1}) - V_{t+i-1}(x_{t+i})] + \sum_{i=1}^{k-1} (\lambda\gamma)^i [V_{t+i}(x_{t+i}) - V_{t+i-1}(x_{t+i})]. \tag{8}$$

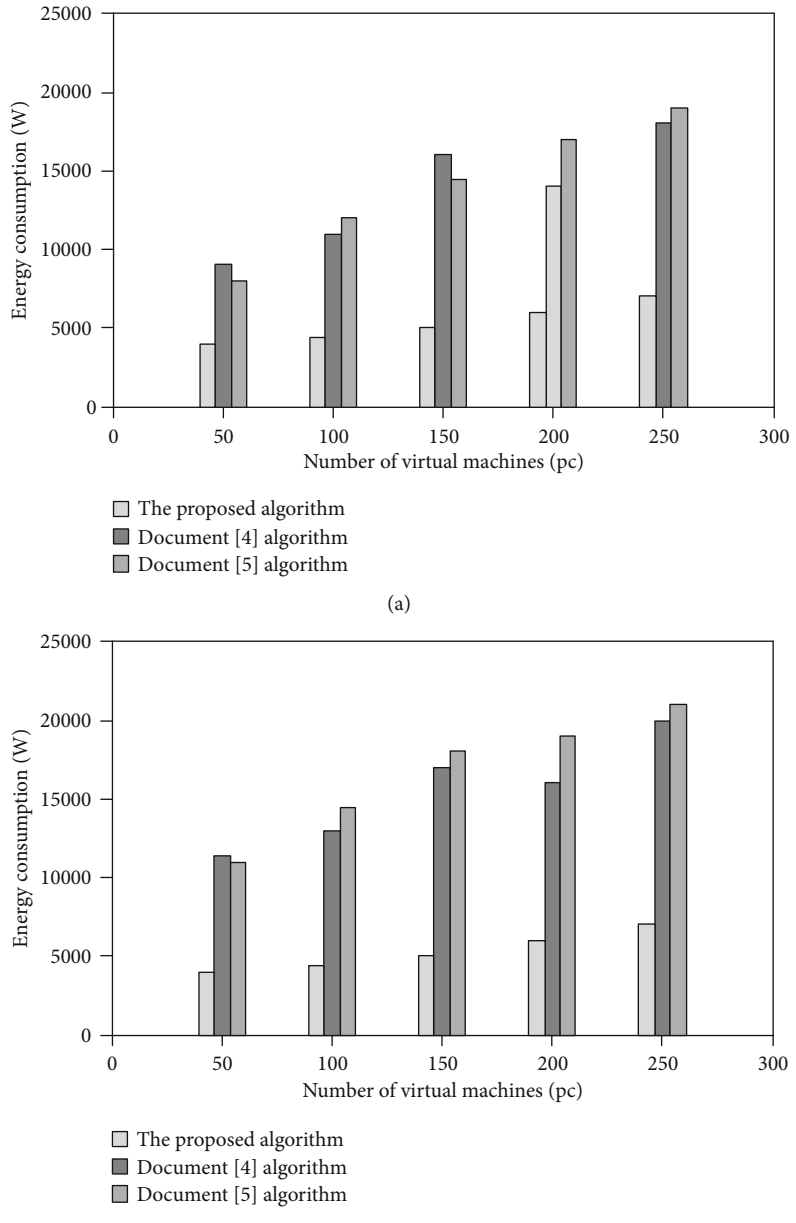

Figure 1: Comparison of energy consumption by different algorithms. (a) Comparison of energy consumption without network congestion. (b) Comparison of energy consumption with network congestion.

When the learning rate α is low, the adjustment speed of the Q value is slow. At this time, the speed of the V value is also reduced. Let $e_t = r_t + \gamma V_t(x_{t+1}) - V_t(x_t)$, $e_t' = r_t + \gamma V_t(x_{t+1}) - Q_t(x_t, a_t)$, and we have

$$r_t^{\lambda,k} = e_t' + \sum_{i=1}^{k-1} (\lambda\gamma)^i e_{t+i} + Q_t(x_t, a_t). \tag{9}$$

Equation (9) is converted to

$$r_t^{\lambda,k} - Q_t(x_t, a_t) = e_t' + \sum_{i=1}^{k-1} (\lambda\gamma)^i e_{t+i}. \tag{10}$$

Through the above process, the update rules of the Q learning mechanism are obtained:

$$Q_{t+1}(x, a) = \begin{cases} Q_t(x, a) + \alpha_t e_t' + \sum_{i=1}^{k-1} (\lambda\gamma)^i e_{t+i}, & x = x_t, \\ & a = a_t, \\ Q_t = (x, a), & \text{other}. \end{cases} \tag{11}$$

The virtual machines are scheduled according to the above rules to realize the adaptive deployment of IaaS cloud virtual machines.

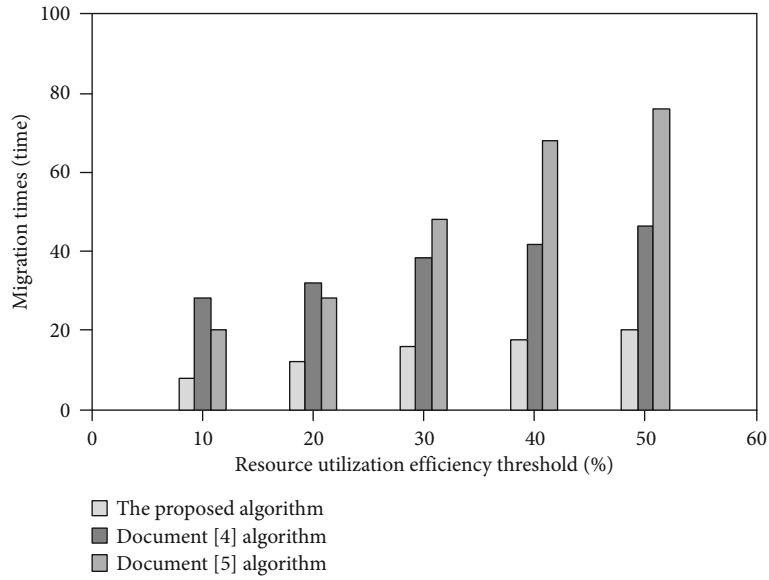

Figure 2: Comparison of the number of migrations by different algorithms.

3. Experiments and Results

In order to verify the overall effectiveness of the adaptive deployment algorithm for IaaS cloud virtual machines based on the Q learning mechanism, it is necessary to conduct related tests on the proposed algorithm. The switch in this test was a three-layer switch, with a power consumption of 80 W, physical machine power consumption of 750 W, and a network bandwidth capacity of 100 M.

The proposed algorithm, Reference [4] algorithm, and Reference [5] algorithm were used for comparison in the following tests.

3.1. Energy Consumption Test. The energy consumption of different algorithms in network congestion and noncongestion conditions was tested. The test results are shown in Figure 1.

From Figure 1, the energy consumption of the proposed algorithm did not change in the states with and without network congestion and was lower than that of Reference [4] algorithm and Reference [5] algorithm. The energy consumption of Reference [4] algorithm and Reference [5] algorithm in the state with network congestion was higher than that in the state without network congestion. Through the above analysis, it could be seen that the energy consumption of the proposed algorithm was not affected by network congestion. The reasons why the proposed algorithm simplified the learning process through a multistep Q learning algorithm based on the Q learning mechanism, and scheduling virtual machines improved the rationality of virtual machine deployment and reduced the energy consumption.

3.2. Analysis of the Number of Migrations. The number of migrations of the virtual machines of the proposed algorithm, Reference [4] algorithm, and Reference [5] algorithm was compared under different resource utilization efficiency thresholds. The analysis results are shown in Figure 2.

From Figure 2, it shows that when increasing the resource utilization efficiency threshold, the number of migrations of the three algorithms gradually increased. Through comparison, it could be seen that the number of migrations of the proposed algorithm was the smallest, indicating that the proposed algorithm completed the deployment of the IaaS cloud virtual machines through the least migrations.

3.3. Average SLA Violation Rate. The average SLA violation rate was used as a test indicator to compare the deployment effectiveness of the proposed algorithm, Reference [4] algorithm, and Reference [5] algorithm. The lower the average SLA violation rate, the better the deployment effect of the algorithm. The average SLA violation rate can be calculated by

$$\mathrm{SLA}_{\mathrm{violation}} = \frac{N_q - N_f}{N_q}, \tag{12}$$

where N_q represents the processing capacity of all requests and N_f represents the processing capacity corresponding to the allocated requests.

The average SLA violation rates of the proposed algorithm, Reference [4] algorithm, and Reference [5] algorithm are shown in Table 1.

From Table 1, it indicates that the average SLA violation rate for the proposed algorithm did not change after the resource utilization efficiency threshold reached 60%. For Reference [4] algorithm and Reference [5] algorithm, the obtained average SLA violation rate increased with the resource utilization efficiency threshold increasing. Through analysis, it could be seen that the average SLA

Table 1: The average SLA violation rates by different algorithms.

Resource utilization efficiency threshold (%)	Average SLA violation rate (%)		
	Proposed algorithm	Reference [4] algorithm	Reference [3] algorithm
10	0	4.2	3.9
20	0	5.6	4.8
30	0	5.9	5.7
40	0	6.5	6.7
50	0	6.8	7.5
60	5.0	7.5	8.8
70	5.0	8.0	9.4
80	5.0	8.4	9.8
90	5.0	8.9	10.4
100	5.0	9.5	11.7

violation rate of the proposed algorithm was the lowest, indicating the best deployment effect by the proposed algorithm.

4. Conclusion

Various cloud service providers have begun to establish big data centers in the context of the continuous reduction of communication traffic costs and the gradual increase of network bandwidth. The energy consumption of big data centers is high. Therefore, enterprises and governments need to construct environmentally friendly and energy-saving cloud data centers. Deploying virtual machines can improve service quality and reduce energy consumption.

At present, the virtual machine deployment algorithm has the problems of high energy consumption, high number of migrations, and high average SLA violation rate. An adaptive deployment algorithm for IaaS cloud virtual machines based on the Q learning mechanism is proposed. First, the deployment problem of the IaaS cloud virtual machines is analyzed. Then, the Q learning mechanism is used to realize the adaptive deployment of IaaS cloud virtual machines, reducing the energy consumption, number of migrations, and average SLA violation rate. The future work is to improve the running speed of the algorithm while ensuring the accuracy.

Data Availability

The labeled dataset used to support the findings of this study is available from the corresponding author upon request.

Conflicts of Interest

The author declares no competing interests.

Acknowledgments

The study is supported by 2019 Guangxi University's Young and Middle-aged Teachers' Basic Research Ability Improvement Project (2019KY1604).

References

[1] S. Qiao, Q. Zhang, and Q. Zhang, "Hybrid seismic-electrical data acquisition station based on cloud technology and green IoT," *IEEE Access*, vol. 8, pp. 31026–31033, 2020.

[2] M. K. Bouza, "Cloud technology is the foundation for designing efficient application," *Artificial Intelligence*, vol. 24, no. 1-2, pp. 14–23, 2019.

[3] M. Mohammadhosseini, A. T. Haghighat, and E. Mahdipour, "An efficient energy-aware method for virtual machine placement in cloud data centers using the cultural algorithm," *The Journal of Supercomputing*, vol. 75, no. 10, pp. 6904–6933, 2019.

[4] Z. Lei and L. Wang, "Virtual machine deployment and migration optimization mechanism for cloud data center," *Computer Engineering and Design*, vol. 40, no. 8, pp. 2216–2223, 2019.

[5] J. Liao, S. Qingxiao, and H. Yang, "Research on preemptible virtual machine instance configuration and scheduling methods that meet the execution time limit of workflow," *Computer Engineering and Science*, vol. 42, no. 11, pp. 1956–1964, 2020.

[6] L. Jiliang, Q. Bing, and L. Wenjiang, "A cloud virtual machine scheduling strategy combining wake-up threshold and semi-sleep mode," *Journal of Yanshan University*, vol. 44, no. 4, pp. 370–378, 2020.

[7] A. Ghasemi and A. T. Haghighat, "A multi-objective load balancing algorithm for virtual machine placement in cloud data centers based on machine learning," *Computing*, vol. 102, no. 9, pp. 2049–2072, 2020.

[8] M. H. Sayadnavard, A. T. Haghighat, and A. M. Rahmani, "A reliable energy-aware approach for dynamic virtual machine consolidation in cloud data centers," *Journal of Supercomputing*, vol. 75, no. 4, pp. 2126–2147, 2019.

[9] S. Jin, X. Qie, W. Zhao, W. Yue, and Y. Takahashi, "A clustered virtual machine allocation strategy based on a sleep-mode with wake-up threshold in a cloud environment," *Annals of Operations Research*, vol. 293, no. 1, pp. 193–212, 2020.

[10] H. Xu, P. Cheng, and Y. Liu, "A fault tolerance aware virtual machine scheduling algorithm in cloud computing," *International Journal of Performability Engineering*, vol. 15, no. 11, 2019.

[11] M. J. Usman, A. S. Ismail, H. Chizari et al., "Energy-efficient virtual machine allocation technique using flower pollination algorithm in cloud datacenter: a panacea to green computing," *Journal of Bionic Engineering*, vol. 16, no. 2, pp. 354–366, 2019.

[12] X. Xi, X. Cao, and P. Yang, "Network resource allocation for eMBB payload and URLLC control information communication multiplexing in a multi-UAV relay network," *IEEE Transactions on Communications*, vol. 69, no. 3, pp. 1802–1817, 2021.

[13] Z. Li and Z. Ding, "Distributed multiobjective optimization for network resource allocation of multiagent systems," *IEEE Transactions on Cybernetics*, 2020.

[14] T. Coorevits, S. Kossman, D. Chicot, F. Hennebelle, A. Montagne, and A. Iost, "Virtual machine concept applied to uncertainties estimation in instrumented indentation testing," *Journal of Materials Research*, vol. 34, no. 14, pp. 2501–2516, 2019.

[15] Z. Liang, Y. Liu, T.-M. Lok, and K. Huang, "Multi-cell mobile edge computing: joint service migration and resource

allocation," *IEEE Transactions on Wireless Communications*, vol. 20, no. 9, 2021.

[16] H. Qian, J. Yu, and L. Hua, "Relay selection algorithm based on social network combined with Q-learning for vehicle D2D communication," *IET Communications*, vol. 13, no. 20, pp. 3582–3587, 2019.

[17] Y. Fan, M. He, L. Su, and X.-. H. Zhou, "A smoothedQ-learning algorithm for estimating optimal dynamic treatment regimes," *Scandinavian Journal of Statistics*, vol. 46, no. 2, pp. 446–469, 2019.

[18] Y. Huang, B. Yang, M. Wang, B. Liu, and X. Yang, "Analysis of the future land cover change in Beijing using CA–Markov chain model," *Environmental Earth Sciences*, vol. 79, no. 2, pp. 1–12, 2020.

[19] L. Ricci, "Asymptotic distribution of sample Shannon entropy in the case of an underlying finite, regular Markov chain," *Physical Review E*, vol. 103, no. 2, article 022215, 2021.

[20] M. Zhang, S. Shi, W. Cheng, and Y. Shen, "Self-adaptive hyper-heuristic Markov chain evolution for generating vehicle multi-parameter driving cycles," *IEEE Transactions on Vehicular Technology*, vol. 69, no. 6, pp. 6041–6052, 2020.

[21] F. Brandon and B. Kosko, "Noise can speed Markov chain Monte Carlo estimation and quantum annealing," *Physical review: E*, vol. 100, no. 5-1, pp. 53309–53309, 2019.

[22] C. Smith, J. R. Lu, R. K. Thomas, I. M. Tucker, J. R. P. Webster, and M. Campana, "Markov chain modeling of surfactant critical micelle concentration and surface composition," *Langmuir*, vol. 35, no. 2, pp. 561–569, 2019.

[23] B. Cai, L. Zhang, and Y. Shi, "Control synthesis of hidden semi-Markov uncertain fuzzy systems via observations of hidden modes," *IEEE Transactions on Cybernetics*, vol. 50, no. 8, pp. 3709–3718, 2020.

Hindawi
Journal of Sensors
Volume 2021, Article ID 4475448, 11 pages
https://doi.org/10.1155/2021/4475448

Research Article

Social Effect Analysis of Intelligent Sports Based on Principal Component Analysis and Fuzzy Control

Xiaobo Chen

Sports Department, Shaanxi University of Science & Technology, Shaanxi Xian 710021, China

Correspondence should be addressed to Xiaobo Chen; chenxiaobo@sust.edu.cn

Received 29 August 2021; Revised 29 September 2021; Accepted 15 October 2021; Published 31 October 2021

Academic Editor: Mu Zhou

In order to explore the social effects of intelligent sports systems, this paper combines principal component analysis technology and fuzzy control technology to construct an intelligent sports social effect analysis system. The original fuzzy data is expressed linearly by structural elements, and the original fuzzy data matrix is divided into a main data matrix part and an error data matrix part. According to the principal component analysis method of fuzzy data represented by structural elements, this paper studies the principal component analysis method of interval data using the left end point matrix, right end point matrix, and midpoint matrix of interval data. In addition, this article uses principal component analysis and fuzzy control to study the response of the intelligent motion system to the masses and conducts experiments to analyze the social effects. It can be seen from experimental research that the intelligent sports system constructed in this article has a high degree of satisfaction of the masses, which proves that the intelligent sports have a certain social effect.

1. Introduction

With the development of wearable device technology, the mobile Internet has been further integrated into people's lives, and the use of smart devices in sports environments has become more frequent. As the wearable device with the largest market share in the current market, smart watches are of great significance to the study of their interface design in a sports environment, and to a certain extent, they have laid a design foundation for the development of the mobile Internet era. After smart watches entered the consumer market on a large scale in 2014, they were once considered to be smart personal terminal products that occupied a large number of markets after smart phones. However, by the second half of 2016, the survey showed that the growth rate of the smart watch market was far from reaching expectations, and the idle rates of purchased fitness trackers and smart watches were 30% and 29%, respectively [1]. The survey shows that 49.5% of the global population wear watches, but most people who buy smart watches are still early adopters of technology products. Although it has a good market prospect, the design ideas of existing smart watches continue to be in smart phones. The screen size limitations, mobility, and context sensitivity of smart watches also pose new challenges for interface design.

With the progress of society and the improvement of the quality of life, more people begin to pay attention to their own health and begin to pursue a healthy lifestyle. The emergence of wearable smart devices provides another new way for people to pursue a healthy lifestyle.

Through these intelligent hardware that can be worn on the human body, it can connect and accommodate a variety of advanced technologies such as wireless communication, microsensing, GPS positioning, virtual reality, and biometric identification. Moreover, it can also integrate the Internet and big data platforms to search, analyze, share, and feedback on the human body anytime and anywhere. There are various types of wearable smart devices, such as smart watches, glasses, necklaces, or clothes. In recent years, wearable smart devices have been popularized and gradually accepted and respected by consumers. Smart watches can detect various data of the user during sports, such as time, distance, heart rate, calories, and other data, and are accepted by more and more young consumers. With the

continuous improvement of technology, wearable smart devices have gradually shifted from focusing on hardware technology to more focusing on user experience. The improvement of interaction design has gradually increased the weight of smart watch design [2].

With the continuous popularization of smart sports equipment, it has caused a certain response in the society [3]. This article combines principal component analysis technology and fuzzy control technology to construct a social effect analysis system of intelligent sports and explores the response of intelligent sports equipment among the public.

2. Related Work

In recent years, the research and development of smart devices in the field of health monitoring at home and abroad have been very rapid, and the research on the detection of various physiological and physical parameters of the human body has been in-depth. The detected parameters mainly focus on body temperature, blood pressure, heart rate, pulse, fall, and so on. Along with the development of smart devices, the construction of sensor networks, big data, and cloud platforms is constantly deepening. The establishment of sports and health data centers is gradually changing the traditional methods of health monitoring and disease prevention and solving the problem of not having real-time performance when only relying on hospitals to diagnose diseases.

Smart watches have great application significance in personal life (for example, medical treatment), and it will become an important terminal in the science and technology ecosystem and penetrate into everyone's life [4]. Smart watches are used in family life and can be used to recognize human body abnormalities, recognize sleep conditions, and recognize gestures and other life situations [5]. Its core function is to monitor the health status at any time, and it is considered as a portable health assistant for humans [6]. In addition to life, smart watches also have better applications in work. Compared with smart phones, smart watches make tasks (for example, receiving notification information) more efficient and easier when completing some specific tasks [7].

When the smart watch is combined with other smart devices, some device interaction functions can be realized. The literature [8] integrated applications into smart watches to make the cross-device interaction between smart watches and smart phones a way to extend the terminal. The literature [9] further developed the joint interaction between smart watch and mobile phone, such as jointly completing touch input and screen expansion. The smart watch can also interact with the computer. When the user wears the watch for keyboard input, through the analysis of the smart watch sensor data, the characters typed by the test can be roughly estimated. When typing an English word with more than 6 characters, there are 10 possible options that can be identified. The loss of visible information causes a certain degree of difficulty in accurate recognition. The wearability of smart watches makes it possible for designers to use built-in sensor technology to capture motion and then perform data analysis and interact with other devices. The literature [10] first analyzed its necessity, and the literature [11] developed a gesture recognition system to solve the problems of high-level interference, transmission data delay, and neglected actions. Based on action recognition, a smart watch-based App was developed, which mainly realizes functions such as controlling the opening and closing of the office door, obtaining information in the house, and simulating door knocking [12]. In addition, literature [13] developed another set of systems involving smart watches and mobile phones to interact with smart TVs. By capturing the movement of the hand wearing the smart watch in the air, the direction the user's hand that is pointing can be recognized. By comparing this method with the method using dedicated forearm sensors (Mypoint) and the method using camera capture technology (Vicon), it is found that the results of the smart watch solution can reach a relatively professional level [14]. In addition, by combining smart watches and smart phones to monitor the user's human activities, the interference of smart device notifications to workers can be reduced. By identifying whether the worker is working or resting, the system under study can adjust the notification push. The results of the research show that this method can significantly reduce the perceived workload of workers [15].

Information processing is the central part, mainly through the central processing unit to analyze and process the signals transmitted by the information detection unit, and schedule other hardware parts to jointly complete the predetermined tasks. This layer is the core layer of the entire smart clothing hardware part, with the function of intelligent decision-making. The pros and cons of information processing technology are directly related to the accuracy of signal processing, the complexity of calculation methods, and the size of power consumption [16]. The central processing unit is the core component of information processing, and the Bluetooth module transmits the data processed by the central processing unit to the external mobile terminal. Information feedback is to transmit the conclusion obtained by the analysis of the information processing unit to the monitoring platform terminal and feedback to the monitoring object in time, so that the monitoring individual or the monitoring center can react in real time. Existing transmission methods can be divided into two categories: wired and wireless transmission. The communication methods described in this article are mainly wireless transmission methods based on Bluetooth. The terminal application module mainly assists users in assessing their own physiological and physical conditions through the analysis of body data and gives users a good experience in a more flexible and intuitive way on the software interface [17].

The literature [18] concluded that wearable acceleration sensors can easily identify the gait performance of walking in daily environments. Compared with other devices, the acceleration sensor has the characteristics of portability and light cost and is considered to be an ideal choice for evaluating human movement and balance changes. Therefore, many researchers have specially designed sensors for acceleration data collection. Considering that the center of gravity of the body is close to the waist of the human body, most of these studies use sensors installed on the waist of the human body to measure gait characteristics [19]. In addition, because acceleration sensors are usually built into smart

handheld devices, some researchers use such off-the-shelf products to measure body acceleration data during walking [20]. The results of the study show that the accuracy of gait measurement using an Android-based smartphone is equivalent to that of a customized three-axis accelerometer sensor [21], which expands new ideas for subsequent research.

2.1. The Main Matrix and Error Matrix of the Fuzzy Data Matrix. The classic principal component analysis method can directly process accurate data, but it cannot directly process fuzzy data represented by structural elements linearly. For this reason, this paper processes the fuzzy data matrix linearly represented by structural elements, divides the fuzzy data matrix into the main matrix part and the error matrix part, and uses the classical principal component analysis method to process the main matrix and the error matrix, respectively.

If there are n observation samples, and p indicators X_1, $X_2, \cdots, X_p$ are observed for each sample, the original sample data matrix is obtained as:

$$X = \begin{bmatrix} x_{11} & x_{12} & \cdots & x_{1p} \\ x_{21} & x_{22} & \cdots & x_{2p} \\ \vdots & \vdots & \ddots & \vdots \\ x_{n1} & x_{n2} & \cdots & x_{np} \end{bmatrix} = (X_1, X_2, \cdots, X_p). \tag{1}$$

In the formula, $X_i = (x_{1i}, x_{2i}, \cdots, x_{ni}), i = 1, 2, \cdots, p$.

For fuzzy principal component analysis, the object it studies is fuzzy data; that is, the data matrix under the condition that all samples is fuzzy data.

$$\tilde{X} = \begin{bmatrix} \tilde{x}_{11} & \tilde{x}_{12} & \cdots & \tilde{x}_{1p} \\ \tilde{x}_{21} & \tilde{x}_{22} & \cdots & \tilde{x}_{2p} \\ \vdots & \vdots & \ddots & \vdots \\ \tilde{x}_{n1} & \tilde{x}_{n2} & \cdots & \tilde{x}_{np} \end{bmatrix}. \tag{2}$$

It is assumed that all fuzzy data can be linearly generated by the fuzzy structure element E, namely:

$$\tilde{x}_{ij} = a_{ij} + b_{ij}E(b_{ij} \geq 0), i = 1, 2, \cdots, n; j = 1, 2, \cdots, p. \tag{3}$$

Then, there is

$$\begin{aligned} \tilde{X} &= \begin{bmatrix} a_{11} + b_{11}E & a_{12} + b_{12}E & \cdots & a_{1p} + b_{1p}E \\ a_{21} + b_{21}E & a_{22} + b_{22}E & \cdots & a_{2p} + b_{2p}E \\ \vdots & \vdots & \ddots & \vdots \\ a_{n1} + b_{n1}E & a_{n2} + b_{n2}E & \cdots & a_{np} + b_{np}E \end{bmatrix} \\ &= (\tilde{X}_1, \tilde{X}_2, \cdots, \tilde{X}_p). \end{aligned} \tag{4}$$

In the formula,

$$\tilde{X}_j = \begin{pmatrix} a_{1j} + b_{1j}E \\ a_{2j} + b_{2j}E \\ \vdots \\ a_{nj} + b_{nj}E \end{pmatrix} = A_j + B_jE, j = 1, 2, \cdots, p. \tag{5}$$

The fuzzy data matrix $\tilde{X}$ can be divided into two parts:

$$\begin{aligned} \tilde{X} &= \begin{bmatrix} a_{11} + b_{11}E & a_{12} + b_{12}E & \cdots & a_{1p} + b_{1p}E \\ a_{21} + b_{21}E & a_{22} + b_{22}E & \cdots & a_{2p} + b_{2p}E \\ \vdots & \vdots & \ddots & \vdots \\ a_{n1} + b_{n1}E & a_{n2} + b_{n2}E & \cdots & a_{np} + b_{np}E \end{bmatrix} \\ &= \begin{bmatrix} a_{11} & a_{12} & \cdots & a_{1p} \\ a_{21} & a_{22} & \cdots & a_{2p} \\ \vdots & \vdots & \ddots & \vdots \\ a_{n1} & a_{n2} & \cdots & a_{np} \end{bmatrix} + \begin{bmatrix} b_{11} & b_{12} & \cdots & b_{1p} \\ b_{21} & b_{22} & \cdots & b_{2p} \\ \vdots & \vdots & \ddots & \vdots \\ b_{n1} & b_{n2} & \cdots & b_{np} \end{bmatrix} E \\ &= M + \mathrm{WE}. \end{aligned} \tag{6}$$

The matrix M is called the main matrix of the fuzzy data matrix $\tilde{X}$, and W is called the error matrix of the fuzzy data matrix $\tilde{X}$. The main matrix M and the error matrix W divide the fuzzy data into the main data part and the error data part.

In fuzzy analysis, interval number, as a special case of fuzzy number, represents a kind of uncertainty and has a wide range of applications in various fields. When conducting principal component analysis, if the data obtained is not deterministic data but interval data, how to obtain the principal components of interval data is the research focus.

If there are n observation samples, and P indicators X_1, $X_2, \cdots, X_p$ are observed for each sample, the original sample data matrix is obtained as:

$$X = \begin{bmatrix} x_{11} & x_{12} & \cdots & x_{1p} \\ x_{21} & x_{22} & \cdots & x_{2p} \\ \vdots & \vdots & \ddots & \vdots \\ x_{n1} & x_{n2} & \cdots & x_{np} \end{bmatrix} = (X_1, X_2, \cdots, X_p). \tag{7}$$

In the formula, $X_i = (x_{1i}, x_{2i}, \cdots, x_{ni})^T, i = 1, 2, \cdots, p$.

For the principal component analysis method based on interval data, the object it studies is interval data; that is, all samples are interval data. Then, there is

Cloud security management	Cloud computing management
Traditional applications and services	Big data applications and services
Virtualization resource tools	Investigate analysis and extract parallel algorithms
Flexible resource plan management	Parallel computing
Virtualization technology	Distributed storage
Cloud computing resources and platforms	

Figure 1: Key contents of cloud computing.

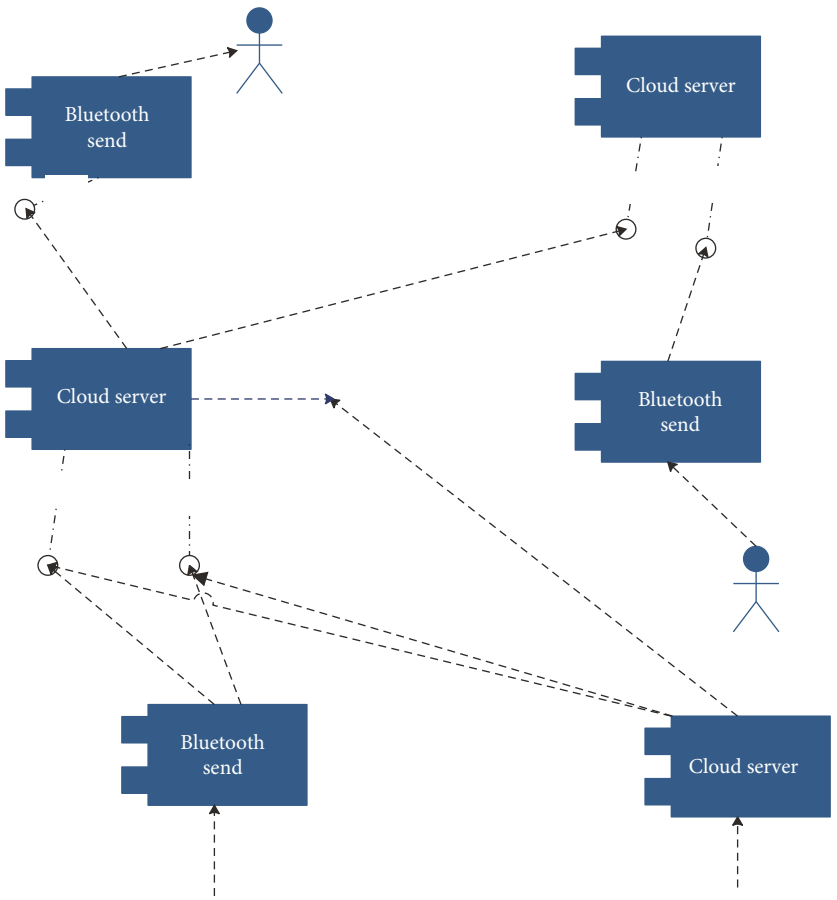

Figure 2: WebSocket protocol agreement.

$$\tilde{X} = \begin{bmatrix} \tilde{x}_{11} & \tilde{x}_{12} & \cdots & \tilde{x}_{1p} \\ \tilde{x}_{21} & \tilde{x}_{22} & \cdots & \tilde{x}_{2p} \\ \vdots & \vdots & \ddots & \vdots \\ \tilde{x}_{n1} & \tilde{x}_{n2} & \cdots & \tilde{x}_{np} \end{bmatrix}. \quad (8)$$

In the formula, $\tilde{x}_{ij} = [a_{ij}, b_{ij}], i = 1, 2, \cdots, n; j = 1, 2, \cdots, p$ is the interval number, so the obtained interval data sample matrix is

$$\tilde{X} = \begin{bmatrix} [a_{11}, b_{11}] & [a_{12}, b_{12}] & \cdots & [a_{1p}, b_{1p}] \\ [a_{21}, b_{21}] & [a_{22}, b_{22}] & \cdots & [a_{2p}, b_{2p}] \\ \vdots & \vdots & \ddots & \vdots \\ [a_{n1}, b_{n1}] & [a_{n2}, b_{n2}] & \cdots & [a_{np}, b_{np}] \end{bmatrix} = \left(\tilde{X}_1, \tilde{X}_2, \cdots, \tilde{X}_p\right). \quad (9)$$

In the formula,

$$\tilde{X}_j = \begin{pmatrix} [a_{1j}, b_{1j}] \\ [a_{2j}, b_{2j}] \\ \vdots \\ [a_{nj}, b_{nj}] \end{pmatrix}, j = 1, 2, \cdots, p. \quad (10)$$

We set $c_{ij} = ((a_{ij} + b_{ij})/2), i = 1, 2, \cdots, n; j = 1, 2, \cdots, p$ is the midpoint of a_{ij} and b_{ij}, and

$$\begin{aligned} A &= \left(a_{1j}, a_{2j}, \cdots, a_{nj}\right), j = 1, 2, \cdots, p, \\ B &= \left(b_{1j}, b_{2j}, \cdots, b_{nj}\right), j = 1, 2, \cdots, p, \\ C &= \left(c_{1j}, c_{2j}, \cdots, c_{nj}\right), j = 1, 2, \cdots, p. \end{aligned} \quad (11)$$

Then, A, B, and C are three data matrices. A is the matrix formed by the left end of the interval data, B is the matrix formed by the right end of the interval data, and C is the matrix formed by the midpoint of the interval data. Next, according to the classic principal component analysis method, the coefficient vectors $a_j^0, b_j^0, c_j^0, j = 1, 2, \cdots, m$ of the principal components of the three data matrices A, B, and C are, respectively, obtained.

For the principal component analysis of fuzzy data, the original fuzzy data is divided into the main data part and the error data part. For the principal component analysis of interval data, the interval data matrix is divided into three data matrices A, B, and C, namely, the left end data matrix, the right end data matrix, and the midpoint data matrix. Then, the classical principal component analysis method is used to obtain the coefficient vector $a_j^0, b_j^0, c_j^0, j = 1, 2, \cdots, m$ of the three principal components, and the coefficient vector $k_j^0, j = 1, 2, \cdots, m$ of the principal component of the original interval data is obtained through the combination of the coefficient vector a_j^0, b_j^0, c_j^0 of the principal component.

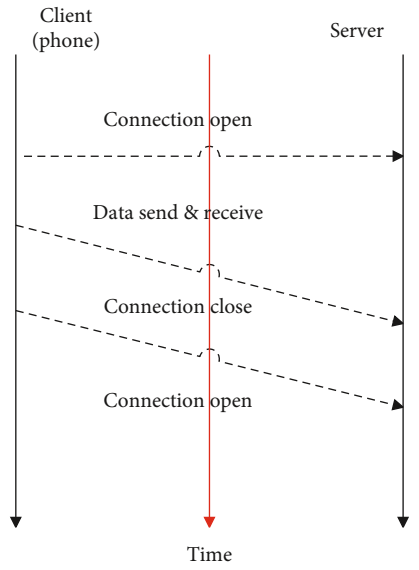

Figure 3: The communication process between the mobile phone and the server implemented by WebSocket.

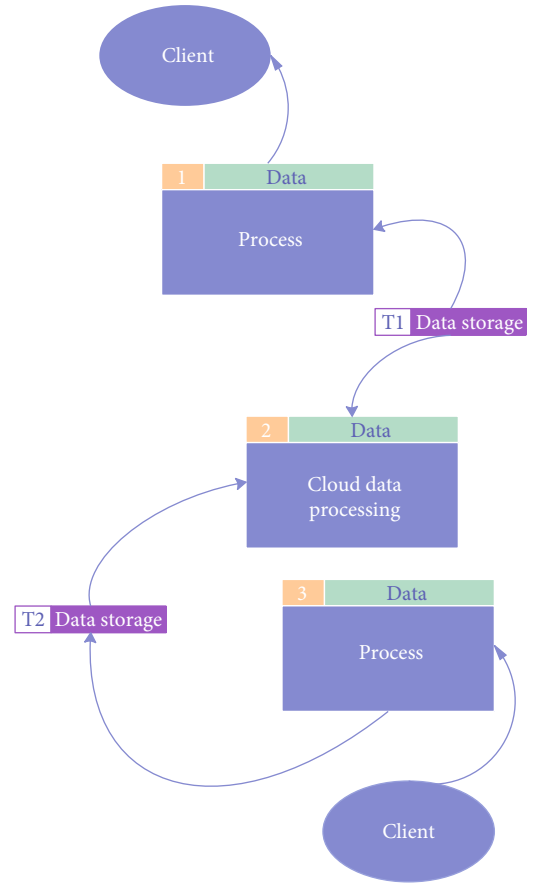

Figure 4: Data cloud storage model.

We assume that the coefficient vector of the principal component of the original interval data is k_j^0, the coefficient vector of the principal component of the left endpoint data

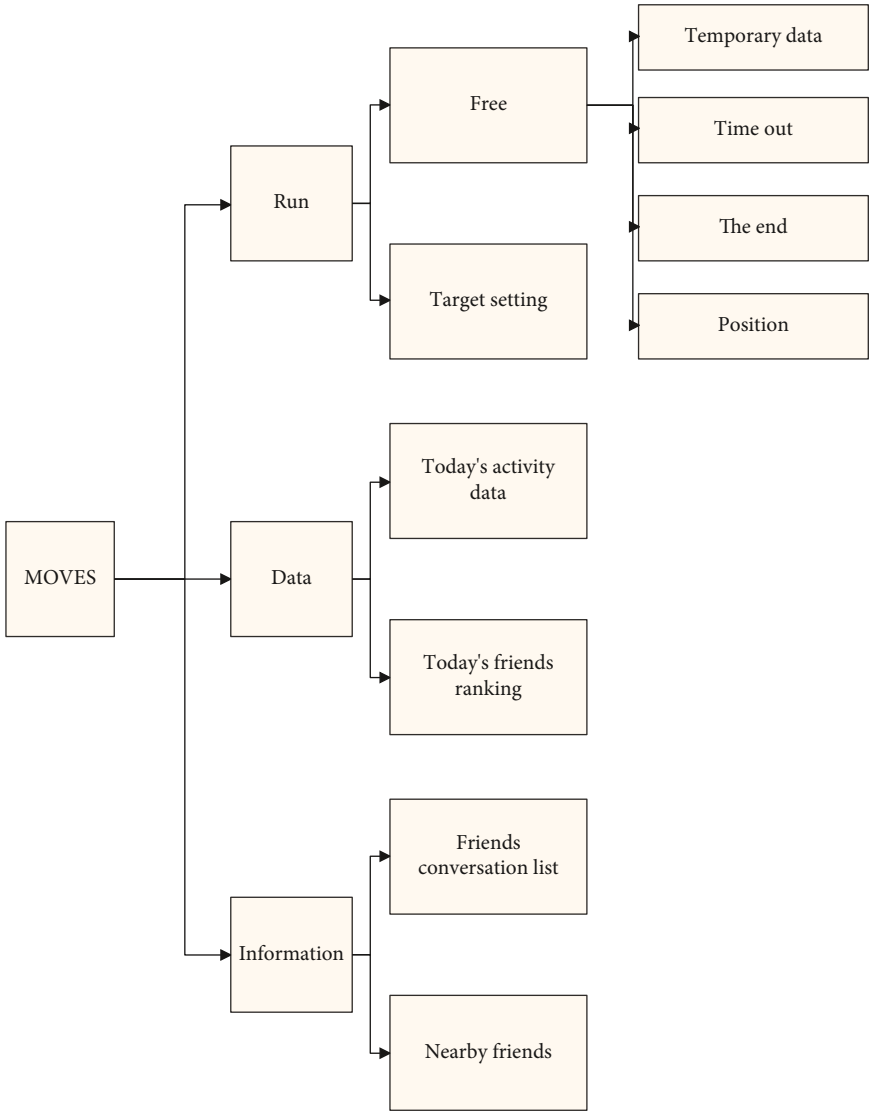

Figure 5: Information architecture diagram 1.

matrix A is a_j^0, the coefficient vector of the principal component of the right endpoint data matrix B is b_j^0, and the coefficient vector of the principal component of the midpoint data matrix c is c_j^0. Then, the relationship between $k_j^0, a_j^0, b_j^0, c_j^0$ can be expressed as:

$$\begin{aligned} &k_j^0 = \lambda a_j^0 + \omega b_j^0 + (1-\lambda-\omega)c_j^0, \\ &\lambda, \omega \in [0,1], \lambda + \omega < 1, j = 1, 2, \cdots, m. \end{aligned} \tag{12}$$

After selecting the value of λ, ω, $k_j^0, j = 1, 2, \cdots, m$ is obtained.

If $(k_1^0)^2 + (k_2^0)^2 + \cdots + (k_m^0)^2 = 1$, the principal component expression of interval data is

$$\tilde{F}_1 = k_1^0 \tilde{X}_1 + k_2^0 \tilde{X}_2 + \cdots + k_m^0 \tilde{X}_m, \tag{13}$$

$$\tilde{F}_i = k_1^i \tilde{X}_1 + k_2^i \tilde{X}_2 + \cdots + k_m^i \tilde{X}_m. \tag{14}$$

If $(k_1^0)^2 + (k_2^0)^2 + \cdots + (k_m^0)^2 \neq 1$, in order to make $(k_1^0)^2 + (k_2^0)^2 + \cdots + (k_m^0)^2 = 1$, we set

$$\left(k_1^0\right)^2 + \left(k_2^0\right)^2 + \cdots + \left(k_m^0\right)^2 = D, \tag{15}$$

$$\left(\frac{k_1^0}{\sqrt{D}}\right)^2 + \left(\frac{k_2^0}{\sqrt{D}}\right)^2 + \cdots + \left(\frac{k_m^0}{\sqrt{D}}\right)^2 = 1. \tag{16}$$

Then, the coefficient vector of the principal component analysis of the interval data is

$$\beta_1^0 = \frac{k_1^0}{\sqrt{D}}, \beta_2^0 = \frac{k_2^0}{\sqrt{D}}, \cdots, \beta_m^0 = \frac{k_m^0}{\sqrt{D}}. \tag{17}$$

The principal component expression of interval data is

$$\tilde{F}_1 = \beta_1^0 \tilde{X}_1 + \beta_2^0 \tilde{X}_2 + \cdots + \beta_m^0 \tilde{X}_m, \tag{18}$$

$$\tilde{F}_i = \beta_1^i \tilde{X}_1 + \beta_2^i \tilde{X}_2 + \cdots + \beta_m^i \tilde{X}_m. \tag{19}$$

We assume that the coefficient vector of the principal component of the original interval data is k_j^0, the coefficient vector of the principal component of the left endpoint data matrix A is a_j^0, the coefficient vector of the principal component of the right endpoint data matrix B is b_j^0, and the coefficient vector of the principal component of the midpoint data matrix c is c_j^0. Then, the relationship between $k_j^0, a_j^0, b_j^0, c_j^0$ can be expressed as:

$$k_j^0 = \frac{\left|a_j^0\right|}{\left|a_j^0\right| + \left|b_j^0\right| + \left|c_j^0\right|} a_j^0 + \frac{\left|b_j^0\right|}{\left|a_j^0\right| + \left|b_j^0\right| + \left|c_j^0\right|} b_j^0 + \frac{\left|c_j^0\right|}{\left|a_j^0\right| + \left|b_j^0\right| + \left|c_j^0\right|} c_j^0. \tag{20}$$

According to the relevant steps, the principal component expression of the interval data is finally obtained.

2.2. Intelligent Sports System Based on Principal Component Analysis and Fuzzy Control. Before constructing the motion system, first analyze the system requirements.

Clear and visible at a glance: use black as the background of the smart device, and try not to use bright background colors in the background of the interface. On the one hand, it is to improve the readability of graphics and text. On the other hand, the black background can be seamlessly integrated with the black frame of the device, giving users no visual effect on the edge of the screen. At the same time, it will save power and extend the standby time. It is still necessary for small size equipment.

High efficiency: stable application, smooth animation, and convenient interaction are all high efficiency performance. The interaction of applications on smart devices should be in the simplest state, reducing the frequency of interface jumps, using very few interface completion functions to increase continuity, and minimize application interaction costs. Keep the text of the current page visually, set global functions, flatten the usage path, and reduce the user's memory burden.

Mobile design: the interface design of smart devices is different from that of mobile phones. It is more limited by a smaller visual space and more mobile usage scenarios. Therefore, to redesign, you cannot directly move the ready-made applications on the mobile phone, but the design style must be consistent with the style of the mobile application interface, including color tone, flattening, dynamic effects, or some special effects.

Color: try to choose bright and strong colors. Strong contrasting colors can increase the readability of pictures and text. Different colors can also be used to distinguish interactive areas. As a mobile device, the use environment of a smart device may include strong light or a dim environment.

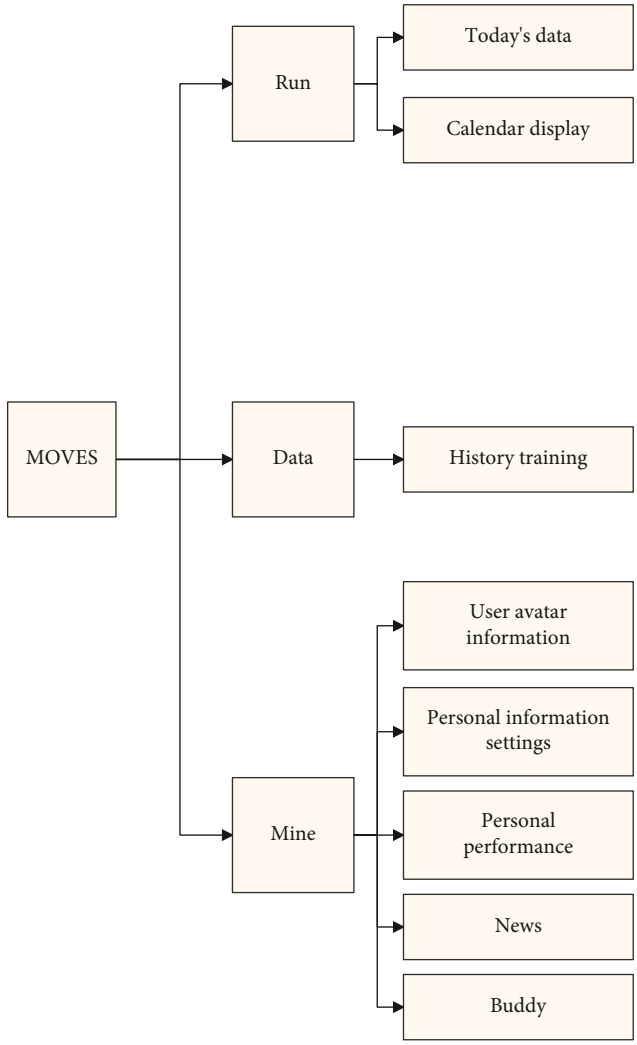

Figure 6: Information architecture diagram 2.

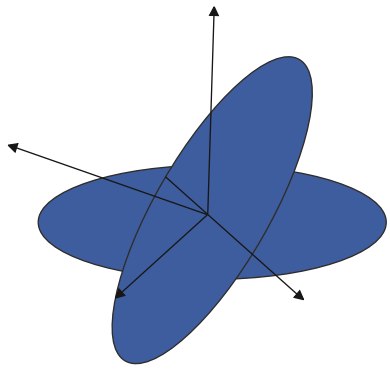

Figure 7: Euler space angle system.

Therefore, in order to ensure that pictures and text can be clearly seen in different environments, the choice of color is very important. To avoid low-saturation and softer colors, bright colors or high-saturation colors are better choices. Combining these colors with black or white fonts will achieve extremely high visual effects.

Table 1: Statistical table of the health information collection effect of the intelligent sports system.

Num	Health information collection effect	Num	Health information collection effect	Num	Health information collection effect
1	85.97	25	88.36	49	89.56
2	88.60	26	80.08	50	90.39
3	90.49	27	87.36	51	89.20
4	86.48	28	88.42	52	90.55
5	89.31	29	88.78	53	80.62
6	86.53	30	81.25	54	82.44
7	79.79	31	88.15	55	86.75
8	84.88	32	89.94	56	85.41
9	83.23	33	84.11	57	80.10
10	80.20	34	82.81	58	89.70
11	79.86	35	86.90	59	86.73
12	82.24	36	81.95	60	85.43
13	90.76	37	88.65	61	83.06
14	85.03	38	83.73	62	87.45
15	79.17	39	83.72	63	84.70
16	83.28	40	80.94	64	83.50
17	87.79	41	90.49	65	88.14
18	84.49	42	81.14	66	82.38
19	88.91	43	80.16	67	90.46
20	83.30	44	90.46	68	81.99
21	89.69	45	80.59	69	84.17
22	84.23	46	79.44	70	84.27
23	88.01	47	89.06	71	87.87
24	79.85	48	79.28	72	79.65

The establishment of big data and cloud computing platforms relies on some basic technologies, including the establishment of sensor networks and data centers. For big data, a flexible hardware infrastructure is a crucial part of realizing data storage. These hardware infrastructures include a large amount of flexible and shared information and communication technology resources. These information and communication technologies can be expanded and contracted horizontally or vertically and dynamically configured according to different application requirements. The advantages of cloud computing over the years have changed the way people obtain and use hardware infrastructure and software services. This view is mainly derived from the evolution of public computing and virtualized infrastructure. The key components of cloud computing are described in Figure 1.

For big data, the data center is not only the center of data storage but also needs to bear more responsibilities such as obtaining data, managing data, and mining the potential value and functions of data. The main focus of the data center is on the "data" rather than the "center." A data center has a large amount of data and managers and manages the data according to its core goals and development path, which is more valuable than having a good website and resources. The development of big data brings more development opportunities to the establishment of future data centers and at the same time faces greater challenges.

Big data requires strong back-end support from the data center. Big data places more stringent requirements on data centers in terms of storage capacity, processing capacity, and network transmission capacity. Only when a highly efficient, stable, secure, and scalable data center is established can the application of big data be ensured. The growing application of big data has also accelerated the reform of data centers. Many big data applications have developed their own unique structures and directly promoted the development of storage, network, and computing technologies related to data centers. With the continuous growth of structured and semi-structured data forms, the means of analyzing data become more diversified, and data centers should strengthen their data processing and computing capabilities. Big data has given the data center more functions. For big data, the data center should not only focus on the establishment of hardware infrastructure but also strengthen software capabilities. This capability includes the acquisition, processing, management, analysis, and application of big data. The establishment of a monitoring center that sports and body temperature monitoring smart clothing will rely on in the future will place more emphasis on analysis and application, which will be an innovation in monitoring methods.

WebSocket is a technology invented to connect the client and the server. The WebSocket protocol is essentially a TCP-based protocol. It first initiates a special http request through the HTTP/HTTPS protocol for handshake and then creates

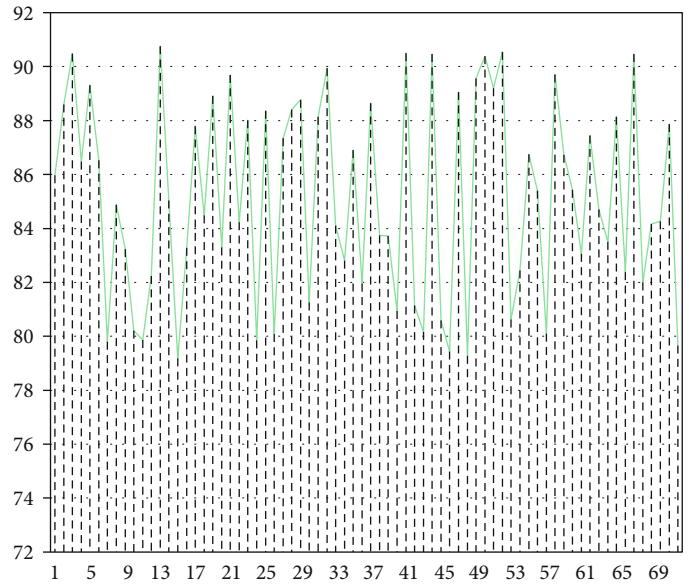

Figure 8: Statistical diagram of the health information collection effect of the intelligent sports system.

Table 2: Statistical table of crowd satisfaction of intelligent sports system.

Num	Crowd satisfaction	Num	Crowd satisfaction	Num	Crowd satisfaction
1	92.20	25	94.16	49	82.03
2	88.89	26	92.15	50	92.09
3	92.87	27	92.12	51	88.88
4	85.43	28	93.32	52	91.05
5	94.67	29	91.54	53	83.30
6	89.80	30	90.92	54	87.24
7	85.64	31	94.07	55	84.45
8	82.18	32	93.03	56	91.89
9	92.92	33	94.45	57	91.38
10	85.67	34	86.51	58	87.85
11	83.17	35	83.88	59	82.65
12	85.35	36	87.62	60	91.34
13	85.35	37	90.53	61	82.85
14	83.47	38	86.43	62	91.20
15	86.69	39	83.26	63	90.59
16	91.87	40	90.97	64	92.22
17	85.29	41	89.80	65	85.98
18	86.36	42	85.30	66	86.92
19	83.13	43	92.51	67	82.04
20	82.63	44	82.65	68	88.98
21	86.63	45	92.15	69	89.01
22	83.77	46	90.82	70	93.48
23	88.82	47	88.54	71	84.53
24	88.34	48	85.21	72	88.14

a stable TCP connection to facilitate data exchange. After the connection is established, the server and the client can carry out real-time communication services through this TCP connection, and this communication mode is two-way communication, as shown in Figure 2. Figure 3 shows the communication process between the mobile phone and the server through WebSocket.

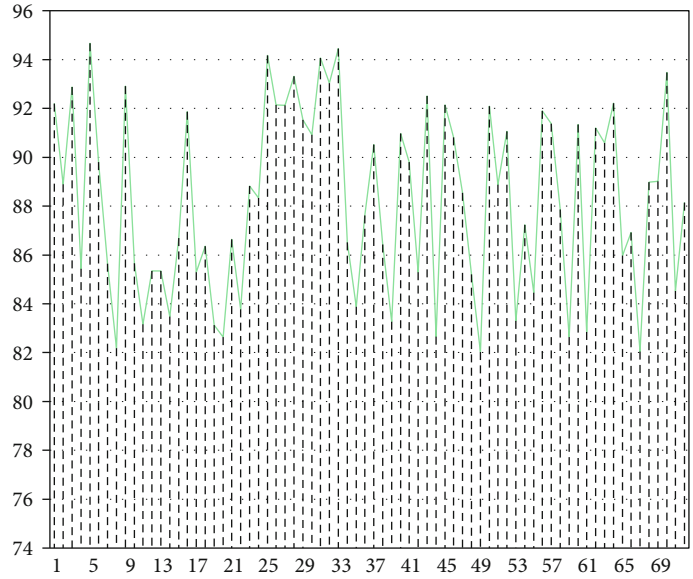

Figure 9: Statistical diagram of crowd satisfaction of intelligent sports system.

Because Mongo has a powerful query language and its syntax is a bit similar to object-oriented, most functions such as single-table query of relational database can be realized by it, and the form index function can be easily realized. The data cloud storage model is shown in Figure 4.

The system information architecture diagram constructed in this paper is shown in Figures 5 and 6.

This article draws on Euler's angle system in the aspect of system induction. As shown in Figure 7, an Euler space angle system is used to determine the position of a fixed-point rotating rigid body with a set of three independent angle parameters, consisting of nutation angle α, precession angle (i.e., precession angle) β, and rotation angle γ. Relative to the spatial reference system (blue), the reference system (red) fixed to the rigid body undergoes spatial rotation. At this time, the angle between the z axis and the Z axis is α, the angle between the x axis and the N axis (the intersection line of the xy plane and the XY plane) is β, and the angle between the X axis and the N axis is γ.

2.3. Analysis of Social Effects of Intelligent Sports Systems Based on Principal Component Analysis and Fuzzy Control. This article analyzes the effects of the intelligent sports system in the society and combines the intelligent sports system constructed in this article to study the reaction of the intelligent system in the masses through experimental analysis. On the basis of the above analysis, this article designs experiments to first verify the system's function of collecting people's health information through grouping experiments. The data obtained is shown in Table 1 and Figure 8.

From the above analysis results, the system constructed in this paper basically meets the basic requirements of sports health information collection. On this basis, this article uses the satisfaction survey method to study the response of the intelligent sports system in the masses. The results are shown in Table 2 and Figure 9.

From the above statistical results, the intelligent sports system constructed in this article has a good response in the masses. It can be seen that the intelligent sports system has a certain social effect and will definitely play a more important role in the health management of the masses in the future.

3. Conclusion

This article makes a systematic review of the current research status of smart sports equipment and analyzes the direction and focus of the next research. This paper develops the research content of the predecessors through experimental methods and continuously refines the information volume and information density presentation based on the previous research on the model structure, system display form, and layout. Moreover, this article conducts an in-depth study on the interface operation and gesture operation of using smart sports equipment in the sports state.

The research purpose of this article is mainly to conduct research on the reaction of the intelligent motion system in the social masses through principal component analysis and fuzzy control. Moreover, this article combines the intelligent motion system constructed in this article to analyze and study the response of the intelligent sports system in the masses through experiments. From the research results, it can be seen that the intelligent sports system constructed in this article has a good response among the masses, and it can be seen that the intelligent sports have a certain social effect.

Data Availability

The labeled dataset used to support the findings of this study are available from the corresponding author upon request.

Conflicts of Interest

The author declares no competing interests.

Acknowledgments

This study is sponsored by the Project of special scientific research plan of Shaanxi Provincial Department of Education, development and research of college students' fitness prescription system based on Wed database management system (No. 11jk0435).

References

[1] C. A. Emery and K. Pasanen, "Current trends in sport injury prevention," *Best Practice & Research Clinical Rheumatology*, vol. 33, no. 1, pp. 3–15, 2019.

[2] V. M. Shulyatyev and M. A. Bulavina, "Sport interview: strategy, design and content," *Theory and Practice of Physical Culture*, vol. 9, pp. 18–18, 2019.

[3] L. J. Ferguson, K. T. Carlson, and D. Rogers, "Moving towards reconciliation through sport: Sharing our process of exploring team Saskatchewan experiences at the North American Indigenous Games," *Journal of Exercise, Movement, and Sport (SCAPPS refereed abstracts repository)*, vol. 51, no. 1, pp. 99–99, 2019.

[4] K. Kimasi, V. Shojaei, and M. R. Boroumand, "Investigation of safety conditions at gymnasia in different organizations," *Journal of Humanities Insights*, vol. 3, no. 2, pp. 70–74, 2019.

[5] K. Reinhart and B. Wichmann, "The TuS Fortschritt Magdeburg-Neustadt (soccer section) in the GDR–an example of amateur socialist sport," *Soccer & Society*, vol. 21, no. 4, pp. 408–420, 2020.

[6] C. Abanazir, "E-sport and the EU: the view from the English Bridge Union," *The International Sports Law Journal*, vol. 18, no. 3-4, pp. 102–113, 2019.

[7] A. Gerke, K. Babiak, G. Dickson, and M. Desbordes, "Developmental processes and motivations for linkages in cross-sectoral sport clusters," *Sport Management Review*, vol. 21, no. 2, pp. 133–146, 2018.

[8] A. I. Pogrebnoy and I. O. Komlev, "Sport institutions reporting to Ministry of Sport of Russian Federation: intellectual property, invention activity, patenting and legal consulting service analysis," *Theory and Practice of Physical Culture*, vol. 2, 2018.

[9] D. C. Ilies, R. Buhas, and M. Ilies, "Sport activities and leisure in Nature 2000 protected area-Red Valley, Romania," *Journal of Environmental Protection and Ecology*, vol. 19, no. 1, pp. 367–372, 2018.

[10] A. I. Kondrukh, "Practical shooting sport in Russian sport system: essential specifications and features," *Theory and Practice of Physical Culture*, vol. 5, pp. 27–27, 2017.

[11] R. Giulianotti and D. Numerato, "Global sport and consumer culture: an introduction," *Journal of Consumer Culture*, vol. 18, no. 2, pp. 229–240, 2018.

[12] A. G. Gurinovich and G. V. Petrova, "Key priorities of physical education and sport sector budgeting laws and regulations in the Russian Federation," *Theory and Practice of Physical Culture*, vol. 4, pp. 34–34, 2019.

[13] M. Mountjoy, A. Costa, R. Budgett et al., "Health promotion through sport: international sport federations' priorities, actions and opportunities," *British Journal of Sports Medicine*, vol. 52, no. 1, pp. 54–60, 2018.

[14] J. J. Pulido, D. Sánchez-Oliva, P. A. Sánchez-Miguel, D. Amado, and T. García-Calvo, "Sport commitment in young soccer players: a self-determination perspective," *International Journal of Sports Science & Coaching*, vol. 13, no. 2, pp. 243–252, 2018.

[15] J. Cristiani, J. C. Bressan, and B. L. Pérez, "Clubs socio-deportivos en un municipio brasileño: espacio, equipos y contenidos [Sport clubs in Brazil: facilities, equipment and content in][Clubes socio-esportivos em município brasileiro: Espaço, equipamentos e conteúdos]," *E-balonmano. com: Revista de Ciencias del Deporte*, vol. 13, no. 2, pp. 105–112, 2017.

[16] E. Happ, M. Schnitzer, and M. Peters, "Sport-specific factors affecting location decisions in business to business sport manufacturing companies: a qualitative study in the Alps," *International Journal of Sport Management and Marketing*, vol. 21, no. 1/2, pp. 21–48, 2021.

[17] M. Castro-Sánchez, F. Zurita-Ortega, and R. Chacón-Cuberos, "Motivation towards sport based on sociodemographic variables in university students from Granada," *Journal of Sport and Health Research*, vol. 11, no. 1, pp. 55–68, 2019.

[18] S. M. Hadlow, D. Panchuk, D. L. Mann, M. R. Portus, and B. Abernethy, "Modified perceptual training in sport: a new classification framework," *Journal of Science and Medicine in Sport*, vol. 21, no. 9, pp. 950–958, 2018.

[19] J. H. Du Plessis and M. Berteanu, "The importance of prosthetic devices in sport activities for Romanian amputees who compete in Paralympic competitions," *Medicina Sportiva: Journal of Romanian Sports Medicine Society*, vol. 16, no. 1, pp. 3197–3204, 2020.

[20] M. Stylianou, A. Hogan, and E. Enright, "Youth sport policy: the enactment and possibilities of 'soft policy' in schools," *Sport, Education and Society*, vol. 24, no. 2, pp. 182–194, 2019.

[21] S. A. Richmond, A. Donaldson, A. Macpherson et al., "Facilitators and barriers to the implementation of iSPRINT: a sport injury prevention program in junior high schools," *Clinical Journal of Sport Medicine*, vol. 30, no. 3, pp. 231–238, 2020.

Hindawi
Journal of Sensors
Volume 2021, Article ID 2017208, 12 pages
https://doi.org/10.1155/2021/2017208

Research Article

Fast Construction of the Radio Map Based on the Improved Low-Rank Matrix Completion and Recovery Method for an Indoor Positioning System

Zhuang Wang, Liye Zhang, Qun Kong, and Kangtao Wang

School of Computer Science and Technology, Shandong University of Technology, Zibo 255000, China

Correspondence should be addressed to Liye Zhang; zhangliye@sdut.edu.cn

Received 12 August 2021; Accepted 29 September 2021; Published 28 October 2021

Academic Editor: Mu Zhou

With the development of information technology, indoor positioning technology has been rapidly evolving. Due to the advantages of high positioning accuracy, low cost, and wide coverage simultaneously, received signal strength- (RSS-) based WLAN indoor positioning technology has become one of the mainstream technologies. A radio map is the basis for the realization of the WLAN positioning system. However, by reasons of the huge workload of RSS collection, the instability of wireless signal strength, and the disappearance of signals caused by the occlusion of people and objects, the construction of a radio map is time-consuming and inefficient. In order to rapidly deploy the WLAN indoor positioning system, an improved low-rank matrix completion method is proposed to construct the radio map. Firstly, we evenly arrange a small number of reference points (RP) in the positioning area and collect RSS data on the RP to construct the radio map. Then, the low-rank matrix completion method is used to fill a small amount of data in the radio map into a complete database. The Frobenius parameter (F-parameter) is introduced into the traditional low-rank matrix completion model to control the instability of the model solution when filling the data. To solve the noise problem caused by environment and equipment, a low-rank matrix recovery algorithm is used to eliminate noise. The experimental results show that the improved algorithm achieves the expected goal.

1. Introduction

Location-based services (LBS) play an indispensable role in the information technology industry. As one of the key technologies of LBS, indoor positioning technology has also attracted widespread attention with the rapid development of mobile Internet and the popularity of smartphones in recent years [1–3]. An indoor positioning system is the continuation of the outdoor positioning system, which largely fills the vacancy of traditional positioning technology and has broad application prospects, such as navigation to specific stores in large shopping malls and indoor personnel positioning in fire scenes. Although outdoor positioning has already had very mature technologies such as Beidou and Global Positioning System (GPS), in the indoor environment, because of the interference of many factors, such as object occlusion, personnel walking, multipath effect in the process of signal propagation, and other noises, the difficulty of realizing indoor positioning technology is increased [4].

In order to achieve accurate indoor positioning, a variety of positioning systems have been proposed by researchers, such as positioning systems based on WLAN, RFID, and other technologies [5–7]. Since there is no need to add special sensors to the fingerprint-based WLAN indoor positioning system, we use the existing WLAN system and the user's intelligent mobile terminal as the hardware platform and develop software on the intelligent mobile terminal to provide positioning services for users. Therefore, the WLAN indoor positioning system has the value of large-scale promotion and application. The fingerprint-based WLAN indoor positioning system is divided into two phases: offline phase and online phase. In the offline phase, we uniformly set a large number of reference points (RP) in the positioning environment and collect RSS values from access points (AP) on the RPs. Each fingerprint is obtained by combining

RSS with its corresponding coordinate, and the set of all fingerprints is the radio map. In the online phase, users' locations can be calculated by matching the real-time collected RSS with the RSS in the radio map [8].

For the fingerprint-based WLAN indoor positioning system, the radio map is the basis for realizing the system [9]. The radio map keeps the mapping relationship between the signal space and location space. In the traditional radio map establishment method, a large number of reference points need to be set in the target area and multiple measurements need to be taken at each reference point to improve the positioning accuracy [10]. This approach consumes a lot of labor and time costs. Therefore, to reduce the time and labor cost of radio map establishment, many effective methods have been proposed. In Reference [11], a hybrid radio map construction method called Hidden Environment Model (HEM) is proposed. In HEM, an Environment Factor Matrix (EFM) is built to model the distinct effects of the indoor environment on signal attenuation, and the EFM is constructed using theoretical interpolations and approximations combined with on-site signal measurements. A precise Indoor Locating System (PILS) is proposed in Reference [12], and the self-correlation between RSS data of reference points is used to interpolate the radio map, which increases the number of reference points and reduces the workload of offline acquisition. However, the interpolation method cannot achieve accurate RSS value estimation in the complex electromagnetic environment indoors. Reference [13] used unlabeled user trajectories for radio map building and achieved interpolation of the radio map by labeling the unlabeled data using the Bayesian theory and hidden Markov model. The paper [14] investigates the influence of signal change on the radio map and obtains the intrinsic relationship of RSS data at different times by a linear model, which effectively reduces the updating workload of the radio map. However, this method requires additional equipment, which reduces the effectiveness of the method. The semisupervised learning algorithm is proposed in Reference [15] to construct a radio map. A small amount of labeled data and a large number of unlabeled data are collected in the offline phase, and the label propagation is calculated on the unlabeled data by a semisupervised learning algorithm. A variety of machine learning algorithms and the collected labeled data are used to calculate the label of unlabeled data and expand the radio map; as a result, the purpose of reducing the radio map construction workload was achieved. These algorithms give us many hints. For example, the widely used reference point expansion methods are spatial interpolation methods, including inverse distance weighted interpolation [16], linear interpolation [17], kriging interpolation [18], and spline interpolation [19]. However, the spatial interpolation methods utilize the local information of the data rather than the global information, and the interpolation results are affected by the order of data arrangement, so the global optimal solution cannot be obtained by the spatial interpolation methods. In 2006, Donoho proposed compressed sensing theory in Reference [20], which has become one of the research hotspots in signal processing, data acquisition, and other related fields. By mining the sparse characteristics of massive signals, under the condition of far less than the Nyquist sampling rate, the original signal can be reconstructed accurately by the compressed sensing algorithm. The development of compressed sensing theory in the matrix space is matrix completion. The matrix completion algorithm uses the low rank of matrix singular value to recover the original matrix by sampling some elements of the matrix. In order to achieve accurate matrix completion, a series of efficient solution algorithms have been proposed. Among these algorithms, the fixed point algorithm proposed in Reference [21] and the inaccurate Lagrange multiplier method proposed in Reference [22] can achieve excellent completion results.

Inspired from the above articles, an improved low-rank matrix completion method is proposed to fast construct the radio map in the indoor positioning system. Because the RSS data matrix in the radio map has a low-rank characteristic, the construction problem of the radio map can be modeled as a low-rank matrix completion problem. Therefore, we only need to collect RSS data at some reference points, and the complete radio map can be filled by the matrix completion algorithm. To eliminate the noise in the RSS data, the F-parameter and the sparse noise term are introduced to the traditional matrix completion model, and an improved algorithm is obtained. In the process of solving the model, the solution is performed by the alternating direction multiplier method (ADMM).

The main contributions of this paper are as follows:

(1) The low-rank matrix completion model is proposed to achieve the fast establishment of the radio map, while the F-parameter is used to eliminate the instability of the model solution

To construct a complete radio map, the accuracy of the data used for filling needs to be guaranteed. When collecting data, due to the influence of the environment (such as human walking and wall blocking), the collected RSS data contain a lot of noise. In the traditional model, only the kernel function is considered by the low-rank matrix complete model, and the low rankness of the model is guaranteed by the kernel parameters. In this paper, the regularization term is introduced into the traditional low-rank matrix completion model, and the F-parameter is used to eliminate the model instability.

(2) A sparse term is introduced to the low-rank matrix completion model to eliminate the sparse noise in RSS data

Due to the influence of the environment, RSS data not only brings Gaussian noise but also contains a small amount of outliers, called sparse noise. In the low-rank completion model, the F-parameter only has a good processing effect on Gaussian noise, but it does not solve the problem caused by outliers. Inspired by the low-rank recovery matrix model, we introduce the sparse term of the recovery model to solve the problem of outliers. Therefore, using the new L1

parameter to characterize the sparse noise can effectively solve the instability problem caused by outliers.

The remainder of this paper is organized as follows. The related works are discussed in Section 2. In Section 3, the fingerprint-based WLAN indoor positioning system is introduced, and the framework of the fast construction algorithm of the radio map is given. In Section 4, we theoretically derive and realize this method. The experimental results and analysis are presented in Section 5. Finally, Section 6 draws the conclusion of this paper.

2. Related Works

In order to reduce the acquisition workload in the offline phase, various low-rank completion methods have been proposed in recent years.

Assuming that the data matrix has low-rank characteristics, the matrix completion algorithm can be used to estimate the value of missing data, and the synthesis matrix closest to the target matrix is obtained under the constraint conditions. However, the robustness of most matrix completion algorithms is not satisfactory when Gaussian noise is added. Li et al. [23] proposed a new robust matrix completion method. The method has better robustness and accuracy when the data are destroyed by Gaussian noise. Zhang and Tan introduced a total variance constraint term based on the original kernel parametric constraint for low-rank matrices [24]. A weighting algorithm was introduced to improve the low rankness of the low-rank matrix and the sparsity of the sparse matrix. This method not only ensures the detailed information of low-rank completion but also ensures the denoising effect.

The above researches on low-rank matrix completion are only optimized in static aspects, and Song and Wang applied the matrix completion model to the field of data mining according to the structural characteristics of web links [25]. Mapping the data into a high-dimensional space makes the nonlinear relationships in dynamic links convert to linear relationships, thus making the model more complete of handling complex network structures. Besides, Reference [26] proposes an efficient algorithm for alternate iterative solution of subproblems for low-rank completion models. The algorithm uses the nonlocal self-similarity of data to propose an interpolation method for the nonlocal low-rank reconstruction model. Reference [27] proposed a weighted kernel parametric minimum model with initial value bootstrap. By constructing weights of opposite magnitude to the singular values, the approximation matrix is made to approximate the original matrix well. Second, the linear search is improved to accelerate the proximal gradient algorithm solution model, which improves the convergence speed of the algorithm.

After continuous optimization, the low-rank matrix completion model has achieved better results. In recent years, improved low-rank matrix completion algorithms have also been widely used in the construction of the radio map. Hu et al. [28] represented the RSS data space as a low-rank matrix and constructed a complete radio map from sparse measurements by the improved low-rank matrix completion method. Experiments proved that the method effectively reduced the number of collected RSS data. An experimental model for constructing a radio map was proposed by Xue et al. in Reference [29]. Based on the indoor RSS map, the signal feature points are proposed and the radio map is reconstructed using the grid points in a geometric space and the signal feature points in an RSS space. The model is significantly better than the traditional positioning method. Tan et al. [30] proposed an improved optimization model based on the traditional matrix completion model. The optimized model converts the kernel parameter into a weighted kernel parameter and introduces both the L1 parameter and F-parameter to recover the unknown data more accurately. Ma et al. [31] proposed a radio map recovery method based on the inexact incremental Lagrange multiplier (IALM) algorithm, which accurately recovered the RSS data in the radio map and effectively reduced the noise. In addition, Ma et al. [32] proposed a radio map noise reduction method using the Hankel matrix. The special structure of the Hankel matrix is used to effectively separate the noise from the signal. This method can achieve a better noise reduction effect and thus improve the localization accuracy. Zhang and Ma [33] proposed a method based on sparse representation and low-rank matrix recovery in order to update the radio map accurately. The method combines the fingerprint correlation of sparse representation with the low rank of the fingerprint matrix to update the radio map more accurately.

3. System Model

The typical fingerprint-based WLAN positioning system includes two phases. In the offline phase, the main task is to construct a radio map to realize the mapping between RSS data and position coordinates. In the online phase, the user's location is calculated using the radio map. The block diagram of the WLAN indoor positioning system is shown in Figure 1. Suppose m APs and n RPs are deployed in the location area. In order to build the radio map, we collect RSS values from all APs on each RP, and a $1 \times m$ dimension RSS vector $\mathbf{RSS}_i = (\mathbf{X}_{i1}, \mathbf{X}_{i2}, \cdots, \mathbf{X}_{im})$ can be gotten after preprocessing on each RP, where $\mathbf{X}_{ik}$ is the received signal strength measured on the i-th RP from the k-th AP. The i-th fingerprint $(\mathbf{RSS}_i, \mathbf{C}_i)$ is obtained combining $\mathbf{RSS}_i$ with its corresponding coordinates $\mathbf{C}_i = (c_{i1}, c_{i2})$. The set of all fingerprints is the radio map, as shown in Figure 1. In the online phase, the user's location can be calculated by matching the collected RSS with the RSS data in the radio map.

For this positioning system, in order to get accurate positioning results, we need to construct an accurate radio map. Therefore, it is necessary to set as many RPs as possible in the indoor positioning area to collect more RSS data. Therefore, the positioning accuracy depends on the accuracy of the radio map and the number of fingerprints in the radio map. However, two problems hinder the establishment of an accurate radio map. First, collecting RSS data on all RPs takes a lot of time and labor costs. Secondly, due to the complex indoor electromagnetic environment, the collected RSS data contain a lot of noise. According to the signal

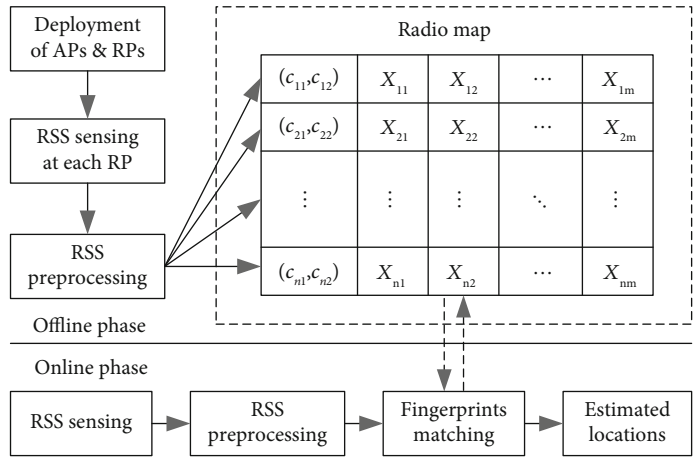

Figure 1: Typical fingerprint-based WLAN indoor positioning system.

propagation model, WLAN signal strength decreases with the increase in distance. The wireless signal propagation model is shown in [34]

$$P_r(d) = Pt - P(d0) - 10n \log 10\left(\frac{d}{d0}\right), \quad (1)$$

where d denotes the distance between the location of the collected signal and the AP, $P_r(d)$ represents the received signal strength of AP, Pt is the transmit power of AP, and $P(d0)$ represents the received signal strength at a distance of $d0$. n is a known parameter that represents the path loss.

Since the received signal strength decreases with the increase in distance and the distance between the adjacent reference point and AP is close, the adjacent reference point has highly similar signal strength. As a result, there is a spatial correlation between RSS data, and the RSS matrix in the radio map has low-rank characteristics. Using the low-rank characteristic of the RSS matrix, we only need to collect a small amount of RSS data at some reference points, and the complete RSS matrix can be obtained by the low-rank matrix completion algorithm. Then, the low-rank matrix recovery algorithm is used to separate RSS data from noise, so as to reduce the noise in the radio map and improve the accuracy of the radio map. Therefore, the construction process of the complete radio map is shown in Figure 2.

4. Methods

4.1. Low-Rank Matrix Completion with the F-Parameter. With the explosive growth of data volume, the dimension of data is increasing, and there is more correlation between high-dimensional data. Therefore, the growth of information content of the data itself is slower than that of the data dimension. For example, after feature extraction, a large number of the same features of the image will be discarded. After the wave transformation, only a small number of coefficients are relatively significant in numerical size. If the image is regarded as a pixel matrix, after singular value decomposition, a small number of singular values often contain 90% of the information of the whole image. These examples show that in high-dimensional data, there are often varying degrees of correlation, which can greatly reduce the storage space of data.

Assume that the original data matrix is low-rank, but the matrix contains many unknown elements. Completion of an incomplete matrix into a complete matrix is called a low-rank matrix completion problem. The low-rank matrix completion model is shown in Figure 3.

The matrix completion problem is aimed at estimating the information of unknown elements through partial observation data of the matrix. Without other constraints, such problems are completely unsolvable. However, if the data matrix has some special properties, it will make the matrix completion problem possible. Low rank is such a property. If the matrix M is known to be low-rank in advance, the matrix completion problem can be formulated as the following optimization problem.

$$\min_x \operatorname{rank}(X) \quad \text{s.t.} X_{i,j} = M_{i.j}, (i,j) \in \Omega, \quad (2)$$

where Ω is the set of observable sample subscripts, X is the matrix filled by the low-rank completion algorithm, M is the true matrix with missing elements, Xi, j is the element of the i-th row and j-th column of the X matrix, and Mi, j is the element of the i-th row and j-th column of the M matrix.

If we set the data on the RP outside the coordinate set Ω to 0, we get

$$\left[M_{i,j}(X)\right] = \begin{cases} X_{i,j}, & (i,j) \in \Omega, \\ 0, & \text{otherwise.} \end{cases} \quad (3)$$

The above problem is NP-hard. The complexity of the problem increases with the increase in matrix dimension, and the convex hull of function rank (X) is the kernel norm $\|X\|$ of matrix X, that is, the sum of all singular values of matrix X, so the problem is converted into a convex

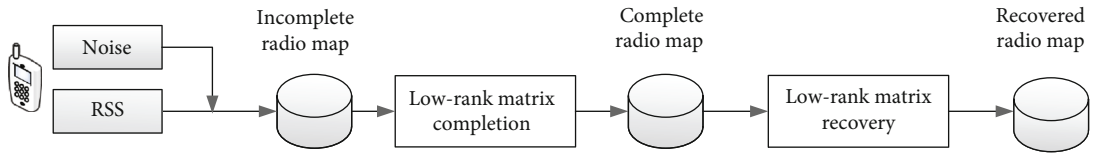

Figure 2: The construction process of the complete radio map.

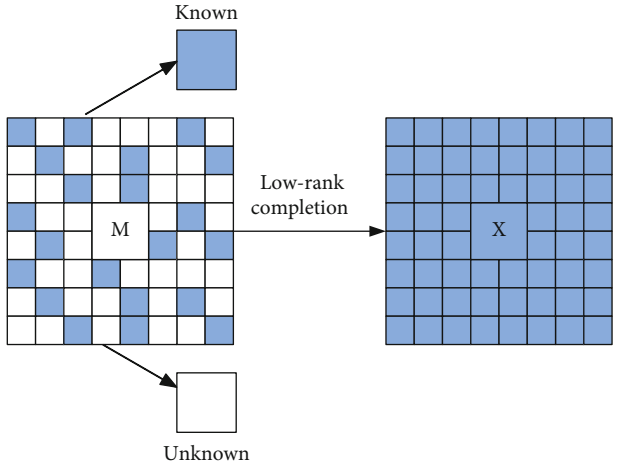

Figure 3: Low-rank matrix completion framework.

optimization problem.

$$\min_x \|X\|_* \quad \text{s.t.} X_{i,j} = M_{i.j}, (i,j) \in \Omega. \tag{4}$$

In Reference [35], the authors point out that the solution of equation (4) is equivalent to the solution of rank (X) under strong incoherent conditions. Reference [36] has proven that the kernel norm is a convex hull with a spectral norm of 1. Therefore, this is a convex relaxation problem of NP-hard problems. If the position of m reference points of the collected data is randomly uniformly distributed, then when $m \geq Cn6/5r \log n$, the observation matrix M has a great probability to receive the optimal solution for the optimization problem, where n is the constraint parameter, r is the rank of the matrix M, satisfying $1 < = r < = m < = n$, and C is a positive constant.

Although the model can produce low-rank solutions, the kernel norm of the matrix to be filled is only considered by the model, which may lead to the instability of the solution obtained by the completion problem of the matrix with a strong correlation. Therefore, on the basis of this model, the F-parameter of the matrix to be filled is introduced as a new regularization term, and a joint regularization term is formed with the original kernel norm [22]. Therefore, the uniqueness and low rank of the solution are controlled by the kernel norm, and the stability of the solution is controlled by the F-parameter. The regularized model is

$$\min_x \tau\|X\|_* + \frac{1}{2}\|X\|_F^2 \quad \text{s.t.} p\Omega(X) = p\Omega(M), (i,j) \in \Omega, \tag{5}$$

where $\tau > 0$. When $\tau \longrightarrow \infty$, the optimal solution of the above optimization problem converges to the optimal solution of the kernel function. Define $P_\Omega(X)$ as the projection operator; $P_\Omega(X) = M_{i,j}(X)$. Construct the Lagrange function of the optimization problem after the regularization model:

$$L(X,Y) = \|X\|_* + \frac{1}{2}\|X\|_F^2 + \langle Y, P_\Omega(M-X)\rangle, \tag{6}$$

where the Lagrange multiplier $Y \in R_{m*n}$. Let $X \in R_{m*n}$ be defined by

$$X = U\Sigma VT, \tag{7}$$

where U and V are orthogonal matrices, Σ is a diagonal matrix, and the elements on the diagonal are singular values of the matrix X. There are three properties of singular values.

Property 1: nonnegativity, i.e., singular values $\sigma i \geq 0$.

Property 2: the number of nonzero singular values of the matrix is equal to the rank of the matrix.

Property 3: the maximum singular value of the matrix is equal to the spectral norm, i.e., σ max $= \|X\|2$.

For $X = U\Sigma VT$, $\Sigma = \text{diag}(\{\sigma i\})$, $1 \leq i \leq r$, and for each $\tau \geq 0$, we have

$$D_\tau(X) = UD_\tau(\Sigma)V^T, \tag{8}$$

where $D_\tau(X) = \text{diag}(\{\sigma i - \tau\} +)$ is the soft threshold operation, diag refers to the diagonal elements of the singular value matrix, and + indicates that the singular value σi is guaranteed to be nonnegative when it tends to 0. It is defined as follows:

$$D_\tau(X) = \begin{cases} x - \tau, & x > \tau, \\ x + \tau, & x < \tau, \\ 0, & \text{otherwise.} \end{cases} \tag{9}$$

Since the above operation is an approximation of the

kernel function, the above equation can be converted to

$$D_\tau(Y) = \arg\min \frac{1}{2}\|X - Y\| + \tau\|X\|_*. \tag{10}$$

The optimization problem is solved using alternating iterations, and the specific iteration format of which can be simply stated as follows:

$$\begin{aligned} X^k &= D_\tau(Yk-1), \\ Yk &= Yk - 1 + \delta k\, P\Omega(M - Xk), \end{aligned} \tag{11}$$

where Y is the auxiliary matrix, M is the measurement matrix (containing missing values), P_Ω is the position of the known elements, and δk is the iteration step. The object of $D\tau(X)$ is the matrix which can be specifically described as the following equation:

$$D_\tau(X) = \begin{cases} [\text{usv}] = \text{svd}(X), \\ \Sigma = \text{sgn} .* \max(\text{abs}(\Sigma) - \tau, 0), \\ X' = U * \Sigma * V^T. \end{cases} \tag{12}$$

The final convergence discriminant is

$$\frac{\|P\Omega(M - Xk)\|F}{\|P\Omega(M)\|F} < \varepsilon. \tag{13}$$

4.2. Low-Rank Matrix Recovery. Large-scale data processing is often accompanied by data missing, damage, and other issues. For example, in the face recognition model, the face images to be recognized in the training set contain shadows, highlight, occlusion, deformation, etc. In structure from motion (SFM) problems, large matching errors often exist in feature extraction and feature matching. Correct and efficient recovery of original data from damaged data is crucial for the analysis and processing of modern large-scale data. Assume that the original data matrix is low rank and the matrix elements contain a lot of noise. To recover a complete low-rank matrix from a matrix containing noise is a low-rank matrix recovery problem. The recovery framework of the low-rank matrix is shown in Figure 4.

When there is no noise or Gaussian noise in the data, the classical data recovery method is principal component analysis [37].

$$X = A_0 + E_0, \tag{14}$$

where X is the observation matrix, $A0$ is a low-rank matrix, and $E0$ is a Gaussian matrix with the independent identical distribution. However, when the matrix $E0$ does not satisfy the Gaussian distribution but a sparse noise matrix, the principal component analysis method is no longer applicable to solve this problem. In this case, the matrix is decomposed into a low-rank matrix part A and a sparse noise matrix part E.

$$X = A + E. \tag{15}$$

Because the noise is sparse, it can be characterized by the L0 norm. The original sparse noise problem can then be modeled as the following optimization problem.

$$\begin{aligned} &\min_{A,E} \text{rank}\,(A) + \lambda\|E\|_0 \\ &\text{s.t.} P_\Omega(X) = P_\Omega(M), (i,j) \in \Omega, \end{aligned} \tag{16}$$

where $X, A, E \in Rm * n$ and X is the observation matrix. Since this problem is NP-hard, the L0 norm of the matrix is relaxed to the L1 norm, and the following equation is obtained:

$$\begin{aligned} &\min \|A\|* + \lambda\|E\|_1 \\ &A, E \\ &\text{s.t.} P_\Omega(X) = P_\Omega(A + E). \end{aligned} \tag{17}$$

The method to solve this problem is called robust principal component analysis. If the singular value distribution of the low-rank matrix A is reasonable and the nonzero elements of the coefficient matrix are evenly distributed, the original low-rank matrix A can be recovered from any unknown error by the convex optimization problem with the probability of close to 1.

The augmented Lagrangian function was constructed for the optimization problem in equation (17).

$$L(A, E, Y, u) = \|A\|_* + \lambda\|E\|_* + < Y, X - A - E > + \frac{u}{2}\|X - A - E\|2F. \tag{18}$$

When $Y = Y_k$ and $u = u_k$, the optimization problem is solved using the inexact Lagrange multiplier method:

$$\min_{A,E} L(A, E, Y_k, u_k). \tag{19}$$

Then, the update equation of A and E is

$$\begin{aligned} A_{k+1} &= \arg\min_A L(A, E_{k+1}, Y_k, u_k) \\ &= D_{1/u_k}\left(X - E_k + 1 + \frac{Y_k}{u_k}\right), \\ E_{k+1} &= \arg\min_E L(A_{k+1}, E, Y_k, u_k) \\ &= S_{1/u_k}\left(X - A_k + 1 + \frac{Y_k}{u_k}\right), \end{aligned} \tag{20}$$

where $D_{1/u_k}(*)$ is singular value operations, regarding equation (14). $S_{1/u_k}(*)$ are soft threshold operations as follows:

$$S_{1/u_k}(x) = \text{sign}\,(x)\left(|x| - \frac{1}{uk}\right). \tag{21}$$

Then, the update equation of the matrix Y is

$$Y_{k+1} = Y_k + u_k(X - A_{k+1} - E_{k+1}). \tag{22}$$

The formula for parameter u_k is as follows:

$$u_{k+1} = \begin{cases} \rho u_k, & \dfrac{u_k \|E_{k+1} - E_k\|_F}{\|X\|_F} < \varepsilon, \\ u_k, & \text{otherwise}, \end{cases} \tag{23}$$

where $\rho(\rho > 1)$ is a constant and $\varepsilon(\varepsilon > 0)$ is a small positive number.

4.3. Indoor Positioning System with Low-Rank Completion. According to the above theory, if the matrix has low-rank characteristics, the missing elements of the matrix can be filled by the low-rank matrix completion algorithm. When collecting data, due to personnel movement, mobile phone orientation, and other reasons, the collected RSS value contains a lot of environmental noise, and the internal sensors of the equipment also produce equipment noise. Therefore, the established radio map contains a lot of noise. Because of the existence of noise, the low-rank matrix completion algorithm cannot achieve ideal results. In order to solve the above problem, we add a sparse noise term to the matrix completion model, and the proposed algorithm combines the completion and recovery algorithms of the low-rank matrix, which is more stable and robust than the original model. The indoor positioning system framework with the low-rank completion and recovery algorithm is shown in Figure 5.

The improved model is

$$\begin{aligned} &\min_{A,E} \operatorname{rank}(A) + \lambda \|E\|_0 + \mu \|A\|_F \\ &\text{s.t.} P_\Omega(X) = P_\Omega(A + E). \end{aligned} \tag{24}$$

The nonconvex problem in equation (24) can be transformed into the following convex optimization problem.

$$\begin{aligned} &\min_{A,E} \|A\| * + \lambda \|E\|_1 + \mu \|A\| F2 \\ &\text{s.t.} X = A + E, P_\Omega(E) = 0. \end{aligned} \tag{25}$$

For the optimization problem in equation (25), the augmented Lagrange function is constructed as follows:

$$\begin{aligned} L(A, E, Y) = {} & \|A\| * + \lambda \|E\| 1 + \mu \|A\| 2F + < Y, X - A - E > \\ & + \frac{\rho}{2} \|X - A - E\| 2. \end{aligned} \tag{26}$$

The optimal solution of the problem is solved by using the alternating direction multiplier method.

$$\begin{aligned} &(A, E) = \arg\min L(A, E, Y). \\ &A, E, Y \in Rm * n \end{aligned} \tag{27}$$

In order to facilitate the derivation of the formula, B is used to replace the regularization term of the F-parameter to distinguish the kernel parameter and the F-parameter. We can get

$$\begin{aligned} &\min_{A,E} \|A\|_* + \lambda \|E\|_1 + \mu \|B\|_F^2 \\ &\text{s.t.} X = A + E, P_\Omega(E) = 0 \\ &\text{s.t.} B = A. \end{aligned} \tag{28}$$

Since two constraints are added, the impact should be divided into two parts. Therefore, the penalty factor is divided into two parts. Let $Y = \langle Y_1, Y_2 \rangle$ and $\rho = \langle \rho_1, \rho_2 \rangle$, and reestablish the Lagrange function as follows.

$$\begin{aligned} L(A, B, E, Y1, Y2) = {} & \|A\| * + \lambda \|E\| 1 + \mu \|B\| 2F + < Y, X - A \\ & - E > + \frac{\rho_1}{2} \|X - A - E\| 2F + < Y, B \\ & - A > + \frac{\rho_2}{2} \|B - A\| 2. \end{aligned} \tag{29}$$

Equation (29) was further rewritten as follows:

$$\begin{aligned} L(A, B, E, Y_1, Y_2) = {} & \|A\| * + \lambda \|E\|_1 + \mu \|B\| 2F \\ & + \frac{\rho_1}{2} \left\| X - A - E + \frac{1}{\rho_1} Y_1 \right\| 2F \\ & + \frac{\rho_2}{2} \left\| B - A + \frac{1}{\rho_2} Y_2 \right\| 2F. \end{aligned} \tag{30}$$

The formulas are updated by alternating variables for iterative solutions. The formulas for each variable are listed below.

$$A = \|A\| * + \frac{\rho 1}{2} \left\| X - A - E + \frac{1}{\rho 1} Y1 \right\| 2F + \frac{\rho 2}{2} \left\| B - A + \frac{1}{\rho 2} Y2 \right\| 2F, \tag{31}$$

$$B = \mu \|B\| 2F + \frac{\rho 2}{2} \left\| B - A + \frac{1}{\rho 2} Y2 \right\| 2F, \tag{32}$$

$$E = \lambda \|E\| 1 + \frac{\rho 1}{2} \left\| X - A - E + \frac{1}{\rho 1} Y1 \right\| 2F. \tag{33}$$

The solution of A can be expressed by the singular value threshold operator, so that the solution of A is

$$\begin{aligned} Ak + 1 = {} & \frac{1}{\rho_1 + \rho_2} D \frac{1}{\rho_1 + \rho_2} \left(\rho_1 \left(X - Ak - Ek + \frac{1}{\rho_1} Y1k \right) \right. \\ & \left. + \rho_2 \left(Bk + \frac{1}{\rho_2} Y2k \right) \right). \end{aligned} \tag{34}$$

The solution of B can be obtained optimally by finding the partial derivative.

$$Bk + 1 = \frac{\rho_2 Ak + Y2k}{2\mu + \rho_2}. \tag{35}$$

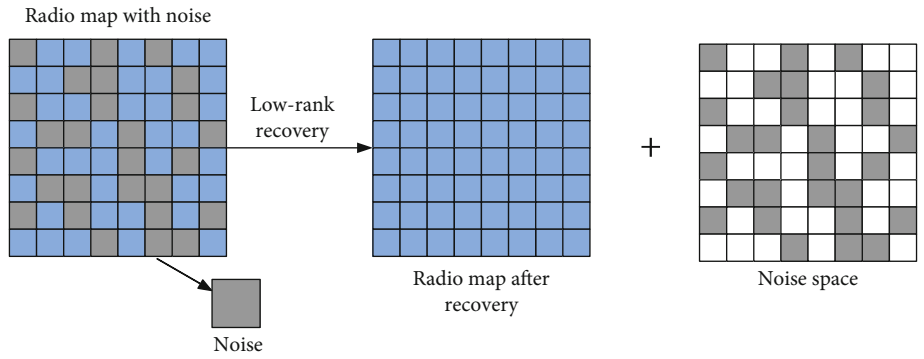

Figure 4: Matrix recovery framework.

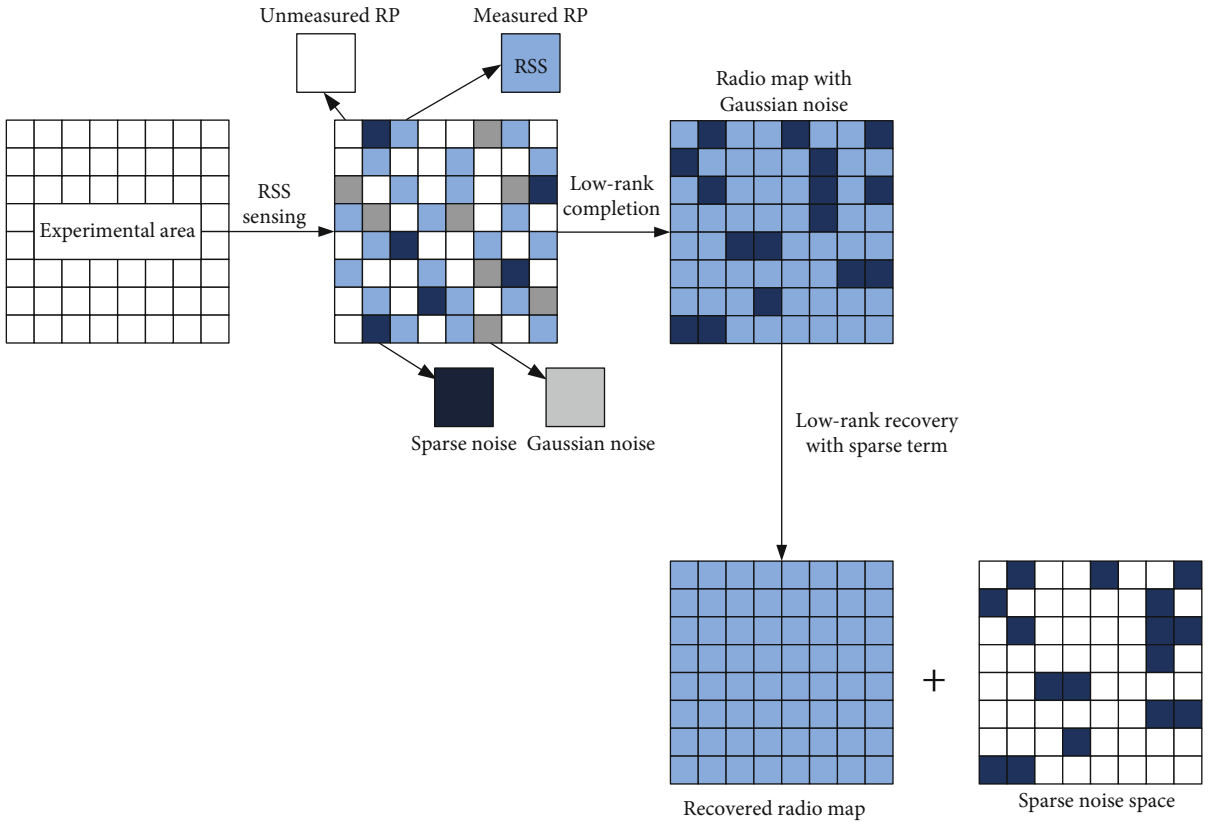

Figure 5: Improved low-rank matrix completion framework.

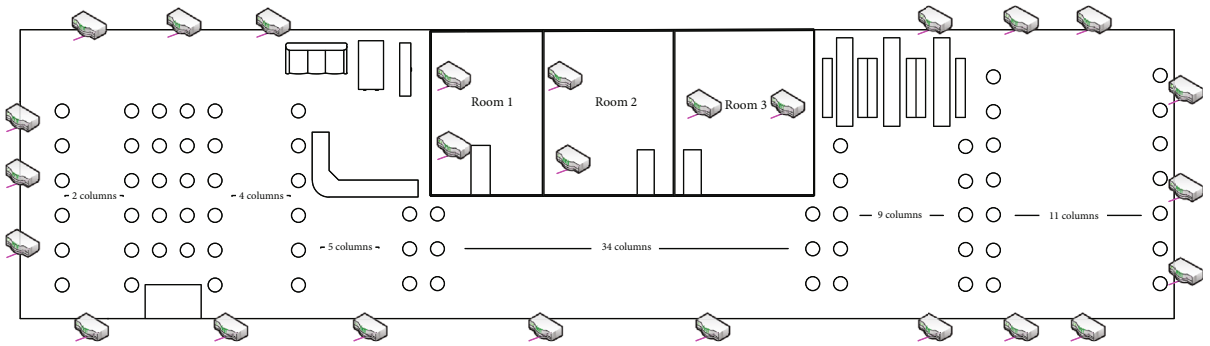

Figure 6: Floor plan for indoor positioning.

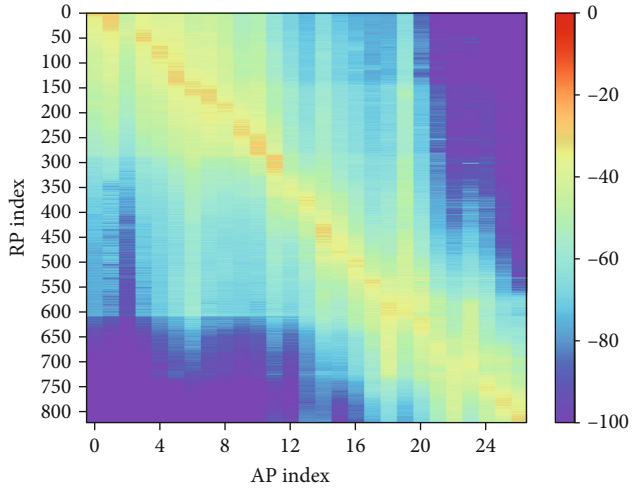

Figure 7: Complete radio map.

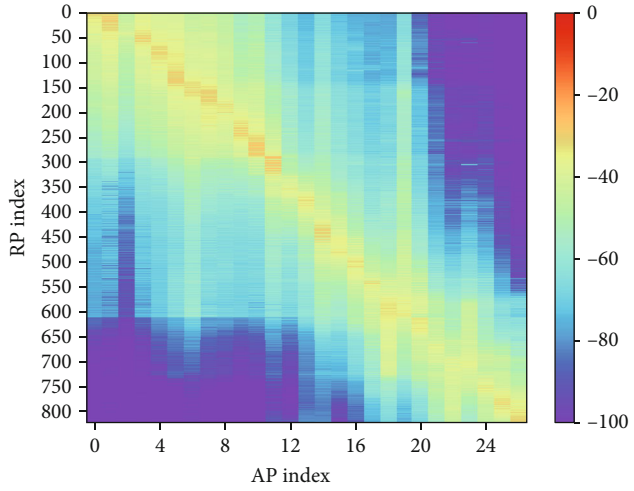

Figure 8: 40% data acquisition constructed by the radio map.

The solution of E can be expressed by the soft threshold operator, so that the solution of E is

$$Ek+1=\frac{1}{\rho_1}S\frac{\lambda}{\rho 1}(\rho_1(X-Ak+1-Ek)+Y_1). \tag{36}$$

Finally, update Y_1 and Y_2.

$$Y1k+1=Y1k+\rho_1\left(X-A^{k+1}-E^{k+1}\right), \tag{37}$$

$$Y2k+2=Y2k+\rho_2\left(B^{k+1}-A^{k+1}\right). \tag{38}$$

5. Experimental Results and Analysis

This section provides details on the experimental results of the proposed method using both simulations and implementations. The positioning area is located in the 4th floor of building 9 at Shandong University of Technology. In this location area, we divide the whole location area into several grids, and each grid spacing is 0.5 m, with a total of 342 reference points, as shown in Figure 6.

A total of 26 APs are installed in this positioning area, and a Redmi K30 Pro mobile phone is used to collect RSS values. In order to verify the effectiveness of our algorithm, we construct a database without missing elements. We collected 100 RSS data at each reference point, removed the singular values, and used the remaining RSS values to calculate the average. Using the average value to establish the radio

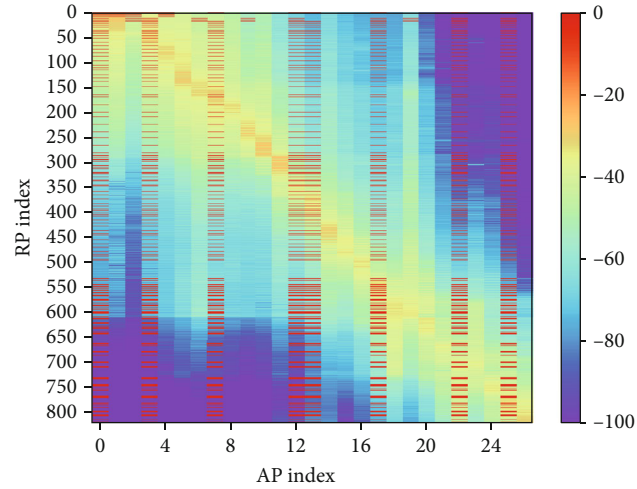

Figure 9: The radio map calculated by the improved low-rank completion method.

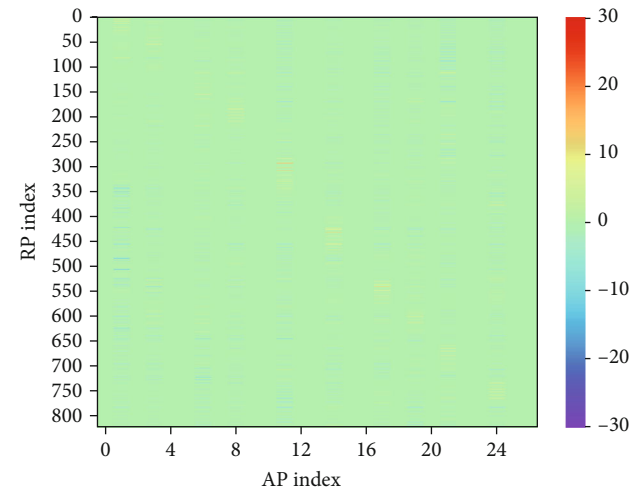

Figure 10: Completion error diagram.

Table 1: Completion errors of different algorithms.

Algorithm	Err (dBm)
Low-rank completion	9.83
Improved low-rank completion	6.52
Spline interpolation (x)	25.48
Spline interpolation (y)	11.69
Spline interpolation (0.0)	50.13

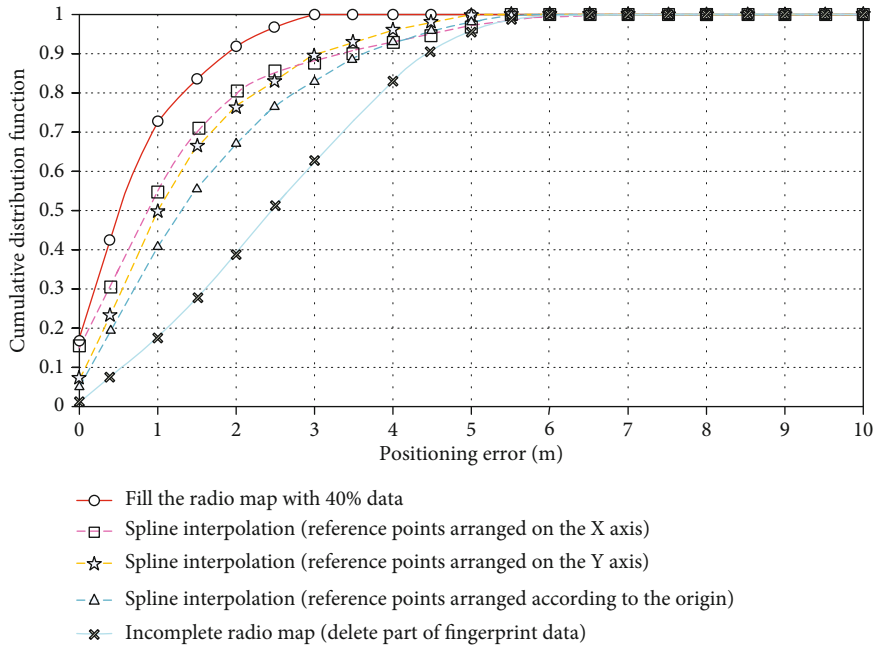

Figure 11: Cumulative distribution function of positioning error.

map can effectively improve the positioning accuracy. However, it took us weeks and a lot of manpower costs to build the radio map. The complete radio map is shown in Figure 7. In Figure 7, horizontal coordinates represent different APs and ordinates represent different RPs, and different colors represent the intensity of the RSS.

In order to quickly establish the radio map, we reduce the scale of data collection and only collect RSS data at 40% RPs. The obtained incomplete radio map is shown in Figure 8. Then, the low-rank matrix completion method is used to expand the RP data, and the complete radio map is obtained. The experimental results are shown in Figure 9.

To demonstrate the completion effect after completion, we define the difference between the complete radio map and the radio map filled from the 40% data using the proposed completion algorithm as the completion error, and the definition equation is

$$\theta = X' - X, \tag{39}$$

where X' denotes the complete radio map and X denotes the result of completion of the radio map constructed from 40% data using the proposed completion algorithm. θ denotes the completion error. That is, the smaller the value is, the closer the completion result is to the ideal radio map and the better the completion effect is. The completion error result is shown in Figure 10. As illustrated in Figure 10, most completion errors are less than 3 dBm.

As shown in Figure 10, the RSS values at unmeasured RPs can be filled effectively by the improved low-rank matrix completion algorithm, and the completion effect is satisfactory. In order to further show the completion effect of the algorithm, we use a cubic spline interpolation method to interpolate the incomplete radio map and calculate the completion error. The results are shown in Table 1.

It can be seen from Table 1 that since the interpolation algorithm is greatly affected by the data arrangement, the completion effect is not ideal by using the interpolation method. When the low-rank completion algorithm is used to fill the reference point, the inherent relationship between the low-rank characteristics of the RSS matrix and the RSS value between adjacent reference points is used, so the radio map obtained has high accuracy and small completion error. In order to show the influence of the algorithm on the actual positioning results, the complete radio map, the incomplete radio map, and the radio map filled with the proposed algorithm and the cubic spline interpolation algorithm are used as the fingerprint database in the offline training phase. In the online positioning phase, we use the classic KNN algorithm ($K = 3$) to calculate the user location, and the cumulative distribution function curves of positioning error for different algorithms are shown in Figure 11.

It can be seen from Figure 9 that when the incomplete radio map is directly used for positioning, the probability of error within 2 m is 63%, and the positioning accuracy cannot meet the actual requirements. When the reference points are arranged according to the distance from the x-axis, the y-axis, and the distance from the origin, the interpolation method is used to expand the reference point, which can improve the positioning accuracy to a certain extent. The probability of error within 2 m is increased to 78%, 77%, and 67%, respectively. When the reference points are arranged according to the distance from the x-axis, the y-axis, and the origin, the interpolation method is used to fill the radio map, and the filled radio map is used to analyze the positioning error. The probability of error within 2 m is increased to about 78%, 77%, and 67%, respectively.

However, the completion effect of the radio map is affected by the order of RPs. Since it is impossible to know how to arrange before completion to ensure the strongest correlation between RSS data, it is difficult to achieve the best completion effect and positioning accuracy. The improved low-rank completion algorithm uses the low-rank characteristics of the RSS matrix and the correlation between RSS data to fill the radio map, and the completion result has a unique solution. Therefore, the probability of positioning error within 2 m is increased to more than 90%, and the positioning accuracy is higher than that of the interpolation method.

In summary, the low-rank matrix completion algorithm proposed in this paper can significantly reduce the workload of building a radio map while ensuring high positioning accuracy.

6. Conclusions

In this paper, an improved low-rank matrix completion method is proposed to realize the rapid establishment of the radio map. To reduce the workload of building the radio map in the offline phase, the matrix completion algorithm is introduced to build the radio map by using the low-rank characteristic of the RSS matrix. The F-parameter is introduced to the traditional low-rank matrix completion model to improve the stability of the algorithm, and the sparse noise term is also introduced to solve the noise interference due to environmental factors. The experimental results show that under the premise of ensuring the same positioning accuracy, the time and labor cost of radio map establishment in the offline phase can be effectively reduced and the influence of noise on the radio map is eliminated simultaneously.

Data Availability

The radio map data used to support the findings of this study were supplied by Liye Zhang under license and so cannot be made freely available. Requests for access to these data should be made to Liye Zhang (zhangliye@sdut.edu.cn).

Conflicts of Interest

The authors declare that they have no competing interests.

Acknowledgments

This work is supported by School of Computer Science and Technology, Shandong University of Technology. This paper is supported by the Shandong Provincial Natural Science Foundation, China (grant number ZR2019BF022), and National Natural Science Foundation of China (grant number 62001272).

References

[1] M. Alakhras, M. Hussein, and M. Oussalah, "Location fixing and fingerprint matching fingerprint map construction for indoor localization," *Journal of Sensors*, vol. 2020, Article ID 7801752, 14 pages, 2020.

[2] W. Shao, H. Luo, F. Zhao, H. Tian, S. Yan, and A. Crivello, "Accurate indoor positioning using temporal–spatial constraints based on Wi-Fi fine time measurements," *IEEE Internet of Things Journal*, vol. 7, no. 11, pp. 11006–11019, 2020.

[3] L. Zhang, X. Meng, and C. Fang, "Linear regression algorithm against device diversity for the WLAN indoor localization system," *Wireless Communications and Mobile Computing*, vol. 2021, Article ID 5530396, 15 pages, 2021.

[4] L. Zhang, Z. Wang, X. Meng, C. Fang, and C. Liu, "Noise reduction for radio map crowdsourcing building in WLAN indoor localization system," *EURASIP Journal on Advances in Signal Processing*, vol. 2021, no. 1, 2021.

[5] P. Davidson and R. Piché, "A survey of selected indoor positioning methods for smartphones," *IEEE Communications Surveys & Tutorials*, vol. 19, no. 2, pp. 1347–1370, 2017.

[6] Y. Wang, Y. Shu, X. Jia, M. Zhou, L. Xie, and L. Guo, "Multi-feature fusion-based hand gesture sensing and recognition system," *IEEE Geoscience and Remote Sensing Letters*, pp. 1–5, 2021.

[7] B. Jang and H. Kim, "Indoor positioning technologies without offline fingerprinting map: a survey," *IEEE Communications Surveys & Tutorials*, vol. 21, no. 1, pp. 508–525, 2019.

[8] P. Bahl and V. Padmanabhan, "RADAR: an in-building RF-based user location and tracking system," in *in INFOCOM 2000 Nineteenth Annual Joint Conference of the IEEE Computer and Communications Societies*, vol. 2, pp. 775–784, Tel Aviv, Israel, 2000.

[9] L. Zhang, M. Lin, Y. Xu, and L. Cheng, "Linear regression algorithm against device diversity for indoor WLAN localization system," in *2017 IEEE Global Communications Conference*, pp. 1–6, Singapore, 2017.

[10] W. Yang, C. Xiu, J. Ye et al., "LSS-RM: using multi-mounted devices to construct a lightweight site-survey radio map for WiFi positioning," *Micromachines*, vol. 9, no. 9, p. 458, 2018.

[11] Z. Xiang, H. Zhang, and J. Huang, "A hidden environment model for constructing indoor radio maps," in *Sixth IEEE International Symposium on a World of Wireless Mobile and Multimedia Networks*, pp. 395–400, Taormina-Giardini Naxos, Italy, 2005.

[12] T. C. Tsai, C. L. Li, and T. M. Lin, "Reducing calibration effort for WLAN location and tracking system using segment technique," in *IEEE International Conference on Sensor Networks, Ubiquitous, and Trustworthy Computing*, pp. 46–51, Taichung, Taiwan, 2006.

[13] X. Chai and Q. Yang, "Reducing the calibration effort for probabilistic indoor location estimation," *IEEE Transactions on Mobile Computing*, vol. 6, no. 6, pp. 649–662, 2007.

[14] J. Yin, Q. Yang, and L. M. Ni, "Learning adaptive temporal radio maps for signal-strength-based location estimation," *IEEE Transactions on Mobile Computing*, vol. 7, no. 7, pp. 869–883, 2008.

[15] J. J. Pan, S. J. Pan, J. Yin, L. M. Ni, and Q. Yang, "Tracking mobile users in wireless networks via semi-supervised colocalization," *IEEE Transactions on Pattern Analysis & Machine Intelligence*, vol. 34, no. 3, pp. 587–600, 2012.

[16] D. Denkovski, V. Atanasovski, and L. Gavrilovska, "Reliability of a radio environment map: case of spatial interpolation techniques," in *2012 7th International ICST Conference on Cognitive Radio Oriented Wireless Networks and Communications*, pp. 248–253, Stockholm, Sweden, 2012.

[17] C. Koweerawong, K. Wipusitwarakun, and K. Kaemarungsi, "Indoor localization improvement via adaptive RSS fingerprinting database," in *The International Conference on Information Networking 2013 (ICOIN)*, pp. 412–416, Bangkok, Thailand, 2013.

[18] H. Zhao, B. Huang, and J. Bing, "Applying kriging interpolation for WiFi fingerprinting based indoor positioning systems," in *Wireless Communications & Networking Conference*, pp. 1–6, Doha, Qatar, 2016.

[19] M. Zhou, Y. Tang, Z. Tian, and X. Geng, "Semi-supervised learning for indoor hybrid fingerprint database calibration with low effort," *IEEE Access*, vol. 5, pp. 4388–4400, 2017.

[20] D. L. Donoho, "Compressed sensing," *IEEE Transactions on Information Theory*, vol. 52, no. 4, pp. 1289–1306, 2006.

[21] S. Ma, D. Goldfarb, and L. Chen, "Fixed point and Bregman iterative methods for matrix rank minimization," *Mathematical Programming*, vol. 128, no. 1-2, pp. 321–353, 2011.

[22] Z. Lin, M. Chen, and Y. Ma, "The augmented Lagrange multiplier method for exact recovery of corrupted low-rank matrices," 2013, arXiv:1009.5055v3.

[23] K. Li, B. Xu, and K. Gao, "Low-rank matrix completion with self-identification of outliers," *Journal of Frontiers of Computer Science and Technology*, vol. 13, no. 8, pp. 1272–1279, 2019.

[24] M. Zhang and W. Tan, "Salt-and-pepper denoising based on total variation and reweighted low-rank matrix recovery," *Computer Engineering and Design*, vol. 37, no. 6, pp. 1579–1583, 2016.

[25] G. Song and L. WANG, "Utilizing matrix completion optimization model on dynamic network link prediction," *Computer Engineering and Applications*, vol. 56, no. 16, pp. 37–44, 2020.

[26] J. Zhang, R. Zhang, and G. Wang, "Image interpolation based on non-local low-rank matrix reconstruction," *Application Research of Computers*, vol. 35, no. 6, pp. 1914–1916, 2018.

[27] W. Feng and D. Xie, "Low rank matrix approximation with weighted nuclear norm and its application," *Journal of Computer Applications*, vol. 40, no. S01, pp. 128–131, 2020.

[28] Y. Hu, W. Zhou, Z. Wen, Y. Sun, and B. Yin, "Efficient radio map construction based on low-rank approximation for indoor positioning," *Mathematical Problems in Engineering*, vol. 2013, 226 pages, 2013.

[29] W. Xue, Q. Li, X. Hua, K. Yu, W. Qiu, and B. Zhou, "A new algorithm for indoor RSSI radio map reconstruction," *IEEE Access*, vol. 6, pp. 76118–76125, 2018.

[30] T. Tan, L. Zhang, and Q. Li, "An efficient fingerprint database construction approach based on matrix completion for indoor localization," *IEEE Access*, vol. 8, pp. 130708–130718, 2020.

[31] L. Ma, J. Li, Y. Xu, and W. Meng, "Radio map recovery and noise reduction method for green WiFi indoor positioning system based on inexact augmented Lagrange multiplier algorithm," in *2015 IEEE Global Communications Conference (GLOBECOM),*, pp. 1–5, 2015.

[32] L. Ma, W. Zhao, Y. Xu, and C. Li, "Radio map noise reduction method using Hankel matrix for WLAN indoor positioning system," in *GLOBECOM 2017 - 2017 IEEE Global Communications Conference*, pp. 1–72, 2017.

[33] Y. Zhang and L. Ma, "Radio map crowdsourcing update method using sparse representation and low rank matrix recovery for WLAN indoor positioning system," *in IEEE Wireless Communications Letters*, vol. 10, no. 6, pp. 1188–1191, 2021.

[34] S. Nikitaki, G. Tsagkatakis, and P. Tsakalides, "Efficient training for fingerprint based positioning using matrix completion," in *2012 Proceedings of the 20th European Signal Processing Conference*, pp. 195–199, Bucharest, Romania, 2012.

[35] M. A. Davenport and J. Romberg, "An overview of low-rank matrix recovery from incomplete observations," *IEEE Journal of Selected Topics in Signal Processing*, vol. 10, no. 4, pp. 608–622, 2016.

[36] J. Cai, E. J. Cand, and Z. Shen, "A singular value thresholding algorithm for matrix completion," *SIAM Journal on Optimization*, vol. 20, no. 4, pp. 1956–1982, 2010.

[37] T. Yu, X. Wang, and A. Shami, "Recursive principal component analysis-based data outlier detection and sensor data aggregation in IoT systems," *IEEE Internet of Things Journal*, vol. 4, no. 6, pp. 2207–2216, 2017.

Hindawi
Journal of Sensors
Volume 2021, Article ID 5194700, 15 pages
https://doi.org/10.1155/2021/5194700

Research Article

Coastal Ecological Environment Monitoring and Protection System Based on Multisource Information Fusion Decision

Lijuan Xu,[1] Lihong Zhang,[2] and Zhenhua Du[3]

[1]*School of Law, Dongguan City College, Dongguan 523419, Guangdong, China*
[2]*School of Intelligent Manufacturing, Dongguan City College, Dongguan 523419, Guangdong, China*
[3]*School of Foreign Languages, Dongguan City College, Dongguan 523419, Guangdong, China*

Correspondence should be addressed to Zhenhua Du; duzh@ccdgut.edu.cn

Received 9 August 2021; Revised 18 September 2021; Accepted 28 September 2021; Published 28 October 2021

Academic Editor: Mu Zhou

With the problem of nuclear leakage being concerned by more and more industries, the research of coastal ecological environment monitoring has become more and more important. Therefore, it is necessary to study the current unsystematic coastal ecological environment monitoring and protection system. Aiming at the accuracy of feature fusion and representation of single short environment information, this paper compares the classification effects of the three fusion methods on four classifiers: logistic regression, SVM, random forest, and naive Bayes, to verify the effectiveness of LDA and DS model fusion and determine the consistency vector representation method of short environment information data. This paper collects and analyzes the coastal data in recent years using multisource information fusion decision-making. In this paper, DS (Dempster Shafer) evidence algorithm is used to collect the data of coastal salinization degree and air relative humidity, and then, the DS feature matching model is introduced to fuse the whole index system. The method in the article completes the standardized and standardized processing of monitoring data digital conversion, quality control, and data classification, forms interrelated four-dimensional spatiotemporal data, and establishes a distributed, object-oriented, Internet-oriented dynamic management real-time and delayed database. Finally, this paper carries out tree decision processing on the coastal ecological environment monitoring data of multisource information fusion, to achieve the extraction and intuitive analysis of special data, and puts forward targeted protection strategies for the coastal ecological environment according to the data results of the DS algorithm. The research shows that the number of indicators in multisource information fusion in this paper is 16, a total of 3251 data, 2866 meaningful information, and 1869 data including ecological cycle. These data are the results of the collection of multi-information data. Based on the multilevel nature of the existing marine environment three-dimensional monitoring system, the study established a comprehensive resource-guaranteed framework and divided it into four levels according to the level of the marine monitoring system: country, sea area, locality, and data access point. In specific analysis, the guarantee resources involved in each level are introduced. On the basis of in-depth analysis of the requirements of the marine environment three-dimensional monitoring system operation guarantee and the guarantee resource structure, the marine environment three-dimensional monitoring operation comprehensive guarantee system is described from the internal structure and the external connection. The DS algorithm extracts the status information resources of various marine environment three-dimensional monitoring systems, through the interaction of various subsystems, realizes the operation and maintenance of the monitoring system, and provides various technical supports such as system evaluation and failure analysis. After multisource information fusion and decision-making, it is obtained that the index equilibrium module in the DS algorithm in this paper is 0.52, the sensitivity is 0.68, and the independence is 0.42. Among them, the range of sensitivity is the largest. In the simulation results, the eco-economic coefficient can be increased from 12% to 36%. Therefore, using the method of multisource information fusion for quantitative index analysis can provide data support for coastal ecological environment detection, to establish a more perfect protection system.

1. Introduction

With the development of the marine economy and the intensification of breeding activities, the coastal ecological environment is deteriorating day by day, resource destruction and water pollution are serious, and disasters such as red tides and Enteromorpha are frequent. The traditional collection of coastal resources and environmental background data is still in a semimanual and semiautomatic state, scientific equipment and detection methods are not mature enough, and imported equipment and complete systems are very expensive. In China, the research on the application of SAR (synthetic aperture radar) images to the extraction of surface feature information in the island coastal zone started late, but good results have also been achieved. Facing the current coastal ecological disaster risk, there is a contradiction between improving the fortification standard of protective facilities and the existing urban residential density and development needs in the coastal zone of the Pearl River Delta. Based on the experience and lessons of the earthquake and tsunami in Jidong, Japan, this paper puts forward the coastal disaster response planning strategy of combining prevention and reduction, which can be used for reference to China.

At present, the main technical means of marine environmental monitoring in my country is the field sampling experiment analysis method, and the real-time and continuity of the data is poor. However, the existing coastal deep-water exploration buoys are generally fixed at a certain position for many years, and the detected data is covered by points and partial coverage, which lacks representativeness. Many scholars use SAR image analysis to study the coastal ecological environment. For example, Wei uses a complex neural network to classify polarimetric SAR, which has achieved good results. Based on the idea of Strassen matrix multiplication, it reduces the training time by reducing the amount of calculation of convolution neural network, which has achieved good results [1]. Law proposes a deep supervised compression neural network to extract ground object information from SAR images. The supervision and punishment mechanism of the network can fully mine the relevant information between features and labels. Compression constraints can enhance the robustness of the network and have better classification performance compared with traditional methods [2]. Rochman et al. introduce the active learning method to verify the effectiveness and feasibility of active learning for feature information extraction through experiments on the full polarization SAR data of the coastal zone of Washington County, North Carolina [3]. Besseling et al. apply the sparse self-encoder to the ground feature classification of polarimetric SAR. This method can learn multilevel features and improve classification accuracy [4]. Fadare et al. use the improved FCM algorithm combined with Claude Pottier decomposition to explore the application ability of SAR image in Jiangsu coastal beach classification [5].

In recent years, scholars have also proposed acceleration methods based on cloud computing. For example, Gigault et al. use the polarization features extracted by Freeman decomposition and cloud Pottier decomposition to construct a feature set combined with Shannon entropy and extract deep features through self-encoder to make the data more separable. The research results show that the introduction of Shannon entropy can significantly improve the efficiency of seawater. Distinguish different ground features such as beach and mudflat, to effectively distinguish different island features in full polarization SAR images [6]. El Hadri et al. construct a convolutional neural network with overlapping denoising and automatic coding to realize the classification of coastal ecological objectives [7]. Wagner and Reemtsma use a convolution neural network based on complex contour wave to extract ground feature information in San Francisco Bay area, approximate the images to be classified in different directions and scales, and obtain a more sparse representation of SAR images, with an overall accuracy improvement of 5.29% [8]. The influence of lime contrast sample and slice size on the classification result verifies the effectiveness of convolutional neural network applied to SAR ground object classification [9]. Cheung and Fok use a convolutional neural network to classify the five target datasets of port, an oil tanker, cargo ship, offshore platform, and wind turbine provided by TerraSAR-X high-resolution image and has been widely used [10]. However, how to integrate short environmental information with coastal zone ecological data description and image description, to give a more accurate vectorial representation, to better serve coastal zone ecological construction, has not been seen in relevant research.

In this paper, the multisource information fusion decision-making method is used to collect and analyze the recent coastal data. In this paper, the DS evidence algorithm is used to collect the data of coastal salinization, relative humidity, and other indicators, and a DS function matching model is introduced to cover the whole index system for integration. Finally, this paper uses the multisource information fusion of coastal ecological monitoring data for tree decision-making to realize the extraction and intuitive analysis of special data. Combined with the data results of the DS algorithm, this paper puts forward the protection mechanism of coastal ecological environment protection.

2. Experiments and Methods

2.1. Research Content. Taking the planning countermeasures of postdisaster reconstruction, the laws and policies extended to the whole country, and the diversified implementation of local governments as the analysis context, this paper extracts the key planning countermeasures of disaster prevention and reduction in the coastal zone of Japan after the East Japan earthquake and provides the overall idea, specific practical disaster prevention, and reduction countermeasures for the ecological disaster prevention and reduction planning of the coastal zone of the Pearl River Delta. The multiagent cooperation mechanism puts forward optimization suggestions from three aspects.

2.2. Experimental Setup and Case Study. Aiming at the accuracy of feature fusion and representation of single short environment information, this paper compares the classification

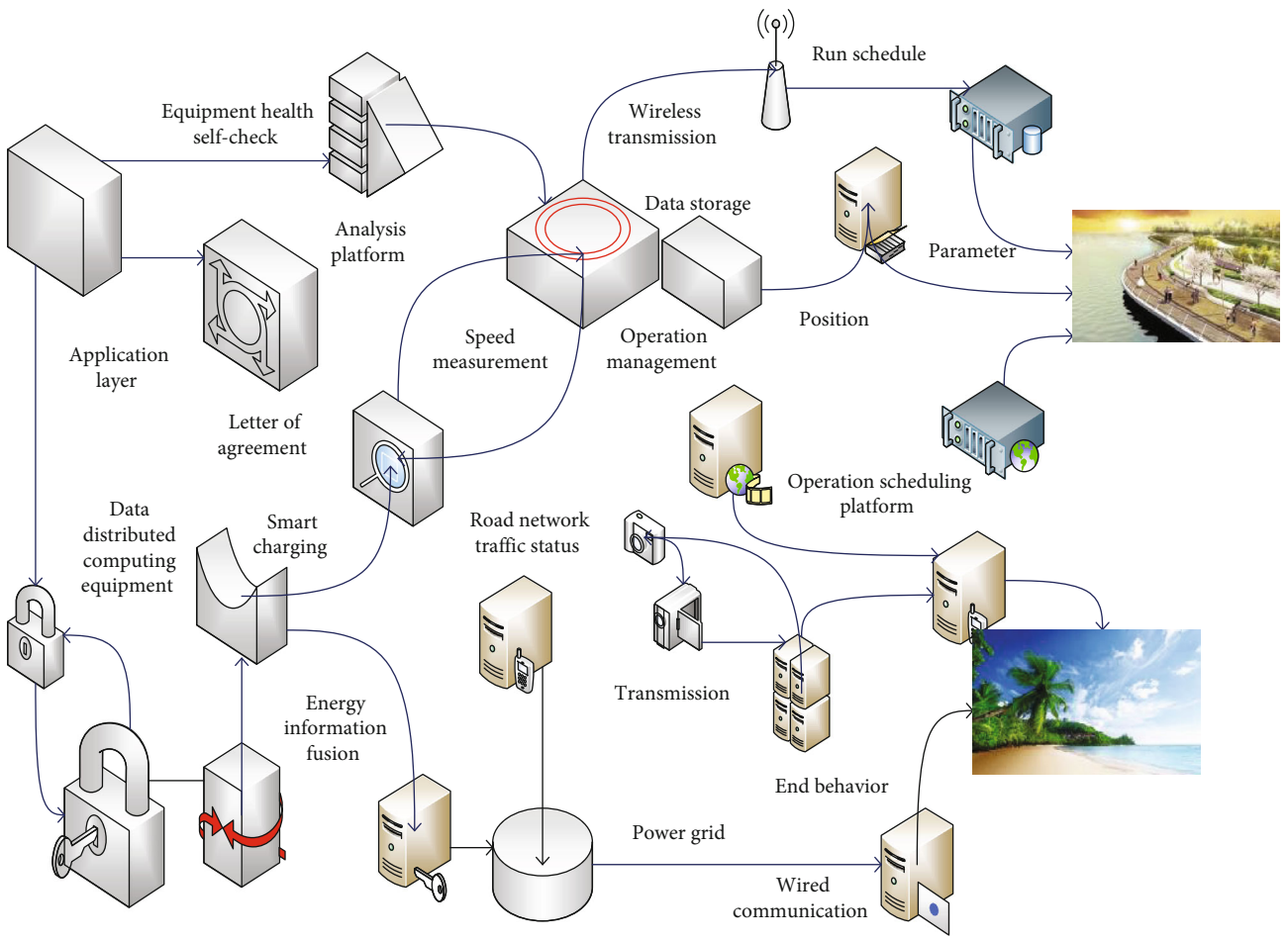

Figure 1: Environment information description framework coastal zone.

effects of the three fusion methods on four classifiers: logistic regression, SVM, random forest, and naive Bayes, to verify the effectiveness of LDA and DS model fusion and determine the consistency vector representation method of short environment information data. Based on the accurate representation of the short environmental information review data of the coastal zone, this paper adds the environmental information description data of the coastal zone and uses the same method as the environmental information collection for verification and analysis, to determine the number of fused coastal zone reviews required to fully express the coastal zone information. The structural network is shown in Figure 1.

The environmental information review data selected in this paper are randomly selected without considering the correlation between evaluations. Here, we continue to verify the rationality of selecting users' environmental information based on Pearson similarity between environmental information [11]. Based on the above experiments, the effectiveness of the proposed algorithm in the learning of multisource heterogeneous fusion representation of environmental information and images is verified by improving the classification accuracy [12]. In this paper, the planning countermeasures for postearthquake recovery and reconstruction in East Japan—laws and policies extended to the whole country—the diversified implementation of local areas are taken as the context, and the key planning countermeasures for disaster prevention and reduction of ecological disasters in the coastal zone of Japan after the East Japan earthquake are extracted and analyzed, to provide a reference for the formulation of ecological disaster prevention and reduction planning in the coastal zone of the Pearl River Delta in China [13]. In the position of Japan's disaster prevention and reduction planning system, Japan's disaster prevention and reduction planning system presents the characteristics of central and local levels [14]. Including the three programmatic legal documents formulated by the Japanese cabinet office to guide the whole country (basic law on disaster countermeasures, basic plan for disaster prevention, and business plan for disaster prevention), based on the characteristics of the region, the regional disaster prevention plan at the county level (at the same level as China's province) formulated by the prefectural government, and the regional disaster prevention plan at the city level formulated by the municipal government [15]. For the special disaster prevention and reduction planning for specific disaster forms, the relevant national departments also formulate principled provisions, and then, the governments of all prefectures, counties, cities, towns, and villages determine the specific implementation scheme based on the

characteristics of their natural and social conditions [16]. Based on the experience and lessons of previous major disasters, Japan revised and adjusted the disaster prevention and reduction planning system from top to bottom [17]. For example, as one of the main research objects of this paper, the tsunami disaster prevention area construction law was put forward in 2017 based on the practice of tsunami countermeasures in the postearthquake reconstruction of East Japan. It is a special national disaster prevention and reduction plan. Based on the above tsunami disaster prevention area construction law, the government under the jurisdiction of the case city made corresponding adjustments to a series of implementation plans within its coastal zone, including the preparation planning of protective facilities, land use planning, and building construction specifications [18].

2.3. Determination of Environmental Detection Scheme and Protection Countermeasures. The coastal zone affected by the East Japan earthquake and tsunami is zoned according to the L1 and L2 immersion lines [19]. Since it is necessary to ensure the safety of life and property, the continuation of economic activities, and the necessary harbor function in the embankment after the L1 tsunami, the fortification standard of protective facilities is usually determined by the L1 tsunami, that is, the L1 immersion line coincides with the dampproof embankment to ensure that the embankment is free from the impact of tsunami [20]. In principle, normal residential, commercial, or production activities can be carried out outside the L2 flooding line (outside the sea and inside the land) and within the L1 flooding line, as long as it is ensured that residents can take effective refuge in case of disaster [21]. However, because the tsunami caused by the East Japan earthquake has caused heavy damage to a large area within the tidal embankment on the coast of Xiantai, the housing loss is serious, the saline-alkali problem of the land within the flooded area also needs to be solved, and the affected residents have psychological difficulty to accept that the location of their damaged housing is still considered safe; the town and village governments of the affected cities along the coast of Xiantai also included an l2-2m flood line as the basis for postdisaster land use and housing reconstruction site selection [22]. The l2-2m flooding line refers to the flooding line caused by the tsunami with a height of 2 m lower than the height of the most serious tsunami once in a thousand years calculated by simulation [23]. This l2-2m flooding line coincides with the flooding line of the tsunami caused by the East Japan earthquake [24]. According to the planning of the local government, residential buildings affected by disasters within the range between L1 and l2-2m lines can be relocated to safe areas with the support of government reconstruction funds; disaster public housing can be built in the area within l2-2m line [25]. Since the area beyond the L2 line is the flooding area of the once-in-a-thousand-year tsunami, refuge towers and buildings need to be set in the area to ensure that residents can realize effective refuge.

2.4. Coastal Zone Data Analysis Model and Dempster Shafer Evidence Algorithm. In accordance with the proposed comprehensive guarantee framework for the operation of the coastal marine environment three-dimensional monitoring system, the detailed design of the comprehensive guarantee was further completed, and the development environment and tools and multiple modules of the realized comprehensive guarantee system were introduced. The prototype development of a comprehensive guarantee framework for the operation of the marine environment three-dimensional real-time monitoring information service system has been realized. In this paper, DS and LDA models are used to represent the vector characteristics of coastal zone ecological data and environmental description environmental information, and then, they are integrated to accurately obtain the environmental vectorial representation that comprehensively reflects user preferences. Let the vector dimension of DS output be LC. Based on the trained PV-dm environment information vectorization representation model, if the i user of the j environment of class k evaluates the environment information as $T1$, then all the environment information evaluation vectors of the environment are K. Similarly, if the description phrase environment information D of the environment is input, its vector representation as t can also be obtained; then, for all user evaluations of the j environment in class k, the environment information processed by DS constitutes a vector space. For the LDA model, to facilitate its integration with DS, the dimension of its feature extraction module is also set as LC, that is, the number of topics selected for LDA is $C1$. For the evaluation environmental information t, the topic vector can be obtained after learning the LDA topic model, expressed as

$$C(A) = K(y(T-1), \cdots, y(t-n), u(T-d-\varphi), \cdots, u(k-d-n)). \tag{1}$$

The subject word vector corresponding to the description phrase is

$$K(Y_i, y_i) = -\frac{1}{n}\sum_{i=1}^{n}[L_i \log(L_i) + (1-L_i)\log(1-L_i)]. \tag{2}$$

In recent years, with the development of new and intelligent marine environmental elements, multiplatform sensing technology, multiplatform remote sensing technology, real-time data communication technology, relational distributed database management technology, networked data processing, and information product development technology, standardized data sharing the development of information service technology has laid a technical foundation for the establishment of a marine environment monitoring system, the implementation of long-term, continuous, comprehensive, and accurate marine environment observation and data processing, product production, data sharing, and information services. Therefore, the establishment of a marine environment monitoring system driven by the overall needs of the country is an inevitable trend in the development of marine monitoring technology. Then, for the j environment in class k, the subject word vector l of user evaluation will increase. By fusing the semantic

information of evaluation environment information extracted based on DS and the subject word distribution information obtained from the LDA model, we can obtain the quantitative feature representation of user evaluation environment information with rich information. Three different fusion methods are considered here, as follows.

Connect the same user evaluation in series in the same environment to form a vector, as shown in

$$G_{\mathrm{LDA}} = \|R_1 - R_O\|_2. \tag{3}$$

The first mock exam is transformed from a single LC to a symbol definition and description. M has an m environment, which can be regarded as a feature extension. Splicing and fusion are simple and easy to operate, but they may bring feature redundancy or noise interference. Add the corresponding elements to form a new vector with dimension LC, as shown in

$$H_i = F\left(\sum_{j=1}^{k} \omega_{ij} y_j - \theta_i\right) - C * Y, \quad i \neq j. \tag{4}$$

Additive fusion does not change the feature dimension and directly accumulates the output vectors of the two types of models. It is simple and easy to operate, but it is also likely to bring noise disturbance. When the two vectors are fused by the Cartesian product, the interactive information between the dimensions of the vector to be fused can be obtained. Here, the sensor fusion method is used to fuse the DS environment information vector and LDA subject vector, as shown in

$$S_F = \frac{n}{\Delta_{\mathrm{LDAl}}} \sqrt{\sum_{s=1}^{n} (x_{ik}(F) - x(F))^2 \Delta_{\mathrm{LDAl}}(Y)}. \tag{5}$$

The fused feature vector $V(T)$ can be obtained by expanding it by line. Obviously, among the three fusion strategies, the dimension of tensor fusion is greatly increased, which is C, but the fusion method can cover more comprehensive features and information between feature interactions. Similarly, by using the above tensor fusion strategy, the fusion vector representation of environment description based on DS and LDA can be obtained. For environment j, if all the obtained user evaluation environment information vectors and environment description environment information vector $V(d)$ are directly fused, the evaluation environment information with less correlation between evaluation content and description content may bring noise and disturbance and increase the amount of calculation. Therefore, equation (6) is used for further calculation.

$$D(c) = \frac{2n1n(c)}{n^2 1n(T)} + n\left\{\frac{n + tr(c)}{n - 2 - tr(c)}\right\} - V, \tag{6}$$

$$V(d_i, w_j) - P(w_j|d_i) = \frac{P(d_i)}{\sum_{k=1}^{K} b(w_j|z_k) P(z_k|d_i)} P(w_j|d_i). \tag{7}$$

P is Pearson correlation, and the user evaluation environmental information with large correlation V and coastal zone description environmental information are selected for fusion:

$$F(Y) = \left[\frac{\zeta_1 c_1(t) + \zeta_2 c_2(p) + \zeta_3 c_3(p)}{\zeta_4 c_4(p) + \zeta_5 c_5(p) + \zeta_6 \omega_{ik}}\right]. \tag{8}$$

ζ is the mean of X and Y; Y_i is the variance of X_i. Select $V(T)$ of P as the representative evaluation vector of the evaluated environment, add these vectors directly to ensure that their dimensions remain unchanged, and then fuse them with $V(d)$. Strategies such as splicing, addition, or tensor fusion can be adopted to obtain the vectorized representation of the environmental information of environment J in class k, which is recorded as $V(Y)$.

For the expression of coastal zone information, the environmental platform often provides a large number of picture information in addition to using words to describe and evaluate the environment. The fusion of multisource environmental information data can more accurately represent the user's environmental information description of the environment. If the image and other data can be further integrated, it can further enrich the UGCS data's description of the environment, making it more accurate and comprehensive to represent the overall information of the user's attention to the environment. The RESNET model is used to extract the image feature information related to the coastal zone with user evaluation. Firstly, the residual network is pretrained using the ImageNet dataset, and then, the network is migrated to the environmental image feature extraction in this paper for fine-tuning. A collection of images related to the environment K

$$K_i = R * \beta(hp_i, v_i) + \varepsilon_j \beta_j + \sum_{j=1}^{p} \beta_j(x, y) \mathrm{x}_{ij}. \tag{9}$$

Input the fine-tuning RESNET network, and the vector output by the network is obtained as the feature of each picture.

$$Y(T) = K(y(k2 - 1), u(p2 - c2 - 1)). \tag{10}$$

For the feature vector set n of all image sets of the environment, the average weighting operation is adopted to obtain the vector after synthesizing all picture information. Equation (11) is the image feature representation of the environment.

$$P_0(N) = \begin{cases} 0, & x_{ik}(e) = \dfrac{N}{A}, \quad x_{jl}(e) = \dfrac{N}{A}, \\ 1, & x_{ik}(e) = Y_i \log(y_1) + (1 - Y_1) \log(1 - y_1), \quad x_{jl}(e) = \dfrac{N}{A}. \end{cases} \tag{11}$$

Environmental information and images have obvious heterogeneous characteristics. The information they represent is not only different but also complementary. Their feature extraction models are completely different, and their feature dimensions are also obviously different. Therefore, it is very important to design a heterogeneous feature data fusion strategy. Inspired by a convolution neural network, this paper proposes a heterogeneous data feature fusion method based on convolution operation. For the comprehensive characteristics of environmental information of environment K,

$$K = \left\{ \frac{1}{N} - \log_m F - \frac{D}{W} \right\} + \lambda \frac{1}{N} |X - G|, \tag{12}$$

$$G = \sum_{i=1}^{g} \left\{ P_i | \sum_{j=1}^{k} p_j^{(i)} \right\}, \tag{13}$$

$$\sqrt{R} = \frac{R^g \cap R^r \| G_0 - G|}{R^g \cap R^r}. \tag{14}$$

The fusion of two types of features based on convolution is shown in

$$\frac{Y}{H} = \sum_{S-1}^{U} \sum_{d-1}^{K} f_s, DV_s, d, \tag{15}$$

$$H(D_i, w_j) = Y(d_i) \frac{P(w_j | d_i)}{\sum_{k=1}^{K} (w_j | z_k) P(z_k | d_i)} + D(w_j | d_i). \tag{16}$$

Compared with other fusion methods such as LDA, DS, and SVM, the fusion method proposed in this study is highly efficient and reliable and uses advanced information processing and management technologies to target the ocean power and ecology obtained by the system data integration module. Environmental monitoring real-time, quasi-real-time, history, business guidance, and other available data in the demonstration area are very applicable in the article.

In the above formula, the number of user evaluation texts of the k environmental information set Y, the t environmental information set D is $h(D, w)$, which does not need to consider the dimension of the features to be fused, and the feature dimension after fusion is far lower than that of tensor fusion. Compared with stitching fusion, convolution fusion can not only fully consider the interaction of heterogeneous data features in all dimensions but also enhance the important features in the data and filter the noise features.

In response to the overall needs of marine environmental monitoring data and marine monitoring information for marine rights maintenance, disaster prevention and mitigation, ecological protection, resource development, marine engineering and shipping, and national defense construction, new and intelligent multiplatform sensing and data acquisition of marine environmental elements are carried out technology, multiplatform remote sensing monitoring and surveillance application technology, and mobile target detection and recognition technology. This paper selects relevant datasets to verify the performance of the proposed algorithm. As shown in Figure 2, the experiments are applied to the evaluation of short environmental information + category environmental information fusion representation learning and environmental information + image fusion representation learning, respectively. In the short environmental information comment feature representation experiment, the comment data of five types of coastal zones such as automobile, outdoor sports environment, office supplies, toys and games, and Android software are selected, the environmental information comment data in the comment data are extracted and labeled to build a balanced experimental dataset, and then it is divided into training set and test set at the ratio of 3 : 1, for example, verification. In the experiment of determining the minimum number of comments required to characterize the coastal zone and image fusion representation of environmental information, due to the loss and damage of some categories of coastal zone image data in the dataset, the categories in Amazon dataset are pet supplies, software, and office supplies; the review text field in the comment dataset of toys and games and the description field in the meta dataset are combined correspondingly according to the coastal zone number as in field.

3. Results and Analysis

3.1. Multisource Fusion Coastal Zone Data Acquisition and Analysis. The completion of a function often requires many function calls back and forth between the client and the server to complete. In the network environment, the impact of these calls on the response speed and stability of the system can be ignored. However, in the network environment, these factors are often a key determinant of whether the entire system can work normally. Therefore, multisource heterogeneous UGCS recommends the use of large data volume for one-time information exchange. This paper proposes a learning strategy for environment vectorization representation based on multisource heterogeneous UGCS data. The coastal zone "chair" not only has the environmental information description and image provided by the sensor but also the evaluation provided by the buyer. This information is fused, expressed, and learned to form a vector containing the information features of different angles of the environment. In this paper, the DS model in Gensim library is used to train the preprocessed coastal zone comments, and then, the basic parameters of DS with the best classification effect are determined through cross-validation and grid search, as shown in Table 1.

Parameter value and parameter description min_ COUNT1 discards words with word frequency less than 1.

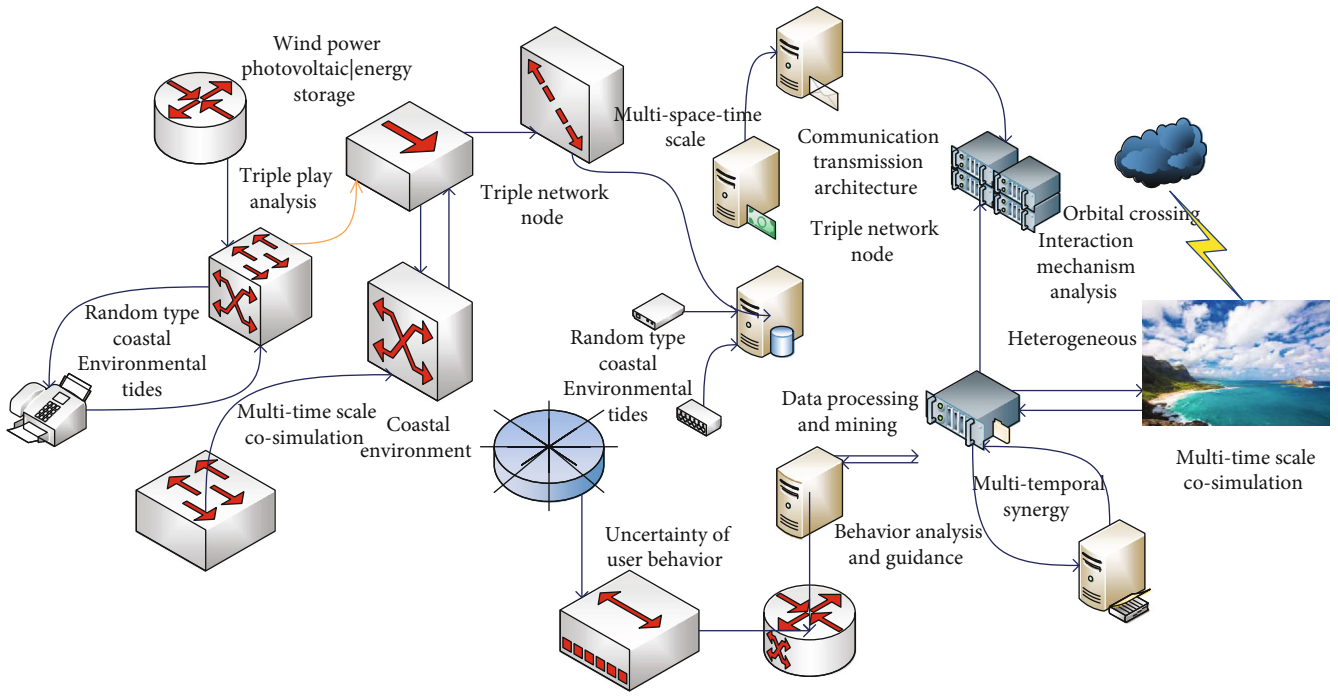

Figure 2: Category environmental information fusion learns.

Table 1: Basic parameters of DS with the best classification effect.

Item	Parameter	End behavior	Smart charging	Orbital crossing
Application layer	6.11	7.35	4.58	9.51
Information fusion	4.97	7.6	4.7	7.8
Run schedule	4.78	6.57	2.42	8.55
Operation management	2.4	4.66	0.66	8.65
Data storage	1.12	3.76	0.45	6.53
Analysis platform	-0.53	3.41	0.82	6.6

The maximum distance vector between the current word and the predicted word in window2_ Dimension HS0 of size200 eigenvector calls negative sampling negative 5 noise word frequency alpha 0.25 initial learning rate min_ Alpha0.00025 minimum learning rate DM1 uses pv-dm algorithm to extract environmental information feature vector by DS, and the vector dimension has an important impact on subsequent fusion. Therefore, the classification accuracy of environmental information features with different dimensions on each classifier is considered here to determine the dimension of DS output. If the feature vector dimension of the DS model is too small, it cannot fully represent the environment information of the corpus, and if the feature vector dimension is too large, it will increase the time complexity of training and operation. Therefore, the feature vector dimension is set to increase from 50 to 300 dimensions, and the classification accuracy is recorded every 50 dimensions.

As shown in Table 2, the reference water level not only determines the elevation of the refuge but also determines the floor elevation of specific buildings in the disaster warning area. The reference water level refers to the total height of the wave height (tsunami, storm surge, or overtopping) superimposed by the surge caused by the obstruction of the building. Refuge places include refuge towers, refuge buildings, and refuge platforms. The elevation of the refuge layer shall be above the reference water level of the area. In the specific calculation, the disaster warning area is divided into several cells (e.g., 10 m × 10 m), and the reference water level height of the cell where the facility is located is obtained through simulation calculation. The prerequisite for human development and use of the ocean is to understand and master the ocean. However, the basis for understanding and mastering the ocean is the implementation of long-term, continuous, comprehensive, and accurate observation of the marine environment in order to grasp the status and changing laws of the marine environment to make correct predictions and evaluations of the marine environment. In turn, it provides the necessary basic data and scientific basis for the rational development and utilization of the ocean, marine environmental protection, marine engineering design, and safety guarantee for marine operations so that marine development enters an orderly and sustainable development track.

In view of the particularity of the marine environment three-dimensional monitoring, this paper takes the integrated guarantee of the marine environment three-dimensional monitoring system operation as the main research objective. Based on the original marine environment monitoring system,

Table 2: Elevation height of the standard refuge area.

Item	Dimension	Heterogeneous	Multisource	Massive
Power grid	3.73	3.1	6.23	5.24
Charge	2.84	5.47	7.5	7.1
Environment	2.03	7.82	10.35	8.59
Speed measurement	3.39	7.23	9.84	8.41
Position	5.66	7.21	11.16	10.71

Table 3: Fortification height of the dyke.

Item	Operational control	Technology	Interaction	Mechanism	Driven users
Random type	8.12	14.58	19.46	6.74	9.69
Coastal	8.86	14.82	17.81	6.08	8.98
Environmental	7.15	13.38	17.73	5.72	7.82
Multitemporal	5.93	13.14	17.97	6.41	7.2
Multispace	6.34	12.68	18.89	6.71	6.65
Time scale	4.78	11.03	17.99	6.4	5.49

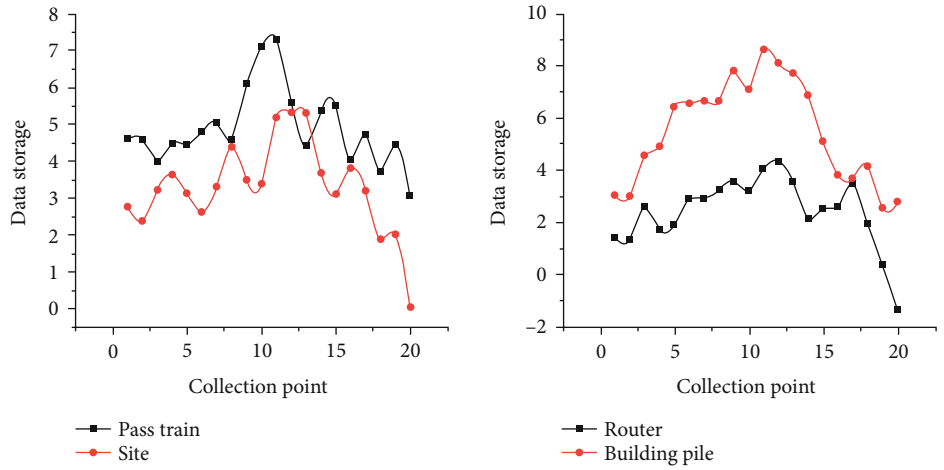

Figure 3: The flooded zone of the tsunami caused by the earthquake.

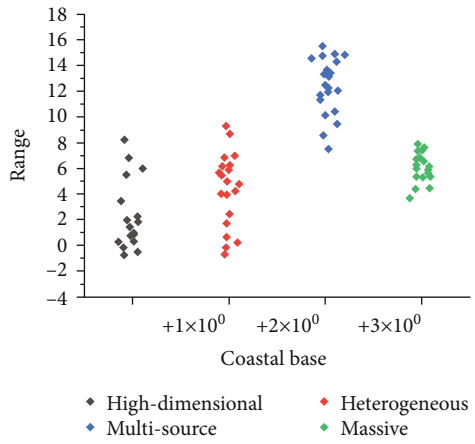

Figure 4: The range and depth of the tsunami flooding.

the research on the LDA and DS model fusion of the relevant operation guarantee technology is carried out. As shown in Table 3, the fortification height of the dampproof embankment is determined by the design tsunami level of the tsunami group with high frequency in decades and hundreds of years and the highest value of the design storm surge tide level after superposition of wave factors. For Tokyo Bay, the storm surge design tide level is always greater than the tsunami design water level. UPI international urban planning combination of prevention and reduction: land use and refuge countermeasures in the coastal zone of Sendai City and Osaka City. Because the key factor determining the immersion depth and scope of the Tokyo Bay is the height of the storm surge, therefore, the promotion of tsunami disaster prevention area construction has not had too much impact on the land use and refuge machines in its coastal zone.

As shown in Figure 3, the outermost layer of the coastal zone is the flooded zone caused by the tsunami caused by the

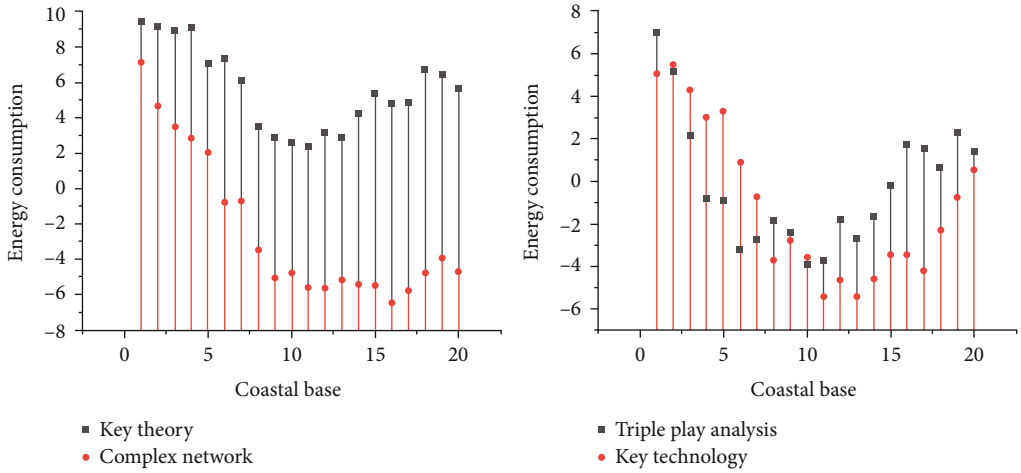

Figure 5: Distance between flooding depth and coastline.

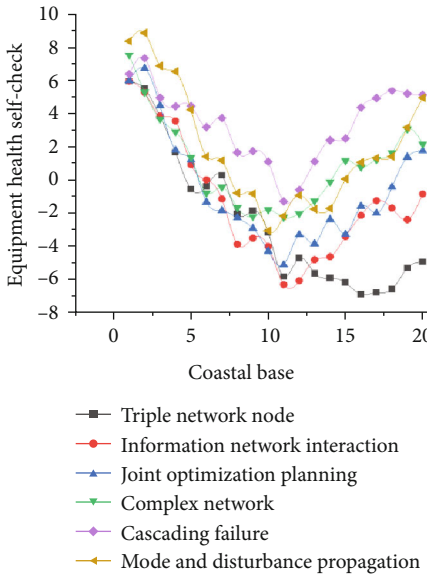

Figure 6: Coastal ecological disaster.

East Japan earthquake. It is planned to be a coastal park and a beach in the future. The second floor is farmland and scattered residential colonies, such as the Okada colony and Pushing colony. Set up main motor vehicle refuge roads between the colonies, and delimit pedestrian refuge paths according to people's behavioral characteristics. The refuge paths are perpendicular to the coast and move towards the highlands away from the coast, which is also known as "run up!" Asylum training is carried out by communities.

After the Ministry of Land, Resources, and Transportation gradually prepared the relevant draft of tsunami disaster prevention area construction, the immersion range and depth of the largest tsunami that may occur in Osaka Bay were simulated and calculated, and the tsunami immersion scenario was obtained, as shown in Figure 4. According to the existing flooding scenario, it can be determined that the refuge path in the coastal zone of Osaka City is still generally perpendicular to the coast and moves inland away from the coast. In some areas, it is necessary to take refuge away from the river.

As shown in Figure 5, as a dense urban coastal zone, its immersion depth depends not only on the distance from the coastline but also on the terrain height, urban building density, distance from the river, and drainage conditions. Some peninsula areas close to the coastline still have low immersion depth due to flat terrain and low building density. Even if there is a certain distance from the coastline, it still has a high risk of flooding due to its proximity to rivers, high building density, and poor drainage conditions. Therefore, it is necessary to closely combine the local natural and social conditions when formulating the construction specifications of buildings in the disaster warning area. The delimitation and specific implementation plan of tsunami disaster warning areas in Osaka city are still in progress.

3.2. Coastal Ecological Environment Monitoring and Construction. As shown in Figure 6, the enlightenment to China's Pearl River Delta coastal zone ecological disaster prevention and mitigation planning, the Pearl River Delta coastal zone presents the contradiction between the improvement of fortification standards under the risk of coastal zone ecological disasters and the living density and development needs of existing coastal zones. A series of coastal zone ecological disaster response planning strategies combined with prevention and reduction after the East Japan earthquake can provide a reference for this.

Running real-time monitoring client software is deployed in each monitoring terminal to achieve status information extraction and reporting, running real-time monitoring server software is deployed in the data center to achieve real-time display and remote control of monitoring service system status information, and information sharing and application service software are deployed on shared servers to realize the security system information sharing service and application and achieve timely warning. As shown in Figure 7, the Pearl River Delta coastal zone should comprehensively consider the ecological disaster risk of the coastal

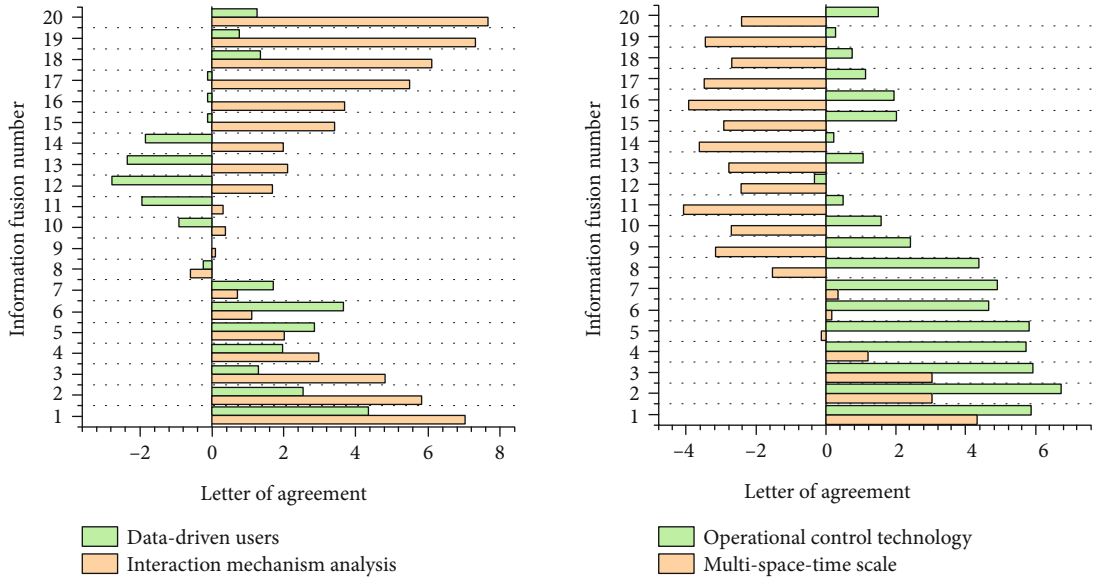

Figure 7: Coastal ecological disaster risk.

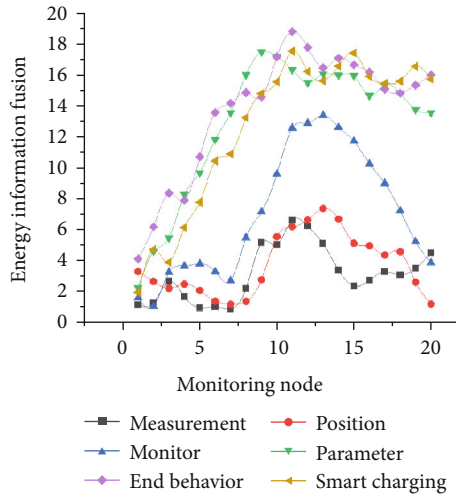

Figure 8: Storm surge level in overseas seas.

zone and divide the disaster risk into the highest tide level of tsunami group or storm surge with high frequency during the facility supply period and the tide level of tsunami or storm surge with the largest possible level. Revise the fortification level of protective facilities according to the tide level with high frequency. Limit the land use and building construction according to the maximum level tide level, to achieve effective refuge and minimize the losses caused by disasters.

As shown in Figure 8, the maximum tidal level of storm surge in Zhuhai offshore caused by typhoons is 4.29 m. The coastal area of the Pearl River Delta measured by simulation calculation has a high tsunami risk below 9 m, and the design tidal level of Zhuhai coastal protective facilities is 3.11 m or even lower. It can be preliminarily considered that the fortification standard of Zhuhai coastal zone protection facilities is determined by storm surge. The tsunami risk of 9 m and below can be used as the standard for dividing dangerous areas and become the basis for regional land use and building construction norms.

China's current disaster response strategy still focuses on disaster prevention countermeasures, as shown in Figure 9. The increased disaster reduction dimension based on Japan's experience is the key to improve China's disaster response system and also provides an important idea to solve the spear between the improvement of fortification standards and residential density and development needs in the coastal zone of the Pearl River Delta, that is, whether to admit that disasters cannot be resisted completely through technical means. Therefore, it is necessary to enhance and give full play to the self-help power of the community to ensure the safety of life and property and minimize the losses caused by disasters. The delimitation of disaster risk areas and the provisions on land and buildings within its scope essentially recognize that the area can be impacted by disasters. It is the setting of prevention and control standards after comprehensive consideration of disaster reduction countermeasures. In this paper, it is still classified as disaster prevention countermeasures for ease of understanding. On this basis, the possible disaster reduction countermeasures are summarized as follows.

As shown in Figure 10, for the built-up area of the coastal zone, the existing dampproof embankment shall be verified according to the tide level height of the once-in-a-century storm surge, and the measures of improving the fortification standard or strengthening and maintenance shall be taken. Delimit the tsunami risk area according to the tsunami of 9 m and below, and take waterproof countermeasures for specific buildings in the area (such as hospitals, welfare facilities for children and the elderly, and residential buildings, whose users have high requirements for safety), including changing the location of their residential part, improving the floor of their residential part, and strengthening the main structure of the building with earthquake and

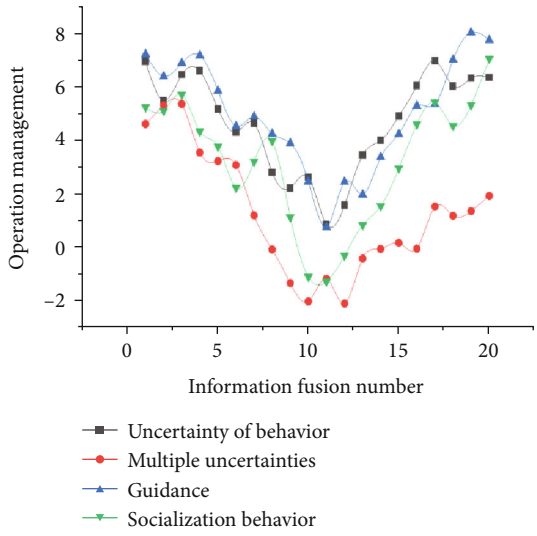

Figure 9: Coastal fortification standards.

water resistance; waterproof board and water stop door shall be set in the area below the immersion line, and important electrical equipment shall be moved to a high place. The floor elevation standard can be determined through the simulation calculation of the reference water level height of the cell.

As shown in Figure 11, the postdisaster reconstruction of Sendai City is one of the prototype cities for formulating the relevant planning for the construction of a tsunami disaster prevention area. Its disaster warning area is bounded by the l2-2 m line, which is equivalent to the flooded area of the East Japan earthquake and tsunami, and most of it is located outside the East Road of Sendai in the figure. In the warning area, its land use shows obvious stratification characteristics parallel to the coast. To realize the above coastal zone ecological disaster response strategy combining disaster prevention and reduction, the coordination and cooperation of water conservancy, transportation, housing, planning, construction, and other government functional departments, social organizations, and community residents are required. This puts forward requirements for clarifying the rights and responsibilities of various departments, formulating multiagent cooperation mechanisms, and determining the action process in advance, which should be paid attention to.

As shown in Figure 12, in the field of personalized services, various application apps have become indispensable tools for life and even work. In the process of using apps, users will not only produce a large amount of real-time communication information but also provide a large amount of data such as dynamically changing environmental information comments, scoring, labels, pictures, and videos. Obviously, under the current network technology, users have become active creators of data, providing a large number of user-generated content (UGCS), which has become a data component with extremely important application value in the field of personalized services. UGC data reflecting user personalized information has obvious multisource heterogeneous characteristics. Its multisource is reflected in that the description and evaluation of the same object are given by different people in a variety of different data forms (such as environmental information, image, or video) from different angles.

Shown in Figure 13 is the zoning planning of the Osaka Bay coastal zone. In addition, compared with the tsunami disaster prevention regional construction planning, which emphasizes the zoning of land use, building construction, and refuge countermeasures perpendicular to the coast, the coastal preservation planning of Osaka Bay also highlights the zoning planning parallel to the coastline due to specific regional conditions. Therefore, according to different coastal types, ecology, and hinterland characteristics, Osaka prefecture divides the coastal zone horizontally into living area, rest area, and production and living integration area. In the planning for the preparation of coastal protection facilities, the specific implementation scheme shall be formulated in close combination with the characteristics and requirements of the zoning where the facility points are located, such as not only improving the fortification standard of protection facilities but also planning and designing its hydrophilicity and its effect on the surrounding environment of the land.

As shown in Figure 14, the number of indicators in multisource information fusion in this paper is 16; there are 3251 data, 2866 meaningful information, and 1869 data including ecological cycle. After multisource information fusion and decision-making, it is obtained that the index equilibrium module in the DS algorithm in this paper is 0.52, the sensitivity is 0.68, and the independence is 0.42. Among them, the range of sensitivity is the largest. In the simulation results, the eco-economic coefficient can be increased from 12% to 36%. There is a high risk of tsunami impact along the coast with a tide height of 9 m and below. Due to the evolution of urban development, the coastal areas of Zhuhai have high residential density and development needs.

4. Discussion

How to achieve efficient personalized search and recommendation in a large number of user-generated data environments has attracted extensive attention in the current personalized service field. To achieve the above tasks, the vectorial representation learning of UGC multisource heterogeneous data is very important. Many research achievements have been made in the fields of environmental information and image classification. For multisource heterogeneous UGC data, because the data comes from the evaluation environment information of different users, the label description of the environment, and the picture information of the environment, the evaluation environment information is mostly oral, fragmented, and noisy short environment information, the label is not unique, and the picture quality is uneven; therefore, it is difficult to fuse and represent this kind of multisource heterogeneous data.

The commercial operation of the marine environment three-dimensional monitoring system directly affects the operation and development of various marine applications.

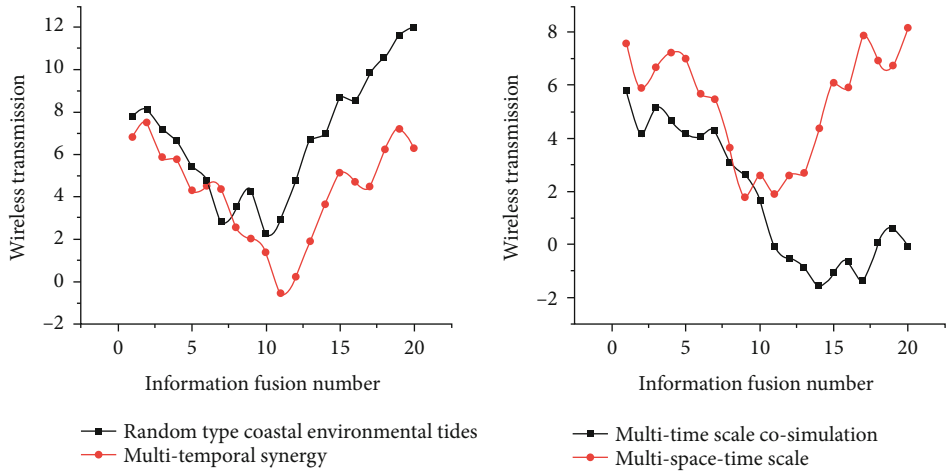

Figure 10: Verification of storm surge level and existing dykes.

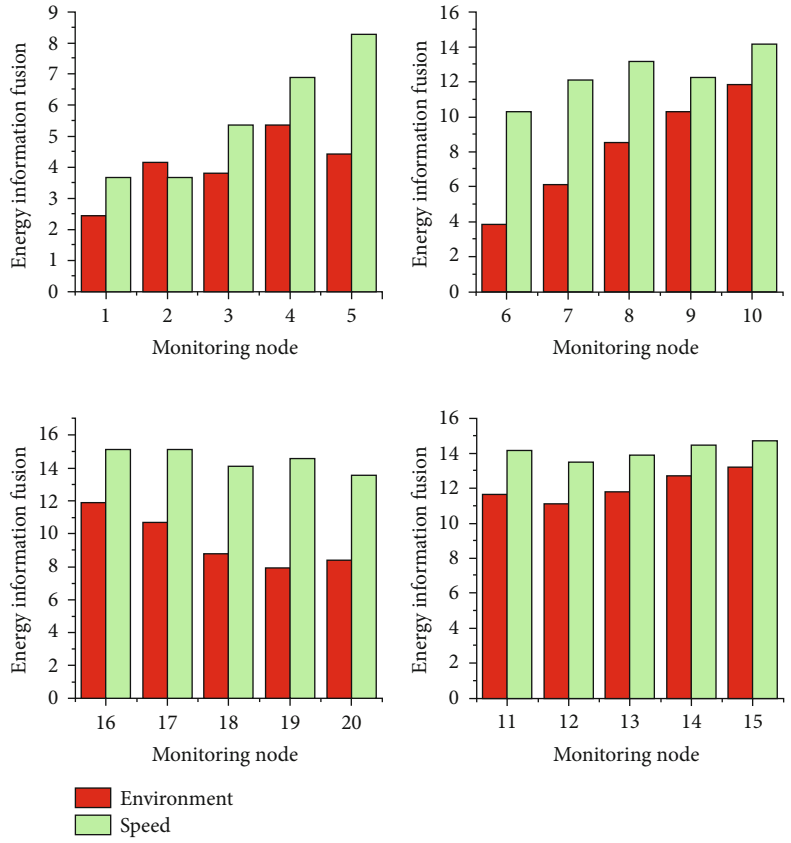

Figure 11: Planning related to tsunami disaster prevention area construction.

Starting from mastering the status and changing laws of the marine environment, the only way to implement long-term, continuous observation and application services of the marine environment is to ensure that the marine environment monitoring system is in a state of operationalization. In response to the need for the stable operation of the marine environment three-dimensional monitoring system, this paper researches and develops the structure of guarantee resources, the framework of the comprehensive guarantee system and the various technologies involved, and realizes a set of operations and maintenance plans for the marine environment three-dimensional monitoring system.

The marine environment three-dimensional monitoring system provides the necessary basic resources and data basis for the maintenance of marine rights and interests, disaster prevention and mitigation, ecological protection, resource development, and decision-making assistance and provides the possibility for the sustainable development of marine

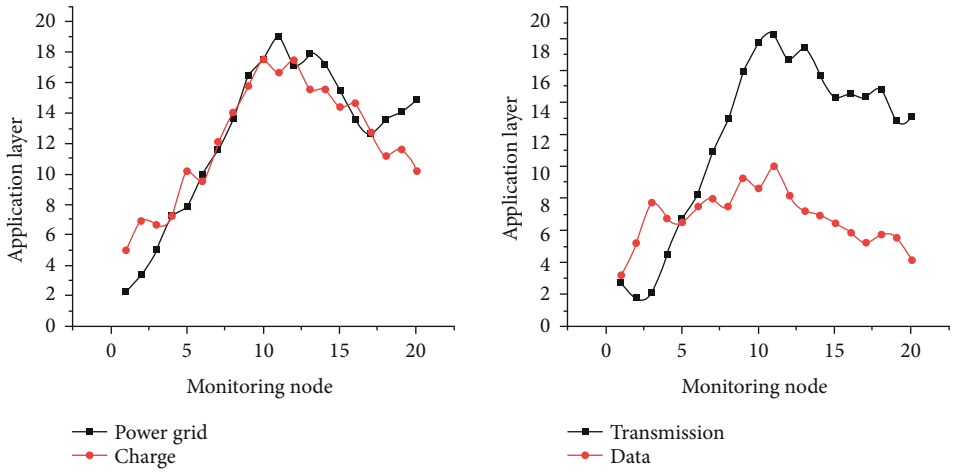

Figure 12: Real-time information exchange environment.

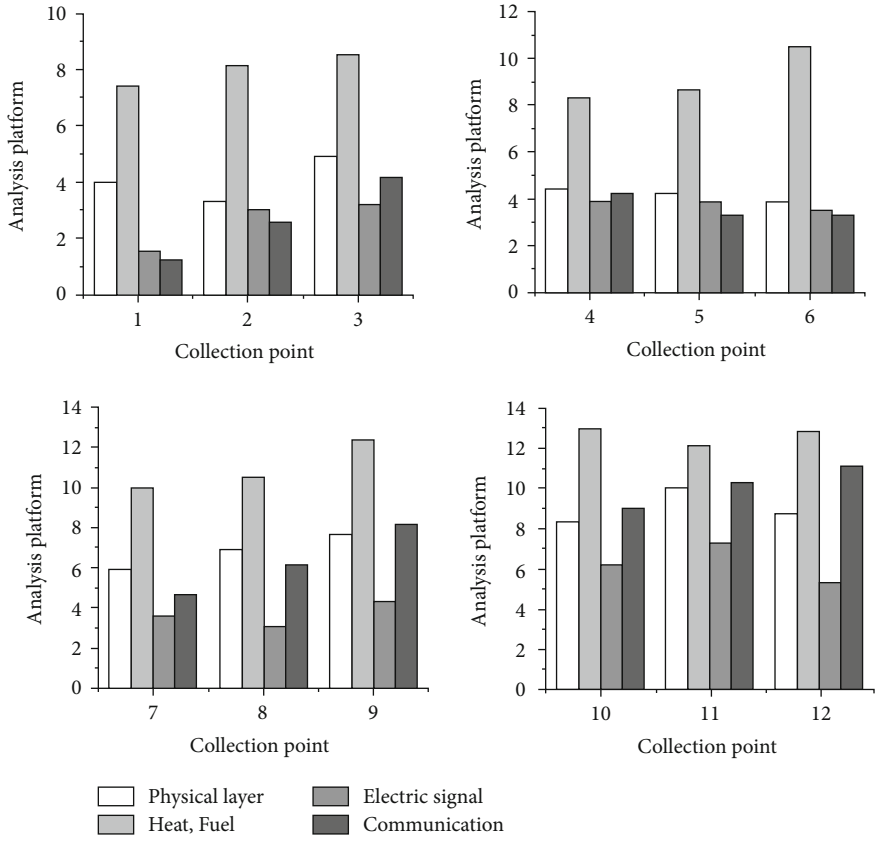

Figure 13: Coastal zone regional construction planning.

undertakings. A complete marine environment monitoring system consists of three parts: three-dimensional observation of the marine environment, data communication and management, and data processing and application. The experience and lessons of the East Japan earthquake once again proved that there is no upper limit for the fortification of natural disasters. Therefore, based on the experience and lessons of the Hanshin earthquake, Japan further put forward a new tsunami response strategy with the concept of "combination of prevention and reduction": disasters with high frequency should be strictly prevented and controlled through scientific means. In the face of a wide area, a complex and long-term disaster such as the East Japan earthquake, we should consider preset the most unfavorable situation of the disaster, delimit its risk area, ensure the life safety of the victims in the area, and make full use of the community self-help ability so that they can take refuge effectively and minimize the losses caused by the disaster

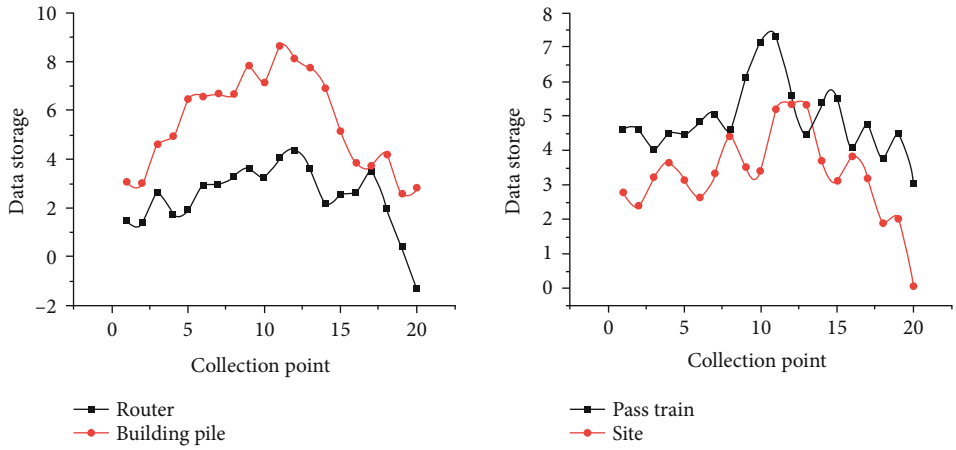

Figure 14: Number of indicators in multisource information fusion.

and recover from the disaster as soon as possible. Due to the frequent occurrence of natural disasters, Japan has accumulated rich experience in disaster response and adjusted and improved its disaster prevention and reduction planning based on the experience and lessons of previous disasters. Taking Zhuhai City after the "Tiange" typhoon as an example, the net hydrological observation facility of "Tiange" typhoon recorded the tide level in the open sea of Zhuhai as high as 4.29 m, breaking through the historical highest tide level of 3.37 m. As a wave protection facility and an important traffic and landscape function, the design tide level area of some sections of Lovers Road along the coast of Zhuhai is only 3.11 m, and the length of damaged areas is more than 45 km. The fortification standard needs to be improved. Set refuge places, including high platforms, refuge towers, and refuge buildings. The refuge elevation is also determined according to the reference water level height of the cell. It is necessary to carry out disaster prevention education for residents in ordinary times, guide residents on how to correctly obtain disaster risk information, carry out refuge training, and guide them on the time when they should take refuge action according to the behavior characteristics of different residents.

5. Conclusions

The research on resource management of intelligent buildings is mainly to integrate the resources of daily property management such as property equipment, property services, and information release of smart buildings by property companies to form a unified comprehensive information platform. The multisource information platform can provide users with advanced security protection, information services, property management, and other services, in order to create a safe, comfortable, convenient, and efficient living space for users and enhance the competitiveness of the enterprise market. This paper uses the method of multisource information fusion for quantitative index analysis, which can provide data support for coastal ecological environment detection, to establish a more perfect protection system. Therefore, although the Pearl River Delta coastal zone has the requirements of improving the fortification height of protective facilities and avoiding disasters, it is in contradiction with the existing urban structure and residential density, good coastal landscape vision, and the development demand for coastal land. The two typhoon disasters exposed the lack of wave protection facilities along the Pearl River Delta. In the existing meteorological disaster, early warning system including typhoons, rainstorms, and blizzard in China, based on early warning of river water volume, the flooding risk early warning mechanism of tsunami or storm surge in specific areas can be added according to the scenario simulation calculation of tide level and protective facilities. Within the disaster risk area, the refuge path shall be set in advance. According to the characteristics of coastal disasters, the refuge direction shall be the highland or inland area away from the coast and away from the river entering the sea.

Data Availability

No data were used to support this study.

Conflicts of Interest

There are no potential competing interests in our paper.

Authors' Contributions

All authors have seen the manuscript and approved to submit to your journal.

Acknowledgments

This paper is the phased achievement of the major scientific research and cultivation project of the Dongguan City College, "The Study of the Legal System of Marine Ecological Restoration," project number 2021YZDYB04R.

References

[1] R. WEI and W. ZIMMERMANN, "Microbial enzymes for the recycling of recalcitrant petroleum-based plastics: how far are we?," *Microbial Biotechnology*, vol. 10, no. 6, pp. 1308–1322, 2017.

[2] K. LAW, "Plastics in the marine environment," *Annual Review of Marine Science*, vol. 9, no. 1, pp. 205–229, 2017.

[3] C. M. Rochman, M. A. Browne, B. S. Halpern et al., "Classify plastic waste as hazardous," *Nature*, vol. 494, no. 7436, pp. 169–171, 2013.

[4] E. BESSELING, P. REDONDO-HASSELERHARM, and E. M. FOEKEMA, "Quantifying ecological risks of aquatic micro- and nanoplastic," *Critical Reviews in Environmental Science and Technology*, vol. 49, no. 1, pp. 32–80, 2019.

[5] O. O. Fadare, B. Wan, L.-H. Guo, Y. Xin, W. Qin, and Y. Yang, "Humic acid alleviates the toxicity of polystyrene nanoplastic particles to Daphnia magna," *Environmental Science: Nano*, vol. 6, no. 5, pp. 1466–1477, 2019.

[6] J. GIGAULT, A. TER HALLE, and M. BAUDRIMONT, "Current opinion: what is a nanoplastic?," *Environmental Pollution*, vol. 235, no. 45, pp. 1030–1034, 2018.

[7] H. EL HADRI, J. GIGAULT, and B. MAXIT, "Nanoplastic from mechanically degraded primary and secondary microplastics for environmental assessments," *Nano Impact*, vol. 17, no. 4, pp. 100206–100206, 2020.

[8] S. WAGNER and T. REEMTSMA, "Things we know and don't know about nanoplastic in the environment," *Nature Nanotechnology*, vol. 14, no. 4, pp. 300-301, 2019.

[9] O. S. Alimi, J. F. Budarz, L. M. Hernandez, and N. Tufenkji, "Microplastics and nanoplastics in aquatic environments: aggregation, deposition, and enhanced contaminant transport," *Environmental Science & Technology*, vol. 52, no. 4, pp. 1704–1724, 2018.

[10] P. K. Cheung and L. Fok, "Characterisation of plastic microbeads in facial scrubs and their estimated emissions in Mainland China," *Water Research*, vol. 122, no. 6, pp. 53–61, 2017.

[11] H. ZHANG, K. U. O. Y-Y, and A. C. GERECKE, "Co-release of hexabromocyclododecane (HBCD) and nano-and microparticles from thermal cutting of polystyrene foams," *Environmental Science & Technology*, vol. 46, no. 20, pp. 10990–10996, 2012.

[12] B. STEPHENS, P. AZIMI, and Z. EL ORCH, "Ultrafine particle emissions from desktop 3D printers," *Atmospheric Environment*, vol. 79, no. 5, pp. 334–339, 2019.

[13] S. A. Carr, J. Liu, and A. G. Tesoro, "Transport and fate of microplastic particles in wastewater treatment plants," *Water Research*, vol. 91, no. 45, pp. 174–182, 2016.

[14] D. E. N. VAN, P. BERG, E. HUERTA-LWANGA, and F. CORRADINI, "Sewage sludge application as a vehicle for microplastics in eastern Spanish agricultural soils," *Environmental Pollution*, vol. 261, no. 4, pp. 114198–114198, 2020.

[15] M. CLAESSENS, L. VAN CAUWENBERGHE, and M. B. VANDEGEHUCHTE, "New techniques for the detection of microplastics in sediments and field collected organisms," *Marine Pollution Bulletin*, vol. 70, no. 2, pp. 227–233, 2019.

[16] O. Hollóczki and S. Gehrke, "Can nanoplastics alter cell membranes?," *Chem Phys Chem*, vol. 21, no. 1, pp. 9–12, 2020.

[17] L. RUBIO, R. MARCOS, and A. HERNáNDEZ, "Potential adverse health effects of ingested micro- and nanoplastics on humans. Lessons learned fromin vivoandin vitromammalian models," *Journal of Toxicology and Environmental Health, Part B*, vol. 23, no. 2, pp. 51–68, 2020.

[18] C. ZHANG, X. CHEN, and J. WANG, "Toxic effects of microplastic on marine microalgae _Skeletonema costatum_: interactions between microplastic and algae," *Environmental Pollution*, vol. 220, no. Part B, pp. 1282–1288, 2017.

[19] I. BRANDTS, M. TELES, and A. GONçALVES, "Effects of nanoplastics on _Mytilus galloprovincialis_ after individual and combined exposure with carbamazepine," *Science of the Total Environment*, vol. 643, no. 4, pp. 775–784, 2018.

[20] R. TREVISAN, C. VOY, and S. CHEN, "Nanoplastics decrease the toxicity of a complex PAH mixture but impair mitochondrial energy production in developing zebrafish," *Environmental Science & Technology*, vol. 53, no. 14, pp. 8405–8415, 2019.

[21] D. K. Tripathi, S. S. Shweta, S. Singh et al., "An overview on manufactured nanoparticles in plants: uptake, translocation, accumulation and phytotoxicity," *Plant Physiology and Biochemistry*, vol. 110, no. 4, pp. 2–12, 2017.

[22] S. VAN WEERT, P. E. REDONDO-HASSELERHARM, and N. J. DIEPENS, "Effects of nanoplastics and microplastics on the growth of sediment-rooted macrophytes," *Science of the Total Environment*, vol. 654, no. 6, pp. 1040–1047, 2019.

[23] S. U. N. X-D, Y. U. A. N. X-Z, and Y. JIA, "Differentially charged nanoplastics demonstrate distinct accumulation in _Arabidopsis thaliana_," *Nature Nanotechnology*, vol. 15, no. 9, pp. 755–760, 2020.

[24] J. DAVID, Z. STEINMETZ, and J. I. KUČERÍK, "Quantitative analysis of poly (ethylene terephthalate) microplastics in soil via thermogravimetry–mass spectrometry," *Analytical Chemistry*, vol. 90, no. 15, pp. 8793–8799, 2018.

[25] J. C. Prata, J. P. da Costa, A. C. Duarte, and T. Rocha-Santos, "Methods for sampling and detection of microplastics in water and sediment: a critical review," *TrAC Trends in Analytical Chemistry*, vol. 110, no. 56, pp. 150–159, 2019.

Hindawi
Journal of Sensors
Volume 2021, Article ID 2292267, 13 pages
https://doi.org/10.1155/2021/2292267

Research Article

Application of Cloud Computing and Information Fusion Technology in Green Investment Evaluation System

Pengwu Wang

School of Accounting, Harbin University of Commerce, Harbin, 150028 Heilongjiang, China

Correspondence should be addressed to Pengwu Wang; wangpengwu2021@126.com

Received 11 August 2021; Revised 15 September 2021; Accepted 7 October 2021; Published 27 October 2021

Academic Editor: Mu Zhou

As an important part of the development of green economy, the green investment evaluation system provides a method to identify the performance of the investment environment and also guides the design of green investment plans. This article is aimed at analyzing the application of cloud computing and information fusion technology in the green investment evaluation system, using empirical analysis, qualitative and quantitative analysis, data integration, and distributed computing algorithms to carry out research. Data acquisition is mainly through cloud platform information fusion, to evaluate the investment subject, investment object, and investment vehicle of green investment. Qualitative and quantitative analysis is mainly through the definition of prerequisites by stipulating certain aspects of green, and the analysis of the country's data changes in a certain time zone. Focus on the qualitative analysis and research on the green benefit attributes of a certain thing. In addition, by analyzing the influencing factors of the investment development status of green industries in different countries, such as green products, green projects, and green funds, it proves that the application of cloud computing and information fusion technology has a huge effect on the green investment evaluation system. Experimental data shows that in the past five years, investment in fixed assets in my country's major industries accounted for the proportion of fixed asset investment in the whole society, and investment in environmental protection and energy supply industries has continued to rise. This upward trend is manifested in the fact that the amount of energy investment is increasing year by year. The development trend is the strongest during the development period and the entry period, and its data grows the most rapidly, while investment in the transportation industry has always been listed in the tables. For the first place in the industry, the highest was 20.84%.

1. Introduction

Cloud computing technology is a key technology to realize the Internet of Things. The computing and storage capabilities of the sensor and other information collection parts in the Internet of Things are relatively weak, and the powerful computing and storage capabilities of the cloud computing center are required [1]. Cloud computing and the Internet of Things will promote each other and develop together. With the advent of the era of big data, a new information environment has been formed with its huge data scale, diverse data, rapid dissemination, and low value density. While bringing development opportunities, it also enables information resource organization and services facing greater challenges. Ultra-large-scale "cloud" has a considerable scale and can obtain various supercapable services through network services, while supporting the operation of different applications and meeting the needs of application and user scale growth, and automated management to greatly reduce the cost of data center management. Based on the characteristics of cloud computing itself, the use of cloud computing technology can avoid the repeated construction of information resources and improve the sharing of information resources. It greatly saves the capital investment of information service subjects, reduces the management and maintenance costs of servers and storage, and reduces the demand for management and maintenance personnel. At present, search engines based on database technology and information retrieval technology are the main information resource organization and service tools. The organization and retrieval of massive information resources on the Internet are mainly done by search engines. However,

poor accuracy of search results, lack of intelligence and interactivity, lack of special search, and single interface are the main problems [2]. As an important aspect of information resource organization, information resource storage also has many problems [3].

In real life, we must face multiple information systems obtained from different angles and different starting points, for example, the reliability, comprehensiveness, novelty, and scientific nature of information, which determine the workload of the information screening and fusion process. For green investment, the needs of investment entities, investment targets, and other multiple entities are also different, and the effects pursued are also different. How to obtain more accurate and high-precision data from these multiple information systems has become a problem we have to face; therefore, people put forward the concept of information fusion [4]. Information fusion is just like the human brain that processes complex information. Humans obtain the information they want from various channels and then use the brain to unify the information for consideration and then draw conclusions for decision-making. The merging method of unfinished information systems is applied to anonymous information systems, and a new binary relationship is established by defining a new degree of similarity, and a merging model is established on this basis. For example, in the data analysis process of this experiment, considering that China and Japan are closer to each other in geographic location and climate, while the United States and the United Kingdom are related to each other for classification and comparison, this is different from the traditional thinking angle. It is the new establishment of a dual relationship [5]. How to fuse less information sources has become the focus of multisensor information integration technology. With the continuous deepening of scientific research, processing large amounts of data in different fields has become more and more important [6].

The research on the application of cloud computing and information fusion technology at home and abroad is mainly concentrated in the fields of information technology such as electronics, communications, computers, and education. Pumchalerm et al. adopt qualitative and quantitative methods for the intelligent cooperative education process management model of cloud computing technology. It uses the opinions of 15 cooperative education experts with ICT experience as a sample group to conduct in-depth interviews and open and closed questionnaires, using a conceptual framework designed to process management model of intelligent cooperative school running based on cloud computing technology [7]. Vithayathil believes that software as a service (SaaS) is an important part of making human machine interfaces (HMI) in the cloud. In its research, the cloud interface compares the project screen of the HMI server in any device with a standard browser and allows the user to monitor any screen object, view and receive alarms, and control it through the appropriate screen object [8]. Information and communication technology (ICT) basically uses ICT tools to store and retrieve information. Appiahene et al. integrate the latest technology into the teaching and learning of ICT. Apply cloud computing to ICT research by sharing IT services based on platforms, software, and infrastructure in the cloud, and focus on the role of cloud computing in ICT research in the education system of Ghana [9]. Cloud computing integrates technology into a hybrid environment of network, virtualization, and cluster environments, creating a new era full of opportunities, thereby making the business highly scalable. However, there are several challenges to be solved, especially safety, which Kumar has listed as one of the most important issues in his research [10]. Attaran's research discussed the potential strategic advantages of the technology, highlighted its evolving technology and trends and its future impact, reviewed the different stages required to deploy the technology, highlighted key adoption factors, and investigated its use in different industries. Potential applications in the use of cloud computing technology will make collaboration between companies easier and may create financial and operational benefits [11]. The distributed information fusion (DIFFUSION) strategy of sharing local information between sensors is one of the key aspects of this intelligent network. Braca et al. use alternative methods of distributed fixed and mobile sensors to form an intelligent network that achieves high performance and has the remarkable characteristics of scalability, robustness, and reliability. In this paper, two DIFFUSION schemes are proposed, in which the information shared between sensors includes (1) contacts generated by the local detection stage and (2) trajectories generated by the local tracking stage [12]. At present, the R&D project "Carbon Neutral Road Technology Development" sponsored by the Ministry of Land, Infrastructure and Transportation of South Korea has been implemented, and sustainable development related to global climate change is being discussed. Noh and Baek proposed a plan to expand the application of these technologies and build a sustainable road system considering the concept of sustainability, in order to obtain the draft of the green road certification system, the design and construction technology of low-carbon and environmentally friendly roads, and the road green road technology investment evaluation system (GTIES), estimating and managing scientific and technological achievements of highway carbon emission research and development projects [13]. Through the above research, it can be found that the research on cloud computing technology and information fusion technology, combined with the green investment evaluation system, compares and analyzes the evaluation elements as a whole, whether it is for the development and establishment of a new system or the improvement and improvement of the existing system. All have great reference significance. However, these studies have focused on cloud computing itself and information fusion technology. It is very vague about how cloud computing and information fusion create value, and the research methods lack innovation, and the experimental data is too single.

Green investment is a new trend in international investment. This paper studies the green investment evaluation system based on cloud computing and information fusion technology. On the basis of introducing the basic principles of cloud computing technology, it discusses the principles of information resource organization and service in cloud

computing. The feasibility of using cloud computing technology to build information resource cloud organization and cloud services was analyzed; an information resource organization and service cloud platform model on the basis of connotation definition, demand analysis, and function realization was built, and a platform for promoting green investment efficient operation mechanism was proposed. Through qualitative and quantitative evaluation of the status analysis, problem analysis, feasibility analysis, model construction, empirical analysis, etc. of the green investment platform, systematically discuss the application of cloud computing and information fusion technology in the organization and service of information resources in the field of green investment. The use of computing technology to obtain and analyze data can make the experimental data more credible. The content of the above experimental arrangements can be combined with the general characteristics of investment differentiation between entities in different countries and can make green investments in my country based on the characteristics of the data. The status quo of development and improvement methods brings certain innovations [14].

2. Application of Green Investment Evaluation System

2.1. Cloud Computing and Green Investment Industry. With the rapid development of network technology and economic technology, companies need to be able to quickly respond to market changes and take innovative measures to understand how to develop in fierce competition [15]. The scientific research and probability orientation of green enterprise investment has just begun. Scientific research is also included in the macrolevel green investment research, from the perspective of green enterprise investment that is closely related to the microlevel. On the other hand, investing in green company projects also is the creation of company clusters by individual companies. Based on the theory of industrial equilibrium development and economic and social development theory, it puts forward the necessity of green industry investment development, pointed out that the development of green industry investment is the industrialization requirement of developing green investment, and further pointed out that the development of green industry investment is not only international. The requirements of development trends are also an urgent need to achieve sound and rapid development of my country's economy—that is, green industry investment can be a good medicine to solve China's economic overheating, overcapacity, resource shortage, and other problems and a new profit growth point for economic development [16]. The implementation of green investment is an international trend. As soon as possible, from a single project investment to a green industry investment, completing the establishment and implementation of the green industry investment evaluation system is an objective requirement put forward by the international situation and an inevitable choice to solve domestic problems. Although the traditional computer system has the characteristics of accurate and fast calculation and judgment, good versatility, easy to use, and can be combined into a network, it still has certain limitations in its ability to play in the face of complex and huge data. The calculation accuracy will also be affected by various factors. As an emerging technology, cloud computing technology is composed of many traditional computer technologies and information technologies. If you only study the cloud computing technology as a whole, you will not be able to get an accurate judgment on the future development of the technology. Therefore, it is necessary to subdivide cloud computing technology into several subtechnologies to conduct a detailed research one by one. The most important thing is to analyze the focus of attention on these subtechnologies by various organizations and countries in the society. Cloud computing is the latest development of information technology. It has also begun to be popularized and applied. Many countries regard it as a typical new technology that drives economic growth in the posteconomic crisis era and occupies the commanding heights of science and technology. It is a new solution to promote enterprise agility to respond to dynamic and complex environments and create value [17].

Green investment is in line with the general trend of economic and social development in the world today and is in line with the strategic national policy of sustainable development, but green investment can not only be a product of ideology but also be reflected in the behavior of economic activities [18]. However, so far, there is very little research on green investment. Research on the green economic chain and corporate social responsibility investment is the requirement and constraint on corporate investment from a microperspective, and they have not integrated various fields to rise to the perspective of green industry for research [19].

2.2. Cloud Computing Technology. The information resource organization and service platform based on cloud computing technology is an intelligent, personalized, one-stop service platform for the big data environment [20]. The cloud storage model requires a large amount of Internet data to be processed, coupled with the data access generated by the platform's support for mobile devices, which brings a high load to the platform. The cloud computing platform model is shown in Figure 1. The platform has big data storage and processing functions, and cloud providers need to provide server clusters and memory clusters to have super storage and computing capabilities. These are the infrastructure-as-a-service modules of cloud computing [21]. The central cloud platform divides data services into national and regional services. National services include the data retrieval of the higher education system, foreign language periodical network, and joint catalogues, and regional services include data storage, higher education system software services, and foreign language periodical network software service. Because "cloud computing" has changed the computing power and the mode of software use, using the existing knowledge base, the data set to be processed is determined by the classification of the universe object and the situation where the partition falls into the data object to determine the approximate area. Parallel computing digital mining is usually used to mean that multiple parts of a program run on multiple processors on a computer at the

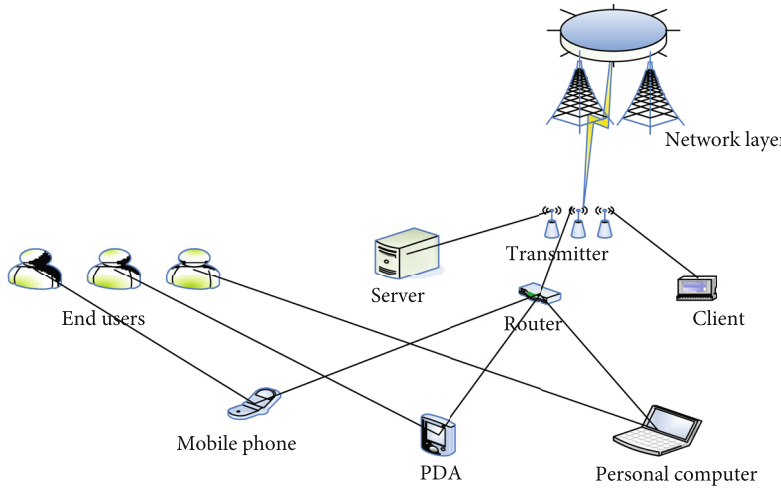

Figure 1: Cloud computing platform.

same time, and the uncertainty of the data object to be studied is described by the approximate area. Computing power has a great impact on system operating efficiency, accuracy, and reliability. Virtualization technology can integrate a large number of scattered, underutilized computing powers into computers or servers with high computing loads to achieve unified scheduling of resources across the entire network. It is used, so as to achieve high efficiency in multiple calculations such as storage, transmission, and calculation [22]. In the research of cloud computing technology, network link data is collected as basic data. Use special monitoring, social network analysis, and other methods to extract network links between multiple business entities and countries. It has achieved the six milestones of cloud computing technology for enterprises [23]. The different attribute knowledge of each division of the investment industry is regarded as a single node in different grids. The utility model of the distributed data collaborative processing process of cloud computing can be expressed as

$$W = k_i \sum_{i=1}^{\alpha} \left\{ \sin a_{i-1} - \beta \frac{k_i^{1+i}}{a + 1/(\alpha+\beta)} \right\},$$
$$K_i = \left[\sum_{i=0}^{\alpha} \beta_{a-1} (a)^{1/i} \right]. \tag{1}$$

$\sin a_{i-1}$ represents the ith node in a typical partition, and k_i^{1+i} is the replacement elasticity value of a single processor. Each area block of investment is input as a whole data node and aggregated according to the different characteristics, but there are three common factors, namely, the investment object, the investment subject, and the effect that the investment can obtain. A compound function calculation that organizes data according to the server cluster of the cloud provider and the internal domain of the software is as follows:

$$N_x^i = \frac{R_i(x)^{-\alpha} e_i}{\sum_{i=1}^{N_i} R_i(x)/2^{i+1}},$$
$$D_l = (1-\eta) h \left[\frac{H_{i+1} + \pi_{i+1}(L_{i+1})}{1 + I_{l+1} - \eta^{i+1}} \right], \tag{2}$$

which represents the number of data selected by H_{i+1} to enter a single program, and its calculated value is determined by η^{i+1}. If the data aggregation of this process is denoted as $G(e)$, then there is

$$G(e) = MI_O^v (1-E) \phi_i \sqrt{\left(1 + e_{i=1}^{i-1}\right) e^{\alpha}}. \tag{3}$$

M is the domain of the cloud computing platform information system, and the set of node attributes constituting the information function is E. Green products, green industries, green projects, and green funds have different impacts on different domains, but there are data nodes that overlap between their values. These overlapping parts are attribute combinations. Part of the similarity is recorded as the approximate value judgment attribute. An approximate value evaluation of decision information system is produced by the combination of attribute and form:

$$f(v) = \frac{\sum_{(a \epsilon \gamma)} \left| \gamma\left(b_i^0\right) \right|}{\underset{a, a+1}{\longrightarrow}} \int (1-e)\gamma,$$
$$F_v : T_v = \frac{\vartheta A (R_{i-1})^{1-\omega} (H_{i-1})^{\omega-1}}{\min rh}. \tag{4}$$

F_v, T_v represent the missing value and the complete value of the approximate value.

The accuracy and ambiguity of cloud computing are also measurable [24]. Suppose there is a being order information (x, y, z, and u), compare the internal advantages of the relationship and shrink it into a set:

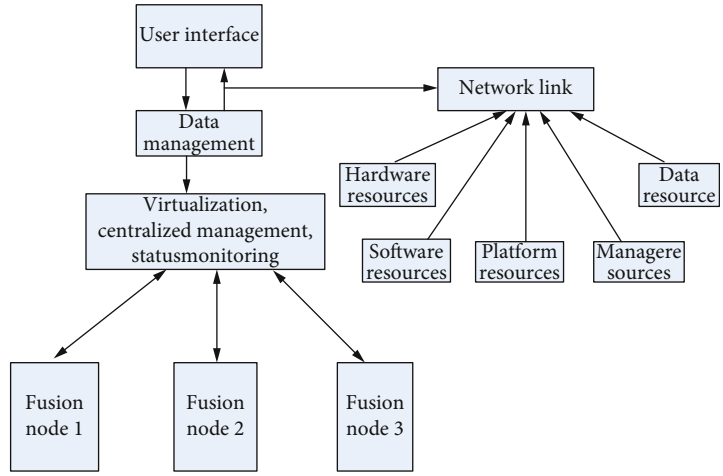

Figure 2: Information fusion process.

$$\forall_{\tau}^{t} A(s) = \underset{(x,y,z,u)}{\wedge} \left\{ A(x) : y\left(|u|^2, z\right) < 1 - \zeta \right\},$$
$$\forall_{\tau}^{t} \max s = \vee_{(x,y,z,u)-1} \left\{ A(x,y) \_ |A|^{i-1}(z,u) \right\}. \tag{5}$$

$\underset{(x,y,z,u)}{\wedge}$ represents the upper approximation of the order information sets, and $\vee_{(x,y,z,u)-1}$ represents the lower approximation of the order information set. Max s is the descriptability when the degree is S.

2.3. Information Fusion Method. With the advancement of computer technology, microelectronics technology, and network communication level, information integration technology has developed rapidly [25]. The embodiment and application of the theory of industrial equilibrium development can enhance the application of information fusion technology. The economy is proportionally restricted and supports development. Computer technology and other technologies are used to maintain the balanced development of the industry and form a balanced development situation. At present, the construction of national knowledge is one of the most important tasks of social construction, and information integration technology is a trivial technology in modern information writing. In general, multisource data integration has obvious advantages over homologous data integration, because many different sensors can capture multiple characteristic data to improve the accuracy of the integration results. An important condition for data-level integration is that the sensor types must be the same in order for data-level integration to be used for system computing power and network communication speed. Information fusion is a theory and method that uses multisensor, multilevel data and subjectively obtained information to make judgments, decision-making, and practical activities. The purpose is to obtain more accurate and valuable information than using a single sensor or decentralized use of multilevel data [26]. Information fusion is a process of information enhancement and systematic optimization. The flow chart of information fusion is shown in Figure 2.

At present, the methods of information fusion mainly include Bayesian estimation, statistical decision-making method, and rough set theory [27]. In this study, a linear filtering system is used to perform statistics on the signal characteristics of information fusion, and the constraints are firstly applied.

$$\begin{bmatrix} r_{11}^{a} \\ (r_{12} - r_{21})^{a} \end{bmatrix} b = 0,$$
$$x \begin{bmatrix} r \\ s \\ 1 \end{bmatrix} = j[r_1\ r_2\ r_3\ s] < r_{ij}^{s}. \tag{6}$$

The estimation of each signal element in the matrix is optimized, and the optimal estimation is

$$L(s, t_i, r_i, 1) = \frac{1}{\sqrt{2\pi}} r^{\sum_{i=1}^{1} s \sum_{t=1}^{r} \sigma / \nu^2},$$
$$l = \sqrt{(t-r)_{ij}} \frac{-1}{\sum_{i=0}^{s-1} (s+t)}. \tag{7}$$

Using the self-adaptive characteristics of data, the relative transformation of information is carried out, and the transformed position information is

$$\Delta s^2 = \min_{\Delta t} \frac{1}{3} \left[f(t) + \int (t_{i+1}) \Delta t \right]^2,$$
$$(\chi(s), \chi(t)) = \langle \gamma(1,s), \gamma(1,t) \rangle = \rho(s,t). \tag{8}$$

$\chi(s)$ is the output signal, which is transformed into relative position $\chi(t)$. The position loss value and the target loss value are

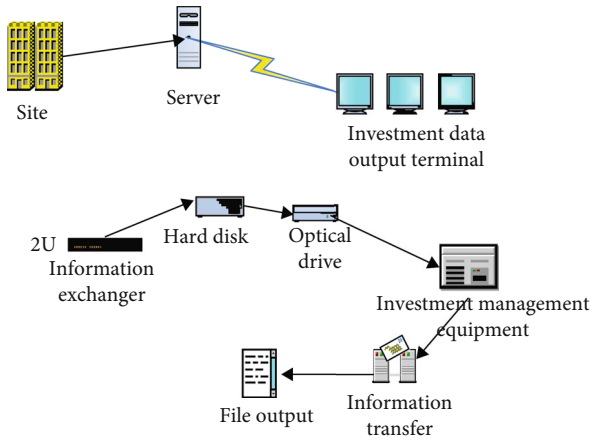

Figure 3: Application model of information fusion and cloud computing in green investment.

Table 1: Comparison of the total green investment rate, total investment contribution rate, and total investment pull rate between my country and the United States, Japan, and the United Kingdom in the past 5 years.

Country	Investment rate	Investment contribution rate	Investment pull rate
China	127.972	87.16	15.93
US	109.46	72.14	10.75
Japan	121.84	85.18	13.71
UK	109.54	69.94	9.07

$$I(r,s,t) = \frac{1}{m}(I(r,s) + \mu I(r,s,t)),$$
$$I(r,s,t) = \sum_{r \notin I}^{S-1} \sum_{\{R_{i+1}, S_{i+1}, T_{i+1}\}} (s_i^r, t_{i+1}^r). \tag{9}$$

Among them, μ is the number of matches between the loss value and the actual value, and I is the cross-validation. The information enhancement of information fusion technology is calculated [28], and the dimension with the largest enhancement probability is calculated by the following formula:

$$S^t = b \max_g \rho\left(\overset{\bullet}{x}^i = 1 \int \kappa(s)\right),$$
$$Z^t = \sum_{i=1}(r,s) + \delta \sum_{j=1}^{1} t\left(z_{i+j}^{j-i}\right) + f(z). \tag{10}$$

Z contains the size of the weight of each dimension of information fusion, $\kappa(s)$ represents the initial function value, and δ represents its weight. The reconstruction of information fusion involves the multimodal problem of data, which can be expressed as

$$p(t) = \sum_{a=1}^{h} \sum_{b=1}^{i} l\left\{\max_l \vartheta_{a,b}\right\} |a-b|,$$
$$f(a,b) = \exp - \left(\frac{\|a-b\|^2}{2\theta^2}\right)\left(a', b'\right). \tag{11}$$

(a', b') represents the modal model of the saved data [29].

3. Experiment Arrangement and Development

3.1. Experimental Content

(1) Related content of fixed asset investment in my country's main industries

(2) The status and influencing factors of green investment development, a detailed analysis of green investment from all aspects of the four fields of green products, green industry, green engineering, and green funds

(3) Summarize the current domestic and foreign research status of cloud computing technology and its application in business intelligence and in-depth study of cloud computing-related technologies and business intelligence-related theories, including cloud computing platforms, massive data storage and processing technologies, data warehouses, and data mining method

(4) Comparative analysis of the evaluation elements of the evaluation system (evaluation object, evaluation institution, evaluation stage, evaluation method, and evaluation index system) and then specific evaluation indicators of China, the United States, Japan, and the United Kingdom, such as the total green investment rate. The total investment contribution rate is compared with the total investment pull rate, and the differences and causes are analyzed and discussed

3.2. Cloud Computing and Information Fusion Technology and Green Investment Evaluation System. A large number of network applications and users have generated huge data storage. Cloud computing is only a change of analysis platform, and data mining is an improvement of analysis tools. When a variety of complex applications are running on it, cloud computing can maximize resource utilization, and different applications can be isolated without interfering with each other. Distributed computing and cloud computing technology are regarded as the third revolution in the information industry. Making computing services similar to public services such as water, electricity, and gas, with on-demand access and on-demand payment, is the main form of social informatization in the future. It is also the main carrier of the country's future information strategy security and has broad prospects for development. In order to solve the main problems existing in the construction of statistical informatization, including the serious waste of statistical information resources, the security of statistical data

Table 2: The proportion of fixed asset investment in my country's main industries in fixed asset investment in the whole society in the past 5 years.

Industry	Time				
	2016	2017	2018	2019	2020
Total investment in fixed assets	100	100	100	100	100
Environmental protection industry	6.91	8.93	9.42	11.7	16.9
Mining industry	7.13	8.39	6.97	8.92	8.88
Energy supply industry	7.54	9.76	10.59	15.01	13.27
Construction industry	7.23	9.79	8.39	12.21	13.49
Transportation	20.84	17.61	19.47	20.12	16.54

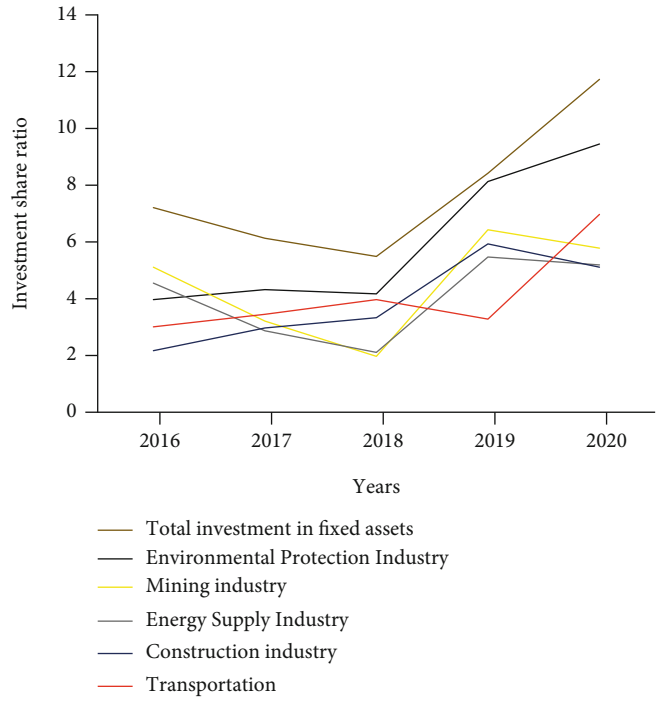

Figure 4: The ratio of investment in fixed assets in my country's major industries to GDP in the past five years.

services and storage, the lack of unified data management in the deployment of application systems, and the lack of unified planning and management of statistical information system resources, using cloud computing and information fusion technology to obtain valuable data, it analyzes and compares data, information, knowledge, and wisdom to identify the knowledge assets in the organization and give full play to the leverage of knowledge assets to help companies gain competitive advantages. For this reason, this article adds the concept of knowledge base to the existing data integration method, thereby abstracting the business logic from the complex data, which is more conducive to the use of users and the management of information. The business logic of cloud computing is mainly to determine certain standards in supporting applications in the investment environment. These standards are integrated and supervised according to the regional blocks of different green investments and then organized in the way of data integration during the application process. Although environmental protection investment, as a part of green industry investment, cannot fully reflect the overall situation of green investment, it has a decisive effect on green investment. Exploring the evaluation system of green investment is conducive to perfecting the theory of economic and social development, conducive to perfecting the theory of industrial equilibrium development, and conducive to the development of related ideas and practices into a complete emerging discipline. The operation model of cloud computing and information fusion technology is shown in Figure 3.

Use cloud computing and information fusion technology to collect data on the green investment evaluation system between my country and the United States, Japan, and the United Kingdom in the past five years. Table 1 shows the total green investment rate and total investment contribution between my country and the United States, Japan, and the United Kingdom in the past five years. Table 2 shows the proportion of fixed asset investment in my country's main industries in the total fixed asset investment in the

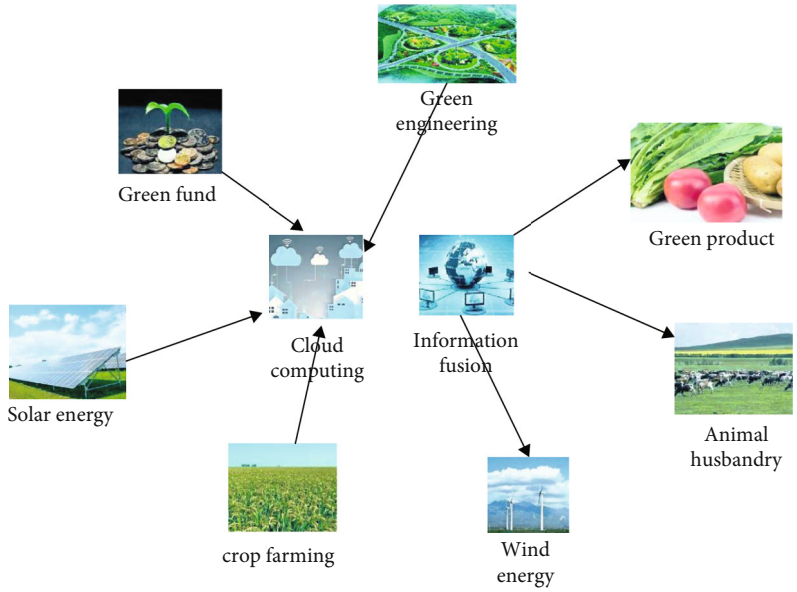

Figure 5: Green investment simulation diagram.

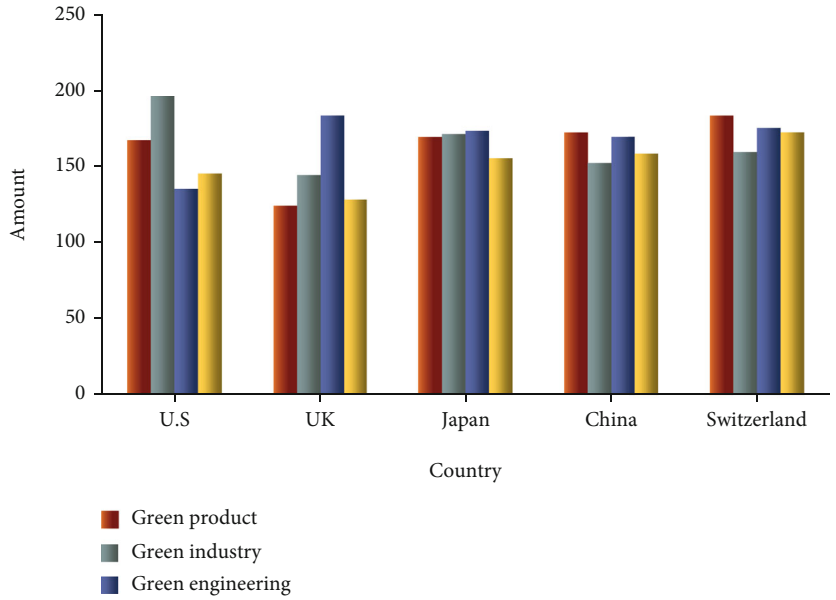

Figure 6: Development status of green products, green industries, green projects, and green funds at home and abroad.

whole society in the past five years; Figure 4 shows the proportion of fixed asset investment in my country's major industries in the total domestic product in the past five years. For the proportion of values, all data has been statistically checked many times.

From the data analysis in Tables 1 and 2, it can be concluded that my country's total green investment rate, total investment contribution rate, and total investment pull rate in the past five years ranked first, followed by Japan. In the past five years, my country's investment in fixed assets in major industries accounted for the proportion of investment in fixed assets in the whole society. The investment in environmental protection and energy supply industries has continued to rise; and the investment in the transportation industry has always been among the industries mentioned in Table 2. The highest is 20.84%. In the statistics of the proportion of investment in fixed assets in my country's main industries in the past five years, the total investment in fixed industries reached the lowest in five years in 2018, the mining industry accounted for the highest proportion in 2019, and the environmental protection industry has been continuously investing funds. In order to conduct a more detailed research, sort out the relevant data on green investment. Cloud computing and information fusion technology are simulated in green investment-related industries, as shown in Figure 5.

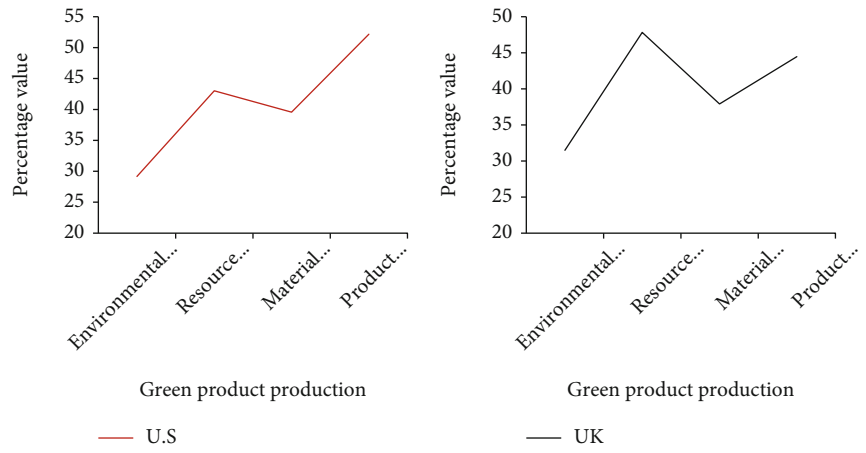

Figure 7: Analysis of green product production in the US and the UK.

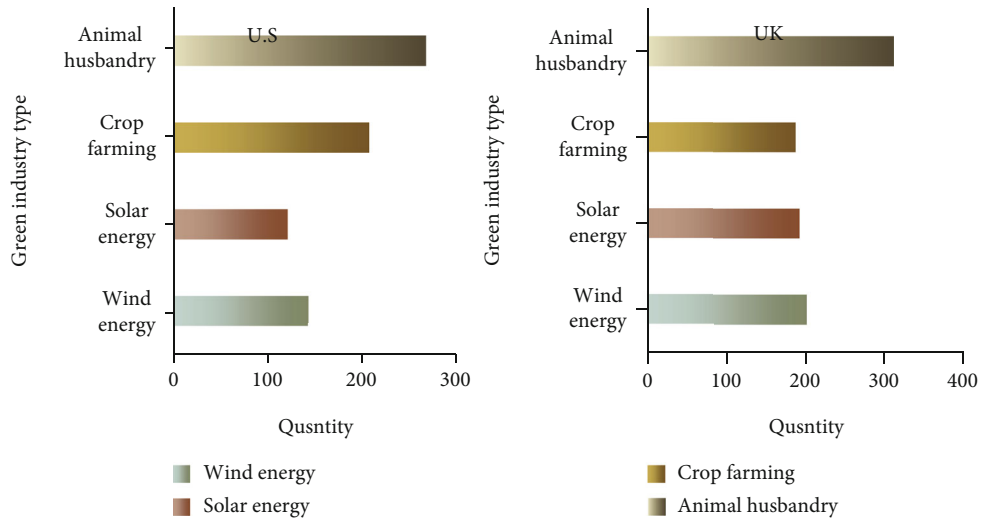

Figure 8: Green industry comparison between the US and the UK.

This research mainly focuses on data analysis on green products, green industries, green projects, and green funds and analyzes the status of green investment. Up to now, the development status data of green products, green industries, green projects, and green funds at home and abroad are shown in Figure 6, mainly for China, the United States, Japan, Switzerland, and the United Kingdom.

The data collected by cloud computing takes into account various aspects such as green products, green industries, green projects, and green funds. It analyzes clustering algorithms and analyzes and compares data, information, knowledge, and wisdom. This can facilitate data management and planning. According to the data in Figure 6, the green industry in the above five countries has received the most attention and development in the United States; among the five countries, Switzerland ranks first, while the UK ranks last; and the green engineering UK ranks first. China is in a type with green products, green industry, green projects, and green funds which are all taken care of, and each field develops in a balanced manner. Secondly, we make comparisons based on the different levels of attention each country has to green investment in various industries. For green products, this experiment compares the United States and the United Kingdom in terms of environmental protection rate, resource utilization, material recovery rate, and product quality, as shown in Figure 7.

The data shows that the priority of the abovementioned factors of green products in the United States is ranked as product quality > resource utilization rate > material recovery rate > environmental protection rate; the priority of the appeal factors for green products in the United Kingdom is ranked as resource utilization rate > product quality > material recovery rate > environmental protection rate. Among them, the product quality of green products in the United States is higher than that of the United Kingdom, and the United States is at a relatively disadvantage in terms of environmental protection rate, resource utilization rate, and recycling rate. To this end, a comparative study of the green industries in the United States

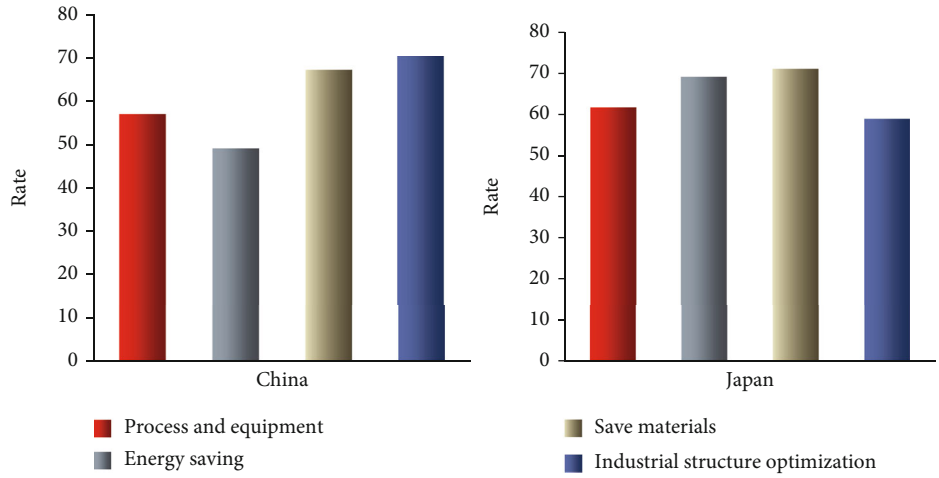

Figure 9: Green engineering development in China and Japan.

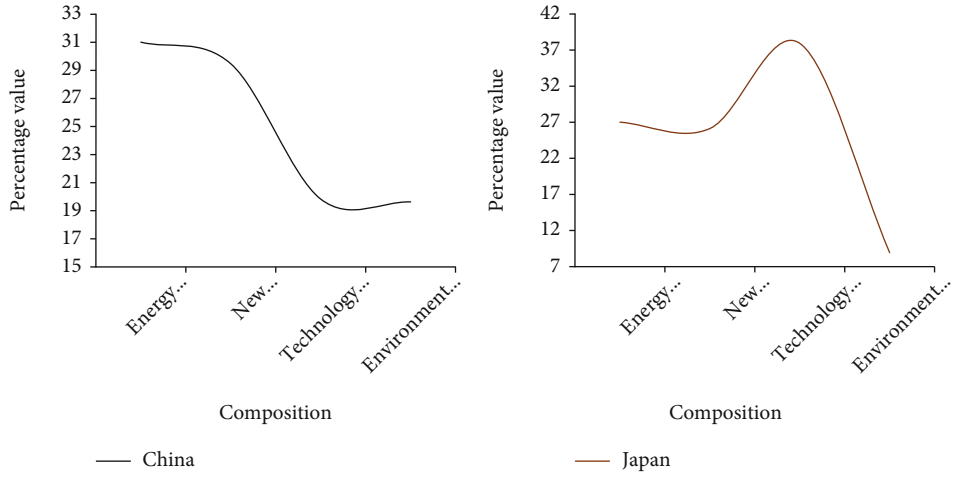

Figure 10: Comparison of green funds between China and Japan.

and the United Kingdom mainly centered on the four major industries of wind energy, solar energy, plantation, and animal husbandry for data processing, as shown in Figure 8.

The above statistics show that, overall, the UK has more wind energy, solar energy, and animal husbandry industries than the US, and the US only surpasses the UK in farming. After comparison, it is found that the animal husbandry industry has the largest gap between the two, followed by wind energy. The development of green engineering has always been paid attention. According to the status quo of the development of green engineering in China and Japan, statistics are carried out around technology and equipment, energy saving, material saving, and industrial structure optimization, as shown in Figure 9.

The industrial structure rate of China's green engineering is as high as 70%, and the technology and equipment, energy-saving rate, and material saving rate are at a disadvantage compared with Japan. The comparison of green funds between China and Japan focuses on data analysis on the components of green funds, such as energy conservation and emission reduction, new energy, technological content, and environmental optimization, as shown in Figure 10.

The composition ratio of China's green funds is energy saving and emission reduction > new energy > technology content > environmental optimization; the composition ratio of Japan's green funds is technology content > energy saving and emission reduction > new energy > environmental optimization. Therefore, China's green fund investment is mostly in energy-saving and emission reduction industries, while Japan's green fund investment is most in technology. Industries with a high degree of investment concern mark the focus of the country's policy preference. Regardless of the type of investment, it is focused on the development of green industries. China's investment in new energy is likely to be balanced with the energy-saving and emission-reduction industries. The best development is to balance the gaps between industries. We have also made statistics on the reasons for the status quo of green investment development presented by the above data, as shown in Figure 11.

Figure 11 mainly analyzes the influencing factors of green investment in different periods, such as investment

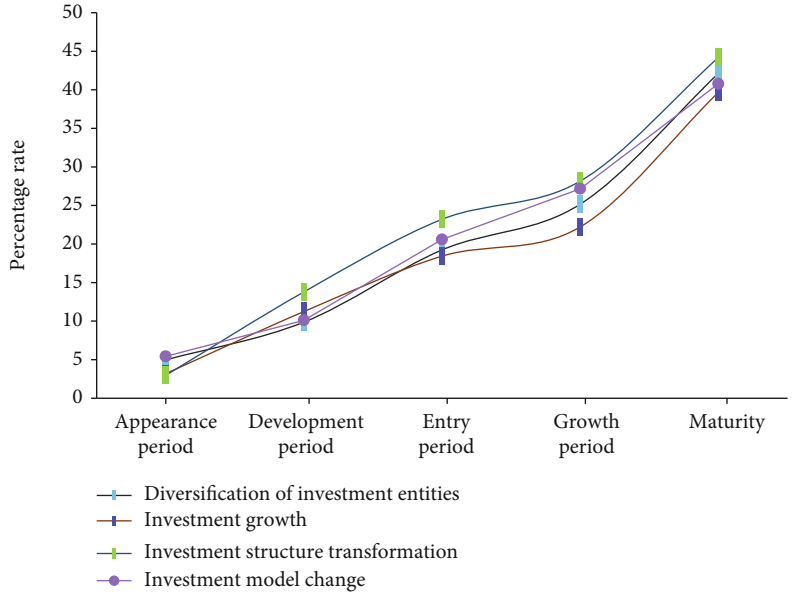

Figure 11: Analysis of influencing factors of green investment.

subject, investment amount, investment structure, and urgency of investment mode. On the whole, the investment entities are diversified, the investment amount is growing rapidly, the investment structure is constantly changing, and the investment model is constantly changing. The development trend is the strongest in the development period and the entry period. Refer to the green investment evaluation system (as shown in Table 3, the highest score is 60) to evaluate the investment subjects, investment objects, and investment vehicles of green products, green industries, green projects, and green funds, as shown in Figure 12.

Among green investments, the investment subject of green funds has the highest evaluation, the investment objects of green projects and green industries are at the same standard, and the investment vehicle evaluation of green industries reaches 9.

Table 3: Quantitative and pricing evaluation methods to establish an investment evaluation system.

Evaluation item	Excellent	Middle	Poor
Develop a comprehensive investment operation process management manual	10	5	0
Clear division of labor and regular training	10	5	0
Investment evaluation level	10	5	0
Effective reward, punishment, and supervision mechanism	10	5	0
Emergency response system for emergencies	10	5	0
Other	10	5	0

4. Discussion

Analyze data from different aspects of different green investment types, and compare and analyze between countries, between influencing factors, and between investment entities. The data provided are all mining and processing through the application of cloud computing and information fusion technology. This argument proves that the application of cloud computing and information fusion technology has great value. Cloud computing is an emerging mode of work. Through cloud computing, software, applications, and services can be provided for green investment, which reduces the cost of software and applications and can efficiently and conveniently meet the different needs of system enterprises at different stages of development. Therefore, cloud computing can solve the information problems of SMEs in terms of cost, information, technology, etc. and meet the unique and sensitive needs of SMEs in the development of green investment. This research establishes a cloud service selection index system, uses a nondistributed approach to evaluate different green investments in different countries, and verifies the feasibility of cloud computing and information fusion technology in green investment evaluation. In order to promote the further development of modern energy management systems, people are building energy cloud platforms to solve the common problems of equipment access, data storage, and service management in the energy management system and reduce the development and maintenance costs of energy management systems. The research on the development of green investment has solved a series of problems including the above. Based on the integration of Internet of Things technology and cloud computing technology, this research provides safe, reliable, meticulous, and timely data storage services for green investment-related energy management and realizes the analysis and processing of massive energy data. It strengthened the interconnection between the green investment management system and the Internet.

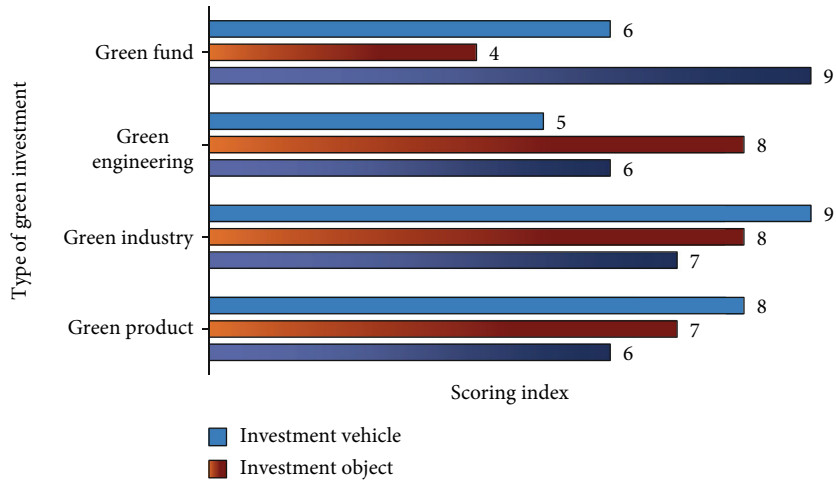

Figure 12: Evaluation of investment subjects, investment objects, and investment vehicles of different investment projects.

5. Conclusion

This experiment takes cloud computing service user companies as the research object and discusses the effect of cloud computing and information fusion technology on green investment companies, in order to achieve the purpose of filling the current research gaps in the field of cloud computing technology to a certain extent. The practice in the field of green investment in my country provides scientific guidance and constructive suggestions. The current green development of society has to deal with standardized and produce modulation for the connection between social development and the natural environment. Green investment economy is a sustainable development model based on the interests of present and future generations. In the current economic development, the scale of the economy must adapt and be active under the control of resource regeneration and environmental sustainability. It is necessary to consider both the development and utilization needs of contemporary people's resources and the viability of future generations. Continue to use the rules. The strategic height of green investment under the new normal has gradually increased. In order to promote my country's energy saving and emission reduction work and build a two-oriented society, it is of far-reaching significance to popularize the concept of green finance and green investment and to study the relationship between them and the optimization of industrial structure. Compared with the traditional investment concept, its distinguishing feature is to consider the quality of the human ecological environment. According to the analysis of experimental data, the structure and direction of regional environmental protection investment are unreasonable, and there are significant regional differences in environmental protection investment benefits, and there is an imbalance between various regions. Giving play to the important role of green finance and green investment in the process of optimizing my country's industrial structure can promote the practice of scientific development concepts and further implement the concept of sustainable development. The scientific development concept advocates improving the economic development model, optimizing the industrial structure, and building a two-oriented society. The orderly expansion of the green industry also relies on the stable development of green finance and green investment, which in turn promotes the continuous optimization of green finance and green investment, and ensures the sustainable development of the financial investment industry itself.

Data Availability

The data that support the findings of this study are available from the corresponding author upon reasonable request.

Conflicts of Interest

The authors declare that they have no conflicts of interest.

Acknowledgments

This work was supported by 2020 Heilongjiang philosophy and social sciences research and planning project "Research on the sustainable deepening path of mixed ownership reform of Heilongjiang Province under the perspective of sharing economy" (20JLE361), 2019 Heilongjiang natural science research planning project "Research on driving system innovation, financial governance and enhancing the development vitality of state-owned enterprises in Heilongjiang Province" (LH2019G018), 2021 Harbin University of Commerce graduate innovation research support project "Impact of green innovation on sustainable growth of energy enterprise performance and improvement path under the goal of carbon peak and carbon neutralization" (YJSCX2021-691HSD), and General project of NSFC "Research on Green Governance Mechanism and policy guarantee of landscape village integration from the perspective of Rural Revitalization" (21BJY189).

References

[1] M. Schmack, G. Ho, and M. Anda, "Technical evaluation of simple condenser devices for a bubble column desalinator," *Desalination and Water Treatment*, vol. 57, no. 40, pp. 18573–18587, 2016.

[2] I. Attiya and X. Zhang, "Cloud computing technology: promises and concerns," *International Journal of Computer Applications*, vol. 159, no. 9, pp. 32–37, 2017.

[3] Z. Li, "Application of a resource-sharing platform based on cloud computing technology," *Agro Food Industry Hi Tech*, vol. 28, no. 1, pp. 2205–2209, 2017.

[4] O. Kopishynska, Y. Utkin, A. Kalinichenko, and D. Jelonek, "Efficacy of the cloud computing technology in the management of communication and business processes of the companies," *Polish Journal of Management Studies*, vol. 14, no. 2, pp. 104–114, 2016.

[5] M. Zhou, X. Li, Y. Wang, S. Li, Y. Ding, and W. Nie, "6G multi-source information fusion based indoor positioning via Gaussian kernel density estimation," *IEEE Internet of Things Journal*, vol. 8, no. 20, p. 15117, 2021.

[6] Y. Liu, X. Fan, C. Lv, J. Wu, L. Li, and D. Ding, "An innovative information fusion method with adaptive Kalman filter for integrated INS/GPS navigation of autonomous vehicles," *Mechanical Systems and Signal Processing*, vol. 100, pp. 605–616, 2018.

[7] S. Pumchalerm, P. Nilsook, and N. Jeerungsuwan, "Intelligent cooperative education process management model on cloud computing technology for higher education institutes in Thailand," *International Journal of Information and Education Technology*, vol. 6, no. 10, pp. 791–794, 2016.

[8] J. Vithayathil, "Will cloud computing make the information technology (IT) department obsolete?," *Information Systems Journal*, vol. 28, no. 4, pp. 634–649, 2018.

[9] P. Appiahene, B. Yaw, and C. Bombie, "Cloud computing technology model for teaching and learning of ICT," *International Journal of Computer Applications*, vol. 143, no. 5, pp. 22–26, 2016.

[10] R. Kumar, "Aggregation of SOA and cloud computing: a recent emerging technology," *International Journal on Data Science and Technology*, vol. 2, no. 1, pp. 5–8, 2016.

[11] M. Attaran, "Cloud computing technology: leveraging the power of the internet to improve business performance," *Journal of International Technology & Information Management*, vol. 26, no. 1, pp. 112–137, 2017.

[12] P. Braca, R. Goldhahn, G. Ferri, and K. D. LePage, "Distributed information fusion in multistatic sensor networks for underwater surveillance," *IEEE Sensors Journal*, vol. 16, no. 11, pp. 4003–4014, 2016.

[13] K. S. Noh and J. D. Baek, "Suggestions of the construction and management for sustainable highways," *Ecology and Resilient Infrastructure*, vol. 3, no. 3, pp. 156–161, 2016.

[14] M. Zhou, Y. Wang, Z. Tian, Y. Lian, Y. Wang, and B. Wang, "Calibrated data simplification for energy-efficient location sensing in internet of things," *IEEE Internet of Things Journal*, vol. 6, no. 4, pp. 6125–6133, 2019.

[15] Q. Zhou, P. Jiang, X. Shao, J. Hu, L. Cao, and L. Wan, "A variable fidelity information fusion method based on radial basis function," *Advanced Engineering Informatics*, vol. 32, pp. 26–39, 2017.

[16] X. Zhou and P. Jiang, "Variation source identification for deep hole boring process of cutting-hard workpiece based on multi-source information fusion using evidence theory," *Journal of Intelligent Manufacturing*, vol. 28, no. 2, pp. 255–270, 2017.

[17] H. Wu, X. Dang, L. Wang, and L. He, "Information fusion-based method for distributed domain name system cache poisoning attack detection and identification," *IET Information Security*, vol. 10, no. 1, pp. 37–44, 2016.

[18] H. Li, Y. Song, and C. Chen, "Hyperspectral image classification based on multiscale spatial information fusion," *IEEE Transactions on Geoscience & Remote Sensing*, vol. 55, no. 9, pp. 5302–5312, 2017.

[19] Z. Ming and Z. Jiang, "Reciprocating compressor fault diagnosis technology based on multi-source information fusion," *Chinese Journal of Mechanical Engineering*, vol. 53, no. 23, pp. 1–8, 2017.

[20] Y. Xu, L. Gui, and T. Xie, "Intelligent recognition method of turning tool wear state based on information fusion technology and BP neural network," *Shock and Vibration*, vol. 2021, no. 8, Article ID 7610884, 2021.

[21] X. Wei, "A classification method of tourism English talents based on feature mining and information fusion technology," *Mobile Information Systems*, vol. 2021, no. 8, Article ID 5520079, 2021.

[22] S.-B. Tsai, Y.-M. Wei, K.-Y. Chen, L. Xu, P. du, and H.-C. Lee, "Evaluating green suppliers from a green environmental perspective," *Environment and Planning B-Planning & Design*, vol. 43, no. 5, pp. 941–959, 2016.

[23] Y. Zhou, L. Chang, and B. Qian, "A belief-rule-based model for information fusion with insufficient multi-sensor data and domain knowledge using evolutionary algorithms with operator recommendations," *Soft Computing*, vol. 23, no. 13, pp. 5129–5142, 2019.

[24] C. C. Oniga, D. Mocuta, S. Cristea, and Ş. Jurcoane, "Economic efficiency of conversion of classical fish farm in organic by use of wastes fish in green houses," *Romanian Biotechnological Letters*, vol. 25, no. 6, pp. 2174–2179, 2020.

[25] S. Ghosh, V. K. Yadav, V. Mukherjee, and P. Yadav, "Evaluation of relative impact of aerosols on photovoltaic cells through combined Shannon's entropy and data envelopment analysis (DEA)," *Renewable Energy*, vol. 105, pp. 344–353, 2017.

[26] J. Y. Wang, Q. W. Zhai, Q. Guo, and Y. Z. Tao, "Study on water environmental carrying capacity evaluation in Taihu Lake Basin," *China Environmental Science*, vol. 37, no. 5, pp. 1979–1987, 2017.

[27] L. Chen and P. Han, "The construction of a smart city energy efficiency management system oriented to the mobile data aggregation of the Internet of Things," *Complexity*, vol. 2021, no. 2, Article ID 9988282, 2021.

[28] P. Albertario, "System of self-financing strategy for the policies aimed at the eco-innovation in the productive sectors," *Procedia Engineering*, vol. 3, no. 1, pp. 8–11, 2016.

[29] Z. Zhong, X. Zhang, and X. Yang, "Benefit evaluation of energy-saving and emission reduction in construction industry based on rough set theory," *Ecological Chemistry and Engineering S*, vol. 28, no. 1, pp. 61–73, 2021.

Hindawi
Journal of Sensors
Volume 2021, Article ID 1527467, 10 pages
https://doi.org/10.1155/2021/1527467

Research Article

Application of New Sensor Technology in the Field of Education in the Era of Internet of Things

Haijun Chen,[1] **Cong Ma**,[2] **and Yiwei Wang**[3]

[1]*School of Business, Wuzhou University, Wuzhou 543003, China*
[2]*School of Economics and Management, Guangxi University of Science and Technology, Liuzhou 545006, China*
[3]*School of Culture and Communication, Henan Finance University, Zhengzhou 450000, China*

Correspondence should be addressed to Yiwei Wang; wangyiwei@hafu.edu.cn

Received 13 August 2021; Revised 18 September 2021; Accepted 7 October 2021; Published 26 October 2021

Academic Editor: Mu Zhou

In order to explore the intelligent education mode in the context of the Internet of Things, this paper combines the Internet of Things technology and sensor technology to improve the sensor technology and proposes a multisensor information fusion technology based on Kalman filtering. Moreover, this paper combines the wireless network technology to construct the system and structure, obtains the functional modules of the intelligent education system based on the Internet of Things technology and the new sensor technology, and analyzes the system realization process. In addition, this paper constructs a smart education system based on the Internet of Things and new sensors and designs experiments to verify the system. The research shows that the method proposed in this paper has good data transmission effect, can effectively improve the effect of intelligent education, and meet the actual needs of current education.

1. Introduction

After years of development, the Internet of Things is no longer a connection between things based on RFID technology, and its definition has been extended and changed very much. In general terms, the current Internet of Things refers to connecting all devices through Internet technology, allowing them to exchange data and information, and completing the intelligent management and control of devices [1]. More specifically, the Internet of Things acts as an information aggregation platform and provides a common language for the interaction of different devices and applications. The transmission of encrypted data is completed between the device and the Internet of Things platform. The Internet of Things integrates data from various devices and applications and realizes data interaction between applications through data analysis [2].

With the development and maturity of information technology and multimedia technology, classrooms have evolved from traditional multimedia classrooms to intelligent and intelligent classrooms [3]. It can be expected that with the maturity and popularization of the Internet of Things technology, mobile devices represented by smartphones, as well as terminal devices such as cameras and sensors, can extend and strengthen the various senses of classroom participants. At the same time, wearable devices can assist teachers and students in teaching activities to directly experience virtual reality/augmented reality (VR/AR) and assist classroom learning [4].

With the maturity and popularization of technologies such as artificial intelligence and deep learning, learning data will be analyzed using deep learning methods in the learning process to provide guidance or feedback for teaching behavior and provide analysis and prediction for teaching results. By analyzing the learning process data recorded by smart cameras, wearable devices, and various sensors, the smart classroom can automatically analyze the facial expressions and gestures of learning in real-time, so that teachers can get more teaching feedback information and improve teaching and learning. The purpose is to improve student learning efficiency.

As the most typical teaching environment application for the development of educational informatization, "smart

classroom" has different understandings from different countries, experts, and scholars. The smart classroom is a new type of smart classroom that includes five dimensions: "presentation of teaching content," "classroom environment management," "teaching resource acquisition," "timely classroom interaction," and "environmental situational awareness." It is an intelligent learning environment. Concentrated embodiment, high-end multimedia and network classrooms and smart classrooms are able to satisfy administrators to intelligently control all the teaching equipment in the classroom, and at the same time, it can promote teaching activities between teachers and students through remote teaching and other methods. It is characterized by computer interaction, relying on smart space technology to improve and expand the functions that can be provided in the classroom; the smart classroom is an enhanced classroom based on electronic technology; the smart classroom can push different learning content to students according to the differences of different students and really do to personalized teaching. The entire classroom is people-oriented, and the effective interaction between people and smart devices promotes the achievement of learning goals; the function of the smart classroom is to use smart teaching equipment to collect and store the behavior data of students in teaching and to improve the teaching content through feedback information. Some smart devices that can quickly collect and find information can also be used to enhance the intelligence of the classroom. It can be found that the definition of the smart classroom is very broad, and the realization of different intelligent functions of the smart classroom depends on the corresponding different technical foundations.

This article combines the Internet of Things technology and new sensor technology to study the intelligence of the education field and combines the contemporary education needs to construct an intelligent education system to improve the effect of subsequent intelligent education.

2. Related Work

In the early stage of classroom construction, the data source of education and teaching was relatively single, the data structure was relatively single, and the main type is relational data. Moreover, the storage method is mainly based on relational databases, among which the more representative ones are MYSQL, Oracle, etc. With the rise of computers and the Internet and the development of the electronics industry, the application of computers in all walks of life, data sources have become widespread, and data types have become diverse. It is mainly divided into structured data and unstructured data. Databases used to store data are divided into two categories: relational databases and NoSQL (not only structured query language) databases. The application and development of these technologies have expanded the source of data. However, these data are stored independently in different systems. They are all data in a single field. There is no data circulation and data sharing, which has caused the phenomenon of data closure and formed a block of data [5]. Moreover, the source of the data is based on the transaction flow, so there is a lack of behavioral data, humanistic data, and social activity data associated with people. At the same time, due to technical limitations, these data have not been well utilized [6].

The high integration of sensors, collaborative sensing technology, mobile sensing technology [7], and other technologies are widely used in various fields to promote the development of sensing technology. Navigation is a typical application of location-based perception technology, which is mainly divided into two categories: car navigation and mobile phone navigation. In the early days, GPS- (Global Positioning System-) based location-aware technology achieved real-time recording and reporting of bus arrivals in modern urban traffic. Real-time information acquisition has improved travel convenience and made public travel more inclined to choose public transportation. In modern transportation systems, perception technology and intelligent technology are used to realize unmanned driving technology [8]. The development of mobile communication technology and wireless communication has played down the acquisition of geographic information. Even if the location of the other party is not known, instant communication can still be carried out. With the development of spatial information, it has emerged in various fields, especially situational awareness. In order to solve the problem that sensor devices in the Internet of Things need to manually set up the Internet, the context-aware dynamic discovery of things (CADDOT, Context-Aware Dynamic Discovery of Things) model [9], which can automatically identify, add and set sensor devices to expand perception range and perception data types. Pervasive perception is also a newly proposed concept. In intelligent sensing devices (mobile phones, tablets) with highly integrated sensors, the perception of smartphones has also become a research hotspot of data perception [10]. According to different perception objects and different application purposes, it can be roughly divided into five categories: physical environment perception, object information system identification perception, human body-related biological characteristics perception, spatial perception, and interactive information perception. The data included in physical environment perception is mainly structured data, and it is widely used in industry and agriculture. Object information system identification perception is widely used in logistics and other aspects, mainly for identification of objects. Spatial perception is the most widely used for location positioning. Interactive information perception has been widely used in applications such as personalized recommendation. Sensors with physiological related characteristics have also been widely used, and personal information data has been expanded to include personal information, personal behavior, personal physiological, and social activities and other related information [11].

In early research, foreign scholars believed that smart classrooms are classrooms enhanced by information technology [12]. At present, the concept of smart classroom has undergone significant changes. Foreign countries no longer define the concept of smart classroom from the aspect of classroom information technology, but from the learning environment [13]. The literature [14] pointed out that the classroom is a learning environment. Moreover, it is believed

that the classroom not only includes all aspects of technology and resources but should also include various methods of education, and the classroom is a learning environment composed of teachers and learners. This literature incorporates the main body of teaching and learning into the study of the learning environment of the smart classroom. The literature [15] put forward the concept of an upside-down classroom. This teaching method gives students more freedom and further reflects the concept of education and teaching that students are the main body of learning.

3. New Sensor Technology Based on the Internet of Things

Sensor technology is one of the main contents of modern information technology. The sensor is a device that converts the amount of external environment information that can be felt into a required output signal through a set rule. It is generally composed of conversion components and sensitive components. The sensitive element refers to the part that can perceive external environmental information, and the conversion element refers to the part where the sensor transforms and outputs the external environmental information sensed by the sensitive element through certain rules.

The basic requirement for the static characteristics of the sensor is that when the input is 0, the output is also 0, or the output should maintain a certain corresponding relationship with the input. As shown in Figure 1, if the input of the sensor is x and the output is y, then $y = f(x)$, and x/y is preferably a constant proportional relationship [16].

Sensitivity and SN: sensitivity is the primary consideration when selecting a sensor. If the sensitivity required for measurement is not achieved, this sensor cannot be used. However, sensors with high sensitivity are susceptible to noise. In addition to environmental noise, there is also noise from the sensor itself [17].

Linear: there is a linear proportional relationship between input and output, which is called linear relationship. In fact, most sensors have a nonlinear relationship.

Hysteresis: when the input quantity increases to X_1, if the output quantity is Y_1, the input quantity continues to increase and then decreases to X_1, and the output quantity is Y_2 at this time. In fact, the output Y_1 and Y_2 are not equal, and there is a certain difference, which is a time lag. In this way, there is no one-to-one correspondence between input and output.

Environmental characteristics: the biggest influence on the sensor is the temperature in the surrounding environment. Moreover, many sensor materials choose semiconductors with high sensitivity and easy signal processing. However, semiconductors are sensitive to the environment, so special care must be taken when using them.

Stability: when sensors with ideal characteristics are added with the same input, the output is always the same. In actual use, the sensor changes with time, and the output may be different for the same input. During continuous work, temperature drift may also occur [18].

Accuracy degree: accuracy degree is used to evaluate the degree of excellence of the system. Accuracy is divided into

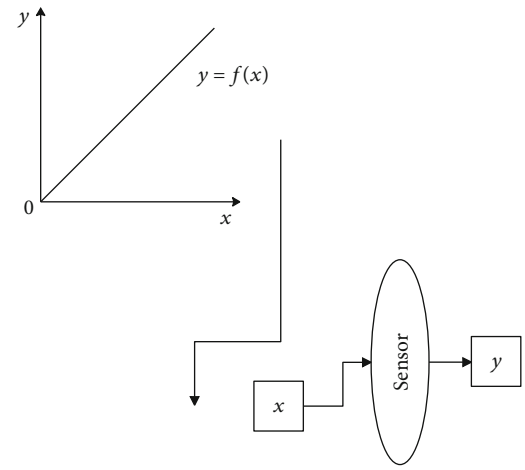

Figure 1: The relationship between input and output.

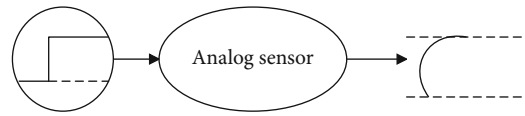

Figure 2: The relationship between input and response.

accuracy and precision. Accuracy refers to the deviation between the measured value and the true value, and correction is needed to correct this deviation. Precision refers to the same object, and each measurement will get a different measurement value, which is the discrete deviation.

The input signal to be detected by the sensor changes with time, and the characteristics of the sensor should be able to track the change of the input signal, so that an accurate input signal can be obtained. If the change is too fast, it may not be tracked. This is the response characteristic, that is, the dynamic characteristic. The dynamic characteristic is one of the important characteristics of the sensor. The relationship between sensor and response is shown in Figure 2.

Among the functional models of multisource information fusion systems, the JDL model and its evolutionary version occupy an important position, and it is currently a widely recognized model. The recommended information fusion model based on JDL is shown in Figure 3.

Level 0 signal/feature estimation: it estimates the state of the signal or feature. Signals and characteristics can be defined as data obtained from observations or measurements.

Level 1 entity estimation: it estimates the state or characteristics of the observed entity.

Level 2 situation estimation: it is an estimation of the actual observed environmental structure, that is, an estimation of the relationship between entities.

Level 3 impact estimation: it is an estimation of the availability and cost of signals, entities, and situational states.

Level 4 process estimation: the process of self-estimation of the system performance completed by comparing with the expected performance and efficiency.

As can be seen from the above figure, the recommended information model clearly divides the functions of each level

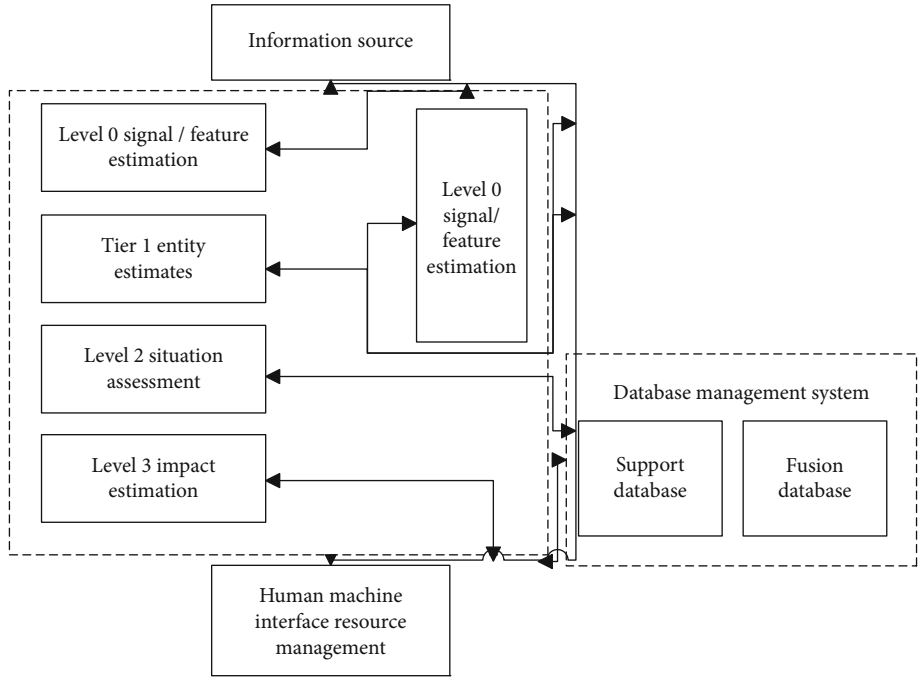

Figure 3: Recommended information fusion model.

of information fusion from the aspects of input data, model, output data, and reasoning type.

Multisensor information fusion is very different from previous single-sensor systems. The key is that the multisensor information of information fusion has a more complex form and can work at different information levels. There are many classification methods for data fusion. One is to classify the sensor data according to the degree of processing before it is sent to the data fusion processing center, which can be divided into sensor data fusion, central-level data fusion, and hybrid data fusion. The so-called hybrid data fusion means that it includes both sensor fusion and central-level fusion in its fusion process [19].

3.1. Sensor Data Fusion. Sensor data fusion is a distributed fusion structure. The basic principle is that different sensors collect the data of their respective observation targets and then input them to different local processors for local processing. After local processing, a local analysis result is formed. Finally, each local processor transmits different local estimates to the fusion center, and then the fusion center performs final processing on the data to form a global estimate.

It can be seen from the above that the sensor data fusion structure can perform simple partial processing on the data after the sensor collects the data, optimizes the data, and makes the system very simple, so it is widely used at present, and its structure is shown in Figure 4.

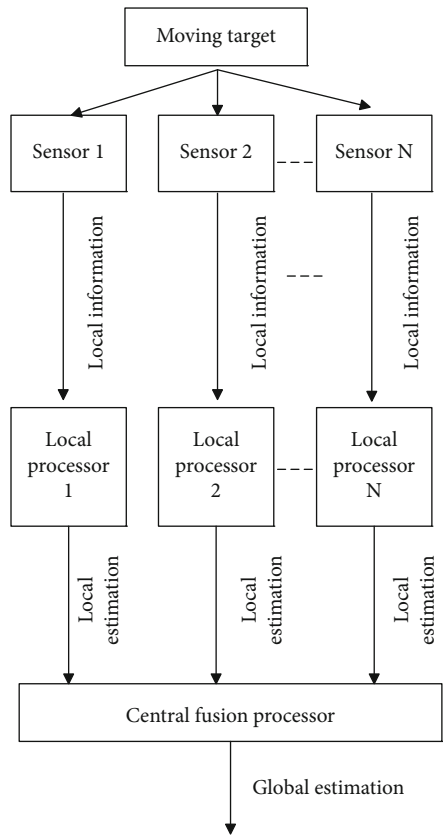

Figure 4: Sensor fusion structure model.

3.2. Central Fusion. Central fusion is also called centralized fusion, which means the fusion of original observation data. It transfers the data of each sensor to the data fusion center and performs data calibration, data association, track/point-track fusion, prediction, and tracking in the data fusion center. Its structure is shown in Figure 5. If the data collected by each independent sensor can be accurately fused in the fusion center, the structure of the central fusion is the method that can obtain the most accurate observations.

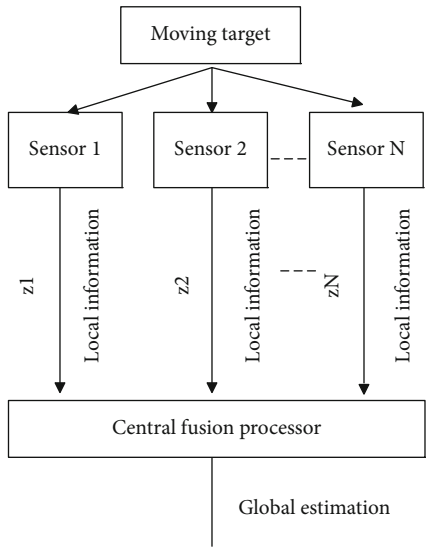

Figure 5: Central fusion structure model.

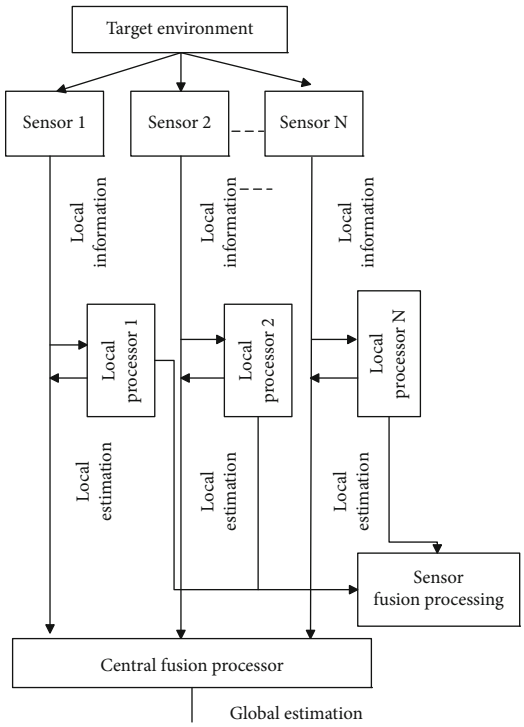

Figure 6: Hybrid fusion structure model.

However, under actual conditions, due to the large number of sensors, the data collected by some sensors may have serious errors that cannot be collected. Moreover, it is sometimes difficult to distinguish which sensors are collecting data from the same target. This makes the processing accuracy of the central-level data fusion structure higher, but the cost is also high and the stability is poor.

The hybrid fusion structure emphasizes the monitoring fusion process and effective scheduling data-level fusion, so it has strong adaptability, and takes into account the advantages of centralized fusion and distributed fusion structure, and has strong stability, as shown in Figure 6. However, this structure increases the complexity of data processing and needs to increase the data transmission rate, so it is time-consuming in communication and calculations [20].

As an intelligent education system, angle sensors can be installed in the classroom to detect the rotation joints of the camera device, so that the angle between the joints can be accurately obtained. After the angle is obtained, the calculation can be performed according to Equation (1) to obtain the pose equation of the wrist joint [21].

$$ {}^{0}T_{3} = {}^{0}T_{1}\,{}^{1}T_{2}\,{}^{2}T_{3}, \tag{1} $$

$$ {}^{0}T_{1} = \begin{bmatrix} c\theta_1 & 0 & -s\theta_1 & 0 \\ s\theta_1 & 0 & c\theta_1 & 0 \\ 0 & -1 & 0 & 0 \\ 0 & 0 & 0 & 1 \end{bmatrix}^{1} T_{2} = \begin{bmatrix} c\theta_2 & -s\theta_2 & 0 & a_2 c\theta_2 \\ s\theta_2 & c\theta_2 & 0 & a_2 c\theta_2 \\ 0 & 0 & 1 & 0 \\ 0 & 0 & 0 & 1 \end{bmatrix}, \tag{2} $$

$$ {}^{2}T_{3} = \begin{bmatrix} c\theta_3 & -s\theta_3 & 0 & a_3 c\theta_3 \\ s\theta_3 & c\theta_3 & 0 & a_3 c\theta_3 \\ 0 & 0 & 1 & 0 \\ 0 & 0 & 0 & 1 \end{bmatrix}. \tag{3} $$

$c\theta_1 = \cos\theta_1$, $s\theta_1 = \sin\theta_1$, and a_2 are the length of the big arm, and a_3 is the length of the forearm.

That is, as long as the value of $\theta_1, \theta_2, \theta_3$ is known, the pose of the wrist relative to the origin of the shoulder joint can be calculated according to Formula (1).

In actual working conditions, the data collected by the sensor may contain errors due to environmental interference, and the data collected by a traditional single sensor loses the characteristics after the information combination.

Kalman filtering has a good filtering effect in the field of linear filtering, especially the optimal state estimation can be obtained in the filtering process under the assumption of linear Gaussian white noise. Because the Kalman filtering method is simple and the linear filtering effect is good, it has been widely used in various fields, especially in the application of target tracking.

A discrete-time system described by the vector difference equation is considered. Due to the influence of Gaussian noise in the system, the state equation of the system is

$$ X(k+1) = F(k)X(k) + G(k)u(k) + v(k), k = 0, 1, 2, \cdots. \tag{4} $$

In the formula, $X(k) \in R$ is the state vector and $u(k) \in R$ is the known input vector. $v(k) \in R$ is the white noise sequence of the mean Gaussian process, and its covariance is

$$ E\left[\left(v(k)v(k)^{T}\right)\right] = Q(k). \tag{5} $$

The measurement equation of the system is

$$ z(k) = H(k)X(k) + w(k). \tag{6} $$

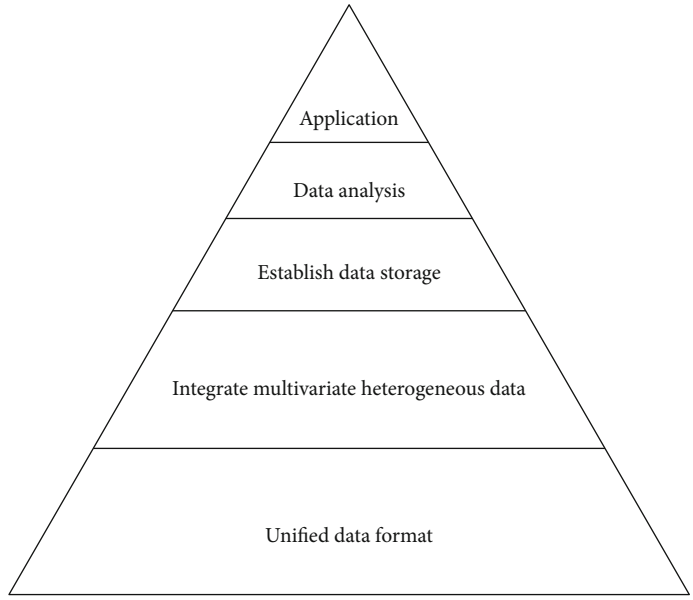

Figure 7: Multisource heterogeneous data processing model.

In the formula, $z(k) \in R$ is the observation vector, $w(k) \in R$ is the zero Gaussian noise sequence with mean value, and its covariance is

$$E\left[\left(w(k)w(k)^T\right)\right] = R(k). \tag{7}$$

The matrices $F(k)$, $G(k)$, $H(k)$, $Q(k)$, and $R(k)$ are assumed to be known and may change over time. That is, the system may change with time, and the noise may also be non-stationary random noise.

Kalman filtering has two types of algorithms: continuous and discrete. Among them, the discrete algorithm is currently widely used in the state estimation of linear systems.

The algorithm flow of Kalman filter is as follows: filter estimation [22]:

$$\widehat{X}(k+1 \mid k+1) = F\widehat{X}(k \mid k) + K(k+1)\left[Z(k) - HF\widehat{X}(k \mid k)\right]. \tag{8}$$

Filter gain:

$$X(k+1) = P(k+1 \mid k)H^T\left[HP(k+1 \mid k)H^T + R(k)\right]^{-1}. \tag{9}$$

Single-step prediction error covariance matrix:

$$P(k+1 \mid k) = FP(k \mid k)F^T + \Gamma Q(k)\Gamma^T. \tag{10}$$

Filtering error covariance matrix:

$$P(k+1 \mid k+1) = [I - K(k+1)H]P(k+1 \mid k). \tag{11}$$

It should be pointed out that $P(k+1 \mid k+1)$ can be regarded as the performance evaluation of Kalman filtering, because:

$$P(k+1 \mid k+1) = E\left[\left(X(k+1) - \widehat{X}(k+1 \mid k+1)\right)(X(k+1) - X\wedge(k+1 \mid k+1))^T\right]. \tag{12}$$

It can be seen from the Kalman filter process that the algorithm process of Kalman filter is actually a set of recursive formulas. The calculation process is a process of continuous prediction and correction according to the set initial value, state equation, and prediction equation. First, according to the state estimation at the previous moment, the next prediction value at the observation moment is obtained from the state equation; then, the correction value of the prediction value is calculated by combining the current real-time observation value and information, so as to obtain the optimal estimated value and complete the prediction.

In the design process of the Kalman filter, an important step is to determine the state vector of the filter, because the state vector often has an important influence on the entire algorithm. In the algorithm design process, considering the derivative relationship between speed and acceleration, speed can be regarded as a state vector. For the selection of another state vector, since once the deviation value of the acceleration is determined, the acceleration can be accurately estimated, so this deviation value can be selected as another state vector instead of directly estimating the acceleration.

We set

$$v = f(x) + w_v, \tag{13}$$

$$a = a(x) - \rho + w_a. \tag{14}$$

In formulas (13) and formula (14), v is the measured value of the speed sensor, a is the measured value of the acceleration sensor, w_v and w_a are the noise interference of the speed sensor and acceleration sensor, respectively, and

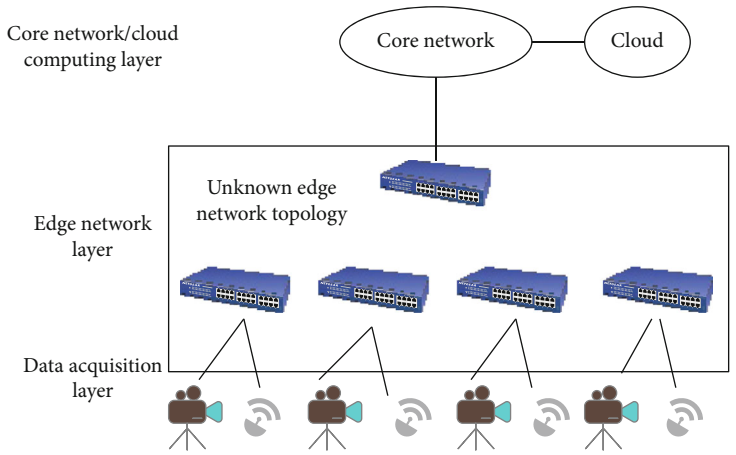

Figure 8: Edge big data processing model based on IoT cloud computing.

ρ is the measured deviation value of the assumed acceleration sensor.

The matrix equation is established as follows:

$$\begin{bmatrix} v \\ \rho \end{bmatrix} = \begin{bmatrix} 0 & -1 \\ 0 & 0 \end{bmatrix} \begin{bmatrix} v \\ \rho \end{bmatrix} + \begin{bmatrix} 1 \\ 0 \end{bmatrix} a + \begin{bmatrix} w_a \\ 0 \end{bmatrix}, \tag{15}$$

$$v = [10] \begin{bmatrix} v \\ \rho \end{bmatrix} + w_v. \tag{16}$$

Since the state vector selects the speed value and the deviation value from the acceleration, respectively, $x = [v \quad \rho]^T$, and the sampling time interval of the system is Δt, and

$$x(k+1) = x(k) + \Delta t \cdot a. \tag{17}$$

By combining formula (15) with formula (13), after sorting, we get

$$x(k+1) = \begin{bmatrix} 1 & -\Delta t \\ 0 & 1 \end{bmatrix} x(k) + \begin{bmatrix} \Delta t \\ 0 \end{bmatrix} a(k) + \begin{bmatrix} w_a(k) \cdot \Delta t \\ 0 \end{bmatrix}. \tag{18}$$

After completing the design of the Kalman filter, the simulation environment is designed according to the known algorithm flow.

3.3. Selection of Simulation Tools. The selection of simulation tools should take into account the simplicity of algorithm writing and the ability to intuitively generate simulation results. Since the Kalman filter algorithm involves matrix operations and recursive operations, the MATLAB tool, which has powerful numerical analysis and matrix operations, and can intuitively generate graphs, is selected for simulation in this design.

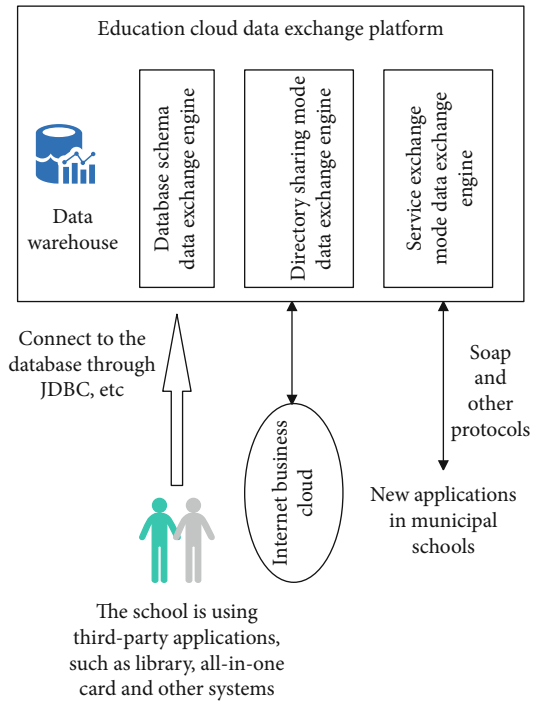

Figure 9: Data exchange function of education platform based on wireless network.

3.4. Determination of the Initial Value of the Filter. After determining the simulation tool to be used, it is necessary to program and simulate the filter. In order to find the derivative more convenient, and to control the upper and lower boundaries of the function, we can choose the sine function and cosine function for simulation, as follows:

$$v = \sin(4t) + w_v, \tag{19}$$

$$a = 4\cos(4t) - 5 + w_a. \tag{20}$$

Formula (18) is derived from formula (17) and obtained by setting the deviation value. w_v and w_a represent the variance values of the velocity function and acceleration function noise, respectively, and the values of w_v and w_a can be

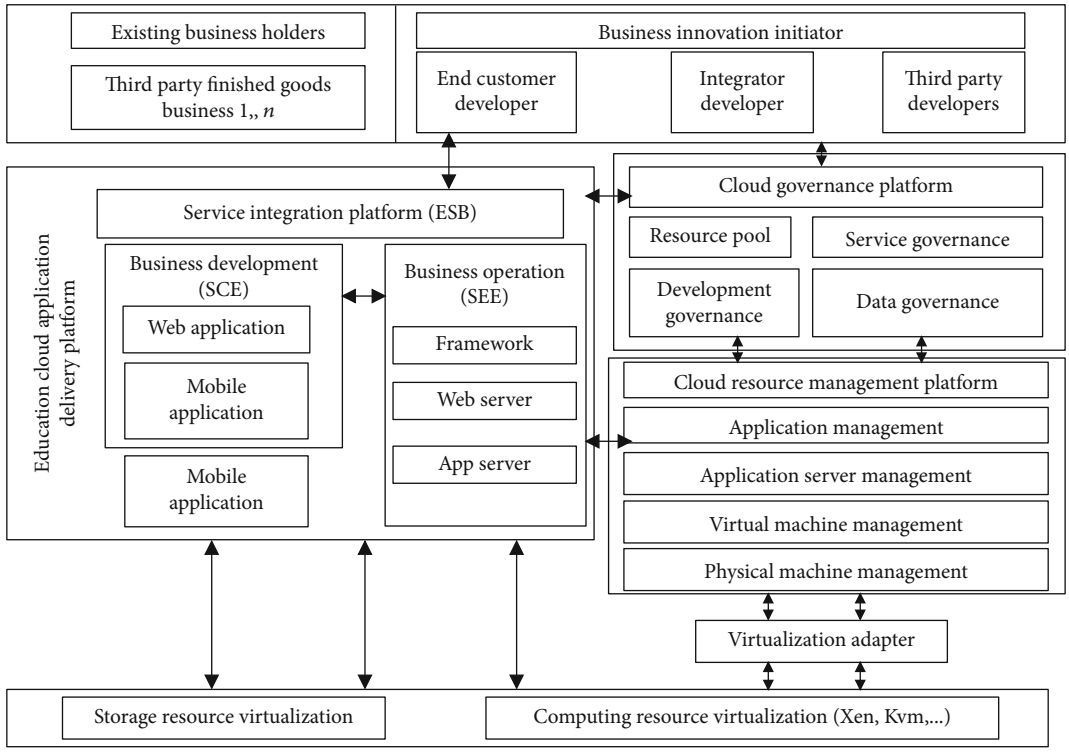

Figure 10: The framework of an intelligent education system based on the Internet of Things and new sensors.

set to 0.04 and 1, respectively. When the time interval of the system is set to $\Delta t = 0.01s$, the matrix function is as follows:

$$f = \begin{bmatrix} 1 & -\Delta t \\ 0 & 1 \end{bmatrix}, F = [\Delta t \quad 0]^T, p = \begin{bmatrix} 0 & 1 \\ 1 & 0 \end{bmatrix}, H = [1 \quad 0], Q = \begin{bmatrix} \Delta t^2 & 0 \\ 0 & 0 \end{bmatrix},$$

$$sgm\Gamma = 0.2, x = [0 \quad 0]^T. \tag{21}$$

Multisource heterogeneous data has the characteristics of large quantity, many data types, low value density, and authenticity. In order to realize the full application of multisource heterogeneous data, effectively carry out systematic analysis and data mining of multisource heterogeneous data, and obtain higher use value, this paper summarizes the multisource heterogeneous data processing requirements into a five-layer model, as shown in Figure 7.

4. Smart Education System Based on Internet of Things and New Sensor Technology

Figure 8 shows the processing model of big data at the network edge based on cloud computing. The model is divided into data collection layer, edge network layer, core network, and cloud computing layer. The data collection layer is responsible for collecting data, which is transmitted via the edge network and the core backbone network to the cloud computing center for processing. Among them, the edge network will be quite different according to different application scenarios. In this paper, it is assumed that the topology of the edge network is unknown.

The data exchange function of the education cloud platform can solve the problem of interconnection of business data generated within the smart class card system and external data such as education cloud, Internet commercial cloud, and school in-use information system. The data source of data exchange includes not only the business data generated by the smart class card system but also a large amount of event data using the smart class card system. Based on these two types of data sources, it satisfies the data query and retrieval, data mining, statistical analysis, and in-depth analysis. Figure 9 shows an example of the data exchange function of the education cloud platform.

As shown in Figure 10 is the overall architecture of the smart cloud platform, then all the subsystems, such as the teaching resource sharing subsystem, the educational administration system, and the all-in-one card system, will run on the service integration platform. Each application developer conducts unified planning to share and manage school, student personal information, and other data.

After constructing an intelligent education system based on the Internet of Things and new sensors, the performance of the system is verified. This article carries on simulation experiment through this Matlab, evaluates the performance of the intelligent education system through many groups of experiments, and counts the data transmission speed and teaching effect; the statistical result is shown in Table 1.

It can be seen from the above research that the method proposed in this paper has a good data transmission effect, can effectively improve the effect of intelligent education, and meet the actual needs of current education.

Table 1: Performance evaluation of intelligent education system based on the Internet of Things and new sensors.

Number	Transmission speed (ms)	System performance	Number	Transmission speed (ms)	System performance
1	143.45	76.51	26	134.23	75.39
2	113.42	88.45	27	119.01	77.73
3	100.33	74.88	28	143.80	80.42
4	106.09	77.87	29	142.81	79.10
5	113.67	77.38	30	121.02	75.02
6	146.11	76.42	31	151.60	76.14
7	148.37	86.08	32	122.74	83.42
8	130.98	86.80	33	101.36	88.04
9	141.18	95.17	34	107.95	96.79
10	106.53	91.82	35	134.78	88.74
11	144.50	92.93	36	138.67	92.91
12	112.72	77.97	37	131.45	90.50
13	99.11	77.21	38	106.24	85.88
14	143.73	90.97	39	149.93	91.22
15	122.87	79.51	40	106.84	79.17
16	147.93	88.36	41	112.80	75.14
17	143.05	95.58	42	107.42	87.91
18	105.97	85.13	43	120.06	75.27
19	112.06	85.46	44	122.07	88.08
20	140.26	77.05	45	114.44	74.16
21	98.70	78.29	46	148.19	78.95
22	115.72	88.06	47	102.28	96.76
23	131.77	78.57	48	126.43	83.35
24	133.41	77.19	49	139.90	81.90
25	110.05	74.91	50	113.15	91.13

5. Conclusion

With the further in-depth integration of computer technology, information technology, Internet technology, artificial intelligence, and other technologies and education, the appearance of smart education will undergo earth-shaking changes. This article discusses the basic principles and related knowledge of sensor technology and multisensor information fusion theory, as well as the application of Kalman filter in sensor data fusion, including the definition, classification, characteristics, and selection of sensors.

This article focuses on the analysis of the business needs of the cloud application platform. The cloud application platform of the smart campus requires basic platform construction, smart portal construction, smart teaching construction, and smart management construction. At the same time, this paper mainly elaborates the construction plan of the smart campus cloud service network platform and implements it. In addition, this paper constructs a smart education system based on the Internet of Things and new sensors and designs experiments to verify the system. Through the research results, it can be seen that the method proposed in this paper has a good data transmission effect, can effectively improve the effect of intelligent education, and meet the actual needs of current education.

Data Availability

The labeled dataset used to support the findings of this study are available from the corresponding author upon request.

Conflicts of Interest

The authors declare no competing interests.

Acknowledgments

This study is sponsored by Henan Finance University.

References

[1] S. M. Chaware, S. Dighe, A. Joshi, N. Bajare, and R. Korke, "Smart garbage monitoring system using internet of things (IoT)," *Ijireeice*, vol. 5, no. 1, pp. 74–77, 2017.

[2] W. Tushar, N. Wijerathne, W. T. Li et al., "Internet of things for green building management: disruptive innovations through low-cost sensor technology and artificial intelligence," *IEEE Signal Processing Magazine*, vol. 35, no. 5, pp. 100–110, 2018.

[3] J. H. Abawajy and M. M. Hassan, "Federated internet of things and cloud computing pervasive patient health monitoring system," *IEEE Communications Magazine*, vol. 55, no. 1, pp. 48–53, 2017.

[4] D. He, R. Ye, S. Chan, M. Guizani, and Y. Xu, "Privacy in the internet of things for smart healthcare," *IEEE Communications Magazine*, vol. 56, no. 4, pp. 38–44, 2018.

[5] P. P. Ray, "Internet of things for smart agriculture: technologies, practices and future direction," *Journal of Ambient Intelligence and Smart Environments*, vol. 9, no. 4, pp. 395–420, 2017.

[6] Y. A. Qadri, A. Nauman, Y. B. Zikria, A. V. Vasilakos, and S. W. Kim, "The future of healthcare internet of things: a survey of emerging technologies," *IEEE Communications Surveys & Tutorials*, vol. 22, no. 2, pp. 1121–1167, 2020.

[7] B. H. Dobkin, "A rehabilitation-internet-of-things in the home to augment motor skills and exercise training," *Neurorehabilitation and Neural Repair*, vol. 31, no. 3, pp. 217–227, 2017.

[8] J. Yao and N. Ansari, "Caching in energy harvesting aided internet of things: a game-theoretic approach," *IEEE Internet of Things Journal*, vol. 6, no. 2, pp. 3194–3201, 2019.

[9] J. E. Siegel, S. Kumar, and S. E. Sarma, "The future internet of things: secure, efficient, and model-based," *IEEE Internet of Things Journal*, vol. 5, no. 4, pp. 2386–2398, 2018.

[10] M. A. Abd-Elmagid, N. Pappas, and H. S. Dhillon, "On the role of age of information in the internet of things," *IEEE Communications Magazine*, vol. 57, no. 12, pp. 72–77, 2019.

[11] A. Sheth, U. Jaimini, and H. Y. Yip, "How will the internet of things enable augmented personalized health?," *IEEE Intelligent Systems*, vol. 33, no. 1, pp. 89–97, 2018.

[12] G. J. Joyia, R. M. Liaqat, A. Farooq, and S. Rehman, "Internet of medical things (IOMT): applications, benefits and future challenges in healthcare domain," *The Journal of Communication*, vol. 12, no. 4, pp. 240–247, 2017.

[13] N. Kshetri, "The evolution of the internet of things industry and market in China: an interplay of institutions, demands and supply," *Telecommunications Policy*, vol. 41, no. 1, pp. 49–67, 2017.

[14] S. Siboni, V. Sachidananda, Y. Meidan et al., "Security testbed for internet-of-things devices," *IEEE Transactions on Reliability*, vol. 68, no. 1, pp. 23–44, 2019.

[15] Y. Yang, M. Zhong, H. Yao, F. Yu, X. Fu, and O. Postolache, "Internet of things for smart ports: technologies and challenges," *IEEE Instrumentation & Measurement Magazine*, vol. 21, no. 1, pp. 34–43, 2018.

[16] Z. Li, Y. Liu, A. Liu, S. Wang, and H. Liu, "Minimizing convergecast time and energy consumption in green internet of things," *IEEE Transactions on Emerging Topics in Computing*, vol. 8, no. 3, pp. 797–813, 2020.

[17] P. P. Ray, "A survey on internet of things architectures," *Journal of King Saud University-Computer and Information Sciences*, vol. 30, no. 3, pp. 291–319, 2018.

[18] M. Mayer and A. J. Baeumner, "A megatrend challenging analytical chemistry: biosensor and chemosensor concepts ready for the internet of things," *Chemical Reviews*, vol. 119, no. 13, pp. 7996–8027, 2019.

[19] M. Saez, F. P. Maturana, K. Barton, and D. M. Tilbury, "Real-time manufacturing machine and system performance monitoring using internet of things," *IEEE Transactions on Automation Science and Engineering*, vol. 15, no. 4, pp. 1735–1748, 2018.

[20] V. Jagadeeswari, V. Subramaniyaswamy, R. Logesh, and V. Vijayakumar, "A study on medical internet of things and big data in personalized healthcare system," *Health information science and systems*, vol. 6, no. 1, pp. 1–20, 2018.

[21] S. Smys, A. Basar, and H. Wang, "Hybrid intrusion detection system for internet of things (IoT)," *Journal of ISMAC*, vol. 2, no. 4, pp. 190–199, 2020.

[22] I. Butun, P. Österberg, and H. Song, "Security of the internet of things: vulnerabilities, attacks, and countermeasures," *IEEE Communications Surveys & Tutorials*, vol. 22, no. 1, pp. 616–644, 2020.

Hindawi
Journal of Sensors
Volume 2021, Article ID 4942657, 9 pages
https://doi.org/10.1155/2021/4942657

Research Article

Case Investigation Technology Based on Artificial Intelligence Data Processing

Jianwei Ding

Department of Investigation, Railway Police College, Zhengzhou 450053, China

Correspondence should be addressed to Jianwei Ding; dingjianwei@rpc.edu.cn

Received 19 August 2021; Accepted 7 October 2021; Published 26 October 2021

Academic Editor: Mu Zhou

Through data mining technology, the hidden information behind a large amount of data is discovered, which can help various management services and provide scientific basis for leadership decision-making. It is an important subject of current police information research. This paper conducts in-depth research on the investigation analysis and decision-making of public security cases and proposes a case-based reasoning model based on two case databases. Moreover, this paper discusses in detail the use of data mining technology to automatically establish a case database, which is a useful exploration and practice for the public security department to establish a new and efficient case investigation auxiliary decision-making system. In addition, this paper studies the method of using data mining technology to assist in the establishment of a case database, analyzes the characteristics of traditional case storage methods, and constructs a case investigation model based on artificial intelligence data processing. The research results show that the model constructed in this paper has certain practical effects.

1. Introduction

Information construction has been initially applied to police work. However, because it is in its infancy, information business processing can only play its most basic functions, such as simple search, add files, delete files, storage, and statistic, but lack real substantive analysis and prediction functions. With the continuous development of work, the information system has realized the transformation of the database from small to large. Therefore, fully integrating the functions of analysis, judgment, and decision-making into data construction can make a reasonable transformation of data between micro and macro data as required.

At present, the informatization of police work in our country has not been popularized. Even if information technology is used in the work, the technical level is generally low. Therefore, scientific and technological means cannot be effectively used to collect and manage information resources. In order to severely crack down on crimes such as high-tech and high-IQ crimes, it is also necessary to combine police work with information construction [1]. By using advanced technology and the high efficiency of information resources, the level of scientific and technological knowledge of police officers can be improved. The full application of modern information technology to police work can improve the detection capabilities of police officers and effectively combat various forms of crime. Moreover, it is also the best way to improve the efficiency of detection and can fundamentally control the crime rate and achieve social stability and harmony [2]. At the same time, information technology is used to fully reflect the substantive potential problems behind things and find out the rules, so as to meet the detection and investigation needs of police officers. The current development of our country is facing diversification, globalization, popularization of information, and deepening of technology. However, with the rapid development of society, the unstable factors in the social environment are increasingly exposed [3]. How to better maintain social stability and harmony has become the biggest challenge facing police officers in public security organs. Police officers must adhere to the strategic strategy of driving science and technology and fully integrate information technology into practical work to improve the scientific and technological content of our country's police work. Building the modernization of

police work in an all-round way and making police work more efficient and dynamic are the focus of the current work of our police officers [4].

This paper conducts in-depth research on the investigation analysis and decision-making of public security cases and proposes a case-based reasoning model based on two case databases. Moreover, this paper discusses in detail the use of data mining technology to automatically establish a case database, which is a useful exploration and practice for the public security department to establish a new and efficient case investigation auxiliary decision-making system.

2. Related Work

As an important content in database information technology, Knowledge Discovery in Database (KDD) was first used when database technology was in the development stage [5]. Later, it was used as an academic research topic, and the academic community would regularly hold seminars on KDD technology. At the meeting, someone vividly combined data with mineral deposits, and the term "data mining" came from this. After that, the United States continued to hold seminars on data mining content, and the research content became more and more professional, and the number of people and experts participating in data mining research increased, even reaching several thousand. Moreover, academic papers on KDD are increasing, and data mining has become a new topic in the field of information technology [6]. With the deepening of research, data research has developed from the initial basic research to comprehensive research and development. It not only incorporates a variety of research strategies but also applies scientific knowledge in various fields. Data mining has become a hot topic in various seminars, and it has been continuously discussed and studied in depth by scholars from various countries [7]. This paper takes the Chicago Police Department (Chicago Police Department, hereinafter referred to as CPD) 2013 prevention work large-scale data as an example. CPD is working to create a social graph similar to Facebook. In order to combat gang violent crimes, it uses network analysis to track active gang members and issue warnings to them to prevent possible violent crimes [8]. In 2012, there were more than 500 murders in Chicago. So far this year, the city's murder rate has dropped by 22%, many of which are related to violent criminal gang activities [9]. Data mining is a network tool that can analyze the conversations, hobbies, and social activities of its members and provide accurate search results. On this basis, CPD constructed a model. The model includes data variables such as the number of times each gang member has been shot and the number of criminal records, so as to identify the "most active" residents of Chicago, that is, those who are most likely to be involved in violent activities [10]. At the beginning of 2013, CPD announced the list of the top 20 "most active" members of the 22 police districts under the jurisdiction of the city of Chicago. After the list was confirmed, the Chicago Police Department and the "Violent Crime Reduction Strategy" organization cooperated to continuously send warning messages to those included in the gang. Some members of these gangs were surprised to receive such news [11]. A piece of Rigel software written in [12] is a criminal tracking software based on "geographic analysis technology." Through the analysis of the distribution of crime scenes, it unearthed the distribution of criminals' (especially criminals in serial cases) residences and other criminal hiding places. The practice of police application has proved that data mining technology can help police analyze past cases, discover crime patterns and characteristics, and find commonalities and similarities. Moreover, data mining can assist leaders in decision-making and serve the various fields of public security work such as combating, preventing, managing, and controlling. In the past, the analysis of police situation and series and parallel cases required manual force to complete, which wasted huge manpower and material resources, and the analysis results were incomplete and unreliable. At present, by using the latest data mining technology, the above problems can be completed in a few hours, which greatly improves the work efficiency of the public security organs [13]. In the long run, big data and data mining technology can optimize the allocation of police resources and enhance the ability of public security organs to fight crime, thereby enhancing the level of social and economic development and the people's sense of security and satisfaction [14].

3. Search Criminal Cases

This article combines machine learning data processing methods to process case investigation data and then calculates and exercises the algorithm.

The purpose of case retrieval is to retrieve one or more cases that are most similar to the target case from the case database, so case retrieval can be attributed to the comparison of similarities between the two cases. In case reasoning systems, there are three commonly used retrieval methods: nearest neighbor method, inductive index method, and knowledge guidance method. We can use only one, or we can use multiple methods to share.

When searching for similar cases, this paper adopts the nearest neighbor method. The meaning of nearest neighbor is as follows: if case Z is the nearest neighbor of case X, that is, Z and X are the most similar, then for any case Y, there must be the following [15]:

$$\text{sim}(X, Y) \leq \text{sim}(X, Z), \tag{1}$$

Among them, sim() is the similarity calculation function, and the larger the value, the more similar the objects. Similarity is not only the core content of the nearest neighbor retrieval method, but also the key to case retrieval.

In the case described in a DBML document, x_n is an element or attribute value of the document, and it may also be a complex data type element (such as victim object information). If it is a complex data type element, we must first calculate the weighted sum of the local similarity of the corresponding nested element (attribute) (the calculation method is the same) and use the calculated weighted sum value as the similarity of the complex data type element to participate in the similarity calculation of the entire case [9].

We set the source case (cases in the typical case database) as $X(x_1, x_2, \cdots, x_n)$ and the target case as $Y(y_1, y_2, \cdots, y_n)$. x_n, y_n is the nth attribute of the case. According to the nearest neighbor method, the similarity between the source case and the target case is defined as follows:

$$\mathrm{sim}(X, Y) = \sum_{i=1}^{n} \omega_i \mathrm{sim}(x_i, y_i). \quad (2)$$

In the formula, ω_i represents the weight of each attribute.

$$1 \geq \mathrm{sim}(x_i, y_i) \geq 0, \quad \sum_{i=1}^{n} \omega_i = 1. \quad (3)$$

For criminal cases, after data preprocessing operations, the types of attributes can be summarized into four types: numeric types, binary variables, enumeration types, and string types. Different attribute types have different similarity calculation methods, here are divided into four cases:

(1) Numerical type

It uses the minimum method to calculate the similarity [16]:

$$\mathrm{sim}(X_i, Y_i) = \frac{\min(x_i, y_i)}{\max(x_i, y_i)}. \quad (4)$$

In the formula, when $x_i = y_i$, there is $\mathrm{sim}(x_i, y_i) = 1$. Among them, $\min(x_i, y_i)$ represents the smaller value in x_i , y_i, and $\max(x_i, y_i)$ represents the larger value in x_i, y_i.

For example, the age of a person can be calculated as a continuous numeric type.

(2) Binary variables

It determines similarity based on whether it is equal or not [17]:

$$\mathrm{sim}(X_i, Y_i) = 0(\mathrm{similar}) \mathrm{or} \mathrm{sim}(X_i, Y_i) = 1(\mathrm{not\ similar}). \quad (5)$$

For example, smoking can take two values, 1 means smoking, and 0 means not smoking. If both smoke or neither smoke, it is represented as $\mathrm{sim}(X_i, Y_i) = 1$, and if one smokes and the other does not, it is represented as $\mathrm{sim}(X_i, Y_i) = 0$.

(3) Enumeration type

This type is divided into two situations, when the enumeration value is a numeric type [6]:

$$\mathrm{sim}(X_i, Y_i) = 1 - \frac{|X_i - Y_i|}{\max(R) - \min(R)}. \quad (6)$$

In the formula, R represents the set of enumerated values, $\max(R)$ represents the largest one in the set R, and $\min(R)$ represents the smallest one in the set R. At the same time, $\max(R) - \min(R)$ is the interval distance of the set R.

When the enumeration value is a string type,

$$\mathrm{sim}(X_i, Y_i) = 0(\mathrm{similar}) \mathrm{or} \mathrm{sim}(X_i, Y_i) = 1(\mathrm{not\ similar}). \quad (7)$$

For example, the case type is an enumerated string.

(4) String type

It determines similarity based on whether it is equal or not [17]:

$$\mathrm{sim}(X_i, Y_i) = 0(\mathrm{not\ similar}) \mathrm{or} \mathrm{sim}(X_i, Y_i) = 1(\mathrm{similar}). \quad (8)$$

It can use the "keyword fuzzy matching" method to calculate the similarity value of two strings, instead of simply using 0 and 1 to indicate similarity. This calculation method is more suitable for calculating the similarity of large sections of text.

Tree construction steps. This phase breaks the two phases of the traditional FP-growth (Frequent Pattern Tree) algorithm, that is, the insertion phase and the remanagement phase. In the insertion phase, the item sets of a transaction are inserted into the tree in descending order of frequency. Moreover, the biggest feature of this method is that if I_n is now responsible for inserting, I_{n-1}'s affairs must be considered. To put it another way, the frequency of items in transactions before I_{n-1} needs to be considered. The proportion of this tree in the project edit distance exceeds a certain threshold.

In the frequent item mining stage, the tree mining stage follows the FP-growth mining technology. The FP-growth algorithm is used to mine frequent items, and the frequency must be within the threshold specified by the user to mine the constructed ISPO-tree (reedispO tree). The mining technology of the FP-growth algorithm is also used in CP-tree (compressible-prefix tree) and Cantree methods.

The source of this unstable dataset is that these data may be slightly modified, as shown in Figure 1. First, we introduce an example of the ISPO-tree method without a small amount of data change, that is, flag is in the inserted state, and there is flag = 0.

It can be expressed by a formula [18].

$$\sum_{i}^{n} \max(i - 1, m - 1) = \frac{i(i-1)}{2} + \mathrm{floor}\left(\frac{i^2}{4}\right). \quad (9)$$

Then, after the algorithm adjusts the tree, the distance D value is cleared. The transaction that has been inserted is shown in Figure 2, and flag is replaced with 1.

This is mainly to be closely related to the characteristics of electronic evidence analysis. For electronic evidence, it is not only necessary to ensure its durability, but also to maintain its validity. Then, some evidences must be copied from the source data before and cannot be modified. However, in the electronic evidence analysis system, in order to analyze the validity of the evidence, it can correct the existing copied data according to the correct modification. For example,

Items	1	2	3	4	5	6	7	8	9	10
D_0										9
D_1									8	8
D_2								7	7	7
D_3							6	6	6	6
D_4						5	5	5	5	5
D_5					4	4	4	4	4	5
D_6				3	3	3	3	5		6
D_7			2	2	2	3	4	5	6	7
D_8		1	1	2	3	4	5	6	7	8
D_9	0	1	2	3	4	5	6	7	8	9
∑D	0	2	5	10	16	24	33	44	56	70

Figure 1: Distance comparison table.

$I1$
$a:1$
$b:1$
$c:1$
$d:1$
$e:1$

$I1$	$I2$	D
$a:1$	$a:2$	
$b:1$	$b:2$	
$c:1$	$e:2$	
$d:1$	$c:1$	
$e:1$	$d:1$	
	$f:1$	

$I2$	$I3$	D
$a:2$	$b:3$	+1
$b:2$	$a:2$	−1
$e:2$	$e:2$	+2
$c:1$	$c:1$	−1
$d:1$	$d:1$	−1
$f:1$	$f:1$	

$I3$	$I4$	D
$b:3$	$b:4$	
$a:2$	$a:3$	
$e:2$	$e:2$	
$c:1$	$d:2$	+1
$d:1$	$c:1$	−1
$f:1$	$f:1$	

$I4$	$I5$	D
$b:4$	$b:5$	
$a:3$	$a:4$	
$e:2$	$e:2$	
$d:2$	$d:2$	+1
$c:1$	$c:2$	−1
$f:1$	$f:1$	

Figure 2: The diagram of result of adding from I_1 to I_5.

when a suspect forges identity, time, location, etc., we need to modify the data to better find evidence in the future. However, this kind of modification is definitely a small amount. If all the analysis is rerun, a lot of time and resources will be wasted. Therefore, in this case, a small amount of modified algorithm is proposed to improve efficiency [19].

In Figure 3, the ISPO-tree generated after modifying I_5 is shown. After the remodification of item I_5 is completed, flag bit flag is preset to 1 by us. Then, we recalculate the D value to determine whether the threshold is greater than or equal to the minimum character and determine whether the tree needs to be reconstructed [21].

D_Trans represents the affairs to be changed. If D_Trans is not empty, it proves that there is a task to modify the transaction, and then, the flag bit is changed to 0. The method of calculating the distance is the same as in the previous section. In the method adopted, the "-" sign represents deleting an element, and the "+" sign represents adding an element. For example, in the following table, a transaction

$I4$	$I5$	D
$b:4$	$b:5$	
$a:3$	$a:3$	
$e:2$	$e:2$	+1
$d:2$	$d:2$	−1
$c:1$	$c:1$	
$f:1$	$f:2$	

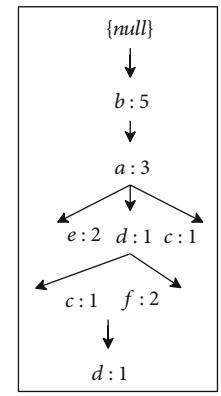

Figure 3: The modified result of I_5.

is added, the flag bit is set to 1, and I_5 is to be changed. Then, the meaning in the table is to change a to f [20].

Since the item header table in FP-tree will be linked to the item's position in the tree, the algorithm finds the position of the element from the first changed transaction to modify the frequency and recalculate the threshold. After that, according to the threshold, the algorithm decides whether to reconstruct the tree. Therefore, the branch tree constructed by the ISPO-tree algorithm is less than the branch tree constructed by the previous two algorithms, and it supports the modification of a small number of elements.

4. DC-STree Improved Algorithm

The algorithm defines $\Omega(o_1, o_2, \cdots, o_n)$ as a dataset. Each object is described by some characteristics. The algorithm defines $R(r_1, r_2, \cdots, r_n)$ as a tuple $(v_1, v_2, \cdots, v_m)$, $v_i \in D_i$ (D_i is the domain of r_i, $1 \le i \le m$). The feature subset $S \in R$ of an object is defined as $I_S(O)$, that is, the feature attribute set in S. $O_{[r]}$ represents the value of the feature. For each feature subset, $S \in R, S \ne \Phi S$ has a Boolean similarity function f_s to describe the relationship between objects. For example, the algorithm gives two definitions, $I_S(O), I_S(O')$ and $O, O' \in \Omega, f_s(O, O') = 1$, which means S is similar to O'. On the contrary, $f_s(O, O') = 0$ is not similar. The following two formulas are examples of Boolean similar functions [22].

$$f_s\left(O, O'\right) = \begin{cases} 1, & \forall r \in S \middle| C_r\left(O[r], O'[r]\right) = 1, \\ 0, & \text{otherwise}, \end{cases} \tag{10}$$

$$f_s\left(O, O'\right) = \begin{cases} 1, & \dfrac{|r \in S | C_r\left(O[r], O'[r]\right) = 1}{|S|} \ge \alpha, \\ 0, & \text{otherwise}. \end{cases} \tag{11}$$

In the formula, $C_r : D_r \times D_r \longrightarrow \{0, 1\}$ is the comparison function of r characteristic attribute value. The following two example formulas are as follows:

$$C_r(x,y) = \begin{cases} 1, & x = y, \\ 0, & \text{otherwise}, \end{cases} \tag{12}$$

$$C_r(x,y) = \begin{cases} 1, & |x-y| \le \varepsilon, \\ 0, & \text{otherwise}. \end{cases} \tag{13}$$

We need to pay attention to the use of similar functions. Equation (10) uses a comparison function like Equation (12), and Equation (12) creates an equivalent function. However, the use of similar functions in formula (10) or formula (11) combines the comparison function formula (12) and also the comparison function formula (13), $\varepsilon \neq 0$. Equation (13) creates a similar function, but different from equality.

We define in $I_S(O)$, there is $O \in \Omega, S \in R, S \neq \Phi$, the Boolean similarity function is not f_s, and then, the frequent number of $I_S(O)$ (that is, the degree of support) is defined as follows:

$$f_s - \text{freq}(O) = \frac{\left|\left\{o' \in \Omega \middle| f_s\left(O, O'\right) = 1\right\}\right|}{|\Omega|}. \tag{14}$$

If $f_s - \text{freq}(O)$ (support) is not less than threshold min freq, $I_S(O)$ is called frequent similarity pattern. If you want to find all the frequent similar patterns contained in the Ω object set, a useful property will be introduced below, which can reduce the number of mining and improve efficiency. The structure of STree is shown in Figure 4.

For any s_1, s_2, there is $s_1 \in s_2 \in R, s_1 \neq \Phi, o \in \Omega$. Then, the following conclusions will be obtained [2]:

$$\left[f_{s_1} - \text{freq}(O) > \min \text{Freq}\right] \longrightarrow \left[f_{s_2} - \text{freq}(O) < \min \text{Freq}\right]. \tag{15}$$

5. Model Building

The data in this article comes from the Internet. The data in this article is processed by machine learning methods and combined with mathematical statistics tools to process statistical charts.

The model system in this paper uses the association rule algorithm in data mining technology to mine the database source data in the existing electronic evidence management system, find frequent item sets, generate association rules, and present results. Moreover, it is used to analyze the relationship between cases and the relationship between criminal suspects and predict possible cases and the motives of criminal suspects. This prototype system is mainly an electronic evidence analysis system. The data source of this analysis system can come from the existing computer forensic system and electronic evidence management analysis system and can be obtained from the hard disk, such as text files, video and audio files, email clients, browser records, QQ client and Fetion client chat records. Mobile devices include mobile hard disks, mobile phones, and U disks, as well as mobile phone address books, short messages, and chat

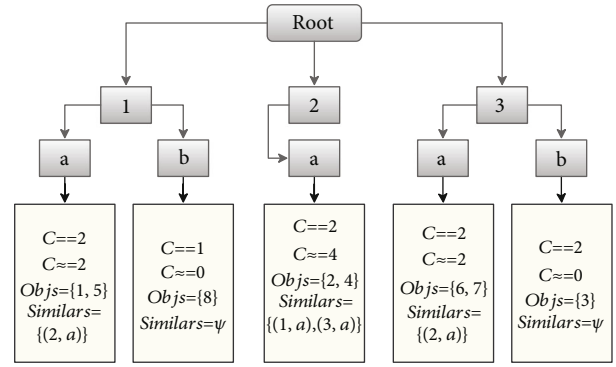

Figure 4: The structure of STree.

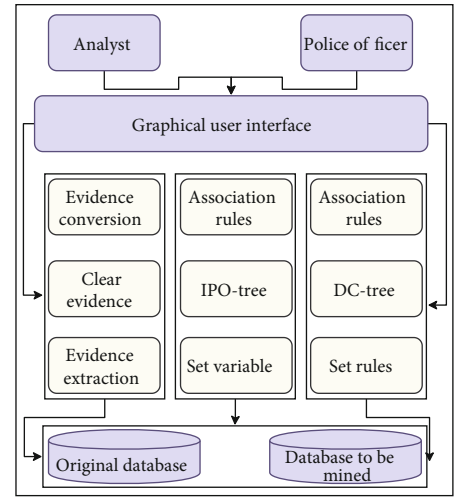

Figure 5: Structure diagram of electronic evidence analysis system based on data mining.

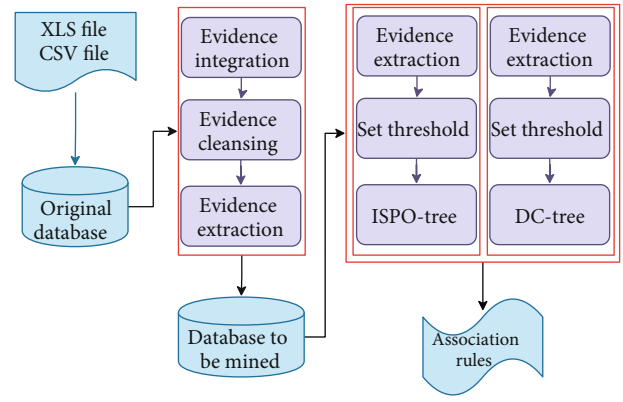

Figure 6: System business flow chart.

records of smart phone clients. The data obtained by these forensic tools will be stored in the database or data warehouse in the electronic evidence analysis system. The focus of this paper is to use association rule algorithms to mine tacit knowledge from these databases or data warehouses that store electronic evidence and finally present it and store it in the knowledge base. The entire system architecture diagram is shown in Figure 5.

Table 1: Comparison of mining time between similar frequent patterns and frequent patterns.

	Similar frequent pattern mining		Frequent pattern mining	
	Data preprocessing time	Mining time		Data preprocessing time
1 K	70 s	56 s	1 K	70 s
10 K	125 s	73 s	10 K	125 s
100 K	672 s	132 s	100 K	672 s

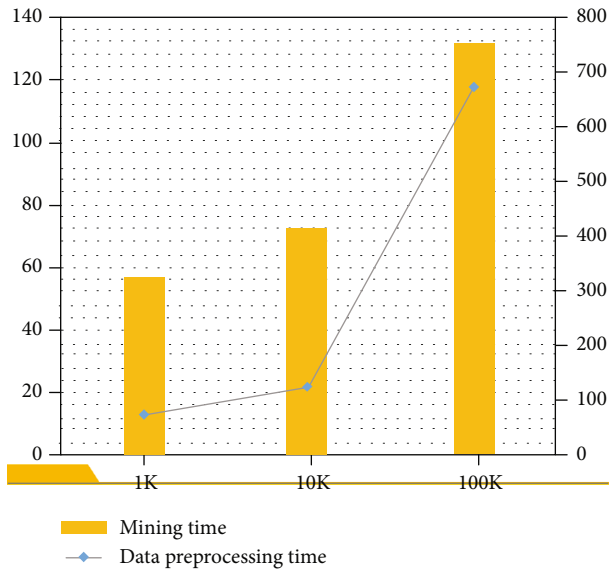

Figure 7: Statistical diagram of mining time of similar frequent patterns.

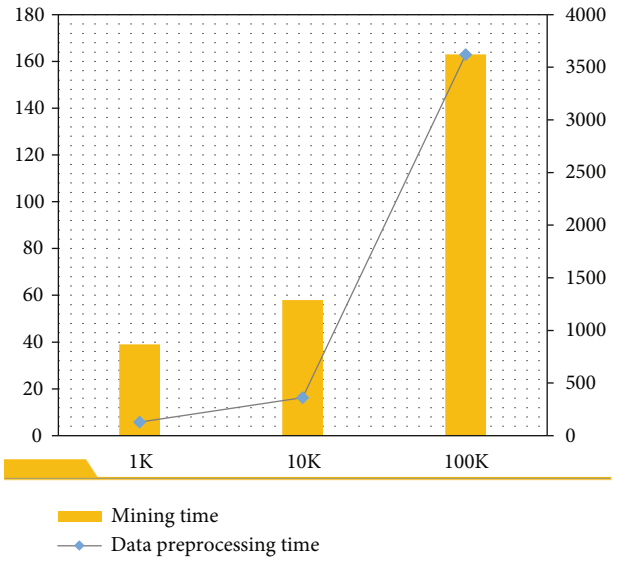

Figure 8: Statistical diagram of the mining time of frequent patterns.

After analysis and certification, the system first preprocesses the evidence data in the original database, extracts useful evidence data from the database, and removes some irrelevant evidence data. After that, the system hierarchizes

Table 2: Number of cases and loss interval from category 1 to category 10.

Classification	Number of cases	Minimum	Max
1	1764	0	1194
2	1634	1211	1919
3	1120	1949	2626
4	827	2656	3656
5	1007	3666	5050
6	886	5070	7323
7	747	7346	12070
8	705	12080	23634
9	529	23699	69112
10	207	69690	2532070

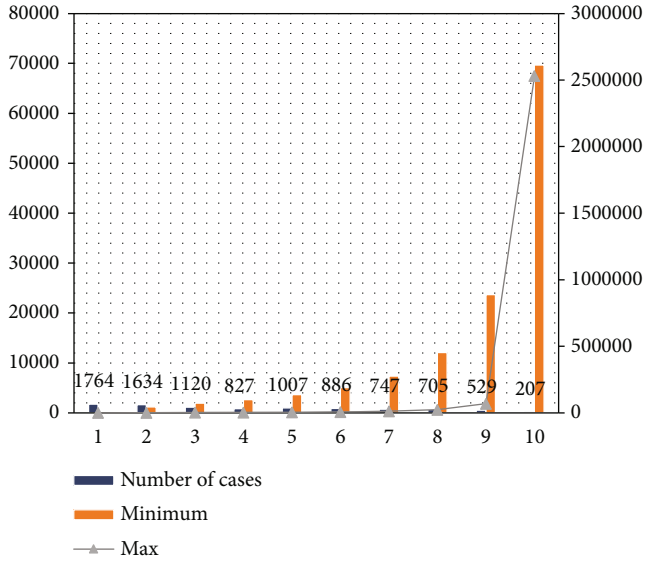

Figure 9: Statistical diagram of the number of cases and loss interval from category 1 to category 10.

and transforms these evidence data concepts and selects some related attributes to transform into the form required by data mining technology. After the preprocessing of the evidence data is completed, the analysts use the data in the improved FP-growth algorithm proposed in this paper to use association rules for data mining. System business flow chart is shown in Figure 6.

The electronic evidence similarity frequent mining algorithm first proposed in this paper has two advantages. The first point is that the time in the data preprocessing part is saved. By formulating similar rules, the work of frequently

Table 3: Statistical table of the case detection rate of the model.

No.	Case detection rate (%)	No.	Case detection rate (%)	No.	Case detection rate (%)	No.	Case detection rate (%)
1	64.4	21	62.5	41	47.8	61	48.5
2	55.3	22	54.4	42	60.1	62	45.6
3	59.2	23	46.4	43	60.9	63	49.4
4	59.9	24	51.8	44	53.1	64	45.9
5	64.9	25	58.2	45	51.4	65	57.2
6	49.5	26	51.7	46	56.8	66	55.1
7	52.7	27	61.3	47	52.2	67	63.8
8	64.9	28	61.8	48	46.6	68	59.9
9	48.9	29	56.7	49	49.5	69	49.0
10	58.7	30	50.5	50	53.2	70	54.3
11	48.1	31	50.7	51	57.5	71	55.5
12	55.2	32	61.6	52	57.6	72	58.6
13	57.1	33	60.6	53	64.4	73	54.7
14	57.9	34	46.5	54	53.6	74	46.9
15	52.7	35	64.0	55	55.1	75	54.7
16	58.2	36	48.3	56	48.7	76	51.0
17	48.8	37	45.1	57	64.4	77	56.4
18	63.5	38	52.4	58	45.4	78	51.4
19	49.7	39	47.8	59	54.5	79	53.7
20	49.6	40	58.6	60	62.5	80	47.2

modifying data items compared to the data preprocessing stage is saved. Moreover, the time spent in the execution of the entire algorithm is much smaller than that of data preprocessing, as shown in Table 1 and Figures 7 and 8.

6. Model Performance Analysis

This paper analyzes the data processing performance of the model. First, this paper studies the classification effect of the model on criminal cases. In the classification profile, the specific distribution interval of the 10 classifications and the number of cases contained in each classification are reflected. In order to make the boundaries of the 10 classifications clearer, an accurate classification boundary interval is obtained by drilling. The specific money value distribution of 10 classifications is shown in Table 2 and Figure 9.

Next, this paper analyzes the accuracy of case investigation by the model constructed in this paper. This paper collects the case data that has been solved in the past 3 years, inputs the case data into the model for data processing, and compares the obtained results with the real results to calculate the correct rate of case detection. The results are shown in Table 3 and Figure 10.

As shown in Figure 10 and Table 3, after inputting real data from the investigation scene of the case, this paper found that the detection rate after the investigation of the case was distributed between 45% and 65%. It can be seen that the practical effect of the model constructed in this paper is very good and can be applied to practice in the later stage.

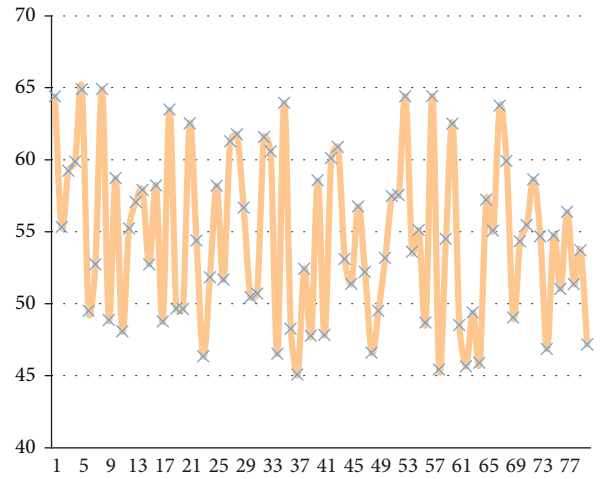

Figure 10: Statistical diagram of the case detection rate of the model.

7. Conclusion

This paper conducts in-depth research on the investigation analysis and decision-making of public security cases and proposes a case-based reasoning model based on two case databases. Moreover, this paper discusses in detail the use of data mining technology to automatically establish a case database, which is a useful exploration and practice for the public security department to establish a new and efficient case investigation auxiliary decision-making system. In addition, this paper studies the method of using data mining

technology to assist in the establishment of a case database, analyzes the characteristics of traditional case storage methods, and designs and implements a CBML criminal case modeling language that conforms to the XML standard. In order to mine traditional case data to extract effective case information, this paper discusses how to perform data preprocessing, including operations such as data cleaning, data integration, data transformation, and data reduction. Then, this paper applies outlier data analysis and cluster analysis techniques to case mining and designs an electronic evidence analysis system model based on data mining. The model proposed in this question mainly includes three parts: electronic evidence preprocessing, electronic evidence frequent pattern mining, and electronic evidence similar frequent pattern mining. The experimental results show that the model constructed in this paper has good performance.

This paper mostly uses simulation research combined with a small amount of data for analysis. The model studied in this paper needs further practical research in the follow-up.

Data Availability

The labeled dataset used to support the findings of this study is available from the corresponding author upon request.

Conflicts of Interest

The author declares no competing interests.

Acknowledgments

This research is supported by the following: (1) General Project of Humanities and Social Science Research in Colleges and Universities in Henan Province in 2022: Research on the Countermeasures of Telecommunication Network Fraud Crimes in the Post-epidemic Era (2022-ZZJH-014) and (2) Henan scientific and technological research projects (202102310487).

References

[1] A. A. Al-Musawi, A. A. H. Alwanas, S. Q. Salih, Z. H. Ali, M. T. Tran, and Z. M. Yaseen, "Shear strength of SFRCB without stirrups simulation: implementation of hybrid artificial intelligence model," *Engineering with Computers*, vol. 36, no. 1, pp. 1–11, 2020.

[2] H. Lu, Y. Li, M. Chen, H. Kim, and S. Serikawa, "Brain intelligence: go beyond artificial intelligence," *Mobile Networks and Applications*, vol. 23, no. 2, pp. 368–375, 2018.

[3] R. Ferrari, C. Mancini-Terracciano, C. Voena et al., "MR-based artificial intelligence model to assess response to therapy in locally advanced rectal cancer," *European Journal of Radiology*, vol. 118, pp. 1–9, 2019.

[4] T. Fu and C. Wang, "A hybrid wind speed forecasting method and wind energy resource analysis based on a swarm intelligence optimization algorithm and an artificial intelligence model," *Sustainability*, vol. 10, no. 11, p. 3913, 2018.

[5] X. Sun, J. Young, J.-H. Liu, and D. Newman, "Prediction of pork loin quality using online computer vision system and artificial intelligence model," *Meat Science*, vol. 140, pp. 72–77, 2018.

[6] A. Zappone, M. Di Renzo, M. Debbah, T. T. Lam, and X. Qian, "Model-aided wireless artificial intelligence: embedding expert knowledge in deep neural networks for wireless system optimization," *IEEE Vehicular Technology Magazine*, vol. 14, no. 3, pp. 60–69, 2019.

[7] X.-N. Bui, H. Nguyen, Y. Choi, T. Nguyen-Thoi, J. Zhou, and J. Dou, "Prediction of slope failure in open-pit mines using a novel hybrid artificial intelligence model based on decision tree and evolution algorithm," *Scientific Reports*, vol. 10, no. 1, pp. 1–17, 2020.

[8] Z. M. Yaseen, A. El-shafie, O. Jaafar, H. A. Afan, and K. N. Sayl, "Artificial intelligence based models for stream-flow forecasting: 2000-2015," *Journal of Hydrology*, vol. 530, pp. 829–844, 2015.

[9] J. E. Laird, C. Lebiere, and P. S. Rosenbloom, "A standard model of the mind: toward a common computational framework across artificial intelligence, cognitive science, neuroscience, and robotics," *AI Magazine*, vol. 38, no. 4, pp. 13–26, 2017.

[10] K. Chapi, V. P. Singh, A. Shirzadi et al., "A novel hybrid artificial intelligence approach for flood susceptibility assessment," *Environmental Modelling & Software*, vol. 95, pp. 229–245, 2017.

[11] M. R. Hashemi, M. L. Spaulding, A. Shaw, H. Farhadi, and M. Lewis, "An efficient artificial intelligence model for prediction of tropical storm surge," *Natural Hazards*, vol. 82, no. 1, pp. 471–491, 2016.

[12] J. Ma, J. Yu, G. Hao et al., "Assessment of triglyceride and cholesterol in overweight people based on multiple linear regression and artificial intelligence model," *Lipids in Health and Disease*, vol. 16, no. 1, p. 42, 2017.

[13] T. Sustrova, "A suitable artificial intelligence model for inventory level optimization," *Trends Economics and Management*, vol. 10, no. 25, pp. 48–55, 2016.

[14] B. T. Pham, M. D. Nguyen, D. Van Dao et al., "Development of artificial intelligence models for the prediction of Compression Coefficient of soil: an application of Monte Carlo sensitivity analysis," *Science of the Total Environment*, vol. 679, pp. 172–184, 2019.

[15] A. Enshaei, C. N. Robson, and R. J. Edmondson, "Artificial intelligence systems as prognostic and predictive tools in ovarian cancer," *Annals of Surgical Oncology*, vol. 22, no. 12, pp. 3970–3975, 2015.

[16] Z. Ghahramani, "Probabilistic machine learning and artificial intelligence," *Nature*, vol. 521, no. 7553, pp. 452–459, 2015.

[17] D. T. Bui, B. Pradhan, H. Nampak, Q.-T. Bui, Q.-A. Tran, and Q.-P. Nguyen, "Hybrid artificial intelligence approach based on neural fuzzy inference model and metaheuristic optimization for flood susceptibilitgy modeling in a high- frequency tropical cyclone area using GIS," *Journal of Hydrology*, vol. 540, pp. 317–330, 2016.

[18] S. Keel, P. Y. Lee, J. Scheetz et al., "Feasibility and patient acceptability of a novel artificial intelligence- based screening model for diabetic retinopathy at endocrinology outpatient services: a pilot study," *Scientific Reports*, vol. 8, no. 1, pp. 1–6, 2018.

[19] H. A. Afan, A. El-shafie, W. H. M. W. Mohtar, and Z. M. Yaseen, "Past, present and prospect of an Artificial Intelligence (AI) based model for sediment transport prediction," *Journal of Hydrology*, vol. 541, pp. 902–913, 2016.

[20] D. T. Bui, Q.-T. Bui, Q.-P. Nguyen, B. Pradhan, H. Nampak, and P. T. Trinh, "A hybrid artificial intelligence approach using GIS-based neural-fuzzy inference system and particle swarm optimization for forest fire susceptibility modeling at a tropical area," *Agricultural and Forest Meteorology*, vol. 233, pp. 32–44, 2017.

[21] F. Fathian, S. Mehdizadeh, A. K. Sales, and M. J. S. Safari, "Hybrid models to improve the monthly river flow prediction: integrating artificial intelligence and non-linear time series models," *Journal of Hydrology*, vol. 575, pp. 1200–1213, 2019.

[22] X. Zhao, C. Wang, J. Su, and J. Wang, "Research and application based on the swarm intelligence algorithm and artificial intelligence for wind farm decision system," *Renewable Energy*, vol. 134, pp. 681–697, 2019.

Hindawi
Journal of Sensors
Volume 2021, Article ID 7066304, 8 pages
https://doi.org/10.1155/2021/7066304

Research Article

A Study on RB-XGBoost Algorithm-Based e-Commerce Credit Risk Assessment Model

Weimin Yang[1] **and Lili Gao**[2]

[1]*Jiangsu Vocational Institute of Commerce, Nanjing, Jiangsu 211168, China*
[2]*Southeast University, Nanjing, 211189 Jiangsu, China*

Correspondence should be addressed to Lili Gao; gaolili0919@seu.edu.cn

Received 6 August 2021; Revised 30 August 2021; Accepted 27 September 2021; Published 25 October 2021

Academic Editor: Mu Zhou

The current method's e-commerce credit risk assessment is prone to poor data balance and low evaluation accuracy. An RB-XGBoost algorithm-based e-commerce credit risk assessment model is proposed in this study. The adaptive random balance (RB) method is used to sample and process the obtained data to improve the balance degree of the data. An assessment index system is constructed based on the processed data. Based on the risk evaluation index system and the XGBoost algorithm, this paper constructed an e-commerce risk assessment model and assessed the e-commerce credit risk using this model. The experimental results show that the proposed method has good data balance, a high kappa coefficient, and a large receiver operating characteristic (ROC) curve area, which can effectively improve e-commerce credit risk assessment accuracy.

1. Introduction

At present, e-commerce has entered society, and informatization has become an inevitable trend and core content of e-commerce, which has a significant impact on the fields of culture, society, and politics [1, 2]. In network economic activities, this technology effectively improves resource allocation and enhances China's economic competitiveness. Therefore, the progress of e-commerce technology is of great significance in economic growth, industrial structure optimization, and economic operation quality and efficiency in China. However, the problem of the credit crisis will lead to great risks in the practical application of e-commerce and seriously restrict the steady development of e-commerce. Therefore, it is necessary to analyze and study the e-commerce credit risk assessment methods to avoid the risks in e-commerce transactions.

Wu et al. minimizes e-commerce credit assessment indicators by a rough set method to obtain important influencing factors of assessment in [3]. A C-XGBoost model is first established to forecast for each cluster of the resulting clusters based on a two-step clustering algorithm, incorporating sales features into the C-XGBoost model as influencing factors of forecasting in [4]. Aiming at the customer characteristics of social network e-commerce, Zhuang builds a customer value model that integrates the value of social network to help companies subdivides the customer accurately in [5]. To improve and enhance the predictive ability of consumer purchasing behaviours on e-commerce platforms, a new method of predicting purchasing behaviour on e-commerce platforms is created in [6]. In the support vector regression method, a particle swarm optimization algorithm is introduced to optimize the model parameters, and the optimized model is used to complete the assessment of e-commerce credit risk. This method has good effectiveness, but the data imbalance rate obtained by this method is high, leading to a poor data balance degree. Chang et al. determines the risk assessment indicators based on the actual transaction situation and relevant literature and constructs a two-layer hybrid model to evaluate the credit risk of e-commerce combined with the back propagation (BP) neural network and naive Bayesian algorithm [7]. This method has relatively high assessment stability but does not process the data set before assessment, resulting in the

unsatisfactory effect of the ROC curve obtained by this method and the problem of low assessment accuracy. An e-commerce credit risk assessment model based on the RB-XGBoost algorithm is proposed to solve the issues in the above methods.

2. System and Model Description

2.1. e-Commerce Credit Risk Assessment Index System

(I) Data balance processing

The e-commerce credit risk assessment model based on the RB-XGBoost algorithm is used to sample and process e-commerce risk data through the adaptive random balance RB method to reduce the imbalance of data [8–10]. The specific process is shown in Figure 1.

(II) Grey correlation analysis of data

We set that m stands for the number of e-commerce enterprises, n stands for the number of risk assessment indicators, and $x_i = \{x_{i(1)}, x_{i(2)}, \cdots, x_{i(n)}\}$ is used to describe the i th e-commerce enterprise sample, where $i = 1, 2, \cdots, m$.

An ideal sequence $x_j^0 = \{x_1^0, x_2^0, \cdots, x_n^0\}$ is established, where $x_j^1 = \max_i \{x_{ij}\}$ represents a positive index and $x_j^2 = \min_i \{x_{ij}\}$ represents a negative index.

There are differences between the dimensions corresponding to different risk assessment indices, so it is necessary to eliminate the data dimensions before data comparison [11, 12]. The negative index is replaced with the positive index and normalizes by the following formula:

$$x'_{ij} = \frac{x_{ij} - x_{\min}}{x_{\max} - x_{\min}}, \tag{1}$$

where $x_{\min}$ and $x_{\max}$, respectively, represent the minimum and maximum values of the jth risk assessment index and x_{ij} represents the corresponding value of the jth indicator in the ith e-commerce enterprise.

A correlation coefficient ξ_{ij} is set, and its calculation formula is as follows:

$$\xi_{ij} = \frac{\min_i \min_j \left|x_{ij} - x_j^1\right| + \partial \left|x_{ij} - x_j^2\right|}{\left|x_{ij} - x_j^1\right| + \partial \min_i \min_j \left|x_{ij} - x_j^2\right|}, \tag{2}$$

where ∂ represents the resolution coefficient.

The correlation degree r_j is calculated according to the correlation coefficient:

$$r_j = \frac{1}{m} \sum_{i=1}^{m} \xi_{ij}. \tag{3}$$

(III) Risk assessment index system

The risk assessment indices are sorted according to their relevance. In the assessment process, the assessment indices of $r_j > r_0$ are selected to build the risk assessment index system [13, 14], as shown in Figure 2.

2.2. e-Commerce Credit Risk Assessment Model. The establishment of the e-commerce credit risk assessment model based on the RB-XGBoost algorithm uses the XGBoost algorithm.

The basic elements for XGBoost model establishment are the tree set. The binary tree structure in the classification regression tree can reflect the actual results of the decision tree. In the decision tree structure, there are two branches of "no" and "yes," which correspond to the branches on the right and left, respectively. Each feature variable is divided by a binary tree, and the feature space is divided to obtain several leaf nodes.

A set $D = \{(x_i, y_i)\}$ is set, in which there are m variables and n samples. The prediction model is obtained based on the regression tree integration model through K functions, and $\hat{y}$ is an output:

$$\hat{y} = \sum_{k=1}^{T} f_k(x_i), f_k \in \Gamma, \tag{4}$$

where $\Gamma = \{f(x) = \omega_{q(x)}\}(q : R^m \longrightarrow T, \omega_i \in R^m)$ represents the regression tree space, ω_i represents the score corresponding to the ith leaf, T represents the number of leaf nodes in the tree structure, q stands for the tree structure, f_k stands for tree, and x_i represents the independent variable corresponding to the ith sample.

For the tree model, objective function ϑ is used for training:

$$\vartheta = \sum_i l(\hat{y}_i, y_i) + \sum_k \Omega(f_k), \tag{5}$$

where l is the convex loss function to measure the difference between the real value y_i and the predicted value $\hat{y}_i$ and Ω represents the penalty term, and its expression is as follows:

$$\Omega(f) = \gamma T + \frac{1}{2}\lambda \|\omega\|^2, \tag{6}$$

where $(1/2)\lambda\|\omega\|^2$ describes the regular term and γ represents leaf node penalty, which is mainly used to avoid overfitting problems.

In the process of e-commerce credit risk assessment, European space cannot be directly used to optimize the objective function [15, 16]. Therefore, the RB-XGBoost algorithm-based e-commerce credit risk assessment model trained the model through boosting learning strategy. The specific process is as follows:

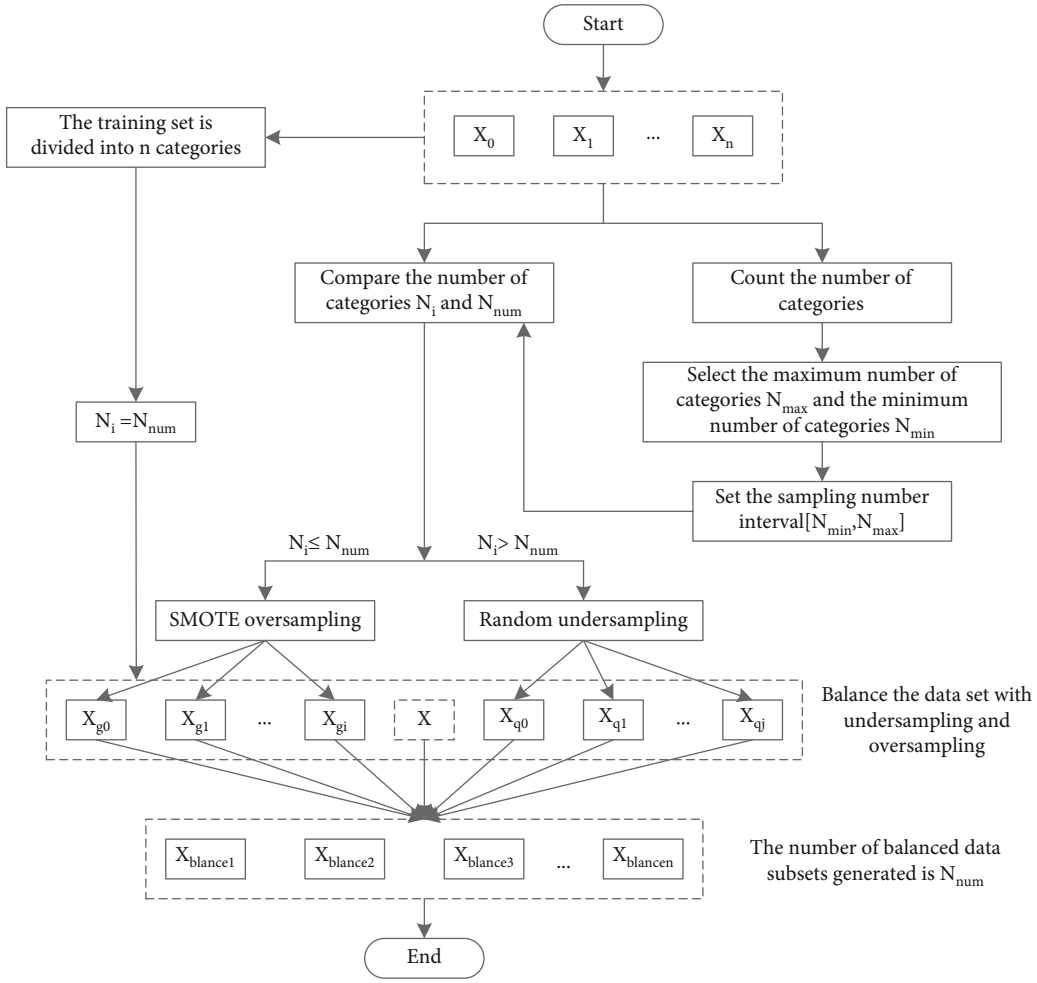

Figure 1: Data balance sampling processing flow.

$$\begin{cases} \widehat{y}_i^{(0)} = 0, \\ \widehat{y}_i^{(1)} = f_1(x_i) = \widehat{y}_i^{(0)} + f_1(x_i), \\ \widehat{y}_i^{(2)} = f_1(x_i) + f_2(x_i) = \widehat{y}_i^{(1)} + f_2(x_i), \\ \vdots \\ \widehat{y}_i^{(t)} = \sum_{k=1}^{t} f_k(x_i) = \widehat{y}_i^{(t-1)} + f_t(x_i), \end{cases} \tag{7}$$

where $\widehat{y}_i^{(t)}$ represents the output corresponding to the accumulation model in the tth round of training and $f_t(x_i)$ represents the function newly added to the tth round training.

According to the above process, the objective function is transformed into the following formula:

$$\vartheta = \sum_{i=1}^{n} l\left(y_i, \widehat{y}_i^{(t-1)} + f_t(x_i)\right) + \Omega(f_t) + \text{constant}, \tag{8}$$

where constant is a constant term.

The fitting results of the model and training data in the assessment process can be measured by the loss function $L = \sum_{i=1}^{n} l(\widehat{y}_i, y_i)$, in which the logical loss function $l(\widehat{y}_i, y_i) = y_i \ln\left(1 + e^{-y\wedge_i}\right)$ and the square loss function $l(\widehat{y}_i, y_i) = (y_i - y\wedge_i)^2$ are widely used in the assessment process [17, 18]. The RB-XGBoot algorithm-based e-commerce credit risk assessment model brings the square loss function into the target function to obtain the following formula:

$$\begin{aligned} \vartheta &= \sum_{i=1}^{n} l\left(y_i, \left(y\wedge_i^{(t-1)} + f_t(x_i)\right)\right)^2 + \Omega(f_t) + \text{constant} \\ &= \sum_{i=1}^{n} \left[2\left(\widehat{y}_i^{(t-1)} - y_i\right) f_t(x_i) + f_t(x_i)^2\right] + \Omega(f_t) + \text{constant}, \end{aligned} \tag{9}$$

where $\widehat{y}_i^{(t-1)} - y_i$ represents the residual.

The loss function can be approximated by the Taylor expansion to obtain the following formula:

$$f(x + \Delta x) \approx f(x) + f'(x)\Delta x + \frac{1}{2} f''(x)(\Delta x)^2. \tag{10}$$

$g_i = \partial_{\widehat{y}_i^{(t-1)}} l(y_i, y\wedge^{(t-1)})$ and $h_i = \partial^2_{\widehat{y}_i^{(t-1)}} l(y_i, y\wedge^{(t-1)})$ are set; then, we obtain the following formula:

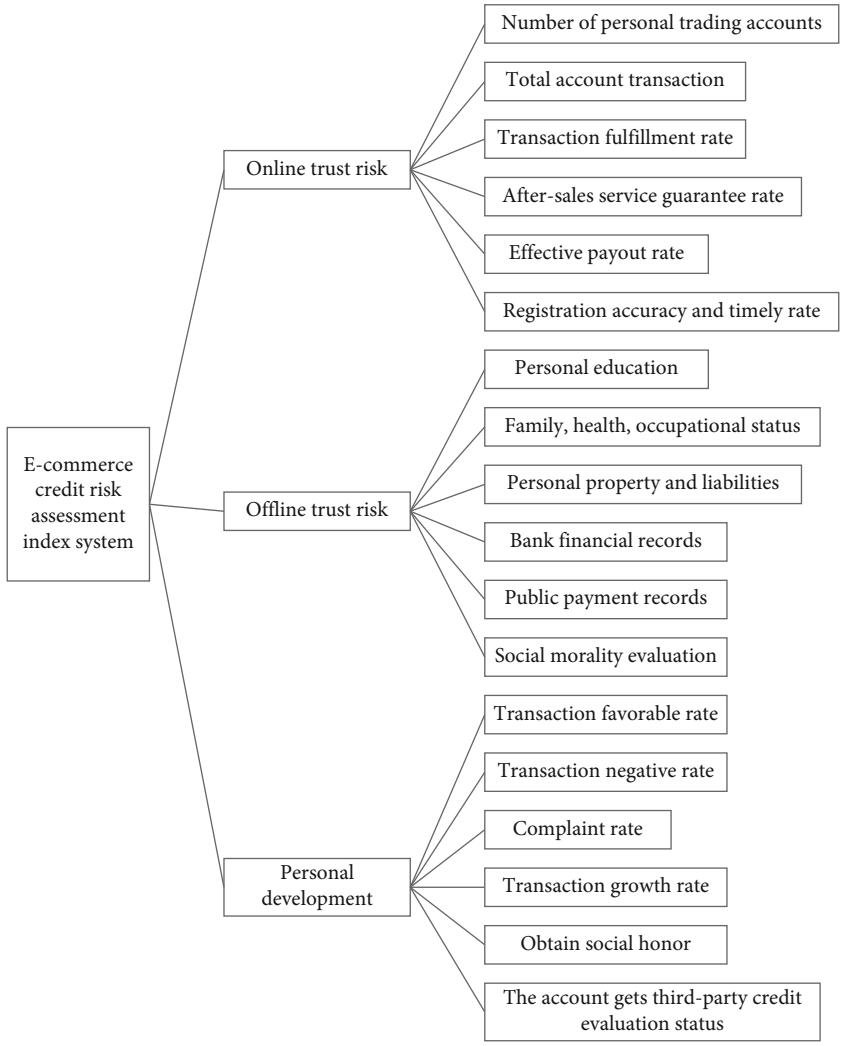

Figure 2: E-commerce credit risk assessment index system.

$$l\left(y_i, y\wedge^{(t-1)} + f_t(x_i)\right) \approx l\left(y_i, y\wedge^{(t-1)}\right) + g_i f_t(x_i) + \frac{1}{2} h_i f_t^2(x_i). \tag{11}$$

The objective function is substituted into the above loss function to obtain

$$\vartheta = \sum_{i=1}^{n} \left[l\left(y_i, y\wedge^{(t-1)}\right) + g_i f_t(x_i) + \frac{1}{2} h_i f_t^2(x_i) \right] + \Omega(f_t) + \text{constant}. \tag{12}$$

When the loss function belongs to square loss in the training process, there is the following formula:

$$\begin{cases} g_i = \partial_{\widehat{y}_i^{(t-1)}} l\left(y_i, y\wedge^{(t-1)}\right) = 2\left(\widehat{y}_i^{(t-1)} - y_i\right), \\ h_i = \partial^2_{y\wedge^{(t-1)}} l\left(y_i, y\wedge^{(t-1)}\right) = \partial^2_{y\wedge^{(t-1)}} \left(y\wedge^{(t-1)} - y_i\right)^2 = 2. \end{cases} \tag{13}$$

The parameters g_i and h_i are substituted into the objective function to obtain the following formula:

$$\vartheta = \sum_{i=1}^{n} \left[y_i - \left(y\wedge_i^{(t-1)} + f_t(x_i) \right) \right]^2 + \Omega(f) + \text{constant}, \tag{14}$$

where $\widehat{y}_i^{(t-1)}$ describes the output result of the model during the $t-1$th round training and y_i describes the dependent variable existing in the objective function. If the dependent variable y_i is known, the above objective function can be simplified to obtain the following formula:

$$\vartheta = \sum_{i=1}^{n} \left[g_i f_t(x_i) + \frac{1}{2} h_i f_t^2(x_i) \right] + \Omega(f) + \text{constant}. \tag{15}$$

In the formula, g_i and h_i are the parameters existing in the loss function. The values of the above parameters are different in different loss functions, so the values of parameters g_i and h_i can be determined in the form of the loss function.

Each tree is redefined by the following formula:

$$f_t(x) = \omega_{q(x)}, \omega \in R^T, q : R^d = \{1, 2, \cdots, T\}, \tag{16}$$

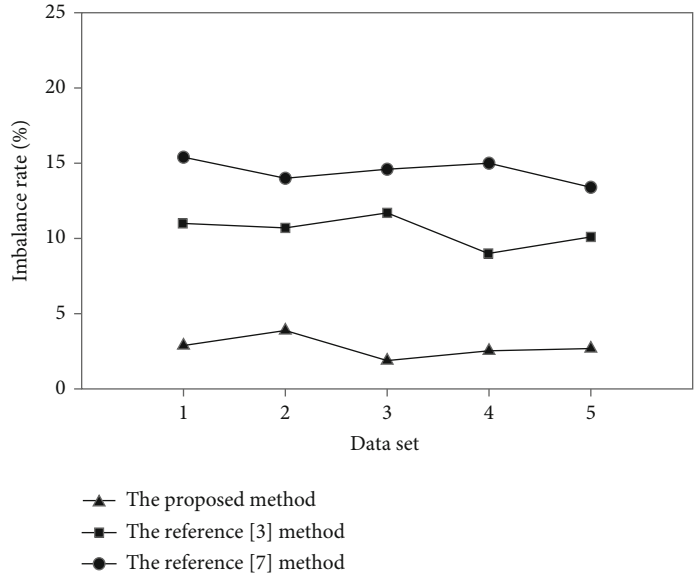

Figure 3: Imbalance rate of different methods.

where ω describes the weight corresponding to the leaf node in the tree structure, $\omega_{q(x)}$ describes the predicted value obtained by the tree model, and $q : R^d = \{1, 2, \cdots, T\}$ represents the structure of the tree.

Model complexity includes L2 regularization of leaf node score and the total number of leaf nodes T [19, 20]. Model complexity $\Omega(f_t)$ can be obtained through tree definition:

$$\Omega(f_t) = \gamma T + \frac{1}{2}\lambda \sum_{J=1}^{T} \omega_j^2. \tag{17}$$

The smoothness of leaf nodes can be improved by L2 regularization to solve the overfitting problem [21, 22]. In the objective function, when the complexity of the model increases, there are two different types of accumulation, one of which is $I_j = \{i|q(x_i) = j\}$, where I_j represents the set of samples in the leaf node j. After adding complexity to the objective function, the final objective function is obtained, that is, the e-commerce credit risk assessment model [23, 24]:

$$\begin{aligned} \mu &= \sum_{i=1}^{n} \left[g_i f_t(x_i) + \frac{1}{2} h_i f_t^2(x_i) \right] + \gamma T + \frac{1}{2}\lambda \sum_{J=1}^{T} \omega_j^2 \\ &= \sum_{j=1}^{T} \left[\left(\sum_{i \in I_j} g_i \right) \omega_j + \frac{1}{2} \left(\sum_{i \in I_j} h_i + \lambda \right) \omega_j^2 \right] + \gamma T. \end{aligned} \tag{18}$$

Based on the selected risk assessment indices, the risk assessment is performed using the e-commerce credit risk assessment model.

3. Experiments and Results

To verify the effectiveness of the RB-XGBoot algorithm-based e-commerce credit risk assessment model, it is necessary to carry out a test. The proposed method, literature [3] method, and literature [4] method are used for comparative experiments. The imbalance rate τ is used as the experimental index to test the data balance degree of different methods. The calculation formula of imbalance rate τ is as follows:

$$\tau = \frac{N_{\max}}{N_{\min}}, \tag{19}$$

where $N_{\max}$ and $N_{\min}$ represent the maximum and minimum values of the sample data in the set. The larger the imbalance rate τ, the more unbalanced the data. The imbalance rate τ of the proposed method, the reference [3] method, and the reference [7] method are shown in Figure 3.

Based on the data in Figure 3, the data imbalance rate obtained by the proposed method is less than 5% when testing different data sets, while the imbalance rate obtained by the methods of literature [3] and literature [7] fluctuates around 10% and 15%, respectively. It can be seen that the imbalance rate obtained by the proposed method is low, indicating that the data obtained by the proposed method is well balanced. This is due to the data sampling and processing by the adaptive random balance RB method before constructing the e-commerce credit risk assessment model, which ensures the balance of the data.

The assessment accuracy of the proposed method, literature [3] method, and literature [7] method is verified by the kappa coefficient and ROC curve. The kappa coefficient can weigh the difference between the assessment results and the real results. The calculation formula of kappa coefficient K is as follows:

$$K = \frac{p_o - p_e}{1 - p_e}, \tag{20}$$

where p_o represents the proportion of correctly evaluated samples in the total number of samples and p_e represents

Table 1: Kappa coefficients for different methods.

Number of iterations (time)	Kappa coefficient		
	The proposed method	The reference [3] method	The reference [7] method
100 s	0.951	0.745	0.695
200 s	0.964	0.715	0.648
300 s	0.978	0.764	0.668
400 s	0.971	0.770	0.678
500 s	0.983	0.721	0.814

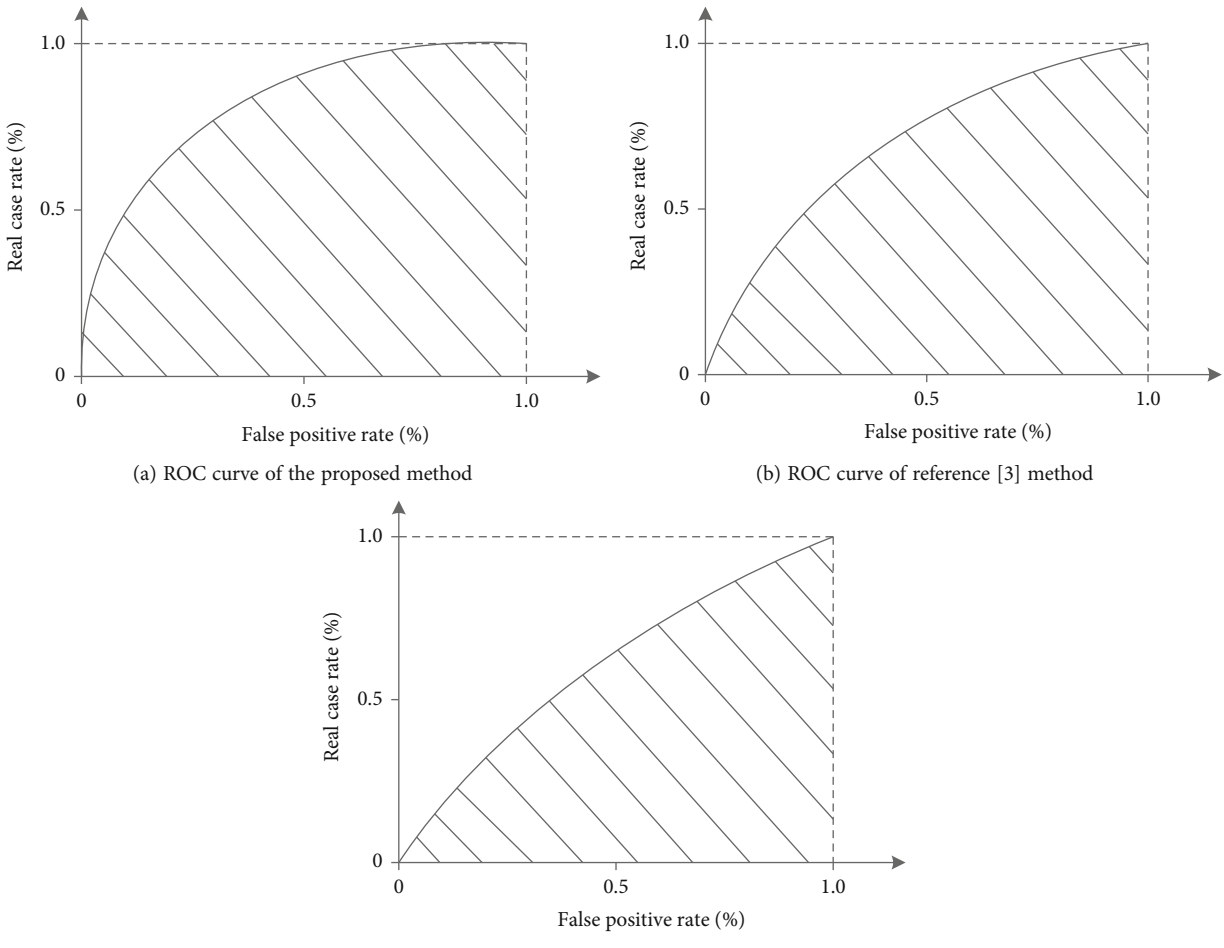

(a) ROC curve of the proposed method

(b) ROC curve of reference [3] method

(c) ROC curve of reference [7] method

Figure 4: ROC curves of different methods.

the randomness ratio. The higher the kappa coefficient K, the more accurate the evaluation results of the method are. The kappa coefficients of the proposed method, the literature [3] method, and the literature [7] method are shown in Table 1.

From the data in Table 1, we can see that the kappa coefficients of the proposed method in multiple iterations are higher than those obtained by the methods in literature [3] and literature [7], indicating that the proposed method can accurately complete the assessment of e-commerce credit risk. This is because this method constructs a risk assessment index system based on the data with a high balance and completes the assessment of the e-commerce credit risk based on the high-precision risk assessment indices.

The abscissa is the true positive rate in the ROC curve, and the ordinate is the false positive case rate. The larger the area enclosed by the ROC curve and the abscissa, the higher the accuracy of the assessment results of the method. The proposed method, literature [3] method, and literature [7] method are, respectively, used to evaluate the credit risk of different e-commerce enterprises, and the obtained ROC curves are shown in Figure 4.

By analyzing Figure 4, it can be seen that the area enclosed by the ROC curve of the proposed method and

abscissa is larger than that enclosed by the ROC curve of the methods of literature [3] or literature [7] and abscissa, indicating that the proposed method has higher assessment results accuracy and can complete credit risk assessment accurately in e-commerce enterprises.

4. Conclusion

Aiming at the problems of high data imbalance rate and low accuracy of assessment results in the current e-commerce credit risk evaluation methods, an e-commerce credit risk evaluation model based on the RB-XGBoost algorithm is proposed. The risk assessment index system is first constructed by using the data with a high balance rate, and then, the risk assessment model is established by the XGBoost algorithm. This model realizes the assessment of e-commerce credit risk, solves the problems existing in the current methods, ensures the degree of data balance, and improves the accuracy of risk assessment. Future work includes improving the risk assessment model and further enhances the accuracy of risk assessment.

Data Availability

The labeled dataset used to support the findings of this study is available from the corresponding author upon request.

Conflicts of Interest

The authors declare no competing interests.

Acknowledgments

This study is sponsored by Qing Lan Project.

References

[1] Y. Liu, Y. Tian, Y. Xu et al., "TPGN: a time-preference gate network for e-commerce purchase intention recognition," *Knowledge-Based Systems*, vol. 220, no. 2, p. 106920, 2021.

[2] A. Vera-Baquero, O. Phelan, P. Slowinski, and J. Hannon, "Open source software as the Main driver for evolving software systems toward a distributed and performant E-commerce platform: a Zalando fashion store case study," *IT Professional*, vol. 23, no. 1, pp. 34–41, 2021.

[3] J. Wu, "E-commerce credit risk assessment based on rough set and support vector regression," *Statistics and Decision*, vol. 35, no. 23, pp. 51–54, 2019.

[4] S. Ji, X. Wang, W. Zhao, and D. Guo, "An application of a three-stage XGBoost-based model to sales forecasting of a cross-border E-commerce enterprise," *Mathematical Problems in Engineering*, vol. 2019, 15 pages, 2019.

[5] Y. Zhuang, "Research on E-commerce customer churn prediction based on improved value model and XG-boost algorithm," *Management Science and Engineering*, vol. 12, no. 3, pp. 51–56, 2018.

[6] P. Song, "An XGBoost algorithm for predicting purchasing behaviour on E-commerce platforms," *Technical Gazette*, vol. 27, no. 5, pp. 1467–1471, 2020.

[7] Z. Chaohui, L. Jiajia, and R. Hui, "Research on E-commerce credit evaluation method based on Bayesian and neural network hybrid algorithm," *Information Science*, vol. 38, no. 2, pp. 81–87, 2020.

[8] W. Wei, B. Zhou, D. Polap, and M. Wozniak, "A regional adaptive variational PDE model for computed tomography image reconstruction," *Pattern Recognition*, vol. 92, pp. 64–81, 2019.

[9] Y. Zhang, S. Qiao, R. Lu, N. Han, D. Liu, and J. Zhou, "How to balance the bioinformatics data: pseudo-negative sampling," *BMC Bioinformatics*, vol. 20, no. 25, pp. 695–695, 2019.

[10] D. Zachariah and P. Stoica, "Effect inference from two-group data with sampling bias," *IEEE Signal Processing Letters*, vol. 26, no. 8, pp. 1103–1106, 2019.

[11] U. P. Shukla and S. J. Nanda, "Designing of a risk assessment model for issuing credit card using parallel social spider algorithm," *Applied Artificial Intelligence*, vol. 33, no. 1-4, pp. 191–207, 2019.

[12] F. Assef, M. T. Steiner, P. J. Steiner Neto, and D. G. . B. Franco, "Classification algorithms in financial application: credit risk analysis on legal entities," *IEEE Latin America Transactions*, vol. 17, no. 10, pp. 1733–1740, 2019.

[13] F. Li, L. Chen, W. Chen et al., "Antibiotics in coastal water and sediments of the East China Sea: distribution, ecological risk assessment and indicators screening," *Marine pollution bulletin*, vol. 151, pp. 110810–110810. 11, 2020.

[14] W. Wang, X. Liu, J. Qin et al., "An extended generalized TODIM for risk evaluation and prioritization of failure modes considering risk indicators interaction," *IIE Transactions*, vol. 51, no. 11, pp. 1236–1250, 2019.

[15] B. Song, W. Yan, and T. Zhang, "Cross-border e-commerce commodity risk assessment using text mining and fuzzy rule-based reasoning," *Advanced Engineering Informatics*, vol. 40, pp. 69–80, 2019.

[16] J. Lv, T. Wang, H. Wang, J. Yu, and Y. Wang, "A SECPG model for purchase behavior analysis in social e-commerce environment," *International Journal of Communication Systems*, vol. 33, no. 6, article e4149, 2020.

[17] S. Savoldelli, C. Cattò, F. Villa et al., "Biological risk assessment in the History and Historical Documentation Library of the University of Milan," *Science of The Total Environment*, vol. 790, no. 5, p. 148204, 2021.

[18] W. Wei, X. Fan, H. Song, X. Fan, and J. Yang, "Imperfect information dynamic stackelberg game based resource allocation using hidden Markov for cloud computing," *IEEE Transactions on Services Computing*, vol. 11, no. 1, pp. 78–89, 2016.

[19] V. Srikrishnan and K. Keller, "Small increases in agent-based model complexity can result in large increases in required calibration data," *Environmental Modelling and Software*, vol. 138, no. 5, p. 104978, 2021.

[20] F. Kong, "Development of metric method and framework model of integrated complexity evaluations of production process for ergonomics workstations," *International Journal of Production Research*, vol. 57, no. 7-8, pp. 2429–2445, 2019.

[21] F. Zheng, S. Derrode, and W. Pieczynski, "Parameter estimation in switching Markov systems and unsupervised smoothing," *IEEE Transactions on Automatic Control*, vol. 64, no. 4, pp. 1761–1767, 2019.

[22] M. Pitek, A. Lisowski, and M. Dbrowska, "The effects of solid lignin on the anaerobic digestion of microcrystalline cellulose and application of smoothing splines for extended data analysis of its inhibitory effects," *Bioresource Technology*, vol. 320, p. 124262, 2021.

[23] M. Soui, I. Gasmi, S. Smiti, and K. Ghédira, "Rule-based credit risk assessment model using multi-objective evolutionary algorithms," *Expert Systems with Applications*, vol. 126, pp. 144–157, 2019.

[24] E. Brons-Piche, G. J. Eckert, and M. Fontana, "Predictive validity of a caries risk assessment model at a dental school," *Journal of Dental Education*, vol. 83, no. 2, pp. 144–150, 2019.

Hindawi
Journal of Sensors
Volume 2021, Article ID 2258625, 10 pages
https://doi.org/10.1155/2021/2258625

Research Article

Singing and Nervous System Regulation Based on Wireless Sensor Network Perception

Feng Yu

School of Music, Guizhou Normal University, Guiyang 550001, China

Correspondence should be addressed to Feng Yu; 460023011@gznu.edu.cn

Received 12 August 2021; Revised 15 September 2021; Accepted 7 October 2021; Published 25 October 2021

Academic Editor: Mu Zhou

In order to build an intelligent platform that can be applied to singing and nervous system adjustment, this paper optimizes the positioning and information processing algorithms for wireless sensor network perception. Moreover, this article combines binocular vision to realize the singer's real-time positioning, combines the singer's emotion recognition with the intelligent sensor system, and combines the emotion recognition with the adjustment of the nervous system, so that the singer can better control the intelligent platform. In addition, in order to solve the problem of multisensor information fusion, this paper improves the sensor fusion algorithm to make it suitable for the information fusion of vision sensors and information sensors. Finally, this paper designs the functional structure of the system, transmits data through wireless sensor networks, simulates human emotion models, and studies the process of singing and the adjustment of the nervous system. It can be seen from the experimental research results that the method proposed in this paper has a certain effect.

1. Introduction

The process of singing is not only a vocal process, but also an emotional transmission process, and people's emotions are mainly controlled by the nervous system. Therefore, in order to improve the effect of singing, it is necessary to improve the regulation of singing and nervous system while singing, so as to improve the effective regulation and control between singing and emotion [1].

In vocal music learning and singing, only by correctly playing the musical instrument "voice" can singers make a correct sound. However, due to the special attribute of voice, singers cannot intuitively operate the "voice" instrument. They can only experience their own singing movement state through various internal feelings and adjust their singing behavior activities in time, so as to make a good and high-quality voice [2]. This makes singing complex and difficult to control. When a singer sings, on the one hand, the brain and nervous system direct the coordinated movement of the singer's physiological organs; on the other hand, they also dispatch internal psychological activities to make a correct response, so as to interact with the singer's physiological body and jointly assist the voice. Singing behavior activity is the combination of singer's body physiology and psychology. This process not only makes each organ of singing physiology in a positive movement state, but also correctly guides singer's psychology, which makes singer's body physiology in an effective movement and cooperates with singing psychology to carry out artistic practice. It can be seen that in vocal music learning and singing, only by effectively grasping the combination of singer's body physiology and psychology can we effectively carry out vocal music artistic activities. Furthermore, we can reproduce the connotation and artistic plot of vocal music works and send out the voice that moves the audience to make the internal psychology of the audience consistent with the emotional expression of the song, so as to infect the audience and make them affirm the singer's artistic behavior [3].

The singer's body physiology is not only the basis of singing, but also the basis of the emergence and development of singing psychological activities. In the study and singing of vocal music, the comprehensive training of singer's physiological function is also the basis of singer's vocal music practice. The training of singers' physiological

skills is the basis of singing. In the early stage of vocal music learning, because the physiological organs of singing body have not been systematically and scientifically trained, there will be some problems in singing, such as broken sound, hoarseness, tension of laryngeal muscle tissue, shallow breath, and inability to reasonably open and apply the resonance chamber. These problems are the result that the singer's psychology cannot reasonably regulate the coordinated movement of the body's physiological organs and muscle tissues without training.

Based on the above analysis, this paper applies wireless sensor network to the regulation of singing and nervous system, transmits data through wireless sensor network, and simulates human emotion model, so as to study the regulation process of singing and nervous system.

2. Related Work

The purpose of WSN is to perceive, collect, and transmit data information related to monitoring objects in the monitoring area, process the information, and finally provide the processed data to users [4]. A typical WSN network system consists of sensor node, sink node, transportation network, and monitoring center. A large number of sensor nodes are randomly deployed in or near the monitoring area, which can form a network through self-organization. The data monitored by the sensor node is transmitted through the transmission network. In the transmission process, the data information may be processed by multiple nodes and routed to the sink node after multiple hops [5].

Data aggregation is an important research problem in wireless sensor networks [6]. For the study of data aggregation, either the algorithm based on energy balance consideration or the algorithm in the case of multiple base stations or the algorithm in the case of single base station or the real-time algorithm in the routing layer, literature [7] proves that the data aggregation problem of reducing delay is NP difficult. They also designed an algorithm for data aggregation with an approximate coefficient of Δ-1 (Δ is the degree of the largest node). Literature [8] studies the optimal forwarding moment problem as a policy node for the decision process model to determine the optimal decision of the sensor. In [9], an algorithm is designed which has a delayed binding $O(\log(N))$. It is believed that each node can learn the nearest neighbors and has a special collision detection function, although this situation cannot always guarantee that the network is normal. The data aggregation model studied in literature [10] is based on a tree structure. Literature [11] proposed a scheduling algorithm based on the maximum independent set, which has a delayed binding of $23R + \Delta - 18$. They focused their main energy on a special scene.

Literature [12] proposed the Ken algorithm, which uses two dynamic probability models; one runs on the sink node (sink node), and the other runs on each node in the network, passing these two models under the premise of a small loss of precision, a model to reduce the amount of data transmission as much as possible. Literature [13] proposed the ALVQ algorithm, which uses historical data to construct a cipher to explore the inherent characteristics of the data and then uses this cipher to piecewise linearly compress other data to reduce the amount of data transmission. Literature [14] proposed a piecewise linear approximation algorithm, which uses a straight line to approximate the current but uncompressed data point under the condition of a given error limit, until a new data point makes this limit be broken. Then similarly, starting from this new data point, use a new straight line to approximate the subsequent arrival point. Literature [15] proposed the EAQ algorithm, which first converts the original time series into a special time series description MVA (multiversion array). Using this MVA prefix, an approximate version of the original time series with a certain error can be recovered. As the prefix increases, the error gradually decreases. The time series approximation with variable error is realized. In addition, researchers have also proposed algorithms for data compression using Discrete Fourier Transform [16], Discrete Cosine Transform [17], and Discrete Wavelet Transform [18], which are all based on time series time correlation algorithms. But its computational complexity is high, so it is not suitable for WSN.

3. General Framework for Multisensor Fusion Positioning of Singing Voice Based on Graph Optimization

Graph optimization is a method for processing optimization problems. The variables and constraint equations between variables that are specifically solved in the optimization problem are expressed as nodes and edges in an undirected graph, and the variables to be optimized are calculated iteratively through methods such as gradient descent. The positioning algorithm framework proposed in this section uses the idea of graph optimization to convert the amount of motion and sensor observations on a certain segment of the singer's trajectory into constraints and variables in the graph optimization and iteratively calculate the optimal singer's pose.

The singer's motion model and viewing model are usually modeled as nonlinear equations with Gaussian noise [19]:

$$\begin{aligned} x_l &= g_l(x_{l-1}, \mathrm{u}_l) + w_l, w_l \sim N\left(0, \Delta_{w_l}^{-1}\right), \\ z_l &= h_i(x_l) + v_l, v_l \sim N\left(0, \Delta_{v_l}^{-1}\right). \end{aligned} \tag{1}$$

x_l is the system state vector to be calculated at the main time, z_l is the observation vector of the sensor at time i, and z_l is the system motion equation that maps the system state vector from time i to time $i+1$. u_l is the system control variable input at time i, and h_l is the system observation equation that maps the state of the system to the observation space at time i. w_l and v_l are the motion noise and observation noise of the system, which are Gaussian white noise with variances $\Delta_{w_l}^{-1}$ and $\Delta_{w_l}^{-1}$, respectively, and Δ_{w_l} and Δ_{w_l} are the signal matrix of motion noise and the information matrix of observation noise, respectively. This state vector can be calculated by solving the following least squares optimization problem:

$$
\begin{aligned}
x^* &= \min_x \sum_l \left(\left\| x_l - g_l(x_{l-1}, u_l) \right\|^2_{\Delta_{w_l}} + \left\| z_i - h_i(x) \right\|^2_{\Delta_{w_l}} \right) \\
&= \min_x \sum_l \left(\left\| r_{g_l}(x) \right\|^2_{\Delta_{w_l}} + \left\| r_{h_l}(x) \right\|^2_{\Delta_{w_l}} \right) \\
&= \min_x \sum_l \left\| r_l(x) \right\|^2_{\Delta_{w_l}}.
\end{aligned} \tag{2}
$$

r_{g_l} and r_{h_l} are the residual expressions of the motion equation and the observation equation, respectively, which can usually be approximated by the Gauss-Newton method. Since it is a nonlinear equation and needs to be linearized by Taylor expansion, the expression of the update amount for each iteration should be

$$
\delta x = \min_{\delta x} \sum_l \left\| r_l(\hat{x} \boxplus \delta x) \right\|^2_{\Delta_{w_l}} \sim \min_{\delta x} \sum_l \left\| r_l(\hat{x}) + J_1 \delta x \right\|^2_{\Delta_{w_l}}. \tag{3}
$$

Among them, $J_l \coloneqq \partial r_l(\hat{x} \boxplus \delta x) / \partial \delta x |_{\delta x = 0}$ is the covariance matrix of the error state. $\boxplus$ is the lie algebra operators. By expanding the above formula, the expression of δx is obtained [20].

$$
\delta x = -\left(J^T \wedge J \right)^{-1} J^T \wedge r. \tag{4}
$$

By superimposing this amount of change on the state amount at the previous moment, the updated state amount at the next moment can be obtained.

$$
x = \hat{x} \boxplus \delta x. \tag{5}
$$

In the positioning problem, the state equation of the above optimization problem may include pose, geosphere point, and parameters. The pose is usually represented by SE3 manifold, and the map point is represented by its Euclidean coordinates. The motion model is related to the singer's motion sensor, and the observation model is related to the singer's sensory sensor. The motion model is to constrain the states of two singers at different times, and the observation model is to constrain the states of the singers and the map points. Therefore, the above optimization model can be expressed as an undirected graph shown in Figure 1.

The general positioning framework is used to describe specific positioning problems, which will greatly help the subsequent system observability analysis and system matrix decomposition. The reason is that the undirected graph here is often similar to the sparse matrix of the system in terms of spatial structure, which facilitates the analysis of the system. At the same time, graph representation is also helpful to the realization of algorithms, because many algorithms in the computer field are implemented based on graph representation.

Aiming at the binocular camera and IMU, combined with the feature-based visual positioning algorithm, a visual positioning system based on binocular-IMU fusion is designed and implemented. The visual mileage estimation is performed by extracting feature points from the binocular image, combined with IMU preintegration. Carry out tight coupling optimization to achieve high-precision and high-stability visual positioning. This method uses the high frequency and high dynamics of the IMU to improve the accuracy and robustness of the feature-based visual positioning algorithm and to ensure the computational efficiency. Experiments show that even in high-speed motion and undertextured scenes, the method can still estimate the singer's motion stably and accurately.

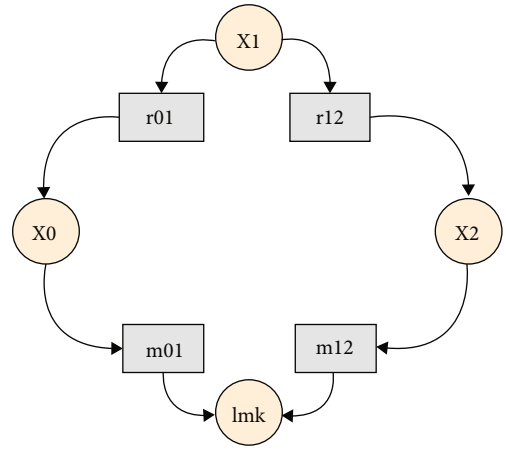

Figure 1: Schematic diagram of the general framework of multisensor fusion positioning.

The structural block diagram of the system is shown as in Figure 2. First, the visual inertial registration algorithm is introduced, and then, the IMU preintegration and binocular visual information are tightly coupled and optimized using the fusion algorithm framework based on graph optimization. Finally, the performance of the algorithm is verified through experiments.

With IMU preintegration, the relative constraints between poses can be obtained for a certain period of time. However, the IMU preintegration is calculated in the IMU local coordinate system and needs to be fused with the result of the calculation in the visual coordinate system. In the visual positioning algorithm, the world coordinate system usually selects the first frame camera coordinate system, and the acceleration of gravity measured by the IMU is in the IMU coordinate system. For the multisensor fusion algorithm, only one coordinate system can be selected as the navigation coordinate system. In this paper, the camera coordinate system is selected as the navigation coordinate system, and the world coordinate system is the camera coordinate system of the first frame. Under this assumption, within a period of time from the beginning of the binocular vision and IMU fusion positioning algorithm proposed in this paper, it is necessary to initialize the visual positioning algorithm to obtain the camera trajectory and the constructed environment map during this period, and corresponding. The IMU preintegration is calculated between adjacent key frames to realign the gravity in the IMU coordinate system to the visual coordinate system. This process is called visual inertial registration.

Unlike a monocular camera, a binocular camera can obtain the left and right images at the same time every time

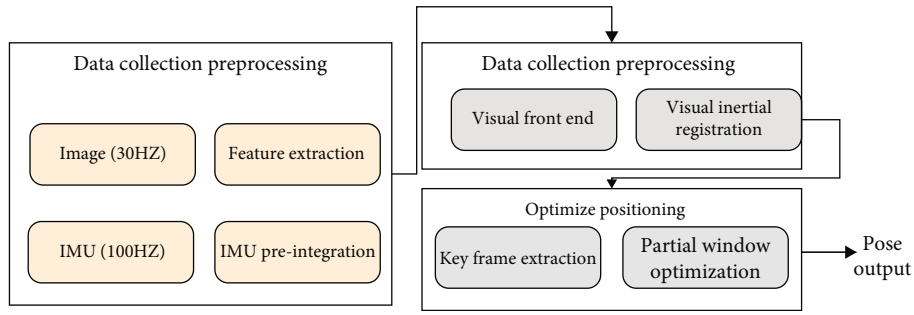

Figure 2: IMU binocular vision fusion algorithm frame.

it samples and can directly restore the feature point depth through the binocular matching algorithm. After the first frame of the binocular image is acquired, the initial visual feature map can be constructed through binocular matching, and through this map and the subsequent binocular images, the PnP algorithm is performed to calculate the pose tracking result. The specific steps are shown in Figure 3.

3.1. Feature Extraction. On binocular images, ORB feature points are extracted to ensure that 1000-1500 feature points can be extracted from each image. In order to make the extracted feature points evenly distributed on the image, this paper divides the image into grids of the same size. The number of feature points extracted in each grid is roughly the same to ensure that enough feature points can be extracted in each image area.

3.2. Three-Dimensional Reconstruction. The binocular vision method can reconstruct the visual feature map from the left and right camera images at the same time. The most commonly used is the module matching algorithm, referred to as the BM algorithm. The binocular image needs to be preprocessed by the binocular alignment algorithm. After this step, the same pixel blocks in the left and right images are the same in height. Then, when performing the BM algorithm, searching for a pixel in the left image to the corresponding pixel block in the right image can simply search on a pixel of the same height, which greatly improves the search efficiency. However, because the binocular alignment algorithm cannot perfectly align the left and right images, when searching, we can not only search for a certain pixel in the right image, but should also search for a certain pixel and its surrounding area to improve the accuracy of the search. After the correct matching point pair is obtained by the BM algorithm, the depth recovery of the feature points can be carried out through the binocular stereo. A schematic diagram of binocular depth recovery is shown in Figure 4. The calculated depth is the Z-direction coordinate of point X, which can be solved by solving the triangle constructed in the figure.

3.3. Pose Solution. Through binocular depth recovery, a feature point map can be reconstructed. Some points in this map can be observed by the current image and associated through feature matching. The method of calculating the pose of the current image through the association between the map points in the three-dimensional space and the pixels on the image is called the PnP algorithm (Perspective n Point). As shown in Figure 5, the map point obtained by binocular recovery at time $k-1$ is a small blue circle in the figure. Some of these map points are observed by the image at time k, that is, the map points connected to the image at time k with a purple line. These map points are projected back to the image at time k and are associated with the feature points in the image through feature matching. In order to calculate T_k^{k-1}, we set the projection matrix at time k to P_k [21].

$$P_k = K \begin{bmatrix} R_k^{k-1} & p_k^{k-1} \\ 0 & 1 \end{bmatrix}. \tag{6}$$

K is the camera internal parameter matrix. The coordinates of a certain map point in space in the $k-1$ camera coordinate system are denoted as X; then, the pixel coordinates x of X in the camera at time k can be calculated by P_k as follows:

$$x = P_k X. \tag{7}$$

The corresponding T_k^{k-1} can be solved by solving the above projection equation. There are a total of 6 degrees of freedom for T_k^{k-1}, and each projection point can provide two linear equations, that is to say theoretically, there are 3 projection point pairs to calculate the relative motion T_k^{k-1}. However, due to factors such as mismatches in the matching process of map points and feature points, we cannot correctly calculate the accurate relative motion T_k^{k-1} by selecting only three projection point pairs in practice, but a large amount of sampling is required. Therefore, this paper uses an optimized method to calculate a result that is closest to the true value.

In addition to the above three modules, key frames are also selected in the visual front end. This paper proposes the following two criteria for selecting key frames. The first is to calculate the average disparity between the current frame and the previous frame. If the average disparity exceeds a certain threshold, it is considered that the current frame should be selected as a key frame. The disparity is obtained by calculating the coordinate pixel difference between the matching feature points of the current frame

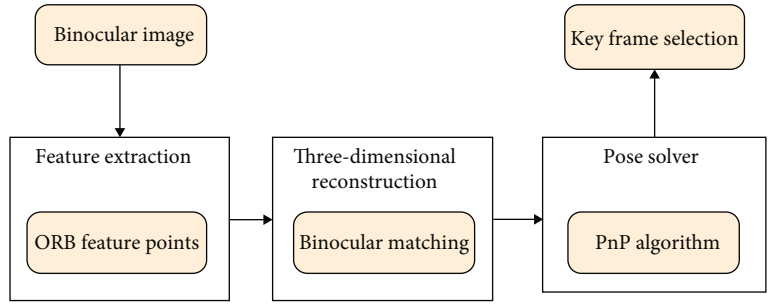

Figure 3: Flow chart of binocular vision front end.

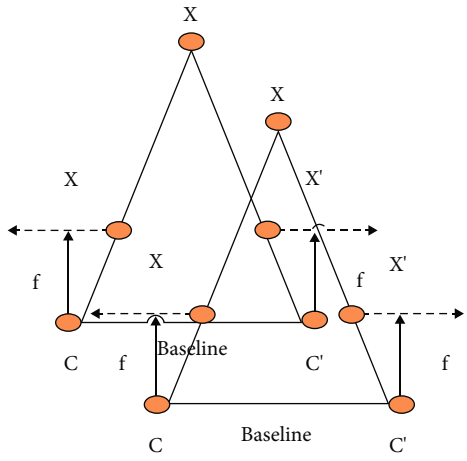

Figure 4: Schematic diagram of binocular depth recovery.

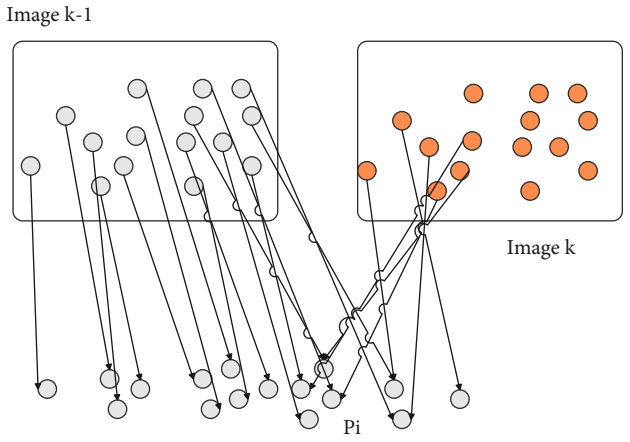

Figure 5: Schematic diagram of PnP algorithm.

and the previous frame. It is worth noting that not only translation will produce parallax, but also rotation. However, it is difficult to reconstruct visual features under pure rotation. In order to avoid this situation, this paper integrates the gyroscope signal in a short period of time and separates it during the calculation of the parallax, so as to ignore the influence of rotation on the visual reconstruction. The second is to consider the quality of pose tracking. If the number of points obtained by matching the current frame with the previous frame is less than a certain threshold, the current frame will be selected as a key frame. This criterion can greatly reduce the probability of pose tracking failure.

The relative pose between the key frames is obtained through IMU preintegration, and the relative pose of the key frames is obtained through the visual front end. Because the coordinate systems are different, the registration needs to be performed in a loose coupling manner, which is mainly to convert the gravity in the IMU coordinate system to the visual coordinate system. Figure 6 is a schematic diagram of a visual inertial registration.

Through the visual front end and IMU preintegration, it is possible to independently calculate the movement trajectory of the camera and the movement of the IMU coordinate system within a period of time. Since the rotation obtained by the preintegration of the gyroscope has nothing to do with gravity, we can first preintegrate the gyroscope to obtain a measurement with offset and compare it with the rotation obtained by the camera motion estimation to estimate the gyroscope offset. The rotations of two adjacent key frames estimated by vision are $R_{C_k}^{C_0}$ and $R_{C_{k+1}}^{C_0}$, and the rotations of the IMU coordinate system can be obtained by the external parameters of the camera and IMU as $R_{B_k}^{C_0}$ and $R_{B_{k+1}}^{C_0}$. Compared with the result of IMU preintegration, there is a relation [22]:

$$R_{B_k}^{C_0\,T} R_{B_{k+1}}^{C_0} \approx \Delta R_{k,k+1}. \tag{8}$$

The gyroscope bias b_g is included in $\Delta R_{k,k+1}$, so the optimization objective equation can be obtained.

$$\begin{aligned} &\min_{\delta b_g} \sum \left\| \log\left(R_{B_{k+1}}^{C_0\,T} R_{B_{k+1}}^{C_0} \Delta R_{k,k+1} \right) \right\|^2, \\ &\Delta R_{k,k+1} \approx \Delta \tilde{R}_{k,k+1} \exp\left(\delta_g\right). \end{aligned} \tag{9}$$

By iteratively optimizing this objective equation, the gyroscope bias b_g in the registration phase can be solved.

The gravitational acceleration is coupled in the acceleration measurement of the IMU. In order to register the gravitational acceleration with the visual coordinate system, it is considered to associate the translation component estimated by the visual motion with the velocity and position measurement in the IMU preintegration. The relationship between the position of the visual coordinate system at time k and

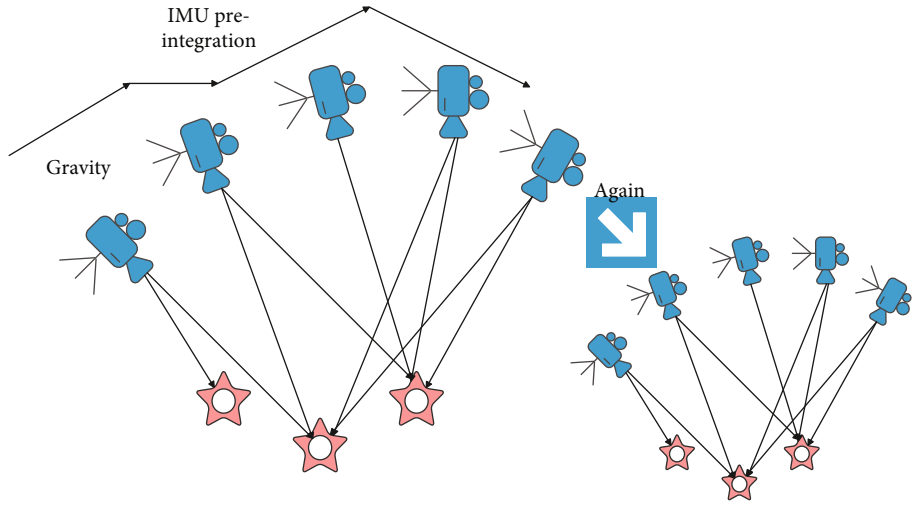

Figure 6: Schematic diagram of visual inertial registration.

the position of the IMU coordinate system is as follows:

$$p_{B_k}^{C_0} \approx p_{C_k}^{C_0} - R_{B_k}^{C_0} p_C^B. \tag{10}$$

In order to convert the gravitational acceleration to the visual coordinate system C_0, the IMU preintegration from time k to $k+1$ is rewritten as follows:

$$\begin{aligned} \Delta p_{k,k+1} &= R_{B_k}^{C_0\,T}\left(p_{C_{k+1}}^{C_0} - p_{C_k}^{C_0} + \frac{1}{2}{}^{C_0} g\Delta t^2 - R_{B_k}^{C_0} v_{B_k}\Delta t\right), \\ \Delta v_{k,k+1} &= R_{B_k}^{C_0\,T}\left(R_{B_{k+1}}^{C_0} v_{B_{k+1}} + {}^{C_0} g\Delta t - R_{B_k}^{C_0} v_{B_k}\right). \end{aligned} \tag{11}$$

Visual motion estimation and IMU preintegration are integrated to obtain the linear observation equation:

$$z_{B_{k+1}}^{B_k} = \begin{bmatrix} \Delta p_{k,k+1} - p_C^B + R_{B_k}^{C_0\,T} R_{B_{k+1}}^{C_0} p_C^B \\ \Delta v_{k,k+1} \end{bmatrix} = H_{B_{k+1}}^{B_k}\chi + n_{B_{k+1}}^{B_k}. \tag{12}$$

Among them, $H_{B_{k+1}}^{B_k} = \begin{bmatrix} -I\Delta t & 0 & 1/2R_{B_k}^{C_0\,T}\Delta t^2 \\ & -I & \end{bmatrix}$ is the variable to be optimized, including $H_{B_{k+1}}^{B_k} = \begin{bmatrix} -I\Delta t & 0 & 1/2R_{B_k}^{C_0\,T}\Delta t^2 \\ & -I & \end{bmatrix}$, v_{B_k}, and $v_{B_{k+1}}$, and $H_{B_{k+1}}^{B_k} = \begin{bmatrix} -I\Delta t & 0 & 1/2R_{B_k}^{C_0\,T}\Delta t^2 \\ & -I & \end{bmatrix}$ is as follows:

$$H_{B_{k+1}}^{B_k} = \begin{bmatrix} -I\Delta t & 0 & \frac{1}{2}R_{B_k}^{C_0\,T}\Delta t^2 \\ -I & R_{B_k}^{C_0\,T} R_{B_{k+1}}^{C_0} & R_{B_k}^{C_0\,T}\Delta t \end{bmatrix}. \tag{13}$$

Just by solving the linear equations, $H_{B_{k+1}}^{B_k} = \begin{bmatrix} -I\Delta t & 0 & 1/2R_{B_k}^{C_0\,T}\Delta t^2 \\ & -I & \end{bmatrix}$ can be calculated and obtained.

$$\min_{\chi} \sum \left\| Z\wedge_{B_{k+1}}^{B_k} - H_{B_{k+1}}^{B_k}\chi \right\|^2. \tag{14}$$

In the multisensor fusion problem, there are usually two fusion methods, namely, loose coupling and tight coupling. Loose coupling means that each sensor in a multisensor system uses its own information to perform calculations and then fuse the results calculated by each sensor. Tight coupling means that the algorithm directly integrates the information obtained by each sensor for processing without preprocessing the information. It can be seen that under the loose coupling optimization method, each sensor is independent of each other and cannot really restrict each other. The tight coupling is to directly unify the raw data of each sensor for processing, and the sensor information is coupled with each other to obtain a better estimation effect. In most applications of multisensor fusion algorithms, tight coupling optimization methods are adopted.

The so-called tight coupling optimization is actually adding the IMU preintegration and visual observation and the camera pose to be optimized into a partial window for optimization. In this partial window, the variables to be optimized are as follows:

$$\begin{aligned} \chi &= [x_0, x_1, \cdots, x_n, l_0, l_1, \cdots l_m], \\ x_k &= \left[p_{B_k}^W, v_{B_k}, R_{B_k}^W, b_a, b_g\right], k \in [0, n] \times, \\ l_j &= [x, y, z], j \in [0, m]. \end{aligned} \tag{15}$$

Among them, x_k is the system state of the k-th captured camera, including the position $p_{B_k}^W$ of the IMU coordinate system relative to the world coordinate system, the speed v_{B_k} and the rotation $R_{B_k}^W$ relative to the world coordinate system, and the offset b_a, b_g in the IMU measurement. Here,

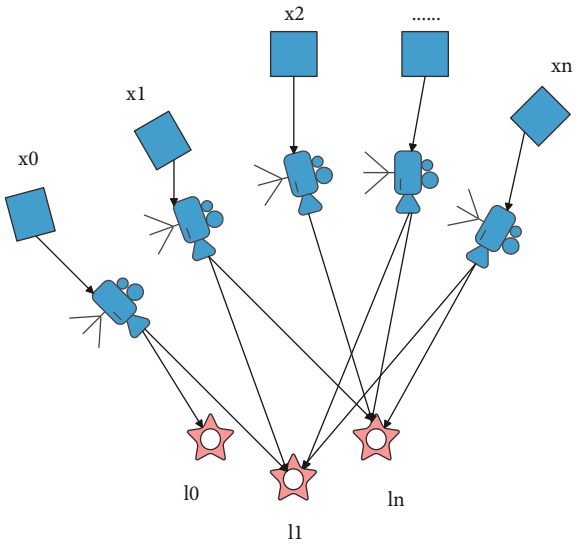

Figure 7: Schematic diagram of partial window.

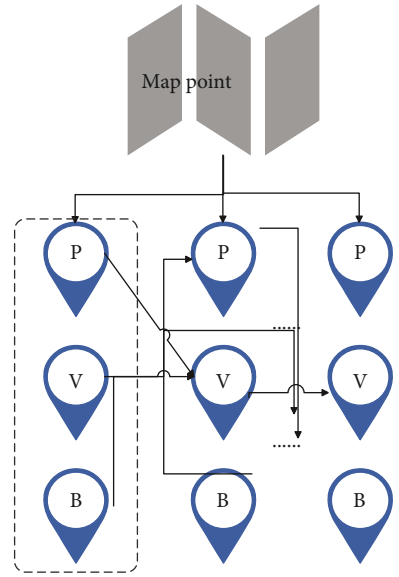

Figure 8: Schematic diagram of graph optimization.

the IMU coordinate system is selected as the navigation coordinate system, and the calculated pose is updated to the camera coordinate system through the external parameters between the IMU and the camera.

Figure 7 is a schematic diagram of partial window optimization in a certain period of time. The combination of the blue rectangle and the blue trapezoid is the camera, the blue rectangle is the IMU, and the black line connecting them is the external parameter. The red five-pointed star is the visual map point, and the dotted line between the camera and the visual map point indicates that the camera observes the map point. Figure 7 is a schematic diagram of map optimization corresponding to the partial window in Figure 8, and the map points are all summarized in blue ellipses. The yellow circle represents the state quantity to be estimated, P is the pose of the IMU, V is the speed of the IMU, and B is the partial mass measured by the IMU. The squares represent constraints, and the blue squares are the constraints of the reprojection error between the visual feature map points and the camera. The green square is the IMU preintegration constraint, and the relationship between the state to be estimated and the constraint is represented by a thin black line. For example, the blue square connects P and the map point.

The optimization problem represented by the above graph optimization is as follows:

$$\chi^* = \min_{\chi} \left(\sum_{k} E_{\text{proj}}(k,j) + E_{\text{IMU}}(i,j) \right). \tag{16}$$

The green square in the figure is the preintegration constraint of $E_{\text{IMU}}(i,j)$, and the blue square is the reprojection error constraint $E_{\text{proj}}(k,j)$. When the k-th map point and the j-th camera are given, the projection error $E_{\text{proj}}(k,j)$ between them is defined as follows:

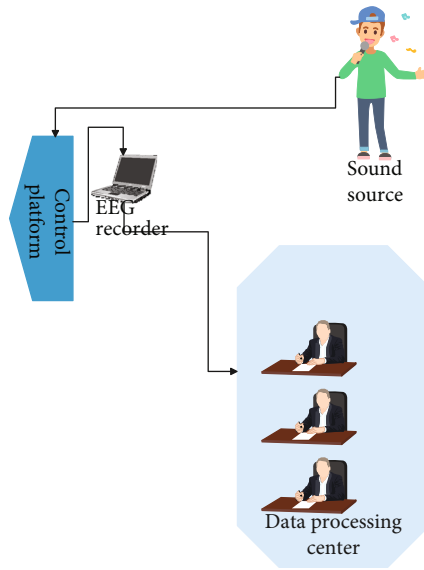

Figure 9: Singing and nervous system regulation platform based on wireless sensor perception network.

Among them, p_k represents the pixel coordinates of the feature point matching the k-th map point to the image, and $\pi(\cdot)$ represents the projection transformation, which projects a point l_c^k in the visual coordinate system onto the image. $\rho(\cdot)$ is a function of error mode detection. When the internal error exceeds a certain threshold, the weight of this error in the optimization is reduced to reduce the impact on the final estimation result. $\sum_k$ is the information matrix of the reprojection error, which is related to the error model of the projection. The larger the error, the smaller the information value. l_c^k is converted from the pose in the IMU coordinate system and the camera IMU external parameter l_k. For the IMU preintegration constraint $E_{\text{IMU}}(i,j)$, there are

Table 1: Experimental research results of singing and nervous system regulation platform based on wireless sensor network perception.

Number	System assessment	Number	System assessment	Number	System assessment	Number	System assessment
1	93.37	14	95.44	27	96.31	40	94.58
2	93.99	15	85.41	28	84.21	41	85.68
3	86.76	16	95.52	29	93.39	42	94.53
4	92.27	17	88.17	30	91.51	43	84.71
5	96.50	18	86.79	31	91.04	44	91.44
6	85.98	19	84.70	32	86.38	45	85.68
7	94.75	20	85.05	33	92.13	46	89.26
8	85.93	21	90.95	34	92.56	47	85.79
9	89.06	22	94.82	35	93.93	48	84.47
10	92.73	23	91.69	36	89.98	49	90.47
11	85.60	24	95.35	37	95.54	50	95.64
12	94.33	25	84.12	38	85.40		
13	87.07	26	93.79	39	94.34		

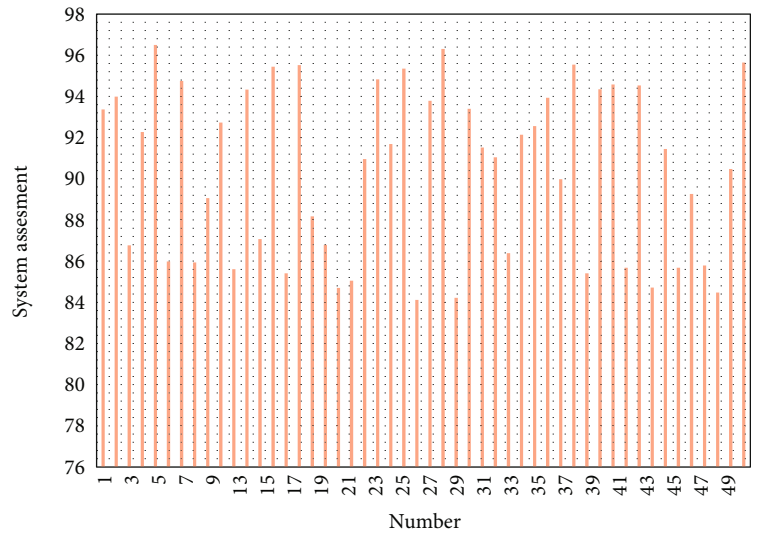

Figure 10: Histogram of experimental research results of singing and nervous system regulation platform based on wireless sensor network perception.

$$
\begin{aligned}
E_{\mathrm{IMU}}(i,j) &= \rho\left(\left[e_R^T, e_v^T e_p^T\right]\sum_l\left[e_R^T, e_v^T e_p^T\right]^T\right) + \rho\left(e_b^T\sum_b e_b\right),\\
e_R &= \log\left(\left(\Delta R_{ij}\exp\left(\delta b_{gi}\right)\right)^T R_W^{B_i} R_{B_j}^W\right),\\
e_v &= R_W^{B_i}\left(v_{B_j} - v_{B_i} - {}^w g\Delta t\right) - \Delta v_{ij},\\
e_p &= R_W^{B_i}\left(p_{B_j}^W - p_{B_i}^W - v_{B_i}\Delta t - \frac{1}{2}{}^W g\Delta t^2\right) - \Delta p_{ij},\\
e_b &= b_j - b_i.
\end{aligned}
\tag{17}
$$

Among them, $\sum_l$ is the information matrix of preintegration, and $\sum_b$ is the information matrix of partial quality. For the above graph optimization structure, an optimization solver is constructed, such as a Gauss-Newton solver or an LM solver. Therefore, the number of poses in the partial window designed in this section is limited to 10, which takes into account the calculation efficiency and accuracy of the algorithm.

4. Singing and Nervous System Regulation Based on Wireless Sensor Perception Network

This paper constructs a mental emotion recognition system when singing, in which emotion recognition is directly linked to the nervous system. The data collection and

transmission of the system in this paper are realized through the wireless sensor network perception system. The system constructed in this paper is shown in Figure 9.

After constructing the system platform as shown in Figure 9, this paper evaluates the performance of this system through experimental research and studies the reliability of this system. This paper selects 50 volunteers from college vocal music majors with normal hearing and good health as the experimental subjects. Before the experiment, the subjects did not take any drugs that could affect the EEG and did not drink alcohol. At the same time, in order to ensure good electrical conductivity between the scalp and the electrode cap and improve the signal-to-noise ratio, all subjects are asked to wash their hair and dry their hair before the experiment started. Moreover, this paper uses a sensor network to simultaneously identify and locate 50 experimental subjects at the same time and calculate the effectiveness of this platform. The experimental results are shown in Table 1 and Figure 10.

From the above research results, it can be seen that the singing and nervous system regulation platform based on the wireless sensor network perception built in this paper has certain effects, and the system built in this paper can continue to be experimentally studied in the follow-up practice to explore its practical effects.

5. Conclusion

Singing is a manifestation of human beings' perception of the outside world or their own emotions. The content and emotions of singing are expressed through voice and body language. This is inseparable from the singer's own emotional mobilization and the coordination of the body's physiology. Moreover, whether the physical movement of the singer's body is correct or not directly affects the quality of the singer's voice and the expression of singing psychology. Therefore, the correct physiological movement of singing is inseparable from the guidance and regulation of correct singing psychological activity. Singing physiology is mainly composed of the physiological structure of the voice, respiratory system, resonance system, language system, and other elements. They affect and restrict the learning, teaching, and practical activities of vocal music. Only the coordinated movement of various singing physiological organs and parts can produce a beautiful singing voice. However, the production of the voice is inseparable from the scheduling and control of the singer's psychological activities, and the correct guidance of the singing psychological activities can lead to the correct physiological movements of the body. This article uses wireless sensor network applications to regulate singing and the nervous system, uses wireless sensor networks for data transmission, and simulates the human emotion model to study the regulation of singing and the nervous system. Through experimental research, it can be known that the singing and nervous system regulation platform based on wireless sensor network perception built in this paper has certain effects.

Data Availability

The labeled dataset used to support the findings of this study are available from the corresponding author upon request.

Conflicts of Interest

The author declares no competing interests.

Acknowledgments

This study is sponsored by the Guizhou Normal University.

References

[1] G. Bedi, G. K. Venayagamoorthy, R. Singh, R. R. Brooks, and K. C. Wang, "Review of Internet of Things (IoT) in electric power and energy systems," *IEEE Internet of Things Journal*, vol. 5, no. 2, pp. 847–870, 2018.

[2] I. Bisio, A. Delfino, A. Grattarola, F. Lavagetto, and A. Sciarrone, "Ultrasounds-based context sensing method and applications over the Internet of Things," *IEEE Internet of Things Journal*, vol. 5, no. 5, pp. 3876–3890, 2018.

[3] A. Chamberlain, M. Bødker, A. Hazzard et al., "Audio technology and mobile human computer Interaction," *International Journal of Mobile Human Computer Interaction*, vol. 9, no. 4, pp. 25–40, 2017.

[4] D. B. Ç. Kiliç, "Pre-service music teachers' metaphorical perceptions of the concept of a music teaching program," *Journal of Education and Learning*, vol. 6, no. 3, pp. 273–286, 2017.

[5] D. L. Hoffman and T. P. Novak, "Consumer and object experience in the internet of things: an assemblage theory approach," *Journal of Consumer Research*, vol. 44, no. 6, pp. 1178–1204, 2018.

[6] B. Jia, L. Hao, C. Zhang, H. Zhao, and M. Khan, "An IoT service aggregation method based on dynamic planning for QoE restraints," *Mobile Networks and Applications*, vol. 24, no. 1, pp. 25–33, 2019.

[7] J. Waldron, R. Mantie, H. Partti, and E. S. Tobias, "A brave new world: theory to practice in participatory culture and music learning and teaching," *Music Education Research*, vol. 20, no. 3, pp. 289–304, 2018.

[8] J. Zhang and D. Tao, "Empowering things with intelligence: a survey of the progress, challenges, and opportunities in artificial intelligence of things," *IEEE Internet of Things Journal*, vol. 8, no. 10, pp. 7789–7817, 2021.

[9] E. Gun, "The opinions of the preservice music teachers regarding the teaching of orchestra and chamber music courses during distance education process," *Cypriot Journal of Educational Sciences*, vol. 16, no. 3, pp. 1088–1096, 2021.

[10] G. Muhammad, S. K. M. M. Rahman, A. Alelaiwi, and A. Alamri, "Smart health solution integrating IoT and cloud: a case study of voice pathology monitoring," *IEEE Communications Magazine*, vol. 55, no. 1, pp. 69–73, 2017.

[11] X. Shengmin, "Analysis on the innovative strategy of national music teaching in colleges from the perspective of visual communication," *Studies in Sociology of Science*, vol. 7, no. 6, pp. 52–55, 2017.

[12] Z. Lian, "Research on aesthetic education in instrumental music teaching," *Journal of Literature and Art Studies*, vol. 10, no. 5, pp. 435–439, 2020.

[13] S. K. Kim, N. Sahu, and M. Preda, "Beginning of a new standard: Internet of Media Things," *KSII Transactions on internet and information systems*, vol. 11, no. 11, pp. 5182–5199, 2017.

[14] A. Kaplan and M. Haenlein, "Siri, Siri, in my hand: who's the fairest in the land? On the interpretations, illustrations, and implications of artificial intelligence," *Business Horizons*, vol. 62, no. 1, pp. 15–25, 2019.

[15] F. L. Reyes, "A community music approach to popular music teaching in formal music education," *The Canadian Music Educator*, vol. 59, no. 1, pp. 23–29, 2017.

[16] V. K. Jones, "Voice-activated change: marketing in the age of artificial intelligence and virtual assistants," *Journal of Brand Strategy*, vol. 7, no. 3, pp. 233–245, 2018.

[17] P. S. Aithal and S. Aithal, "Management of ICCT underlying technologies used for digital service innovation," *International Journal of Management, Technology, and Social Sciences (IJMTS)*, vol. 4, no. 2, pp. 110–136, 2019.

[18] C. Johnson, "Teaching music online: changing pedagogical approach when moving to the online environment," *London Review of Education*, vol. 15, no. 3, pp. 439–456, 2017.

[19] P. L. Lin, "Trends of internationalization in China's higher education: opportunities and challenges," *US-China Education Review B*, vol. 9, no. 1, pp. 1–12, 2019.

[20] S. Y. Hong and Y. H. Hwang, "Design and implementation for iort based remote control robot using block-based programming," *Issues in Information Systems*, vol. 21, no. 4, pp. 317–330, 2020.

[21] J. G. Bayley and J. Waldron, ""It's never too late": adult students and music learning in one online and offline convergent community music school," *International Journal of Music Education*, vol. 38, no. 1, pp. 36–51, 2020.

[22] L. F. Luque Vega, E. Lopez Neri, A. Santoyo, J. Ruíz Duarte, and N. Farrera Vázquez, "Educational methodology based on active learning for mechatronics engineering students: towards educational mechatronics," *Computación y Sistemas*, vol. 23, no. 2, pp. 325–333, 2019.

Hindawi
Journal of Sensors
Volume 2021, Article ID 6943970, 12 pages
https://doi.org/10.1155/2021/6943970

Research Article

Research on the Dynamic Model of Entrepreneurship Based on Improved Machine Learning

Mengbin Zhu,[1] Yan Yang,[1] and Huaying Cao[2]

[1]*The Open University of Shaanxi, Xi'an 710119, China*
[2]*Zhengzhou Shengda University, Zhengzhou 451191, China*

Correspondence should be addressed to Huaying Cao; 100740@shengda.edu.cn

Received 13 August 2021; Revised 10 September 2021; Accepted 29 September 2021; Published 23 October 2021

Academic Editor: Mu Zhou

There are many influencing factors in the entrepreneurial process, which lead to a variety of unknown situations in the entrepreneurial process and affect the entrepreneurial process. In order to improve the effect of entrepreneurial analysis, this paper improves the traditional machine learning algorithm and proposes an entrepreneurial dynamic model based on improved machine learning. Aimed at the opportunistic behavior of the following venture capital institution under joint investment, this paper constructs an evolutionary game model between the leading venture capital institution and the following venture capital institution under joint investment and constructs an industrial cluster knowledge fusion and entrepreneurial innovation model. Moreover, this paper confirms through the structural equation model that the use of information fusion technology can improve the effectiveness and comprehensiveness of internal and external knowledge of industrial clusters. In addition, this paper uses experimental analysis methods to evaluate the performance of the entrepreneurial dynamic model constructed in this paper. From the research results, it can be seen that the system constructed in this paper has a certain effect.

1. Introduction

Today's economy has been dubbed a series of names such as knowledge economy, information economy, high-tech economy, and new economy, which is quite different from the previous economy characterized by low-intellectual labor. It is essentially an economy characterized by highly intelligent labor. The development of reality has increasingly confirmed Schumpeter's view that "the central issue of economics is not balance but structural change." Entrepreneurship will play a central role in this structural change. Moreover, the development of entrepreneurial activities has a positive effect on maintaining China's economic development, promoting a smooth transition of the economy, and smoothly realizing the adjustment and transformation of the economic structure [1].

In the context of global economic integration, how to avoid the impact of the external economy and how to overcome the limitations of the internal economic structure are major issues facing the sustainable development of our country's economy. Under the current situation, in order to be in line with the fundamental interests of economic development, the long-term stable development of China's economy must enable rapid and stable adjustments to the economic structure and gradually transform China's economic development mode. The emergence and development of the entrepreneurial economy are closely related to the knowledge economy, which is very different from the management economy. Labor, capital, and land are the main factors driving economic growth in the traditional management economy model; the core content of the entrepreneurial economy is to regard entrepreneurs and entrepreneurial spirit as an indispensable and important element of the economic form and also to promote economic development. The main factors can promote enterprise innovation and promote economic growth. In today's China, the role of entrepreneurial activities and new ventures in economic development has been recognized by all sectors of society. At the same time, research on entrepreneurs and entrepreneurial behavior has also become a hot topic in the field of

entrepreneurship. With the progress of China's reform and opening up, the adjustment of the economic structure, the continuous deepening of the reform of state-owned enterprises, and the rapid rise of non-state-owned enterprises, new ventures have become an indispensable main component of China's national economy. As the largest developing country in the world, China's economic aggregate continues to grow, and its impact on the world economy is increasing. Improving the inherent quality of economic development and achieving steady and sustained economic growth are important issues that we face. It can be seen that entrepreneurial activities are of great significance to technological innovation, productivity improvement, employment increase, and national economic growth. This point has been recognized and confirmed by many scholars.

Entrepreneur research and the design and implementation of entrepreneurial support policies and measures have received great attention from countries and regions around the world, and entrepreneurship has become a global hot topic [2].

Based on this, this paper constructs a dynamic model of entrepreneurship with the support of improved machine learning algorithms. Through effective analysis of the model, the entrepreneurial process is studied, and on this basis, the efficiency of entrepreneurial analysis is further improved.

2. Related Work

Studies have shown that new ventures contribute to the growth of wealth, economic prosperity, and job creation in economic regions, thereby having a positive effect on the economic system [3]. With the implementation of entrepreneurial support policies, the scale of entrepreneurs is increasing, so how to identify entrepreneurs, how to distinguish the differences between entrepreneurs and nonentrepreneurs, and how entrepreneurs will develop have become topics of concern in the field of entrepreneurship research. Based on different entrepreneurial processes, the individual characteristics of entrepreneurs have different effects on entrepreneurial behavior. For example, in the entrepreneurial environment where the startup is a small- and medium-sized enterprise, the overall atmosphere and development direction of the entire startup will be directly affected by the entrepreneur's individual characteristics and spirit. Therefore, entrepreneurial research cannot ignore the research on the individual characteristics of entrepreneurs. The establishment and future development of new ventures will be affected by the individual characteristics of entrepreneurs. Therefore, the relationship between entrepreneurial characteristics and entrepreneurial inclination needs to be further studied.

Entrepreneurship process research is a hot spot in the field of entrepreneurship. Most of these studies focus on the analysis of resource development and value creation from the perspective of entrepreneurial team building, entrepreneurial opportunity identification, and entrepreneurial resource acquisition. Although the results of entrepreneurial research are becoming more and more abundant, there are not many studies on the identification of potential entrepreneurs and the antecedents of entrepreneurial behavior. The literature [4] points out that the antecedent factor of all entrepreneurial activities is entrepreneurial tendency. The research mainly focuses on the issue of entrepreneurial propensity and plans to deeply analyze the correlation between entrepreneurial antecedents, introduce path adjustment variables and intermediary variables, and finally establish a path model of entrepreneurial antecedents and entrepreneurial propensity.

Early entrepreneurial research described entrepreneurs as individuals with a high degree of confidence and risk taking in the face of uncertain and ambiguous situations and believed that entrepreneurs have distinct characteristics compared with nonentrepreneurs. Scholars believe that it is the inherent characteristics of individuals that make individuals take risky actions, which promote entrepreneurial behavior. Therefore, the research orientation of entrepreneurial characteristics tries to find the intrinsic characteristics of individuals that can identify entrepreneurs [5]. Entrepreneurs' individual characteristics, such as achievement needs, risk taking, internal control sources, and other individual psychological characteristics, have been confirmed by relevant empirical studies. This helps distinguish entrepreneurs from nonentrepreneurs and explain and predict the conversion of potential entrepreneurs to actual entrepreneurship. Among them, achievement demand is considered to be one of the most commonly used individual characteristic indicators that can successfully predict entrepreneurs [6]. However, some scholars believe that the research on entrepreneurial characteristics has not been able to explain in depth the internal causes of individuals participating in entrepreneurial activities [7]. Some scholars even question the research orientation of entrepreneurial characteristics and believe that the identification of entrepreneurs cannot be predicted only from individual characteristics [8]. The research on the cognitive process of entrepreneurship attempts to make up for the shortcomings of the research on entrepreneurial characteristics by exploring the cognitive factors that can stimulate entrepreneurship. The literature [9] believes that entrepreneurs and nonentrepreneurs have significant differences in the way of thinking and conducts research on the cognitive mechanisms that trigger entrepreneurs to identify entrepreneurial opportunities and engage in entrepreneurial activities. Moreover, it believes that from the perspectives of entrepreneurial cognitive mechanism, entrepreneurial decision-making types, entrepreneurial intentions, etc., it is possible to explore the important characteristics of entrepreneurs. Based on the study of the cognitive process of entrepreneurship, the literature [10] believes that the strength of individual entrepreneurial aspirations will be affected by entrepreneurial self-efficacy, and the essential factor that affects individual entrepreneurial behavior is individual entrepreneurial intentions. Individual entrepreneurial intention is the desire of an individual to actively prepare and strive to achieve the expected value of entrepreneurial behavior. The stronger this intention, the stronger its ability to predict actual entrepreneurial behavior.

The literature [11] points out that entrepreneurs are those who invent at the right time and transform their

inventions into innovations, and it emphasizes the core role that entrepreneurs play in the innovation process. At the same time, these resource combinations established by entrepreneurs, including the supply of new raw materials, new product combinations, new production methods, new market development, and new organizational combinations, have become the guarantee for the implementation of economic reforms. The entrepreneurial process describes the process of a series of events triggered by the discovery of entrepreneurial opportunities and ultimately leading to the creation of a new enterprise [12]. The literature [13] points out that the description dimensions of the entrepreneurial process can be divided into three dimensions: the pursuit of profit in the market, the establishment of an organization, and the economic innovation. The literature [14] believes that there are three factors that will promote the entrepreneurial process, namely, entrepreneurs and entrepreneurial teams, entrepreneurial opportunities, and entrepreneurial resources. The literature [15] established a model for the establishment of new ventures. This mechanism model includes opportunity identification, commitment to the entrepreneurial process, production technology construction, organization establishment, product creation, market entry, and customer feedback. In order to feed back the abstract, driven, and actual entrepreneurial process, the mechanism model is repetitive and nonlinear. The framework developed in the literature [16] is based on the study of entrepreneurs and their enterprises and the sum of variables in previous studies. The individual variables of this framework include attitude, experience, and background. Although the use of psychological variables to study entrepreneurs was highly questioned before this, the three variables of achievement demand, control source, and risk tolerance are introduced into the research model of literature [17]. However, it can be seen from the four variables of the model that the process only enumerates some of the actions mentioned in the creation of new enterprises that are generally recognized in the society. The environment column mentions the various dimensions that will be involved in the social environment. The model in the literature [18] does not fundamentally fully explain the relationship between each column such as environment and process, individual and organization, or the other two, and there is even no relationship between variables.

3. Model Solving and Stability Analysis

The expected return of the leading venture capital institution M to choose supervision and nonregulation is U_0^1 and U_0^2, respectively. The average return of the group of the leading venture capital institution M is $\bar{U}^0$. According to the related theory of an evolutionary game [19],

$$\begin{aligned} U_0^1 &= y[\alpha(R+\gamma\Delta V)-C_0]+(1-y)(\alpha R-C_0+\lambda R_3),\\ U_0^2 &= y[\alpha(R+\Delta V)]+(1-y)\alpha R,\\ \bar{U}_0 &= xU_0^1+(1-x)U_0^2. \end{aligned} \tag{1}$$

In the same way, the expected return of the following venture capital institution N to choose active management and opportunism is U_1^1 and U_1^2, respectively. The average return of the group of the following venture capital institution N is $\bar{U}_1$. According to the related theory of an evolutionary game,

$$\begin{aligned} U_1^1 &= x[\beta(R+\gamma\Delta V)-C]+(1-x)[(\beta(R+\Delta V)-C)],\\ U_1^2 &= x(\beta R+R_1-\lambda R_2)+(1-x)(\beta R+R_1),\\ \bar{U}_1 &= yU_1^1+(1-y)U_1^2. \end{aligned} \tag{2}$$

According to the dynamic equation of replication, the growth rate of the leading venture capital institution and the following venture capital institution to choose supervision and active management, respectively, is

$$\begin{aligned} F(x) = \frac{dx}{dt} &= x\left(U_0^1-\bar{U}_0\right)\\ &= x(1-x)[y(\alpha\gamma\Delta V-\alpha\Delta V-\lambda R_3)+(\lambda R_3-C_0)], \end{aligned}$$

$$\begin{aligned} G(y) = \frac{dy}{dt} &= y\left(U_1^1-\bar{U}_1\right)\\ &= y(1-y)[x(\beta\gamma\Delta V-\beta\Delta V+\lambda R_2)+(\beta\Delta V-C-R_1)]. \end{aligned} \tag{3}$$

We set $dx/dt = 0$ and $dy/dt = 0$. When the replication dynamic equations of venture capital institutions M and N are set to zero, by solving the local equilibrium points of venture capital institutions M and N strategic interactions, five local equilibrium points of the system can be obtained, and they are, respectively, $(0,0)$, $(0,1)$, $(1,0)$, $(1,1)$, and (x_0, y_0). Among them,

$$\begin{aligned} x_0 &= \frac{R_1+C-\beta\Delta V}{\beta\gamma\Delta V-\beta\Delta V+\lambda R_2},\\ y_0 &= \frac{C_0-\lambda R_3}{\alpha\gamma\Delta V-\alpha\Delta V-\lambda R_3}. \end{aligned} \tag{4}$$

When $0 \le x_0, y_0 \le 1$, (x_0, y_0) exists [20].

The Jacobian matrix of the joint investment strategy selection system is

$$J = \begin{pmatrix} \dfrac{\partial F(x)}{\partial x} & \dfrac{\partial F(x)}{\partial y} \\ \dfrac{\partial G(x)}{\partial x} & \dfrac{\partial G(y)}{\partial y} \end{pmatrix} = \begin{pmatrix} a_{11} & a_{12} \\ a_{21} & a_{22} \end{pmatrix}. \tag{5}$$

Among them,

$$\begin{aligned} a_{11} &= (1-2x)[y(\alpha\gamma\Delta V - \alpha\Delta V - \lambda R_3) + (\lambda R_3 - C_0)], \\ a_{12} &= x(1-x)(\alpha\gamma\Delta V - \alpha\Delta V - \lambda R_3), \\ a_{21} &= y(1-y)(\beta\gamma\Delta V - \beta\Delta V + \lambda R_2), \\ a_{22} &= (1-2y)[x(\beta\gamma\Delta V - \beta\Delta V + \lambda R_2) + (\beta\Delta V - C - R_1)]. \end{aligned} \tag{6}$$

Five partial equilibrium points are substituted into a_{11}, a_{12}, a_{21}, a_{22} to get their specific values.

$$\begin{aligned} Q &= x_0(1-x_0)(\alpha\gamma\Delta V - \alpha\Delta V - \lambda R_3), \\ R &= y_0(1-y_0)(\beta\gamma\Delta V - \beta\Delta V + \lambda R_2). \end{aligned} \tag{7}$$

To make the solution process simple, we set

$$\begin{aligned} A &= \lambda R_3 - C_0, \\ B &= \alpha\gamma\Delta V - \alpha\Delta V - C_0, \\ E &= \beta\Delta V - C - R_1, \\ F &= \beta\gamma\Delta V + \lambda R_2 - C - R_1. \end{aligned} \tag{8}$$

Because $\gamma \geq 1, \lambda \in (0,1), R_2 > 0, F > E$. At this time,

$$\begin{aligned} x_0 &= \frac{-E}{F-E}, \\ y_0 &= \frac{-A}{B-A}. \end{aligned} \tag{9}$$

(x_0, y_0) is the center point. For leading venture capital institutions, if the initial state is $y = y_0$, then all x are in a stable state. That is, when the proportion of the follow-type venture capital institution choosing active management strategies is y_0, the proportion of leading venture capital institutions choosing supervision at any level can reach a stable state. When $y > y_0, F(x) > 0, F'(0) > 0, F'(1) < 0$, according to the stability theorem of differential equations, $x = 1$ is an evolutionary stable state. When $y < y_0, F(x) < 0$, $F'(0) < 0, F'(1) > 0$, then $x = 0$ is an evolutionary stable state [21].

For the following venture capital institutions, if the initial state is $x = x_0$, then all y are in a stable state. That is, when the leading venture capital institution chooses a supervisory strategy ratio of x_0, the ratio of any level of the following venture capital institution choosing active management can reach a stable state. When $x > x_0, G(x) > 0, G'(0) > 0, G'(1) < 0$, according to the stability theorem of differential equations, $y = 1$ is an evolutionary stable state. When $x < x_0, G(x) < 0, G'(0) < 0, G'(1) > 0$, $y = 0$ is an evolutionary stable state.

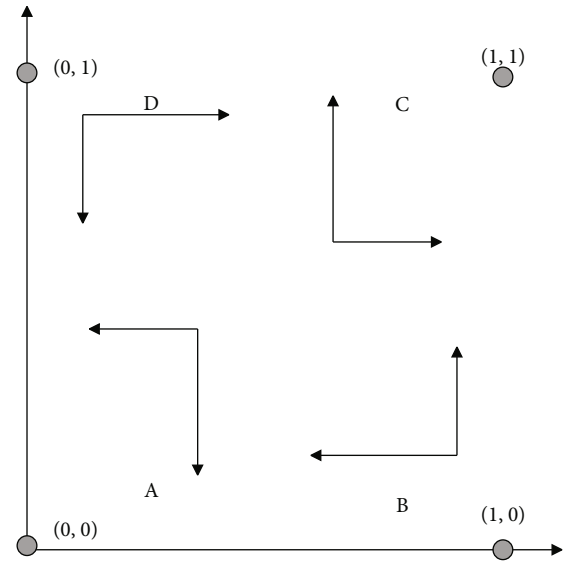

Figure 1: Phase diagram of the evolutionary game between the leading venture capital institution and the following venture capital institution.

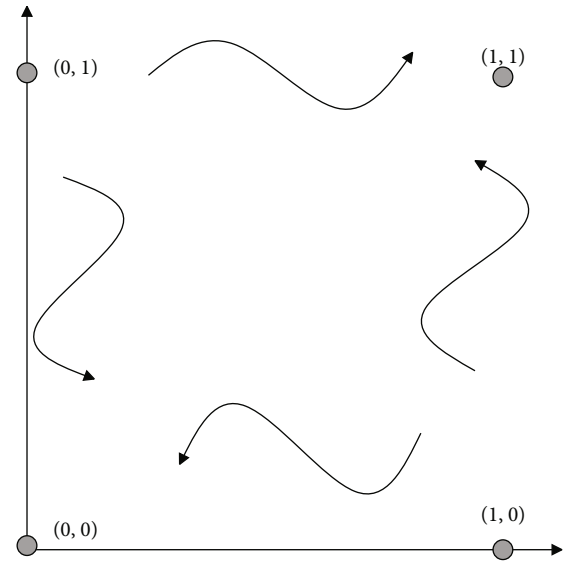

Figure 2: Evolution path diagram of the leading venture capital institution and the following venture capital institution.

According to the above stability analysis, the evolutionary game phase diagram shown in Figure 1 can be obtained.

According to the related theory of an evolutionary game and Figure 1, the evolution path diagram shown in Figure 2 can be obtained [22].

The final evolutionary stability strategy of the system is related to the initial state of the leading venture capital institution and the following venture capital institution. When the initial state of both parties falls in the OAEC area, the system will converge to point $O(0,0)$; that is, the leading venture capital institution chooses a nonregulatory strategy,

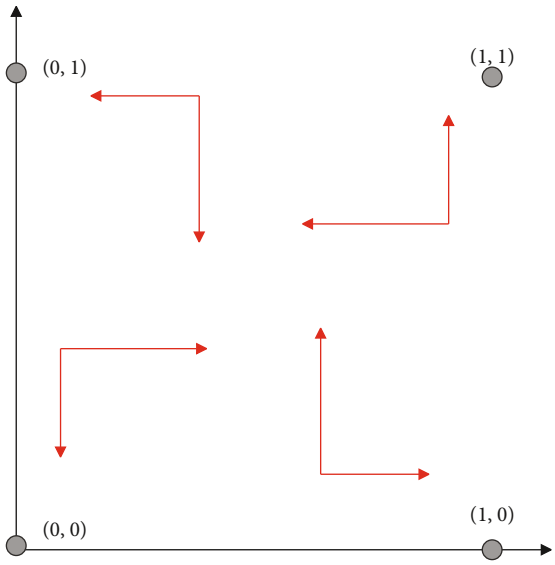

Figure 3: Evolution phase diagram of the leading venture capital institution and the following venture capital institution.

and the following venture capital institution chooses an opportunistic strategy. When the initial state of both parties falls in the CEAB area, the system will converge to point B $(1, 1)$; that is, the leading venture capital institution chooses a regulatory strategy, and the following venture capital institution chooses an active management strategy.

The following analysis is to solve the "prisoner's dilemma" that both parties tend to point O and analyze which parameters will affect the final evolutionary stability strategy of both parties to converge to point B. Moreover, we analyzed which parameters will affect the area of the polygon CEAB from a geometrical point of view. The larger the S_{CEAB} is, the easier it is for the leading venture capital institution and the following venture capital institution to form a win-win situation of cooperation with supervision and active management [23].

$$\begin{aligned} S_{CEAB} &= 1 - S_{OCEA} = 1 - \left(\frac{x_0}{2} + \frac{y_0}{2}\right) \\ &= 1 - \frac{R_1 + C - \beta\Delta V}{2(\beta\gamma\Delta V - \beta\Delta V + \lambda R_2)} \\ &\quad - \frac{C_0 - \lambda R_3}{2(\alpha\gamma\Delta V - \alpha\Delta V - \lambda R_3)}. \end{aligned} \tag{10}$$

(1) The influence of the profit ratio α, β of the leading venture capital institution and the following venture capital institution on the cooperation strategy is as follows:

$$\begin{aligned} \frac{dS_{CEAB}}{d\alpha} &= \frac{(C_0 - \lambda R_3)(\gamma\Delta V - \Delta V)}{2(\alpha\gamma\Delta V - \alpha\Delta V - \lambda R_3)^2} > 0, \\ \frac{dS_{CEAB}}{d\beta} &= \frac{(R_1 + C - \beta\Delta V)(\gamma\Delta V - \Delta V)}{2(\beta\gamma\Delta V - \beta\Delta V - \lambda R_2)^2} > 0. \end{aligned} \tag{11}$$

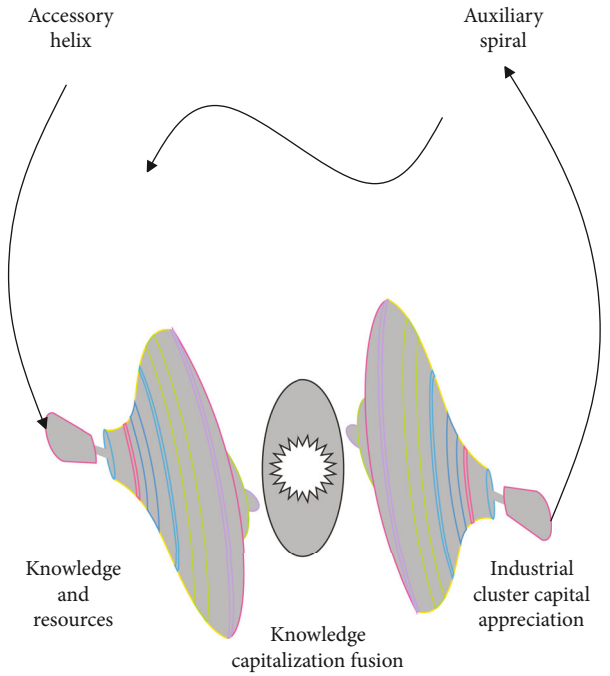

Figure 4: Process model of the knowledge capitalization of entrepreneurial talents to promote the technological upgrading of industrial clusters.

It can be seen that S_{CEAB} is positively correlated with the respective incomes of both parties. It shows that when other conditions remain the same, the greater the α, β, the greater the probability that the initial state of the two parties will fall into the regional CEAB, so that the leading venture capital institution and the following venture capital institution are more likely to form a cooperation and win-win situation of supervision and active management.

Conclusion: the greater the profit ratio of the leading venture capital institution and the following venture capital institution, the easier it is to form a cooperation situation.

(2) When the following venture capital institution chooses opportunistic behavior, the influence of probability λ that is discovered on the cooperation strategy is as follows:

$$\begin{aligned} \frac{dS_{CEAB}}{d\lambda} &= \frac{R_2(R_1 + C - \beta\Delta V)}{2(\beta\gamma\Delta V - \beta\Delta V - \lambda R_2)^2} \\ &\quad + \frac{R_3(\alpha\gamma\Delta V - \alpha\Delta V - \lambda R_3) - R_3(C_0 - \lambda R_3)}{2(\alpha\gamma\Delta V - \alpha\Delta V - \lambda R_3)^2} > 0. \end{aligned} \tag{12}$$

It can be seen that S_{CEAB} is positively correlated with the probability λ of being discovered when the following venture capital institution chooses opportunistic behavior. It shows that under the circumstance that other conditions remain the same, the greater the λ, the greater the probability that the initial state of both parties will fall into the regional

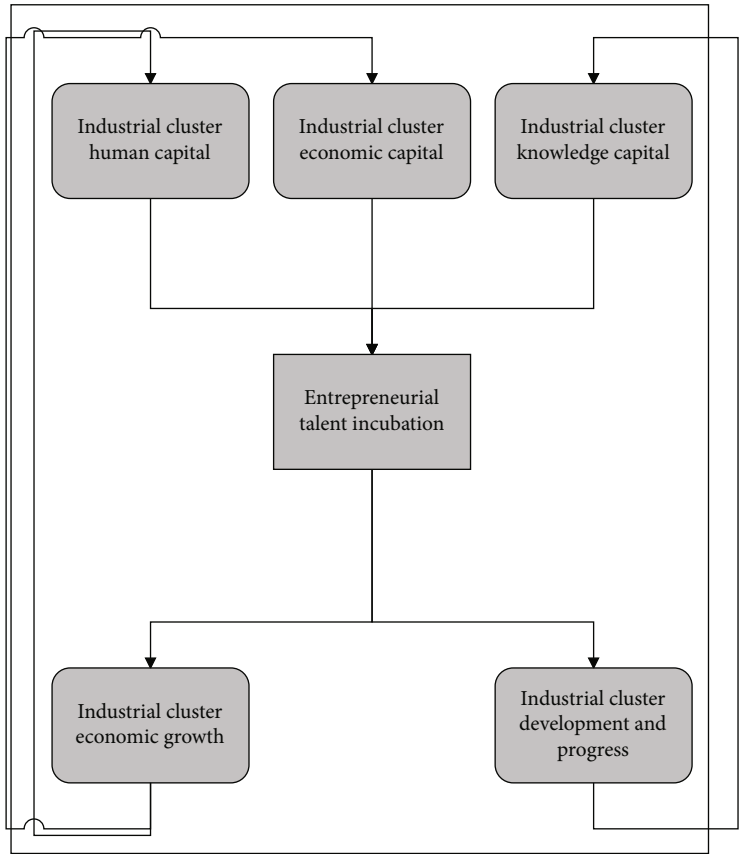

Figure 5: The structural model of the interaction model between entrepreneurial talents and industrial clusters.

CEAB, so that the leading venture capital institution and the following venture capital institution are more likely to form a cooperation and win-win situation of supervision and active management.

Conclusion: the greater the probability of finding opportunistic behavior, the easier it is to form a cooperative situation.

(3) The influence of the synergy coefficient γ of both parties on the cooperation strategy is as follows:

$$\frac{dS_{\mathrm{CEAB}}}{d\gamma} = \frac{\beta\Delta V(R_1 + C - \beta\Delta V)}{2(\beta\gamma\Delta V - \beta\Delta V - \lambda R_2)^2} + \frac{\alpha\Delta V(C_0 - \lambda R_3)}{2(\alpha\gamma\Delta V - \alpha\Delta V - \lambda R_3)^2} > 0. \tag{13}$$

It can be seen that S_{CEAB} is positively correlated with the synergy coefficient γ of both parties. It shows that under the condition that other conditions remain unchanged, the greater the γ, the greater the probability that the initial state of both parties will fall into the regional CEAB, so that the leading venture capital institution and the following venture capital institution are more likely to form a cooperation and win-win situation of supervision and active management.

Conclusion: the greater the synergy coefficient between the leading venture capital institution and the following venture capital institution, the easier it is to form a cooperation situation.

(4) The influence of the leading venture capital institution's regulatory costs C_0 on cooperation strategies and the leading venture capital institution is as follows:

$$\frac{dS_{\mathrm{CEAB}}}{dC_0} = -\frac{1}{2(\alpha\gamma\Delta V - \alpha\Delta V - \lambda R_3)} < 0. \tag{14}$$

It can be seen that S_{CEAB} is negatively related to the regulatory cost C_0 of the leading venture capital institution. It shows that under the circumstance that other conditions remain unchanged, the larger the C_0, the smaller the probability that the initial state of the two parties will fall in the regional CEAB, so that the leading venture capital institution and the following venture capital institution are less likely to form a cooperation and win-win situation of supervision and active management.

Conclusion: the lower the cost of supervision of the leading venture capital institution, the easier it is to form a cooperation situation.

(5) The influence of the active management cost C of the following venture capital institution on the cooperation strategy is as follows:

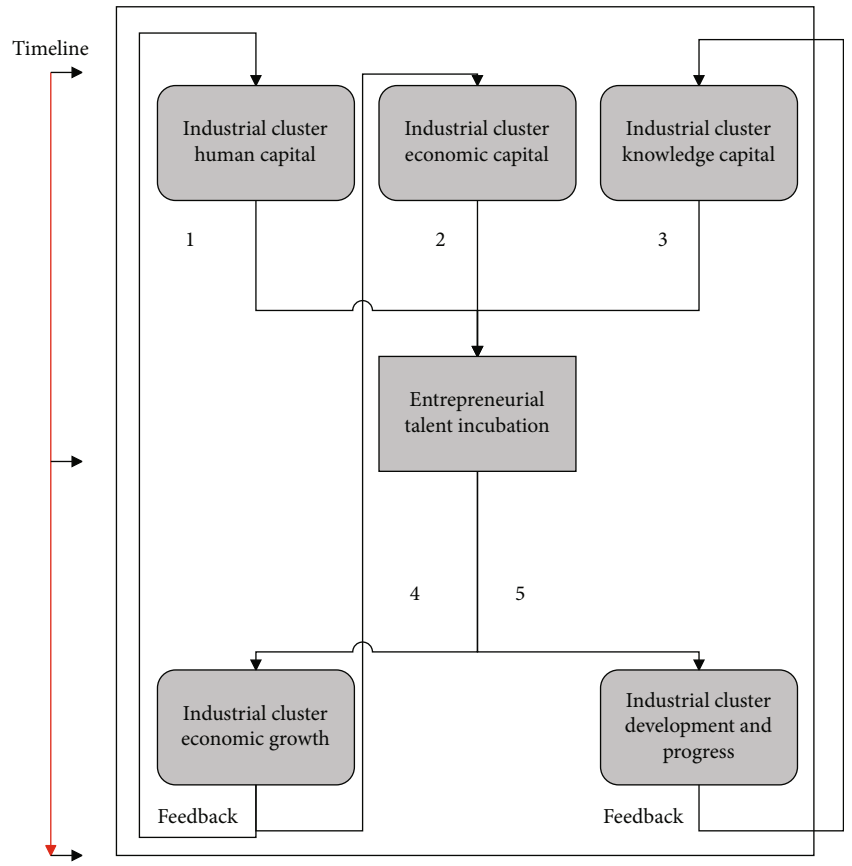

Figure 6: Test results of the interactive structure model between entrepreneurial talents and industrial clusters.

$$\frac{dS_{\mathrm{CEAB}}}{dC} = -\frac{1}{2(\beta\gamma\Delta V - \beta\Delta V + \lambda R_2)} < 0. \tag{15}$$

It can be seen that S_{CEAB} is negatively related to the active management cost C of the following venture capital institution. It shows that under the circumstance that other conditions remain unchanged, the larger the C, the smaller the probability that the initial state of the two parties will fall in the regional CEAB, so that the leading venture capital institution and the following venture capital institution are less likely to form a cooperation and win-win situation of supervision and active management.

Conclusion: the lower the active management cost of the following venture capital institution, the easier it is to form a cooperation situation.

(6) The influence of the following venture capital institution's additional profits R_1 brought by opportunistic behavior on the cooperation strategy is as follows:

$$\frac{dS_{\mathrm{CEAB}}}{dR_1} = -\frac{1}{2(\beta\gamma\Delta V - \beta\Delta V + \lambda R_2)} < 0. \tag{16}$$

It can be seen that S_{CEAB} is negatively correlated with the following venture capital institution's additional profits R_1 brought by opportunistic behavior. It shows that under the circumstance that other conditions remain unchanged, the larger the R_1, the smaller the probability that the initial state of the two parties will fall in the regional CEAB, so that the leading venture capital institution and the following venture capital institution are less likely to form a cooperation and win-win situation of supervision and active management.

Conclusion: the lower the additional benefits brought by opportunistic behavior, the easier it is to form a cooperative situation.

(7) The influence of the loss of profits R_2 on the cooperation strategy when the opportunistic behavior of the following venture capital institution is discovered is as follows:

$$\frac{dS_{\mathrm{CEAB}}}{dR_2} = -\frac{1}{2(\beta\gamma\Delta V - \beta\Delta V + \lambda R_2)} > 0. \tag{17}$$

It can be seen that S_{CEAB} is positively correlated with the loss of profits R_2 when the following venture capital institution's opportunistic behavior is discovered. It shows that under the circumstance that other conditions remain unchanged, the greater the R_2, the greater the probability that the initial state of both parties will fall into the regional CEAB, so that the leading venture capital institution and the following venture capital institution are more likely to form

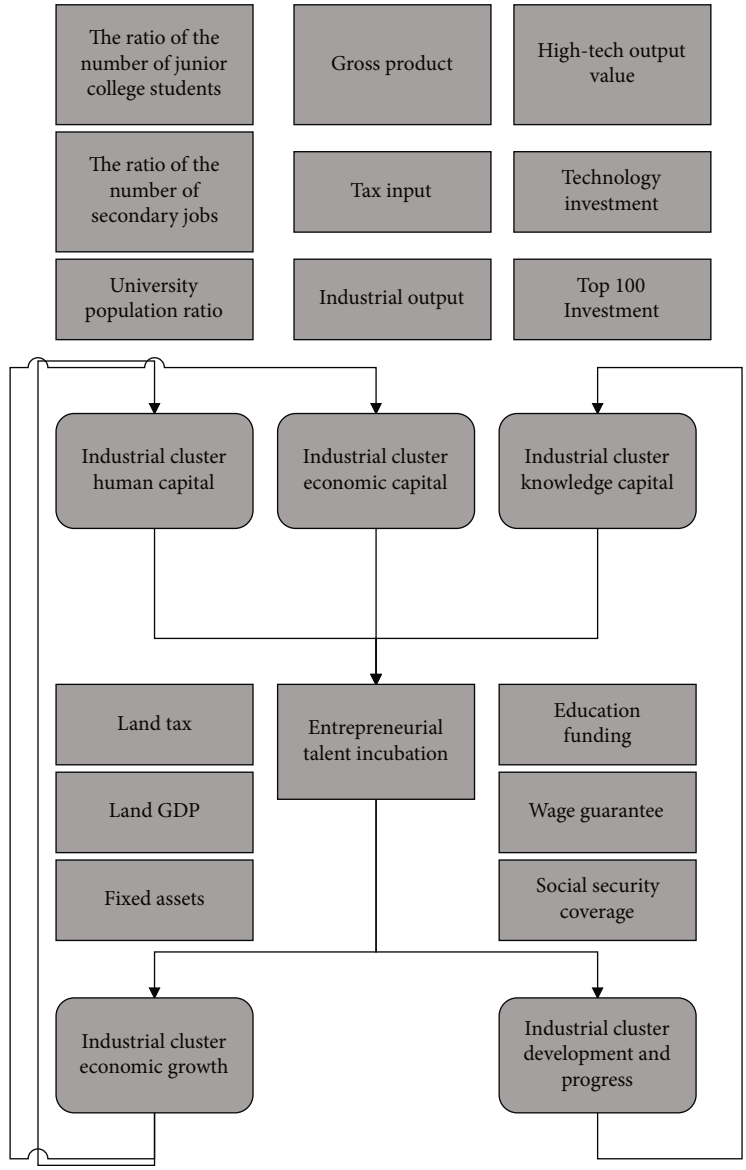

Figure 7: Simulation structure model.

a cooperation and win-win situation of supervision and active management.

Conclusion: the greater the loss when the opportunistic behavior of the following venture capital institution is discovered, the easier it is to form a situation of cooperation.

(8) The influence of fines R_3 collected by the leading venture capital institutions for discovering opportunistic behaviors of the follow-type venture capital institution on cooperation strategies is as follows

$$\frac{dS_{\mathrm{CEAB}}}{dR_3} = \frac{\lambda(\alpha\gamma\Delta V - \alpha\Delta V - \lambda R_3) - \lambda(C_0 - \lambda R_3)}{2(\alpha\gamma\Delta V - \alpha\Delta V - \lambda R_3)^2} > 0. \quad (18)$$

It can be seen that S_{CEAB} is positively correlated with the fine R_3 collected by the leading venture capital institution for discovering opportunistic behaviors of the following venture capital institution. It shows that under the circumstance that other conditions remain the same, the larger the R_3, the greater the probability that the initial state of the two parties will fall into the regional CEAB, and thus, the leading venture capital institution and the following venture capital institution are more likely to form a cooperation and win-win situation of supervision and active management.

Conclusion: the more fines the leading venture capital institution charges for the following opportunistic behavior, the easier it is to form a cooperative situation.

Table 1: Statistical table of the effect of the entrepreneurial dynamic model on data processing of entrepreneurial factors.

No.	Entrepreneurship data analysis	No.	Entrepreneurship data analysis	No.	Entrepreneurship data analysis
1	92.7	30	86.4	59	86.7
2	84.3	31	92.8	60	79.7
3	87.8	32	93.6	61	92.5
4	81.3	33	80.8	62	87.4
5	84.0	34	83.3	63	84.3
6	80.3	35	88.8	64	81.1
7	84.9	36	84.0	65	88.7
8	90.0	37	89.4	66	88.5
9	83.5	38	90.3	67	80.6
10	92.0	39	82.4	68	87.5
11	79.6	40	79.8	69	89.3
12	86.9	41	80.0	70	87.0
13	85.0	42	84.9	71	82.8
14	86.9	43	82.1	72	90.1
15	92.9	44	92.6	73	79.3
16	89.0	45	87.3	74	90.9
17	93.2	46	86.7	75	93.2
18	91.7	47	84.7	76	90.5
19	90.4	48	87.2	77	80.7
20	81.9	49	84.8	78	88.9
21	87.4	50	82.8	79	92.7
22	84.8	51	93.3	80	91.8
23	92.4	52	92.2	81	93.3
24	80.5	53	82.3	82	82.5
25	81.5	54	90.7	83	81.1
26	87.1	55	93.1	84	88.4
27	92.2	56	90.6	85	88.3
28	83.8	57	82.8	86	80.8
29	83.3	58	86.0	87	80.9

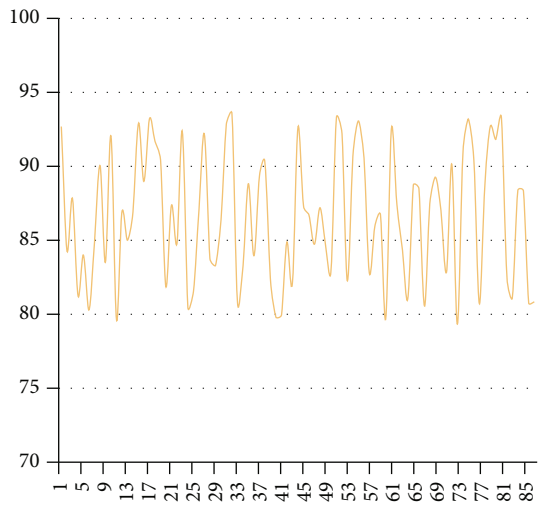

Figure 8: Statistical diagram of the effect of the entrepreneurial dynamic model on data processing of entrepreneurial factors.

In condition 7, the system has no evolutionary stable solution. The evolutionary game phase diagram is shown in Figure 3.

It can be seen from Figure 3 that there is no evolutionary stable solution in the four quadrants. Therefore, the entire system will be in constant change.

4. Entrepreneurship Dynamic Model Construction

Entrepreneurial talents gather the knowledge competitiveness of industrial clusters, transform capital competitiveness, and promote the development of industrial clusters in a process similar to the way in which auxiliary spirals and auxiliary spirals function in the natural world. There are two kinds of spirals in meteorology. One kind of spirals accumulates matter centripetally and gathers a large amount of energy at the tip of the spiral to form matter fusion. This is called auxiliary spiral; the other is to separate matter and energy. The spiral cone tip is released through the

Table 2: Statistical table of the entrepreneurial analysis effect of the entrepreneurial dynamic model.

No.	Entrepreneurial effect	No.	Entrepreneurial effect	No.	Entrepreneurial effect
1	69.4	30	82.5	59	73.6
2	84.4	31	83.0	60	89.5
3	79.1	32	77.9	61	69.6
4	84.9	33	82.3	62	74.1
5	88.1	34	90.8	63	69.0
6	72.0	35	86.7	64	72.2
7	68.8	36	72.6	65	82.0
8	68.5	37	88.1	66	75.4
9	80.8	38	71.3	67	79.9
10	73.6	39	89.6	68	68.2
11	72.4	40	69.4	69	74.0
12	85.5	41	76.7	70	71.6
13	76.8	42	73.7	71	69.2
14	85.4	43	80.0	72	80.0
15	74.7	44	69.0	73	86.5
16	72.8	45	71.5	74	74.7
17	84.5	46	78.2	75	75.7
18	86.5	47	87.8	76	90.4
19	70.8	48	77.7	77	69.3
20	68.9	49	77.3	78	76.6
21	69.0	50	89.6	79	77.5
22	87.3	51	72.7	80	83.0
23	72.5	52	76.8	81	83.2
24	86.3	53	68.8	82	86.1
25	70.6	54	77.2	83	85.9
26	83.5	55	86.3	84	85.2
27	85.2	56	83.2	85	68.6
28	86.8	57	89.7	86	80.2
29	77.0	58	83.5	87	78.3

centrifugal rotation orbit, which is called the auxiliary scattered spiral.

There is no pure auxiliary spiral or pure auxiliary spiral in nature. If there is material or energy spiraling in from the periphery of the spiral, there must be an equal amount of energy spiraling out from the tip of the spiral. It is the focus of qualitative energy and the gate of qualitative change of matter. This phenomenon is similar to the process of entrepreneurial talent incubation to promote the development of industrial clusters. In the interactive model of industrial clusters and entrepreneurial talents, the two precession spirals of industrial cluster development and entrepreneurial talent incubation share a spiral tip, in which entrepreneurial talents accumulate knowledge. It forms a complementary spiral with resources and realizes the capitalization transformation at the tip of the cone. After the capitalization transformation, knowledge and resources can be more widely recognized by other individuals and then form a complementary spiral through a wide range of knowledge spillovers within the industrial cluster. Finally, it spreads among other individuals in the cluster and drives the overall development of the cluster. The developed cluster can better support the accumulation of material and energy for entrepreneurial talents to generate a complementary spiral.

The process model is shown in Figure 4.

In order to more clearly define regional development and progress and economic growth, this study combines existing empirical research in this area and summarizes the promotion of entrepreneurial talents on industrial clusters into two aspects: capital appreciation and noncapital factors. In terms of entrepreneurial talents regarding the economic growth of regional development, entrepreneurial talent is a group that seeks to maximize profits and can discover the profit space and entrepreneurial opportunities in the market. In terms of noncapital factors (economic development), entrepreneurial talent can drive the region. The self-realization process of internal individuals brings new knowledge and technology to industrial clusters, promotes the diversified development of market technology, and promotes regional knowledge spillover and technology diffusion. A thorough consideration of these two aspects can systematize the relationship between entrepreneurial talents

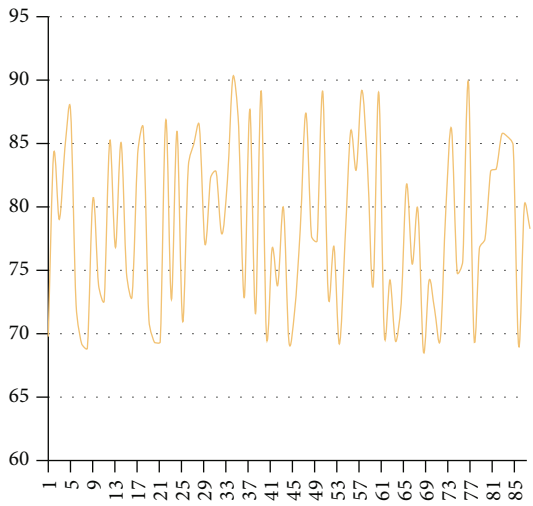

Figure 9: Statistical diagram of the entrepreneurial analysis effect of the entrepreneurial dynamic model.

and the development of industrial clusters. Hypothesis a: there is a positive correlation between entrepreneurial talent incubation and the economic growth of high-tech industrial clusters. Hypothesis b: there is a positive correlation between entrepreneurial talent incubation and the economic growth of traditional industrial clusters. Hypothesis 2a: there is a positive relationship between entrepreneurial talent incubation and the development and progress of high-tech industrial clusters. Correlation hypothesis 2b: there is a positive correlation between entrepreneurial talent incubation and the development and progress of traditional industrial clusters.

The interactive system of entrepreneurial talents and industrial clusters includes three components. The first is the economic capital, human capital, and knowledge capital of industrial clusters. This level of factors constitutes the foundation for the incubation of entrepreneurial talents. The second layer is the incubation of entrepreneurial talents, and the third layer is the economic growth of industrial clusters and the overall development and progress of industrial clusters. The model construction is shown in Figure 5.

Through the machine learning algorithm constructed in this paper, the size of the entrepreneurial equilibrium value and the relationship between the entrepreneurial equilibrium value and the economic development level of the industrial cluster can be obtained. It can be seen that hypothesis a passes the test and hypothesis b fails the test. Therefore, the test result of the interactive structure model of entrepreneurial talents and industrial clusters is shown in Figure 6.

After the input and output variables are determined, this research studies the construction model of the double helix interaction hypothesis between industrial clusters and entrepreneurial talents. Since previous studies have also pointed out that the contribution of entrepreneurial talents varies from region to region with different development models, and industrial clusters with different development models have different influencing factors when interacting with entrepreneurial talents. Therefore, before proceeding with the interaction hypothesis, this study classifies the development models of industrial clusters. The simulation structure model diagram is shown in Figure 7.

5. Performance Verification of the Entrepreneurial Dynamic Model Based on Improved Machine Learning

This paper constructs the entrepreneurial dynamic model based on the improved machine learning algorithm and evaluates the performance of the constructed system after constructing the entrepreneurial dynamic model. Since the entrepreneurial dynamic model requires a large number of entrepreneurial factor analysis data, this paper inputs a large number of factor analysis data through simulation software, and the results obtained are shown in Table 1 and Figure 8.

From the above analysis, it can be seen that the system constructed in this paper has a stable performance in the data analysis of entrepreneurial factors. On this basis, the entrepreneurial analysis effect of the entrepreneurial dynamic model is evaluated. The results are shown in Table 2 and Figure 9.

From the above analysis results, it can be seen that the entrepreneurial dynamic model constructed in this paper can basically meet the basic needs of entrepreneurial analysis.

6. Conclusion

The economic environment, entrepreneurial conditions, and the stock and flow of intellectual capital of industrial clusters are important determinants that affect the incubation of entrepreneurial talents. Previously, many scholars conducted research on entrepreneurial talents in the context of the country, rather than in specific industrial clusters. This paper combines improved machine learning algorithms to construct a dynamic model of entrepreneurship. Moreover, in response to the opportunistic behavior of following venture capital institutions under joint investment, this paper constructs an evolutionary game model between leading venture capital institutions and following venture capital institutions under joint investment. In addition, by solving the dynamic replication equation and the evolutionary stability strategy, this paper constructs the system model according to the actual investment situation. Finally, after constructing the model, this article analyzes the system performance through simulation. From the research and results, it can be seen that the entrepreneurial dynamic model constructed in this article has a certain effect.

Data Availability

The labeled dataset used to support the findings of this study are available from the corresponding author upon request.

Conflicts of Interest

The authors declare no competing interests.

Acknowledgments

This study is sponsored by 2020 Special Project of Humanities and Social Sciences of Shaanxi Provincial Education Department: "Research on the Evaluation of Innovation and Entrepreneurship Ecosystem Based on Grey Association Law - Take Xi'an City as an Example" (20JK0046).

References

[1] J. Albrecht, M. Robayo-Abril, and S. Vroman, "Public-sector employment in an equilibrium search and matching model," *The Economic Journal*, vol. 129, no. 617, pp. 35–61, 2019.

[2] P. Barbieri, R. Bozzon, S. Scherer, R. Grotti, and M. Lugo, "The rise of a Latin model? Family and fertility consequences of employment instability in Italy and Spain," *European Societies*, vol. 17, no. 4, pp. 423–446, 2015.

[3] C. Barnard, "EU employment law and the European social model: the past, the present and the future," *Current Legal Problems*, vol. 67, no. 1, pp. 199–237, 2014.

[4] G. R. Bond and R. E. Drake, "Making the case for IPS supported employment," *Administration and Policy in Mental Health and Mental Health Services Research*, vol. 41, no. 1, pp. 69–73, 2014.

[5] G. R. Bond, S. J. Kim, D. R. Becker et al., "A controlled trial of supported employment for people with severe mental illness and justice involvement," *Psychiatric Services*, vol. 66, no. 10, pp. 1027–1034, 2015.

[6] M. Bornay-Barrachina, A. López-Cabrales, and R. Valle-Cabrera, "How do employment relationships enhance firm innovation? The role of human and social capital," *The InTernaTIonal Journal of human resource managemen T*, vol. 28, no. 9, pp. 1363–1391, 2017.

[7] J. H. Fede, K. S. Gorman, and M. E. Cimini, "Student employment as a model for experiential learning," *The Journal of Experimental Education*, vol. 41, no. 1, pp. 107–124, 2018.

[8] P. Frijters, D. W. Johnston, and M. A. Shields, "The effect of mental health on employment: evidence from Australian panel data," *Health Economics*, vol. 23, no. 9, pp. 1058–1071, 2014.

[9] U. Huws, N. H. Spencer, and D. S. Syrdal, "Online, on call: the spread of digitally organised just-in-time working and its implications for standard employment models," *New Technology, Work and Employment*, vol. 33, no. 2, pp. 113–129, 2018.

[10] F. Latorre, D. Guest, J. Ramos, and F. J. Gracia, "High commitment HR practices, the employment relationship and job performance: a test of a mediation model," *European Management Journal*, vol. 34, no. 4, pp. 328–337, 2016.

[11] C. C. Lo and T. C. Cheng, "Race, employment disadvantages, and heavy drinking: a multilevel model," *Journal of Psychoactive Drugs*, vol. 47, no. 3, pp. 221–229, 2015.

[12] L. Lynas, "Project ABLE (autism: building links to employment): a specialist employment service for young people and adults with an autism spectrum condition," *Journal of Vocational Rehabilitation*, vol. 41, no. 1, pp. 13–21, 2014.

[13] T. Marshall, R. W. Goldberg, L. Braude et al., "Supported employment: assessing the evidence," *Psychiatric Services*, vol. 65, no. 1, pp. 16–23, 2014.

[14] C. Dillahunt-Aspillaga, R. Nakase-Richardson, T. Hart et al., "Predictors of employment outcomes in veterans with traumatic brain injury: a VA traumatic brain injury model systems study," *Journal of Head Trauma Rehabilitation*, vol. 32, no. 4, pp. 271–282, 2017.

[15] L. Ottomanelli, S. Barnett, L. Goetz, and R. Toscano, "Vocational rehabilitation in spinal cord injury: what vocational service activities are associated with employment program Outcome?," *Topics in Spinal Cord Injury Rehabilitation*, vol. 21, no. 1, pp. 31–39, 2015.

[16] F. Portella-Carbo, "Effects of international trade on domestic employment: an application of a global multiregional input–output supermultiplier model (1995–2011)," *Economic Systems Research*, vol. 28, no. 1, pp. 95–117, 2016.

[17] M. Shirmohammadi, M. Beigi, and J. Stewart, "Understanding skilled migrants' employment in the host country: a multidisciplinary review and a conceptual model," *The International Journal of Human Resource Management*, vol. 30, no. 1, pp. 96–121, 2019.

[18] D. Tavani and L. Zamparelli, "Endogenous technical change, employment and distribution in the Goodwin model of the growth cycle," *Studies in Nonlinear Dynamics & Econometrics*, vol. 19, no. 2, pp. 209–216, 2015.

[19] G. Topa, C. M. Alcover, J. A. Moriano, and M. Depolo, "Bridge employment quality and its impact on retirement adjustment: a structural equation model with SHARE panel data," *Economic and Industrial Democracy*, vol. 35, no. 2, pp. 225–244, 2014.

[20] C. Topsakal, "Policy on teacher employment model in Turkey: contracted teachers," *International Journal of Educational Methodology*, vol. 5, no. 4, pp. 671–682, 2019.

[21] E. Totty, "The effect of minimum wages on employment: a factor model approach," *Economic Inquiry*, vol. 55, no. 4, pp. 1712–1737, 2017.

[22] S. Van de Walle, B. Steijn, and S. Jilke, "Extrinsic motivation, PSM and labour market characteristics: a multilevel model of public sector employment preference in 26 countries," *International Review of Administrative Sciences*, vol. 81, no. 4, pp. 833–855, 2015.

[23] J. F. Wen and D. V. Gordon, "An empirical model of tax convexity and self-employment," *Review of Economics and Statistics*, vol. 96, no. 3, pp. 471–482, 2014.

Hindawi
Journal of Sensors
Volume 2021, Article ID 7927415, 11 pages
https://doi.org/10.1155/2021/7927415

Research Article

Dance Movement Recognition Technology Based on Multifeature Information Fusion

Xin Liu[1] **and Jiazhe Hu**[2]

[1]*Sports Art Institute, Harbin Sport University, Harbin, 150008 Heilongjiang, China*
[2]*Academic Affairs Office, Harbin Sport University, Harbin, 150008 Heilongjiang, China*

Correspondence should be addressed to Xin Liu; liuxin125228@cau.ac.kr

Received 11 August 2021; Revised 17 September 2021; Accepted 28 September 2021; Published 22 October 2021

Academic Editor: Mu Zhou

Multifeature data integration technology uses computer technology to automatically analyze and process the observation data obtained by multiple sensors in chronological order according to a defined threshold. And it can complete the necessary decision-making and evaluation tasks in the data processing process. This article is aimed at studying the effect of multifeature information fusion on dance movement recognition technology. The article mainly adopts the principle of structural risk mitigation and the image thresholding method to effectively obtain the binarized image of the dancer's moving image, so as to select an appropriate threshold, use the threshold as its distinguishing standard, and then segment the pixel threshold. The method of multifeature information fusion and dance movement recognition technology is introduced. The performance of image classification algorithms is compared, and the experiment of dance video movement, human behavior recognition, and gait phase recognition are carried out. The experimental data show that in the power identification algorithm of this article, when the peak value is 1000 bits, the experimental data is 256 bits, the analysis and comparison data is 457 bits, and the experimental environment is 812 bits. When the peak value is 2000 bits, the experimental data is 451 bits, the analysis and comparison data is 635 bits, and the experimental environment is 947 bits. The experimental data is 562 bits, the analysis and comparison data is 546 bits, and the experimental environment is 774 bits. The experimental results show that the dance action recognition technique based on multifeature information fusion is studied well.

1. Introduction

In recent years, action recognition has become a hotspot in computer vision research. And it has greatly research value. Scholars and research institutions at home and abroad have done a lot of research and achieved great success. However, there are few researches on the application of motion recognition technology in dance videos. The main reason is that the complexity of human movements in dance videos is quite high. At the same time, there is still a problem to be solved in dance. This reduces the accuracy of motion perception; so, the development of motion detection and recognition in dance videos is relatively slow. With the continuous development of multi feature data integration technology and sensor based human behavior recognition technology, it is developed rapidly and widely used in motion detection and other fields. Sensor-based methods can better reflect the nature of motion and have excellent advantages in portability, cost, and ease of maintenance. Although sensor-based human behavior recognition has made great progress in various fields, there are still some important issues need to be resolved, such as the possibility of exporting in a more efficient way and how to make a high-precision, low-complexity classifier.

With the development of computer technology, human-computer interaction is constantly innovating. From the traditional mouse and keyboard to the popular touch screen to the advanced voice control technology, human-computer interaction technology is becoming more human than traditional human-computer interaction. Gesture interaction has the advantage of nontouch functionality. Therefore, it is very important for human computer interaction technology

research to be based on gestures. In the 21st century, mobile phones have entered a period of rapid growth. With the rapid development of mobile phones and the emergence of smart phones, the mobile Internet has also emerged and developed rapidly. As the era of mobile Internet changes, most people mainly rely on touch screens to interact with their phones. Touch screen is a convenient and natural way of man-machine interaction. It is capable of using speech for human-computer interaction. Modern human-computer interaction based on speech interaction has become a research center. Say a word to a machine using voice commands and it will perform specific tasks that are more natural and in line with today's human interaction. This is due to improved computer performance and rapid advances in deep learning, voice, face, and gesture recognition. Computer vision and intelligent robotics are advancing even faster. And natural and effective human-computer interaction began to attract. The most effective and intelligent human-computer interaction is not just a machine for understanding human natural language but it also helps to understand human body language. Gestures are an important form of body language. Therefore, gesture interaction has become an indispensable part of intelligent human-computer interaction. With the rapid development of information technologies such as computers, communications, and the Internet, the importance of electronic information security has become more and more prominent than ever. The necessary prerequisite for system security is identity authentication. People register for network services, online shopping, and bank access. Money, consumer credit cards, e-government, finance, e-commerce, and other application fields require identification [1].

Many scholars at home and abroad have made their own judgments based on the research of dance movement recognition technology based on multifeature information fusion. Zhai uses the semantic inference and information transfer function of graph convolutional networks to mine and deduce the relationship between attribute features and dancer features and obtain more expressive action features, thereby achieving high-performance dance action recognition. The test and analysis results of the data set show that the algorithm can recognize dance movements, effectively improve the accuracy of dance movement recognition, and realize the dancer's movement correction function [2]. In view of the delay and energy consumption of terminal equipment caused by high-speed data transmission and calculation of virtual technology, Xu and Chu proposed a sports dance movement transmission scheme with equal power distribution on the uplink [3]. In order to improve the ranging accuracy and active measurement range based on peak discriminator (PD), Jie proposed a ranging method based on the differential time domain method (DTDM). We developed a mathematical model and concluded that the zero crossing sensitivity is an important factor affecting the DTDM ranging error. In addition, the zero crossing sensitivity is determined by the delay time [4]. Lee et al. need to conduct prospective studies using standardized injury and exposure measures to consolidate our understanding of the incidence of injuries and risk factors related to musculoskeletal injuries among preprofessional dancers. The purpose of their research was to investigate the incidence of injuries among preprofessional dancers attending a full-time training school in New Zealand. The secondary purpose of this study is to investigate the relationship between dance exposure and injury risk, as well as the relationship between risk factors (especially the MCS result score) and injury risk [5]. Jeon's research compares the effects of positive and negative feedback on dance students. 28 female students took 60 lessons in two weeks and learned Jangguchu, a traditional Korean inspiration. Half of the students received positive feedback on their performance in the learning phase, while the other half received negative feedback [6]. Byczkowska-Owczarek's article introduces examples of culture, dance, and body in the field of communication (with self, community, God), social hierarchy, social values, relationship between individuals and groups, and relationships between people from the perspective of dance sociology. Sociological perspectives also indicate the various historical and ritual, controlling and regulating roles played by traditional and modern dances in the communities where they appeared and performed [7]. Liu researched line dance moving target detection technology based on machine vision to improve target detection. For this reason, the frame difference of the improved background modeling technology is combined with the target detection algorithm. Extract moving targets and perform postmorphological processing to make target detection more accurate. On this basis, the tracking target is determined on the time axis of the moving target tracking stage, the position of the target in each frame is found, and the most similar target is found in each frame of the video sequence [8].

The above scholars do not have a comprehensive understanding of multifeature information fusion and virtual technology. Therefore, this paper makes a far-reaching study on dance movement recognition technology on the basis of the above scholars' views and makes a prospect for the future development of dance movement recognition technology based on multifeature information fusion.

2. Dance Movement Recognition Technology Based on Multifeature Information Fusion Method

2.1. Multifeature Information Fusion. The multifeature recognition technology of human motion is widely used in many fields such as intelligent video surveillance. Video content retrieval has high research value and is a very difficult and popular research topic in the field of computer vision. This article discusses the two key aspects of deep recognition of human actions from the current research and development status at home and abroad and how to recognize existing actions, by examining the combination of multiple features such as action representation and action classification, and the motion attributes describe the motion information of the object [9]. And it is generally regarded as a necessary feature in the isolation feature of action recognition. The optical flow method is often used to extract motion

information. Abstract luminous flux refers to the instantaneous speed of an object due to changes in surface pixels when it is moving. Then, apply grayscale pixel ratio changes to dance videos. And the relationship between the pixels to be determined the position change of a single pixel, and the generation of luminous flux is generally caused by the movement of the camera. In this paper, the optical flow method is used to distinguish the movement attributes, and two descriptors are used: optical flow direction histogram and motion limit histogram [10, 11]. Optical flow direction histogram statistics, optical flow information, traffic limit histogram statistics, and optical flow tilt in two directions. Both of these data are based on optical flow calculations. Multibiological feature recognition technology improves the accuracy of overall decision-making by combining data provided by multiple biological features. The multibiological character recognition system has two ways to combine multiple identical biological traits and multiple different biological traits [12]. The multifeature recognition technology of human motion has a very wide range of uses. For example, it can be used for face recognition in traffic systems, filtering and screening of criminals, and attendance systems for schools and formulas. Since the biometric recognition process is actually the adopted biometric pattern recognition process, the pattern recognition can be roughly divided into attribute extraction, pattern matching, and decision-making [13]. Therefore, according to the degree of fusion, the fusion processing of multiple biological features can generally be divided into "feature layer fusion," that is, fusion-decision layer fusion. Gesture interaction also has some shortcomings and problems. Although it is convenient, it is also easy for users to expose their own information, which causes unnecessary trouble.

In the process of multitarget monitoring, data association is the key technology. Data association is the process of comparing the observation data received by the sensor with the known target part, and finally determining the correct observation/monitoring coupling, or create a new track. Most related methods include a method. The most common representative is the Joint Likelihood Data Link (JPDA) method [14]. The NN method is effective. The statistical distance is measured for the closest target prediction. Observation is the goal, and JPDA believes that all valid observations can come from the goal, but each valid observation has a different probability relative to the target, using a weighted sum of probabilities. The NN method is a statistical distance calculation. When JPDA calculates the relative probability, it only uses the data directly related to the calculation of the target state vector. The data can also receive additional information about the target and how to use other functions. This information is used to improve the effectiveness of the target link. In the active radar position, multitarget consistency is the only extended NN method, and it is still the most suitable algorithm in the machine. Biodiversity fusion recognition technology is a technology that combines multiple biological characteristic data to provide complete recognition. Data fusion technology is a new theory and technology for efficiently processing multisource data. Processed is by multiple sensors. It can obtain new and more complete information. These new data cannot be compared with a single sensor [15]. The main goal of data aggregation is to obtain more accurate data from a single input through aggregation.

2.2. Dance Movement Recognition Technology. The choreography of dancers is very different from the daily choreography of normal people. Many movements require the dancer's arms and legs to be brought together. When selecting the target area for background recognition, it is necessary to obtain the dancer's whole body motion data. The correct understanding of their behavior and the perception of dancers' movements can be divided into several categories: static characteristics, which are mainly manifested in size, color, body shape, depth, etc. [16, 17]. The target is of the dancer's face. It can convey comprehensive information about the dancer's movements, for example, through the dancer's shadow. You can draw the current basic shape. The dancer's movement path remembers these characteristics to calculate the nature of the dancer's movement direction. To create conditions for modeling, the characteristics of time and space are mainly expressed in descriptive ways, such as the shape of time and space and points of interest, such as dancers' scenes, surrounding objects, and gestures. Dance video image recognition takes into account the obstacles of dance background and clothing to motion recognition [18]. The movements must be memorized in order to accurately record and fully reflect the dancer's movement data, static data collection technology, and dancer's body movement data. From existing research, this document provides a specific memory method. These methods are suitable for the nature of dancers' movements, can accurately detect and recognize dancers' movements in dance images, improve the accuracy and efficiency of recognition, and have great value applications. Enter average trajectory, distance, direction of travel, and average speed to describe the trajectory of the target. First, each attribute area is grouped using the mean shift algorithm to retrieve potential traffic categories. More attribute fusion algorithms are designed to fuse the classification data by calculating the relationship between the categories in different attribute regions and finally get the clustering results of the data combination of multiple attribute regions [19]. This is because data integration occurs at the grouping level. Therefore, when combining at the spatial level, the problem of dimensional integration can be effectively avoided. The study of human behavior perception can be summarized into three levels according to the content of behavior from simple to complex: visual movement. There are mainly the following two problems: one is in the identification process [20]. Most of the information in the video action frame is repetitive or has little relevance to action recognition. This not only increases the computational complexity but also affects the accuracy of action recognition. Secondly, in the process of selecting and understanding attributes, the main method is to combine representation and posture features, but the choreography scenes and costumes are variable. And based on the nature of information gestures, it is easy to ignore the static state of the human body [21].

As a branch of human behavior perception, dance action recognition based on multifeature fusion has received extensive attention from research institutions at home and abroad and is widely used in many fields such as authentication. In exoskeleton robots and rehabilitation medical equipment, most of the current domestic and foreign researches use unobstructed indoor tents, and the collected plantar pressure data is also local plantar pressure data. Recognize the effective walking distance under complex road conditions, such as blind roads and grass. This article will introduce how to identify walking distance in complex road conditions and consider a combination of many features in terms of total tread pressure. An important issue in the study of data association algorithms is how to improve the quality of data association when multiple targets fly over. Because when multiple targets fly over, due to the influence of measurement noise and various interferences [22], the uncertainty of the measurement value is relatively serious, and related errors are prone to occur, leading to track exchange. Incorrect related results will cause serious consequences. Countless losses the effective way to solve this problem is to use multiple target feature information obtained from radar measurement data as a basis for judging whether the measurement is related to a known target. View the real and complete data acquisition method of ethnic dance movement records and use it as a guide for collecting dance data. At the same time, this article takes the creation of dance movements as an example to introduce the follow-up digitization of ethnic dance. Making models with national characteristics, it is supplemented by tying the bones and then connecting the role model with the action. The dance performance information and motion capture data drive the character model to create animation goals and improve the efficiency of animation production. It shows how to use dynamic technology to protect our country's art and dance culture. The use of motion technology to promote digital folk dance will bring positive social and economic benefits. The method of creating 3D dance data based on motion capture is the process of recording the actions of entities (dancers) and then mapping the recorded actions to virtual objects generated by the computer. The current motion capture systems are mainly divided into five types: mechanical motion capture systems, acoustic motion capture systems, electromagnetic motion capture systems, inertial motion capture systems, and optical motion systems. Optical motion capture technology is currently the most widely used and mature shooting technology [23]. The optical motion system uses optical principles to capture the 3D motion process as follows: first, the equipment detects errors, calibrates the camera, and determines the range of motion of the performer. At the same time, in order to facilitate collection and processing, performers are usually required to wear casual clothes and to stick reflector "marks" on key parts of the body. Multiple cameras are then used to capture the actor's movements through "marked" points on the body and images. In digital image processing, the binary image occupies a very important position. The binary image of the image greatly reduces the amount of data in the image, which can highlight the contour of the target [24]. The sequence is stored for analysis and processing, determining the signal points and calculating their spatial position at any given time and mathematically plotting the three-dimensional coordinates of each reflected signal. When the data is recognized by the computer, the data can be combined with the animation, the character can be combined into an animation, and then the animation can be easily edited into a computer-generated download.

2.3. Algorithm of Dance Action Recognition Technology Based on Multifeature Information Fusion. In the K-means algorithm, the final clustering effect is affected by the initial clustering center. The proposal of the K-means++ algorithm provides a basis for choosing a better initial clustering center. However, in the algorithm, the clustering categories are the number k still needs to be determined in advance. For a data set whose number of categories is unknown in advance, it will be difficult for K-means and K-means++ to accurately solve it. For this, some improved algorithms have been proposed to deal with the unknown number of clusters' k situation.

Image thresholding can effectively obtain the binarized image of the dancer's moving image, so as to select an appropriate threshold, use the threshold as its distinguishing standard, and then segment the pixel threshold [25]. The threshold usually takes the following form:

$$T = T[x, y, f(x, y), p(x, y)], \tag{1}$$

$$A_n = \frac{n+1}{\pi} \sum_{i=1}^{\text{image}} \sum U(i, \mu, \lambda)[V_{\min}(r, \theta)], \tag{2}$$

$$T = \{(x_1, y_1), (x_2, y_2), \cdots, (x_n, y_n) - \sum_{i=1}^{i} \alpha_j, \tag{3}$$

$$\min \frac{1}{2} \sum_{i=1}^{i} \sum_{j=1} y_i y_l \alpha_i K(x_1, x_i). \tag{4}$$

Select appropriate functions and appropriate parameters [26] and construct and solve the optimization problem, as shown in the following formula:

$$\text{st} \sum_{\text{j}=1}^{\text{i}} \text{y}_\text{i} \alpha_j = 0, 0 \le \alpha \le C, \tag{5}$$

$$\beta = y_j - \sum_{i=1}^{l} y_i \alpha_i^2 K(x_1 - x_2), \tag{6}$$

$$f(x) = \text{sgn}\left(\sum_{i=1}^{l} \alpha_2^1 y_i K(x, x_1) + b^2\right), \tag{7}$$

$$U(i, \mu, \gamma) = (x_1 - x_{i-1})^{\mu} (y_i - y_{i-1}). \tag{8}$$

The similarity measurement of dance moves is based on

Figure 1: Prospects of dance moves.

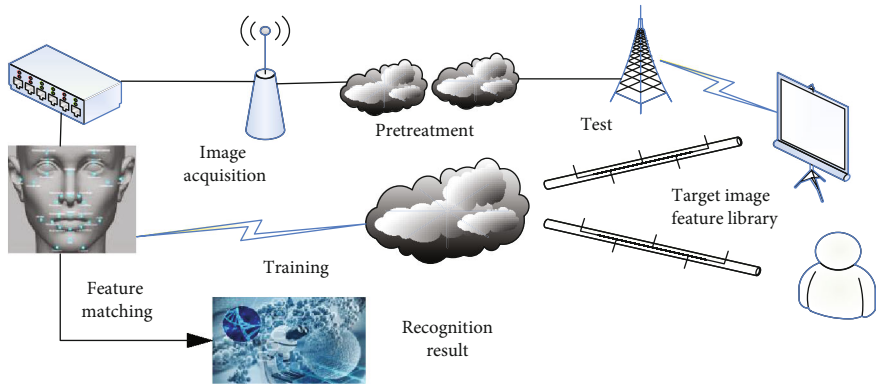

Figure 2: Action recognition system.

whether the directions of the vectors are similar [27], and the similarity coefficient can be expressed as

$$\cos(x,y) = x^t y / \left[\left(x^t x\right)\left(y^T y\right)\right]^{\frac{1}{2}}, \tag{9}$$

$$g(x,y) = \text{media}\{f(x-i,y-i)\}(i,j) \in W. \tag{10}$$

Adding formulas (9) and (10), the following formula will be obtained.

$$f(a,b) = 1 - \frac{2\sqrt{(a+1)} + (b+1)}{(a+1)+(b+1)} \times \frac{2\sqrt{(212-a)} + (256-b)}{(256-a)}. \tag{11}$$

After the period detection is performed on a video sequence, a normalization process can be performed [28], so that the period calculation is performed by using the distance from the center of mass to the outer contour of the human body. The calculation formula is

$$x_c = \frac{\sum_{x,y} xI(x,y)}{\sum_{x_1,y_2} I(x,y)}, \tag{12}$$

$$y_c = \frac{\sum_{x,y} yI(x,y)}{\sum_{x,y} I(x,y)}, \tag{13}$$

$$D_T(x,y) = \begin{cases} f_t(x,y), t=0 \\ \|f_t(x,y) - f_{t-1}(x,y)\|, t>o \end{cases}, \tag{14}$$

$$S = \sum_{i=1}^{n} \frac{Z_i Z_t}{2} + 1. \tag{15}$$

Recognizing the image of a given set of dance moves and minimizing the target, the objective function is obtained as follows:

$$\min \sum_{i,j} \frac{1}{2} \|y_i - y_t\|^2 S_i, \tag{16}$$

$$\arg\min = Av - i \times v^T A^T (L \otimes I_m), \tag{17}$$

$$\mu_i(X,c) = \frac{1/\|X-c\|^{2/(a-1)}}{\sum_{j=1}^{k} 1/\|X - X_1\|}. \tag{18}$$

Through the above formula, the average value formula of the video can be obtained:

$$g_c(X) = \max \sum_{i=1}^{2} \mu_1, \text{ then } X \in c, \tag{19}$$

$$Z = [z_1, z_2, .., z_k]^T, z_i = x_i + jy_1. \tag{20}$$

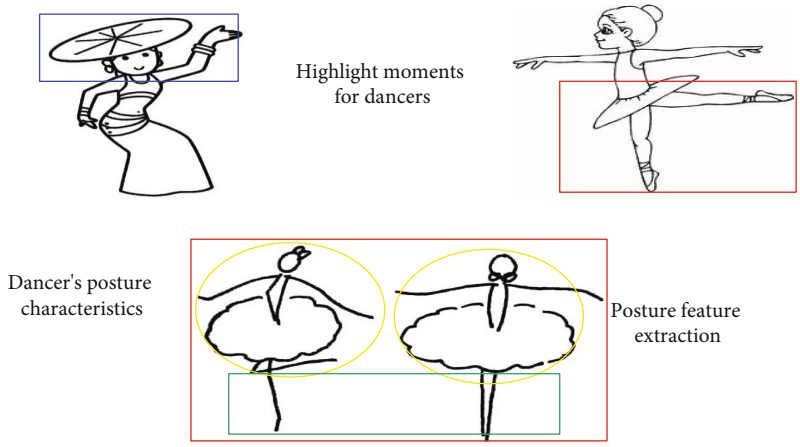

Figure 3: Change of dancer's movements.

3. Experiment of Dance Movement Recognition Technology Based on Multifeature Information Fusion

In the dance image, in addition to the dancer's first goal, there are many other backgrounds, such as space equipment, environment, and lighting. The existence of these different backgrounds increases the complexity of the scene. The first goal can be achieved by removing the background: the total area of the human body. This can reduce the difficulty of remembering actions. There is a lot of research on removing background. According to the particularity of the dance video image, this article chooses the Gaussian composite model, which can remove the background. After the calculation of the cycle, we can get the specific calculation method of the human body recognition technology, and through this method, the result corresponding to each technology can be detected.

3.1. Experimental Description and Experimental Strategy. This article focuses on the application and impact of motion recognition technology on video images. Especially for dance videos, this article divides grayscale, binary, and images into action video images and then calculates the 3DZemike interval of the processed binary image as the action classification feature. Then, the 3DZemike torque similarity factor is applied to the standard classification criteria, and finally, the KTH database and the A-go-go dance video database are classified and recognized by the SVM supporter, and good recognition is obtained. This research explores the vision-based video action recognition technology. This technology performs preprocessing tasks such as grayscale and background removal and reduces filters in the generated video dance images. Then, perform character actions in the video series. Next, use the SVM support engine to extract some fragments from the object attribute sample set for model learning and training. Then, after completing the training, perform action classification and other perception areas. The indepth application of computer-assisted teaching has not only enriched the teaching content. It also makes up for many shortcomings of traditional teaching methods. The

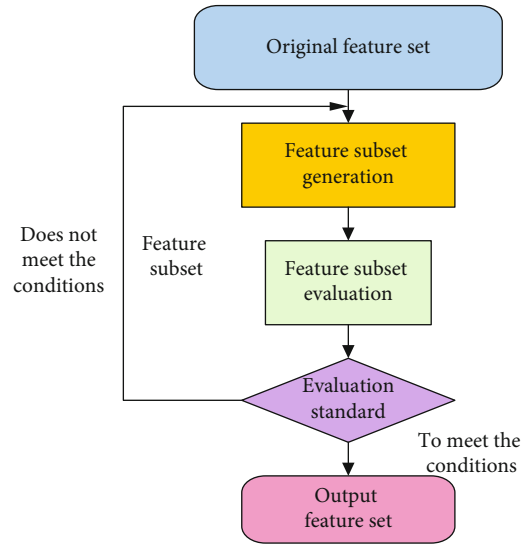

Figure 4: Feature selection process.

powerful combination of motion capture technology and dance teaching is a form of computer-assisted teaching. This creates a perfect fusion of 3D virtual world and augmented reality technology. "In recent years, researchers have conducted extensive research on the application of motion capture and described the technology of animation elements and the elimination of rolling steps in the animation production process." This shows that the use of motion capture technology is widespread, and dance is a body in sync with the rhythm of the movement, but learning to dance is not as easy as individual differences and rhythm. In order to improve this situation, the author recommends the use of motion capture technology to assist dance teaching and research and to transform dancers' 3D movement data into digital subtraction movements to create a three-dimensional foundation, as human movement data creation teaching cartoon is very important to change the disadvantages of traditional dance teaching. And it can improve the quality of education and teaching. GMM refers to the linear combination of multiple Gaussian distribution functions. In theory,

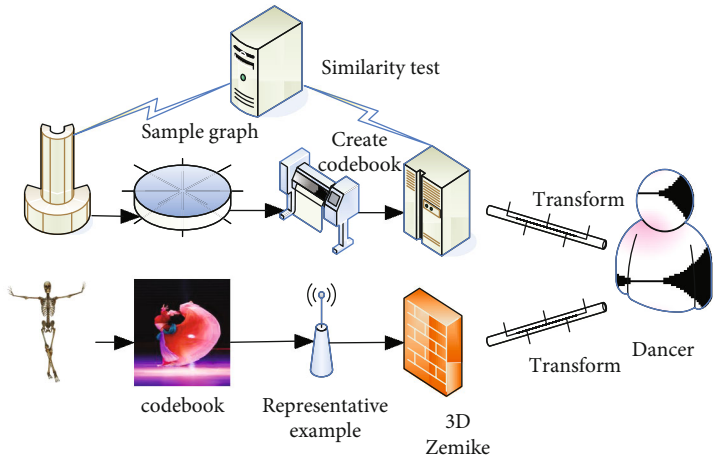

Figure 5: Cycle similarity measure.

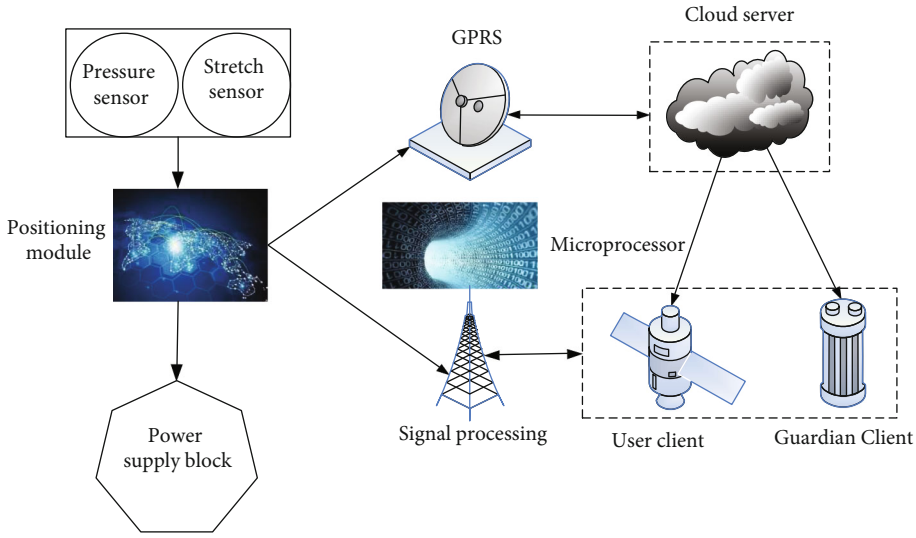

Figure 6: Dancer node recognition model.

GMM can fit any type of distribution. It is usually used to solve the situation where the data in the same set contains multiple different distributions.

3.2. Sample Collection. Understanding of human behavior in videos is the focus of computer research today. Its purpose is to isolate and analyze the actions in the video through image processing and various recognitions and classification techniques. Determining the actions of the characters in the video provides useful information for a variety of purposes. The key to recognizing human actions in the video is to rationally process the original video and export the video image attributes. Research on the integration of motion recognition technology and dance art has just started in China. Dance videos use human movement recognition technology, which can effectively identify rhythmic movements. Compare video actions with standard actions, you can evaluate the dancer's attitude and make suggestions on how to adjust. This is an advanced, high-intensity training. This paper proposes a method of grouping moving target trajectories based on the convergence of multiple attributes. Perform independent trajectory grouping for each attribute area to obtain a set of basic trajectory classification results and then combine these groups corresponding to each attribute category result area to avoid the problem of regional flatness. First, consider the characteristics of spatial location. Direction is angel of movement. The method of complete interpretation is the speed of the trajectory data and the trajectory data. This feature is convenient for better identification of the target. Aiming at the motion law of the target in the scene, the mean-shift method is used to group each trajectory area to realize the distribution of the trajectory area or trajectory. This is because the mode of distributing motion between feature gaps is partial. Finally, the grouping results between feature spaces can be combined to fully extract the motion distribution pattern in the trajectory data. The most

Table 1: Image classification algorithm performance comparison results.

Index	Algorithm	Traditional algorithm	Image classification algorithm
Peak signal-to-noise ratio/dB	21.3	13.6	23.5
Execution time/ms	20.6	21.5	24.1
Performance	2.2	3.6	5.6

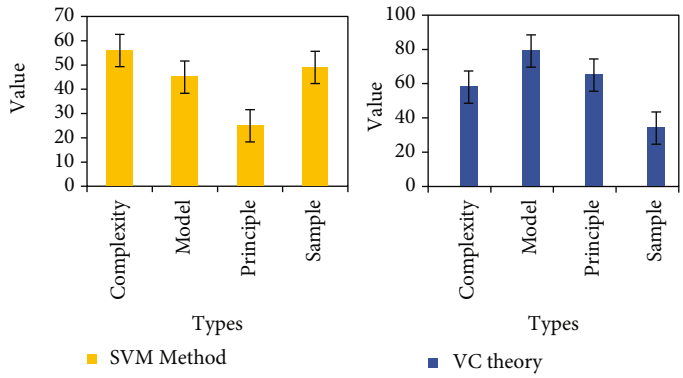

Figure 7: SVM method.

important of these is the environment and space equipment, which will affect the dance athlete's posture, movement performance, and angle estimation.

3.3. Experimental Data and Result Analysis. Normally, in many dance videos, the stage is mainly characterized by the prospect of the dancer as the main object. Different pixels in the video dance image are used to match the Gaussian model. If the match is successful, it can be regarded as a reference point. If the match fails, it can be judged as the first point to separate the background from the foreground, as shown in Figure 1:

Match the dance action features to be recognized with the images in the template library, as shown in Figure 2:

The stop level sensor can be used when using the gesture separation method. It is widely used in robot detection and motion vision to judge the movement direction of the dancer. The light flux value in the detection system can be used to filter the background information in the image to obtain the dancer's approximate coordinates. This removes the influence of factors such as "the dancer's shadow and clothes" and also affects the dancer's movements. Engineering robots are teleoperation multijoint manipulators or multi-degree-of-freedom robots that rely on their own power and control capabilities to perform engineering construction operations in high-risk and special environments. It not only has the advantages of high-power, multifunction, and wide application range of construction machinery but also has various functions such as flexible movement of robots, environment perception, and intelligent recognition. The dancer's posture is shown in Figure 3.

There are two main methods for feature selection attributes. How to directly select attributes and how to reduce the size and direct attribute selection methods that directly analyze the attributes, select the features that have

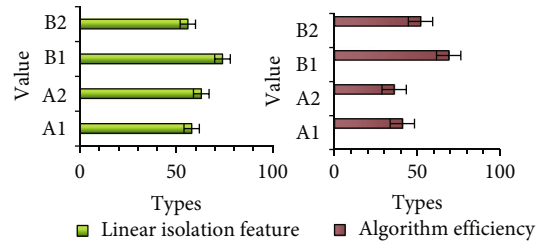

Figure 8: Kernel function.

the greatest impact on the ranking and memory results, and delete the attributes that have less impact on the classification results, as shown in Figure 4:

The codebook contains most of the representative examples in the example area. These examples can distinguish this category from other categories in this article. Use the cluster analysis method to create a codebook. First, define the similarity of each category to describe the similarity between the categories. This algorithm belongs to feature surface matching. Compared with terrain matching based on feature points and feature lines, theory and practice have proved that this algorithm has higher matching probability and matching accuracy. This document uses the 3DZemike period similarity metric to create a codebook, as shown in Figure 5:

Establishing dancer node recognition modeling can better recognize and help dancers better correct dance movements, as shown in Figure 6:

Through the comparison of the performance of image classification algorithms, we can see the results of each classification algorithm, as shown in Table 1:

The SVM method uses the VC dimension theory of statistical learning theory and the principle of structural risk

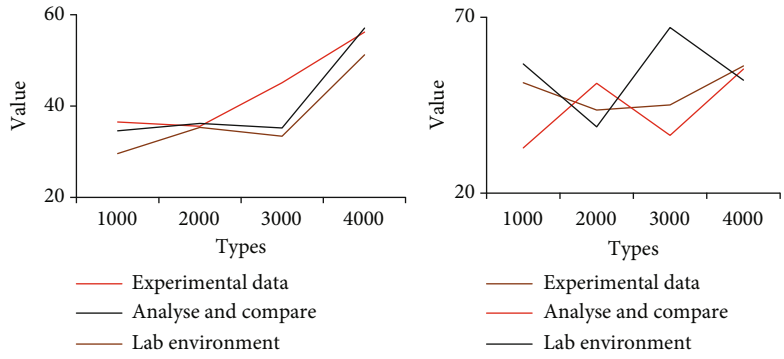

Figure 9: Power recognition algorithm.

mitigation. A limited data sample finds the best balance between model complexity and acquired learning ability. The basic idea to obtain the best generalized capacitance is to convert the input vector into high-dimensionality through a certain type of nonlinear mapping, and the feature region allows linear separation of nonlinear and traditional nonlinear isolated feature spaces, as shown in Figure 7:

The core function of the dance movement recognition technology based on multifeature information fusion is to match the linearly isolated feature area with the high-dimensional space and then proceed to the internal operation of the product. You can change the high-dimensional area. The inner product of the space is equivalent to the inner product of the original low-dimensional space. This greatly reduces the dimensionality of data processing and avoids spatial dimensionality and improves algorithm efficiency, as shown in Figure 8:

The efficiency of the power recognition algorithm in this paper has been confirmed in various video data sets. The main content is experimental data.

Video analysis and comparison are erimental environment, experimental design, and experimental results, as shown in Figure 9 and Table 2:

To test human behavior recognition and gait phase recognition in the same way, completely different experimental results can be obtained, as shown in Tables 3 and 4:

The experimental results of the dance video movement show that, during the action training process and the action test process, each process includes multiple feature extraction and description, as shown in Figure 10 and Table 5:

Table 2: Power recognition algorithm.

	1000	2000	3000
Experimental data	256	451	562
Analyse and compare	457	635	546
Lab environment	812	947	774

Table 3: Dance behavior recognition.

	Test data	Test result	Result analysis
Optimize feature classification	4517	5112	4365
Plantar pressure	561	442	324
Dance behavior recognition	28	17	32

Table 4: Human gait recognition.

	Test data	Test result	Result analysis
Optimize feature classification	254	352	411
Plantar pressure	2031	1459	1547
Human gait recognition	31	16	28

4. Discussion

In the passive positioning system, the target state carrier can be directly calculated by measuring DOA, TOA, and Doppler frequency. This is referred to below as target state measurement. The general target data reported here includes target state measurements. The working frequency pulse width and pulse repetition time are similar to the BPAF of the D2S hypothesis theory, and we put forward the concept of correlation. Correlation refers to the degree of correlation between the effective observation of the individual in the gateway and the actual target based on certain characteristic data. Evidence integration is the process of combining evidence into a new body of evidence within a framework. Evidence-based multifeature data integration refers to the combination of multifeature data based on effective observations in the gateway. The correlation degree of attribute data determines the correlation degree between each effective observation in the gateway and the actual target. Most of the images in the dance video are in color. If you directly enter the computer vision system without conversion, the amount of data input from the image increases. As a result, the amount of subsequent calculations is increased, and processing color images in grayscale videos can reduce the number of subsequent calculations and improve the efficiency of computer vision recognition operations. The gesture recognition method based on pattern matching mainly acquires

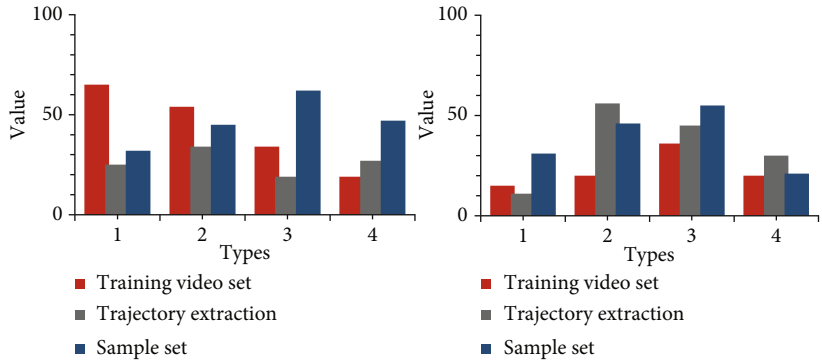

Figure 10: Video release rate.

Table 5: The main process of the experiment.

	Number	Results	Process
Construct a dictionary	1542	5321	1324
Quantitative training video	654	721	459
Video classifier	23	54	61

gesture patterns by learning different types of gesture data. The specific idea of this method is to match the previously learned gesture images with known patterns. The degree of similarity between the standards the process of dynamic gesture recognition can be divided into the following steps: first, the gesture is converted and simulated into a static gesture sequence. Then, the sequence of gestures to be recognized corresponds to the sequence of learning gestures and their similarities.

5. Conclusions

In the past few years, with the continuous development of computer vision, deep learning and human-computer interaction technology, which is more personalized than mouse and keyboard, have become a new research topic. And there are other technologies and more that are also applicable to humans, such as machine interaction, face detection, and face recognition. Human-computer interaction such as speech recognition and synthetic facial expression recognition, which is more mature than gesture recognition, human-computer interaction assessment, and examination, is indispensable in people's daily life and as one of the important components of modern human-computer interaction. Gesture recognition based on vision has also made great progress and become an important issue of people's attention. When using the gesture feature extraction method, gesture sensor can be used, which is widely used in the field of motion monitoring and robot vision, and can set the direction of the dancer's movements. The value of the image stream in the pose estimator can be used to filter the background data in the image to obtain the coordinate space of the dancer's joints.

Data Availability

The data that support the findings of this study are available from the corresponding author upon reasonable request.

Conflicts of Interest

The authors declare that they have no conflicts of interest.

Acknowledgments

Business Expense Project of Fundamental Scientific Research of Undergraduate Universities within Heilongjiang Province (2020KYYWF—FC08).

References

[1] Q. Wang, Y. Li, and X. Liu, "The influence of photo elements on EEG signal recognition," *Eurasip Journal on image and video processing*, vol. 2018, no. 1, 2018.

[2] X. Zhai, "Dance movement recognition based on feature expression and attribute mining," *Complexity*, vol. 2021, no. 21, Article ID 9935900, 2021.

[3] F. Xu and W. Chu, "Sports dance movement assessment method using augment reality and mobile edge computing," *Mobile Information Systems*, vol. 2021, no. 1, Article ID 3534577, 2021.

[4] J. Cao, Q. Hao, Y. Cheng et al., "differential time domain method improves performance of pulsed laser ranging and three-dimensional imaging," *Applied Optics*, vol. 55, no. 2, pp. 360–367, 2016.

[5] L. Lee, D. Reid, J. Cadwell, and P. Palmer, "Injury incidence, dance exposure and the use of the movement competency screen (MCS) to identify variables associated with injury in full-time pre-professional dancers," *International Journal of Sports Physical Therapy*, vol. 12, no. 3, pp. 352–370, 2017.

[6] H. J. Jeon, J. H. Baek, and S. An, "The effects of positive and negative feedback on dance learning," *International journal of Human Movement Science*, vol. 11, no. 2, pp. 49–58, 2017.

[7] D. Byczkowska-Owczarek, "Dance as a sign: discovering the relation between dance movement and culture," *Kultura i Społeczeństwo*, vol. 63, no. 3, pp. 63–74, 2020.

[8] L. Liu, "Moving object detection Technology of line dancing based on machine vision," *Mobile Information Systems*, vol. 2021, no. 2, Article ID 9995980, 2021.

[9] S. H. Malling, "Book review: dance/movement therapists in action: a working guide to research options (3rd edition)," *American Journal of Dance Therapy*, vol. 41, no. 1, pp. 133–135, 2019.

[10] H. Mcilveen, "Dance movement Psychotherapist's experience of their body image when working with an eating disorder client group: a feminist auto-ethnographic exploration," *European Eating Disorders Review*, vol. 24, no. 4, pp. E19–E19, 2016.

[11] S. W. Goodill, S. Chaiklin, and H. Wengrower, Eds., "Dance and creativity within dance/movement therapy: international perspectives. Routledge," *American Journal of Dance Therapy, 2021*, vol. 43, no. 1, pp. 1–5, 2021.

[12] B. Burger and P. Toiviainen, "See how it feels to move: relationships between movement characteristics and perception of emotions in dance," *Human Technology*, vol. 16, no. 3, pp. 233–256, 2020.

[13] E. L. Lydia, J. S. Raj, R. Pandi Selvam, M. Elhoseny, and K. Shankar, "Application of discrete transforms with selective coefficients for blind image watermarking," *Transactions on Emerging Telecommunications Technologies*, vol. 32, no. 2, 2021.

[14] R. D. Renard, "Creating the other requires defining Thainess against which the other can exist: early-twentieth century definitions (Redefining"otherness"from Northern Thailand)," *tōnan ajia kenkyū*, vol. 44, no. 3, pp. 295–320, 2017.

[15] O. Poutanen, S. Ylirisku, and P. Hoppu, "Technology choreography: studying interactions in Microsoft's future visoins through dance," *Human Technology*, vol. 13, no. 1, pp. 10–31, 2017.

[16] J. H. Lee, H. S. Kim, and E. S. Shin, "A kinetic analysis of "Suyangsumurepdipimu" movement for Korean dance "Cheoyong-mu"," *Korean Journal of Sports Science*, vol. 29, no. 2, pp. 1121–1132, 2020.

[17] O. Millard, "Dance as a social practice," *IDEA JOURNAL*, vol. 17, no. 2, pp. 335–349, 2020.

[18] H. Jing and S. Ravn, "Sharing the dance – on the reciprocity of movement in the case of elite sports dancers," *Phenomenology & the Cognitive Sciences*, vol. 17, no. 1, pp. 1–18, 2017.

[19] M. S. Hossain and M. A. Yousuf, "Real time facial expression recognition for nonverbal communication," *International Arab Journal of Information Technology*, vol. 15, no. 2, pp. 278–288, 2018.

[20] Y. Li, D. K. Jha, A. Ray, and T. A. Wettergren, "Information fusion of passive sensors for detection of moving targets in dynamic environments," *IEEE Transactions on Cybernetics*, vol. 47, no. 1, pp. 93–104, 2017.

[21] J. Xia, Y. Feng, L. Liu, and D. Liu, "An information fusion model of innovation alliances based on the bayesian network," *Tsinghua Science and Technology*, vol. 23, no. 3, pp. 347–356, 2018.

[22] H. L. Li and Y. F. Ma, "Target recognition method based on multi feature fusion and hybrid kernel SVM," *Shenyang Gongye Daxue Xuebao/Journal of Shenyang University of Technology*, vol. 40, no. 4, pp. 441–446, 2018.

[23] Y. Cai, J. Liu, Y. Guo, S. Hu, and S. Lang, "Video anomaly detection with multi-scale feature and temporal information fusion," *Neurocomputing*, vol. 423, no. 5, pp. 264–273, 2021.

[24] X. Liu, Y. Li, and Q. Wang, "Multi-view hierarchical bidirectional recurrent neural network for depth video sequence based action recognition," *International Journal of Pattern Recognition and Artificial Intelligence*, vol. 32, no. 10, article 1850033, 2018.

[25] F. Qi, W. Tianjiang, L. Fang, and L. HeFei, "Research on multi-camera information fusion method for intelligent perception," *Multimedia Tools & Applications*, vol. 77, no. 12, pp. 15003–15026, 2018.

[26] M. S. Chen, L. Huang, C. D. Wang, D. Huang, and J. H. Lai, "Relaxed multi-view clustering in latent embedding space," *Information Fusion*, vol. 68, no. 9, pp. 8–21, 2021.

[27] S. Bahrami, F. Dornaika, and A. Bosaghzadeh, "Joint auto-weighted graph fusion and scalable semi-supervised learning," *Information Fusion*, vol. 66, no. 1, pp. 213–228, 2021.

[28] W. Xu, L. Jing, J. Tan, and L. Dou, "A multimodel decision fusion method based on DCNN-IDST for fault diagnosis of rolling bearing," *Shock and Vibration*, vol. 2020, no. 1, Article ID 8856818, 2020.

Hindawi
Journal of Sensors
Volume 2021, Article ID 8427336, 10 pages
https://doi.org/10.1155/2021/8427336

Research Article

Analysis of Driving Factors of Innovation and Entrepreneurship Based on Time Series Analysis

Jing Feng

Henan Finance University, Zhengzhou 450046, China

Correspondence should be addressed to Jing Feng; sightfj@hafu.edu.cn

Received 11 August 2021; Revised 9 September 2021; Accepted 23 September 2021; Published 8 October 2021

Academic Editor: Mu Zhou

In order to analyze the driving factors of innovation and entrepreneurship, based on the time series analysis algorithm, this paper combines the analysis requirements of innovation and entrepreneurship driving factors to improve the time series, uses decomposition methods to decompose the complex original data into relatively simple components and reconstruct them, and predicts the reconstructed components to integrate the final predicted value. Moreover, this paper introduces entrepreneurial attitude as an intermediary variable and verifies it through data collection and statistical analysis, so that entrepreneurial traits influence entrepreneurial propensity through entrepreneurial attitude. The test results show that entrepreneurial attitude can better explain the influence of entrepreneurial traits on entrepreneurial propensity. In addition, this paper constructs an analysis model of driving factors for innovation and entrepreneurship, obtains experimental data through questionnaire survey methods, and conducts experimental research in combination with mathematical statistics. From the statistical results, it can be seen that the innovative and entrepreneurial driving factor analysis model based on time series analysis proposed in this paper is effective.

1. Introduction

From ancient times to the present, the phenomenon of entrepreneurship has always existed, but it has not received everyone's attention. In particular, it has never entered the research vision and research framework of mainstream economists. It was not until the emergence of the New Austrian School of Economics in the 1970s and 1980s that entrepreneurship became a hot topic for mainstream economists [1]. Moreover, due to the accelerated growth of the global economy, domestic and foreign researchers have begun to increase their efforts to study entrepreneurship issues. In the past two decades, entrepreneurship research has become the fastest growing field in management research. Why is entrepreneurial research so popular? The first point is that entrepreneurship provides a virgin field for research, which needs to be enriched by scholars. Second, entrepreneurship can weaken the inefficient mechanism of an economy and improve efficiency. Finally, entrepreneurship is an important source of social change and innovation.

Entrepreneurship activities are playing an increasingly important role in the economy and society and have aroused widespread concern in the academic community. At the same time, entrepreneurship involves management, cognitive theory, sociology, psychology, and other theories and methods. Therefore, it is not to study entrepreneurial activities as an independent discipline. At present, research results in entrepreneurship and related fields show a trend of diversification and diversification. In particular, the research on entrepreneurial cognition, entrepreneurial ability, entrepreneurial awareness, entrepreneur traits, entrepreneurial opportunity identification, entrepreneurial propensity, entrepreneurial decision-making, and entrepreneurial performance is constantly changing. Among them, the research on the concepts and issues related to entrepreneur traits and entrepreneurial inclination has attracted much attention [2].

Regardless of the content of entrepreneurship and related fields, the research on entrepreneurial activities has important practical significance. Entrepreneurship activities play a positive role in promoting economic progress, integrating

resource allocation, and promoting social progress, and they also bring a variety of elements to active markets. At present, entrepreneurial theory still lacks localized research, and most of its research methods and models are borrowed from or based on western research results. In a small number of empirical studies in China, the subject is a group of college students. Because college students lack practical work experience and their cognition of entrepreneurial activities is mostly at the level of theoretical research, the results of the research have a low success rate. In view of the phenomenon that the selection of subjects may cause deviations in the research results, the subjects selected in this study are subjects with higher education, knowledge, and culture, rich work and practical experience, entrepreneurial capabilities, and mature thoughts, especially MBA. This will not only broaden the scope of research subjects, increase the accuracy of data, and make empirical research more convincing, but at the same time enrich the content of entrepreneurial theory and expand the scope of research on entrepreneurial theory. Innovation is essential to the development and progress of a country. Among them, entrepreneurship is a typical manifestation of innovation [3].

This paper analyzes the driving forces of innovation and entrepreneurship based on time series algorithms, and on this basis, it studies the problems of innovation and proposes relevant strategies.

2. Related Work

Literature [4] believed that for entrepreneurial companies, team members must have strong learning ability and knowledge absorption ability. Only in this way, when facing the dynamic market environment and the ever-changing competitive situation, the enterprise can face it calmly and flexibly.

For entrepreneurs, the importance of the three driving forces and the difficulty of obtaining them are not constant. As time changes, the effects of the environment and time will also change, and the importance of the three elements will also appear in a state of imbalance. At this time, successful entrepreneurs need to make flexible and dynamic balance arrangements for the three elements in accordance with external competitors and dynamic changes in the environment. Although the importance of the three major driving forces is dynamically changing, for enterprises, the three major driving forces are indispensable at any stage of development. Therefore, the process of entrepreneurship will not stop; it will continue in the process of constant adaptation and balance of the three driving forces [5].

Literature [6] shows that entrepreneurship and innovation have the same root and the same relationship, and the two are related to each other and complement each other. The source of entrepreneurship is innovation, and innovation can develop and flourish in entrepreneurial activities. Moreover, entrepreneurship ultimately transforms innovation into a commodity with social value and realizes the value of innovation. From the perspective of the transformation of scientific and technological achievements of enterprises, literature [7] analyzed the driving factors of innovation and entrepreneurship of Chinese enterprises through cases and summarizes 4 modes. Literature [8] regarded the driving forces of innovation and entrepreneurship as the same. Literature [9] tried to introduce Timmons' entrepreneurial model into the field of innovation. Literature [10] constructed a technological innovation cultivation model for technological enterprises based on the Timmons entrepreneurial management model.

Literature [11] believed that the identification of innovation opportunities is essential to the continuous innovation of enterprises, and the decision-making behavior preferences of corporate decision-makers play a moderating role in the identification of major corporate opportunities. This literature formally emphasizes the two driving factors of opportunity and team. Literature [12] studied the impact of corporate absorptive capacity and knowledge integration capacity on corporate innovation performance and found that the team's absorptive capacity and knowledge integration resource acquisition capacity improved corporate innovation performance to a certain extent. Literature [13] further pointed out that entrepreneurial opportunities can be a new product/service, new material, or even a new organization method, but it must finally enter the mass production stage and obtain revenue through market sales. Literature [14] adopted Schumpeter's classic definition and believed that opportunity is a possibility for creative integration of resources to meet market demand and realize value. Therefore, opportunity recognition refers to the behavior of companies identifying new ideas and transforming ideas into business concepts that can create value through resource integration. The concept of opportunity recognition originated in the field of entrepreneurship. Existing research also specifically emphasized the concept of opportunity recognition in the field of innovation. Literature [15] studied the impact of cultural differences on the ability to identify innovation opportunities. The definition of opportunity recognition is the ability of individuals to associate changes, events, and trends to produce new products or services. It can be found that the definition of opportunity identification has transitioned from the field of entrepreneurship to the field of innovation. Literature [16] defined opportunity recognition as the behavior of individuals or organizations linking changes, events, and trends to identify new ideas and generate new products or services through resource integration to create value.

Regarding the research on the relationship between opportunity recognition and innovation, most scholars agree that opportunity recognition is the front-end process of innovation. Some scholars have found that opportunity identification has a positive effect on corporate performance, comprehensive innovation, business model innovation, and open innovation. In addition, there are studies that specifically emphasize the relationship between opportunity identification and exploratory/breakthrough innovation [17]. Literature [18] found in case analysis that only disruptive innovation can build a company's competitive advantage, and opportunity identification is an important part of it. Breakthrough innovation is usually the result of the integration of various new technologies after the identification of corporate opportunities. However, few studies have explored

the relationship between opportunity identification and incremental innovation/utilization innovation. The conclusion of the relationship between opportunity recognition and exploitative innovation is not clear, and further exploration is needed. Before literature [19] clearly proposed the concept of resource patchwork, resource patchwork was often confused with improvisation. This shows that resource patchwork and improvisation have similarities, and they are mostly temporary solutions. Literature [20] believed that patchwork is a "loose coupling between intention, plan, behavior, and performance," that is, patchwork can have a certain degree of planning, but the plan is not strong. Literature [21] believed that resource patchwork has the attributes of rapid response, low planning, and action preferences, and companies often use this to deal with opportunities and problems that require rapid response.

Literature [22] divided the patchwork into "the exploration of the creative layer" patchwork and the "utilization of the resource layer" patchwork. On the one hand, resource patchwork is dedicated to the creative reorganization of resources, which is exploratory. On the other hand, it also follows the "satisfaction model," emphasizing temporary quick response, which in turn makes the resource patchwork less innovative and easy to form utilization innovation.

3. Time Series Analysis

The first step of MFCM is to decompose the complex original FTS, which can effectively reduce the complexity of the original data and the difficulty of predictive modeling. Therefore, the decomposition effect will greatly affect the analysis and prediction of FTS. At present, the widely used decomposition method with good effect is the empirical mode decomposition series model. As early as more than 30 years ago, literature [23] proposed an epoch-making signal analysis method called Hilbert-Huang Transform (HHT). The core part of the algorithm is empirical mode decomposition (EMD). Essentially, the EMD method is to smooth the original data and obtain the time-frequency-energy characteristics of the signal. This signal analysis method has been widely used, including various fields in many industries, such as the following: in the medical field, it can be used to detect arrhythmia, the spread of dengue fever, and blood pressure changes; in the transportation field, it can be used to detect the safety of highways and bridges; in the security field, it can be used to identify the speaker's identity; in the geographic field, it can be used in earthquake engineering; in the aerospace field, it can be used in satellite data analysis, etc. This method has made a great contribution to the development of these fields. Later, this analysis method was also applied to the financial field.

The basic goal of the EMD algorithm is to adaptively decompose the original signal into components with different frequencies and a residual term (trend component). These different frequency components are called eigenmode functions (IMFs). IMF is defined as a function that satisfies the following conditions: (a) in the entire time series, the number of local extreme points of the data and the number of zero-crossing points of the data should not be much different, and the difference should not exceed 1; (b) anything in the entire data for a time, the local upper and lower envelopes are symmetrical, where the upper (lower) envelope refers to the envelope of the local maximum (small) value, that is, the average value of the two envelopes is equal to zero. Among the two conditions, the former requirement is similar to the narrowband requirement of Gauss signal. Item (b) is a new requirement, which reduces the previous global requirement to a local requirement, so that the fluctuation of the asymmetric waveform does not affect the instantaneous frequency. For nonstationary FTS, calculating the local mean involves a local time scale that is difficult to determine. Therefore, in condition (b), the local mean value of the two envelopes is required to be zero, so that the signal waveform is locally symmetric. Under normal circumstances, using this method, the instantaneous frequency will still conform to the physical meaning of the research system. IMF represents the inherent vibration mode of the sequence. Since most of the FTS studied are not IMF, in any time dimension, FTS often contains many fluctuation patterns. Because of such a simple Hilbert transform cannot fully characterize the frequency characteristics of FTS, further EMD decomposition of FTS is a better choice.

The EMD decomposition method has three assumptions, which are explained below. (a) There are at least two extreme values, namely, at least one maximum value and at least one minimum value. (b) The time scale between extreme points uniquely determines the local time domain characteristics of the data. (c) If there is no extreme point in the sequence, but there is an inflection point, the extreme value can be obtained by differentiating the data n times and then integrating to obtain the decomposition result. This process can be vividly called "sifting." After the "sifting" process, IMFs with different frequencies and a monotonic residual term that can no longer be decomposed are obtained, which is also called the trend term $R(t)$. IMF is selected from high frequency to low frequency in order, and there is no direct connection between them. The decomposition result can be expressed as the following formula:

$$X(t) = \sum_{i=1}^{n} \mathrm{IMF}_i(t) + R(t). \tag{1}$$

Next, we will introduce the specific decomposition steps of the EMD method.

(1) The algorithm finds all the local extreme points of the data $X(t)$

(2) The algorithm uses cubic spline interpolation to fit the maximum and minimum points, respectively, and construct the upper envelope $u(t)$ and the lower envelope $l(t)$

(3) After obtaining $u(t), l(t)$, the algorithm calculates its mean value, obtains the mean value curve, and records it as $m_1(t)$. The expression is as follows:

$$m_1(t) = \frac{1}{2}(u(t) + l(t)) \tag{2}$$

(4) The algorithm sifts out $m_1(t)$ from the original data $X(t)$ and denotes the remaining part as $h_1(t)$:

$$h_1(t) = X(t) - m_1(t) \tag{3}$$

(5) The algorithm judges whether $h_1(t)$ is IMF, that is, whether it meets the two basic conditions of IMF. In an ideal situation, $h_1(t)$ should be the IMF, because the $h_1(t)$ obtained through the above process seems to have met all the requirements of the IMF. However, in reality, new extreme values are usually generated, and existing extreme values are shifted or exaggerated. Therefore, under normal circumstances, the screening process needs to be repeated many times to achieve a true eigenmode function. If $h_1(t)$ is not IMF, the algorithm continues to replace $X(t)$ with $h_1(t)$ and repeat the above steps until the remaining part meets the two conditions of IMF. Specifically, the algorithm repeats the process from 1 to 5 k times until ${h_1}^k(t)$ is IMF. So far, the first eigenmode component $\mathrm{IMF}_1(t)$ is obtained, where

$$h_1^k(t) = h_1^{k-1}(t) - m_1^k(t) \tag{4}$$

In particular, the criteria for stopping the screening process can be limited to a certain range based on the value of the standard deviation (SD) of two adjacent results in order to retain sufficient physical information of the IMF. The following conditions must be met:

$$\mathrm{SD} = \sum_{t=0}^{T} \left[\frac{\left| h_1^{k-1}(t) - h_1^k(t) \right|^2}{\left(h_1^{k-1}(t) \right)^2} \right] \le \alpha. \tag{5}$$

Among them, α represents the screening threshold, and a value between 0.2 and 0.3 is often used in operation.

(6) The algorithm replaces $X(t)$ with $X(t) - \mathrm{IMF}_1(t)$ and repeats the above steps 1 to 5 in the next screening process to continue to find the next IMF until all IMFs are screened out. At this time, there is only one monotonic residual sequence left, which is denoted as $R(t)$, that is, the trend component. The flow chart of the EMD algorithm is summarized as Figure 1

The EMD algorithm has some good characteristics, such as decomposition adaptability, completeness, and subsignal orthogonality. The adaptability is embodied in three aspects, namely, the adaptive basis function, frequency, and filtering process, which can automatically decompose the components with decreasing frequency according to the characteristics of FTS itself; completeness refers to the decomposition of the original data through the EMD algorithm. Each IMF and trend item can be added together to form the original data, and the original book order data can be completely recovered from the decomposed components with small errors. Therefore, the EMD algorithm has high completeness; the orthogonality of the subsignals is obvious. It means that the decomposed components are orthogonal to each other.

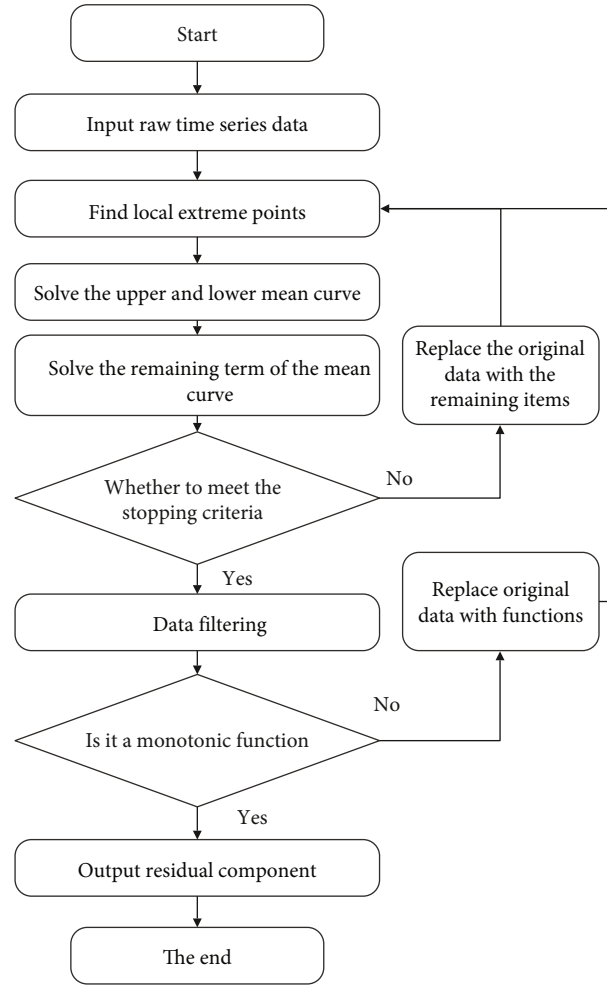

Figure 1: Flow chart of the EMD algorithm.

At the same time, the EMD algorithm also has some unavoidable shortcomings, including the error accumulation of the decomposition results and the aliasing of submodes. In response to the above problems, relevant scholars continue to study and put forward some improvement methods.

Add Gaussian white noise with uniform spectrum distribution to the original data. In the subsequent averaging process, the added white noise can basically cancel each other through multiple integrations and at the same time solve the problem of modal aliasing in EMD decomposition. The effective realization of data decomposition is an important improvement of EMD.

The following describes the specific decomposition steps of EEMD on the basis of EMD:

(1) The algorithm adds the Gaussian white noise sequence $\varepsilon_m(t)$ to the original data $X(t)$ to obtain the mixed time series data, denoted as $X_m(t)$, and the expression is as follows:

$$X_m(t) = X(t) + \varepsilon_m(t) \tag{6}$$

Among them, m represents the number of times of mixing, and $m = 1, 2, 3, \cdots, N$, and N represents the total number of times of mixing white noise in the original data.

(2) The algorithm implements the EMD method on the mixed data $X_m(t)$ to obtain n IMF components and 1 residual component $R_{mn}(t)$. The expression is as follows:

$$X_m(t) = \sum_{j=1}^{n} \mathrm{IMF}_{mj}(t) + R_{mn}(t) \tag{7}$$

(3) The algorithm repeats the above process until $m = N$, that is, N times of EMD decomposition is performed

(4) The algorithm, respectively, averages the IMF components and remainders obtained by N times of EMD decomposition, and the result is used as the output of EEMD. The expression is as follows:

$$X(t) = \sum_{j=1}^{n} \overline{\mathrm{IMF}}_j(t) + \bar{R}(t) \tag{8}$$

Among them, n indicates that a total of n IMFs are decomposed, and $\overline{\mathrm{IMF}}_j(t)$ and $\bar{R}(t)$ indicate the mean value of the decomposition results of m noise data. The flow chart of the EEMD method is shown in Figure 2.

The EEMD method improves the inherent defects of EMD modal aliasing by adding Gaussian white noise with uniform spectral distribution to the original data. Under the premise of ensuring the original characteristics of the data, it improves the accuracy of the decomposition and in turn makes the application of EMD-like methods more extensive and more valuable. However, the introduced Gaussian white noise will cause some pollution to the original data, and the increased integration times will also cause serious calculation time.

For FTS with complex nature, the decomposition effect will greatly affect the analysis and prediction of FTS, so the improvement of decomposition method is of great significance to model optimization.

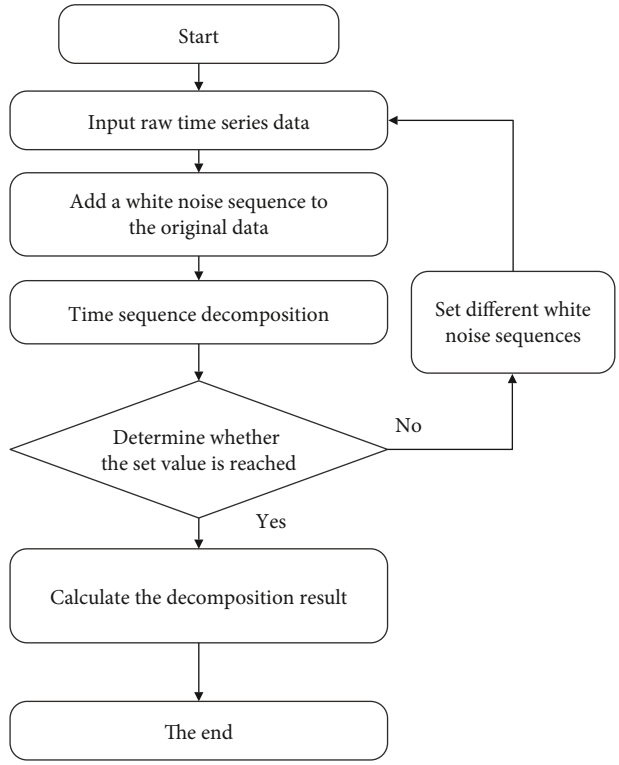

Figure 2: EEMD algorithm flow chart.

Reconstructing component prediction is the most critical step of the MFCM model, and the result of component prediction will directly affect the final model effect. At present, the prediction part of MFCM usually uses the support vector regression (SVR) model with good effect. The application of this method in the field of FTS has been fully studied by scholars, and it has been successfully applied to the prediction of reconstructed components after decomposition, and certain results have been achieved.

Among the existing MFCM models, the support vector regression model (SVR) has been successfully applied to the prediction of reconstruction components and has good performance due to its relatively simple structure, fast learning rate, and strong generalization ability. Support vector machine (SVM) starts from a certain amount of sample data, based on the VC dimension theory, and follows the principle of structural risk minimization. At the same time, it takes into account the two aspects of ensuring the accuracy of the model and reducing the complexity to solve the global optimal solution, thereby constructing the optimal learner. SVM is usually suitable for classification problems. After the original SVM model was researched and developed by related scholars, a support vector regression model (SVR) suitable for regression problems was derived. In this paper, we mainly focus on Least Squares Support Vector Regression (LS-SVR), which is widely used and faster to solve in MFCM.

We set a set of training data $\{(x_0, y_0), \cdots, (x_l, y_l)\}$, where x_i is an input and y_i is the target output, and for $i = 0, 1, \cdots,$

$l, x_i \in R^d, y_i \in R$. The core idea of SVR is to determine the function $f(x, w)$, and its predicted value can be accurately close to the actual value in the future, which can be expressed as follows:

$$y = f(x, w) = w\varphi(x) + b. \tag{9}$$

Among them, w and b represent the weight vector and the deviation, respectively, $w \in R^{n_k}$, $b \in R$ and the input vector x will be mapped to the high-dimensional feature space through a certain nonlinear function $\varphi : R^d \longrightarrow R^{n_k}$.

LS-SVR solves the regression problem by minimizing the following constrained objective function to solve w and b.

$$\begin{aligned} \min_{w \in R^{n_k}, b \in R} J(w, \xi) &= \frac{1}{2} w^T w + \gamma \frac{1}{2} \xi^T \xi, \\ s.t. y &= z^T w + b 1_l + \xi. \end{aligned} \tag{10}$$

Among them, $Z = (\varphi(x_1), \varphi(x_2), \cdots, \varphi(x_l)) \in R^{n_k \times l}$, and $\xi = (\xi_1, \xi_2, \cdots, \xi_l)^T \in R^l$ contain the relaxation variable, $\gamma \in R_+$ is a positive real regularization parameter, and $1_l = [1, 1, \cdots, 1]^T \in R^l$. The Lagrange function of the above formula is as follows:

$$L(w, b, \xi, \alpha) = J(w, \xi) - \alpha^T \left(z^T w + b 1_l + \xi - y \right). \tag{11}$$

Among them, $\alpha = (\alpha_1, \alpha_2, \cdots, \alpha_l) \in R^l$ is a vector composed of Lagrange multipliers. The KKT condition of the optimization problem is as follows:

$$\begin{cases} \dfrac{\partial L}{\partial w} = 0 \Rightarrow w = Z\alpha, \\ \dfrac{\partial L}{\partial b} = 0 \Rightarrow \alpha^T 1_l = 0, \\ \dfrac{\partial L}{\partial \xi} = 0 \Rightarrow \alpha = \gamma \xi, \\ \dfrac{\partial L}{\partial \alpha} = 0 \Rightarrow z^T w + b 1_n + \xi - y = 0_l. \end{cases} \tag{12}$$

By offsetting w and ξ, the following linear system can be obtained:

$$\begin{bmatrix} 0 & 1_l^T \\ 1_l & H \end{bmatrix} \begin{bmatrix} b \\ \alpha \end{bmatrix} = \begin{bmatrix} 0 \\ y \end{bmatrix}. \tag{13}$$

Among them, $H = K + \gamma^{-1} I_l \in R^{l \times l}$ is a positive definite matrix, where $K = Z^T Z \in R^{l \times l}$, and the elements are

$$K_{i,j} = \varphi(x_i)^T \varphi(x_j) = K(x_i, x_j). \tag{14}$$

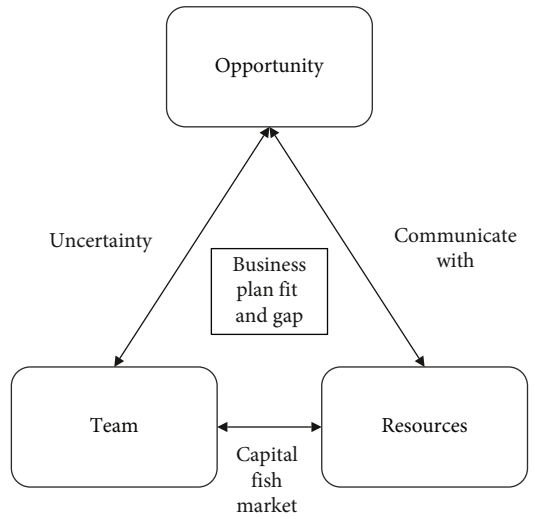

Figure 3: Timmons entrepreneurial model.

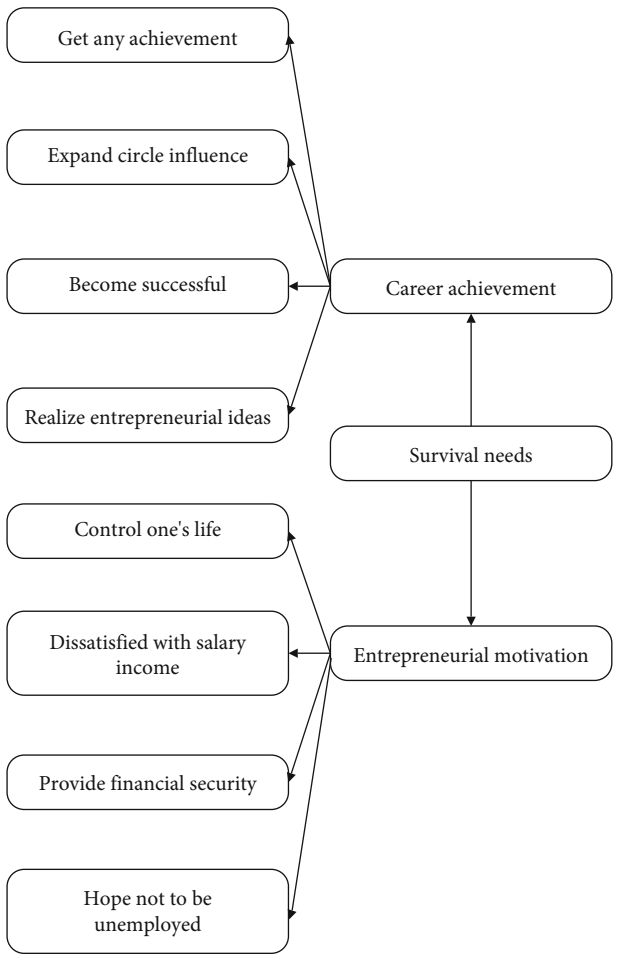

Figure 4: Two-factor model of entrepreneurial motivation.

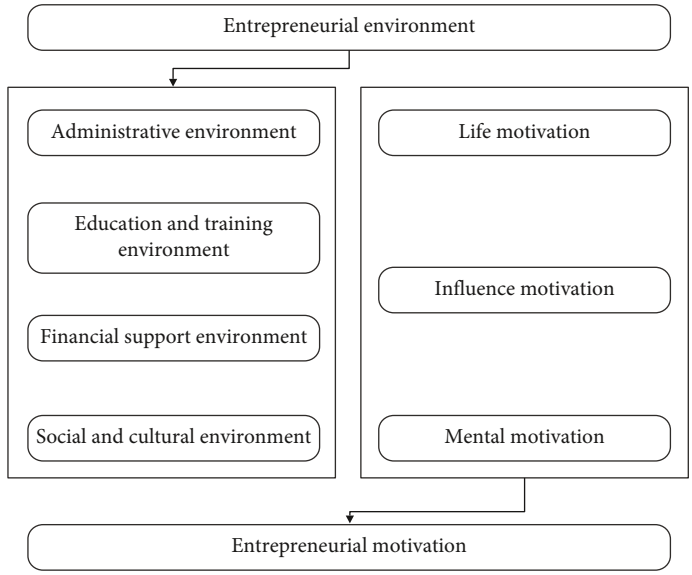

Figure 5: Theoretical structure diagram.

$K(\cdot,\cdot)$ is the kernel function. For $\forall(i,j) \in N_l \times N_l$, if the solution of formula (13) is $\alpha^* = (\alpha_1^*, \alpha_2^*, \cdots, \alpha_1^*)^T$ and b^*, then the corresponding decision function is as follows:

$$y = f(x, w^*) = \varphi(x)^T w^* + b^* = \varphi(x)^T Z\alpha^* + b^* = \sum_{i=1}^{l} \alpha_i^* \varphi(x)^T \varphi(x_i) + b^* = \sum_{i=1}^{l} \alpha_i^* K(x, x_i) + b^*. \quad (15)$$

4. Model Building

Successful entrepreneurial activities require constant matching and adaptation of resources, business opportunities, and teams, so that the three can maintain a dynamic balance. Among them, business opportunities are the core and origin of the entire entrepreneurial activity. Therefore, in the early stage of entrepreneurship, the discovery and selection of opportunities is crucial, and companies should identify as many business opportunities as possible to help improve the performance of entrepreneurial activities. At the same time, resources are the supporting elements of the entrepreneurial process, and they are important for the identification and development of opportunities. Therefore, entrepreneurs need to try to develop and establish multiple channels to obtain abundant resources. Figure 3 shows the Timmons entrepreneurial model.

The theoretical model is obtained by exploratory factor analysis method, and the confirmatory factor analysis is carried out, and finally, a two-factor model is obtained. The model is shown in Figure 4.

On the basis of studying the results of domestic and foreign scholars, this paper combines the influence mechanism of entrepreneurial environment and entrepreneurial motivation, takes entrepreneurial environment as an independent variable, and divides entrepreneurial environment into four dimensions. At the same time, this paper takes entrepreneurial motivation as the dependent variable, which includes three dimensions: life-type motivation, influence-type motivation, and spiritual-type motivation. In order to explore the mechanism of entrepreneurial environment on motivation,

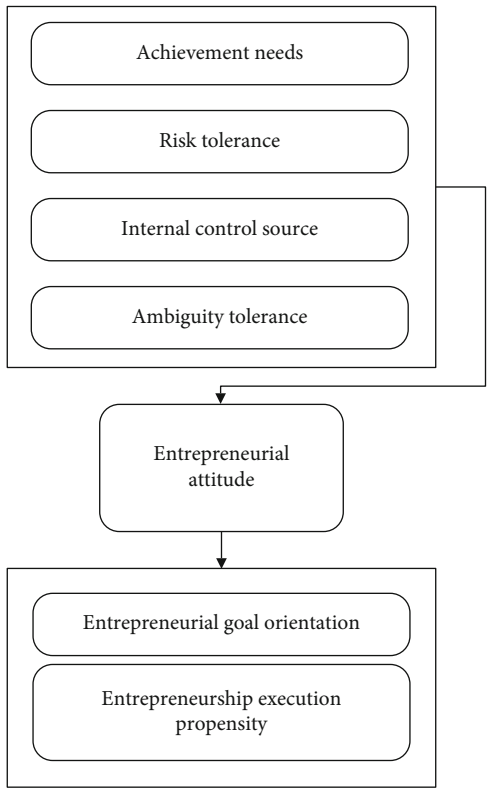

Figure 6: The relationship model of entrepreneur traits, entrepreneurial attitude, and entrepreneurial propensity.

Table 1: Statistical table of data mining effect.

Number	Data mining	Number	Data mining	Number	Data mining
1	82.4	28	90.7	55	85.5
2	91.3	29	83.9	56	80.8
3	84.0	30	82.9	57	85.8
4	89.2	31	81.9	58	80.4
5	85.0	32	87.3	59	80.8
6	86.5	33	86.3	60	88.0
7	80.8	34	80.6	61	80.0
8	85.9	35	79.1	62	87.5
9	93.4	36	94.0	63	82.2
10	90.5	37	82.6	64	79.5
11	86.1	38	83.0	65	86.7
12	79.9	39	88.4	66	86.8
13	81.3	40	83.3	67	89.3
14	87.7	41	93.8	68	80.3
15	80.3	42	83.5	69	84.2
16	89.2	43	81.8	70	82.5
17	90.4	44	91.5	71	85.4
18	85.1	45	92.1	72	86.7
19	90.7	46	82.3	73	82.7
20	80.7	47	83.1	74	86.2
21	92.0	48	93.4	75	88.7
22	92.4	49	85.0	76	87.3
23	81.6	50	88.2	77	85.3
24	92.0	51	83.0	78	80.6
25	81.4	52	84.1	79	90.6
26	86.3	53	84.6	80	88.9
27	82.5	54	92.8	81	81.0

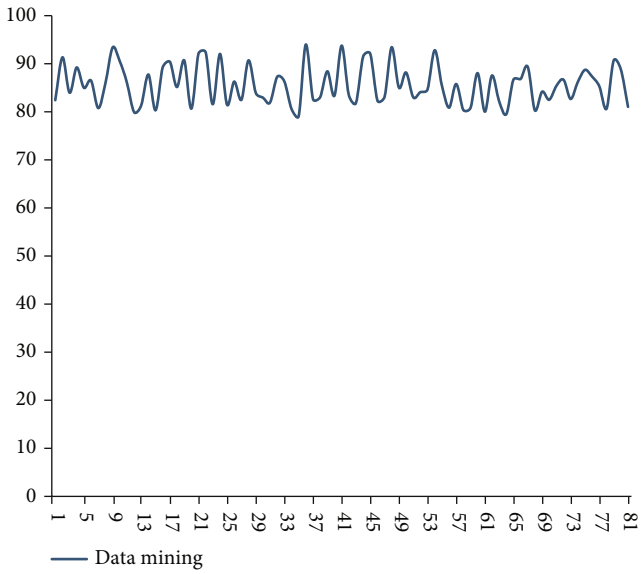

Figure 7: Statistical diagram of data mining effect.

Table 2: Statistical table of the evaluation of the decision-making effect of innovation and entrepreneurship.

Number	Decision effect	Number	Decision effect	Number	Decision effect
1	85.1	28	90.0	55	74.4
2	80.1	29	82.0	56	86.4
3	71.5	30	69.8	57	88.0
4	80.4	31	86.3	58	80.9
5	89.0	32	71.5	59	75.1
6	86.0	33	73.3	60	77.8
7	70.1	34	82.0	61	69.9
8	90.2	35	75.1	62	69.1
9	90.2	36	85.2	63	83.8
10	75.7	37	88.0	64	69.2
11	72.9	38	84.1	65	75.2
12	69.9	39	90.4	66	84.9
13	77.7	40	73.0	67	71.9
14	80.5	41	86.7	68	81.5
15	89.7	42	78.2	69	75.3
16	82.4	43	71.2	70	75.1
17	78.2	44	77.6	71	83.0
18	73.2	45	84.5	72	77.0
19	85.9	46	83.1	73	69.4
20	83.3	47	70.6	74	90.5
21	77.8	48	82.0	75	68.3
22	83.3	49	72.9	76	74.5
23	72.4	50	73.5	77	86.9
24	90.6	51	77.8	78	88.5
25	75.5	52	69.7	79	73.2
26	89.2	53	82.3	80	83.8
27	73.6	54	89.0	81	88.8

this paper constructs the theoretical model of this paper by reading a large number of documents, as shown in Figure 5.

The purpose of this paper is to explore the relationship between entrepreneurial traits, entrepreneurial attitude, and entrepreneurial propensity. Through the analysis and combing of relevant literature, it is not difficult to find that the characteristics of entrepreneurs have an impact on entrepreneurial propensity. However, there are few empirical studies that show that the traits of entrepreneurs are directly related to entrepreneurial propensity, and when the personal traits of entrepreneurs or potential entrepreneurs are regarded as the only cause of entrepreneurial propensity, the research results will be one-sided. This article introduces entrepreneurial attitude as an intermediary variable and validates it through data collection and statistical analysis, so that entrepreneurial traits influence entrepreneurial propensity through entrepreneurial attitude. The test results found that entrepreneurial attitude can better explain the influence of entrepreneurial traits on entrepreneurial propensity. In summary, this paper constructs a conceptual model of the research, as shown in Figure 6.

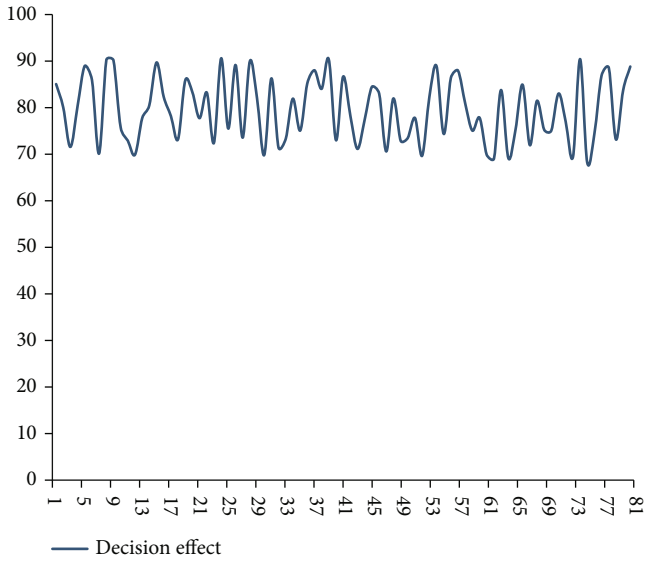

Figure 8: Statistical diagram of the evaluation of the decision-making effect of innovation and entrepreneurship.

5. Analysis of Driving Factors for Innovation and Entrepreneurship Based on Time Series Analysis

In order to test the effect of the model proposed in this paper, this paper will obtain data by issuing questionnaires and collect the questionnaires within a certain time limit. The questionnaire is mainly distributed by means of two-dimensional code sharing and web links, and the coverage is expanded through communication platforms such as WeChat, Weibo, and Qzone.

After obtaining the data, this paper examines the data mining effect of the innovative and entrepreneurial driving factor analysis model based on time series analysis proposed in this paper. The results are shown in Table 1 and Figure 7.

From the above research results, the innovative and entrepreneurial driving factor analysis model based on time series analysis proposed in this paper has a certain effect. On this basis, the effect of system innovation and entrepreneurship decision-making is evaluated, as shown in Table 2 and Figure 8 below.

Through experimental research, we can see that the innovative and entrepreneurial driving factor analysis model based on time series analysis proposed in this paper has a certain effect.

6. Conclusion

China's economy has entered a new normal, and Chinese companies are gradually moving from past imitative innovation to independent innovation. In this context, the voice of the business community for improving innovation performance is even higher, and entrepreneurs hope to develop more exploratory innovation while maintaining utilization innovation. Based on the time series analysis algorithm, this paper introduces the concept of resource patchwork on the basis of the Timmons entrepreneurial model and its three major elements (opportunities, resources, and teams). Moreover, this paper believes that resource patchwork, as an informal innovation hidden in the daily work of an enterprise, can quickly respond to identified opportunities through the rational development and recombination of resources at hand. In addition, this paper constructs an analysis model of innovation and entrepreneurship driving factors based on time series analysis and validates the model in this paper through case analysis. The research results show that the model constructed in this paper has a certain effect.

Data Availability

The data used to support the findings of this study are available from the corresponding author upon request.

Conflicts of Interest

The author declares no competing interests.

Acknowledgments

This study is sponsored by the Henan Finance University.

References

[1] E. Totty, "The effect of minimum wages on employment: a factor model approach," *Economic Inquiry*, vol. 55, no. 4, pp. 1712–1737, 2017.

[2] J. H. Fede, K. S. Gorman, and M. E. Cimini, "Student employment as a model for experiential learning," *The Journal of Experimental Education*, vol. 41, no. 1, pp. 107–124, 2018.

[3] S. Van de Walle, B. Steijn, and S. Jilke, "Extrinsic motivation, PSM and labour market characteristics: a multilevel model of public sector employment preference in 26 countries," *International Review of Administrative Sciences*, vol. 81, no. 4, pp. 833–855, 2015.

[4] P. Barbieri, R. Bozzon, S. Scherer, R. Grotti, and M. Lugo, "The rise of a Latin model? Family and fertility consequences of employment instability in Italy and Spain," *European Societies*, vol. 17, no. 4, pp. 423–446, 2015.

[5] U. Huws, N. H. Spencer, and D. S. Syrdal, "Online, on call: the spread of digitally organised just-in-time working and its implications for standard employment models," *New Technology, Work and Employment*, vol. 33, no. 2, pp. 113–129, 2018.

[6] J. F. Wen and D. V. Gordon, "An empirical model of tax convexity and self-employment," *Review of Economics and Statistics*, vol. 96, no. 3, pp. 471–482, 2014.

[7] C. Dillahunt-Aspillaga, R. Nakase-Richardson, T. Hart et al., "Predictors of employment outcomes in veterans with traumatic brain injury: a VA traumatic brain injury model systems study," *Journal of Head Trauma Rehabilitation*, vol. 32, no. 4, pp. 271–282, 2017.

[8] M. Bornay-Barrachina, A. López-Cabrales, and R. Valle-Cabrera, "How do employment relationships enhance firm innovation? The role of human and social capital," *The InTernaTIonal Journal of Human Resource Managemen T*, vol. 28, no. 9, pp. 1363–1391, 2017.

[9] G. R. Bond and R. E. Drake, "Making the case for IPS supported employment," *Administration and Policy in Mental Health and Mental Health Services Research*, vol. 41, no. 1, pp. 69–73, 2014.

[10] D. Tavani and L. Zamparelli, "Endogenous technical change, employment and distribution in the Goodwin model of the growth cycle," *Studies in Nonlinear Dynamics & Econometrics*, vol. 19, no. 2, pp. 209–216, 2015.

[11] P. Frijters, D. W. Johnston, and M. A. Shields, "The effect of mental health on employment: evidence from Australian panel data," *Health Economics*, vol. 23, no. 9, pp. 1058–1071, 2014.

[12] F. Portella-Carbo, "Effects of international trade on domestic employment: an application of a global multiregional input–output supermultiplier model (1995–2011)," *Economic Systems Research*, vol. 28, no. 1, pp. 95–117, 2016.

[13] G. R. Bond, S. J. Kim, D. R. Becker et al., "A controlled trial of supported employment for people with severe mental illness and justice involvement," *Psychiatric Services*, vol. 66, no. 10, pp. 1027–1034, 2015.

[14] G. Topa, C. M. Alcover, J. A. Moriano, and M. Depolo, "Bridge employment quality and its impact on retirement adjustment: a structural equation model with SHARE panel data," *Economic and Industrial Democracy*, vol. 35, no. 2, pp. 225–244, 2014.

[15] M. Shirmohammadi, M. Beigi, and J. Stewart, "Understanding skilled migrants' employment in the host country: a multidisciplinary review and a conceptual model," *The International Journal of Human Resource Management*, vol. 30, no. 1, pp. 96–121, 2019.

[16] G. P. Clarkson, "Twenty-first century employment relationships: the case for an altruistic model," *Human Resource Management*, vol. 53, no. 2, pp. 253–269, 2014.

[17] C. Topsakal, "Policy on teacher employment model in Turkey: contracted teachers," *International Journal of Educational Methodology*, vol. 5, no. 4, pp. 671–682, 2019.

[18] L. Ottomanelli, S. Barnett, L. Goetz, and R. Toscano, "Vocational rehabilitation in spinal cord injury: what vocational service activities are associated with employment program outcome?," *Topics in Spinal Cord Injury Rehabilitation*, vol. 21, no. 1, pp. 31–39, 2015.

[19] C. C. Lo and T. C. Cheng, "Race, employment disadvantages, and heavy drinking: a multilevel model," *Journal of Psychoactive Drugs*, vol. 47, no. 3, pp. 221–229, 2015.

[20] E. E. Dean, K. M. Burke, K. A. Shogren, and M. L. Wehmeyer, "Promoting self-determination and integrated employment through the self-determined career development model," *Advances in Neurodevelopmental Disorders*, vol. 1, no. 2, pp. 55–62, 2017.

[21] G. R. Bond, R. E. Drake, and A. Luciano, "Employment and educational outcomes in early intervention programmes for early psychosis: a systematic review," *Epidemiology and Psychiatric Sciences*, vol. 24, no. 5, pp. 446–457, 2015.

[22] K. Y. Huang and Y. R. Chuang, "Aggregated model of ttf with utaut2 in an employment website context," *Journal of Data Science*, vol. 15, no. 2, pp. 187–201, 2017.

[23] E. J. Bartelsman, P. A. Gautier, and J. De Wind, "Employment protection, technology choice, and worker allocation," *International Economic Review*, vol. 57, no. 3, pp. 787–826, 2016.

Hindawi
Journal of Sensors
Volume 2021, Article ID 7166142, 10 pages
https://doi.org/10.1155/2021/7166142

Research Article

Image Sensory Experience of Artistic Design Based on the Role of Omnidirectional Vision Sensors

Zhen Tong

Department of Teacher Education, Nanchong Vocational and Technical College, Nanchong, 637000 Sichuan, China

Correspondence should be addressed to Zhen Tong; ty13890837297@163.com

Received 12 July 2021; Revised 1 September 2021; Accepted 27 September 2021; Published 6 October 2021

Academic Editor: Mu Zhou

As a sensor with a wide field of view, the panoramic vision sensor is efficient and convenient in perceiving the characteristic information of the surrounding environment and plays an important role in the experience of artistic design of images. The transformation of visual and other sensory experiences in art design is to integrate sound, image, texture, taste, and smell with each other through reasonable rules, to create more excellent crossborder art design works. To improve the sensory experience that art design works bring to the audience, the combination of vision and other sensory experiences can maximize the advantages of multiple information dissemination methods and combine the omnidirectional visual sensor with the sensory experience of art design images. In the method part, this article introduces the omnidirectional vision sensor, art design image, and sensory experience modes and content and introduces the hyperbolic concave mirror theory and the Micusik perspective projection imaging model. In the experimental part, the experimental environment, experimental objects, and experimental procedures of this article are introduced. In the analysis part, this article analyzes the six aspects of image database dependency test, performance, comparison of different distortion types, false detection rate and missing detection rate, algorithm time-consuming comparison, sensory experience analysis, and feature point screening. Among the feelings of the art design image, for the first image, 87.21% of the audience's feelings are happy, indicating that the main idea of this image can bring joy to people. In the second image, the audience's feelings are mostly sad. For the third image, more than half of the audience's feelings are melancholy. For the fourth image, 69.34% of the audience's inner feelings are calm. It explains that the difference in the content of art design images can bring different sensory experiences to people.

1. Introduction

At present, the research of panoramic video acquisition equipment has become a hot research topic. Any point in the panoramic image corresponds to a certain point in the surveillance space; so, the spatial position calibration algorithm is simple, and there is no need to aim at the target during monitoring, making the algorithm for acquiring, detecting, and tracking moving objects in the surveillance range more visual information. Simple, it is a fast and reliable means of collecting panoramic visual information. The image collected by the omnidirectional camera uses the principle of specular reflection, which makes the omnidirectional image and the image seen by the human eye very different, and there is a certain degree of deformation. The use of omnidirectional cameras for video capture has the advantages of low cost, easy installation and debugging, and no dead corners for monitoring. It provides strong technical support for realizing dynamic image understanding and further improves the economy, safety, and intelligence of the entire security system. Images are obtained by various observation systems observing the objective world in different forms and methods. They are entities that can directly or indirectly act on the human eye to produce visual perception. About 75% of the information we get from this world comes from the visual system, which is the image we see. Human image recognition ability is very strong. The image stimulates human sensory organs, and people recognize it as a certain image, know its purpose, etc. In the process of human image recognition, it is necessary to have both the image information that enters the sensory organs at the time and the image information stored in the brain. By searching for the existing

image information in the memory, and comparing the image information that enters the sensory organs at the time, we can identify the image to be identified. If there is no information about this image in the brain, then the brain will open up a place to put the image in. After multiple recognitions, the image will form a memory in the brain. When you see the image again, you can compare it and identify it. Based on the swift mode of the big data era of modern society, the social population has not enough time to read cumbersome social information and emotional communication through much text. The maverick young group mainly uses image and visual communication methods to rush. Because image vision has more circulation and rendering than text language and can change real life, it saves time to a certain extent and enhances the viewer's visual experience of the world. At present, with abundant information, the surrounding social life is also full of various and wonderful image visions, most of which include advertising posters and film packaging. The application of image vision is also very wide. It can be said that it is ubiquitous. The reason social culture is a visual culture is that it is more influential than written language from many angles.

Based on the role of omnidirectional visual sensors in the sensory experience of artistic design images, many scholars at home and abroad have conducted related research. Zhou proposed an omnidirectional stereo vision sensor based on a single camera and a reflection system. As a key component, a camera and two pyramid mirrors are used for imaging. Four pairs of virtual cameras can realize omnidirectional measurements in different directions in the horizontal field, with good synchronization and compactness. In addition, the invariance of perspective projection is ensured during the imaging process, and the imaging distortion caused by curved mirror reflection is avoided. The research established the structural model of the sensor and designed the sensor prototype. It also discussed the influence of the structural parameters on the field of view and measurement accuracy. In addition, actual experiments and analyses were carried out to evaluate the performance of the proposed sensor in measurement applications. The results proved the feasibility of the sensor and showed considerable accuracy in 3D coordinate reconstruction. The author has conducted research on the omnidirectional stereo vision sensor, but has no prospects for the application of this sensor [1].Svetlichnaya studied the variants of artistic activities aimed at adapting a person's existing external image to various social and cultural situations. The communication practice of using art design to shape a person's external image is positioned as a "flexible" image model. Recommended for communication between different communities, a person's external image is considered to be a means of providing instant information exchange between communicators of different social groups, pointing out the visual components of the person's external image that affect the translation of social and cultural information, such as clothing and hairstyle. The artistic design method in modern culture is defined as creative, which helps to form a unified visual image of the social group participating in it. The method of artistic design, in the context of designing a person's external image, will affect its purposeful formation and adaptation, and this image will be transformed into a social group. According to the research results, combined with the communication goals of representatives of different social groups, suggestions are made on the choice of artistic design methods in the process of designing the external image of the characters. The author created a relevant model for art design in the research, but did not combine relevant data and diagrams to illustrate [2]. Abusaada believes that in the literary works of phenomenological theory, emotion is conceptualized as an important factor related to changing people's emotions in urban environment research. The research is aimed at demonstrating a toolkit for creating an emotional city atmosphere based on communication between people and places. To better understand the relationship between the sensory body theory and the reconstruction of the emotional urban atmosphere in the urban environment, the research conducted a literature survey of reasonable approaches and proposed a toolkit related to multisensory experiences. The research groundbreakingly discussed the concepts of sensory bodies, important driving forces, and daily multisensory experiences as a contribution to urban research applications. In addition, the author also clarified the possibility of creating an emotional city atmosphere by using emotional concepts as a predesign stage process. The work of multisensory experience in the urban environment needs to solve the important driving force of the sensory body and becomes a set of perceptual dimension urban research tools. The research carried out sentiment analysis on works of art, but the authors did not combine some modern techniques to illustrate [3]. The subject matter described here includes methods, systems, and computer-readable media for reducing Wi-Fi scanning using cellular network to Wi-Fi access point mapping information and uses mobile communication devices to receive Wi-Fi and cellular signals and create or obtain a database of mapping between Wi-Fi access points and cellular network information. The mobile communication device detects the signal from the base station in the cellular network. The mobile communication device determines at least one recommended access point based on the data derived from the database. In response to determining that there is at least one Wi-Fi signal, the mobile communication device attempts to connect to at least one recommended access point. However, whether the mobile communication device determines whether there is any Wi-Fi signal still cannot be proven [4, 5].

This paper studies the sensory experience of art design images based on omnidirectional visual sensing. In the method part, this article introduces the omnidirectional vision sensor, art design image, and sensory experience modes and content and introduces the hyperbolic concave mirror theory and the Micusik perspective projection imaging model. In the experimental part, the experimental environment, experimental objects, and experimental procedures of this article are introduced. In the analysis part, this article analyzes the six aspects of image database dependency test, performance, comparison of different distortion types, false detection rate and missing detection rate, algorithm time-consuming comparison, sensory experience analysis,

and feature point screening. The innovation of this article lies in the application of omnidirectional visual sensors to the sensory experience of art design images, combined with related schematic diagrams for explanation, and this article also studies the relationship between human multisensory organs and art design to obtain sensory elements importance in art design. The experience of applying the senses in art design will make the design more humane, more participatory, and interactive. However, this article uses an omnidirectional vision sensor. When faced with a more complicated actual environment, precise positioning may not be possible, or even positioning may not be completed. If you want to solve all situations with only omnidirectional vision sensors, it is still not realistic.

2. Image Sensory Experience Method Based on Omnidirectional Visual Sensor in Art Design

2.1. Omnidirectional Vision Sensor. The omnidirectional vision sensor is the direct source of information for the entire machine vision system. It is mainly composed of one or two graphic sensors, sometimes with light projectors and other auxiliary equipment. An instrument that uses optical elements and imaging devices to obtain image information of the external environment usually uses image resolution to describe the performance of a visual sensor. The accuracy of the vision sensor is not only related to the resolution, but also related to the detection distance of the measured object. The farther the measured object is, the worse its absolute position accuracy. Below, we explain it using the omnidirectional vision lens, the imaging of the omnidirectional vision system, and the omnidirectional image.

The emergence of omnidirectional vision lenses solves the defects of ordinary lenses. The omnidirectional image collected by the omnidirectional vision sensor contains horizontal environmental information, and a picture can contain the image information that can be captured by several ordinary cameras at the same time. For systems that require a large field of vision applications, omnidirectional vision undoubtedly provides a good solution.

The imaging of the panoramic vision system is divided into two projection processes: First, the light around the panoramic vision sensor hits the surface of the curved mirror, which belongs to the projection from the surrounding environment to the surface of the curved mirror. The projection on the surface of the curved mirror may cause distortion of the image of the object in the surrounding environment; the other projection is the projection of the curved mirror to the plane of the image. The mechanism of this projection is equivalent to the usual camera projection. Through these two projections, the objects around the panoramic vision sensor are generated as distorted panoramic images on the imaging plane [6, 7].

It can be seen from the panoramic image: (1) the effective field of view of the panoramic vision sensor is relatively wide. With the UP-OmniVision panoramic vision sensor as the center, the imaging within a radius of 4 m is quite clear [8]. (2) Objects in the image inevitably have a certain degree of distortion, such as curved floor tiles and deformed wooden boards. (3) The artificial road signs on the same area in the panoramic image are different from the panoramic vision sensor in the distance, resulting in different pixel areas occupied by the artificial road signs in the panoramic image [9]. For example, the red and orange artificial road signs closer to the panoramic vision sensor are relatively large, while the green and purple artificial road signs farther from the panoramic vision sensor occupy a relatively small pixel area. Figure 1 shows two different catadioptric cameras. Though different kinds of reflex cameras to capture the scenery, the omnidirectional images obtained are different. When some reflex cameras project the image onto the curved mirror of the camera, it may cause distortion of the object images in the environment. Using a suitable reflex camera, we can get the projection of the corresponding image plane, so that the image is complete and undistorted, as shown in Figure 2.

The advantages of omnidirectional vision sensor applied to image detection are as follows: (1) a omnidirectional vision sensor can monitor a large range of scenes; (2) the cumbersome work of image fusion of multiple cameras is avoided when the image is tracked, and the detection algorithm is more simple; and (3) when acquiring scene images, the placement of omnidirectional vision sensors in the scene is more free, and real-time images of the scene can be obtained without aiming at the target. In systems that require panoramic real-time processing, the use of omnidirectional vision sensors to obtain images is a fast and reliable way to collect visual information [10].

2.1.1. Hyperbolic Concave Mirror Theory. Establish the relationship between the horizontal coordinate $m(s)$ of the object point and the horizontal coordinate s of the image point. The expression of this hyperbola is as follows:

$$\frac{(v-l-b)^2}{c^2} - \frac{m^2}{d^2} = 1. \tag{1}$$

Among them, $b^2 = c^2 + d^2$.

The lower half of the hyperbola can be expressed as

$$v = -\sqrt{\left(\frac{m^2}{d^2} + 1\right)} + l + b. \tag{2}$$

Here, suppose the horizontal coordinate $m(s)$ of the object point is a function of the horizontal coordinate s of the image point, the relationship between $m(s)$ and s is deduced against the optical path. The reflected light passes through the points $(s, 0)$ and $(0, -r)$; so, the straight line where the light lies can be expressed as a two-point formula:

$$\frac{m-0}{s-0} = \frac{v+r}{0+r}. \tag{3}$$

After finishing,

$$v = \frac{r}{s}m - r. \tag{4}$$

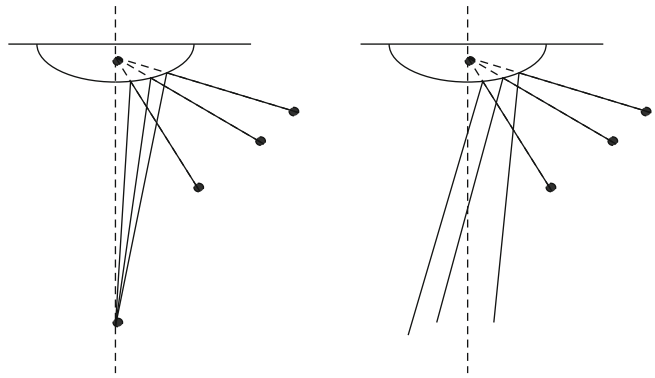

Figure 1: Two different catadioptric cameras.

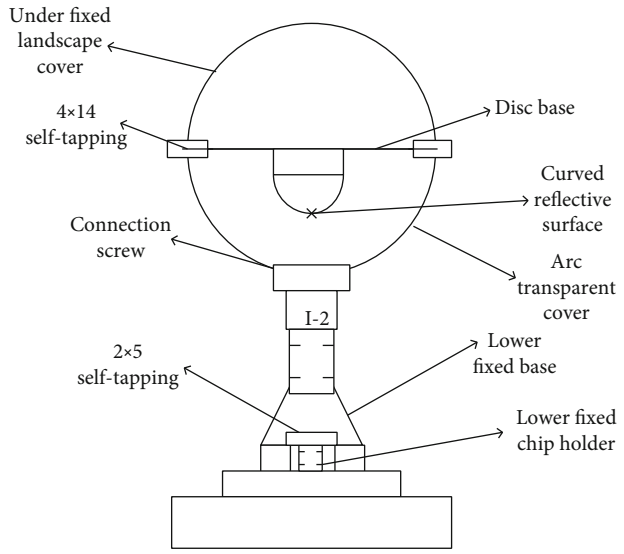

Figure 2: Vision sensor structure diagram.

The intersection point of the incident ray and the hyperbolic concave mirror is $q(m_q, v_q)$, the equation about x is obtained simultaneously, the equation is solved, and two solutions are obtained. The reflected light intersects the lower half of the hyperbola. Take the smaller solution m_q and substitute it to get v_q. Taking the derivation, we can know that the tangent slope of the hyperbola at point q is

$$k = -\frac{c}{d^2}\left(\frac{m_q^2}{d^2} + 1\right)^{-\frac{1}{2}} m_q. \tag{5}$$

Since the normal line is the perpendicular line of the tangent line, and the slope of the normal line and the slope of the tangent line have a negative reciprocal relationship, the normal slope of the hyperbola at point q is

$$k' = -\frac{d}{c^2}\left(\frac{m_q^2}{d^2} + 1\right)^{-\frac{1}{2}} \frac{1}{m_q}. \tag{6}$$

It can be known from the point oblique formula that the normal equation of the hyperbola at point P is

$$v - v_q = \frac{d}{c^2}\left(\frac{m_q^2}{d^2} + 1\right)^{-\frac{1}{2}} \frac{1}{m_q}\left(m - m_q\right). \tag{7}$$

From the law of light reflection, we know that; so, there is

$$\tan\delta = \tan\left(2\alpha - \beta\right) = \frac{\tan 2\alpha - \tan\beta}{1 + \tan 2\alpha \tan\beta}. \tag{8}$$

Moreover, because

$$\tan 2\alpha = \frac{2\tan\alpha}{1 - \tan^2\alpha} = \frac{2k'}{1 - k'^2}. \tag{9}$$

Substituting it in to get the slope of the incident light $k = \tan\delta$, from the point oblique formula, the straight line where the incident light lies is

$$v - v_q = k\left(m - m_q\right). \tag{10}$$

Substituting $v = -l$ into the position of the horizontal coordinate of the object point, the object-image relation function of this position is

$$m(s) = m_q(s) - \frac{l + v_q(s)}{k(s)}. \tag{11}$$

2.1.2. Micusik Perspective Projection Imaging Model. The sensor plane is a virtual plane perpendicular to the visible axis of the reflector. The center origin is the intersection of the image axis and the plane. The coordinate system is created based on the viewpoint of the mirror. Each possible image format of a microscope camera describes the process of creating a point on the image from a local point to a mirror point, that is, from the mirror point to the sensor surface and from the sensor surface to the camera surface point [11, 12].

(1) Conversion from Mirror Surface to Sensor Plane. The area vector generated by the single-view mirror a and the mirror point b projects the vertical point W onto the sensor plane through the optical center O of the perspective camera:

$$t' = \begin{bmatrix} w'^{R} \\ c' \end{bmatrix} = \begin{bmatrix} l\left(\|v'\|\right)v' \\ h\left(\|v'\|\right) \end{bmatrix}. \tag{12}$$

Among them, the function h represents the geometric shape of the mirror, and the function l represents the relationship between v' and $l(\|v'\|)v'$. This is determined by the reflection parameters of the reflector refracting mirror based on the projection transformation geometry. The relationship between the orthogonal point W and the space vector t' is as follows.

$$\eta t' = \eta \begin{bmatrix} w'^{R} \\ c' \end{bmatrix} = \eta \begin{bmatrix} l\left(\|v'\|\right)v' \\ h\left(\|v'\|\right) \end{bmatrix} = T.W, \eta > 0. \tag{13}$$

(2) Conversion from Sensor Plane to Image Plane. Since the optical axis of the SLR camera cannot form a certain angle with the plane O, the center of the image is centered on the sensor, and there is a certain distortion in the digital processing of the image. It is the conversion relationship from the sensor plane to the image plane, and the relationship between the two reference planes can be expressed by affine.

$$v' = Fv' + e. \tag{14}$$

Among them, $F \in P^{2\times2}$, $e \in P^{2\times1}$.

2.2. Art Design Image. Since the entry of art design into the 21st century, the rapid development of science and technology, the substantial improvement of design expression techniques, the increasing improvement of design tools, and the rapid development of output technology have all promoted the steady development of the field of art design. Due to the development of science and technology, the field of design has been strongly influenced by it, not only the efficiency of production has been greatly improved but also the realization of the design has made a substantial leap [13]. Moreover, the emergence of new materials has provided designers with more possibilities and enlightenment. People's pursuit is improving, the means and expressions of design must be constantly innovated, and the development from a single dimension to a multidimensional direction is a favorable way to achieve this goal. Secondly, in today's society, whether it is an audience or a designer, because of the fast paced life, people are receiving more and more pressure from work and life, and people cannot breathe. Therefore, people's demand for entertainment is becoming stronger and stronger. Entertainment can not only separate people from the tense atmosphere and get a moment of rest but also allow people to discover the beauty of life and the warmth of the world when they relax [14]. Therefore, if the designer can cut in at this point, it will definitely bring a sense of visual joy to the audience.

The performance of traditional art design is that whether the design elements used are abstract or realistic, most of the information presented to the audience is a flat image, and this image still uses the principle of designing a gestalt. The basic elements such as color, texture, dots, lines, and planes are consciously combined. This is also to more effectively and intuitively understand the content of the information to be expressed and to meet the aesthetic psychology of the audience [15, 16]. Nowadays, under the influence of factors such as the development of science and technology and people's desire for emotional enhancement, art design has shown a different form from the past, with multidimensional characteristics. It has broken the traditional paper medium's situation of covering the sky on one hand using a single paper medium, like the development of emerging media, from two-dimensional to$N$-dimensional development, from static viewing to dynamic interactive experience transformation. This kind of change is like the change brought to music by harmony. Those who have studied music know that when they first start, they must be a single syllable, which sounds boring and boring. With the improvement of skills and understanding, there will be gradually the addition of Hexuan, and the addition of Hexuan is like an injection of fresh blood, bringing new life to quiz and a new auditory feast. The relationship between intervals is like the relationship between the audience and the work. One to three or more variable parameters are called sound in harmony. According to the superimposed relationship of three degrees, combined in depth, it becomes the multidimensional "harmony" of artistic design and "Spin." However, in the traditional art design, its unique temperament has not been obscured or obliterated it, multidimensional art design only uses different media, and the multidimensional expression of art design uses various media that can magnify its advantages., in order to highlight the purpose of its design and more complete and efficient information visual services. When doing art design, we cannot simply start from people's visual sensory experience, but should consider the comprehensive application of multiple senses [17, 18]. Table 1 shows the relationship between color and sense in art design.

2.3. Sensory Experience. Sensory experience is an experience that integrates vision, hearing, touch, smell, and taste. It is the mental and physical changes that people recognize through their own sensory organs. In the context of the experience economy era, when people receive external information, they need the participation of various sensory systems. Today's society pays more and more attention to the humanization and individualization of design and emphasizes the basis of people's experience; so, art design should pay attention to other sensory functions [19, 20]. The content of sensory experience mainly includes the following three aspects:

2.3.1. Sensory Impact. Visual impact can change people's temporary "numbness." In the art design, strong color

Table 1: The relationship between color and sense.

Color	Hearing	Tactile	Taste	Smelling
Red	Lively, noise	Hot and rough	Spicy	Thick, burnt
Yellow	Bright and cheerful	Smooth and soft	Sweet	Fragrant
Orange	Loud, tragic	Fever, warmth	Hot and sour	Strong
Green	Clear, soft, calm	Relaxed and cool	Sour	Fresh, mint
Blue	Steady and elegant	Cold and hard	Jerky, fresh	Sea salt
White	Quiet and bright	Clean and flat	Tasteless and bland	Fragrant
Black	Heavy and vigorous	Hard	Bitter	Smoke

Table 2: Analysis of the stimulation form of the five senses.

Sensory type	Receptor	Stimulus input	Source of stimulus	Reactive properties
Sight	Eye	390-800 nm light wave	External	Shape, size, color, movement direction, etc.
Hearing	Ear	20-20000 Hz	External	The loudness, pitch, timbre, direction of sound source, and distance of the sound
Tactile	Skin	The effect of physical or chemical substances on the skin	Direct or indirect contact	Touch, pressure, pain, hot and cold, etc.
Smell	Nose	Volatile and dispersive substance	External	Floral, fruity, and other scents
Taste	Tongue	Substances dissolved in saliva	Direct or indirect contact	Sweet, bitter, spicy, and salty

contrast is often used to achieve the effect of visual impact. Auditory impact is generally the arrangement of music and the processing of special sounds in the process of brand image design and the use of auditory channels to convey important brand information [21].

2.3.2. Sensory Pleasure. Sensory pleasure refers to obtaining sensory comfort and enjoyment through people's vision, hearing, touch, taste, and smell. It is a method often used in brand image design. Although this way of expression is simple and direct, the effect it produces should not be underestimated [22, 23].

2.3.3. Sensory Interaction. "Interaction" means to relate to each other and communicate with each other. It is the communication process of emotional changes between people and things. Sensory interaction refers to participating in the environment through people's sensory organs, resulting in a kind of interesting communication [24, 25].

Table 2 shows the analysis of the stimulus form of the five senses.

3. Image Sensory Experience Experiment Based on Omnidirectional Visual Sensor in Art Design

3.1. Experimental Environment. In this paper, the recognition of artistic design images is developed by the Eclipse platform and realized by the Java language [26, 27]. The software development environment of the whole system is shown in Table 3.

Table 3: System software development environment.

Items	Development environment
Operating system	Windows XP sp3
Development tools	JDK 1.5,JMF2.1.2,Open CV
Development platform	Eclipse 3.1.1

3.2. Sources of Subjects. Most of the current image databases have not established special image collections for the study of image color casts. To conduct "case study" and "statistical research" on the color cast evaluation method proposed in this article, the two methods of downloading on the Internet and camera shooting are used to collect a large number of images, and these images are randomly divided into two groups, one is the "training group," which is used for related exercises before the formal test, and the other is the "experimental group," which is used for the formal test. First, 30 volunteers were selected, ranging in age from 15 to 55 years old, with normal vision and normal color vision.

3.3. Experimental Procedure. Before the formal test, the volunteers explained the purpose and operation process of the test in detail and conducted the corresponding training, so that the volunteers have a comprehensive and correct understanding and cognition of the "color cast," and the arbitrary color the image can correctly judge the color characteristics of the image. The entire 50 test process is divided into multiple stages, and the interval between the two stages is provided for volunteers to rest to avoid visual fatigue. 25 images are displayed at each stage. The first 5 images are selected from the training group to stabilize the subjective evaluation results of volunteers. The score data of these 5 images are not included in the result set. The last 20 images

are from the "experimental group" and the evaluation result income result set. In the formal test, volunteers are required to record the evaluation results one by one to avoid memory deviation. The evaluation results are divided into "essential color cast images," "true color cast images" (color cast images), "normal non-color cast images," "Unrecognized images." After each volunteer has completed the subjective evaluation of all images of the "experimental group," the result set needs to be preprocessed to remove the images with disputed classification results: the number of people only when a certain image is judged to be a certain category when it is not less than 18, and the image is marked as this category image and kept in the result set. If the number of people classified into the 4 categories is less than 18, the image is removed. After the preprocessing is completed, each image in the result set has an effective subjective evaluation mark, and the custom image library is now completed.

3.4. Experimental Description. Randomly select 200 images from the result set as the test image library for the effectiveness of the objective evaluation method, including 60 "true color cast" images, 35 "essential color cast" images, 85 "normal no color cast" images and 20 "unrecognizable" images; the remaining images in the result set are used as the training image library in the objective evaluation method research process. When the parameters are determined, according to the difference between the subjective evaluation results in the training library and the objective evaluation results obtained, correct the parameter threshold. The SIFT feature matching algorithm used in this article includes two stages: the first stage is the generation of SIFT feature;, that is, the feature vectors that are independent of scale, scaling, rotation, and brightness changes are extracted from multiple images to be matched; the second stage is the SIFT feature vector matching.

4. Image Sensory Experience Analysis Based on Omnidirectional Visual Sensor in Art Design

4.1. Image Database Dependency Test. Because the algorithm proposed in this paper that is only tested on the LIVE2 image database, it is impossible to ensure that the performance of this method can maintain a good advantage in other image databases. It can be seen from Table 4 that, compared with SSIM, 56BLIINDS-II, DIIVINE, and BRISQUE, the method in this paper maintains good consistency in the test results of degraded images in these two databases and is mature in terms of performance. The image quality evaluation algorithm is comparable. Therefore, based on the above data analysis, it can be concluded that the superior performance of the algorithm in this paper does not depend on a specific image database, and the test results of other image databases still maintain a high degree of credibility.

It can be seen from Table 4 that for JP2K images, using this algorithm is the best in performance; for JPEG images, although both SSIM and BLINDS-II algorithms have higher performance advantages than this algorithm, the algorithm proposed in this article is not bad. For blurred images, the performance advantage of this algorithm is significantly higher than other algorithms; for WN image performance, the overall evaluation can also be ranked second. Therefore, it can be seen that the algorithm proposed in this paper can maintain good consistency.

Table 4: Test results of the algorithms listed in this article on the TID2013 database.

	JP2K	JPEG	BLUR	WN
This algorithm	0.8124	0.8775	0.9345	0.9487
SSIM	0.9583	0.9313	0.8372	0.9721
BLIINDS-II	0.9014	0.8987	0.6731	0.8523
DIICINE	0.9198	0.8723	0.8473	0.8682
ROI-BRISQUE	0.8472	0.9174	0.8512	0.8988
BRISQUE	0.8387	0.9173	0.8289	0.8900

4.2. Performance Comparison of Different Distortion Types. Distortion, also known as "distortion," refers to the deviation of a signal from the original signal or standard during transmission. In an ideal amplifier, the output waveform should be the same as the input waveform except for amplification, but it cannot be done. When the output waveform is the same as the input waveform, this phenomenon is called distortion.

It can be seen from Figure 3 that whether it is a single distortion type or multiple distortion types coexisting, the PLCC evaluation index value of this algorithm is higher than the performance evaluation index value obtained by the BRISQUE algorithm and the RMSE value obtained by the algorithm in this paper. They are also smaller than the RMSE value obtained by the BRISQUE algorithm. Generally speaking, the performance of the algorithm in this paper is better than the BRISQUE algorithm. At the same time, the accuracy of the prediction results of this algorithm is better than that of the BRISQUE algorithm for the five types of degraded images in the LIVE2 database. The algorithm makes full use of the human visual characteristics, so that its evaluation results are more in line with the subjective evaluation results. Compared with the current mature objective quality evaluation algorithms, the algorithm in this paper shows superior performance in all aspects. The method given in this paper belongs to a new type of nonreference image quality evaluation algorithm, which maintains good consistency with the visual perception characteristics of the human eye.

4.3. False Detection Rate and Missed Detection Rate

4.3.1. False Detection Rate. Figure 4 shows the error detection rate of the three methods. Among these methods, the false detection rate of the SSC method is relatively the highest. The contour detected by this method has a lot of texture interference. Combined with the detected images, it can be seen that the method does not perform the same operation in texture suppression. Although the integrity of the main contour is very high, the texture will interfere with the highlights of the contour, resulting in a detection effect which is not ideal. In terms of error detection, the method in this

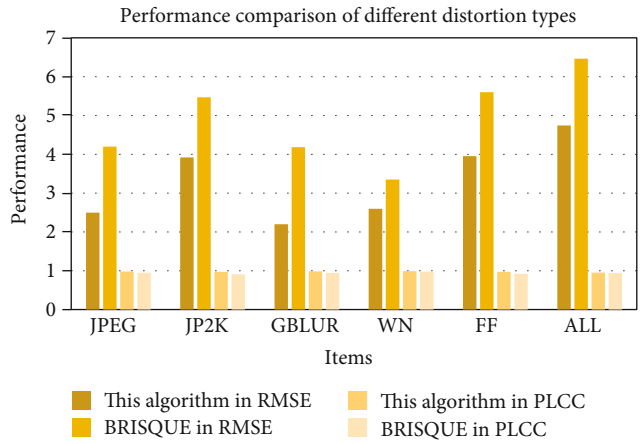

Figure 3: Performance comparison of different distortion types.

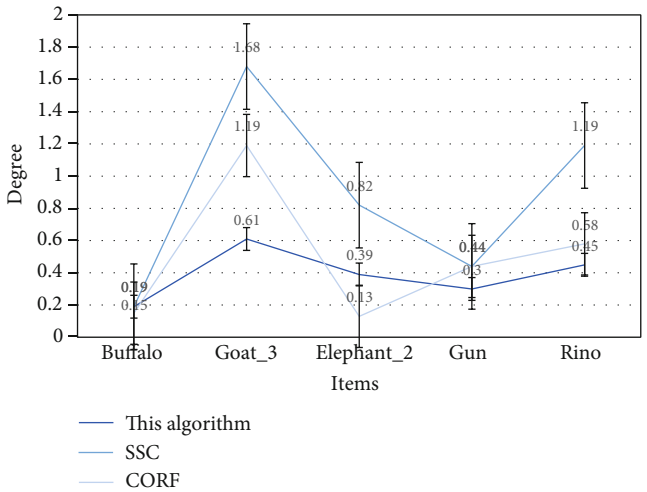

Figure 4: False detection rate.

paper performs relatively well and can maintain a relatively stable error detection rate, indicating that the method performs well in suppressing background texture. Combined with the detected images, it can be seen that the contour details of the image are seriously lost.

4.3.2. Missed Detection Rate. Figure 5 shows the missed detection rate. Among these methods, the SSC method performs better in missing detection, and the missed detection rate is relatively low, indicating that the method detects better contour integrity. In terms of missed detection rate, CORF is relatively high, indicating that the texture is excessively suppressed. Combined with the detected images, it can be seen that the contour details of the image are seriously lost. Compared with the SSC method and the CORF method, the method in this paper has an absolute advantage in the balance of missing detection and false detection.

4.4. Algorithm Time-Consuming Comparison. For image quality evaluation, the computational complexity of the algorithm is another important indicator for judging the performance of the algorithm. Table 5 shows the average

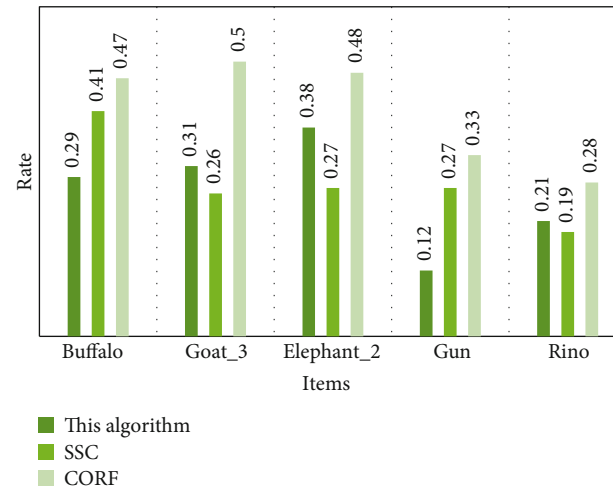

Figure 5: Missed detection rate.

Table 5: The average calculation speed of the algorithm in this paper and the existing algorithm in SIQAD.

Model	Time cost
This algorithm	0.4118
PSNR	0.0298
SSIM	0.0512
VIF	1.2987
IFC	1.2981
GSS	0.1389
SIQM	0.1241

computational complexity of each full-reference image quality evaluation method. The computational complexity of the full-reference image quality evaluation method can be divided into three levels. The first level is PSNR and SSIM. They run much faster than other algorithms, but their predicted scores do not fit well with subjective scores. The second level is SIQM, GSS, and the algorithm of this paper. They run fast and have excellent performance. The algorithm of this paper has achieved the best performance indicators. The third level is VIF and IFC, which have relatively high computational complexity. According to the weighing calculation accuracy and calculation efficiency of the screen image quality evaluation method, the algorithm can achieve excellent results.

4.5. Sensory Experience Analysis. As shown in Figure 6, it shows the audience's four feelings for four different art design images. The four feelings include happiness, sadness, melancholy, and peace. Clearly, for the first image, 87.21% of the audience's feelings are happy, indicating that the main idea of this image can bring joy to people. In the second image, the audience's feelings are mostly sad. For the third image, more than half of the audience's feelings are melancholy. For the fourth image, 69.34% of the audience's inner feelings are calm, explaining that the difference in the content of artistic design images can bring different sensory experiences to people.

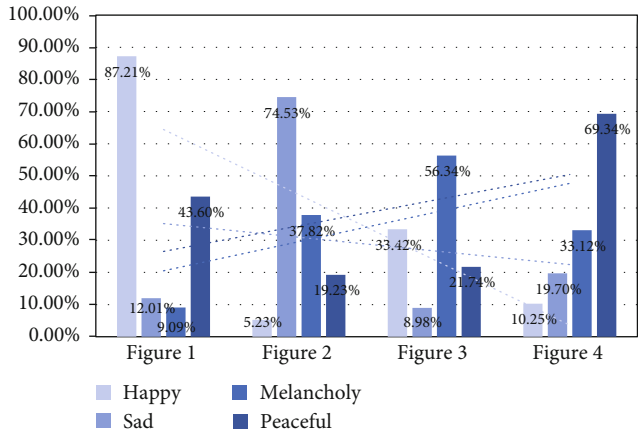

Figure 6: The audience's feelings about different art designs.

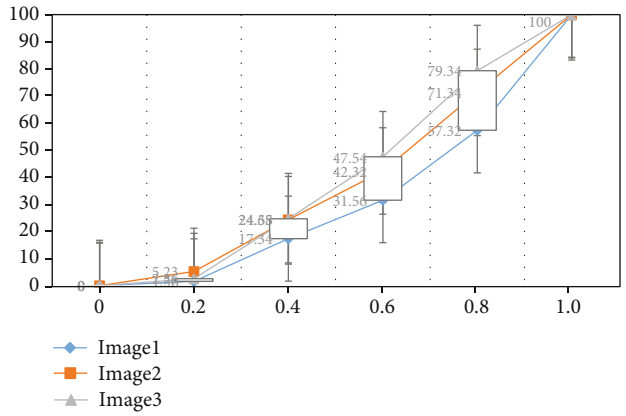

Figure 7: The number of final matching points under different thresholds.

4.6. Feature Point Selection. Figure 7 shows the number of feature points under different thresholds. The threshold in this paper can be determined by the results of multiple experiments. Taking the actual PCB image as an example, if 1000 matching point pairs are obtained by rough matching, the final matching point pairs that pass the nearest neighbor ratio test when different thresholds are set are shown in the figure. When the threshold is a higher value, the number of matching point pairs will increase, but the computational complexity will also increase, resulting in a decrease in overall efficiency; when a lower value is taken, the result is the opposite. In general, a good balance can be achieved between efficiency and accuracy.

5. Conclusion

Image is the most intuitive way of visual language and information reading, it helps the public to quickly and accurately read useful information. This article reanalyzes information design from the perspective of artistic aesthetics and proposes that artistic images should be used to accurately convey information. Artistic images are aesthetic and can meet people's aesthetic needs. Aesthetic activities are the unity of sensibility and rationality. Through artistic images, they have a perceptual understanding of information, which arouses the emotional resonance of readers and leaves a deep impression in their minds. At the same time, this article also has certain limitations and deficiencies. The sensor used in this article is a panoramic vision sensor, and the positioning effect obtained is still good, but this is for the more structured scene of the experimental environment; if the real environment is more complicated, it may not be possible to have such precise positioning or even unable to complete the positioning. It is difficult to truly perform positioning and navigation tasks in life by relying on a single sensor. Therefore, a method of combining multiple sensors is required. This is not only the best way to improve positioning accuracy and success rate, but also a hot trend in future positioning research. To improve the artificial intelligence and object-oriented nature of art design, an art design system design method based on image processing technology is proposed. The color difference compensation method is used for the image brightness balance restoration processing for the artistic design image, the image fusion is combined with the pixel quantization tracking method, and the wavelet noise reduction technology is used to realize the image noise reduction processing, thereby completing the image processing in the artistic design. In the future, the use of image recognition can more effectively realize the image output in art and improve the output quality of art design images, the output signal-to-noise ratio of the image is high, and the human-computer interaction performance of the system is better.

Data Availability

The data underlying the results presented in the study are available within the manuscript.

Conflicts of Interest

The author declares that he has no conflict of interest regarding the publication of the research article.

References

[1] F. Zhou, X. Chai, X. Chen, and Y. Song, "Omnidirectional stereo vision sensor based on single camera and catoptric system," *Applied Optics*, vol. 55, no. 25, pp. 6813–6820, 2016.

[2] I. Svetlichnaya, "Methods of art Design in the Design of the External Image of a person," *Scientific Research and Development Modern Communication Studies*, vol. 9, no. 4, pp. 68–75, 2020.

[3] H. Abusaada, "Strengthening the affectivity of atmospheres in urban environments: the toolkit of multi-sensory experience," *International Journal of Architectural Research Archnet-IJAR*, vol. 14, no. 3, pp. 379–392, 2020.

[4] L. Wu, C.-H. Chen, and Q. Zhang, "A mobile positioning method based on deep learning techniques," *Electronics*, vol. 8, no. 1, p. 59, 2019.

[5] N. Chen, B. Rong, X. Zhang, and M. Kadoch, "Scalable and flexible massive MIMO precoding for 5G H-CRAN," *IEEE Wireless Communications*, vol. 24, no. 1, pp. 46–52, 2017.

[6] Z. Yang, S. Lu, T. Wu, G. Yuan, and Y. Tang, "Detection of morphology defects in pipeline based on 3D active stereo omnidirectional vision sensor," *IET Image Processing*, vol. 12, no. 4, pp. 588–595, 2018.

[7] D. L. Stone, G. Shah, Y. Motai, and A. J. Aved, "Vegetation segmentation for sensor fusion of omnidirectional far-infrared and visual stream," *IEEE Journal of Selected Topics in Applied Earth Observations and Remote Sensing*, vol. 12, no. 2, pp. 614–626, 2019.

[8] J. Cui, H. Yoon, and B. D. Youn, "An omnidirectional biomechanical energy harvesting (OBEH) sidewalk block for a self-generative power grid in a Smart City," *International Journal of Precision Engineering and Manufacturing-Green Technology*, vol. 5, no. 4, pp. 507–517, 2018.

[9] A. K. Sood, G. Pethuraja, R. E. Welser et al., "Development of large area nanostructured antireflection coatings for EO/IR sensor applications," *Advances in Computational Sciences & Technology*, vol. 9, no. 1, pp. 87–100, 2016.

[10] J. Schneider, C. Stachniss, and W. Forstner, "On the accuracy of dense fisheye stereo," *IEEE Robotics & Automation Letters*, vol. 1, no. 1, pp. 227–234, 2016.

[11] K. Qiu, T. Liu, and S. Shen, "model-based global localization for aerial robots using edge alignment," *IEEE Robotics and Automation Letters*, vol. 2, no. 3, pp. 1256–1263, 2017.

[12] Z. Xiang, S. Chen, L. Luo, and N. Zou, "compact omnidirectional multi-stereo vision system for 3D reconstruction," *Applied Optics*, vol. 57, no. 34, pp. 9929–9935, 2018.

[13] Z. Wang, D. Liang, J. Zhang, and H. Liu, "A SLAM method based on inertial/magnetic sensors and monocular vision fusion," *Jiqiren/Robot*, vol. 40, no. 6, pp. 933–941, 2018.

[14] P. Lo, A. Cho, M. Leung, D. K. W. Chiu, E. H. T. Ko, and K. K. W. Ho, "use of smartphones by art and design students for accessing library services and learning," *Library Hi Tech*, vol. 34, no. 2, pp. 224–238, 2016.

[15] L. Jieun, "The effects of stylistic information about an art image on consumers' aesthetic responses in package design," *The Korean Journal of Consumer and Advertising Psychology*, vol. 17, no. 2, pp. 251–270, 2016.

[16] H. Ji and Y. Shang, "Using color difference compensation method to balance and repair the image of art design," *Complexity*, vol. 2021, no. 2, Article ID 3516745, 2021.

[17] S. Breakell, "The handbook of art and design librarianship," *Journal of the Society of Archivists*, vol. 39, no. 2, pp. 265–267, 2018.

[18] L. Chen, "Research on the art design innovation based on computer 3D aided system optimization," *Revista de la Facultad de Ingenieria*, vol. 32, no. 12, pp. 248–254, 2017.

[19] R. Ezhilarasi and K. Venkatalakshmi, "Low complexity orthogonal transforms for low cost image/video codec design," *Journal of Computational and Theoretical Nanoscience*, vol. 15, no. 3, pp. 859–865, 2018.

[20] H. Wang and Y. Tang, "Application of art design semiotics in environmental art," *Boletin Tecnico/Technical Bulletin*, vol. 55, no. 20, pp. 238–243, 2017.

[21] Y. Xu and Y. Li, "Research on computer aided environmental art design based on 3D studio max," *Revista de la Facultad de Ingenieria*, vol. 32, no. 3, pp. 149–155, 2017.

[22] A. R. Mardinly, I. Spiegel, A. Patrizi et al., "Sensory experience regulates cortical inhibition by inducing IGF1 in VIP neurons," *Nature*, vol. 531, no. 7594, pp. 371–375, 2016.

[23] K. P. Wiedmann, F. Labenz, J. Haase, and N. Hennigs, "The power of experiential marketing: exploring the causal relationships among multisensory marketing, brand experience, customer perceived value and brand strength," *Journal of Brand Management*, vol. 25, no. 2, pp. 101–118, 2018.

[24] F. Ferri, Y. S. Nikolova, M. G. Perrucci et al., "A neural "tuning curve" for multisensory experience and cognitive-perceptual schizotypy," *Schizophrenia Bulletin*, vol. 43, no. 4, pp. 801–813, 2017.

[25] J. Zhang, "Tasting tea and filming tea: the Filmmaker's engaged sensory experience," *Visual Anthropology Review*, vol. 33, no. 2, pp. 141–151, 2017.

[26] A. Y. Shishelova, R. R. Aliev, and V. V. Raevskii, "Effect of early sensory experience on the exploratory activity in adult animals," *Doklady Biological Sciences*, vol. 468, no. 1, pp. 101–103, 2016.

[27] Y. S. Baek, "A study on the process of meaning-making in art education: focusing on the sensory experience of Locke and Hume," *Journal of Research in Art Education*, vol. 21, no. 3, pp. 47–65, 2020.

Hindawi
Journal of Sensors
Volume 2021, Article ID 8592558, 10 pages
https://doi.org/10.1155/2021/8592558

Research Article

Automatic Parking Path Planning Based on Ant Colony Optimization and the Grid Method

Guo Liang Han

School of Artificial Intelligence, Beijing Technology and Business University, Beijing 100048, China

Correspondence should be addressed to Guo Liang Han; 1830302005@st.btbu.edu.cn

Received 17 June 2021; Revised 30 June 2021; Accepted 31 July 2021; Published 5 October 2021

Academic Editor: Mu Zhou

This paper analyzes the path planning problem in the automatic parking process, and studies a path planning method for automatic parking. The grid method and the ant colony optimization are combined to find the shortest path from the parking start point to the end point. The grid method is used to model the parking environment to simulate the actual parking space of automatic parking; then this paper makes some improvements to the basic ant colony optimization, finds the destination by setting the ants' movement rules in the grid, and finds the shortest path after N iterations; since the optimal path found is a polyline, it will increase the difficulty of controlling vehicle path tracking and affect the accuracy of vehicle path tracking. The bezier curve is used to generate a smooth path suitable for vehicle walking. Finally, through matlab simulation, the obstacles in the environment are simulated, and the parking trajectory is obtained. The results show that the path planning method proposed in this paper is feasible.

1. Introduction

The problem of automatic parking path planning is to find a better movement path from the parking start point to the end point in the known parking environment, so that the vehicle can reach the expected parking location safely and without collision during the movement.

The current research status of automatic parking path planning at home and abroad is as follows:

Piao CH, Zhang L, Lu S [1] and others combined the actual environment and used several arcs to form an automatic parking trajectory. It has strong adaptability to the environment and is similar to traditional parking trajectory generation methods. Compared with the method, the success rate and adaptability of this method are better; Jiang H, Guo KH, Zhang JW [2] analyzed and backed up the possibility of vehicle collision in the parking space, provided trajectory constraints for subsequent parking, realized parking path planning, and verified the correctness of the above strategy in actual simulations; Liang Z, Zheng G, Li J [3] studied the possible collisions of vehicles with obstacles in the parking space, using Ackerman geometric steering formula to generate parking arcs, and using Bezier curves to make the generated parking trajectory smoother, so as to get the final parking trajectory; Choi S, Boussard C, D'Andrea-Novel B, et al. and Vorobieva H, Glaser S, Minoiu Enache N, et al. [4, 5] calculated the parking trajectory of vehicle using a purely geometric method based on the geometry and maximum turning angle of the vehicle; Ge Y, Chen Y, Dai G [6] and others realized that when the vehicle is parked at the initial point, the vehicle can be in any position.

Wu Bing, Qian Lijun and others of Hefei University of Technology analyzed the possible collision points of parallel parking process and calculated the minimum parking space required for parking through reverse path planning, replacing the initial points of traditional path planning with the initial parking area. The use of different data samples for the particle swarm optimization RBF neural network avoids the analysis of various constraint relations such as safety distance, so that the planned parking path can be better suitable for the parking process [7]. Li Hong and Guo Konghui of Hunan University analyzed the design requirements of the

parking trajectory curve and integrated the characteristics of the B-spline curve, and proposed a method for automatic vertical parking trajectory planning based on the B-spline curve theory by optimizing the trajectory control points [8].

Throughout the research on automatic parking trajectory planning at home and abroad, one-time global planning is mainly used to obtain a safe path from the parking start point to the end point, and some algorithms are used to optimize the path, such as genetic algorithm [9], B-spline curve algorithm and fuzzy algorithm, but these methods have problems such as large search space, complex algorithm, and low efficiency. The genetic algorithm's ability to explore new spaces is limited, and it is easy to converge to a local optimal solution. The processing scale is small. When the problem is complex, the calculation time is very long. While using the B-spline curve for parking trajectory planning, although a B-spline curve can be drawn, it is necessary to repeatedly calculate the cubic polynomial of each coordinate component. The calculation amount is also quite large, and the drawing and fitting speed is extremely slow, which is difficult to satisfy actual needs. At the same time, the above method cannot effectively avoid obstacles when there are other obstacles in the parking environment (except for the already parked vehicles).

Chen Xin and Lan Fengchong of South China University of Technology [10] used reinforcement learning to realize automatic parking, and proposed a staged training method based on curriculum learning for parking problems, which accelerated the algorithm convergence, and the planning success rate reached 90.6%; Wang Qiming and Zong Gaoqiang of the University of Shanghai for Science and Technology [11] proposed a multi-stage parking path planning for the narrow parallel parking path and the discontinuity of the parking trajectory. The final parking attitude angle is the smallest as the index for finding the optimal solution; Song Jie of Shanghai University of Engineering and Technology [12] combined panoramic vision and lidar to improve the accuracy of parking space detection when there is no nearby vehicle or parking space marking line, and proposed a parking path planning method based on B-spline theory.

Ren-Fang Zhou, et al. [13], aiming at the error of the tracking algorithm in the automatic parking system, proposed a secondary path plan, updated the parking path, and divided the path into 24 Segment model, using traversal strategy to select path mode, using secondary planning algorithm to fine-tune the path model to achieve the best effect. Jiangbo Meng, et al. [14] have proposed a parking path tracking algorithm combining fuzzy control and Kalman filter for the low accuracy of automatic parking path tracking caused by sensor noise, and the actual driving is established based on the vehicle kinematics equations. The deviation model of the path and the reference path, the Kalman filter is used to reduce the measurement noise in the vehicle position and heading angle measurement data, and the simulation model is established through Matlab/Simulink to verify the effectiveness of the proposed algorithm. Hao Ye, et al. [15] proposed a linear model predictive control path tracking control strategy with softening constraints on how to improve the accuracy of automatic parking path tracking control. Establish a linear time-varying prediction model of the vehicle, predict the future state of the vehicle, add a relaxation factor in the optimization process, calculate the control increment of each cycle through quadratic programming, roll optimization and feedback correction, and correct various deviations in the control process in time. Ti-chun Wang, et al. [16] discussed the AGV Navigation Analysis method based on multi-sensor data fusion.

In addition, the above-mentioned methods only start from a fixed parking starting point, and then complete the parking route planning and the entire parking process. However, in real life, the starting position is found by the driver. Since each driver's driving skills and driving habits are different, it is difficult to ensure that each driver can drive to the ideal starting point during normal parking position. If the driver is strictly required to park the car at the specified starting position before parking, it will increase the difficulty of driving for the driver, and the driver will spend a lot of energy in determining the starting position, so that it will not be convenient for the driver to park in parallel into the parking space.

In view of the shortcomings of the above-mentioned automatic parking path, this paper conducts a new research on the automatic parking algorithm, and proposes a more adaptable solution, which combines the ant colony optimization with the grid method to find the shortest path from a starting point to the end point, and the bezier curve function is added to obtain a trajectory that allows the vehicle to park, which can not only effectively increase the range for the driver to find the starting parking position, but also avoid obstacles when other obstacles are involved in the parking environment, which increases the adaptability of automatic parking to the environment.

2. Environmental Description and Modeling

A reasonable representation of the environment is conducive to the planning of the best path during the parking process. The grid method is a representation method of the spatial geographic environment. It divides the geographic space into regular grids, which have the characteristics of uniform size and binary value. The size of the grid is the same, and the selection of the grid size affects the effect of path planning. Smaller grids increase storage space and computing power. At the same time, interference signals will also increase. Larger grids make environmental planning unclear, and the results are not credible. Setting the grid size as the basic step length of the vehicle is a feasible solution; Binary means that each grid has only two values with different values, free grid and obstacle grid, depending on whether there are obstacles in the grid. The raster is stored in the form of a raster array, where there is an obstacle 1 to indicate, and there is no obstacle 0 to indicate. During the movement of the vehicle, the grid remains stationary, and the movement of the vehicle is converted into the movement of the vehicle from one grid to another.

The establishment of the environmental model is a very important part of the automatic parking path planning of

vehicles. The actual parking environment of the vehicle is an actual physical space, but the space processed by the path planning algorithm is an abstract representation of the environment.

In this paper, the grid method [17] is used to establish an environment model to simulate the actual parking space of automatic parking. In the application of the grid method, the grid method uses the basic element as the minimum grid granularity to divide the map into grids. The basic element is located in the free area and the value is 0, and the obstacle area or the obstacle-containing area is 1; Then the model recursively divides the environment into 4 equal-sized subregions until the basic units contained in each region are all 0 s or all 1 s.

For the automatic parking environment, a limited number of vehicles parked can be regarded as obstacles. These obstacles are easy to map due to their coordinate positions and can be regarded as known environmental information. After ergodic learning the two-dimensional space of automatic parking, a grid map can be established.

Ignoring the information in the height direction of the vehicle, the two-dimensional space where the vehicle is parked is recorded as LOL, and a limited number of vehicles are parked in its internal parking space, which can be regarded as an obstacle. For automatic parking in a static environment, the position and size of obstacles can be detected, and they will not change during the movement of the vehicle. In LOL, the lower left corner is the coordinate origin, the direction parallel to the car body is the X axis, and the direction perpendicular to the car body is the Y axis to establish a system rectangular coordinate system Σ. All the following diagrams are created in this way, and will not be repeated. The maximum value of LOL in the x-axis and y-axis directions is $X_{\max}$ and $Y_{\max,}$ respectively.

If there are no obstacles in a certain grid size range, the grid is called a free grid and expressed in white; otherwise, it is called an obstacle grid and expressed in gray. When $X_{\max}= Y_{\max}=17$, the grid model of the vehicle parking space is shown in Figure 1. In the figure, the side length of each grid is 0.5 m, and the ants can only move from one grid center point to another grid center point at a time during the ant's marching process, which stipulates that they cannot walk diagonally.

In Figure 1, the lower two black areas represent vehicles that have parked in the parking spaces, and the blank area between the two vehicles is the empty parking space to be parked. According to the relevant vehicle size information, the length of the vehicle is approximately 2.5 times the width of the vehicle. Therefore, for the convenience of description, in the grid environment, the size of the vehicle occupies 10 grids, and it is specified that the vehicle close to the lower left origin is car A, and the vehicle on the right is car B. Here we specify the grid number occupied by each vehicle is 1, 2, 3, 4, 5, 6, 7, 8, 9, 10 from the upper left corner to the right.

In addition, we introduced the serial number method to identify all grids:

As shown in Figure 1, starting from the upper left corner of the grid array, each grid is numbered in the order from left to right and top to bottom, and the sequence number n is from 1 to 289 in turn. The grid identified by the serial number method is recorded asG_n, for example, the grid with serial number 1 is recorded as G_1.

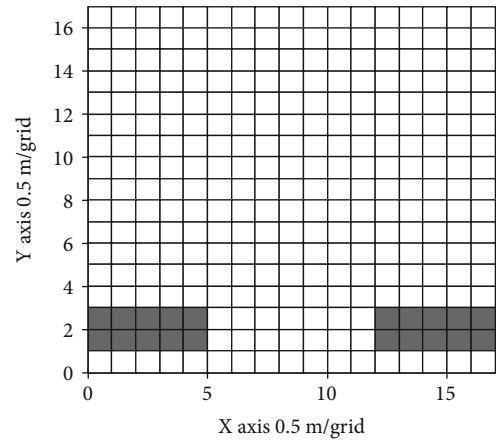

Figure 1: The grid figure of vehicle parking environment.

For grid environments of other scales, the relationship between grid number and grid coordinates is the same as this type.

In order to verify the feasibility of the ant colony optimization in automatic parking path planning, in this study, the starting position $G_{209}$of the vehicle path planning is the ant nest and the target position $G_{266}$is the food source. Set the 10th grid in the lower right corner of the 10 grids occupied by the vehicle as the research point of the vehicle so that it coincides with G_{209}, and the trajectory of the vehicle during operation is the trajectory of the vehicle's automatic parking. In the grid environment of 17×17, during the parking process, from the starting point G_{209} to G_{266}, if no obstacles are detected in the forward direction of the parking, the two squares on the top right of the fifth square of car A, the grid G_{227} and G_{228} are set as a safe area, and the vehicle path cannot pass through this square. At this time, the first two steps in the ant's pathfinding can only be two squares in the direction parallel to the vehicle body, and then go down in the direction closer to the destination. In such a grid environment, with the restriction of the safe area, not only can the vehicle to be parked avoid collision with car A, but at the same time, when the Bezier function is used to obtain the parking trajectory at the end, it can also ensure that the radius of the curve is larger than the minimum turning radius of the vehicle.

In the same way, if an obstacle is detected in the forward direction of the parking at the beginning of parking, only set square G_{227}as the safe area, and the surrounding obstacle square is set as a safe area, so that the vehicle can avoid collision with car A and obstacles during parking, and also ensure that the final Bezier curved path meets the parking conditions.

The proof is as follows:

According to the theory of calculus, the curvature of the curve is:

$$k = \left|\frac{d\varphi}{ds}\right| = \left|\frac{\left(y/1 + y'2\right)dx}{\sqrt{1 + y'2}dx}\right| = \left|\frac{y''}{\left(1 + y'2\right)^{3/2}}\right| \tag{1}$$

Then the radius of curvature is:

$$\rho = \frac{1}{k} \tag{2}$$

According to the quadratic Bezier curve:

$$Q(t) = \sum_{t=0}^{2} B_{i,2}(t) \cdot P_i = (P_2 - 2P_1 + P_0)t^2 + 2(P_1 - P_0) \cdot t + P_0 \tag{3}$$

and so,

$$\begin{aligned} \frac{dy}{dt} &= (Y_2 - 2Y_1 + Y_0)t + (Y_1 - Y_0) \\ \frac{dx}{dt} &= (X_2 - 2X_1 + X_0)t + (X_1 - X_0) \end{aligned} \tag{4}$$

Therefore, the radius of curvature is:

$$\rho = \left|\frac{\left[(dx/dt)^2 + (dy/dt)^2\right]^{3/2}}{(dy/dt)' \cdot (dx/dt) - (dy/dt) \cdot (dx/dt)'}\right| \tag{5}$$

(1) In the case of obstacles, because the vehicle has to avoid obstacles, the first three points of its forward path are: starting point A, intermediate point B_1, and intermediate point B_2. The coordinates are

$$\begin{aligned} A(X_0, Y_0) &= (4.5, 4.5) \\ B_1(X_1, Y_1) &= (6.5, 4.5) \\ B_2(X_2, Y_2) &= (6.5, 2.5) \end{aligned} \tag{6}$$

Putting the above coordinates into the curvature radius formula, we get

$$\begin{aligned} \frac{dy}{dt} &= (2.5 - 2 \times 4.5 + 4.5)t + (4.5 - 4.5) = -2t \\ \frac{dx}{dt} &= (6.5 - 2 \times 6.5 + 4.5)t + (6.5 - 4.5) = -2t + 2 \end{aligned} \tag{7}$$

Then, We can get

$$\rho = \left|\frac{\left[(2 - 2t)^2 + (-2t)^2\right]^{3/2}}{-2 \times (2 - 2t) + 2t \times (-2)}\right| = \left|\frac{\left(8t^2 + 4 - 8t\right)^{3/2}}{-4}\right|, t \in (0, 1) \tag{8}$$

When t takes 0 or 1,ρ=2,that is, the curve composed of the first three points of the bezier curve is equivalent to a quarter circle, and the bezier curve in the presence of obstacles is a curve composed of more than three control points. Therefore, the curvature of the bezier curve is greater than ρ=2.

In addition, according to the calculation formula of the vehicle's minimum turning radius [14]:

$$R = \frac{L}{\sin \theta_{\max}} + \frac{b - M}{2} \tag{9}$$

Among them: L is the wheelbase, $\theta_{\max}$ is the maximum turning angle of the outer wheel of the steering wheel, b is the front track, and M is the center distance of the main pin.

After consulting the relevant vehicle size, for the convenience of calculation, this article reduces the vehicle ratio to a ratio of vehicle length to vehicle width of 2.5, that is, the vehicle length is 2.5 m and the vehicle width is 1 m. In this way, we can get the corresponding wheelbase L =1.42 m, front wheelbase b =0.81 m, and kingpin center distance M =0.65 m,$\theta_{\max}$=40°.

It can be obtained from the above data that the minimum turning radius of the vehicle is R =1.96 m.

It can be seen from the above calculation that $\rho$is greater than the minimum turning radius R =1.96.Therefore, in the presence of obstacles, the vehicle can park along the path.

(2) In the absence of obstacles, since the safe area is two square spaces, the first three points of the path of the vehicle to be parked are the starting point A, the middle point B_1, and the middle point B_2

$$\begin{aligned} A(X_0, Y_0) &= (4.5, 4.5) \\ B_1(X_1, Y_1) &= (7.5, 4.5) \\ B_2(X_2, Y_2) &= (7.5, 1.5) \end{aligned} \tag{10}$$

In the same way, it can be known from the formula of the radius of curvature of the Bezier function that the radius of curvature at this time must be greater than the radius when there are obstacles.

In this way, while the grid environment is established and the safe area is set, it is ensured that the radius of curvature of the parking path is greater than the minimum turning radius of the vehicle.

3. Description and Definition of Parking Path Planning Problem

Problem Description: The path planning of automatic parking is to find a suitable parking trajectory from the parking start point to the parking end point, so that the vehicle can be parked into the empty parking space smoothly. Since this article uses the Bezier function to curve, it can fit any number of control points, and the curvature is relatively small. Therefore, the mathematical description of ant colony optimization applied to automatic parking can be find a path

from the starting point A through the intermediate point $B = \{b_1, b_2, \cdots \cdots b_n\}$ to the ending point C, so that the objective function:

$$D = \sum_{1}^{n} d(A, b_1) + d(b_2, b_3) + \cdots + d(b_{n-2}, b_{n-1}) + d(b_n, C) \tag{11}$$

Get the minimum value, which $d(A, b_1), d(b_{n-2}, b_{n-1}), d(b_n, C)$ are all equal to 1, when each ant is walking, it cannot walk along the diagonal. This can ensure that the middle point will not be far away from the target point during the path finding process, making the bezier curve fitting more suitable for parking.

In order to simulate the foraging behavior of the actual ant colony, in this study, the starting position of the vehicle path planning G_{209} is the ant nest, and the target position G_{266} is the food source. If the starting point select G_{208}, then the vehicle can also be parked, so there is no need to search for the starting point artificially.G_{209} is selected in the 10 grids above the A car and a row apart from the A car. The vehicle parking path planning based on the ant colony optimization is actually through the interaction and cooperation between the ants in the ant colony to avoid the front and rear cars of the parking space and finally find an optimal path from the ant nest to the food source. For the convenience of the following description, the variables used here are defined as follows:

n is the total number of grids, in the environment studied in this paper, n =289. That is, when the vehicle perceives the entire parking environment, it is modeled as a 17×17 grid environment. For a more refined grid environment, further research is needed.

K is the number of iterations, that is, how many waves of ants are dispatched in total; M is the number of ants (the number of ants in each wave), in this algorithm, m =50.

S represents the starting point, E represents the end point, Alpha represents the parameter that characterizes the importance of the pheromone, Beta represents the parameter that characterizes the importance of the heuristic factor, Rho represents the pheromone evaporation coefficient, Q represents the pheromone increase intensity coefficient, and Tau represents the output dynamics Corrected pheromone.

d_{ij} is a matrix that records the distance between all grids. d_{ij}represents the distance between $G_i$and G_j, (the distance between the geometric center points of the two grids is defined as the distance between the grids), and there are:

$$d_{ij} = \sqrt{[a(i) - a(j)]^2 + [b(i) - b(j)]^2} \tag{12}$$

Among them, $a(i)$and $a(j)$are the abscissas of grids G_i and G_j, respectively, and $b(i)$ and$b(j)$are the ordinates of grids G_i and G_j, respectively.

In the basic ant colony optimization, the ants decide the next transfer direction based on the amount of pheromone on each path and the heuristic information on the path. The state transition rule used is called the random proportional rule, which gives the probability that the ant k at the node i chooses the node j as the transition direction:

$$P_{ij}^{k}(t) = \begin{cases} \dfrac{\tau_{ij}^{\alpha}(t)\eta_{ij}^{\beta}(t)}{\sum_{s \in allowed_k} \tau_{is}^{\alpha}(t)\eta_{is}^{\beta}(t)} & j \in allowed_k \\ 0 & otherwise \end{cases} \tag{13}$$

Where: η_{ij}represents the visibility in the direction i, j.

$\tau_{ij}(t)$ represents the amount of residual information on the line segment ij at time t.

α represents the relative importance of pheromones ($\alpha \geq 0$).

β represents the relative importance of visibility ($\beta \geq 0$).

4. Automatic Parking Path Planning Based on Ant Colony Optimization and Grid Method

The ant colony optimization is a probabilistic algorithm used to find the optimal path. It was proposed by Marco Dorigo in 1992. It was inspired by ants finding the path when looking for food. It is a bionic algorithm, in the process of foraging, ants can always find the optimal path. The behavior of a single ant when looking for food is relatively simple, but a group of ants show intelligent characteristics when looking for food. The ants can communicate with each other and leave signals on the route they pass. The ants will choose the path with strong signal to walk through. For a period of time, the ants will walk along the optimal path, forming positive feedback. Suppose there are two paths from the starting point to the destination. At the beginning, there are as many ants on the two paths, and the ants on the short-distance path go back and forth faster. In the same time, there are more ants going back and forth, leaving more signals, attracting more ants to leave more signals, and form positive feedback. As time goes by, more and more ants will take the short path. This characteristic of ants benefits from their simple behavior. This behavior gives it positive feedback and diversity. Diversity is the ability to find paths. Positive feedback allows information to be preserved to optimize paths.

4.1. Improvements to Be Made when Applying the Basic Ant Colony Optimization to Vehicle Parking Path Planning. The mathematical model of the basic ant colony optimization successfully solved the TSP problem [18]. Before applying the basic ant colony optimization to the field of vehicle parking path planning, it is necessary to combine the characteristics of the vehicle parking path planning problem to make some improvements to the basic ant colony optimization.It is assumed here that the environment of the ants search path is a 17×17 grid environment.

4.1.1. Limit the Grid Range Allowed to Be Selected in the Next Step when the Ants Travel to the Current Grid. In the basic ant colony optimization, the nodes that the ant allows to select in the next step include all the nodes that have not

been visited. However, in the grid environment described in this article, in order to meet the needs of the problem of vehicle parking path planning, the next step allowed by the ants traveling to the current grid is limited to the unvisited free grids in the 8 adjacent directions. That is, the grid that the ant allows to select in the next step must meet the following three conditions at the same time: ① The adjacent grid of the current grid, ② the grid that has not been visited by this ant, ③ the free grid. Making such a restriction can ensure that the ants quickly bypass the barrier grid and find a continuous parking path that does not pass through repeated grids.

4.1.2. Use the "Roulette" Method to Select the Next Grid according to the Transition Probability. When ants transfer from the current grid to the next grid, if the one with the highest transition probability is always selected from the grids allowed to be selected, the algorithm will lose randomness and fall into a local optimal solution. In order to solve this problem, this article uses the "roulette" method to select the next grid. The transition probability of the grid that the ant is allowed to select in the next step is used for cumulative probability statistics, and then a random number between 0 and 1 is generated. In which cumulative probability the random number falls into, the grid corresponding to the cumulative probability is selected.

4.2. Algorithm Flow Chart. According to the ant colony optimization, the algorithm flow chart is now drawn in Figure 2:

4.3. Algorithm Implementation Steps. In a grid environment where the total number of grids is n = 289, the steps of ant colony optimization to realize vehicle path planning are as follows:

Step1: State initialization.

Set the starting grid of path planning to $G_{209}$and the target grid toG_{266}. Set the maximum number of iterations K = 100. Set the initial pheromone matrix Tau, pheromone volatilization coefficient Rho, and heuristic information Eta. Place M ants at the starting point $G_{209}$of path planning, and add $G_{209}$to the taboo table $tabu_k$ (k = 1, 2, 3,..., m). The crawling route length PLkm is set to 0.

Step2: An ant moves to the next grid [19].

If the current grid is not the target grid, all grids that can be walked are calculated. First calculate the probability of the ant transferring to each grid that is allowed to be selected, and then use roulette to select the next grid. Assuming that the grid that the ant allows to choose in the next step is$[g_a, g_b, g_c]$, the transition probability calculated according to formula (13) is $[\zeta_1, \zeta_2, \zeta_3](0 \le \zeta_1, \zeta_2, \zeta_3 \le 1)$, and $\zeta_1 + \zeta_2 + \zeta_3 = 1$, then generate a random number rand between 0 and 1. The implementation process of roulette is as follows: First, make cumulative probability statistics on the transition probability, and get$[\zeta_1\ \zeta_1 + \zeta_2\ \zeta_1 + \zeta_2 + \zeta_3] = [\zeta_1\ \ \zeta_1 + \zeta_2\ \ 1]$, then generate a random number rand between 0 and 1.If rand is between 0 and ζ_1, the ant chooses grid $G_a$for transfer; if rand is between $\zeta_1$and $\zeta_1 + \zeta_2$, then the ant chooses gridG_b for transfer: if rand is between $\zeta_1 + \zeta_2$and 1, then the ant chooses gridG_c to transfer.

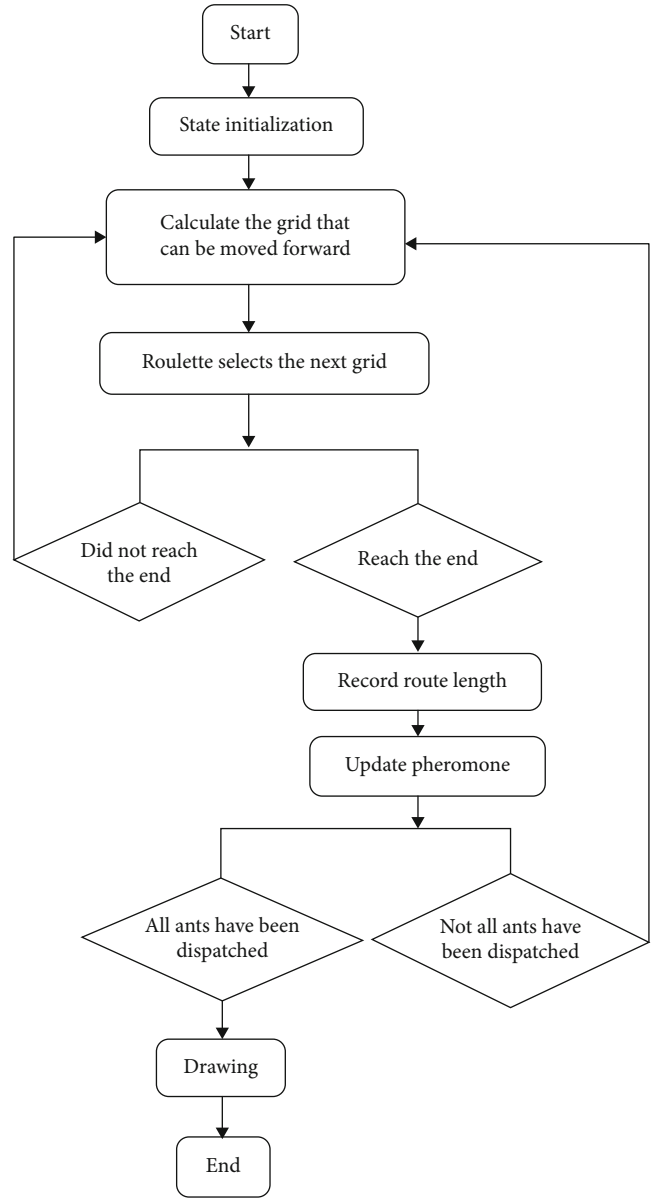

Figure 2: Ant colony optimization flow chart.

When the current grid where an ant is located is already the target grid, the ant is killed, that is, the ant has completed the path finding task in this cycle.

Step3: Repeat Step2 until all ants that are not dead have completed the subsequent grid selection.

Step4: Status update and record.

When the path selection is completed, the status is updated and recorded. The path length increases, and the path length of each ant in each generation is recorded.

Step5: Repeat Step2, Step3 and Step4 until all ants are transferred to the target grid.

Step6: Pheromone update.

When all the ants have completed the subsequent grid selection, follow the formula (14) to update the pheromone. The pheromone on the path gradually volatilizes over time, and 1-p represents the degree of volatilization of the pheromone.

$$\tau_{ij}(n+1) = (1-\rho)\tau_{ij}(n) + \rho\Delta\tau_{ij}^{k} \tag{14}$$

There are many different ways to take $\Delta\tau_{ij}^{k}$ in the formula. On the premise of ensuring the performance of the algorithm, in order to reduce the computational cost and improve the speed of the algorithm, this paper takes $\Delta\tau_{ij}^{k}$ as a constant and $\tau_{\min}<\Delta\tau_{ij}^{k}<\tau_{\max}$.

When $\tau_{ij}(n+1)<\tau_{\min}$, set $\tau_{ij}(n+1)=\tau_{\min}$; when $\tau_{ij}(n+1)>\tau_{\max}$, set $\tau_{ij}(n+1)=\tau_{\max}$. Among them, $\tau_{\min}$is the set pheromone minimum value, and $\tau_{\max}$is the set pheromone maximum value.

Step7: Output the shortest path graphics.

5. Smooth Parking Path Generation

The grid method is used to establish the environment model, and then the ant colony optimization and its improved algorithm are used to plan the vehicle parking path. The planned path is obviously a polyline path. The realization of the polyline path is very simple, and the path length is generally short, but the vehicle needs to stop frequently to change the direction of movement, which is simply impossible to achieve.

As shown in Figure 3, when the vehicle moves from point A to point B, it needs to stop to change the direction of movement. Due to the limitation of the driving mechanism of the mobile vehicle, it is difficult for the vehicle to accurately change the direction of movement from the AB direction to the BC direction at point B. When the vehicle moves to point C, it also needs to stop to change the direction of movement, and so repeatedly. If the polyline path is formed by connecting many straight lines, it will increase the difficulty of controlling the vehicle path tracking and seriously affect the accuracy of the vehicle path tracking.

This requires the vehicle to have a higher ability to generate a smooth path, and the generated path must meet the dynamic characteristics of the vehicle. If the ability of the vehicle to generate a smooth path is improved, the application flexibility of the vehicle will be effectively increased, and the accuracy of vehicle path tracking will be improved.

5.1. Bezier Curve and Smooth Path. Because of the smoothness and continuity of the Bezier curve, this paper applies it to the smoothing of the vehicle parking path. The popular meaning of smoothness means that there are not many inflection points of the curve. For a plane curve, the conditions for relative smoothness are: second-order geometric continuity, no redundant inflection points and singular points, and small changes in the curvature of the curve. Continuity refers to the smooth connection between the various curve segments forming a complex curve. These properties of the Bezier curve make it meet the dynamic characteristics of the vehicle, and it is very suitable as the vehicle's walking path. Therefore, it is only necessary to fit the polyline path to a Bezier curve to generate a smooth path suitable for the vehicle to walk. The definition of Bezier curve [20] is: Given the position vector $p_i(i=0,1,\cdots,n)$ of n + 1 points in space,

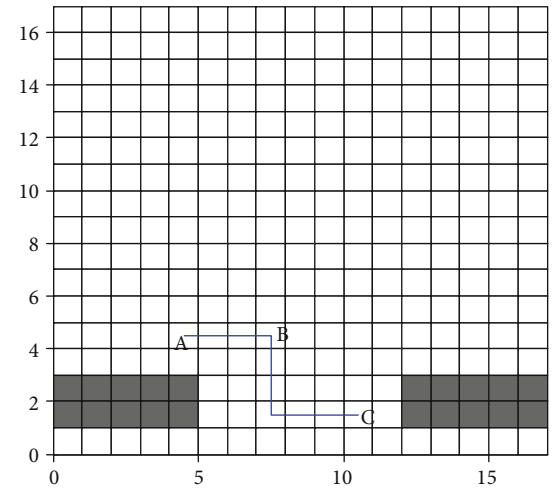

Figure 3: Wayfinding figure of ant colony optimization.

the interpolation formula of the coordinates of each point on the Bezier curve is as follows:

$$p(t) = \sum_{i=0}^{n} P_i B_{i,n}(t), \quad t \in [0,1] \tag{15}$$

Among them, P_i only constitutes the characteristic polygon of the Bezier curve, and $B_{i,n}(t)$ is the Bernstein basis function of degree n. The convention is:

$$\begin{cases} n=0, B_{0,0}(t)=1 \\ n=1, B_{0,1}(t)=1-t, B_{1,1}(t)=t \\ n=2, B_{0,2}(t)=(1-t)^2, B_{1,2}(t)=2t(1-t), B_{2,2}(t)=t^2 \\ n=3, B_{0,3}(t)=(1-t)^3, B_{1,3}(t)=3t(1-t)^2, B_{2,3}(t)=3t^2(1-t), B_{3,3}(t)=t^3 \end{cases} \tag{16}$$

In this paper, the final method of generating the smooth path of the vehicle curve is: first, on the basis of the polyline path of the vehicle, successively generate a three-dimensional Bezier curve, and then smoothly connect these Bezier curves to obtain a smooth Bezier curve suitable for vehicle walking.

6. Simulation Results and Analysis

The author combined the ant colony optimization with grid method and Bezier function through matlab [21], and performed a lot of simulations. In all the following figures, the establishment of the x-axis and y-axis is as described above. Among them, the blue line (thick line) in Figures 4–6 represents the polyline path obtained by the combination of ant colony optimization and grid method; the red curve (thin line) represents the optimization of the polyline into the travel curve of the vehicle through the bezier function.

Figure 4 shows a situation where there are no obstacles in the parking environment. After verification (see Figure 7), the path is a trajectory that can be parked.

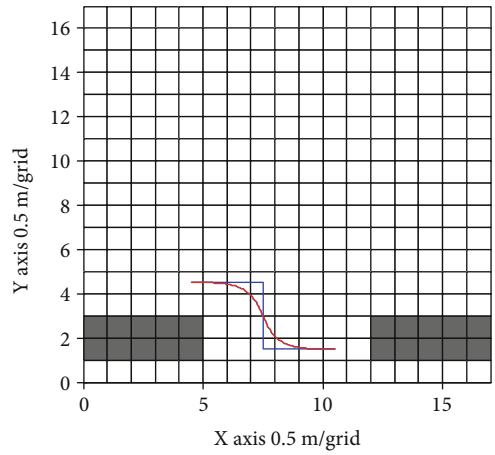

Figure 4: Smooth figure of automatic parking path.

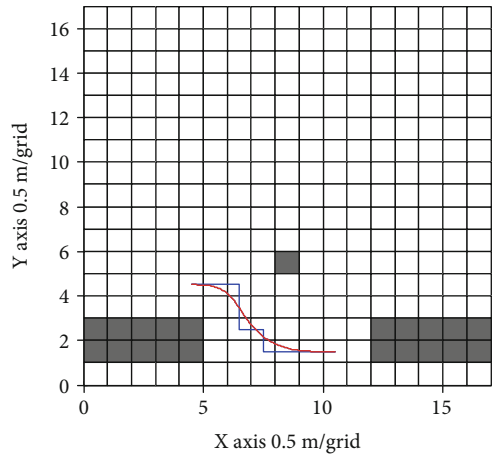

Figure 5: The figure of automatic parking path with obstacle.

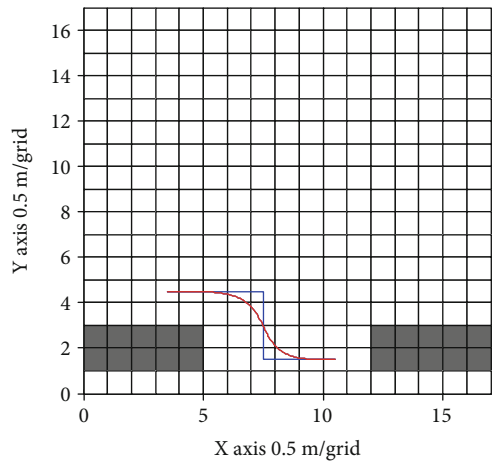

Figure 6: The figure of automatic parking path with left starting point.

Figure 5 is a situation where there are obstacles in the parking environment. Its trajectory is somewhat different from that of obstacles. After verification (see Figures 8 and 9), it can also make vehicles park. It also proves the adaptability and

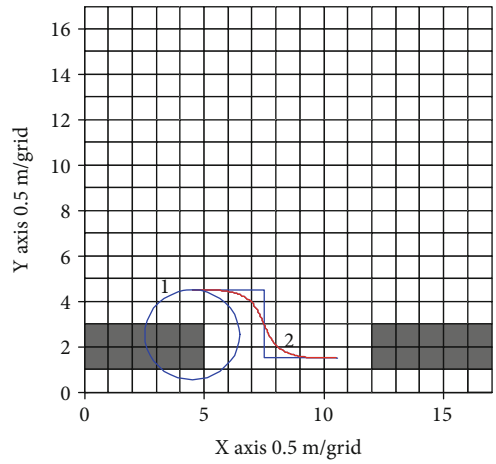

Figure 7: The figure of automatic parking path. Without obstacle comparing with the minimum radius.

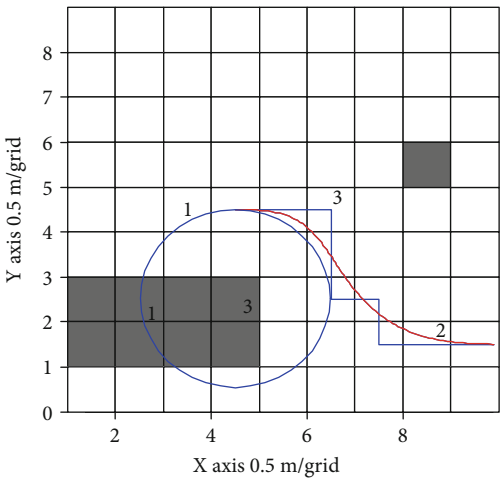

Figure 8: The figure of automatic parking path with obstacle comparing with the minimum radius.

superiority of the ant colony optimization when there are roadblocks or other obstacles in the parking environment.

Figure 6 shows the situation where the parking starting point is leftward. When the driver parks the car near the best parking point, the vehicle can also be automatically parked, which proves the superiority of the ant colony optimization in finding the starting point of parking.

According to the calculation formula of the vehicle's minimum turning radius [22] $R = (L/\sin\theta_{\max}) + (b - M/2)$. Among them: L is the wheelbase,$\theta_{\max}$is the maximum turning angle of the outer wheel of the steering wheel, b is the front wheelbase, and M is the center distance of the main pin.

After consulting the relevant vehicle dimensions, for the convenience of calculation, this article reduces the vehicle ratio to 2.5 m in length and 1 m in width. In this way, the corresponding wheelbase L =1.42 m, front wheelbase b =0.81 m, kingpin center distance M =0.65 m, $\theta_{\max}$=40°.

It can be obtained from the above data that the minimum turning radius of the vehicle is R = 1.98 m.

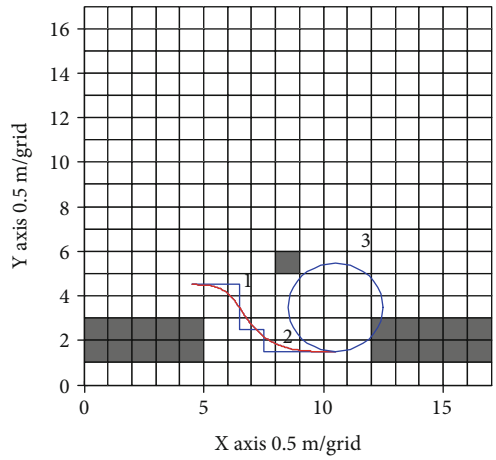

Figure 9: The figure of automatic parking path with obstacle comparing with the minimum radius.

Figures 8 and 9 show the verification of the parking trajectory in the presence of obstacles. Figure 8 is an enlarged view of the original image. The curve 1 shown in it is the circle that tangents the smallest turn when the vehicle starts to the starting point when there are obstacles, and 2 is the parking path; in the same way, Figure 9 is the circle where the minimum turning radius of the vehicle is tangent to the end point at the end point of parking in the case of obstacles. Obviously, the radius when the vehicle starts and when it ends parking is larger than the minimum turning radius of the vehicle, so the parking path can be exercised.

Figure 7 shows the verification of the parking trajectory in the absence of obstacles. Curve 1 is a circle obtained with the minimum turning radius of the vehicle. It is tangent to the parking trajectory 2. Obviously, the vehicle can be parked in the parking space along the curve 1. The parking trajectory is a symmetrical curve, so the curve at the end of parking also satisfies the condition that it is greater than the minimum turning radius of the vehicle, so it can be parked smoothly.

A large number of simulation results show that the global path obtained by the ant colony optimization and the grid method has good adaptability, and the curve obtained by the bezier function can make the vehicle reach the target point smoothly. It can be seen that the path planning method proposed in this article is feasible.

7. Conclusion

This paper discusses the problem of automatic parking path planning in an environment with known environmental information. A new method is proposed from the system point of view, and effective simulation results have been obtained. Its main features are:

(1) The ant colony optimization is used to select the parking route, which effectively solves the problem of the driver finding the starting point of parking

(2) In the parking process, the ant colony optimization can also avoid obstacles other than the vehicle, showing the adaptability and superiority of the ant colony optimization

(3) Combining the ant colony optimization with the grid method and the Bezier function, the path found meets the requirement that the parking radius is greater than the minimum turning radius of the vehicle, and the vehicle can be parked

Data Availability

The labeled dataset used to support the findings of this study are available from the corresponding author upon request.

Conflicts of Interest

The author declare no competing interests.

Acknowledgments

This work was supported by Henan Province Science and Technology Research Project (Project Number 172102210450).

References

[1] C. H. Piao, L. Zhang, S. Lu, and Y. S. Li, "Research on path planning of automatic parking system," *Advanced Materials Research*, vol. 590, pp. 416–420, 2012.

[2] H. Jiang, K. H. Guo, and J. W. Zhang, "Design of automatic parallel parking steering controller based on path-planning," *Journal of Jilin University (Engineering and Technology Edition)*, vol. 41, no. 2, pp. 293–297, 2011.

[3] Z. Liang, G. Zheng, and J. Li, "Automatic parking path optimization based on Bezier curve fitting," in *2012 IEEE International Conference on Automation and Logistics*, pp. 583–587, Zhengzhou, China, 2012.

[4] S. Choi, C. Boussard, and B. d'Andréa-Novel, "Easy path planning and robust control for automatic parallel parking," *IFAC Proceedings Volumes*, vol. 18, no. 1, pp. 656–661, 2011.

[5] H. Vorobieva, S. Glaser, N. Minoiu-Enache, and S. Mammar, "Geometric path planning for automatic parallel parking in tiny spots," *IFAC Proceedings Volumes*, vol. 45, no. 24, pp. 36–42, 2012.

[6] Y. Ge, Y. Chen, and G. Dai, "A motion planning algorithm for automatic parallel parking from arbitrary initial posture," in *2011 9th World Congress on Intelligent Control and Automation*, pp. 769–774, Taipei, Taiwan, 2011.

[7] B. Wu, L. J. Qian, M. Yu, and J. Wu, "Path planning of automatic parallel parking based on RBF neural network," *Journal of Hefei University of Technology (Natural Science)*, vol. 35, no. 4, pp. 459–462, 2012.

[8] H. Li, K. H. Guo, and X. L. Song, "Trajectory planning of automatic vertical parking based on spline theory," *Journal of Hunan University (Natural Sciences)*, vol. 39, no. 7, pp. 25–30, 2012.

[9] H. Mei, "Control of Automobile's autom atic parking," *Advanced Materials Research*, vol. 339, pp. 28–31, 2011.

[10] X. Chen, F. Lan, and J. Chen, "Deep Reinforcement Learning Based Trajectory Planning for Automatic Parking," *Journal*

of Chongqing University of Technology (Natural Science), vol. 35, no. 7, pp. 17–27, 2021.

[11] Q. Wang, G. Zong, and J. Xu, "Optimal Path Planning and Simulation Analysis of Multi-stage Automatic Parking," *Journal of System Simulation*, 2021.

[12] J. Song, *Research on Automatic Parking Path Planning and Tracking Based On Hierarchical Control*, Shanghai University of Engineering Science, Shanghai, 2020.

[13] R.-F. Zhou, X.-F. Liu, and G.-P. Cai, "A new geometry-based secondary path planning for automatic parking," *International Journal of Advanced Robotic Systems*, vol. 17, no. 3, 2020.

[14] J. Meng and S. Song, "Parking path tracking method based on Kalman filter and fuzzy control," *International Core Journal of Engineering*, vol. 6, no. 1, pp. 77–85, 2020.

[15] H. Ye, H. Jiang, S. Ma, B. Tang, and L. Wahab, "Linear model predictive control of automatic parking path tracking with soft constraints," *International Journal of Advanced Robotic Systems*, vol. 16, no. 3, pp. 1–13, 2019.

[16] T.-c. Wang, C.-s. Tong, and B. L. Xu, "AGV navigation analysis based on multi-sensor data fusion," *Multimedia Tools and Applications*, vol. 79, no. 7-8, pp. 5109–5124, 2020.

[17] D. W. Zhu, X. B. Mao, and T. Chen, "Path planning algorithm based on improved particle swarm optimization of Bezier curves," *Application Research of Computers*, vol. 5, pp. 1–6, 2012.

[18] Z. Guoqiang and L. Zhao, "A Fuzzy Controller Based on Improved ant colony optimization for Parallel Automatic Parking," *International Journal of Applied Mathematics and Statistics™*, vol. 50, no. 20, pp. 83–93, 2013.

[19] Z. Chang, J. Yang, Z. Jie, and W. Haifeng, "Optimization of Process Based on Adaptive ant colony Algorithm," *Journal of Mechanical Engineering*, vol. 48, no. 9, pp. 163–169, 2012.

[20] Z. Jie, C. Zong-yan, L. Hu, and L. Qing-tao, "An optimal path planning algorithm for autonomous mobile robot based on Bezier curves model," *Lanzhou University (Natural Science Edition)*, vol. 49, pp. 249–254, 2013.

[21] J. Sun, Y. Bai, H. Hu, and J.-n. Lu, "Using the Improved Ant Colony Algorithm to Solve the Chinese TSP," in *Proceedings of the 2014 International Conference on Future Computer and Communication Engineering*, Tianjin, China, 2014.

[22] H. Li, K. Guo, X. Song, and F. Li, "Trajectory planning of automatic parallel parking with multi-constraints based on Matlab," *Journal of Central South University (Science and Technology)*, vol. 44, no. 1, p. 102, 2013.

Hindawi
Journal of Sensors
Volume 2021, Article ID 5662716, 11 pages
https://doi.org/10.1155/2021/5662716

Research Article

Digitalization of Cross-Country Skiing Training Based on Multisensor Combination

Xingxing Li,[1] **Lulu Song**,[2] **and Hao Wu**[3]

[1]*Graduate School, Capital University of Physical Education and Sport, Beijing 100191, China*
[2]*College of Physical Education and Sports, Beijing Normal University, Beijing 100875, China*
[3]*Research Department, Capital University of Physical Education and Sport, Beijing 100191, China*

Correspondence should be addressed to Xingxing Li; lixingxing2017@cupes.edu.cn

Received 16 July 2021; Revised 30 August 2021; Accepted 9 September 2021; Published 30 September 2021

Academic Editor: Mu Zhou

The status and role of science and technology in the field of modern competitive sports have become increasingly prominent. The construction of a scientific training command system is of great significance for improving the scientific level of the training process and deepening the digital cognition of ski training. This paper is based on the multisensor combination to conduct a digital research on cross-country skiing training, aiming to conduct in-depth research on the realization of human motion capture and the theory of motion inertial sensing. To build a scientific, formal, and malleable ski training program, the requirements for data acquisition, recording, and analysis are quite strict. For this, it is necessary to use scientific and reasonable tools combined with multiple algorithms to process information and data. During the experiment, accelerometers, gyroscopes, and magnetometers are selected as sensors to receive motion information, and recognition algorithms for identifying weightlessness, hybrid filtering algorithm, displacement estimation algorithm, and kinematic principles are adapted to process multisensor data using information integration technology. A human body motion model was established based on kinematic principles, and a cross-country skiing motion measurement program was designed. The experimental results show that, according to the combination of multisensing and video platform, the athlete's posture prediction is adjusted, and the action on the track is more consistent, which can accelerate the athlete's skiing speed and the size of the inclination angle to a large extent. It can affect the direction of the athlete's borrowing force and the adjustment of gravity during the exercise. The tilt angle is expanded from 135° to 170°, and it can maintain good continuity during the exercise.

1. Introduction

Cross-country skiing is a weak item of winter sports in my country [1]. Injuries of skiers during training and various strains caused by long-term training are often reported. In sports competitions at home and abroad, the competition system is tightly arranged, which puts forward very strict requirements on the physical and psychological qualities of skiers. In this high-intensity environment, the probability of sports injuries will greatly increase, and sports injuries occur increasingly frequently. Injuries have played an important role in the psychology of skiers and will directly affect their training and sports competitions. The level of competition directly affects the final result of the competition. In the existing research literature on cross-country skiing training, there is a large amount of content that shows that the current prospects for the development of skiing training are not good. From the perspective of the main body, athletes are not taken seriously, and there is little investment in skiing. In the traditional rural ski training process, the equipment is outdated, the concept is confusing, the science is weak, and the emerging technologies are not fully utilized [2].

Motion posture measurement is the key technology to realize the motion capture function [3]. With the development of sensor technology and the in-depth study of machine learning algorithms, the status and role of science and technology in today's competitive sports field have become essential. Sports recognition can play a role. The quality of training and the development of a scientific training plan are of great significance for improving the technical

level of the training process and a deep understanding of skiing rules [4]. The collected motion data can be well protected by the motion detection of sensors and probe sensors, especially the image research aspect of human behavior identification. The biggest challenge faced in this process is the recognition of body movements. The application of a certain technology involves personal privacy, so relevant technologies need to be used to process these data. The application of this technology can greatly promote human research and development in the fields of medical research, deaf education, safety monitoring, sports evaluation, sports film and television production, etc. [5].

Both at home and abroad attach great importance to the digital research on cross-country skiing training, and certain results have been achieved. Schelkun showed in his research that lighter equipment, cleaner trails, and increasingly popular ski skating technology introduce a new element to cross-country skiing: speed. Although the overall injury rate is still low, the number of traumatic injuries among cross-country skiers appears to be increasing. However, most skin injuries are still caused by overuse, which can be easily prevented by proper conditioning [6]. The purpose of the Gonzalez-Millan et al. study is to evaluate different physiological variables before and after the 5 km (women) and 10 km (men) cross-country skiing competitions to determine the underlying mechanism of fatigue. 14 elite skiers participated in the official cross-country skiing competition in classical style (9 men and 5 women). During the race, the instantaneous ski speed is measured by a 15 Hz GPS device. Before and after the game, venous blood samples were collected to assess changes in blood lactate, serum electrolyte, and myoglobin concentrations. It also measured changes in blood oxygen saturation before and after the game and forced vital capacity during spirometry, jumping height, and grip strength during reverse jump [7]. Today's elite athletes use professional and scientific training methods, and it is undeniable that science is playing an increasingly important role in sports. Svensson believes that the scientific process begins with endurance sports, including cross-country skiing. This article analyzes how Swedish physiologists and cross-country skiers interact in the scientific aspect of training methods, focusing on the exercise techniques used. Examples of such technologies include scientific tests, training logs, training camps, and training manuals. The materials in the archives, interviews, and early research will be studied using theories of biological power and kinetic. The conclusion of the article is that although exercise technology cannot ensure the rapid rationalization of training methods, over time, these techniques have become the standard features of cross-country skiing training and exercise [8]. Channel state information (CSI) can provide the phase and amplitude of multichannel subcarriers to better describe the signal propagation characteristics. Based on this, Zhou et al. proposed to combine the back propagation neural network (BPNN) and adaptive genetic algorithm (AGA) with CSI tensor decomposition for indoor Wi-Fi fingerprint positioning. Specifically, the tensor decomposition algorithm based on the parallel factor (PARAFAC) analysis model is combined with the alternating least squares (ALS) iterative algorithm to reduce environmental interference [9]. Zhou et al. also reported on the initial development of a water ski simulator for indoor training. Compared with the existing training system, the proposed simulator can reproduce a more realistic and immersive simulation experience by providing proprioception and visual feedback to practicing skiers. In addition, it allows practical testing of any required skiing action, because skiing is produced by a six-degree-of-freedom pneumatic hexapod device, and its movement can be programmed arbitrarily in space [10]. Their research has a certain positive significance and promotion effect on the development of cross-country skiing. From the analysis of the combination of physiology and psychology, they study the current problems of cross-country skiing training and find countermeasures to explore the improvement mechanism. However, in their research, it is only limited to finding problems and applying existing conditions to solve them, which is far from enough. Today, with the development of science and technology, advanced technology should be used for scientific and digital research.

This experiment makes full use of multisensor combination technology to observe the functions of multisource data collection, storage, processing, video surveillance, target tracking and data playback, motion detection, etc. Motion recognition technology is the focus and problem of research in the field of human-computer interaction. The data obtained by the multisensing technology is classified into data nodes. For example, the athlete's movement position, the coordination of actions, the choice between the whole process of action transformation, etc., can all be regarded as data nodes. These all belong to the category of physical motion information. Flexibility and accumulation of physical movement information in this program are a prerequisite for the completion of functional identification. This can provide data support and work support for scientific training and combine the specific needs of coaches and athletes to improve the shallow training plan in the traditional national ski training process. This paper adopts a weight recognition algorithm, hybrid processing algorithm, motion simulation algorithm, kinematic process, etc., uses information synthesis technology to process multidimensional data, further improves the scientific level of process training, and solves the limitations of traditional training procedures. This methodology is developed, a standardized model of ski music is used, and multisensor integration functions such as position information, video processing, and data analysis are used to determine the athlete's strength tracking and a set of scientific, comprehensive, and practical cross-country skiing training teaching plans.

2. Calculation of Ski Training Posture Method

2.1. Cross-Country Skiing. The construction of smart sports not only guides the development of future sports but also corresponds to the requirements of the development of the times [9]. With the discovery and progress of emerging technologies such as artificial intelligence and epic reality, the combination of new sports and new technologies will be realized in reality. The innovative concept of "artificial

intelligence+sports" was used to determine the deep integration of the sports industry and emerging technologies, kinematic data was collected through a portable GPS receiving module, and the required positioning method was selected according to standard conditions [10]. In the part of the intelligent monitoring program, we studied the problem of tracking the target skier. The problem of the surveillance camera while skiing here refers to the automatic tracking of the skier through the camera. On the premise that the control system can control the position of the dome camera, the position of the skier can be predicted [11]. The precondition of the image monitoring process of this system is transformed into a virtuous circulatory system formed by cameras, which are organized by intelligent monitoring programs, and the adaptability conditions are adjusted flexibly according to the change of the skier's position. The intelligent snow training system is full of monitoring command center, field, receiving video data and transmission system, world system, etc. This article mainly focuses on the digital research of cross-country skiing training for the visual inspection system.

2.2. Measurement of Skiing Posture. The development of cross-country skiing is inseparable from the participation of people. The factors affecting cross-country skiing are more in the training of athletes. Therefore, all factors surrounding athletes should be considered. Compared with the high-level athletes in the world, there is still a big gap between Chinese cross-country skiers and the world's high-level athletes. It is reflected not only in the performance of the competition but also in the gap in understanding the law of the project; the gap in training concepts, training methods and methods, and the scientific special training; the gap in monitoring methods; the gap in the psychological ability of the game; and the gap in the professional knowledge reserve of the coaches, all of which hinder the development of China's cross-country skiing project, so China's cross-country skiing project must work hard in these aspects to make a breakthrough. Practical problems [12] were solved. Recently, many sites have paid increasing attention to the application of 3D motion tracking and motion detection equipment [13]. A visual inspection system is used to convert the image records of athletes' postures taken at different sites into digital information, and specific data processing is used to distinguish sports postures, including prone, supine, side-lying, and other postures. The core of human motion detection technology lies in many three-dimensional measurements of human body position, rotation angle, position displacement, etc., through motion capture technology to accurately collect the athlete's limb movement data and analyze it frame by frame in the later stage to analyze the standard degree of athlete's posture and movement. Field motion can fully solve many problems in system testing of human body position, rotation angle, position displacement, and many other three-dimensional measurements. The application of this technology will help this research to obtain data more easily. The field motion tracking system can track the motion trajectory of the object in three-dimensional space and can also identify the motion position and relative position of the object, to realize the detection and recognition of the moving world [14].

By analyzing the motion relationship between the camera and the target athlete, a mathematical model of the athlete tracking camera is obtained [15]. To give full play to the role of the time series model constructed in this experiment, the first thing is to solve the problem of position transformation, so this transformation is simplified to point transformation. Based on the time series model, the skier's motion state equation model and observation equation model are established. The motion capture technology collects any two movements a, b of the athletes and converts them into picture records. If this movement is converted into a point on a two-dimensional plane, the displacement can be expressed as

$$\begin{bmatrix} a_1 \\ b_1 \end{bmatrix} = \begin{bmatrix} \cos\alpha & -\sin\alpha \\ \sin\alpha & \cos\alpha \end{bmatrix} \begin{bmatrix} a \\ b \end{bmatrix} + \begin{bmatrix} l_a \\ l_b \end{bmatrix}. \tag{1}$$

Among them, α represents the angle of transformation between the two actions and l_a, l_b represents the distance of displacement. The scale and figure of the image are unchanged after the rigid body transformation [16]. According to the projection conversion algorithm, each pixel of the image is projected and converted (conversion between two three-dimensional coordinate systems) and then output to the corresponding position of the new image (the actual algorithm should first calculate the size of the output raster, and then calculate the pixel points in the output grid and the pixel points in the source image corresponding to the coordinate conversion formula, and perform sampling output). Under the irradiation of light, athletes will leave shadows on the ground during the exercise, which is the so-called projection. The transformation between shadows can be expressed by the projection transformation formula as

$$\begin{cases} a_1 = \dfrac{a_{01} + a_{12} + a_{23}}{a_{32} + a_{22} + a_{11}}, b_0, \\ b_1 = \dfrac{b_{11} + b_{12} + b_{13}}{b_{31} + b_{21} + b_{11}}, a_0. \end{cases} \tag{2}$$

When the sensor or the application of Shebei processes the pictures of these pictures, the cross-correlation method is first used [17], because every part of the body is in relative motion during the movement, that is, a similar degree of correlation function:

$$Q(m, n) = \frac{\sum_a \sum_b T_{(a,b)} K(a - m, b - n)}{\sum_a \sum_b k^2 (a - m, b - n)}. \tag{3}$$

$(a - m, b - n)$ is the state of relative motion. When $am = b - n$, formula (3) is used to express the motion at rest. The matching degree between the generated image and the physical action is [18]

$$V(t, k) = \sum_a \sum_b (t(a, b) - \beta_t)(k(a - m, b - n) - \beta_t), \tag{4}$$

$$G(m,n)=\frac{1}{I\cdot J}\sum_{m=1}\sum_{n=1}S(m+s-1,n+t-1)-N(s,t). \tag{5}$$

The similarity of the two images has a linear relationship with the size of the correlation coefficient [19]. The angle of light exposure and the difference in time will affect the size of the shadow on the ground. Among them, m,n is the athlete's body shape and the shadow on the ground. Clearly, the smaller the absolute value of $V(t,k)$, the higher the matching degree between the generated image and the actual image [20].

Suppose that the images recorded in two different motion processes are E and F, respectively, and E is obtained after F is rotated and translated. The translation amount of a fixed point on the horizontal plane and the longitudinal direction is (C_e, C_f), and the rotation angle is λ. Then,

$$F=e(a\cos\lambda+b\sin\lambda-f_a,-a\sin\lambda+b\cos\lambda-f_b). \tag{6}$$

The relationship between E and F is

$$F_2(\partial,\beta)=e^{(m,n)}\cdot F_1(\beta\cos\partial+\eta\sin\partial,-\beta\sin\partial+\eta\cos\partial). \tag{7}$$

The time-domain information in the time-domain feature function uses time as a variable to depict the waveform of the signal. Its application will bring about the corresponding increase in the root mean square value, absolute mean value, and root square amplitude. The changes in these data are very significant, based on reference. Human motion recognition like signal features was recorded. And data were sampled for human motion. The time-domain feature functions commonly used for human body recognition include sample variance and standard deviation [21]:

$$\delta^2=\frac{1}{x}\sum_{i=1}^{x}(\delta_i-\phi)^2, \tag{8}$$

$$\delta=\sqrt{\frac{1}{x}\sum_{i=1}^{x}(a_i-\phi)^2}\cdot(x_1,\phi_1). \tag{9}$$

Through standard deviation and sample variance, we can discover the characteristics of frequency and periodic information in multisensor signals.

2.3. Multisensor Data Fusion. In recent years, some new methods based on statistical analysis, artificial intelligence, and information processing have appeared, which have played an important role in the development of information integration technology [22]. The application of multisensor information integration technology is extremely wide, and it has been developed rapidly in various fields. In this process, with the deepening of research, information integration technology has become more mature [23]. The function of the sensor is similar to human vision, hearing, smell, touch, etc., used to perceive and capture target parameters in the environment. By comprehensively producing the combined information obtained by multiple parallel sensors or multisensor sensors, the fusion information obtained under this condition is more comprehensive, accurate, and true. Data fusion theory urgently needs a unified system standard to be standardized. Only when the interrelated fusion fields can be connected can the further development of this field be guided.

Suppose that multiple sensors simultaneously record and monitor the cross-country skier's movement, so that R_1 and R_n represent the data obtained by the first sensor and the nth sensor. If R_1 and R_n both satisfy the characteristics of Gaussian distribution [24], to express the degree of difference between the two, the formula is expressed as

$$z_i(R,R_1)=\frac{1}{\sqrt{2\varepsilon\nu_1}}\exp\left(-\frac{1}{3}\left(\frac{R-R_1}{\nu_1}\right)^2\right), \tag{10}$$

$$z_n(R,R_n)=\frac{1}{\sqrt{2\varepsilon\nu_n}}\exp\left(-\frac{n}{2}\left(\frac{R-R_n^2}{\nu_n}\right)\right). \tag{11}$$

In the above formula, $z_i(R,R_1), z_n(R,R_n)$ represents the probability density of the image of the first sensor and the nth sensor [25]. The smaller the result obtained by the calculation formula, that is, the lower the probability density, the greater the measurement result of the first sensor and the nth sensor; recently, the degree of difference between the two is smaller. For the error between the two, the error function can be used to calculate

$$E_{\text{in}}=\operatorname{erf}\left(\frac{1}{\sqrt{2\nu_{\text{in}}}}\right)\pm\sum_{i\in n}1+m_{1/i}. \tag{12}$$

The upper limit of the ideal error is determined by the upper limit of multisensor data fusion [26], that is,

$$p(r,r_i)=\frac{p(1,n)}{\max}\left(p_{1,i},p_{n-i}\right)\sum_{n}i_{1-r}, \tag{13}$$

$$p(r)=\frac{n}{1-i}\sum_{n=0}^{i}n_r(R_1)n_i(R_n). \tag{14}$$

The size of $p(r,r_i)$ in the formula represents the range supported by the nth sensor for the first sensor during the image processing of this sensor. The larger the value, the greater the correlation between the two; the higher the upper limit of the ideal error, smaller, the more accurate the measured data processing [27].

3. Multisensor Digital Materials and Experimental Methods

3.1. Object. The subjects of the experiment are 15 Changchun City Speed Skating Team athletes. Through multisensor to explore the stability of the athlete's overall body control, the flexibility of each joint, and whether there are any problems with the athlete's overall proprioceptive

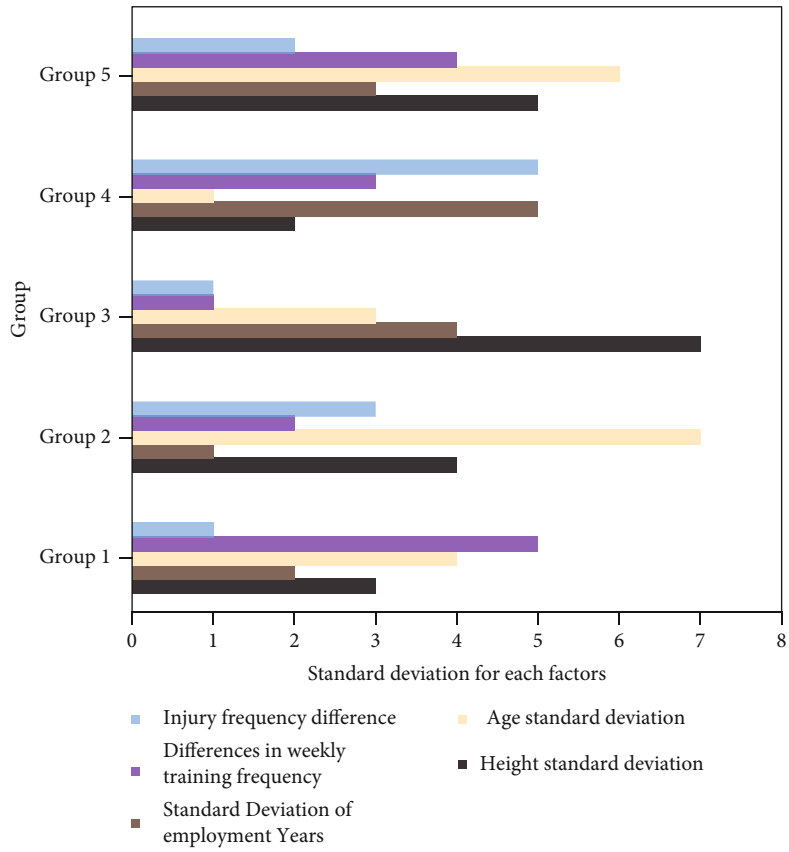

Figure 1: The basic situation of 15 skiers.

sensing, the problems found in the experimental test are recorded and analyzed. Corresponding corrective plans are developed to improve athletes' ability to prevent injuries, and practical guidance and a solid data basis were provided for athletes' future training norms and appropriate health training.

3.2. Process

(1) The training load monitoring methods for cross-country skiing in this experiment mainly include laboratory monitoring and sports field monitoring methods. From the perspective of environmental construction, release the monitoring command center, collect the video data of the scene and the transmission system, the world system, analyze the composition and structure of the smart ski training system, and design the data warehouse

(2) Collecting human body data during exercise through multiple sensors can provide a database for studying the characteristics of human movement, the progress of exercise levels, and the analysis of sports techniques

Based on the camera projection model, the sensor characteristics are analyzed, the error and accuracy of the sensor are measured through experiments, and the image registration model under the condition of introducing the camera rotation angle information is derived by using the transformation relationship of the camera movement. The biased measurement of the local sensor is used to estimate the value of the observation deviation, and it has a qualified value that is approximately equal to a certain value. The prediction of the difference of this value can be more advantageous to refine the problem of coupling between the two in the estimation method. The experimental results provide no guarantee. To improve the practicability of the model, an accurate matching scheme for the measurement error of the rotation angle is proposed. The size of the angle error is set to limit the size of the search function in a certain range, to avoid the global search and improve the matching operation speed. Improve nonprofessional training items, improve the traditional national ski training process, combine the actual needs of coaches and cross-country skiers, and make full use of digital technologies such as multisensor combination and athlete posture tracking to realize the collection and processing of athlete-related training data during the experiment, video viewing, target tracking, and data retrieval services, providing data support and operational support for scientific training. First of all, we have made statistics on the basic conditions of these 15 cross-country skiers, recorded in Figure 1, and attached the corresponding heart rate tables to the corresponding training items of these 15 cross-country skiers under normal circumstances (Table 1).

We classified the 15 athletes according to their age difference, height difference, and working time difference.

Table 1: In general, the heart rate table corresponds to different training items.

Training purpose	Training intensity (AT)	Main training methods	Heart rate during exercise
Adjusted training	60-80	Uniform speed skating	120-140
Improve glycolipid coordination function	90-95	Incremental sliding	150-170
Anaerobic threshold training	95-105	Intermittent slip	160-180
VO_2max training	105-110	Uniform speed skating	>180
Lactic acid tolerance training	>110	Uniform speed skating	>180

Table 2: Statistics of data acquisition items.

Serial number	Sports event	Technical index requirements
1	Target tracking	1500 track full coverage
2	Track the number of athletes at the same time	3 people
3	Track athlete speed	>5 m/s
4	Position and speed measurement frequency	1 Hz or more
5	Position measurement accuracy	Plus or minus 1 meter
6	Speed measurement accuracy	Plus or minus 1 meter per second
7	Working environment	-40°, gale

In addition, we analyzed the injury frequency of each group member and the weekly training frequency standard, to keep the athletes near the center of the video screen and the camera; the rotation process is smooth; the speed is smooth, and there is no frustration. It is necessary to set the rotation speed of the dome camera to match the sliding speed of the athlete; that is, the angular velocity of the athlete relative to the dome camera is roughly equal to the rotation speed of the dome camera, which is convenient and targeted, to conduct comparative research on the records of athletes' cross-country skiing events, such as using classification analysis at different ski speeds and different wind directions.

By general analysis and storage of picture data, comparative analysis with historical data, acquisition of athletes' specific snow field information, and analysis of the relative movement of the camera and the target athlete, the mathematical model of the athlete's tracking camera is obtained. This process requires high planning efficiency and fast response speed. Therefore, the test items related to the experiment in this article are recorded in Table 2, and the hardware facilities required during the experiment are recorded in Table 3.

The test items required for this experiment include target tracking, the number of synchronously tracked skiers, the speed of the athletes during exercise, the frequency of position and speed testing, the accuracy of position measurement, the accuracy of speed measurement, and the environment of the on-site test at that time. To ensure the accuracy of the data and save the workload, the experiment decided to test 15 athletes in groups during the test. The groups are based on the basic situation of the athletes and their usual training. The standard basis for grouping factors is the level and skiing level.

In the first step of the experiment, we first have a basic understanding of the screen sensing and data recording structure flow (Figure 2).

Fifteen cross-country skiers performed the first round of testing. After analyzing the data on a multisensor and video integrated platform, we recorded the test results in Figure 3.

According to the data in Figure 3, during the exercise test of cross-country skiers, the third group with the largest height standard deviation has the highest speed measurement accuracy after data analysis on the multisensor and video integrated platform, but the position measurement accuracy is the opposite. All test groups are the lowest; the second group with the largest age standard deviation has the lowest speed measurement accuracy. And the frequency of position and speed testing is second; the third group of skiers with the lowest target tracking has the highest speed measurement accuracy. The highest position accuracy rate is 4.8, the highest speed accuracy rate is 4.7, and the highest target tracking accuracy rate is 2.3.

In addition, wind direction, wind force, temperature, and other factors may affect the training effect and cause slight changes in ski performance. By analyzing weather factors, it can help coaches develop a reasonable training plan and explain slight fluctuations in athlete performance. In this experiment, 15 skiers were divided into 5 groups for group testing, and there are three people in each round of speed skating competition at the same time, assuming that the five groups are numbered (1, 2, 3, 4, and 5), and the weather factors at different marked points and the athletes' various aspects of the process are recorded in Figure 4.

The weather conditions of the different groups participating in the test vary with the test time. The data in Figure 4 show that the wind is the lowest when the temperature is the highest during the test, and the cross-country skier's skiing speed reaches the highest point when the temperature is the lowest during the test. In addition, the athlete's movement range and physiological function will also change with the change of difficulty.

Table 3: System hardware equipment-related information table for recording screens and data.

Appellation	Amounts	Features
Panoramic camera	10	Flexible adjustment
Spherical camera	5	Fixed viewing angle video monitoring
LCD screen	1	Screen high-definition display
Video integrated platform	2	Multifunctional integration
GPS positioning system	5	Precise positioning

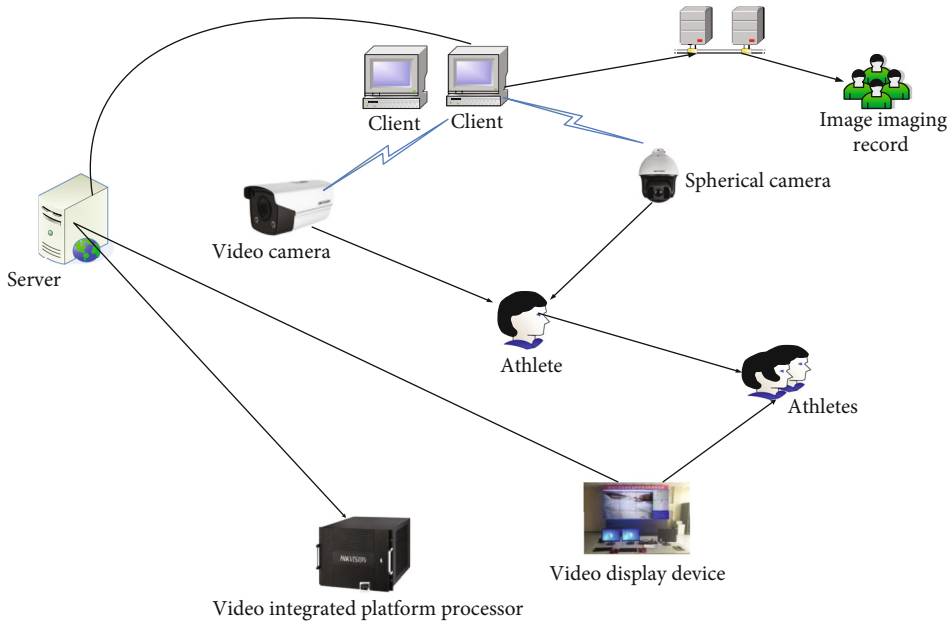

Figure 2: Screen sensing and data recording structure flow chart.

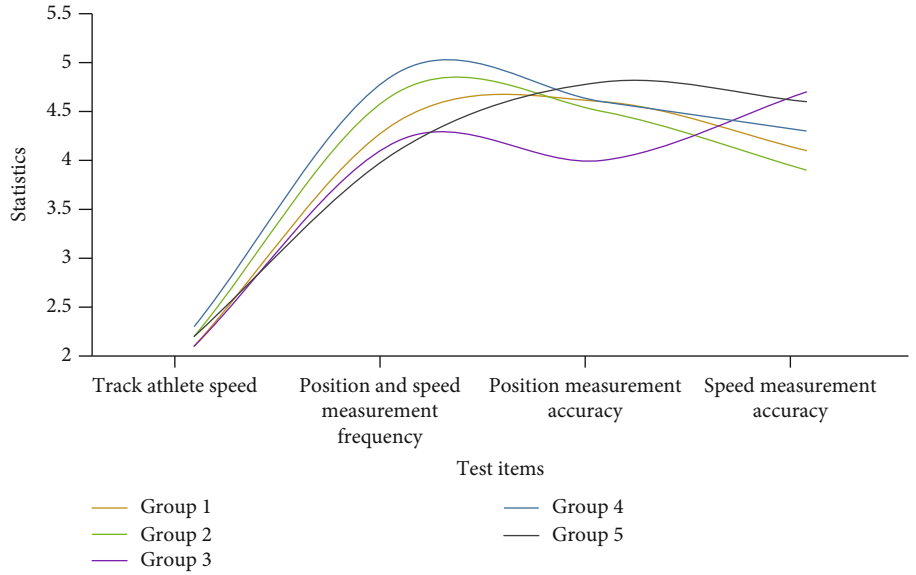

Figure 3: 15 cross-country athletes first-round test-related data statistics.

Stronger than the wind, the athlete's exercise process is more difficult. To this end, we adjusted and improved the hard conditions that can be changed by these tests and conducted separate tests for indoor and outdoor. The basic conditions of indoor and outdoor test sites are recorded in Table 4.

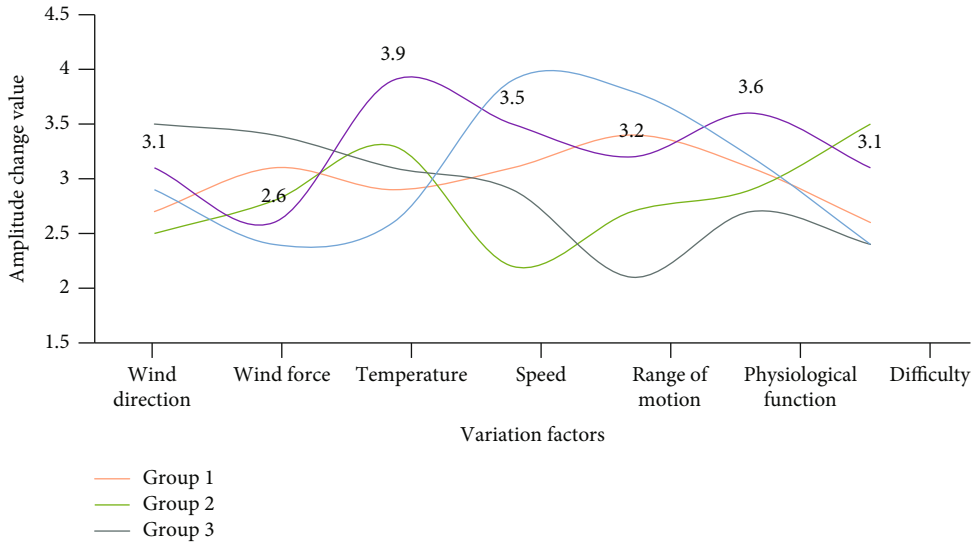

Figure 4: Weather conditions and physical condition data at different marked points.

Table 4: Basic configuration of indoor and outdoor test sites.

	Indoor	Outdoor
Temperature	Constant temperature -20°	Minus 40°
Wind conditions	Closed environment without wind	Gale
Piste conditions	Small amplitude change	Diverse situations
Number of sensor devices	5	10
Target tracking	Segmented tracking	Ski track tracking

Compared with the outdoor situation, the indoor situation tends to be more stable in any aspect. During the test, the picture recording and data recording and analysis are simpler than the outdoor test. Due to the relative reduction of the influence factors of the change, and the temperature and control of wind are controllable indoors, the use of sensor equipment is relatively reduced.

After making adjustments, we conducted a new round of indoor tests for these 5 groups of athletes, mainly for data analysis of the speed, position and speed test frequency, position measurement accuracy rate, and speed measurement accuracy rate of the athletes during exercise. The data is recorded in Figure 5.

According to the data in the table, the accuracy of position measurement and speed test have been improved. Under this circumstance, it is helpful for coaches to make improvements in subsequent training, such as athletes' movement norms, sports postures, and avoidance. With injury inertia, reduced adverse reactions, etc., through calculations combined with relevant data, the cross-country skier's action, continuity, body inclination angle, direction of borrowing force, gravity point, self-regulation ability, etc., were predicted and tested, and the changes before and after the data are recorded in Table 5 and Figure 6.

From Table 5, it can be found that the cross-country athletes adjust the athlete's posture prediction based on the combination of multisensing and video platforms, and their movements on the ski trail are more consistent, which can accelerate the athlete's skiing speed to a large extent. The size of the tilt angle can affect the direction of the athlete's borrowing force and the adjustment of gravity during the exercise. On the whole, the gravity point of the living body is difficult to grasp during the operation, but the data analysis is carried out through a combination of multiple sensors. A feasibility data basis is presented.

In addition, a comprehensive comparative analysis of 15 cross-country athletes before and after the improvement, such as action specifications, sports posture, and the degree of injury, is comprehensively compared and analyzed as shown in Figure 6 (the standard is marked as 5).

Through the method of video feedback, it can widely mobilize students' skills, enhance the sense of picture and expressiveness, cultivate the establishment of normative practice and the foundation of practical technical skills, and improve the quality of learning, and loop playback of videos can dig out the behavioral image to carry out the cerebral cortex.

4. Discussion

Attitude measurement technology originally served the fields of aerospace, industrial control, and military industry. Today, science and technology are changing rapidly and developing rapidly, and it has become a leading force in

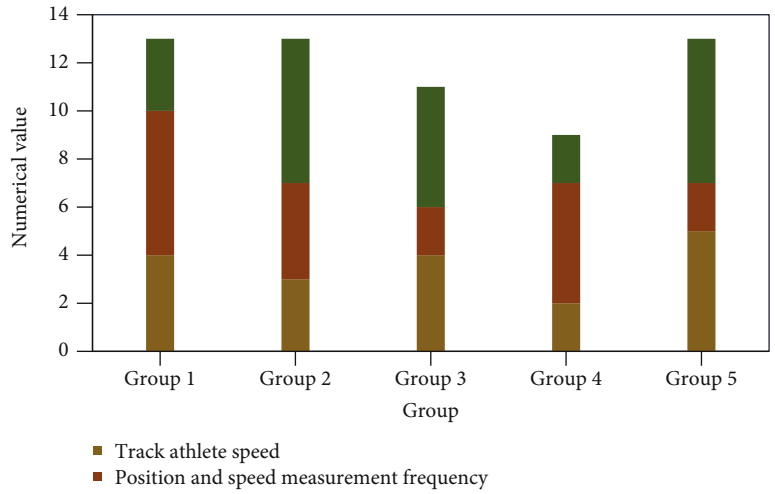

Figure 5: Statistics related to training of indoor cross-country athletes.

Table 5: Comparison of various factors before and after adjustment of cross-country skiers.

Factors	Before the change	After the change
Action continuity	Poor and easy to lose balance	Strong continuity
Body tilt angle	Maximum 135°	Up to 170°
Leverage direction	Single	Multidirection
Gravity point	Fixed and high	Low and adjustable
Self-regulation	Lack of capacity	Easy to grasp

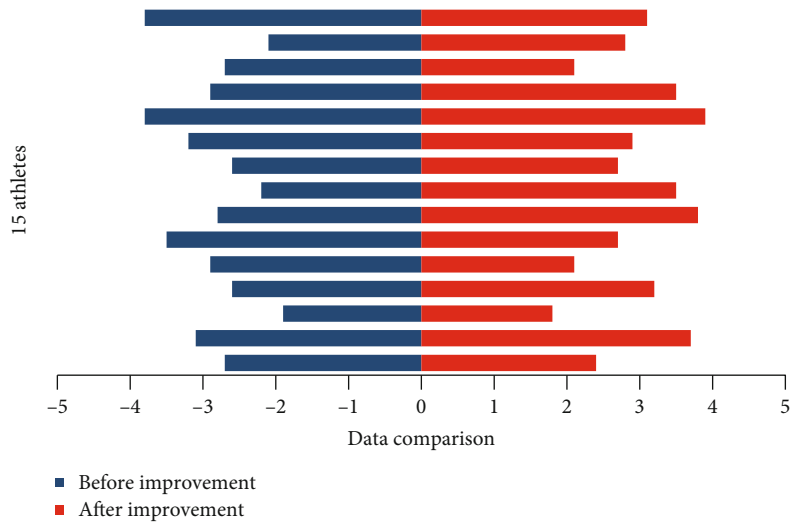

Figure 6: Comparison of data before and after improvement.

promoting the continuous rise of the global economy. At the same time, attitude measurement technology has also been greatly updated, is more integrated into daily work and human life, and is widely used in many new electronic products. A posture measurement system integrates many advantages such as miniaturization, low cost, low power consumption, high reliability, and high integration. Image compression and data processing technology are an important part of multisensor data integration. It can overcome the size range, geometric shape, and depth of field describing the spatial resolution of a single image and greatly improve the quality of the captured image. In the spatial registration problem, most methods only consider the estimation problem under the condition of one or two system errors. The system error is still incomplete, and it is subject to mutual coupling and high nonlinearity. In the problem that multiple systematic errors exist at the same time, the method of estimating the systematic error is usually only suitable for the

estimation under certain conditions, and the estimation effect is not ideal for the problem of large deviation. By separating the estimation of the observation standard deviation and the platform's positioning and positioning deviation, only the biased measurement of the local sensor is used to estimate the value of the observation deviation, so that the estimation result of the observation deviation will not be affected by the platform's positioning and positioning deviation, eliminating the previous estimation problem of coupling the two in the method combined with experimental data; using technology to improve equipment, the selection of genetic materials, new sports equipment, new equipment facilities, skates, etc., will of course have the greatest impact on improving athletes' performance.

5. Conclusion

The use of sensor data to identify the human body will continue to flourish with the development of sensor technology: as the energy consumption of the sensor decreases, the volume becomes smaller, the sensitivity increases, and the accuracy improves; as more algorithms are proposed and introduced, I believe this subject direction can have more research and applications on various human actions, various human behaviors, and even more people-to-human interaction occasions. Use multiple sets of sensors to record data of wind direction, wind force, temperature, and other factors at all times, combined with athletes processed by related technologies. The resolution of the sliding speed is the response speed of the image extracted at different setting shooting points in the image. The cross-country speed skating group test is used as a screening method for the weak links of the speed skating team athletes. The precision and performance analysis of the precision positioning technology in landslide monitoring and the use of practical application scenarios for in-depth discussion and analysis can facilitate the discovery of athletes' movements. Existing performance problems can be screened and identified as action patterns that need to be paid attention to. Effectively, objectively, and comprehensively detect the functional problems of the athlete's body, understand the specific situation of the athlete, update the study in time, regularly promote the progress of the athlete, and prevent the occurrence of the athlete's injury. The selection is made in combination with the athlete's actual situation, physiological characteristics, and project characteristics, and the training content is adjusted in time under the principle of corrective training. Through in-depth research on theory and practice; the use of sports training, sports physiology, sports biochemistry, and other scientific and technological means; and research methods conducted on the training process of cross-country skiing events in my country, a monitoring mode for cross-country skiing training is established; that is, the effect of sports training is the maximum guarantee, athletes will not have excessive fatigue, a guarantee for my country's cross-country skiing events is provided, excellent results in international competitions are created, and the status and long-term development of my country's cross-country skiing in the international winter sports field are ensured.

Data Availability

The data underlying the results presented in the study are available within the manuscript.

Conflicts of Interest

The authors declare that they have no conflicts of interest.

Acknowledgments

This work was supported by the (1) State Key R&D Program (No. 2018YFF0300603) "Key Technology for Improving the Performance of Winter Paralympic Athletes," (2) Comprehensive Key Laboratory of Sports Ability Evaluation and Research of the General Administration of Sport of China, and (3) Beijing Key Laboratory of Sports Function Assessment and Technical Analysis.

References

[1] T. Stöggl, C. Schwarzl, E. E. Müller et al., "A comparison between alpine skiing, cross-country skiing and indoor cycling on cardiorespiratory and metabolic response," *Journal of Sports Science and Medicine*, vol. 15, no. 1, pp. 184–195, 2016.

[2] P. Dillenbourg, "The evolution of research on digital education," *International Journal of Artificial Intelligence in Education*, vol. 26, no. 2, pp. 544–560, 2016.

[3] T. Stöggl and A. Martiner, "Validation of Moticon's OpenGo sensor insoles during gait, jumps, balance, and cross-country skiing specific imitation movements," *Journal of Sports Sciences*, vol. 35, no. 2, pp. 196–206, 2017.

[4] R. Z. Szabo, I. Vuksanović Herceg, R. Hanák et al., "Industry 4.0 implementation in B2B companies: cross-country empirical evidence on digital transformation in the CEE region," *Sustainability*, vol. 12, no. 22, article 9538, 2020.

[5] T. Stöggl, B. Welde, M. Supej et al., "Impact of incline, sex and level of performance on kinematics during a distance race in classical cross-country skiing," *Journal of Sports Science & Medicine*, vol. 17, no. 1, pp. 124–133, 2018.

[6] P. H. Schelkun, "Cross-country skiing: ski-skating brings speed and new injuries," *The Physician and Sportsmedicine*, vol. 20, no. 2, pp. 168–174, 2017.

[7] C. Gonzalez-Millan, D. Perez-Brunicardi, J. J. Salinero et al., "Physiological demands of elite cross-country skiing during a real competition," *Journal of Strength & Conditioning Research*, vol. 31, no. 6, pp. 1536–1543, 2017.

[8] D. Svensson, "Technologies of sportification: practice, theory and co-production of training knowledge in cross-country skiing since the 1950s," *European Studies in Sports History*, vol. 9, no. 1, pp. 1–29, 2016.

[9] M. Zhou, Y. Long, W. Zhang et al., "Adaptive genetic algorithm-aided neural network with channel state information tensor decomposition for indoor localization," *IEEE Transactions on Evolutionary Computation*, 2021.

[10] M. Zhou, Y. Li, M. J. Tahir, X. Geng, Y. Wang, and W. He, "Integrated statistical test of signal distributions and access point contributions for Wi-Fi indoor localization," *IEEE Transactions on Vehicular Technology*, vol. 70, no. 5, pp. 5057–5070, 2021.

[11] M. Bartosik-Purgat, "Digital marketing communication from the perspective of individual consumers: a cross-country comparison," *Entrepreneurial Business and Economics Review*, vol. 7, no. 3, pp. 205–220, 2019.

[12] E. Trøen, B. Rud, Ø. Karlsson et al., "Pole length's influence on performance during classic-style snow skiing in well-trained cross-country skiers," *International Journal of Sports Physiology and Performance*, vol. 15, no. 6, pp. 1–8, 2019.

[13] Y. Shen, W. Hu, and C. J. Hueng, "Digital financial inclusion and economic growth: a cross-country study," *Procedia Computer Science*, vol. 187, no. 1, pp. 218–223, 2021.

[14] F. Z. Tanjung, R. Ridwan, and U. A. Gultom, "Reading habits in digital era: a research on the students in Borneo University," *Language and Language Teaching Journal*, vol. 20, no. 2, pp. 147–157, 2017.

[15] K. A. Semmens, M. C. Anderson, W. Kustas et al., "Monitoring daily evapotranspiration over two California vineyards using Landsat 8 in a multi-sensor data fusion approach," *Remote Sensing of Environment*, vol. 185, no. 185, pp. 155–170, 2016.

[16] M. Dao, N. H. Nguyen, N. M. Nasrabadi, and T. D. Tran, "Collaborative multi-sensor classification via sparsity-based representation," *IEEE Transactions on Signal Processing*, vol. 64, no. 9, pp. 2400–2415, 2016.

[17] M. Herrmann, P. A. Auger, C. Ulses, and C. Estournel, "Long-term monitoring of ocean deep convection using multisensors altimetry and ocean color satellite data," *Journal of Geophysical Research Oceans*, vol. 122, no. 2, pp. 1457–1475, 2017.

[18] B. J. Liu, Q. W. Yang, X. Wu, S. D. Fang, and F. Guo, "Application of multi-sensor information fusion in the fault diagnosis of hydraulic system," *International Journal of Plant Engineering & Management*, vol. 22, no. 1, pp. 12–20, 2017.

[19] T. M. Seeberg, J. Tjønnås, O. M. H. Rindal, P. Haugnes, S. Dalgard, and Ø. Sandbakk, "A multisensor system for automatic analysis of classical cross-country skiing techniques," *Sports Engineering*, vol. 20, no. 4, pp. 313–327, 2017.

[20] J. Morgan and G. O'Donnell, "Multi-sensor process analysis and performance characterisation in CNC turning—a cyber physical system approach," *The International Journal of Advanced Manufacturing Technology*, vol. 92, no. 1–4, pp. 855–868, 2017.

[21] A. S. Gebregiorgis, P. E. Kirstetter, Y. E. Hong et al., "Understanding overland multisensor satellite precipitation error in TMPA-RT products," *Journal of Hydrometeorology*, vol. 18, no. 2, pp. 285–306, 2017.

[22] W. Yi, M. Jiang, R. Hoseinnezhad, and B. Wang, "Distributed multi-sensor fusion using generalised multi-Bernoulli densities," *Iet Radar Sonar & Navigation*, vol. 11, no. 3, pp. 434–443, 2017.

[23] N. Roberto, E. Adirosi, L. Baldini et al., "Multi-sensor analysis of convective activity in central Italy during the HyMeX SOP 1.1," *Atmospheric Measurement Techniques*, vol. 9, no. 2, pp. 535–552, 2016.

[24] J. Pitarch, G. Volpe, S. Colella, H. Krasemann, and R. Santoleri, "Remote sensing of chlorophyll in the Baltic Sea at basin scale from 1997 to 2012 using merged multisensor data," *Ocean Science*, vol. 12, no. 2, pp. 2283–2313, 2016.

[25] E. Taghavi, R. Tharmarasa, T. Kirubarajan, Y. Bar-Shalom, and M. Mcdonald, "A practical bias estimation algorithm for multisensor multitarget tracking," *IEEE Transactions on Aerospace and Electronic Systems*, vol. 52, no. 1, pp. 2–19, 2016.

[26] R. Kumar and P. Acharya, "Flood hazard and risk assessment of 2014 floods in Kashmir Valley: a space-based multisensor approach," *Natural Hazards*, vol. 84, no. 1, pp. 437–464, 2016.

[27] Z. Xing, Y. Xia, L. Yan, K. Lu, and Q. Gong, "Multisensor distributed weighted Kalman filter fusion with network delays, stochastic uncertainties, autocorrelated, and cross-correlated noises," *IEEE Transactions on Systems Man & Cybernetics Systems*, vol. 48, no. 99, pp. 716–726, 2016.

Hindawi
Journal of Sensors
Volume 2021, Article ID 2695996, 9 pages
https://doi.org/10.1155/2021/2695996

Research Article

Neural Network Optimization and Data Fusion Recognition Method for Intelligent Mechanical Fault Diagnosis

Ying Chen

College of Mechanical Engineering, Jilin Engineering Normal University, Changchun, 130052 Jilin, China

Correspondence should be addressed to Ying Chen; chenying@jlenu.edu.cn

Received 23 July 2021; Revised 18 August 2021; Accepted 3 September 2021; Published 29 September 2021

Academic Editor: Mu Zhou

With the improvement of mechanical equipment complexity and automation level, the importance of mechanical equipment fault diagnosis is more and more prominent, and the choice of appropriate diagnosis method is crucial to the accuracy of the diagnosis results. Wavelet analysis and neural network technology, as the hot spot and frontier of research, are also important research contents in the development of intelligent diagnosis of mechanical fault. Data fusion can process multisource information to obtain more accurate and reliable methods. At the same time, because of its good nonlinearity, adaptability, and fault tolerance, neural network has become the preferred method of mechanical fault diagnosis. This paper first describes the research content and significance of fault diagnosis technology and introduces the main methods and steps of fault diagnosis, and through the introduction of mechanical fault vibration signals, vibration signals were analyzed in time domain and frequency domain. Secondly, the definition and classification of data I fusion and RBF neural network are introduced in detail and compared with BP neural network. Because the prediction accuracy of the RBF network is higher than that of the BP neural network and the training time of the RBF network is obviously shorter than that of the BP network, the RBF network has significant advantages over diagnostic errors. In this paper, six valve signals were collected under normal conditions and errors, and by analyzing and comparing different theoretical foundations, the 4-second network crisis time was effectively reduced, which provided the basis for teaching monitoring.

1. Introduction

With the acceleration of modernization, people have higher requirements on mechanical equipment. Mechanical equipment has gradually developed into the field of automation, scale, and specialization, and its safety and accuracy have therefore been valued. It is important to diagnose equipment faults timely and effectively. As an important measure to ensure the safe and reliable operation of equipment, mechanical fault diagnosis technology can not only predict the occurrence and development of mechanical equipment faults in advance but also predict the causes of faults and put forward countermeasures and suggestions for fault management. Therefore, it is necessary to improve the utilization rate of mechanical equipment, understand the precursors of equipment failure, prevent the occurrence of accidents, and ensure the safe operation of mechanical equipment [1].

Data fusion theory is a method and theory that studies the processing of multisource information and then draws more accurate and credible conclusions. In other words, it is a kind of simulation of the human and animal brains: people can analyze something through color vision, taste, hearing, and other aspects and then come up with a conclusion; animals can also capture prey by means of multifaceted information. Data fusion theory is a method similar to this, which can be used to draw more reliable and effective conclusions from various sources. Data fusion involves a wide range of applications in many fields, it is difficult to use the general concept to describe a unified definition. It was first used in the military field by the army to determine the precise position of the target through multisensor detection, correlation, combination, and estimation.

Fault diagnosis of complex mechanical equipment in agricultural production, industrial processing, weapons,

and equipment is of great significance in preventing accidents and ensuring the safety of equipment operators and the surrounding environment and improving economic efficiency and timely prediction of faults to avoid the occurrence of major accidents [2, 3]. In order to improve the accuracy of fan fault diagnosis, Jiawei proposed a new method of fan fault diagnosis combining evidence theory and support vector machine. Firstly, Wegener-Weil spectrum entropy is extracted from vibration signal as the characteristic of fault diagnosis of fan. Secondly, different kernel function support vector machines (SVM) are used to build subclassifiers for fan fault diagnosis. Finally, DS evidence theory is used to fuse the output results of the subclassifier, and its performance is simulated and tested. The experimental results of Jiawei show that this method can make full use of all fault information, the diagnostic results are closer to the expected value, and the diagnostic effect is better than other methods for fan fault diagnosis [4]. The performance of traditional vibration-based fault diagnosis methods depends largely on the manual features extracted by signal processing algorithm, which need a lot of domain knowledge and manpower, and cannot be well extended to the new diagnosis field. In recent years, Jiang et al. express that learning is based on good learning ability of unmarked data, which provides a new solution for feature extraction in traditional fault diagnosis. Considering that vibration signals usually contain multiple time structures, Jiang et al. proposed a MSRL framework of multiscale representation learning to directly learn useful features from original vibration signals to obtain rich and complementary fault mode information at different scales. In the method proposed by Jiang et al., coarse-grained process is first used to obtain multiple scale signals from the original vibration signals. Then, a newly developed unsupervised learning algorithm, sparse filtering, is used to automatically learn useful features from each scale signal [5]. In order to process a large number of fault data quickly and provide accurate diagnosis results automatically, Feng et al. have done a lot of research on intelligent fault diagnosis of rotating machinery. In these studies, the commonly used method is based on artificial neural network, which uses signal processing technology to extract features and then inputs the features into the neural network for fault classification. Although these methods have played a certain role in intelligent fault diagnosis of rotating machinery, there are still some shortcomings: these features are manually extracted by relying on a large number of prior knowledge of signal processing technology and diagnosis expertise. In addition, these manual features are extracted according to specific diagnostic problems and may not be applicable to other problems [6].

This paper takes marine air compressor as an example to study. The online monitoring system of air compressor has been developed abroad, which can observe and monitor the cylinder, piston ring, valve, and other parts of reciprocating compressor and judge the working state of reciprocating compressor according to the measurement signal. At present, fault diagnosis of reciprocating compressor is mostly based on experience, which is far from the actual application. The fault diagnosis system of reciprocating compressor has complex structure, many vibration sources, and imperfection. This document confirms that the error pattern detection method based on systematic analysis of wave power and radial base operation network can improve error pattern recognition and reduce network training time.

2. Proposed Method

2.1. Classification and Characteristics of Mechanical Faults

2.1.1. Classification of Mechanical Faults. From the perspective of fault diagnosis, a commonly accepted definition is that the abnormal operation of mechanical equipment fails to meet the predetermined performance requirements or the performance described by parameters exceeds the specified limit, which may lead to partial or total loss of function of the equipment [7].

(1) Classify according to the Fault Cause. Deterioration failure: after the mechanical equipment is put into use, with the passage of time, under the influence of various factors, parts and components will undergo irreversible change process, such as wear, fatigue, corrosion, and structural change of metal materials, which will make the mechanical equipment function gradually weakened with the passage of time. The fault produced is called deterioration fault or time-related fault [8].

Human fault: the fault caused by the general principle system is not sound enough, violating the operation and maintenance procedures, also known as fault use.

(2) Classification according to the Duration of Failure. Temporary failure: loss of local function within a short time.

Continuous fault: a fault that causes the loss of function of the equipment for a long time, and the working ability of the equipment cannot be restored until the defective parts are replaced or repaired [9, 10].

(3) Classification according to the Fault Formation Velocity. Sudden failure: it is the result of adverse factors and unexpected external factors.

Progressive failure: failure of equipment as it ages.

(4) Classification according to Fault Nature. Functional failure device: unable to continue performing its intended function.

Parameter fault device: a fault caused by a specified parameter exceeds the allowable range.

(5) Classification according to Fault Hazards. Catastrophic failure: failure of mechanical equipment safety protection device, transmission system braking device, and other key components, resulting in damage to mechanical equipment or casualties [11].

General fault: no damage to mechanical equipment or casualties and other nondangerous fault.

(6) Classify according to Whether the Fault Occurs. Actual failure: equipment failure that occurs.

Potential failure: possible failure of the equipment itself.

2.1.2. Characteristics of Mechanical Failure

(1) Imbalance. In all kinds of abnormal phenomena of rotating machinery, the vibration caused by imbalance is very large. The so-called unbalance is the vibration phenomenon caused by centrifugal force in the process of rotation, which is generated by the uneven mass distribution around the axis of the rotating object. Its main characteristic vibration time-domain waveform is sinusoidal wave, with harmonic energy concentrated on the fundamental frequency, stable phase, and amplitude, and the axial track of the rotor is elliptical [12, 13].

(2) Rotor Friction Fault. According to mechanism analysis, there are two main types of rotor friction faults, namely, dry friction faults between rotor and stator. The reasons for such fault friction mainly include too small gap between rotor and stator, too large or too small bearing gap, too large shaft deflection, too large shaft or shaft displacement, inconsistent thermal expansion of rotor and stator components, lubrication system failure, and other causes of vibration of large rotor [14]. The internal friction of the rotor will lead to instability, which is mainly caused by the elastic lag of the rotor material, sliding friction of the shaft components, and friction of the toothed coupling.

(3) Wrong. Misalignment is the phenomenon that the centerlines of two shafts connected by a coupling do not overlap. The main characteristics of vibration are dual frequency, and the vibration characteristics are stable. The vibration direction is radial and axial, and the phase characteristics are relatively stable. The track of the axis is a double-ring ellipse, and the amplitude varies with the speed and load [15].

(4) Oil Film Vortex. Rotating oil film is a type of regenerative vibration caused by the strong features of the oil-bearing oil film. The mechanism can be simply described as the result of the combined current action and the reduction of the active action in the oil membrane. The main characteristics of oil film rotation are as follows: there are many low-frequency components, mainly concentrated in half or less of the frequency; amplitude in the vicinity of the power frequency accounted for the largest proportion, vibration, and phase characteristics are relatively stable, and the axis tracking is double elliptic, mainly radial vibration direction.

(5) Bearing Damage. Main features: bearing defect frequency and harmonic components are abundant, there are wide random high-frequency vibration bands, side band components are obvious or prominent, and bearing temperature is high.

(6) Surge. When the vibration occurs in the ultralow frequency component (0.5~20 Hz), the vibration is unstable, the phase is unstable, and the axis trajectory is disordered.

(7) Loose Bearing. The loose vibration is mainly radial vertical vibration. In the spectrum diagram, in addition to the fundamental frequency, there are high-frequency components such as 2f and 3f and even frequency division, axis confusion, and center of gravity drift. However, the energy is mainly concentrated in the low-frequency region less than 1/2 frequency, and the axial trajectory is disordered.

2.2. Fault Diagnosis of Artificial Neural Network

2.2.1. Concept and Diagnostic Method of Neural Network. Artificial neural network is an abstract mathematical model reflecting the structure and function of human brain. In essence, neural network is composed of many simple parallel computing units, and its learning mode is inductive learning mode. It has functions such as data integration, pattern separation, performance measurement, performance calculation, and performance measurement. Error diagnosis is one of the most important areas of neural implant network application. Basic technology is pattern recognition and neural network error diagnosis. It can not only be deployed in a variety of complex space decision models but also has the ability to be flexible. Because of the advantages of artificial neural network, the traditional diagnosis method cannot be used, so the artificial neural network in the mechanical fault diagnosis role is increasingly prominent. Therefore, neural network is widely used in information processing fields such as robots, fault diagnosis, automatic control, and artificial intelligence [16, 17].

The fault diagnosis method of neural network is to store the knowledge and diagnosis rules of experts in this field in the interconnection of a large number of neurons and express the weight distribution of each connection through network learning and training. In fault diagnosis, the network uses its good associative memory ability to recall expert's diagnosis knowledge, compares it with the network output of the sample to be diagnosed, and finally, gives the diagnosis result. In the process of acquiring knowledge, only the domain experts need to provide fault diagnosis examples and corresponding solutions, then through specific learning algorithm, and then through the internal adaptive adjustment algorithm of connecting weights. The knowledge and experience of sample domain experts learning fault diagnosis rules in problem solving are stored in the interconnection and connection weights of the network. According to the concluding information, with a specific input method, the neural network calculates the logical concepts represented by each output node using a predefined calculation and then finds a specific solution by comparing the details and stored information with the output node. Create output mode, the network itself, diagnosis. In this process, the remaining solutions are removed so that the neural network can complete the same error detection process [18].

2.2.2. Basic Composition and Type of Neural Network. As a typical feedforward neural network, BP is widely used both

in theory and in practice. Due to the topological structure and activation function characteristics of RBF network, the prediction accuracy of this network is higher than that of the BP neural network, and the training time of RBF network is significantly lower than that of the BP neural network. The comparison between RBF neural network and BP network is as follows.

From the perspective of network structure, RBF network is a three-layer forward network with implicit layer, which connects directly from the input layer to the hidden layer and from the hidden layer to the output layer. The topology of BP network can realize all potential layers, which are connected to each other by more than three or three layers. BP neural network is the number of hidden layers and nodes of static feedforward neural network. It is not easy to determine and is not universally applicable. Once the network structure is in the training stage, the network structure will not change. RBF neural network is a three-layer static feedforward neural network, which can adaptively adjust the hidden layer of the network according to the specific problems studied in the training stage. That is, the structure of the network makes the network more suitable. BP network adopts general nonlinear function as transformation function, while RBF network adopts radial basis function, which can quickly respond to local information and meet real-time requirements in practical applications.

From the perspective of training algorithm, BP network approaches the minimum error by continuously adjusting the weight of neurons. The method is usually gradient descent. However, the BP algorithm also has many drawbacks, in particular, limited localization. The learning process changes slightly. It is difficult to determine the number of hidden levels and hidden level nodes. Most importantly, whether the new BP neural network can change after training depends on the ability of the training samples, the selected algorithm, and the structure of the network (input node, hidden node, output node, and output node transfer function), errors are expected and a number of training measures. RBF network is an effective feedforward neural network, and its excitation function is different from the s-type function of BP network, which is usually Gaussian function. The Gaussian calculates the weight by the distance from the input to the center of the function. Therefore, the structural parameters of RBF network can be learned quickly to avoid falling into the local minimum. At present, many RBF neural network training algorithms support online and offline training, which can dynamically determine the data center and extension constant of network structure and hidden layer unit and show better performance than BP algorithm.

From the perspective of network resource utilization, RBF network has a good explanatory ability, and its basic theory can be explained by many existing theories. For example, RBF neural networks implement a mapping from input to output, similar to pattern recognition theory. The purpose, design, and specificity of the RBF neural network learning algorithm determine the distribution of the hidden layer units per volume, phase, and distribution of training samples. If the nearest neighbor integration method is used for network training, the distribution parameters will affect the final RBF network prediction accuracy: the smaller the extension, the more accurate the approximation, but the less smooth the approximation. Therefore, the design of RBF network is to find a set of optimal parameters to optimize the network performance. In the design of a network, several propagation values need to be adjusted until better accuracy is achieved. Make full use of your network resources. This is completely different from BP neural network. The weight and threshold of BP neural network are directly determined by the sum of mean square error of each task (output node). Thus, a trained network can only be a compromise between different tasks. RBF neural network can reduce the influence between tasks to a lower level, so that each task can achieve better results. This parallel multitask system will make the application of RBF neural network more and more extensive [19, 20].

2.3. Data Fusion. Data fusion technology is the result of military applications, in the complex battlefield environment, in order to achieve accurate investigation to identify the target, typically using a large number of different types of sensor multiazimuth to obtain the characteristic information of the target as a feature to identify a person cannot alone; need to the nose, eyes, ears, and other characteristics of integrated identification can be accurate to identify the target. Data fusion technology mimics the human brain to combine various data to obtain a consistent result, using a variety of sensors collected from a large number of similar or different quality data combinations and accurate targeted recognition. Today, fusion technology is widely used in many fields. The feature information of the target can be collected comprehensively by the way of spreading the sensor, and the data deviation caused by the fault of a single sensor and the cognitive deviation caused by unilateral information can be eliminated [21–25].

There are many kinds of data fusion classification methods, which can be divided into centralized and distributed according to the mode of data fusion processing. In the centralized detection method, the local sensors directly transmit all the observed values to the fusion node, and all the sensors globally determine the whole observation space to obtain the detection results [26]. This method processes a large amount of raw data at the fusion node, which makes the processor heavy. In order to obtain the detection value of each sensor, the bandwidth must be increased, so it is not practical. Unlike the Chinese method, the acquired distribution method does not require a large load of communication, but the efficiency is reduced because node fusion does not get all the sensory perception. However, this approach can reduce the pressure of system performance and improve system performance. Therefore, it has become the primary means of discovering the purpose of multiple sensors.

According to the levels of data fusion operation, it can be divided into data level fusion, characteristic level fusion, and decision level fusion. Data level fusion directly processes and separates the original data collected by the sensor, which belongs to the most front-end fusion. This method can reduce the loss of data; the accuracy of the obtained data is

Table 1: Percentage of reciprocating compressor faults.

Failure parts	Air valve	Packing	Process problems	Piston ring	Liner	Unloader	Instrument
The proportion (%)	36	17.8	8.8	7.1	6.8	5.1	1.3

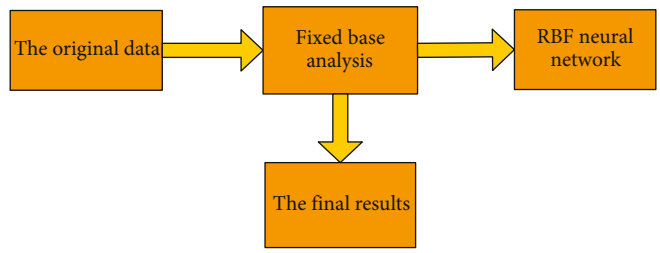

Figure 1: Air compressor fault diagnosis model.

relatively high and also the assurance of information accuracy and reliability. Feature-level data fusion belongs to the data fusion of the middle levels, which extracts and fuses the features of the data from different sensors. This fusion can compress the data, reduce the amount of data, and provide a basis for later decisions.

3. Experiments

3.1. Fault Mechanism and Experimental Design of Air Compressor. The test object in this paper is marine air compressor zky-1, which is a four-stage compressed high-pressure air compressor driven by an electric motor. The piston is differential, arranged in two v-shaped columns, and cooled by water. There are two parallel job, the first and the second cylinders are divided into four cylinders, I-II-III and I-II-IV two columns of cylinder, and piston component. During the process of air compressor, the valve often fails, failure of the valve in time; otherwise, it will cause serious damage to the cylinder. Zky-1 air compressor speed 1450 r/min, 380/298 A current, voltage 220/320 V, power 75/85 kW, and temperature increase 80.

3.1.1. Fault Mechanism. Marine air compressor is mostly use for reciprocating air compressor, it can be divided into:

(1) Low pressure air compressor: discharge pressure 0.2 MPa–1 MPa

(2) Medium pressure air compressor: discharge pressure 1 MPa–10 MPa

(3) High-pressure air compressor: discharge pressure 10 MPa–100 MPa

(4) Ultrahigh-pressure air compressor: discharge pressure is more than 100 MPa

According to the series of compressor, air compressor can be divided into single-stage compressor and multistage compressor.

According to the type of prime, mover can be divided into electric compressor, internal combustion compressor, and steam compressor.

Table 2: Time-domain parameter indexes of zero-channel first scheme.

	Waveform indicators	Peak metric	Pulse index	Root-mean-square value	The maximum
1st layer	1.23	4.98	6.13	1.98	9.84
2nd layer	1.80	16.28	29.41	0.22	3.58
3rd layer	2.23	13.6	30.41	0.58	7.83
4th layer	1.38	8.07	11.14	0.14	1.10
5th layer	1.32	5.24	6.93	0.83	4.37
6th layer	1.52	7.63	11.62	0.36	2.78

According to the form of cylinder, centerline can be divided into vertical, horizontal, V, and W compressor.

3.1.2. Working Principle of the Experiment. The prime mover rotates by driving the crankshaft, and this connecting rod drives the piston to move back and forth. As the piston moves from TDC to TDC, the volume around the piston and cylinder increases, and the pressure decreases. When the pressure is less than the external pressure of the suction valve, the pressure difference on both sides of the suction valve can exceed the spring strength and open the suction valve. The air from the suction hose flows into the cylinder and begins to smell. When the piston passes to the lower stop position, the closing value is no longer increased, the suction valve closes automatically, and the suction force is eliminated by elastic power and the whole suction process. As the piston moves from BDC to BDC, the closing volume of the piston and cylinder decreases, and the intake and exhaust valves close. The air in the enclosed space is compressed, the pressure increases, and the air temperature increases. When the pressure in the volume is higher than the pressure outside the exhaust valve, the pressure difference overcomes the spring elasticity, the exhaust valve opens, the compression ends, and the exhaust process begins. When the piston moves to TDC, the closed volume no longer decreases, the exhaust valve closes, and the exhaust process ends.

When the piston reaches TDC, there is a gap between the cylinder head and the top of the piston. At the end of

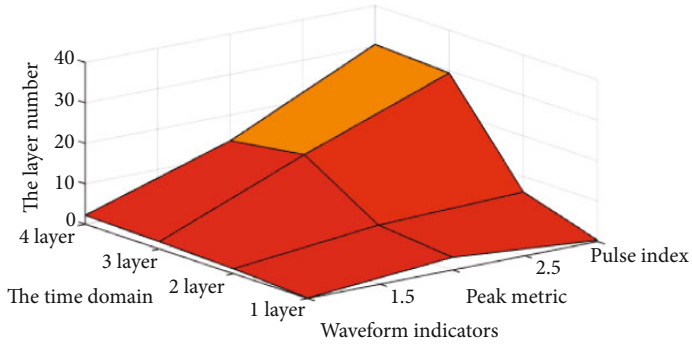

Figure 2: Time-domain parameter changes of zero-channel fourth scheme.

the exhaust, air in the gap cannot be removed. The volume of the gap is called the volume of the gap. When the piston is moved from the TDC to the TDC, the air in the room is compressed, and the pressure is high, so that the air will not smell faster. The air in the gap expands and compresses, beginning the expansion process. When the pressure is lower than the external pressure of the suction valve, the suction valve opens, the expansion process ends, and the suction begins. Piston reciprocating motion, compressor cylinder in turn to perform suction, compression, elimination, and expansion of four processes of motion can complete a cycle.

4. Discussion

On marine air compressor, ZKY-type 1 valve fault signal is studied; the experimental collection of valve under normal and fault condition of six signal multiresolution analysis is shown in Table 1, using waveform index, peak index, pulse index, and root-mean-square value of the maximum five indicators, each index comparison of the six state. It is impossible to extract fault features by observing only the indicators of the original signal. Wavelet multiresolution analysis can extract fault feature models of each layer, as shown in Figure 1, and obtain fault features of each indicator. When the method of fixed-time base point is applied in the wavelet transform and multiresolution analysis, the waveform index, peak index, pulse index, root-mean-square value, and maximum value of the valve under the fault state are all larger than the waveform index, peak index, pulse index, root-mean-square value, and maximum value of the valve under the normal state. In the analysis of multiple wavelet transform solutions, waveform index, peak index, pulse index, root-mean-square value, and the maximum number of other errors are all below the waveform index, peak index, pulse index, and mean root equivalent value in the normal condition of the air valve. Because wavelet transform does not have time-shift invariance, the method using fixed-time base point is more effective than ordinary wavelet analysis. Wavelet fixed-time base analysis can effectively eliminate the redundancy in the fault signal of compressor valve, reduce the input dimension of neural network, and improve the convergence performance of the network.

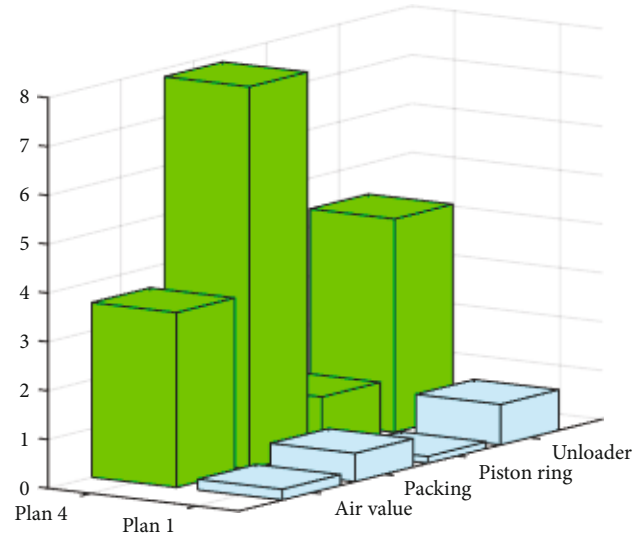

Figure 3: Time-domain parameter changes of the first and fourth schemes of the first layer of zero channel.

4.1. Application of Multiresolution Analysis in Compressor Fault Diagnosis. The waveform difference between normal state and fault state can be clearly seen on the sixth layer. The time-domain parameters commonly used in mechanical fault diagnosis include waveform index, peak index, pulse index, and effective value. For the first scheme, when ch0 measures the new exhaust valve and ch1 measures the new intake valve, the waveform index, peak index, pulse index, effective value, and maximum value of each channel are obtained (as shown in Table 2).

For the fourth scheme, when ch0 measures the fault exhaust valve and ch1 measures the fault suction valve, the waveform index, peak index, pulse index, effective value, and maximum value of each channel are obtained (as shown in Figure 2).

Comparing Table 2 and Figure 2, in the first, second, fourth, and sixth layers, each index of the valve in the fault state is larger than that of the valve in the normal state. In the third layer, the root means that the square value of the valve in case of error is greater than the root-mean-square value and the highest value of the valve under normal conditions. The waveform index, altitude index, and pulse voltage

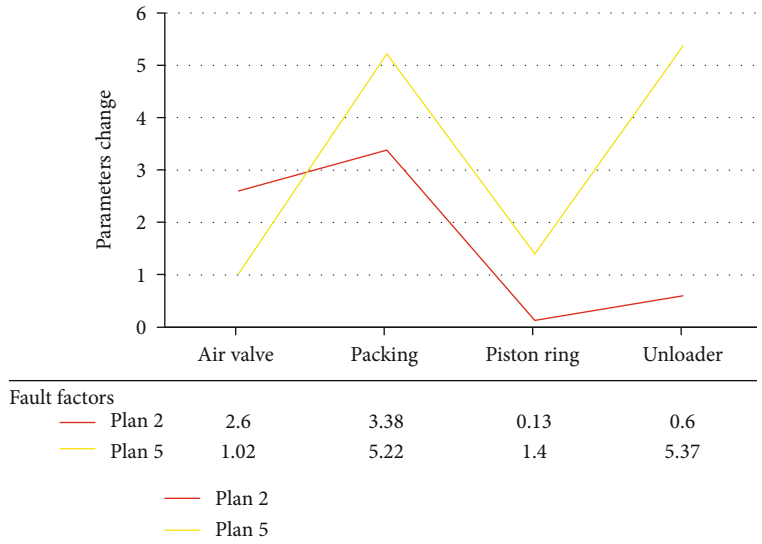

Figure 4: Time-domain parameter changes of the first layer of zero-channel of the second scheme and the fifth scheme.

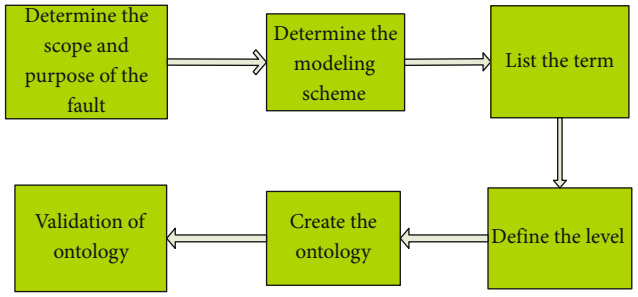

Figure 5: Output flow of output volume in the field of fault diagnosis.

index in the third layer are lower than under normal conditions.

4.2. Wavelet Fixed-Time Basis Analysis of Zero Channel. It can be seen from Figure 3 that the waveform index, peak index, pulse index, root-mean-square value, and maximum value of the valve under the fault state are all larger than the waveform index, peak index, pulse index, root-mean-square value, and maximum value of the valve under the normal state.

As shown in Figure 4, the waveform index, peak index, pulse index, root-mean-square value, and maximum value of the valve under the fault state are all larger than the waveform index, peak index, pulse index, root-mean-square value, and maximum value of the valve under the normal state.

4.3. Design Principle of RBF Neural Network in Experiment

4.3.1. Selection of Input Quantity. It is better to choose flexible ones that have a big impact on the output and are easy to find or remove. In addition, the relationship between each input must be kept very small and it is often not possible to send inputs directly to the neural network. A variety of signal processing techniques and feature detection technology

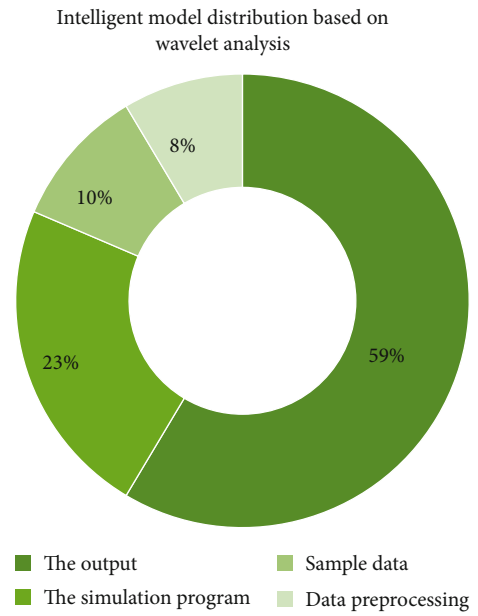

Figure 6: Content distribution of neural network intelligent diagnosis model for wavelet analysis.

are required, and parameters that best reflect the input characteristics are extracted from the original input as the input of the network (as shown in Figure 5).

4.3.2. Selection of Output. The output actually refers to the expected output of neural network, such as classification of problems. The output can be expressed either verbally or numerically. Common language representations are "n choose 1" notation and "n-1" notation. However, numerical representation is only applicable to the classification of two types of contradictions, and it is difficult to apply it to progressive classification. The neural network BP typically accepts a function as a neuron transfer function, and the output range is 0~1 or -1~1. Without data processing, the

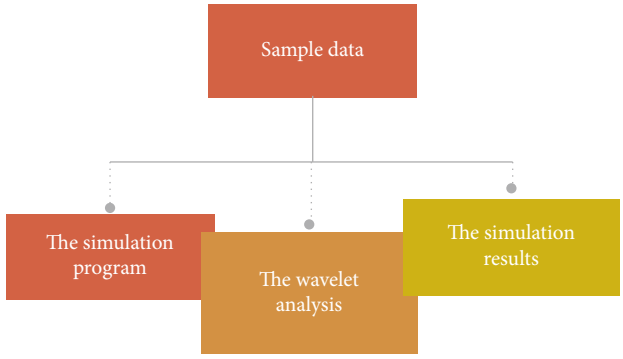

Figure 7: Input and output steps.

total network error to the total error will increase, which will significantly affect learning speed and training and network error. Therefore, the frequency is required to normalize the input and output and to convert the sample distribution to an irrational distribution. The neural network intelligent diagnosis model based on wavelet analysis is shown in Figure 6.

(1) Collect and normalize the sample data of air compressor valve in normal and fault state

(2) Write the simulation program

(3) Conduct simulation experiments. The normalized samples were used for network training, and the expected output during network training was set as a logical value corresponding to the state of the input samples and then sent to the trained neural network for identification

(4) Output corresponding simulation results (as shown in Figure 7)

5. Conclusion

In recent years, the study of mechanical fault intelligent diagnosis system has become a hot spot in the field of mechanical fault diagnosis. The degree of intelligence and diagnostic accuracy of the system depends on the quantity and quality of knowledge in the system knowledge base, as well as the organization, classification, and further knowledge sharing and reasoning. Through the development of the theory of mechanical fault diagnosis system, this paper analyzes the mechanism of typical rotating machinery faults, studies the related theories of mechanical equipment diagnosis technology, and chooses the vibration diagnosis technology based on neural network and data fusion recognition as the theoretical basis of mechanical equipment fault diagnosis.

In the experiment of this paper, 6 signals of the valve under normal and fault conditions were collected, and the 6 signals of the valve were analyzed with multiresolution, and the analysis results with time-domain fault characteristics were extracted. Waveform index, peak index, pulse index, root-mean-square value, and maximum value are selected to compare each index under 6 conditions. Since it is impossible to extract fault features only by observing each indicator of the original signal, multiresolution analysis can extract fault features of each layer and obtain fault features of each indicator. In the process of fault signal wavelet analysis, it is found that the wavelet transform does not have time-shift invariance, and the spectra obtained at different time starting points are also different. By this method, the waveform index and peak value of each layer and the waveform index, peak value, pulse index, root-mean-square value, and maximum value under the fault state of the valve are greater than the waveform index, peak value, pulse index, root-mean-square value, and maximum value under the normal state of the valve. RBF neural network is used for pattern recognition of the obtained data, and the fault can be accurately judged by MATLAB simulation. Wavelet pretreatment can effectively eliminate the redundancy of compressor valve fault signal, reduce the input dimension of neural network, improve the convergence performance of the network, reduce the training time of the network, and avoid the network falling into local minima.

The novelty of this paper is that it proposes a fixed-time method to overcome the variable wavelength of the nonvariable wave, and the RBF neural network is effectively used in air compressor fault detection. The implementation of this project provides another effective case for the application of air compressor condition monitoring and diagnostic errors, which have a certain value of reliability.

Data Availability

No data were used to support this study.

Conflicts of Interest

The author states that this article has no conflict of interest.

References

[1] H. Sofuoglu and M. E. Cetin, "An investigation on mechanical failure of hip joint using finite element method," *Biomedizinische Technik/biomedical Engineering*, vol. 60, no. 6, pp. 603–616, 2015.

[2] S. Hajilar and B. Shafei, "Mechanical failure mechanisms of hydrated products of tricalcium aluminate: a reactive molecular dynamics study," *Materials & Design*, vol. 90, pp. 165–176, 2016.

[3] E. Newton, "The investigation of aircraft accidents with particular reference to those caused by mechanical failure, their diagnosis and lessons learnt from them," *Aeronautical Journal*, vol. 68, no. 639, pp. 156–164, 1964.

[4] L. I. Jiawei, "Intelligent diagnosis of fan fault based on evidence theory and support vector machine," *Journal of Jilin University*, vol. 54, no. 3, pp. 609–612, 2016.

[5] G.-Q. Jiang, P. Xie, X. Wang, M. Chen, and Q. He, "Intelligent fault diagnosis of rotary machinery based on unsupervised multiscale representation learning," *Chinese Journal of Mechanical Engineering*, vol. 30, no. 6, pp. 1314–1324, 2017.

[6] F. Jia, Y. Lei, J. Lin, X. Zhou, and N. Lu, "Deep neural networks: a promising tool for fault characteristic mining and

intelligent diagnosis of rotating machinery with massive data," *Mechanical Systems and Signal Processing*, vol. 72-73, pp. 303–315, 2016.

[7] R. Batash, R. Debi, and D. Grinberg, "Mechanical failure of plate breakage after open reduction and plate fixation of displaced midshaft clavicle fracture-a possible new risk factor: a case report," *Journal of Medical Case Reports*, vol. 13, no. 1, p. 127, 2019.

[8] Y. Shang, L. Sun, and C. Li, "Test of mechanical failure for via holes and solder joints of complex interconnect structure," *Journal of Electronic Testing*, vol. 33, no. 4, pp. 491–499, 2017.

[9] C. Zhang, J. Xu, and L. Cao, "Constitutive behavior and progressive mechanical failure of electrodes in lithium-ion batteries," *Journal of Power Sources*, vol. 357, pp. 126–137, 2017.

[10] L. U. Zhaoqing, S. U. Zhiping, and Z. H. A. N. G. Meiyun, "Mechanical behavior and failure mechanism of phosphoric acid modified para-aramid fiber," *Chinese Journal of Materials Research*, vol. 31, no. 8, pp. 597–602, 2017.

[11] Y. Ganin, E. Ustinova, and H. Ajakan, "Domain-adversarial training of neural networks," *Journal of Machine Learning Research*, vol. 17, no. 1, 2015.

[12] M. Havaei, A. Davy, and D. Warde-Farley, "Brain tumor segmentation with deep neural networks," *Medical Image Analysis*, vol. 35, pp. 18–31, 2017.

[13] Y.-G. Jiang, Z. Wu, and J. Wang, "Exploiting feature and class relationships in video categorization with regularized deep neural networks," *IEEE Transactions on Pattern Analysis & Machine Intelligence*, vol. 40, no. 2, pp. 352–364, 2018.

[14] R. M. V. Pidaparti and M. J. Palakal, "Material model for composites using neural networks," *AIAA Journal*, vol. 31, no. 31, pp. 1533–1535, 2015.

[15] M. H. S. Segler, M. Preuss, and M. P. Waller, "Planning chemical syntheses with deep neural networks and symbolic AI," *Nature*, vol. 555, no. 7698, pp. 604–610, 2018.

[16] Y. Li, X. Yang, and L. Shi, "Finite-time synchronization for competitive neural networks with mixed delays and non-identical perturbations," *Neurocomputing*, vol. 185, no. 10, pp. 242–253, 2016.

[17] M. A. Fernández-Gámez, A. M. Gil-Corral, and F. Galán-Valdivieso, "Corporate reputation and market value: evidence with generalized regression neural networks," *Expert Systems with Applications*, vol. 46, pp. 69–76, 2016.

[18] L. Sheng, Z. Wang, E. Tian, and F. E. Alsaadi, "Delay-distribution-dependent H∞ state estimation for delayed neural networks with (x,v)-dependent noises and fading channels," *Neural Networks the Official Journal of the International Neural Network Society*, vol. 84, pp. 102–112, 2016.

[19] K. Yu and M. Salzmann, "Second-order convolutional neural networks," *Clinical Immunology & Immunopathology*, vol. 66, no. 3, pp. 230–238, 2017.

[20] L. N. Smith, "Cyclical learning rates for training neural networks," in *2017 IEEE Winter Conference on Applications of Computer Vision (WACV)*, pp. 464–472, 2015.

[21] M. Zhou, X. Li, Y. Wang, S. Li, and W. Nie, "6g multi-source information fusion based indoor positioning via gaussian kernel density estimation," in *IEEE Internet of Things Journal*, 2020.

[22] F. Xiao, "Multi-sensor data fusion based on the belief divergence measure of evidences and the belief entropy," *Information Fusion*, vol. 46, pp. 23–32, 2019.

[23] Z. Lv and H. Song, "Mobile Internet of Things under data physical fusion technology," in *IEEE Internet of Things Journal*, 2019.

[24] W. Elsayed, M. Elhoseny, S. Sabbeh, and A. Riad, "Self-maintenance model for wireless sensor networks," *Computers & Electrical Engineering*, vol. 70, pp. 799–812, 2018.

[25] M. Zhou, Y. Long, W. Zhang et al., "Adaptive genetic algorithm-aided neural network with channel state information tensor decomposition for indoor localization," *IEEE Transactions on Evolutionary Computation.*, p. 1, 2021.

[26] M. Zhou, Y. Li, M. J. Tahir, X. Geng, Y. Wang, and W. He, "Integrated statistical test of signal distributions and access point contributions for Wi-Fi indoor localization," *IEEE Transactions on Vehicular Technology.*, vol. 70, no. 5, pp. 5057–5070, 2021.

Hindawi
Journal of Sensors
Volume 2021, Article ID 6232968, 11 pages
https://doi.org/10.1155/2021/6232968

Research Article

Method of Analyzing and Managing Volleyball Action by Using Action Sensor of Mobile Device

Xu Sun,[1] Kai Zhao,[2] Wei Jiang,[2] and Xinlong Jin[3]

[1]*Volleyball Teaching and Research Section, Shenyang Sport University, Shenyang, 110000 Liaoning, China*
[2]*China Volleyball College, Beijing Sport University, Beijing, 100089 Beijing, China*
[3]*Academic Affairs Office, Dalian University of Science and Technology, Dalian, 116000 Liaoning, China*

Correspondence should be addressed to Kai Zhao; paiqiu@bsu.edu.cn

Received 22 July 2021; Revised 26 August 2021; Accepted 1 September 2021; Published 21 September 2021

Academic Editor: Mu Zhou

With the development of electronic technology and sensor technology, more and more intelligent electronic devices integrate micro inertial sensors, which makes the research of human action recognition based on action sensing data have great application value. Data-based action recognition is a new research direction in the field of pattern recognition, which is essentially a process of action data acquisition, feature extraction, feature extraction, and recognition, the process of classification and recognition. Inertial motion information includes acceleration and angular velocity information, which is ubiquitous in daily life. Compared with motion recognition based on visual information, it can more directly reflect the meaning of action. This study mainly discusses the method of analyzing and managing volleyball action by using the action sensor of mobile device. Based on the motion recognition algorithm of support vector machine, the motion recognition process of support vector machine is constructed. When the data terminal and gateway of volleyball players are not in the same LAN, the classification algorithm classifies the samples to be tested through the characteristic data, which directly affects the recognition results. In this paper, the support vector machine algorithm is selected as the data classification algorithm, and the calculation of the classification process is reduced by designing an appropriate kernel function. For multiclass problems, the hierarchical structure of directed acyclic graph is optimized to improve the recognition rate. We need to bind motion sensors to human joints. In order to realize real-time recognition of human motion, mobile devices need to add windows to the motion capture data, that is, divide the data into a small sequence of specified length, and provide more application scenarios for the device. This method of embedding motion sensors into devices to read motion information is widely used, which provides a convenient data acquisition method for human motion pattern recognition based on motion information. The multiclassification support vector machine algorithm is used to train the classification algorithm model with action data. When the signal strength of the sensor is 90 t and the speed is 2.0 m/s and 0.5 m/s, the detection accuracy of the adaptive threshold is 93% and 95%, respectively. The results show that the SVM method based on hybrid kernel function can greatly improve the recognition accuracy of volleyball stroke, and the recognition time is short.

1. Introduction

In recent years, more and more researchers have begun to analyze the movements of the human body, and the field of research is also expanding. From medical rehabilitation engineering, motion sensing games to the production of movies and TV works, virtual reality, and professional sports analysis, human action analysis and recognition technologies are more and more widely used and have produced huge value. Most of the mature research on the understanding of human behavior is based on the analysis of video or image sequences. The motion recognition method based on optical motion capture has obvious advantages. But it also has the most basic disadvantage: the acquisition of motion data is uncertain.

Using quantitative posture data as input data, the basic characteristics of motion can be reconstructed. In the aspect of action recognition, this method uses the support vector

machine algorithm to classify the longest common part as a kernel function to integrate, train, and compare the similarity of the time series of daily sports and realize common classification and recognition. Using the longest common subsequence as the kernel function of the support vector machine is completely different from the traditional time-based single point information. Using the time series information contained in sports, design a classification system for volleyball actions based on spatial methods.

Motion sensor technology and automatic fall detection systems have become reliable and low-cost solutions for falls. Yu et al. have developed a fall detection system based on Hidden Markov Model (HMM), which can use a single motion sensor to automatically detect falls for actual home monitoring scenarios. They proposed a new representation for the acceleration signal in HMM to avoid feature engineering and developed a sensor orientation calibration algorithm to solve the problem of sensor misalignment in actual scenes (misaligned sensor position and misaligned sensor orientation). The HMM classifier is trained to detect falls based on the acceleration signal data collected from the motion sensor. They collect data sets from experiments that simulate falls and normal activities. Their research process lacks theoretical foundation [1]. The smart phone sensor can measure the unique behavioral characteristics of the user when interacting with the smart phone according to the user's different habits, gestures, and angle preferences of touch operations. Shen et al. studied the reliability and applicability of active and continuous smart phone authentication using motion sensor behavior in various operating scenarios and systematically evaluated the uniqueness and durability of behavior. For each sample of sensor behavior, motion information sequences must be extracted and analyzed. These information sequences have statistics, frequency, and wavelet domain characteristics to provide accurate and fine-grained representations of user touch actions. Their research process lacks data [2]. Yurtman and Barshan proposed a novel noniterative direction estimation method based on the physical and geometric characteristics of acceleration, angular velocity, and magnetic field vector to estimate the direction of the motion sensor unit. They obtain the orientation of the sensor unit according to the rotation quaternion transformation between the sensor unit frames. He evaluated the proposed method by incorporating it into an activity recognition scheme for daily and sports activities, which requires accurate estimation of the orientation of the sensor unit in order to achieve the invariance of the orientation of the unit on the body. His research process lacks experimental data [3]. Signature recognition is to identify the owner of the signature, and verification is the process of finding the authenticity of the signature. Although both are important in the field of forensic science, verification is even more important for banks and credit card companies. Behera et al. proposed a method to analyze 3D signatures captured using leap motion sensors. They extended the original 2D function from the original signature to 3D and applied a well-known classifier for identification and verification. They used the leap sports interface to create a large data set containing more than 2,000 signatures registered by 100 volunteers. Their research method is not novel enough [4].

This research mainly uses the support vector machine method based on the hybrid kernel function to determine the movement recognition of the human body in the volleyball movement database. First, the moving images in the database are processed, and an action database suitable for the SVM algorithm is established. Then, PCA dimensionality reduction was performed before classification. Finally, the SVM classifier was used to identify the action type. In the research process of volleyball motion recognition, this research will focus on the SVM algorithm based on the hybrid kernel function and compare it with the experimental template matching method. The SVM algorithm based on the hybrid kernel function proves that the recognition of volleyball stroke is effective and fast.

2. Volleyball Stroke

2.1. Internet of Things Technology. The Internet of Things technology can use smart terminals, communication base stations, data processing, and other display devices to optimize the collection, processing, and monitoring of information. The Internet of Things needs to meet special needs when applied, such as low power consumption, strong coverage, and low cost. In order to meet these needs, various industry organizations have formulated a series of communication standards. The current system based on the Internet of Things technology can meet the requirements of low cost and low power consumption, but there are still problems in security and capacity, so the demand for new Internet technology standards is becoming more and more urgent [5, 6]. The combination of wireless communication technology and wireless automatic identification technology is a network based on the computer Internet. On the basis of the Internet, sensors and controllers are particularly important. What we expect is that all devices or test objects on the network can communicate information without manual intervention [7].

2.2. Motion Feature Recognition. Motion detection is a general preprocessing process for computer vision applications, but motion detection is easily affected by the environment, for example, in scenes such as changes in light, dynamic background, camera movement, and shadows. It is very difficult to correctly detect moving targets. Currently, background subtraction, interframe difference, and optical flow have been widely used in motion detection [8, 9].

Median filtering is a type of nonlinear filtering that can effectively remove noise. The values around the calculated points are arranged in accordance with the gray value, and the gray value of the median value of the placed point is substituted by the gray value of the calculated point, thereby realizing the filtering function. This method can effectively remove noise and high-frequency deviation in Fourier space, so that the image is smoother and the resolution will not be reduced. If the pixel value of the point (x, y) is $f(x, y)$, and the pixel value of the corresponding point after median filtering is $g(x, y)$, the relevant formula is as follows [10]:

$$g(x, y) = \text{median}\{f(x - m, y - n), (m, n) \in Q\}. \quad (1)$$

Among them, Q is the size of the module. After feature representation, classifiers in machine learning are often used to recognize actions. Supervised learning is to build a model that represents the distribution between the classification label and the input features. The unsupervised learning mode is to directly learn training actions from the entire training data, that is, without inputting classification labels. The choice of the number of median filter banks depends on the actual situation. If the number is too small, the texture feature of the image cannot be fully expressed, and if the number is too large, the calculation will be complicated. Particularly during deep training, since deep neural networks can automatically learn image features, if the number of channels is set too much, the training speed will be greatly reduced, the memory footprint will be large, and the learning will be repeated between features, which will affect the overall robustness of the network [11, 12]. The parameters of the Gaussian function most suitable for pixel n can be obtained by a_n and k_n [13].

$$D(\alpha_n, k_n, z_n) = \frac{1}{2} \log \det \sum(\alpha_n, k_n) + \frac{1}{2}[z_n - \mu(\alpha_n, k_n)]^T \cdot \sum(\alpha_n, k_n)^{-1}[z_n - \mu(\alpha_n, k_n)]. \quad (2)$$

Among them, z_n is the RGB value of pixel n. In actual application scenarios, the observation of the target is often multiangle and multidirectional, so these properties are very important for the effective extraction of texture features. They also directly determine the application field of the median filter, and compared to other edge filters, the median filter is closer to the continuously variable condition [14, 15].

2.3. Support Vector Machine. Support vector machine (SVM) is a classic method in the field of pattern recognition and machine learning. It is a supervised learning model related to learning and training. It can be used for data analysis, pattern recognition classification, and regression. The support vector machine algorithm is based on the structural risk minimization of statistical learning methods and the VC dimension theory. Specifically, the support vector machine is constructed by eigenvalue dimensions, a high-dimensional space, in which a hyperplane is established so that the data categories are distributed on both sides of the hyperplane, and the hyperplane is optimized to make the separation between the separated data categories and the hyperplane. Maximize to get the optimal hyperplane. Motion characteristics are obtained by estimating continuous interframe changes. The local motion feature is based on a nonpredetermined target area motion analysis method, which directly searches for points of interest or regions from images or videos and describes their motion information [16]. The discrete form of the transformation function is

$$s_k = T(r_k) = \sum_{j=0}^{k} P_r(r_j) = \sum_{j=0}^{k} \frac{n_k}{n} k = 0, 1, 2, \cdots, L - 1, \quad (3)$$

where n is the sum of pixels in the image and n_k is the number of pixels whose gray level is n. Compared with the global shape feature, the different subshapes in the local shape feature are considered relatively independent, so the description of the shape is not as good as the global feature complete and accurate. However, because the local shape features are relatively less affected by the human body detection and tracking results, they can be used in complex scenes [17, 18]. Therefore, the heart in the initial state probability σ is defined as

$$\left(\sigma_{t+1}^{i}\right)^2 = (1 - \rho)(\sigma_u)^2 + \rho(x - \mu)^T\left(x_i - \mu_j\right). \quad (4)$$

It represents the probability that the first frame of this type of action is in the state ρ. Different initial models will produce different training results. The key issue of the application of the SVM model in action recognition is the determination of the hidden state. The traditional method is to divide each action sequence into N segments, and each segment corresponds to a state in the SVM model. In this way, we have added a penalty for samples that are out of bounds in the problem of maximizing the interval [19]. The trade-off between the two is controlled by the parameter C. The Lagrange equation [20, 21] at this time becomes

$$L(w, b, a) = \frac{1}{2}w^2 + C\sum_{n=1}^{N}\xi_n - \sum_{n=1}^{N} a_n\{y_n(w^T x_n + b) - 1\} - \sum_{n=1}^{N}\mu_n\xi_n. \quad (5)$$

Among them, a is the Lagrangian multiplier.

2.4. Motion Sensor. Generally, when selecting sensor positions, researchers often only consider the importance of different sensor positions to the action category. When a position is selected, the subsequent position selection will be selected according to the importance of the remaining position to the action category [22, 23]. If each position is not related to each other, then there is no problem with this method. However, in practice, the positions are related to each other, and they may contain the same information. If only the correlation between the sensor position and the action category is considered, the result will be the positions that cause serious overlap are selected at the same time, and the importance is relatively small, but the position and the selected position do not have any overlap are often ignored, so that some action categories that can only be distinguished by the ignored position cannot be well recognized [24]. When a single-turn optical fiber coil with a diameter of D rotates, two light waves are emitted clockwise (CW) and counterclockwise (CCW) from point P of the circular optical path, then

$$T_{CW} = \frac{\pi D}{V_{CW}} = \frac{\pi D}{V_f - \Omega D} = \frac{\pi D}{(c/n) - \Omega D}. \quad (6)$$

Among them, c is the speed in a vacuum [25, 26].

3. Volleyball Stroke Management Experiment

3.1. Support Vector Machine (SVM) Action Recognition Algorithm Flow Design. The sensor node is the core of the system, and each node is fully integrated with the accelerometer and the inertial measurement unit of the magnetometer. The motion capture system connects all sensor nodes through wires and finally collects the motion capture data on the hub and realizes wired or wireless output through the hub based on the Internet of Things technology. The design process of the SVM algorithm is shown in Figure 1.

(1) The foreground part of the image is further segmented by the method based on image segmentation. Assign a pixel value to each divided block. In this way, the finally obtained image is composed of several pixel blocks, which have different pixel values for distinguishing each other

(2) After the first step, we will get the segmented image block. Refine each image block and extract bones. After all the image blocks are extracted, the results are added together to form the image T

(3) Perform vertical expansion on the obtained image T. The purpose of this expansion is to connect the obtained bone points to each other, because there may be gaps between the bone points obtained in the previous step, and they are not connected to each other

(4) Set a threshold, filter the image T, and filter out the smaller area (less than the threshold). Used to eliminate the interference of some noise points

3.2. Design of Foreground Detection Module. The foreground detection module takes the current frame as the input signal and then judges the value of each pixel to obtain a binary image of the same size as the current frame. If the pixel value is 1, then the pixel is the detected moving image pixel. If the pixel value is 0, it means that the pixel is a background pixel. Foreground detection is the basis of the entire support vector machine algorithm. In practical applications, the quality of the foreground detection module will directly affect the detection effect, and the foreground detection module processes pixel-level data, so the amount of calculation is very large. Generally, the relationship between algorithm complexity and foreground extraction effect is considered [27, 28].

3.3. Status Query Module Design. The cloud server functions as a WAN gateway in the Internet of Things technology. When the data terminal and the gateway of the volleyball swimmer are not in the same local area network, the cloud server needs to be used for communication and connection. In addition, the security key comparison, the user's mode settings, and other configuration files are also stored in the cloud server.

3.4. Design of Volleyball Data Acquisition Module. To achieve the overall range of motion capture of the human body motion, more than 10 sensor nodes are required, and motion sensors need to be bound to the limb joints of the human body for motion capture. The sensors can detect the human body through the built-in angular rate gyroscope and accelerometer. Collect the motion information in the motion process. For the motion data collected by the motion sensor, the data acquisition module is required to process and collect the data. After the system is initialized, these sensor nodes will automatically build a sensor network using ZigBee technology to calculate the posture of each part of the human body independently and in real time. Then, under the scheduling of the sink node, the posture information of each part of the human body in the wireless sensor network is orderly sent to the sink node. Finally, the sink node uniformly uploads the data of each sensor node to the host computer, which calculates the final action form of the human body.

The function of the motion sensor data acquisition module is to process the motion data collected by the motion sensor equipment, including the following: (1) Analyze the obtained binary data to obtain the real data information of the motion. (2) Perform initial calculations on exercise data. (3) Convert the format of the motion data to a format that is easy to handle. (4) The movement data is handed over to the data transmission module, and the transmission module transmits the data to the terminal PC.

3.5. Design of Volleyball Data Storage Module. For the storage of sports data, the SaveDataFile method is implemented in the CDataManager class. The data storage format is completely in accordance with the data format received by the serial port and is saved in a txt file in binary form. The advantage of using this storage format is that the same data decoding method as when the serial port receives data can be used when the system software performs historical movement reproduction. According to the stored data in the form of a matrix, the effective data during the volleyball movement process are extracted, including the offset position information and the rotation angle information. Combining these two sets of data, the posture analysis algorithm is used to calculate the movement trajectory of the discrete data at the main joint points of the human body.

3.6. Trajectory Image Generation Module Design. The trajectory generation module takes the clump information, foreground mask information, and volleyball stroke data information as input information and then draws the corresponding motion trajectory information according to the position information of each clump and finally retains the motion trajectory information in the designated file. The trajectory generation module is the basis of the subsequent OPENCV program. If the module can give an effective moving object trajectory curve, it will greatly facilitate the

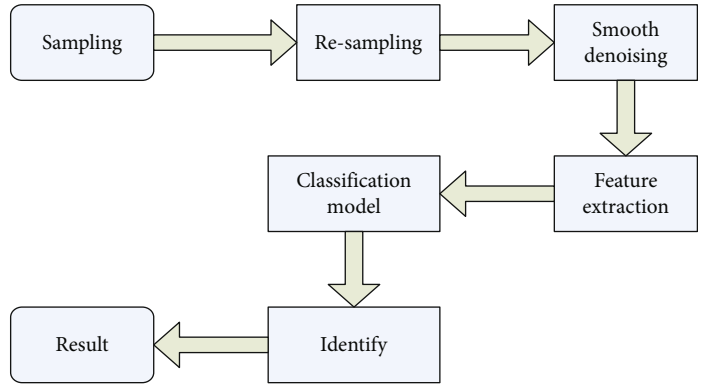

Figure 1: SVM algorithm design process.

convenience of the subsequent program to study the moving object. In real life, the algorithm itself is generally not considered complexity, usually choose the movement trend that can smoothly draw the trajectory curve, and prepare for the program to run.

3.7. Data Windowing. In order to realize the real-time recognition of human movements, it is necessary to window the motion capture data, that is, to divide the data into a short sequence of specified length. At the same time, in order to enhance the ability to describe actions, there is a 50% overlap between adjacent windows. The length of the window is related to the frequency of the human body's behavior. If the length of the window is shorter, the cycle of the human body motion included is also less, and the recognition effect is worse. If the length of the window is longer, the cycle of the human body motion included is also more, the more stable the recognition effect. But the length of the window should not be too large; otherwise, it will cause system delay. Considering that the sampling rate of the motion sensor used in this study is 100 Hz, this study sets the length of the window to 230.

3.8. Denoising Processing of Volleyball Image. The key to median filtering is to replace the local average value with the local median value. In the $N \times N$ $(N = 2n + 1)$ mask window centered on the pixel (x, y) of the gray image F, the gray values of the $N \times N$ pixels are arranged in descending order. The gray value of the middle position is defined as a, a is called the median value, and then $f(x, y) = a$. The median filter will affect the impact function. When half of the window is larger than the width of the alluvial function, the impact function tends to disappear, and the upper part of the triangular function is flattened, so edge blur can be avoided and discrete impact noise can be reduced. In this study, the median filtering method was mainly used to denoise the volleyball image.

3.9. SVM Parameter Training. Using the multiclass SVM algorithm, use the action data to train the classification algorithm model. Randomly select 650 groups from the 1300 groups of sample data as the training set, and the remaining 650 groups as the test set. The final training process of the classification algorithm is to input the training action data in the parameters of the volleyball, and the SVM classifier model for action recognition can be obtained. For different parameters, the recognition results and time are different.

3.10. Network Simulation Program Realization. In the process of network simulation, when the density of network nodes is small, the positioning calculation based on cooperation mode is selected. The simulation program is composed of two parts: one is a user interface program written with VisualC++ development tools; the other is a simulation example program for volleyball wireless monitoring sensor network technology written with OMNeT++ discrete event simulation software. The latter is the core part of the simulation program, which is composed of application layer simulation sample program and MAC/route simulation sample program, which are embedded in the user interface program, and the two simulation sample programs can be started in the user interface program.

3.11. Interactive Communication Design between the Client and the Server. The server publishes related programming interfaces through UDDI, and the client queries these interfaces through UDDI and programs these interfaces to realize the secure communication between the client and the server.

3.12. System Test. The accelerometer data used for training needs to be tagged, and the experimenter needs to enter the type of volleyball style used. Four common volleyball styles can be selected: breaststroke, freestyle, backstroke, and volleyball. Add nickname information to prevent data confusion during the experiment. In addition, the experiment recorder needs to manually record the time point when each experimenter swims and turns and the number of strokes. Click the start button before volleyball, and click the end button after going back and forth through the pool. Then, the acceleration data can be exported to the mobile phone SD card in the txt format through the export button. The txt data format contains the system's time stamp and the *xyz* three-axis data components of the acceleration sensor. The naming format is id+stroke style+pool distance +sensor data source category.

Table 1: SVM parameter identification results.

Method	GS	GA	PSO
Parameter	(0.743, 0. 188)	(0.673, 0.981)	(0.665, 0.100)
Training sample accuracy	90.33 (542/600)	91.5% (549/600)	92.2% (553/600)
Test sample accuracy	92.0 (552/600)	96% (576/600)	93.8% (563/600)
Support vector number	305	179	289
Training time	26	20 s	24 s

4. Analysis of Volleyball Stroke Management

4.1. Analysis of Parameter Recognition Results. SVM parameter identification results are shown in Table 1. Compare the combined training results of three parameters (C, g). Looking at the test accuracy of the three classifiers as a whole, except for the genetic algorithm, the other two have an accuracy close to 94%. Further analysis of the impact of different parameters on the accuracy rate found that the smaller the penalty factor C, the greater the number of support vectors, the larger the C, the less the number of corresponding support vectors. This is in line with the definition of C. The smaller the C, the smaller the emphasis on noise points. During training, more noise points are treated as data samples. However, when the parameter g is 0.1, the test accuracy is higher, and the genetic algorithm has the highest accuracy in the training samples, which indicates that the kernel function affects the generalization ability of the classifier, and the effect of processing unknown samples is better. In summary, the parameter combination obtained by the grid search algorithm corresponds to the classifier with higher accuracy and better performance. The actual test time of the three methods is within 0.5 seconds. For a well-trained interactive system, it meets the real-time requirements. The training process is performed offline and does not affect real-time recognition. There is also a positive correlation between training time and the number of support vectors, indicating that more support vectors require a lot of training time. It can be seen from Table 1 that even if only the relative position features between the pair of bone nodes are used, the average recognition rate of this study is the highest. This shows that the SVM based on the two-layer AP can select a more representative posture. Taking the selected posture as the hidden variable of SVM, this method can achieve good results for action recognition. After adding bone angle features, the average recognition rate of this study can reach 96%. It can be seen that for the UTKinect database, the combination of special recognition features can enrich the feature information and improve the recognition rate.

4.2. Area Window Size on the Detection Effect. After SVM detects the peak, it needs to detect the window of the area where the peak is located and eliminate the influence of some spike interference on the detection effect. The setting of different area windows will affect the monitoring effect of the algorithm. This research will find the best through experiments. The size of the area window makes the detection accuracy the highest. The experiment extracts the complete data of 4 users from the volleyball data and measures the accuracy of the measurement in different area windows through the above algorithm. The effect of the area window size on the detection effect is shown in Table 2. In the data collection, when each subject is recording the acceleration data during volleyball while wearing the equipment, the experimenter in charge of recording will observe with his eyes and record the number of strokes. By comparing the actual recorded data with the measured data, the accuracy of the algorithm can be obtained. Observe the average accuracy of the experiment by setting different sizes of time windows in the algorithm. The ideal recognition accuracy is the dynamic threshold detection method and the regional peak detection method proposed in this paper. As the acceleration curve is difficult to avoid, there are some spike interference signals that make the curve difficult to be completely smooth. Therefore, some of the peak signals may be misjudged as arm stroke behavior, resulting in experimental detection results generally greater than actual results. The dynamic threshold detection method will miss the detection situation, resulting in the detection result is generally less than the actual result. Based on the results of volleyball style detection, the measured value of the regional peak detection method is the closest to the actual situation, which can show that the method proposed in this study is feasible.

Table 2: Influence of area window size on detection effect.

Numbers	Time window	Check accuracy
1	2	93%
2	4	95%
3	6	97%
4	8	98%

4.3. Different Dimensionality Reduction Methods on the Performance of Action Recognition. In this study, the selected part of the action sequence and the collected action sequence in the action database are used as the research data set, and the angle characteristic sequence of each action sequence is extracted, and each sequence is further extracted by windowing each sequence. The time-frequency characteristics of the data. Part of the collected human movement data is used as training data, the movement data selected from the CMU movement database and the rest of the collected data are used as test data. Three different feature reduction methods are used to reduce the dimensionality of the test data. It can be seen from the figure that in the dimensionality reduction results obtained by linear discriminant analysis, the same types of action data are almost clustered

together, but the action data between different types are too close and the degree of discrimination is too small. In the dimensionality reduction results obtained by principal component analysis, all the motion data are intertwined in a mess, which is difficult to distinguish with the naked eye. In contrast, in the dimensionality reduction results obtained by the generalized discriminant analysis, the same type of action data has good aggregation, and different types of actions have a large degree of distinction, which lays a good foundation for the classification of the next step.

In order to further quantitatively study the impact of different dimensionality reduction methods on the performance of action recognition, this study uses the collected action data as the training set, and the data selected from the CMU action database as the verification set. The hierarchical SVM classifier is used to compare the three different dimensionality reduction methods compared. The verification results obtained by different dimensionality reduction methods are shown in Figure 2. The action recognition rate obtained by generalized discriminant analysis dimensionality reduction is the highest, followed by linear discriminant analysis, and principal component analysis is the lowest. The worst results obtained by using principal component analysis to reduce dimensionality can be explained as follows: principal component analysis is a linear dimensionality reduction method, and it is also an unsupervised dimensionality reduction method. The effect of sample labels is not considered in the process of dimensionality reduction. Important information is not extracted. In contrast, linear discriminant analysis, as a supervised dimensionality reduction method, has better feature extraction capabilities. Due to the introduction of the kernel function, generalized discriminant analysis can map nonlinear motion characteristics to high-dimensional space and then perform linear discriminant analysis, so generalized discriminant analysis has a stronger ability to extract information from human movements.

4.4. Feasibility Analysis of SVM. According to the best effect of this feature, this study set the number of joints to 6 and the segmentation window to 60. The SVM descriptor has the fastest recognition time. This is because the descriptor has only a few simple operations in the process of extracting time-frequency features, and the dimensionality reduction process can be obtained only by multiplying with the projection matrix. In addition, the descriptor applied generalized discriminant analysis to effectively extract the important information in the action features, so a good recognition result was obtained. Through comparison, it can be found that the method proposed in this study is superior to other methods in recognition rate and recognition time. The two descriptors proposed based on the topic model, LDA and LDA+SVM, have the best recognition accuracy, which can be explained as follows: the topic model-based method refines the difference of different types of actions to the difference of the posture frame. Sampling makes action words with smaller discrimination in similar types of actions have greater weight, which makes action descriptors of similar action types have greater differences. The feature recognition result of SVM for volleyball stroke is shown in Figure 3. Since the types of actions in this study are few and simple, it uses fewer action words and action topics to achieve the optimal recognition effect and has a shorter recognition time. Compared with the two types of action descriptors proposed in this study, both HOD and SMIJ have longer recognition time. Since the HOD descriptor needs to count the sum of the displacement of each joint point in different directions in different dimensions, the calculation amount is large and noise is easily introduced, so the effect of the descriptor is relatively poor. The SMIJ descriptor needs to select the first 6 joints with the largest amount of information from all joints in each time window. The selection process is more complicated and consumes a lot of time. The experimental results show that although the accuracy of the SVM method based on the hybrid kernel function in the action recognition result is only slightly higher than that of the template matching method, the time it takes to recognize the action is much lower than the template matching method. This is because when using the template matching method, to identify the input action category, it is necessary to traverse the entire template library, which greatly increases the running time of the program. When using the SVM method of the mixed kernel function, due to the principal component analysis method, only need to extract the features of the picture, no need to traverse and analyze each image, which greatly shortens the recognition time, so it proves that the SVM method based on the hybrid kernel function is feasible in action recognition, and it is a kind of higher efficiency. Method. The template matching method and the SVM method based on the hybrid kernel function are used to identify the action category of the person in the image. The results show that for nondatabase images, the calculation speed of the two methods is basically unchanged, and the recognition rate is reduced. This is mainly because the types of actions in the database are limited, they are all actions under the same background, and the direction of application is the same.

4.5. Sample Size and Time Interval on Recognition Results. The influence of sample size and time interval on the recognition result is shown in Figure 4. The recognition accuracy rate of volleyball stroke is represented by a blue curve and a red curve with a star. The number of samples increases from 1 to 5, and the recognition accuracy increases faster, while from 5 to 50, it increases more and more slowly, until it reaches the highest value at 50. The sampling interval is in seconds, starting from 0.1 s and ending at 0.5 s, respectively, 0.1, 0.2, 0.3, 0.4, and 0.5 seconds. From the experimental results, the recognition accuracy of the DTW algorithm will indeed increase as the number of template samples increases, and the recognition accuracy of the corresponding DTW+SVM hierarchical recognition method will also increase as the number of template samples increases. However, when the number of samples reaches 50, the recognition accuracy reaches the maximum, which means that only 50 high-quality samples need to be found from 200 samples as template samples. The internal voting method is adopted, and the number of votes is selected from more

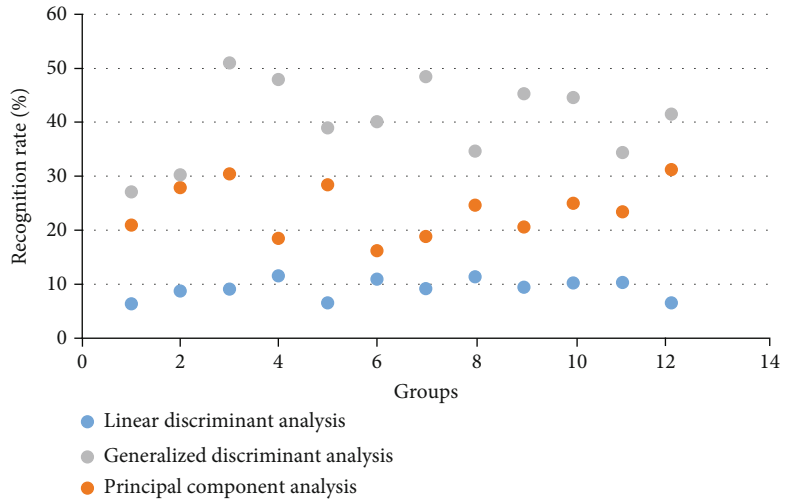

Figure 2: Recognition results of verification data obtained by different dimensionality reduction methods.

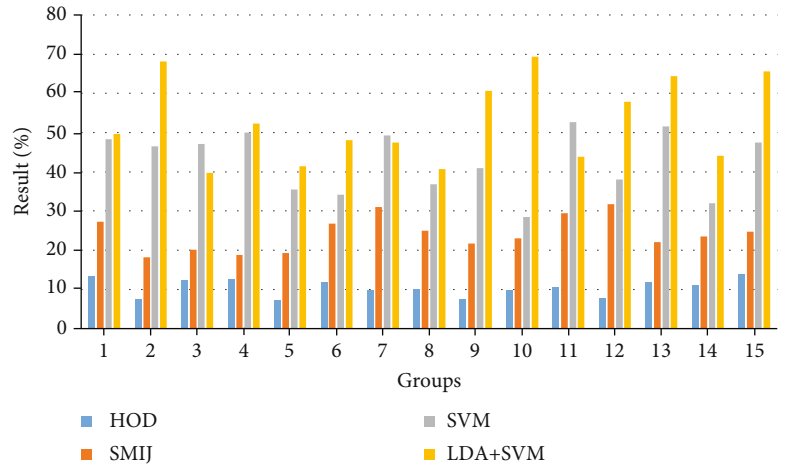

Figure 3: SVM feature recognition results for volleyball stroke.

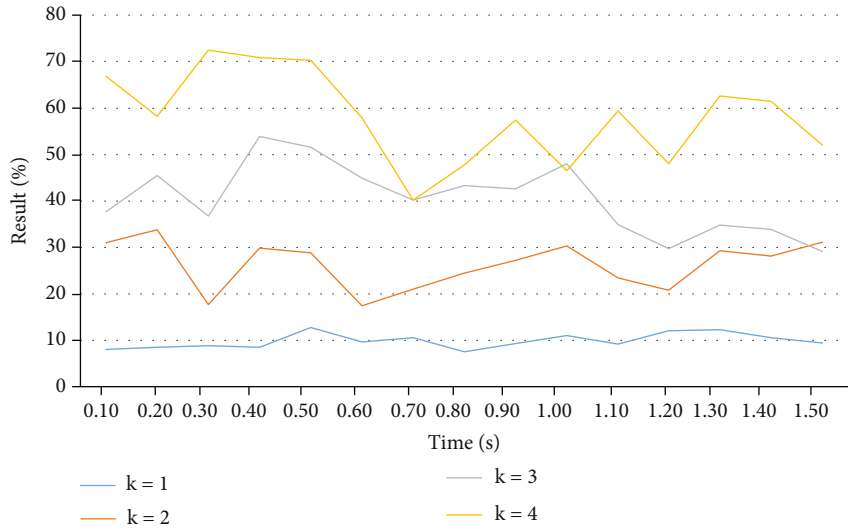

Figure 4: Influence of sample size and time interval on identification results.

to less. Arrange, take the first 50 samples. It can be seen from Figure 4 that the recognition time is closely related to the number of samples, which means that the more samples, the longer the recognition time. The reason is that the number of samples increases, and the number of template matches for the DTW algorithm to recognize simple arm movements will also be corresponding; the identification time will also increase. From Figure 4, it can be seen that the sample size range is between 10 and 50. It is more appropriate to combine the sample size between 10 and 30. If you need to improve the recognition accuracy, increase the number of samples, and if you need to shorten, recognition consumes time and reduces the number of samples. It can be seen from Figure 4 that both the red curve and the blue curve will decrease as the sampling interval increases, that is, the recognition accuracy of simple arm movements and the recognition accuracy of arm movements will decrease as the sampling interval increases; the decreasing range is getting bigger and bigger. When the sampling interval is 0.5 seconds, the recognition accuracy of arm movements is only about 60%. The time spent on recognition decreases as the sampling interval increases. It can be seen that it is more appropriate to set the sampling interval to less than 0.8 seconds. If you need to improve the recognition accuracy, reduce the sampling interval, and if you need to reduce the identification consumption time, increase the sampling interval. Considering the number of candidate segments, the number of candidate segments k performs length statistics on all simple arm motion templates and sorts them from high to low according to the number of occurrences. The first k lengths are selected as the length of the candidate segments, so the larger the value of k, the more the number of candidate segments, the better the segmentation effect, the higher the recognition accuracy, and the smaller the k value, the less the number of candidate segments, the worse the segmentation effect, and the lower the recognition accuracy. And when k is from 1 to 2, the degree of improvement in recognition accuracy is small, and the degree of improvement from 3 to 4 is very small, so the number of suitable candidate segments k is selected between 3 and 4; if you need to improve the recognition accuracy, it can be appropriate. Modifying the value of the number of candidate segments k, increasing k can slightly improve the recognition accuracy, but it will also increase the recognition time. The larger the value, the more the number of candidate segments, the better the segmentation effect, the higher the recognition accuracy, and the longer the recognition time. Conversely, the smaller the k value, the worse the segmentation effect, the lower the recognition accuracy, and the more expensive the recognition, the shorter the time.

4.6. Analysis of Median Filter Denoising Results. First, divide the pixels into three groups, namely, P1, P2, and P3. Then, sort the three groups separately to find the maximum, middle, and minimum of the three groups. Finally, take the smallest value among the three sets of maximum values, the middle value among the three sets of intermediate values, and the largest value among the three sets of minimum values, and then compare the intermediate values. This

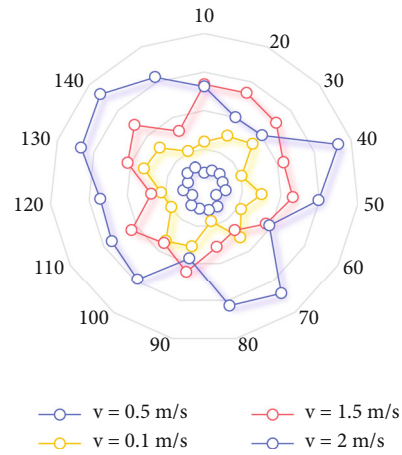

Figure 5: Median filter denoising results.

intermediate value is the required pixel value. This is the content of the quick sort module 2, a total of 3 rows, 3 columns, and 6 sorts; each sorting only needs to delay 3 clock cycles to get the result. Human body movements are characterized by high complexity and style diversity, and it is difficult to avoid the introduction of noise when using wearable sensors to collect movement data. Therefore, the time-frequency features extracted from movement data have a nonlinear relationship with different types of movements. In the actual design, only one value sorting module is needed, and the design can be completed by including them in the top file, respectively. The median filter denoising result is shown in Figure 5. It can be seen from Figure 5 that using the pipeline method for design, after the first group of 9 pixels are quickly arranged, after a delay of three clock cycles, the final median value is the value of data 2. The median value obtained in the second and third groups is also delayed by three clock cycles before getting the result, which shows that the design meets the requirements. It can be seen from Figure 5 that the gray image has more noise, and after median filtering, most of the noise can be filtered out. When the signal strength is 90 T, at 2.0 m/s and 0.5 m/s speed, the detection accuracy of the adaptive threshold reaches 93% and 95%, respectively. Since the adaptive threshold dynamically adjusts the detection threshold according to the signal conditions, it maintains a high detection rate under the low signal condition of 9 T, and the accuracy of 3.0 m/s and 0.5 m/s motion detection reaches 84% and 92%.

5. Conclusion

In this study, firstly, the analysis and management method of volleyball action using a mobile device's action sensor is proposed, and a two-layer AP gesture selection SVM action recognition algorithm is proposed, and the effectiveness of the algorithm is simulated and analyzed. The second is to make use of resources. Based on Visual Studio programming technology, a motion recognition software system platform based on MFC is designed and developed, which can recognize the trained motion captured by Kinect in real time. In the aspect of feature selection of action recognition, a SVM action

recognition method based on two-layer AP gesture selection is proposed. This method can quickly, accurately, and stably select multiple gestures that can represent this kind of action and accurately recognize them through support vector machine. It avoids the shortcomings of the traditional clustering initialization algorithm which is complex or unstable.

According to different application scenarios and information acquisition methods, human action recognition is roughly divided into two categories: image-based and inertial sensor-based. With the development of electronic technology, information shows that the national surveillance cameras have reached 30 million, recording a lot of video information every day. In this study, under the basic framework of traditional video surveillance, the access detection module, motion tracking module, motion recognition module, intelligent SMS notification module, cheek control module, and analysis result display module are added, which basically realizes the intelligent video surveillance function in a simple environment. Because the development of an ordinary video surveillance system has been quite mature, in each module, action recognition is the most difficult, and the algorithm is also the most complex. This paper will briefly introduce the related research of video surveillance, focusing on the related research of action recognition module. Adapt to more changing application scenarios. By embedding the motion sensor into the small wearable device, it is not affected by the external environment, such as light, background, range of motion, and obstacles. There is no need for complex additional equipment, such as cameras; the user's personal real environment does not affect the recognition effect, so it has more application scenarios. More direct access to motion data. Inertial sensors can directly obtain the acceleration and angular velocity information in the process of motion. Through filtering the measured data, high-precision measurement can be achieved, which greatly improves the accuracy of feature extraction in the process of recognition quality.

Through the effective processing of acceleration information, we can extract the corresponding action information and infer the intention of the action executor. On the basis of consulting a large number of fields of human motion capture and behavior recognition, the behavior referred to in pattern recognition is what we call action. Most human activities can be divided into a single combination of actions, so the recognition of behavior can be summed up as the recognition of a series of actions. Data-based action recognition is a new research field in the field of pattern recognition. The process can be simplified as the following steps: firstly, the motion sensor obtains the acceleration and angular velocity data generated during the motion and transmits the measured data to the mobile device through wireless transmission. Secondly, the mobile device processes the data and extracts the characteristic value of the action. Finally, the action is classified and recognized according to the characteristic value through the pattern recognition algorithm.

Data Availability

No data were used to support this study.

Conflicts of Interest

The author states that this article has no conflict of interest.

References

[1] S. Yu, H. Chen, and R. A. Brown, "Hidden Markov model-based fall detection with motion sensor orientation calibration: a case for real-life home monitoring," *IEEE Journal of Biomedical and Health Informatics*, vol. 22, no. 6, pp. 1847–1853, 2018.

[2] C. Shen, Y. Li, Y. Chen, X. Guan, and R. A. Maxion, "Performance analysis of multi-motion sensor behavior for active smartphone authentication," *IEEE Transactions on Information Forensics & Security*, vol. 13, no. 1, pp. 48–62, 2018.

[3] A. Yurtman and B. Barshan, "Novel noniterative orientation estimation for wearable motion sensor units acquiring accelerometer, gyroscope, and magnetometer measurements," *IEEE Transactions on Instrumentation and Measurement*, vol. 69, no. 6, pp. 3206–3215, 2020.

[4] S. K. Behera, D. P. Dogra, and P. P. Roy, "Analysis of 3D signatures recorded using leap motion sensor," *Multimedia Tools and Applications*, vol. 77, no. 11, pp. 14029–14054, 2018.

[5] M. Hirata, R. Watanabe, Y. Koyano et al., "Using a motion sensor-equipped smartphone to facilitate CT-guided puncture," *Cardiovascular & Interventional Radiology*, vol. 40, no. 4, pp. 609–615, 2017.

[6] J. K. Min, E. J. Cheon, J. M. Kim, S. C. Lee, and K. Choi, "Comparison of the 6-DOF motion sensor and stain gauge data for ice load estimation on IBRV ARAON," *Journal of the Society of Naval Architects of Korea*, vol. 53, no. 6, pp. 529–535, 2016.

[7] I. I. Duma and S. Giurgiu, "Circadian activity and nest use of Dryomys nitedula as revealed by infrared motion sensor cameras," *Folia Zoologica*, vol. 61, no. 1, pp. 49–53, 2018.

[8] L. B. Huang, W. Xu, C. Zhao et al., "Multifunctional water drop energy harvesting and human motion sensor based on flexible dual-mode nanogenerator incorporated with polymer nanotubes," *ACS Applied Materials And Interfaces*, vol. 12, no. 21, pp. 24030–24038, 2020.

[9] T. A. Donaldson, "Inline calibration of motion sensor," *Journal of Chinese Pharmaceutical ences*, vol. 48, no. 23, pp. 2022–2025, 2016.

[10] G. Marin, F. Dominio, and P. Zanuttigh, "Hand gesture recognition with jointly calibrated leap motion and depth sensor," *Multimedia Tools and Applications*, vol. 75, no. 22, pp. 14991–15015, 2016.

[11] H. Jin, Q. Chen, Z. Chen, Y. Hu, and J. Zhang, "Multi-Leap-Motion sensor based demonstration for robotic refine tabletop object manipulation task," *Caai Transactions on Intelligence Technology*, vol. 1, no. 1, pp. 104–113, 2016.

[12] Z. Wei, W. Zhang, and W. Liu, "Attitude theory and experimental research of micro-aircraft based on MEMS sensor," *Piezoelectrics & Acoustooptics*, vol. 40, no. 4, pp. 516–520, 2018.

[13] D. Laurijssen, S. Truijen, W. Saeys, W. Daems, and J. Steckel, "An ultrasonic six degrees-of-freedom pose estimation sensor," *IEEE Sensors Journal*, vol. 17, no. 1, pp. 151–159, 2017.

[14] D. Korpi, J. Tamminen, M. Turunen et al., "Full-duplex mobile device - pushing the limits," *IEEE Communications Magazine*, vol. 54, no. 9, pp. 80–87, 2016.

[15] L. Zhou, "Mobile device-to-device video distribution: theory and application," *ACM Transactions on Multimedia Computing Communications and Applications*, vol. 12, no. 3, pp. 1–23, 2016.

[16] E. Noei, M. D. Syer, Y. Zou, A. E. Hassan, and I. Keivanloo, "A study of the relation of mobile device attributes with the user-perceived quality of Android apps," *Empirical Software Engineering*, vol. 22, no. 6, pp. 3088–3116, 2017.

[17] K. F. Chiang and H. H. Wang, "Nurses' experiences of using a smart mobile device application to assist home care for patients with chronic disease: a qualitative study," *Journal of Clinical Nursing*, vol. 25, no. 13-14, pp. 2008–2017, 2016.

[18] X. Du and K. Yang, "A map-assisted WiFi AP placement algorithm enabling mobile device's indoor positioning," *IEEE Systems Journal*, vol. 11, no. 3, pp. 1467–1475, 2017.

[19] R. Gotor, P. Ashokkumar, M. Hecht, K. Keil, and K. Rurack, "Optical pH sensor covering the range from pH 0-14 compatible with mobile-device readout and based on a set of rationally designed indicator dyes," *Analytical Chemistry*, vol. 89, no. 16, pp. 8437–8444, 2017.

[20] M. I. Gofman and S. Mitra, "Multimodal biometrics for enhanced mobile device security," *Communications of the ACM*, vol. 59, no. 4, pp. 58–65, 2016.

[21] C. Hauptmann, A. Wegener, H. Poppe, M. Williams, G. Popelka, and P. A. Tass, "Validation of a mobile device for acoustic coordinated reset neuromodulation tinnitus therapy," *Journal of the American Academy of Audiology*, vol. 27, no. 9, pp. 720–731, 2016.

[22] R. D. Keegan, M. C. Oliver, T. J. Stanfill et al., "Use of a mobile device simulation as a preclass active learning exercise," *Journal of Nursing Education*, vol. 55, no. 1, pp. 56–59, 2016.

[23] W. Sun, F. Brännström, and E. G. Ström, "Network synchronization for mobile device-to-device systems," *IEEE Transactions on Communications*, vol. 65, no. 3, pp. 1193–1206, 2017.

[24] H. X. Zhang, F. F. Sheng, P. Y. Xu, and Y. Tang, "Visualizing user characteristics based on mobile device log data," *Journal of Software*, vol. 27, no. 5, pp. 1174–1187, 2016.

[25] S. J. Lofgreen, K. Ashack, K. A. Burton, and R. P. Dellavalle, "Mobile device use in dermatologic patient care," *Current Dermatology Reports*, vol. 5, no. 2, pp. 77–82, 2016.

[26] H. Chen and W. Li, "Mobile device user's privacy security assurance behavior: a technology threat avoidance perspective," *Information & Computer Security*, vol. 25, no. 3, pp. 330–344, 2017.

[27] M. Zhou, Y. Long, W. Zhang et al., "Adaptive genetic algorithm-aided neural network with channel state information tensor decomposition for indoor localization," *IEEE Transactions on Evolutionary Computation*, p. 1, 2021.

[28] Y. L. Zhou, Y. Li, M. J. Tahir, X. Geng, Y. Wang, and W. He, "Integrated statistical test of signal distributions and access point contributions for Wi-Fi indoor localization," *IEEE Transactions on Vehicular Technology.*, vol. 70, no. 5, pp. 5057–5070, 2021.

Hindawi
Journal of Sensors
Volume 2021, Article ID 4853183, 10 pages
https://doi.org/10.1155/2021/4853183

Research Article

Semantic-Based Sports Music Information Fusion and Retrieval in Wireless Sensor Networks

Qiaolin Yu,[1] Xiaofei Liu,[2] Sihui Li,[1] Lei Hou,[1] Chengdong Zhu,[2] and Ying Lin[3]

[1]*School of Music, Liaoning Normal University, Dalian, 116021 Liaoning, China*
[2]*School of Sport, Liaoning Normal University, Dalian, 116021 Liaoning, China*
[3]*Omnimedia Tech Center, Shenyang Radio and Television Station, Shenyang, 110300 Liaoning, China*

Correspondence should be addressed to Chengdong Zhu; zhuchengdong104321@lnnu.edu.cn

Received 12 July 2021; Revised 23 August 2021; Accepted 27 August 2021; Published 18 September 2021

Academic Editor: Mu Zhou

The wireless sensor network has developed rapidly in recent years. It is formed by the intersection of multiple disciplines. It integrates embedded technology, sensor technology, distributed technology, wireless communication technology, and modern networks. It is a brand new information acquisition platform. The characteristics of sensor networks determine that information fusion technology is a hot spot in the research of wireless sensor networks. Information fusion can achieve high performance and low cost in terms of energy and communication, which is of great significance to the research of sensor networks. This paper is aimed at studying the semantic-based sports music information fusion and retrieval research in wireless sensor networks. WSNs may face various attacks including eavesdropping attacks, replay attacks, Sybil attacks, and DOS attacks. Therefore, they are designing sensor network solutions. It is necessary to consider the network security issues. This article summarizes and analyzes the existing WSN security data fusion solutions for this issue and compares them by classification. This paper proposes methods and theories such as the spatial correlation detection algorithm, CBA algorithm, FTD algorithm, and DFWD algorithm, which enriches the research of information fusion and retrieval in wireless sensor networks, which is of exploratory significance, and it also establishes this problem. The model was studied, and reliable data was obtained. The experimental results of this paper show that when using these methods to diagnose faults in WSN, the correct rate of model diagnosis is higher than 77%.

1. Introduction

1.1. Background. WSNs are currently attracting international attention, a highly integrated frontier research field involving multiple disciplines and a high degree of intersecting knowledge. Developments in sensor technology, in microelectrical systems technology, computer technology, and radio communication have promoted the emergence and development of modern WSN. After the Internet, WSNs are IT hotspot technologies that have a significant impact on human lifestyles in the 21st century. As early as 1999, it was listed by US Business Weekly as the most influential machine of the 21st century, and in 2000 by the US Department of Defense as one of the five cutting-edge areas of national defense. These miniature, inexpensive, and low-power sensor nodes (devices) have the function of sensing the surrounding environment and data processing and can form a sensor network spontaneously through wireless communication technology, which is convenient for people to collect useful information and analyze and process. In many fields in the real environment, WSNs have very broad application prospects. For example, it has good applications in military, target tracking, environmental monitoring, health monitoring, and other fields. Later, in 2003, MIT's *Technology Review* magazine listed WSN as the first emerging technology among the top ten emerging technologies in the future; in 2003, *Business Week* published a report in its "Future Technology Special Edition." The article pointed out that WSN is one of the four high-tech industries in the world in the future. Since the promotion of sports dance in China in the 1980s, in order to make it quickly become one of the fitness programs of national sports, to

harmoniously integrate with the international sports dance culture, and to enhance the cultural taste of Chinese sports dance, some experts and scholars have advocated. Under the influence of the theory of Chinese sports dance, sports dance uses Chinese elements in music and clothing, making this sport quickly accepted by the Chinese people and effectively promoting the development of national fitness sports.

1.2. Significance. The basic function of WSNs is to sense, collect, process, and return data information in the monitoring area. The resources of the sensor nodes are very limited, especially the battery energy resources of the nodes, which are directly related to the service life of the entire network. WSN usually contains many wireless sensor nodes, which are composed of embedded processors, sensing components, power modules, and communication parts. The sensor nodes are usually deployed by random placement. At any time, the sensor nodes use wireless communication to self-organize the network topology. Each node has a strong collaboration ability, and the network system is "intelligent" from the perspective of the overall behavior of the system. At the same time, due to the characteristics of reciprocal measurement and distributed collaboration, wireless sensor networks have a wider application range, flexible operation, high measurement accuracy, and intelligence and have broad application prospects in many fields such as military, industry, and agricultural production. At the same time, the reliability and sustainability of the network are also increasing. The fault diagnosis of sensor nodes is very important. Real-time understanding of the state of the network plays an important role.

1.3. Related Work. Since the end of the 19th century, the wireless sensor network has been a highly interdisciplinary field. It highly integrates sensors, embedded computing, wireless network, and communication technologies. Scholars at home and abroad have paid more and more attention to its research due to many unavoidable factors. Due to the influence of factors, the environment in which WSN is used is extremely complex and harsh, so the probability of sensor node failure is much higher than that of other systems. Li and Wang proposed that wireless sensor networks, as an emerging technology integrating information acquisition, transmission, and processing, play an important role in the field of computer networks. Reliable information fusion is a key technology for reducing energy consumption and data transmission in wireless sensor networks and has broad prospects. In recent years, with the development of information technology, the research of WSN reliable information fusion method has attracted wide attention from domestic and foreign scholars and gradually diversified [1]. Wu et al. proposed the wireless sensor network holmium wshn41, which has been widely used in military, transportation, medical, and other fields. The design of a wireless sensor network routing protocol is limited by the characteristics of local information and power supply. The communication ability and access point of sensor networks are limited. How to improve the energy efficiency of node and network life cycle is the current research hotspot, and an improved leach holmium algorithm is proposed [2]. Wang et al. said that the class state estimation problem of wireless sensor networks (WSNs) with finite energy is studied. Firstly, the multirate estimation model is established, and then, the calculation is carried out on the basis of matrix weighting. Based on the optimal fusion criterion, there is a new development. A two-step information fusion algorithm is designed. Compared with the existing methods, the proposed fusion algorithm can greatly reduce the communication cost. A wireless sensor network can effectively save the energy cost of sensors [3]. Although the analysis is in place, some of the theories put forward do not have practical significance. The disadvantage of the research is that there is no specific analysis of the research process.

1.4. Innovation. Innovative points of this article are the following: (1) Innovation is from the perspective of topic selection. From the perspective of topic selection, this article is a brand new perspective. It has exploratory significance in researching wireless sensor networks, sports music, information fusion, and retrieval. (2) The innovation of the method part is to use the spatial correlation detection algorithm, CBA algorithm, FTD algorithm, and DFWD algorithm in the research for sports music information fusion and retrieval. (3) The other is the innovation of project practice. Due to the characteristics of peer-to-peer measurement and distributed collaboration, wireless sensor networks have a wider application range, flexible operation, high measurement accuracy, and intelligence and have broad application prospects in many fields such as military, industry, and agricultural production.

2. Overview of Wireless Sensor Network Detection Methods

2.1. Overview of Detection Methods. Wireless sensor networks have an important application value in many fields, such as detecting whether an event has occurred and reporting it to users. The application research of event detection is the design of effective event detection technology. Since the 21st century, many domestic and foreign scholars have conducted research on this. This paper summarizes the existing event area detection algorithms, which can be roughly divided into two categories: algorithms based on spatial correlation and algorithms based on spatiotemporal correlation [4].

2.1.1. Detection Algorithm Based on Spatial Correlation. Krishnamachari et al.'s research on event detection technology in the sensor network environment is relatively early. According to the spatial correlation characteristics between nodes, they proposed a Bayesian fault-tolerant algorithm (BFTA). The first is the need to calculate the prior probability; the second is the error rate of the classification decision; the third is that it is very sensitive to the expression of the input data; the fourth is the use of the assumption of the independence of the sample attributes, so if the sample attributes are related, the effect is not good. The BFTA algorithm [5] is executed on the premise that normal nodes have

spatial relevance but error nodes do not have spatial relevance characteristics, all nodes have the same error rate, and the missed alarm rate and false alarm rate [6] are consistent. Define the node error rate, then

$$P = P(S_i = 0|D_i = 1) = P(S_i = 1|D_i = 0). \quad (1)$$

Among them, it is defined as the actual condition of the event, which is defined as the state observed by the node, and the value is "1" or "0." Assume L_n indicates normal conditions. Lower node perception data,$L_e/2$, represents node perception data under abnormal conditions; the best decision threshold is equal to $L_n + L_e/2$. If the environmental noise obeys the normal distribution $N(0, \partial^2)$, then the value of P can be obtained according to formula (1):

$$P = \Re\left(\frac{L_e - L_n}{2\partial}\right). \quad (2)$$

2.2. Detection Algorithm. The CBA algorithm, FTD algorithm, and DFWD algorithm are all three different improved algorithms for the above BFTA fault-tolerant OTDS algorithm. The CBA algorithm improved algorithm performance, such as reducing the incident missed alarm rate. The FDT algorithm reduced the communication between network nodes on the premise of effectively completing event detection. The DFWD algorithm improves the reliability of event detection and reduces the false positive rate. The improved methods and advantages and disadvantages are shown in Table 1.

2.2.1. CBA Algorithm. In the algorithm, T_j represents the credibility of each sensor node [7], and the mean value of the product of X_i and the node observation value is used to determine whether an event has occurred, and the discriminant function is set to $f(X_i, \bar{X}_i)$. If the mean value meets certain conditions, the other is $f(X_i, \bar{X}_i)$; otherwise, it is 0. If X_i is defined as the neighbor node of node s_j, the observation data of $s_j(j = 1, 2, \cdots, k)$, and the initial value of the node's credibility is $T_{\max}$, the average value of node s_j and its neighbor node s_i is calculated as $\bar{X}_i$:

$$\bar{X}_i = SDG\{X_f|j = 2\} = \frac{\sum_{j=1}^{k} T_j}{\sum_{j=1}^{k} T_j}. \quad (3)$$

Secondly, use the judgment function $f(X_i, \bar{X}_i)$ to judge the state of node s_i, namely,

$$s(X_i, \bar{X}_i) = \begin{cases} 1, & \text{if } |x_i x_j| > \delta, \\ 0, & \text{otherwise.} \end{cases} \quad (4)$$

2.2.2. FTD Algorithm. The algorithm implements event detection according to the neighbor node of the node and the neighbor node status of its node neighbors [8]. Each node in the algorithm sets different credibility according to the neighbor's neighbor nodes and judges whether the node realizes the reliable detection of the event through the credibility. First, calculate the sum of the observations of the neighbor nodes of node s_i, namely,

$$t_i = \sum_{j=3}^{n_2} f_{dfg}. \quad (5)$$

Calculate the credibility of s_i node:

$$W_i^{\text{self}} = \frac{1 + D_{ai}}{2n_2} = \begin{cases} \dfrac{2}{(3 * n_1), S_{ai}} = 0, \\ \dfrac{2}{n_1, S_{ai} = 1}. \end{cases} \quad (6)$$

Calculate the credibility of neighbor nodes of s_i node neighbor:

$$W = \sum_{i=1}^{b_1} W_i^{\text{neighbor}} * W_i^{\text{self}},$$

$$W = \sum_{i=2}^{n_2}\left[\frac{t_1}{n_2} * \frac{2}{3n_2}(1 + s_{as})\right], \quad (7)$$

$$W = \sum_{i=1}^{g_k}\left[\frac{g_k}{n_2}\frac{1}{2n_1}(2 + 2)\right] + \sum_{n=2}^{n_1}\left[\frac{t_e}{n_3}\frac{1}{3n}(2 + 0)\right].$$

2.2.3. DFWD Algorithm. The DFWD algorithm is an algorithm based on hypothesis testing. If most of its neighbor nodes also meet the hypothesis testing conditions, it is considered that node s_j has detected an abnormality. The conditions to be met are

$$\frac{\left|X_t^i - \text{Exp}_r(t)\right|}{SarSR_e(t)} < \partial. \quad (8)$$

Among them, the variance function that defines the node perception data is $SarSR_e(t)1$, and it is determined by the following formula:

$$A_{rh}(t) = \frac{\text{Exp}_n(t) + \text{Exp}_e(t)}{3}. \quad (9)$$

$\text{Exp}_n(t)$ and $\text{Exp}_e(t)$, respectively, represent the expected function of the node perception data in the normal area and the event area.

2.3. The Information Processing Method of the Convergence Node of the Wireless Sensor Network. In WSNs, the sensor information of ordinary nodes in the monitoring area is transmitted to the sink node, and the data packet transmission method and the ability of the ordinary sampling points in the monitoring area to fuse data information [9] and information processing methods can be divided into centralized and distributed. The characteristic of the centralized structure is that the sensor node directly transmits the

Table 1: Three different improved algorithms.

Algorithm	Ways to improve	Advantage	Disadvantage
CBA algorithm	Modify the relevant theoretical knowledge and change the threshold from $0.5(n-1)$	Improved algorithm performance, such as reducing incident missed alarm rate	Few types of errors are considered, ignoring the impact of transient errors on event detection
FDT algorithm	Set an upper limit for the missed alarm rate	Reduce the communication between network nodes on the premise of effectively completing event detection	Few types of errors are considered, and the threshold is calculated every time the algorithm is executed, which increases the amount of calculation
DFWD algorithm	Define different weights according to the distance between nodes	Improve the reliability of event detection and reduce the false positive rate	Few types of errors are considered, ignoring the impact of transient errors on event detection

associated information to the sink node and then performs data fusion through it. This structure minimizes loss of information, but wireless sensor network nodes are very tightly deployed, so there are multiple sensor nodes corresponding to obstacles, or multiple to one situations. This kind of redundant information will make the wireless sensor network. The energy is severely lost. The distributed method is also called information processing in the sensor network [10]. When the sensor node uses the cluster head node in the network to transmit information, the cluster head node will flip through the scanned information and then preprocess the information accordingly. A method for sinks in wireless sensor networks to collect information when they are moving: first establish a two-layer grid in the entire network, and perform hierarchical monitoring based on the two-layer grid, and perform event-driven or query-driven monitoring of events of interest in the environment. For monitoring applications, when the sink is moving, the agent mechanism is used to reselect the direct agent and the main agent to ensure that the sink can continue to collect data from the event source or the node of the query source. Then, the cluster head node transmits the fault information to the sink node, and finally, it implements information processing. In this way, the information collection of the wireless sensor network can be carried out efficiently, and the two open can reduce the scale of information transmission [11] and then can reduce energy consumption [12]; the channel utilization rate has been improved, and the wireless sensor network has expanded usage time. Therefore, for wireless sensor networks with high energy-saving requirements like this article, a distributed structure is used to process data. In the wireless sensor network, there are many ways to classify the data fusion method of the sink node. The main method of data fusion is shown in Figure 1.

3. Simulation Experiment

3.1. Feasibility Experiment. The experimental scenario assumes that 4000 nodes are randomly generated in 633 RCs distributed on a 6400 square meter site. The node distribution is shown in Figure 2. The sensing radius [13] is 15 meters, and the initial energy of the nodes is 90 joules, as shown in Figure 2.

First of all, consider the energy consumption of the wireless sensor network without attack and without other network nodes [14], the transmitter radius of SORCA-W being ten meters and the transmitter radius of SORCA being 40 meters, as shown in Figure 3.

It can be seen from the power consumption model that when the communication node distance is greater than 0, the power consumption of the transmitter is proportional to the square of the distance; otherwise, it is proportional to the fourth power of the distance. It does not affect the normal communication of nodes [15, 16]; a large amount of energy can be saved by shortening the transmitting radius of the node.

3.2. Continuous Wiener Acceleration Model. When studying the state estimation problem of linear systems, use the Wiener process to describe the product performance degradation trajectory. In the test, when the product performance degrades to a certain threshold, the stress level is changed, so that the stress level change time of the product is a random variable that obeys the inverse Gaussian distribution. Based on this situation, the step stress accelerated degradation of the product is an established model. CWPA is the most basic model. The purpose of designing this experiment is mainly as follows:

(1) Through this experiment, how to model the physical system is understood and the obtained continuous time-invariant state differential equation is converted into a discrete form state equation suitable for Kalman filter, numerical data processing noise reduction, Kalman data processing technology, Kalman data processing noise reduction, real-time computing, parallel programming, real-time programming, real-time updating, Kalman filter, navigation, control, etc.

(2) Because in the simulation experiment the measurement data of the sensor needs to be generated artificially, this experiment also explains how to simulate the dynamic system to generate the sensor measurement data close to the actual value

(3) The influence of the type and error of the physical quantity measured by the sensor on the experimental results is explained

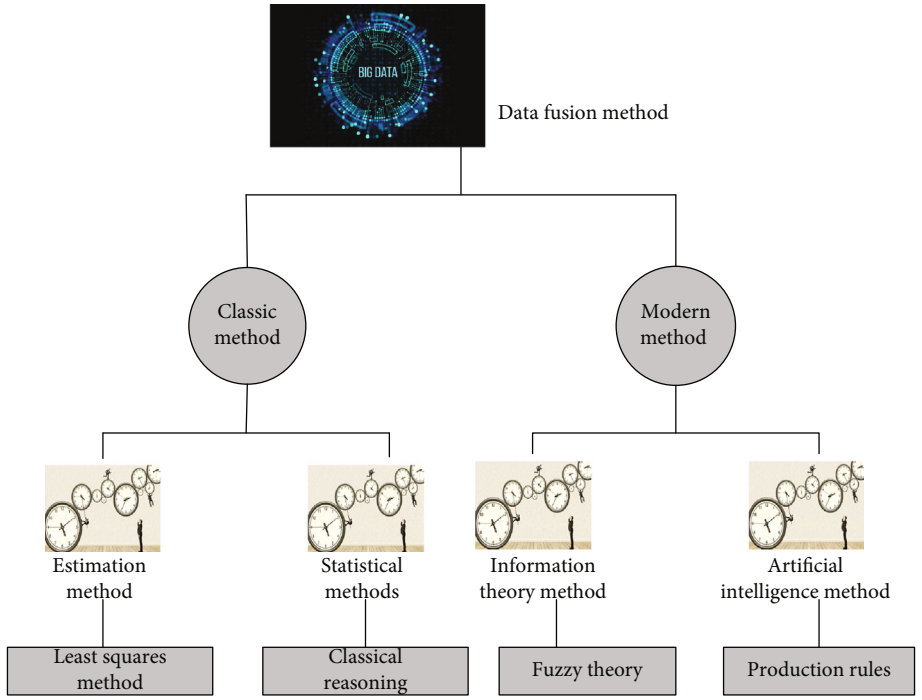

Figure 1: The main ways of information fusion.

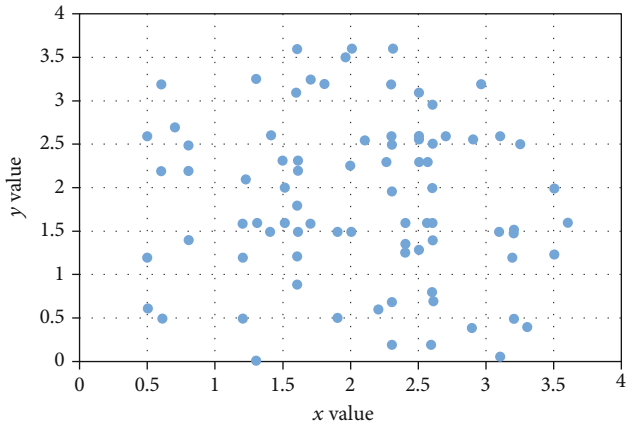

Figure 2: Node distribution in the simulation scene.

In the mathematical modeling of actual linear time-invariant physical systems [17] (linear time-invariant models), they often need to be expressed in the form of continuous time-invariant state differential equations, namely,

$$\frac{dX(i)}{df} = AR(i) + Dw(t). \tag{10}$$

In the simulation experiment, the target motion trajectory and measured value generated by the simulation are shown in Figure 4.

According to the above-measured values, the following position and velocity estimates can be obtained by the standard Kalman filter [18], as shown in Figures 5 and 6.

The feedback of this figure is that the greater the error covariance of the generated measurement, the greater the D, the more intuitive. This is because the value of the coordinate is much larger than the value of the speed. After normalizing the error, it can be known that the relative error of the position is lower than the relative error of the speed. This is because the sensor directly measures only the target position, while the speed is obtained by indirect calculation. If the observation matrix H [19] is modified to measure the target position and speed at the same time, then the accuracy of the filtered position and speed estimation will be improved.

3.3. Experimental Data Set. This experiment uses the KDD99 data set [20], which is used by most researchers in training and testing network intrusion detection systems. The experimental network topology consists of more than 500,000 network connection records for training and more than 200,000 network connection records for testing, as shown in Figure 7.

Each record of this data contains 3 class identifiers and 42 fixed characteristic attributes, of which there are 5 symbolic variables, 7 discrete variables, and 32 continuous variables in the characteristic attributes. The data text format is shown in Table 2.

The last column is the category identifier, which is used to mark whether the record is normal. There are 24 types of attacks here, and the test set contains another 18 types of attacks [21]. The data includes a large amount of normal network traffic data and various intrusion behavior data, which are relatively representative. The intrusion data involves 3 categories and 21 subcategories of intrusion attacks. The specific categories include DOS, Probe, R2L,

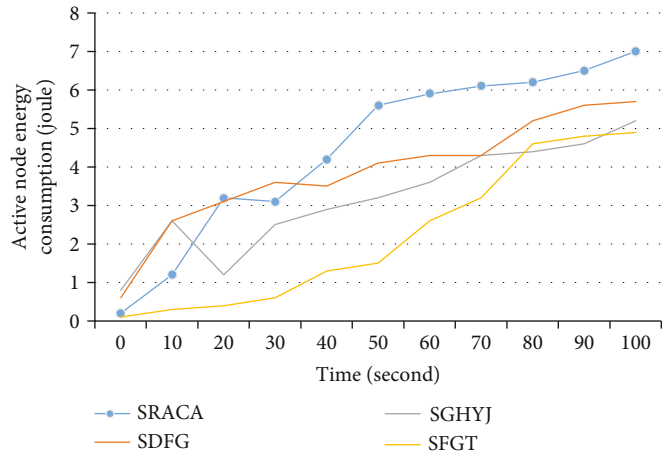

Figure 3: Comparison of energy consumption without attack.

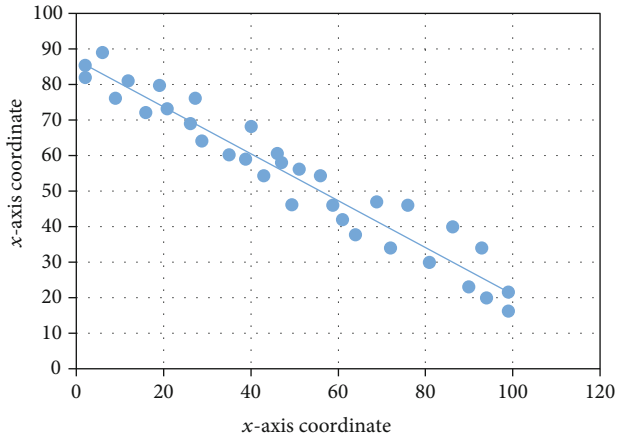

Figure 4: Target motion trajectory and analog sensor measurement value.

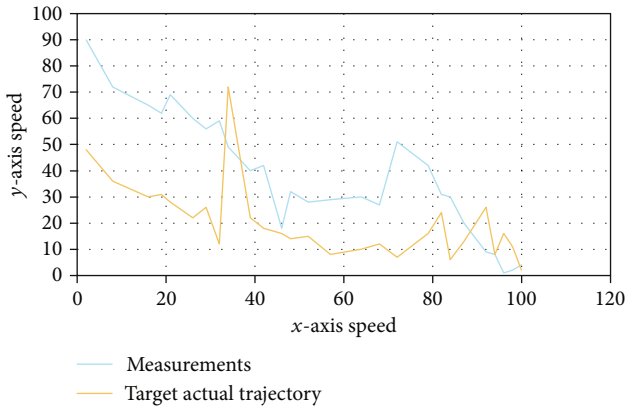

Figure 5: Coordinate estimation of filter.

and U2R. For the four types of attacks in the data set and normal [22], respectively, the intrusion detection classification is performed. Taking into account the total number of samples and the balance rate of the data, the attack data in the data set is marked as abnormal [23].

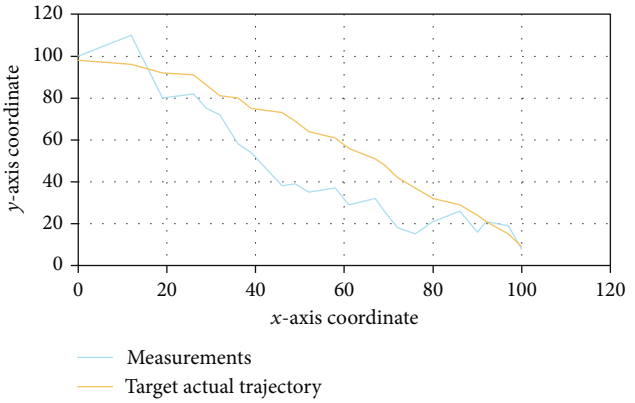

Figure 6: Coordinate estimation of filter.

4. Experiment and Result Analysis

4.1. The Relationship between S-LEACH Algorithm and Improved Bp Neural Network Algorithm. Since the model uses a network model based on a clustering mechanism, the S-LEACH routing algorithm provides a reasonable data collection and transmission mechanism for model construction. That is to say, the network is clustered according to the improved cluster head election algorithm, and then, we use the improved BP neural network fusion algorithm in each cluster routing structure to fuse the data collected by the sensors to extract different types of members in the cluster. The node collects the characteristic value of sensor data fusion and transmits the characteristic value to the sink node through a combination of single-hop and multihop. In this way, the sink node receives the characteristic data that reflects the current entire network situation, rather than the original sensor data. This method will greatly reduce the energy consumption caused by large amounts of data transmission. The S-LEACH routing algorithm is a data fusion algorithm at the network level. It uses cluster heads to summarize data to improve the energy consumption efficiency of the WSN network, while the BP neural network algorithm can extract and reflect the collected data through the trained neural network model. At the level of integration,

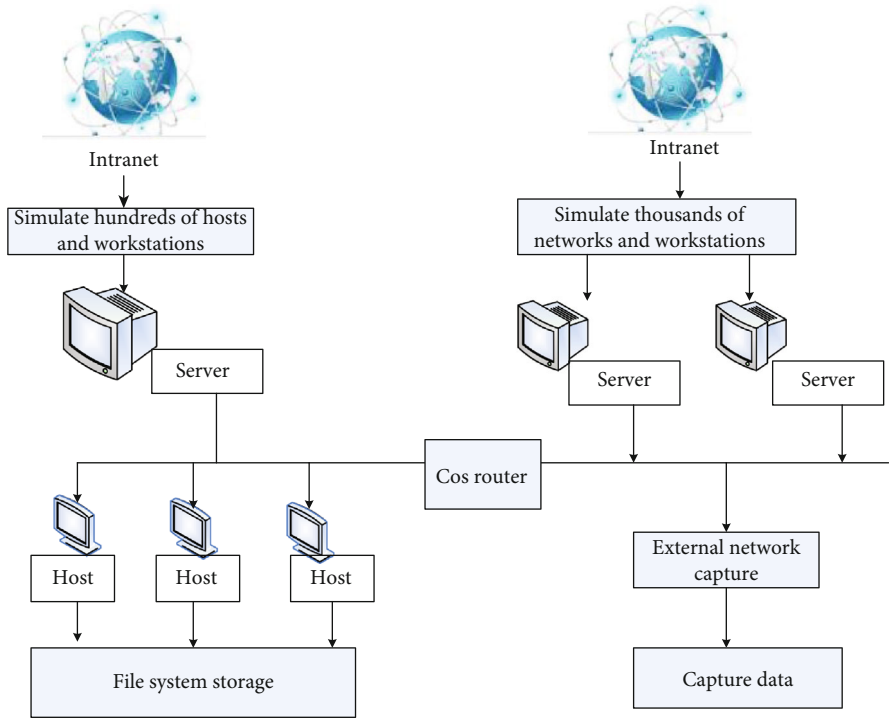

Figure 7: KDD99 intrusion detection network environment.

Table 2: KDD99 data format.

1	tcp	http	SF	5483	5698	2	3	1	2	1	3	2	3	1	00	0
2	1	3	0	000	15	0	02	15	26	0	0	2	56263	12235	1	3
5	6	23	00	00	4	0	0	0	00	48	00	00	0	0	00	Back
0	tcp	http	SF	242	00	12	0	0	0	0	0	1	0	0	0	123
245	265	236	268	0	00	0	0	0	0	0	1	0	2	0	3	0
0	1	2	0	0	12	0	0	0	15	0	00	15	102	157	11	Normal

the two complement each other and can make up for their own shortcomings. Using the combination of two algorithms to build a WSN-based data fusion model can effectively improve the efficiency of data collection and extend the life cycle of the network. In WSN, the data collected by the node is used as the input of the BP neural network, and the characteristic value of the sensor data can be extracted through the neural network model [24]. In this way, we can convert the sensor data occupying different types of data bytes into simple special values and send it to the convergence center, thus realizing the fusion processing of the data. In view of the above assumptions, we will establish a multilevel data fusion model in this chapter, including the first-level fusion model and the second-level fusion model. Since the S-LEACH algorithm in this paper is based on multihop between clusters, the two-level fusion adopts the intercluster fusion model based on the weighted average algorithm.

4.2. Data Analysis. In this article, the one-to-one method is used to realize multiclass fault classification. First, the training samples are used to train the LS-SVM diagnosis model, and then, the trained model is used to diagnose the simulation fault. In this paper, RBF kernel function is used as the kernel function of LS-SVM, and a cross-validation method is used to determine the model parameters, namely, hyperparameter δ and RBF kernel parameter ∂. The reduced fault sample data is randomly divided into 6 nonintersecting subsets $S_1, S_2, S_3, S_4, S_5, S_6$. In each training process, 5 of the subsets are used as training samples, and the remaining subset is used as the test set. In this way, the classification result can be compared with the original fault type of the test sample, and the classification ability of the classifier for unknown samples can be reflected according to its accuracy. This article uses a combination of cross-validation method and grid search method to determine the best parameter (δ, ∂) and make the classification accuracy the highest. According to experience, this article gives a set of parameters $\partial = (0.02, 0.06, 10, 50)$, $\delta = (5, 10, 50, 300)$. Table 3 is part of experimental result analysis.

From the results in Table 3, it can be seen that $\delta = 0.5$, $\partial = 1$ when the training accuracy and test accuracy are the highest, respectively, 0.99 and 0.98, so the optimal parameter combination is $\delta = 0.5$, $\partial = 1$.

Table 3: Analysis of classification accuracy using LS-SVM.

δ / ∂	0.5		1		10		50	
	Training accuracy	Test accuracy	Training accuracy	Test accuracy	Training accuracy	Test accuracy	Training accuracy	Test accuracy
1	0.95	0.86	0.96	0.86	0.78	0.99	0.89	0.95
5	0.23	0.56	0.45	0.75	0.65	0.68	0.75	0.56
10	0.56	0.25	0.36	0.36	0.56	0.85	0.36	0.75
100	0.95	0.23	0.36	0.42	0.45	0.56	0.57	0.85

Table 4: Analysis of assortment accuracy using SVM.

δ / ∂	0.5		1		10		50	
	Training accuracy	Test accuracy	Training accuracy	Test accuracy	Training accuracy	Test accuracy	Training accuracy	Test accuracy
1	0.96	0.9	086	0.89	0.79	0.88	0.9	0.97
5	0.23	0.56	0.45	0.75	0.65	0.25	0.36	0.36
10	0.32	0.36	0.59	0.75	0.62	0.26	0.62	0.86
100	0.95	0.23	0.36	0.42	0.45	0.23	0.56	0.45

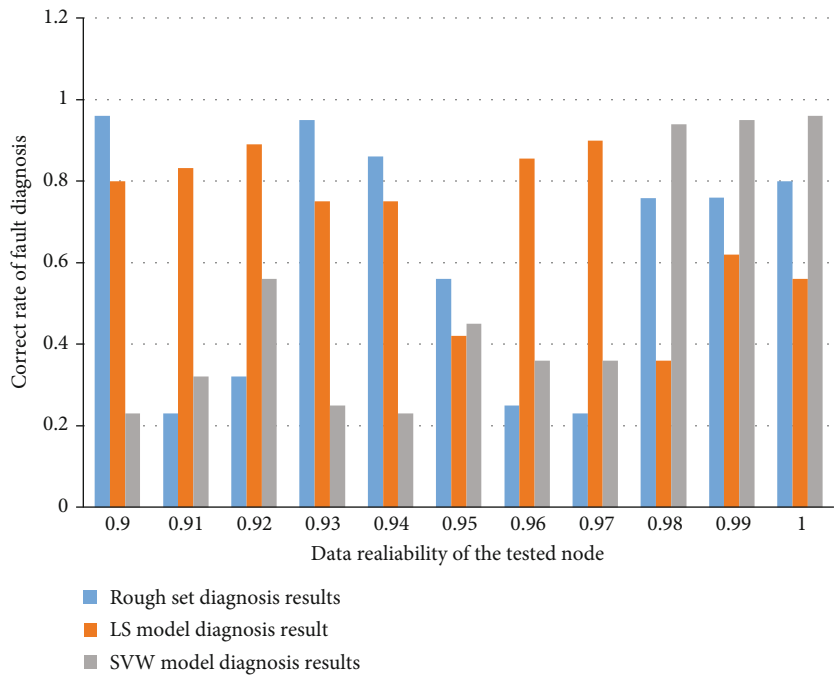

Figure 8: Comparison of reliability simulation results of different data.

Some conclusions obtained by using SVM to train it are shown in Table 4.

By comparing Tables 3 and 4, it can be found that although the highest classification accuracy obtained by LS-SVM training is not as high as that of SVM, on the whole, the classification accuracy obtained by SVM is very dependent on the choice of parameters. Choose different parameters. The difference in classification accuracy will be very large. As shown in Table 4, the highest classification accuracy can reach about 98%, while the lowest classification accuracy is only about 30%. For LS-SVM, it can be seen from Table 3 that no matter which set of parameters is selected, the difference in classification accuracy will not be too large due to different model parameters, and it will usually not be less than 55%. This also shows that LS-SVM has stronger generalization ability than SVM.

4.3. Experimental Results. Since WSN is generally used in a complex environment, meteorological conditions and changes in the ionospheric state will interfere with the short-wave channel. At the same time, some factors such as noise will also cause a certain deviation in the data measured by the node. Therefore, this paper selects another 200 sets of test sample data whose faults are interfered with by external

environmental noise. The reliability of the data is reduced to 99.5%, 99%, 98.5%, and 97%, respectively. Rough set, LS-SVM model, and RSLS-SVM model are used, respectively. The fault test samples are compared with diagnostic experiments. The comparison chart of simulation results with MATLAB under different data reliability conditions is shown in Figure 8.

It can be seen from Figure 8 that the correct rate of diagnosis using the RSLS-SVM model is significant and rough set diagnosis. The accuracy of the LS-SVM model and rough set method is only 80% and 70% when the data reliability is 90%. When the reliability of the data reaches about 98.5%, the accuracy of diagnosis using the RSLS-SVM model has reached a stable level, reaching 95%, while the LS-SVM model and rough set method cannot achieve stability, only 85% and 77%. When the data reliability reaches about 99%, the correct rate of diagnosis using the LS-SVM model is stable, and the correct diagnosis rate is 88%; when the data reliability reaches about 99%, the rough set is used for fault diagnosis. In order to achieve a stable rate, the correct diagnosis rate is 71%. This shows the feasibility and superiority of the combination of rough set theory and LS-SVM. From the above experimental results, it can be seen that the use of a rough set for fault diagnosis takes 1.213 s, and the diagnosis accuracy rate is only 79%, which is the lowest, while the use of the LS-SVM model for diagnosis takes 0.321 s, which greatly reduces the diagnosis time. At the same time, the RSLS-SVM model that uses the combination of rough set and LS-SVM takes only 0.180 s, and the diagnostic accuracy rate reaches 98%, which is better than using the rough set or LS-SVM model alone. The efficiency of diagnosis is much higher, and the accuracy of diagnosis is also improved, and the fault tolerance performance is better. It can be seen from the whole diagnosis process that when using this method to diagnose WSN faults, the diagnostic personnel only need to collect the symptoms when the WSN node fails without having to have a deep understanding of the WSN domain knowledge, which improves the fault, the vitality of diagnostic algorithms, and the wide range of applications.

5. Conclusions

In the modern era of rapid scientific development, information fusion participates in more and more human production processes, such as aviation and railway information, environmental monitoring, and forest fire prevention. Many scholars are committed to the research and mining of a fusion algorithm in order to make the application scope of the algorithm wider and more efficient. The main work includes the following points: (1) research on the theory and technology of multisensor data fusion; (2) in view of the fact that the fusion threshold is limited in the data-level fusion algorithm, the accuracy of the fusion result is affected; this paper proposes a data fusion algorithm applied to homogeneous multisensor. With the continuous application of WSNs, the research on secure data fusion methods in WSNs will continue to improve, including the research on specific data fusion methods, the research on the types of attacks that can be resisted, the research on encryption methods, and the research on network efficiency. Compared with the existing schemes, the two different WSN security data fusion schemes proposed in this paper perform well, but it does not mean that it is perfect and still needs to be improved.

Data Availability

No data were used to support this study.

Conflicts of Interest

There are no potential competing interests in our paper.

Authors' Contributions

All authors have seen the manuscript and approved it to submit to your journal.

Acknowledgments

This study was supported by the Liaoning Provincial Social Science Youth Project "Study on the Improvement of Students' Physical Fitness from the Perspective of Smart Sports" (No. L19CTY002).

References

[1] J. Li and C. Wang, "Research on efficient fusion methods for reliable information in wireless sensor networks," *Revista de la Facultad de Ingenieria*, vol. 32, no. 11, pp. 583–587, 2017.

[2] W. Wu, N. Xiong, and C. Wu, "Improved clustering algorithm based on energy consumption in wireless sensor networks," *IET Networks*, vol. 6, no. 3, pp. 47–53, 2017.

[3] N. Wang, Y. Li, G. Qi, and A. Sheng, "Distributed two-stage state estimation with event-triggered strategy for multirate sensor networks," *International Journal of Adaptive Control and Signal Processing*, vol. 33, no. 7, pp. 1174–1188, 2019.

[4] Y. Liu, D. Liu, Y. Zhao, and L. Wang, "The reliability analysis of wireless sensor networks based on the energy restrictions," *International Journal of Wireless & Mobile Computing*, vol. 10, no. 4, pp. 399–406, 2016.

[5] M. Abu and G. P. Hancke, "Localised information fusion techniques for location discovery in wireless sensor networks," *International Journal of Sensor Networks*, vol. 26, no. 1, pp. 12–25, 2018.

[6] Z. Zhang, J. Li, and L. Liu, "Distributed state estimation and data fusion in wireless sensor networks using multi-level quantized innovation," *Christophorus Daniel Beurer, : Pharmacopoeus Nofodochialis as Sp St*, vol. 59, no. 2, pp. 1–22316, 2016.

[7] X. Guo, Y. He, S. Atapattu, S. Dey, and J. S. Evans, "Power allocation for distributed detection systems in wireless sensor networks with limited fusion center feedback," *IEEE Transactions on Communications*, vol. 10, p. 1, 2018.

[8] J. Zhang, S. Gao, X. Qi, J. Yang, J. Xia, and B. Gao, "Distributed robust cubature information filtering for measurement outliers in wireless sensor networks," *IEEE Access*, vol. 8, pp. 20203–20214, 2020.

[9] P. Kar and S. Misra, "Reliable and efficient data acquisition in wireless sensor networks in the presence of transfaulty nodes,"

IEEE Transactions on Network and Service Management, vol. 13, no. 1, pp. 99–112, 2016.

[10] H. A. Sanchez-Hevia, D. Ayllon, R. Gil-Pita, and M. Rosa-Zurera, "Maximum likelihood decision fusion for weapon classification in wireless acoustic sensor networks," *IEEE/ACM Transactions on Audio Speech & Language Processing*, vol. 25, no. 6, pp. 1172–1182, 2017.

[11] K. P. Rajput, A. Kumar, S. Srivastava, A. K. Jagannatham, and L. Hanzo, "Bayesian learning-based linear decentralized sparse parameter estimation in MIMO wireless sensor networks relying on imperfect CSI," *IEEE Transactions on Communications*, vol. 99, p. 1, 2021.

[12] J. Wang, I. S. Ahn, Y. Lu, T. Yang, and G. Staskevich, "A distributed least-squares algorithm in wireless sensor networks with unknown and limited communications," *International Journal of Handheld Computing Research*, vol. 8, no. 3, pp. 15–36, 2017.

[13] Department of Electronics and Communication Engineering, S G Balekundri Institute of Technology, Belagavi, India, V. I Puranikmath, S. S Harakannanavar, S. Kumar, and D. Torse, "Comprehensive study of data aggregation models, challenges and security issues in wireless sensor networks," *International Journal of Computer Network and Information Security*, vol. 11, no. 3, pp. 30–39, 2019.

[14] P. Y. Chen, S. M. Cheng, and H. Y. Hsu, "Analysis of information delivery dynamics in cognitive sensor networks using epidemic models," *IEEE Internet of Things Journal*, vol. 99, p. 1, 2017.

[15] W. Liu, "Real-time obstacle detection based on image semantic segmentation and fusion network," *Traitement du Signal*, vol. 38, no. 2, pp. 443–449, 2021.

[16] M. Zhou, Y. Li, M. J. Tahir, X. Geng, Y. Wang, and W. He, "Integrated statistical test of signal distributions and access point contributions for Wi-Fi indoor localization," *IEEE Transactions on Vehicular Technology.*, vol. 70, no. 5, pp. 5057–5070, 2021.

[17] S. Teng, G. Chen, Z. Liu, L. Cheng, and X. Sun, "Multi-sensor and decision-level fusion-based structural damage detection using a one-dimensional convolutional neural network," *Sensors*, vol. 21, no. 12, p. 3950, 2021.

[18] A. Argyriou, "Distributed estimation in wireless sensor networks with an interference canceling fusion center," *IEEE Transactions on Wireless Communications*, vol. 15, no. 3, pp. 2205–2214, 2016.

[19] X. Xue, C. Jiang, J. Zhang, H. Zhu, and C. Yang, "Matching sensor ontologies through Siamese neural networks without using reference alignment," *PeerJ Computer Science*, vol. 7, no. 4, article e602, 2021.

[20] C. Warden, ""Queer music-hall sport": all-in wrestling and modernist fakery," *Modernism/Modernity*, vol. 27, no. 1, pp. 147–164, 2020.

[21] A. Doletsky, I. V. Khvastunova, and N. Sentyabrev, "Neurophysiological criteria of functional states modification in sportsmen through aromatherapy and music effects," *Physical Education and Sport*, vol. 33, no. 3, pp. 40–46, 2020.

[22] L. Gao, L. Qi, E. Chen, and L. Guan, "Discriminative multiple canonical correlation analysis for information fusion," *IEEE Transactions on Image Processing*, vol. 99, p. 1, 2017.

[23] S. Roy, D. Sarkar, and D. De, "Entropy-aware ambient IoT analytics on humanized music information fusion," *Journal of Ambient Intelligence and Humanized Computing*, vol. 11, no. 1, pp. 151–171, 2020.

[24] M. Zhou, Y. Long, W. Zhang et al., "Adaptive genetic algorithm-aided neural network with channel state information tensor decomposition for indoor localization," *IEEE Transactions on Evolutionary Computation.*, 2021.

Hindawi
Journal of Sensors
Volume 2021, Article ID 7741881, 9 pages
https://doi.org/10.1155/2021/7741881

Research Article

Electrochemical Characteristics Based on Skin-Electrode Contact Pressure for Dry Biomedical Electrodes and the Application to Wearable ECG Signal Acquisition

Jinzhong Song,[1,2] **Tianshu Zhou**,[3] **Zhonggang Liang**,[2] **Ruoxi Liu**,[4] **Jianping Guo**,[2] **Xinming Yu**,[2] **Zhongping Cao**,[2] **Chuang Yu**,[2] **Qingjun Liu**,[1] **and Jingsong Li**[1,3]

[1]*Key Laboratory for Biomedical Engineering of Ministry of Education, Engineering Research Center of EMR and Intelligent Expert System, Ministry of Education, College of Biomedical Engineering and Instrument Science, Zhejiang University, Hangzhou 310027, China*
[2]*State Key Laboratory of Space Medicine Fundamentals and Application, China Astronaut Research and Training Center, Beijing 100094, China*
[3]*Research Center for Healthcare Data Science, Zhejiang Lab, Hangzhou 311100, China*
[4]*Pony Testing International Group Co. Ltd, Zhejiang Lab, Beijing 100095, China*

Correspondence should be addressed to Jingsong Li; ljs@zju.edu.cn

Received 25 June 2021; Revised 15 August 2021; Accepted 25 August 2021; Published 16 September 2021

Academic Editor: Ying-Ren Chien

Based on one simulated skin-electrode electrochemical interface, some electrochemical characteristics based on skin-electrode contact pressure (SECP) for dry biomedical electrodes were analysed and applied in this research. First, 14 electrochemical characteristics including 2 static impedance (SI) characteristics, 11 alternating current impedance (ACI) characteristics and one polarization voltage (PV), and 4 SECP characteristics were extracted in one electrochemical evaluation platform, and their correlation trends were statistically analysed. Second, dry biomedical electrode samples developed by the company and the laboratory, including textile electrodes, Apple watch, AMAZFIT rice health bracelet 1S, and stainless steel electrodes, were placed horizontally and vertically on the "skin" surface of the electrochemical evaluation platform, whose polarization voltages were quantitatively analysed. Third, electrocardiogram (ECG) collection circuits based on an impedance transformation (IT) circuit for textile electrodes were designed, and a wearable ECG acquisition device was designed, which could obtain complete ECG signals. Experimental results showed SECP characteristics for dry electrodes had good correlations with static impedance and ACI characteristics and the better correlation values among 2-10 Hz. In addition, polarization voltages in vertical state were smaller in horizontal state for dry biomedical electrodes, and polarization voltage of electrode pair (PVEP) values for Apple watch bottom was always smaller than ones for Apple watch crown and LMF-2 textile electrode. And the skin-electrode contact impedance of IT textile electrodes was less than the traditional textile electrodes.

1. Introduction

With the development of biomedical engineering technologies, the need for low-load, noninvasive medical supervision is becoming more and more prominent. People's health data can be obtained not only in hospitals but also at home by health monitoring equipment, whose own physical state can be known conveniently.

Biomedical signals (such as ECG, EMG, EEG, and EOG) were usually used to evaluate cardiovascular and other functions for human bodies widely, which was usually extracted by traditional wet paste electrodes (Ag/AgCl) nowadays. While it presents many problems [1, 2], for example, it needs to stick to the skin and easily causes allergic reaction. Recently, dry biomedical electrode, as one new biosensor, has attracted researchers' attention because they can obtain

biomedical signals from human bodies with some advantages such as without glues, reused, convenient to find the location, and very useful for wearable health monitoring.

In recent years, many kinds of dry biomedical electrodes have been produced, such as stainless-steel dry electrode, noncontact electrodes, textile electrodes, microneedle electrodes, and smart bracelet electrode [2–4]. Stainless-steel dry electrode is mainly composed of a stainless-steel sheet plated with Ag/AgCl, which is used to extract ECG signals from human body surface according to touching the skin directly without conductive paste.

One kind of textile electrode was designed by Song et al. using Jacquard [3], and Ag was plated in the fiber in the weft direction; it was found that this method was more stable than the weaving structure and had a lower loosening effect. Pola and Vanhala used embroidery to make textile electrodes, which increased the skin-electrode contact area [5], and other kinds of textile electrodes were used to extract ECG signals [6, 7]. Conductive fabrics were made of a variety of wire fibers, where the main metal elements used to transmit bioelectrical signals were Ag, AgCl, AgNy, AgCu, Cu, Ni, etc. Some textile electrodes were developed by Professor Tao Xiaoming's research team in Hong Kong Polytechnic University [8].

Microneedle-shaped dry electrodes had a variety of preparation methods: Silicon as an electrode material [9], multiwall carbon nanotubes (MWCNT) [10], and polymers for molds [11]. In order to ensure electrode conductivity and take into account biological compatibility, some metal materials were deposited on the electrode surface, which were mainly Au, Ag and Pt, and IrO [12].

However, dry biomedical electrodes are easy to form a big contact impedance and a large polarization voltage in skin-electrode interface when they were attached to the surface of human skins when collecting biomedical signals, and they often come across noise interference [13, 14]. And a complete biomedical signal acquisition requires a good contact impedance (needing a good contact between electrode and skin), while it often causes people's discomfort [14, 15].

In recent years, some dry electrodes were used to collect ECG signals, and a number of products using dry electrode technologies had also been developed. Apple Watch Series 4 was on the market in 2018.09, whose important feature was the addition of ECG detection function. And ECG signals were detected from people's fingers and arms with two dry electrodes. AMAZFIT rice health bracelet 1S was also on the market, with whom ECG signals could be can be recorded for 24 hours with dry electrodes.

Many electrochemical characteristics based on skin-electrode contact pressure (SECP) for dry biomedical electrodes were analysed and applied in this research. First, some electrochemical and skin-electrode contact pressure characteristics for dry electrodes were quantitatively extracted, and the correlation trends between electrochemical characteristics and SECP characteristics were statistically analysed. Second, dry biomedical electrode samples on the market developed by the company and the laboratory, including textile electrodes, apple watch, AMAZFIT rice health bracelet 1S, and stainless steel electrodes, were placed horizontally and vertically on the skin surface, whose polarization voltage was quantitatively analysed. Third, a wearable ECG acquisition device based on textile electrodes was developed: One kind of impedance transformation circuit for textile electrodes was designed, whose electrode-skin contact impedance was analysed compared with the traditional textile electrode, and a wearable collection device for ECG signals was designed, which could obtain the complete ECG signals.

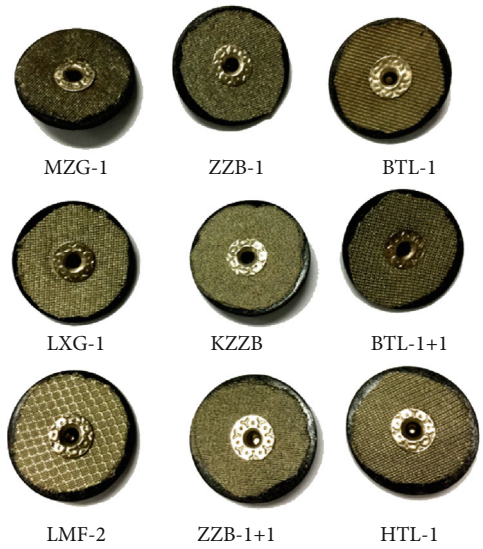

Figure 1: Textile electrode samples.

Figure 2: Watch bottom and watch crown for Apple Watch Series 4.

Figure 3: AMAZFIT rice health bracelet 1S.

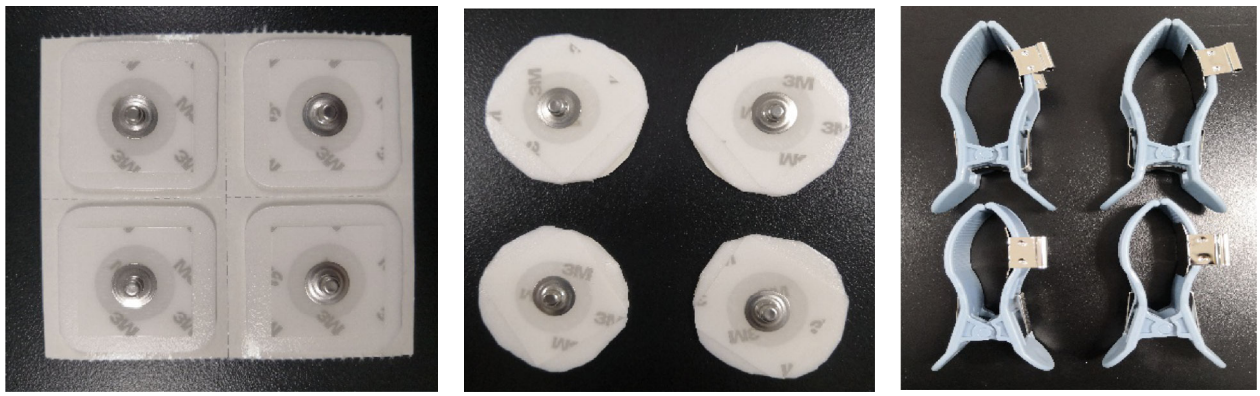

(a) (b) (c)

Figure 4: Traditional paste ECG electrodes in hospitals: (a) 3M ECG electrode; (b) 3M circle ECG electrode; (c) stainless-steel electrode.

2. Materials and Methods

2.1. Evaluation Platform. In this research, an electrochemical evaluation platform was set up to quantitatively evaluate dry biomedical electrodes [16], which could simulate the electrochemical interface between the dry biomedical electrodes and the skin surface.

2.2. Characteristic Settings for Dry Electrodes. Based on a passive electrochemical evaluation platform (PEEP) in the evaluation platform [16], the static impedance (SI) between electrode 1 and electrode 2 was measured by a CHI660 electrochemical workstation, and the SI values were measured by an impedance-time method. The parameters in this testing platform were set as follows: initial potential 0 V, potential amplitude 0.01 V, time 60 s, and frequency 1000 Hz. The dry electrodes in this research were intended for extraction of biomedical signals with amplitudes in the range of approximately $0 \sim 10$ mV, so the potential amplitude was set to the mV level.

Alternating current impedance (ACI) values were measured by a CHI660 electrochemical workstation. The parameters in this testing platform were set as follows: initial potential 0.1 V, high frequency 100 Hz, low frequency 0.1 Hz, and potential amplitude 0.1.

Polarization voltage (PV) between electrode 1 and electrode 2 was measured by a digital mustimeter (Agilent Technologies U3402A).

Skin-electrode contact pressure (SECP) was measured by a pressure device, and the pressure range was set as $0 \sim 3$ N.

2.3. Electrochemical Characteristics and Skin-Electrode Contact Pressure

2.3.1. Electrochemical Characteristic Extraction. 14 electrochemical characteristics were extracted in the evaluation platform [16], which were 2 static impedance characteristics, denoted by Z_{se}_static and Φ_{se}_static, 11 alternating current impedance characteristics, denoted by $Z_{ACI-1} \sim Z_{ACI-11}$, and one polarization voltage denoted by U_{p-se}.

2.3.2. Skin-Electrode Contact Pressure (SECP) Characteristic Extraction. For skin-electrode contact pressure characteristics, 4 characteristics were extracted [16], which including upper skin-electrode contact pressure (USECP, denoted by F_{USECP}), lower skin-electrode contact pressure (LSECP, denoted by F_{LSECP}), the difference between USECP and LSECP (SECP_D, denoted by F_{SECP_D}), and the sum of USECP and LSECP (SECP_S, denoted by F_{SECP_S}).

3. Results and Discussion

3.1. Dry Biomedical Electrode Samples. More and more wearable dry biomedical electrodes were used to obtain biomedical signals (such as ECG, EEG, and EOG) from the human body without skin pretreatment and conductive paste. Several types of dry biomedical electrodes had been produced, such as textile electrodes, stainless steel electrode, and smart bracelet electrode.

3.1.1. Textile Electrode Samples. Textile electrode as one type of dry biomedical electrodes was studied in this research, 9 kinds of conductive textile samples with different plating processes and different textile processes, whose definition was introduced in literature [16], were produced as shown in Figure 1.

3.1.2. Dry Biomedical Electrode Samples in the Market. Apple Watch Series 4 was on the market in 2018.09, whose important feature was the addition of ECG detection function. And ECG signals were detected from people's fingers and arms with two dry electrodes, which were watch bottom and watch crown for Apple Watch Series 4, as shown in Figure 2.

On the other hand, AMAZFIT rice health bracelet 1S was on the market in 2018.09, with whom ECG signals could be recorded for 24 hours with dry electrodes. And their dry electrodes were watch button and watch bottom shown in Figure 3.

To evaluate different dry biomedical electrodes, some common ECG electrodes in the market were analysed, which included 3M ECG electrode, 3M circle ECG electrode with a diameter 2 cm, and stainless-steel electrode as shown in Figure 4.

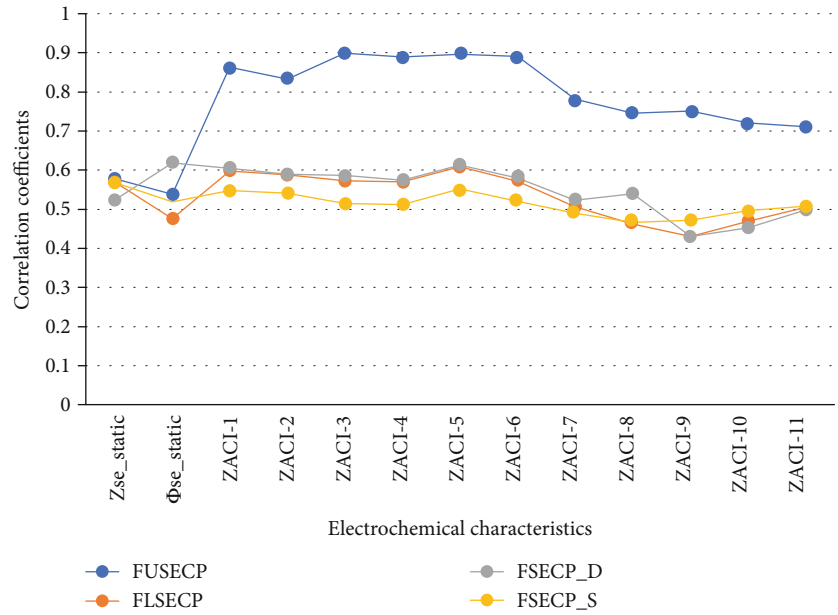

Figure 5: Trends of correlation coefficients between electrochemical and SECP characteristics.

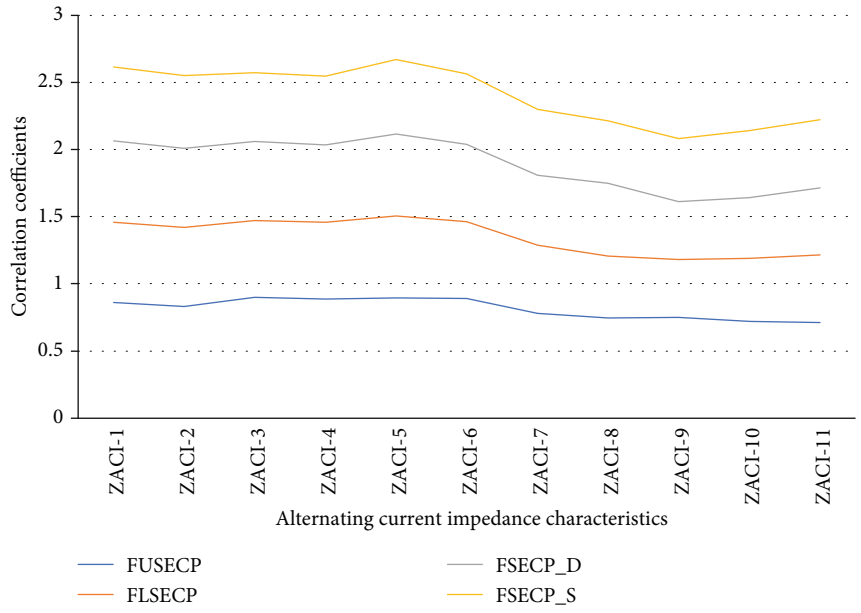

Figure 6: Four trends of correlation coefficients between alternating current impedance and SECP characteristics (note: F_{USECP}: +0; F_{LSECP}: +1; F_{SECP_D}: +2; F_{SECP_S}: +3).

3.2. Correlation Analysis. Based on 9 textile electrodes in Section 3.1.1, the trends of correlation coefficients between electrochemical characteristics and SECP characteristics versus for 4 skin-electrode contact pressure (SECP) characteristics are shown in Figure 5.

As could be seen from Figure 5 4 SECP characteristics (denoted by F_{USECP}, F_{LSECP}, F_{SECP_D}, and F_{SECP_S}), especially F_{USECP}, had good correlations with Z_{se}_static and alternating current impedance characteristics, and better correlation values occurred among 2-10 Hz ($Z_{ACI-3} \sim Z_{ACI-6}$); therefore, the influence of contact pressure on signal qualities should be considered when signals among 2-10 Hz were collected by textile electrodes.

As shown as Figure 6, each correlation coefficient curve for alternating current impedance characteristics in Figure 5 was shown separately. In order to describe the change trend of correlation coefficient better, the correlation coefficients of F_{USECP}, F_{LSECP}, F_{SECP_D}, and F_{SECP_S} were plotted by adding 0, 1, 2, and 3, respectively, as shown in Figure 6.

With the increasing of frequency, the correlation coefficient between ACI and SECP characteristics decreased

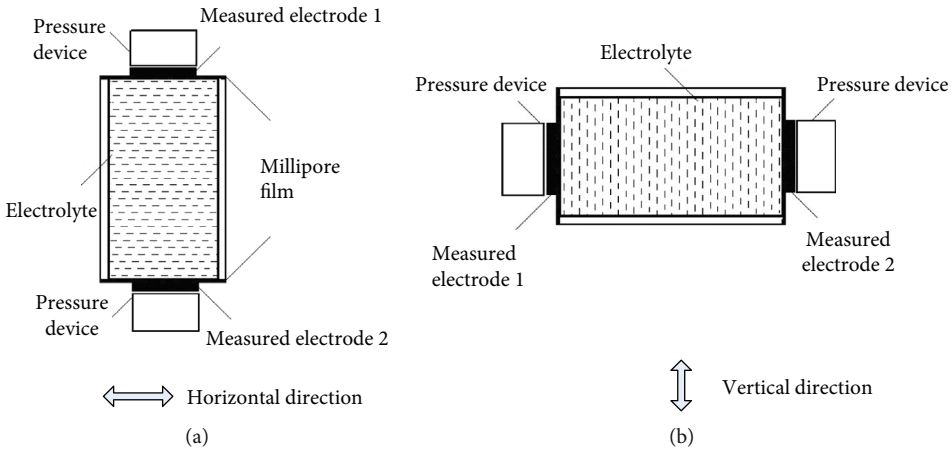

Figure 7: Horizontal and vertical model: (a) horizontal model; (2) vertical model.

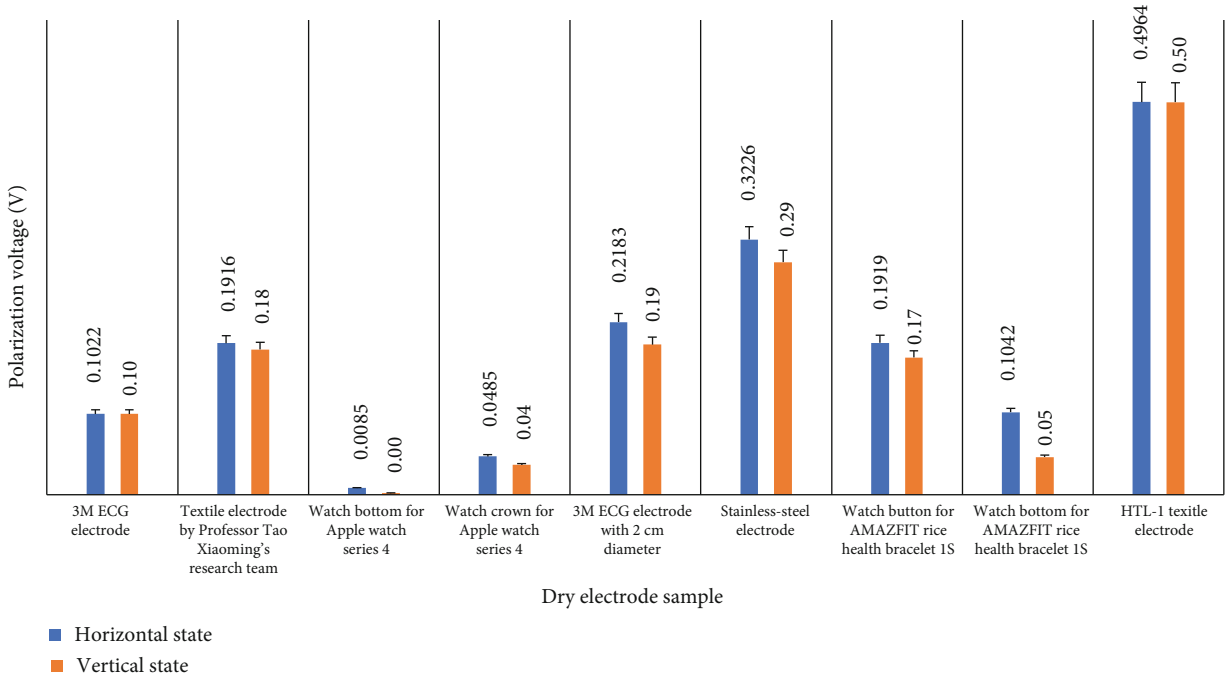

Figure 8: Polarization voltage in horizontal state and vertical state for different electrodes.

(especially above 10 Hz), which showed that the quality of signals in low frequency could be improved by contact pressure.

Based on a variety of biomedical electrodes developed by the company and the laboratory, including 3M ECG electrode (shown in Figure 4), textile electrodes (shown in Figure 1), Apple watch (shown in Figure 2), AMAZFIT rice health bracelet 1S (shown in Figure 3), and stainless steel electrodes (shown in Figure 4), these electrodes were placed horizontally and vertically on the skin surface, whose polarization voltages were quantitatively analysed as shown in Figure 7. The horizontal model is shown in Figure 7(a), and the electrode was placed horizontally on the skin surface, while the vertical model is shown in Figure 7(b), and the electrode was placed vertically.

Based on above 9 kinds of biomedical electrodes, skin-electrode polarization voltages were measured in horizontal and vertical stations as shown in Figure 7, where the upper surface contact pressure in Figure 7(a) and the left surface contact pressure in Figure 7(b) were set as 40.12 cN, and the lower surface contact pressure in Figure 7(a) and the right surface contact pressure in Figure 7(b) were set as 5.11 cN.

Means and variances of polarization voltages in horizontal state and vertical state are shown in Figure 8.

As shown in Figure 8, polarization voltages in vertical state were smaller in horizontal state, which indicated that there was a significant difference for polarization voltages between the electrodes on the surface of the skin in the horizontal and vertical directions.

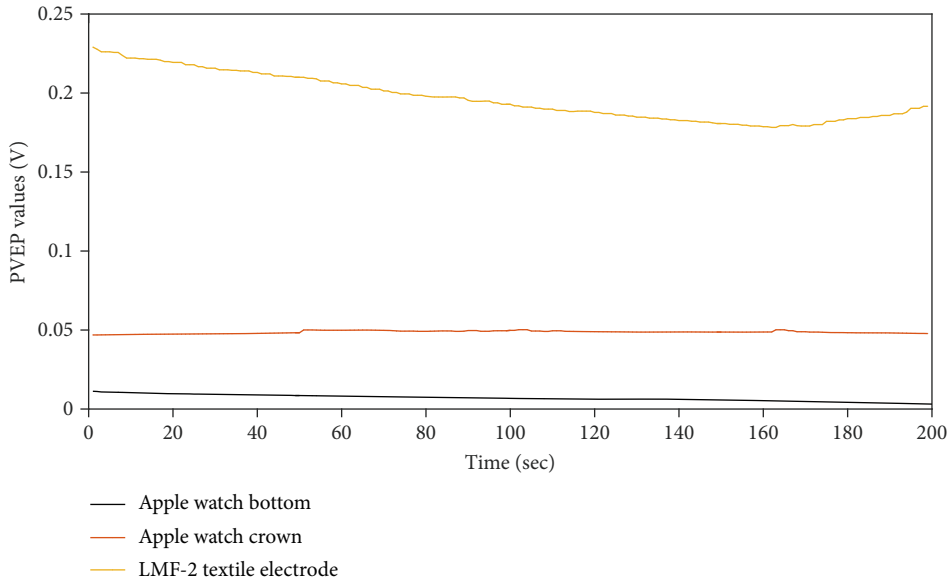

Figure 9: Polarization voltage for different dry electrodes.

The polarization voltage of electrode pairs (PVEP), defined as the sum of skin-electrode polarization voltage of electrode 1 and electrode 2 at the upper and lower Millipore film based on a passive electrochemical evaluation platform (PEEP) [16], was evaluated for the watch bottom and watch crown of Apple Watch Series 4 and one kind of conductive textile sample (LMF-2) from Qingdao Tianyin Textile Co., Ltd.

Based on PEEP [16], electrode 1 was the dry electrode sample, and electrode 2 was 3M electrode (model: 2560). F_{USECP} and F_{LSECP} were set as 40.12 cN and 5.11 cN separately. PVEP values for three kinds of dry electrodes (including Apple watch bottom, Apple watch crown, and LMF-2 textile electrode) are obtained as shown in Figure 9.

As shown in Figure 9, PVEP values showed a consistent change trend with time for three kinds of dry electrode samples, and PVEP values for Apple watch bottom were always smaller than ones for Apple watch crown and LMF-2 textile electrode.

3.3. A Wearable Device for ECG Collecting

3.3.1. Design of Impedance Transformation (IT) Textile Electrode. The textile electrode samples shown in Figure 1 were integrated into impedance transformation circuits to reduce the contact resistance between skin and electrodes. The circuit is shown in Figure 10. The voltage is changed from 200 k to 100, and the multiple is nearly 20,000. As a result, an impedance transformation textile electrode (IT textile electrode) was produced (Figure 11).

In addition, the skin-electrode contact impedance of IT textile electrodes and traditional textile electrodes was quantitatively compared and analysed based on the electrochemical evaluation platform [16]. Experimental results showed that the electrode-skin contact impedance of IT textile electrodes was less than traditional textile electrodes, as shown in Figure 12.

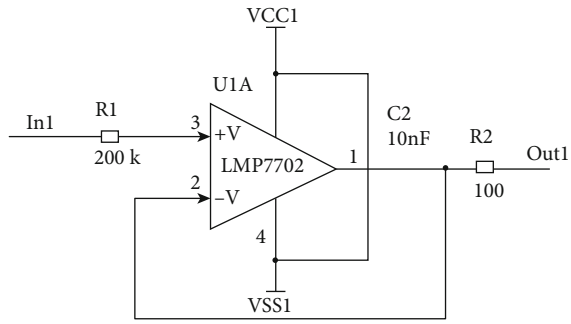

Figure 10: An impedance transformation circuit.

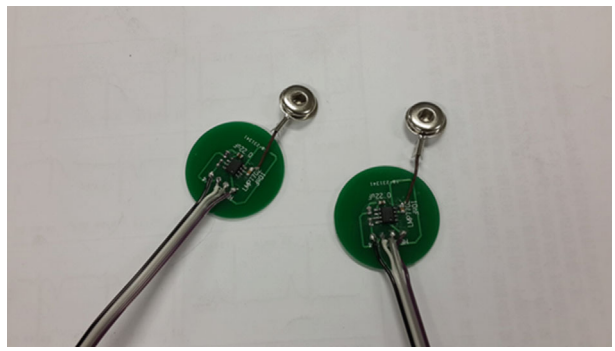

Figure 11: IT textile electrodes.

3.3.2. Chinese Aerospace ECG Lead System. Two-lead ECG signals were collected using Chinese aerospace ECG lead system including chest sword (CW) and chest axillary (CA), as shown in Figure 13.

3.3.3. ECG Conditioning Circuit. AD8221 was selected as an instrument amplifier, which had high common mode

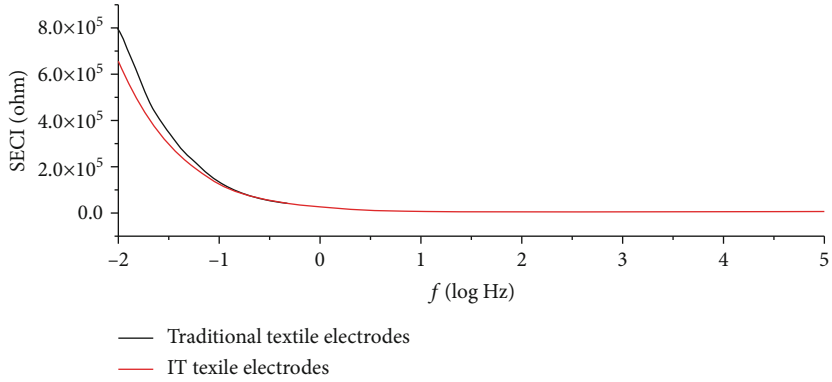

Figure 12: Contact impedance curve of IT and traditional textile electrode.

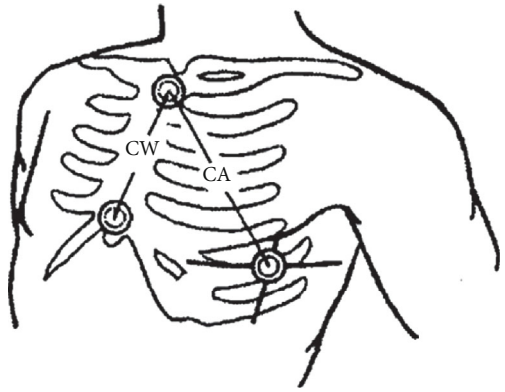

Figure 13: Chinese aerospace ECG lead system.

suppression ratio (CMRR). AD8221 gain (denoted by G) was programmed through the resistance R_G, which could be calculated by the following formula:

$$R_G = \frac{49.4k\Omega}{G-1}. \quad (1)$$

In this research, G value (the gain of an instrument amplifier) was designed to be 200 when R_G value was selected by 248 Ω.

3.3.4. Right Leg Drive Circuit. The right leg drive circuit was introduced to suppress the influence from common mode interference. A voltage follower was used to separate the drive circuit from the main circuit, and common signals were amplified 20 times and fed back to the human body.

3.3.5. Power Conversion Circuit. The ECG amplifier circuit was supplied by ±5 V, and a single power supply was used in this paper. 3.3 V reference level was provided for AD acquisition chips, which required high accuracy and less noise. A conversion circuit for 3.3 V reference level, 5 V, and -5 V are shown separately in Figures 14–16.

3.3.6. AD Acquisition and Wireless Communications. The ECG baseline level was not raised in the circuit design in this research for the miniaturization circuit design. Instead, AD7606 (positive and negative AD acquisition chips) was adopted, and Zigbee communication protocol was used for the wireless transmission.

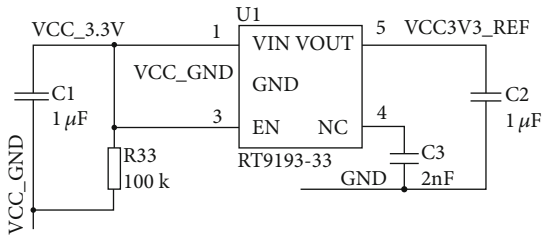

Figure 14: Conversion circuit for 3.3 V reference level.

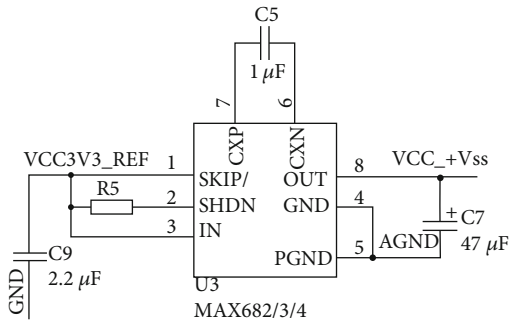

Figure 15: Conversion circuit (3.3 V to 5 V).

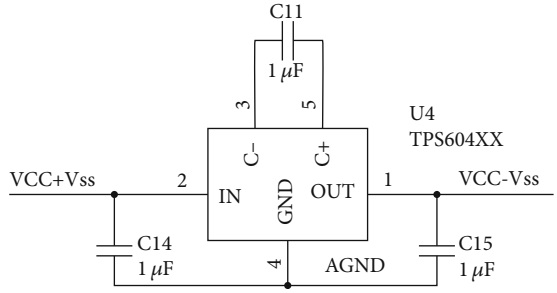

Figure 16: Conversion circuit (5 V to -5 V).

3.3.7. Results for the Wearable ECG Acquisition Device. A wearable ECG acquisition device was developed based on a

(a) (b) (c)

Figure 17: A wearable ECG collection device.

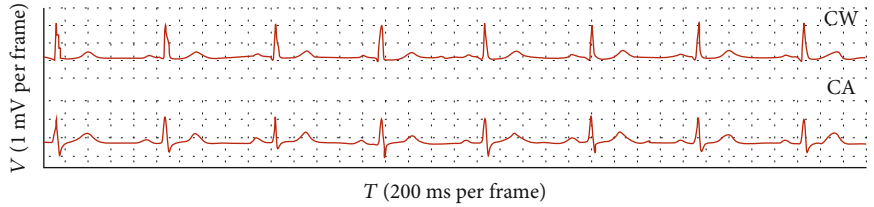

Figure 18: Two-lead ECG waveform.

garment integrating by IT textile electrodes, lead lines, and ECG collection circuit, which could extract two lead ECG signals in a low-load and unconstrained way.

The front of the garment for the wearable ECG signal acquisition is showed in Figure 17(a), and the reverse of the wearable ECG signal acquisition garment is showed in Figure 17(b), which combined IT electrodes, ECG lead lines, and ECG acquisition device. During the use for some subjects, if the garment is put on and the ECG acquisition device is turned on, collected ECG signals can be seen at the display terminal. The ECG acquisition device on the garment is showed in Figure 17(c).

Based on the above principle of ECG acquisition, it was proved by human experiments that the wearable ECG acquisition device developed in this paper could collect complete ECG waveform. The experimental results are shown in Figure 18.

4. Conclusions

Based on a variety of biomedical electrodes developed by the company and the laboratory, including 3M ECG electrode, textile electrodes, Apple watch, AMAZFIT rice health bracelet 1S, and stainless steel electrodes, correlations between electrochemical characteristics and skin-electrode contact pressure were analysed. Experimental results showed that SECP characteristics for dry electrodes had good correlations with static impedance and ACI characteristics and the better correlation values among 2-10 Hz. And polarization voltages in vertical state were smaller in horizontal state for dry biomedical electrodes.

In addition, one kind of textile electrode named by IT textile electrode was designed, whose electrode-skin contact impedance was analysed compared with traditional textile electrodes based on an electrochemical evaluation platform [16], and the electrode-skin contact impedance of IT textile electrodes was less than traditional textile electrodes. Then, a wearable device for ECG acquisition was designed, which could obtain the complete ECG waveform. Experimental results showed that the ECG signal acquisition based on IT textile electrode was feasible, which provided a basis for the production, evaluation, and application of dry biomedical electrodes. Issues such as cost, usability, and pandemic should be taken into account in the selection of devices and electrodes for actual health monitoring, experiments, sensing under daily activities, and health management.

Data Availability

The data that support the findings of this study are available from the corresponding author upon reasonable request.

Conflicts of Interest

The authors declare that there are no conflicts of interest regarding the publication of this paper.

Authors' Contributions

Jinzhong Song and Tianshu Zhou contributed equally to this work.

Acknowledgments

This work was supported by the National Key Research and Development Program of China (No. 2018YFC0116901), the National Natural Science Foundation of China (No. 81771936, No. 81801796), the Fundamental Research Funds for the Central Universities (No. 2021FZZX002-18), the Major Scientific Project of Zhejiang Lab (No. 2020ND8AD01), the Research Funds of China space medical engineering (2021SY54B0709, SMFA20C02), and the "Fei Tian" Foundation of Astronaut Center of China (2021SY54B0704).

References

[1] J. Song, H. Yan, Y. Li, and K. Mu, "Research on electrocardiogram baseline wandering correction based on wavelet transform, QRS barycenter fitting, and regional method," *Australasian Physical & Engineering Sciences in Medicine*, vol. 33, no. 3, pp. 243–250, 2010.

[2] J. Song, H. Yan, G. Gong, Y. Zhang, Z. Cao, and L. Zhang, "Research progress of textile electrode technologies applied in electrocardiogram signal acquisition," *Transducer and microsystem technologies*, vol. 34, no. 10, pp. 4–7, 2015.

[3] H. Song, J. Lee, D. Kang et al., "Textile electrodes of jacquard woven fabrics for biosignal measurement," *The Journal of the Textile Institute*, vol. 101, pp. 768–770, 2010.

[4] J. Song, H. Yan, Z. Xu, X. Yu, and R. Zhu, "Myocardial ischemia analysis based on electrocardiogram QRS complex," *Australasian Physical & Engineering Sciences in Medicine*, vol. 34, no. 4, pp. 515–521, 2011.

[5] T. Pola and J. Vanhala, "Textile electrode in ECG measurement," in *Proceedings of 3rd international conference on intelligent sensors*, pp. 635–639, Melbourne, 2007.

[6] J. Baek, J. An, J. Choi, K. S. Park, and S. H. Lee, "Flexible polymeric dry electrodes for the long-term monitoring of ECG," *Sensors and Actuators A*, vol. 143, pp. 423–429, 2008.

[7] J. Yoo, L. Yan, S. Lee, H. Kim, and H. J. Yoo, "A wearable ECG acquisition system with compact planar-fashionable circuit board-based shirt," *IEEE Transactions on Information Technology in Biomedicine*, vol. 13, no. 6, pp. 897–902, 2009.

[8] P. Xu, "Skin-electrode mechanical interaction and motion artifacts of textile electrodes for body surface ECG signal monitoring," in *Textile material and textiles design*, pp. 1–19, Donghua University, Shanghai, China, 2012.

[9] P. Griss, P. Enoksson, H. Tolvanen-Laakso, P. Merilainen, S. Ollmar, and G. Stemme, "Micromachined electrodes for biopotential measurements," *Journal of microelectro-mechanical systems*, vol. 10, no. 1, pp. 10–16, 2001.

[10] G. Ruffini, S. Dunne, L. Fuentemilla et al., "First human trials of a dry electro-physiology sensor using a carbon nanotube array interface," *Sensors and Actuators A: Physical*, vol. 144, pp. 275–279, 2008.

[11] W. Ng, H. Seet, K. Lee et al., "Micro-spike EEG electrode and the vacuum-casting technology for mass production," *Journal of Material Processing Technology*, vol. 209, no. 9, pp. 4434–4438, 2009.

[12] N. Dias, J. Carmo, A. da Silva, P. M. Mendes, and J. H. Correia, "New dry electrodes based on iridium oxide (IrO) for non-invasive biopotential recordings and stimulation," *Sensors and Actuators A*, vol. 164, pp. 28–34, 2010.

[13] Y. Chi, T. Jung, and G. Cauwenberghs, "Dry-contact and noncontact biopotential electrodes: methodological review," *IEEE Reviews in Biomedical Engineering*, vol. 3, pp. 106–119, 2010.

[14] D. Duxi, S. Kim, N. Van Helleputte et al., "Correlation between electrode-tissue impedance and motion artifact in biopotential recordings," *IEEE Sensors Journal*, vol. 12, no. 12, pp. 3373–3383, 2012.

[15] J. Song, H. Chen, H. Zhang, W. Chen, and X. Yu, "Detection methods for skin-electrode contact impedance of textile electrodes," *Progress in modern biomedicine*, vol. 15, no. 24, pp. 4777–4781, 2015.

[16] J. Song, Y. Zhang, Y. Yang et al., "Electrochemical modeling and evaluation for textile electrodes to skin," *Biomedical Engineering Online*, vol. 19, no. 1, pp. 1–27, 2020.

Hindawi
Journal of Sensors
Volume 2021, Article ID 1089266, 12 pages
https://doi.org/10.1155/2021/1089266

Research Article

Correlation Analysis of Stocks and PMI Index Based on Logistic Regression Model

Qiong Kang

Henan Industrial Vocational and Technical College, Nanyang 473000, China

Correspondence should be addressed to Qiong Kang; 2009013@hnpi.edu.cn

Received 15 July 2021; Revised 14 August 2021; Accepted 18 August 2021; Published 15 September 2021

Academic Editor: Mu Zhou

In order to explore the correlation between stocks and the PMI index, based on the generalized logistic loss and margin distribution, this paper designs a margin distribution logistic regression model that is easy to optimize, has robustness, and generalization ability, and gives a multiclass margin distribution logistic regression framework. This framework can be used to perform two-classification, multiclassification, and feature selection tasks. Moreover, this paper gives a training algorithm for margin distribution logistic regression on large-scale data sets through the pairwise stochastic gradient descent method. In addition, this paper combines the logistic regression model to construct a correlation analysis model between stocks and PMI index and uses the PMI data of the National Bureau of Statistics as a sample to design experiments to verify the performance of the system model constructed in this paper. From the experimental analysis, it can be seen that the algorithm constructed in this paper has a certain effect, and the strong correlation between PMI and stocks has been further verified.

1. Introduction

At this stage, the international and domestic economic environment is becoming more and more complicated, and there are many uncertain risk factors. Therefore, we need comprehensive and advanced economic indicators to express our country's economic conditions, and the purchasing manager index is just such an indicator [1].

In recent years, the PMI has received widespread attention from government agencies, financial circles, and even ordinary people. After the official PMI is released on the first working day of each month, the major financial media and financial institutions will reprint it as soon as possible and use this as a basis for a reasonable analysis of the economic trend in the future. The release and continuous application of the PMI system in the actual economy are one of the important manifestations of my country's continuous economic development and embracing the world [2]. Therefore, research on the origin of the PMI system is conducive to the continuous progress of my country's PMI system. Official PMI and HSBC PMI are one of the important products of the rapid development of market economy. The influence of the financial market on the international economy is becoming more and more significant, and the stock market, as an extremely important part of the financial market, has developed rapidly in recent years [3]. The volatility of stock prices is one of the universal laws of the stock market, and it is also a key point of concern to the general public and regulatory authorities. Therefore, the accuracy and timeliness of stock price analysis are an important goal for all relevant practitioners. Many authoritative media and security companies pay more attention to the PMI index, and reprint it as soon as the monthly PMI index is released, and use it as an important basis for analyzing the future stock market trend, and the PMI index is also familiar to more ordinary people.

2. Related Work

Through research, the literature [4] found that PMI has a good role in predicting macroeconomic information such as business cycles and economic growth, can provide early clues to the transition of economic development, and can improve the accuracy of prediction; that is, the biggest feature of PMI is its advancement. The literature [5] indicates that economists are very concerned about PMI, especially when the turning point of economic development is approaching. The literature [6] studied the critical value of PMI in prediction. When the purchasing manager index is >47, it generally means that the manufacturing industry is in a state of expansion and the development prospects are optimistic. When the purchasing manager index is >47, the gross national product (GDP) generally maintains a positive growth, and the overall economic situation is good. When PMI > 52.5, it is often accompanied by an increase in short-term interest rates. The literature [7] found that PMI and other related indicators of the manufacturing industry are consistent, which can reflect the overall real situation of the entire manufacturing industry. The literature [8] found through descriptive statistics that the trend of purchasing manager index and GDP growth rate is highly correlated. Moreover, it analyzed the growth rate of PMI and GDP and the growth rate of personal income and found that PMI can improve the prediction accuracy of both in the current period, and the prediction of the next period can improve the prediction accuracy more greatly. The literature [9] used the sum of the production index PMI in the manufacturing and nonmanufacturing purchasing manager index systems and its first-order difference ΔPMI to perform an OLS regression analysis on GDP growth rates and concluded that the single diffusion index in the PMI system can also predict economic growth. The literature [10] carried out a weighted average of the two individual indicators of new orders and supplier delivery time in the PMI system. The research results show that the new indicators are highly correlated with GDP. The literature [11] shows the effectiveness of the Professional Forecast Survey (SRF) and PMI for forecasting actual economic activities.

The literature [12] gave a brief introduction to the establishment background and preparation process of the PMI system and pointed out the important significance of the establishment of the PMI system. The literature [13] proposed to establish a PMI system in line with national conditions to enhance the authority and persuasiveness of the indicators. The literature [14] put forward two suggestions for the establishment and development of the PMI system. The first is to be in line with international standards; to learn the survey methods, sample selection, and calculation methods of the foreign mature and advanced PMI system; and to discuss the advantages of the current PPS sampling method. The second is to continuously improve the system structure based on actual national conditions, ensure the scientificity of sample selection, increase the participation of sample units, and ensure the truth and validity of statistics. The literature [15] made a brief analysis of PMI from three aspects: first, the concept and impact of the PMI system; second, the investigation and calculation method of PMI; and third, the indicative role of PMI on economic operations. The literature [16] studied the relationship between manufacturing purchasing manager indices and obtained relevant conclusions by establishing a VAR model and using impulse response and variance decomposition methods.

The literature [17] carried out a meaningful conversion and reduction of the individual diffusion data in the PMI system and found that PMI is ahead of related indicators such as fixed asset investment (FAI), factory price of industrial products (PPI), and customs import and export and further verifies the predictive effect of PMI on the macroeconomic cycle. Based on the significant impact of total inventory investment on GDP fluctuations, the literature [18] used PMI, an indicator widely used in economic fluctuation forecasting, to analyze the periodicity of finished product inventory investment and raw material inventory investment, and found that the former is counter-cyclical and the latter is vice versa. The literature [19] used the VAR model to conduct Granger causality test and Johnson cointegration test and concluded that PMI is the Granger cause of GDP growth, and there is a long-term equilibrium relationship between the two, and PMI can be used to effectively predict economic growth.

3. Margin Distribution Logistic Regression Model

A classification model is mainly composed of two parts:

$$\text{Loss} = l\left(y, w^T x\right) + r(w). \tag{1}$$

The first part is the loss function l of the classification, and the second part is the regularization term r of the model. When designing a classification model, the robustness of the model and the generalization ability of the model need to be considered. From the perspective of loss function, the huge loss function value caused by unreasonable outliers cannot have an excessive impact on the normal classification loss, which is caused by several unreasonable outliers. With unreasonable classification function, so the robustness of the model should be mainly considered from the perspective of the loss function of the model. From the perspective of the generalization ability of the model, there are often a lot of noise points in real data. These noise samples may be flooded in the vicinity of the two types of classification and discrimination hyperplanes, making it difficult for the model to find the true classification function. And how to resist the influence of these noise points is a key factor in the generalization ability of the model. The regularization technology in the model can help introduce some a priori assumptions, such as soft interval, maximize minimum interval, and optimize interval distribution. In this article, we mainly consider how to build a classification model with robustness and generalization ability from the loss function of the model and the introduction of a priori assumptions, specifically by introducing a smooth, convex, and generalized weakly

sensitive to outliers generalized logistic loss; abandoning the prior assumption of maximizing the minimum interval successfully obtained in the support vector machine; introducing the optimization goal of interval distribution; and transforming from highlighting the minimum interval formed by specific sample points to highlighting the distribution of the overall data features, thereby weakening the influence of noise data on training and improving the generalization ability of the model [20].

Furthermore, the interval distribution logistic regression model is extended to the task of multiclassification, and by introducing structured regularization, the defect of independent classifiers in the traditional multiclassifier construction is improved, and the shared information in multiple categories is used to improve the overall effect of the model. At the same time, a general framework in the linear case of interval distribution logistic regression is derived. Under this general framework, tasks such as binary classification, multiclassification, and feature selection can be completed at the same time [21]. Moreover, since there are a lot of linear inseparable data in real data, how to use interval distribution logistic regression to construct nonlinear classifiers is also an important content in interval distribution logistic regression research. In this article, by introducing the kernel method, due to interval distribution logistic regression, the simplicity of the model itself can easily be extended to the logistic regression of the kernel interval distribution and successfully used in the scenario of nonlinear classification.

Robustness is an important attribute of a classification model. Robustness is mainly reflected in the ability of the model to adapt to outliers. This ability mainly comes from the definition of the loss function. An ideal loss function should exist in the structure in Figure 1. But the ideal loss function is a nonconvex loss function, which will bring optimization difficulties. Therefore, an ideal and reasonable robust loss function needs to have monotonically decreasing properties and be insensitive to outliers; that is, for classification, the error gives linear loss growth.

Different loss functions are discussed. The squared loss or exponential loss is much more sensitive to outliers than the hinge loss or logistic loss, and it will impose penalties on correctly classified sample points. Among them, the hinge loss is adopted by the support vector machine, and the logistic loss is adopted by the logistic regression. However, since the Hinge Loss is a non-smooth loss term, it may introduce some complexity to the model optimization. Therefore, logic loss is a better alternative. A lot of work focuses on the ability to further explore the logic loss. Vapnik compared logistic regression and support vector machines and proved that chain loss can be approximated by logistic loss. Furthermore, Zhang and Ole proposed generalized logic loss (GLL). The generalized logic loss can approximate the soft-margin support vector machine (Soft-Margin SVM) well under certain conditions, which shows that the logic loss is very important for constructing a simple and robust classifier [22].

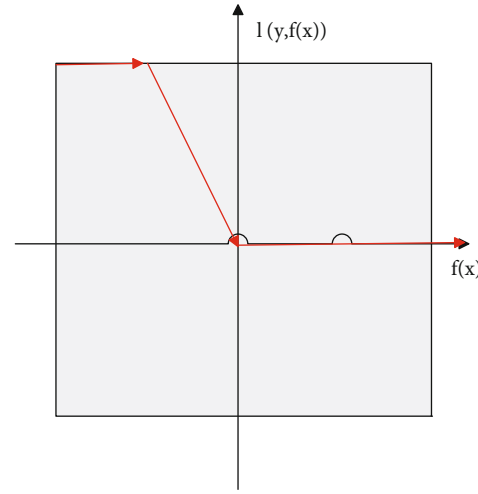

Figure 1: Ideal classification loss function.

When $x \in R^{D\times 1}$ represents a data point and $y \in \{-1,+1\}$ represents the corresponding binary label, the logistic regression model can be expressed as

$$\Pr(y|x) = \frac{1}{1+\exp(-yw^T x)}. \tag{2}$$

Among them, $\Pr(y|x)$ represents the conditional probability of label y in a given sample x, and $w^T x = 0$ defines a classification hyperplane in the feature space. The category conditional probabilities of data points on this classification hyperplane are all 0.5. It should be noted that these data points need to be centralized. Otherwise, x and w should be augmented to [23]

$$\begin{aligned} x &= [x_1, x_2, \cdots, x_D, 1]^T \in R^{(D+1)\times 1},. \\ w &= [w_1, w_2, \cdots, w_D, w_0]^T \in R^{(D+1)\times 1}. \end{aligned} \tag{3}$$

In order to optimize this logistic regression model, we need to optimize the log likelihood function for w:

$$\mathrm{NLL}(w) = -\mathrm{In}\prod_{i=1}^{N}\Pr(y_i|x_i) = \sum_{i=1}^{N}\mathrm{In}\left(1+\exp\left(-y_i w^T x_i\right)\right). \tag{4}$$

The above formula represents the logic loss. The generalized logistic regression loss is proposed to approximate the chain loss used in support vector machines:

$$\mathrm{GLL}\left(\alpha, yw^T x\right) = \frac{1}{\alpha}\mathrm{In}\left(1+\exp\left(-\alpha\left(yw^T x-1\right)\right)\right). \tag{5}$$

The main difference between GLL and logistic loss is that GLL defines the function margin between the two categories. The optimization objective function of GLL is

defined as [24]

$$w = \arg\min_{w} \frac{1}{N}\sum_{i=1}^{N}\frac{1}{\alpha}\mathrm{In}\left(1+\exp\left(-\alpha\left(y_i w^T x_i - 1\right)\right)\right)$$
$$= \arg\min_{w} \frac{1}{N\alpha} 1_N^T \mathrm{In}\left(1_N + \exp\left(-\alpha\left(Y \odot X^T w - 1_N\right)\right)\right). \tag{6}$$

The generalized logic loss is a loss function that can be adjusted by the parameter. When α increases, the generalized logic loss can approximate the chain loss very well. As shown in Figure 2, when $\alpha = 10$, the generalized logic loss is almost exactly the same as the chain loss. Since chain loss is a nonsmooth loss function and logic loss does not impose zero loss on any correctly classified data, which will lead to overlearning of correctly classified samples, generalized logistic loss is a better replacement for loss function.

The success of support vector machines shows that the a priori hypothesis of maximizing the minimum interval can significantly improve the generalization ability of the model. The assumption of maximizing the minimum interval is also applied to logistic regression. Under the framework of generalized logistic loss, the chain loss in support vector machine is replaced with generalized logistic loss, and the maximum interval logistic regression is proposed to approximate support vector machine. Furthermore, the maximum interval logistic regression is also extended to feature selection and sparse learning. But even if the maximum interval strategy is effective most of the time, this strategy is easily affected on noisy data.

The interval distribution, by considering the interval distribution of all data points, rather than the minimum interval of the data points closest to the decision boundary, is proved to have better performance than the minimum interval strategy.

Studies have shown that all data points have an impact on the generalization error boundary, and the impact of a data point on the generalization error and its distance from the decision boundary show an exponential decrease; that is, the closer the point to the decision boundary, the more impact on the generalization error (big). The traditional support vector machine is proved to have a lower bound on the divergence between data classes, but it ignores the important prior distribution information in the data classes [25].

Theorem 1.

$$\Pr_D[yf(x) < 0] \le \frac{1}{m^{50}} + \inf_{\theta\in(0,1]}\left[\Pr_S[yf(x) < \theta] + m^{-2/\left(1-E_S^2[yf(x)+\theta/9]\right)}\right] + \frac{3\sqrt{\mu}}{m^{3/2}} + \frac{7\mu}{3m} + \sqrt{\frac{3\mu}{m}\widehat{L}(\theta)}. \tag{7}$$

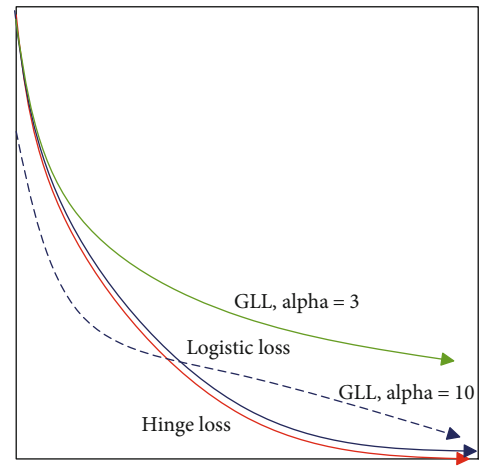

Figure 2: Comparison of different loss functions.

Among them,

$$\mu = \frac{144InmIn(2|H|)}{\theta^2} + \mathrm{In}\left(\frac{2|H|}{\delta}\right),$$
$$\widehat{L}(\theta) = \Pr_S[yf(x) < \theta]\Pr_S\left[yf(x) > \frac{2\theta}{3}\right]. \tag{8}$$

$Es[yf(x)]$ is the mean of the margin, and $\widehat{L}(\theta)$ is the variance of the margin.

Theorem 1 proves that the margin mean and margin variance play a key role in the generalization of the classifier. The margin distribution is defined as the first and second moments of the margin, that is, the margin mean $(\bar{\eta})$ and the margin variance $(\widehat{\eta})$. The optimization goal of the margin distribution is to simultaneously maximize the margin mean and minimize the margin variance:

$$\bar{\eta} = \frac{1}{N}\sum_{i=1}^{N} y_i w^T x = \frac{1}{N}(XY)^T w, \tag{9}$$

$$\widehat{\eta} = \frac{1}{N}\sum_{i=1}^{N}\left(y_i w^T x_i - \bar{\eta}\right)^2. \tag{10}$$

The margin distribution has a significant impact on the learned classification hyperplane. It will help the classification model to fully consider the statistical information hidden in the training data:

Theorem 2. *The margin mean value in formula (9) will help expand the class center distance of the two types, and the margin variance constraint in formula (10) will force the hyperplane to be in a direction with higher data uncertainty and prevent the hyperplane from deviating too much from the centers of the two types.*

3.1. Certification. N_+ and N_- are the numbers of positive and negative samples, S_+ and S_- are the sets of positive and negative samples, respectively, $\bar{x}_{+--}$ and $\bar{x}_-$ are the centers of positive and negative samples, respectively, and S_W^+ and S_W^-

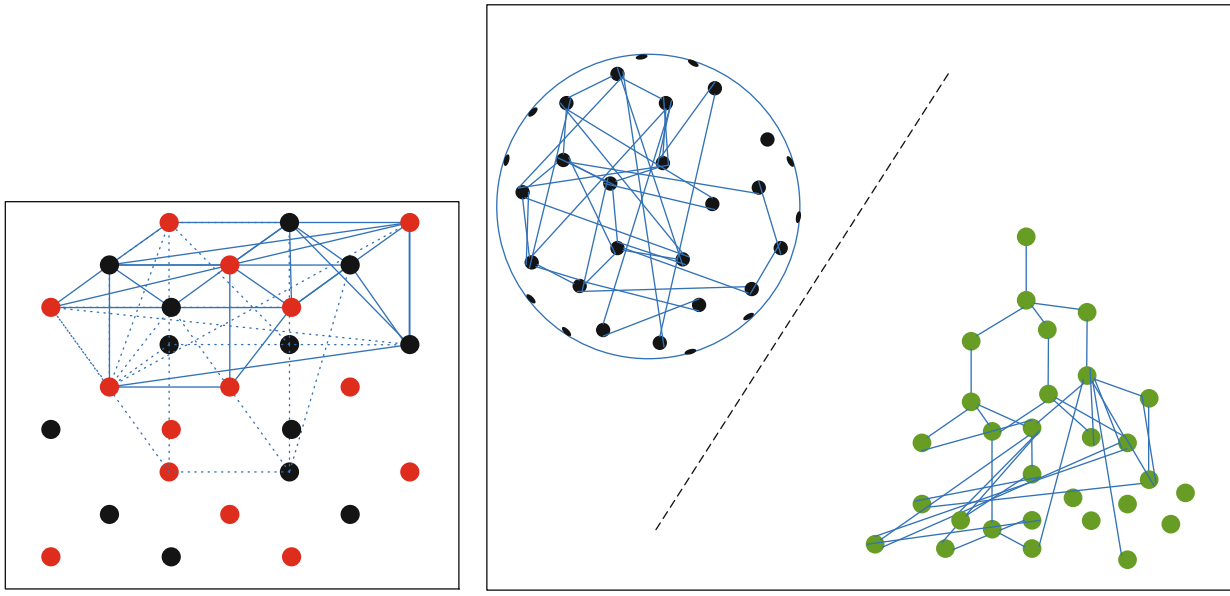

(a) Hyperplanes in feature space (b) Projected points in logistic space

Figure 3: Comparison of logistic regression and margin distribution logistic regression.

are the covariance matrices of positive samples and negative samples, respectively. The mean margin can be correspondingly expressed as

$$\begin{aligned}\bar{\eta} &= \frac{1}{N}\sum_{i=1}^{N} y_i w^T x_i = \frac{1}{N}\left(\sum_{x_i \in S_+} w^T x_i - \sum_{x_i \in S_-} w^T x_i\right) \\ &= \frac{N_+}{N} w^T \bar{x}_{+--} - \frac{N_-}{N} w^T \bar{x}_{---}.\end{aligned} \tag{11}$$

Similarly, the margin distribution can be rewritten as

$$\begin{aligned}\hat{\eta} &= \frac{1}{N}\sum_{i=1}^{N} \left(y_i w^T x_i - \bar{\eta}\right)^2 \\ &= \frac{1}{N}\left(\sum_{x_i \in S_+} \left(w^T x_i - \bar{\eta}\right)^2 - \sum_{x_i \in S_-} \left(w^T x_i + \bar{\eta}\right)^2\right).\end{aligned} \tag{12}$$

Part of the above formula is expressed as

$$\begin{aligned}\sum_{x_i \in S_+} \left(w^T x_i - \bar{\eta}\right)^2 &= \sum_{x_i \in S_+} \left(w^T x_i - \left(\frac{N_+}{N} w^T \bar{x}_{+--} - \frac{N_-}{N} w^T \bar{x}_{---}\right)\right)^2 \\ &= N_+ w^T S_W^+ w + \frac{N_+^2 N_-}{N^2} w^T \left(\bar{x}_+ + \bar{x}_{----}\right)^2 w.\end{aligned} \tag{13}$$

Thus, the margin variance can be further rewritten as

$$\hat{\eta} = \frac{1}{N} w^T \left(N_+ S_W^+ + N_- S_W^-\right) w + \frac{N_+ N_-}{N^2} w^T \left(\bar{x}_{+--} + \bar{x}_-\right) w. \tag{14}$$

For the margin mean formula, when the margin mean is optimized, the distance between the two categories is enlarged, thereby improving the discriminative ability of the model. For the margin variance, it can be decomposed into two parts. The first part represents the margin variance of each category. When the margin variance is minimized, the discriminant hyperplane will be along the direction with the greatest data uncertainty, thereby reducing the possibility of data crossing the discriminant hyperplane. When the second part of the margin variance is maximized, the discriminant hyperplane will not deviate too much from the two types of center points, thereby obtaining a more reasonable discriminant hyperplane and ensuring the discriminative ability of the model.

Through the analysis of the margin distribution characteristics, it can be known that when adjusting the parameters of the margin distribution constraint, it can help the model to better adapt to the distribution of the training data. When the model can make better use of the statistical information in the data, the model can have better adaptability to noise and outliers.

A margin distribution logistic regression model with robustness and generalization ability is defined as

$$\arg\min_{w} \frac{1}{N\alpha} 1_N^T \mathrm{In}\left[1_N + \exp\left(-\alpha\left(Y \odot X^T w - 1_N\right)\right)\right] + \lambda_1 \hat{\eta} - \lambda_2 \bar{\eta}. \tag{15}$$

In the above formula, the classification error is minimized by GLL, while the margin variance is reduced and the margin mean is increased. The margin is the functional distance of a sample point to distinguish the hyperplane. However, after the logistic regression projection, the margin corresponds to the distance of the $w^T x$ from the origin of the coordinate after the data point is projected. Among them, the origin of the coordinates represents the position where the classification probability is 0.5, and the slope of the curve

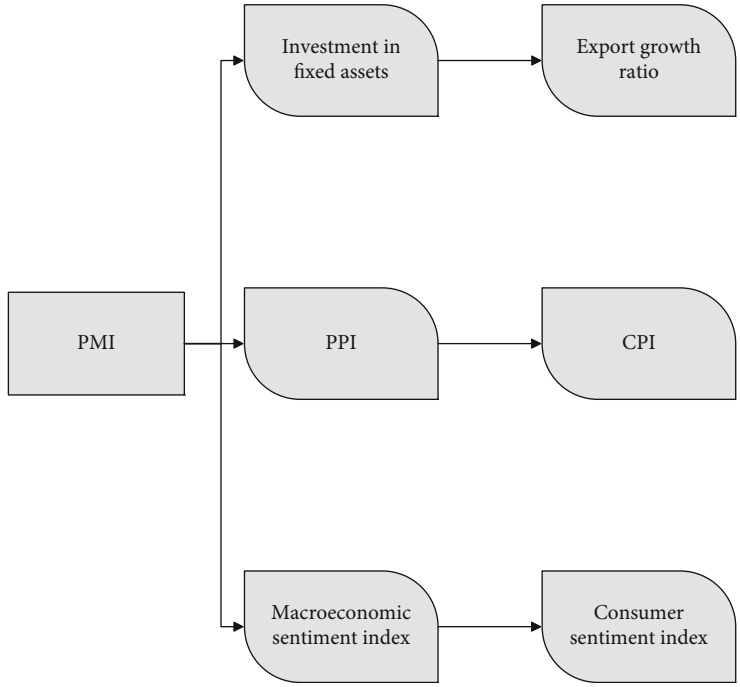

Figure 4: Mechanism analysis of PMI and different indicators.

here is the highest. Obviously, data points near the origin are more likely to be classified incorrectly. When we increase the mean margin, as shown in Figure 3(b), we can make a larger safety margin between the two categories and make the classification confidence higher. Moreover, the margin distribution also makes the corresponding discriminant hyperplane changes to the data distribution, as shown in Figure 3(a). When the control margin variance is small, the discrimination hyperplane can be along the direction of greater data uncertainty. At the same time, due to the optimization of the margin mean, the learned classification hyperplane can still maintain its most critical discriminative ability in the classification task.

In real applications, most data is composed of multiple categories. Therefore, it is of great significance to extend the two classifiers to multiple classifiers. In this paper, we extend the margin distribution logistic machine (MDLM) to a multiclass version.

Generally speaking, a multiclass classifier determines the final category by combining a group of one-to-many two-classifiers or a group of one-to-one two-classifiers through voting. However, these two combination strategies have a common flaw. That is, there is no way for these independent two classifiers to share information, resulting in the information between categories cannot be shared. For example, there is a feature subset that is effective for this multiclassification task, but an independent set of classifiers cannot help capture this important information. Therefore, we need to adopt a method that can not only classify at the same time but also help the model capture the information that exists between the categories. There are also studies that combine a C-class classification task into an optimization and avoid the complexity of training a large number of independent

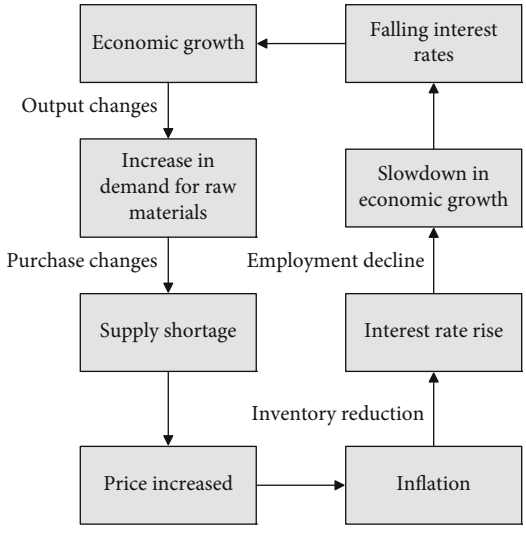

Figure 5: The connection between the PMI system and the business cycle.

classifiers at the coding and logic levels. Through the following method, a multiclass support vector machine is constructed, and this multiclass support vector machine can be optimized by a model:

$$\begin{aligned} \min \quad & \left\{ C \sum_{i=1}^{n} \sum_{k \neq y_i} \xi_i^k + \frac{1}{2} \sum_{k=1}^{C} \sum_{j=1}^{m} \left(w_{k,j} \right)^2 \right\} \\ \text{s.t.} \quad & w_{y_i}^T x_i \geq w_k^T x_i + 2 - \xi_i^k \\ & \xi_i^k \geq 0 \quad (i = 1, 2, \cdots, n\,; k \neq y_i). \end{aligned} \tag{16}$$

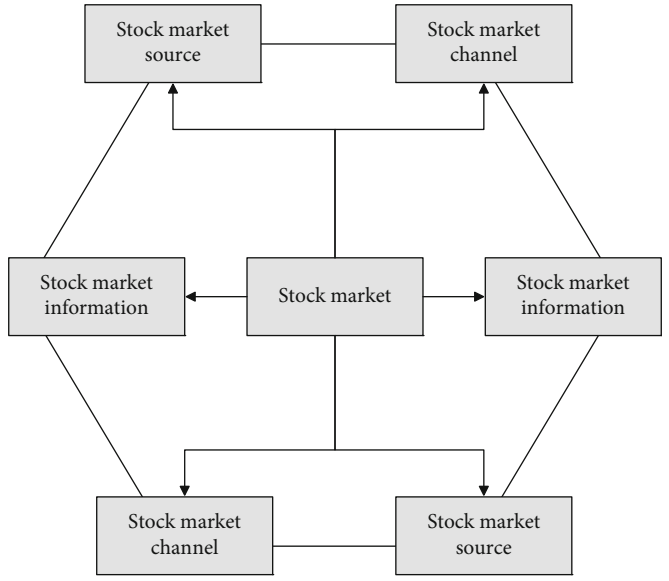

Figure 6: The information transmission model of the stock market.

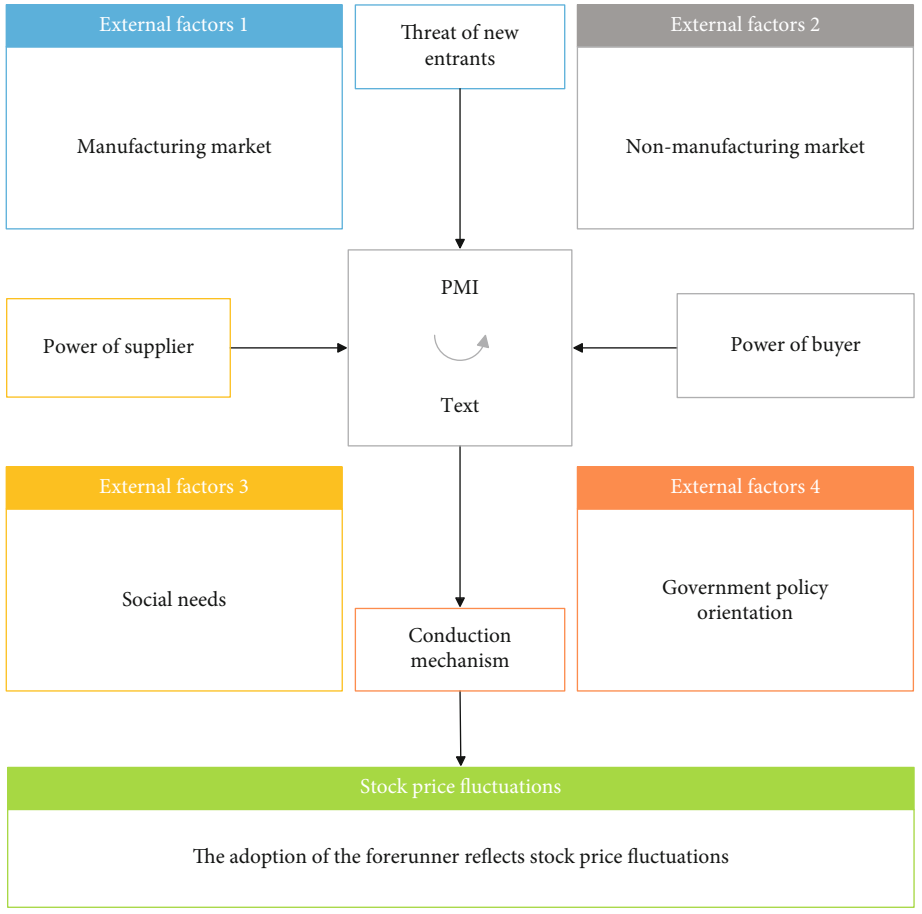

Figure 7: Correlation analysis model of stocks and PMI index based on logistic regression model.

GLL is used to replace the nonsmooth chain loss in support vector machines. Similarly, the SVM using GLL has also been extended to a multiclass model. This multi-class maximum margin logistic regression (MLR) is given in the following form. This mode can also complete the learning of a multiclass classifier in an optimization

Table 1: Statistical table of China's PMI from December 2017 to March 2021.

	Manufacturing PMI	Year-on-year growth	Nonmanufacturing PMI	Year-on-year growth
1-Mar-21	51.9	-0.19%	56.3	7.65%
1-Feb-21	50.6	41.74%	51.4	73.65%
1-Jan-21	51.3	2.60%	52.4	-3.14%
1-Dec-20	51.9	3.39%	55.7	4.11%
1-Nov-20	52.1	3.78%	56.4	3.68%
1-Oct-20	51.4	4.26%	56.2	6.44%
1-Sep-20	51.5	3.41%	55.9	4.10%
1-Aug-20	51	3.03%	55.2	2.60%
1-Jul-20	51.1	2.82%	54.2	0.93%
1-Jun-20	50.9	3.04%	54.4	0.37%
1-May-20	50.6	2.43%	53.6	-1.29%
1-Apr-20	50.8	1.40%	53.2	-2.03%
1-Mar-20	52	2.97%	52.3	-4.56%
1-Feb-20	35.7	-27.44%	29.6	-45.49%
1-Jan-20	50	1.01%	54.1	-1.10%
1-Dec-19	50.2	1.62%	53.5	-0.56%
1-Nov-19	50.2	0.40%	54.4	1.87%
1-Oct-19	49.3	-1.79%	52.8	-2.04%
1-Sep-19	49.8	-1.97%	53.7	-2.19%
1-Aug-19	49.5	-3.51%	53.8	-0.74%
1-Jul-19	49.7	-2.93%	53.7	-0.56%
1-Jun-19	49.4	-4.08%	54.2	-1.45%
1-May-19	49.4	-4.82%	54.3	-1.09%
1-Apr-19	50.1	-2.53%	54.3	-0.91%
1-Mar-19	50.5	-1.94%	54.8	0.37%
1-Feb-19	49.2	-2.19%	54.3	-0.18%
1-Jan-19	49.5	-3.51%	54.7	-1.08%
1-Dec-18	49.4	-4.26%	53.8	-2.18%
1-Nov-18	50	-3.47%	53.4	-2.55%
1-Oct-18	50.2	-2.71%	53.9	-0.74%
1-Sep-18	50.8	-3.05%	54.9	-0.90%
1-Aug-18	51.3	-0.77%	54.2	1.50%
1-Jul-18	51.2	-0.39%	54	-0.92%
1-Jun-18	51.5	-0.39%	55	0.18%
1-May-18	51.9	1.37%	54.9	0.73%
1-Apr-18	51.4	0.39%	54.8	1.48%
1-Mar-18	51.5	-0.58%	54.6	-0.91%
1-Feb-18	50.3	-2.52%	54.4	0.37%
1-Jan-18	51.3	0.00%	55.3	1.28%
1-Dec-17	51.6	0.39%	55	0.92%

problem:

$$\min \frac{1}{n\alpha}\sum_{i=1}^{n}\sum_{k\neq y_i}\mathrm{In}\left(1+\exp\left(-\alpha\left(w_{y_i}^{T}-w_k^{T}\right)X-2\right)\right) + \lambda\sum_{k=1}^{C}\sum_{j=1}^{m}\left(w_{k,j}\right)^2. \tag{17}$$

In this paper, using the core idea of multiclass classifiers, an equivalent multiclass learning model is given. We assume that a given data set has different categories of C and construct a multiclass label matrix $Y=[y_1,y_2,\cdots,y_C]\in\{-1,1\}^{N\times C}$ of this data set and $y_i=[-1,\cdots-1,\underbrace{1,\cdots,1}_{i-\text{thclass}},-1,\cdots-1]^T$. This multiclass classifier is

built on the basis of MDLM. Its optimization objective function is

$$\arg\min w = [w_1,\cdots,w_C]\sum_{i=1}^{C}\frac{1}{N\alpha}1_N^T\mathrm{In}\left[1_N+\exp\left(-\alpha\left(y_i\odot X^T w_i-1_N\right)\right)\right] + \lambda_1\widehat{\eta}_i-\lambda_2\bar{\eta}_i+\beta\|w\|_{2,1}. \tag{18}$$

This multiclass MDLM model tries to learn C one-to-many multiclassifiers at the same time. It is worth noting that it is different from the L2 norm regularity imposed in SVM and large margin logistic regression; in this paper, we use the L21 norm to capture the information implicit in each subtask in this multiclass task, especially the feature validity information. In particular, when the number of categories C is equal to 2, the model can be adjusted to the L1 norm, that is, the two-class sparse margin distribution logistic machine model (SMDLM). The L1 norm has also been proven to be a very effective technique for classification problems, and the SMDLM model can be well applied in many feature selection problems. When the parameter β is equal to 0, the model degenerates to MDLM. Therefore, such a multiclass MDLM model can be well applied in the expansion of two classification, feature selection, multiclassification, multimodel learning, multimodal feature selection, and so on.

In real applications, nonlinear classification is also a very important research content, because there are a large number of linear inseparable data sets.

Research on the nonlinear model of logistic regression has also received a lot of attention. The objective function of linear margin distribution logistic regression is

$$\arg\min_{w}\frac{1}{N\alpha}1_N^T\mathrm{In}\left[1_N+\exp\left(-\alpha\left(Y\odot X^T w-1_N\right)\right)\right]+\lambda_1\widehat{\eta}-\lambda_2\bar{\eta}. \tag{19}$$

Any function can be expressed in the following form:

$$f(x)=\sum_{i=1}^{n}\alpha_i K(x,x_i). \tag{20}$$

Among them, $K(x,x_i)$ represents the kernel function, which can use linear kernel function, polynomial kernel function, radial basis kernel function, and so on. This paper defines K as the radial basis kernel function:

$$K(x,x_i)=e^{-\left(\|x-x_i\|^2\right)/2\sigma^2}. \tag{21}$$

If we define K as the sample kernel matrix, $K\in R^{N\times N}$, then,

$$f(x)=w^T x=\sum_{i=1}^{n}\alpha_i K(x,x_i)=\alpha^T K_i. \tag{22}$$

The objective function of the nonlinear margin distribution logistic regression is obtained:

$$\arg\min_{\alpha}\frac{1}{N\alpha}1_N^T\mathrm{In}\left[1_N+\exp\left(-\alpha\left(Y\odot K^T\alpha-1_N\right)\right)\right] -\frac{\lambda_2}{N}Y^T K^T\alpha+\frac{\lambda_1}{N}K^T\alpha\alpha^T K-\frac{\lambda_1}{N^2}\alpha^T KYY^T K^T\alpha. \tag{23}$$

The nonlinear margin distribution logistic regression algorithm is a smooth and convex model, which can be directly optimized by the gradient descent algorithm.

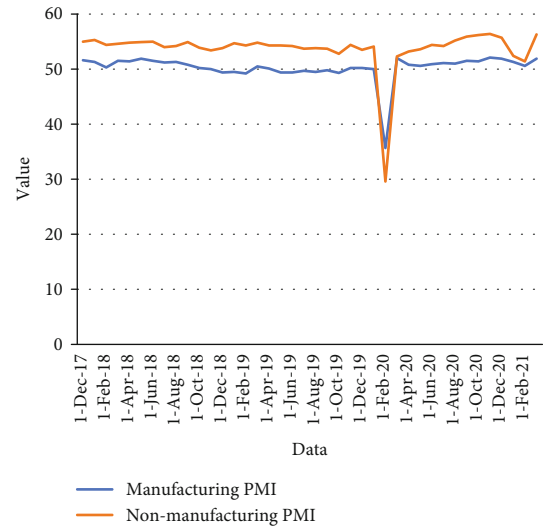

Figure 8: Statistical diagram of China's PMI from December 2017 to March 2021.

4. Analysis Model of the Correlation between Stocks and PMI Index Based on Logistic Regression Model

PMI has a linkage relationship with the early warning index of the macroeconomic prosperity index, the consumer expectations index, and the real estate prosperity index. PMI is also an indicator of economic prosperity. Therefore, this paper empirically analyzes the correlation between PMI and other economic prosperity indexes, which are also economic prosperity indexes. PMI has the leading value in the economic climate index and reflects the characteristics of different economic cycles of economic fluctuations, as shown in Figure 4.

The mechanism of PMI's effect on the macro economy is shown in Figure 5.

According to the theory of supply and demand, the prices of labor and raw materials will rise, and therefore, the price level of the society as a whole will rise, and the economy as a whole is in a state of inflation. At this time, the country will take control of the supply of currency to ensure the stability of the price level, and the reduction of the supply of money will make it difficult for companies to meet the demand for funds, and interest rates will rise. The increase in interest rates will increase the cost of inventories of enterprises, reduce inventories, and relatively decrease

Table 2: Statistical table of the correlation between stock price and PMI from December 2017 to March 2021.

Data	Manufacturing PMI	Share price	Data	Manufacturing PMI	Share price
1-Mar-21	51.9	13.8	1-Jul-19	49.7	15.3
1-Feb-21	50.6	15.9	1-Jun-19	49.4	14.9
1-Jan-21	51.3	17.1	1-May-19	49.4	14.2
1-Dec-20	51.9	15.5	1-Apr-19	50.1	15.5
1-Nov-20	52.1	17.4	1-Mar-19	50.5	15.2
1-Oct-20	51.4	16.6	1-Feb-19	49.2	16.6
1-Sep-20	51.5	14.7	1-Jan-19	49.5	16.3
1-Aug-20	51	16.9	1-Dec-18	49.4	14.3
1-Jul-20	51.1	15.6	1-Nov-18	50	15.7
1-Jun-20	50.9	16.2	1-Oct-18	50.2	16.5
1-May-20	50.6	16.4	1-Sep-18	50.8	15.1
1-Apr-20	50.8	8.6	1-Aug-18	51.3	16.0
1-Mar-20	52	15.2	1-Jul-18	51.2	16.2
1-Feb-20	35.7	15.6	1-Jun-18	51.5	16.3
1-Jan-20	50	16.9	1-May-18	51.9	15.6
1-Dec-19	50.2	14.4	1-Apr-18	51.4	14.7
1-Nov-19	50.2	15.2	1-Mar-18	51.5	15.3
1-Oct-19	49.3	15.3	1-Feb-18	50.3	15.8
1-Sep-19	49.8	14.5	1-Jan-18	51.3	15.1
1-Aug-19	49.5	14.4	1-Dec-17	51.6	13.7

production. On the other hand, the increase in interest rates will also slow down the momentum of overall investment and consumption. In turn, our country's economy, which currently mainly relies on these two methods to drive economic growth, has gradually slowed down its growth rate.

The manufacturing PMI data is authoritatively published by the China Logistics Purchasing Federation, while the HSBC Manufacturing PMI is published by HSBC. The channels of the stock market mainly include relevant channels for the transmission of economic information, such as the Internet, newspapers, research reports, mobile phones, and other media. The information sink of the stock market is the investors of all kinds of stock markets. Investors use their own analysis and judgment of economic information and make corresponding stock trading behaviors, thereby affecting the fluctuation or trend of the stock market. Noise in the stock market refers to the fact that macroeconomic information is inevitably affected by other external factors in the process of transmission, including both human and nonhuman factors. Under the combined influence of these factors, macroeconomic information will be disturbed by noise such as exaggeration, reduction, and distortion, which will affect the transmission of information and ultimately affect investors' investment decisions. The information transmission model of the stock market is shown in Figure 6.

Combining the demand for stock price fluctuation analysis, the correlation analysis model of stock and PMI index based on logistic regression model constructed in this paper is shown in Figure 7.

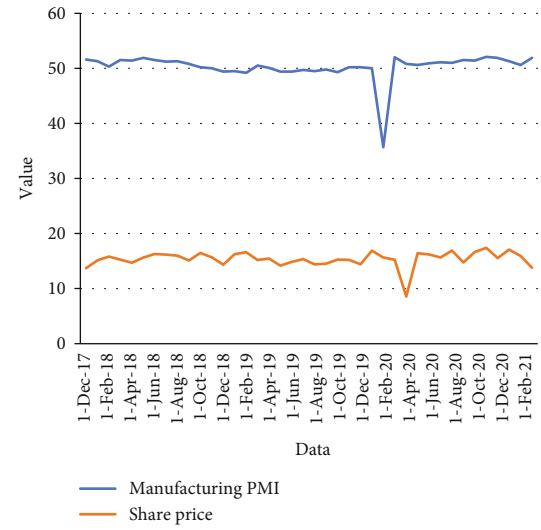

Figure 9: Statistical diagram of the correlation between stock price and PMI from December 2017 to March 2021.

5. Test Analysis

According to actual needs, a correlation analysis model of stocks and PMI based on logistic regression model is constructed. On this basis, this paper obtains data from the National Bureau of Statistics to analyze the performance of the model and count the PMI data of China in recent years, as shown in Table 1 and Figure 8.

This article takes the stock price of a listed company as the evaluation object and analyzes the correlation with PMI. The research object of this paper is manufacturing

enterprises, so the manufacturing PMI is selected as the research object. The statistical results are shown in Table 2 and Figure 9.

Through the analysis of the above chart and table, we can see that the stock price has a strong correlation with the PMI. In addition, compared with stock prices, PMI is at least two months forward-looking. Therefore, the system model constructed in this paper shows that there is a clear correlation between PMI and stocks.

6. Conclusion

Based on the reality that the Purchasing Managers Index is widely used in the forecast of economic growth and is known as the "barometer" of the stock market, this paper first theoretically analyzes the forecasting and functioning mechanism of the Purchasing Manager Index for the macroeconomy and the stock market. Moreover, this paper designs a margin distribution logistic regression model that is easy to optimize and has robustness and generalization ability on the basis of generalized logistic loss and margin distribution and gives a multiclass margin distribution logistic regression framework. This framework can be used to perform two-classification, multiclassification, and feature selection tasks. In addition, this paper constructs an analysis model of the correlation between stocks and the PMI index based on a logistic regression model and combines actual data to carry out the analysis. From the experimental results, it can be seen that the algorithm model constructed in this paper has certain practical effects.

Data Availability

The labeled datasets used to support the findings of this study are available from the corresponding author upon request.

Conflicts of Interest

The authors declare no competing interests.

Acknowledgments

This study is sponsored by Henan Industrial Vocational and Technical College.

References

[1] C. J. Adam, "How firms shape income inequality: stakeholder power, executive decision making, and the structuring of employment relationships," *Academy of Management Review*, vol. 41, no. 2, pp. 324–348, 2016.

[2] M. B. Alexandri and W. K. Anjani, "Income smoothing: impact factors, evidence in Indonesia," *International Journal of Small Business and Entrepreneurship Research*, vol. 3, no. 1, pp. 21–27, 2014.

[3] T. Alquraan, A. Alqisie, and S. A. Al, "Do behavioral finance factors influence stock investment decisions of individual investors?(Evidences from Saudi Stock Market)," *Journal of American Science*, vol. 12, no. 9, pp. 72–82, 2016.

[4] N. Apergis, B. Simo-Kengne, and R. Gupta, "The long-run relationship between consumption, house prices, and stock prices in South Africa: evidence from provincial-level data," *Journal of Real Estate Literature*, vol. 22, no. 1, pp. 83–99, 2014.

[5] N. Arshed, A. Anwar, M. S. Hassan, and S. Bukhari, "Education stock and its implication for income inequality: the case of Asian economies," *Review of Development Economics*, vol. 23, no. 2, pp. 1050–1066, 2019.

[6] S. R. Baker, "Debt and the response to household income shocks: validation and application of linked financial account data," *Journal of Political Economy*, vol. 126, no. 4, pp. 1504–1557, 2018.

[7] M. Banam and A. Mehrazeen, "The relationship of information asymmetry, institutional ownership and stock liquidity with income smoothing in Tehran Stock Exchange," *Journal OF Management and Accounting Studies*, vol. 4, no. 3, pp. 6–11, 2016.

[8] E. Bengtsson and D. Waldenström, "Capital shares and income inequality: evidence from the long run," *The Journal of Economic History*, vol. 78, no. 3, pp. 712–743, 2018.

[9] L. Carvalho and C. Di Guilmi, "Technological unemployment and income inequality: a stock-flow consistent agent-based approach," *Journal of Evolutionary Economics*, vol. 30, no. 1, pp. 39–73, 2020.

[10] S. Chen and B. Komal, "Impact of stock market development on economic growth: evidence from lower middle income countries," *Management and Administrative Sciences Review*, vol. 5, no. 2, pp. 86–97, 2016.

[11] Y. Dafermos and C. Papatheodorou, "Linking functional with personal income distribution: a stock-flow consistent approach," *International Review of Applied Economics*, vol. 29, no. 6, pp. 787–815, 2015.

[12] R. Gantino, "Effect of managerial ownership structure, financial risk and its value on income smoothing in the Automotive Industry and Food & Beverage Industry Listed in Indonesia Stock Exchange," *Research Journal of Finance and Accounting*, vol. 6, no. 4, pp. 48–56, 2015.

[13] M. Gao, J. Meng, and L. Zhao, "Income and social communication: the demographics of stock market participation," *The World Economy*, vol. 42, no. 7, pp. 2244–2277, 2019.

[14] J. P. Gómez, R. Priestley, and F. Zapatero, "Labor income, relative wealth concerns, and the cross section of stock returns," *Journal of Financial and Quantitative Analysis*, vol. 51, no. 4, pp. 1111–1133, 2016.

[15] M. Hoffmann, "The consumption–income ratio, entrepreneurial risk, and the U.S. stock Market," *Journal of Money, Credit and Banking*, vol. 46, no. 6, pp. 1259–1292, 2014.

[16] B. F. Jones, "The human capital stock: a generalized approach," *American Economic Review*, vol. 104, no. 11, pp. 3752–3777, 2014.

[17] H. H. Khan, I. Naz, F. Qureshi, and A. Ghafoor, "Heuristics and stock buying decision: evidence from Malaysian and Pakistani stock markets," *Borsa Istanbul Review*, vol. 17, no. 2, pp. 97–110, 2017.

[18] H. J. Kleven and E. A. Schultz, "Estimating taxable income responses using Danish tax reforms," *American Economic Journal: Economic Policy*, vol. 6, no. 4, pp. 271–301, 2014.

[19] G. Li, "Information sharing and stock market participation: evidence from extended families," *Review of Economics and Statistics*, vol. 96, no. 1, pp. 151–160, 2014.

[20] M. Y. Mohammadi and M. H. Arman, "The survey of accounting variables effect on incomesmoothing in stock exchange companies," *Journal of Fundamental and Applied Sciences*, vol. 8, no. 2, pp. 1257–1271, 2016.

[21] S. N. Nazar, T. Ekowati, and H. Setiyawan, "Does income smoothing improve informativeness of stock prices?," *Econosains Jurnal Online Ekonomi dan Pendidikan*, vol. 15, no. 2, pp. 225–239, 2017.

[22] T. Nguyen, H. N. Duong, and H. Singh, "Stock market liquidity and firm value: an empirical examination of the Australian market," *International Review of Finance*, vol. 16, no. 4, pp. 639–646, 2016.

[23] E. Saez and G. Zucman, "Wealth inequality in the United States since 1913: evidence from capitalized income tax data," *The Quarterly Journal of Economics*, vol. 131, no. 2, pp. 519–578, 2016.

[24] S. H. Shin and K. T. Kim, "Income uncertainty and household stock ownership during the great recession," *Journal of Financial Counseling and Planning*, vol. 29, no. 2, pp. 383–395, 2018.

[25] J. Voelzke, "Individual labour income, stock prices and whom it may concern," *Applied Economics Letters*, vol. 23, no. 13, pp. 965–968, 2016.

Hindawi
Journal of Sensors
Volume 2021, Article ID 6941258, 12 pages
https://doi.org/10.1155/2021/6941258

Research Article

Sports Information Acquisition and Functional Training System Based on Multisensor Information Fusion

Zhonglin Ma,[1] Zhihao Yu,[1] and Jingshan Zhang[2]

[1]*College of Physical Education, Jilin Normal University, Siping, 136000 Jilin, China*
[2]*Department of Sports Humanities, Sichuan Sports College, Chengdu, 610043 Sichuan, China*

Correspondence should be addressed to Jingshan Zhang; zhangjingshan2007@126.com

Received 9 July 2021; Revised 5 August 2021; Accepted 16 August 2021; Published 2 September 2021

Academic Editor: Mu Zhou

Since entering the 21st century, multisensor information fusion technology has developed rapidly, and multisensor information fusion is a trend in the coming years and even decades. This article is aimed at studying how the traditional sports information acquisition and functional training system can be implemented under the multisensor information fusion. This article proposes the use of multisensor information fusion technology to conduct an in-depth study on the traditional ways of acquiring sports information and the cognition of sports information by different groups of people, as well as the use of multisensor information fusion technology to update the functional training system and discuss whether this new functional training system is in line with the speed and rhythm of the current era compared with the traditional training system. The results of obtaining sports information from different groups of people show that more people know about sports events at home and abroad, reaching 22.5%. Under the same circumstances, 60% of the elderly are willing to pay attention to sports information, while only 30% of the young people are willing to pay attention to sports information. And from 2016 to 2021, the number of people in functional training nationwide has increased from 200,000 to 1.5 million.

1. Introduction

With the accelerated development of information and the Internet of Things era, information acquisition, comprehensive analysis, and processing of information and information fusion have become research hotspots in the field of information technology. Information system is our most important carrier for obtaining information resources, and it will inevitably become the information science main research object. The huge amount of information in the information system brings obvious uncertainty. There are many uncertainties in the source, true and false, and quality of the information. These uncertain information are also important topics in data mining and knowledge discovery. It can be seen everywhere in our daily life, which greatly affects all aspects of life, and is one of the very important social components. The Internet has become an important media tool for sports communication by virtue of its advantages such as rapid transmission, strong interactivity, fast release, and large amount of information. Especially since the integration of the Internet, traditional media, and mobile phone new media, the network's advantages in sports communication have been exerted. Nowadays, people have attached great importance to daily sports. Online sports information is quietly affecting people's sports awareness, interest, attitude, and other sports awareness and changing people's sports behaviors such as participation in physical exercise, sports consumption, and acquisition of sports information. However, since the 2010s, various techniques have been combined with functional training, which has led to the prevalence of functional training in our country. Many scholars have proposed systematic research in theory; some have proposed functional training theories, and the proposed integration technology, coupled with a detailed combination method that fits our country's national conditions, has led to functional training in many places in our country.

The idea of multi-information fusion is like the human brain. It fully integrates the data information of multiple sensors. Through the reasonable analysis and use of the observed multidimensional information, the multidimensional sensors

are spatially redundant or complementary. The information completes the fusion operation according to the established rules and finally obtains the desired combined result. The basic principles of multi-information fusion include the following: sensors in multiple dimensions receive the information of the target system, the information obtained by the sensor is processed with a certain algorithm, and finally, a data vector that can represent our needs is obtained; the output data of the sensor is used by the information fusion algorithm. According to specific rules, the mathematical description of the described system is obtained. And huge sports information resources. The Internet is constantly spreading vast and ever-changing sports information, and it provides uninterrupted reports on sports events and sports news. The speed of Internet communication is now developing rapidly. Compared with traditional media, Internet media has a big update in the amount of information and has strong interactivity. Now people's main source of information is from the Internet and various mobile terminal capabilities. It is more convenient and quicker than traditional methods to allow people to obtain information anytime and anywhere. Traditional media dissemination of sports information is a relatively single one-way transmission, while the network can present strong interactivity when disseminating sports information and it can spread in multiple directions. For example, in the live broadcast of a sports game, the audience can comment and exchange views in real time.

Multisensor information fusion (IF) has attracted the attention of many researchers in different fields because it can improve modeling accuracy by integrating information collected from multiple sensors. Traditionally, the input to multisensor IF problem is mostly quantitative data. However, in order to provide more comprehensive decision support, quantitative data and expert domain knowledge should be integrated in the IF process. In addition, there may be insufficient data in many practical situations, which makes many conventional methods unsuitable. Because the belief rule base (BRB) has advantages in nonlinear modeling with insufficient data and expert domain knowledge, the BRB-IF model is proposed for the multisensor intermediate frequency problem. Yu et al. proposed a specific optimization model for BRB-IF and its corresponding specific optimization algorithm, which can greatly improve efficiency. The model they proposed can test the optimization algorithm of particle swarms, so that particle swarms can be more efficient for activities, and differential evolution algorithm as an optimization engine, it can greatly improve the calculation speed of solving operator recommendation strategies. The effectiveness of the proposed BRB-IF is verified through actual case studies of threat level assessment, in which a comparison between BRB-IF and neural network is carried out. When training radial basis function neural network (RBFNN), the position of Gaussian neurons is usually determined by clustering. However, Yu et al. did not use a large amount of data information to conduct a comprehensive analysis and introduction of multisensor information fusion and finally got a convincing result [1]. The training input can be clustered in a completely unsupervised manner (input clustering), or some supervision can be introduced, for example, by concatenating the input vector with the weighted output vector (input-output clustering). Raitoharju et al. recommend applying clustering (class-specific clustering) to each class separately. This idea has been used in some previous work, but the benefits of this method have not been evaluated. When training RBFNN, we compared class-specific, input, and input-output clustering methods in terms of classification performance and computational efficiency. To achieve this goal, we applied three different clustering algorithms and conducted experiments on 25 benchmark data sets. The process of the experiment shows that the specific class-based method significantly reduces the overall complexity of clustering. The experimental results of Raitoharju et al. show that this method can significantly improve the classification ability and is widely used in functional training, fusion principles, etc., especially in terms of lack of Gaussian neuron network. Among other clustering algorithms, Raitoharju et al. combine dynamic evolutionary optimization, multidimensional particle swarm optimization, and specific clustering to optimize the number and location of cluster centroids for the first time. However, Raitoharju et al. did not make a summary explanation with their experimental results in the functional training systems, leading to their theory may still be insufficient [2]. Raquel et al. used distributed and centralized fusion methods to study the problem of information fusion estimation for a class of multisensor linear systems affected by different types of random uncertainties. It is assumed that the measurement output is disturbed by one-step autocorrelation and cross-correlation additive noise, and Raquel et al. also consider the random uncertainty caused by multiplicative noise and random loss of measured values in the sensor output. At each sampling time, each sensor output is sent to the local processor, and due to some kind of transmission failure, a step-related random delay may occur. Only the covariance information is used, and the evolution model of the signal process is not required. The local minimum squares (LS) filter based on the measured value received from each sensor is designed through an innovative method. Then, use the LS optimality criterion to fuse all these local filters through matrix-weighted linear combination to generate the best distributed fusion filter. In addition, a recursive algorithm of centralized fusion filter is proposed, and the accuracy of the estimator measured by the estimation error covariance is analyzed through simulation examples. However, Raquel et al. did not conduct an analysis of the uncertain multisensor information fusion technology to support their experimental logic [3].

The research on functional training in this article is carried out on the basis of multi-information fusion and uses the latest network, communication, 5G, and other technologies. Network technology can control the transmission of information in the local area network, and communication technology can enable information to be transmitted wirelessly and can be very good for the acquisition of sports information and the realization of related functional training. It can also be said to be multisensor information convergence. It is the correlation, fusion, and update of specific

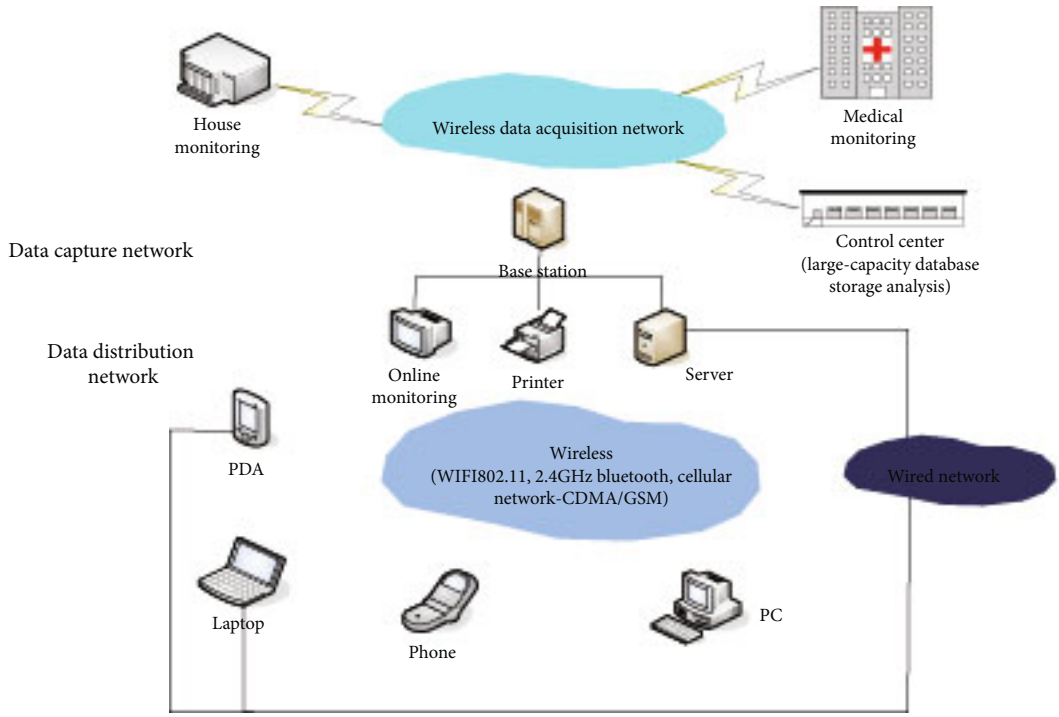

Figure 1: Comprehensive map of multisensor information fusion.

experimental data such as data core information that people obtain from multiple different information sources to achieve acquisition, very accurate location, and corresponding identity estimation, including the processing of information obtained from a very comprehensive assessment of the situation and threats and their importance. This process is a continuous process of estimating and evaluating the needs of other information sources. At the same time, it is also a process of continuous self-correction of information in the process of processing and finally gets the results you want. At present, people's acquisition of sports information may still remain in the traditional and single method, including traditional media and the current network. Traditional techniques are also used when performing functional training, which has not kept up with the changes in this era. On the basis of traditional theory, this article uses new multi-information fusion technologies, as well as the Internet, 5G, and communication technologies to have a new way to obtain sports information, while the traditional functional training is updated. The previous methods used more scientific and practical methods and methods for training.

2. Multisensor Information Fusion Method and Information Acquisition

2.1. Multisensor Information Fusion Technology. The so-called multisensor information fusion (MSIF) is the use of computer technology to automatically analyze and synthesize information and data from multiple sensors or sources under certain criteria to complete the required decisions and estimates [4]. Multisensor information fusion is an information processing technology used to include multiple sensors in different locations, as shown in Figure 1. In the mature development of modern sensor technology, data processing technology, computer software and hardware technology, and industrialized control technology, data processing technology can process the information collected by sensors correspondingly, and computer software and hardware can play a basic role in the transmission process. Industrialization of the control can carry out the control operation of the sensor, and now the multi-information sensor information fusion technology has become a very popular technology. Nowadays, my country's related research on sensor information fusion technology has been used in ordinary engineering to locate and identify information [5]. The positioning of information can accurately locate the products produced, and subsequent maintenance updates and identification technology have been carried out and can effectively identify relevant information. And it is believed that with the advancement of science, multisensor information fusion technology will become a specialized technology for comprehensive processing and research of intelligent and refined data, information, and images [6].

It can be obtained from the statistical method of probability theory. Information entropy is the average uncertainty of the information source. It is defined in Shannon information theory as the elimination or reduction of people's understanding of uncertain things. This method can be achieved through sensor technology. The purpose of collecting and fusing information can provide good statistics on the information transmitted [7]. According to the principle of information theory, the information content of multidimensional information fused by single-dimensional information is greater than that of any single-dimensional information.

This is the purpose of multisensor information fusion [8]. The proof is as follows:

Because the entropy $H(X)$ of the random variable X can only be a function of its probability distribution p_1, $p_2, \cdots, p_n$, it is also recorded as follows:

$$H(X) = H(p_1, p_2, \cdots, p_n) \cong -\sum_{i=1}^{n} p_i \log p_i. \tag{1}$$

In Equation (1), $0 \le p_i \le 1$, so

$$H(p_1, p_2, \cdots, p_n) \ge 0. \tag{2}$$

If and only if each item is $-P_I \sum \log p_i = 0 (i = 1, 2, \cdots, n)$, the equal sign is true, namely, $p_i = 0$ or $p_i = 1$. And because of $\sum_{i=1}^{n} p_i = 1$, if and only if $p_i = 1, p_k = 0 (k \ne i, k = 1, 2, \cdots, n)$, the equal sign of Equation (2) holds [9].

Supposing the two sets of random variables are X and Y and the information entropy is $H(X)$ and $H(Y)$, respectively, then there is an additivity of information entropy to obtain the information entropy of the joint set XY:

$$H(XY) = H(X) + H(Y \mid X). \tag{3}$$

Supposing the probability distribution of events in the X set is $p_1, p_2, \cdots, p_n$, the conditional transition probability between the X set and the Y set is p_{ij}, and Equation (3) is expressed in the form of Equation (1), the information entropy of the two-dimensional random variable can be obtained as follows:

$$\begin{aligned} &H(P_1P_{11}, P_1P_{12}, \cdots, P_1P_{1n}, P_2P_{21}, P_2P_{22}, \cdots, P_2P_{2n}, \cdots, P_mP_{m1}, P_mP_{mn},) \\ &\quad = H(p_1, p_2, \cdots, p_n) + \sum_{I=1}^{m} P_I H(p_{i1}, \cdots, p_{im}). \end{aligned} \tag{4}$$

Among them,

$$\sum_{j=1}^{m} p_{ij} = \sum_{j=1}^{m} p_{i1} + p_{i2} + \cdots + p_{im}, \quad i = 1, 2, \cdots, n. \tag{5}$$

From Equation (2) and Equation (4), we can get the following:

$$\begin{aligned} &H(P_1P_{11}, P_1P_{12}, \cdots, P_1P_{1n}, P_2P_{21}, P_2P_{22}, \cdots, P_2P_{2n}, \cdots, P_mP_{m1}, P_mP_{mn}) \\ &\quad \ge H(p_1, p_2, \cdots, p_n). \end{aligned} \tag{6}$$

When N is a random variable $X_1, X_2, \cdots, X_n$, according to the additivity of information entropy, we can get the following:

$$H(X_1, X_2, \cdots, X_n) = H(X) + H(X_1 \mid X_2) + \cdots + H(X_n \mid X_1X_2, \cdots, X_{n-1}). \tag{7}$$

From Equations (6) and (7), it can be obtained that the information content of multidimensional information is greater than that of any single-dimensional information [10].

2.2. Sports Information Acquisition. At present, most people generally obtain sports information by some traditional methods, for example, through traditional media methods such as the Internet, TV, and newspapers. Such methods are very simple and require a large amount of data and support and require a lot of media to follow closely to obtain information [11]. The sports information acquisition based on the multisensor information fusion method we studied is completely different from the traditional method, and it is also very suitable for this fast-paced era [12]. The flow chart of obtaining sports information is shown in Figure 2:

CoreConnect is an integration technology developed and designed by IBM. It can connect many different chips to form a whole, and use this technology to reuse integration and core applications. In this experiment, we use this technology and the system can not only save costs but also improve system performance to a certain extent [13]. The CoreConnect bus contains its own bus (PLB), on-chip peripheral bus (OPB), 1 bus bridge, 2 arbiters, and 1 device control register (DCR) bus. The kernel needs to go through the OPB to access other system resources. Although the OPB bus is a synchronous bus, it is actually in an independent bus layer, providing unrelated 32-bit address bus and 32-bit data bus [14, 15]. Moreover, it is not directly connected to the core to connect to the processor core; the core can access peripherals through the "PLB to OPB" bridge, and the peripherals can access the memory through the "OPB to PLB" bridge. The logical structure of the self-designed IP core is shown in Figure 3, which includes the NAND FLASH control part, DMA high-speed data storage part, sensor data transmission part, and USB control part [16].

The three-axis accelerometer and the three-axis gyroscope in the MIMU sensor are composed of three orthogonal coordinate axes. The three measurement axes have different measurement properties, and the three measurement axes cannot guarantee two-by-two orthogonally [17]. The zero error can be expressed as follows:

$$g_0 = \begin{bmatrix} g_{x0} & g_{y0} & g_{z0} \end{bmatrix}^{\mathrm{T}}. \tag{8}$$

Among them, g_{x0} g_{y0} g_{z0} is the zero deviation of the x-axis, y-axis, and z-axis, respectively [18].

The sensitivity error is mainly caused by the different characteristics of the signal amplifier circuit on the three axes of the sensor.

$$S = S_n \begin{matrix} 1 & 0 & 0 \\ 0 & 1 & 0 \\ 0 & 0 & 1 \end{matrix} + \begin{matrix} \partial S_x & 0 & 0 \\ 0 & \partial S_y & 0 \\ 0 & 0 & \partial S_z \end{matrix} = \begin{matrix} S_x & 0 & 0 \\ 0 & S_y & 0 \\ 0 & 0 & S_z \end{matrix}. \tag{9}$$

Among them is the rated sensitivity of the MIMU sensor, and S_x, S_y, S_z is the sensitivity of the three axes [19].

The three coordinate axes of the MIMU sensor are completely orthogonal, but the three axes cannot be

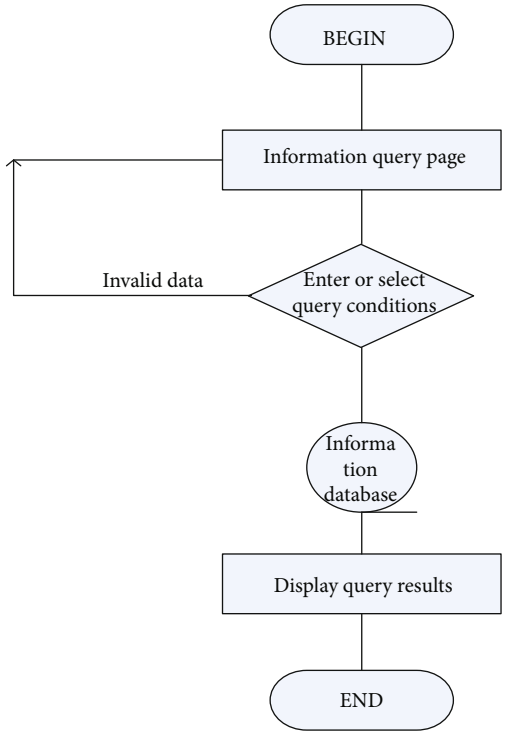

Figure 2: Flow chart of exercise information acquisition function.

guaranteed to be orthogonal in the sensor production process, resulting in nonorthogonal errors [20]. The nonorthogonal error can be expressed as follows:

$$C = \begin{matrix} \cos\alpha & 0 & \sin\alpha \\ \sin\beta\cos\gamma & \cos\beta\cos\gamma & \sin\gamma \\ 0 & 0 & 1 \end{matrix} \approx \begin{matrix} 1 & 0 & \alpha \\ \beta & 1 & \gamma \\ 0 & 0 & 1 \end{matrix}. \quad (10)$$

Generally, the nonorthogonal error angle of the MIMU sensor provided by the manufacturer is less than 0.5, so Equation (10) can be simplified [21]. Considering the above errors of the acceleration sensor, the true value g_e and the measured value g_m are as follows:

$$g_m = S \bullet C \bullet g_e + g_0 = D \bullet g_e + g_0. \quad (11)$$

Among them,

$$D = \begin{matrix} S_x & 0 & \alpha S_x \\ \beta S_y & S_y & \gamma S_y \\ 0 & 0 & S_z \end{matrix}. \quad (12)$$

Then,

$$g_e = E(g_m - g_0). \quad (13)$$

Among them,

$$E = A^{-1} = \begin{matrix} \frac{1}{S_x} & 0 & -\frac{\delta}{S_z} \\ -\frac{\gamma}{S_x} & \frac{1}{S_y} & \frac{\beta\gamma - \vartheta}{S} \\ 0 & 0 & \frac{1}{S_z} \end{matrix}. \quad (14)$$

Therefore, by calculating the zero error g_{x0}, g_{y0}, g_{z0}, the sensitivity error S, and the nonorthogonal error angles α, β, and γ, the measured value can be accurately calibrated to obtain the true value [22].

Ideally, the measured value A satisfies the following equation:

$$A^T \bullet A = (1G)^2. \quad (15)$$

That is, the acceleration modulus $\sqrt{(g_x)^2 + (g_y)^2 + (g_z)^2}$ of an ideal three-axis acceleration sensor in any posture is a fixed value g. The trajectory of the measured value A is a gravitational spherical surface with a radius of 1 g. Actually, due to various errors in the three axes of the acceleration sensor, the output trajectory will be an ellipsoid whose center deviates from the origin of the coordinates [23].

2.3. Functional Training System. After entering the 2010s, functional training entered our country and began to spread widely. Until now, although everyone has known that this is very beneficial for human training and recovery, the parties have not yet reached a consensus on the definition of a functional training system [24]. Gary Cook (1997) first put forward the concept of functional training. Functional training is an increase process that gradually improves athletic performance. At the very beginning, a model with high standard and high quality should be established. Firstly, it should correct poor posture and accelerate recovery from injuries. On this basis, the basic abilities of the human body, such as strength, speed, and balance, are further developed and repaired, and then, targeted repairs are carried out according to the different injury parts of different people. In the development of different movements according to specific abilities, the whole is similar to a pyramid [25]. The starting point of active-duty training is the mode of action. It can combine various functions by practicing human gestures and motion patterns in order to optimize the most basic exercise ability of the human body. Through functional spine strength energy chain recovery and regeneration, speed, explosive power, energy system, etc., it is used for systematic training and continuously strengthening the method system of cultivating sports talents. Execution system is the basic content of on-duty training. Studies have shown that healthy people have some limitations in completing their course of action. The main goal of functional training is to improve its implementation [26]. In daily life, it is necessary

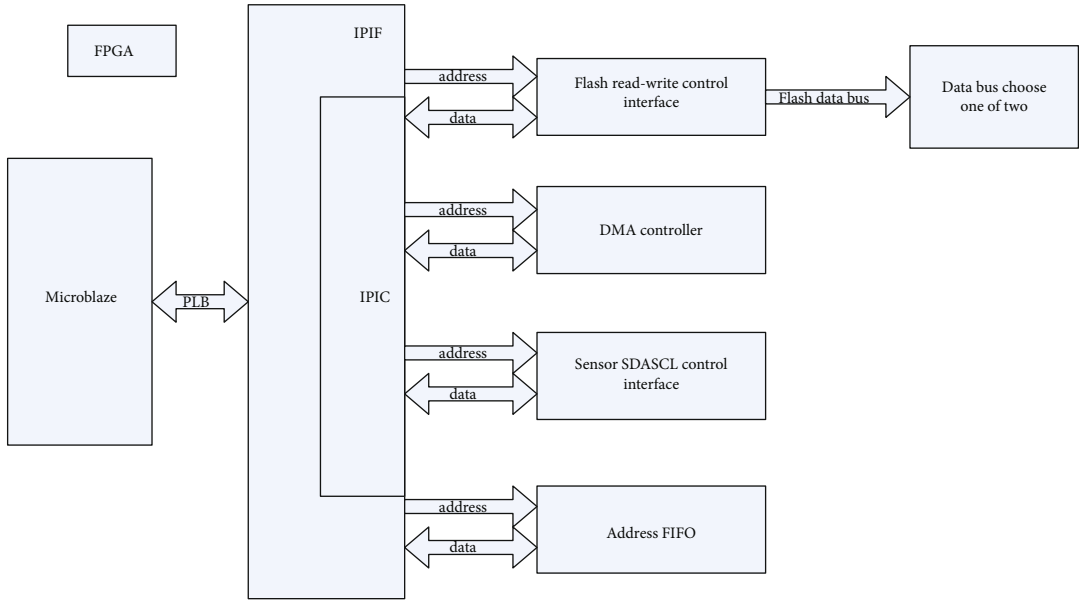

Figure 3: Internal logic diagram of self-designed IP core.

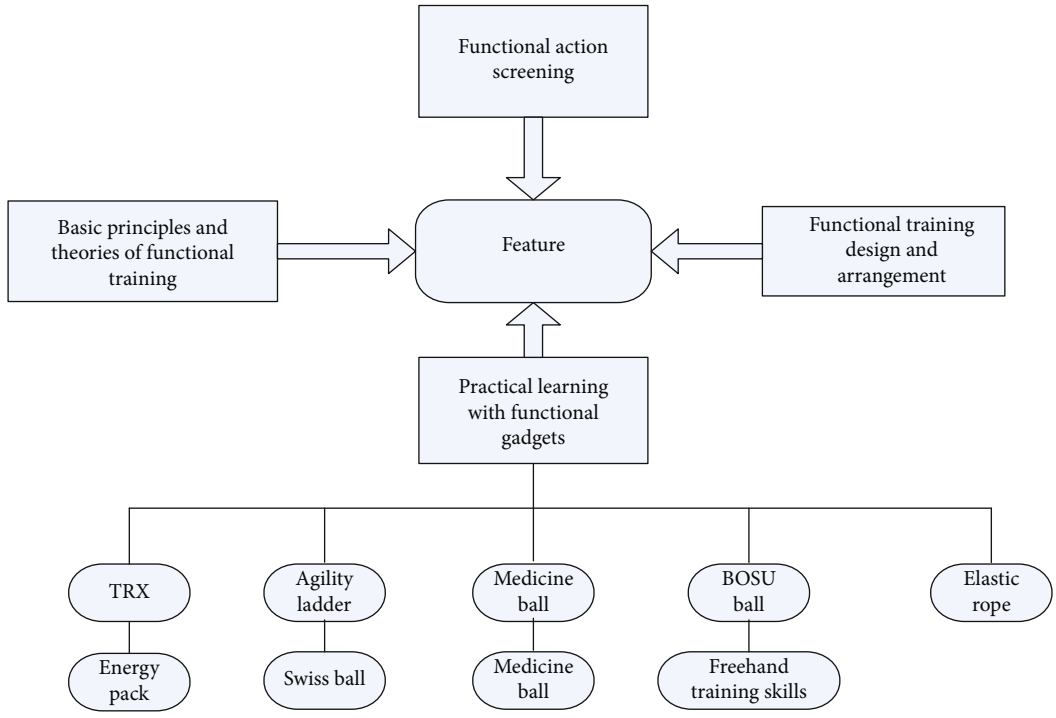

Figure 4: Detailed schematic diagram of the logical relationship of functional training.

to warm up and perform detailed system training and to ensure that you are not injured; you must train before you can enhance your physical fitness. Functional training is based on the principle of first evaluation and practice before you can carry out good training to improve our physical capabilities. In competitive sports, it seems to improve the ability of competitive athletes [27], as shown in Figure 4.

3. Multisensor Information Fusion Platform

3.1. Hardware Design. STMicroelectronics has developed the STM32 series of microarithmetic controllers. Its embedded application software system design has the advantages of high performance, low cost, and low power consumption. It has 32 bits developed based on the ARM Cortex-M3 core. Microcontroller uses the software in the experiment to

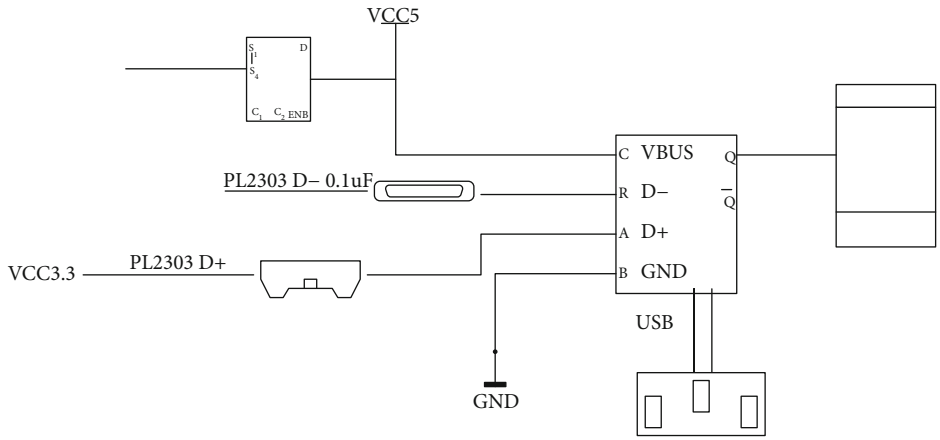

Figure 5: Detailed design drawing of the power circuit.

perform calculation and storage functions of related information. The power consumption of the code read and executed from flash is only 36 mA, which is equivalent to 0.5 mA/MHz. Compared with all 32-bit microprocessors on the market, the power consumption of STM32F103 is the lowest. At the beginning of the design, the serial port was designed to communicate with the PC. Since the notebook is more convenient to carry and easy to debug, and the PC does not have a serial port, it is designed to use USB power supply. This power supply mode is convenient, simple, and fast, compared to the conventional power supply mode which has great flexibility. Considering that the power cord needs to be tightly connected to the development board when power is supplied, and cannot be loosened, based on this principle, the USB interface type at the PCB board adopts the way of USB to square port. The USB power supply circuit is shown in Figure 5. This method is relatively simple and fast and can obtain a stable 5 V voltage directly from the USB. If the 5 V voltage is self-made, the power supply voltage may not be stable enough due to the operation of the manufacturing process or the device. In addition, at the beginning of the design, it was considered that the power consumption of all devices when working at the same time was less than 2 W, and the maximum power of USB power supply reached 2.5 W, which can meet the power consumption requirements of the system of 3.3 V power supply requirements of some devices.

3.2. Software Design. This article uses the USB interface protocol as the communication interface between the system and the PC and sends command codes to the system through the PC to control system formatting, acquisition, and configuration parameters. The most important thing is to save the data collected by the system to the PC for analysis. This system uses FIDI's high-speed FT256 chip as the control chip for USB communication. The USB read and write control signals DR and WR and RXF and TXE status signals are directly connected to the FPGA chip. Directly address the registers through the MicroBlaze soft core, control the read and write modules, and read the status of RXF and TXE. The MicroBlaze soft core in the FPGA performs data reading and writing by controlling the coordination of various modules. There is a FIFO buffer area inside the USB chip. When RXF is low, it means that the FIFO-receiving buffer has received a byte of data from the host computer. When the RD read signal arrives at a low level, The FIFO controller in the chip will release the data bus. The FIFO data is released to the 8-bit data bus. At this time, the data on the bus is transferred to the soft core through the PLB bus, and the data at the 28PC end is transmitted to the system. After that, the RD signal is pulled high, and the RXF signal is also pulled high, indicating that the FIFO-receiving buffer is already empty and waiting for new data to be added.

3.3. Multisensor Information Fusion Platform. This article is based on the fusion of multisensor information to obtain traditional sports information and conduct an in-depth study on the way of functional training. Multisensor information fusion (MSIF) technology uses the latest computer science and technology to obtain data and information from a large number of ordinary sensors under certain rules or guidelines. The rules and guidelines include sensor technology, fusion principles, and information transmission. The rules are established by the parties. Information or data is researched or comprehensively analyzed to finally achieve the real-time information processing process for the desired results and decision-making. With the gradual development and maturity of various sensor application technologies, computer software and hardware technologies, and data information processing technologies since the 21st century, multi-information sensing technology has become a very popular technology in recent years. It is also very popular. Place multiple ordinary sensors in different locations to perform operations such as data perception, collection, processing, and the ability to give feedback to the processed information to the background for subsequent operations. This technology is called multi-information sensing technology. The technology can collect information operation because there are many different sensors placed in different locations. With the gradual deepening of science and technology, multi-information sensor fusion technology will be more and more in-depth research, and in the future, it will surely become a professional technology that integrates refined data, intelligent information, and image processing.

However, the multisensor information fusion platform is also an immature platform technology. The multi-information fusion system is also a complex system with very strong uncertainty. The processing method of the platform has also received existing technology, equipment, theoretical knowledge, and limits. Although this is a newly developing subject, there are still many theoretical knowledge shortages. However, with the continuous development of science and technology and related subjects in the future, I believe that we will gradually come into contact with it and experience it in our future study and life to the convenience it brings us.

4. Analysis and Discussion

4.1. Data Analysis Based on Multisensor Information Fusion. Relying on the multisensor information fusion platform, this paper uses multisensor information fusion technology to study the acquisition of traditional sports information and functional training. Among them, we have done some questionnaires for the acquisition of sports information. Information is a survey and research conducted on different people of different ages and classes within the whole school. People's motivation for contact is shown in Table 1. People's motivations for acquiring sports information include increasing sports knowledge, understanding domestic and foreign sports competitions, studying, enjoying sports, wanting to improve conversation skills, leisure and entertainment, coping with exams, passing time, and others.

There are commonalities among different individuals, but there are also personalities between them. Differences in gender, age, and occupation affect the ways and motivations of different people to contact sports information. Table 2 shows that gender differences make different groups of people have great differences in their exposure to sports information. In terms of increasing sports knowledge, understanding domestic and foreign sports competitions, and enjoying sports, men far surpass women. However, in terms of learning and leisure and entertainment, there are far more women than men in dealing with exams and so on. People of different ages also have different purposes for acquiring sports information. The younger ones are mostly motivated to improve communication skills, leisure and entertainment, and pass time, while the older ones are to increase their sports knowledge and understand domestic and foreign sports competitions. Wait. The level of income also affects the motivation of obtaining sports information to a certain extent. Those with high income have slightly lower motives than those with lower incomes except for understanding domestic and foreign sports events, learning, and other motives, and other motives are higher than those with lower incomes. People with low levels rely more on sports information to meet their own needs.

In daily life, people have different ways to obtain sports information, including newspapers, television, Internet, and radio, and the types of sports-related information obtained based on different ways are also diverse. According to the different functions and attributes of the media, the sports information obtained is roughly divided into news, entertainment, and knowledge. There are six types of people getting more sports information: news, entertainment, knowledge, comprehension, education, and comment. Our research is based on specific data obtained on this basis. The details of the data are shown in Table 3.

Table 1: People's motivation for obtaining sports information.

	Number of people	%
Increase sports knowledge	1085	21.3
Understand domestic and foreign sports competitions	1145	22.5
Learn	821	16.0
Love sport	395	7.7
Want to improve conversation skills	263	5.1
Leisure and entertainment	956	18.7
Overcome exam	204	4.0
Kill time	196	3.8
Others	35	0.6

Sports information cognition means that sports participants have a systematic understanding and understanding of some basic sports and common knowledge. With more and more knowledge and understanding, they have a higher level of awareness of sports. The promotion function makes it easier to obtain detailed sports information, which is also of great benefit to the formation of sports behaviors. As shown in Figure 6, when conducting surveys and researches on people at various stages, it was found that different groups of people have different degrees of agreement on the cognitive impact of sports information, but in general, sports information has a significant impact on the sports of most people. The increase of sports knowledge and the understanding of sports have a very obvious effect; that is, obtaining sports information helps different people's cognition of sports.

The gradual improvement process of actual sports performance is fast and standardized. A cumulative process that gradually increases with the performance in the experiment is called functional training. At the very beginning, a standard and high-quality model is established instead of starting from the basics. Establishing a high standard for experimentation can achieve an expected experiment purpose. First, correct poor posture and accelerate recovery from injuries. On this basis, it is necessary to improve the basic abilities of the human body, such as strength, speed, balance, which are further developed and repaired, and then, targeted repairs are carried out according to different injured parts of different people. Different actions are developed according to specific abilities. The whole is similar to a pyramid. The basic action patterns of the human body are shown in Table 4. When receiving different information, the feedback of the human body's perception in the brain is reflected in different areas.

In recent years, as the number of exercisers has increased year by year, the number of injured people has also increased year by year. Excluding professional athletes, in daily learning exercises, failure to master the correct exercise methods can easily cause injuries, o professional functions are important and the most basic. Sex training becomes very

Table 2: Motivation of different groups of people to contact sports information.

Motivation	Male	Female	Old	Young	Low	High
Increase sports knowledge	54.8	39.4	52.0	42.9	47.2	46.7
Understand domestic and foreign sports competitions	63.4	36.3	54.9	45.5	47.8	52.1
Learn	33.2	38.5	38.9	30.0	40.0	34.4
Love sport	26.8	8.3	19.9	15.7	17.1	17.8
Want to improve conversation skills	11.6	10.7	9.0	12.1	12.3	8.5
Leisure and entertainment	56.9	60.2	56.0	60.1	62.6	53.5
Overcome exam	5.5	11.4	8.1	8.7	10.1	6.3
Kill time	19.2	27.0	19.0	26.0	23.7	22.5
Others	0.7	0.7	0.41	0.9	0.5	1.0

Table 3: Types of people getting more sports information.

	News	Entertainment	Knowledge	Comprehension	Education	Comment
Number	1366	1427	890	708	478	514
%	59.4	62.1	38.7	30.8	20.8	22.3
Sorting	2	1	3	4	6	5

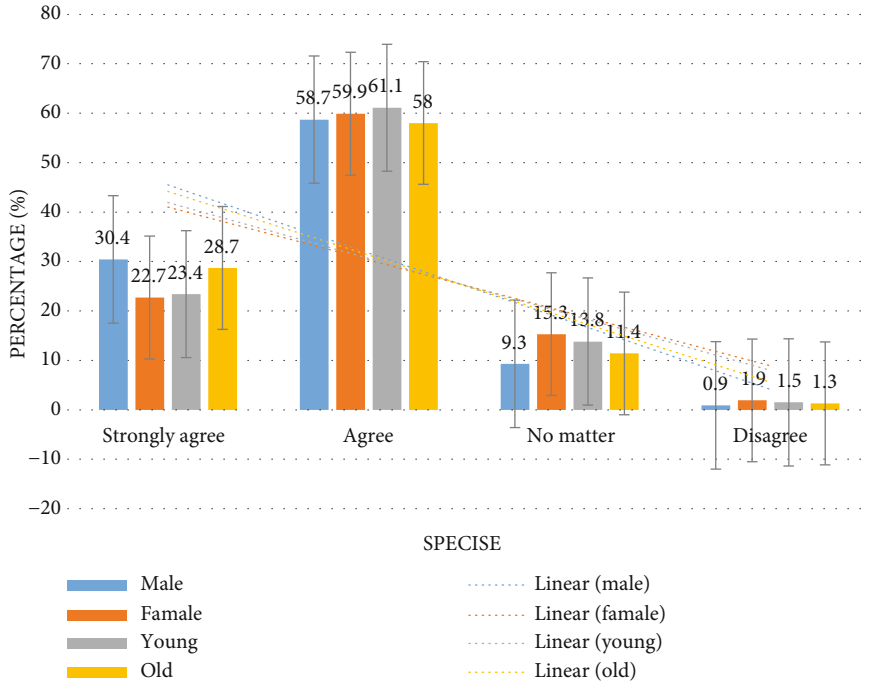

Figure 6: The influence of obtaining sports information on sports cognition of different groups of people.

Table 4: Patterns of basic human movements.

Basic action mode	Daily life example	Examples of fitness life
Squat	Sit and stand	Weight-bearing squat exercise
Lunge	Go up the stairs	Lunge walking practice
Gait	Walking or running	Rhythm running
Body flexion	Bent over to pick up things	Back lifting exercises
Body rotation	Turn around to take something	Upper body diagonal pull exercise
Push support	Push the door or prop up the body	Push-up exercises

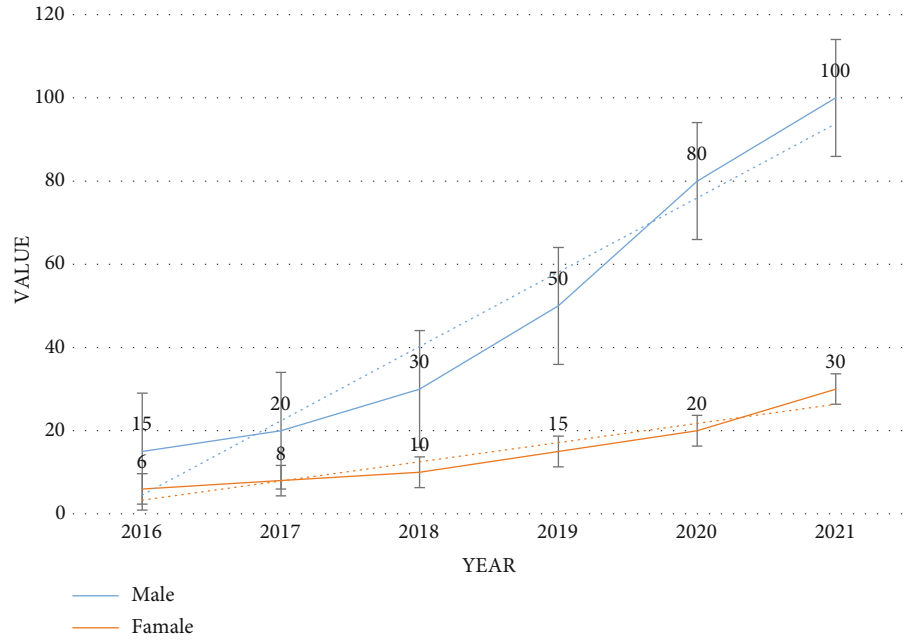

Figure 7: The total number of people in functional training in different places across the country.

Table 5: Selective functional action assessment content and purpose.

Serial number	Name	Evaluation purpose
1	Cervical spine assessment	Neck spine flexion and extension degree, atlanto-occipital joint flexibility, and neck The degree of spinal rotation and lateral flexion
2	Evaluation of upper limb movement patterns	The entire range of shoulder movement, including internal and external rotation, abduction, adduction, extension, and flexion The activity of the song
3	Multistep buckling assessment	Normal flexion of both hips and spine
4	Multistep stretch evaluation	Normal extension of the shoulders, hips, and spine
5	Standing on one foot assessment	Static and dynamic single-leg stability
6	Squat with arms up head	Symmetrical flexibility of both hips, knees, and ankles

important. This paper conducts functional training research on the basis of multisensor information fusion. As shown in Figure 7, the number of functional training in different parts of the country in the past 6 years has changed greatly compared with before. This makes our research very meaningful.

After the initial screening and finding out the functional actions, we can formulate different training programs for different people according to the specific results and start targeted training. If there is damage or bad actions during training it can be adjusted in time. In this case, a selective functional movement assessment (SFMA) is required to carry out strict and standardized training in the later stage according to the patient's adaptability and personal physique, as shown in Table 5:

4.2. Discussion. Multisensor information fusion technology is to use the most popular computer, 5G, Internet of Things, and other technologies and use a variety of different sensors or information and data from a variety of different sources. Information or data is summarized and analyzed, and a detailed result is finally obtained to complete an information processing process for the final decision. There are many ways to obtain sports information. People use different ways and methods to obtain different sports information. With the support of a multisensor information fusion platform, we can go through a variety of ways. Different information sources can easily obtain a lot of sports information, so as to finally get the information you want to get. Traditional functional training is a training that teaches people how to use strength with the help of professionals. It is a complete, systematic, and planned training and functional training based on multisensor information fusion; it is more suitable for the current era than the traditional ones and can help people complete the corresponding training faster.

5. Conclusions

This article is a research on sports information acquisition and functional training based on multisensor information

fusion technology. In the past, traditional ways to obtain sports information included newspapers, radio, and television. The advantage is that the information source of the traditional method is single but true and reliable. The disadvantage is that the transmission is slower than the latest information, and the efficiency is very low. Functional training is a very professional technology before, and it requires professional staff to operate. It is difficult for ordinary people to perform after being injured, so based on the functionality of multisensor information fusion technology, training can facilitate scientific and systematic training. Since the beginning of the 21st century, the multisensor information fusion technology has developed rapidly. Some people are focusing on and developing new calculation models, while others want to modify the original traditional algorithms to achieve better results. Information fusion is a development direction in the future. It will be a trend in the world in the next few years and even decades, and our research will follow the trend in the future sports information acquisition and functional training be utilized.

Data Availability

No data were used to support this study.jjj

Conflicts of Interest

The authors declare that there is no conflict of interest with any financial organizations regarding the material reported in this manuscript.

Acknowledgments

This study was funded by the fund project of the State Ethnic Affairs Commission (No. 2020-GMD-080) and the National Social Science Fund of China (No. 17CTY008).

References

[1] Z. Yu, L. Chang, and B. Qian, "A belief-rule-based model for information fusion with insufficient multi-sensor data and domain knowledge using evolutionary algorithms with operator recommendations," *Soft Computing*, vol. 23, no. 13, pp. 5129–5142, 2019.

[2] J. Raitoharju, S. Kiranyaz, and M. Gabbouj, "Training radial basis function neural networks for classification via class-specific clustering," *IEEE Transactions on Neural Networks and Learning Systems*, vol. 27, no. 12, pp. 2458–2471, 2016.

[3] C. Á. Raquel, H. C. Aurora, and L. P. Josefa, "Fusion estimation from multisensor observations with multiplicative noises and correlated random delays in transmission," *Mathematics*, vol. 5, no. 3, pp. 45–45, 2017.

[4] X. Zhou and P. Jiang, "Variation source identification for deep hole boring process of cutting-hard workpiece based on multi-source information fusion using evidence theory," *Journal of Intelligent Manufacturing*, vol. 28, no. 2, pp. 255–270, 2017.

[5] M. Zhou, Y. Long, W. Zhang et al., "Adaptive genetic algorithm-aided neural network with channel state information tensor decomposition for indoor localization," *IEEE Transactions on Evolutionary Computation*, p. 1, 2021.

[6] P. Gong, Y. Fei, and L. Song, "Road recognition method of wheel-tracked robot based on multi-sensor information fusion," *Shanghai Jiaotong Daxue Xuebao/Journal of Shanghai Jiaotong University*, vol. 51, no. 4, pp. 398–402, 2017.

[7] M. Mosalanejad and M. M. Arefi, "UKF-based soft sensor design for joint estimation of chemical processes with multi-sensor information fusion and infrequent measurements," *IET Science, Measurement & Technology*, vol. 12, no. 6, pp. 755–763, 2018.

[8] W. Bohuai, "Research on data acquisition and fusion system based on wireless sensor," *Acta Technica CSAV (Ceskoslovensk Akademie Ved)*, vol. 62, no. 1, pp. 469–477, 2017.

[9] J. Li and C. Wang, "Research on efficient fusion methods for reliable information in wireless sensor networks," *Revista de la Facultad de Ingenieria*, vol. 32, no. 11, pp. 583–587, 2017.

[10] K. H. Byun, S. J. Kim, and J. W. Kwon, "Development of a multi-sensor fusion-based traffic information acquisition system with robust to environmental changes using mono camera, radar and infrared range finder," *The Journal of the Korea Institute of Intelligent Transport Systems*, vol. 16, no. 2, pp. 36–54, 2017.

[11] L. Zheng, R. Ji, W. Liao, and M. Li, "A positioning method for apple fruits based on image processing and information fusion," *IFAC-Papers OnLine*, vol. 51, no. 17, pp. 764–769, 2018.

[12] X. Xu, M. Wang, L. Luo, Z. Meng, and E. Wang, "An indoor pedestrian localization algorithm based on multi-sensor information fusion," *Journal of Computer and Communications*, vol. 5, no. 3, pp. 102–115, 2017.

[13] Y. Xu, L. Chen, Z. Yuan, and T. Xie, "Intelligent recognition of tool wear conditions based on the information fusion," *Zhendong yu Chongji/Journal of Vibration and Shock*, vol. 36, no. 21, pp. 257–264, 2017.

[14] R. Miyagusuku, A. Yamashita, and H. Asama, "Data information fusion from multiple access points for WiFi-based self-localization," *IEEE Robotics & Automation Letters*, vol. 4, no. 2, pp. 269–276, 2018.

[15] M. Zhou, Y. Li, M. J. Tahir, X. Geng, Y. Wang, and W. He, "Integrated statistical test of signal distributions and access point contributions for Wi-Fi indoor localization," *IEEE Transactions on Vehicular Technology.*, vol. 70, no. 5, pp. 5057–5070, 2021.

[16] Q. Bi, X. Jiang, X. Liu, L. He, and T. Cheng, "Information fusion of imaging that high dynamic range in welding region based on image registration," *Shanghai Jiaotong Daxue Xuebao/Journal of Shanghai Jiaotong University*, vol. 50, no. 12, pp. 1915–1920, 2016.

[17] J. Yang and Q. Na, "Avoiding obstacle system of intelligent vehicle based on multi-sensor information fusion," *IPPTA: Quarterly Journal of Indian Pulp and Paper Technical Association*, vol. 30, no. 8, pp. 800–807, 2018.

[18] H. Yuan and G. Wu, "Fault diagnosis of transformer based on multi-information fusion," *Gaoya Dianqi/High Voltage Apparatus*, vol. 54, no. 9, pp. 103–110, 2018.

[19] D. Xu, M. Xing, J. Fu, and G. Sun, "Multi-aspect components extraction and fusion based on attributed scattering center model," *Xi Tong Gong Cheng Yu Dian Zi Ji Shu/Systems Engineering and Electronics*, vol. 39, no. 6, pp. 1197–1202, 2017.

[20] B. J. Liu, Q. W. Yang, W. U. Xiang, S. D. Fang, and F. Guo, "Application of multi-sensor information fusion in the fault

diagnosis of hydraulic system," *International Journal of Plant Engineering & Management*, vol. 22, no. 1, pp. 12–20, 2017.

[21] L. Li, L. Hui, and S. Li, "Intelligent fire monitoring system based on the information fusion algorithm," *Sensor Letters*, vol. 14, no. 11, pp. 1094–1098, 2016.

[22] M. Liu, J. Chen, X. Zhao, L. Wang, and Y. Tian, "Dynamic obstacle detection based on multi-sensor information fusion," *IFAC-Papers OnLine*, vol. 51, no. 17, pp. 861–865, 2018.

[23] X. Ouyang, W. He, W. Lu, and Z. Bian, "Study on 3D border surveillance system and multi-sensor information fusion technology," *Bandaoti Guangdian/Semiconductor Optoelectronics*, vol. 39, no. 2, pp. 298–304, 2018.

[24] Z. Ming, L. Yun, and H. Gang, "Multi-sensor information fusion predictive control algorithm," *International Journal of Multimedia and Ubiquitous Engineering*, vol. 11, no. 4, pp. 49–58, 2016.

[25] X. Zhu, T. Shi, X. Jin, and Z. Du, "Multi-sensor information fusion based control for VAV systems using thermal comfort constraints," *Building Simulation*, vol. 14, no. 4, pp. 1047–1062, 2020.

[26] L. Yue, D. K. Jha, A. Ray, and T. A. Wettergren, "Information fusion of passive sensors for detection of moving targets in dynamic environments," *IEEE Transactions on Cybernetics*, vol. 47, no. 1, pp. 93–104, 2016.

[27] W. Cai, S. Guo, S. Zhang, and J. Lin, "Unified framework of modeling and simulations for multi-platforms multi-sensors multi-objects source information fusion (M3SIF) system," *Journal of Information Hiding and Multimedia Signal Processing*, vol. 9, no. 3, pp. 760–767, 2018.

Hindawi
Journal of Sensors
Volume 2021, Article ID 6140914, 9 pages
https://doi.org/10.1155/2021/6140914

Research Article

Passive Localization of Moving Target with Channel State Information

Xiaolong Yang, Jiacheng Wang, Wei Nie, and Yong Wang

School of Communication and Information Engineering, Chongqing University of Posts and Telecommunications, Chongqing 400065, China

Correspondence should be addressed to Xiaolong Yang; yangxiaolong@cqupt.edu.cn

Received 26 June 2021; Accepted 17 August 2021; Published 31 August 2021

Academic Editor: Bin Gao

With the popularity of wireless networks and smart devices, wireless signal-based passive target sensing and localization have become a hot research topic and attracted numerous researchers' interests. The existing passive localization solutions require multiple receivers, which is not practical for real-world applications. In response to this compelling problem, in this paper, we propose a practical single access point-based passive moving target localization system. Concretely, it first utilizes multiple antennas of the access point to form an antenna array and extended antenna, to capture channel state information (CSI) at different spatial locations. Then, leveraging the obtained CSI, the signal parameters, including the angle of arrival (AoA) and time of flight (ToF), are estimated. Based on the estimated signal parameters and the locations of the antenna array and extended antenna, finally, the passive localization of the moving target is realized. Comprehensive experiments are conducted under the real-world scenario with two different test platforms, and the experimental results show the proposed algorithm's median localization can reach 1.087 m when the number of antennas is 4 and the signal bandwidth is 80 MHz, demonstrating the effectiveness of the proposed algorithm.

1. Introduction

With the ubiquitous penetration of wireless signals and high levels of public acceptance of smart devices, passive localization has become a research hotspot, with important applications, including security surveillance [1] and elderly care [2]. During the last few years, diverse methods have been used for the passive localization, such as visible light [3, 4], infrared [5, 6], and ultrasound [7, 8]. Some of these systems can realize an impressive localization accuracy. However, for the real-world passive localization, the Wi-Fi-based system stands out as a particularly promising method, due to the pervasive availability of Wi-Fi access points (APs) [9], especially with the emergence and use of PHY channel state information (CSI) in recent years [10].

Typically, Wi-Fi-based localization systems can be divided into two main categories. The first one works in an active manner, which always employs multiple receivers (or single receiver) to capture signal travels from the transmitter to the receiver directly and extract signal parameters, such as received signal strength (RSS) [11], angle of arrival (AoA) [12], time of flight (ToF) [13], and angle of departure (AoD) [14], to realize indoor localization of the transmitter. For example, BMW [15] employs the output of the 9-axis sensor coupled with the pedestrian dead reckoning (PDR) algorithm to get a location estimation. On this basis, BMW fuses the estimated location with the RSS localization result via Kalman filter, to realize the localization of the user. Leveraging the CSI obtained by multiple receivers, the classic system SpotFi [16] estimates the signal AoA and combines the extracted AoA with the received signal strength (RSS) to realize the localization of the signal transmitter. Combining the CSI with deep learning, DeepFi [17] trains all weights of the deep network as fingerprints in the off-line training phase and employs a greedy learning algorithm to reduce complexity. During the online localization phase, DeepFi uses a probabilistic method based on the radial basis function to realize localization. ToneTrack [18] proposes a novel algorithm, which combines time-of-arrival (ToA) data from different transmissions as a mobile device hops across different

channels, approaching time resolutions previously not possible with a single narrowband channel. On this basis, it can accurately estimate the signal ToF and achieve localization based on the estimated ToF. Recent work *M3* [19] jointly estimates AoA, relative ToF (rToF), and AoD based on the CSI extracted from a single receiver and pinpoints the transmitter based on these extracted parameters, under the line-of-sight (LoS) scenario. Some other researchers [20] first construct constraints by using ToF differences between reflection paths and direct path. Then, with the help of AoA, they develop a Particle Swarm Optimization- (PSO-) based searching algorithm to realize the target and reflection point localization.

The other one is the device-free localization system, which works in a passive manner, indicating they achieve the localization without the requirement for having the user carry any wireless-enabled devices [21–25]. Essentially, this kind of system focus on estimating parameters of the signal reflected from the target. On this basis, these systems utilize the estimated signal parameters and the spatial location of the receiver to construct geometric constraints, so as to realize passive localization of the target. For instance, IndoTrack [12] estimates the Doppler and AoA of the signal reflected by the target through the CSI obtained by multiple receivers, which are deployed in different spatial locations. Then, it estimates target velocity and location to rebuild the absolute trajectory of the moving target through the proposed probabilistic comodeling of spatialtemporal Doppler and AoA information, which are estimated from the CSI obtained by multiple receivers. Leveraging the incoherence between the direct signal and target-induced reflection (TIR), MaTrack [26] estimates the AoA of the TIR and combines the estimated AoA with the locations of receivers to achieve passive target localization. By using the three-dimensional multiple signal classification (3D-MUSIC) algorithm and the proposed interference cancellation algorithm, our previous work [27] estimates the AoA, ToF, and Doppler frequency shift (DFS) of the TIR under the through-the-wall (TTW) scenario, so as to achieve TTW passive moving target localization. Some other systems, such as Widar 2.0 [28] and mD-Track [14], use SAGE [29], cross-correlation, and other algorithms to estimate more signal parameters, including ToF, AoA, AoD, and DFS, and construct geometric constraints based on the estimated signal parameters and locations of transmitter and receiver, to achieve passive localization of the target. These systems rely on accurate signal parameters estimation, indicating the resolvability is important for these systems. So, some recent works attempt to enlarge the antenna array by physically moving the antenna and form a larger bandwidth by combining adjacent channels via channel hopping [30, 31], so as to further improve the signal parameter estimation accuracy and localization accuracy.

Although promising, it is not difficult to see that all above mentioned passive localization systems strongly rely on the assumption, that is, no matter how many receivers are involved in passive localization, the location of the transmitter is fixed and preacquired. This assumption could be broken easily under the real-world scenario, since the user may move their device (such as laptop and cell phone, which may act as the signal transmitter), driving the location of transmitter unpredictable and finally lead to a failure in passive localization. So, we ask the following question: is it possible to realize the passive localization with only one receiver, while holding no requirement for the preobtaining location of the transmitter?

In this paper, we propose a single receiver-based passive localization system SR-PLoc, which employs the CSI measurements obtained by a single receiver to achieve passive localization of the target without preobtaining the location of the transmitter or assuming it is never changed. The essential observation lies in SR-PLoc is that the phase errors [31], including carrier frequency offset (CFO), sample frequency offset (SFO), and packet detection delay (PDD), are caused by the unsynchronization between transmitter and receiver and hardware imperfection, indicating all propagation paths (including the direct path from the transmitter to the receiver and the TIR) recorded by CSI, undergo the same phase error. Leveraging this fact, SR-PLoc first uses multiple antennas of the receiver to form an antenna array and extended antenna, so as to capture the CSI at different locations. Based on the obtained CSI, SR-PLoc estimates AoA and ToF of the direct signal and TIR. Finally, SR-PLoc combines the estimated signal parameters with the locations of the antenna array and extended antenna to construct geometric constraints, so as to realize the passive localization of the moving target. Unlike the previous works, the proposed SR-PLoc achieves the passive localization of the moving target with only one receiver, while holding no need for preobtaining the location of the transmitter. We build two test platforms and carry out rich experiments under the real-world scenario. The experimental results demonstrate the effectiveness and practicability of the proposed algorithm.

2. Materials and Methods

SR-PLoc aims to realize passive localization of moving target with a single receiver; the whole localization process mainly includes three steps, as Figure 1 shows.

2.1. CSI Obtaining and Signal Parameter Estimation. Considering a receiver with multiple antennas, SR-PLoc builds a uniform linear array (ULA) with antenna spacing of half-wavelength and extended antenna to capture the CSI at different locations, as Figure 1 shows. At time t, the reported CSI measurements extracted from ULA and extended antenna can be expressed as

$$\begin{cases} \mathbf{h}(t) = \begin{bmatrix} h_{1,1}(t) & \cdots & h_{1,K}(t) \\ \vdots & \ddots & \vdots \\ h_{I,1}(t) & \cdots & h_{I,K}(t) \end{bmatrix}, \\ \mathbf{c}(t) = [c_1(t) \cdots c_K(t)] \end{cases} \tag{1}$$

where $h_{i,k}$ is the CSI corresponding to kth subcarrier of the i th antenna of the ULA, $c_k(t)$ is the CSI extracted from the k th subcarrier of the extended antenna, and I and K are the

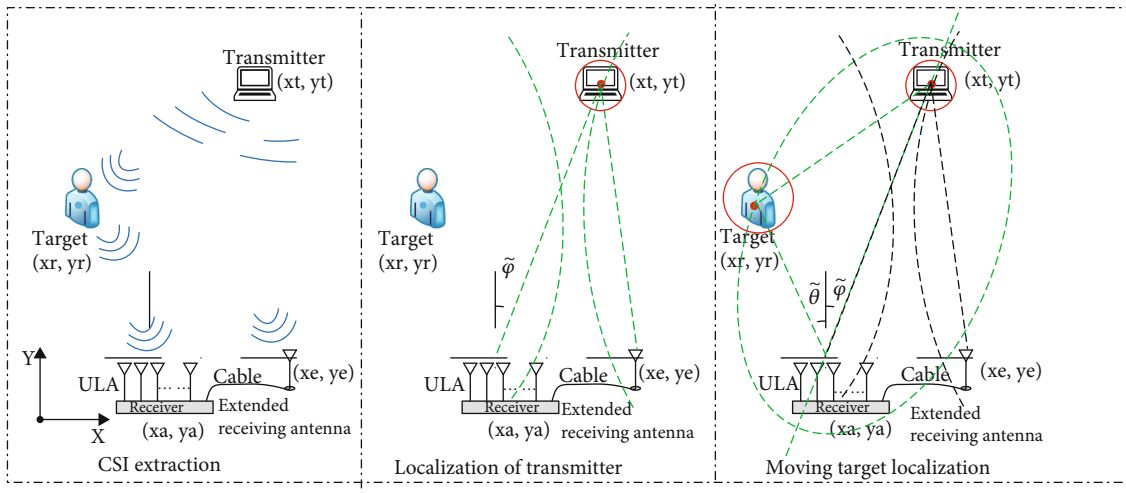

Figure 1: System overview of SR-PLoc.

number of antenna and subcarrier, respectively. Taking the multipath effect into consideration, the received signal is a superposition of multiple signals. Thereby, we have

$$\begin{cases} h_{i,k} = \sum_{r \in G_R} h_{i,k}^r + \sum_{d \in G_D} h_{i,k}^d + n_{i,k}, \\ c_k = \sum_{r \in G_R} c_k^r + \sum_{d \in G_D} c_k^d + n_k, \end{cases} \tag{2}$$

where $h_{i,k}$ is the CSI extracted from the kth subcarrier of the ith antenna; G_R and G_D are the sets of the direct path and reflection path components, respectively; c_k is the CSI extracted from the kth subcarrier of the extended antenna; and $n_{i,k}$ and n_k are the noise. Without loss of generality, for any propagation path $l \in \{G_D \cup G_R\}$, one can see that the CSI extracted from ULA and extended antenna can be denoted as

$$\begin{cases} h_{i,k}^l = \alpha_l e^{-j2\pi f_k \tau_l} \times e^{-j\pi(i-1)\times(f_k/f_c)\times \sin(\theta_l)} + n_{i,k}^l, \\ c_k^l = \alpha_l' e^{-j2\pi f_k \tau_l'} + n_k^l, \end{cases} \tag{3}$$

where α_l, τ_l, θ_l, and $n_{i,k}^l$ are the attenuation, ToF, AoA, and noise of the lth propagation path, respectively, corresponding to the ULA; f_c is the central frequency; $f_k = f_c + (k-1)\Delta f$ is the frequency of the kth subcarrier; Δf is the frequency spacing between two adjacent subcarriers; and α_l', τ_l', and n_k^l are the attenuation, ToF, and noise of the lth propagation path, respectively, corresponding to the extended antenna. In practice, due to the phase error induced by PDD, CFO, SFO, the real CSI extracted from the antenna array and extended antenna can be denoted as

$$\begin{cases} h_{i,k}^l = \alpha_l e^{-j2\pi f_k \tau_l} \times e^{-j\pi(i-1)\times(f_k/f_c)\times \sin(\theta_l)} \times e^{-j2\pi f_k(\lambda_b+\lambda_o)} e^{-j2\pi\beta} + n_{i,k}^l, \\ c_k^l = \alpha_l' e^{-j2\pi f_k \tau_l} \times e^{-j2\pi f_k(\lambda_b+\lambda_o)} e^{-j2\pi\beta} + n_k^l, \end{cases} \tag{4}$$

where λ_b and λ_o are the time offset introduced by the PDD and SFO, respectively, and $e^{-j2\pi\beta}$ is the phase offset induced by CFO. When the target moves within the detection area, the propagation path length of the TIR changes accordingly, which introduces a nonnegligible DFS to the human-induced reflection (HIR) $f_{D=}f_c \times v_t/c$, where v_t is the speed of path length change and c is the speed of light. Considering the time interval between two adjacent CSI packets is Δt, at time $(t + \Delta t)$, we have

$$\begin{cases} \mathbf{h}(t+\Delta t) = \mathbf{h}(t) \times e^{-j2\pi\Delta t \times f_D} = \mathbf{h}(t)\varphi(v), \\ \mathbf{c}(t+\Delta t) = \mathbf{c}(t) \times e^{-j2\pi\Delta t \times f_D} = \mathbf{c}(t)\varphi(v). \end{cases} \tag{5}$$

Taking the first CSI measurements as a reference, for a CSI trace with M measurements, we have

$$\begin{cases} \mathbf{H} = \left[1, \varphi(v), \cdots, \varphi^{M-1}(v)\right] \otimes \mathbf{h}(t), \\ \mathbf{C} = \left[1, \varphi(v), \cdots, \varphi^{M-1}(v)\right] \otimes \mathbf{c}(t), \end{cases} \tag{6}$$

where $\otimes$ represents the Kronecker product. Based on the above analysis, it can be seen that, through the phase difference between antennas, subcarriers, and measurements, the CSI trace describes the AoA, ToF, and the DFS, respectively. So, the 3D-MUSIC algorithm, presented in our previous work [27], is used to estimate signal AoA, ToF, and DFS jointly. Taking the CSI received by the array as an example, here, we briefly describe the estimation process. First, we rewrite the CSI trace as

$$\begin{aligned} \mathbf{H} = \exp(-j2\pi f_1 \tau) \left[1, \varphi(v), \cdots, \varphi^{M-1}(v)\right]^{\mathrm{T}} \\ \otimes \left[1, \omega(\theta), \cdots, \omega^{I-1}(\theta)\right]^{\mathrm{T}} \otimes \left[1, \xi(\tau), \cdots, \xi^{K-1}(\tau)\right]^{\mathrm{T}}, \end{aligned} \tag{7}$$

where

$$\begin{cases} \xi(\tau) = e^{-j2\pi\Delta f \tau}, \\ \omega(\theta) = e^{-j2\pi f_k(d \sin\theta/c)}. \end{cases} \tag{8}$$

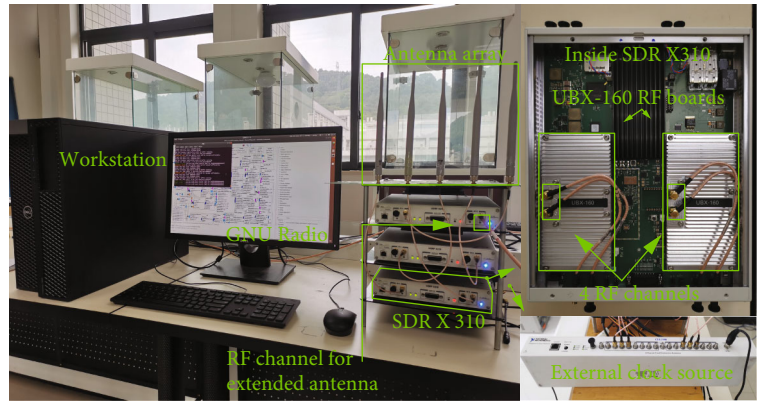

FIGURE 2: The receiver of the SDR test platform. The receiver is composed of three independent X310, which can provide 6 RF channels to receive the wireless signal, and the signal bandwidth can reach up to 100 MHz.

Then, the three-dimensional smoothing is performed on $\mathbf{H}$ to eliminate the influence of coherent signals on parameter estimation. After that, the eigenvalue decomposition is conducted on the autocorrelation matrix of $\mathbf{H}'$, which is the smoothed form of $\mathbf{H}$. Based on the Minimum Description Length (MDL) criterion [32], the dimension of noise subspace is estimated, so the noise subspace $\mathbf{E}_n$, spanned by small eigenvalues, can be extracted. At last, the signal AoA, ToF, and DFS is estimated via the function

$$P(\theta, \tau, \nu)_{3D} = \frac{1}{\left(\mathbf{a}^{\mathrm{H}}(\theta, \tau, \nu)\mathbf{E}_n\mathbf{E}_n^{\mathrm{H}}\mathbf{a}(\theta, \tau, \nu)\right)}, \tag{9}$$

where $\mathbf{a}(\theta, \tau, \nu)$ is the corresponding steering matrix and $\{\cdot\}^{\mathrm{H}}$ is the conjugate transpose operator. In a similar way, SR-PLoc uses the CSI extracted from the extended antenna to realize the joint estimation of DFS and ToF. Due to the phase error introduced by the PDD, CFO, and SFO, the estimated ToF is not the absolute signal ToF. However, the signal AoA and rToF between different propagation paths are not contaminated, since the phase error is the same for all paths, as discussed above. So, based on the estimated signal parameters, SR-PLoc filters out moving target introduced reflection by analyzing the DFS and employs its AoA and rToF to achieve passive moving target localization.

2.2. Passive Moving Target Localization. Assuming the coordinates of the transmitter, moving target, antenna array, and extended antenna are $\mathbf{l}_T[x_t, y_t]$, $\mathbf{l}_R[x_r, y_r]$, $\mathbf{l}_A[x_a, y_a]$, and $\mathbf{l}_E[x_e, y_e]$, respectively, as Figure 2 shows, then, based on the estimated signal parameters and previous discussion, we have

$$\begin{cases} \|\mathbf{l}_T - \mathbf{l}_A\|_2 + \Delta\tau \times c + \varepsilon_{TA} = \tilde{\tau}_{ta} \times c, \\ \|\mathbf{l}_T - \mathbf{l}_E\|_2 + \Delta\tau \times c + \varepsilon_{TE} = \tilde{\tau}_{te} \times c, \\ \|\mathbf{l}_R - \mathbf{l}_T\|_2 + \|\mathbf{l}_R - \mathbf{l}_A\|_2 + \Delta\tau \times c + \varepsilon_{TRA} = \tilde{\tau}_r \times c, \end{cases} \tag{10}$$

where $\|\cdot\|_2$ is two-norm operator; $\Delta\tau \times c$ is the distance corresponding to the ToF offset induced by phase error; ε_{TA}, ε_{TE}, and ε_{TRA} are the estimating error; $\tilde{\tau}_{ta}$ and $\tilde{\tau}_{te}$ are the estimated ToF of the direct path from transmitter to the antenna array and extended antenna, respectively; and $\tilde{\tau}_r$ is the estimated ToF of the moving target induced reflection arrives at the antenna array. Combining the AoA of the direct path estimated by the antenna array with the first two equations in Equation (10), the following constraints can be built

$$\begin{cases} \|\mathbf{l}_T - \mathbf{l}_A\|_2 - \|\mathbf{l}_T - \mathbf{l}_E\|_2 + \varepsilon_{TA} - \varepsilon_{TE} = (\tilde{\tau}_{ta} - \tilde{\tau}_{te}) \times c, \\ \dfrac{(x_t - x_a)}{(y_t - y_a)} = \tan\left(\tilde{\varphi} + \varepsilon_{\varphi}\right), \end{cases} \tag{11}$$

where $\tilde{\varphi}$ is the estimated AoA of the direct path from the transmitter to the antenna array and ε_{φ} is the AoA estimating error. Leveraging Equation (11), the location of the transmitter can be calculated

$$\begin{cases} x_t = \tan\left(\tilde{\varphi} + \varepsilon_{\varphi}\right)(y_t - y_a) + x_a, \\ y_t = \dfrac{W \times y_a - (x_a - x_e)^2 - y_e^2 + y_a^2 + (d_1 + \varepsilon_{TE} - \varepsilon_{TA})^2 + \Gamma y_a}{W - 2y_e + 2y_a + \Gamma}, y_t < y_a, \\ y_t = \dfrac{W \times y_a - (x_a - x_e)^2 - y_e^2 + y_a^2 + (d_1 + \varepsilon_{TE} - \varepsilon_{TA})^2 - \Gamma y_a}{W - 2y_e + 2y_a - \Gamma}, y_t > y_a, \end{cases} \tag{12}$$

where

$$\begin{cases} W = 2\tan\left(\tilde{\varphi} + \varepsilon_{\varphi}\right)(x_a - x_e), \\ d_1 = (\tilde{\tau}_{ta} - \tilde{\tau}_{te}) \times c, \\ \Gamma = 2\dfrac{(d_1 + \varepsilon_{TE} - \varepsilon_{TA})}{\cos\left(\tilde{\varphi} + \varepsilon_{\varphi}\right)}. \end{cases} \tag{13}$$

When $y_t = y_a$, it indicates the AoA of the direct path reaches 90 degrees. At this time, the localization of the transmitter can be achieved via the rToF. After obtaining the location of the transmitter, one can see that

$$(\tilde{\tau}_r - \tilde{\tau}_{ta}) \times c = \|\mathbf{l}_R - \mathbf{l}_T\|_2 + \|\mathbf{l}_R - \mathbf{l}_A\|_2 - \|\mathbf{l}_T - \mathbf{l}_A\|_2 + \varepsilon_{TRA} - \varepsilon_{TA}, \tag{14}$$

which is an elliptic equation, indicating the moving target is located on an ellipse whose focus is transmitter and antenna array. Meanwhile, based on the estimated AoA of the moving target induced reflection, we have

$$\arctan\left[\frac{(x_r - x_a)}{(y_r - y_a)}\right] = \widetilde{\theta} + \varepsilon_\theta, \tag{15}$$

where $\widetilde{\theta}$ is the estimated AoA of the TIR and ε_θ is the AoA estimating error. Leveraging the constraints given in Equations (14) and (15), finally, the location of the moving target can be calculated as

$$\begin{cases} x_r = \tan\left(\widetilde{\theta} + \varepsilon_\theta\right)(y_r - y_a) + x_a, \\ y_r = \dfrac{Z \times y_a - (x_a - x_t)^2 - y_t^2 + y_a^2 \pm \left(2Uy_a/\cos\left(\widetilde{\theta} + \varepsilon_\theta\right)\right) + U^2}{Z - 2y_t + 2y_a \pm \left(2U/\cos\left(\widetilde{\theta} + \varepsilon_\theta\right)\right)}, \end{cases} \tag{16}$$

where

$$\begin{cases} Z = 2\tan\left(\widetilde{\theta} + \varepsilon_\theta\right)(x_a - x_t), \\ U = \sqrt{(x_t - x_a)^2 + (y_t - y_a)^2} + (\tilde{\tau}_r - \tilde{\tau}_{ta}) \times c - \varepsilon_{TRA} + \varepsilon_{TA}, \end{cases} \tag{17}$$

So far, by using the AoA (extracted from the CSI obtained by the antenna array) and the rToF (extracted from the CSI obtained by the antenna array and extended antenna), SR-PLoc realizes the passive moving target localization. Since the reflection paths are weaker than the direct signal traveling from the transmitter to the receiver, SR-PLoc employs the CSI-CR algorithm proposed in our previous work [33] to reduce the direct path induced interference to further improve the ToF estimation accuracy, during the parameter estimation process.

3. Results and Discussion

3.1. Implementation. To verify and evaluate the performance of SR-PLoc, comprehensive experiments are carried out in a typical indoor office room, which, as Figure 3 shows, contains office furniture such as computers, work desks, and bookcases. Multiple test locations, which are denoted as blue dots, are selected for the moving target. At the same time, to fully analyze the system performance, multiple test locations are selected for the transmitter and extended antenna, which are denoted as green and red boxes, respectively. To accurately obtain the ground truth of the reflection, the tester is asked to stand at the test reflection locations and wave an iron plate to generate the reflection path.

To test the performance of the proposed algorithm with different configurations (i.e., different bandwidth and the number of antennas), two test platforms are constructed, as Figures 2 and 4 show.

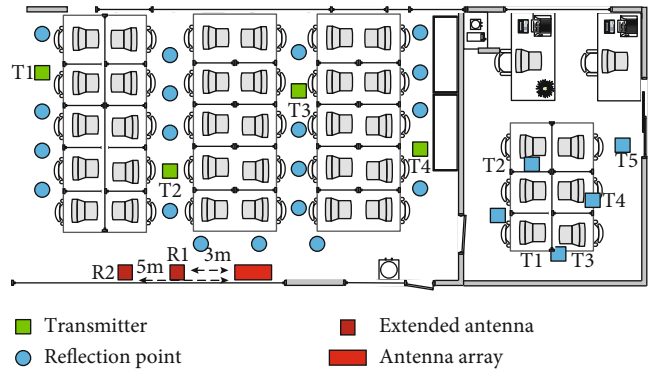

Figure 3: The diagram of the testbed.

(i) As presented in Figure 2, the first one is the Software Defined Radio (SDR) platform. The receiver includes three USRP X310 devices [34] with six RF UBX-160 cards, which are synchronized via the OctoClock-G [35] to ensure antennas (including antenna array and extended antenna) can sample the spatial signal simultaneously. The transmitter contains a USRP X310 device with two RF UBX-160 cards to send the signal. The workstation equipped with GNU radio is used to control SDR equipment, to send the signal, or extract CSI from the received OFDM signal, which can cover a bandwidth up to 100 MHz

(ii) The second one is a commercial access point (AP) equipped with Broadcom 4366C0 wireless NIC and NexMon tool [36]. A computer with Ubuntu 18.04 operating system controls an AP, which acts as the receiver, to complete the CSI data extraction via instructions set. Another AP with the same configuration is used as the transmitter to send the signal. The receiver of this platform contains four antennas, which can collect CSI with a bandwidth up to 80 MHz based on the IEEE 802.11 ac protocol

During the experiment, the default signal bandwidth is 80 MHz, the central frequency is 5G Hz, the number of antennas in the antenna array is 3, the CSI packet transmission rate is 200 Hz (i.e., the transmitter sends 200 packets per second), and the number of the extended antenna is 1. Both transmitter and receiver are placed 1.5 meters above the ground. Before the test, the power splitter is used to measure the phase difference among different RF channels. The measured phase difference will be used to compensate for the initial phase offset to make sure the AoA can be estimated effectively. Leveraging the data collected from these platforms, the system evaluation is conducted from three aspects. At first, the localization accuracy of the transmitter is briefly analyzed. Next, the impact of the transmitter's location on the moving target localization accuracy is analyzed. At last, the localization accuracy of the moving target with different configurations is inspected, including the impact of the signal bandwidth, number of antennas in the ULA, and location of the extended antenna.

Figure 4: The receiver of the IEEE 802.11n protocol-based Broadcom 4366C0 test platform. This receiver can provide 4 RF channels to receive the wireless signal and the signal bandwidth can reach up to 80 MHz.

3.2. Performance Evaluation. At first, the transmitter localization performance of SR-PLoc is analyzed via the comparison with SIFI [37], which expands multiple antennas of a single receiver to capture CSI at different locations and estimate ToA to realize localization. The localization performance comparison is presented in Figure 5, via the Cumulative Distribution Function (CDF) of the localization error. One can see from the result, SR-PLoc's median localization error is about 1.016 m, which is slightly better than SIFI's 1.110 m when the extended antenna is at R1. The error under the ratio of 66.7% of SR-PLoc can reach 1.220 m, which is 0.121 m lower than that of SIFI, demonstrating the effectiveness of the proposed SR-PLoc in transmitter localization. When the extended antenna is at R2, one can see that the transmitter localization accuracy is further improved. Concretely, SR-PLoc's median localization error and error under the ratio of 66.7% can reach 0.821 m and 1.088 m, respectively. The reason for this enhancement is that the layout of the receiver is more suitable for localization when the distance between the extended antenna and the antenna array is increased within a reasonable range. However, for the real-world application, this distance should not be too large; otherwise, it will cause inconvenience to the deployment of the receiver.

After the transmitter localization performance evaluation, next, the impact of the transmitter's location on the moving target localization accuracy is analyzed and the result is presented in Figure 6. Overall, it can be seen that, on the one hand, SR-PLoc performs better when the extended antenna is at R2. This can be explained by that the transmitter localization accuracy is higher when the extended antenna is at the R2, resulting in an improvement of moving target localization accuracy. On the other hand, when the transmitter is at T2 and T3, the localization accuracy moving target is better than that of the transmitter at T1 and T4. Taking the median localization error as an example, when the extended antenna is at R1, the median localization error can reach 1.592 m, 0.959 m, 0.759 m, and 1.211 m when the transmitter is at T1, T2, T3, and T4, respectively. A similar trend can be observed when the extended antenna is at R2. This is because T1 and T4 are at the edge of the test area, indicating the transmitter is close to the wall and furniture, which may introduce strong reflection and cause a decrease in the accuracy of parameter estimation and finally lead to a failure in filtering out the moving target induced reflection.

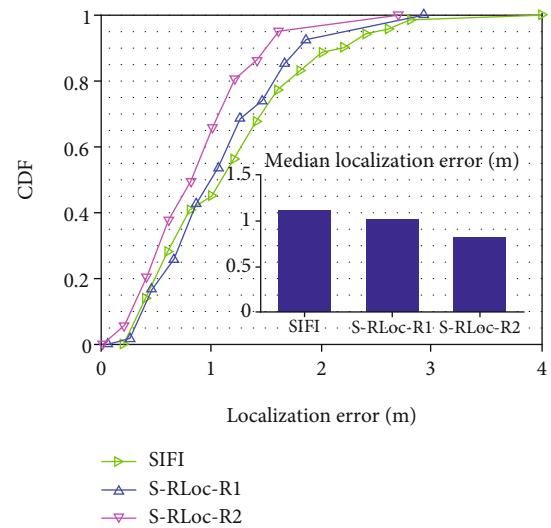

Figure 5: The transmitter localization accuracy comparison.

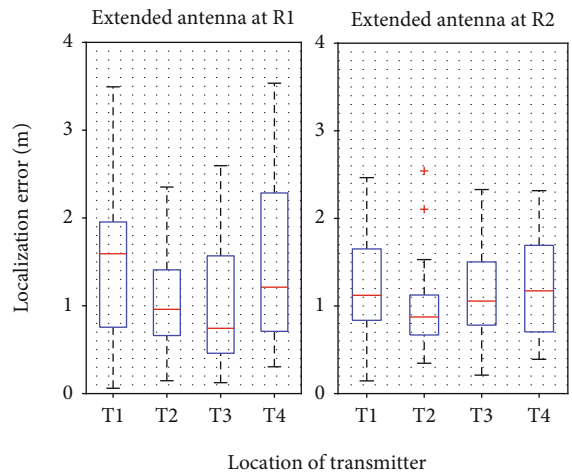

Figure 6: The impact of transmitter's location on the moving target localization accuracy.

With different signal bandwidths, the localization accuracy of the moving target is analyzed. From Figure 7, it is not hard to observe that the moving target localization performance is boosted with the increase of the signal

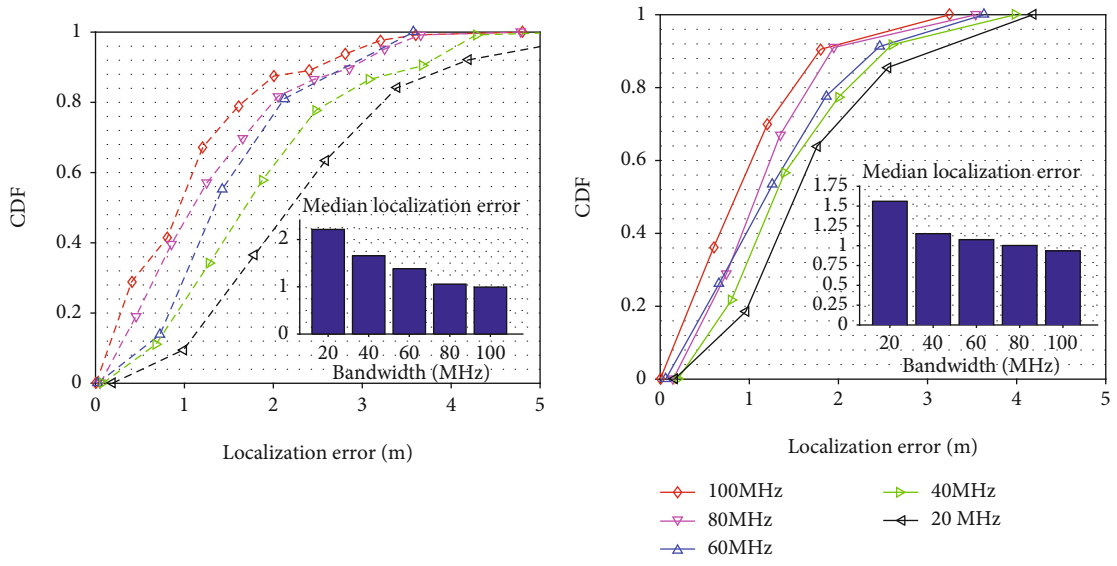

(a) Extended antenna at R1 (b) Extended antenna at R2

FIGURE 7: The localization accuracy of moving target versus the signal bandwidth. (a) Shows the localization accuracy under different bandwidths when the extended antenna is at the test location R1. (b) Demonstrates the localization accuracy under different bandwidths when the extended antenna is at the test location R2.

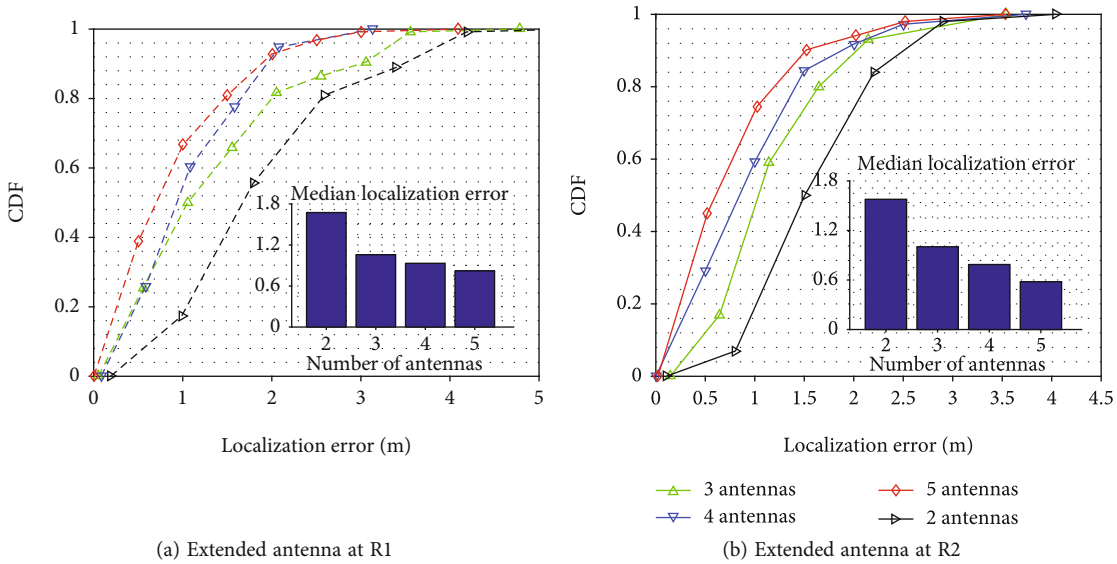

(a) Extended antenna at R1 (b) Extended antenna at R2

FIGURE 8: The localization accuracy of moving target versus the number of antennas. (a) Shows the localization accuracy when the extended antenna is at the test location R1 and the antenna array is equipped with a different number of antennas. (b) Demonstrates the localization accuracy when the extended antenna is at the test location R2 and the antenna array is equipped with a different number of antennas.

bandwidth. Specifically, when the extended antenna is at R1, the median localization error of SR-PLoc can reach 0.902 m, 1.087 m, 1.303 m, 1.675 m, and 2.214 m, with the signal bandwidth of 100 MHz, 80 MHz, 60 MHz, 40 MHz, and 20 MHz, respectively. We believe this is because the increase of signal bandwidth improves the signal ToF estimation resolution, driving the estimated signal ToF more accurate and ultimately leading to an enhancement in localization accuracy. Comparing two subfigures in Figure 7, one can see that the moving target localization accuracy is improved when the extended antenna is moved to R2. This can be also interpreted by that the layout is more suitable for localization when the distance between the extended antenna and the antenna array is increased.

At last, we analyze the impact of the number of antennas on the moving target localization accuracy. As Figure 8 shows, it can be seen that the median localization error of SR-PLoc can reach 1.708, 1.087 m, 0.931 m, and 0.710 m, with 2, 3, 4, and 5 antennas in the antenna array, respectively, when the extended antenna is at R1. This phenomenon means the localization accuracy is positively correlated with the number of antennas. Since the increase in the

number of antennas improves the AoA estimation accuracy and finally results in the improvement of localization accuracy. Comparing two subgraphs in Figure 7, one can see that the median localization error of SR-PLoc is reduced by about 0.104 m, 0.101 m, 0.104, and 0.113 m, with 2, 3, 4, and 5 antennas in the antenna array, respectively, when the extended antenna is moved to the location R2. Similar to the previous result, this enhancement is also introduced by the improvement in transmitter localization accuracy.

4. Conclusions

In this paper, we propose SR-PLoc, a single receiver-based passive moving target localization system. Taking the nonsynchronization between the transmitter and the receiver-induced phase errors recorded in CSI into full consideration, the proposed algorithm constructs an antenna array and an extended antenna, by using multiple antennas from a single receiver, to capture the wireless signal at different spatial locations. On this basis, SR-PLoc estimates the signal AoA and ToF and combines the estimated parameters with locations of the antenna array and extended antenna to realize the passive localization of the moving target. Different from the existing solutions, which rely on the assumption that the transmitter's location is preacquired and unchanged, SR-PLoc holds no requirement for that, making it more promising for real-world applications. Comprehensive experiments are conducted based on the two test platforms, which are built upon the SDR equipment and commercial AP. The experimental results verify the effectiveness and practicality of the proposed algorithm, which lays a solid foundation for ubiquitous passive localization for the moving target.

Data Availability

The data that support the findings of this study are available from the corresponding author upon reasonable request.

Conflicts of Interest

The authors declare that there is no conflict of interest regarding the publication of this paper.

Acknowledgments

First, we would like to thank Dr. Kaikai Liu, who has given us suggestions when constructing the SDR test platform and helped us to complete the localization test. Then, we sincerely thank the anonymous reviewers for their valuable feedback. This work is partially supported by the Science and Technology Research Program of Chongqing Municipal Education Commission (KJQN2018 00625, KJZD-K202000605, KJQN202000630), the Chongqing Natural Science Foundation Project (cstc2019jcyj-msxmX0635, cstc2020jcyj-msxmX0842), the National Natural Science Foundation of China (61771083, 61771209), and the Chongqing University of Posts and Telecommunications PHD Talents Training Project (BYJS201904).

References

[1] Y. Qiao, O. Zhang, W. Zhou, K. Srinivasan, and A. Arora, "PhyCloak: obfuscating sensing from communication signals," in *13th {USENIX} Symposium on Networked Systems Design and Implementation ({NSDI} 16)*, pp. 685–699, Santa Clara, CA, 2016.

[2] F. Adib, Z. Kabelac, D. Katabi, and R. C. Miller, "3d tracking via body radio reflections," in *11th {USENIX} Symposium on Networked Systems Design and Implementation ({NSDI} 14)*, pp. 1–14, Seattle, WA, 2016.

[3] L. Li, P. Hu, C. Peng, G. Shen, and F. Zhao, "Epsilon: a visible light based positioning system," in *11th {USENIX} Symposium on Networked Systems Design and Implementation ({NSDI} 14)*, pp. 331–343, Seattle, WA, 2014.

[4] T. Li, C. An, Z. Tian, A. T. Campbell, and X. Zhou, "Human sensing using visible light communication," in *Proceedings of the 21st Annual International Conference on Mobile Computing and Networking*, pp. 331–344, New York, NY, USA, 2015.

[5] M. F. Norazman and N. M. Thamrin, "Landmark scanning by using infrared sensor for simultaneous localization and mapping application," in *2018 IEEE 14th International Colloquium on Signal Processing & Its Applications (CSPA)*, pp. 145–149, Penang, Malaysia, 2018.

[6] N. Faulkner, F. Alam, M. Legg, and S. Demidenko, "Device-free localization using privacy-preserving infrared signatures acquired from thermopiles and machine learning," *IEEE Access*, vol. 9, pp. 81786–81797, 2021.

[7] N. Priyantha, A. Chakraborty, and H. Balakrishnan, "The cricket location-support system," in *Proceedings of the 6th annual international conference on Mobile computing and networking - MobiCom '00*, pp. 32–43, New York, NY, USA, 2000.

[8] R. S. Bandaru, A. Sornes, J. D'hooge, and E. Samset, "2D localization of specular reflections using ultrasound," in *2014 IEEE International Ultrasonics Symposium*, pp. 2209–2212, Chicago, IL, USA, 2014.

[9] M. Zhou, Y. Li, M. J. Tahir, X. Geng, Y. Wang, and W. He, "Integrated statistical test of signal distributions and access point contributions for Wi-Fi indoor localization," *IEEE Transactions on Vehicular Technology*, vol. 70, no. 5, pp. 5057–5070, 2021.

[10] J. Liu, H. Liu, Y. Chen, Y. Wang, and C. Wang, "Wireless sensing for human activity: a survey," *IEEE Communications Surveys & Tutorials*, vol. 22, no. 3, pp. 1629–1645, 2020.

[11] Q. Pu, J. K. Y. Ng, and M. Zhou, "Fingerprint-based localization performance analysis: from the perspectives of signal measurement and positioning algorithm," *IEEE Transactions on Instrumentation and Measurement*, vol. 70, pp. 1–15, 2021.

[12] X. Li, D. Zhang, Q. Lv et al., "IndoTrack: device-free indoor human tracking with commodity Wi-Fi," *Proceedings of the ACM on Interactive, Mobile, Wearable and Ubiquitous Technologies*, vol. 1, no. 3, pp. 1–22, 2017.

[13] J. Wang, Z. Tian, X. Yang, and M. Zhou, "CSI-based ToF estimation for reflection path under the TTW scenario," *IEEE Wireless Communications Letters*, vol. 10, no. 5, pp. 1010–1013, 2021.

[14] Y. Xie, J. Xiong, M. Li, and K. Jamieson, "mD-Track: Leveraging multidimensionality in passive indoor Wi-Fi tracking," in *The 25th Annual International Conference on Mobile Computing and Networking*, pp. 1–16, New York, NY, USA, 2019.

[15] M. Zhou, B. Wang, Z. Tian, and L. Xie, "Hardware and software design of BMW system for multi-floor localization,"

EURASIP Journal on Wireless Communications and Networking, vol. 2017, no. 1, Article ID 139, 2017.

[16] M. Kotaru, K. Joshi, D. Bharadia, and S. Katti, "SpotFi: decimeter level localization using WiFi," in *Proceedings of the 2015 ACM Conference on Special Interest Group on Data Communication*, pp. 269–282, New York, NY, USA, 2015.

[17] X. Wang, L. Gao, S. Mao, and S. Pandey, "CSI-based fingerprinting for indoor localization: a deep learning approach," *IEEE Transactions on Vehicular Technology*, vol. 66, no. 1, pp. 763–776, 2016.

[18] J. Xiong, K. Sundaresan, and K. Jamieson, "ToneTrack: leveraging frequency-agile radios for time-based indoor wireless localization," in *Proceedings of the 21st Annual International Conference on Mobile Computing and Networking*, pp. 537–549, New York, NY, USA, 2015.

[19] Z. Chen, G. Zhu, S. Wang et al., "M^3: multipath assisted Wi-Fi localization with a single access point," *IEEE Transactions on Mobile Computing*, vol. 20, no. 2, pp. 588–602, 2019.

[20] Z. Li, Z. Tian, and M. Zhou, "Decimeter level indoor localization using hybrid measurements of a distributed single receiver," *IEEE Transactions on Instrumentation and Measurement*, vol. 70, pp. 1–14, 2021.

[21] J. Wang, J. Xiong, H. Jiang et al., "Low human-effort, device-free localization with fine-grained subcarrier information," *IEEE Transactions on Mobile Computing*, vol. 17, no. 11, pp. 2550–2563, 2018.

[22] R. Palmeri, M. T. Bevacqua, A. F. Morabito, and T. Isernia, "Noncooperative localization and tracking through the factorization method," *IEEE Geoscience and Remote Sensing Letters*, vol. 16, no. 8, pp. 1205–1209, 2019.

[23] Y. Xie, J. Xiong, M. Li, and K. Jamieson, "Xd-track: Leveraging multidimensional information for passive Wi-Fi tracking," in *Proceedings of the 3rd Workshop on Hot Topics in Wireless*, pp. 39–43, New York, NY, USA, 2016.

[24] Z. Zhou, Z. Yang, C. Wu, L. Shangguan, and Y. Liu, "Omnidirectional coverage for device-free passive human detection," *IEEE Transactions on Parallel and Distributed Systems*, vol. 25, no. 7, pp. 1819–1829, 2014.

[25] K. Joshi, D. Bharadia, M. Kotaru, and S. Katti, "WiDeo: fine-grained device-free motion tracing using RF Backscatter," in *12th {USENIX} Symposium on Networked Systems Design and Implementation ({NSDI} 15).*, pp. 189–204, Oakland, CA, 2015.

[26] X. Li, S. Li, D. Zhang, J. Xiong, Y. Wang, and H. Mei, "Dynamic-MUSIC: accurate device-free indoor localization," in *Proceedings of the 2016 ACM International Joint Conference on Pervasive and Ubiquitous Computing*, pp. 196–207, New York, NY, USA, 2016.

[27] J. Wang, Z. Tian, X. Yang, and M. Zhou, "TWPalo: through-the-wall passive localization of moving target with Wi-Fi," in *2019 IEEE Global Communications Conference (GLOBECOM)*, pp. 1–6, Waikoloa, HI, USA, 2019.

[28] K. Qian, C. Wu, Y. Zhang, G. Zhang, Z. Yang, and Y. Liu, "Widar2.0: passive human tracking with a single Wi-Fi link," in *Proceedings of the 16th Annual International Conference on Mobile Systems, Applications, and Services*, pp. 350–361, New York, NY, USA, 2018.

[29] J. A. Fessler and A. O. Hero, "Space-alternating generalized expectation-maximization algorithm," *IEEE Transactions on Signal Processing*, vol. 42, no. 10, pp. 2664–2677, 1994.

[30] S. Kumar, S. Gil, D. Katabi, and D. Rus, "Accurate indoor localization with zero start-up cost," in *Proceedings of the 20th annual international conference on Mobile computing and networking*, pp. 483–494, New York, NY, USA, 2014.

[31] Y. Xie, Z. Li, and M. Li, "Precise power delay profiling with commodity Wi-fi," *IEEE Transactions on Mobile Computing*, vol. 18, no. 6, pp. 1342–1355, 2019.

[32] M. Wax and T. Kailath, "Detection of signals by information theoretic criteria," *IEEE Transactions on Acoustics, Speech, and Signal Processing*, vol. 33, no. 2, pp. 387–392, 1985.

[33] J. Wang, Z. Tian, X. Yang, and M. Zhou, "CSI component reconstruction-based AoA estimation for subtle human-induced reflection under the TTW scenario," *IEEE Communications Letters*, vol. 23, no. 8, pp. 1393–1396, 2019.

[34] Ettus Research, "USRP X310," July 2020 https://www.ettus.com/all-products/x310-kit/.

[35] Ettus Research, "OctoClock-G CDA-2990," July 2020 https://www.ettus.com/all-products/octoclock-g/.

[36] M. Schulz, D. Wegemer, and M. Holick, "DEMO: using NexMon, the C-based WiFi firmware modification framework," in *Proceedings of the 9th ACM Conference on Security & Privacy in Wireless and Mobile Networks*, pp. 213–215, New York, NY, USA, 2016.

[37] W. Gong and J. Liu, "SiFi: pushing the limit of time-based WiFi localization using a single commodity access point," *Proceedings of the ACM on Interactive, Mobile, Wearable and Ubiquitous Technologies*, vol. 2, no. 1, pp. 1–21, 2018.

Hindawi
Journal of Sensors
Volume 2021, Article ID 3812145, 9 pages
https://doi.org/10.1155/2021/3812145

Research Article

Design and Implementation of High-Skilled Talent Information Management System Based on Multisensor Information Fusion

Shui Liu

College of Union Cadre Education and Training, Shandong Management University, Jinan, 250357 Shandong, China

Correspondence should be addressed to Shui Liu; 14438120130326@sdmu.edu.cn

Received 12 June 2021; Revised 27 July 2021; Accepted 10 August 2021; Published 21 August 2021

Academic Editor: Mu Zhou

With the rapid development of science and technology, the global network and informatization process is changing people's lives, and it has also brought profound changes to the management of enterprises. Traditional management still relies heavily on offline management and paper delivery of information. The traditional management model in the past cannot meet the needs of the continuous development of enterprises. The purpose of this article is to design a high-skilled talent information management system to meet the needs of users and enterprises. This paper combines the BP multisensor information fusion algorithm to screen and process the data and designs a multisensor information fusion-based competency evaluation model for highly skilled talents. A high-skilled talent information management system has been established with modules such as basic personnel information, skills identification information, high-skilled talent management, competence, key research teams, common reports, comprehensive query, and system maintenance. In the test of the system's usability, 156 users rated the system above 3 points, accounting for 78% of the survey population, indicating that the system has a certain ease of use. This system realizes the electronicization of the basic information of skilled personnel, which plays an important role in regulating the professional management of skilled personnel and improving the management efficiency of skilled personnel.

1. Introduction

With the rapid development of artificial intelligence technology, informatization construction and paperless office have become the signs of the modern office. The application of multisensor information fusion in robotics makes people pay more and more attention to the development of artificial intelligence. With the development of computer technology and management science, information management systems have emerged, which has greatly improved the quality and effectiveness of management and decision-making. The information technology of the international developed countries has been produced relatively early, has always occupied a leading position, and occupied a certain Chinese market. Although the domestic information technology started late, it is also developing rapidly. At present, the development of domestic management information systems is not inferior in technology to the same industry abroad, but there are certain differences in the types of applications and management functions.

The information management system can effectively manage enterprise data, so that these data can be efficiently stored, used, and shared and promote the standardization and modernization of enterprise management [1, 2]. The realization of a high-skilled talent information management system can provide enterprises with powerful intellectual resources, enable enterprises to better grasp, and reasonably allocate information on high-skilled talent resources, so that these talents can make full use of them [3]. As the enterprise continues to develop, the function of the information management system needs to be able to meet the changing needs of the enterprise, and it must have strong adaptability and scalability. Can draw on the application of multisensor information fusion in robot technology, design artificial intelligence network-based high-skilled talents information management system, to achieve professional management of standardized skilled talents, and improve the management efficiency of skilled talents [4, 5].

Chettibi's team used multisensor information fusion to develop an intelligent power management system that will

automatically control load shedding in local power distribution areas and utilize different types of generator sets such as conventional and unconventional energy sources. If the power generation is insufficient to meet the load demand, the multisensor information fusion will predict and predict when the load demand is greater than the power generation amount and specifically propose a suitable load reduction area. Utilizing and processing different types of seasonal and occasional loading data, they designed multisensor information fusion to automatically show them that local power restrictions would be better based on priority. Therefore, the area that needs to minimize the load is a priority [6]. Peng's team established the development of an information database and information data management system to facilitate the multisource, multidisciplinary data generated by the data management work in the geological repository in China during the site selection process. Through this management system, basic functions such as creation, retrieval, update, deletion, full-text retrieval, and download can be realized. It can even provide some professional data statistics and analysis functions. Finally, data from many different disciplines was successfully integrated, stored, and managed. At the same time, the management system can also provide an important reference for data management in related research fields such as decommissioning and management of nuclear facilities, resource exploration, and environmental protection [7]. Yue's team has developed an air pollution and health impact monitoring information system that includes data collection, data management, data quality control, statistics, and visual display. Through the B/S architecture, the design concept of separation of authority management from professional applications and centralized data management, authority process management, and quality control is integrated into the entire process of data collection, data processing, data review, and statistics. Key functions such as data collection, three-level auditing, statistics, visual display, and system management of the information system were realized. The system has been applied in national projects in 31 provinces, 65 cities, and 126 monitoring points. So far, more than 16 million business records have been stored in the system, and the amount of data has reached more than 10 g. It not only meets the monitoring requirements but also provides basic support for research and decision-making [8].

This article designs a high-skilled talent information management system to meet the needs of users and enterprises. This paper combines the BP multisensor information fusion algorithm to screen and process the data and designs a multisensor information fusion-based competency evaluation model for high-skilled talents. It establishes basic personnel information, skills identification information, high-skilled talent management, competence, key research teams, a highly skilled talent information management system with modules such as reports, comprehensive query, and system maintenance. By testing the system, it is concluded that the system can meet the needs of users and enterprises. It can meet the corresponding requirements in many aspects such as functionality, reliability, software design, compatibility, and security. The realization of the electronicization of the basic information of skilled personnel has played an important role in regulating the professional management of skilled personnel and improving the management efficiency of skilled personnel.

2. Proposed Method

2.1. Multisensor Information Fusion

2.1.1. Characteristics of Multisensor Information Fusion. Multisensor information fusion is a simulation of the human brain system. It reflects many basic characteristics of human brain function. But it is not a true portrayal of the human brain nervous system, it is to simplify and abstract it [9]. It processes information by simulating the way a brain multisensor information fusion processes memory information. Its characteristics are the following:

(1) *Nonlimiting.* A multisensor information fusion can usually do calculations in the process of information transmission and can also store it. This source is formed by the connection of multiple neurons. The prediction of a certain behavioral result of the system requires the interaction and interconnection of multiple neurons, which mimics the characteristics of human neural connections, so that the operation efficiency is very high, which is the advantage of multisensor information fusion

(2) *Nonlinear.* The wisdom of the brain is a nonlinear phenomenon. It is a parallel structure and processing order. According to mathematical theory, the two states of activation or inhibition of artificial neurons are what people call excited or unexcited states, so they are understood as a nonlinear relationship

(3) *Nonconvex.* Multisensor information fusion under certain conditions, a certain state function changes, and a system state will also change. Multisensor information fusion is the same. A state function has multiple extreme values, and the system also has multiple stable states. The information is not only stored in a unit; there may be multiple evolution directions of the system. This is that multisensor information fusion has a relatively strong fault tolerance feature

(4) *Very Qualitative.* Multisensor information fusion has the ability to self-organize, self-learn, and adapt, which is very similar to the human brain. Therefore, if the final output is incorrect, the system will also add weights to produce new results, and there are multiple changes in the information to be processed. People often use iterative processes to represent the process evolution of dynamic systems

According to these four characteristics, multisensor information fusion has been applied to a variety of fields: in the information field, multisensor information fusion for nonlinear signal processing and adaptive signal processing [10], for example, spectrum estimation and noise

cancellation. It can also be applied to pattern recognition, such as handwritten Chinese character recognition function and fingerprint recognition system in smartphones [11]. In the field of automation, intelligent monitoring and detection of comprehensive indicators such as environmental comfort are often used in daily life [12]. In the engineering field, such as the optimization of automobile fuel consumption rate and smoke exhaust degree, dense steel decentralized storage, voice switch, fingerprint switch function [13]. In the economic field, credit analysis and accurate and objective evaluation results can be obtained based on key data to reduce financial risks. At the same time, the performance of stock trends is particularly outstanding. It can build a more accurate and reliable stock market model based on a variety of factors and determine the future price trend [14].

Multisensor information fusion has developed rapidly over the years in the field of computational intelligence, which is characterized by simulating biological multisensor information fusion and learning from nature. Three branches of multisensor information fusion, evolutionary computation, and fuzzy logic have been formed, which provide new ideas, theories, and methods for the research and development of computer science and many disciplines. The organic combination of multisensor information fusion, evolutionary computing, and fuzzy logic to creatively solve complex problems belonging to the category of image thinking has become a research hotspot in computational intelligence and its applications [15].

The emergence of multisensor information fusion has changed the application of computers in many aspects. The main features of a computer are a centralized structure, a serial execution of a sequence of instructions, and a storage component separated from a computing component. During information processing, the problems to be implemented need to be programmed and executed by the computer. The problems must be structured problems that can be accurately expressed; otherwise, the computer will not be able to handle them [16]. The traditional artificial intelligence expert system has initially solved this problem, but it is based on planning. It requires people to clearly express their knowledge in advance. Only when the computer centrally stores these knowledge and rules summarized through human wisdom, it has intelligence. So in essence, the traditional artificial intelligence only makes logical reasoning in the form of simulating the human brain from the aspect of external functions. Multisensor information fusion is another sublimation on the basis of the former two. It is a network structure composed of a large number of parallel nonlinear processing units through connection rights, so it simulates part of the image thinking of the human brain from the internal structure. As a result, the ability to solve some non-linear and unstructured problems has become stronger and has been proven in many already implemented systems.

On the other hand, there are still some deficiencies and problems in the application of multisensor information fusion. First, for large-scale distributed systems, the execution time of multisensor information fusion is almost proportional to the square of the number of nodes. Considering the response time of the system, the computer is required to have a high operating speed, so the hardware requirements are very high, and sometimes special hardware is required, and the corresponding cost will be greatly increased. Therefore, hardware research is also an aspect of multisensor information fusion technology. Second, from the characteristics of the multisensor information fusion described above, it can be seen that modifying permissions in the network is a very complicated machine learning process. The network itself cannot give the reason for the output results; it just gives a mapping from the input space to the output space. The information processing process is a black box, and the knowledge distribution is stored in the connection right, so as information storage, the entire network after learning must be stored [17]. In addition, the learning algorithm converts the input and output problem of the example into a nonlinear optimization problem. There is a local minima problem in mathematics. It is likely that the system will fall into a local minima. No matter how many iterations, the error is decline. So at present, the improvement of learning algorithms is still one of the research directions of multisensor information fusion. In addition, the widening of application fields is also one of the research directions. Experts in many fields have tried to use the idea of multisensor information fusion to achieve problems such as prediction, evaluation, identification, and analysis, which have improved the development of productivity in various fields [18].

2.1.2. BP Multisensor Information Fusion. The BP learning algorithm generally consists of an input layer, a thousand intermediate layers, and an output layer, and each layer performs function mapping with weights. As shown in Figure 1, a number of factors, that is, the function independent variable is set as the input layer, and the corresponding output value is obtained by calculating the intermediate layer weights and adjusting the function. The corresponding error is obtained by comparing the output value with the actual value in the sample value. The error value is adjusted by the back-propagation of the multisensor information fusion to adjust the weights and adjustment functions of the middle layer, and the model is adjusted to an acceptable error range.

The input variables are x_j, the output variables are θ_k, w_{ki}, and w_{ij} are the weights θ_i and a_k of the network connection as the node thresholds, and $f(x)$ represents the excitation function of the network.

During the forward propagation of the signal, the input of the ith node in the middle layer is

$$\text{net}_i = \sum_{j=1}^{M} w_{ij} x_j + \theta_i. \tag{1}$$

The output of the ith node in the middle layer is

$$y_i = \Phi(\text{net}_i) = \Phi\left(\sum_{j=1}^{M} wi_j x_j + \theta_i\right). \tag{2}$$

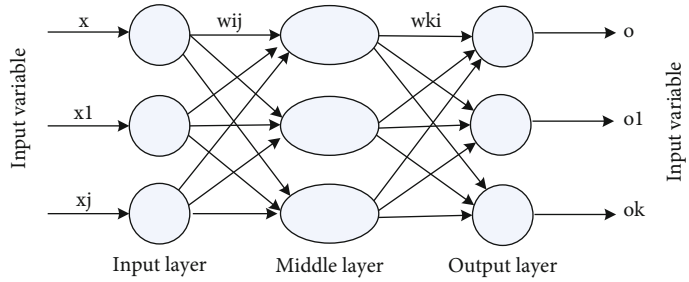

Figure 1: BP-ANN model structure.

The input of the kth node of the output layer is

$$\text{net}_k = \sum_{j=1}^{M} w_{ki} x_i + a_i = \sum_{j=1}^{M} w_{ki} \Phi\left(\sum_{j=1}^{M} w_{ki} x_j + \theta_i\right) + a_i. \quad (3)$$

The output of the kth node of the output layer is

$$o_k = \Phi(\text{net}_k) = \Phi\left(\sum_{j=1}^{M} w_{ki} \Phi\left(\sum_{j=1}^{M} w_{ki} x_j + \theta_i\right) + a_i\right). \quad (4)$$

During the back-propagation of errors, the back-propagation adjusts the weight value through the output error, so that the output continuously tends to the expected value. For the pth training sample, its error function is

$$E_p = \frac{1}{2} \sum_{k=1}^{1} \left(T_k^p - o_k^p\right)^2. \quad (5)$$

The total error function is

$$E = \frac{1}{2} \sum_{p=1}^{p} \sum_{k=1}^{1} \left(T_k^p - o_k^p\right)^2. \quad (6)$$

Determine each correction value by inverse calculation

$$\begin{aligned}
\Delta w_{ki} &= -\beta \sum_{p=1}^{p} \sum_{k=1}^{1} \left(T_k^p - o_k^p\right)^2 \cdot \Psi'(\text{net}_k) y_i, \\
\Delta a_k &= -\beta \sum_{p=1}^{p} \sum_{k=1}^{1} \left(T_k^p - o_k^p\right)^2 \cdot \Psi'(\text{net}_k), \\
\Delta w_{ij} &= -\beta \sum_{p=1}^{p} \sum_{k=1}^{1} \left(T_k^p - o_k^p\right)^2 \cdot \Psi'(\text{net}_k) w_{ki} \phi'(\text{net}_k) x_j, \\
\Delta \theta_i &= -\beta \sum_{p=1}^{p} \sum_{k=1}^{1} \left(T_k^p - o_k^p\right)^2 \cdot \Psi'(\text{net}_k) w_{ki} \phi'(\text{net}_k).
\end{aligned} \quad (7)$$

The multisensor information fusion can implement the nonlinear mapping process without considering the interference and correlation coefficients between various influencing factors of the input layer. There is no bottleneck that the computer cannot calculate within the effective time due to NP difficulties. With the help of computer programming, fast-convergent computing power can be achieved.

2.2. Highly Skilled Talents. High-skilled talent is a dynamic, historical category. With the changes of the times and the adjustment of the industrial structure, its connotation and extension have continued to develop [19]. At the current stage of our country, high-skilled talents refer to between the leadership and decision-making level and the technical operation level. Mainly refers to having solid professional theoretical knowledge, mastering contemporary high-level application technology, strong hands-on ability, superb ability, and technology in key skill areas, and being able to independently solve difficult technical and operational problems in this field; highly skilled talents promote technology. Progressive translators put scientific research results into practice. They are a group of compound application-oriented talents who fully meet the needs of the society [20]. Its main characteristics are embodied in complexity, professionalism, practicality, innovation, and modernity [21, 22].

Through specialized training and training, high-skilled personnel have mastered the current high-level applied technology, skills, and theoretical knowledge and have high-quality employees with innovative ability, entrepreneurial ability, and ability to independently solve critical problems [23]. With the continuous improvement of the high-skilled talent growth environment and incentive and guarantee mechanism of the group company, the skilled talent team has continued to grow in recent years. Every year, the graphic and textual materials retained by skilled personnel in terms of training, use, and evaluation are mostly based on raw paper, and the number is constantly increasing. In addition, most of the business offices of group companies have inconvenience in consulting and statistically reviewing a large amount of historical data, and lack of electronic files for changes in skilled personnel. To this end, research and design high-skilled talent information management system to grasp the construction and development of skilled talents, understand the changes of skilled talents, and build a large database of skilled talents information based on the intranet of the group company. Collect high-skilled talent information globally, realize unified information management and resource sharing, timely grasp the changes in the basic data of the skills of employees in all units, make a reserve of skilled talent resources, and improve the management of statistics, query, and evaluation of high-skilled talents.

2.3. Information Management System. The construction of an information management system plays an increasingly important role in the economic activities of enterprises. The application of our country's information management system is developing in a large-scale and networked direction. At the same time, information management technology is also continuously automated and intelligent. However, the traditional information management system still stays in the simple classification and storage of data in the form of tables. It has a low degree of intelligence and low information utilization efficiency. It does not really realize the functions of forecasting, decision-making, and optimization. Meet the needs of enterprise development [24].

An information management system (IMS) is a system composed of people, computers, and other related equipment. It is mainly used to manage the information required by users. It has data processing and auxiliary decision-making functions and is an information system for management services [25]. Like other disciplines, the information management system also has a process of continuous development and improvement, and various references have different opinions on its origin. Early IMS was limited by computer software, hardware, and network communication technology at that time, and many of them were developed based on CP-ALN. In this system mode, the database is built on the file server, but the database management system and database applications are still running on the workstation (usually the CP machine). The performance of servers and workstations in this type of system is difficult to make full use of the network transmission speed is very slow, and it is easy to cause network bottlenecks. When developing IMS, you can only consider more workstations with poor performance. Various IMS development standards are not unified, it is difficult to exchange information with the outside world, and it is impossible to use today's rich Internet resources. Because the traditional IMS development cycle is long and difficult to develop; if the user's needs change, it is difficult to modify the system to meet new requirements. Traditional IMS can only deal with narrowly defined information such as finance, sales, and inventory and cannot handle nonbusiness broad information such as internal management information, corporate culture information, and daily administrative communication of enterprises. It is inconvenient to operate, and the user interface is not uniform and not intuitive, which causes inconvenience to use, difficult training, and complicated maintenance [26]. With the rapid development of information technology applications, the inherent disadvantages of traditional IMS have become increasingly prominent. Information technology is developing rapidly, new technologies are constantly emerging, and the requirements of IMS for various parties are constantly increasing [27].

With the development of society, the improvement of computer performance and cost reduction, and the improvement of public computer operation skills, the management work of enterprises, institutions, and government agencies will develop in the direction of information, paperless, digital, and network. The popularity of information management systems is and will greatly change our way of life in the future. The information management system can not only complete the basic functions of traditional information systems but also have many functions that traditional information systems cannot achieve, such as information prediction and auxiliary decision-making. Information system security is an issue that information systems must consider, to ensure the integrity, availability, and confidentiality of information. Information system security planning is a very detailed and very important task. There are many common security threats to information systems, such as information leakage, illegal use, bypass control, counterfeiting, infringement of authorization, theft, and business fraud.

In order to meet the needs of the daily management of skilled personnel in the group company, from the perspective of actual management work and functions, the basic unit can guide the basic information and identification information of employees according to the Excel template. When there is an error in the guide data, the basic unit can download the error data and continue to guide after the maintenance is correct. The interface must be beautiful, concise, and easy to operate, and it is convenient for the basic units to maintain data. Facilitate comprehensive query and statistics of skilled personnel data. The ability to automatically generate reports is required for daily management. According to various conditions, you can query the data results required for statistics.

3. Experiments

3.1. Development Environment. This system is based on Windows operating system, the development tool is Microsoft Visual Studio 2008, the development language is ASP.NET, C #, the network platform architecture is B/S architecture, and the Web service middleware uses IIS7.5, as shown in Table 1. Strictly follow web security specifications, double authentication in front and back, and parameter encoding transmission.

3.2. System Architecture Design. According to the needs of business operations, in order to meet the needs of the group company to access the technical personnel management information system through the intranet to perform technical personnel information management, to achieve information sharing, comprehensive application, and visual analysis and statistics of technical personnel, the system adopts a three-layer software structure that is currently popular in distributed systems and is divided into an interaction layer, a service layer, and a data layer, as shown in Figure 2.

The interaction layer is the external interface between the system and the user. It only provides the user interface of the application and is responsible for interacting with the user. The results of various functions in the service layer are displayed in a centralized manner to provide a visual form of the basic services required by the user and the expected results.

The service layer is the key to the application system. Responsible for processing all user requests, performing specific calculations, and processing business processes. According to the specific data provided by the data layer,

Table 1: System development environment configuration standards.

System environment	Configuration standard
Operating system	Windows
Development tools	Microsoft Visual Studio 2008
Development language	ASP.NET, C#
Network platform architecture	B/S
Web service	IIS7.5

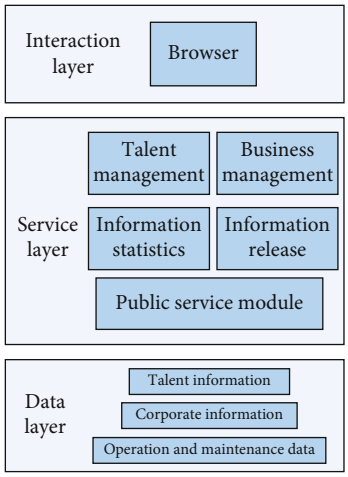

Figure 2: System framework structure.

specific functions such as user information management and maintenance, information statistics, and information release are realized. It also manages specific parameter settings during system operation and the interaction between the system and other systems.

The data layer stores the underlying data related to system operation, as well as personal information registered by individual users and corporate users. The data layer uses database technology to maintain and update applications. System resources are accessed in an authorized manner, and user passwords and access authorization are implemented for sensitive resources. Ensuring controllable and traceable sensitive resources will effectively ensure data security.

3.3. System Database and Module Design

3.3.1. System Function Module. Reporting needs and business processes based on skilled talent information. It is determined that the high-skilled talent information management system mainly includes eight modules of basic personnel information, skills identification information, high-skilled talent management, competency evaluation, key research teams, common reports, comprehensive query, and system maintenance, as shown in Figure 3.

3.3.2. Evaluation Design of Competence of High-Skilled Talents Based on Multisensor Information Fusion. The high-skilled talent management system can be based on the

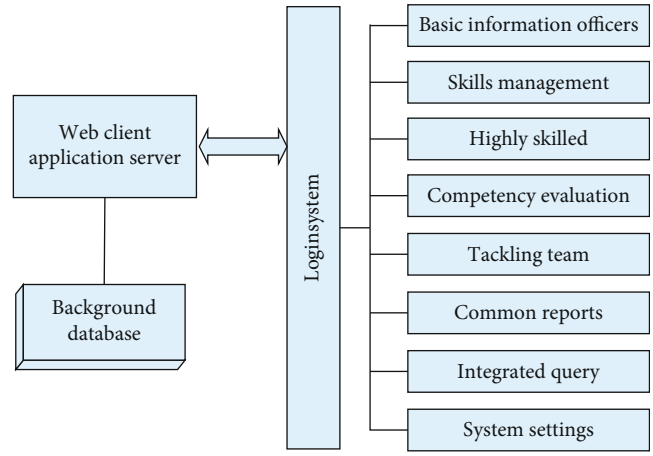

Figure 3: System function module division.

competency model to help companies find talents that meet the quality characteristics of project implementation requirements, in order to avoid the adverse consequences and losses caused by talent errors. When selecting competent high-skilled talents for the project, not only the knowledge and skills should be examined but also the inherent personal qualities such as their personal qualities and role positioning. The influencing factors for determining competence are academic qualifications, professional titles, honors, skills competitions, assessment results, technical papers, and competence levels. The evaluation is classified as excellent (0.9-1), consistent (0.7-0.9), and not consistent (0-0.7). The BP multisensor information fusion algorithm is used here, and the influencing factors are used as the input layer input. The calculation steps of the established multisensor information fusion model are as follows.

The selection range of connection weight and threshold is uniformly distributed at (-0.3, 0.3) random numbers; the range of threshold value $\theta_0, \theta_1, \theta_2$ is (0, 0.3) uniformly distributed random numbers. Activation function selection is

$$f(x) = \frac{1}{1 + e^{-x}}. \tag{8}$$

Randomly assign a smaller value to w_1, w_2, θ_0, θ_1, and θ_2 and get the activation value of the input layer:

$$\begin{aligned} &\text{data\_training\_in-data\_training} + \theta^0, \\ &\text{data\_input\_out} = f(\text{data\_training\_in}). \end{aligned} \tag{9}$$

Calculate the inputs and activations of the output layer:

$$\begin{aligned} &\text{data\_hide\_in} = w_2 * \text{data\_hide\_out} + \theta_2, \\ &\text{data\_output} = f(\text{data\_output\_in}). \end{aligned} \tag{10}$$

Output layer error signal is

$$w_1 + w_1 + \beta * \text{data\_input\_out} * \delta^y. \tag{11}$$

Calculate the hidden layer error signal:

$$\delta^{y} = \text{data\_hide\_out} * (1 - \text{data\_out}) * \sum_{1}^{k} w_2 * \delta^{0}. \quad (12)$$

Utilizing a mature multisensor information fusion model, when the quantitative numbers of factors affecting the competency evaluation of a high-skilled talent are collected, they can be entered into the model, so that the level of competence of high-skilled talents (excellent, consistent, noncompliant).

4. Discussion

4.1. Design and Implementation of User Login Module and Main Interface

4.1.1. Design and Implementation of User Login Window. In order to improve the security of the information, under the premise of ensuring the security of the system, when setting the user to log in to the system, the user enters a user name and password, and the system will transfer this information to the server for review and verification. The login flow chart is shown in Figure 4. All the information entered is correct. If the verification is passed, the system will jump to the next interface, and the user can successfully select the required module for operation. If the user name or password is wrong or one of them is wrong, the system will prompt you to enter the wrong user name and password and keep logged in, as shown in Figure 5; if the user forgets the original password, the user can follow the instructions in the password recovery module The original password needs to be restored. To do this, the user must enter the password set by the user to restore the question prompt. If the prompt is answered correctly, the original password will be successfully retrieved.

4.1.2. Design and Implementation of Main Interface. After the username and password are entered correctly, the system will automatically jump to the main user interface. This interface includes basic personnel information, skill identification information, high-skilled talent management, competency evaluation, key research team, common reports, comprehensive query, and system maintenance. As shown in Figure 6, it is the main user interface.

4.2. System Test

4.2.1. System Module Test. The system function test is used to ensure that the operation results of the system are as expected. During the test process, the black box test method is used to test each functional module. In the test, the tester compares the required functions to determine the test cases, so as to test the operating results of the entire system. Unit testing is usually used to achieve functional coverage testing. The method used in the testing process is white box testing to test each module. Write corresponding test cases during the test to verify the difference between test results and test expectations. If there

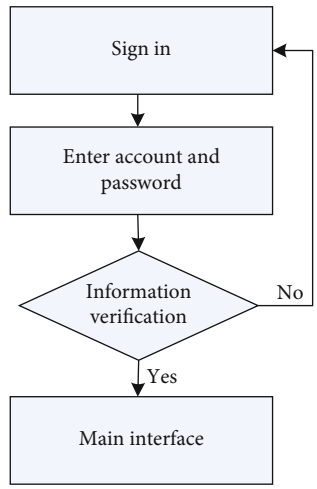

Figure 4: Login flowchart.

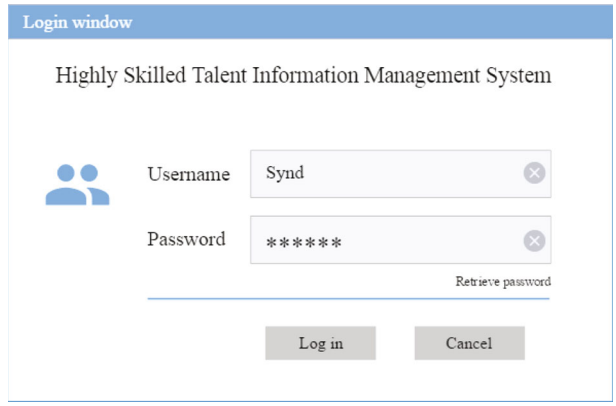

Figure 5: User login window.

are differences, make corresponding adjustments, as shown in Figure 7, which is a user login failure graph.

By testing the system modules, the test results are the same as the expected results, indicating that the system modules operate normally and can meet the needs of users.

4.2.2. System Usability Test. Regarding the ease of use of the system, a survey was conducted for public users, talent users, enterprise users, and system administrators, with 50 people in each category and 200 people in total. Using the analytic hierarchy process, various users rate the system's use, with 0 being the lowest in ease of use and 5 being the highest in ease of use. The survey results of various users are shown in Figure 8.

It can be seen that 156 users rated the system above 3 points, accounting for 78% of the survey population, indicating that the system has certain ease of use. Test effectiveness through test cases can help testers find defects faster. Through testing, we know that under the simulated operating environment, the highly skilled personnel information management system including hardware, software, network,

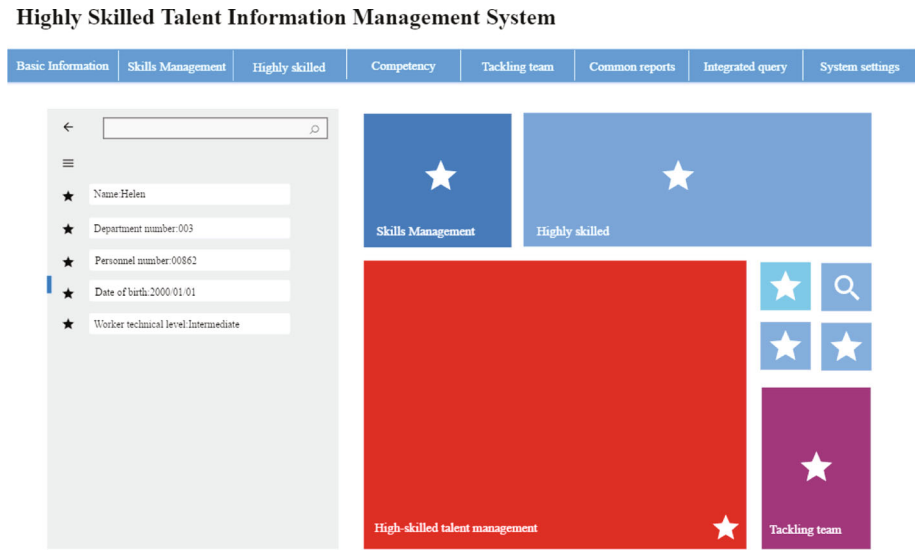

Figure 6: User main interface design.

Figure 7: User login failure prompt window.

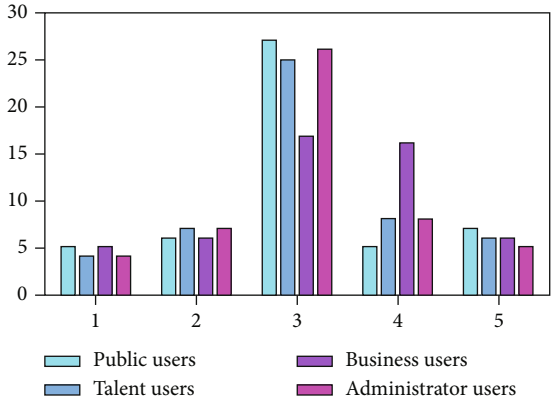

Figure 8: Usage survey results.

and support platforms is properly configured and connected to meet user needs. It can meet the corresponding requirements in many aspects such as functionality, reliability, software design, compatibility, and security.

5. Conclusions

This article designs and implements a high-skilled talent information management system based on multisensor information fusion. Through system testing, we know that under the environment of simulating system operation, the highly skilled personnel information management system includes hardware, software, network, and support platforms, which are properly configured and connected, which can meet users' functional requirements and system design for the system, and has certain applicability.

The high-skilled talent information management system designed based on multisensor information fusion in this paper has realized the transformation from artificial paper records to information management methods, electronicized the basic data of skilled talents, and quickly grasped the distribution of employee skills information data in the unit. It plays an important role in standardizing the professional management of skilled personnel and improving the management efficiency of skilled personnel. Multisensor information fusion-based competency evaluation design for high-skilled talents helps companies find qualified talents that meet the requirements and avoids the negative consequences and losses caused by human error.

At present, the information management system of high-skilled talents provides a development environment for standardizing the professional management of high-skilled talents. In view of the scalability and information resources of the information management system, the future research direction can connect the information management system message with SMS and WeChat and realize the application in the field of intelligent mobile.

Data Availability

No data is involved in this article.

Conflicts of Interest

The author declared no potential conflicts of interest with respect to the research, authorship, and/or publication of this article.

References

[1] C. Ialongo, M. Pieri, and S. Bernardini, "Artificial neural network for total laboratory automation to improve the management of sample dilution," *SLAS TECHNOLOGY: Translating Life Sciences Innovation*, vol. 22, no. 1, pp. 44–49, 2017.

[2] H. Wang, X. B. Zhang, X. G. Ge et al., "Design and implementation of information management system for Chinese materia medica resources survey," *China Journal of Chinese Materia Medica*, vol. 42, no. 22, pp. 4287–4290, 2017.

[3] C. Yuan, X. Zhao, and Y. Liu, "The design and implementation of the university alumni management system," *International Journal of Advanced Pervasive & Ubiquitous Computing*, vol. 8, no. 1, pp. 13–29, 2016.

[4] B. Chenglin, "The design and implementation on the network environment of the multimedia information processing system," *Computer Engineering & Software*, vol. 4, pp. 90–94, 2016.

[5] L. Huan-Zhang, X. Jing-Bo, Q. Men-Bao et al., "Design and implementation of field questionnaire survey system of taeniasis/cysticercosis," *Chinese Journal of Schistosomiasis Control*, vol. 30, no. 2, pp. 211–214, 2018.

[6] N. Chettibi, A. Mellit, G. Sulligoi, and A. Massi Pavan, "Adaptive neural network-based control of a hybrid AC/DC microgrid," *IEEE Transactions on Smart Grid*, no. 99, pp. 1–13, 2016.

[7] P. Wang, S.-T. Huang, J. Wang et al., "Development of geoinformation data management system and application to geological disposal of high-level radioactive waste in China," *Nuclear Technology and Radiation Protection*, vol. 32, no. 3, pp. 294–301, 2017.

[8] Y. Liu, S. Hao, Y. Lü, J. Liu, and D. Xu, "Implementation and application of the new information system of air pollution and health impact monitoring," *Journal of Hygiene Research*, vol. 47, no. 1, pp. 97–102, 2018.

[9] R. Weijian, Z. Shan, and H. Fengcai, "Design and implementation of oilfield archive management system based on petri net and custom technology," *Journal of Jilin University*, vol. 34, no. 5, pp. 635–644, 2016.

[10] L. Zhang, A. Bose, A. Jampala, V. Madani, and J. Giri, "Design, testing, and implementation of a linear state estimator in a real power system," *IEEE Transactions on Smart Grid*, vol. 8, no. 4, pp. 1782–1789, 2017.

[11] W. Kim, "A design and implementation of the real time 4-channel image processing system for vehicle using the smart phone," *Journal of Computational and Theoretical Nanoscience*, vol. 23, no. 4, pp. 3763–3766, 2017.

[12] P. Yue, Z. Wu, and B. Shangguan, "Design and implementation of a distributed geospatial data storage structure based on spark," *Wuhan Daxue Xuebao (Xinxi Kexue Ban)/Geomatics and Information Science of Wuhan University*, vol. 43, no. 12, pp. 2295–2302, 2018.

[13] Y.-J. Zhang, Z. Li, and Q. Liu, "Design and implementation of remote monitoring system for high frequency vibrator," *Chung-kuo Tsao Chih/China Pulp and Paper*, vol. 37, no. 12, pp. 51–55, 2018.

[14] J. Li, "Information integration management system for spiral bevel gear networked manufacturing process," *Transactions of the Chinese Society of Agricultural Engineering*, vol. 33, no. 15, pp. 227–236, 2017.

[15] W. Ma, J. Ren, and X. Wei, "Design and implementation of CORS-based mobile field geographic information verification and acquisition system," *Journal of Geomatics*, vol. 42, no. 4, pp. 98–101, 2017.

[16] S. C. Ripamonti and L. Galuppo, "Work transformation following the implementation of an ERP system," *Journal of Workplace Learning*, vol. 28, no. 4, pp. 206–223, 2016.

[17] M. K. Hassan and S. Mouakket, "ERP and organizational change," *International Journal of Organizational Analysis*, vol. 24, no. 3, pp. 487–515, 2016.

[18] S. Shen, L. I. Zhe, J. I. Qinghui, and X. Chen, "Design and implementation of construction management information system for North Hubei water transfer project," *Journal of Yangtze River Scientific Research Institute*, vol. 33, no. 11, pp. 68–72, 2016.

[19] G. Wang, Z. Li, and Y. Li, "Design and implementation of mobile information system for electric power engineering environment evaluation water conservation," *Journal of Geomatics*, vol. 43, no. 5, pp. 100–103, 2018.

[20] B.-q. Chen, X.-d. Tian, H. Cao, J. K. Jia, and Y. Zhang, "Design and implementation of 3-D GIS-based monitoring and warning system for geological hazard in Danjiangkou reservoir area," *Journal of Yangtze River Scientific Research Institute*, vol. 33, no. 7, pp. 51–54, 2016.

[21] M. Zhou, Y. Long, W. Zhang et al., "Adaptive genetic algorithm-aided neural network with channel state information tensor decomposition for indoor localization," *IEEE Transactions on Evolutionary Computation*, p. 1, 2021.

[22] M. Zhou, Y. Li, M. J. Tahir, X. Geng, Y. Wang, and W. He, "Integrated statistical test of signal distributions and access point contributions for Wi-Fi indoor localization," *IEEE Transactions on Vehicular Technology*, vol. 70, no. 5, pp. 5057–5070, 2021.

[23] Y. Lee and J. Cho, "RFID-based sensing system for context information management using P2P network architecture," *Peer-to-Peer Networking and Applications*, vol. 11, no. 6, pp. 1197–1205, 2018.

[24] N. Maarop, K. Thamadharan, G. N. Samy et al., "Information security management system implementation success factors: a review," *Advanced Science Letters*, vol. 22, no. 10, pp. 3023–3026, 2016.

[25] N. Maarop, G. N. Samy, P. Magalingam, W. M. H. W. Affandi, W. Z. Abidin, and S. Ya'acob, "Exploring usability key issues regarding research management information system: a case study in research institute," *Advanced Science Letters*, vol. 24, no. 1, pp. 695–698, 2018.

[26] X. Mei and Y. Lu, "Development of implantable medical device traceability management information system," *Chinese Journal of Medical Instrumentation*, vol. 40, no. 5, pp. 359–362, 2016.

[27] O. Yigitbasioglu, "Firms' information system characteristics and management accounting adaptability," *International Journal of Accounting and Information Management*, vol. 24, no. 1, pp. 20–37, 2016.

Hindawi
Journal of Sensors
Volume 2021, Article ID 4284249, 7 pages
https://doi.org/10.1155/2021/4284249

Research Article

Application of Posture Recognition Service System Based on Information Fusion Smart Sensor in Dance Training

Yan Gao[1,2] **and Dazhi Xu**[3,4]

[1]*College of Art, Hunan University of Arts and Science, Changde, 415000 Hunan, China*
[2]*School of Management, Shinawatra University, Bangkok 12160, Thailand*
[3]*College of Economics and Management, Hunan University of Arts and Science, Changde, 415000 Hunan, China*
[4]*School of Public Administration, Central South University, Changsha, 410083 Hunan, China*

Correspondence should be addressed to Dazhi Xu; xudazhi@huas.edu.cn

Received 4 June 2021; Revised 30 June 2021; Accepted 30 July 2021; Published 10 August 2021

Academic Editor: Mu Zhou

With the development and extension of the Internet of Things technology, many fields have already involved the Internet of Things technology, and its application in dance training has gradually emerged. In order to guide dance training and solve the hidden dangers of dance training, this article mainly introduces the application of posture recognition service system based on information fusion intelligent sensor in dance training. This article uses human body detection, computer interactive Boosting algorithm calculations and establishes standard dance poses. The difference between the trainer's posture and the standard posture can be clearly seen on the posture recognition service platform. The error is only less than 5%, and it can also help the trainer find their own mistakes in time. Dance and correct your posture in time, and it can reduce the error rate of difficult dances and reduce the error rate of 10%-20%. In addition, through the survey on the satisfaction survey of the security services of the gesture recognition service platform, the satisfaction rate is as high as 90%. Thereby, while ensuring safe training, the dance quality and level of trainers are improved.

1. Introduction

1.1. Research Background and Significance. The Internet of Things technology can combine the sensor personnel and terminal equipment by using local network and other communication technologies to realize the connection of people and things to form an intelligent network for remote management and control. It can provide targeted services for dance training under the condition of realizing resource sharing. Connecting dance training with the gesture recognition service platform is of great significance to the dance training process and results. In the current dance training process, the learner usually achieves the purpose of training by watching the video repeatedly or by seeking corrective guidance from the coach himself. This not only consumes a lot of time and energy but also brings certain difficulties and challenges to the trainer. Therefore, this article combines the posture recognition service platform based on information fusion smart sensors to collect standard dance moves, analyze the gap between the trainer and the standard dance, so that the trainer can intuitively feel the gap, and help the trainer discover themselves in time during dance training. By combining dance training with information fusion smart sensors to recognize postures, apply information fusion smart sensors and other technologies to capture the entire training movement and collect dance movement data and then match and compare with standard movements to analyze user movements and standards The size of the gap in the direction of the action bones allows the user to find the gap more intuitively. This method enables the majority of dance teaching workers, dancers, and dance learners who have a strong demand in teaching and self-study to make accurate adjustments to their unstandardized dance gestures, thereby ensuring the accuracy of dance gestures in training.

At the same time, it is not restricted by time and geographical location and can be trained at any convenient time and place, which broadens the teaching methods.

1.2. Related Content. With the development of the Internet of Things technology, related research on the Internet of Things has also become an important focus. Zamanifar et al. proposed a distributed self-healing motion prediction scheme for IoT applications, namely, DSHMP-IOT, to predict the motion direction of mobile IP-based sensors in multiuser environments (such as healthcare systems) [1]. This is the first time that an AI solution has been applied to predict the direction of mobile nodes in an IP-based mobile network. The proposed scheme utilizes an implicit semi-Markov model (HSMM) to predict the direction of motion with high accuracy and low overhead. A previous work for estimating the direction of a mobile node in an IP-based mobile network was based on AOA (a hardware-specific method) [2]. Compared with similar methods, his scheme has advantages in power consumption, switching delay, and packet loss. However, there are limitations in identifying differences [3, 4]. Wilson and Bobick proposed a new method for representing, recognizing, and interpreting parametric poses [5]. The so-called parameterized posture refers to the posture that shows the spatial change of the system; the first is the point posture, where the relevant parameter is the two-dimensional direction. His method is to extend the standard hidden Markov model method of gesture recognition by including global parameter changes in the output probability of the HMM state [6]. He used the visually obtained and directly measured three-dimensional body position measurement value as input. The results he gave proved the recognition advantage of PHMM over standard HMM technology and the parameter estimation compared with the noise in the input feature and higher pertinence [7, 8]. His method is pertinent, but not universal. Chakraborty et al. found that intensive whole-body dance training may cause the fibers connecting different brain regions to spread out in a larger fan shape, increase the cross fibers, or increase the axon diameter [9]. In contrast, musicians show lower diffusion and greater fiber coherence in similar areas. Crucially, diffusion measures are related to performance in dance and music tasks, thereby distinguishing groups. This shows that dance and music training have opposite effects on the structure of WM [10, 11]. Therefore, music training may result in a more focused focus on a specific approach to the effector. This finding emphasizes that different types of training can have different long-term effects on brain structure, thereby expanding the understanding of brain plasticity [12]. However, there is no comparative study from other aspects, and there is a certain degree of one-sidedness.

1.3. Main Content and Innovation. Through the human body detection, computer interactive calculation, and the establishment of standard dance poses, the posture recognition method based on the angle of the human joint points is improved, which can automatically collect and recognize the dance movements of the trainer. Evaluate the dance posture of the trainer in two aspects of the angle formed by the joints, and give an action comparison chart and guidance suggestions. The innovation of this paper is to use the combination of smart sensors and gesture recognition services and make full use of the advantages of smart sensors of the Internet of Things to give play to the construction and use of the gesture recognition service platform, thereby providing assistance to dance training and promoting the combined development of dance field and technology [13, 14].

2. Establish a Database and Research Methods

2.1. Boosting Algorithm. Each training set selected by the Boosting algorithm depends on the results of the previous learning. In sampling and calculation according to the error rate, it can effectively combine the errors of the last dance in dance training to achieve dance training progress [15, 16]. The Boosting algorithm can significantly reduce model prediction bias. Since the entire Boosting model is a serial combination of multiple base learners, resulting in a strong correlation between the models, the Boosting algorithm generally cannot significantly reduce the prediction variance [17]. By changing the weight distribution, the classifier can strengthen the learning of data that is defined as difficult to classify and then integrate multiple weak classifiers into a strong classifier. The algorithm deviation value is shown by

$$\text{Bias} = E\left(\sum_{n-1}^{N} y_n * f_n\right) = y * \sum_{n-1}^{N} E(f_n). \tag{1}$$

Among them, Bias represents the parameter of Boosting, E represents the number of dances, and f_n represents the dancer's mastery of the dance.

2.2. Establish a Standard Dance Movement Database. The human body is represented as a whole that is rigidly connected by multiple joint points. Each joint point is connected by a rigid body, and each joint point represents a characteristic point, and the length of the rigid connection body is unchanged, so the human body can be. Movement is simplified to the movement of the human skeleton. In order to correct the dance moves of the trainer, there must be a standard dance move as a comparison template. In this part, by acquiring the dance moves of the dance coach, the joint points of the body are detected to form standardized motion data [18, 19]. This article invites professional dance coaches to demonstrate standard dance moves, collects dance movement data using the gesture recognition service platform, marks each group of data with the corresponding action name, and saves it as movement information as a comparison template for trainers. The database records the standard movements of teachers of different dance styles, which can meet the training needs of beginners, and its service platform can also record new standard movements according to the different needs of trainers in the later stage.

2.3. Questionnaire Method. This article conducted a satisfaction survey on the safety of the dance studio's gesture recognition service platform. The survey respondents included dance teachers, trainers, and trainers' parents. Among them,

there were 50 dance teachers and 100 trainers and trainers' parents. The survey questions are mainly about the satisfaction and opinions of the safety reminder service.

3. Gesture Recognition Processing Technology and Processing Flow

3.1. Key Points of Gesture Recognition. In dance, gesture recognition mainly relies on the recognition of joints for gesture recognition. By dividing the dancer's hand steps to be composed of nodes, using sensors to collect the key nodes of the hand, the dancer's hand data can be obtained. Through comparison, the accuracy of the dancer's hand movements can be effectively improved. The joint points of the human body are to connect the human body through the joint points. The key to joint recognition is as follows:

It can be seen from Table 1 that the key points have four parts, namely, input model diagram, extraction of body part distribution points, body joint point detection, and output of human skeleton. In this way, the dancer's posture can be more comprehensively identified and analyzed.

3.2. Gesture Recognition Processing Model. This article selects three operations of rotation, scaling and flipping. Assuming that the position of the person in the input image has been detected, this formula is calculated by recognizing the posture. The data enhancement is generated in a given detection frame [20]. Rotation includes clockwise or counterclockwise rotation around the center position. Take the first pixel in the upper left corner as the origin of the coordinates, specify the origin coordinates as $(1, 1)$, rotate the original picture with the size (G_x, G_y) around the center, and convert the labels of each key point into the rotated coordinate system:

$$x_i^s = \left(x - \frac{G_x}{2}\right)\cos\theta - \left(y - \frac{G_y}{2}\right)\sin\theta + \frac{G_x^s}{2}. \quad (2)$$

x is the value of the coordinate system of the i-th key point after the rotation, the picture after the rotation is G, and the size is

$$G_x^s = \left(G_y - G_x\tan\theta\right)\sin\theta + G_x\cos\theta. \quad (3)$$

Scaling means that the image is enlarged or reduced. The image size will be larger than the original size when it is enlarged, and it needs to be cropped according to the original image size; when it is reduced, it is necessary to make assumptions about things outside the image boundary, resulting in a variety of scale transformations [21, 22]. Flip includes horizontal flip and vertical flip. It is a kind of mirror-like flip. Vertical flipping of the posture of the human body will make the human body upside down. Therefore, this article chooses horizontal flip to change the posture of the human body left and right. Suppose the coordinates (x, y) of a certain key point in the original image are flipped to obtain the corresponding j-th key point coordinates:

Table 1: Key points of human joint recognition.

Serial number	Key point
1	Input model diagram
2	Extract the distribution points of body parts
3	Body joint point detection
4	Output human skeleton

$$\begin{cases} x_j^s = G_x^r - x_i^r, \\ y_y^s = y_s^r. \end{cases} \quad (4)$$

Flip in the last step to reduce the operation cost, and increase the data set while seeing the potential changes of the image; the authenticity is higher. The horizontal flip does not affect the coordinate changes of the joint points of the head, but the marking order of the corresponding joints is changed in the wrist, elbow, and other parts. By using rotation, scaling, and flipping operations on the image data, the training set of the image is enriched, so that the model has as many samples as possible, avoiding the over-fitting of a limited number of samples and improving the generalization ability of the model [23, 24].

3.3. Human Target Detection without Pose Restriction. Human gesture recognition can generally be divided into direct methods and indirect methods. The direct method is to establish a human body pose model, compare the collected human body data with the model one by one, and find the most similar human body pose. The indirect method is a method based on predictive generative model, which predicts the characteristic contour according to the collected human body data and recognizes the human posture according to the characteristic contour.

First, quickly find many candidate human bodies from the image to be detected. Due to the influence of noise, etc., there are many nonfalse positive human targets in the candidate body. Then, we calculate the HOG descriptors of the candidate body coverage area in the image and input the calculated HOG features into the support vector machine for classification, so that the false positive sample points of the candidate body set obtained in the first step can be removed [25]. Use the shape context to quickly detect the human target from the inside and outside of the contour image of the shape to obtain a set of points. The shape of the object in the image can be represented by these discrete points. To describe these points, they proposed a shape context descriptor. Comparing whether two points are similar can be achieved by comparing the shape context descriptors of the two points, and the similarity of the two shapes can be judged by matching the context descriptors of a discrete point set. The context descriptor of a discrete point p_i on the shape S is represented by a histogram h_i of the relative coordinates of p_i and other points:

$$h_{i(k)} = \#\{q \neq p_i : (q - p_i) \in bin(k)\}. \quad (5)$$

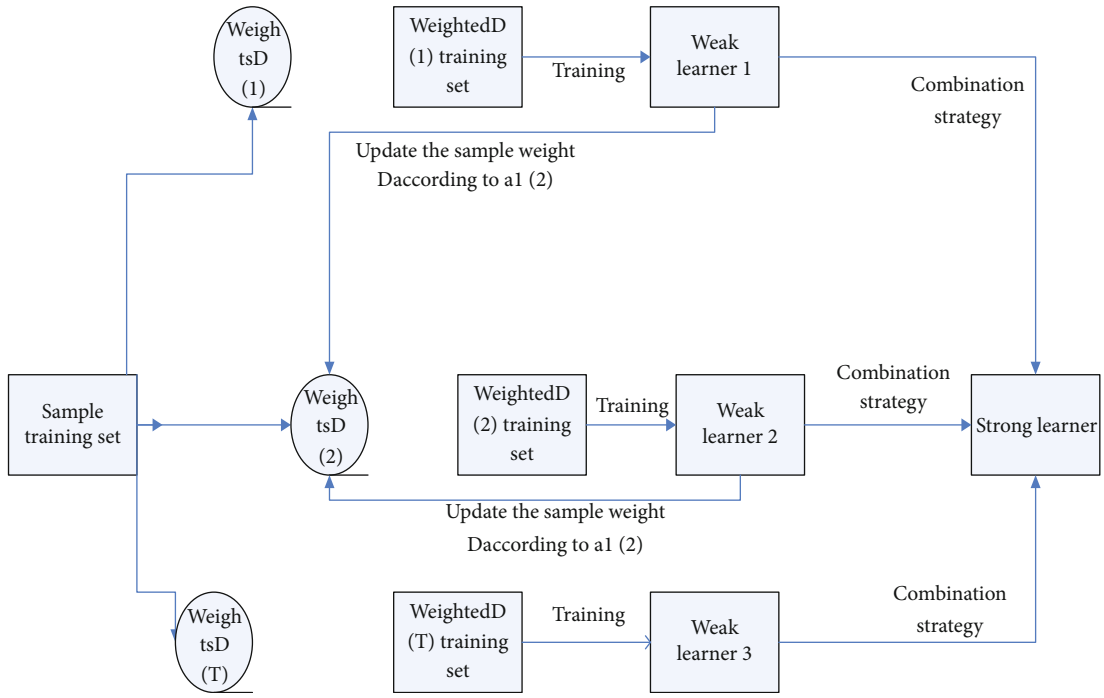

Figure 1: Boosting algorithm flow.

Next, we describe the process of applying shape context descriptor matching. We have used the human body image set to establish three human body shape templates from different perspectives [26]. For each shape template, we obtain a point set through sampling and then calculate the shape context descriptor of each point in the point set and use this set of context descriptors as the human body shape feature. Randomly sample from the image boundary to get r (approximately take the set S_s of 1/8 points of the total boundary pixels). For any point p_i of the set S_s, calculate the matching degree with any point qj in the template shape T. The distance is defined as follows:

$$C_{ij}^{t} = \frac{1}{2}\sum \frac{\left[h_i(k) - h_j^t(k)\right]^2}{h_i(k) + h_j^t(k) + \varepsilon}. \tag{6}$$

In formula (2), h_i and h_j are the shape context descriptors of the point p_i on the image to be detected and the point on the template image qj, respectively, and $h_i(k)$ and $h_j(k)$ are the k-th component of the descriptor. To prevent the denominator on the right side of the formula from being zero, add a small positive value to the denominator. In the scene with noisy background, the boundary obtained by applying the edge detection algorithm contains a large number of noise points [27]. In order to reduce the influence of noise, we modify the matching cost function of formula (2). In formula (2), if $h_j(k)$ is equal to zero and $h_i(k)$ is not equal to zero, we discard the difference of this component and redefine the matching distance:

$$C_{ij}^{t} = \frac{1}{2}\sum \frac{\left[h_i'(k) - h_j^t(k)\right]^2}{h_i'(k) + h_j^t(k) + \varepsilon}. \tag{7}$$

In formula (3), h' is the modified shape context descriptor, which is defined as follows:

$$h_i'(k) = \begin{cases} 0, & \text{if } h_i^t(k) = 0, \\ h_i(k), & \text{else.} \end{cases} \tag{8}$$

The lines in the two images have similar shapes and are located at corresponding positions. The distance between the shape context descriptors should be as small as possible. The distance calculated by formula (3) is calculated by using our modified descriptor. Since the influence of noise points in the image is removed, the distance between the two descriptors is small, which is much smaller than the former. Therefore, through comparative analysis, we can effectively suppress the influence of image noise points on shape context matching by modifying the distance calculation formula. In this way, the dance form can be accurately judged.

3.4. Boosting Algorithm Flow. It can be seen from Figure 1 that the process is as follows: first, set the same weight value for each training sample, and train a weak divider under this training sample distribution. Use the weak classifier to update the weight of each sample, classify incorrectly classified samples as difficult to classify, and increase their weight, while reducing the weight of correctly classified samples to form a new weight distribution; under the new weight distribution, train a new weak classifier and update the weight

Table 2: Comparison of trainer's movements and standard joint coordinates.

Location	Standard dance joint point coordinates		Trainer's joint point coordinates	
	Abscissa	Y-axis	Abscissa	Y-axis
Head	-50	100	-55	95
Neck	-20	20	-25	25
Left shoulder	-100	-50	-105	-40
Left hand	-500	-60	-505	-100
Right hand	100	-10	300	300
Right shoulder	50	500	90	100

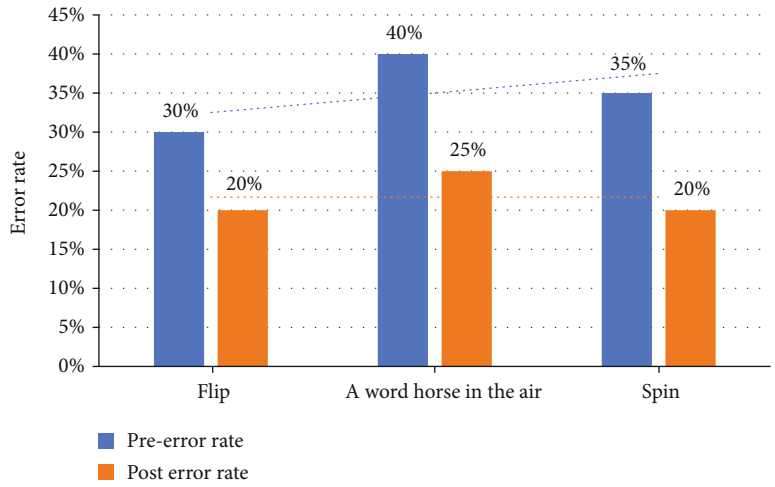

Figure 2: The error rate before and after the assistance of the dance recognition service platform.

value with reference to the second step. Repeat the above process T times to obtain T new weak classifiers. By changing the weight distribution, the classifier can strengthen learning for those data that are defined as difficult to classify. And then integrate multiple weak classifiers into a strong classifier.

4. Dance Training Effect and Safety Satisfaction

4.1. Dance Posture Correction Training. The correction training collects the joint coordinates of each movement of the trainer and then compares it with the standard movement of the dance instructor, as shown in the figure below. By comparing the movement trajectory of the joint points, the gap between the trainer and the standard movement can be found intuitively, and then, the learner's dance posture can be corrected.

It can be seen from Table 2 that the position coordinates of the head, neck, shoulders, and hands of the trainer and the standard dance. The dance position of the trainer's head, neck, and left shoulder is not much different from the standard dance position, and they are all within plus or minus 50 of the standard dance position. However, there is a big difference between the trainer's hand and right shoulder and the standard dance. The ordinate of the left hand differs by 50 points, and the abscissa and ordinate of the right hand differ by 200 and 290 points, respectively. At the same time, the right shoulder the ordinate also differs by 400 points. This shows that the ascending height of the trainer's arm does not meet the standard requirements, and the ascending height should be increased, and the closing movement is too fast, and it does not agree with the standard movement, resulting in a difference in the right shoulder. Therefore, trainers can follow up their own training adjustments according to the dance posture recognition service platform, perfect one's dancing posture, correct their unqualified dance postures, and reach a higher level of dance.

4.2. Strengthen the Learning of Difficult Dances. It can be seen from Figure 2 that the error rate before the assist of the flip dance is 30%, the error rate after the assist is reduced to 20%, the error rate of the air horse is reduced from 40% to 25%, and the error rate of the rotating dance is reduced from 35%. It is 20%. It can be seen that the learning of difficult dance poses has been assisted by the dance recognition service platform, which reduces the difficulty and error rate of difficult dance learning, making the dancer's learning more intuitive and simple, and can easily find errors and timely correct your mistakes and show perfect dance.

4.3. Ensure the Safety of Dance Training. The dancing posture recognition service system has a calculation of the distance of the safe joint points. The safety of the dancing posture is judged by the human body in the shape context and the distance between the joint point and the joint line. When the safe distance is exceeded, the dancing posture service

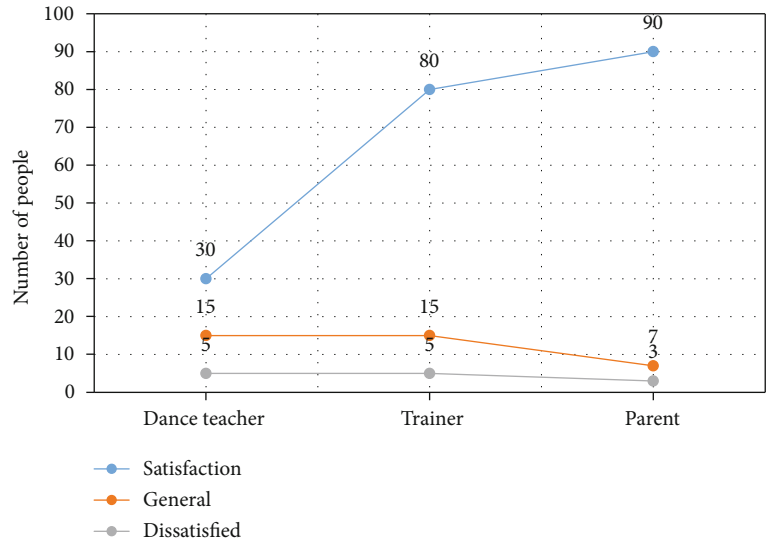

Figure 3: Service platform security service reminder satisfaction.

platform will use the camera and the connected mobile phone to perform safety reminder. The picture below is a satisfaction survey on the safety dance reminder service.

Figure 3 shows that the number of satisfied dance teachers is 30, the number of trainers is 80, and the number of parents of trainers is 90. Those who feel average and dissatisfied are only a very small part of the survey population. It can be explained that the safety reminder service style in the dancing posture recognition service platform has been recognized by everyone. Especially, parents have the highest satisfaction. It also shows that the safety of dance training is an aspect that everyone attaches great importance to.

5. Discussion

In this paper, a dance assisted training system is designed, which can analyze and evaluate the trainer's movements from the joint point coordinates and the angle formed by the joint and provide the trainer with intuitive error correction prompts. Experiments show that the system can accurately give the difference between the trainer's movement and the standard movement, and the trainer can adjust the movement posture according to the prompts, improve the dance level, and achieve the purpose of auxiliary training. With the rapid development of technologies such as human-computer interaction, smart sensors will be widely used in various aspects such as competitive sports, rehabilitation therapy, and somatosensory games. In addition, the safe posture detection in the posture recognition service system provides real-time tripartite joint reminders, which provides a safety guarantee for the safety of dance postures in dance training. This system only collects the basic dance training movement information of some dance coaches and cannot meet the needs of a large number of dance movement training. In the future, more professional coaches' dance moves can be collected to enrich the database.

Data Availability

No data were used to support this study.

Conflicts of Interest

The authors declare that there is no conflict of interest with any financial organizations regarding the material reported in this manuscript.

Acknowledgments

This work was supported by the Project of Hunan Provincial Social Science Achievement Review Committee, China (Grant No. XSP21YBC376), and the Excellent Youth Project of Department of Education of Hunan Province, China (Grant No. 20B395).

References

[1] A. Zamanifar, E. Nazemi, and M. Vahidi-Asl, "DSHMP-IOT: a distributed self healing movement prediction scheme for internet of things applications," *Applied Intelligence*, vol. 46, no. 3, pp. 569–589, 2017.

[2] M. McNinch, D. Parks, R. Jacksha, and A. Miller, "Leveraging IIoT to improve machine safety in the mining industry," *Mining, Metallurgy & Exploration*, vol. 36, no. 4, pp. 675–681, 2019.

[3] T. Hang, Y. Zheng, K. Qian et al., "WiSH: WiFi-based real-time human detection," *Tsinghua Science and Technology*, vol. 24, no. 5, pp. 615–629, 2019.

[4] M. Zhou, Y. H. Li, M. J. Tahir, X. L. Geng, Y. Wang, and W. He, "Integrated statistical test of signal distributions and access point contributions for Wi-Fi indoor localization," *IEEE Transactions on Vehicular Technology*, vol. 70, no. 5, pp. 5057–5070, 2021.

[5] A. D. Wilson and A. F. Bobick, "Parametric hidden Markov models for gesture recognition," *IEEE Transactions on Pattern*

Analysis and Machine Intelligence, vol. 21, no. 9, pp. 884–900, 1999.

[6] R. Dhall and V. K. Solanki, "An IoT based predictive connected car maintenance approach," *Ijimai*, vol. 4, no. 3, pp. 16–22, 2017.

[7] Z. Lu, X. Chen, Q. Li, X. Zhang, and P. Zhou, "A hand gesture recognition framework and wearable gesture-based interaction prototype for Mobile devices," *IEEE Transactions on Human-Machine Systems*, vol. 44, no. 2, pp. 293–299, 2014.

[8] F. Despinoy, D. Bouget, G. Forestier et al., "Unsupervised trajectory segmentation for surgical gesture recognition in robotic training," *IEEE Transactions on Biomedical Engineering*, vol. 63, no. 6, pp. 1280–1291, 2016.

[9] B. K. Chakraborty, D. Sarma, M. K. Bhuyan, and K. F. MacDorman, "Review of constraints on vision-based gesture recognition for human–computer interaction," *IET Computer Vision*, vol. 12, no. 1, pp. 3–15, 2018.

[10] M. C. Chiu and J. Y. Chiou, "Technical service platform planning based on a company's competitive advantage and future market trends: a case study of an IC foundry," *Computers & Industrial Engineering*, vol. 99, pp. 503–517, 2016.

[11] D. Liu, "Research on the construction of fitness service platform in colleges and universities," *International Core Journal of Engineering*, vol. 6, no. 4, pp. 110–114, 2020.

[12] P. Liu, W. Jiang, X. Wang, H. Li, and H. Sun, "Research and application of artificial intelligence service platform for the power field," *Global Energy Interconnection*, vol. 3, no. 2, pp. 175–185, 2020.

[13] G. Plouffe and A. M. Cretu, "Static and dynamic hand gesture recognition in depth data using dynamic time warping," *IEEE Transactions on Instrumentation and Measurement*, vol. 65, no. 2, pp. 305–316, 2016.

[14] L. M. Sampaio, S. Subramaniam, R. Arena, and T. Bhatt, "Does virtual reality-based kinect dance training paradigm improve autonomic nervous system modulation in individuals with chronic stroke?," *Journal of Vascular and Interventional Neurology*, vol. 9, no. 2, pp. 21–29, 2016.

[15] L. Laberge-Côté, "The porous body: cultivating malleability in traditional dance training," *Journal of Dance & Somatic Practices*, vol. 10, no. 1, pp. 65–77, 2018.

[16] F. A. Maruf, A. O. Akinpelu, B. L. Salako, and J. O. Akinyemi, "Effects of aerobic dance training on blood pressure in individuals with uncontrolled hypertension on two antihypertensive drugs: a randomized clinical trial," *Journal of the American Society of Hypertension*, vol. 10, no. 4, pp. 336–345, 2016.

[17] A. V. Maerle, D. V. Voronina, K. L. Dobrochaeva et al., "Immuno-PCR technology for detection of natural human antibodies against Lec disaccharide," *Glycoconjugate Journal*, vol. 34, no. 2, pp. 199–205, 2017.

[18] H. Ragb and V. Asari, "Multi-hypothesis approach for efficient human detection," *Journal of Imaging Science and Technology*, vol. 63, no. 2, pp. 20503-1–20503-13, 2019.

[19] M. Zhou, Y. M. Wang, Y. Y. Liu, and Z. S. Tian, "An information-theoretic view of WLAN localization error bound in GPS-denied environment," *IEEE Transactions on Vehicular Technology.*, vol. 68, no. 4, pp. 4089–4093, 2019.

[20] T. Kefi-Fatteh, R. Ksantini, M. B. Kaâniche, and A. Bouhoula, "Human face detection improvement using incremental learning based on low variance directions," *Signal, Image and Video Processing*, vol. 13, no. 8, pp. 1503–1510, 2019.

[21] M. Man, "Kitchen contemporary dance classes in times of COVID-19, dance objects (DO): dancing the onion," *Theatre, Dance and Performance Training*, vol. 11, no. 4, pp. 487–487, 2020.

[22] C. Crickmay, "Drawing as part of a performance practice," *Theatre, Dance and Performance Training*, vol. 11, no. 4, pp. 522-523, 2020.

[23] R. Karafistan, "The five continents of theatre: facts and legends about the material culture of the actor," *Theatre, Dance and Performance Training*, vol. 12, no. 1, pp. 129–131, 2021.

[24] K. Beswick, "Playing to type: industry and invisible training in the National Youth Theatre's 'Playing Up 2," *Theatre, Dance and Performance Training*, vol. 9, no. 1, pp. 4–18, 2018.

[25] D. Kotler, M. Lynch, D. Cushman, J. Hu, and J. Garner, "Dancers' perceived and actual knowledge of anatomy," *Journal of Dance Medicine & Science*, vol. 21, no. 2, pp. 76–81, 2017.

[26] C. Edinborough, "Editorial," *Journal of Theatre Dance & Performance Training*, vol. 9, no. 2, pp. 139–141, 2018.

[27] B. Jennings, "Answer the question," *Journal of Theatre Dance & Performance Training*, vol. 9, no. 3, pp. 430–430, 2018.

Hindawi
Journal of Sensors
Volume 2021, Article ID 1970896, 10 pages
https://doi.org/10.1155/2021/1970896

Research Article

NNT: Nearest Neighbour Trapezoid Algorithm for IoT WLAN Smart Indoor Localization Leveraging RSSI Height Estimation

Wilford Arigye,[1] **Mu Zhou**,[1] **Muhammad Junaid Tahir**,[1] **Waqas Khalid**,[1] **and Qiaolin Pu**[2]

[1]*School of Communication and Information Engineering, Chongqing University of Posts and Telecommunications, Chongqing 400065, China*
[2]*Hong Kong Baptist University, Hong Kong*

Correspondence should be addressed to Wilford Arigye; l201910017@stu.cqupt.edu.cn

Received 4 May 2021; Accepted 11 July 2021; Published 2 August 2021

Academic Editor: Abdellah Touhafi

Indoor localization as a technique for assisting, or replacing outdoor satellite and cell tower localization systems, has taken a toll in the recent Internet of Things (IoT) era. This IoT drive has prompted increased research towards indoor localization, where fingerprinting, radio mapping as a cost-effective and efficient scheme, is emerging as the best enterprise entrepreneurs choose. However, indoor complex environments comprise of trackable devices (TD) at various heights, such as child trackers, dog tags, TD on the table, TD's in the pockets, and situations such as pedestrians talking on the phone: that is at the height of the ear, amongst others. This paper first investigates and analyses "experimentally" the impact of received signal strength indicator (RSSI) fingerprinting height to construct radio maps for indoor localization. Secondly, it proposes the novel trapezoid path loss model for RSSI estimation and finally the nearest neighbour trapezoid (NNT) algorithm for IoT smart indoor localization leveraging and mitigating the impact of height considered during the offline signal fingerprinting. We further propose approximately 1 meter above the flooring of the target space as the effective fingerprinting height for indoor localization approaches.

1. Introduction

Realization of Internet of Things (IoT) technology in recent years for smart cities, smart homes, and integrated government infrastructure services have raised the applicability of location-based services (LBS). Localization fingerprinting in complex Wi-Fi indoor environments as a technique to achieve precise indoor positioning has attracted affordable and reliable accuracy ever since the introduction of the RADAR [1, 2] and Horus indoor localization systems [3]. Indoor localization usage covers a wide range of aspects, such as emergency response [4], location-based targeted advertising [5, 6], indoor robotics navigation [7], and capability that falls short to outdoor satellite navigation systems indoors due to signal fluctuations within complex indoor environments [8]. Indoor positioning technologies such as Bluetooth [9], ultra-wideband [10], radiofrequency technologies [11], microelectromechanical systems [12], wireless local area networks [13], computer vision [14], magnetic field [15], ultrasonic [16], and infrared signal have been proposed [17].

In this paper, we first experimentally evaluate, test, and analyse the effect of fingerprinting height to indoor localization accuracy using machine learning nearest neighbour in signal space approaches such as nearest neighbour (NN) and k-nearest neighbour (KNN) algorithms with various radio maps constructed at different heights. The KNN algorithms return the location estimate as the average of the coordinates of the k neighbours corresponding to the smallest RSS distances to the query RSSI values [2]. Then, we propose and test the performance of the trapezoid path loss model to estimate the RSSI and the trapezoid nearest neighbour algorithm to accurately estimate the mobile location with minimal distance error. Experimental results show better localization accuracy performance by the proposed trapezoid signal distance model than the Euclidean distance deploying the proposed NNT algorithm than the native NN algorithm.

The contributions of this paper can be summarized as follows:

(1) The proposed system deploys the RSSI-based approach, which requires no additional hardware and easily implemented on/off the shelf mobile devices equipped with the 802.11 family chipsets. Other than relaying of the internal inertia sensors, our proposed technique utilizes the received RSSI to estimate the height of the trackable device

(2) We propose trapezoid signal distance, instead of the Euclidean distance of the received RSSI signal and the fingerprint, as the evaluation function that proves better positioning accuracy

(3) We propose a novel trapezoid model for signal prediction in free space based on proposed trapezoid signal distance other than the log distance model

(4) We propose the nearest neighbour trapezoid algorithm (NNT) for indoor complex fingerprinting localization. Furthermore, we state that the proposed model can be used in any other location system. It provided better and robust localization

Indoor localization systems are discussed in Section 2. Empirical fingerprint construction is presented in Section 3. In Section 4, we describe our proposed trapezoid construction process, the trapezoid path loss model, and the localization algorithm. Section 5 presents the experimental evaluation. Finally, Section 6 concludes this paper.

2. Related Works

Indoor localization research has seen a great deal of interest over the decade cutting across various architectures. Several solutions have been proposed by multinational industries and researchers, some requiring dedicated infrastructures such as infrared [18], ultrasound [19], and radiofrequency identification (RFID) [20, 21], thus increasing the cost of deployment. However, RFID emerging techniques to resolve collision detections, such as the enhanced collision detection (ECD) [22], can improve identification rate, time, and slot efficiencies at low cost, whereas some solutions leverage already existing sensor infrastructures, such as Bluetooth [9, 23], frequency modulation (FM) [24], GSM cellular [25], and wireless fidelity (Wi-Fi) signal strengths [2, 3, 26, 27]. They deploy techniques such as the angle-of-arrival (AoA) leveraging the angle of incidence of the received signal vectors [28], time-difference-of-arrival (TDOA), the time-of-flight (TOF) [29] leveraging the arrival time sequence to measure the delay of the signal, and signal strength fingerprinting. Fingerprint techniques map indoor propagated signals to a specific reference point, without the need to know the transceiver's location and transmit power, as opposed to techniques that rely on building signal propagation models for localization.

WLAN indoor localization system based on fingerprinting comprises of basic two stages. The first stage is radio map construction during the offline surveying stage: During this stage, site survey calibration is carried out to obtain specific reference points at which RSSI sample vectors are sampled at a predetermined height and then saved in the localization server. The second stage is the localization query stage: During this stage, sensor device queried fingerprint vectors at unknown locations are compared to fingerprints in the radio map database in the localization server and then returns the corresponding location estimate that minimizes the mean errors in accordance to the localization algorithms' criterion. Indoor complex environments comprise devices tractable at different heights, such as child trackers, dog tags, mobile devices on the table or in pockets, and pedestrians on phone talking, amongst other height orientations. These diverse height orientations would have an impact on RSSI signal fluctuations; thus, different localization accuracy estimation results during online localization; this is because in most cases offline fingerprints are sampled and constructed at a specific height. This paper, therefore, presents an in-depth experimental evaluation to validate this height effect, proposes a novel trapezoid path loss model, and finally proposes novel trapezoid nearest neighbour localization approach.

3. Fingerprint Localization

The fingerprint-based localization process consists of offline data collection, radio map construction phase, and online localization estimation phase. Offline construction of the radio map is initialized by the site survey, with grid formation calibrating of the target indoor environment. At each calibrated reference point (RP), we use a prerequisite Wi-Fi enabled tractable device (TD) to scan and sample the received signal strength indicator (RSSI) value from hearable transmitter access points (APs) in a predefined time stamp. When a discoverable number of APs are less than 3, the fingerprint signature at that specific RP point is not viable for complex indoor localization environments; thus, the fingerprint surveyor should take note of the AP population within the target environment signal coverage.

Let N be the number of RPs and L be the total number of APs deployed in the signal coverage target floor. We denote the RSSI value form AP l at RP i as f_i^l (dBm). We sample multiple random fingerprint signals at each predefined RP and then averaged the signal values to find the mean RSSI $\bar{f}_i^l$ at each RP i from AP l denoted as

$$\bar{\mathrm{f}}_i^l = \frac{1}{S_i^l}\sum_{s=1}^{S_i^l} f_i^l(s), i = 1, \cdots, N.l = 1, \cdots, L \tag{1}$$

where $f_i^l(s)$ is the s^{th} RSSI sample (in dBm) at RP i from AP l, and S_i^l is the total number of RSSI samples collected within the predefined time stamp. Then, the fingerprint at RP i is defined as

$$\mathbf{F}_i = \left[\bar{f}_i^1, \bar{f}_i^2, \cdots, \bar{f}_i^L\right]. \tag{2}$$

Forming an interactive radio map matrix as

$$\Psi = \begin{pmatrix} \bar{f}_1^1 & \cdots & \bar{f}_1^L \\ \vdots & \ddots & \vdots \\ \bar{f}_N^1 & \cdots & \bar{f}_N^L \end{pmatrix}. \quad (3)$$

Secondly, for each predefined time stamp, we calculate the mean and standard deviation of the RSSI per AP to store in a radio map at the back end of the server. Let σ_n^l (dBm) be the corresponding standard deviation of S_n^l collected RSSIs.

Similarly, given the online query target measured RSSI R^l from AP l, the RSSI vector at the target, denoted as ϑ, can be defined as

$$\vartheta = \left[R^1, R^2, \cdots, R^L\right]. \quad (4)$$

During the data processing, to differentiate the RSSI values within indoor environment, mW, instead of dBm, is used when we consider the random signal level mean, i.e.,

$$\bar{f}_i^l\Big|_{\mathrm{mW}} = 10^{\left(\bar{f}_i^l\big|_{\mathrm{dBm}}\right)/10}, \quad (5)$$

which transforms RSSIs from smartphones to values for better signal differentiation. Correspondingly, we also transform RSSI values $t^{l'}s$ in ϑ from dBm into mW.

4. NNT Algorithm

As IoT indoor environments are comprised of localization of persons of interest and transceivers at diverse heights, we propose a novel approach to solve the disparity of the pairwise cluster of the fingerprint RSSI and receiver RSSI by the trapezoidal area between the fingerprint perpendicular heights. Assuming a transceiver Tx at height $H1$ on $(x0, y0)$ coordinate location in the equal space calibrated indoor space, fingerprint Fp at height $H2$ on $(x1, y1)$ coordinate and receiver Rx at a height $H3$ on $(x2, y2)$ coordinate, as shown in Figure 1 and the two-dimensional distance relationship in Figure 2.

In order to measure the degree of neighbour's closeness at varying heights, we propose minimizing the proposed trapezoidal distance, which is further achieved by several other minimizations such as the hypotenuse signal distance, the floor distance between the fingerprint and the location device, the differential height between the two. From Figure 1,

$$\tan Q = \frac{C1}{(H1 - H2)} = \frac{C2}{(H2 - H3)} = \frac{C1 + C2}{(H1 - H3)}, \quad (6)$$

where

$$C1 = \sqrt{(x1 - x0)^2 + (y1 - y0)^2}, \quad (7)$$

$$h1 = \sqrt{(C1)^2 + (H1 - H2)^2}. \quad (8)$$

4.1. RSSI Distance Model. Natively, during the offline calibration stage, the average RSSI at various fingerprint reference points at different distances $C1$ from the Tx transceiver antenna can be associated with the RSSI distance model as in

$$\bar{f}_i^l = 10n \log (\mathrm{C1}) + \bar{A}_l + X_\sigma, \quad (9)$$

where $\overline{A_l}$ is the average RSSI at a 1 m distance from Tx. Assuming a close neighborhood from the Tx antenna nodes in the wireless fidelity network, the transmission indoor space-dependent parameter n remains the same. Thus, n can be determined by

$$n = \frac{\bar{f}_i^l - \bar{A}_l}{10 \log (C1)}. \quad (10)$$

During online, the target received RSSI R^l of the surrounding transceivers are compared to the fingerprint database RSSI values. Similarly obeying the anticipated RSSI distance model as in

$$R^l = 10n \log (\mathrm{C2}) + \bar{f}_i^l. \quad (11)$$

The distance at which the receiver is anticipated is obtained as

$$\mathrm{C2} = 10^{\left(\left(R^l - \bar{f}_i^l\right)/10n\right)}. \quad (12)$$

Further, we derive the height estimate at which the RSSI is estimated to be recorded as

$$H3 = \frac{H2(C1/(H1 - H2)) - C2}{(C1/(H1 - H2))}. \quad (13)$$

4.2. Trapezoid Path Loss Model. In this section, we propose and define our trapezoid path loss model for indoor radio propagation. Existing models have approximately predicted the RSSI fingerprints, though extremely challenging due to multipath effect and environmental site-specific parameters. From Figure 2, we can derive the following relationship:

$$Q + 90 + \alpha = 180, \alpha = 90 - Q, \quad (14)$$

$$\sin (90 - Q) = \sin 90 \cos Q - \cos 90 \sin Q = \cos Q = \frac{(H2 - H3)}{h2}, \quad (15)$$

$$\cos \left(\arctan \left(\frac{C2}{H2 - H3}\right)\right) = \frac{1}{\sqrt{1 + (C2/(H2 - H3))^2}} = \frac{H2 - H3}{h2}. \quad (16)$$

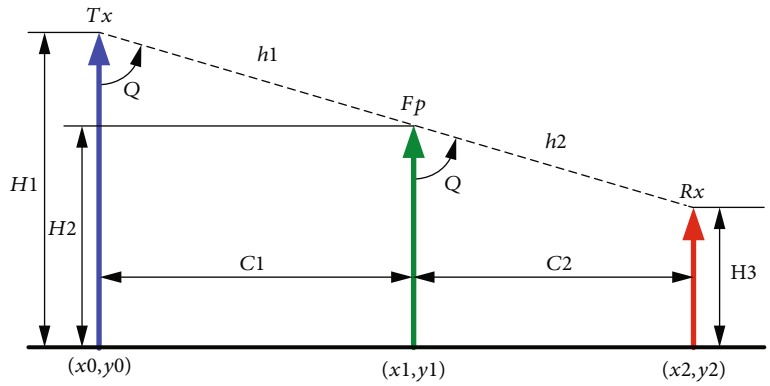

Figure 1: Fingerprinting system perpendicular relationship. The height relationship of the transmitter, fingerprint, and receiver.

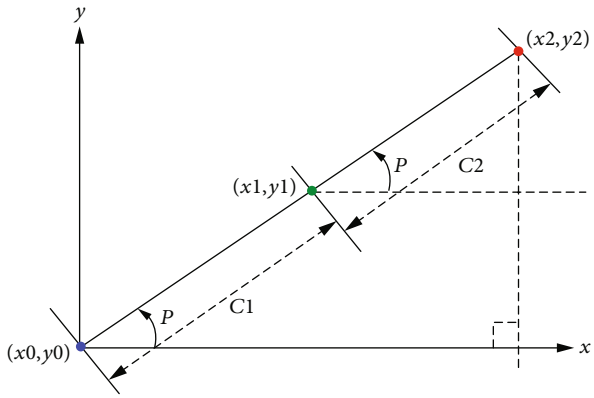

Figure 2: Fingerprinting system floor relationship. The floor distance relationship of the transmitter, the fingerprint, and the receiver.

From Equation (16),

$$h2 = (H2 - H3) \times \sqrt{1 + \left(\frac{C2}{H2 - H3}\right)^2}. \tag{17}$$

The trapezoid nearest neighbour area A is defined as

$$A = \frac{C2}{2}(H2 + H3) = \frac{(H2 + H3)}{2}\sqrt{(h2)^2 - (H2 - H3)^2}. \tag{18}$$

The proposed trapezoid path loss model that leverages the trapezoid distance can be defined as

$$Rx^l = \bar{f}_i^l + \frac{10n \log (C2)}{h2}, \tag{19}$$

where averaged Rx^l is the estimated received RSSI, $C2$ is the estimated distance between the transceiver and receiver, $\bar{f}_i^l$ is the fingerprint RSSI, and $h2$ is the proposed trapezoid factor to signal distance that affects the signal between the transceiver and the receiver.

4.3. Proposed Algorithm. Amongst existing main machine learning typical deterministic method for classifying objects based on closest neighbour training examples in the radio map such as NN and KNN, we propose novel height-specific NNT and KNNT algorithm for the online localization stage. KNNT aims at returning the position estimate of the current location query as an average of the k-neighbours in the radio map resulting from the minimum pairwise trapezoid signal distance d, used to query fingerprint in a 2-dimensional space.

$$\widehat{\ell}(\mathbf{R}) = \frac{1}{K}\sum_{i=1}^{K} \text{argmin}_{\ell_i}(d_i), \tag{20}$$

where the proposed trapezoid signal distance as in Equation (20) between the reference fingerprint and the observed test fingerprint is calculated as

$$d_i^2 = h2_i^l * \text{sqrt}\left(\sum_{l=1}^{L}\left(\bar{f}_i^l - R^l\right)^2\right). \tag{21}$$

5. Experimental Evaluation

Raw data fingerprinting experiment was carried out on the office floor of our faculty administration building of Chongqing Posts and Telecommunications University (CQUPT), a test bed of about 66 m wide by 17.1 m long, whose schematic experimental test floor plan is shown in Figure 3. Several stages include the experimental setup and data acquisition steps in Section 5.1, the initial experiment to determine the effect of height on radio fingerprinting, the proposed trapezoid path loss model, and the proposed trapezoid localization algorithm based on accuracy results and cost of construction.

5.1. Setup and Data Acquisition. In the test bed setup, initial prescans discover various RSSI readings that could be resulting from tethered devices in various offices, which in turn could increase the preprocessing computational cost of the collected data due to increased discoverable TD's. To minimize the processing, we filter out and simplify the process by setting up 5 D-Link APs (DAP 2310) operating at 2.4 GHz IEEE 802.11b/g/n Wi-Fi standard as baseline testing

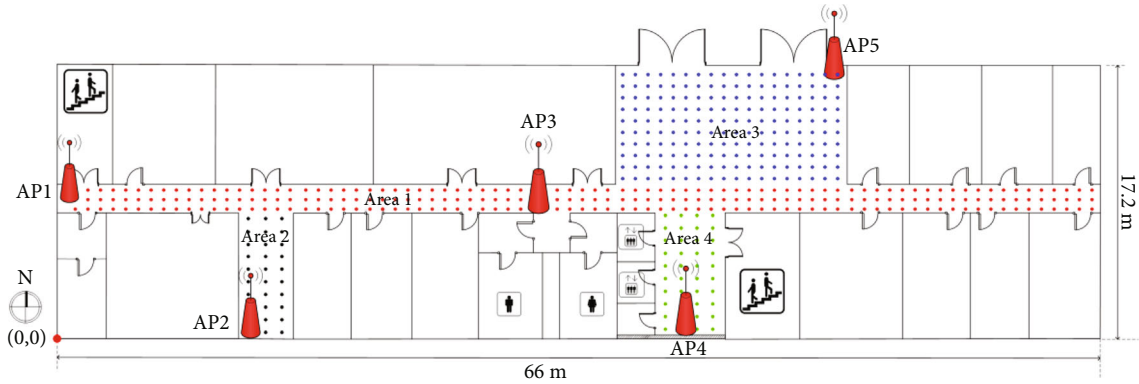

Figure 3: Test bed. Five APs installed on the target floor. 327 RPs calibrated at an interval of 0.8 m.

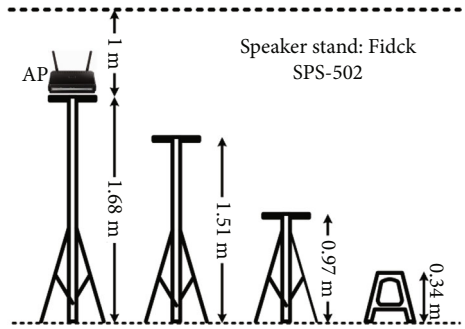

Figure 4: Configuration of the heights.

transceivers. Installed at a height of 1.68 m on the adjustable Fidck SPs-502 speaker stands, whereas the sampling TDs are at respective heights as described in Figure 4.

During the one-time offline training phase, we calibrate RPs on the floor at respective scaling intervals of 0.8 m forming a grid. At each grid RP, we sample 120 RSSI values (in dBm) as fingerprints within a 1-second time interval using our developed android application facing the northing direction, installed it on a prerequisite Samsung Galaxy GT-S7568, and averaged and stored as fingerprints in the localization server, at different heights of 1.51 m, 0.97 m, 0.34 m, respectively, as illustrated in Figure 4, as well as Figure 5 showing the real image of the various height setups in the test bed. Meanwhile, we further calibrate test RP's, at which respective 120 RSSI values are sampled, averaged, and stored for online unknown locality testing.

Considering the amount of time for the surveyor to interact with the developed APP, our developed android platform sampling APP is simpler and user friendly than in [30], requiring only the reference point name, the interval at which we sample the RSSI. On scan initialization for a predefined time stamp, it records the interval, the RSSI value followed by MAC address of the source transceiver AP. Saving the sampled data into a text file (.txt) format in the security digital (SD) card, from which we later extract RSSI values using MATLAB R2015b running on 64-bit Windows 7 Ultimate desktop equipped with i3 4160 CPU@3.60 GHz processor and 4 GB RAM to form an interactive matrix, thus empirical RSS database.

5.2. Height Effect on Localization Accuracy. We experimentally evaluate the localization accuracy of various Wi-Fi fingerprints constructed at different heights for indoors localization to enable use for determining the extent to which the height factor impacts our fingerprint. We use nearest neighbour algorithms of NN and KNN, where NN is a special case of the KNN algorithm when the number of neighbours in the localization formulation is equal to one ($k = 1$).

$H1$ vs. $T1$ represents radio map fingerprints at height 1 ($H1 = 0.34$ m) versus testing fingerprints at height 1 ($T1 = 0.34$ m); this notation is adopted for all the possible height combinations used in the testing (Figure 6), summarized in Table 1. We can see a radio map constructed with fingerprints at heights $H2$, and test fingerprints at height $T3$, that is "$H2$ vs. $T3$" performing better than other comparison fingerprint height combinations. This confirms that when a localization device is at the height of 1.51 m, location fingerprints constructed at $H2$ result in reduced localization mean error greatly than $H1$, and $H3$ fingerprints, respectively, with the same online query test fingerprints at height $T3$. We further observe that, under different values of the well-known parameter k used by the KNN, the attained localization accuracy differs greatly, with $k = 3$ resulting in better performance with combinations of $H2$ vs. $T3$. When the number of neighbour's used during the localization algorithm is equal to 1 ($k = 1$), resulting results are attributed to the NN algorithm. From this point, we select and proposed $H2$ as our fingerprinting height for the analysis of the proposed trapezoid path loss model and finally the proposed localization technique.

5.3. Trapezoid Pass Loss Model Analysis. Efficient, applicable RSSI signal prediction is a key to indoor localization in the era of IoT, however, due to the diversity of the height of location-based devices, accurate signal modelling at different receiver heights on the same location possesses a challenge due to multipath effect, refraction, diffraction, and reflection of the signal by the complex indoor environments. Considering the lobby area (Area 3), we perform a comparison to the choices of minimization factors from the following enabling features such as the proposed trapezoid signal distance (blue colour), the signal distance (red colour), the floor distance (green colour), and the trapezoid area (black colour). From

Figure 5: Configuration of the heights picture. $H1$ vs. $T1$, $H2$ vs. $T2$, and $H3$ vs. $T3$.

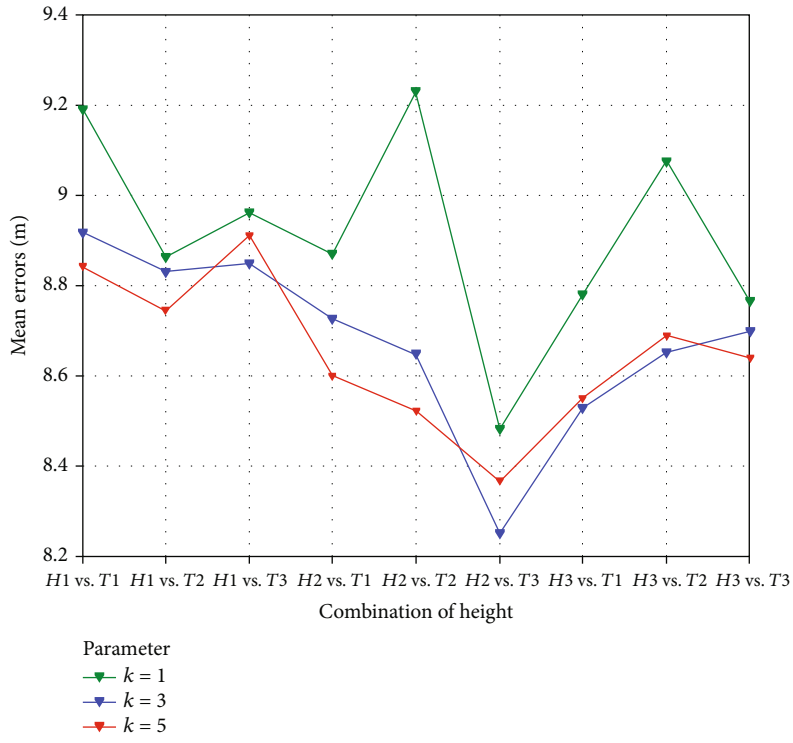

Figure 6: Comparison of location mean errors under difference combinations of heights and k parameter values.

Table 1: Summary of height combinations.

Height	0.34 (m)	0.97 (m)	1.51 (m)
0.34 (m)	$H1$ vs. $T1$	$H1$ vs. $T2$	$H1$ vs. $T3$
0.97 (m)	$H2$ vs. $T1$	$H2$ vs. $T2$	$H2$ vs. $T3$
1.51 (m)	$H3$ vs. $T1$	$H3$ vs. $T2$	$H3$ vs. $T3$

the comparison, we observe overall superior localization accuracy performance of the proposed prediction path loss model leveraging height estimation than peers, as seen in Figure 7. Furthermore, analysing the localization accuracy by the NNT algorithm that leverages trapezoid path loss model at each TP location in Area 3, as seen in Figure 8. We observe robustness with NNT localization mean errors of range 0 meters (floor) such as TP location 6, TP location

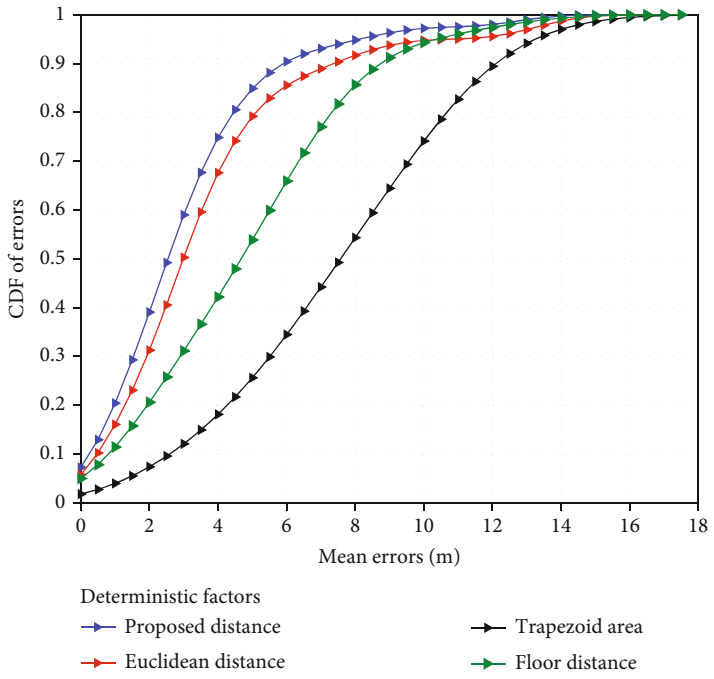

Figure 7: CDF comparison of deterministic factors.

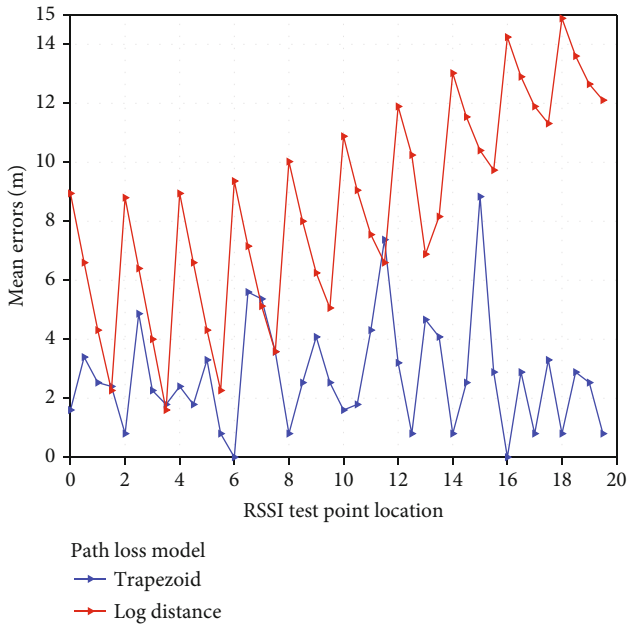

Figure 8: Comparison of location accuracy by path loss models. Area 3 location mean errors at 40 test TPs.

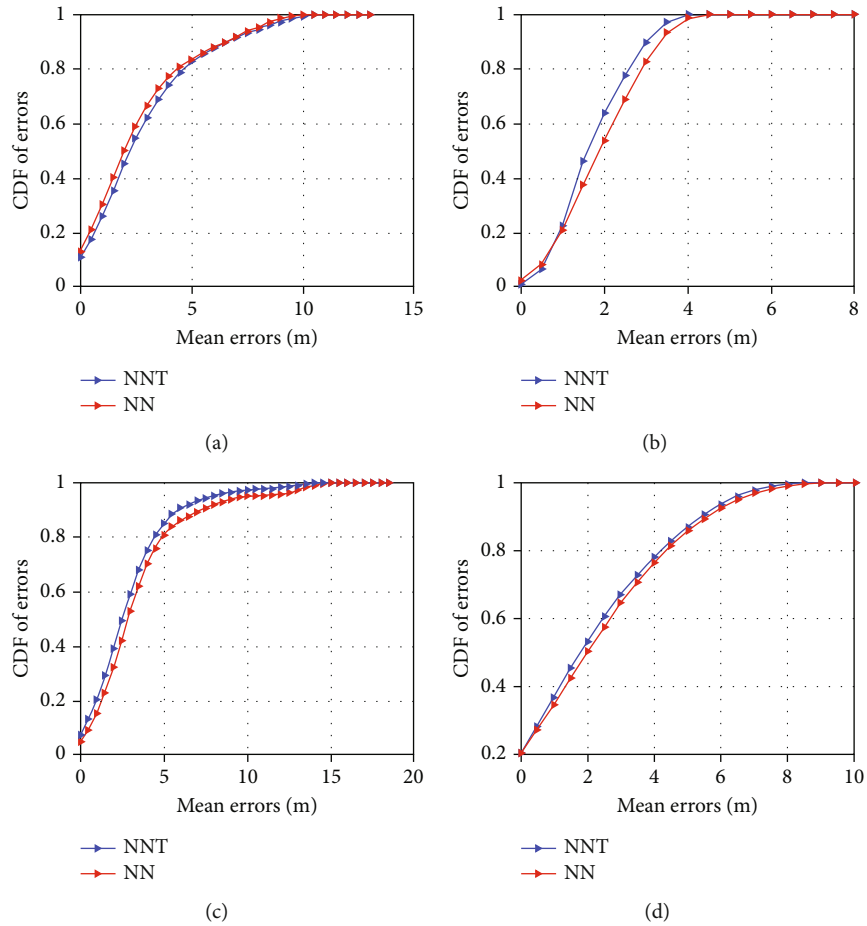

Figure 9: Localization sub area accuracy. (a) Area 1 corridor with LoS AP1 and AP3. (b) Area 2 left lower space with LoS AP2. (c) Area 3 middle lobby with LoS AP5. (d) Area 4 lower middle lobby with LoS AP4.

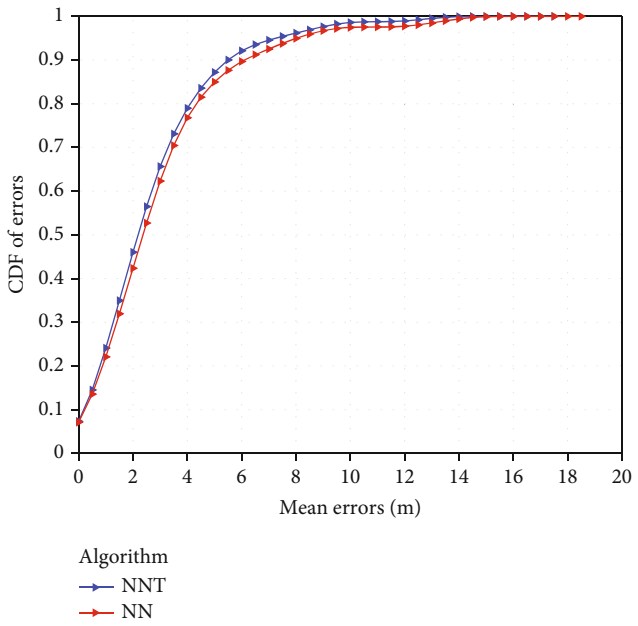

Figure 10: Total floor. Localization mean errors in meter within a complex environment, total floor coverage.

16 and 9 meters (ceiling), with a median of 2 meters compared to NN range of 2 meters (floor) to 15 meters (ceiling) with all RSSI test RP's.

5.4. Localization Accuracy Analysis. We evaluate the accuracy of the proposed NNT localization algorithm by computation of the mean error with the well-known NN algorithm in different environments, as seen from the Figure 9, below for each areas subsection, and the general total floor, we observe the NNT algorithm (blue) outperforming the native NN algorithm (red), both in room base localization and total floor base localization Figure 10.

6. Conclusions

As the demand increases for indoor LBSs in the IoT era, Wi-Fi-based fingerprinting as a key low-cost approach to precise indoor navigation and positioning keeps increasing. This paper firstly presents an extensive experimental analysis on the effect of the height, chosen by the offline site surveyor for sampling RSSI data in one-sided heading, as a minimum measure during the fingerprint radio map construction. We further note that pedestrians and traceable valuables indoors can be found at diverse heights; thus, the same could

reversibly affect the localization radio map, directly impacting the localization accuracy. From this evaluation, we observe the effect of AP's installation heights versus the localization height in complex environments and further propose that radiofrequency-based indoor fingerprinting to be sampled at approximately 1 m above the floor of localization interest.

Secondly, we propose a novel trapezoid path loss model to better estimate indoor RSSI fingerprint characteristics due to changing height. On the same basis, we finally propose a novel trapezoid-based nearest neighbour indoor localization scheme that leverages online RSSI to dynamically predict and update the RSSI in real time. Comparing with the classic nearest neighbour algorithm for localization accuracy performance, the experimental findings clearly show that the proposed algorithms can better predict RSSI with dynamic indoor coverage and improve the positioning accuracy.

Data Availability

The data is available on request.

Conflicts of Interest

The authors declare that there is no conflict of interest regarding the publication of this paper.

Acknowledgments

This work was supported in part by the Science and Technology Research Program of Chongqing Municipal Education Commission (KJZD-K202000605, KJQN202000630), the Chongqing Natural Science Foundation Project (cstc2020jcyj-msxmX0842), the National Natural Science Foundation of China (61771083, 61771209), and the Program for Changjiang Scholars and Innovative Research Team in the University (IRT1299).

References

[1] D. Macagnamo, G. Destino, and G. Abreu, "Indoor positioning: a key enabling technology for IoT applications," in *2014 IEEE World Forum on Internet of Things (WF-IoT)*, pp. 117-118, Seoul, Korea, 2014.

[2] P. Bahl and V. N. Padmanabhan, "RADAR: an in-building RF-based user location and tracking system," in *Proceedings IEEE INFOCOM 2000. Conference on Computer Communications. Nineteenth Annual Joint Conference of the IEEE Computer and Communications Societies (Cat. No.00CH37064)*, Tel Aviv, Israel, 2000.

[3] M. Youssef and A. Agrawala, "The Horus WLAN location determination system," in *Proceedings of the 3rd international conference on Mobile systems, applications, and services - MobiSys '05*, pp. 205–218, ACM: New York, 2005.

[4] E. D. Manley and J. Deogun, "Location learning for smart homes," in *21st International Conference on Advanced Information Networking and Applications Workshops (AINAW'07),*, Niagara Falls, ON, Canada, May 2007.

[5] P. Bellavista, A. K, and S. Helal, "Location-based services: back to the future," *IEEE Pervasive Computing*, vol. 7, no. 2, pp. 85–89, 2008.

[6] L. Aolto, N. Gothlin, J. Korhonen, and T. Ojala, "Bluetooth and WAP push based location-aware mobile advertising system," in *Proceedings of the 2nd International Conference on Mobile Systems, Applications, and Services, ser. MobiSys '04*, pp. 49–58, New York, NY, USA: ACM, 2004.

[7] B. Sohn, J. Lee, H. Chae, and W. Yu, "Localization system for mobile robot using wireless communication with IR landmark," in *The Proceedings of First International Conference on Robot Communication and Coordination*, Piscataway, NJ, USA: IEEE Press, 2007.

[8] P. Dana, *Global positioning system overview*, Department of Geography university of Colorado, 1999.

[9] P. Davidson and R. Piche, "A survey of selected indoor positioning methods for smartphones," *IEEE Communications Surveys & Tutorials*, vol. 19, no. 2, pp. 1347–1370, 2017.

[10] A. Ren, F. Zhou, A. Rahman, X. Wang, N. Zhao, and X. Yang, "A study of indoor positioning based on UWB base-station configurations," in *2017 IEEE 2nd Advanced Information Technology, Electronic and Automation Control Conference (IAEAC)*, pp. 1939–1943, Chongqing, China, March 2017.

[11] S. S. Saab and Z. S. Nakad, "A standalone RFID indoor positioning system using passive tags," *IEEE Transactions on Industrial Electronics*, vol. 58, no. 5, pp. 1961–1970, 2011.

[12] G. Li, E. Geng, Z. Ye, Y. Xu, J. Lin, and Y. Pang, "Indoor positioning algorithm based on the improved RSSI distance model," *Sensors*, vol. 18, no. 9, p. 2820, 2018.

[13] C. Wu, Q. Mu, Z. Zhang, Y. Jin, Z. Wang, and G. Shi, "Indoor positioning system based on inertial MEMS sensors: design and realization," in *2016 IEEE International Conference on Cyber Technology in Automation, Control, and Intelligent Systems (CYBER),*, pp. 370–375, Chengdu, China, June 2016.

[14] Y. Tian, D. Shigaki, W. Wang, and C.-J. Ahn, "A weighted least-squares method using received signal strength measurements for WLAN indoor positioning system," in *2017 20th International Symposium on Wireless Personal Multimedia Communications (WPMC),*, pp. 310–314, Bali, Indonesia, December 2017.

[15] J. Kim and H. Jun, "Vision-based location positioning using augmented reality for indoor navigation," *IEEE Transactions on Consumer Electronics*, vol. 54, no. 3, pp. 954–962, 2008.

[16] V. Pasku, A. de Angelis, M. Dionigi, G. de Angelis, A. Moschitta, and P. Carbone, "A positioning system based on low-frequency magnetic fields," *IEEE Transactions on Industrial Electronics*, vol. 63, no. 4, pp. 2457–2468, 2016.

[17] J. Qi and G. P. Liu, "A robust high-accuracy ultrasound indoor positioning system based on a wireless sensor network," *Sensors*, vol. 17, no. 11, p. 2554, 2017.

[18] T. Raharijaona, R. Mawonou, T. V. Nguyen et al., "Local positioning system using flickering infrared LEDs," *Sensors*, vol. 17, no. 11, p. 2518, 2017.

[19] N. B. Priyantha, A. Chakraborty, and H. Balakrishman, "The Cricket location-support system," in *Proceedings of the 6th annual international conference on Mobile computing and networking - MobiCom '00*, pp. 32–43, New York, NY, USA: ACM, 2000.

[20] D. Hahnel, W. Burgard, D. Fox, K. Fishkin, and M. Philipose, "Mapping and localization with RFID technology," in *IEEE International Conference on Robotics and Automation, 2004. Proceedings. ICRA '04. 2004*, New Orleans, LA, USA, April 2004.

[21] L. M. Ni, Y. Liu, Y. C. Lau, and A. P. Patil, "LANDMARC: indoor location sensing using active RFID," in *Proceedings of*

the First IEEE International Conference on Pervasive Computing and Communications, 2003. (PerCom 2003),, pp. 407–415, Fort Worth, TX, USA, 2003.

[22] J. Su, R. Xu, S. Yu, B. Wang, and J. Wang, "Idle slots skipped mechanism based tag identification algorithm with enhanced collision detection," *KSII Transactions on Internet and Information Systems*, vol. 14, no. 5, pp. 2294–2309, 2020.

[23] M. Hossain and W. S. Soh, "A comprehensive study of Bluetooth signal for localization," in *2007 IEEE 18th International Symposium on Personal, Indoor and Mobile Radio Communications*, Athens, Greece, Sept 2007.

[24] Y. Chen, D. Lymberopoulos, J. Liu, and B. Priyantha, "FM-based indoor localization," in *Proceedings of the 10th international conference on Mobile systems, applications, and services - MobiSys '12*, pp. 169–182, ACM: New York, 2012.

[25] H. Buyruk, A. K. Keskin, S. Sendil et al., "RF fingerprinting based GSM indoor localization," in *2013 21st Signal Processing and Communications Applications Conference (SIU),*, Haspolat, Turkey, 2013.

[26] A. Goswami, L. E. Ortiz, and S. R. Das, "WiGEM," in *Proceedings of the Seventh COnference on emerging Networking EXperiments and Technologies on - CoNEXT '11*, New York, NY, USA: ACM, 2011,.

[27] E. Martin, O. Vinyals, G. Friedland, and R. Bajcsy, "Precise indoor localization using smart phones," in *Proceedings of the international conference on Multimedia - MM '10*, pp. 787–790, New York, NY, USA: ACM, 2010.

[28] S. Sen, J. Lee, K.-H. Kim, and P. Congdon, "Avoiding multipath to revive inbuilding WiFi localization," in *Proceeding of the 11th annual international conference on Mobile systems, applications, and services - MobiSys '13*, ACM: New York, 2013.

[29] S. Lanzisera, D. Zats, and K. S. J. Pister, "Radio frequency time-of-flight distance measurement for low-cost wireless sensor locazation," vol. 11, Tech. Rep. 3, IEEE Sensors Journal, 2011.

[30] D. Mascharka and E. Manley, "LIPS: learning based indoor positioning system using mobile phone sensors," in *2016 13th IEEE Annual Consumer Communications & Networking Conference (CCNC)*, pp. 968–971, Las Vegas, NV, USA, 2016.

Hindawi
Journal of Sensors
Volume 2021, Article ID 4024737, 11 pages
https://doi.org/10.1155/2021/4024737

Research Article

A Novel Optimization Method for Bipolar Chaotic Toeplitz Measurement Matrix in Compressed Sensing

Rui Zhang, Chen Meng, Cheng Wang, and Qiang Wang

Shijiazhuang Campus, Army Engineering University, Shijiazhuang 050003, China

Correspondence should be addressed to Cheng Wang; 810134271@qq.com

Received 1 June 2021; Revised 27 June 2021; Accepted 14 July 2021; Published 31 July 2021

Academic Editor: Mu Zhou

In this paper, a bipolar chaotic Toeplitz measurement matrix optimization algorithm for alternating optimization is presented. The construction of measurement matrices is one of the key techniques for compressive sensing from theory to engineering applications. Recent studies have shown that bipolar chaotic Toeplitz matrices, constructed by combining the intrinsic determinism of bipolar chaotic sequences with the advantages of Toeplitz matrices, have significant advantages over other measurement matrices in terms of memory overhead, computational complexity, and hard implementation. However, problems such as strong correlation and large interdependence coefficients between measurement matrices and sparse dictionaries may still exist in practical applications. To address this problem, we propose a new bipolar chaotic Toeplitz measurement matrix alternating optimization algorithm. Firstly, by introducing the structure matrix, the optimization problem of the measurement matrix is transformed into the optimization problem of the generating sequence, thus ensuring that the optimization process does not destroy the structural properties of the matrix; then, constraints are added to the values of the generating sequence during the optimization process, so that the optimized measurement matrix still maintains the bipolar properties. Finally, the effectiveness of the optimization algorithm in this paper is verified by simulation experiments. The experimental results show that the optimized bipolar chaotic Toeplitz measurement matrix can effectively reduce the reconstruction error and improve the reconstruction probability.

1. Introduction

Compressed sensing (CS) [1, 2] is a new framework for signal sampling. It enables to sample sparse signals at a sampling rate much lower than Nyquist's and to achieve accurate recovery of the original signal with high probability. The signal processing method based on compressed sensing theory does not depend on the bandwidth of the signal and can break the limitation of the sampling process by Nyquist's sampling theory. CS has broad application prospects in the fields of broadband signal acquisition [3], medical imaging [4, 5], and data compression [6], etc.

The measurement matrix design is one of the cores of compressed sensing theory [7]. On the one hand, the nature of the measurement matrix directly determines whether the compressive sampling process can fully retain the useful information of the original signal, and on the other hand, the design of the measurement matrix needs to take into account the implementation capability of the compressed sampling system [8, 9]. Although the widely used random measurement matrices such as Gaussian and Bernoulli have good applicability, there are too many free elements in the matrices, and they are not conducive to hardware implementation. Based on the above two factors, the bipolar chaotic sequence is used to construct Toeplitz matrix as a measurement matrix for compressed sensing—called the bipolar chaotic Toeplitz measurement matrix—in the literature [10]. This measurement matrix is simple to generate and has few free elements, which greatly reduces the difficulty of hardware implementation and, at the same time, supports fast algorithms that can solve numerous problems related to convolutional operations. Although the restricted isometry property (RIP) of the bipolar Toeplitz measurement matrix was proved [11, 12], the constructed bipolar chaotic Toeplitz

measurement matrix may still have a large correlation with the sparse dictionary during practical applications, which affects the compressed sampling reconstruction of the signal.

Measurement matrix optimization is an effective way to solve the above problem; the current optimization algorithms on the measurement matrix mainly focus on the optimization of random measurement matrix, such as the Elad algorithm [13], the Duarte-Carvajalino algorithm [14], and the Abolghasemi algorithm [15]. The strategy of alternating optimization between the matrix to be optimized and the target matrix in the Abolghasemi algorithm can effectively expand the search space and improve the optimization effect. Based on the idea of alternating optimization, a weighted measurement matrix optimization objective function was proposed in the literature [16] to improve the robustness of the compressive sampling system under the condition of considering both signal adaptation and the matrix's own characteristics. The literature [17] introduced the concept of parameter update in K-SVD to improve the measurement matrix update and improve the efficiency of matrix optimization. The literature [18] proposed a new joint optimization algorithm of the measurement matrix and sparse dictionary to improve the signal compression-aware reconstruction effect by constructing a new objective function. However, the above alternating optimization algorithm does not consider the possible structural constraints of the measurement matrix itself, so the structural properties of the measurement matrix itself will be destroyed after optimization. On the premise of considering the structural properties of the matrix, the literature [19] proposed an alternating optimization algorithm for sparse measurement matrices, and the literature [20] proposed an alternating optimization algorithm for cyclic matrices, but both algorithms are not applicable to the bipolar Toeplitz measurement matrix.

From the above analysis, it can be seen that the existing measurement matrix optimization methods do not meet the optimization needs of the bipolar Toeplitz measurement matrix. The reasons for this are mainly the following two aspects. On the one hand, the bipolar Toeplitz measurement matrix has a special matrix structure, and the existing measurement matrix optimization algorithms cannot guarantee that the matrix structure remains unchanged after optimization. On the other hand, the matrix elements of the bipolar Toeplitz measurement matrix have only two values, and the existing measurement matrix optimization algorithm will destroy the bipolar characteristics of the matrix elements.

To address the above problems, a new bipolar chaotic Toeplitz measurement matrix alternation optimization algorithm is proposed in this paper. In this paper, starting from the structural characteristics of Toeplitz matrix, the Toeplitz matrix is decomposed into the form of weighted summation of multiple structural matrices, thus converting the matrix optimization problem into the optimization problem of matrix generation sequence, which ensures that the original structure of the matrix optimization process remains unchanged. Second, a threshold function is introduced to constrain the values of the generated sequence during the iterative process, which ensures that the optimized matrix still maintains the bipolar property. The experimental results show that the optimized bipolar chaotic Toeplitz measurement matrix compression-aware reconstruction error is reduced and the reconstruction probability is significantly improved.

2. Description of the Problem

2.1. Bipolar Chaotic Sequence. Before constructing a bipolar chaotic Toeplitz measurement matrix, a bipolar sequence needs to be constructed first. The pseudorandom sequences based on chaotic systems have deterministic generating functions and good statistical independence, which are more conducive to hardware implementation, and for this reason, a bipolar sequence generation method based on chaotic systems is used in this paper.

A logistic chaotic system is a commonly used method to generate chaotic sequences. Considering the problem of generating bipolar Toeplitz measurement matrix, the following mapping function for the logistic chaotic system is used in [21]:

$$x_{j+1} = \mu\left(1 - 2x_j^2\right), j \in \mathbb{N}, \tag{1}$$

where $x_j \in [-1, 1]$ and $\mu \in [0, 1]$; this function is more suitable for the modulation of digital signals. When $\mu \geqslant 0.8371$, the logistic chaotic system has a positive Lyapunov exponent and the system enters a chaotic state; when $\mu = 1$, the mapping is traversed on the interval [-1, 1]. As can be seen from Figure 1, the time series goes through three different evolutionary stages of unstable immobility⟶cycle⟶chaos in turn. The closer μ is to 1, the closer the range of values of x distributed over the entire region of -1 to 1; this means that the more obvious the chaos is. When the logistic mapping is extremely sensitive to changes in the initial value after the value of μ is determined, the structure of the entire chaotic system is very different when a small change in the initial value occurs.

The invariant probability density function of the logistic chaotic sequence is

$$\rho(x) = \begin{cases} \dfrac{1}{\pi\sqrt{1 - x^2}}, & x \in [-1, 1], \\ 0, \text{else}. \end{cases} \tag{2}$$

Then, the mean value of the series is

$$\bar{x} = \lim_{J \longrightarrow \infty} \frac{1}{J} \sum_{j=1}^{J} x_j = \int_{-1}^{1} x\rho(x)dx = 0. \tag{3}$$

By repeated iterations of Equation (1), a set of logistic real-valued chaotic sequences $\{x_j\}_{j=0}^{\infty}$ can be generated.

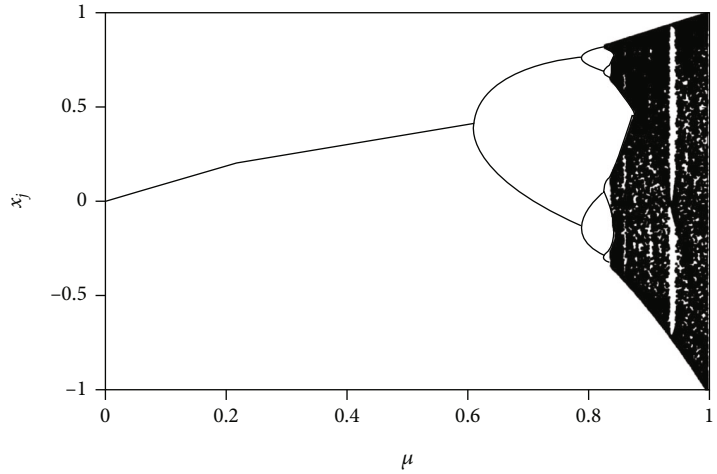

Figure 1: Logistic map bifurcation diagram.

Subsequently, a bipolar chaotic threshold function is introduced for this chaotic sequence $\{x_j\}_{j=0}^{\infty}$, which is

$$A_j = T(x_j) = \begin{cases} +1, & x_j \geq 0, \\ -1, & x_j < 0. \end{cases} \tag{4}$$

Then, the sequence A_j constitutes a set of bipolar chaotic sequences. When A_{j+1} obtains ±1, the value interval of x_j is taken as follows, respectively:

$$A_{j+1} = \begin{cases} +1, & x_j \in \left(-\frac{1}{\sqrt{2}}, \frac{1}{\sqrt{2}}\right), \\ -1, & x_j \in \left(-1, -\frac{1}{\sqrt{2}}\right) \cup \left(\frac{1}{\sqrt{2}}, 1\right). \end{cases} \tag{5}$$

Then, using Equation (2), we can get the equal probability of A_{j+1} obtaining ±1, both being 0.5.

2.2. Bipolar Chaotic Toeplitz Measurement Matrix. To ensure the applicability of the bipolar Toeplitz matrix alternating optimization algorithm in this paper, two Toeplitz measurement matrices are constructed using the bipolar chaotic sequence described above [10].

$$\mathbf{\Phi}_1 \in \mathbb{R}^{M\times N} = \frac{1}{\sqrt{M}} \begin{pmatrix} A_N & A_{N-1} & \cdots & A_2 & A_1 \\ A_{N+1} & A_N & \cdots & A_3 & A_2 \\ \vdots & \vdots & \ddots & \vdots & \vdots \\ A_{M+N-1} & A_{M+N-2} & \cdots & A_{M+1} & A_M \end{pmatrix}, \tag{6}$$

and $\mathbf{\Phi}_2 \in \mathbb{R}^{M\times N} = [\mathbf{\Phi}^{(1)}\mathbf{\Phi}^{(2)} \cdots \mathbf{\Phi}^{(b)}]$, where

$$\mathbf{\Phi}^{(i)}(i = 1, 2, \cdots, b) \in \mathbb{R}^{M\times N/b} = \frac{1}{\sqrt{M}} \begin{bmatrix} A_N^{(i)} & A_{N-1}^{(i)} & \cdots & A_2^{(i)} & A_1^{(i)} \\ A_{N+1}^{(i)} & A_N^{(i)} & \cdots & A_3^{(i)} & A_2^{(i)} \\ \vdots & \vdots & \ddots & \vdots & \vdots \\ A_{M+N-1}^{(i)} & A_{M+N-2}^{(i)} & \cdots & A_{M+1}^{(i)} & A_M^{(i)} \end{bmatrix}. \tag{7}$$

The scalar $1/\sqrt{M}$ in Equation (6) is used to normalize the columns of $\mathbf{\Phi}$ to ensure that the energy of the original signal x is consistent with the energy of the measured sample signal y during the dimensionality reduction$\mathbb{R}^N \longrightarrow \mathbb{R}^M$. $\mathbf{\Phi}_2$ is the multiblock Toeplitz measurement matrix, and when $b = 1$, the multiblock Toeplitz measurement matrix degenerates to the conventional single-block Toeplitz measurement matrix. Since the generating sequences of both measurement matrices are bipolar chaotic sequences, the two measurement matrices are collectively referred to as bipolar chaotic Toeplitz measurement matrices in this paper.

The RIP properties of the bipolar chaotic Toeplitz measurement matrix have been effectively demonstrated in [9] and are not repeated here. The focus of this paper is on the optimization of the bipolar chaotic Toeplitz measurement matrix. Although the bipolar chaotic Toeplitz measurement matrix constructed using Equation (6) can satisfy the RIP property with high probability, there may still be problems such as strong correlation between the measurement matrix and the sparse dictionary and large interdependence coefficients during practical applications, so it is necessary to optimize the constructed bipolar chaotic Toeplitz measurement matrix to further improve the performance of the measurement matrix.

Currently, the core idea of measurement matrix optimization is to reduce the interdependence coefficients of the measurement matrix by reducing the values of the

nondiagonal elements of the Gram matrix. And the main methods to reduce the values of nondiagonal elements are threshold shrinkage, gradient descent, and singular value decomposition. However, the above methods all destroy the structural properties of the measurement matrix and the bipolar properties of the matrix elements, so they are not suitable for the optimization of bipolar chaotic Toeplitz measurement matrices. Based on this, this paper presents a new bipolar chaotic Toeplitz measurement matrix alternation optimization algorithm.

3. Bipolar Chaotic Toeplitz Matrix Alternating Optimization Algorithm

3.1. Optimization of the Objective Function. For a one-dimensional signal $x \in \mathbb{R}^N$, the compressed perception process can be expressed as

$$y = \Phi x = \Phi \Psi s, \tag{8}$$

where $\boldsymbol{y} \in \mathbb{R}^M$ is the measurement data, Φ is the measurement matrix, Ψ is the sparse dictionary, s is the sparse vector, and when the signal x is sparse, Ψ is the identity matrix.

The first attempt to consider the optimal design of measurement matrix was made in [12]. It states that by reducing the correlation between the measurement matrix and the sparse dictionary, the compression-aware reconstruction of the signal can be effectively improved. We define the Gram matrix:

$$\mathbf{G} = \Psi^T \Phi^T \Phi \Psi. \tag{9}$$

The measurement matrix objective function can be expressed as follows:

$$\min_{\mathbf{G},\mathbf{G}_{\text{ideal}}} \|\mathbf{G} - \mathbf{G}_{\text{ideal}}\|_F^2. \tag{10}$$

The bipolar chaotic Toeplitz matrix used in this paper has obvious structural properties. In order to ensure that the measurement matrix optimization process still maintains its original structural properties, the measurement matrix is decomposed as follows:

$$\Phi = \sum_{j=1}^{J} A_j \Phi^j, \tag{11}$$

where J is the number of free elements in the measurement matrix, and J in Φ takes the value of $M + N - 1$, and Φ^j is the structure matrix corresponding to element A_j. The matrix consists of 0 and $1/\sqrt{M}$ elements and has the same matrix dimension as Φ. If the matrix element in a is $1/\sqrt{M}$, it means that the matrix element in that position in Φ is A_j. So Φ can be expressed as

$$\begin{aligned}
\Phi_1 &= \begin{pmatrix} A_N & A_{N-1} & \cdots & A_2 & A_1 \\ A_{N+1} & A_N & \cdots & A_3 & A_2 \\ \vdots & \vdots & \ddots & \vdots & \vdots \\ A_{M+N-1} & A_{M+N-2} & \cdots & A_{M+1} & A_M \end{pmatrix} \\
&= \begin{pmatrix} 0 & \cdots & A_1 \\ \vdots & \ddots & \vdots \\ 0 & \cdots & 0 \end{pmatrix} + \cdots + \begin{pmatrix} 0 & \cdots & 0 \\ \vdots & \ddots & \vdots \\ A_{M+N-1} & \cdots & 0 \end{pmatrix} \\
&= A_1 \Phi^1 + \cdots + A_{M+N-1} \Phi^{M+N-1},
\end{aligned} \tag{12}$$

that is,

$$\Phi^1 = \begin{pmatrix} 0 & \cdots & \frac{1}{\sqrt{M}} \\ \vdots & \ddots & \vdots \\ 0 & \cdots & 0 \end{pmatrix}, \cdots, \Phi^{M+N-1} = \begin{pmatrix} 0 & \cdots & 0 \\ \vdots & \ddots & \vdots \\ \frac{1}{\sqrt{M}} & \cdots & 0 \end{pmatrix}. \tag{13}$$

Similarly, in Φ_2,

$$\Phi_2 = A_1 \Phi^1 + \cdots + A_{bM+N-b} \Phi^{bM+N-b}, \tag{14}$$

where

$$\begin{aligned}
\Phi^1 &= \begin{pmatrix} 0 & \cdots & \frac{1}{\sqrt{M}} & & 0 & \cdots & 0 \\ \vdots & \ddots & \vdots & \cdots & \vdots & \ddots & \vdots \\ \underbrace{0 \quad \cdots \quad 0}_{\mathbb{R}^{M \times N/b}} & & & & \underbrace{0 \quad \cdots \quad 0}_{\mathbb{R}^{M \times N/b}} & & \end{pmatrix}, \cdots, \\
\Phi^{bM+N-b} &= \begin{pmatrix} 0 & \cdots & 0 & & 0 & \cdots & 0 \\ \vdots & \ddots & \vdots & \cdots & \vdots & \ddots & \vdots \\ \underbrace{0 \quad \cdots \quad 0}_{\mathbb{R}^{M \times N/b}} & & & & \underbrace{\frac{1}{\sqrt{M}} \quad \cdots \quad 0}_{\mathbb{R}^{M \times N/b}} & & \end{pmatrix}.
\end{aligned} \tag{15}$$

Although Φ_1 and Φ_2 have different structures, they can both be expressed in the form of Equation (11) and, given a value of b, the measurement matrix is determined by the generating sequence A_j only. To ensure that the structural properties of the measurement matrix are not destroyed by the optimization process, the measurement matrix optimization objective function is further expressed as

$$\min_{\{A_j\},\mathbf{G}_{\text{ideal}}} f\left(\{A_j\},\mathbf{G}_{\text{ideal}}\right)=\left\|\boldsymbol{\Psi}^T\left(\sum_{j=1}^{J}A_j\left(\boldsymbol{\Phi}^j\right)^T\right)\left(\sum_{j=1}^{J}A_j\boldsymbol{\Phi}^j\right)\boldsymbol{\Psi}-\mathbf{G}_{\text{ideal}}\right\|_F^2. \tag{16}$$

This ensures that the structure matrix remains unchanged during the optimization process and only the sequence A_j is optimized.

3.2. The Proposed Method. For the multiparameter optimization problem in Equation (16), the following alternating optimization strategy is used in this paper:

(i) Fixed the latest $\{A_j\}$, updated G_{ideal}

(ii) Fixed the latest G_{ideal}, updated $\{A_j\}$

G_{ideal} is updated using the following contraction operation for a fixed $\{A_j\}$:

$$\mathbf{G}_{\text{ideal}}^{i+1}\left(n,n'\right)=\begin{cases}1, & n=n',\\ \text{sign}\left(\mathbf{G}^i\right)\min\left(\left|\mathbf{G}^i\left(n,n'\right)\right|,\eta\right), & n\neq n',\end{cases} \tag{17}$$

where i is the number of iterations, $\mathbf{G}^i=\boldsymbol{\Psi}^T(\sum_{j=1}^{J}A_j^i(\boldsymbol{\Phi}^j)^T)(\sum_{j=1}^{J}A_j^i\boldsymbol{\Phi}^j)\boldsymbol{\Psi}$, and sign $(\cdot)$ is the sign function, $\eta=\sqrt{(M-N)/(N(M-1))}$.

The elements in the sequence $\{A_j\}$ are updated one by one using the gradient descent algorithm under the condition that the G_{ideal} is fixed:

$$A_j^{i+1}=A_j^i-\beta\nabla f_{A_j^i}\left(A_j^i,\mathbf{G}_{\text{ideal}}^i\right), \tag{18}$$

where β is the gradient descent step and $\nabla f_{A_j^i}(\cdot)$ is the gradient operator. In this paper, the expression for $\nabla f_{A_j^i}(A_j^i,\mathbf{G}_{\text{ideal}}^i)$ is derived as follows:

$$f\left(\{A_j\},\mathbf{G}_{\text{ideal}}\right)=\left\|\boldsymbol{\Psi}^T\left(\sum_{j=1}^{J}A_j\left(\boldsymbol{\Phi}^j\right)^T\right)\left(\sum_{j=1}^{J}A_j\boldsymbol{\Phi}^j\right)\boldsymbol{\Psi}-\mathbf{G}_{\text{ideal}}\right\|_F^2, \tag{19}$$

let

$$\begin{aligned}a&=\left(\boldsymbol{\Phi}^j\boldsymbol{\Psi}\right)^T\boldsymbol{\Phi}^j\boldsymbol{\Psi},\\ b&=\left(\boldsymbol{\Phi}^j\boldsymbol{\Psi}\right)^T\sum_{j}{}'^{\neq j}JA_j{}'\boldsymbol{\Phi}^{j'}\boldsymbol{\Psi}+\sum_{j}{}'^{\neq j}JA_j{}'\left(\boldsymbol{\Phi}^{j'}\boldsymbol{\Psi}\right)^T\boldsymbol{\Phi}^j\boldsymbol{\Psi},\\ c&=\sum_{j}{}'^{\neq j}JA_j{}'\left(\boldsymbol{\Phi}^{j'}\boldsymbol{\Psi}\right)^T\sum_{j}{}'^{\neq j}JA_j{}'\boldsymbol{\Phi}^{j'}\boldsymbol{\Psi}-\mathbf{G}_{\text{ideal}}.\end{aligned} \tag{20}$$

Then Equation (19) can be simplified as

$$f\left(\{A_j\},\mathbf{G}_{\text{ideal}}\right)=\left\|A_j^2a+A_jb+c\right\|_F^2. \tag{21}$$

$\nabla f_{A_j^i}(A_j^i,\mathbf{G}_{\text{ideal}}^i)$ can be calculated by the following equation:

$$\begin{aligned}&\nabla f_{A_j^i}\left(A_j^i,\mathbf{G}_{\text{ideal}}^i\right)=\\ &\left(4A_j^i\text{vec}^T(a)+2\text{vec}^T(b)\right)\text{vec}\left(\mathbf{G}^i-\mathbf{G}_{\text{ideal}}^i\right),\end{aligned} \tag{22}$$

where vec$(\cdot)$ is the matrix vectorization operator. The derivation process converts the F-parametrization of the matrix to the 2-parametrization of the vector by the vec$(\cdot)$ operator, which gives the result in Equation (22).

3.3. Constraints for Generating Sequences. The introduction of the structure matrix $\boldsymbol{\Phi}^j$ ensures that the structural properties of the measurement matrix are not destroyed during the alternating optimization process, but it is not guaranteed that the elements of the optimized matrix maintain their original bipolar properties. For this reason, this paper introduces a bipolar threshold function in sequence construction to constrain the sequence $\{A_j\}$ during the iterative process from the perspective of bipolar chaotic sequence construction:

$$A_j^{i+1}=\begin{cases}+1, & A_j^{i+1}\geq 0,\\ -1, & A_j^{i+1}<0.\end{cases} \tag{23}$$

Then, by combining Equation (18) and Equation (23), the bipolar properties of the matrix elements will be effectively preserved during the optimization process. When the iterations converge, the optimized measurement matrix can be given by (11). At this point, the alternating optimization algorithm for the bipolar chaotic Toeplitz matrix in this paper is shown in Algorithm 1.

4. Experiments and Analysis

In order to verify the effectiveness of the bipolar chaotic Toeplitz measurement matrix alternating optimization algorithm in this paper, numerical simulation experiments are conducted to analyse the optimization effect of the measurement matrix and the compression-aware reconstruction effect of the optimized matrix.

4.1. Optimization Performance Analysis. The bipolar chaotic sequence is constructed using the logistic mapping and the bipolar threshold function, and then, the single block Toeplitz measurement matrix $\boldsymbol{\Phi}_1$ and the multiblock Toeplitz measurement matrix $\boldsymbol{\Phi}_2$ are constructed according to Equations (6) and (7), respectively. The parameters of the measurement matrix are set as follows: $N=256$, $M=128$, $b=2$. Setting the sparse dictionary as an identity matrix and the maximum number of iterations as 30, the optimization effect of the two measurement matrices is shown in Figure 2.

Input: Measurement matrix $\boldsymbol{\Phi}$, sparse dictionary $\boldsymbol{\Psi}$
Output: Optimized measurement matrix $\boldsymbol{\Phi}_{\text{opt}}$
Step 1: Using the input measurement matrix $\boldsymbol{\Phi}$, construct the sequence $\{A_j\}$ as well as the structure matrix $\{\boldsymbol{\Phi}^j\}$.
Step 2: Complete the update of G_{ideal} by Equation (15)
Step 3: Using Equation (18), complete the update of sequence element A_j one by one
Step 4: Constrain the updated element A_j using Equation (23)
Step 5: Determine if the iteration termination condition is met, if so, go to Step 6, otherwise, go back to Step 2.
Step 6: Output optimized measurement matrix $\boldsymbol{\Phi}_{\text{opt}}$ using Equation (11)

Algorithm 1: The process of the proposed optimization method.

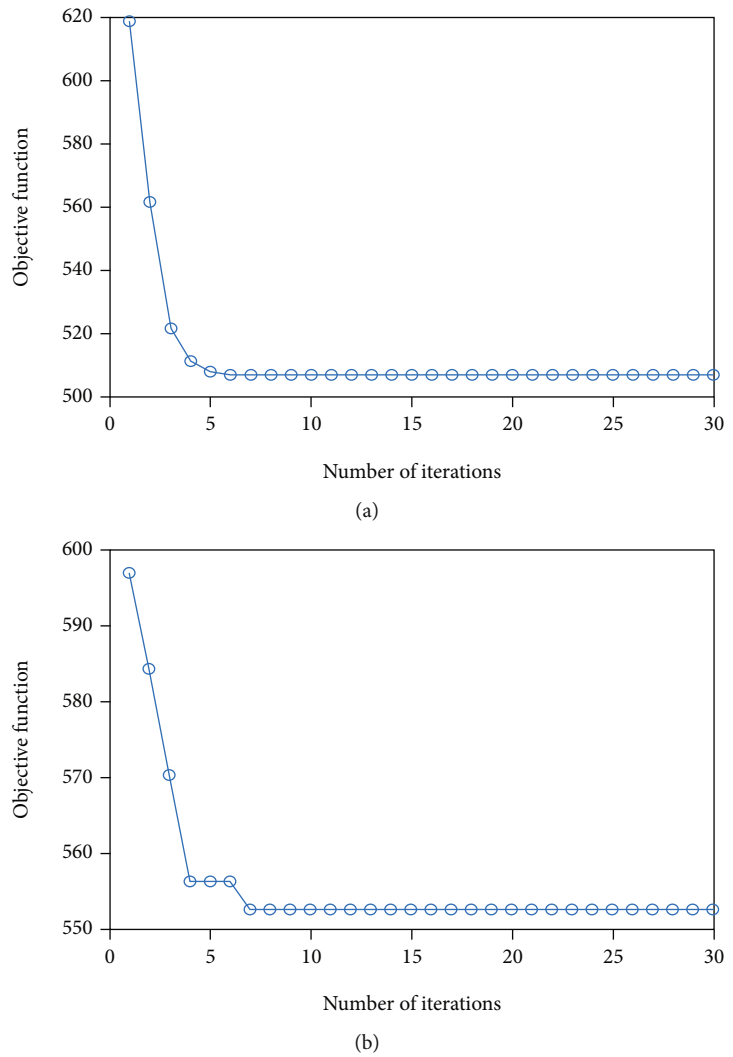

Figure 2: Optimization performance: (a) single-block bipolar chaotic Toeplitz measurement matrix and (b) multiblock bipolar chaotic Toeplitz measurement matrix.

As can be seen from the Figure 2, the optimization objective function decreases with the increase in the number of iterations and finally converges to stability. Compared with other measurement matrices, the structural properties of the bipolar chaotic Toeplitz measurement matrix and the bipolar nature of the matrix elements largely limit the

Table 1: Correlation coefficients.

	Original		Optimized	
	$\mu_{\max}$	μ_{av}	$\mu_{\max}$	μ_{av}
$\boldsymbol{\Phi}_1$	0.4587	0.0965	0.3437	0.0662
$\boldsymbol{\Phi}_2$	0.5781	0.1001	0.3594	0.0724

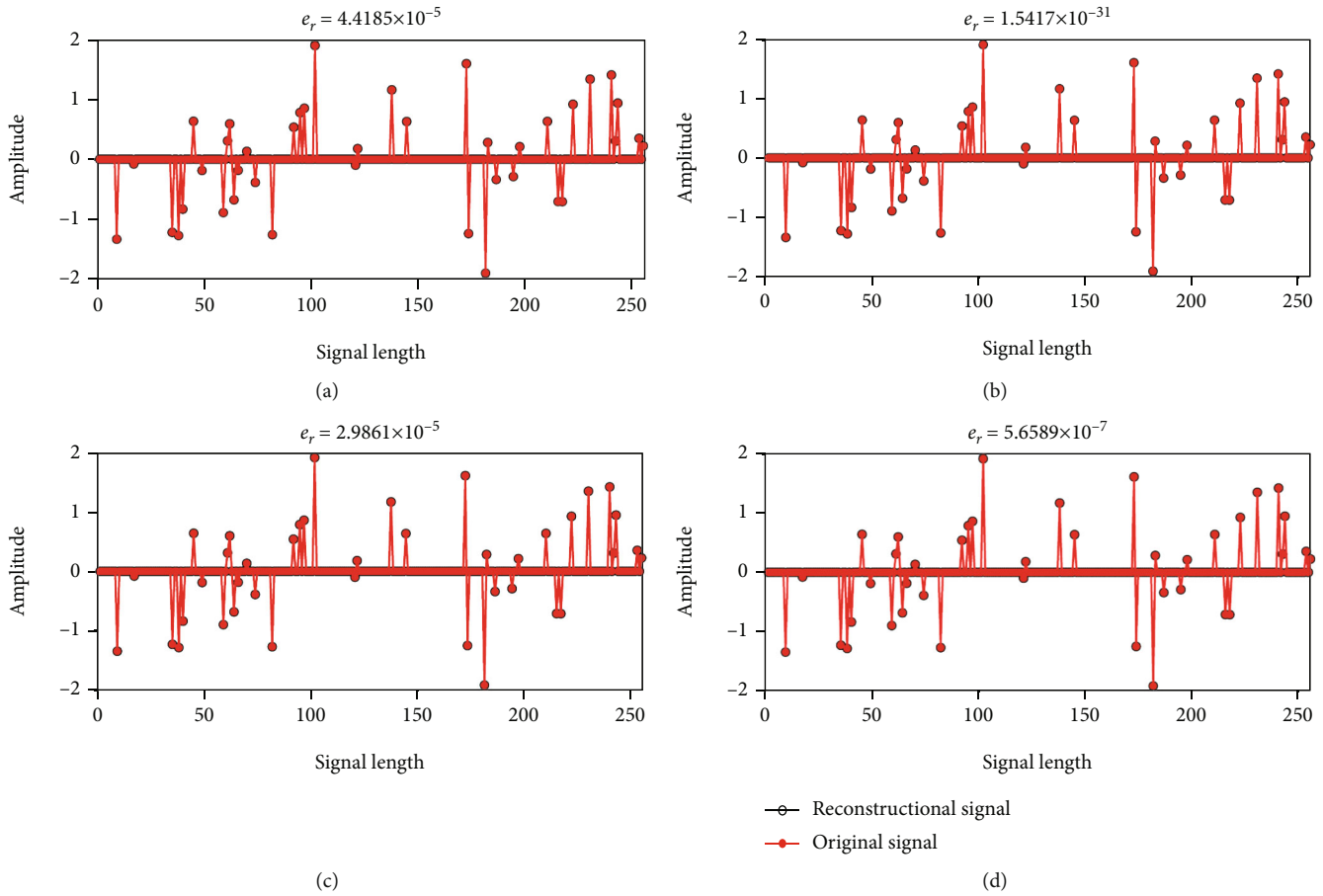

Figure 3: Reconstruction performance: (a) single-block bipolar chaotic Toeplitz measurement matrix, (b) optimized single-block bipolar chaotic Toeplitz measurement matrix, (c) multiblock bipolar chaotic Toeplitz measurement matrix, and (d) optimized multiblock bipolar chaotic Toeplitz measurement matrix.

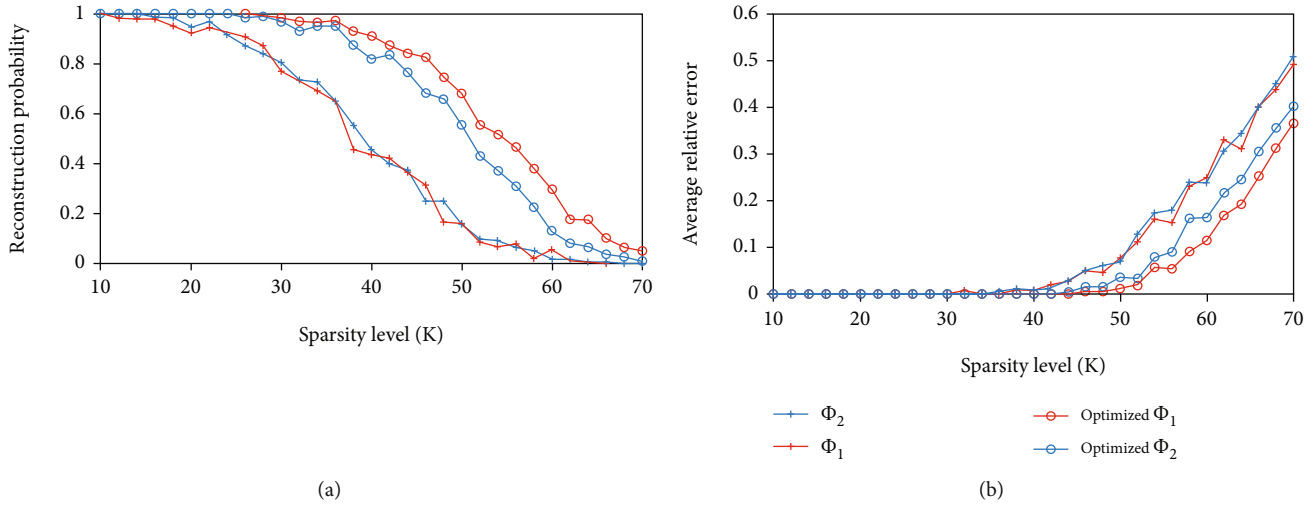

Figure 4: Reconstruction performance with different K: (a) reconstruction probability and (b) average relative error.

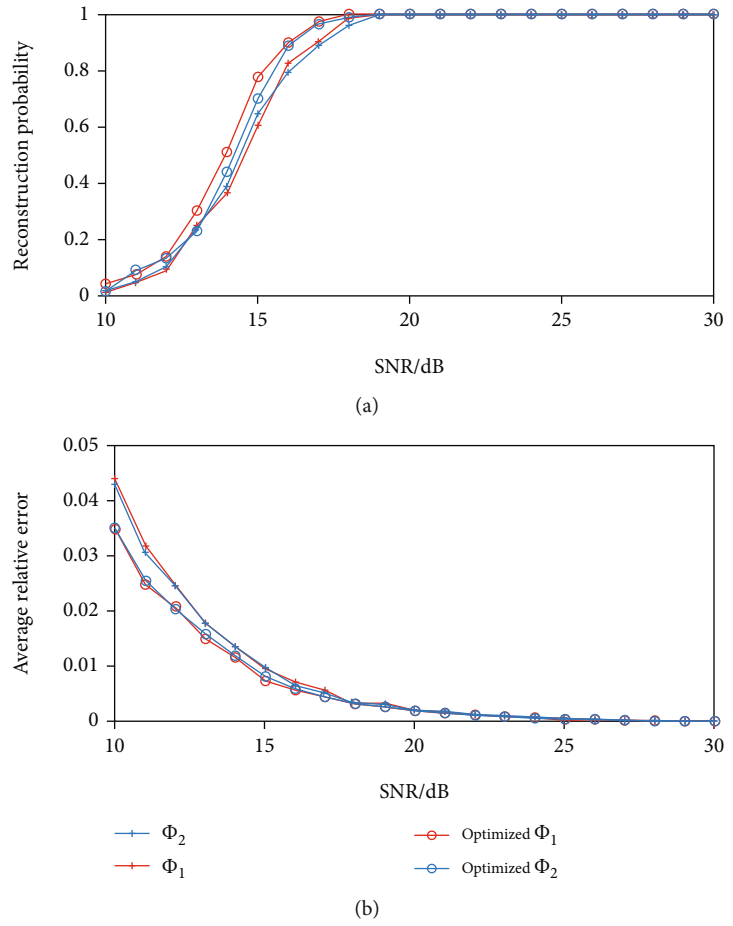

Figure 5: Reconstruction performance with different SNRs: (a) reconstruction probability and (b) average relative error.

optimizable space of the measurement matrix, so the iterative convergence of this matrix is faster. After optimization, the correlation coefficients of the measurement matrix are shown in Table 1, where

$$\mu_{\max} = \max_{1\le n,n'^{\le N,n\ne n'}} \left|\mathbf{G}\left(n,n'\right)\right|, \tag{24}$$

$$\mu_{\text{av}} = \frac{1}{N(N-1)} \sum_{1\le n,n'^{\le N,n\ne n'}} \left|\mathbf{G}\left(n,n'\right)\right|. \tag{25}$$

As can be seen in Table 1, the optimized measurement matrix correlation coefficients $\mu_{\max}$ as well as μ_{av} have been significantly reduced.

4.2. Analysis of the Effect of One-Dimensional Signal Reconstruction. The optimized measurement matrix was used to carry out simulation experiments on the compressive-perceptual reconstruction of one-dimensional signals and to analyse the effect of the optimized measurement matrix on the compressive-perceptual reconstruction effect of one-dimensional signals. During the simulation, a time-domain sparse signal was used for the one-dimensional signal, at which time the sparse dictionary was an identity matrix. Setting the sparsity $K = 30$, the effect of compressive-aware reconstruction for four different measurement matrices (single bipolar chaotic Toeplitz measurement matrix, optimized single bipolar chaotic Toeplitz measurement matrix, multiblock bipolar chaotic Toeplitz measurement matrix, and optimized multiblock bipolar chaotic Toeplitz measurement matrix) is shown in Figure 3. The reconstruction algorithm uses an orthogonal matching tracking algorithm [22], and to further quantify the reconstruction effect, the relative error is introduced as follows:

$$e_r = \frac{\|\widehat{\boldsymbol{x}} - \boldsymbol{x}\|_2^2}{\|\boldsymbol{x}\|_2^2}. \tag{26}$$

From the reconstruction results, it can be seen that all four measurement matrices achieve an effective reconstruction of the original signal at $M = 128$, but a comparison of the reconstruction relative error shows that the optimized single/multiblock bipolar chaotic Toeplitz measurement matrix has significantly lower values of reconstruction relative error than the unoptimized single/multiblock bipolar chaotic Toeplitz measurement matrix.

(a) (b)

Figure 6: Original images: (a) "Barbara" and (b) "Boat."

(a) (b) (c) (d)

Figure 7: Reconstructed "Barbara": (a) single-block bipolar chaotic Toeplitz measurement matrix, $e_r = 2.3077 \times 10^{-4}$; (b) optimized single-block bipolar chaotic Toeplitz measurement matrix, $e_r = 1.4181 \times 10^{-4}$; (c) multiblock bipolar chaotic Toeplitz measurement matrix, $e_r = 2.0132 \times 10^{-4}$; and (d) optimized multiblock bipolar chaotic Toeplitz measurement matrix, $e_r = 1.8460 \times 10^{-4}$.

A different sparsity K is set, and the reconstruction effect of the measurement matrix on different sparse signals is analysed. In the experiment, the position and amplitude of the sparse signals are generated randomly. 1000 Monte Carlo experiments were conducted under the same experimental conditions, and the reconstruction was successful when the relative error of reconstruction was lower than 10^{-4}; otherwise, the reconstruction failed. The reconstruction probabilities of the four measurement matrices under different conditions of sparsity K and the average relative errors are shown in Figure 4, where the average relative error is the average of 1000 Monte Carlo experiments.

As can be seen in Figure 4, the increasing sparsity leads to a decreasing reconstruction probability and an increasing reconstruction error. The optimized measurement matrices are more suitable for one-dimensional signals with different sparse locations and amplitudes, as the correlation coefficients $\mu_{\max}$ and μ_{av} are significantly reduced. At this point, it can be seen from Figure 4 that the reconstruction probabilities of the optimized $\mathbf{\Phi}_1$ and $\mathbf{\Phi}_2$ are higher than those of the unoptimized $\mathbf{\Phi}_1$ and $\mathbf{\Phi}_2$ for the same sparsity, while the average relative errors are significantly lower than those of the unoptimized $\mathbf{\Phi}_1$ and $\mathbf{\Phi}_2$.

In practical applications, the signal measurement process will inevitably be noisy, so the noise of different signal-to-noise ratios (SNR) is added to the compressed sampling process to analyse the reconstruction effect of the optimized bipolar chaotic Toeplitz measurement matrix under noisy conditions. In the experiments, the sparsity was set to 12, and the reconstruction probability of the four measurement matrices without noise was close to 1. Under the noisy condition, the reconstruction was successful when the reconstruction relative error was below 10^{-2}; otherwise, the reconstruction failed. The reconstruction probabilities and the average relative errors of the four measurement matrices with different SNRs are shown in Figure 5.

4.3. Analysis of the Effect of Two-Dimensional Image Reconstruction. The optimization of the bipolar chaotic Toeplitz measurement matrix was further validated using two-dimensional images. The two natural images ("Barbara" and "Boat") shown in Figure 6 were chosen as the experimental objects, both with a dimension of256×256. The above image was divided into 256 image blocks which were 16×16 for a compressed perceptual reconstruction experiment. The sparse dictionary used in the experiments is an orthogonal cosine dictionary. Setting the sampling rate to 0.5, the reconstructed images after compressive sampling with different measurement matrices are shown in Figures 7 and 8.

As the images are not ideally sparse signals under the orthogonal cosine dictionary, there is local blurring in the reconstructed images after compressive sampling compared to the original images. Further comparison of the reconstruction errors shows that the optimized single/multiblock bipolar chaotic Toeplitz measurement matrix has a lower relative reconstruction error than the unoptimized single/multiblock bipolar Toeplitz measurement matrix. Thus, after optimization, the bipolar chaotic Toeplitz measurement matrix is effectively improved for compression-aware reconstruction in 2D images.

(a) (b) (c) (d)

Figure 8: Reconstructed "Boat": (a) single-block bipolar chaotic Toeplitz measurement matrix, $e_r = 3.172 \times 10^{-4}$; (b) optimized single-block bipolar chaotic Toeplitz measurement matrix, $e_r = 1.7814 \times 10^{-4}$; (c) multiblock bipolar chaotic Toeplitz measurement matrix, $e_r = 2.8183 \times 10^{-4}$; and (d) optimized multiblock bipolar chaotic Toeplitz measurement matrix, $e_r = 2.4414 \times 10^{-4}$.

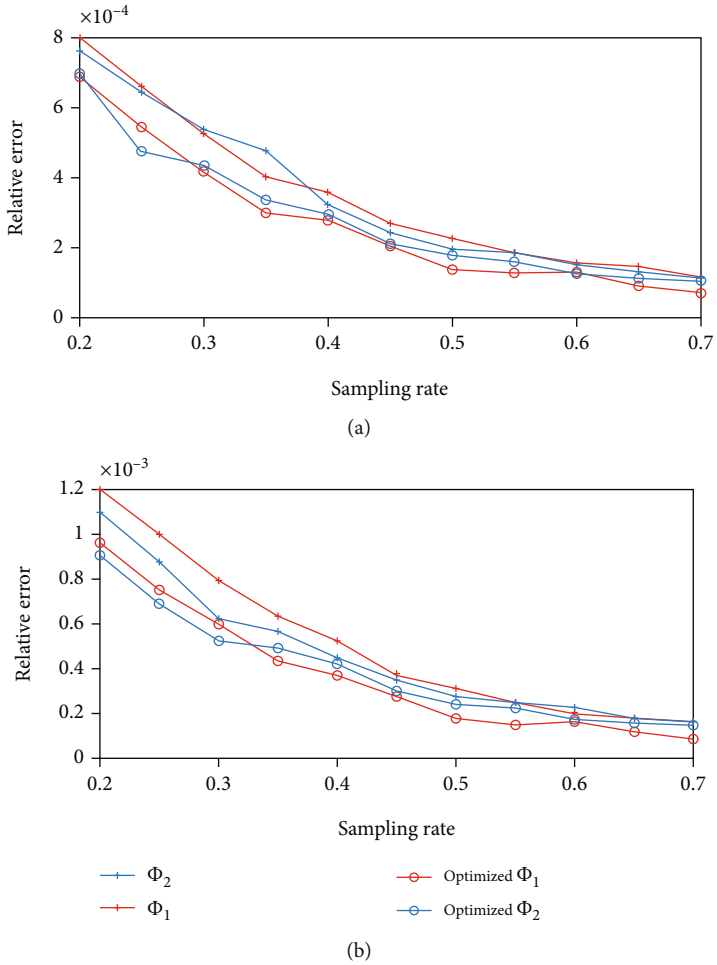

Figure 9: Reconstruction error with different sampling rates: (a) "Barbara" and (b) "Boat."

To further analyse the effect of sampling rate on the effect of image compression-aware reconstruction, the sampling rate was set to increase from 0.2 to 0.7, and the relative error after compression-aware reconstruction of the four measurement matrices was analysed at different sampling rates, and the experimental results are shown in Figure 9. In the figure, as the sampling rate increases, the number of sampling points keeps increasing; therefore, the relative error of compressed sensing reconstruction keeps decreasing. And comparing the four measurement matrices, it can be seen that at the same sampling rate, the optimized single/multiblock bipolar chaotic Toeplitz measurement matrix has a lower relative reconstruction error than the unoptimized single/multiblock bipolar chaotic Toeplitz measurement matrix. This experimental result shows that the alternating optimization algorithm of the bipolar chaotic Toeplitz measurement matrix in this paper can effectively improve the compression-aware reconstruction performance of the measurement matrix at different sampling rates.

5. Conclusions

In this paper, a bipolar chaotic Toeplitz measurement matrix optimization algorithm with alternating optimization is proposed to address the problem that existing measurement matrix optimization algorithms are not applicable in bipolar chaotic Toeplitz measurement matrices. The algorithm in this paper ensures that the structural properties of the optimized measurement matrix remain unchanged by introducing a structure matrix and then ensures that the bipolar properties of the optimized matrix elements remain unchanged by introducing constraints. The experimental results show that the optimization process effectively reduces the correlation coefficient of the measurement matrix, and the reconstruction error is effectively reduced, and the reconstruction probability is significantly improved when the optimized measurement matrix is applied to compressed perceptual reconstruction of 1D signals and 2D images.

Data Availability

The data used to support the findings of this study are available from the corresponding author upon request.

Conflicts of Interest

The authors declare that they have no conflicts of interest.

Acknowledgments

This work was funded by the National Natural Science Foundation of China (Grant No. 61501493).

References

[1] D. L. Donoho, "Compressed sensing," *IEEE Transactions on Information Theory*, vol. 52, no. 4, pp. 1289–1306, 2006.

[2] E. J. Candes, J. Romberg, and T. Tao, "Robust uncertainty principles: exact signal reconstruction from highly incomplete frequency information," *IEEE Transactions on Information Theory*, vol. 52, no. 2, pp. 489–509, 2006.

[3] H. Zhao, L. Qiao, J. Zhang, and N. Fu, "Generalized random demodulator associated with fractional Fourier transform," *Circuits Systems & Signal Processing*, vol. 37, no. 11, pp. 5161–5173, 2018.

[4] M. Ambrosanio, P. Kosmas, and V. Pascazio, "A multithreshold iterative DBIM-based algorithm for the imaging of heterogeneous breast tissues," *IEEE Transactions on Biomedical Engineering*, vol. 66, no. 2, pp. 509–520, 2019.

[5] C. Dai, H. Che, and M. F. Leung, "A neurodynamic optimization approach for L1 minimization with application to compressed image reconstruction," *International Journal on Artificial Intelligence Tools*, vol. 30, no. 1, article 2140007, 2021.

[6] Q. Wang, C. Meng, W. Ma, C. Wang, and L. Yu, "Compressive sensing reconstruction for vibration signals based on the improved fast iterative shrinkage-thresholding algorithm," *Measurement*, vol. 142, pp. 68–78, 2019.

[7] Z. Wei, J. Zhang, Z. Xu, Y. Liu, and K. Okarma, "Measurement matrix optimization via mutual coherence minimization for compressively sensed signals reconstruction," *Mathematical Problems in Engineering*, vol. 2020, Article ID 7979606, 18 pages, 2020.

[8] R. Arie, A. Brand, and S. Engelberg, "Compressive sensing and sub-Nyquist sampling," *IEEE Instrumentation and Measurement Magazine*, vol. 23, no. 2, pp. 94–101, 2020.

[9] T. Ragheb, J. N. Laska, H. Nejati, S. Kirolos, and Y. Massoud, "A prototype hardware for random demodulation based compressive analog-to-digital conversion," in *2008 51st Midwest Symposium on Circuits and Systems*, pp. 37–40, Knoxville, TN, USA, 2008.

[10] H. Gan, S. Xiao, T. Zhang, and F. Liu, "Bipolar measurement matrix using chaotic sequence," *Communications in Nonlinear Science and Numerical Simulation*, vol. 72, pp. 139–151, 2019.

[11] L. Yu, J. P. Barbot, G. Zheng, and H. Sun, "Toeplitz-structured chaotic sensing matrix for compressive sensing," in *2010 7th International Symposium on Communication Systems, Networks & Digital Signal Processing (CSNDSP 2010)*, pp. 229–233, Newcastle Upon Tyne, UK, 2010.

[12] B. Zhang, J. Zhou, and J. Li, "Improved shrinkage estimators of covariance matrices with Toeplitz-structured targets in small sample scenarios," *IEEE Access*, vol. 7, no. 99, pp. 116785–116798, 2019.

[13] M. Elad, "Optimized projections for compressed sensing," *IEEE Transactions on Signal Processing*, vol. 55, no. 12, pp. 5695–5702, 2007.

[14] J. M. Duarte-Carvajalino and G. Sapiro, "Learning to sense sparse signals: simultaneous sensing matrix and sparsifying dictionary optimization," *IEEE Transactions on Image Processing*, vol. 18, no. 7, pp. 1395–1408, 2009.

[15] V. Abolghasemi, S. Ferdowsi, and S. Sanei, "A gradient-based alternating minimization approach for optimization of the measurement matrix in compressive sensing," *Signal Processing*, vol. 92, no. 4, pp. 999–1009, 2012.

[16] H. Bai, G. Li, S. Li, Q. Li, Q. Jiang, and L. Chang, "Alternating optimization of sensing matrix and sparsifying dictionary for compressed sensing," *IEEE Transactions on Signal Processing*, vol. 63, no. 6, pp. 1581–1594, 2015.

[17] T. Hong and Z. Zhu, "An efficient method for robust projection matrix design," *Signal Processing*, vol. 143, pp. 200–210, 2018.

[18] H. Bai and X. Li, "Measurement-driven framework with simultaneous sensing matrix and dictionary optimization for compressed sensing," *IEEE Access*, vol. 8, no. 99, pp. 35950–35963, 2020.

[19] T. Hong, X. Li, Z. Zhu, and Q. Li, "Optimized structured sparse sensing matrices for compressive sensing," *Signal processing*, vol. 159, pp. 119–129, 2019.

[20] J. Guo and R. Wang, "Alternating optimisation seeking generates elemental amplitudes combined with chaotic random phases to construct a circular measurement matrix," *Acta Physic Sinica*, vol. 64, no. 13, pp. 55–66, 2015.

[21] X. Kong, H. Bi, D. Lu, and N. Li, "Construction of a class of logistic chaotic measurement matrices for compressed sensing," *Pattern Recognition and Image Analysis*, vol. 29, no. 3, pp. 493–502, 2019.

[22] S. Zhang, D. Wang, and Y. Yan, "Instrumental variable-based OMP identification algorithm for Hammerstein systems," *Complexity*, vol. 2018, Article ID 8420426, 10 pages, 2018.

Hindawi
Journal of Sensors
Volume 2021, Article ID 7047119, 12 pages
https://doi.org/10.1155/2021/7047119

Research Article

Tourism Information Data Processing Method Based on Multi-Source Data Fusion

YaoGuang Li and HeChi Gan

College of Culture and Tourism, Jeonju University, Jeonju 55069, Jeollabub-do, Republic of Korea

Correspondence should be addressed to HeChi Gan; hechigan@163.com

Received 7 May 2021; Revised 1 July 2021; Accepted 15 July 2021; Published 31 July 2021

Academic Editor: Mu Zhou

Urban social civilization and the quality of life of residents are gradually improved, and the development scale and trend of the leisure tourism industry have been growing. This paper constructs a multi-source data fusion model based on an ensemble learning algorithm, uses Ctrip 2020 open data set to train the model, and then obtains the tourism information data processing and prediction results. This paper takes the data of Ctrip as the training set and compares the trained model with the data of tunic and Feizhu. In this paper, sensor detection technology is used to analyze many famous scenic spots in China, including tourist type, gender, and location. The results show that tourism feature extraction results are consistent with data from trending flying bamboo, tunics, and other websites, according to the results of a multi-source fusion of tourism information. Among them, in the data of the first half of 2020, the prediction accuracy of the model after data processing is about 62%. Affected by the epidemic situation, the accuracy of the model is low. In the second half of the year, the prediction accuracy is 78%, which can be used to fuse tourism information in a short time. Therefore, the data show that the model has high learning ability and high trend prediction ability in tourism data processing, which can provide necessary information support for tourists.

1. Introduction

Tourism information processing technology usually uses a POI model related to specific human social activities to represent a group of points in arc tourism information. This paper analyzes the distribution and agglomeration characteristics of leisure tourism space and discusses how to coordinate the relationship with urban construction and development, which plays a vital role in the construction of livable cities, the development of tourism, and the sustainable development of cities.

At present, many studies refer to the urban landscape and tourism data. For example, Chen y divides the urban leisure space into four categories by analyzing the world's major parks [1]. Shang CF discusses and analyzes the research status of the concept of leisure tourism at home and abroad. As a new data source and research idea, it can further analyze the urban leisure tourism space [2]. Oberoi analyzes the distribution characteristics of tourism information services in Guangzhou by using the nearest neighbor distance method and other spatial analysis methods [3]. In terms of coupling analysis of tourism information data and scenic spot data, Bernardi PD uses landscape pattern index, gravity model, gravity model, and coupling analysis to analyze the urban spatial distribution structure of Anhui Province Based on DMSP/OLS image, statistical data, and tourism information data [4]. PON W C selects tourism information data and NPP remote sensing data for kernel density analysis and further analyzes the characteristics of the urban spatial structure of Wuhan City [5].

In data fusion, a new artificial intelligence technology proposed by poetry y a proposes that multi-source data fusion is that a central server coordinates multiple clients to complete a learning task without disclosing data [6]. Ramadhan GR proposes a user-level differential privacy training algorithm, which effectively reduces the possibility of recovering personal information from the transmission model by adding privacy protection to the aggregation algorithm [7]. On the other hand, Huyan w proposed a differential privacy hybrid model, which partitions users by their trust

preferences, to reduce the size of the required user base [8]. Oezturan m combines gradient selection and secret sharing algorithm, which greatly improves the communication efficiency while ensuring user privacy and data security [9]. In terms of resource optimization in multi-source data fusion, Liu P considered multi-source data fusion through the wireless network and proposed the problem of optimizing energy consumption and global multi-source data fusion time [10–11]. The above research in the data source processing is not fully integrated, so the tourism data prediction cannot achieve accurate prediction.

This paper constructs a multi-source data fusion model based on an ensemble learning algorithm, uses Ctrip 2020 open data set to train the model, and then obtains the tourism information data processing and prediction results [11–12]. This white paper uses Ctrip data as a training set and compares the trained model with tunic and flying bamboo data. This treatise mainly analyzes some of China's famous scenic spots, such as tourist type, gender, and location. According to the results of the multi-source fusion of tourism information, the results of tourism feature extraction are consistent with the data of Feizhu, tunic, and other websites in the trend.

2. Tourism Data Processing and Multi-Source Data Fusion

2.1. Distributed Tourism Data Processing Method. In the information age, massive tourism data will bring many problems to the centralized data processing mode with the cloud computing model as the core [13]. First, the processing mode of uploading all data to the cloud will not only cause low efficiency but also cause additional bandwidth overhead, at the same time, the network delay will also increase [14]. Second, due to the improvement of users' privacy awareness, the data of edge devices are likely to leak in the upload link, and the security of personal privacy cannot be guaranteed [15]. The distributed data processing mode can effectively solve the delay and efficiency problems of traditional cloud computing [16]. At the same time, aiming at the problem of "data island", Google proposed a new concept of "multi-source data fusion" for the first time [17]. The model is individually trained on multiple edge devices using training samples, and sharing of multi-source information is achieved by aggregating model parameters without disclosing user privacy. In addition, due to the diversity of edge devices, the data collected by the devices exhibits diversity in annotations, semantics, and existing formats [18]. For example, for the description of the same object, there are text class, picture class, video class, and audio class data, and multi-modal data widely exists [19]. Different modal data can describe the target object from many aspects [20]. By eliminating redundant data and fusing various data sources for correlation and supplementary analysis, more valuable new information can emerge from the data, to achieve the effect of $1 + 1 > 2$. Multimedia data collected from the Internet and mobile devices are typical unstructured data, which is significantly different from the traditional structured data format [21]. Therefore, the processing of multi-source heterogeneous data collected by different edge devices becomes an urgent problem in big data research [22]. In the traditional multi-source heterogeneous data fusion algorithm, data centralized processing has the risk of data privacy leakage in practical application [23]. Therefore, there are still many problems in multi-source heterogeneous data processing without disclosing user privacy: first, due to enterprise competition and user privacy protection awareness, data exchange is blocked for a long time, and information sharing cannot be realized, so the value of heterogeneous data cannot be fully exploited. Secondly, the neural network is used to process the data, and the model designed according to the data cannot be changed once it is determined [24]. However, in edge computing, there are differences in data structure and the number of types collected by edge devices. If we design a neural network for the data of each network edge device, the workload is huge [25–26]. At the same time, the model can only be applied to a single node or the edge device with the same data characteristics as the node, the universality is not high, and it can not give full play to the value of other heterogeneous data in the Internet of things [26]. To solve the problem of multi-source heterogeneous data fusion without disclosing user privacy in edge computing, this paper proposes a multi-source heterogeneous data fusion algorithm based on multi-source data fusion [27–30]. Starting from the data structure characteristics collected by edge devices, combined with tensor tucker decomposition theory, this paper studies the adaptive processing of multi-source heterogeneous data model on different edge devices, and solves the single adaptability problem caused by the disunity of the heterogeneous data model in multi-source data fusion.

2.2. Multi-Source Data Fusion System Model. In this paper, we aim at the problem of heterogeneous data fusion without data exchange, consider the introduction of multi-source data fusion to edge computing, and learn the potential characteristics of multi-user without invading user privacy. The basic architecture of its intelligent sensor system is shown in Figure 1.

In this framework, the system is composed of an edge node, Internet of things, and cloud server. The edge node connects with the cloud server through the Internet of things (such as gateway and router). Multi-source data fusion is a distributed learning framework, in which the original data is collected and stored on multiple edge nodes, and the model training is performed at the nodes, and then the model is gradually optimized through the interaction between node n and cloud server h. The formula is as follows

$$H = \frac{\sum_{j=1}^{k}\sum_{h=1}^{k}\sum_{t=1}^{n_j}\sum_{r=1}^{n_h}\left|y_{ij} - y_{hr}\right|}{2n^2u} \tag{1}$$

Based on the above framework, multi-source data fusion can use local data from multiple independent edge nodes sharing model, and use model transmission instead of data transmission to avoid the risk of user privacy leakage in the process of transmitting the collected original data from multiple edge nodes to the cloud server.

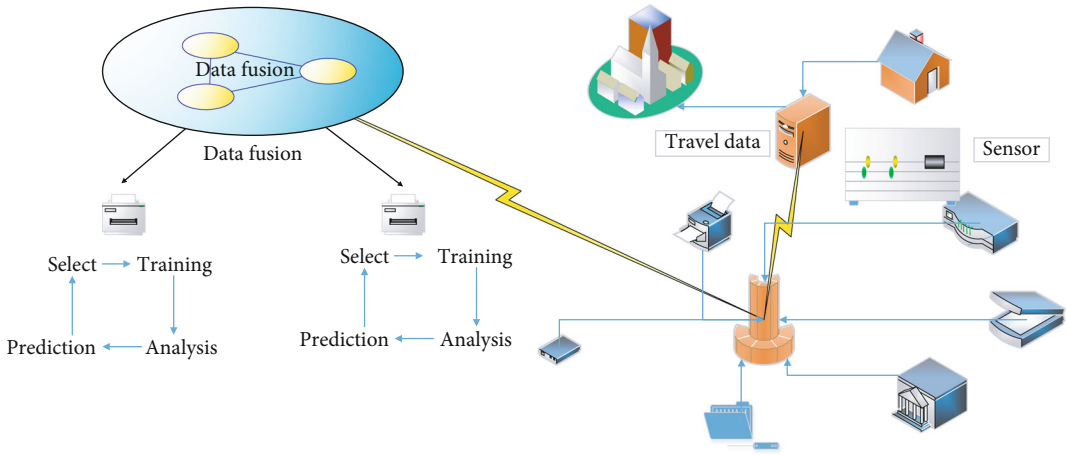

Figure 1: Multivariate data fusion framework diagram.

The multi-source heterogeneous data fusion algorithm proposed in this paper is mainly divided into feature extraction modules, feature fusion modules, and feature decision modules. The feature extraction module is composed of feature extraction sub-networks corresponding to various heterogeneous data. In the initialization stage, the central control node randomly initializes the network parameters of the feature extraction module, feature fusion module, and feature decision module, and sends them to the edge node T, where the fusion parameter is C.

$$\sum_{T} = \mathrm{C}(\max(\sigma_i, \upsilon, 0))$$
$$\mathrm{E}_j = \frac{1/2u_j \sum_{i=1}^{n_j} \sum_{r=1}^{n_j} \left| y_{ji} - y_{jr} \right|}{n_j^2} \tag{2}$$

In the model training stage, after receiving the model from the central control node, the edge node selects the corresponding feature extraction module according to the data set structure of the local node and uses the local data set to train the feature extraction module, feature fusion module, and feature decision module. The termination condition of a new round of edge node training is that the number of local node training rounds exceeds the given number of training rounds. After training, the training model is returned to the central control node for model aggregation. The first practice test is to use the average aggregation algorithm for the function fusion module and the function determination module. For the feature extraction module, the average sub-module is extracted according to the corresponding feature extraction submodule to ensure that the same mode data extract features are similar. Finally, the updated model is redistributed to the edge nodes for a new round of training. This paper assumes that the heterogeneous data to be processed are audio, visual, and textual data. In the feature extraction module, according to the features of different modes, different feature extraction sub-networks are used to extract the features of audio, visual, and text information. Audio and visual feature sub network: for audio information and visual information, covered acoustic analysis framework and face facial expression analysis framework is used to sample and extract features from MoSi data sets (sampling frequency is 100 Hz and 30 Hz, respectively). In this section, it is assumed that the heterogeneous data features to be processed are audio data features

$$\mathrm{V}_{jh} = \frac{\sum_{z=1}^{hj} \sum_{r=1}^{n_h} \left| y_{ji} - y_{hr} \right|}{n_j n_h \left(u_j + u_h \right)} \tag{3}$$

Visual data features:

$$\mathrm{V}_{nb} = \sum_{j=2}^{k} \sum_{h=1}^{j-1} G_{jh} \left(p_j s_h + p_h s_j \right) D_{jh} \tag{4}$$

Text data features:

$$\mathrm{V}_0 \int_0^{\infty} dF_j(y) \int_0^{y} (y - x) dF_h(x) \tag{5}$$

After the feature fusion module, the feature output is v0. Next, taking the above assumption as the basic condition, the basic principle of the proposed heterogeneous data fusion algorithm based on tucker decomposition is described. The first mock exam module introduces a high tensor W with heterogeneous data feature space, and each mode of the tensor corresponds to spatial mapping of heterogeneous data characteristics. Therefore, when fusing the features of each heterogeneous data, the high-order tensor w can not only introduce the features of other heterogeneous data modes for correction but also memorize the ongoing heterogeneous data modal features. When the features of the heterogeneous data to be processed are P and S, the memory unit W is a third-order tensor, and the three dimensions of the tensor corresponding to the feature spaces of the three heterogeneous data features. In the heterogeneous data feature fusion proposed in this section, the memory unit with the heterogeneous data feature can be obtained by modular multiplication of the heterogeneous data feature and the feature space

corresponding to the memory unit, and further feature fusion operation can be carried out. The fusion operation is mainly divided into three stages. The memory unit W is modulo multiplied with the heterogeneous data feature AZ along the first order to obtain a new memory unit with AZ feature.

$$W_{jh}\frac{\mathrm{AZ}_{jh}-P_{jh}}{\mathrm{AZ}_{jh}+P_{jh}} \tag{6}$$

Secondly, memory unit W is modulo multiplied with heterogeneous data features along the second-order to obtain memory unit w with AZ features. Finally, the memory unit W is modularly multiplied with the heterogeneous data features along with the third order, and finally, the fusion tensor with the three features is obtained Z。 The specific process can be expressed as follows:

$$E_{\mathrm{AZ}}=\sum_{j=1}^{k}G_{jj}p_j s_j \tag{7}$$

Among them:

$$P_j=\int_0^{\infty}dF_h(y)\int_0^{y}(y-x)dF_j(y) \tag{8}$$

For the fused data, this chapter uses the traditional full connection layer to make decisions based on the global characteristics, including the prediction of regression model and the probability prediction of a classification model. In this module, the L1 norm loss function is used to measure the error between the target value and the predicted value. Its et expression is

$$\mathrm{E}_T\sum_{j=2}^{k}\sum_{h=1}^{j-1}G_{jh}\left(p_j s_h+p_h s_j\right)D_{jh}\left(1-L1_{jh}\right) \tag{9}$$

The expression of NL is:

$$\mathrm{NL}_t=\tanh\left(w_c,x_t+u_c(r_t\Theta h_{t-1})+b_c\right) \tag{10}$$

Then, it is assumed that n edge nodes participate in the training of the shared model, and all edge nodes collect m kinds of heterogeneous data. In the initialization stage, according to the collected m kinds of heterogeneous data, the cloud designs the corresponding feature extraction module F, feature fusion module I and feature decision module C. Then the shared model G can be expressed as:

$$\mathrm{G}=\mathrm{F}*\mathrm{f}/\mathrm{C}=\frac{\sqrt{1/M\sum_{i=1}^{n}\left(I_{it}-I_{it}\right)^2}}{I_{it}} \tag{11}$$

Where $*$ represents the model splicing operation. Specifically, in the feature extraction module F, the corresponding feature extraction sub-network MF is designed from kinds of heterogeneous data, which can be expressed as:

$$1\mathrm{n}\left(\frac{MF_{it}}{MF_{it}-1}\right)=\alpha+\beta\,1\mathrm{n}MF_{it}-1+\varphi X_{it}-\tau_t \tag{12}$$

Where x is the feature extraction sub-network of the I heterogeneous data. In feature fusion module I, a high-order tensor with spatial dimension characteristics of heterogeneous data is constructed. After training, the parameters of the tensor expanded along the I module can reflect the spatial dimension characteristics of the I heterogeneous data. In the feature decision-making module C, through the training of the fused heterogeneous data features, the potential relationship between heterogeneous data is mined in a deeper level, and the feature expression of the model in multi-source heterogeneous data is improved. Due to the diversity of data collected by edge devices, the data processed by each edge node is different. Therefore, in the premise of not disclosing user privacy, multi-source heterogeneous data fusion has the problem of insufficient adaptability. The size of the tensor after fusion is consistent with that of memory unit W. Therefore, when the factor matrix satisfies the square matrix constraint, there is an identity relationship between the core tensor and the original tensor in the spatial dimension. Using this feature, in the initialization phase, the global is further set, and the feature extraction sub-network fi feature graph is defined

$$1\mathrm{n}\left(\frac{FI_{it}}{FI_{it}-1}\right)=\alpha+\beta\,1\mathrm{n}FI_{it}-1+\nu_i+\mathfrak{F}_t \tag{13}$$

Thus, the problem of heterogeneous data fusion caused by the uncertainty of heterogeneous data in edge computing is solved. In the model training stage, n edge nodes participate in the training according to the heterogeneous data types they have

$$N_t z_t\Theta h_{t-1}+(1-z_t)\Theta h_t \tag{14}$$

The corresponding feature extraction sub-network FZ is adaptively selected for training. In the feature fusion module, because the feature graph of the feature extraction subnetwork r is set to FR in the global initialization definition stage, the tensor size after heterogeneous data fusion is constrained to a fixed value

$$\begin{aligned}\mathrm{R}&=\frac{\mathrm{FR}}{1-\mathrm{FZ}}\\ \mathrm{FR}&=-\frac{1}{T}1\mathrm{n}(1+\beta)\end{aligned} \tag{15}$$

Suppose that all the heterogeneous data types to be processed are N, X, and H, respectively, and the three dimensions of the corresponding memory unit w correspond to the feature spaces of the three heterogeneous data. The

heterogeneous data types collected by node 1 and node n are different. In the model training stage, the features are obtained, respectively

$$f(\mathrm{N}) = \frac{1}{Nh}\sum_{i=1}^{N} k\left(\frac{X_i - x}{h}\right)$$
$$\mathrm{W} = k(\mathrm{H}) = \frac{1}{\sqrt{2\pi}}\ \exp\ \left(-\frac{x^2}{2}\right) \tag{16}$$

According to the number of heterogeneous data types on the node, the feature fusion stage is divided into two parts: first, memory unit W is modulo multiplied with AF feature along the first order to get a new memory unit w with AF feature. Secondly, the memory unit w multiplies the VF features along the second-order to obtain the fusion tensor with the above two heterogeneous data features Z。 The process can be expressed as follows:

$$\mathrm{W1}_j \sum_i c_{ij} u_{(\mathrm{AF|AV})} \tag{17}$$

W1 is the fusion of VF features based on AF features. In this process, the model first uses the memory unit to memorize the AF features, and obtains the model with AF features, and takes this as a priori condition for the fusion of VF features. Thus, in the process of model training, the memory unit can not only learn the spatial dimension features of each heterogeneous data but also capture the potential relationship between different heterogeneous data. The training mechanism on node n is similar to that on node 1. The above process can be expressed as follows:

$$k_{t1}[\mathrm{N}] = \sum_j \cos\left(w_i^1, w_j^2\right)/\mathrm{K} \tag{18}$$

Where n is the node K in the j-round global iteration, using the heterogeneous data collected locally, the learning rate is η The gradient descent algorithm is used to get the local model. In the model aggregation stage, because each edge node uses the adaptive selection mechanism of feature extractor to train the feature extraction module, it is necessary to merge the feature extraction sub-networks selected and trained by each edge node, and then use the average aggregation algorithm to get the shared model with global heterogeneous data features

$$u_{(j|i)} = w/\mathrm{N} *_{ij} A_i \tag{19}$$

Where a is a shared model with global characteristics obtained by aggregating the local models on n edge nodes through the joint average algorithm. J is the number of all heterogeneous samples and the total number of all heterogeneous samples on the edge node.

3. Multivariate Fusion Data Model

3.1. Methods. This paper constructs a multi-source data fusion model based on an ensemble learning algorithm, uses Ctrip 2020 open data set to train the model, and then obtains the tourism information data processing and prediction results. This paper takes the data of Ctrip as the training set and compares the trained model with the data of tunic and Feizhu. In this paper, sensor detection technology is used to analyze many famous scenic spots in China, including tourist type (youth, adult), gender, and location.

3.2. Data Acquisition and Processing. Through a comprehensive comparison of other online tourism service platforms such as tunics and Hitake, this paper has the highest number of online comments on http://Trip.com/'s Saikei Wetland, and Ctrip's online comments are rich in content and have interference factors. Few, positive and negative comments, and most of them are the true feelings of tourists. Therefore, it is common and effective to choose Ctrip online game reviews as your data source. Through Python technology, this paper grabs the online comments of tourists in Xixi Wetland scenic spot on Ctrip from May 1, 2020, to May 1, 2021, removes the invalid online comments that deviate from the research theme, and collates 3052 effective online comments, and makes specific research and analysis of the collected online comments. In addition, in cooperation with Xixi Wetland Tourism Development, the research group carried out an offline questionnaire survey on tourists' comprehensive satisfaction of Xixi National Wetland Park during the long holidays of May Day and national day in 2020, and obtained 102 valid questionnaires, which fully investigated the customer source market and tourists' satisfaction of Xixi National Wetland Park, as a supplementary means of network big data survey, this paper puts forward more relevant and targeted suggestions for the future development of Xixi National Wetland Park.

According to the text data of tourists' online reviews and the comprehensive satisfaction offline questionnaire, the research results of Xixi Wetland Park's tourism image perception are relatively consistent. When analyzing the influencing factors of tourism perception experience, there are many overlapping problems, that is, the important concerns when improving the tourism brand image. For example, given the insufficient setting of public toilets, rest chairs, and free drinking water points, drinking water, and lunch supply points should be added accordingly; For the lack of a single tour line of battery car and battery boat in the park and long waiting time for tourists to enter and leave the park, we should provide parking guidance service; Continuously improve service awareness and management level, and focus on ticket and catering prices, safety management of cruise terminal, queuing guidance, increase the number of sanitation personnel, increase recreational equipment, strengthen the integration of tourism formats and products, and improve the effective supply of products.

Figure 2: Word frequency statistics for comment texts of famous scenic spots.

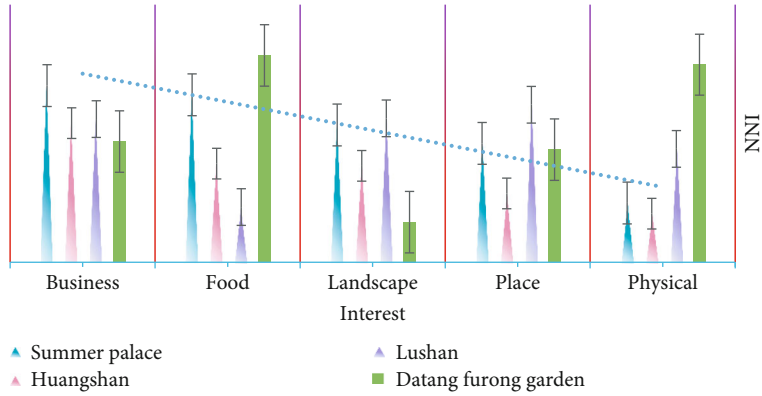

Figure 3: Overall NNI of leisure and tourism space.

4. Results and Discussion

4.1. Multi-Source Information Fusion Tourism Information Processing Method. Use Python to perform word frequency statistics on the comment texts of scenic spots and famous scenic spots in China, and extract the top 50 high-frequency feature words, as shown in Figure 2. Key terms such as "travel" and "attractions" are ranked high, indicating that projects that attract tourists to Tiger Beach are primarily special venues and ropeways across the ocean. The most attractive to tourists is the third-ranked "performance", such as "dolphin show". In addition, the characteristic words such as "getting tickets", "buying tickets" and "tickets" indicate that tourists pay great attention to the purchase of tickets, and the innovation and improvement of tourist ticket purchase methods in scenic spots should be highly valued. Compared with China's famous scenic spots, "shows" ranked first, indicating that watching performances are the main activity of tourists in Shengya.

As shown in Figure 3, the overall NNI (neural network intelligence) of leisure tourism space is less than 1, and the NNI of different types of space is also less than 1, among which catering services and commercial services are lower, indicating that these two types are more inclined to cluster development, and the cluster scale is larger. Catering and business services have a strong economic effect on agglomeration and are affected by factors such as economic level, population density and convenience of transportation. The NNI of sports leisure and cultural entertainment services were 0.35 and 0.52, respectively, which also showed a general trend of agglomeration. The NNI of scenic spot service is the largest, which is 0.46. Because of the influence of natural ecological conditions and urban open space, the agglomeration degree of all scenic spots is relatively low.

As shown in Figure 4, it has passed the significance test at the level of 5%, and the influence coefficient is positive, indicating that the innovation and technological progress of the tourism industry will play a promoting role in the growth of local tourism consumption without considering other factors. As the main platform of scientific and technological innovation in the industry, tourism colleges and research institutes, represented by coastal areas, have formed a certain scale. A large number of tourism colleges and universities have formed mature curriculum and perfect talent training systems, with rich research results, which are applied to the development and design of tourism creative products and tourism service supply management.

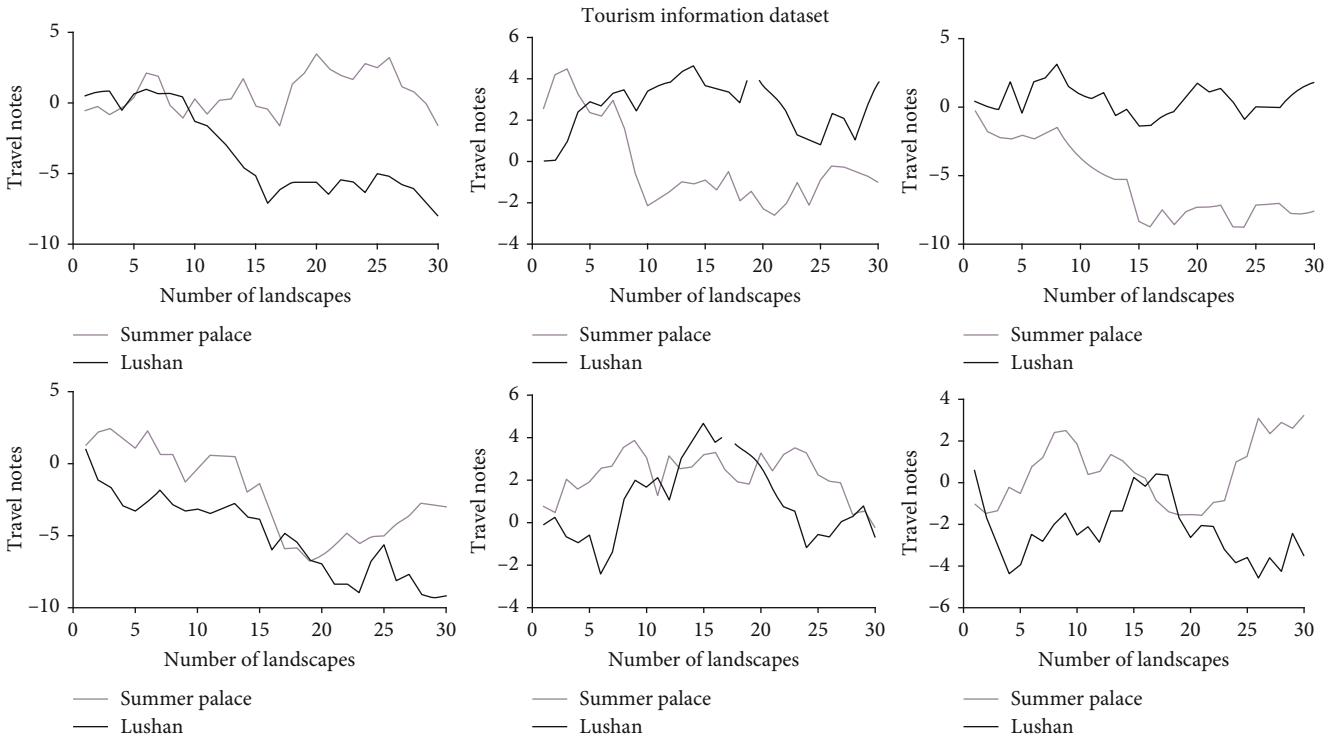

Figure 4: Tourism Information Dataset.

Under the special evaluation content, the target layer, criterion layer, and index layer of urban physical examination are established, and the index system reflecting the urban natural background and the operational signs of tourism information is constructed, as shown in Table 1. At the same time, according to the national standards of relevant indicators, the vertical establishment of planning expectation value and the horizontal comparison of the level of cities at the same level, the standard value and reference interval is determined, and the evaluation and calculation are carried out according to the positive and negative direction of the indicators. According to the data sources and evaluation contents of each index, the calculation methods can be divided into two categories: tourism information spatial analysis and statistical data analysis. For the smaller-scale spatial data of urban districts and counties and below, the methods of tourism information computing geometry, buffer analysis and overlay analysis can be used, such as calculating the coverage of public service facilities through buffer analysis and overlay analysis. Using the statistical data, we can summarize the static data of the basic elements of the city, calculate the average value, per capita value, proportion, number statistics, and coverage analysis.

As shown in Figure 5, the distribution and total amount of tourism information are always increasing. To analyze the change direction and trend of the center of gravity of urban space and leisure tourism space more intuitively, the migration trajectory of the center of gravity of urban space is drawn by using tourism information. It shows that the overall development of urban space and leisure tourism space is first to the northwest, then to the southwest, and the spatial growth is mainly in the southwest cities.

Table 1: The Index System of Tourism Information Operation Signs.

Item	Summer palace	Huangshan	Lushan	Datang Furong garden
Business	4.8	3.78	3.89	3.28
Food	4.55	2.68	1.5	5.62
Landscape	3.73	2.62	3.91	1.09
Place of interest	3.23	1.87	4.28	3.06
Physical education	1.61	1.32	3.08	5.39

Among the famous scenic spots in China, there are "dinosaur museum", "Ocean Museum" and "undersea tunnel". The reason why the "dinosaur museum" ranks high is that it is far away from the other four museums, which is also one of the important reasons why "walking" ranks high. As shown in Figure 6, the second-highest frequency word in the two scenic spots is "children", which indicates that the two scenic spots have a strong attraction for children and are the choice of many families for parent-child travel. In addition, "a lot of people", which ranks third among the famous scenic spots in China, ranks 50th among the characteristic words of tiger beach. The main reason is that Tiger Beach covers a large area and tourists are more evacuated. China's famous scenic spots are more attractive to tourists.

As shown in Table 2, tourists have a higher perception of tourism attractions and experience of tiger beach and Shengya, but a lower perception of tourism environment and facilities and services, and there are obvious differences

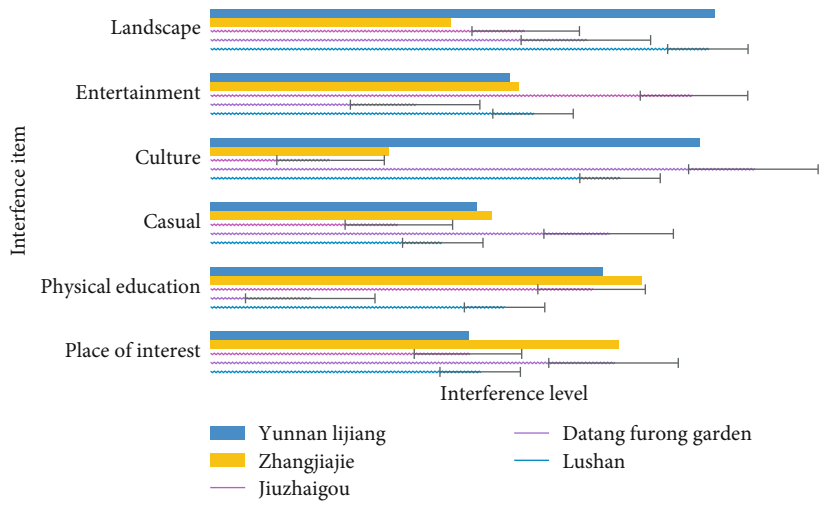

Figure 5: Distribution and Total Change Trend of Tourism Information.

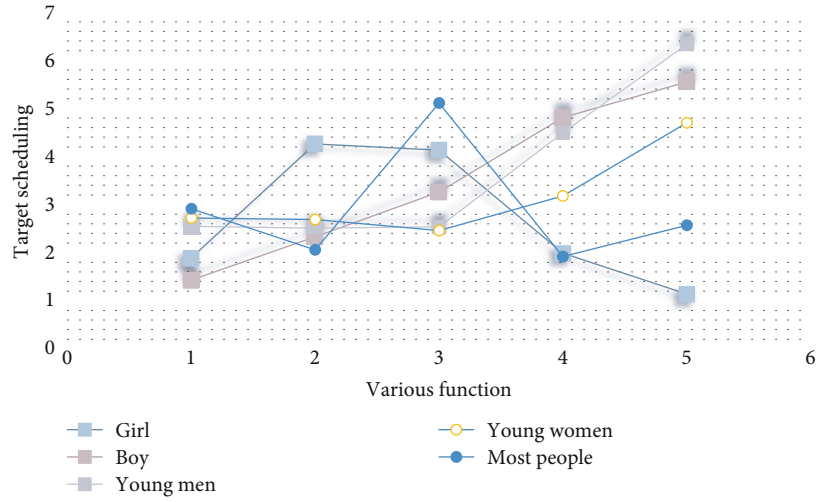

Figure 6: Projects that attract tourists among China's famous attractions.

Table 2: Perception of tourist attractions and tourist experience.

Item	Landscape	Place of interest	Physical education	Casual
Summer palace	0.8	0.12	1.62	0.86
Huangshan	2.06	3.46	2.95	3.87
Lushan	5.23	3.86	3.47	3.19
Datang Furong	4.1	5.08	4.55	2.36
Jiuzhaigou	1.64	1.76	3.54	4.43
Zhangjiajie	4.66	2.31	2.96	5.06

Table 3: Tourists' cognitive evaluation and emotions.

Item	Datang Furong garden	Jiuzhaigou	Zhangjiajie	Yunnan Lijiang
Place of interest	4.96	3.17	5.02	3.18
Physical education	1.23	4.69	5.31	4.83
Casual	4.9	2.32	3.46	3.28
Culture	6.68	1.48	2.19	6.02
Entertainment	2.52	5.95	3.79	3.68

between the two scenic spots. In the overall perception of scenic spots, tiger beach and Shengya have little difference. The two scenic spots belong to marine theme scenic spots, in which leisure and entertainment are all around the ocean, which is a romantic ocean trip for tourists; Children are attracted by all kinds of interesting marine creatures and performances in the scenic area, which is also a good choice for parent-child travel. Among the tourist attractions, tiger beach and Shengya are quite different, which indicates that tourists pay more attention to the tourist attractions, and

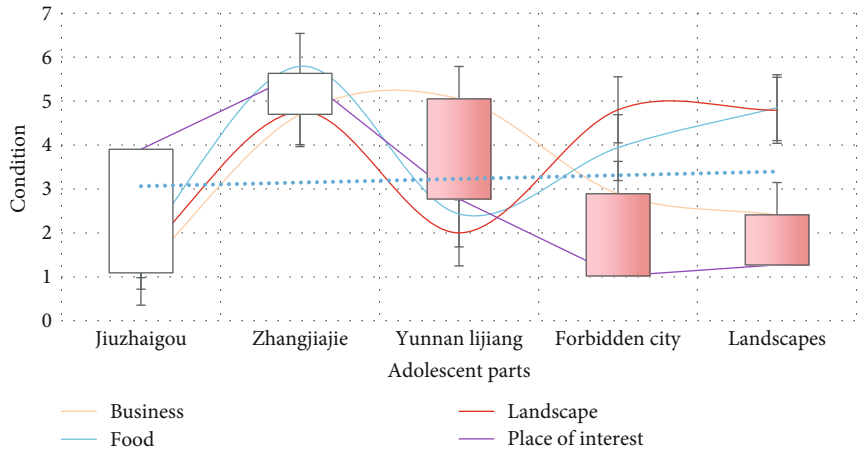

Figure 7: The overall trend of tourism information.

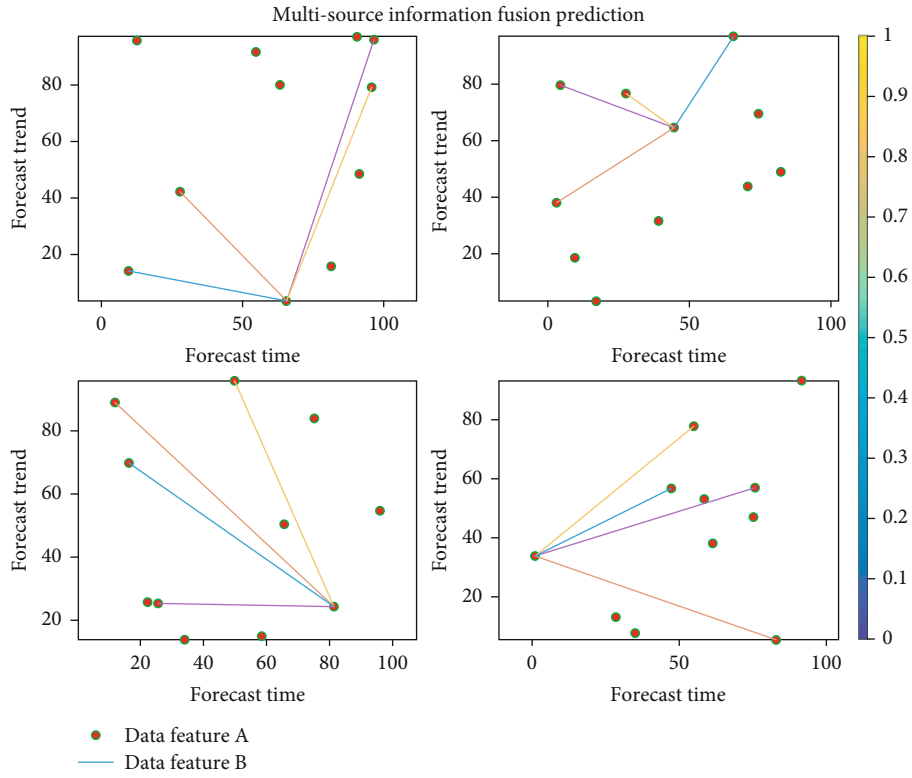

Figure 8: Multi-source information fusion prediction.

Shengya is more attractive. Tourists have a higher perception of Shengya theme venues and special performances.

As shown in Table 3, among the famous scenic spots in China, tourists' cognitive evaluation is more positive and there are not too many negative emotions. This shows that tourists are more satisfied with the service of famous scenic spots in China. Tourists' perception of the tourism environment and facilities of tiger beach and Shengya is weak. In the level of tourism environment perception factors, there are obvious differences in social environment perception. Among them, China's famous scenic spots are located in urban areas and are very close to Xinghai Square, which makes "Xinghai Square" stand out. Dalian Xinghai Square itself is one of the scenic spots that Dalian must visit. Tourists will take two scenic spots as a one-day tour plan, while Tiger Beach Ocean Park is relatively remote, this is also one of the important reasons why tourists sometimes choose Shengya when they choose two marine theme scenic spots.

As shown in Figure 7, through the coupling analysis of tourism information data and scenic spot data, it can be found that the overall tourism information is gradually decreasing from the central urban area to the surrounding areas, and there is a high coupling between the two data, and the areas showing coupling differences can also reflect the buildings with the same nature, such as stations, airports, industrial development zones, and other large areas. There is

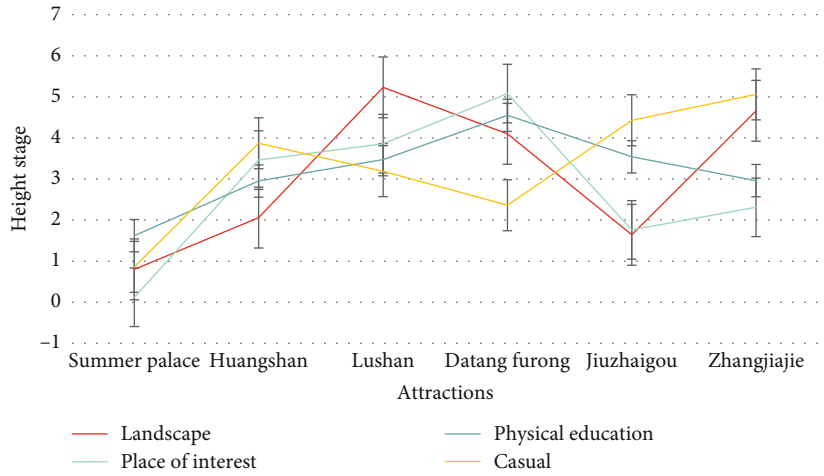

Figure 9: The center of gravity of urban space and leisure tourism space.

a wide range of low low coupling around the central city because the economic construction of suburban towns is relatively backward, so the value of tourism information and various leisure tourism service facilities are low, which is in line with the reality.

The center of gravity of urban space and leisure tourism space is shown in Figure 8. This paper finds that with the increase of human activity intensity and urban construction, the area of tourism information increases year by year, and the direction of gravity shift is from southwest to northwest. The results show that the multi-method comprehensive analysis based on big data can better describe the spatial distribution attributes and spatiotemporal evolution characteristics of the region. For example, this paper objectively and comprehensively reveals the agglomeration characteristics of leisure tourism space and provides indispensable reference information for land space planning. But at the same time, there are some limitations. The analysis of the characteristics of regional spatial agglomeration in this paper is more about the results, and the analysis of its driving factors or influencing factors is still lacking.

As shown in Figure 9, according to the results of the multi-source fusion of tourism information in this model, the results of tourism feature extraction are consistent with the data of Feizhu, tunic, and other websites in the trend. Among them, in the data of the first half of 2020, the prediction accuracy of the model after data processing is about 62%. Affected by the epidemic situation, the accuracy of the model is low. In the second half of the year, the prediction accuracy is 78%, which can be used to fuse tourism information in a short time. Therefore, the data show that the model has high learning ability and high trend prediction ability in tourism data processing, which can provide necessary information support for tourists.

4.2. Discussion. Given the target redundancy in the reconstruction results of specific scenic spots, this paper constructs a multi-source data fusion model based on an ensemble learning algorithm. In the field of 3D reconstruction, the irrelevant objects in a specific scene are eliminated by data fusion to achieve 3D scene reconstruction! Firstly, the lightweight algorithm is used to extract and match the features of different types of feature points, and the point clouds at different times are fused to complete the reproduction of the point cloud map. Then, for the irrelevant targets that may exist in the constructed point cloud map, with the help of multi-source sensor data and deep learning application technology in the field of computer vision, the target detection and elimination are carried out in three-dimensional space. For the two different processes of point cloud map modeling and target detection, the point cloud registration method is used to fuse them, and finally, the scene reappearance in the scenic spot environment is completed! The experimental results show that the method based on multi-source data fusion can effectively combine the two processes of 3D modeling and target detection, and complete the construction of a point cloud map without redundant targets in scenic spots.

By comparing the online comment text data of tourists and the offline comprehensive satisfaction survey questionnaire, it is found that the survey results of the tourism image perception of West Wetland Park are relatively consistent. Based on multi-source data integration of leisure travel space based on tourist information data and tourist attraction data, it is found that the leisure travel space in the central city area is distributed in a clear central multipoint layout, and the overall leisure travel is there. In the urban area, there is a trend of high agglomeration of scenic spots, which shows that scenic spots are the most concentrated areas of leisure tourism, while the agglomeration effect of peripheral counties is weak. In addition, the overall distribution pattern of leisure tourism space shows obvious characteristics of denseness and sparseness and a trend from northwest to southeast.

5. Conclusions

The multi-source fusion of tourism information of this model shows that the results of this model are consistent with the data of Feizhu, tunic, and other websites in the trend. Among them, in the data of the first half of 2020, the

prediction accuracy of the model after data processing is about 62%. Affected by the epidemic situation, the accuracy of the model is low. In the second half of the year, the prediction accuracy is 78%, which can be used to fuse tourism information in a short time. Therefore, the data show that the model has high learning ability and high trend prediction ability in tourism data processing, which can provide necessary information support for tourists. Based on the online comments on Ctrip, combined with the survey results of tourists' comprehensive satisfaction in the same period, the online tourism big data and offline questionnaire verify each other, comprehensively analyze the tourism image perception of Xixi National Wetland Park, and innovate the means and methods of tourism image perception research, However, there are still some deficiencies in the number and period of tourists' online comments. In the follow-up research, it is necessary to further increase the number of online tourism big data and offline questionnaire survey samples, and enrich the correlation analysis of tourists' attributes, temporal and spatial behavior characteristics and tourism image perception, try to reduce the error caused by the difference of online and offline survey samples.

Data Availability

The data underlying the results presented in the study are available within the manuscript.

Conflicts of Interest

The author(s) declare (s) that they have no conflicts of interest.

References

[1] Y. Chen, "A survey on industrial information integration 2016-2019," *Journal of Industrial Integration and Management*, vol. 5, no. 4, pp. 56–59, 2020.

[2] C. F. Shang, Y. F. Wang, and J. L. Du, "Information integration for motor generation," *Current Opinion in Physiology*, vol. 8, no. 4, pp. 116–120, 2019.

[3] A. Oberoi, M. Arora, and V. K. Garg, "A novel approach for dynamic information integration," *International Journal of Reasoning-based Intelligent Systems*, vol. 13, no. 2, pp. 76-77, 2021.

[4] P. de Bernardi, A. Bertello, and R. Shams, "Logics hindering digital transformation in cultural heritage strategic management: an exploratory case study," *Tourism Analysis*, vol. 24, no. 3, pp. 315–327, 2019.

[5] W. C. Poon and K. Y. Koay, "Hong Kong protests and tourism: Modelling tourist trust on revisit intention," *Journal of Vacation Marketing*, vol. 4, no. 4, pp. 1356–1359, 2021.

[6] Y. A. Poetra, "Upaya Pemerintah Dalam Mengkomunikasikan Tradisi Malamang Menjadi Objek Pariwisata Budaya Di Kabupaten Padang Pariaman," *Jurnal Pustaka Budaya*, vol. 5, no. 2, pp. 52–61, 2018.

[7] G. R. Ramadhan and I. Buchori, "Strategi Integrasi Sistem Transportasi Umum Dalam Menunjang Pariwisata Kota Yogyakarta," *Jurnal Pengembangan Kota*, vol. 6, no. 1, pp. 84-85, 2018.

[8] W. Huyan and J. Li, "Research on rural tourism service intellectualization based on neural network algorithm and optimal classification decision function," *Journal of Ambient Intelligence and Humanized Computing*, vol. 9, no. 4, pp. 1–21, 2021.

[9] M. Özturan, M. Mutlutürk, B. Çeken, and B. Sarı, "Evaluating the information systems integration maturity level of travel agencies," *Information Technology & Tourism*, vol. 21, no. 2, pp. 237–257, 2019.

[10] P. Liu, H. Zhang, J. Zhang, Y. Sun, and M. Qiu, "Spatial-temporal response patterns of tourist flow under impulse pretrip information search: from online to arrival," *Tourism Management*, vol. 73, no. 8, pp. 105–114, 2019.

[11] M. Zhou, Y. Li, M. J. Tahir, X. Geng, Y. Wang, and W. He, "Integrated statistical test of signal distributions and access point contributions for Wi-fi indoor localization," *IEEE Transactions on Vehicular Technology*, vol. 70, no. 5, pp. 5057–5070, 2021.

[12] G. Xiao, Q. Cheng, and C. Zhang, "Detecting travel modes using rule-based classification system and Gaussian process classifier," *IEEE Access*, vol. 7, pp. 116741–116752, 2019.

[13] X. Guangnian and Z. Wang, "Empirical Study on Bikesharing Brand Selection in China in the Post-Sharing Era," *Sustainability*, vol. 12, p. 3125, 2020.

[14] T. Arenas, M. N. Martínez, H. Xu, O. Morales, and M. Chávez, "Integrating VSM and network analysis for tourism strategies-case: Mexico and the Chinese outbound market," *Systemic Practice and Action Research*, vol. 32, no. 3, pp. 315–333, 2019.

[15] R. Strulak-Wójcikiewicz, N. Wagner, A. Łapko, and E. Hącia, "Applying the business model canvas to design the E-platform for sailing tourism," *Procedia Computer Science*, vol. 176, no. 5, pp. 1643–1651, 2020.

[16] M. Shiraishi, H. Ashiya, A. Konno et al., "Development of real-time collection, integration, and sharing Technology for Infrastructure Damage Information," *Journal of Disaster Research*, vol. 14, no. 2, pp. 333–347, 2019.

[17] K.-Y. Kwon, "A study on the path-dependent in Korea and China's early cultural industry policy," *The Journal of Chinese Cultural Research*, vol. 39, no. 6, pp. 88-89, 2018.

[18] D. E. Setyowati, Y. Antariksa, E. Haryati, H. Haryono, and I. P. P. Salmon, "Local tourism? Why not! Integrating tourism geographic spatial in Ngawi Regency, Indonesia," *Modern Applied Science*, vol. 14, no. 9, pp. 1–8, 2020.

[19] V. V. Yavorska, I. V. Hevko, V. A. Sych, O. I. Potapchuk, and K. V. Kolomiyets, "Features of application of information technologies in modern tourism," *Journal of Geology Geography and Geoecology*, vol. 28, no. 3, pp. 591–599, 2019.

[20] W. Zhu, Y. Hou, E. Wang, and Y. Wang, "Design of Geographic Information Visualization System for marine tourism based on data mining," *Journal of Coastal Research*, vol. 103, no. 1, pp. 30–34, 2020.

[21] K. Y. Chen and S. Y. Yang, "A cloud information monitoring and recommendation multi-agent system with friendly interfaces for tourism," *Applied Sciences*, vol. 9, no. 20, pp. 43–48, 2019.

[22] I. Ramos-Soler, "AM Martínez-Sala, Campillo-Alhama C. ICT and the sustainability of world heritage sites. Analysis of senior Citizens' use of tourism apps," *Sustainability*, vol. 11, no. 11, pp. 32-33, 2019.

[23] S. L. Ratnasari, E. N. Susanti, W. Ismanto, R. Tanjung, D. C. Darma, and G. Sutjahjo, "An experience of tourism development: how is the strategy?," *Journal of Environmental Management and Tourism*, vol. 11, no. 7, pp. 1877–1886, 2020.

[24] T. Melikh, D. Voit, and D. Archybisova, "Aquacultural Integration in recreational tourism: features of development and management of coastal territories," *Baltic Journal of Economic Studies*, vol. 5, no. 5, pp. 84–95, 2020.

[25] M. N. Rifa'I, "Integrasi Pariwisata Halal di Kota Malang," *FALAH Jurnal Ekonomi Syariah*, vol. 4, no. 2, pp. 194–196, 2019.

[26] G. Manyara, "Regional tourism in inter-governmental authority on development: a comparative policy and institutional best practice approach," *International Journal of Tourism Policy*, vol. 9, no. 1, pp. 50–52, 2019.

[27] M. Zhou, Y. Long, W. Zhang et al., "Adaptive genetic algorithm-aided neural network with channel state information tensor decomposition for indoor localization," *IEEE Transactions on Evolutionary Computation*, 2021.

[28] M. Abd, "The integration time-driven activity-based costing (TDABC) and events approach their role in decision-making and their effect on tourism," *African Journal of Hospitality Tourism and Leisure*, vol. 8, no. 2019, pp. 51–53, 2019.

[29] R. Peng, Y. Lou, M. Kadoch, and M. Cheriet, "A human-guided machine learning approach for 5G smart tourism IoT," *Electronics*, vol. 9, no. 6, pp. 947–949, 2020.

[30] Z. Lv, D. Chen, R. Lou, and Q. Wang, "Intelligent edge computing based on machine learning for smart city," *Future Generation Computer Systems*, vol. 115, pp. 90–99, 2021.

Hindawi
Journal of Sensors
Volume 2023, Article ID 9842945, 1 page
https://doi.org/10.1155/2023/9842945

Retraction

Retracted: Course Ideological and Political Teaching Platform Based on the Fusion of Multiple Data and Information in an Intelligent Environment

Journal of Sensors

Received 17 October 2023; Accepted 17 October 2023; Published 18 October 2023

This article has been retracted by Hindawi following an investigation undertaken by the publisher [1]. This investigation has uncovered evidence of one or more of the following indicators of systematic manipulation of the publication process:

(1) Discrepancies in scope
(2) Discrepancies in the description of the research reported
(3) Discrepancies between the availability of data and the research described
(4) Inappropriate citations
(5) Incoherent, meaningless and/or irrelevant content included in the article
(6) Peer-review manipulation

The presence of these indicators undermines our confidence in the integrity of the article's content and we cannot, therefore, vouch for its reliability. Please note that this notice is intended solely to alert readers that the content of this article is unreliable. We have not investigated whether authors were aware of or involved in the systematic manipulation of the publication process.

In addition, our investigation has also shown that one or more of the following human-subject reporting requirements has not been met in this article: ethical approval by an Institutional Review Board (IRB) committee or equivalent, patient/participant consent to participate, and/or agreement to publish patient/participant details (where relevant).

Wiley and Hindawi regrets that the usual quality checks did not identify these issues before publication and have since put additional measures in place to safeguard research integrity.

We wish to credit our own Research Integrity and Research Publishing teams and anonymous and named external researchers and research integrity experts for contributing to this investigation.

The corresponding author, as the representative of all authors, has been given the opportunity to register their agreement or disagreement to this retraction. We have kept a record of any response received.

References

[1] J. Zhou, Z. Wei, F. Jia, and W. Li, "Course Ideological and Political Teaching Platform Based on the Fusion of Multiple Data and Information in an Intelligent Environment," *Journal of Sensors*, vol. 2021, Article ID 1558360, 10 pages, 2021.

Hindawi
Journal of Sensors
Volume 2021, Article ID 1558360, 10 pages
https://doi.org/10.1155/2021/1558360

Research Article

Course Ideological and Political Teaching Platform Based on the Fusion of Multiple Data and Information in an Intelligent Environment

Jieqiong Zhou,[1] Zhenhua Wei,[2] Fengzhen Jia,[1] and Wei Li[1]

[1]*School of Marxism, Xijing University, Xi'an, 710123 Shaanxi, China*
[2]*Faculty of Education, Xi'an Siyuan University, Xi'an, 710038 Shaanxi, China*

Correspondence should be addressed to Zhenhua Wei; james@link.cuhk.edu.hk

Received 7 June 2021; Revised 1 July 2021; Accepted 10 July 2021; Published 31 July 2021

Academic Editor: Mu Zhou

In the current teaching of politics, teachers still focus on the cultivation of the basic intelligence of students' language intelligence, and it is easy to ignore the cultivation of other intelligences that affect the overall development of students. This research mainly discusses the design of curriculum ideological and political teaching platform based on the fusion of multiple data and information in an intelligent environment. This research adopts the MVC architecture, and the web application developed based on the MVC (Model View Controller) architecture pattern is easier to complete the realization of multiple controllers. The front desk ideological and political teaching teacher module includes the login system. In addition, the teacher can view the test status of a specific student and can also pay attention to the total intelligence of all students who have been tested. The process of the student test is to enter the correct account and password to log in to the system and then perform the test. After the test, the test result can be viewed, and the personal information can be maintained at the same time. In addition, the personal login password can be modified. The existence of the database is to ensure that the data is correct and effective. This system uses MySql to design the database, and the name of the database is braintest_db. The data table in relational database is the main object of storing and managing data, and it is also an important task of database design. This system has designed three kinds of user logins, namely, administrator, student, and teacher, and login can be realized according to the account number and password. Among them, teacher's participation is by inquiring about students' test situation, paying attention to students' multiple intelligences, and teaching students in accordance with their aptitude. In addition, the main object of this test is students, and the analysis of multiple intelligences is realized through student tests. Students are vitally physical objects that can be tested and searched for results. In the study, 20% of the students both learn the basic content of the platform and use the forum. This research will help improve students' literacy in an all-round way.

1. Introduction

The fusion of multiple data and information breaks through the traditional education and teaching concepts, and is in line with the concept of quality education in my country. It is a theoretical theory that focuses on the development and diversification of students' intelligence. Consider the strengths and weaknesses of different aspects of intelligence, use strengths to drive weaknesses, and respect the development of students in all aspects of intelligence.

The fusion of multiple data and information is also an effective guiding ideology for the realization of quality education, which is of high value to educational research. The multiple intelligence test system uses this as a theoretical basis, breaks the limitations of traditional tests, establishes scientific and effective coping strategies through more topic tests, evaluates students' intelligence in many aspects, stimulates potential, and helps the development of education to the greatest extent.

The use of multiple data and information fusion is becoming more and more extensive. Perdikaris et al. have

developed a framework for multifidelity information fusion and predictive reasoning in high-dimensional input space and in the presence of a large number of data sets. The method they proposed establishes a new paradigm for constructing the response surface of a high-dimensional stochastic dynamic system and at the same time considers the multifidelity in the physical model and the multifidelity in the probability space. Although they combined these new development results, they can get a linear complexity algorithm, but it is not clear enough when it comes to benchmarking problems [1]. Zhou et al. believe that the integration of multiple functions and the context structure of unlabeled data have proven its effectiveness in enhancing similarity measures in many computer vision applications. First, integrate multiple features into a unified similarity to enhance the discriminative ability of similarity measurement. They uses the diffusion process on the tensor product graph to achieve these goals. Although the method they obtained has been verified on many challenging video sequences, the research process is very complicated [2]. Quing et al. believe that traffic state estimation plays an important role in operational traffic management and is essential for real-time traffic modeling and prediction. With the emergence of more and more heterogeneous traffic data, data fusion has become one of the main challenges of state estimation. Although their research has produced state estimation values, which are better than those obtained by any data source alone, PISCIT has a better performance in the source data. Structural errors and random errors are also very powerful [3]. Wen et al. believe that because timely early fault diagnosis is the key to ensuring operational safety and suppressing fault deterioration, they reviewed the data-driven initial fault research, which has low amplitude and is easily concealed by system interference and noise. In addition, they not only pointed out the problems related to complex systems but also hoped to promote the development of the field by adding new information and using new mathematical tools to mine unused hidden information. Although they proposed four ideas worthy of discussion, diagnosis based on correlation analysis, multisource information fusion, machine learning, and time-frequency transformation, there are too few research process data [4].

This research mainly discusses the design of curriculum ideological and political teaching platform based on the fusion of multiple data and information in an intelligent environment. This research adopts the MVC architecture, and the web application developed based on the MVC (Model View Controller) architecture pattern is easier to complete the realization of multiple controllers. The front desk ideological and political teaching teacher module includes the login system. In addition, the teacher can view the test status of a specific student and can also pay attention to the total intelligence of all students who have been tested. This system has designed three kinds of user logins, namely, administrator, student, and teacher, and login can be realized according to the account number and password. Among them, teacher's participation is by inquiring about students' test situation, paying attention to students' multiple intelligences, and teaching students in accordance with their aptitude. The main object of this test is students, and the analysis of multiple intelligences is realized through student tests. Students are vitally physical objects that can be tested and searched for results.

2. Course Ideological and Political Teaching Platform

2.1. Multivariate Data Information Fusion. In the process of using multiple data and information fusion, students' intelligence is multiple, and teachers should adopt multiple teaching methods. However, the purpose of the teaching method using multiple intelligences is not only to cultivate students' intelligence but to use multiple data and information fusion to enable students to better master the basic knowledge, at the same time, to train students on the world outlook, outlook on life, and values for students' life. Development lays the foundation for ideological and political quality [5, 6].

$$\lambda = e^{-(1/2\sigma)}\left(\tau_{(t)} - T\right)^2 + e^{1/2\sigma}\left(\tau_{(t)} + T\right). \tag{1}$$

λ is a multiple fusion parameter. Some teachers pay attention to the cultivation of multiple intelligences in the ideological and political classroom, but ignore the disciplinary characteristics of ideological and political and the role of the ideological and political classroom, as well as the students' mastery of basic knowledge [1].

$$\mu = \frac{T_{(t)} - T_{(\min)}}{T_{(\max)} - T_{(\min)}}. \tag{2}$$

T is the time for students to study [7].

$$\omega_{(n)} = Y - 0.5\cos\frac{\pi n}{N} + 0.4\cos\frac{\pi n}{N}. \tag{3}$$

2.2. Ideological and Political Teaching. In terms of specific disciplines, the liberal arts disciplines represented by language and history mainly examine students' speech-language intelligence, while the science disciplines represented by mathematics and physics mainly examine students' logic-mathematics. From this point of view, these disciplines are mainly based on a kind of intelligence factor, so these disciplines still mainly rely on speech-language intelligence or logic-mathematics intelligence in the evaluation process. At this time, the course of ideology and politics shows the difference from other disciplines under the fusion of multiple data and information. It is mainly manifested in: although school's ideological and political class is also based on students' speech-language intelligence, it often examines students' understanding and memorization ability, but it also often examines students' logic-mathematics intelligence P, such as economics study the calculation problems in the common sense part [8, 9].

$$P = \frac{1}{n}\sum_{t=1}^{n}\left|\frac{R' - R_i}{R_i}\right|. \tag{4}$$

R the relationship between matter and consciousness. In addition, sometimes, ideological and political classes often allow students to carry out group inquiry discussions and social practice. At this time, the main investigation is students' physical-motor intelligence, interpersonal intelligence, self-cognition intelligence, etc. So, in concrete terms, the focus of multiple intelligence evaluation in ideological and political courses is the comprehensive evaluation of multiple intelligence factors, not just one or two evaluations [10].

$$U = \sqrt{\frac{1}{M}\sum_{i=1}^{M}(X_i - X)}, \tag{5}$$

$$Q = 1 - \frac{H_i - H^2}{H_i - H\bar{H}}\sum_{i=1}^{n}\left(X - \bar{X}\right). \tag{6}$$

Q is a spatial factor, and U is an intellectual factor. Although various disciplines have introduced multiple data and information fusion to enrich the methods and means of evaluation of students in this discipline, so as to play the role of incentive and feedback of evaluation, however, due to the particularity of the school's ideological and political courses, the evaluation results of the school's ideological and political courses are different from other disciplines. Because the purpose of opening school ideological and political courses is to give play to the role of ideological and political education, help young people to establish a good value orientation, and form a positive outlook on life, values, and world outlook. Therefore, the final result of implementing school's ideological and political multiple intelligence evaluation system is to help students form a good character. At the same time, the final result of the evaluation of multiple intelligences in other disciplines is to help students firmly grasp an ability [11]. For example, Chinese, mathematics, and other subjects use the feedback function of the multiple intelligence evaluation system in the teaching process, so that students can firmly grasp the reading ability and calculation ability [12].

$$P_x = K\sum_{i=1}^{T}\left(X - \bar{X}\right)^2\left(X + \bar{X}\right), \tag{7}$$

$$P_y = K\sum_{i=1}^{T}\left(Y - \bar{Y}\right)^2, \tag{8}$$

$$P_Z = G\sum_{i=1}^{t}\left(T - \bar{T}\right)^2(T - X + Y)^{1/N}. \tag{9}$$

P_x means reading ability. P_y represents computing power. P_Z stands for feedback ability [13, 14].

2.3. Teaching Platform. When analyzing a system, feasibility analysis is also an indispensable link. Technical, economic, operational, and social factors will affect a system. These factors should also be taken into account by mature developers. First of all, from the analysis of technical feasibility, the software and hardware equipment of this test system includes ordinary personal computers, stable Windows systems, stable functional Eclipse development tools, and mature and rich MySql databases. I have a good grasp of programming languages such as Java and databases. The situation is good, and the tutor has been engaged in the research and teaching of related majors and has given some help to ensure the normal development and operation of the system. Then, from the analysis of operational feasibility, the system is mainly oriented to students and teachers. The interface of the system is direct and friendly. It has a little foundation in computer or some help and guidance. As long as you enter the system and understand the text prompts of the system, you can proceed related operations [15].

$$Z_x = \phi\sum_{i=1}^{T}\eta\left(X - \bar{X}\right)\left(Y - \bar{Y}\right). \tag{10}$$

Z_x indicates the degree of self-confidence [16, 17].

$$\chi_i = \sum_{n,m\in V}\sum_{j\in C}\mathrm{o}_{m,j} * W_{j,n} * L^i{}_{n,m} * T_n, \quad \forall I \in V. \tag{11}$$

The variable R_n is used to represent the data transmission speed of the ideological and political teaching platform [18].

$$\sum_{i:(i,k)\in E} F_{Lk} = \sum_{j:(k,j)\in E} F_{kJ} + \sum_{j:(k,j)\in H} F_J^k + X_k. \tag{12}$$

Here, f_{ik} represents a link transmission delay connected to the node J where v is set. Then, from the analysis of economic feasibility, the school provides laboratories for students majoring in computer science, and a certain amount of computers are available for students to use [19, 20]. Nowadays, laptops are basically students' academic must-haves. In terms of materials, school libraries, and college materials, relevant information can be provided by libraries, online resources, etc. [21]. The optimization problem solved by this technique can be expressed as follows [22, 23]:

$$\begin{aligned}\arg_{\max} = {} & \mu_1 N(A - A_{\min}) + \mu_2 N(E_{\max} - E) \\ & + \mu_3 N(T_{\max} - T) + \mu_4 N(S_{\max} - S).\end{aligned} \tag{13}$$

Here, A, E, and T represent a problem that needs to be optimized, which can be changed according to the requirements of the task [24, 25]. Finally, from the analysis of social feasibility, the system mainly combines multiple data and information fusion to help students develop various intelligences, develop their advantages and discover deficiencies, fully implement teaching concepts, and improve teaching quality [26].

$$\begin{aligned}W &= -\beta\frac{-\theta_x F_y + \theta_y F_x}{\left[F_x{}^2 + F_y{}^2\right]}\left[F_x{}^2 + F_y{}^2\right]^{1/2} \\ &= \beta\frac{F_{xx}\left(F_y\right)^2 + (F_x)^2 f_{yy} - 2F_x F_y F_{yy}}{\left[F_x{}^2 + F_y{}^2\right]}.\end{aligned} \tag{14}$$

Therefore, the product of the vector of the rate of change in the direction of the gradient $F(X, Y)$ can be represented by the symbol β as the boundary and the magnitude of the gradient [27].

3. Design Experiment of the Course Ideological and Political Teaching Platform

3.1. Overall Structure Design of the System. MVC is the model (Model), view (View), controller (Controller), and web applications developed based on the MVC (Model View Controller) architecture pattern; it is easier to complete the implementation of multiple controllers; when the controller is written, relevant setting of page navigation is relatively troublesome. Through the research of web applications based on the MVC architecture, differences in implementation can be found. Based on these differences, this type of web software can be developed, which adjusts the calling process in accordance with the MVC architecture. For the differences, it is pointed out that the strategy of using external configuration files is used and achieved. With such an ingenious way to set the changed part through the configuration file, the web software can be made into a development platform, allowing the developer to use the previous software to set the basic structure according to the MVC architecture, and the developer only needs to follow his own actual situation. If you need to achieve specific functions, you can achieve the development of Web projects. This kind of Web software is called a Web framework, and the use of this framework can reduce workload, improve implementation efficiency, and effectively reduce maintenance costs.

This system is designed to adopt Struts2+Bootstrap framework mode combination development. Struts2 is developed on the basis of WebWork2. The business controller action is written and implemented by the developer. It can be a simple Java class, separated from the ServletAPI. The processing flow of Struts2 is roughly to send a request through a browser. The central processor finds the corresponding action class for processing the request according to the struts.xml file. The interceptor chain of WebWork automatically applies general functions to the request, such as, WorkFlow, validation, and other functions. When the method parameter is configured in the Struts.xml file, the Method in the action class corresponding to the method parameter is called; otherwise, the general execute method is called to process the user request, and the result returned by the corresponding method in the action class is responded to the browser. The overall structure is shown in Figure 1.

3.2. System Flow. According to the analysis of system requirements and functions, combined with the overall structure design, the system's various functional processes are basically determined. The system administrator mainly manages the accounts of teachers and student users, so that the foreground data and the background data will always be consistent and only need to use the existing permissions to operate.

The process of the front desk teacher includes logging in to the system, and only entering the correct account and password can enter the teacher system interface. If a student forgets his password information, the teacher can help the student modify the information through this interface. In addition, the teacher can view the test status of a specific student and also pay attention to the total intelligence of all students who have been tested.

The process of the student test is to enter the correct account and password to log in to the system and then perform the test. After the test, the test result can be viewed, and the personal information can be maintained. It mainly includes the maintenance of the personal user name and email address, and the individual can be modified login password.

In short, the administrator has the highest authority and can restrict teachers and students as users to perform some specific operations and at the same time master their information. Teachers can manage students in a certain range; on the one hand, it is convenient for teachers to understand students and at the same time protect students' privacy. In addition to operating with their own permissions, student users do not affect other users, but they are the most important users in this system and the basis for other users' operations.

3.3. Database Design. Data is an important element of the project. The existence of the database is to ensure that the data is correct and valid. This system uses MySql to design the database. The name of the database is brain test_db. The data table in the relational database is the main object of storing and managing data, and it is also an important task of database design.

The design of the database is carried out according to the data needs of the system. This system has designed three user logins, namely, administrator, student, and teacher, and login can be realized according to the account number and password. Among them, teacher's participation is to check students' test conditions, pay attention to students' multiple intelligences, teach students in accordance with their aptitude, and help students to progress and develop according to the actual situation. It also includes gender and mailbox, and different attributes can help the system identify users. In addition, the main object of this test is students, and the analysis of multiple intelligences is realized through student tests. Students are vitally physical objects that can be tested and searched for results. Because the login interface of teachers and students are the same, their attributes are the same, including account number, password, name, gender, and email address.

The connection between the teacher and the student is mainly through the test result. The student enters the test interface by logging in and submits the test content to obtain the result, and the teacher can query the test result of a single student or view the intelligent result curve graph of all students and understand the overall situation. The current state of intellectual development of all students.

In addition, the design of test questions is related to the actual development and progress of social life, combined with the classification of intelligence in the concept of multiple data information fusion, and the test questions are classified, which are related to language intelligence, logical

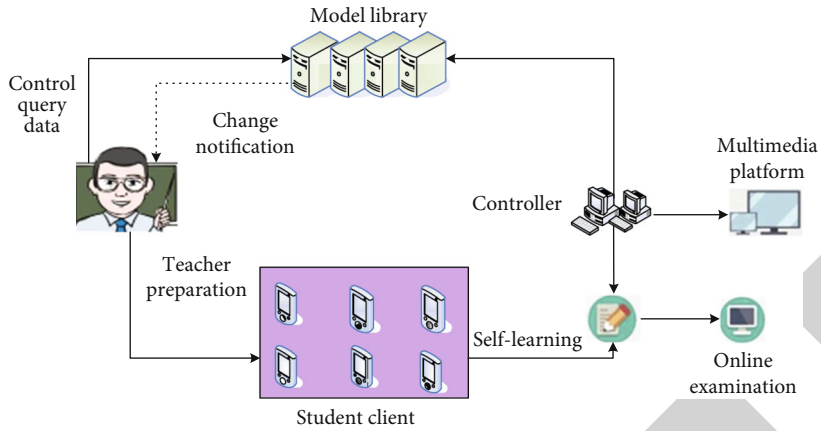

Figure 1: Overall structure.

Table 1: Teacher information.

Data item	Data item meaning	Type of data	Space
Id	Teacher id	Int<20>	No
Account	Account number	Var char<100>	No
Pass word	Password	Var char<100>	No
User_name	Name	Var char<100>	Yes
Sex	Gender	Int<1>	Yes
User_type	User type	Int<1>	No

mathematics intelligence, and spatial intelligence, physical movement intelligence, musical intelligence, interpersonal intelligence, self-cognition intelligence, and natural intelligence topics. Teacher information is shown in Table 1.

3.4. Module Design

3.4.1. Administrator Module. A complete system requires an administrator to lead the overall situation, manage every user who uses the system, and make all operations within the scope of authority. Of course, the administrator also needs to have an account and password. After passing the authentication, the administrator can enter the management interface. Administrator's login interface is shown in Figure 2.

In this interface environment, the administrator can add users. If some users will not register or the client has problems, the administrator can assign an account to them to help users better access the system. Among them, teacher users need to apply for distribution at the administrator to prevent users who are not teachers from registering wantonly and infringing on the information of other users. The design of this function ensures the reasonableness and safety of the system.

In addition, through this interface, when facing some malicious users or needing to organize user information, the administrator can delete some worthless user information, and then, this account will no longer be able to login on the user side.

3.4.2. Teacher Module. The teacher module is a channel for teachers to understand and analyze the intelligence of students through the system. After they have a certain grasp of the intelligence, they can adjust teaching strategies and methods to improve teaching quality. The reflection of multiple intelligences adjusts teachers' view of students. Teachers should adjust teaching according to the uniqueness of each student's intelligence. Different students need different ways of education, especially for students who are relatively backward in performance. Pay attention to the development of its advantages and intelligence, use its advantages to drive disadvantages, build up students' self-confidence, face up to the current social demand for talent types, and fully realize quality education.

If the teacher wants to view the test result of one of the students, check the test result to help the student improve specifically, enter student's account, and click to view the single test result, there will be a histogram of student's test result. In addition to the students, only the teacher has the authority to view the personal test results. Through the understanding

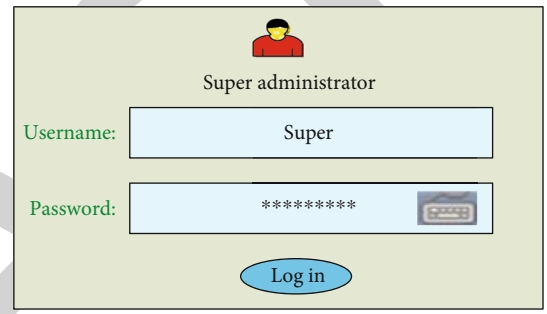

Figure 2: The login interface of the administrator.

Table 2: Student information.

Data item	Data item meaning	Type of data
Id	Student id	Int<10>
Account	Account number	Var char<50>
Pass word	Password	Var char<50>
User_name	Name	Var char<50>
Sex	Gender	Int<1>
User_type	User type	Int<1>

Table 3: Student motivation.

Options	Before the experiment		After the experiment	
	Experimental class	Control class	Experimental class	Control class
Strongly motivated people	3	3	5	3
Motivated average number	3	4	3	4
People with weak motivation	2	2	1	2

of a certain student's intelligence status, combined with the actual communication, the teaching concept of paying attention to each student can be realized. The test result is not an absolute evaluation by the students, but only as a reference item for the smooth progress of the teaching work, to provide teachers with some realistic data of the students, so as to facilitate the adjustment of teaching strategies and teach students in accordance with their aptitude.

If the teacher wants to view the test results of all students, just click view all test results to have all the student result information, and all the results will be fed back to the teacher in the form of a line graph. Teachers can adjust the way of classroom teaching according to the general intelligence of students, adjust the teaching progress according to the development progress of students' intelligence, integrate theory with practice, and complete teaching tasks better and faster. Secondly, the presentation of this result allows teachers to have a relative reference standard for the evaluation of students, to have a relative evaluation of students, and to help students in combination with their specific conditions.

3.4.3. Student Module. The design of student's module is mainly to allow students to understand their own intelligence through the test, in order to help students adjust the pace of development; this module is mainly for testing; the first is to verify whether there is this permission to enter the test system. If you have not registered an account and the administrator has not assigned it, you need to register a user that belongs to you. There are restrictions on what you need to fill in during registration. For example, if the registered user name is already used by others, a prompt message will pop up.

After login verification, you will enter the main interface of the student test. If you want to return or exit, there is a prompt button in the upper right corner to operate. This interface is all the operations that student users can perform, including testing, viewing the results of the test, maintaining personal information, and modifying personal passwords, because the password is a main verification information for a user to log in to the system, and its importance is not unusual, so a label is specifically set to allow users to manage passwords.

After clicking the start exam button, students will enter the main interface of the test. All test questions are presented in the form of single selection, and the options are divided into 5 levels. The tester chooses according to his actual situation and the degree of conformity with the content, and all the questions appear randomly. Each time the user performs a test, the question will be updated. All questions are randomly given by the question bank, to ensure that users will not reduce the reliability of the test because of memorizing the content of the questions.

3.4.4. Smart Homework Evaluation Homework Evaluation Module. It is a relatively traditional evaluation method, and it is also a very effective evaluation method. In actual teaching work, we should actively expand the effect of homework evaluation and gradually transition from the traditional single-intelligent homework evaluation to the multiple-intelligence homework evaluation mode. In order to realize the diversification of the evaluation of students in the school's ideological and political courses, improve the objectivity of the evaluation results, and promote the teaching of the school's ideological and political courses. Intelligent homework evaluation requires teachers to take into account the various intelligences of students in the process of designing homework and organically combine specific knowledge requirements with intelligent evaluation. Only in this way can the objective and perfect evaluation results be achieved, the quality of the homework will be improved, and the quality of the work will be improved. There is an advancement of the teaching reform of ideological and political courses in schools. In the actual homework design, the reasonable allocation of subjective questions and objective questions should be achieved, and the open test questions should be combined with general test questions. Only in this way can the role of evaluation be better realized.

4. Results and Discussion

According to the specific implementation of the system, the data tables designed from this mainly include teacher information table, student information table, multiple intelligence test question table, and test result table. Different tables define different permissions and contents. Student information is shown in Table 2.

Before and after the experiment, students' learning motivation, interest in learning, and attitude to the evaluation of multiple intelligences in ideological and political classes were investigated through interviews, so as to grasp the degree of recognition of students' evaluation of multiple intelligences. At the same time, it was also found through comparison in the teaching of ideological and political classes. Use multiple intelligences to evaluate the role and value. The motivation of students is shown in Table 3.

After the experimental class implemented the multiple intelligence evaluation strategy for a semester, students' interest in the study of ideological and political courses has also been greatly improved. The changes in student interest are shown in Figure 3.

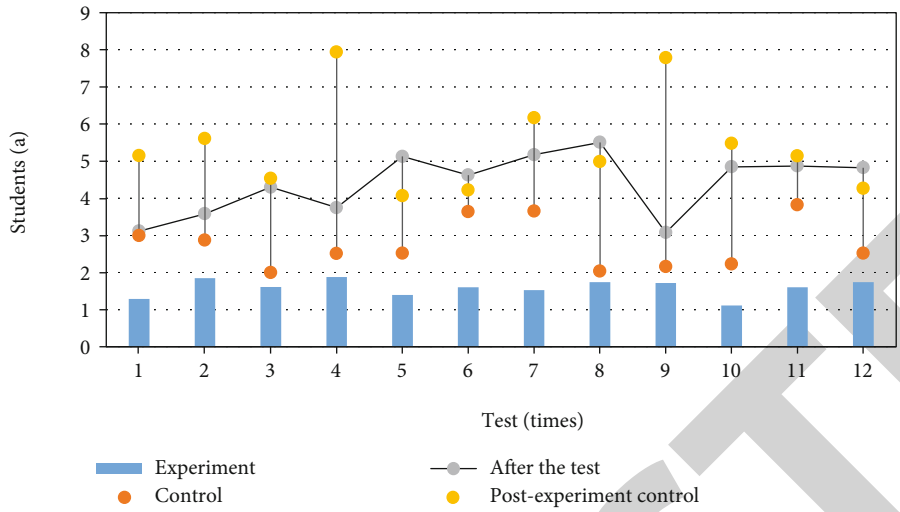

Figure 3: Changes in student interest.

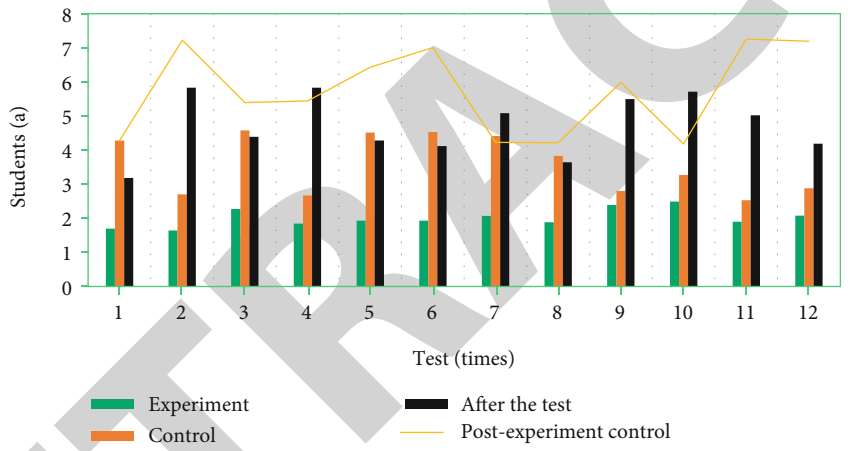

Figure 4: Students' evaluation of multiple intelligences in ideological and political classes.

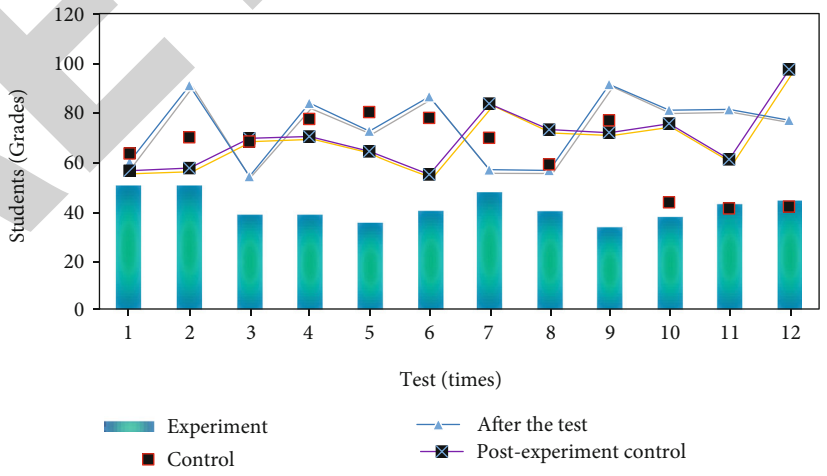

Figure 5: Student performance statistics.

Analyzing the comparative data, we can find that after the experiment, the students in the experimental class have a strong interest in the evaluation of multiple intelligences in the ideological and political class. Before and after the experiment in the control class, there was basically no change in the three indicators of the students. This shows that the

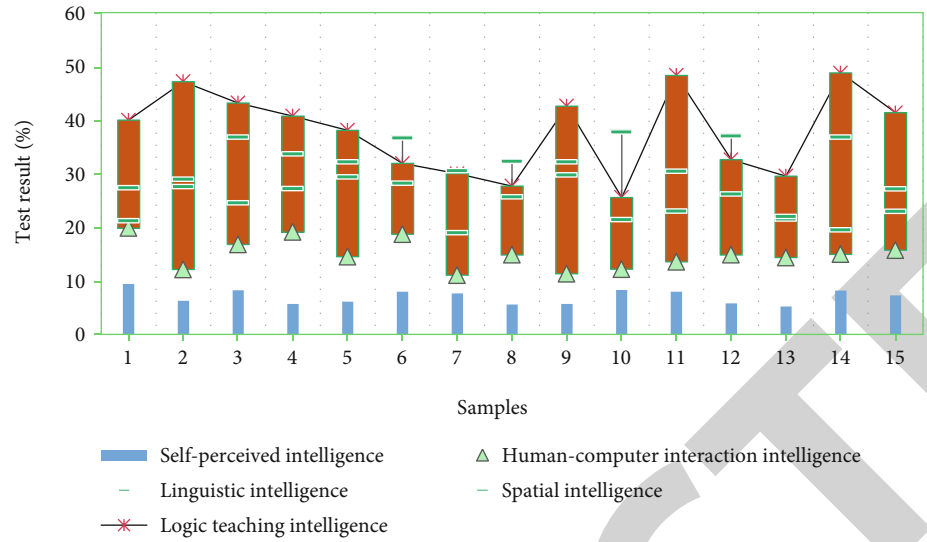

Figure 6: Test results on students.

Figure 7: The use of the platform by students.

evaluation of multiple intelligences in ideological and political courses has a greater effect on improving students' learning motivation and interest in ideological and political courses. At the same time, students prefer the evaluation of multiple intelligences in ideological and political courses and should be actively used in the future teaching process. Students' evaluation of multiple intelligences in ideological and political classes is shown in Figure 4.

Through analysis, we can find that before the experiment, the ideological and political performance of the experimental class and the control class is basically the same, and the average score, variance, and standard deviation data show that there is no big difference. However, after a one-semester evaluation of multiple intelligences in the experimental class, the two classes reuse the same test paper for the test. The average score of the experimental class is nearly 6 points higher than the control class, and the standard deviation and variance have decreased. This shows that the overall performance of the students in the experimental class has made greater progress, and the gap between the students has further narrowed. This shows that the evaluation of multiple intelligences is of great significance to the teaching of ideological and political courses in schools. Student performance statistics are shown in Figure 5.

Each test will produce a test result; in the result, the system will classify and summarize the scores of each intelligence and then feed back to the tester in time in the form of a histogram, which more intuitively reflects the status of each intelligence. Testers can perform multiple tests and have a certain understanding of their own intelligence based on the situation reflected by the system. Although this test does not fully reflect their own strength, it can be used as a

reference to discover their own superior intelligence, develop their expertise, and improve those who are relatively weak. Other intelligence promotes all-round development. Everyone's intelligence distribution is definitely different. Even for students with low overall intelligence, they can find their own shining points and improve self-confidence. The society does not need different types of talents; as long as they have talents, they will be paid attention to. Figure 6 shows the test results for students.

Schools should pay attention to the mutual participation of subjects in interactive evaluation so that they can actively cooperate, participate, communicate, and even evaluate themselves in an equal and democratic atmosphere, so as to effectively improve the effectiveness of multisubject evaluation. According to analysis, more than 6% of students only learn the basic content of online learning platform (oucontent), more than 7% of students only learn knowledge expansion resources (resource), and more than 5% of students only use forums (forumng) for discussion, with nearly 37% of students learn not only the basic content on the platform but also knowledge expansion resources, more than 25% of students only learn supplementary materials through links (url), and 20% of students both learn the basic content of the platform and use forums, and nearly 1% students log in to the subpage to learn. The use of the platform by students is shown in Figure 7.

5. Conclusion

With the in-depth development of basic education curriculum reform, building a developmental evaluation system has become an inevitable trend in the development of teaching evaluation. At present, what changes have taken place in the teaching evaluation of ideological and political courses in schools, what are the problems in teaching evaluation in teaching practice, and how to solve these problems. Based on the above questions, this research has conducted a research on the teaching evaluation of ideological and political courses in schools. This research adopts the MVC architecture, and the web application developed based on the MVC (Model View Controller) architecture pattern is easier to complete the realization of multiple controllers. The front desk ideological and political teaching teacher module includes the login system. In addition, the teacher can view the test status of a specific student and can also pay attention to the total intelligence of all students who have been tested. This system has designed three kinds of user logins, namely, administrator, student, and teacher, and login can be realized according to the account number and password. Among them, teacher's participation is through inquiring students' test situation, paying attention to students' multiple intelligences, and teaching students in accordance with their aptitude. In short, in the future, teachers need to pay more attention to the comprehensive training of students and teach students in accordance with their aptitude.

Abbreviations

MVC: Model View Controller
CPU: Central processing unit
RAM: Random access memory
MAE: Mean absolute error.

Data Availability

Data sharing is not applicable to this article as no datasets were generated or analysed during the current study.

Conflicts of Interest

The authors declare that they have no competing interests.

Acknowledgments

This work was supported by the Educational Research Fund SGH20Y1529 of A Study on the Teaching Status of Humanities General Education Courses in Private Universities and Reform Strategies: A Case Study of Five Private Universities in Shaanxi. This work was supported by educational research fund YBKT-1801 of Shaanxi Education Bureau.

References

[1] P. Perdikaris, D. Venturi, and G. E. Karniadakis, "Multifidelity information fusion algorithms for high-dimensional systems and massive data sets," *SIAM Journal on Scientific Computing*, vol. 38, no. 4, pp. B521–B538, 2016.

[2] Y. Zhou, X. Bai, W. Liu, and L. J. Latecki, "Similarity fusion for visual tracking," *International Journal of Computer Vision*, vol. 118, no. 3, pp. 337–363, 2016.

[3] Q. Ou, J. W. C. van Lint, and S. P. Hoogendoorn, "Piecewise inverse speed correction by using individual travel times," *Transportation Research Record*, vol. 2049, no. 1, pp. 92–102, 2008.

[4] C. L. Wen, F. Y. Lv, Z. J. Bao, and M. Q. Liu, "A review of data driven-based incipient fault diagnosis," *Acta Automatica Sinica*, vol. 42, no. 9, pp. 1285–1299, 2016.

[5] J.-F. Ehlenbröker, U. Mönks, and V. Lohweg, "Sensor defect detection in multisensor information fusion," *Journal of Sensors and Sensor Systems*, vol. 5, no. 2, pp. 337–353, 2016.

[6] M. Yousefi and E. Carranza, "Data-driven index overlay and Boolean logic mineral prospectivity modeling in greenfields exploration," *Natural Resources Research*, vol. 25, no. 1, pp. 3–18, 2016.

[7] B. Rasti, P. Ghamisi, J. Plaza, and A. Plaza, "Fusion of hyperspectral and LiDAR data using sparse and low-rank component analysis," *IEEE Transactions on Geoscience & Remote Sensing*, vol. 55, no. 11, pp. 6354–6365, 2017.

[8] P. Braca, R. Goldhahn, G. Ferri, and K. D. LePage, "Distributed information fusion in multistatic sensor networks for underwater surveillance," *IEEE Sensors Journal*, vol. 16, no. 11, pp. 4003–4014, 2016.

[9] A. de Paola, P. Ferraro, S. Gaglio, G. L. Re, and S. K. Das, "An adaptive Bayesian system for context-aware data fusion in smart environments," *IEEE Transactions on Mobile Computing*, vol. 16, no. 6, pp. 1502–1515, 2017.

[10] B. J. Liu, Q. W. Yang, W. U. Xiang, F. A. Shi-dong, and G. U. Feng, "Application of multi-sensor information fusion in the fault diagnosis of hydraulic system," *International Journal of*

Hindawi
Journal of Sensors
Volume 2021, Article ID 1869281, 9 pages
https://doi.org/10.1155/2021/1869281

Research Article

Construction of an Intelligent Processing Platform for Equestrian Event Information Based on Data Fusion and Data Mining

Zhong Wu[1] **and Chuan Zhou**[2]

[1]*Physical Education School, Wuhan Business University, Wuhan, 430056 Hubei, China*
[2]*Institute of Mechanical Engineering, Wuhan Institute of Shipbuilding Technology, Wuhan, 430062 Hubei, China*

Correspondence should be addressed to Chuan Zhou; 20150459@wbu.edu.cn

Received 29 April 2021; Revised 27 May 2021; Accepted 3 June 2021; Published 24 July 2021

Academic Editor: Mu Zhou

In the past two years, equestrian sports have become more and more popular with the public. Due to the comprehensive development of equestrian preparations for the 2020 Olympic Games in China, the equestrian sports industry presents an unprecedented favorable development environment in China. This article is aimed at studying the construction of an equestrian event information intelligent processing platform based on data fusion and data mining. This article introduces the relevant theoretical knowledge of data mining and data fusion, including the description of the concept of data mining, the common analysis methods and algorithms of data mining, the basic concepts of data fusion, and the functional structure of data fusion. It discusses various algorithms in cluster analysis and focuses on the analysis of distance measurement and similarity coefficient in cluster analysis. In the experimental part, in order to intelligently process and acquire information, an information intelligent processing platform is constructed based on data fusion and data mining technology. The experimental results of this paper show that the precision rate, recall rate, and F-score of the platform under closed test are much higher than those under open test, and the precision rate is increased by about 7.26%.

1. Introduction

China is one of the countries in the world with a long history of horse breeding and one of the countries that develop horse culture. For a long time, horse culture has always been an important part of Chinese national culture, so "horse culture" also represents a kind of "cultural trust." This "cultural trust" equestrian sport is a sport where athletes and horses work together. One of the most obvious differences from other sports is that the object that the athlete grasps is not a lifeless equipment, but a living horse. After the reform and opening up, the rapid development of China's tertiary industry has greatly promoted the development of sports in my country. Although equestrianism is a very special sport, as a high-level sporting event in our country, it has become more and more popular in recent years. Equestrian sports began to show a trend of vigorous development. The rapid economic growth and the improvement of people's spiritual and cultural needs have made equestrian sports possible. With the increasing number of equestrian events held, it is urgent to build an intelligent information processing platform.

National policies have promoted the rapid development of equestrian sports. The holding of equestrian events requires a logical and scientific platform to intelligently process event data. There are various forms of data expression and big data storage capacity in the intelligent data processing platform. Due to the increasing requirements for data processing speed and accuracy, conventional data processing methods can no longer satisfy the platform. In addition, with the rapid development of computer technology and data processing technology, a large amount of information can be processed in real time. In this case, data fusion technology has emerged. In addition, too much information is a problem that people must deal with. In order to obtain useful data from a large amount of information, data mining technology is further introduced. Data mining is a broad interdisciplinary field that gathers researchers in various fields, especially researchers and engineers in databases, artificial intelligence, and data

processing. At the same time, the concept of data mining also points out a new research direction for the use of new technologies and methods to develop intelligent data processing.

The Internet of Things technology has been used as the core technology of converged services that require intelligent information processing, and its importance is gradually emerging. Am-suk proposed a beacon device using acceleration sensors and hole sensors. The beacon device can control the target under specific conditions by sensing the moving target. In addition, we expect to apply it to various types of factory environments, such as detachable installation and optimal management using sensors. Through the internal network construction of the Internet of Things interactive devices, it can be effectively connected with the Internet of Things devices, and diversified services can be provided through the connection with the open platform. However, in addition to the basic functions of the beacon technology, there are still many requirements under specific environments and conditions [1]. With the rapid development of big data technology, a new way of thinking about intelligent transportation has become an obligation. Mendili SE creates a big data modeling method by using a data modeling method called ITS for processing transmission and processing data. The method pays special attention to the creation of multiple layers. Among these layers, you can find the management and processing layer, which contains three layers: processing, analysis, and storage. The disadvantage is that different types of different traffic data are numerous and huge [2]. Quan's research on intelligent data processing is aimed at establishing a theory, algorithm, system and technical method for processing data, complex systems, and uncertainties, researched the theory and methods of processing intelligent information using the sensory mechanism of perception, established usable calculation models, and developed application programs. It has a wide range of applications in complex system modeling, system analysis, decision-making, control, optimization, and design. However, the effectiveness of this research on the modeling method of intelligent information processing has yet to be verified [3].

The innovations of this paper are (1) introduction and improvement of the clustering algorithm, which improves the efficiency of the network monitoring system and paves the way for the intelligent information processing technology to be studied in the experimental part. (2) Combining URL processing, content processing, and port processing and applying this mixed processing method to the platform, through automatic classification, reduce the burden of managing large-scale data processing systems and improve the efficiency of data processing functions.

2. Construction Method of Intelligent Processing Platform for Equestrian Event Information Based on Data Fusion and Data Mining

2.1. Data Mining

2.1.1. The Concept of Data Mining. Data mining is to extract the knowledge that people are interested in from the database [4, 5]. This kind of knowledge is indirect knowledge, which is unknown and may be useful, and can be expressed in the form of concepts, rules, laws, standards, etc. Generally speaking, data mining is a decision support process, a mode used to find and collect facts or observe the results. The object of data mining is not only a database but also a file system or other data collection [6, 7].

The task of data mining is to extract knowledge from it. Divided by function, this knowledge is divided into two categories: predictive and descriptive [8]. The prediction type can accurately determine a specific result based on the value of the data item. Descriptive is the description of the rules contained in the data or data grouping through the similarity of the data. According to the differences in knowledge found, we can classify data mining tasks into the following categories: (1) feature rules: extract feature formulas about these data from a set of data related to the learning task to express the overall characteristics of the data set [9]; (2) classification: search for the concept of a category, which represents the total information of this type of information [10]; (3) clustering: first, group the data and then put it in a cluster. The differences between the groups are as large as possible, and the differences within the groups are as small as possible. The difference between clustering and classification is that clustering does not depend on predefined classes and does not require a training set [11, 12]; (4) association analysis: means that when the value of two or more data elements is represented and the probability is high, at time, there is a specific relationship, and the relationship law of these data elements can be determined [13]; (5) prediction: learn the law of change from the past data, and create a model, and use this model to predict the type and characteristics of future data, etc. [14]; (6) deviation detection (anomaly analysis): deviation detection is to detect significant changes and deviations between the current status of data, historical records, and standards. Bias includes a large category of potentially useful knowledge [15].

2.1.2. Commonly Used Analysis Methods and Algorithms for Data Mining. Data mining technology is widely used in all aspects, so its shortcomings are becoming more and more perfect. The key problem to be solved is the type of problem and the type and scale of data. According to the powerful functions of data mining, the analysis method can be used and divided into the following four types:

(1) Analysis based on the degree of relevance: the purpose of relevance analysis is to dig out the interrelationships hidden in the data [16]

(2) Based on sequence analysis: the focus of sequence pattern analysis is to analyze the before-and-after or causal relationship between data [17]

(3) Classification analysis: the input set of the classification analysis method is a set of records and several kinds of marks. First, a mark is assigned to each record, that is, records are classified by mark, and then, these calibrated records are checked and the characteristics of these records are described [18]

(4) Cluster analysis: the input set of the cluster analysis method is a set of uncalibrated records, which means that the input records have not been classified at this time [19, 20]. Its purpose is to reasonably divide the record set according to certain rules and use explicit or implicit methods to describe different categories. These rules are defined by cluster analysis tools

In the process of using any technology, its used conditions and scope will be limited, and data mining technology is no exception. Therefore, the important selection link in the use process is to select effective data mining models and analysis algorithms for specific fields.

The main data mining methods of database technology are (1) statistical methods; (2) association rules: mining association rules is to search for correlations in the data set [21]; (3) genetic algorithms; (4) rough set methods: never accurate; knowledge is found in fuzzy and uncertain information; traditional set theory can be used to classify and find incorrect information or internal links that interfere with information [22]; (5) fuzzy method: fuzzy logic systems are widely used in the field of classification; (6) neural network method: neural network is used to obtain the classification model [23].

2.2. Data Fusion. Data fusion is the multilayer processing and aggregation of multiple sensor data sets obtained from the same target to generate important new data [24]. The sensors here refer to various data acquisition systems and related databases. Data integration is a method of dealing with multiple data sources. In short, data fusion is a complete multidata algorithm [25, 26]. The purpose of processing is to reason and identify the information received and to evaluate and judge accordingly. By combining data from multiple sensors, data from multiple sensors can be combined to increase confidence, reduce ambiguity, and improve system reliability.

Data fusion is a comprehensive process through which computers can be used to process, control, and make decisions about information from different sources [27]. The functions of most data fusion systems include correlation detection, perception, and estimation, and the functional mode is shown in Figure 1. The fusion system is divided into two levels of low-level processing and high-level processing [28, 29]. Low-level processing includes data extraction, data connection, target state evaluation, and characterization and is numerical processing that produces numerical results. Advanced processing mainly includes behavior prediction evaluation and state evaluation. It is a symbolic processing and can lead to more abstract results.

As show in Figure 2, data detection is the continuous scanning and observation of targets using multiple sensors in a data fusion system, and key detection and key detection are performed at the signal level [1]. The function of the data interface unit is to determine whether the time and space data are different from the same target. The state evaluation is based on the approximate value of the target parameter of the sensor observation and uses these estimated values to predict the state of the next observation target. Target perception is to generate N-dimensional feature vectors based on feature targets measured by different sensors. Each dimension represents the independent characteristics of the target. If it is known in advance that the target has an M type and a single target type, the metric vector can be compared with the known category features to define the target category. According to the location, parts, type, and other information, understand the overall development goals and general situation. In distributed processing, each sensor makes an independent decision and then sends the result of the decision to the fusion center for the CPU to make a final decision. The advantage of this structure is that it requires low channel capacity and is easy to implement in engineering. But each sensor will decide on its own, which will make the fusion process unstable. The hybrid structure has the following two advantages: low data transmission channel requirements and availability of main measurement data.

2.3. Cluster Analysis. Clustering refers to the process of dividing a collection into multiple groups in a certain way. Among them, objects in the same group have a high degree of similarity, but are very different from objects in other groups. Cluster analysis is used as a tool to classify information, observe the characteristics of each category, and discover the hidden information. At present, cluster analysis is used in various industries, such as graphics processing, information retrieval, and statistics.

2.3.1. Definition of Cluster Analysis. In the field of machine learning, unlike classification, clustering is an unsupervised learning process; the result of which is unknown. Here is the mathematical description of cluster analysis:

For the data set $A = \{a_i \mid i = 1, 2, \cdots, n\}$, according to the similarity between the data objects u_i, it is divided into k groups, $\{C_j \mid j = 1, 2, \cdots k\}$, and meets $C_i \cap C_j \neq \varnothing i \neq j$ and $C_i \cup C_j = A$, where C_i is called a cluster.

Assuming that the data to be clustered contains n objects, each object x_i contains m attributes, and x_{ij} represents the jth attribute of the ith object, and the m attributes of the nth object form an $n \times m$ matrix.

$$\begin{pmatrix} x_{11} & x_{12} & \cdots & x_{1m} \\ x_{21} & x_{22} & \cdots & x_{2m} \\ \vdots & \vdots & \ddots & \vdots \\ x_{n1} & x_{n2} & \cdots & x_{nm} \end{pmatrix}. \tag{1}$$

Another representation is called the dissimilarity matrix, which can be used to store the dissimilarity between n objects.

$$\begin{pmatrix} 0 & & & & \\ d(2,1) & 0 & & & \\ d(3,1) & d(3,2) & 0 & & \\ \vdots & \vdots & \vdots & & \\ d(n,1) & d(n,2) & \cdots & \cdots & 0 \end{pmatrix}. \tag{2}$$

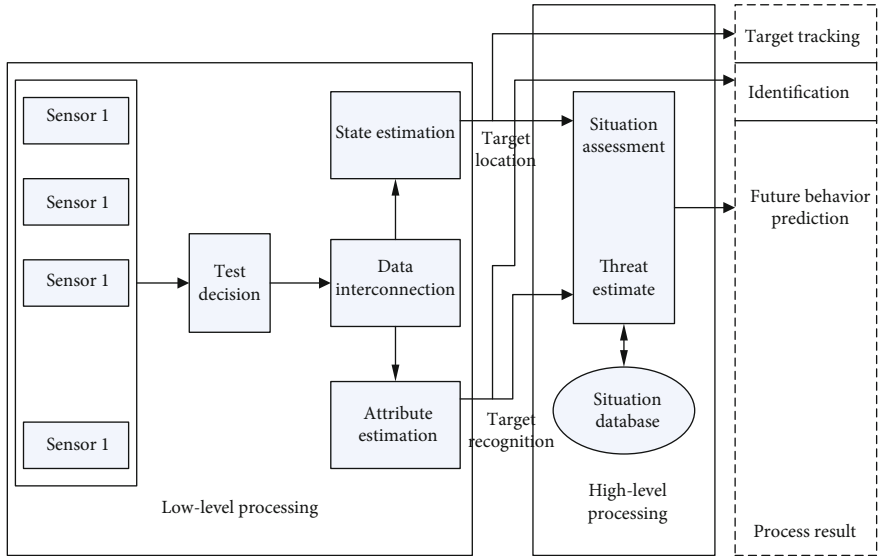

Figure 1: Data fusion functional structure.

The dissimilarity matrix is an $n \times n$ matrix, where $d(i, j)$ represents the dissimilarity between object i and object j. Its value is a nonnegative number, and the larger the value, the greater the difference between the two, and the smaller the value, the more similar the two. Obviously $d(i, j) = d(j, i)$, so the dissimilarity matrix is expressed as a lower triangular matrix.

2.3.2. Distance Measurement in Cluster Analysis. Most clustering algorithms divide data objects into similar clusters. Therefore, the similarity between clusters is very low, but the similarity between cluster objects is high. Generally, the distance of an object is used to measure the similarity of an object. There is a special relationship between inequality and similarity, which can be transformed into the following formula.

$$d = 1 - s, \tag{3}$$

or

$$d = \frac{1}{s} - 1. \tag{4}$$

For objects x_i and x_j with m attributes, the common distance formulas are:

(1) Euclidean distance

$$d(x_i, x_j) = \left\| x_i - x_j \right\| = \left[\sum_{k=1}^{m} \left| x_{ik} - x_{jk} \right|^2 \right]^{1/2}. \tag{5}$$

(2) Manhattan distance

$$d(x_i, x_j) = \sum_{k=1}^{m} \left| x_{ik} - x_{jk} \right|. \tag{6}$$

(3) Chebyshev distance

$$d(x_i, x_j) = \max \left| x_{ik} - x_{jk} \right|, i, j = 1, 2, \cdots, n. \tag{7}$$

(4) Minkowski distance

$$d(x_i, x_j) = \left[\sum_{k=1}^{m} \left| x_{ik} - x_{jk} \right|^q \right]^{1/q}. \tag{8}$$

For $q \in [1, +\infty)$, when $q = 1$, it is the Manhattan distance; when $q = 2$, it is the Euclidean distance, and when $q \longrightarrow \infty$ is the Chebyshev distance.

2.3.3. Mahalanobis Distance. P. C. Mahalanobis proposed Mahalanobis distance, which is an effective method to calculate the similarity between two groups of unknown samples.

$$d(x_i, x_j) = (x_i - x_j) \sum^{-1} (x_i - x_j)^T, \tag{9}$$

where Σ is the covariance matrix.

In addition to distance, similarity coefficients can also be used as a metric. The closer the nature of the transaction, the closer the similarity is to 1, and the closer the similarity of unrelated transactions is to 0. Common similarity coefficients are:

(1) Cosine of included angle

The angle cosine is derived from the similarity. When $\theta_{ij} = 0$, then $\cos \theta_{ij} = 1$; it means that the object i and the object j are completely similar. When $\theta_{ij} = 90°$, then $\cos \theta_{ij} = 0$, which means that the object i and the object j are not related.

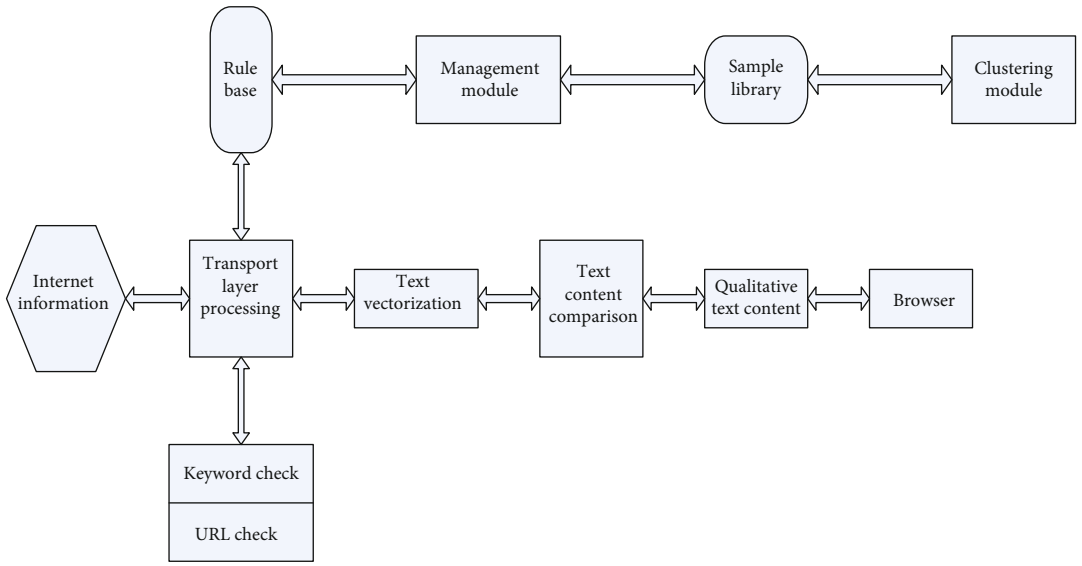

Figure 2: Typical information processing system.

$$\cos\theta_{ij} = \frac{\sum_{a=1}^{p} x_{ia}x_{ja}}{\sqrt{\sum_{a=1}^{p} x_{ia}{}^{2}\sum_{a=1}^{p} x_{ja}{}^{2}}}, 0 \le \cos\theta_{ij} \le 1. \quad (10)$$

(2) Correlation coefficient

The value range of the correlation system is $[-1, 1]$, which is an indicator used to measure the degree of linear relationship between variables with specific values. The correlation coefficient can be positive or negative. The higher the correlation coefficient, the higher the linear relationship between the variables.

$$r_{ij} = \frac{\sum_{a=1}^{p}(x_{ia} - \overline{x_i})(x_{ja} - \overline{x_j})}{\sqrt{\sum_{a=1}^{p}(x_{ia} - \overline{x_i})^2 \sum_{a=1}^{p}(x_{ja} - \overline{x_j})^2}}, -1 \le r_{ij} \le 1. \quad (11)$$

3. Experiments on the Construction of an Intelligent Processing Platform for Equestrian Event Information Based on Data Fusion and Data Mining

3.1. Overall Design. For this network information processing system, in order to be able to grasp the operation flow of data packets in the system, different processing strategies and strengths will be implemented according to different protocol layer data information. For example, in the TCP/IP protocol stack, corresponding to the network layer, transport layer, and application layer, the data processed, respectively, are IP packets, TCP or UDP packets, and complete application protocol data, but for example, the domain name and specific content are different. For the HTTP application layer protocol of the nature of the data, these requirements must be considered separately in the information processing process. Therefore, to design a secure network information processing system, many users will have their own personalized processing strategies, so to divide these users into different grouping levels, it is necessary to implement different processing strategies for different types of content at different levels.

To design an intelligent data processing system based on address processing and web content processing based on data mining technology, we must first create a sample library and maintain a URL list through intelligent web content analysis and then dynamically update the URL list. Before connecting to the remote target network, check whether the address list URL matches the keywords defined on the web page, and then, determine whether to process the URL and bad web page information, and add the web page URL of the bad information to the blacklist. This intelligent information processing can be dynamic, constantly update the address list, and accurately analyze the content of the web page. The intelligent information processing system designed is mainly considered from three aspects: user's personalized processing rule setting, matching processing algorithm, optimization, and sharing of rule library and sample library. Considering the requirements of each of the above key steps, the basic structure of the information processing system is as follows.

The main responsibilities of the main management modules of the system are user personalized management, rule list library management, sample information library management, cluster analysis results, and processing level setting management.

(1) User personalized management: create a user management system based on personalized processing strategies

(2) Rule library management: create a URL address library list and keyword management library

(3) Sample library management: the administrators or ordinary users perform operations such as adding, clearing, refreshing, and changing the harmful sample libraries of the system, as well as the subject ownership of the categories in the sample library

(4) Cluster analysis: perform periodic cluster analysis of the sample library or manually performed by the user, and use it in conjunction with module c, and use the sample library reasonably

(5) Processing level management: the processing level setting is completed by the system administrator according to different processing strategies

3.2. Design Goals. The network information processing monitoring system is mainly used in the Ethernet environment. The network monitoring system gives full play to the monitoring role of the software to effectively monitor and manage all the computers in the system, according to the current network application status and the current network monitoring technology level. The design of the network monitoring system for information processing is as follows:

(1) Comprehensiveness of monitoring: not only need to know the usage of the internal network of the LAN but also to know the specific network information of the current application of a certain computer, to see if it can run hacker software or other illegal network applications

(2) Strong operability: in order to enable network managers to use the system interface simply, quickly, and conveniently, the graphical interface must be designed to be simple and easy to use

(3) High security: the monitoring station program must use password authentication to log in to prevent illegal users from using the monitoring system

(4) High efficiency: the network monitoring system usually analyzes thousands of pieces of data in a very short time. The amount of data processed is quite large, and the analysis results are required to be very accurate. The system must have extremely high operating efficiency. And the detection algorithm must have low time complexity

3.3. Processing Flow. First, the user sends information to make a request to the network. Then, the transmission layer processing module checks the request sent by the network user according to the URL blacklist or the rule setting of the keyword, and judges whether the information is reserved or blocked according to the matching algorithm. Then, obtain the data information from the result of the transport layer inspection, and then, preprocess the web page text. After querying the categories in the sample library, the text is divided into roots based on the similarity to determine the content level of the text. If it is bad information, you need to set a warning or clear the log, and put its address in the blacklist. Give the user prompt information. Perform periodic cluster analysis and other operations on the sample library or other training sample libraries for various topics.

Table 1: Information intelligent processing development environment configuration.

Operating system	Windows Server 2003,Linux
Development tools	VC 6.0,Visual Studio 2008
System programming language	C++,C#
Database access operation component	ADO.NET
System database	Oracle 9i

Table 2: Mixing matrix of the classifier.

Category	Actually a positive example	Actually negative
Classified as positive	TP	FP
Classification as negative	FN	TN

3.4. Development Environment. The monitoring station module of the monitoring system mainly operates the database. It uses Microsoft's .NET visualization and easy-to-operate platform. The development tool uses Visual Studio 2008, which is based on .NET technology and web applications. Program development provides a well-supported integrated development environment [30, 31]. The programming language is C#, and ADO.NET is used for database access operations in Visual Studio 2008, because it can easily and efficiently implement operations such as database connection, access, and editing. In order to meet the real-time data change frequency of the network monitoring system and the requirements for the database of the system with large traffic, the system adopts the Oracle9i database, because the Oracle database has efficient data storage efficiency and powerful data maintenance functions as well as a good database structure design. The detailed development environment configuration of the network monitoring system based on information processing is shown in Table 1.

4. Experimental Results and Analysis

4.1. Matrix Analysis. In actual use, users tend to certain categories. For example, in the process of using the Internet, users may only be interested in documents on a certain topic. Generally speaking, the category that the user is interested in can be called the positive category, and the other categories are called the negative category. The recall rate and precision rate can reflect the accuracy and completeness of affirmative case classification. The hybrid matrix used to analyze these two evaluation criteria is shown in Table 2.

In practical applications, high precision is usually at the expense of recall, and the importance of evaluation criteria depends on actual application needs. If only one standard is needed to measure the performance of two different

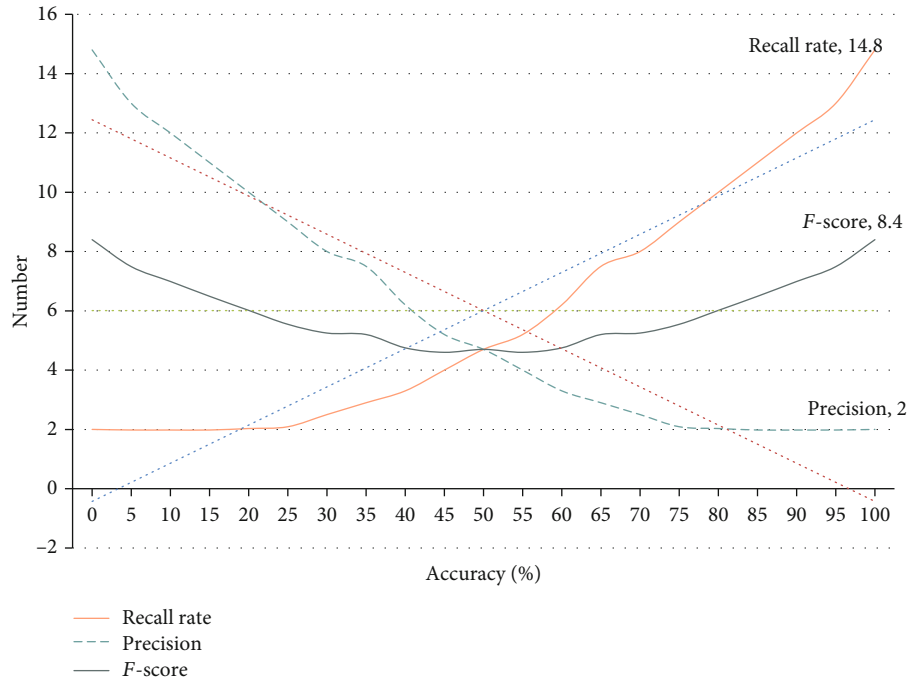

Figure 3: The relationship between precision, recall, and F-score.

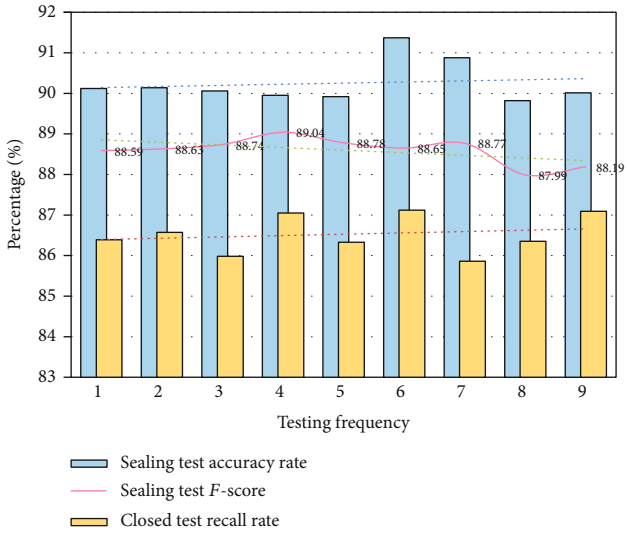

Figure 4: Test results of the closed test.

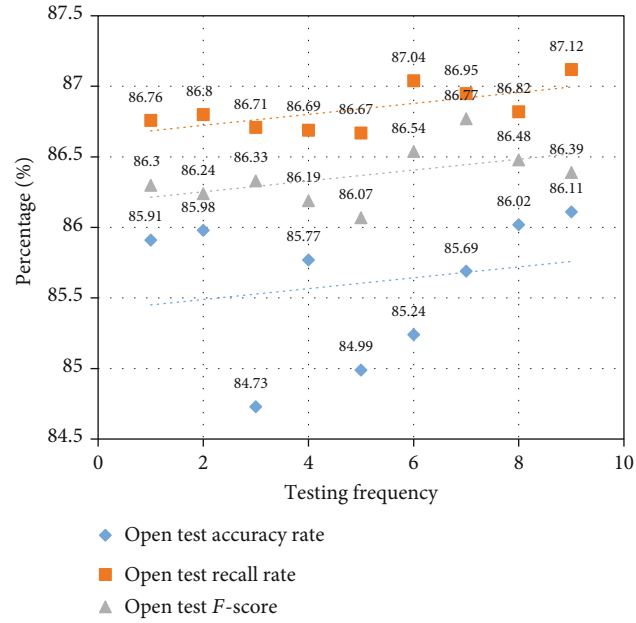

Figure 5: Test results of the open test.

classifiers, F-score is usually used. F-score represents the harmonic average of recall and precision. The relationship between the three is shown in Figure 3.

4.2. Sample Analysis. In order to build an information intelligent processing platform based on data fusion and data mining, 1,800 copies of legal and illegal webpages were collected from the Internet to form a sample database, of which 1,200 were legal webpages, and 600 were illegal webpages. This ratio is close to a general ratio of legal and illegal web pages that we usually encounter. During the testing process, the number of training samples can be added at any time, and the administrator will analyze the test results regularly. The 600 illegal web pages are divided into 8 copies, each with 75 copies, and 1200 legitimate web pages are randomly selected out of 600 copies. Divide into 8 pages, combine these 16 pages according to the cross-integration of illegal pages and legal pages, plus one page used for the open test is composed of 75 normal pages and 75 illegal pages, so there are 9 sets of rules and 150 pages each.

Then, each time, 2 of these 9 web pages are drawn, one is included in the training sample library as a closed test example, and the other is not included in the training sample

Table 3: Test results.

Test method	Sealing test accuracy rate	Closed test recall rate	Closed test F-score	Open test accuracy rate	Open test recall rate	Open test F-score
Test results	93.18%	88.97%	90.93%	85.92%	86.71%	86.25%

library as an open test example and continues to loop according to the above combination rules. Test 9 times and records the results while testing. The test result of the closed test is shown in Figure 4.

The test result of the open test is shown in Figure 5.

It can be seen from Figures 4 and 5 that in the two test environments of closed testing and open testing, the precision, recall, and F-score under closed testing are higher than those under open testing. And F-score, the precision rate under the open test, is much lower than that under the closed test, which is reduced by about 7.26%. The overall calculation results are shown in Table 3.

5. Conclusions

Due to the popularity of the Internet, information technology and equestrian competitions have formed an inseparable relationship among various equestrian events. Intelligent data processing is a pioneering interdisciplinary computer science and a comprehensive applied subject. The purpose is to process large and complex data and study new and advanced theories and technologies. The research of intelligent data processing includes multilevel basic research, applied basic research, basic research technology, and applied research. This article introduces the relevant theoretical knowledge of data mining and data fusion technology and conducts analysis and discussion to build an information intelligent processing platform based on data fusion and data mining. This article focuses on the design of the sample database, the function of the platform interface, and the interception effect of the data mining information processing system. Through experiments, network monitoring and information processing are realized. The platform can control illegal networks or bad data information and effectively process and monitor information. The platform constructed in this article truly embodies the characteristics of "letting the data speak," and when the data sample is particularly large, it also reflects the advantages of rapid and accurate computer automated processing. In theory, although some progress has been made in the construction of a sample database, a database based on web addresses, and web page text content, other factors of the entire network have not been considered in the research, and there is still a lot of work to be continued.

Data Availability

No data were used to support this study.

Disclosure

We confirm that the content of the manuscript has not been published or submitted for publication elsewhere.

Conflicts of Interest

There are no potential competing interests in our paper.

Authors' Contributions

All authors have seen and approved the manuscript.

Acknowledgments

This work was supported by the Wuhan University of Business Doctoral Fund Projects (2021KB002), the Application Foundation Frontier Project (2020010601012294), and the School-Level Academic Team Project of Wuhan Business University (2018TD011).

References

[1] O. Am-suk, "Transmission control method of beacon signal based on Bluetooth of lower electric power," *Journal of the Korea Institute of Information and Communication Engineering*, vol. 20, no. 6, pp. 1136–1141, 2016.

[2] S. el Mendili, "Big data processing platform on intelligent transportation systems," *International Journal of Advanced Trends in Computer Science and Engineering*, vol. 8, no. 1.4, pp. 1099–1199, 2019.

[3] W. Quan, "Intelligent information processing," *Computing in Science & Engineering*, vol. 21, no. 6, pp. 4-5, 2019.

[4] N. Feng, "Research on the modern intelligent healthcare platform from the perspectives of grid based cloud computing and information management system assisted internet of things technology," *International Journal of Grid and Distributed Computing*, vol. 9, no. 11, pp. 35–48, 2016.

[5] Y. Chai, "Design and implementation of English intelligent communication platform based on similarity algorithm," *Complexity*, vol. 2021, Article ID 5575417, 10 pages, 2021.

[6] J. F. Qiao, G. T. Han, and H. B. Zhou, "Knowledge-based intelligent optimal control for wastewater biochemical treatment process," *Zidonghua Xuebao/Acta Automatica Sinica*, vol. 43, no. 6, pp. 1038–1046, 2017.

[7] X. Zhang, "Construction of intelligent network customer service platform based on natural language processing and machine learning," *IPPTA: Quarterly Journal of Indian Pulp and Paper Technical Association*, vol. 30, no. 5, pp. 259–268, 2018.

[8] M. Janssen, S. Chattopadhyay, and N. Z. Rehe, "A reference architecture for context-aware intelligent traffic management platforms," *International Journal of Electronic Government Research*, vol. 14, no. 4, pp. 65–79, 2018.

[9] Z. Jin and D. Y. Ge, "Detection and recognition method of monocular vision traffic safety information for intelligent vehicles," *Journal of Intelligent & Fuzzy Systems*, vol. 2, pp. 1–10, 2020.

[10] W. Ping, "Data mining and XBRL integration in management accounting information based on artificial intelligence," *Journal of Intelligent & Fuzzy Systems*, vol. 40, no. 4, pp. 6755–6766, 2021.

[11] A. Kharbouch, Y. Naitmalek, H. Elkhoukhi et al., "IoT and big data technologies for monitoring and processing real-time healthcare data," *International Journal of Distributed Systems and Technologies*, vol. 10, no. 4, pp. 17–30, 2019.

[12] M. A. Al Mamun, M. A. Hannan, A. Hussain, and H. Basri, "Theoretical model and implementation of a real time intelligent bin status monitoring system using rule based decision algorithms," *Expert Systems with Applications*, vol. 48, pp. 76–88, 2016.

[13] Z. Rong and Z. Gang, "An artificial intelligence data mining technology based evaluation model of education on political and ideological strategy of students," *Journal of Intelligent & Fuzzy Systems*, vol. 40, no. 2, pp. 3669–3680, 2021.

[14] J. Wu, C. Ma, P. Xu, S. Guo, and L. Qiao, "Implementation of the dual-body intelligent inspection robot in substation based on data mining algorithm," *Academic Journal of Manufacturing Engineering*, vol. 16, no. 4, pp. 102–109, 2018.

[15] L. Vladareanu, V. Vladareanu, H. Yu, D. Mitroi, and A. C. Ciocîrlan, "Intelligent control interfaces using Extenics multidimensional theory applied on VIPRO platforms for developing the IT INDUSTRY 4.0 concept," *IFAC-Papers OnLine*, vol. 52, no. 13, pp. 922–927, 2019.

[16] Y. Zhang, J. zhao, and H. Han, "A 3D machine vision-enabled intelligent robot architecture," *Mobile Information Systems*, vol. 2021, Article ID 6617286, 11 pages, 2021.

[17] M. G. Papoutsidakis, C. S. Psomopoulos, G. C. Ioannidis, and D. I. Tseles, "Motion sensors and transducers to navigate an intelligent mechatronic platform for outdoor applications," *Sensors and Transducers*, vol. 198, no. 3, pp. 16–24, 2016.

[18] S. Li and J. Feng, "An optimized data processing model for computer big data platform based on parallel computing," *Boletin Tecnico/technical Bulletin*, vol. 55, no. 8, pp. 318–324, 2017.

[19] E. Kosalendra, G. Leema, V. P. K. Muni, I. Kartheek, and K. C. Hemanth, "Intelligent car anti-theft system through face recognition using Raspberry Pi and global positioning system," *The International Journal of Analytical and Experimental Modal Analysis*, vol. 12, no. 6, pp. 1017–1021, 2020.

[20] S. Dong, Z. Yuan, C. Gu et al., "Research on intelligent agricultural machinery control platform based on multi-discipline technology integration," *Transactions of the Chinese Society of Agricultural Engineering*, vol. 33, no. 8, pp. 1–11, 2017.

[21] H. A. Al-Rubaie and A. S. Abbas, "Software effort estimation using data mining techniques based on improved precision," *Journal of Advanced Research in Dynamical and Control Systems*, vol. 12, no. 5, pp. 176–185, 2020.

[22] D. Li, Z. Zhang, K. Yu, K. Huang, and T. Tan, "ISEE: an intelligent scene exploration and evaluation platform for large-scale visual surveillance," *IEEE Transactions on Parallel and Distributed Systems*, vol. 30, no. 12, pp. 2743–2758, 2019.

[23] C. Choong-Sik, "From electronic government to platform government," *Journal of Platform Technology*, vol. 5, no. 3, pp. 3–10, 2017.

[24] V. O. Filatov, A. L. Yerokhin, O. V. Zolotukhin, and M. S. Kudryavtseva, "Methods of intellectual analysis of processes in medical information systems," *Information extraction and processing*, vol. 2020, no. 48, pp. 92–98, 2020.

[25] A. F. Zhai, B. M. Cheng, C. L. Zhang, D. T. Ding, and E. Y. Liu, "Optimization of agricultural production control based on data processing technology of agricultural internet of things," *Italian Journal of Pure and Applied Mathematics*, vol. 38, pp. 243–252, 2017.

[26] W. Wu and S. Xu, "Application of MapReduce parallel association mining on IDS in cloud computing environment," *Journal of Intelligent & Fuzzy Systems*, vol. 39, no. 2, pp. 1915–1923, 2020.

[27] H. Wang, X. Huang, and L. Li, "Microblog oriented interest extraction with both content and network structure," *Intelligent Data Analysis*, vol. 22, no. 3, pp. 515–532, 2018.

[28] S. Tharunya, A. Manuel, and K. L. Shunmuganathan, "A multi-agent based intelligent query processing system for Hadoop with Foundation for Intelligent Physical Agents-OS using cooperating agent in cloud environment," *Journal of Computational and Theoretical Nanoscience*, vol. 13, no. 5, pp. 2774–2779, 2016.

[29] C. T. Yang, S. T. Chen, W. den, Y. T. Wang, and E. Kristiani, "Implementation of an intelligent indoor environmental monitoring and management system in cloud," *Future Generation Computer Systems*, vol. 96, pp. 731–749, 2019.

[30] M. Zhou, Y. Li, M. J. Tahir, X. Geng, Y. Wang, and W. He, "Integrated statistical test of signal distributions and access point contributions for Wi-Fi indoor localization," *IEEE Transactions on Vehicular Technology*, p. 1, 2021.

[31] M. Zhou, Y. Wang, Y. Liu, and Z. Tian, "An information-theoretic view of WLAN localization error bound in GPS-denied environment," *IEEE Transactions on Vehicular Technology*, vol. 68, no. 4, pp. 4089–4093, 2019.

Hindawi
Journal of Sensors
Volume 2021, Article ID 3782446, 9 pages
https://doi.org/10.1155/2021/3782446

Research Article

Motor Fault Diagnosis Algorithm Based on Wavelet and Attention Mechanism

Yong Yan,[1] **Qiang Liu**,[2] **and Xiao qin Gao**[3]

[1]*The College of Electronics Information and Automation, Aba Teachers University, Aba 623002, China*
[2]*The College of Electronics and Information Engineering, Sichuan University, Chengdu 610065, China*
[3]*The Department of Information Engineering, Sichuan Technology Business College, Dujiangyan 611830, China*

Correspondence should be addressed to Yong Yan; 20069623@abtu.edu.cn

Received 18 May 2021; Accepted 22 June 2021; Published 8 July 2021

Academic Editor: Mu Zhou

In order to improve the maintenance efficiency of the motor and realize the real-time fault diagnosis function of the motor, a motor fault diagnosis algorithm based on wavelet and attention mechanism is proposed. Firstly, the motor vibration signal is decomposed by wavelet transform, and the high-frequency signal is denoised to improve the signal-to-noise ratio. Secondly, the frequency band and time dimension after wavelet decomposition are taken as input data, the convolution neural network is used to fuse the frequency band features of data, and the bidirectional gated loop unit is used to fuse the time series features. Then, the attention mechanism is used to adaptively integrate the features of different time points. Finally, motor fault diagnosis and prediction are realized by classifier recognition. Experimental results show that, compared with the existing deep learning fault diagnosis model, this method has higher diagnosis accuracy and can accurately diagnose the running state of the motor.

1. Introduction

Motor is the most commonly used device to drive all kinds of machinery and industrial equipment. In order to ensure the safe and stable operation of the system, staff often needs to carry out regular overhaul and maintenance of the system [1]. However, this manual method not only requires a lot of manpower, material, and financial resources but also ensures that the fault can be eliminated in time. With the development of computer technology, large- and medium-sized motors are equipped with computer-centered condition monitoring and fault diagnosis system, in order to prevent or repair the functional failure or local failure before the failure, minimize the loss, and prevent the occurrence of catastrophic accidents [2].

The motor system is composed of multiple functional modules, and its faults are often uncertain and nonlinear. In the motor system, any small deviation of function module may lead to the collapse of the whole system. Therefore, it is particularly important to find a reasonable and effective fault diagnosis method. The common faults of large- and medium-sized motors include mass imbalance of moving parts, bearing wear, improper matching of moving parts, oil film oscillation, shaft misalignment, and cracks. The characteristics of these faults are most obvious in the frequency of vibration signal. Therefore, correlation analysis and spectrum analysis are usually used to monitor and diagnose the state of motor vibration signal. These methods usually deal with the data first, extract the characteristic parameters, and then refer to some fault diagnosis specifications [3].

At present, motor fault diagnosis methods mainly include quantitative analysis and qualitative analysis. Quantitative analysis methods include analytical model-based method and data-driven method. At present, the fault characteristic signal processing of rotor and bearing in the motor system usually uses the data driven by quantitative analysis method. In reference [4], the Prony method is combined with band selection and thinning technology to amplify and analyze the small frequency band near the characteristic frequency of broken rotor bars, which improves the calculation accuracy. However, in the low noise background, the diagnosis effect is not ideal. In reference [5], a rotor fault

diagnosis method based on improved matrix beam filtering and detection is proposed. The improved matrix beam algorithm can effectively overcome the influence of noise and has better resolution for short-term data. In reference [6], the Park vector mode transformation technique and rotation invariant signal parameter estimation technique are proposed. The Park vector mode transformation technology is used to eliminate the influence of power frequency components and reduce the amount of calculation on the premise of ensuring the accuracy. In reference [7], a fault diagnosis technology of motor bearing based on wavelet transform and Hilbert transform is proposed. Hilbert transform is used to demodulate the modulation signal, and the effective analysis of fault characteristic signal is realized. At the same time, this method introduces the thselect function into the wavelet transform and uses the adaptive ability of this function to adjust the threshold under different noise conditions. It can eliminate the high-frequency signal and improve the adaptive ability of the algorithm. However, this method ignores the noise interference of low-frequency signal, which will still lead to misjudgment and omission. Although the quantitative analysis method based on data can carry out fault analysis according to characteristic components, the accuracy of fault detection is often affected by interference signals. Therefore, the quantitative analysis method is difficult to meet the requirements of motor system fault diagnosis.

Qualitative analysis is a method of building system model based on internal knowledge of the system [8], mainly including graph theory method, expert system, and qualitative simulation. Petri net is a graph theory method, which uses the relationship between the components in the target system to establish a directed graph combination model and accurately deals with the relationship among the sequence, concurrency, and conflict of discrete events [9]. In recent years, with the research of scholars at home and abroad, the application of Petri net in motor system fault detection is gradually increasing and has achieved good results. Aiming at the uncertainty in the process of fault propagation, a probabilistic transition method of fault Petri nets is defined in reference [10], which solves the shortcoming that the fault diagnosis process of Petri nets only focuses on the state of the repository. But the way of probability change is not adaptive. In reference [11], a colored Petri net model is established by using colored Petri nets and modelling tools cpntools, which improves the efficiency of fault diagnosis and the intuitiveness of the model. In reference [12], Petri net and fuzzy reasoning are combined to solve some stochastic and uncertain fault problems effectively. It greatly improves the ability to locate the fault source in fault diagnosis. In reference [13], fuzzy Petri net (FPN) carries out strict mathematical reasoning and gives the reasoning process of matrix. However, the acquisition of its weight still depends on the experience of experts, and its adaptability is poor.

In the practical use of the motor system, the components of motor vibration signal are more complex. At the same time, due to the fluctuation of working conditions, the vibration signal has strong time varying, and the signal characteristics at different times are very different. Therefore, aiming at the characteristics of complex frequency information and strong time varying of motor vibration signal, a motor fault diagnosis algorithm based on wavelet and attention mechanism is proposed. The wavelet denoising method is used to remove the original signal noise and improve the signal-to-noise ratio. Convolution neural network and bidirectional gating loop unit are used to fuse time-frequency information. The attention mechanism module is used to dynamically weigh the features of different time points in the time dimension, so as to more accurately predict and diagnose motor faults.

2. Method

2.1. Principle of Motor Bearing Vibration. The fault frequency of motor bearing detection is divided into high-frequency detection and low-frequency detection. When a part of motor bearing fails, pulse signal is generated due to periodic motion. Most of the low-frequency signals are generated by the rotation of the fault parts, while the high-frequency signals are generated by the natural frequencies of other parts when the bearing fails. The natural frequency range of bearing components is 1 kHz~10 kHz, and its level is mainly affected by material, structure, processing technology, assembly, and other factors.

The natural frequency of bearing rolling element is

$$f_1 = 0.212\frac{Hg}{r\gamma}. \tag{1}$$

The natural frequency of the inner and outer ring of the bearing is

$$f_2 = \frac{m\left(m^2-1\right)}{2\pi(d_a/2)^2\sqrt{m^2+1}}\sqrt{\frac{HIg}{\gamma A}}, \tag{2}$$

where H is the modulus of elasticity. g is the acceleration of gravity. r is the radius of the steel ball. γ is the material density. I is the moment of inertia of the cross section of the bearing ring. m is the vibration order. A is the cross-sectional area of the bearing ring. d_a is the neutral shaft diameter of bearing cross section.

When the outer ring of the bearing fails, its characteristic frequency is

$$f_3 = \frac{s}{2\times 60}\left(1-\frac{d}{D}\cos\alpha\right)N. \tag{3}$$

When there is bearing inner ring failure, its characteristic frequency is

$$f_4 = \frac{s}{2\times 60}\left(1+\frac{d}{D}\cos\alpha\right)N, \tag{4}$$

where s is the inner ring speed. d is the diameter of roller. N is the number of rollers. D is the diameter of bearing pitch circle. α is the contact angle.

2.2. Wavelet Transform and Noise Reduction. Wavelet transform is a relatively new mathematical theory, which has outstanding characteristics of time-frequency localization. The wavelet transform is an integral transform, while the inner product of the continuous wavelet transform $f(t)$ and the stretching coefficient of the wavelet function is

$$W_f(x,y) = \int_{-\infty}^{+\infty} f(t)p(x,y,t)dt, \tag{5}$$

where

$$p(x,y,t) = |x|^{-1/2} h\left(\frac{t-y}{x}\right), \tag{6}$$

where$p(t)$is the parent wavelet, which is the normalized coefficient. y and x are the translation and stretching factors of the wavelet function, respectively. The resolution of the local structure can be changed by adjusting the translation factor and the stretching factor. The excitation function of the hidden layer of the wavelet neural network [14] is the wavelet basis function, which is obtained by translating and stretching the parent wavelet function.

The principle of wavelet transform denoising is to decompose the collected signal to obtain low-frequency signal and high-frequency signal. The noise is generally contained in the obtained high-frequency signal so that the threshold value can be set to filter out the noise and the remaining signal can be reconstructed to achieve noise reduction.

2.3. Fusion of Time-Frequency Features. According to the characteristics of complex and time-varying frequency information of motor vibration signal, convolution neural network and bidirectional gating loop unit are used to fuse the time-frequency information. Then, the attention mechanism is used to dynamically weigh the time-varying characteristics, and the fault diagnosis of planetary gearbox is realized.

Wavelet packet is another important development of wavelet theory in signal processing. It has the characteristics of multidimensional and multiresolution analysis and can provide more complex signal analysis methods [15]. The signal can be decomposed into a series of frequency bands layer by layer. It further decomposes the undivided high-frequency part of the wavelet analysis and selects the corresponding frequency band according to the characteristics of the analyzed signal to match the signal spectrum. Therefore, the wavelet packet decomposition method is used to decompose the original vibration signal into two-dimensional signals in time domain and frequency domain. For nonstationary signals such as motor vibration signals, wavelet packet decomposition can effectively represent the energy information in different frequency bands and different times and can reflect the rapid change of information in each frequency band in a short time. The process of wavelet packet decomposition is shown in Figure 1. The two-dimensional wavelet coefficient matrix obtained from the original signal decomposition is used as the input of the deep learning model.

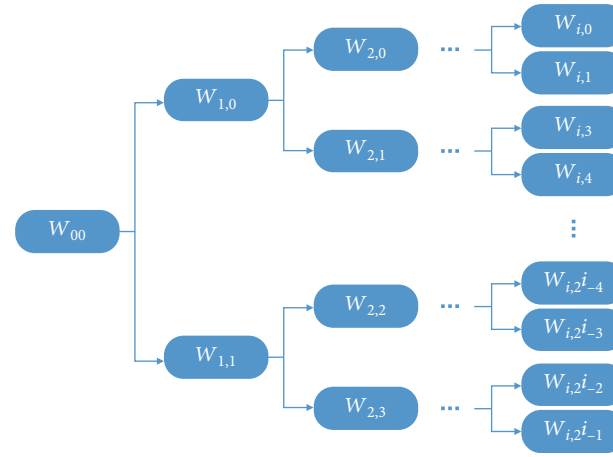

Figure 1: Schematic diagram of wavelet packet decomposition.

2.3.1. Frequency Band Feature Fusion. The vibration information of the motor contains multiple vibration frequencies, which are expressed in the wavelet packet decomposition coefficient matrix of the vibration signal. The amplitude in each frequency band reflects the working state of different structures, and the related information between different frequency bands can reveal the deep health status. Therefore, it is necessary to extract and fuse the band features in the signal and use these features to solve the problem of complex frequency components.

CNN is a neural network structure with local sensing ability. It scans the input data through the convolution check formed by locally connected network nodes and extracts the detailed features of the data. CNN has been widely used in image recognition and other fields because of its powerful feature learning ability. The calculation process of CNN can be expressed as follows:

$$x_j^l = p\left(\sum_i x_i^{l-1} * d_{ij}^l + v_j^l\right), \tag{7}$$

where x_j^l is the jth feature graph output at the l layer and x_i^{l-1} is the ith feature graph of layer $(l-1)$. d_{ij}^l is the convolution kernel of the ith input feature graph connected with the j th feature graph. v_j^l is the offset term. $*$ is the convolution operation. $p(\bullet)$ is the activation function. In this paper, the Rectified Linear Unit (ReLU) is adopted, and its function expression is as follows.

$$p(x) = \max\{0, x\}. \tag{8}$$

In this paper, one-dimensional CNN is used to fuse the wavelet packet characteristic matrix of planetary gearbox vibration signal in frequency domain. Through multiple one-dimensional convolution kernels, the feature information of signals in different frequency bands is fused into new features. Therefore, the model can adaptively learn the complex frequency information in the vibration signal of planetary gearbox and reorganize the original frequency

information into new features. Now, the one-dimensional convolution kernel will scan along the time axis of the wavelet packet characteristic matrix, so the output data still contains the characteristics of the time dimension.

2.3.2. Time Series Feature Fusion. In the vibration signal, in addition to the correlation characteristics between different frequency bands, the amplitude variation characteristics of each frequency band with time also reflect the health status of the planetary gearbox. However, CNN is mainly used to extract the local features of signals, and it is difficult to perceive the overall change features in long sequences. For the vibration signal of planetary gearbox, it is necessary to integrate the time dimension features to improve the recognition ability of its health state.

Strobe recursive unit (GRU) is a kind of improved recurrent neural network, which is specially used to process time series data and can maintain the change characteristics before and after the series, so it can be used to integrate the characteristics of data in time dimension. The internal structure of GRU is shown in Figure 2.

Its calculation process can be expressed as

$$h_t = z_t \otimes \tilde{h}_t + (1 - z_t) \otimes h_{t-1}, \tag{9}$$

$$r_t = (W_r x_t + U_r h_{t-1} + v_r)\sigma_g, \tag{10}$$

$$z_t = (W_z x_t + U_z h_{t-1} + v_z)\sigma_g, \tag{11}$$

$$\tilde{h}_t = (W_h x_t + U_t(r_t \otimes h_{t-1}) + v_h)\sigma_h, \tag{12}$$

where $W \in R^{d\times k}$, $V \in R^{d\times d}$, and $b \in R^d$ are trainable parameters. $\otimes$ is the cross product operation. x_t and h_t are input and output vectors, respectively. z_t and r_t are update and reset gate vectors, respectively. σ_g and σ_h are activation functions.

In this paper, Hard Sigmoid and Tanh are used as activation functions, respectively. The Hard Sigmoid function is expressed as follows.

$$p(x) = \begin{cases} 0, & x<-2.5, \\ 0.2x + 0.5, & -2.5 \le x \le 2.5, \\ 1, & x > 2.5. \end{cases} \tag{13}$$

The Tanh function is expressed as follows.

$$p(x) = \frac{e^x - e^{-x}}{e^x + e^{-x}}. \tag{14}$$

GRU unit receives a group of data each time, feeds back the state of the previous time, and merges it with the current data as input. After the output is calculated, the cycle is used for the next calculation until the last time scale, so as to obtain the overall change characteristics of the input data in the time dimension. Compared with the standard RNN structure, GRU can selectively learn and forget the features in time series by controlling the state of update gate and reset gate and has the ability of long-term memory. In order to further enhance the time feature fusion ability of the model, this paper adopts the bidirectional GRU structure, and its time series expansion is shown in Figure 3. As can be seen from Figure 3, bidirectional GRU can obtain the time series features before the current time through forward scanning and obtain the time series features after the current time through backward scanning. Compared with one-way GRU, the efficiency of feature fusion is greatly improved. We can get the time series characteristics after the current time. Compared with one-way GRU, the efficiency of feature fusion is greatly improved.

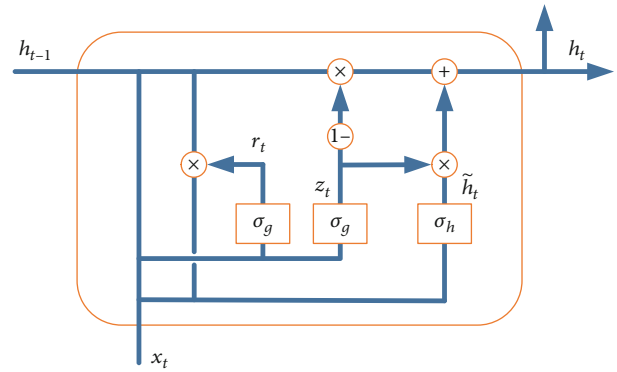

Figure 2: The internal structure of GRU.

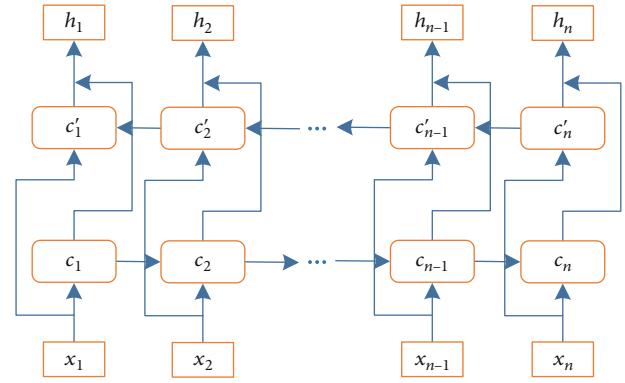

Figure 3: Schematic diagram of time sequence expansion of bidirectional GRU.

2.4. Dynamic Weighted Fusion Based on Attention Mechanism. Under the influence of alternating working conditions, the vibration signal of planetary gearbox on display has strong time-varying characteristics. Therefore, the signals collected at different times have different characteristics, and there are great differences between different samples, which will greatly reduce the generalization ability of deep learning model.

The attention mechanism in deep learning is a bionic concept, which simulates the process of human focusing on the specific part of the observed object and improves the ability of information acquisition by focusing on different parts of the object information. Based on the deep learning model, attention mechanism is added to dynamically fuse the output features of bidirectional GRU layer at different times so that

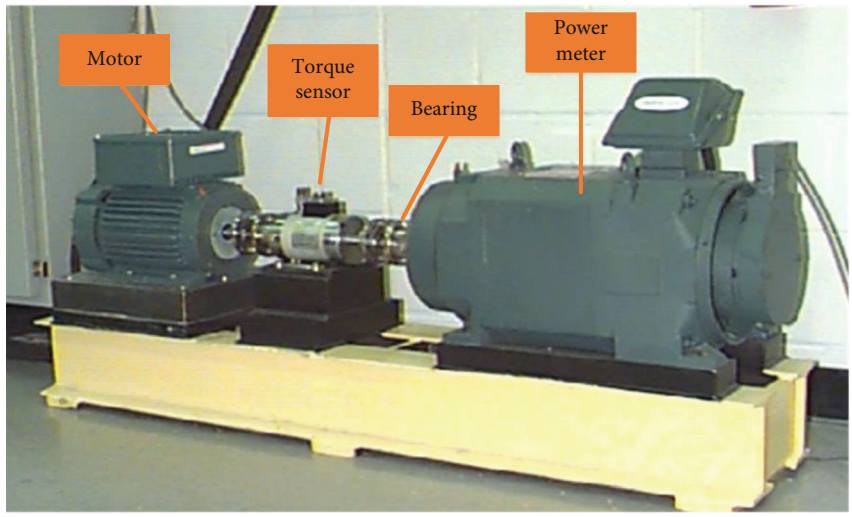

Figure 4: The bearing test system.

the model can adaptively focus attention at different times when facing signals with obvious differences in time features and solve the nonstationary vibration signal caused by sample difference.

The structure of this paper is as follows:

$$e_t = p\left(\sum_i W_t^i h_t^i + v_t^i\right), \tag{15}$$

$$\alpha_t = \frac{\exp\left(e_t\right)}{\sum_{k=1}^{T} \exp(e_k)}, \tag{16}$$

$$s_t = \alpha_t h_t, \tag{17}$$

where $p(\bullet)$ is the activation function. The hidden state sequence of bidirectional GRU is entered into the full connection layer, resulting in a dynamic weight α_t. s_t is the feature vector after dynamic weighted fusion.

The neural network outputs a weight α_t for the feature at every moment by learning the information of the input data itself, which represents the "attention" of the network. The size of the weight represents the degree of focus of attention. Since the vibration signals of the planetary gearbox have different characteristics at different times, the attention machine can help the neural network to dynamically give weight to the characteristics at different times. Thus, it can more effectively improve the utilization degree of useful information and reduce the sensitivity of the mode to the input data.

2.5. The Process of the Proposed Algorithm. The motor fault diagnosis algorithm based on wavelet and attention mechanism can be divided into four steps: signal acquisition and truncation, sample wavelet packet decomposition, deep learning model design and training, and fault diagnosis testing.

(1) Signal acquisition and truncation: the vibration sensor is used to collect the vibration signal of the planetary gearbox, and the collected signal is truncated to the same length to get the sample

(2) Sample wavelet packet decomposition: one-dimensional vibration sample signal is decomposed by wavelet packet to obtain two-dimensional time-frequency diagram samples, which are divided into the training set and the test set

(3) Design and training of deep learning model: use training set data to train model parameters, and constantly adjust super parameters in the training process to achieve better performance

(4) Fault diagnosis test: after the training of the model, the data of the training set is used for fault diagnosis test to verify the diagnosis performance of the model

According to the above methods, the deep learning model is constructed. Among them, batch normalization is to normalize the output data of the convolution layer. It can make the activation of neurons tend to normal distribution and avoid oversaturation. Therefore, it can alleviate the problem of gradient vanishing to a certain extent, accelerate the convergence speed, and improve the accuracy of the model.

The global average pool is used to compress the dimension of the fused feature data to maintain the significance of the feature. It can effectively reduce the number of network parameters, reduce the complexity of the network, and prevent overfitting. In this paper, we use global average pool operation after structure fusion. Statistics and dimension reduction of the fused features are carried out to facilitate the subsequent classification and recognition.

Shedding is an effective way to reduce over assembly. In this process, some weights are discarded randomly when the network parameters are updated in each training. Only retained weights are updated for backpropagation. This can reduce the excessive dependence on some neurons, reduce the complex adaptive relationship between neurons, and

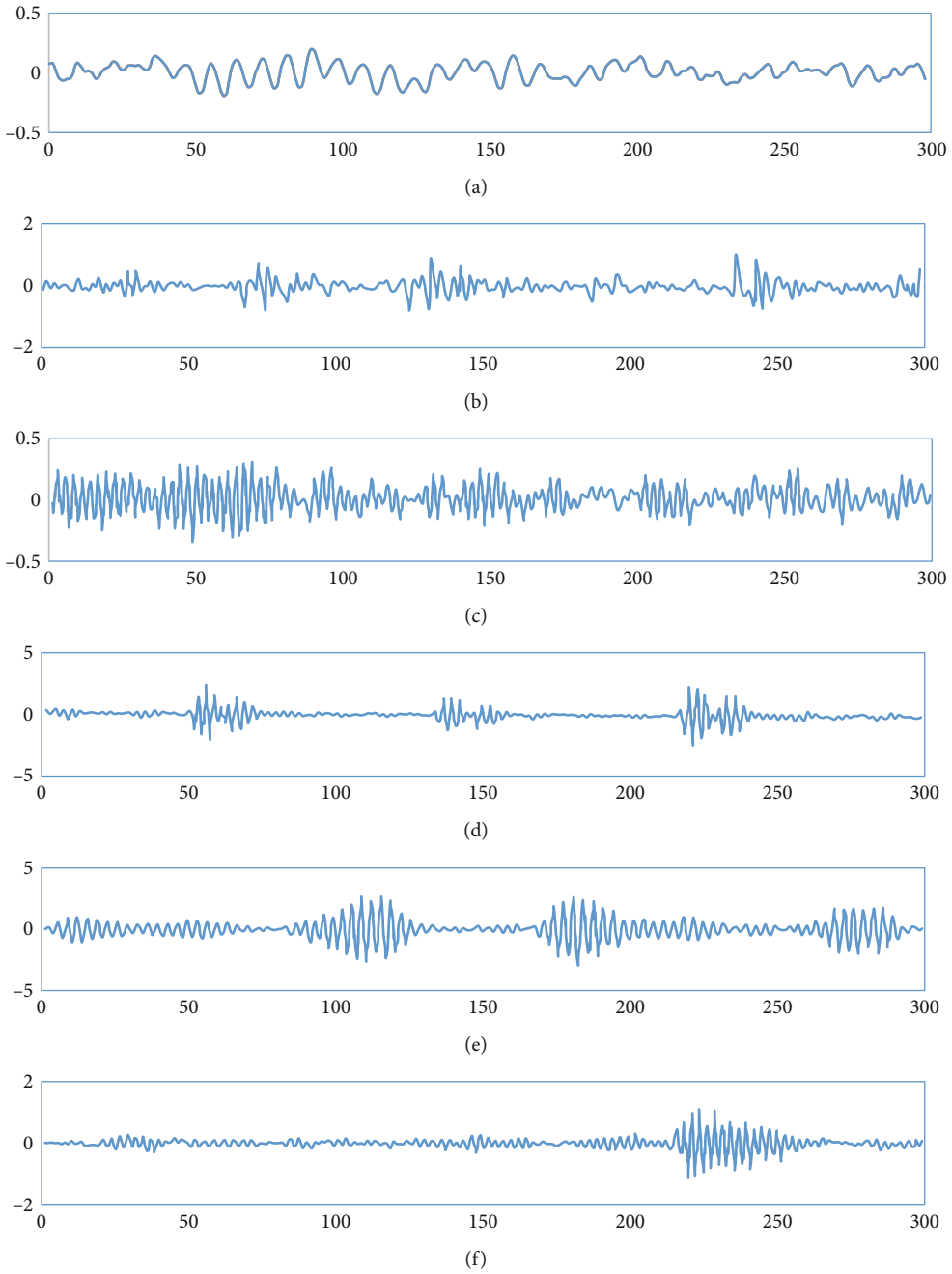

Figure 5: Examples of six vibration data.

improve the generalization ability of the network. In this paper, exit operation is set between all connection layers, which only takes effect during training, but not during testing.

The final output of the deep learning model generates probability distribution through Softmax classifier to judge the fault types of the input data. Its mathematical representation is as follows.

$$y_j = \frac{e^{x_j}}{\sum_{i=1}^{M} e^{x_i}}. \tag{18}$$

In this paper, cross entropy is selected as the loss function to calculate the error between the calculated value and the real value of the deep learning model and promote its back-propagation to update the parameters. The loss function is expressed as follows.

$$L = -\sum_{j=1}^{M} t_j \log y_j, \tag{19}$$

where M is the number of fault types, t_j is the true sample label, and y_j is an estimate of the output of Softmax.

The RMSProp optimization algorithm [16] was used as the optimizer for model training, and the parameters were iterated and updated in the process of backpropagation. It brings the model's predictions closer to the real value. RMSProp limits the oscillations of gradient descent during backpropagation, allowing the network to obtain more accurate results.

3. Experimental Results and Analysis

3.1. Feasibility Verification of the Proposed Algorithm. In this paper, experimental data from the Bearing Data Center of Case Western Reserve University [17] were used to test the effectiveness of the proposed method. Vibration signals were measured by the bearing test system, and the bearing test system is shown in Figure 4.

The bearing model is skf6203, the sampling frequency is 1.2 kHz, the rotating speed is 1797 r/min, and there are four kinds of bearings: normal bearing, inner ring fault bearing, in which the damage diameter is 0.53 mm, rolling element fault bearing, in which the damage diameter is 0.53 mm, and outer ring fault bearing, in which the damage diameter is 0.53 mm (including center @ 6:00, orthogonal @ 3:00, and opposite @ 12:00). For each type of data, 120000 sample points are obtained, which means that the length of time series data is at least 120000. If it is directly used as the input of deep neural network, the training will be too large. Here, a group of vibration signals is grouped according to every 300 sampling points, and a total of 2400 datasets are obtained. Figure 5 shows an example of six vibration data.

In order to verify the performance of the model proposed in this paper, based on the same dataset, it is compared with the AlexNet [18], GoogleNet [19], and ResNet [20] deep learning methods that have been proposed at present.

The 400 hundred groups were selected as the test data, and 500, 1000, 1500, and 2000 samples were selected for training. The algorithm proposed in this paper was used to carry out diagnostic tests, and the comparison of diagnosis rate is shown in Figure 6.

As can be seen from Figure 6, with the increase of the number of training samples, the accuracy rate of the proposed algorithm is gradually increased.

3.2. Actual Experimental Results and Analysis. Field diagnosis tests are carried out on motor bearings, in order to further verify the effectiveness of the improved random forest algorithm and verify whether the diagnosis method proposed in this paper is accurate when the bearing fault signal is weak. The motor model is SEW-DV132M4, the speed is 1430 r/min, the sampling frequency is 1 kHz, the bearing model is SKF6209-2Z, and the vibration data collector is COMMTEST-VB7. There are 4 kinds of bearings: normal, inner ring fault (damage diameter of 10 μm), rolling body fault (damage diameter of 18 μm), and outer ring fault (damage diameter of 9 μm). The number of diagnostic samples was 1000, and the number of collected samples was 2000.

In order to reduce the influence of unexpected factors, the training set and the test set are divided randomly for 10 times. Each group of data was used for independent training and testing, and the experimental results were recorded, respectively. The results of 10 experiments are used as performance evaluation indexes for comparative verification. The specific results are shown in Figure 7. The average accuracy and standard deviation are shown in Table 1. The accuracy of the AlexNet model is poor. Because the model simply overlaps multiple convolution layers, it is difficult to effectively extract complex data features. The GoogleNet model adds convolution kernels of different sizes in each convolution layer, which has certain frequency feature extraction ability, and its accuracy is 1.21% higher than that of AlexNet.

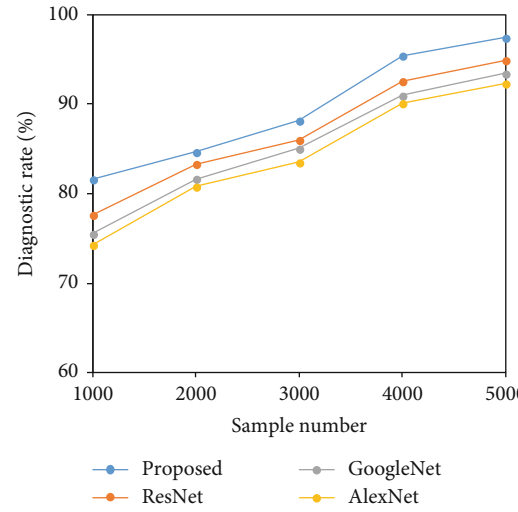

Figure 6: Results of diagnostic rate.

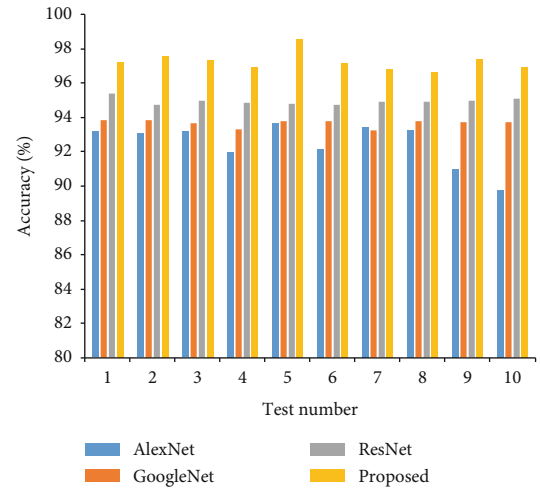

Figure 7: The results of 10 experiments.

Table 1: Experimental results.

Accuracy	Train	Test
AlexNet [18]	96.18	92.47
GoogleNet [19]	97.69	93.68
ResNet [20]	98.23	94.95
Proposed	99.51	97.27

ResNet adds residual structure on the basis of GoogleNet and realizes cross layer connection of convolution layer, and its accuracy is 1.27% higher than that of GoogleNet. However, due to the single network structure for feature extraction, the above models cannot make full use of the information contained in the signal, so the overall accuracy is low. The method proposed in this paper can fully combine the time-frequency characteristics of the signal and introduce the attention mechanism of dynamic weighting. Therefore, in each test, its accuracy is higher than other deep learning models. The above results show that, compared with other deep learning fault diagnosis methods, the proposed fault diagnosis method has obvious advantages [21–24].

4. Conclusion

In order to improve the accuracy of motor fault diagnosis, a motor fault diagnosis algorithm based on wavelet and attention mechanism is proposed. The wavelet denoising method is used to remove the original signal noise and improve the signal-to-noise ratio. Convolution neural network and bidirectional gating loop unit are used to fuse time-frequency information. The attention mechanism module is used to dynamically weigh the features of different time points in time dimension. In the experimental part, the feasibility of the algorithm is verified by the dataset of Case Western Reserve University Bearing Data Center. The field diagnostic test was used for test comparison. Experimental results show that, compared with other deep learning methods, the proposed fault diagnosis method has obvious advantages.

Data Availability

The labeled dataset used to support the findings of this study are available from the corresponding author upon request.

Conflicts of Interest

The authors declare no competing interests.

Acknowledgments

The study was supported by the Aba Science and Technology Bureau (19YYJSYJ0091) and the 13th five-year plan of educational informatization construction in Sichuan Province (Chuan Jiao Guan 2019-142).

References

[1] I. H. Kao, W. J. Wang, Y. H. Lai, and J. W. Perng, "Analysis of permanent magnet synchronous motor fault diagnosis based on learning," *IEEE Transactions on Instrumentation and Measurement*, vol. 68, no. 2, pp. 310–324, 2019.

[2] O. AlShorman, M. Irfan, N. Saad et al., "A review of artificial intelligence methods for condition monitoring and fault diagnosis of rolling element bearings for induction motor," *Shock and Vibration*, vol. 2020, Article ID 8843759, 20 pages, 2020.

[3] Y. M. Hsueh, V. R. Ittangihal, W. B. Wu, H. C. Chang, and C. C. Kuo, "Fault diagnosis system for induction motors by CNN using empirical wavelet transform," *Symmetry*, vol. 11, no. 10, p. 1212, 2019.

[4] W. Dehina, M. Boumehraz, and F. Kratz, "On-line detection and estimation of harmonics components in induction motors rotor fault through a modified Prony's method," *International Transactions on Electrical Energy Systems*, vol. 31, no. 2, article e12737, 2021.

[5] K. C. D. Kompella and G. V. Madhav, "An improved matrix pencil method based bearing fault detection in three phase induction motor," in *2020 IEEE International Conference on Computing, Power and Communication Technologies (GUCON)*, pp. 51–56, NCR New Delhi, India, 2020.

[6] F. Husari and J. Seshadrinath, "Inter-turn fault diagnosis of induction motor fed by PCC-VSI using Park vector approach," in *2020 IEEE International Conference on Power Electronics, Drives and Energy Systems (PEDES)*, pp. 1–6, Jaipur, Rajasthan, India, 2020.

[7] F. Ding and F. W. Qin, "Application of wavelet denoising and Hilbert transform in fault diagnosis of motor bearing," *Electric Machines and Control*, vol. 21, no. 6, pp. 89–95, 2017.

[8] D. Kiel, C. Arnold, and K. I. Voigt, "The influence of the Industrial Internet of Things on business models of established manufacturing companies - a business level perspective," *Technovation*, vol. 68, pp. 4–19, 2017.

[9] D. Angeli and S. Manfredi, "A Petri Net approach to consensus in networks with joint-agent interactions," *Automatica*, vol. 110, article 108466, 2019.

[10] Z. Jiang, Z. Li, N. Wu, and M. Zhou, "A Petri net approach to fault diagnosis and restoration for power transmission systems to avoid the output interruption of substations," *IEEE Systems Journal*, vol. 12, no. 3, pp. 2566–2576, 2018.

[11] G. P. Bhandari, R. Gupta, and S. K. Upadhyay, "Colored Petri nets based fault diagnosis in service oriented architecture," *International Journal of Web Services Research*, vol. 15, no. 4, pp. 1–28, 2018.

[12] K. Q. Zhou, W. H. Gui, L. P. Mo, and A. Zain, "A bidirectional diagnosis algorithm of fuzzy Petri net using inner-reasoning-path," *Symmetry*, vol. 10, no. 6, p. 192, 2018.

[13] Y. Zhang, Y. Zhang, F. Wen et al., "A fuzzy Petri net based approach for fault diagnosis in power systems considering temporal constraints," *International Journal of Electrical Power & Energy Systems*, vol. 78, pp. 215–224, 2016.

[14] Ying Chen, P. B. Luh, Che Guan et al., "Short-term load forecasting: similar day-based wavelet neural networks," *IEEE Transactions on Power Systems*, vol. 25, no. 1, pp. 322–330, 2010.

[15] X. Li, X. Zhang, P. Zhang, and G. Zhu, "Fault data detection of traffic detector based on wavelet packet in the residual subspace associated with PCA," *Applied Sciences*, vol. 9, no. 17, p. 3491, 2019.

[16] D. Xu, S. Zhang, H. Zhang, and D. P. Mandic, "Convergence of the RMSProp deep learning method with penalty for nonconvex optimization," *Neural Networks*, vol. 139, pp. 17–23, 2021.

[17] Y. Li, X. Wang, S. Si, and S. Huang, "Entropy based fault classification using the Case Western Reserve University data: a benchmark study," *IEEE Transactions on Reliability*, vol. 69, no. 2, pp. 754–767, 2020.

[18] C. Alippi, S. Disabato, and M. Roveri, "Moving convolutional neural networks to embedded systems: the alexnet and VGG-16 case," in *2018 17th ACM/IEEE International Conference*

on Information Processing in Sensor Networks (IPSN), pp. 212–223, Porto, Portugal, 2018.

[19] G. Cao, K. Zhang, K. Zhou, H. Pan, Y. Xu, and J. Liu, "A feature transferring fault diagnosis based on WPDR, FSWT and GoogLeNet," in *2020 IEEE International Instrumentation and Measurement Technology Conference (I2MTC)*, pp. 1–6, Dubrovnik, Croatia, 2020.

[20] L. Wen, X. Li, and L. Gao, "A transfer convolutional neural network for fault diagnosis based on ResNet-50," *Neural Computing and Applications*, vol. 32, no. 10, article 4097, pp. 6111–6124, 2020.

[21] S. Deb, Z. Tian, S. Fong, R. Wong, R. Millham, and K. K. L. Wong, "Elephant search algorithm applied to data clustering," *Soft Computing*, vol. 22, article 3076, no. 18, pp. 6035–6046, 2018.

[22] Z. Tang, G. Zhao, and T. Ouyang, "Two-phase deep learning model for short-term wind direction forecasting," *Renewable Energy*, vol. 173, pp. 1005–1016, 2021.

[23] K. K. L. Wong, G. Fortino, and D. Abbott, "Deep learning-based cardiovascular image diagnosis: a promising challenge," *Future Generation Computer Systems*, vol. 110, pp. 802–811, 2020.

[24] D. Yao, H. Liu, J. Yang, and J. Zhang, "Implementation of a novel algorithm of wheelset and axle box concurrent fault identification based on an efficient neural network with the attention mechanism," *Journal of Intelligent Manufacturing*, vol. 32, article 1701, no. 3, pp. 729–743, 2021.

Hindawi
Journal of Sensors
Volume 2021, Article ID 9945187, 10 pages
https://doi.org/10.1155/2021/9945187

Research Article

New Visual Expression of Anime Film Based on Artificial Intelligence and Machine Learning Technology

Yijie Wan[1] **and Mengqi Ren**[2]

[1]*College of Media and Communications, Guangxi University for Nationalities, Nanning 530000, Guangxi, China*
[2]*College of Arts, Guangxi University, Nanning, 530000 Guangxi, China*

Correspondence should be addressed to Yijie Wan; 20100039@gxun.edu.cn

Received 18 March 2021; Revised 20 May 2021; Accepted 13 June 2021; Published 7 July 2021

Academic Editor: Mu Zhou

With the improvement of material living standards, spiritual entertainment has become more and more important. As a more popular spiritual entertainment project, film and television entertainment is gradually receiving attention from people. However, in recent years, the film industry has developed rapidly, and the output of animation movies has also increased year by year. How to quickly and accurately find the user's favorite movies in the huge amount of animation movie data has become an urgent problem. Based on the above background, the purpose of this article is to study the new visual expression of animation movies based on artificial intelligence and machine learning technology. This article takes the film industry's informatization and intelligent development and upgrading as the background, uses computer vision and machine learning technology as the basis to explore new methods and new models for realizing film visual expression, and proposes relevant thinking to promote the innovative development of film visual expression from a strategic level. This article takes the Hollywood anime movie "Kung Fu Panda" as a sample and uses convolutional neural algorithms to study its new visual expression. The study found that after the parameters of the model were determined, the accuracy of the test set did not change much, all around 57%. This is of great significance for improving the audiovisual quality and creative standards of film works and promoting the healthy and sustainable development of the film industry.

1. Introduction

The rapid development of the Internet industry has brought great convenience to users, and at the same time, the amount of information has also exploded at an exponential level [1, 2]. The cost for users to obtain valuable information has greatly increased, and how to help Internet users find the content that is valuable to users efficiently and quickly in massive information data has become an important issue. The visual performance of film is an eternal topic in the field of film. It cannot be separated from the development of the times, the progress of the industry, and the development and application of new technologies [3]. The conception of film works is shown naturally, smoothly, and efficiently, showing the feelings of film characters and explaining the experience of film characters, using visual elements to promote the world view, life view, and value of film works [4]. The visual performance of the film, combined with the informatization and intelligent evolution of the whole society, needs to correspond to the times and continuously improve the visual impact of film works [5, 6]. Therefore, it is very important to innovate the visual performance of movies, explore new ways of visual performance of movies, and meet the characteristics of the times and industry needs [7, 8].

The visual media began with the emergence of printed materials such as newspapers and magazines. As visual designers, they are constantly thinking about the conveyer of information. That is, the delicate relationship between the designer and the audience and the effectiveness of the information transmission [9]. The new visual media is a new generation of media that is more popular and generally accepted by the public. After immersive visual expressions and other types of design opened up a new field of visual experience, visual designers adopted a comprehensive

approach to several senses. Experiments make participants feel the same and thus have synchronicity and interaction [10, 11]. The emergence of interactive media such as the Internet has enriched the scope of traditional visual media. Due to the varying degrees of audience acceptance, the effect of information or emotional expression is not satisfactory [12, 13]. At this time, the visual designer began to think about how to make the audience as empathetic as possible. Only when the designer and the audience resonated would the work reflect the real value [14]. Visual artists are not just the identity of designers, but they are also practitioners of technology and psychologists. The indispensable or even irreplaceable component of information or emotion is the participant, and the pleasure, imagination, comprehension, discovery, and exploration produced in the process itself contribute to the integrity of the expression of artistic ideas [15, 16].

The purpose of artificial intelligence (AI) is to enable machines to perform intelligent tasks that require manual processing. AI-based prediction models have great potential for solving complex environmental applications that include a large number of independent parameters and nonlinear relationships. Due to its predictive ability and nonlinear characteristics, several AI-based modeling techniques have recently been adopted in the modeling of various realistic processes in the field of energy engineering, such as artificial neural networks, fuzzy logic, and adaptive neural fuzzy inference systems [17]. De Raedt et al. discuss the foundations of two widely used AI-based technologies, namely, artificial neural networks and support vector machines, and highlight the important mathematical aspects of these methods. It describes computational problems and the respective advantages of these methods, and many implementations of these models are now available in large numbers in software repositories [18]. In recent years, deep learning has shown encouraging results in various artificial intelligence applications. Therefore, Foulquier et al. studied a comparison of a deep learning architecture called deep neural network (DNN) with classical random forest (RF) machine learning algorithms for malware classification. They studied the performance of classic RF and DNN with 2-, 4-, and 7-layer architectures with 4 different feature sets and found that the classic RF accuracy is better than DNN regardless of the feature input [7]. The research of artificial intelligence has become a hot spot in academia and industry. With this, there has been interest in the ability of artificial intelligence to make the right decisions when compared to human decisions. Due to the complex relationship between interest variables, predicting the outcome of a sporting event has traditionally been considered a difficult task. Because of the limited rationality of human decision-making functions, trying to make accurate predictions is full of bias. Pascual and Zapirain propose that artificial intelligence methods using machine learning will produce a considerable level of accuracy. Random forest classification algorithm is used to predict the results of the 2015 Rugby World Cup. The performance of this model is compared with the comprehensive results of Super Bru and OddsPortal. Machine learning-based systems have accuracy rates of 89.58% and 85.58% at the 95% confidence intervals (77.83, 95.47) and 85.42% confidence intervals (72.83, 92.75), respectively. These results indicate that for rugby, for a limited time in a particular game, the evidence is insufficient to show that at a significance level $\alpha = 0.05$, human agents are superior in terms of accuracy in predicting game results compared to machine learning methods. However, compared with these two platforms, the model is better able to estimate the probability measured by betting on currency wins for the round [1]. Machine learning (ML) is now common. Traditional software engineering can be applied to develop ML applications. However, we must consider the specific issues of ML applications in terms of quality requirements. Nalmpantis and Vrakas presented a survey of software quality for ML applications to see the quality of ML applications as an emerging discussion. Through this survey, they raised issues with ML applications and discovered software engineering methods and software testing research areas to address these issues. They divided the survey goals into academic conferences, magazines, and communities. They targeted 16 academic conferences on artificial intelligence and software engineering, including 78 papers. They targeted 5 journals, including 22 papers. The results indicate that key areas such as deep learning, fault location, and prediction will be studied through software engineering and testing [19]. Azmat et al. compared the application of machine learning algorithms in sensor data collection for aggregation processes. Several machine learning algorithms such as adaptive neural fuzzy inference system, neural network, and genetic algorithm were implemented using the MATLAB software, and the accuracy and robustness of the modeling process (MSE) were compared. The results show that compared with artificially established models, machine learning-based methods can produce more accurate and robust process models, while being more adaptable to new data. Azmat et al. looked forward to the potential advantages of machine learning algorithms and its application prospects in the industrial process industry [20].

This article takes the film industry's informatization and intelligent development and upgrading as the background, uses computer vision and machine learning technology as the basis to explore new methods and new models for realizing film visual expression, and proposes relevant considerations at the strategic level to promote the innovative development of film visual expression. It is of great significance to improve the audiovisual quality and creative standard of film works and promote the healthy and sustainable development of the film industry.

2. Proposed Method

2.1. Artificial Intelligence. Artificial intelligence is a machine that simulates humans in various environments. Like many emerging disciplines, artificial intelligence does not yet have a unified definition. "The next general definition is almost impossible, because intelligence seems to be a hybrid of many information processing and information expression skills." Mainly because the main reason is that different disciplines are different from their respective perspectives. Disciplines from their respective perspectives have different definitions.

In addition, the most fundamental point is what is the nature or mechanism of artificial intelligence (such as hearing, vision, and expression of knowledge), and it is not clear to people at present. The artificial intelligence dictionary is defined as "making computer systems simulate human intelligent activities and accomplish tasks that humans can only accomplish with intelligence, which is called artificial intelligence." To be precise, this cannot be used as a definition of artificial intelligence. Test the functional parameters of the machine in an appropriate way. Some scholars are focusing on the development of artificial intelligence, and they have also made certain achievements in this area and have been applied to many fields. For example, artificial intelligence technologies in medicine, biology, geology, geophysics, aeronautics, chemistry, and electronics have all found applications.

2.1.1. Weak Artificial Intelligence. Weak artificial intelligence (TOP-DOWNAI) refers to the use of designed programs to simulate the logical thinking of animals and humans. Scholars who hold the view of weak artificial intelligence believe that it is impossible to create intelligent machines that can really reason and solve problems. At present, many electronic products have certain intelligence. When the external data input changes, corresponding programs will be run to get different results, which can replace people to complete repetitive simple tasks. Weak artificial intelligence can be seen everywhere. But the application of weak artificial intelligence is also limited to imitating human lower behavior.

2.1.2. Strong Artificial Intelligence. Strong artificial intelligence (BOTTOM-UPAI) belongs to more advanced artificial intelligence. The strong artificial intelligence believes that it is possible to create intelligent machines that have real consciousness, thinking ability and feelings, can solve problems, and can reason. For strong artificial intelligence, not only can computers study consciousness; in other words, computers have certain cognitive abilities after corresponding programming, and it is also conscious to understand computers from this perspective.

2.2. Artificial Intelligence Applications. No matter how the structure of the convolutional neural network changes, its basic process mainly includes four parts: image input, region feature extraction, neural convolution feature calculation, and regional object classification. The core is to organically integrate feature extraction and classifiers. The method of gradient descent is back-propagated, and the parameters of the convolution template and the parameters of the fully connected layer are continuously optimized, so that the finally learned features and classifiers are close to optimal, and the classification features are obtained.

This paper uses a deep recursive convolutional neural network algorithm to implement platform construction, detection, and verification:

(1) Part is the feature extraction of machine learning, i.e., simulating human recognition of category features (so-called "see more knowledge"), the data set used is related to the accuracy of category features, and the public MNIST, ImageNet dataset, PASCALVOC training set, COCO, and other image training data sets to obtain features of major categories, such as people, various animals, and various vehicles

(2) Part is to perform feature vector recognition on specific targets in the specific analysis movie (multitarget objects are possible, and in this case, Jean Agen is used as an example)

(3) Apply deep recursive convolutional neural network CAFFE to classify and identify categories, scenes, and dialogues in movie films (or scenes and lens fragments) and input category features, etc. into the classifier to meet the specific needs of some movie object matching classification

(4) Recognize and calibrate scenes and characters in movies and videos and synthesize movie scenes and lens content semantics

Since the movie video itself contains a large amount of data, it is composed of multiple frames of static images per second, and each frame of image contains rich information. In order to achieve efficient, accurate, and high-precision identification and retrieval of movie content, recursive convolutional neural on the network algorithm was used, the method and strategy of improving the object recognition accuracy by adjusting the LOSS function, to achieve fast and accurate target detection and positioning.

2.3. Classification of Machine Learning. The learning process is a complex knowledge activity closely related to the inference process. Machine learning can be classified according to learning strategies, descriptions of knowledge, or application areas. In general, the form of knowledge expression is determined by the algorithm selection of the mechanical learning system itself. Learners with the same structure can also be applied in different fields. Reasoning strategies can better reflect the description of the form and method of learning and the relationship between the learner and the adjustment of data and knowledge, so the main categories of machine learning are briefly introduced in the following based on the reasoning strategy.

(1) Mechanical learning

Mechanical learning does not require the computer to automatically infer or summarize the input data into knowledge. Instead, the input data is processed step by step according to the designed operating procedures. It mainly considers how to search and use the established facts and knowledge.

(2) Supervised learning

Supervised learning is to provide some correct input and output examples to the learner (similar to the standard answer). The data provider does not need to care about the functional relationship between these inputs and outputs. The learner learns from the examples. The mapping

relationship between input and output is updated to its own knowledge base and maintains compatibility with existing knowledge. Supervised learning is a common learning method for training neural network and decision tree learners.

(3) Deductive learning

At this time, the reasoning form of the learner is deductive reasoning, and the process is to derive some meaningful conclusions through logical transformation by using more basic axioms. This learning process helps computers to explore unknown knowledge to get some more useful knowledge.

(4) Analogy learning is similar to human analogy thinking, assuming that the learner has mastered the knowledge of the source domain and the target domain is an unknown knowledge domain. Analogy learning is the process of comparing the similarity of knowledge in the source domain and the target domain to obtain useful knowledge in the target domain. Analog learning is more complicated than the previous three learning methods. The main reason is that it involves the knowledge of two domains. In order to make the knowledge of the target domain more useful and effective, it is necessary to learn as much as possible of the knowledge in the source domain. One of the powerful functions of analog learning is that a computer system that has been successfully run in a certain field is quickly transformed into a similar field application, which reduces the cost of secondary development

(5) Explain learning

Explain learning is an environment that provides the learner with an example and its criteria under the concept of achieving a certain goal, explains how the example satisfies a given goal concept, and learns the rules of interpretation in the example. A sufficient condition to extend this interpretation to the concept of the goal is based on the inherent knowledge system. Explaining learning is now widely used to streamline the knowledge base and improve system performance.

(6) Inductive learning

Inductive learning is the most complicated learning process compared to the inference process in the aforementioned learning categories. When the learner conducts inductive learning, the environment does not provide a general description of the concepts that need to be learned, but provides some examples or counterexamples that reflect the concept, from which the learner learns the general description of the concept.

2.4. Machine Learning Technology and Its Application in New Visual Expression of Movies. Machine learning is an algorithm to identify new intelligent samples, analyze, and predict the future, and the machine can learn rules from a large amount of historical data. Mechanical learning should follow the following basic steps: determine the training data set, use the training data set for model training or learning and learner construction, use the validation data set to evaluate learner performance and model selection, and predict the final model based on the test data used and the output of the prediction. The ultimate goal of machine learning is to adapt the learning or training model to a new sample. In short, there is a strong generalization ability to avoid overfitting and underfitting. Among them, overfitting is due to proper prediction of known data and insufficient learning ability to make insufficient prediction of unknown data. This reduces the generalization performance of the learner. This is the main obstacle to machine learning and must be mitigated. Insufficient learning is due to poor learning ability, which can be overcome by increasing training samples.

Mechanical learning technology is widely used in computer graphics, movie virtual asset analysis, and 3D animation production. For example, the reuse of 3D motion data has become the focus of attention in the production of 3D animation movies. This is the basic data-driven motion generation technique. Based on a large amount of 3D motion data and expression data, mechanical learning technology can be used to realize the reuse of 3D motion data such as subspace analysis, statistical learning, principal component analysis, and multiple body learning, which can be used for the execution of existing 3D motion data. Analyze, learn, and guide the generation of new motion data. In addition, the automation and intelligent generation of action animation is an important research content for the production of 3D animation movies, and its implementation is to build agents with autonomous decision-making functions and create action animations for virtual characters. It can be applied to mechanical learning technology, such as constructing an introduction mode of action. The establishment of the action and consciousness mode of the virtual character enables the agent to quickly and firmly learn the dialogue action with different users and provides a dialogue-type virtual environment and a dynamic action plan for the virtual character. In addition, 3D motion data and expression data belong to multimedia data. Mechanical learning technology is widely used in the field of multimedia content analysis and image understanding, so it has important application value for 3D motion data and expression data processing.

In addition, semisupervised learning technology plays an important role in the field of virtual filming of movies. In semisupervised learning, learners do not rely on external interactions, but automatically use unlabeled samples to improve learning performance. This can be divided into pure semisupervised learning and direct-driven learning. The latter assumes that the unlabeled samples considered in the learning process are predicted data, and the learning objective is to obtain the best generalized performance among the unlabeled samples. In the collection and analysis of movie's virtual assets, samples without labels are

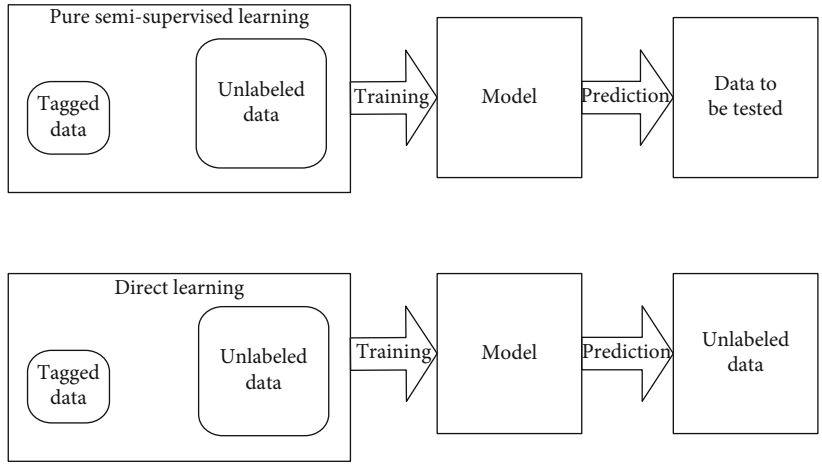

Figure 1: Semisupervised learning (including pure semisupervised learning and direct push learning).

often collected. Obtaining labels requires a lot of time and effort. The combination of a small number of labeled samples and unlabeled samples simplifies the workload of sample labeling, establishes more accurate data models, and completes learning tasks. The semisupervised learning data model is shown in Figure 1.

The basic mode of human beings' understanding of the unknown world is perception→learning→cognition. However, scientific research topics are based on the nature and laws of human beings being known, the mystery of human mind, and the emergence of scientific knowledge based on the future, able to discover more universal mechanisms of human behavior, expressions, and emotions.

3. Experiments

3.1. Experimental Algorithm Steps. This article uses a convolutional neural network algorithm to study the new vision of anime films. The core idea of the convolutional neural network algorithm is to iteratively train, use gradient descent to reduce the loss function, and propagate the adjustment results back to the layers. Constantly adjust and optimize the weight offset according to the difference, and finally, get the parameters of each layer that can fit the training data well. The steps of the convolutional neural network algorithm are as follows:

(1) *Network Initialization*. First, define the number of convolution layers and pooling layers, the number of convolution kernels contained in each convolution layer, the step size to be moved during the convolution operation, the calculation method of the loss function, the number of iterations, and the learning rate.

(2) Initialize weights and offsets randomly with a series of random numbers

(3) Randomly select n input data and corresponding output data from the training set as the training sample

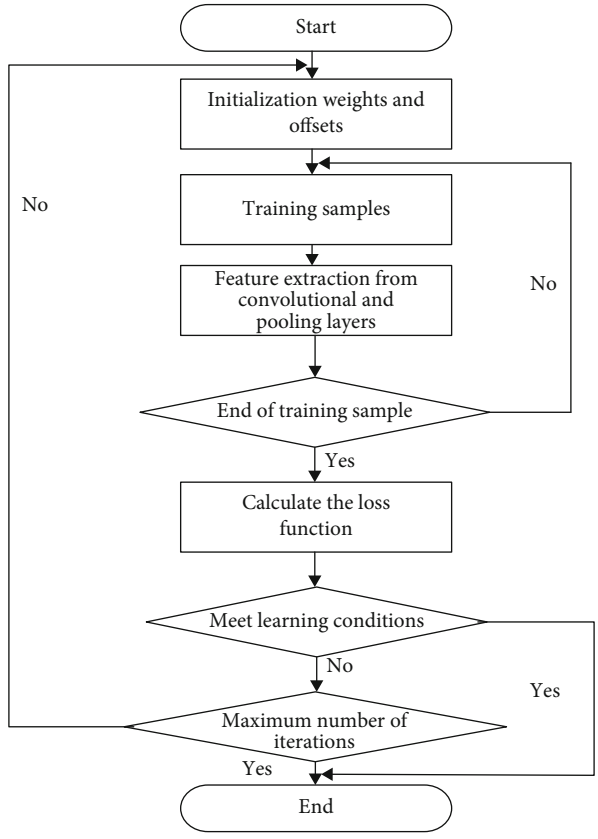

Figure 2: Convolutional neural network training flowchart.

$$X(n) = (x_1(n), x_2(n), \cdots, x_k(n)),$$
$$D(n) = \left(d_1(n), d_1(n), \cdots, d_q(n)\right). \quad (1)$$

(4) Calculate the output according to the input of each layer of neurons until it reaches the tail sensor. The input and output of each layer of neurons are calculated using the following formula

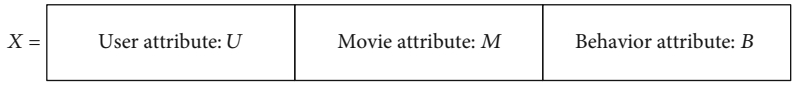

Figure 3: Feature vector data.

Table 1: Hyperparameter combinations and corresponding accuracy of some convolutional neural networks.

Batch size	Number of iterations	Convolutional layers	Learning rate	Dropout	Accuracy
200	200	3	0.001	0.75	25.55%
100	200	3	0.0008	0.75	14.28%
200	200	3	0.0008	0.75	30.22%
200	200	3	0.0008	0.2	3%
200	200	7	0.001	0.75	31.22%
100	200	7	0.0008	0.75	44.98%
200	200	7	0.0008	0.75	48.98%
200	200	7	0.0008	0.2	6.55%
200	200	11	0.001	0.75	44.55%
100	200	11	0.0008	0.75	53.22%
200	200	11	0.0008	0.2	14.99%
200	200	11	0.0008	0.75	57.55%

$$f_{\text{in}}(n) = \sum_{i=1}^{n} (p_i, w_i + b_h), \tag{2}$$

$$f_{\text{out}}(n) = \max\,(0, f_{\text{in}}(n)). \tag{3}$$

(5) After the final result is obtained by the neural network, the training set results and actual output results are used to inversely adjust the corresponding convolution kernel of each convolution layer by calculating the partial derivative of the loss function about the weights and offsets. Define error function (4)

$$e = \frac{1}{2} \sum_{o=1}^{q} (d_o(k) - f_{\text{out}}(n))^2. \tag{4}$$

(6) Constantly correct weights and offsets through iterative learning

(7) Determine whether the requirements are met according to the error function. When the value of the error meets the preset area or the number of iterative learning is greater than the preset value, the training is ended. Otherwise, return to step 3 and continue to the next round of training. The detailed flowchart of network training in the entire process is shown in Figure 2

3.2. Selection of Experimental Data. The training data is Movielens-100 K dataset of Movielens, which contains 400000 rating records of 1882 anime movies by 943 users. The information in the data set includes user ID, user age, user occupation, user gender, user region, anime movie name, anime movie type, and anime movie rating. Feature vector data is shown in Figure 3.

As input data of the convolutional neural network, occupations need to be represented by numbers. The paper uses random assignment to evaluate 21 types of occupations. The initial value is assigned, and the random adjustment is performed according to the different attributes of the occupation and the proportion of the user's interest value in the process of forward adjustment error in the later stage.

3.3. Experimental Data Verification Method

3.3.1. K-Fold Cross-Validation. The main idea of the K-fold cross-validation method is to divide the data set M into K similarly sized nonintersection subsets, each time using the union of $K-1$ subsets as the training data set and the remaining subset as the test data set; in this way, we can obtain the K-group training plus test data set. Since the cross-validation method depends on the value of K, the cross-validation method is also called "K-fold cross-validation."

3.3.2. 2K-Fold Cross-Validation Method. Based on K-fold cross-validation, $2K$-fold cross-validation divides each subset into two. The small sets are denoted as S_0 and S_1; the set S_0 is used as the training set, and S_1 is used as the test set. After the experiment is performed, then S_1 is used as the training set, and S_0 is used as the test set. The advantage of the $2K$-fold cross-validation method is that the test set and the training set are both large enough and can be repeatedly tested according to the number of samples. The parameter $K = 10$ is often taken in the $2K$-fold cross-validation method.

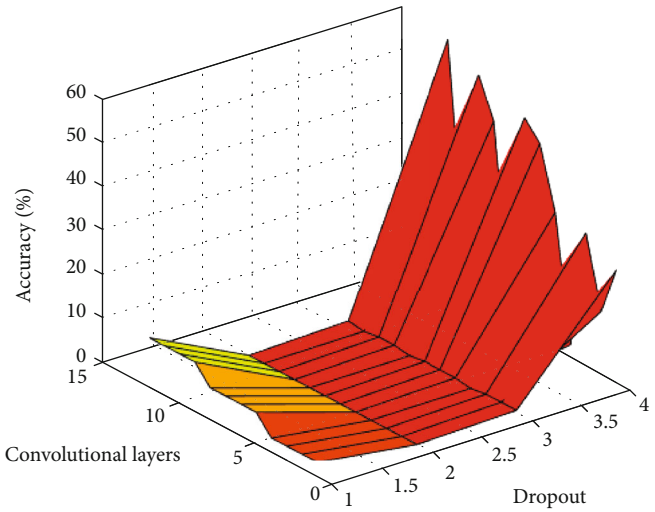

Figure 4: Partial convolutional neural network hyperparameter combinations and corresponding accuracy graphs.

Table 2: Parameter setting diagram of eleven-layer convolutional neural network.

Parameter name	Parameter value
Convolution kernel activation function	RelU
Convolution kernel size	[1, 5]
Number of convolution kernels	598
Dropout ratio	0.64
Batch size	200
Convolutional layers	11
Stride	1
Number of iterations	200

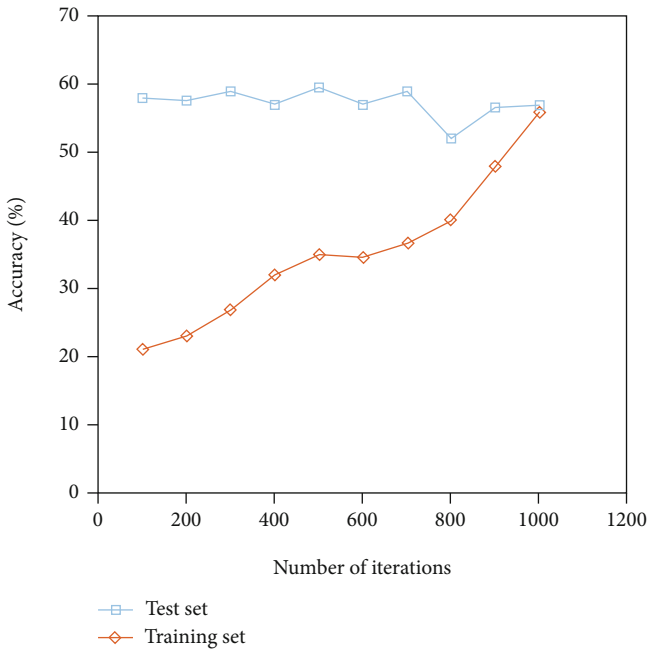

Figure 5: Relationship between training times and accuracy.

Table 3: Comparison of the accuracy of eleven-layer convolutional neural networks and some machine learning.

Number of experiments	Support vector machines	Decision tree	Naive Bayes classifier	Eleven-layer convolutional neural network
1	33.98%	25.88%	28.00%	57.55%
2	34.55%	25.00%	27.00%	55.95%
3	32.55%	27.22%	30.00%	58.22%

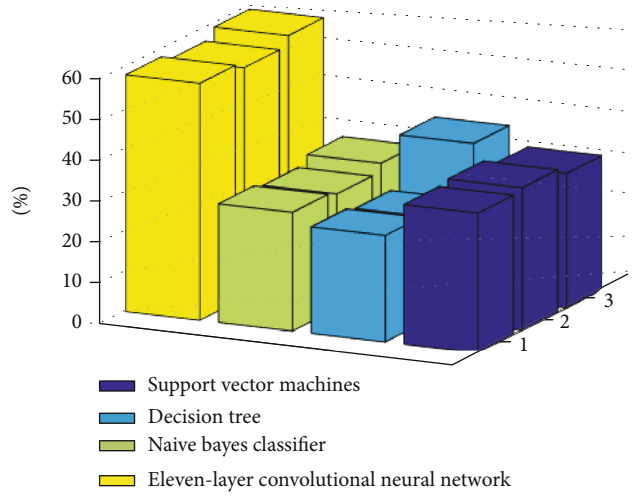

Figure 6: Comparison of the accuracy of eleven-layer convolutional neural networks and some machine learning.

4. Discussion

4.1. Convolutional Neural Network Training Analysis. Since different hyperparameters will have a greater impact on the final result during the training of the neural network, multiple combinations are used to verify the actual effect of the algorithm. It includes the learning rate, the number of convolutional layers, the number of convolution kernels, the number of pooling layers, the number of iterative learning, and

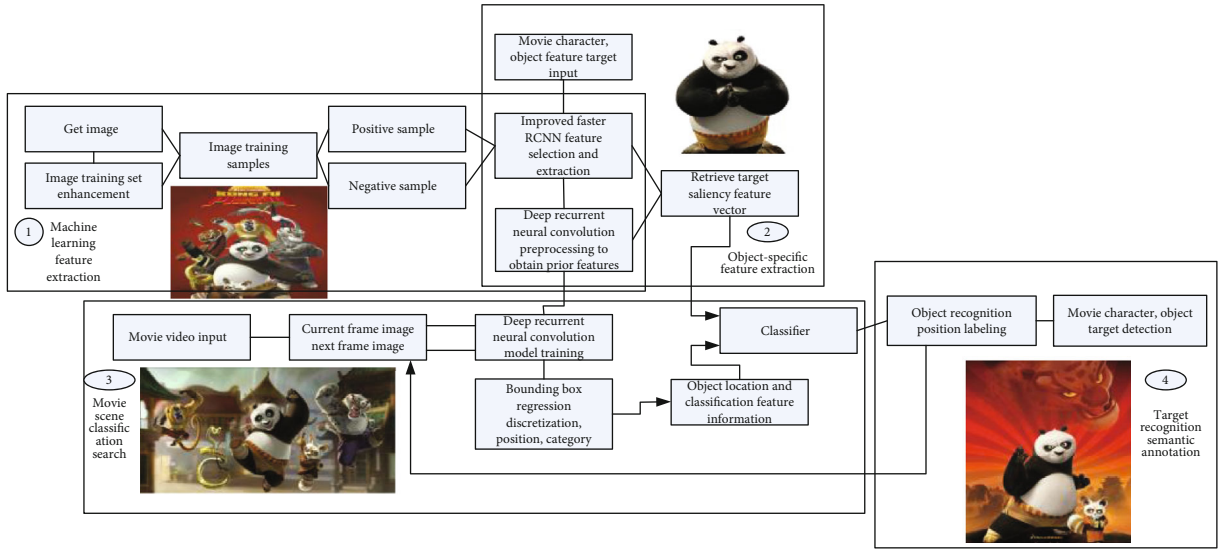

Figure 7: Recursive convolutional neural network for new visual studies of anime films.

the step size. The convolutional neural network hyperparameter combinations and their corresponding accuracy rates are shown in Table 1 and Figure 4.

After continuous training verification, it is found that from the two factors of training time and accuracy, the eleven-layer convolutional neural network can achieve a best training result, so the eleven-layer convolutional neural network is taken as an example to compare. In this paper, the size of the first layer of convolution kernel is selected based on the effective user information and movie information size. Each record has 5 valid attributes, so the size of the first layer of convolution kernel is. Some parameter settings of the eleven-layer convolutional neural network suitable for score prediction are shown in Table 2 and Figure 5:

In this experiment, the number of iterations is not repeated training for the same batch of data sets, but all data is divided into 200 batches, each input of 200 data, and each training is an iteration, so it does not exist for the same batch of data, and the problem of "overfitting" occurs because of too many trainings. During the test, 300 data sets were used for each batch. From the experimental results, it can be found that, for the training set, the accuracy rate continues to increase as the number of iterative trainings increases. After the parameters of the model were determined, the accuracy of the test set did not change much, all around 57%.

4.1.1. Comparative Experimental Analysis of Different Algorithms. In order to test the actual effect of the algorithm in this paper, it needs to be compared with existing algorithms. The higher the accuracy of the score prediction, the better the performance of the score prediction algorithm. For different comparison algorithms, the parameter values are as follows:

(1) *Support Vector Machine*. The regularization parameter C is 100, the kernel function is Gaussian radial kernel function, and Gamma is 0.003.

(2) *Decision Tree*. Criterion is set to "entropy," and Splitter is set to "best."

(3) *Naive Bayes Classifier*. The data dimension is 5, and the feature vector dimension is 5.

The accuracy comparison results of the eleven-layer convolutional neural network and three machine learning methods after three experiments are shown in Table 3 and Figure 6.

As shown in Table 3 and Figure 6, the new visual expression research algorithms for animation films based on convolutional neural networks have higher advantages than other machine learning algorithms, whether they are related to machine learning algorithms or to traditional algorithms in comparison, and the eleven-layer convolutional neural network proposed in this paper has a greater advantage in accuracy.

4.2. New Visual Expression of Artificial Intelligence in Anime Films. At present, artificial intelligence technology is mainly based on Convolutional God Network (CNN), and many excellent algorithms have been generated according to applications in different fields, such as the famous SIFT features, Alex Net, RCNN, GoogLeNet, Faster RCNN, SOLO, and SSD, regardless of the network structure. The core of how to change is to transform its basic process. It mainly includes image input, region feature extraction, region feature classification, partial feature extraction, and classifier implementation. Through the method of stochastic gradient descent, the parameters of intermittent splicing panels and parameters of all connected layers can be optimized to obtain the features and categories closest to the final arrival. This paper uses a deep recursive convolutional neural network algorithm to implement platform construction, detection, and verification, as shown in Figure 7.

The electronic image itself is composed of multiple static images due to the large amount of data. On the movie deep

recursive convolutional neural network algorithm, by adjusting the LOSS function, it provides methods and strategies to improve the accuracy of object recognition to achieve high-speed standard target detection and location.

5. Conclusions

So far, the electronic imaging industry has introduced large-scale data, which has shown massive, multisource, structural features, and data-intensive applications in the film industry. In this article, artificial intelligence technology is the core technology associated with language by independently analyzing electronic content analysis and its characteristics and analyzing electronic content elements to extract content elements individually. Through in-depth study of the content of dynamic images, analysis of the occurrence of a large number of similar effects and formation characteristics is looking for electric effects, in order to improve the level of animated films and promote the creation and marketing innovation of animated films.

After researching and summarizing the relevant knowledge in the recommendation field at this stage, this article analyzes the personalized recommendation algorithms involved in the recommendation system in various fields. This paper proposes the application of convolutional neural networks in deep learning to the new visual expression research of anime films and proposes a new visual research expression algorithm of anime films. After further research on the principle of new vision of animation film, the new visual expression research model of animation film is established according to the research process of new visual expression of movie, and the established algorithm is used in the new vision research expression model of animation film.

Due to the limitation of time and conditions, there are still some shortcomings and to be improved in this article. There are still some shortcomings, including the following: cold start of the algorithm, data setting and initialization, data structure, and the balance between accuracy and recall. With the continuous innovation of artificial intelligence technology, the analysis methods and means of artificial intelligence technology in movies will also be more widely used in movie creation, production, review, appreciation, marketing recommendations, and other links.

Data Availability

No data were used to support this study.

Conflicts of Interest

The authors declare that they have no conflicts of interest.

References

[1] M. Frutos-Pascual and B. G. Zapirain, "Review of the use of AI techniques in serious games: decision making and machine learning," *IEEE Transactions on Computational Intelligence & Ai in Games*, vol. 9, no. 2, pp. 133–152, 2017.

[2] M. Zhou, X. Li, Y. Wang, S. Li, Y. Ding, and W. Nie, "6G multi-source information fusion based indoor positioning via Gaussian kernel density estimation," *IEEE Internet of Things Journal*, 2021.

[3] M. Alkasassbeh, "An empirical evaluation for the intrusion detection features based on machine learning and feature selection methods," *Journal of Theoretical & Applied Information Technology*, vol. 95, no. 22, pp. 5962–5976, 2017.

[4] K. W. Johnson, J. Torres Soto, B. S. Glicksberg et al., "Artificial intelligence in cardiology," *Journal of the American College of Cardiology*, vol. 71, no. 23, pp. 2668–2679, 2018.

[5] C. Prakash, R. Kumar, and N. Mittal, "Recent developments in human gait research: parameters, approaches, applications, machine learning techniques, datasets and challenges," *Artificial Intelligence Review*, vol. 49, no. 1, pp. 1–40, 2018.

[6] T. Dyster, S. A. Sheth, and G. M. McKhann II, "Ready or not, here we go: decision-making strategies from artificial Intelligence based on deep neural networks," *Neurosurgery*, vol. 78, no. 6, pp. N11–N12, 2016.

[7] N. Foulquier, P. Redou, and C. Le Gal, "Pathogenesis-based treatments in primary Sjogren's syndrome using artificial intelligence and advanced machine learning techniques: a systematic literature review," *Human Vaccines & Immunotherapeutics*, vol. 14, no. 3, pp. 1–18, 2018.

[8] Z. Yuan, Y. Lu, and Y. Xue, "Droiddetector: android malware characterization and detection using deep learning," *Tsinghua Science and Technology*, vol. 21, no. 1, pp. 114–123, 2016.

[9] Y. Zhou, P. Li, and S. Wang, "Research progress on big data and intelligent modelling of mineral deposits," *Bulletin of Mineralogy Petrology & Geochemistry*, vol. 36, no. 2, pp. 327–331, 2017.

[10] Á. Baquero-Pecino, "After Human Rights: Literature, Visual Arts, and Film in Latin America, 1990-2010 by Fernando J. Rosenberg," *Arizona Journal of Hispanic Cultural Studies*, vol. 20, no. 1, pp. 307–309, 2016.

[11] D. Valente, A. Theurel, and E. Gentaz, "The role of visual experience in the production of emotional facial expressions by blind people: a review," *Psychonomic Bulletin & Review*, vol. 25, no. 1, pp. 1–15, 2018.

[12] K. Borowski, J. Soh, and C. W. Sensen, "Visual comparison of multiple gene expression datasets in a genomic context," *Journal of Integrative Bioinformatics*, vol. 5, no. 2, pp. 94–103, 2008.

[13] H. Chen, A. Zhang, and S. Hu, "Abrupt motion tracking of plateau pika (Ochotona curzoniae) based on local texture and color model," *Transactions of the Chinese Society of Agricultural Engineering*, vol. 32, no. 11, pp. 214–218, 2016.

[14] N. I. Bloch, "Evolution of opsin expression in birds driven by sexual selection and habitat," *Proceedings of the Royal Society B: Biological Sciences*, vol. 282, no. 1798, pp. 701–715, 2015.

[15] P. Pradhan, N. Upadhyay, and A. Tiwari, "Genetic and epigenetic modifications in the pathogenesis of diabetic retinopathy: a molecular link to regulate gene expression," *New Frontiers in Ophthalmology*, vol. 2, no. 5, pp. 192–204, 2016.

[16] A. Bennis, J. G. Jacobs, and L. A. E. Catsburg, "Stem cell derived retinal pigment epithelium: the role of pigmentation as maturation marker and gene expression profile comparison with human endogenous retinal pigment epithelium," *Stem Cell Reviews and Reports*, vol. 13, no. 5, pp. 659–669, 2017.

[17] M. Zhou, Y. Wang, Y. Liu, and Z. Tian, "An information-theoretic view of WLAN localization error bound in GPS-denied environment," *IEEE Transactions on Vehicular Technology*, vol. 68, no. 4, pp. 4089–4093, 2019.

[18] L. De Raedt, K. Kersting, S. Natarajan, and D. Poole, "Statistical relational artificial intelligence: logic, probability, and computation," *Synthesis Lectures on Artificial Intelligence and Machine Learning*, vol. 10, no. 2, pp. 1–189, 2016.

[19] C. Nalmpantis and D. Vrakas, "Machine learning approaches for non-intrusive load monitoring: from qualitative to quantitative comparation," *Artificial Intelligence Review*, vol. 52, no. 1, pp. 217–243, 2019.

[20] F. Azmat, Y. Chen, and N. Stocks, "Analysis of spectrum occupancy using machine learning algorithms," *IEEE Transactions on Vehicular Technology*, vol. 65, no. 9, pp. 6853–6860, 2016.

Hindawi
Journal of Sensors
Volume 2021, Article ID 7300864, 6 pages
https://doi.org/10.1155/2021/7300864

Research Article

Iris Location Algorithm Based on Union-Find-Set and Block Search

Long-yang Huang,[1] **Li-qiang Zhang**,[2] **and Xiao-li Duan**[3]

[1]*College of Air Traffic Management, Civil Aviation Air Flight University of China, Guanghan 618307, China*
[2]*Electrical Engineering Department, Zhengzhou Technical College, Zhengzhou 450121, China*
[3]*School of Economics & Management, Zhengzhou Normal University, Zhengzhou 450044, China*

Correspondence should be addressed to Li-qiang Zhang; zlq1362386@163.com

Received 23 April 2021; Revised 20 May 2021; Accepted 8 June 2021; Published 6 July 2021

Academic Editor: Mu Zhou

In view of the problem of unstable recognition effect and low robustness of a traditional iris location algorithm, an iris location algorithm based on union-find-set and block search is proposed. Firstly, the inner circle of the iris is roughly positioned by the method of retrieval, and then, the Hough transform is used to accurately locate the pupil. After that, the convolution operation is used to roughly locate the outer circle, and then, the original image is partitioned to search. And the grayscale change in the gray histogram of the screenshot is observed to accurately locate the outer circle. The obtained iris and the iris obtained by the traditional localization algorithm are processed by the same iris recognition algorithm. The results show that the proposed image is more effective in image recognition and has good robustness.

1. Introduction

Due to the uniqueness, noninvasiveness, stability, and natural anticounterfeiting of the iris, the iris has higher accuracy than other biometrics [1]. Therefore, iris recognition technology is one of the most popular biometric recognition technologies.

The iris recognition process is divided into iris image acquisition, iris quality evaluation, iris location, iris normalization enhancement, and iris feature expression and matching [2]. Iris location is used to locate the inner and outer boundaries of the iris and segment the iris ring region between the two boundaries, so as to facilitate the expression and recognition of iris features [3]. Traditional iris location algorithms include the calculus circle template method and Hough method based on edge detection [4, 5]. The inner boundary of the iris is roughly located by using the lower edge of the binary image, and the outer boundary of the iris is roughly located by using the one-dimensional gray mean signal on both sides of the inner boundary center [6]. An iris location algorithm based on edge detection and circle fitting is proposed [7]. The iris location algorithm based on a small-scale search is adopted [8]. Although these algorithms can accurately locate the position of the iris, they have poor robustness and high requirements for the image. Moreover, they have poor anti-interference ability to rough eyelids, illumination, and other noise interference, and the recognition effect is unstable. The algorithm processing flow of this paper is shown in Figure 1.

Therefore, the iris localization algorithm based on union-find-set and block search is proposed in this paper. For the inner circle positioning of the iris, the method of firstly adopting and collecting the method to realize the coarse positioning of the inner circle can overcome the influence of spot factors, and then, the Hough transform is adopted to improve the speed of accurate positioning of the inner circle. For outer circle positioning, the convolution operation is used to roughly locate the outer circle, and then, the original image is partitioned to search. Then, the grayscale change in the gray histogram of the screenshot is observed to accurately locate the outer circle. Experiments show that the proposed algorithm can effectively enhance the robustness of iris

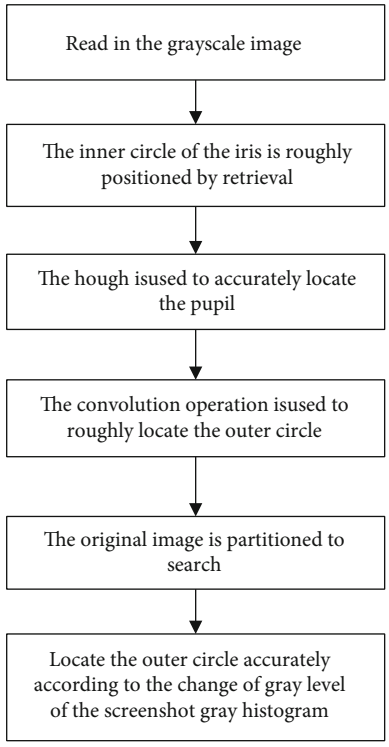

Figure 1: Iris inner and outer circle positioning process.

localization, and the iris images acquired by different collectors under different conditions can be used for iris localization, and the recognition effect is stable.

2. Algorithm Implementation

2.1. The Inner Circle Positioning of the Iris. In some application problems, a set of n elements needs to be divided into several disjoint subsets according to the relationship between the elements. To solve this kind of problem, first make each element form a separate collection. If there are direct or indirect links between elements in different collections, the two collections are merged until there is no contact in any of the elements in the collection. Since the main concern in such problems is the merge and lookup of sets, such sets are referred to as union-find-set. The mathematical model is as follows.

Several mutually disjoint dynamic sets $S = \{A, B, C \cdots\}$ are known, which support the following operations:

(i) initial(A, x). Construct a collection named A that contains only one element x

(ii) merge(A, B). Combine the sets A and B, and the result is named A or B

(iii) find(x). Find the collection of elements x and return the name of the collection

The processing steps of the union-find-set are as follows:

(i) Use the initial(A, x) operation to create a subset of each element in the collection

(ii) The sets A and B of the x and y elements are obtained by using the find(x) operation for each associated element pair (x, y)

(iii) If A and B are different, then x and y are considered to belong to different sets, and then, the merge(A, B) operation is performed

(iv) Go back to step 2 to process the next pair of associated elements until all associated element pairs have been processed

In order to improve the efficiency of union-find-set execution, the tree structure is adopted in this paper to implement and check the set, where the name of the root represents the name of the generated subset and is directly or indirectly associated with any two elements in the tree. There is no direct or indirect association between any two elements in different trees. When the collection tree of two related elements merges, simply find the root of the tree in which each element is located, and then, use one tree as the tree root tree of the other tree.

For example, set set = $\{1, 2, 3, 4, 5, 6, 7, 8, 9, 10\}$, and the associated element pair is $\{5, 1\}$, $\{7, 4\}$, $\{10, 4\}$, $\{4, 2\}$, $\{6, 3\}$, $\{8, 3\}$, $\{9, 3\}$. The processing results of the union-find-set are shown in Table 1, where line 2 of Table 1 is the result of the initial(A, x) processing. The first line is all the elements in the collection, the second line is the collection where each element is located, and the name of the collection is the name of the element. Line 3 of Table 1 is the result of union-find-set execution. The number of sets with the same element and set name in the figure is the final and the result of the collection process.

The grayscale feature of the iris image is that the grayscale of the pupil region is generally smaller than the grayscale of the iris region. The grayscale of the iris region is generally smaller than the grayscale of the sclera region. And the grayscale change in the same region is relatively small, while that at the boundary of different regions is relatively large. Each pixel in the iris image can be regarded as a set element. If the gray level difference between two adjacent pixels i and j is less than a certain threshold k, it can be considered that there is an association relationship between the two pixels, denoted as (i, j). In this way, the division of different types of regions in the iris can be realized by the union-find-set operation. As the gray level of the pupil area is smaller than that of other regions, the final pupil area can be determined according to the size of the obtained gray level of each region. For a visible iris image, the gray value of the area around the light spot in the inner pupil will show a significant jump. Since the area of the light spot is usually smaller than the area of the pupil, the spot only changes the gray level of a small portion of the pupil area, and the gray level of most of the pupil area is still not affected by the spot. Thus, through the union-find-set operation, a pupil with a partial defect is obtained. This defective pupil can be used as a rough positioning of the pupil, as shown in Figure 2. Figure 2(b) is a result of rough positioning of the pupil region by the union-find-set operation of Figure 2(a).

Table 1: The union-find-set set initialization and processing results.

i	1	2	3	4	5	6	7	8	9	10
Initial set(i)	1	2	3	4	5	6	7	8	9	10
Result set(i)	1	2	3	2	1	3	4	3	3	4

On the basis of obtaining the pupil coarse location, the edge tracking method is used to obtain all the edge points of the pupil region. Then, the final inner contour of the iris is obtained by the Hough transform. Because the pupil area is determined before the Hough transform, the search range of the circle center and circle radius is greatly reduced. In addition, because the points used in the Hough transform are edge points obtained by edge tracking, there are no other interference edge points outside the pupil, so the speed of the Hough transform is greatly improved. Figure 2(c) is the final inner contour of the iris obtained by the Hough transform.

The coarse positioning of the iris inner circle by union-find-set can quickly complete the coarse positioning of the iris pupil, and even in the case of spot interference, most of the pupil can be obtained. Then, the Hough transform is used to determine the precise inner circle contour and improve the positioning efficiency of the inner circle.

2.2. The Outer Circle Positioning of the Iris. Although the inner and outer boundaries of the iris are not concentric circles, there is a certain coupling relationship between them. Therefore, the rough location of the center of the pupil circle can be obtained by combining the rough location of the outer ring with the fine location of the inner ring. Firstly, the 5-ary convolution operation is used to process the image. After convolution, the result is binarized. The binary image is shown in Figure 3(b).

In order to calculate the number of white points on the curve of a specified angle range, the number of different radii should be calculated, and the variation range of the radius gradually increases from $(r, 2 \times r)$. Since the upper and lower parts of the iris image are easily interfered by noise such as eyelids, the number of white points under a certain iris angle is only calculated in order to reduce the interference of noise on the positioning of the outer boundary of the iris. It can be seen from Figure 3(b) that the white spot on the lower right side of the iris is more and easy to read. To read as many white points as possible under the condition of less interference, the angle range is selected from the horizontal direction of the pupil center to the right side clockwise 0~60°, which is calculated as the following formula.

$$\max_{(x_c,y_c,r)} \left| \frac{\partial}{\partial r} G_\sigma(r) * \left(\int_{r-t/2(x_c,y_c,r)}^{r+t/2} \oint \frac{I(x,y)}{\pi(r+(t/2))^2 - \pi(r-t/2)^2} dsdr \right) \right|, \tag{1}$$

where $*$ is the convolution operation. $G_\sigma(r)$ is the Gaussian smoothing function.

$$G_\sigma(r) = \frac{1}{\sqrt{2\pi}\sigma} e^{(r-r_c)^2/2\sigma^2}. \tag{2}$$

The pupil center (x_c, y_c) of the inner circle is used as the search point, and the radius is continuously increased. The number of white points of each arc is calculated in turn, and the maximum value is determined to determine the center and radius (x_c, y_c, R). This will roughly establish the position of the outer circle of the iris. The outer circle is roughly positioned as shown in Figure 3(c).

There are two problems in the outer circle coarse positioning of the convolution operation. First of all, the outer circle is a concentric circle centered on the pupil. Secondly, the ratio of the iris radius to the pupil radius cannot be accurately predicted due to the different conditions of each image. According to the physiological practice, the iris radius of the human eye is about 1~2 times of the pupil radius, and the maximum radius is set to be 2 times of the pupil radius. Therefore, it is necessary to use the block search method again to perform the precise positioning of the outer ring. The rough location of the outer circle needs two segmentation detection operators of the cylinder center and radius boundary in the horizontal direction.

According to the gray histogram of the detection operator, the detection operator is moved left and right, and the gray distribution in the gray histogram of the detection operator is compared with the gray distribution in the gray histogram of the eye image. Then, the gray value distributions on the left and right sides are, respectively, obtained to reach the gray value in the sclera region, and the detection operator moves the distance k to the left and the distance to the right to m. The center of the coarse positioning circle is (x_c, y_c) and the radius is R. After moving, the center of the circle $(\widehat{x}_c, \widehat{y}_c)$ can be calculated as follows.

$$\begin{cases} \widehat{x}_c = & x_c - \dfrac{k}{2} + \dfrac{m}{2}, \\ \widehat{y}_c = & y_c. \end{cases} \tag{3}$$

And the radius $\widehat{R}$ can be calculated as follows.

$$\widehat{R} = R + \frac{k}{2} + \frac{m}{2}. \tag{4}$$

The precisely positioned outer circle is shown in Figure 3(d).

3. Experimental Results and Analysis

In the experiments, the CASIA-Iris-Interval iris library [9] of the Chinese Academy of Sciences and the iris library collected by our laboratory were used. In the CASIA-Iris-Interval iris library, 50 of these categories were selected, and 15 images were selected for each category, for a total of 750 images. The visible iris map library collected by our laboratory is mainly from 1200 photos of students and patients, with a resolution of 800×600. The image has passed the quality evaluation and detection in advance, but it contains a variety of types, including images close to the boundary

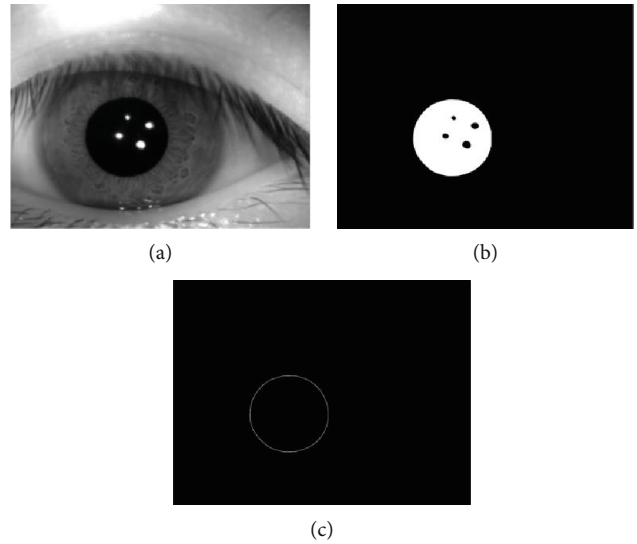

(a) (b) (c)

Figure 2: The inner circle positioning of the iris.

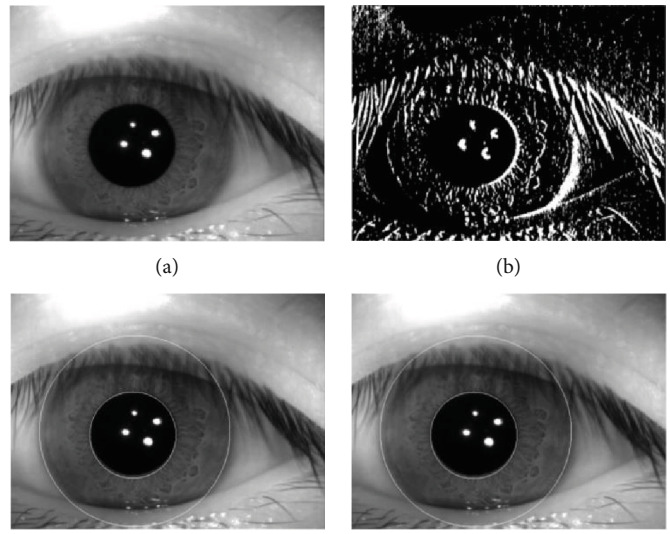

(a) (b) (c) (d)

Figure 3: The outer circle positioning of the iris.

and heavy eye hairs, which are used to detect the robustness of the algorithm.

3.1. Image Feature Expression and Matching. In this paper, the rubber ring model is used to uniformly normalize the iris image, and the circular rainbow is expanded into a 512 rectangle × 64. The strongest part of the texture is intercepted and cut into 256 × 32 fixed rectangular regions to enhance the image texture.

In the experiment, the main frequency of CPU is 2.5 GHz, the memory is 8 GB, and the operating system is Windows 10. Before feature extraction, all normalized iris images are translated horizontally to eliminate the problem of iris rotation. Then, two-dimensional Gabor filter is used to extract feature texture information. The attributes of the iris image are determined by comparing the Euclidean distance between samples.

Table 2: Results of the CASIA-Iris-Interval iris library.

Algorithm	Success number	Pupil time (s)	Iris time (s)	Time (s)	CRR (%)	EER (%)
Literature [4]	728	0.75	1.02	1.76	95.8	1.38
Literature [6]	724	0.67	0.94	1.62	96.1	1.03
Literature [7]	717	0.63	0.76	1.38	97.2	0.84
Proposed	749	0.60	0.68	1.24	97.4	0.65

3.2. Experimental Judgment Indicators and Experimental Results. The ROC curve is a curve indicating the relationship between False Reject Rate (FRR) and False Accept Rate (FAR) [10]. The ROC curve reflects the matching

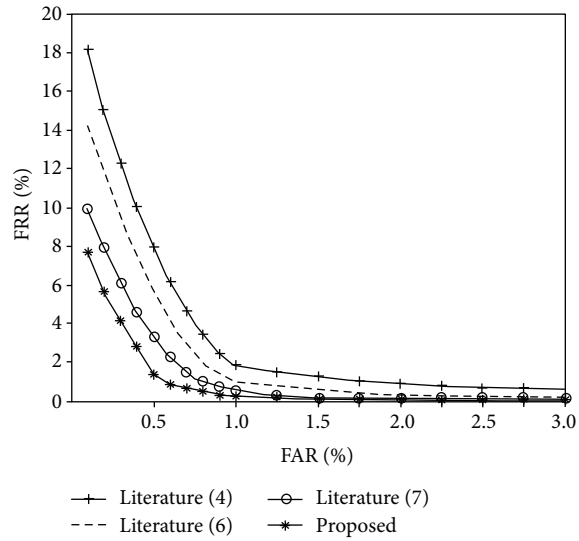

Figure 4: The ROC curve of CASIA-Iris-Interval iris library experiment results.

Table 3: Results of our laboratory.

Algorithm	Success number	Pupil time (s)	Iris time (s)	Time (s)	CRR (%)	EER (%)
Literature [4]	1148	0.75	1.02	1.76	95.5	1.38
Literature [6]	1157	0.69	0.95	1.64	96.8	1.03
Literature [7]	1178	0.63	0.77	1.39	97.7	0.84
Proposed	1188	0.57	0.68	1.26	97.9	0.67

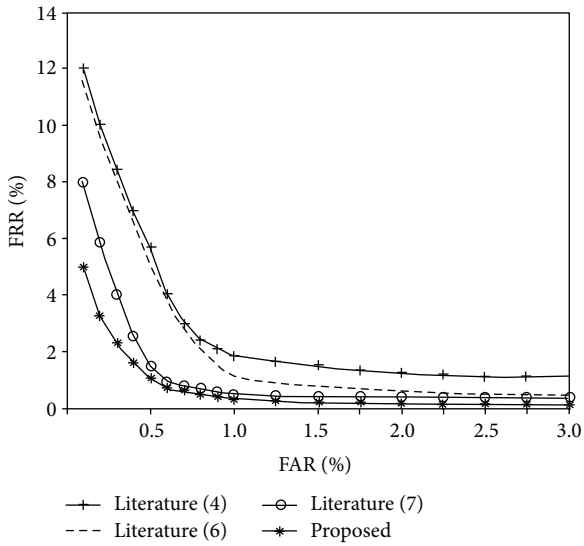

Figure 5: The ROC curve of our laboratory experiment results.

performance of the iris recognition algorithm [11]. The closer to the horizontal and vertical axes, the better the performance of the system. When the FRR is equal to the value of FAR, which is the best system performance, the value is called Equal Error Rate (EER) [12]. The smaller the EER, the better the performance. In addition, the Correct Recognition Rate (CRR) is also one of the performance evaluation indicators of the commonly used iris recognition system [13].

This paper is based on CRR, EER, ROC curve, and algorithm in the average time (pupil time). The outer circle positioning average time (iris time) and the overall average positioning time (time) and the number of irises successfully positioned by the positioning algorithm are compared [14–16].

The experimental results of the CASIA-Iris-Interval iris library are shown in Table 2. The ROC curve is shown in Figure 4. The experimental results of our laboratory are shown in Table 3, and the ROC curve is shown in Figure 5.

4. Conclusion and Future Work

An iris location algorithm based on a joint search set and block search is proposed. The inner circle of the iris is roughly located by the joint search set method, and then, the inner circle of the pupil is accurately located by the Hough transform. Firstly, the convolution operation is used to roughly locate the outer circle of the iris, and then, the block search is used to accurately locate the outer circle of the iris. Under the same feature representation and recognition algorithm, it is compared with other location methods. The experimental results show that the ROC curve of this method is closer to the horizontal and vertical coordinates, and the average time is shortened. This method has high precision and good robustness.

The future work of this paper is the combination of theory and practice, so that the proposed algorithm can meet the needs of actual target detection.

Data Availability

The labeled dataset used to support the findings of this study are available from the corresponding author upon request.

Conflicts of Interest

The authors declare no competing interests.

Acknowledgments

The study was funded by the Civil Aviation Education Talent Project: Discipline Innovation Laboratory Construction for postgraduate student of CAFUC (0252103).

References

[1] J. J. Winston and D. J. Hemanth, "A comprehensive review on iris image-based biometric system," *Soft Computing*, vol. 23, no. 19, pp. 9361–9384, 2019.

[2] X. Li, Y. Jiang, M. Chen, and F. Li, "Research on iris image encryption based on deep learning," *EURASIP Journal on Image and Video Processing*, vol. 2018, 10 pages, 2018.

[3] E. Severo, R. Laroca, C. S. Bezerra et al., "A benchmark for iris location and a deep learning detector evaluation," in *2018*

International Joint Conference on Neural Networks (IJCNN), pp. 1–7, Rio de Janeiro, Brazil, 2018.

[4] J. G. Daugman, "Statistical richness of visual phase information: update on recognizing persons by iris patterns," *International Journal of Computer Vision*, vol. 45, no. 1, pp. 25–38, 2001.

[5] Z. Hu, C. Wang, and L. Yu, "Iris location using improved randomized Hough transforms," *Chinese Journal of Scientific Instrument*, vol. 24, no. 5, pp. 477–479, 2003.

[6] H. I. Kim, J. B. Kim, and R. H. Park, "Efficient and fast iris localization using binary radial gradient features for human–computer interaction," *International Journal of Pattern Recognition and Artificial Intelligence*, vol. 31, no. 11, p. 1756015, 2017.

[7] L. H. Zhong, K. Meng, Y. Wang, Z. Q. Dai, and S. Li, "Iris location algorithm based on the CANNY operator and gradient Hough transform," *IOP Conference Series: Materials Science and Engineering*, vol. 281, no. 1, article 012061, 2017.

[8] L. J. Yu, X. Zhang, Y. Liu, and X. Zhu, "Iris location algorithm based on small regional search," *Journal of Computational Information Systems*, vol. 11, no. 12, pp. 4221–4228, 2015.

[9] D. Kerrigan, M. Trokielewicz, A. Czajka, and K. W. Bowyer, "Iris recognition with image segmentation employing retrained off-the-shelf deep neural networks," in *2019 International Conference on Biometrics (ICB)*, pp. 1–7, Crete, Greece, 2019.

[10] T. D. Yang and C. P. Fan, "Effective scale-invariant feature transform based iris matching technology for identity identification," in *2018 IEEE international conference on consumer electronics-Taiwan (ICCE-TW)*, pp. 1–5, Taichung, Taiwan, 2018.

[11] N. Ahmadi, M. Nilashi, S. Samad, T. A. Rashid, and H. Ahmadi, "An intelligent method for iris recognition using supervised machine learning techniques," *Optics & Laser Technology*, vol. 120, p. 105701, 2019.

[12] L. A. Zanlorensi, E. Luz, R. Laroca, A. S. Britto, L. S. Oliveira, and D. Menotti, "The impact of preprocessing on deep representations for iris recognition on unconstrained environments," in *2018 31st SIBGRAPI conference on graphics, patterns and images (SIBGRAPI)*, pp. 289–296, Parana, Brazil, 2018.

[13] L. Shuai, L. Yuanning, Z. Xiaodong et al., "Constrained sequence iris quality evaluation based on causal relationship decision reasoning," in *Biometric Recognition*, pp. 337–345, Springer, Cham, 2019.

[14] M. Zhou, Y. Long, W. Zhang et al., "Adaptive genetic algorithm-aided neural network with channel state information tensor decomposition for indoor localization," *IEEE Transactions on Evolutionary Computation*, p. 1, 2021.

[15] Y. Jiang, D. Wu, Z. Deng et al., "Seizure classification from EEG signals using transfer learning, semi-supervised learning and TSK fuzzy system," *IEEE Transactions on Neural Systems and Rehabilitation Engineering*, vol. 25, no. 12, pp. 2270–2284, 2017.

[16] Y. Jiang, K. Zhao, K. Xia et al., "A novel distributed multitask fuzzy clustering algorithm for automatic MR brain image segmentation," *Journal of Medical Systems*, vol. 43, no. 5, pp. 1–118, 2019.

Hindawi
Journal of Sensors
Volume 2021, Article ID 8463944, 10 pages
https://doi.org/10.1155/2021/8463944

Research Article

Research on Software Design of Intelligent Sensor Robot System Based on Multidata Fusion

Fenglang Wu, Xinran Liu, and Yudan Wang

Network Information Department, The First Affiliated Hospital of Xi'an Jiaotong University, Xi'an, 710061 Shaanxi, China

Correspondence should be addressed to Fenglang Wu; wufenglang@xjtufh.edu.cn

Received 29 April 2021; Revised 22 May 2021; Accepted 1 June 2021; Published 3 July 2021

Academic Editor: Mu Zhou

With the advent of robots combined with artificial intelligence, robots have become an indispensable part of production and life. Especially in recent years, the collaboration between humans and machines has become a research trend in the field of robotics, with high work efficiency and flexibility. The advantages of safety and stability make intelligent robots the best choice for the current industrial and service industries with high labor intensity and hazardous working environments. This paper is aimed at studying the software design of an intelligent sensor robot system based on multidata fusion. In this paper, through the needle robot's high precision requirements and the problem of fast response, a path design method based on the ant colony optimization (ACO) algorithm is proposed. Path planning is performed by intelligent robots for obstacle avoidance experiments, while global optimization is performed by the ant colony optimization (ACO) algorithm. For adaptive functions including obstacle reduction and path information length, the safest and shortest path is finally achieved through the ant colony optimization (ACO) algorithm. The experimental results show that using the ant colony optimization algorithm to perform simulation experiments and preprocessing operations on the data collected by the sensor can improve the accuracy and effectiveness of the data. The ant colony algorithm performs fusion and path planning, and on the basis of ensuring accuracy, it can speed up the convergence speed. Through the data analysis of obstacle avoidance experiments of intelligent robots, it can be concluded that it is very necessary for intelligent robots to install ultrasonic sensors and infrared sensors in obstacle avoidance, because the error between the test distance of the ultrasonic sensor and the infrared sensor and the actual distance is 0.001.

1. Introduction

1.1. Background of Topic Selection. Robots have become an indispensable part of production and life. Intelligent and standard robots combine mechanical design, computer software technology, advanced signal processing, communication engineering, materials science, computer vision, and other fields to form a complex, reliable, and intelligent system. The advancement and development of robotics fully proved the advancement of science and technology. In terms of industrial technology, military strength, skill level, and human survival services, the development of the country is closely related to the development of robotics. Therefore, the development and implementation of robot technology objectively represent the frontier of high-tech development, represent the country's technological development level, and represent the country's industrial automation and high-tech level. The research, development, and rapid development of robots are an important step for the country to develop advanced technology, and it is also the only way to improve the country's comprehensive national strength.

1.2. Significance of the Research. In the control of intelligent sensor robots, sensors are the means to obtain external information, are the core of the overall perception of external information, and are responsible for receiving information about the external environment of the robot in real time so that the robot can make adjustments. Determine the work sequence and operation content according to changes in the natural working environment. It can more comprehensively reflect changes in the environment, so that correct decisions can be made and the accuracy, speed, and stability of the robot system can be ensured. However, because the information provided by a single sensor is too small to meet the

requirements of the entire robot, we urgently need a technology that can combine the information of many sensors at the same time to accurately guide the entire robot. Compared with single-sensor technology, the multisensor fusion control system has great characteristics. It can be used to enhance and improve the reliability of measurement data, expand the measurement range of the fusion system, and improve the robustness of the system. If some sensors have failed, you can quickly complete the reconfiguration and resume work. Multisensor data collection and calculation belong to the information fusion technology, which collect and calculate the data transmitted from different sensors to the processor, and combine the calculated data into a single interface description method to improve the adaptability of the robot. Multisensor data merging can describe the typical functions of the robot interface in more detail and ensure the safe and stable operation of the robot. Therefore, the development of multisensor fusion is becoming faster and faster, and it has become a research point in the field of robotics.

1.3. Relevant Work on the Software Design and Research of Intelligent Sensor Robot System Based on Multidata Fusion. This paper studies the software design of the intelligent sensor robot system based on multidata fusion, preprocessing the environmental information data collected from each sensor of the robot, processing and fusing the data collected from each sensor, and planning the movement path of the robot. Zhou et al. proposed the use of artificial potential fields to avoid obstacles on the mobile chassis. The target set by the host is defined as gravity, and obstacles in the environment are defined as repulsive forces. Based on this, artificial gravitation and repulsion models are constructed. According to the force function derived from the force field, the force of the robot in the working environment is obtained, and the speed of the robot is obtained to achieve the purpose of avoiding obstacles [1]. Zhang successfully implemented the high-stability and high-precision visual SLAM algorithm, completed the positioning based on the features of the matched image, and improved the stability of the mapping based on the advantages of scale-invariant feature transformation and Harris focus. SLAM's position and attitude estimation provides support. At the same time, the IMU data can be fused according to the Harris focusing method, and the motion of the robot can be predicted according to the posture estimation of the IMU, so that the quaternion can be used to solve the current position and posture of the robot. However, the use of the ant colony optimization algorithm can be better achieved [2]. Semmens et al. uses the extended Kalman filter method and the particle filter method to complete the test calculation of the signal with Gaussian noise distribution and uses the encoder as the sensor and the ultrasonic sensor as the condition estimation standard of the mobile device [3]. In this case, the particle filter requires a higher calculation cost, but the calculation time and calculation accuracy of the particle filter used for sensor fusion are stronger than those of the Kalman filter. However, by analyzing the challenging problems in the big data reaction, their research data volume is not large and the basis is insufficient.

1.4. Innovation Points of This Research

(1) Multisensor information fusion technology can improve the reliability of measurement data, expand the measurement range of the fusion system, and improve the robustness of the system when some sensors fail. It can quickly complete reconfiguration and resume work

(2) Through the ant colony optimization algorithm, the optimal path and faster convergence speed can be obtained during the obstacle avoidance process of the robot

2. Software Design and Research Method of Intelligent Sensor Robot System Based on Multidata Fusion

2.1. Goal of Multiple Data Fusion. Multidata fusion, also known as multisensor information fusion, has become a popular research field. It has been applied to many fields, such as navigation, robots, GPS positioning, and signal processing. In modern electronic warfare, it is difficult for the information provided by a single sensor to reach the target and carry out the requirements of tracking accuracy and state evaluation. The purpose of multisensor information fusion is to combine data from multiple sensors to measure environmental variables, reduce signal uncertainty, and improve measurement accuracy [4]. Therefore, they fuse different types of information at different levels for fusion, and the sensor can directly receive raw data or processed data [5]. In the fusion process, complex reasoning must be performed on this different and changing information to produce the effect of $1 + 1 > 2$, thereby improving the control efficiency of the controller [6].

2.2. Necessity of Multisensor Information Fusion. The collection of sensors and traditional robots that collect environmental information is a kind of intelligent robot. In order to make the robot have the same cognitive and judgment abilities as humans, it is necessary for the robot to perceive as much information about the environment as possible [7]. Intelligent robots based on multisensor information fusion can perceive the robot's environmental information and also enhance the robot's intelligent control capabilities [8, 9].

2.3. Features of Multisensor Information Fusion. Compared with single-sensor information fusion, multisensor information fusion has the following characteristics.

2.3.1. Good Stability. The performance of each sensor is complementary, and the information collected is not related to each other. The entire system receives complete information that cannot be received by any sensor [10]. Therefore, when one of the sensors fails, there will always be another sensor collecting environmental data as supplementary information, which will make the system less sensitive to interference caused by changes in the external environment, thereby improving the stability of the entire system [11].

2.3.2. High Reliability. Since information is obtained from multiple sensors, the possibility of data errors is greatly reduced. At the same time, the environmental information collected by many sensors also improves the system's understanding of the environment and significantly improves the overall reliability of the system [12].

2.3.3. Reduced Ambiguity of Information. When multiple sensors detect the same environmental target, more environmental information can be obtained, which greatly reduces the uncertainty of the detected environment [13].

2.3.4. The Overall Performance of the System Is Enhanced. In theory, it has been proven that sensing the environment or target through multiple sensors and fusing the received data using optimization methods will not reduce the overall performance of the system. In other words, the performance of a system based on multisensor information fusion is better than that of a single sensor. Generally, the performance of a multisensor information fusion system is better than that of a single-sensor system.

2.3.5. Expanded Space Coverage. Since different types of sensors have different capabilities for detecting environmental information, the distance and accuracy of detection are also different. By applying multiple different types of sensors to the same area at the same time, the space coverage can be greatly expanded [14].

2.4. Basic Principles of Multisensor Information Fusion. Multisensor fusion technology is a comprehensive and advanced decision-making process based on measurement results. In a multisensor system, since the information provided by different sensors may be different, they are mutually supportive or complementary [15]. Multisensor fusion technology utilizes multiple sensor resources to integrate redundant multisensor information in time and space, while eliminating errors or unreliable information, so as to obtain a consistent description or explanation of the object described. As a result, the sensor system has better performance than a system composed of various subsets [16].

2.5. Basic Methods of Multisensor Information Fusion

2.5.1. Random Method

(1) *Weighted average method*: the weighted average method is usually suitable for dynamic environments with simple structure and low requirements for fusion accuracy. It is a simple and intuitive sensor data fusion algorithm. The weighted average method uses the weighted average of environmental data collected by sensors [17] and uses the final result as a fusion.

(2) *Kalman filter method*: the Kalman filtering method is mainly used to merge real-time low-level data from multiple sensors. There are two information fusion methods based on the Kalman filter. The centralized Kalman filter directly integrates all the local observation equations to obtain the extended-dimensional fusion observation equation, and then, the global optimal Kalman filter of the state equation is given [18]. However, the distributed Kalman filter uses the local weighted Kalman estimation to provide global optimal or global Kalman fusion [19]. Observation fusion technology can be broadly divided into core fusion technology, centralized fusion technology, and distributed fusion technology. The fusion observation method is the same as other fusion methods, and this variance observation fusion method is also referred to as the weighted observation fusion method. The weighted local observation equation can be used to obtain the weighted local observation equation, and then, the state equation can be used to obtain the Kalman filter fused with the weighted local observation [20]. However, the Kalman filter has two characteristic limitations: the system and the observation value must be nonlinear and in this case must be Gaussian. The actual environmental conditions are often more complicated, so we need to optimize the Kalman filter [21].

(3) *Bayes estimation method*: the main difference between the Bayes estimation algorithm and traditional methods is whether to combine previous information and Bayes estimation model information. The parameter to be estimated is considered to be a random variable with some previous probability distribution constraints. Sample observation is actually a process in which the previous probability density is converted into a posterior probability distribution by calculation, so that the initial estimated parameters can be corrected from the useful sample information [18].

2.5.2. Artificial Intelligence Methods

(1) *Neural network method*: the neural network has powerful self-learning, self-organization, and self-adaptation capabilities and can simulate complex nonlinear mapping. These neural network functions and powerful nonlinear processing capabilities can perfectly meet the requirements of multisensor data fusion processing [22]. In multiple sensor systems, each environmental information source can provide each environmental information because they have a certain degree of uncertainty, and these uncertainties are fused with other information. The process is actually a process derived from reasoning. The neural network determines its classification index based on the similarity of the samples accepted by the current system. This approach to decision-making is mainly reflected in the network weight and structure distribution [23]. At the same time, it also allows us to use a special neural network learning algorithm to obtain knowledge from the network and obtain the mechanism of inference uncertainty from the network. It uses the self-learning and reasoning functions of the neural network to perform multisensor data fusion.

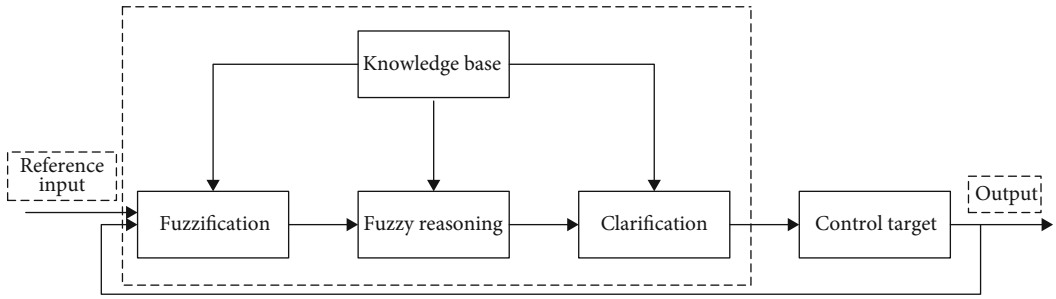

Figure 1: Block diagram of the fuzzy controller.

(2) *Fuzzy logic theory algorithm*: the fuzzy logic theory algorithm is an algorithm for fuzzy general judgment, which simulates the thinking of the human brain. It uses some fuzzy rules to derive key performance indicators, but the key is to construct logical member functions and index functions [24]. In fuzzy reasoning, the subordinate rules are fuzzy rules. The fuzzy input set corresponds to the specific output set through specific functions. This calculation process is a fuzzy inference. In addition, using it with other different types of algorithms can significantly improve the efficiency of information fusion.

The structure diagram of the fuzzy controller is shown in Figure 1:

(3) *Ant colony algorithm*: the ant colony algorithm is a new optimization algorithm inspired by the ant colony behavior in nature. Once the algorithm was proposed, it attracted widespread attention from scholars all over the world and successfully solved many combinatorial optimization problems [25].

The advantages of the ant colony algorithm are as follows: First, it is very robust, and simple modifications to the algorithm can be used to solve other problems. Second, the ant colony algorithm can be combined with some other algorithms for calculation, which can improve the calculation performance of the ant colony algorithm. The flow chart of the ant colony algorithm is shown in Figure 2.

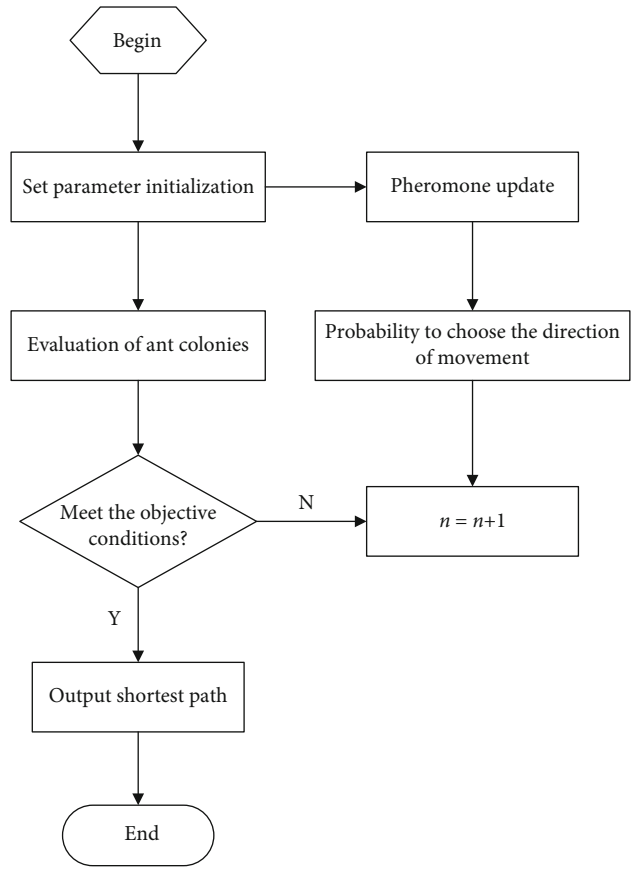

Figure 2: Ant colony algorithm flow chart.

2.6. Comparison of Multisensor Information Fusion Methods

(1) The weighted average method is suitable for low-level data fusion in a dynamic operating environment. The advantage of this method is that there is less information loss and the initial data can be easily merged. The disadvantage is that a suitable mathematical model must be found, and the scope of application is relatively limited

(2) Kalman filtering method is suitable for low-level data fusion in a dynamic operating environment. This information is expressed as a probability distribution with Gaussian noise uncertainty. The advantage is that the amount of information transmitted by the data will not be lost, and the initial data can be easily integrated. The disadvantage is that it needs to build a more accurate mathematical model or know the statistical properties, which limits the scope of application

(3) The Bayes estimation method is suitable for advanced data fusion in a static environment. It is also a way of representing information, which has an unknown probability distribution of Gaussian noise. The advantage is that the theoretical foundation is well supported, so it is easy to understand and implement. The disadvantage is that it is difficult to obtain prior knowledge, which limits its widespread use

(4) The neural network method can run on the bottom data of the dynamic environment or the top data of

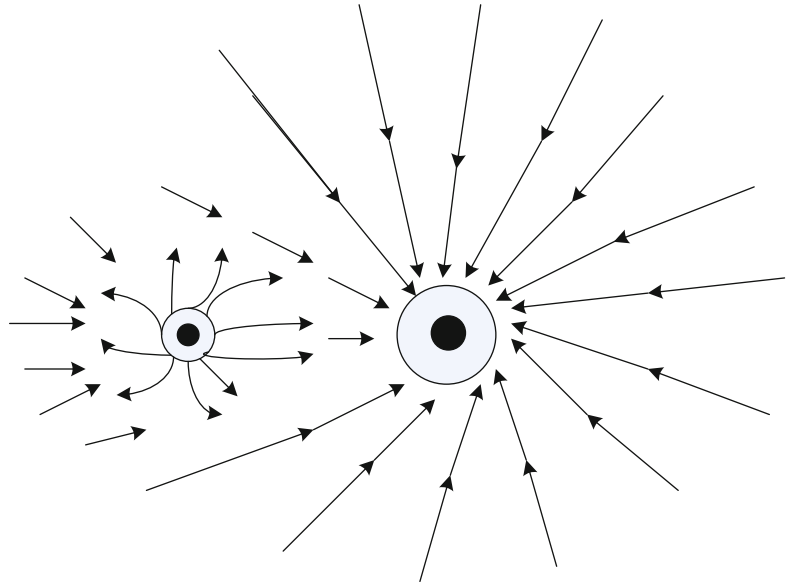

Figure 3: Schematic diagram of artificial potential field.

the static environment. It belongs to the information representation method of the neuron input, and there is the uncertainty of learning errors. The advantage is that the requirements for prior knowledge are not too high or not required, and the ability to adapt is very strong. The disadvantage is the large amount of calculation, and it is difficult to establish effective learning rules

(5) The fuzzy logic theory algorithm is suitable for advanced data fusion in a static operating environment [26], and it is a propositional information expression method with member uncertainty. The advantage is that it can clearly describe the problem, is close to human language habits, and has good scalability. The disadvantage is that the amount of calculation is large

2.7. Path Planning Based on Artificial Potential Field. The basic idea of the artificial potential field is to construct the gravitational potential field of the target point and the repulsive potential field of the obstacle after determining the position of the target point and the obstacle and determining the direction of falling by determining the target position. By finding the descending direction of the combined potential field function of the two possible fields, the best path without collision is determined. The schematic diagram of the artificial potential field is shown in Figure 3:

When the robot moves to the target point, the repulsive force field function generated by the obstacle on the robot is U, and the generated potential energy is related to the distance (d) between the obstacle and the robot. The specific relationship is shown in the repulsive force field function. The form of the field function is

$$U_{\text{rep}}(X) = \begin{cases} \dfrac{K_r}{d}, & d < d_m, \\ 0, & d > d_m. \end{cases} \tag{1}$$

Among them, K_r represents the repulsive force field constant, X represents the position of the robot, Y represents the position of the obstacle, and d_m is the range of influence of the repulsive force field.

The repulsion of obstacles to the robot is generated by the virtual repulsion potential field, and the direction is the negative gradient direction of the repulsion potential field, and its expression is

$$F_{\text{rep}}(X) = -\nabla U_{\text{rep}}(X). \tag{2}$$

When d tends to 0, F tends to infinity, indicating that the robot collides with an obstacle. In order to prevent this from happening, generally set a safety distance threshold d_0; when d tends to d_0, F tends to infinity, and the robot's repulsive force expression is

$$F_{\text{rep}}(X) = \begin{cases} K_r \times \left(\dfrac{1}{(d - d_0)^2} - \dfrac{1}{(d_m - d_0)^2} \right), & d \le d_m, \\ 0, & d > d_m. \end{cases} \tag{3}$$

Gravitation is the attraction of the target point to the robot. As the robot approaches the target, the force will gradually decrease. When the robot is too close to the target, the force tends to zero, which can be ignored. In this article, the gravity field function is considered as

$$U_{\text{rep}}(X) = \frac{1}{2} K_a \cdot d^2. \tag{4}$$

Among them, K_a is the gravitational potential field constant, and the response gravitation generated by the gravitational field is

$$F_{\text{att}}(X) = -\nabla U_{\text{att}}(X). \tag{5}$$

Resynthesize (1) which is the expression of the gravitation on the robot:

$$F_{\text{att}}(X) = K_a \cdot d. \tag{6}$$

The direction of gravity is from the robot to the target point.

The resultant potential field of the robot's running space is the combination of the gravitational field and the repulsive field experienced by the robot. According to the superposition principle of the potential field, the expression of the whole situation field is obtained as

$$U(X) = U_{\text{att}}(X) + U_{\text{rep}}(X). \tag{7}$$

The resultant force experienced by the robot is shown in

$$F(X) = -\nabla U(X) = -\nabla U_{\text{att}}(X) - \nabla U_{\text{rep}}(X) = F_{\text{att}}(X) + F_{\text{rep}}(X). \tag{8}$$

2.8. Realization of Ant Colony Optimization Algorithm and Path Planning. There are two core problems in the ant colony optimization algorithm, ant coding and fitness function construction. For coding, the distance between the planning origin point and the planning target point is divided into $D+1$ equal parts along the X axis, and the ordinate value is the ant code. Assume that the total number of ants is n. The process ant colony optimization algorithm is described in path planning:

Objective function:

$$f(x, y) = \min f(x, y). \tag{9}$$

This is the path length. When moving, $\text{ant}_k k\,(1, 2, \cdots, n)$ determines the next transmission direction based on the amount of information. At time t, the corresponding probability of the ant from position i to position j is shown in

$$p_{ij}^k = \begin{cases} \dfrac{\tau_{ij}^{\alpha}(t) \cdot \eta_{ij}^{\beta}(t)}{\sum_{r \in S^K}^{n} \tau_{ir}^{\alpha}(t) \cdot \eta_{ir}^{\beta}(t)}, & j \in S_i^K, \\ 0, & j \notin S_i^K. \end{cases} \tag{10}$$

Among them, $\eta_{ij}(t)$ is a local heuristic function, the parameters α and β are used to modify the $\tau_{ij}(t)$ and $\eta_{ij}(t)$ for the weight of the entire mobile probability effect, and S_i^K is the feasible region of position i at time K, and the feasible region is updated in the iterative process.

$$\Delta\tau_{ji}(t) = \frac{1}{f(x_i, y_i)}. \tag{11}$$

It is the relative path length.

$$\tau_{ij}(t+1) = \rho \cdot \tau_{ij}(t) + \Delta\tau_{ij}(t). \tag{12}$$

ρ is the coefficient of pheromone volatilization, which is 0.8 in this article. Over time, the update formula is

$$\tau_{ij}(t+1) = \rho \cdot \tau_{ij}(t) + \sum_{k=1}^{n} \tau_{ij}^k. \tag{13}$$

Among them, $\Delta\tau_{ij}^k$ is the amount of information left by k ant; if the ant passes (i, j) in the k-th cycle, then

$$k\Delta\tau_{ij}^k = \frac{\tau_{ij}^0}{L_k}. \tag{14}$$

L_k is the total length of all paths in the k-th cycle, or $\Delta\tau_{ij}^k = 0$.

3. Experiments on Software Design and Research of Intelligent Sensor Robot System Based on Multidata Fusion

3.1. Examples of Multisensor Fusion Robots. At present, intelligent mobile robots basically have visual sensors, tactile sensors, ultrasonic sensors, and infrared sensors through fusion methods. One of the key technologies is to improve the ability of mobile robots to avoid obstacles under sensor data. Some examples of multisensor fusion for mobile robots are shown in Table 1.

3.2. Obstacle Avoidance Experiment

3.2.1. Static Obstacle Avoidance Experiment of Dynamic Window Method. The static obstacle avoidance experiment of the mobile chassis is completed based on the dynamic window method. The mobile chassis will drive forward and will change the driving direction when encountering obstacles, thus avoiding static obstacles and reaching the designated position. During the test, the average running speed of the mobile chassis was 0.29 m/s, and the average time was 30 s. The static obstacle avoidance physical map of the dynamic window method is shown in Figure 4 (the process is from left to right):

3.2.2. Dynamic Window Method Dynamic Obstacle Avoidance Experiment. When the dynamic windowing method is used for local route planning, it is impossible to predict the trajectory of the moving object and replan the route, and it is difficult to deal with dynamic obstacles. When the dynamic target completely blocks the path of the moving chassis, the moving chassis will detect the obstacle, replan the path, and then move backward to avoid encountering obstacles when turning. It can be concluded that the dynamic window method has limitations for the obstacle avoidance of dynamic targets. During the test, the average running speed of the mobile chassis was 0.23 m/s, and the average time was 35 s. The dynamic obstacle

Table 1: Multisensor fusion robot example.

Robot	Sensor type	Fusion technology
HILARE	Sound, vision, laser ranging	Weighted average
DARPA	Vision, sonar, laser ranging	Small range average increase
Stanford	Semiconductor laser, tactile, ultrasonic	Kalman filtering
RANGER	Semiconductor laser, tactile, ultrasonic	Jacobian tensor and Kalman filtering
LIAS	Ultrasonic, infrared	Multiple fusion
Alfred	Sonar, sound, color camera	Logical reasoning
ANFM	Camera, infrared, ultrasonic, GPS	Neural networks

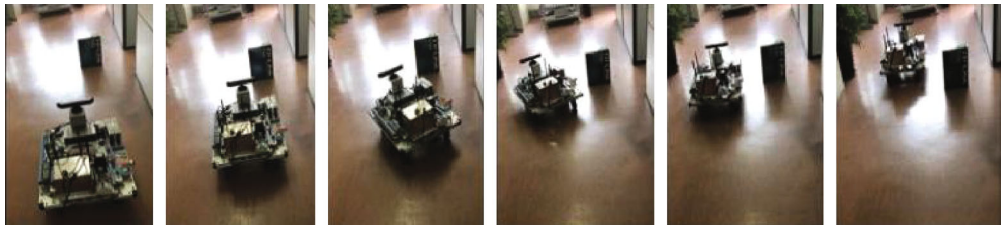

Figure 4: The physical image of static obstacle avoidance based on dynamic window method. (This picture begins with "Research on Mobile Robot System Design and Map Navigation Based on Multisensor Fusion.")

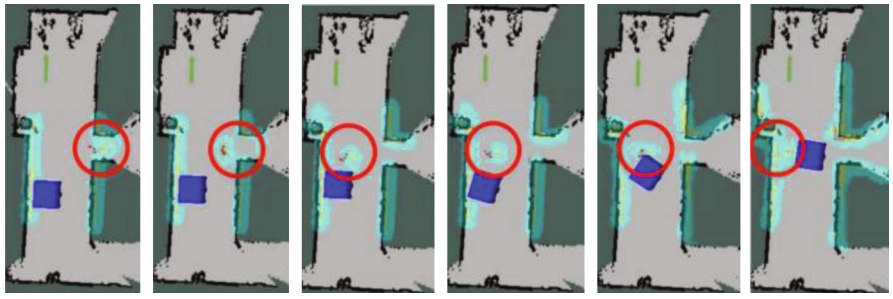

Figure 5: Dynamic obstacle avoidance based on dynamic window method. (This picture begins with "Research on Mobile Robot System Design and Map Navigation Based on Multisensor Fusion.")

avoidance diagram based on the dynamic window method is shown in Figure 5 (the process is from left to right).

3.2.3. Dynamic Obstacle Avoidance Experiment Based on Artificial Potential Field Method. In the human-in-field method, the extracted dynamic obstacle model is used to add the speed term of the obstacle to the method, and the dynamic obstacle avoidance experiment is carried out. The experimental conditions are basically the same as the dynamic window method. The mobile chassis predicts the trajectory of the pedestrian based on the speed of the pedestrian and determines in advance whether a collision will occur, and the local path planning will change the trajectory of the robot in real time to achieve the goal of dynamic obstacle avoidance. During the test, the average running speed of the mobile chassis was 0.23 m/s, and the average time was 29 s. The physical map of dynamic obstacle avoidance based on the improved artificial potential field method is shown in Figure 6 (the process is from left to right).

See Table 2 for the analysis and comparison of the above three groups of mobile chassis obstacle avoidance experiments. It can be seen from the table that the dynamic window method has a good effect when applied to static obstacle avoidance and can meet the requirements of normal use, but it is not well applied in dynamic obstacle avoidance, the path planning efficiency is low, and there is a risk of collision. The artificial potential field method can successfully predict the trajectory according to the moving speed of the obstacle and plan the possible collision path in advance. Compared with the dynamic window method, it greatly improves the success rate and efficiency of obstacle avoidance.

4. Software Design Research of Intelligent Sensor Robot System Based on Multidata Fusion

4.1. Intelligent Robot Obstacle Avoidance System. Sensors are the main tool that connects the robot with the external

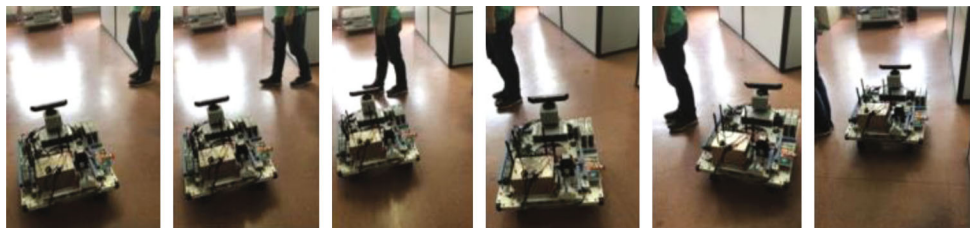

Figure 6: Dynamic obstacle avoidance based on improved artificial potential field method. (This picture begins with "Research on Mobile Robot System Design and Map Navigation Based on Multisensor Fusion.")

Table 2: Obstacle avoidance experiment comparison.

Experimental scene	Local path planning method	Success rate	Moving chassis speed	Average running time
Static obstacle avoidance	Dynamic window method	80%	0.29 m/s	30 s
Dynamic obstacle avoidance	Dynamic window method	40%	0.23 m/s	35 s
Dynamic obstacle avoidance	Improved artificial potential field method	90%	0.23 m/s	29 s

Table 3: Ultrasonic sensor test data.

Actual distance (m)	0.3	0.4	0.6	0.7	0.9	1.4	1.9	2.0
Test distance (m)	0	0.389	0.588	0.679	0.888	1.378	1.898	1.967
Actual distance (m)	2.4	2.8	3.3	4.0	4.6	5.0	5.5	6.0
Test distance (m)	2.365	2.766	3.279	3.999	3.554	4.964	5.454	6.098

environment, and the choice of sensors is the most important for realizing the autonomous movement of intelligent robots. The intelligent robot platform is equipped with 4 ultrasonic sensors and 2 infrared sensors, both of which can realize the ranging function. The ultrasonic sensor has a wide range and cannot detect obstacles at close range. Infrared sensors can make up for the shortcomings of ultrasonic sensors that cannot be detected at close range. Therefore, in this chapter, we mainly study how to use ultrasonic and infrared sensors to avoid obstacles.

4.1.1. Ultrasonic Sensor. Ultrasonic sensors are widely used as noncontact distance measurement sensors. The working principle is that the ultrasonic transmitter emits a pulse signal of a specific frequency in a specific direction. When an obstacle is encountered, the pulse signal is reflected and received by the receiving end. The reflected signal can calculate the distance from the transmitting end to the obstacle by measuring the time difference from transmission to reception and the propagation speed of ultrasonic waves in the medium. Since the working environment of the robot is indoors, the sound wave propagates in the medium at a speed of 340 m/s under the condition that the accuracy of the distance measurement is not high. The distance measurement experiment is performed on a single ultrasonic sensor at room temperature. The experimental test results are shown in Table 3.

The above results are all tested in an ideal experimental environment. The difference between the actual distance and the test distance is very small. When the robot is in motion or the environment is not ideal, the measurement results have greater uncertainty.

Table 4: Infrared sensor characteristics.

GP2Y0A02YK0F parameters	
Distance measurement range	20-140 cm
Output type	Analog voltage
Package dimensions	$28.5 \times 12 \times 12.5$ mm
Current consumption	22 MA
Voltage	4~5 V

4.1.2. Infrared Sensor. The infrared sensor system is a measurement system that uses infrared as the medium. It has the advantages of simple operation, fast measurement speed, and high accuracy. It is widely used in various fields of daily life, especially in the field of robotics, as a distance sensor. In order to reduce the cost of the experiment and improve the accuracy of the system, we carried out the infrared sensor circuit design, carried out the ranging experiment at the same time, and calculated the accuracy of the infrared sensor, laying the foundation for multisensor data fusion.

When the infrared sensor emitted by the infrared sensor encounters an obstacle, it will be reflected to the sensor's receiving head. During this process, the counter will detect the number of clock pulses passed to obtain the distance between the robot and the front of the obstacle. The sensor selected in this article must provide a voltage output proportional to the measured distance. The infrared sensor is a

Table 5: Infrared sensor ranging experiment data.

Actual distance (m)	0.3	0.4	0.6	0.7	0.9	1.4	1.9	2.0
Test distance (m)	0	0.419	0.688	0.699	0.918	1.398	1.888	1.997
Actual distance (m)	2.4	2.8	3.3	4.0	4.6	5.0	5.5	6.0
Test distance (m)	2.335	2.774	3.265	3.976	3.577	4.988	5.464	6.045

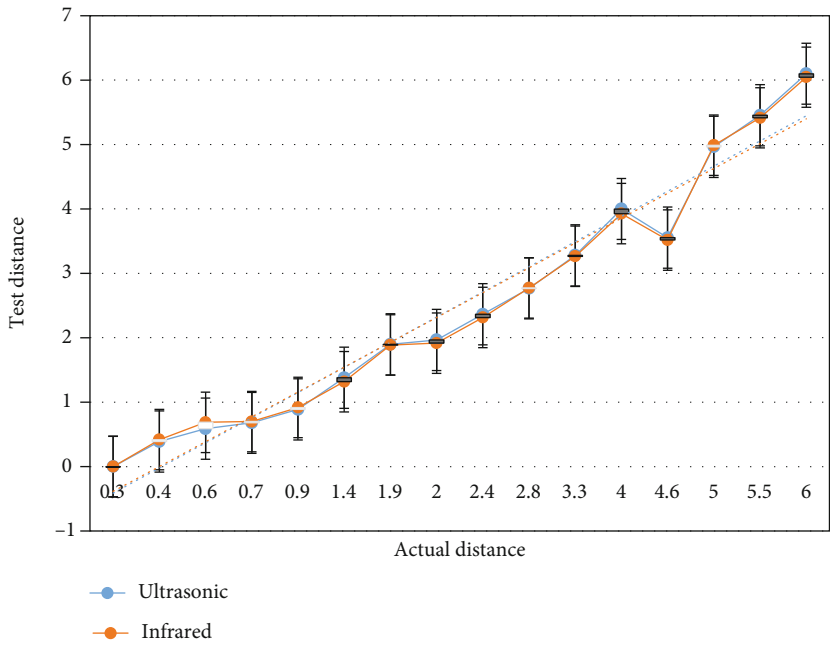

Figure 7: Comparison of actual distance and test distance between ultrasonic sensor and infrared sensor.

Sharp GP2Y0A02YK0F analog distance sensor. The main characteristics of the infrared sensor are shown in Table 4.

Since the working environment of the robot is indoors, the sound wave propagation speed in the medium is 340 m/s under the condition that the accuracy of the distance measurement is not high. The distance measurement experiment is carried out on a single infrared sensor at room temperature. The experimental test results are shown in Table 5.

4.2. Ultrasonic Sensors and Infrared Sensors. Through the above experimental analysis, it can be concluded that whether it is an ultrasonic sensor or an infrared sensor, the error between their test distance and the actual distance is very small. From Tables 3 and 5, we can get that the minimum error between the test distance and the actual distance is 0.001.The comparison between the actual distance and the test distance between the ultrasonic sensor and the infrared sensor is shown in Figure 7.

5. Conclusion

This paper studies the software design of an intelligent sensor robot system based on multidata fusion, preprocessing the environmental information data collected from each sensor of the robot, processing and fusing the data collected from each sensor, and planning the movement path of the robot. Simulating and preprocessing data collected from sensors using ant colony optimization algorithms can significantly improve the accuracy and effectiveness of the data. The ant colony algorithm can perform fusion and path planning and speed up fusion based on ensuring accuracy. Finally, in the obstacle avoidance experiment of intelligent robots, we can conclude that multisensor data fusion technology is very necessary for intelligent robots, because we can make intelligent robots avoid obstacles through ultrasonic sensors and infrared sensors.

Data Availability

No data were used to support this study.

Conflicts of Interest

There are no potential competing interests in our paper.

Authors' Contributions

All authors have seen the manuscript and approved to submit it to this journal.

Acknowledgments

This work was supported by the Institutional Foundation of the First Affiliated Hospital of Xi'an Jiaotong University (No_2018RKX-08).

References

[1] D. Zhou, K. Zhang, A. Ravey, F. Gao, and A. Miraoui, "Online estimation of lithium polymer batteries state-of-charge using particle filter-based data fusion with multimodels approach," *IEEE Transactions on Industry Applications*, vol. 52, no. 3, pp. 2582–2595, 2016.

[2] M. Su and X. Zhang, "95.3D data model acquisition of binocular vision medical instrument based on multi data fusion," *Boletin Tecnico/Technical Bulletin*, vol. 55, no. 20, pp. 667–672, 2017.

[3] K. A. Semmens, M. C. Anderson, W. P. Kustas et al., "Monitoring daily evapotranspiration over two California vineyards using Landsat 8 in a multi-sensor data fusion approach," *Remote Sensing of Environment*, vol. 185, no. 185, pp. 155–170, 2016.

[4] A. R. Di Rosa, F. Leone, C. Scattareggia, and V. Chiofalo, "Botanical origin identification of Sicilian honeys based on artificial senses and multi-sensor data fusion," *European Food Research & Technology*, vol. 244, no. 2, pp. 1–9, 2017.

[5] S. DAS, S. BARANI, S. WAGH, and S. S. SONAVANE, "Extending lifetime of wireless sensor networks using multi-sensor data fusion," *Sādhanā*, vol. 42, no. 7, pp. 1083–1090, 2017.

[6] L. Jiang, L. Yan, Y. Xia, Q. Guo, M. Fu, and K. Lu, "Asynchronous multirate multisensor data fusion over unreliable measurements with correlated noise," *IEEE Transactions on Aerospace & Electronic Systems*, vol. 53, no. 99, pp. 2427–2437, 2017.

[7] M. Bouain, K. M. A. Ali, D. Berdjag, N. Fakhfakh, and R. B. Atitallah, "An embedded multi-sensor data fusion design for vehicle perception tasks," *Journal of Communications*, vol. 13, no. 1, pp. 8–14, 2018.

[8] Z. Xing and Y. Xia, "Comparison of centralised scaled unscented Kalman filter and extended Kalman filter for multi-sensor data fusion architectures," *IET Signal Processing*, vol. 10, no. 4, pp. 359–365, 2016.

[9] M. Zhou, Y. Li, M. J. Tahir, X. Geng, Y. Wang, and W. He, "Integrated statistical test of signal distributions and access point contributions for Wi-Fi indoor localization," in *IEEE Transactions on Vehicular Technology*, p. 1, 2021.

[10] P. Ferrer-Cid, J. M. Barcelo-Ordinas, J. Garcia-Vidal, A. Ripoll, and M. Viana, "Multisensor data fusion calibration in IoT air pollution platforms," *IEEE Internet of Things Journal*, vol. 7, no. 4, pp. 3124–3132, 2020.

[11] P. Shan, H. Lv, L. Yu, H. Ge, Y. Li, and L. Gu, "A multisensor data fusion method for ball screw fault diagnosis based on convolutional neural network with selected channels," *IEEE Sensors Journal*, vol. 20, no. 14, pp. 7896–7905, 2020.

[12] A. Reyana and P. Vijayalakshmi, "Multisensor data fusion technique for energy conservation in the wireless sensor network application "condition-based environment monitoring"," *Journal of Ambient Intelligence and Humanized Computing*, vol. 13, pp. 1–10, 2021.

[13] Y. Yang, "Research on house price prediction based on multi-dimensional data fusion," *International Journal of Advanced Network Monitoring and Controls*, vol. 5, no. 1, pp. 1–8, 2020.

[14] H. Zhang and T. Zhang, "Parallel processing method of inertial aerobics multisensor data fusion," *Mathematical Problems in Engineering*, vol. 2021, no. 4, p. 11, 2021.

[15] R. Liu, K. Greve, P. Cui, and N. Jiang, "Collaborative positioning method via GPS/INS and RS/MO multi-source data fusion in multi-target navigation," *Survey Review*, vol. 1, pp. 1–11, 2021.

[16] G. Muniandi, "Train distance and speed estimation using multi sensor data fusion," *IET Radar, Sonar, Navigation*, vol. 13, no. 4, pp. 664–671, 2019.

[17] S. Liu, D. Zhang, and J. Li, "Study on traffic multi-source data fusion," *International Journal of Cognitive Informatics and Natural Intelligence*, vol. 13, no. 2, pp. 63–75, 2019.

[18] G. Gong and H. Zhu, "A portable embedded explosion gas detection and identification device based on intelligent electronic nose system," *Sensor Review*, vol. 36, no. 1, pp. 57–63, 2016.

[19] A. L. Zhou and D. C. Wang, "Analysis of intelligent casting and present status and key technology of robot application[J]," *Zhuzao/Foundry*, vol. 67, no. 1, pp. 11–13, 2018.

[20] S. Hamaza, I. Georgilas, M. Fernandez et al., "Sensor installation and retrieval operations using an unmanned aerial manipulator," *IEEE Robotics and Automation Letters*, vol. 4, no. 3, pp. 2793–2800, 2019.

[21] S. Sridhar and A. Eskandarian, "Cooperative perception in autonomous ground vehicles using a mobile-robot testbed," *IET Intelligent Transport Systems*, vol. 13, no. 10, pp. 1545–1556, 2019.

[22] W. Ihn-Sik and L. Soon-Geul, "Intelligent robotic walker with actively controlled human interaction," *ETRI Journal*, vol. 40, no. 4, pp. 522–530, 2018.

[23] N. T. Burkhard, M. R. Cutkosky, and S. J. Ryan, "Slip sensing for intelligent, improved grasping and retraction in robot-assisted surgery," *IEEE Robotics & Automation Letters*, vol. 3, no. 4, pp. 4148–4155, 2018.

[24] H. Jian, Y. Xiaoqiang, T. Chunjing, and School of Automation, "Research on intelligent gait detection based on wireless wearable sensor system," *Huazhong Keji Daxue Xuebao (Ziran Kexue Ban)/Journal of Huazhong University of Science and Technology (Natural Science Edition)*, vol. 45, no. 10, pp. 105–110, 2017.

[25] A. A. Mohammed, I. Aris, M. K. Hassan, and N. A. Kamsani, "New algorithm for autonomous dynamic path planning in real-time intelligent robot car," *Journal of Computational and Theoretical Nanoscience*, vol. 14, no. 11, pp. 5499–5507, 2017.

[26] M. Zhou, Y. Wang, Y. Liu, and Z. Tian, "An information-theoretic view of WLAN localization error bound in GPS-denied environment," *IEEE Transactions on Vehicular Technology*, vol. 68, no. 4, pp. 4089–4093, 2019.

Hindawi
Journal of Sensors
Volume 2021, Article ID 7021151, 11 pages
https://doi.org/10.1155/2021/7021151

Research Article

Intelligent Perception System of Big Data Decision in Cross-Border e-Commerce Based on Data Fusion

Xiaheng Zhang,[1,2] Dongpeng Xu,[3] and Lin Xiao[2]

[1]*College of Business and Trade, Nanchang Institute of Science and Technology, Nanchang, 330108 Jiangxi, China*
[2]*Management School, Northwest University of Political Science and Law, Xi'an, 710122 Shaanxi, China*
[3]*Faculty of Finance, City University of Macau, Macao, 999078 Macao, China*

Correspondence should be addressed to Dongpeng Xu; f20092100138@cityu.mo

Received 29 April 2021; Revised 28 May 2021; Accepted 12 June 2021; Published 25 June 2021

Academic Editor: Mu Zhou

There is a gap between supply and demand in cross-border e-trading platforms. The so-called supply and demand gap refers to the existing good companies that cannot meet the needs of buyers. Cross-border e-commerce, the buyer's purchase demand is often included in the buyer's behavior, such as searching for goods by pressing buttons, clicking price, category and other means, and on-site delivery time. It is important for CBEC to analyze the buyer's needs to protect the procurement and provide the seller with reference to supply, so as to solve the supply and demand gap between the buyer and the seller. This paper mainly studies the CBEC big data decision intelligent perception system based on data fusion. It is the same as the innovation process of better application of data fusion to the e-commerce business model. At the same time, the key technologies of data extraction, conversion, data warehouse, and front-end display in the system construction are analyzed and designed. This paper mainly uses data fusion algorithm, data fusion network model, quaternion method, big data decision intelligent sensing system framework design experiment, and CBEC user experiment to study the CBEC big data decision intelligent sensing system based on data fusion, and also with the development of CBEC, I hope more people can participate in CBEC practice. The results show that with the increase of data volume of the CBEC platform from 2016 to 2020, the construction of the CBEC platform business of big data production intelligent perception system considers the situation of users from seven aspects. With the increase of consumption, domestic consumers are increasingly pursuing a better life, cross-border import e-commerce ushered in a great development era.

1. Introduction

Cross-border e-commerce is an important part of Internet services. With the development of the Internet, CBEC has been extended to all aspects of the economy and society, as well as its impact on the manufacturing industry, and other industries are becoming more and more important. Internet users have become a common behavior to shop through the CBEC platform. The basic function of the CBEC platform is to provide a platform for the buyer and seller to trade on the Internet. The criteria to evaluate whether the CBEC platform can provide users with good service include user satisfaction and user experience after-sales service. One of the most important aspects is that the seller users can provide the goods that the buyer users want to buy. Users usually use the search engine of the CBEC platform to search for the items they want to buy and then select the items that meet the users' wishes to purchase in the search results. If users cannot search for the goods they want to buy on the platform, they will give up their willingness to purchase this time or switch to other CBEC platforms for purchase. In order to solve this practical problem, it is necessary to analyze the supply and demand of all goods on the platform on the CBEC platform and solve the problem of asymmetric information between buyer and seller users through supply and demand analysis.

In the current situation of explosive growth of Internet data, it is required that the Internet industry store and process data efficiently. Every day, the CBEC platform will produce a large number of data, such as user behavior data,

transaction data, updated goods information, user information, and customer service information. When these data are stored, there is a need for an efficient platform for data extraction and analysis. According to statistics, the data volume in 2014 will reach 4zb, and 34% of the general data of the Internet can be understood and applied, which has a high utilization value. These data are obtained through CBEC, social networks, video, and entertainment. However, only about 7% of these valuable data are effectively used, and such information has high analytical value. Of all data, only 1 percent of the data is analyzed.

With the development of big data and cloud computing, the consumption of data storage resources and computing cost has been greatly reduced. The construction of these databases has been improved, and data storage is not the main problem in the era of big data. When data acquisition is more and more, how to use data effectively becomes one of the most important problems. Liao et al. believe the results of the 2014 data fusion competition organized by the IEEE Society for image analysis and data fusion technology committee. As in previous years, the technical committee of the space debris federation organized a data fusion contest aimed at fostering new ideas and solutions for multisource remote sensing research. The founders considered the fusion of multiresolution and multisensor between optical data with 20 cm resolution and long-wave infrared hyperspectral data of 1-meter resolution. The competition was proposed as a two-track race: one goal was accurate land cover classification, and the other was to seek innovation in the fusion of thermal hyperspectral and color data, but lack of specific data [1]. Semmens et al. believe that the fusion method of big data sensor estimates the evapotranspiration of vineyards. Combining with Landsat 8, MODIS, goes data, the estimated value of ET of field size is provided. The simulated surface energy flux is in good agreement with the ground flux measurement value, and the spatial distribution of ET is consistent with the output estimation. Therefore, the early inference may be due to the coverage of crops between vines, but the necessary experimental data is not available [2]. Bareinboim and Pearl believe that the concept, principles, and tools of current causal analysis methods are unified, and the new challenges brought by big data are concerned. In particular, the data fusion and merging of the problem data we solve are collected in different conditions to obtain effective answers but lack of numerical analysis content [3]. Berkow et al. think that the performance measurement of the trunk line is the key problem of traffic system management, traveler information, and real-time situation-aware routing. In many urban areas, the latest information on the state of the motorway is available, taking into account the large number of trips that have taken place on these facilities. Since nearly 40 percent of the mileage of vehicles in the United States occurs on the main road, similar information is required, which is not only available for travelers but also available for traffic engineers and managers. Since many main roads are equipped with drive traffic lights, it has been explored to use installed sensors as a source of traffic volume, occupancy, or speed data to inform the main road performance system. With this in mind, it is possible to take advantage of the availability of mobile detector geolocation data, which include automated vehicle positioning systems for buses or taxi fleets, or mobile phones or other GPS-type equipment. Demonstrate the potential value of fusing fixed and mobile monitoring system data, but some of the discussions are not accurate [4].

The innovation of this paper is to study the intelligent perception system of CBEC big data decision-making based on data fusion, such as data fusion algorithm, data fusion network model, quaternion method, and big data decision intelligent perception system design experiment and CBEC user experiment, and at the same time, it is aimed at encouraging more entrepreneurs to join CBEC. The research on the decision-making of the CBEC model can help cross-border enterprises choose the right business model, reduce the possibility of decision-making mistakes, and improve the success rate of CBEC business [5].

2. Data Fusion Algorithm

2.1. Data Fusion. Data fusion in business big data is a process of getting more accurate description of the fusion information of perceived objects through a certain rule, intelligent analysis of multilevel optimization, and finally, the user's needs are completed [6]. In business big data, the perceived information obtained by data fusion technology is usually more persuasive than the data collected and analyzed by a node. Data fusion can ensure the accuracy of perceived data, reduce the network data traffic and reduce redundant data in the network, and play an important role in making reasonable decision-making for application [7, 8]. In the big business data, the energy of nodes is limited. Multidimensional data collected from different nodes can be aggregated by using data fusion technology, so as to eliminate redundant data and reduce the data communication volume in the network to reduce the energy loss [9]. Data fusion technology can be combined with a variety of technologies: data fusion is often combined with clustering technology of topology. When cluster head collects data collected in cluster, it will be fused, and the fusion results will be transmitted to base station. Decision big data fusion by base station can be shown in Figure 1.

2.2. Data Fusion Network Model

2.2.1. Communication Energy Consumption Model. KPCA can change some nonlinear data into linear data by dimension increasing, which solves the problem that PCA cannot effectively extract principal components when dealing with some nonlinear problems [10]. Meanwhile, due to the nonlinear transformation, KPCA may extract more principal components than PCA, which can be expressed as the loss of energy E when a node transmits n bit data to a node whose distance is

$$E(n, a) = E \times n + \varepsilon \times n \times a^2, \tag{1}$$

where e is the unit of transmission (sending or receiving) and the energy lost by the node when bit data is transmitted; M is the power amplification factor of the free space transmission

Figure 1: Internet edge computing (http://alturl.com/qfxtf).

model; M is the power amplifier factor of the multipath attenuation model; a is the threshold, when $a < A$; the spatial transmission model has been adopted; otherwise, the multidimensional suppression transmission model should be adopted [11, 12]. On the contrary, the calculation formula for the energy loss of a bit data received by the receiving node is as follows:

$$H = aE. \tag{2}$$

In addition, the calculation of threshold satisfies the formula:

$$A = \sqrt{\frac{m}{M}}. \tag{3}$$

2.2.2. Optimal Number of Cluster Heads. Suppose that there are m randomly deployed sensor nodes in the $H = a * a$ monitoring area, a is the number of cluster head nodes in the network, that is, the number of clusters, and the energy consumed by data fusion is f [13]. Then, the energy consumption of each round of cluster head in the network is expressed as

$$F = n \times E\left(\frac{M}{a} - 1\right) + n \times \frac{M}{a} + n \times \varepsilon b^2, \tag{4}$$

where B is the average distance from the cluster head to the base station, and B is calculated as follows:

$$b = \iint_s \sqrt{x^2 + y^2}\,\frac{1}{s}\,dxdy. \tag{5}$$

For the completion time of the task, it is not only related to the upload completion time of edge calculation but also related to whether the previous upload edge calculation is completed [14].

2.2.3. The Design of Ceoda Algorithm. According to the ratio of the residual energy to the average residual energy in each region, the nodes are divided into candidate cluster head nodes and common nodes. Candidate cluster head nodes participate in cluster head election. Using the idea of fuzzy logic, the input variables are the average residual energy of the node, the distance from the node to the receiver, and the number of neighbors around the node, the opportunity value of all candidate cluster head nodes is calculated in this round, and the more appropriate cluster head node is selected [15]. The energy consumption E and the whole network of a complete cluster in each round can be calculated; the energy consumption of each round W is expressed as

$$E = W + \left(\frac{M}{a} - 1\right)E. \tag{6}$$

Therefore, by minimizing E and making its derivative to a 0, the optimal number of cluster heads n is calculated, which is expressed as follows:

$$n = \sqrt{\frac{M}{2\pi}}\frac{A}{b}. \tag{7}$$

In the range of N, the more neighbor nodes a, the more extensive the information collected and the wider the information coverage, so it is more suitable to be elected as cluster

Figure 2: Internet business big data (http://alturl.com/xtpfp).

head node. The minimum radius of N ideal cluster is calculated as follows:

$$N = \sqrt{\frac{A}{\pi \times a}}. \tag{8}$$

When sampling data arrives at a specific time slot, an adjustable data similarity ratio C is set at F. The selection strategy is as follows:

$$f \le h + h \times (1 - c). \tag{9}$$

F is the actual monitoring data of a node in a cluster in the current time. H and C represent the maximum and minimum monitoring values of adjacent common nodes, respectively [16].

2.3. Big Data. Big data, as a hot topic in academic research, has attracted the full attention of experts and scholars around the world, and the relevant analysis and research literature have increased year after year [17, 18]. Foreign countries have made in-depth research on the following three aspects, including the basic theory of big data. It usually focuses on the origin and development, basic definition, main characteristics, and basic structure of big data. The characteristics of big data are as follows: large volume, many kinds, and poor accuracy; the reason why big data has attracted more and more attention is that it has great social influence and significance in terms of cultural tradition, professional technology, academic status, and data and information research and analysis; the traditional data information collection, data information acquisition, data information research and analysis, and data information application technology cannot meet the demand [19]. Analysis and research on the quality of big data, there are a lot of low-quality data information in large-scale data databases and the Internet. Big data is shown in Figure 2.

For big data problems, we can use the data preprocessing to deal with and solve the problem of big data quality. The experimental model of big data quality obtained by a kind of operation process can be used to ensure the selection and adaptation of data quality, the evaluation of comprehensive quality of big data, and the analysis and research of reference standards [20].

2.4. Data Fusion Quaternion Method. The quaternion theory is to transform the dynamic measurement problem which is inconvenient to measure into the change mode of the object rotating around the fixed point easily. According to the above definition of quaternion, the quaternion G can be converted into the following form:

$$G = g_0 + g_1 i + g_2 j + g_3 k. \tag{10}$$

Its fixed-point rotation can be described as the rotation of a coordinate or a vector relative to a certain coordinate system:

$$G = \sin i \cos a + \sin j \cos \beta. \tag{11}$$

Table 1: The field meaning of filtering extraction.

Protocol type	Key field	Field meaning	Purpose
Radius	0x0608	Broadband account	Identify user
Http	Network layer	User's public IP	Matches broadband
	Host	Host domain name	User identity
	User agent	User description	Terminal

Table 2: User identity key steps.

Serial number	Step
1	DPI data cleaning
2	Protocol analysis
3	Message suffix filtering
4	Broadband account extraction of radius message
5	Unified decoding
6	Basic message information

Indicates the direction of rotation of the instantaneous shaft, therefore, quaternion can not only represent the direction of rotation of the rotation axis but also represent the size of the rotation angle. Now, this rotation relationship is expressed by the following operation methods:

$$H^a = GH^nG^a. \tag{12}$$

In order to make the filtering algorithm suitable for the nonlinear system, it is necessary to improve it to a certain extent. The Kalman filter has the function of simple algorithm and easy implementation, so either the classical Kalman filter algorithm or the improved extended and unscented Kalman filter algorithm will be applied in various fields, such as navigation guidance, target tracking, and integrated navigation. Let the state equation and measurement equation of the stochastic discrete system at k time be

$$H_k = F_kX_k + W_k. \tag{13}$$

The general solution process of the Kalman filter algorithm is as follows:

$$Y_{k,k-1} = \varphi_{k,k-1}Y_{k,k-1}. \tag{14}$$

State estimation equation:

$$Y_{k,k-1} = Y_{k,k-1} + K_k(F_k - W_kY_{k,k-1}). \tag{15}$$

3. Related Experiments of CBEC Big Data Decision-Making Intelligent Perception System

3.1. Cross-Border e-Commerce. Cross-border e-commerce is derived from CBEC, personal purchase, and other modes. With the development mode of different conditions becoming more and more mature, China's CBEC market is also gradually evolving, which makes researchers explore it from the development process, development ideas, and other aspects. The problems and countermeasures in the development process show that China's e-commerce has broad prospects and great potential, but the development of cross-border logistics is slow. It has seriously restricted the further development of cross-border trade and new logistics, while foreign warehouses are emerging. With the development of the times, it can solve many problems that traditional cross-border logistics cannot solve, such as time-consuming, high cost, and heavy custom clearance. Cross-border e-commerce enterprises also face some problems in using foreign warehouses. For example, the wrong choice of foreign storage facilities and the operation mode of CBEC companies have brought many obstacles to the future operation.

3.2. Cross-Border e-Commerce User Identity Keywords. For a large-scale data analysis system, because there is a lot of unnecessary information in the local broadband business data, in order to meet certain strategic needs, the required data must be deleted for effective data analysis to ensure the accuracy and efficiency of extraction. Most broadband users' network traffic is DPI, which is used to analyze data packets and extract relevant information, evaluate the type of packet protocol, and filter and delete packets other than HTTP and nonbeam, such as FTP, DNS SMTPitp and Nast. Then, other HTTP packets are analyzed through HTTP application layer messages, and fields such as URI, host, UA, refer, cookie, and content are downloaded. The meaning of the extracted fields is shown in Table 1.

For example, in the URI field, ICT, GIF, PNG, JS, JPEG, CSS, and other formats are used as extensions to require image resources and website styles. Since the traffic data are all requests of users for unified data resources, they do not contain enough information about the user's identity, so it is useless to extract the user's identity information, as shown in Table 2.

3.3. Big Data Decision Intelligent Perception System Framework. On the basis of the unique advantages of having more complete user online shopping traffic than other CBEC platforms, operators provide broadband users with personal online shopping recommendation, which not only provides reliable traffic promotion methods for operators but also provides high-quality data services for home broadband users, which has far-reaching significance and value in the field of CBEC [21, 22]. Through the analysis and mining of home broadband user traffic, and through a series of operations such as user feature extraction based on deep packet analysis,

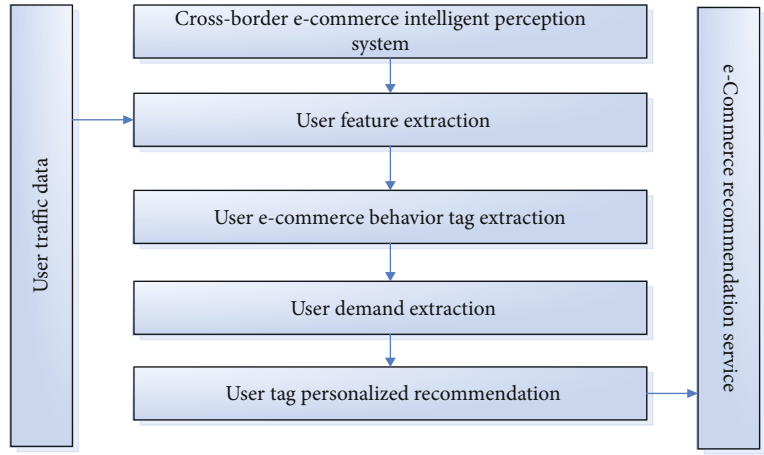

Figure 3: Platform user management module.

Table 3: Ranking of cross-border e-commerce platforms in China.

Popularity	e-Commerce platform
1	Tmall global
2	NetEase koala
3	JD global
4	Little red book
5	Ocean terminal
6	Vipin international

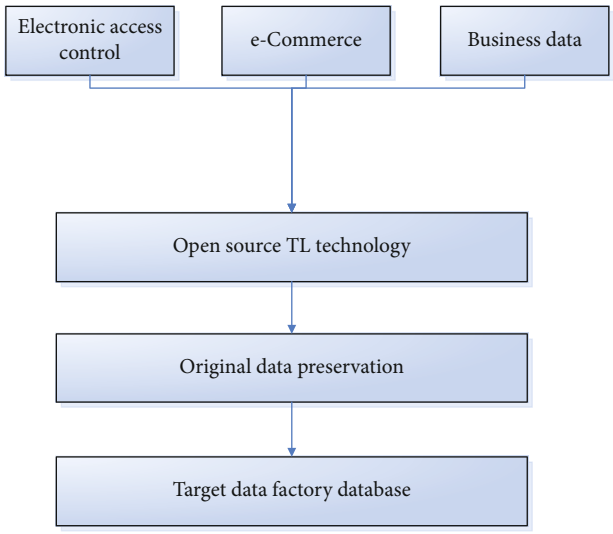

Figure 4: Platform user login.

tag extraction based on user e-commerce behavior, and personalized recommendation based on user tag, the personalized e-commerce recommendation service for home broadband users based on big data analysis is finally realized. The basic framework flow is shown in Figure 3.

3.4. Evolution of Cross-Border Import e-Commerce. The development of CBEC in China has experienced five stages: germination, birth, development, standardization, and standardization. e-Commerce begins with the purchase of foreign goods for Chinese foreign students. They went to foreign supermarkets to buy foreign goods and sent them to China by meat express. With the emergence of national food security and the increase of consumption, the demand of Chinese population for foreign goods increases, and CBEC begins to rise. The state has issued a series of important policies to adapt to the development of CBEC, opening up cross-border registration licenses successively, launching CBEC market, and large amount of funds flowing into cross-border areas. China's CBEC import has entered the peak of growth, and various CBEC companies have emerged. The state then issued a series of policies to regulate the behavior of CBEC enterprises. A number of small- and medium-sized CBEC enterprises began to close, and CBEC entered the brand washing and ranking period, users gradually gather to a complex platform and vertical classification of CBEC enterprises import, and the industrial chain optimization has entered a new stage.

4. Intelligent Perception System of Big Data Decision in CBEC

4.1. Cross-Border e-Commerce Trading Enterprises in China. According to the survey of popularity ranking of China international e-commerce platform in 2019, Tmall international reputation ranks first, NetEase koala ranks second, and JD ranks third in the world, while Hong Kong and JD, respectively, get the fourth and fifth popularity. As a benchmark enterprise of China's e-commerce, Tmall and JD gather a large number of users. Their cross-border import business will grow faster than other companies. However, as a comprehensive procurement platform, they are limited in meeting the personalized needs of cross-border users. Haigou koala relies on NetEase to select CBEC users from NetEase user base. NetEase koala takes the way of direct and independent procurement in commodity supply, which makes the goods have excessive production cost and can transform users. Tmall international, JD global, and NetEase koala are the leading enterprises of CBEC in China. Xiaohongshu

Table 4: e-Commerce platform user rate questionnaire.

Year	Number of users (must)	User rate
2016	40	7.34%
2017	65	12.45%
2018	76	13.25%
2019	78	15.66%
2020	80	18.88%

Table 5: Weighting table of influencing factors.

Factors	Weight
Users	8
Products	7
Experience	5
Talents	6
Technology	7
Capital	5
Logistics	6

works with foreign end-end e-commerce to make vertical segmentation and finally obtain market recognition according to user needs. Vertical e-commerce imports represented by Xiong Hongtu, foreign terminals, and darling constitute the basis of CBEC import in China. The popularity ranking of e-commerce platform is shown in Table 3.

As a cross-border platform and e-commerce, e-commerce can continue to promote economic globalization and play an important role in promoting the development of foreign trade. In terms of development level, the development level of CBEC in developed countries in Europe and America is significantly higher than that in China, However, with the information fusion technology, the decision intelligent perception system is a high-level application based on the existing informatization of the scenic spot. It has strong practicability and advanced nature and can meet the requirements of cross-border business decision support, business data analysis, traffic prediction, data management, and system management. Therefore, the intelligent decision system of scenic spot decision-making based on business intelligence is designed. The overall framework of the system is shown in Figure 4.

The data required by the prediction submodule is distributed in business systems such as electronic access control, e-commerce, and business data or public platforms. In order to make accurate prediction of CBEC by using these data, the ETL Technology must be used to extract and transform these data and then load them into the data warehouse. In order to meet the actual information data decision-making status of CBEC, the ETL Technology must be used to extract and transform these data, so each business system is designed to use different database software storage, which has common representativeness.

4.2. Number of Cross-Border e-Commerce Internet Users. China has a huge Internet user base, so China's CBEC import has a huge consumer market. Since 2016, the number of users of the e-commerce platform has increased significantly. This is due to the vigorous promotion of cross-border enterprise development by China's e-commerce and the high attention paid by various departments to the development of CBEC. The situation of users of the CBEC platform is shown in Table 4.

From Table 4, we can see that the number of Internet users in China reached 610 million in 2016, among which CBEC users exceeded 40 million, and the penetration rate of CBEC users was 7.34%; in 2017, the number of Internet users in China reached 640 million, of which the number of CBEC users reached 65 million, and the penetration rate of CBEC users reached 12.45%; in 2018, the number of CBEC users in China increased to 76 million, with the penetration rate of CBEC users reaching 13.25%; in 2019, the number of CBEC users in China increased to 780 million, and the penetration rate of CBEC users reached 15.66%; in 2020, the number of CBEC users in China will increase to 80 million, and its permeability will be increased to 18.88%.

4.3. Construction of Cross-Border e-Commerce Decision Intelligent Perception System Model. The construction of the CBEC decision model is the application of cross-border import decision matrix in the e-commerce decision model, and it is a practice of the optimal scheme selection. The expert method is used to summarize all the alternative business models. The evaluation criteria are replaced by common factors affecting e-commerce enterprises' decision-making, namely, flow introduction, supply chain integration ability, core management personnel industry experience, Internet product development ability; capital, logistics, and talent factors play an important role in the selection of the CBEC model as shown in Table 5.

It can be seen from Table 5 that the expert method is used to assign values to each factor, and weights are given from 1 to 10 according to the importance of the influencing factors. The weights of each influencing factor are calculated by the average value after the expert group members assign values to them, respectively. China's cross-border import and e-commerce mainly include "online tariff import" and "direct import." Therefore, China's cross-border import and export trade mainly includes "online import" and "direct import" bonded custom clearance and direct mail custom clearance. Therefore, an intelligent system for CBEC big data decision-making is established. The flow chart is shown in Figure 5.

The construction of the cross-border decision-making model of import e-commerce is the application of the cross-border business model decision-making matrix in e-commerce, and it is the practice of system optimization selection: traffic (users), supply (product organization supply), experience (industry experience of core executives), talent, technology (Internet product development ability), capital, and logistics. The expert method is used to give weight to the seven elements. The influencing factors are evaluated according to the evaluation criteria, that is, the influencing factors are evaluated according to the actual situation of the enterprise to be diagnosed. The highest score is the theoretical optimal option. The "influencing factors" and evaluation criteria are determined as shown in Figure 6.

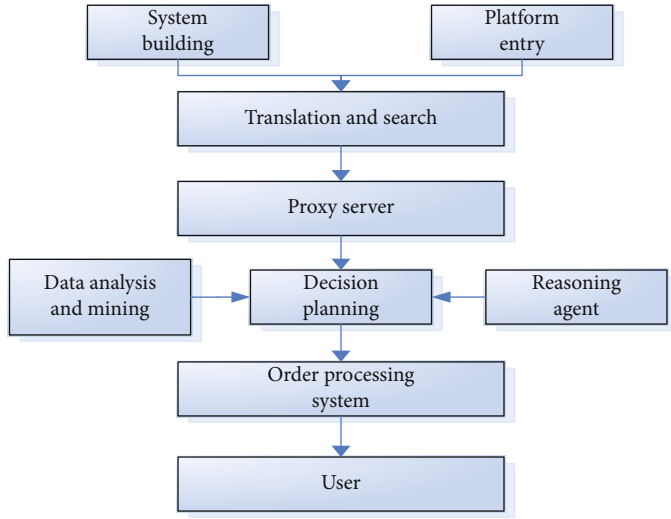

Figure 5: Platform collaborative management.

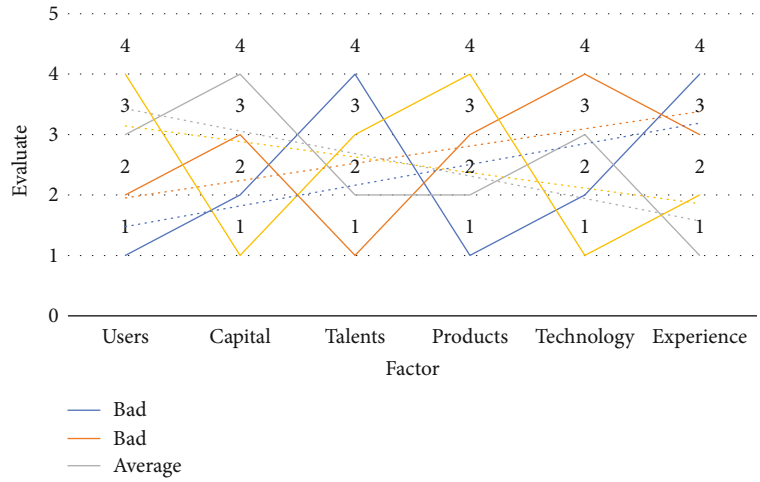

Figure 6: Influencing factors and evaluation criteria.

From the perspective of big data globalization strategy innovation, CBEC enterprises need to continuously strengthen bilateral regional cross-border data flow cooperation and need to carry out data fusion and platform docking with government big data platform. One road policy, the state will not only establish a market leading edge in the region but also promote the integration of industrial optimization and rational allocation of resources. The government and CBEC enterprises need to continuously expand the docking degree of the platform, optimize the trade process, and strengthen the supervision. Through the continuous process optimization and industrial upgrading of the bonded zone and free trade zone, CBEC enterprises can make the innovation of decision-making and operation more suitable for the needs of the rapid development of the market and also enable the government to realize dynamic and real-time supervision, to ensure the healthy and orderly development of CBEC industry, as shown in Figure 7.

Cross-border e-commerce enterprises need to have a full understanding of the globalization strategy. By intervening in the big data factors inside and outside the organization, they can make the organization's information communication more rapid and accurate, make the organization's management level flatter, reduce the decision-making level, simplify the operation process, improve the quality of products and services, and increase customer satisfaction, as shown in Figure 8.

From the perspective of big data platform business strategic innovation, CBEC enterprises need to innovate in the form of platform strategic solutions from the perspectives of product, industry, supply chain, and new economic form. Cross-border e-commerce enterprises need to establish and improve B2B and B2C product visualization trading platform, classify, integrate, and analyze business data with visualization big data, and adopt big data precision marketing strategy to realize the promotion of low-cost and accurate products and services. According to the industrial characteristics of CBEC, establish and improve cross-border financial service platform to achieve industrial agglomeration with low-cost funds.

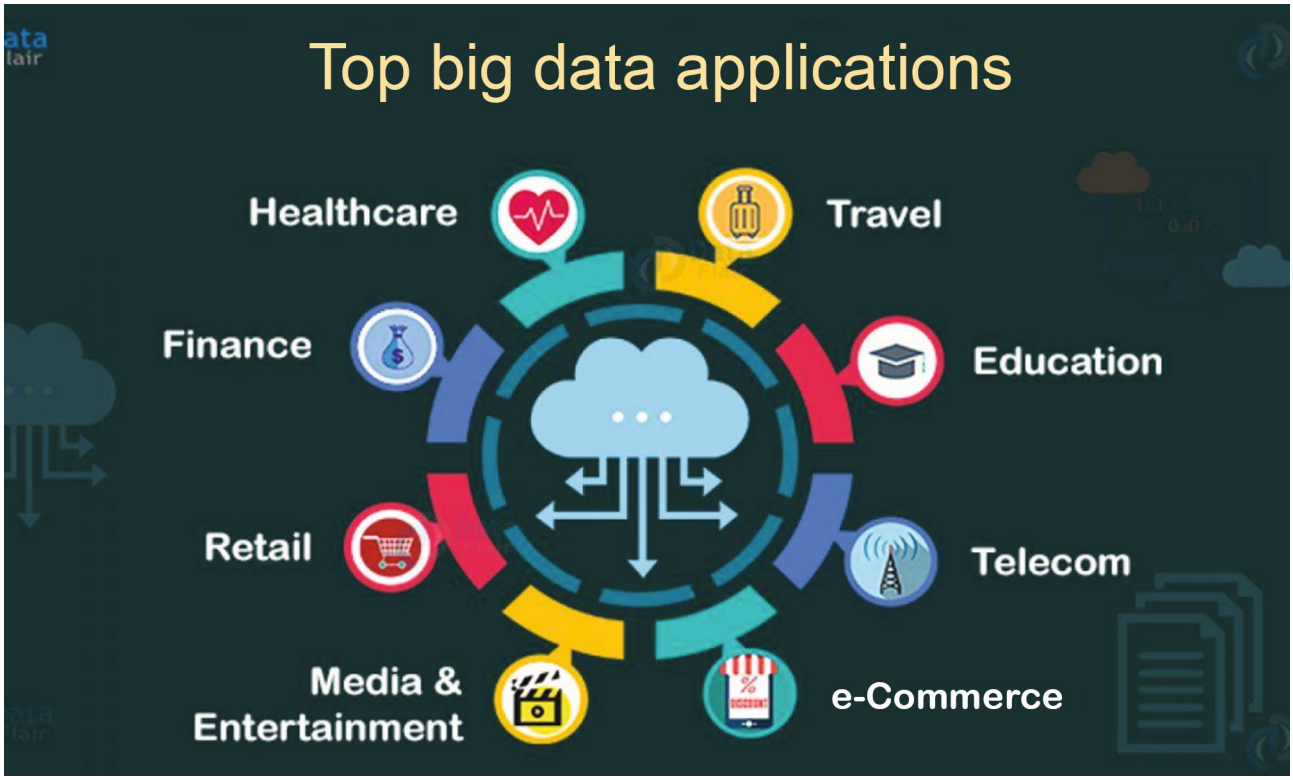

Figure 7: Data fusion of enterprise e-commerce platform (http://alturl.com/9b7yp).

Figure 8: Cross-border e-commerce industry development (http://alturl.com/s2fk4).

5. Conclusion

In this paper, the data fusion algorithm method, data fusion network model, quaternion method, big data decision intelligent perception system framework design experiment, and CBEC user experiment are used to study the CBEC big data decision intelligent perception system based on data fusion. With the continuous development of Internet technology and big data application, data-driven and technology-driven business model innovation of modern enterprises emerges endlessly. With the change of social, economic, and related industrial structure, the external environment of enterprises is also changing rapidly. Customer orientation to meet personalized needs and customized services has become the core business focus of enterprises. Based on previous scholars' research, the thinking and theory of big data and enterprise business model innovation are more perfect. Based on these thoughts and theories, modern enterprises find the theoretical basis and thinking direction in the way of big data application and business model innovation. Few scholars have systematically discussed the driving force of business model innovation, and few scholars have conducted in-depth research and discussion on the relationship between business model innovation and the development of enterprise strategy, industry, and national strategy. Previous scholars have done a lot of research on business model innovation, but most of them focus on the process, evaluation, and concept of business model innovation. When they study the process of business model innovation, they tend to put forward the path of business model innovation from one or two aspects; however, few scholars have conducted systematic or strategic discussions on business model innovation in the era of big data.

Data Availability

No data were used to support this study.

Disclosure

We confirm that the content of the manuscript has not been published or submitted for publication elsewhere.

Conflicts of Interest

There are no potential competing interests in our paper.

Authors' Contributions

All authors have seen the manuscript and approved to submit it to your journal.

Acknowledgments

This work was supported by Jiangxi Provincial Department of Education Science and technology research project "Jiangxi Province cross border e-commerce industry chain cluster research" (GJJ202505) and Nanchang Institute of Science and Technology introduced talents research start project "cross border e-commerce industry chain cluster research" (NGRCZX-20-11).

References

[1] W. Liao, X. Huang, F. Van Coillie et al., "Processing of multiresolution thermal hyperspectral and digital color data: outcome of the 2014 IEEE GRSS data fusion contest," *IEEE Journal of Selected Topics in Applied Earth Observations and Remote Sensing*, vol. 8, no. 6, pp. 2984–2996, 2017.

[2] K. A. Semmens, M. C. Anderson, W. P. Kustas et al., "Monitoring daily evapotranspiration over two California vineyards using Landsat 8 in a multi-sensor data fusion approach," *Remote Sensing of Environment*, vol. 185, no. 185, pp. 155–170, 2016.

[3] E. Bareinboim and J. Pearl, "Causal inference and the data-fusion problem," *Proceedings of the National Academy of Sciences of the United States of America*, vol. 113, no. 27, pp. 7345–7352, 2016.

[4] M. Berkow, C. M. Monsere, P. Koonce, R. L. Bertini, and M. Wolfe, "Prototype for data fusion using stationary and mobile data: sources for improved arterial performance measurement," *Transportation Research Record: Journal of the Transportation Research Board*, vol. 2099, no. 1, pp. 102–112, 2018.

[5] M. Schmitt and X. X. Zhu, "Data fusion and remote sensing: an ever-growing relationship," *IEEE Geoscience and Remote Sensing Magazine*, vol. 4, no. 4, pp. 6–23, 2016.

[6] K. Liu and S. Huang, "Integration of data fusion methodology and degradation modeling process to improve prognostics," *IEEE Transactions on Automation Science and Engineering*, vol. 13, no. 1, pp. 344–354, 2016.

[7] N. Yokoya, C. Grohnfeldt, and J. Chanussot, "Hyperspectral and multispectral data fusion: a comparative review of the recent literature," *IEEE Geoscience and Remote Sensing Magazine*, vol. 5, no. 2, pp. 29–56, 2017.

[8] L. Mou, X. Zhu, M. Vakalopoulou et al., "Multitemporal very high resolution from space: outcome of the 2016 IEEE GRSS data fusion contest," *IEEE Journal of Selected Topics in Applied Earth Observations and Remote Sensing*, vol. 10, no. 8, pp. 3435–3447, 2017.

[9] D. Tuia, G. Moser, B. Le Saux, B. Bechtel, and L. See, "2017 IEEE GRSS data fusion contest: open data for global multimodal land use classification [technical committees]," *IEEE Geoscience and Remote Sensing Magazine*, vol. 5, no. 1, pp. 70–73, 2017.

[10] B. Pradhan, M. N. Jebur, H. Z. M. Shafri, and M. S. Tehrany, "Data fusion technique using wavelet transform and Taguchi methods for automatic landslide detection from airborne laser scanning data and QuickBird satellite imagery," *IEEE Transactions on Geoscience and Remote Sensing*, vol. 54, no. 3, pp. 1610–1622, 2016.

[11] F. C. Chen and R. Jahanshahi, "NB-CNN: deep learning-based crack detection using convolutional neural network and Naïve Bayes data fusion," *IEEE Transactions on Industrial Electronics*, vol. 65, no. 5, pp. 4392–4400, 2018.

[12] F. H. Bijarbooneh, W. Du, E. C.-H. Ngai, X. Fu, and J. Liu, "Cloud-assisted data fusion and sensor selection for internet-of-things," *IEEE Internet of Things Journal*, vol. 3, no. 3, pp. 257–268, 2017.

[13] D. Zhou, K. Zhang, A. Ravey, F. Gao, and A. Miraoui, "On-line estimation of lithium polymer batteries state-of-charge using

particle filter based data fusion with multi-models approach," *IEEE Transactions on Industry Applications*, vol. 52, no. 3, pp. 2582–2595, 2016.

[14] Z. Tao and P. Bonnifait, "Sequential data fusion of GNSS pseudoranges and Dopplers with map-based vision systems," *IEEE Transactions on Intelligent Vehicles*, vol. 1, no. 3, pp. 254–265, 2017.

[15] A. Alofi, A. Alghamdi, R. Alahmadi, N. Aljuaid, and M. Hemalatha, "A review of data fusion techniques," *International Journal of Computer Applications*, vol. 167, no. 7, pp. 37–41, 2017.

[16] A. Kawa and W. Zdrenka, "Conception of integrator in CBEC," *Logforum*, vol. 12, no. 121, pp. 63–73, 2016.

[17] Y. H. Hsiao, M. C. Chen, and W. C. Liao, "Logistics service design for cross-border E-commerce using Kansei engineering with text-mining-based online content analysis," *Telematics & Informatics*, vol. 34, no. 4, pp. 284–302, 2017.

[18] H. Qian, "Status of cross border e-commerce development against the background of "Silk Road Economic Belt" and measures%," *Journal of Urumqi Vocational University*, vol. 25, no. 3, pp. 44–48, 2016.

[19] Y. K. Wang, "Model for evaluating the logistics service quality of cross-border E-commerce enterprises with intuitionistic fuzzy information," *Journal of Computational and Theoretical Nanoscience*, vol. 14, no. 2, pp. 1136–1139, 2017.

[20] Q. Fan, "An empirical study on cross border e-commerce promoting regional economic I nnovation: taking Taicang City as an example," *Jiangsu Science and Technology Information*, vol. 36, no. 15, pp. 1–3, 2019.

[21] M. Zhou, Y. Li, M. J. Tahir, X. Geng, Y. Wang, and W. He, "Integrated statistical test of signal distributions and access point contributions for Wi-Fi indoor localization," *IEEE Transactions on Vehicular Technology*, vol. 70, no. 5, pp. 5057–5070, 2021.

[22] M. Zhou, Y. Wang, Y. Liu, and Z. Tian, "An information-theoretic view of WLAN localization error bound in GPS-denied environment," *IEEE Transactions on Vehicular Technology*, vol. 68, no. 4, pp. 4089–4093, 2019.

Hindawi
Journal of Sensors
Volume 2023, Article ID 9762451, 1 page
https://doi.org/10.1155/2023/9762451

Retraction

Retracted: College English Teaching Quality Evaluation System Based on Information Fusion and Optimized RBF Neural Network Decision Algorithm

Journal of Sensors

Received 17 October 2023; Accepted 17 October 2023; Published 18 October 2023

This article has been retracted by Hindawi following an investigation undertaken by the publisher [1]. This investigation has uncovered evidence of one or more of the following indicators of systematic manipulation of the publication process:

(1) Discrepancies in scope
(2) Discrepancies in the description of the research reported
(3) Discrepancies between the availability of data and the research described
(4) Inappropriate citations
(5) Incoherent, meaningless and/or irrelevant content included in the article
(6) Peer-review manipulation

The presence of these indicators undermines our confidence in the integrity of the article's content and we cannot, therefore, vouch for its reliability. Please note that this notice is intended solely to alert readers that the content of this article is unreliable. We have not investigated whether authors were aware of or involved in the systematic manipulation of the publication process.

Wiley and Hindawi regrets that the usual quality checks did not identify these issues before publication and have since put additional measures in place to safeguard research integrity.

We wish to credit our own Research Integrity and Research Publishing teams and anonymous and named external researchers and research integrity experts for contributing to this investigation.

The corresponding author, as the representative of all authors, has been given the opportunity to register their agreement or disagreement to this retraction. We have kept a record of any response received.

References

[1] Y. Chen, "College English Teaching Quality Evaluation System Based on Information Fusion and Optimized RBF Neural Network Decision Algorithm," *Journal of Sensors*, vol. 2021, Article ID 6178569, 9 pages, 2021.

Hindawi
Journal of Sensors
Volume 2021, Article ID 6178569, 9 pages
https://doi.org/10.1155/2021/6178569

Research Article

College English Teaching Quality Evaluation System Based on Information Fusion and Optimized RBF Neural Network Decision Algorithm

Yajun Chen

School of Humanities, Social Sciences and Foreign Languages, Baotou Medical College, Baotou, 014040 Inner Mongolia, China

Correspondence should be addressed to Yajun Chen; 102013076@btmc.edu.cn

Received 17 April 2021; Revised 13 May 2021; Accepted 22 May 2021; Published 10 June 2021

Academic Editor: Mu Zhou

In the process of deepening and developing the current higher education reform, people pay more and more attention to the research of college English education. The key to improve the college English education is to improve the quality of education, and learning evaluation is the key measure to improve the quality of education and training. This paper mainly studies the college English teaching quality evaluation system based on information fusion and optimized RBF neural network decision algorithm. This paper analyzes the main problems and complexity of creating an ideal learning quality evaluation system. On the basis of analyzing the advantages and disadvantages of the previous learning quality evaluation methods, this paper summarizes the existing learning quality evaluation methods and puts forward some suggestions according to the existing evaluation methods. A learning quality evaluation model based on RBF algorithm of neural network is proposed. RBF regularization network method, RBF neural network decision algorithm, and experimental investigation method are used to study the college English teaching quality evaluation system based on information fusion and optimization of RBF neural network decision algorithm. By innovating teaching methods and enriching teaching means, college students' thirst for English knowledge can be aroused, and teachers' teaching level can be improved. The results show that 50% of college students think that the level of college English teaching is average and needs to be improved. In the performance evaluation system of college English teaching quality based on information fusion and optimized RBF neural network decision algorithm, it is necessary to establish a learning evaluation system, monitor the learning quality in real time, find problems and improve them in time, and recognize the current situation of education.

1. Introduction

With the rapid development of education, more and more children have entered the university. College English has become a subject that college students must learn. The quality of college English teaching in many areas has become the focus of attention. It is not only related to the survival and development of university schools but also directly affects the future and destiny of students. With the expansion of large groups and college students in recent years, a series of development scale has been formed. At present, there are many problems such as lack of teachers, low quality of university, and insufficient teaching and training machines and English service machines. The level of college English education has become a focus of debate and a full reflection of the evaluation of college work.

As a new technology, RBF neural network has its own basic characteristics of nonlinear programming, learning, and real-time optimization. It has unique advantages in pattern recognition, programming, filtering, and other aspects, such as identification, automatic control, and prediction. RBF neural network can detect fairness from many unknown modes. If so, any complex relationship can be fully evaluated in almost all nonlinear relationships. It can be evaluated by a nonlinear method. Compared with the traditional method, RBF neural theory has been trained in the quality evaluation system, not only the quality index problem but also the complexity and complexity of the mathematical model in the

traditional evaluation process a miscellaneous mathematical analysis. The direct evaluation of education quality is based on the neural network theory, which has an important influence on the quality of education.

Jan Friedrich studies that in industrial processes, a variety of sensors are increasingly used to measure and control processes. In an application, one way to process hundreds of thousands of different sensors' simultaneous interpreting data is to use information fusion system. Information fusion system, the result of this information fusion process is regarded as a health index of a complex system. Therefore, the information fusion method is applied to the sensor defect detection algorithm, which uses the structure of sensor fusion algorithm based on multilayer group. The results of the method for different test cases and the ability of the method to detect the defects of several typical sensors are given, but the specific data is not available. Liu BJ believes that a multisensor pressure charge identification method based on BP neural network and D-S evidence theory is proposed to solve the problem of incomplete information and uncertain information in the identification of complex parameter systems. Firstly, two BP neurons are used to detect false data in parallel; then, the evidence theory and local diagnosis results are used to understand the exact and the accurate information, and accurate diagnosis results are obtained. The method can be used for hydraulic identification of a rocket head hydrogen system, fault location, and preliminary diagnosis of main parts of the system. And the ability of effectively improving the system, but it lacks necessary experimental data. China's "one belt, one road" brings new challenges and opportunities to China's new economic norms. Zhou X believes. It also challenges English education, challenges English education of British universities, analyzes this path, and deepens English education. We should train more high-quality talents. But the content of numerical analysis is missing [1]. Braca P believes that with the development of China's economy, the development of market economy, the improvement of competitiveness, and the rapid development of the world economy, the society has put forward higher requirements for students' quality. English is an important tool for students to learn. International competition has changed. In order to better adapt to the needs of market economy, the demand for public English education is becoming larger and larger. It is very important to use effective education to influence education and improve the students' English. This paper proposes different methods to influence college English education, which can be used for reference [2].

The innovation of this paper is to study the quality evaluation system of college English teaching based on information fusion and optimization of RBF neural network decision algorithm by using the investigation experiment method, the calculation of RBF regularization network method, the RBF neural network decision algorithm, and the experimental investigation method [3, 4]. A set of evaluation system is an important part of the education system. It can help the education department evaluate the quality of education from the aspects of class education, educational achievements, school management, and teachers, to the current situation and also need to learn effectively, improve education problems, file the case, and improve the quality of students [5, 6].

Figure 1: InformationsfusionAdlerauge (http://alturl.com/oprin).

2. Information Fusion and Optimization of Decision Algorithm ORbf Neural Network

2.1. Information Fusion. With the development of information technology, information dissemination also appears in many ways. At present, information fusion technology supports complex applications and displays various displays [5, 7]. However, due to the large amount of information, strong processing capacity, complexity, and time limit between various sensors, simple data processing is not enough; in fact, data combination from multiple sensors is not enough; it is a pressure technology produced by multiple sensors. It uses intelligence to create, analyze, and form to best evaluate or describe the United States or define the objectives and nature of the United States, thus reducing costs [8, 9]. It is unacceptable to use sensors. We decide from more accurate and accurate sources of information as shown in Figure 1:

2.2. RBF Neural Network Decision Algorithm

2.2.1. Structure of RBF Neural Network. RBF neural network forms all neural networks with central point activity as hidden layer activity [10, 11]. The specific form of the method is as follows:

$$f_j(x) = \phi_j\left(\left\|x - b_j\right\|\right), \tag{1}$$

where f_j is the implied layer output and ϕ_j RBF neural network takes the distance b between the sample point X and the hidden layer data center as the input of the network, rather than the sample point as the direct input [12, 13]. It is called radial basis function. In RBF neural network, radial basis function activity is usually used as hidden layer activity, as follows:

$$\phi(x) = \exp\left(\frac{\|x - b\|}{2\sigma^2}\right). \tag{2}$$

Gaussian function has local distribution, nonlinearity, and nonnegativity, and its value shows a radial attenuation trend for the center point [14, 15]. In RBF neural network,

when Gaussian function is selected as activation function, the expansion constant is as follows:

$$\sigma = \frac{f_{\max}}{\sqrt{2m}}. \tag{3}$$

2.2.2. Training of Neural Network. According to the sharing strategy of RBF neural network, there are four types: random selection from stable center, self-selection center, selection center, and at least vertical center. By using the self-organizing learning strategy, the relevant parameters of RBF neural network can be determined by selecting the center point [16, 17]. The output layer of RBF neural network is as follows:

$$f_j(x) = \exp\left(\frac{\|x - b_j\|}{2\sigma_j^2}\right). \tag{4}$$

Because in neural networks, the initial value of the activation of the hidden layer of the neural node is usually used as the output of the next layer of the neural node, so we have established the $c_j^{(1)}$; the input value of the activation function of the jth neuron in layer is as follows:

$$c_j^a = \sum_{i=1}^{r_{a-1}} h_{ji}^{a-1} r_i^{a-1} + a_j^{a-1}. \tag{5}$$

Input data $x = (x_1, x_2 \cdots x_i)$. After that, the forward propagation process of multilayer feedforward network is analyzed.

2.2.3. Application of RBF Neural Network. BP algorithm is usually used to train RBF neurons. The main idea is to calculate the real value of neural network, first reduce the error, and then define the function of damage mode:

$$J(h, a; x, y) = \frac{1}{2}\left|f_{h,a}(x) - y\right|^2, \tag{6}$$

where h and a are the weights of the network; this is a sample $f_{h,a}(x)$. The original value y obtained from the direct propagation of the network is the actual value corresponding to the sample$X$, $\{(x^{(1)}, y^{(1)}, \cdots, x^{(m)}, y^{(m)})$. M is the number of samples:

$$J(h, a) = \left[\frac{1}{m}\sum_{i=1}^{m} J\left(h, a; x^i, y^i\right)\right] + \frac{\lambda}{2}\|h\|^2, \tag{7}$$

$$C_{\text{new}}^a = C^a - a\frac{\partial}{\partial c^a} J(h, c), \tag{8}$$

where a is called the learning rate or step size factor, where the partial derivative is calculated as follows:

$$\frac{\partial}{\partial h^a} J(h, c) = \left[\frac{1}{m}\sum_{i=1}^{m} \frac{\partial}{\partial h^a} J\left(h, c; x^{(i)}, y^{(i)}\right)\right] + \lambda h^{(a)}. \tag{9}$$

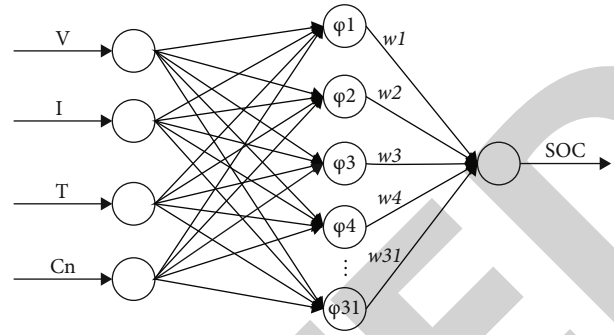

Figure 2: RBF neuronalesNetzwerkdiagramm (http://alturl.com/xwi55).

2.3. RBF Neural Network. BP network has the function of fitting function and connecting the world neurons. All the neurons hidden on the floor affect the results of network training process. In the process of training BP network, it is easy to find the optimal local solution. It is necessary to find a local network quickly and reduce the optimal solution of the local network. In biology, it is the same as the cerebral cortex and the set area and local reception of the cerebral cortex. Its principle is that the previous network only uses one layer to arrive at each job. Compared with BP network, RBF neural network uses radial activity as radial basis, uses hidden layer activity, and uses hidden layer data center to simplify the weight between input layer and hidden layer, as shown in Figure 2:

In many ANN models, RBF neural network has advantages in fitting ability, classification ability, and learning speed. Moreover, its network structure is simple and has good promotion ability. In fact, fault diagnosis is to classify and identify the operation status and judge whether the current operation status is fault and what kind of fault. Therefore, RBF neural network has some advantages in fault diagnosis.

2.4. RBF Regularization Network Method. Some complex valued RBF neural network structures can be divided into two categories according to the output of hidden layer nodes: one is that the output and excitation function of hidden layer are real numbers with complex weights; the other is that the output and weight of hidden layer are complex numbers. But in the latter category, according to the different excitation functions, it can be divided into separate structure and non-complex numerical RBF neural network training algorithm research and application of separate structure. For the convenience of description, we assume that there is only one node in the output layer, and the actual output of the corresponding network can be written as:

$$f_t(y_t) = \sum_{n=1}^{r} h_n \phi_n(\|x_t - b_n\|). \tag{10}$$

Given the same data set $\{a_n b_n\}^M$, now, if we want to use a function to approximate this set of samples, we usually use the approximation function that is found by minimizing the following objective errors

$$S_r(f) = \frac{1}{2}\sum_{n=1}^{M} \lfloor b_n - f(a_n) \rfloor^2. \quad (11)$$

The error function calculates the distance between the expected output and the actual network output. The regularization method is on the basis of standard error; a term limiting the complexity of approximation function is added, that is, grunt. The regularization term must have the following "geometric" properties of the approximation function to obtain:

$$S_r(f) = \frac{1}{2}\|Hf\|^2, \quad (12)$$

where h is the linear differential operator and represents the prior knowledge of $F(x)$

$$S(f) = S_r(f) + \lambda S_n(f), \quad (13)$$

where λ is the regularization coefficient and the above regularization is solved as follows:

$$f(x) = \sum_{n=1}^{M} h_n G(x, x_n). \quad (14)$$

3. Related Experiments of RBF Neural Network College English Teaching Quality Evaluation System

3.1. RBF Neural Network. On the basis of RBF neural network, by optimizing the network structure and introducing other algorithms, it can reduce the network computation and enhance the network function. Considering the complexity of the operation of the basis function in the engineering implementation of RBF neural network and the large amount of calculation of the first partition from the middle layer to the output layer, researchers began to introduce the algorithm ideas such as rce and KNN into RBF neural network. In the network, it can not only reduce the computation of the network but also enhance the function of the network. The basic principle is to map the data set to be classified into high-dimensional space and then divide it linearly. Researchers call this kind of network as RBF like neural network. Of course, the algorithms introduced in RBF like neural network are not the same, and the simplification methods of network structure are also very different. It is emphasized that RBF like neural network is generated by introducing rce and KNN algorithm. This paper introduces rce algorithm and KNN algorithm into RBF neural network. The generated RBF-like neural network is divided into three layers: input layer, middle layer, and output layer. The input layer represents the attributes describing external things, the middle layer stores different sample prototypes, and each node in the output layer represents a category. The specific nodes in each layer need to choose the best number of nodes through later experiments.

Table 1: User information table.

Property name	Varchar	Primary foreign key or not
User ID int	10	Yes
User name	10	No
Password	10	Yes
Role	20	Yes
Contact information	20	No

Table 2: Student evaluation form.

Serial number	Property name
1	Evaluation number
2	Teacher number
3	Scoring results
4	Rating detail number
5	Evaluation time

3.2. Evaluation System Database Table. The purpose of data table design is to meet the requirements of data storage. Therefore, it is necessary to set attributes according to the role of each table in the system. At the same time, it is also necessary to clarify the type and size of each attribute. Otherwise, if it does not meet the requirements, it will not meet the storage requirements. The table structure of each table is described below. User information table is the basis of identity authentication, which contains multiple fields, such as user ID, login name, and password. Based on the analysis of the storage mode of each field, the table structure of user information table can be obtained as shown in Table 1.

The student evaluation form is the basis of getting the evaluation results. It needs to include the fields of evaluation ID, teacher ID, and score detail ID. Based on the analysis of the storage method of each field, the attribute structure of college English teacher of the student evaluation form can be obtained, as shown in Table 2.

3.3. Comparative Experiment of College English Classes. In order to test whether the network has a positive impact on students' college English learning, teacher Zhang decided to conduct a one semester study comparison in the two classes she taught (the English level of the two classes is equal by the long-term teaching situation and understanding of the two classes). First, it is clear that the teaching contents of the two classes are consistent, and the teachers' rating standards are consistent. The difference is that the experimental class uses the sentence cool correction network, and the parallel class does not use it. The difference between the two classes is particularly obvious, whether it is average score, highest score, or lowest score. The scores obtained are all corrected by teachers, so the scoring standards are consistent, and the comparison can be made as shown in Figure 3.

3.4. System Basic Data Management. In order to support the operation of teaching quality evaluation system, many basic data are needed. The existence of these data can reduce the workload of staff and do not need to input data manually.

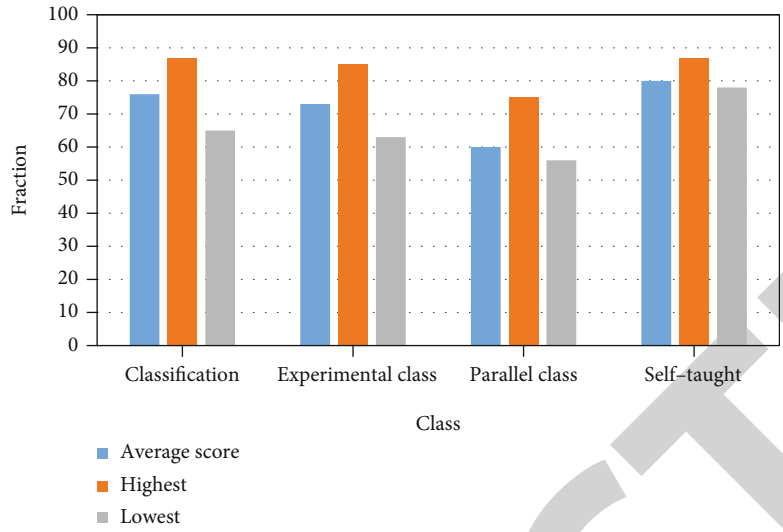

Figure 3: Descriptive views of the family.

Thus, the business processing efficiency can be improved, including the functions of user type management and student management. The number of student information is large, and the efficiency of adding data one by one is very low. In order to solve the above defects, the system introduces the import function to realize the batch addition of data. The following will introduce the function of student information import and student information export in the form of time sequence diagram.

3.5. System Evaluation Scheme Management. Evaluation scheme is the key part of teaching quality evaluation, which is mainly used to determine the student evaluation plan, teacher evaluation plan, and leadership evaluation plan and also needs to clarify the proportion of each part. Each function is to add, delete, and update related schemes. This section will describe the workflow of the evaluation proportion update function. The workflow is as follows:

(1) The function of assessment proportion management is the basis of teaching quality evaluation. Only the staff of the Ministry of Education can manage the weight of each part, namely, rateManage

(2) The system will call the method searchrateinfo to query the current appraisal proportion and display it to the staff of the Academic Affairs Office for updating

(3) Staff of the Ministry of Education enter the new assessment proportion

(4) The system will call the check method to check whether the new appraisal proportion meets the requirements, including digital verification, and whether the sum of the proportion equals 1, etc.

(5) On the basis of meeting the requirements of appraisal proportion, the system will call the updaterate function to save the new appraisal proportion information to the system database, such as:

Table 3: The overall evaluation of college English online teaching.

Semester	2017	2018	2019	2020
Number < 80	15	16	20	30
Number ≥ 80	43	26	24	12
Number > 90	23	45	52	41
Excellent rate	12%	14%	20%	25%
Good rate	78%	76%	50%	55%
Unqualified rate	10%	10%	30%	20%

$$\mathrm{OD}(f,\lambda) = -\log\left(\frac{H(f,\lambda)}{H_0(f,\lambda)}\right). \tag{15}$$

4. Platform Analysis of College English Teaching Quality Evaluation System

4.1. Online Evaluation Results of College English Course. College English teachers actively comply with the reform of curriculum requirements, update teaching ideas, improve teaching links, constantly optimize the teaching process, and strive to improve the teaching effect. In order to let the students participate in the monitoring of classroom teaching quality more actively and effectively and collect the feedback information of students on classroom teaching in time, the Academic Affairs Office of the University conducts online trial evaluation on the courses of each college. The author analyzes the data collected from the academic affairs office and compares the data of nearly 4 years; the overall evaluation of college English online teaching in 2007 is converted, and the specific statistical data are shown in Table 3.

From Table 3, we can see whether English teachers can create the best environment for students' language learning, whether they can stimulate students' interest in college English learning, and whether they can guide students to deepen their understanding of the language and cultural background. There is quite a number of students hope that college English course can also use multimedia-assisted

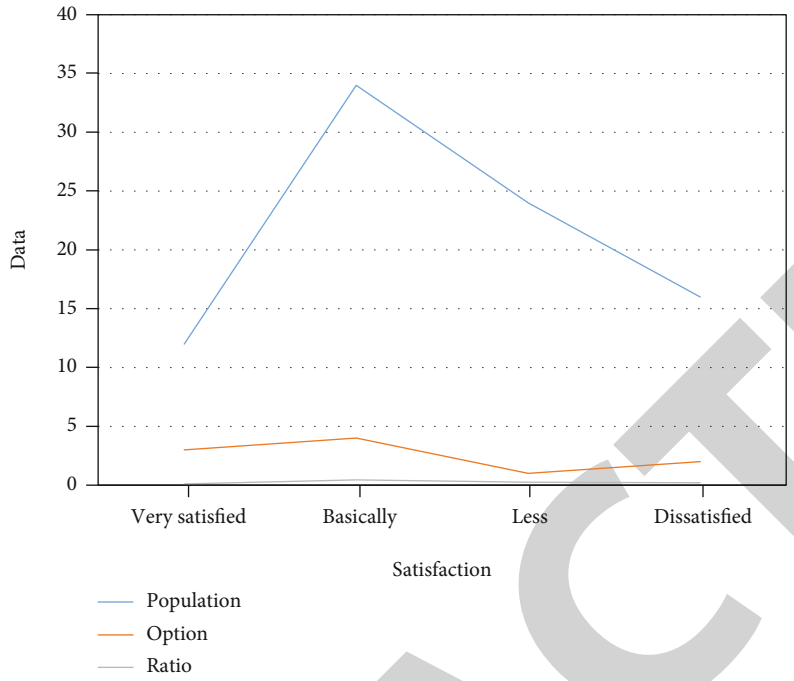

Figure 4: Statistical table of questionnaire survey data on college English curriculum satisfaction.

teaching; combined with audio-visual text, illustrated teaching can eliminate the monotony of English learning. This shows that the quality of college English teaching still needs to be greatly improved, not only to ensure the completion of the "quantity" of teaching tasks but also to make more efforts on the "quality" of the overall teaching level. In other words, English teachers must also change their teaching philosophy, conform to the development of the times, adhere to people-oriented, pay attention to the cultivation of students' comprehensive application ability, and pay attention to students' initiative and innovation consciousness. The overall score of the questionnaire is shown in Figure 4.

Students put forward some requirements in the open-ended response to the questionnaire, such as a large number of students think that foreign teachers are needed to attend the class. Nearly half of the students think that two years after college English study, they should offer continuous courses, and some students think that various English improvement courses or public courses related to English culture should be offered to further improve their understanding of English countries and improve their own language application ability. All of these are urgent needs to be reflected and summarized in time to ensure the improvement of the quality of college English curriculum.

4.2. Data Analysis of Passing Rate of CET-4. CET-4 has a complete set of scientific and authoritative examination system, so the various data it provides is gradually becoming a strong basis for the educational administrative departments to make macrodecisions and to improve the teaching quality of teaching units. It can be said that up to now, it is the only authoritative form that can show the teaching quality of a certain course in colleges and universities in China by means of examination and quantitative hard index. In order to understand the quality of College Public English teaching, examination, teaching, and learning are organically combined and promoted each other. It is necessary to analyze the passing rate of CET-4 in China, collect the passing rate of CET-4 examination for undergraduates in recent years from the Ministry of Education, and make statistics on the results as shown in Table 4.

Table 4: Statistical table of passing rate of CET-4 preliminary examination for college students.

Grade	Number of examinees	Number of first time	Passing rate
2017	5000	1200	20%
2018	4500	1400	24%
2019	4300	1500	22%
2020	5600	1600	34%

It can be seen from Table 4 that the number of professional courses offered by various colleges increases, the difficulty and pressure of learning increase, and the practice and practice courses will also occupy a lot of their time and energy. College students leave the English classroom without the supervision and guidance of teachers. It is more difficult for them to successfully pass CET-4 or even CET-6, and they need to make considerable efforts to reach the corresponding level. Therefore, it requires English teachers to work hard and find more breakthroughs in the short two years of college teaching, constantly improve the teaching level and quality, and strive to make students pass CET-4 smoothly in the two years of college English learning.

4.3. Optimization Scheme of Course Teaching Quality Assurance System. Through the innovation of teaching

Table 5: The basic framework of college English curriculum quality assurance system.

Type	Measurement	Information	Time resolution	Portability	Cost
fNIRS	HbO and Hb	4 ~ 6 cm	Per second	Yes	Medium
fMRI	BOLD	5 mm	Per second	No	High
EEG	Nerve potential	7 ~ 9 cm	Millisecond	No	High
PET	Glucose and oxygen metabolism	6 ~ 10 mm	About 60 seconds	No	High

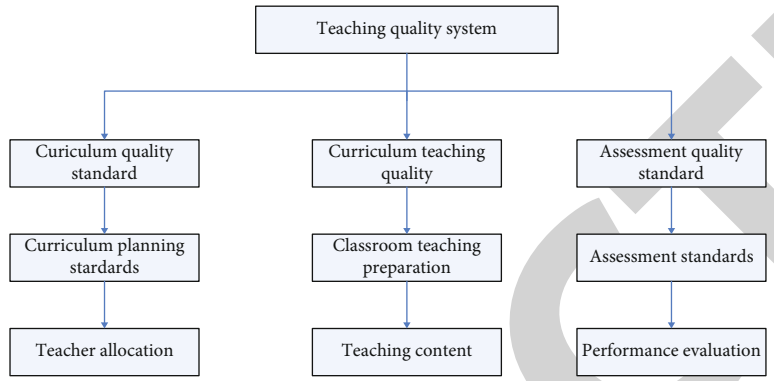

Figure 5: The fNIRS probe is projected onto the brain mode.

methods and the enrichment of teaching methods, teachers can mobilize students' knowledge needs. With the renewal of educational concepts, the main body of classroom teaching gradually changes from teachers to students, encouraging students to actively seek knowledge and play a teaching role. Therefore, college English teachers should stimulate students' curiosity, cultivate students' interest in learning, and improve their interest in classroom teaching by ensuring classroom order, using games, situational performances, and other activities. Encourage students to speak English boldly, let students participate in English teaching, not just a knowledge receiver, and comprehensively strengthen students' English listening, speaking, reading, and writing ability. The basic framework of the existing curriculum quality assurance system of college English is shown in Table 5.

It can be seen from Table 5 that the basic framework of college English curriculum quality assurance system can be divided into three parts: teaching quality standard system, teaching quality supervision system, and teaching quality incentive system. In order to further improve the teaching level and quality of college English course in our university, we must optimize it more reasonably, further refine each link, link each other, and give full play to the force of each link, as shown in Figure 5.

College teaching quality evaluation is more specific to college English teaching quality evaluation. Ralph W. Tyler defines teaching evaluation as a process to determine the extent to which courses and teaching plans effectively achieve teaching objectives in the basic principles of curriculum and teaching. Chinese educational scholars believe that quality assessment teaching is based on the preset teaching objectives. Collect the teaching information related to the evaluation; use scientific measurement means to assess whether the teaching results are consistent with the teaching objectives. The evaluation results of college English teaching quality are shown in Table 6.

Table 6: Framework of college English teaching evaluation system.

Evaluation index	Very good	Relatively good	Bad	Poor
Network resources	0.3	0.4	0.1	0.2
Practicability	0.1	0.5	0.2	0.2
Teaching method	0.6	0.1	0.1	0.2
Professional ethics	0.4	0.3	0.1	0.2

Figure 6: College English teaching classroom (http://alturl.com/t7x8d).

The teaching resources of university change curriculum and teaching into teaching content; combine the teacher level and teachers' quality into teachers' quality; change the result dimension, learning achievement, and student level into teaching effect; keep the teaching quality monitoring; and change it into teaching quality feedback. The teaching resources mainly refer to the various resources provided by the school for English teaching. The application of network technology in modern teaching makes classroom teaching

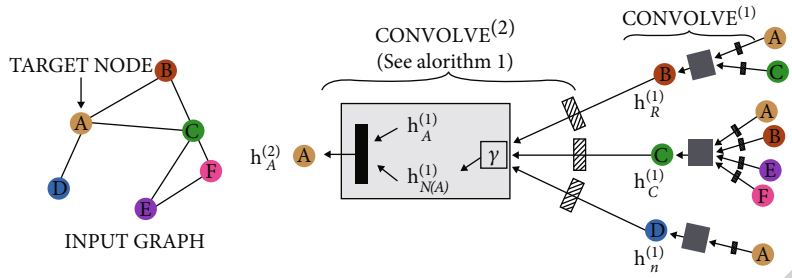

Figure 7: Neural network in college English teaching (http://alturl.com/6gerk).

more vivid and popular with students [18]. In the developed areas of education, the application of network in teaching is very common, so it is unnecessary to be a separate indicator. The network resources of universities, especially for students, are limited, so the network resources are set as the subordinate indicators of teaching resources, judging whether the teaching content is comprehensive and whether the teaching goal is clear. The chart of students' class in college English teaching is shown in Figure 6.

To improve the quality of college English teaching, we must follow the virtuous circle mode of "finding problems, exploring teaching methods and improving teaching quality". The system index system can analyze the problems that affect the improvement of college English teaching, analyze the reasons, and put forward policy suggestions. Through the analysis of the research results, we find that the main factors that affect college English teaching are the English level of schools and students, and the average scores of "teaching resources," "teachers' quality," and "teaching effect" are medium. The improvement of these three elements mainly depends on the efforts of "school authority" and "teachers." The improvement of "teaching resources" mainly depends on school authority, while the improvement of "teachers' quality" and "teaching effect" mainly depends on school authority. Depending on the efforts of school authorities and teachers, the evaluation system of college English teaching quality based on RBF neural network is shown in Figure 7.

From the RBF neural network decision-making college English teaching quality evaluation system, we can see that students' positive thinking will be encouraged and praised by teachers. The interaction between teaching subjects enhances mutual confidence and helps to improve teaching quality. In addition, classroom teaching should be combined with modern teaching methods. On the premise of necessary facilities, such as the application of multimedia means will help students to improve their image thinking through audio-visual. However, the old teaching method and single mode are one of the main factors that restrict the improvement of English education quality in primary schools [19]. This disadvantage can be solved directly from the perspective of teachers. Both the cost of education and the cost of education are very low, and can be used for teachers to "copy" and promote.

5. Conclusion

This paper studies the quality evaluation system of college English teaching based on information fusion and optimization of RBF neural network decision algorithm by using the method of calculating RBF regularization network, RBF neural network decision algorithm, and experimental investigation method. The college English teaching problem is worth further exploration. The quality evaluation should have a practical evaluation system first. By using the evaluation system, the present situation of English teaching can be quantified. Teachers can understand the problems in teaching by quantifying the teaching results and analyzing the reasons, so as to improve the teaching quality. At present, the construction of education evaluation system has begun in the developed areas of education. Because of the differences in teaching resources, teachers, and students' quality, these evaluation systems are not suitable for the backward areas of education. In addition, China has no right to evaluate college English teaching system for single course. Therefore, it is necessary to establish a set of college English teaching evaluation system which is suitable for the college English subject in the underdeveloped areas.

Data Availability

No data were used to support this study.

Conflicts of Interest

There are no potential competing interests in our paper.

Authors' Contributions

All authors have seen the manuscript and approved to submit to your journal.

References

[1] X. Zhou and P. Jiang, "Variation source identification for deep hole boring process of cutting-hard workpiece based on multi-source information fusion using evidence theory," *Journal of Intelligent Manufacturing*, vol. 28, no. 2, pp. 255–270, 2017.

[2] P. Braca, R. Goldhahn, G. Ferri, and K. D. LePage, "Distributed information fusion in multistatic sensor networks for underwater surveillance," *IEEE Sensors Journal*, vol. 16, no. 11, pp. 4003–4014, 2016.

[3] L. Peng, B. Liao, W. Zhu, Z. Li, and K. Li, "Predicting drug–target interactions with multi-information fusion," *IEEE Journal of Biomedical and Health Informatics*, vol. 21, no. 2, pp. 561–572, 2017.

Hindawi
Journal of Sensors
Volume 2021, Article ID 9204123, 11 pages
https://doi.org/10.1155/2021/9204123

Research Article

Volleyball Action Extraction and Dynamic Recognition Based on Gait Tactile Sensor

Limin Qi

College of Sports Science, Harbin Normal University, Harbin, 150025 Heilongjiang, China

Correspondence should be addressed to Limin Qi; 474949287@hrbnu.edu.cn

Received 13 April 2021; Revised 27 April 2021; Accepted 15 May 2021; Published 2 June 2021

Academic Editor: Mu Zhou

At present, the industry research of volleyball technology is relatively in-depth, and the analysis of the muscle strength characteristics and coordination of the jumping ball is less, which is not conducive to the control of technical movements. This study used a wireless portable surface EMG tester (16 lines) to analyze the EMG of the main muscle groups in athletes' volleyball and conducted a video synchronization test method to find the position of the human body. Therefore, a background-based frame difference method is proposed to detect the position and obtain the precise position of the human body. Experiments show that the background-based three-frame difference method effectively eliminates the "hole" effect of the original three-frame difference method and provides an accurate and complete framework for identifying the human body. Adjust the recognition frame according to the proportion of the human body in the image, and use the predefined parameters of the severe frame to perform forward/volleyball background segmentation. The novelty of this document lies in the completion of the complete human body placement of the above three tasks, precapture/background segmentation, and an improved human body position estimation algorithm to extract the human body pose from the video. First, locate the human body in each frame of the video, and then, perform the process of estimating the position of the graphic model based on the color and texture of the unit. After recognizing the gesture of each image in the video, the recognition result will be displayed. Experiments show that after detecting the position of the human body, the predefined frame setting process of the tomb is carried out in two steps, which improves the automation of the human body image detection algorithm, effectively extracts the human motion video, and increases the motion capture rate by more than 30%, to provide a useful reference for the improvement of college volleyball players' movement skills and training competitions.

1. Introduction

The volleyball game began in 1895, and its founder was Holly Walker of Massachusetts, USA, the secretary of the YMCA, William Morgan. At the beginning, his idea was to choose a moderate, moderate sport. This is a leisure sport that can meet the needs of people who cannot adapt to the intense basketball game. Casual timetable, but as time goes by, volleyball has gained more and more public recognition and is developing rapidly. After continuous reform and improvement, it has become a world-class sport. Keeping pace with the times and looking forward to the future, volleyball is also developing rapidly. In addition to the conventional six-sided volleyball and beach volleyball, various volleyball sports are widely used, such as soft volleyball and air volleyball. Volleyball has a variety of forms and comprehensive skills. In China, since the Chinese women's volleyball team won a difficult championship in the 2004 Athens Olympics, China has always had an unlimited volleyball boom. The national sand queuing performance has also improved by leaps and bounds, and soft volleyball has become a competition event in various middle schools. It has gradually appeared in various city offices and enterprises and has become an official event for sports workers.

For humans, understanding the posture of volleyball can be easily solved, but for computers, this understanding is indeed quite difficult. So far, there is no algorithm or system that can accurately describe the motion of an image with a close human comprehension ability under few restrictions. Therefore, this article attempts to do some work in this direction and achieve some results.

Ning believes that after more than 20 years of development, my country's volleyball league has continuously adapted to the reform of the International Volleyball Federation, and social attention and respect have greatly increased. Professional sports companies have intervened, including the Hawkeye referee assistance system, the introduction of foreign aid, and the reform of the competition system. These measures are bound to accelerate the professionalization of my country's volleyball championships, activate the volleyball market, and promote the recurrence of volleyball in our country, but the human body research of volleyball is not perfect [1]. Liu proposed an ultrawideband position calibration method based on motion detection. The realization of this method is based on two experiments. One is to use a total station to check the accuracy of the motion detection system, and through Bursa seven-coordinate parameter conversion, the model will process experimental data, which shows that the accuracy of the motion detection system meets the requirements and can be used to calibrate the motion detection system. The accuracy of the UWB indoor installation system: the second is to calibrate the accuracy of the UWB indoor positioning system through the motion detection system detected by the motion detection system. The data is real. Compare the data recorded by the UWB indoor installation system with the data recorded by the motion detection system. However, the accuracy of the experiment is not high and needs to be improved [2, 3]. Wang proposed a new MOCAP algorithm to recover data distortion. The algorithm first preprocesses the MOCAP data so that the converted data represents the change in the relative position of adjacent markers to receive the volleyball length limiter and then uses it. The sparse display and the limitation of the length of volleyball are used for dictionary training, and finally, the trained dictionary is used to recover the lost data. But this method requires a lot of time and cannot get results quickly [4].

The innovation of this article is to use eye tracking technology to explore and analyze the cognitive processing characteristics of volleyball players of different sports levels when judging the point of serve. It provides a theoretical basis for the cognitive processing characteristics of volleyball players and can be used as a reference for the selection of athletes. The expected research hypothesizes that there are differences in cognitive processing characteristics of volleyball players when judging the drop points of different serve offenses. Therefore, human motion detection and volleyball movement changes can be studied as independent topics or as a comprehensive study of the various steps of a topic. The experimental results of this method show that the target step rate is increased by more than 60%. This article is mainly devoted to the study of target detection and extraction in the analysis of moving objects.

2. Content and Method of Gait Tactile Sensor

2.1. Main Content of the Gait Tactile Sensor System

(1) To systematically develop and research gait tactile sensors and discuss the relevant background and research significance of the topic [5]

(2) Based on the previous work, a simple large-area robot sensor array was developed, focusing on the development of detection circuits, signal processing circuits, and signal receiving circuits for receiving and processing signals

(3) The complete virtual instrument technology data acquisition and analysis system based on NI PCI-6259 data acquisition card can provide data acquisition, analysis and processing, real-time control, and synchronization control. Use OpenGL technology to design the screen software system [6]

(4) The integrity, advantages, and disadvantages of the gait tactile sensor and hardware and software systems are tested through experiments

(5) Analyze the error of the experimental results, discuss the source of the error, summarize the remaining problems, and propose the direction of the next step [7]

2.2. Literature Data Method. Retrieval and screening of relevant literature data are based on "volleyball physical training," "jump serve technique," "core strength," and keywords through Chinese journal databases such as CNKI and Wanfang and the library of Shandong Institute of Physical Education [8, 9]; nearly 110 related documents on the use of core strength in volleyball were obtained, sorted out, refined, and summarized, through the sorting and analysis of reference materials, mastering the research and analysis of core strength and technical movements in volleyball, focusing on the analysis of the concept of core strength and the theoretical basis of training such as jump serve movement analysis, training methods, and stability factors [10, 11].

2.3. Expert Interview Method. On the basis of consulting relevant materials, in order to obtain sufficient theoretical basis such as scientific and reasonable measurement indicators and research methods, the purpose is to consult

(1) about the main factors affecting jump serve training [12]

(2) select measurement indicators related to volleyball jump serve training

(3) issues related to the selection of core strength training methods

This was done through visits to volleyball coaches and related academic experts, according to the starting point and feasibility, actual conditions, rationality and testing methods of this thesis research, the selection of evaluation

indicators and training methods, and consulting experts' opinions [13, 14].

2.4. Questionnaire Survey Method. Before the experiment, in order to obtain reasonable experimental training methods and ensure the effectiveness of various indicators, a list of the core strength training for male volleyball players' jump serve training methods index selection order table was developed. The title of the topic is the research screening table of the influence of core strength training on the jump serve ability of male volleyball players, and the experimental training indicators are determined by the selection and evaluation of experts in all aspects of the volleyball field [15, 16]. The design purpose of the questionnaire is to obtain effective index help and guiding suggestions that are conducive to improving the training methods of volleyball players' jump serve ability [17].

3. Correlation Experiment of Gait Tactile Sensor

In order to perceive the external environment quickly and accurately, many experts and scholars have developed various sensors according to different needs. The sensing principles can be divided into seven types, namely, piezoresistive effect, piezoelectric effect and pyroelectric effect, capacitive, magnetoelectric sensing, photoelectric sensing, mechanical sensing, and ultrasonic sensing. Sensitive materials are used for the conversion and sensitive components in the sensor design. Its performance directly affects the performance indicators of the sensor. Therefore, in order to be able to design a sensor that meets actual requirements, the first problem to be solved is to select the sensitive material [18, 19]. In order to enable the flexible tactile sensor to have efficient sensing and energy conversion capabilities, this paper selects a piece of elastic silica gel as the sensitive element of the flexible tactile sensor and selects a strain gauge as the conversion element of the flexible tactile sensor. According to the requirements of the subject, various factors in the laboratory are comprehensively considered. Due to the advantages of simple structure, strong antifatigue ability, easy signal processing, and low signal hysteresis [20], the strain sensor is selected in this paper, as shown in Figure 1.

It is the schematic diagram of the initial tactile information collection circuit, where the dashed frame represents the unit volume of conductive rubber K (its piezoresistive characteristic curve has been determined), Q is the reference resistance [21, 22], and e is the regulated DC power supply. Since the voltage of e and the resistance of Q are constant, when we apply pressure to the conductive rubber Q, its resistance also changes so that the voltage V shared on Q changes.

$$Q = Q_C \times K \cos e + V. \tag{1}$$

In the first state, the sensitive unit is not under pressure, and the unit volume of conductive rubber Q appears as an open switch in the circuit; in the second state, the sensitive unit is under pressure $Q1$, and the voltage $V1$ is read at R at this time; in the third state, the sensitive unit is under pressure $Q2$, read the voltage $V2$ at R at this time [23, 24].

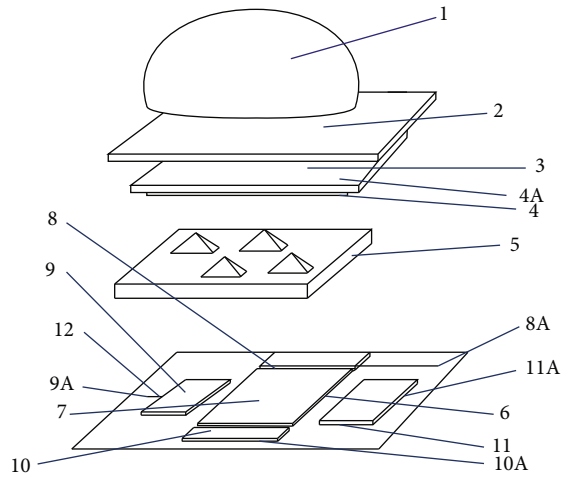

Figure 1: Gait tactile sensor.

$$Q_C = Q1 + Q2 = \gamma \times Q2 - \gamma \times Q1. \tag{2}$$

The value of the resistance Q per unit volume of conductive rubber under pressure can be calculated from the formula, and the coefficient can be found from the piezoresistance curve according to this value.

When the resistance wire is under the action of the tensile force F, the resistance wire elongates L, the cross-sectional area decreases C, and the resistivity changes due to the change of the material lattice, which causes the resistance to also change K. Differentiate and get the relative change of resistance as [25]

$$\frac{dQ}{Q} = \frac{dC}{C} = \frac{dF}{F} + Q^C. \tag{3}$$

Among them, L is the amount of change in length, expressed as strain M as

$$M = \frac{dL}{L} - \sqrt{M} + C. \tag{4}$$

According to the mechanics of materials, in the elastic range, when the metal wire is under tension, the metal wire elongates in the axial direction and shortens in the radial direction so that M is the axial strain of the metal resistance wire and C is the radial direction of the metal resistance wire. Strain, so the relationship between axial strain and radial strain can be expressed as [26]

$$\frac{dQ}{Q} = -\mu\frac{dL}{L} + \sqrt{M} = -\mu M. \tag{5}$$

μ in the formula is Poisson's ratio of the metal resistance wire material, and the negative sign indicates that the strain direction is opposite. Substituting formula (3) into formula (5), we can get

$$\frac{dR}{R} = (1 + 2\mu)C + \frac{dF}{F} - \mu, \tag{6}$$

where R is the leakage resistance of the Kth row and R is the leakage resistance of the Zth column, expressed as

$$\frac{1}{R_i} = \sum_{1}^{n} \frac{1}{r_z} + \frac{1}{R}. \tag{7}$$

In formulas (6) and (7), the insulation resistance is between P and U row and column electrodes. The analysis of the circuit shows that the circuit is a typical reverse addition circuit [27]:

$$V_{\text{cout}} = -P_1\left(\frac{V}{R} + \frac{U}{R}\right) = -\frac{1}{R_i} \times V_i. \tag{8}$$

The line scan method scans one line at a time, thereby greatly improving the readout speed of all information in a single tactile array [28, 29], laying the hardware foundation for the real-time performance of the entire system and improving the sampling speed while better solving the problem between rows and columns, the problem of crosstalk noise. Therefore, in this design, the line scan method is used to scan and collect the tactile signals. The circuit is mainly controlled by a set of pulse sequences, and the gating of eight analog switches is controlled by a six-bit counter [30–32].

4. Volleyball Action Extraction and Dynamic Recognition Analysis

An independent sample T test was performed on the physical fitness indicators of the experimental group and the control group before the experiment. The test results showed that there was no significant difference in the physical fitness indicators of the two groups of athletes ($P > 0.05$), so the experimental group can be defined statistically. There is no significant difference in the physical fitness index of the athletes in the control group before the experiment.

From the results in Table 1, it can be seen that the training methods of the experimental group and the control group have certain differences and many connections in many comparison items. Not all traditional training methods are useless. It shows that there is no significant comparison between the two groups of feet in the vertical jump, approach height, and 30-meter sprint, indicating that the physical fitness indicators are the same.

From Figure 2, we can see that for the training of the core strength and serve speed of volleyball jump serve technology, different forms of training are used to improve the stability of the core muscle group of jump serve hits, so as to improve the stability of the athletes' jump serve hits sexual ability, thereby improving the speed and success rate of jump serve hits in training and competition.

It can be seen from Figure 3 that the use of traditional training methods has certain advantages and foundations, which are mainly to improve the maximum muscle strength by overcoming its own gravity and the external resistance of load bearing. The advantages of the training methods adopted in this article are mainly the action function in the field of training; the action mode has a variety of actions and the method is flexible; the muscle movement has the joint and coordinated force of the large and small muscle groups; the emphasis is on the power chain, coordination chain, joint flexibility and stability, action mode, and training purpose to improve the muscular endurance of the athletic ability and the stability of the specific technical action. The shortcomings of traditional training methods are the movement is relatively single and fixed, the single-joint muscle training, the emphasis is on absolute strength, separation from specific technical movements, and the training purpose is to train with intensity and improve physical fitness.

Table 1: The statistical results of athletes' physical fitness indicators before the experiment.

Index	Prone back extension	Sit-ups	Foot jump	Run up	300 m sprint
Control group	37.95	47.24	52.36	35.26	40.12
Test group	32.77	46.45	39.33	30.16	51.23
P value	0.249	0.857	0.502	0.177	0.172

As shown in Table 2, in the results of the analysis of variance (ANOVA) on the three parameters of gait, the P value is less than 0.05, indicating that the three parameters have significant statistical differences in the three self-selected speed modes. The mean value and error distribution are shown in the figure. The results in the figure also show that the three parameters are statistically different in the three optional speed modes. Therefore, in the subsequent reliability analysis, the reliability of the three speed modes must be investigated separately.

As shown in Figure 4, the reliability coefficients from 2 to 10 measurements are calculated in each speed mode, and their values and changing trends are shown in Figure 2.3. The data in Table 2.3 is the statistical result of the number of measurements required to reach the ICC value of 0.75 and 0.9 in Figure 2.3. Obviously, in order to meet the ICC value of 0.75, only 2 measurements are required in slow walking, normal walking, and fast walking modes; and in order to meet the ICC value of 0.9, at least 3 measurements are required in slow walking mode; and in normal walking and fast walking modes, at least 2 measurements are needed.

The comparison between the gait parameters obtained from the research in Figure 5 and the existing research results is shown. From the comparison, it can be seen that the step length and pace are smaller than the previous research results, but this is consistent with the research results of Chiu, who also used Asian races as the experimental subjects. He limited speeds of 3, 4, and 5 km/h, respectively. It is slow walking, normal walking, and fast walking (Chiu and Wang, 2007). Obviously, the results of different races will be different (Braun et al., 1980). When two points on the touch sensor array are pressed, the waveform window displays two high-level signals. The digital signal represents the corresponding row. The experimental data can also be seen from the saved text table, but due to the large amount of data in the table, it is inconvenient to display, so intuitive graphic display is adopted to prove the correctness of the experimental data.

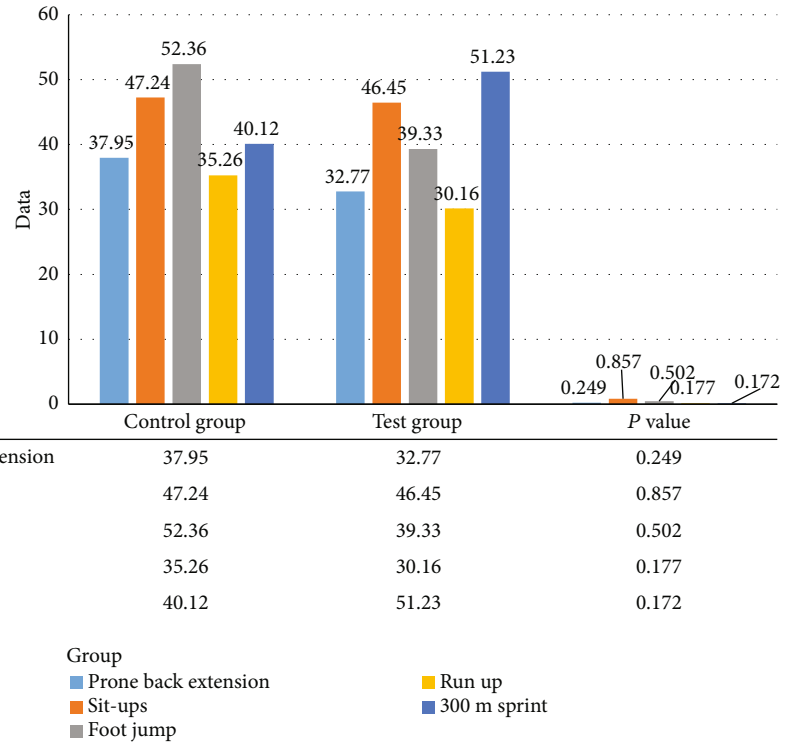

Figure 2: The statistical results of athletes' physical fitness indicators before the experiment.

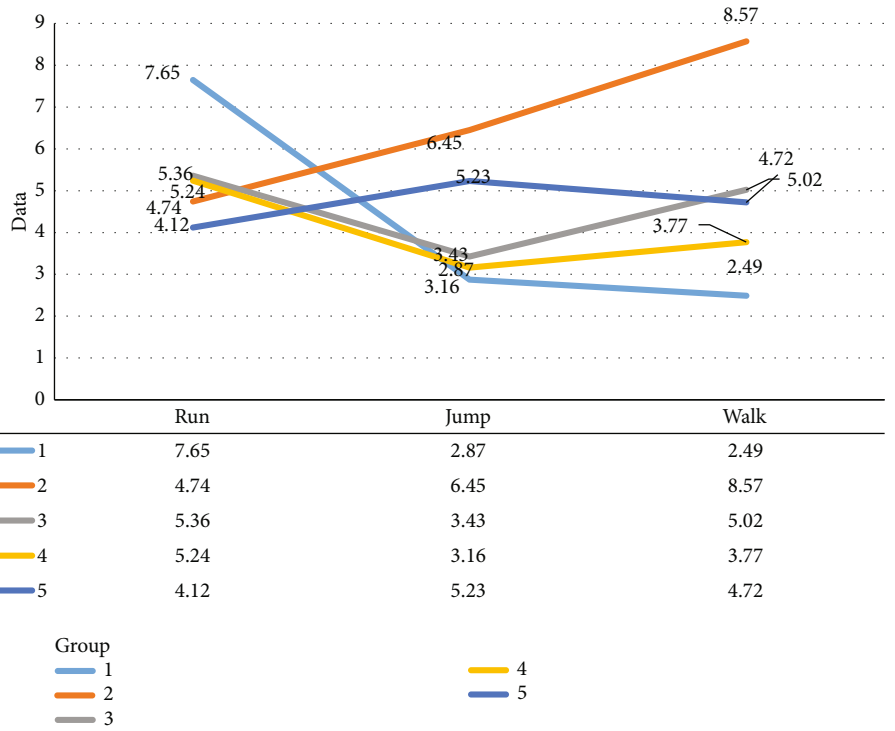

Figure 3: The statistical results of athletes' physical fitness indicators before the experiment.

Table 2: The statistical results of athletes' physical fitness indicators before the experiment.

	Slow	Normal	Fast	Slow normal	Fast normal	Slow fast
Step length	0.57	0.63	0.69	0.53	0.43	0.65
Cadence	0.21	0.13	0.31	0.25	0.21	0.35
Velocity	0.52	0.32	0.53	0.21	0.61	0.28

In addition, we require the subject to be measured barefoot on the electronic trail, which may also be one of the reasons for the relatively small step length.

This experiment verifies that the electronic trail (also known as the digital track) has high reliability when collecting walking time and space parameters and will provide a good reference for researchers who use this instrument in the future. Different speed modes will affect the reliability of step length, step frequency, and pace. The slow walking, normal walking, and fast walking modes at the optional speed have high reliability. When the electronic trail is used in the experimental research of walking test, at least 3 measurements are required to meet the high reliability requirements under different speed modes.

There is relationship between vibration training under different vibration frequencies and the muscle strength of the upper limbs of the shoulder and elbow; there is relationship between vibration training and the explosive force and vibration frequency of the lower limbs of volleyball players. Then, through experimental training, we seek suitable vibration training strategies to maximize the athletes' whole body coordination, flexibility, bounce ability, and balance ability, in order to further apply suitable vibration strength training to the public level and improve the overall quality of citizens lay the foundation. Therefore, according to the research content, this thesis will determine the maximum strength of the shoulder and elbow joint, the flight time, the support time, the explosive force index of the lower limbs (lower extremity explosive force index = the flight time/support time), and other parameters for volleyball players and nonspecialized personnel under different vibration frequencies. The measurement results are compared horizontally and vertically to provide support for quantitative vibration training and volleyball players' strength research.

The intensity of myoelectric activity is triceps > front deltoid > biceps > brachioradialis. The triceps of the upper limb muscles are very excited. The electric discharge is strong. Observing the technical structure of the action at this time, it can be found that the athlete's upper arm is swinging backwards forcefully. This swing makes the upper arm in a more favorable position for exerting force. It is for the next step to quickly swing forward and increase the support leg. The bottom force creates conditions. In the data acquisition system, to complete the signal measurement and analysis, you should first set the device name, sampling rate, trigger mode, and so on. In view of the more commonly used measurement requirements and signal types, we have designed the default values of the data acquisition parameters. Taking into account the diversification of user needs, users can also manually modify the parameter settings.

We can derive from Figure 6 that the jump-off buffer stage of the jump serve is the stage from the moment the jumping leg hits the ground to the maximum buffer moment of the knee joint of the jumping leg. Its main task is to actively complete the concessionary work of the muscles, store elastic potential energy, and serve for subsequent leg extensions. Make effective preparations. At this stage, the lower limbs have to withstand the greater impact of the ground, while the body maintains balance and the arms actively swing back to create the best working conditions for the subsequent kicking and stretching movements. Possible reasons for these results: the daily exercise load of the shoulder-elbow joint flexors of nonspecialized personnel is greater than that of the shoulder-elbow joint extensors, resulting in the training effect of the extensors being better than the flexors; the muscles are more suitable for low-frequency vibration training in the short term. Significant effects are seen inside. It can be seen that the effect of vibration training is still very significant, but it is not suitable for changing the vibration frequency in a short period of time. It takes a period of adaptation to achieve the optimal effect. These research results are all researches on the relationship between vibration training on shoulder and elbow joint upper limb muscle strength and vibration frequency, laying a foundation for further applying appropriate vibration strength training to the public level and improving the overall quality of citizens.

In the buffering stage, it mainly plays the role of pulling and braking the calf to buffer the horizontal speed. At the same time, braking the calf is more conducive to the formation of stable support for the ankle joint. The role of the gluteus maximus is relatively small in the lower limb muscles, with a contribution rate of only 6.18%. The contribution rate of the EMG of the trunk muscles in the buffer phase is not high. The trapezius muscle, the external oblique muscle, and the erector spinae are all involved in the erection of the trunk and the extension of the spine. The sum of the three accounts for 16.41% of the total muscle activity tested. The myoelectric activity of the upper limb muscles is not high at this stage. The total myoelectric contribution rate accounts for 26.32% of all tested muscles, but the biceps myoelectric contribution rate accounts for 9.14%, which produces stronger contraction and work. This is caused by the movement of the arm position during this process. These research results have laid the foundation for the research of vibration training on the relationship between the shoulder and elbow joint upper limb muscle strength and the vibration frequency and also laid the foundation for seeking suitable vibration training strategies to maximize the athlete's whole body coordination. Flexibility, jumping ability, balance, and other abilities lay the foundation for further applying appropriate vibration strength training to the public level and improving the overall quality of citizens.

Judging from the electromyographic characteristics of the jump serve of college volleyball players, the main muscle groups of the whole body are involved in the whole jump serve technique during the jump serve. Therefore, in the

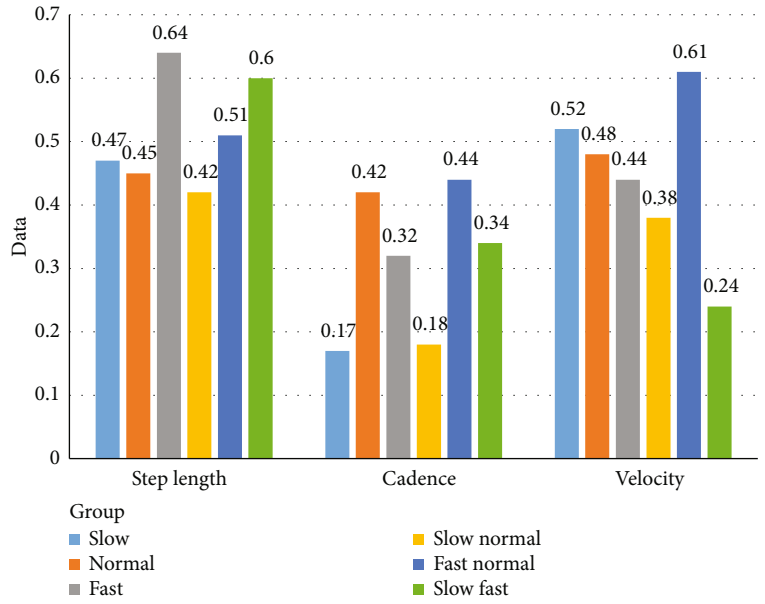

Figure 4: The statistical results of athletes' physical fitness indicators before the experiment.

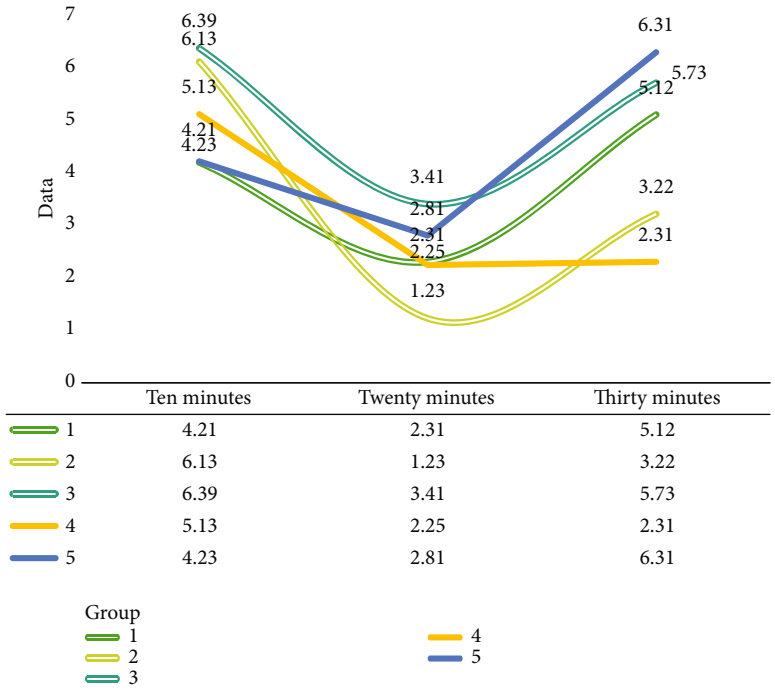

Figure 5: The statistical results of athletes' physical fitness indicators before the experiment.

process of muscle strength training of athletes, it is necessary to pay attention to all-round development. In their physical training, they should include depth jump training of different heights, weight-bearing training of different loads, and combined training formed by different training methods to achieve comprehensive development of the whole body. The role of muscle groups: the strength of the muscle group in the core area plays an important role in promoting the correct sequence of muscle exertion, reducing the loss of force transmitted between the shoulder and the arm, and ensuring the physical fitness required for the jump serve technique. Therefore, to strengthen the strength training in the core area, coaches should design and develop the core area muscle strength training methods on the basis of traditional strength

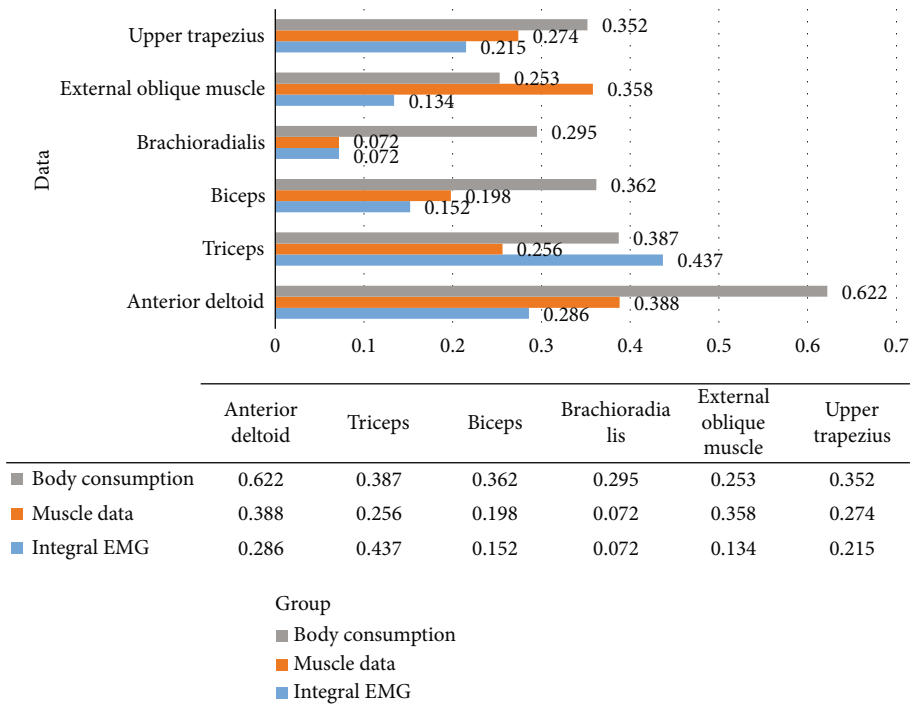

	Anterior deltoid	Triceps	Biceps	Brachioradialis	External oblique muscle	Upper trapezius
Body consumption	0.622	0.387	0.362	0.295	0.253	0.352
Muscle data	0.388	0.256	0.198	0.072	0.358	0.274
Integral EMG	0.286	0.437	0.152	0.072	0.134	0.215

Figure 6: The integral EMG value of each muscle of the athlete in the last step of the jump serve and run-up.

training to supplement and improve the strength training system of volleyball players. From the perspective of the lower limb muscle force of college volleyball players, the coordinated development of lower limb joint muscle strength plays an important role in improving jumping efficiency. Although the special endurance training focuses on improving the flexibility of the lower limbs, the flexion endurance training of the lower limbs cannot be ignored. This is not only related to the coordination of lower extremity muscles to better improve muscle work efficiency and successfully complete jumps but also one of the important methods to prevent sports injuries.

According to the characteristics of the circuit and the degree of integration, MOS analog switch integrated circuits can be divided into many types. The types, names, and characteristics of commonly used analog switch integrated circuits are now listed in Table 3.

According to the needs of the experiment, we chose the CD4051 one-of-eight analog switch as the chip to control the switch circuit. Due to space limitations, only CD4051 is described in detail below. For details of CD4097, please refer to its technical data. CD4051 is a two-way analog switch. In the integrated circuit, there are 4 independent analog switches that can control the transmission of digital and analog signals. Each switch has an input port and an output port. They can be used instead. There is also a strobe terminal (also called a control terminal). When the selected communication terminal is high level, the switch is turned on. The selected communication terminal is usually in an energy-saving state, and the switch is turned off. Do not float the terminal strobe light when using it.

Touch sensors are one of the most important types of robot sensors, and their design also follows the basic principles of sensor design. It is mainly composed of sensitive components, conversion components, and signal conditioning and measurement circuits. The main components of the sensor are shown in Figure 7.

However, not all sensors must contain sensitive components and conversion elements. If the sensitive element directly extracts electricity, it can also be used as a conversion element. In the actual production design, there are many sensors that combine sensitive components and conversion components. For example, when the measured temperature difference is detected, the thermocouple sensor directly exits the electromotive force. Piezoelectric vibrators, piezoelectric pressure sensors, photoelectric devices, etc. are all sensors. Since the output signal of the sensor is usually very weak and one or more interference signals are usually mixed, a signal conditioning circuit is needed to amplify, filter, and configure it. The type of measurement circuit is mainly based on the sensor detection principle, which depends on the type of conversion element, such as bridge circuit, high-impedance input circuit, and differential amplifier circuit. This article uses the row scan method to scan the flexible tactile sensor array. In order to accurately determine the position of the force, the row and column signals collected each time need to be consistent with the row and column signals of the actual sensor array. The scanning circuit of the flexible tactile sensor array uses a piece of four-bit binary counter to change from 0000 to 1111 in the process of cyclically collecting signals. When the counter is 0000, the signals of the first row of the flexible tactile sensor array are collected, and when the

Table 3: Familiar analog multiplexers.

Category	Model	Name	Features
Analog switch	CD4066	Four-way analog switch	Four groups of independent switches, two-way transmission
Multichannel analog switch	CD4051	8 out of 1 analog switch	Level shift, two-way transmission, address selection
	CD4052	Dual 4 out of 1 analog switch	Level shift, two-way transmission, address selection
	CD4053	Three-way, two-way analog switch	Level shift, two-way transmission, address selection
	CD4067	Single 16-channel analog switch	Level shift, two-way transmission, address selection
	CD4097	Dual 8-channel circuit analog switch	Level shift, two-way transmission, address selection
	CD4529	Dual four-way or single eight-way analog switch	Level shift, two-way transmission, address selection

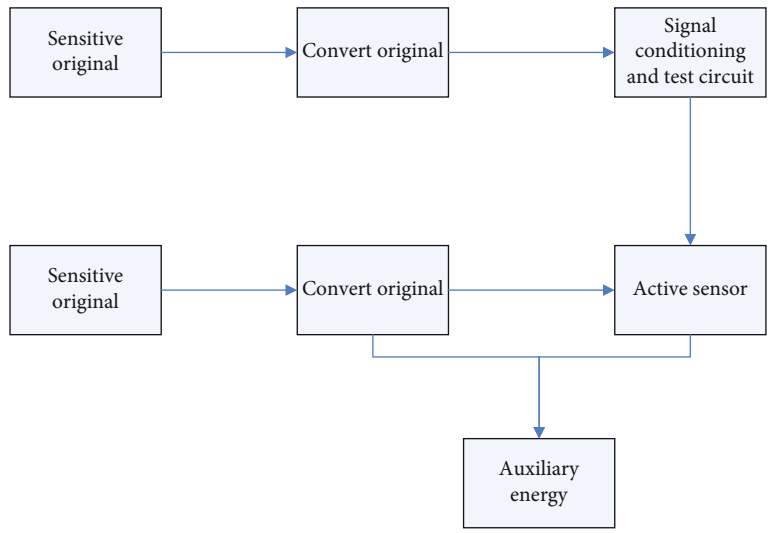

Figure 7: Diagram for sensor's composition.

counter is 0001, the signals of the second row of the flexible tactile sensor array are collected, and so on. Therefore, in this section, a digital signal acquisition program is designed to display the position of the scan line.

5. Conclusions

This article is aimed at developing a set of principle systems that can monitor walking energy consumption in real time. It mainly uses flexible array pressure sensors to detect plantar pressure distribution to obtain the user's gait information in real time and design it into the form of an insole, which is embedded in the sole. In the process of exercise, energy consumption is a very illusory concept after all. The user has a fuller and more specific understanding of speed, distance, and exercise time. Therefore, while effectively estimating exercise energy consumption, it must also be able to record the user's exercise. Time, estimate the speed and distance of the user. Based on these requirements, this article needs to establish two estimation models; one is the estimation model of walking speed, and then, the movement distance is calculated; the other is the estimation model of walking energy consumption, which can estimate the energy consumption of users in real time. These two models are the software part of the embedded sports energy monitoring principle system based on the flexible array pressure sensor insole. Theoretical analysis and experimental research show the new type of rubber-based touch sensor conductive plate and the information collection, analysis, and processing studied in this article. The system is completely feasible and can achieve accurate collection of large-area touch collection information. This is a good method and example, touch sensor panel. This development provides a new method and lays the foundation for the development of smart robotic clothing. The research prospects of this article are as follows. The experiments in this article are objective, the data are real, and the estimation model and experimental process established are reproducible and can stand the test, but they are only preliminary exploratory experiments. For the verification and affirmation of the entire experimental process, there are still many areas for improvement.

Data Availability

No data were used to support this study.

Disclosure

We confirm that the content of the manuscript has not been published or submitted for publication elsewhere.

Conflicts of Interest

There are no potential conflicts of interests in our paper.

Acknowledgments

This work was supported by the Guangdong Philosophy and Social Science Planning Project under Grant No. GD20CTS02.

References

[1] D. Ning and L. Yijun, "Research on the reform of volleyball league in my country," *Sports Culture Guide*, vol. 20, no. 12, pp. 101–105, 2016.

[2] M. Zhou, X. Li, Y. Wang, S. Li, Y. Ding, and W. Nie, "6G multi-source information fusion based indoor positioning via Gaussian kernel density estimation," *IEEE Internet of Things Journal*, 2020.

[3] Z. Lui, J. Li, A. Wang, J. Jia, and J. Wang, "UWB indoor positioning accuracy calibration method based on motion capture system," *Journal of Surveying and Mapping Science and Technology*, vol. 34, no. 2, pp. 147–151, 2017.

[4] Y. Wang, T. Lu, and H. Yonghua, "Distortion recovery of human motion capture data based on bone constraint," *Computer Systems & Applications*, vol. 27, no. 5, pp. 19–27, 2018.

[5] Z. Liang, "The current situation of volleyball teaching in colleges and universities and the improvement of teaching mode," *Journal of Heihe University*, vol. 8, no. 10, pp. 120-121, 2017.

[6] Y. Liu, Y. Feng, Q. Li, Y. Wan, C. Lou, and J. Lou, "Research on characteristics of kinematic parameters of stilt method based on 3D motion capture technology," *Journal of Beijing University of Traditional Chinese Medicine*, vol. 41, no. 3, pp. 235–241, 2018.

[7] F. Huang, Q. Zhang, H. Wang, L. Wang, C. Sun, and Y. He, "Application of motion capture technology in the study of biomechanics of massage techniques," *Chinese Medicine Orthopedics*, vol. 29, no. 11, pp. 41–43, 2017.

[8] H. Yizi, "Motion capture technology process and data processing——facial motion capture and data processing," *Modern Film Technology*, vol. 3, no. 1, pp. 39–42, 2016.

[9] T. Jinghua and Y. Yiguo, "The application of optical three-dimensional motion capture in the research of motion system," *Hainan Medicine*, vol. 29, no. 14, pp. 111–114, 2018.

[10] Y. Tingting and H. Bin, "Human gait analysis based on 3D motion capture technology," *Digital Technology and Application*, vol. 5, no. 2, pp. 232-233, 2017.

[11] C. Zimin, "Human motion segmentation and annotation technology based on motion capture data," *Tomorrow Fashion*, vol. 20, no. 13, pp. 299–299, 2017.

[12] T. Wu, X. Wu, D. Hu, Q. Wang, and F. Wang, "Research progress of shoulder joint kinematics analysis based on optical motion capture system," *Chinese Electronic Journal of Shoulder and Elbow Surgery*, vol. 4, no. 4, pp. 248–250, 2016.

[13] Y. Hou, X. Zhang, B. Li, and W. Li, "Application research of motion capture technology in the virtual environment of substation," *Journal of System Simulation*, vol. 28, pp. 2632–2637, 2016.

[14] C. Ningbo, W. Zhiming, and X. Cundong, "Analysis of human skin deformation during cycling based on motion capture," *Journal of Textile Research*, vol. 39, no. 9, pp. 120–126, 2018.

[15] G. Chunyu, "Motion mechanical parameters and related influencing factors of lumbar spine rotation manipulation in motion capture sitting position," *China Orthopedics and Traumatology*, vol. 32, no. 9, pp. 802–806, 2019.

[16] Z. Haifeng, Z. Can, L. Meixiao, S. Cuirong, and P. Yin, "Analyzing the movement ability of hip joints based on motion capture technology," *Chinese Tissue Engineering Research*, vol. 941, no. 12, pp. 17–21, 2021.

[17] H. Tianyu and L. Qi, "A review of research on motion capture technology and its application in sports," *Electronic Measurement Technology*, vol. 42, no. 3, pp. 146–152, 2019.

[18] Z. Chao, J. Longbin, and H. Cheng, "Cue-guided facial motion capture and data virtual reuse method," *Computer Science*, vol. 45, pp. 198–201, 2018.

[19] P. Shi, J. Lai, P. Lu, and S. Bao, "Real-time attitude measurement algorithm for multi-rotor aircraft based on motion capture system," *Navigation and Control*, vol. 17, no. 72, pp. 104–109, 2018.

[20] F. Liao, S. Jinlong, and G. Xiao, "Three-dimensional motion capture method of point-like feature flexible object," *Computer Systems & Applications*, vol. 27, no. 7, pp. 230–235, 2018.

[21] J. Li, C. Gao, M. Feng et al., "Research on the related issues of motion capture, shaking, pulling and poking in the treatment of ankle sprain movement," *Chinese Journal of Orthopaedics and Traumatology*, vol. 26, no. 9, 2018.

[22] R. Wen, "Research on auxiliary training system based on Kinect motion capture technology," *Electronic Design Engineering*, vol. 27, no. 7, pp. 75–78, 2019.

[23] N. Jingde, "Application analysis of motion capture technology in film and television animation production," *Theoretical Research and Practice of Innovation and Entrepreneurship*, vol. 3, no. 5, pp. 149-150, 2020.

[24] X. Zhong, J. Li, J. Song, W. Lou, and W. Sun, "Application of motion capture technology in power safety simulation training," *Information Technology*, vol. 43, no. 7, pp. 170–174, 2019.

[25] L. Bing, "The application of motion capture technology in film and television animation production," *Television Technology*, vol. 42, no. 10, pp. 46–49, 2018.

[26] L. Shuhua, "Research on the application of performance motion capture technology in film and television performance animation," *Television Technology*, vol. 42, no. 10, 2018.

[27] W. Defang, "Research on the digital processing technology of the original data of the Anzhao dance of the Tu nationality based on the motion capture system," *Journal of Science & Technology Economics Guide*, vol. 27, no. 28, pp. 39–39, 2019.

[28] W. Shixiang, "Research on digital protection of ethnic dances based on motion capture technology," *Public Standardization*, vol. 309, no. 16, pp. 153-154, 2019.

[29] S. Chen and M. Xiangxu, "Application of performance motion capture technology in film and television performance animation," *Southern Agricultural Machinery*, vol. 50, no. 4, p. 187, 2019.

[30] M. Zhou, Y. Wang, Y. Liu, and Z. Tian, "An information-theoretic view of WLAN localization error bound in GPS-denied environment," *IEEE Transactions on Vehicular Technology*, vol. 68, no. 4, pp. 4089–4093, 2019.

[31] S. Yao, L. Li, Y. Wang, F. Chang, and Y. Zeyuan, "Whole body motion capture method based on dual Kinect adaptive weighted data fusion," *Journal of Chongqing University of Technology*, vol. 33, no. 9, pp. 109–117, 2019.

[32] C. Wei, "Application of motion capture technology in 3D computer animation production," *Automation and Instrumentation*, vol. 32, no. 12, pp. 143-144, 2017.

Hindawi
Journal of Sensors
Volume 2023, Article ID 9868193, 1 page
https://doi.org/10.1155/2023/9868193

Retraction

Retracted: Multimode Intelligent Control Based on Multidata Fusion Filtering in High-Speed Train Traffic Signal and Control

Journal of Sensors

Received 31 October 2023; Accepted 31 October 2023; Published 1 November 2023

This article has been retracted by Hindawi following an investigation undertaken by the publisher [1]. This investigation has uncovered evidence of one or more of the following indicators of systematic manipulation of the publication process:

(1) Discrepancies in scope
(2) Discrepancies in the description of the research reported
(3) Discrepancies between the availability of data and the research described
(4) Inappropriate citations
(5) Incoherent, meaningless and/or irrelevant content included in the article
(6) Peer-review manipulation

The presence of these indicators undermines our confidence in the integrity of the article's content and we cannot, therefore, vouch for its reliability. Please note that this notice is intended solely to alert readers that the content of this article is unreliable. We have not investigated whether authors were aware of or involved in the systematic manipulation of the publication process.

Wiley and Hindawi regrets that the usual quality checks did not identify these issues before publication and have since put additional measures in place to safeguard research integrity.

We wish to credit our own Research Integrity and Research Publishing teams and anonymous and named external researchers and research integrity experts for contributing to this investigation.

The corresponding author, as the representative of all authors, has been given the opportunity to register their agreement or disagreement to this retraction. We have kept a record of any response received.

References

[1] B. Huang and Y. Huang, "Multimode Intelligent Control Based on Multidata Fusion Filtering in High-Speed Train Traffic Signal and Control," *Journal of Sensors*, vol. 2021, Article ID 6081999, 10 pages, 2021.

Hindawi
Journal of Sensors
Volume 2021, Article ID 6081999, 10 pages
https://doi.org/10.1155/2021/6081999

Research Article

Multimode Intelligent Control Based on Multidata Fusion Filtering in High-Speed Train Traffic Signal and Control

Bin Huang and Ying Huang

School of Automatic Control, Liuzhou Railway Vocational Technical College, Liuzhou, 545616 Guangxi, China

Correspondence should be addressed to Ying Huang; hy@ltzy.edu.cn

Received 15 April 2021; Revised 26 April 2021; Accepted 6 May 2021; Published 1 June 2021

Academic Editor: Mu Zhou

As the speed of high-speed trains continues to increase, the intelligent monitoring of high-speed trains has become a concern of people. This research mainly discusses the application of multimode intelligent control of multidata fusion filtering in high-speed train traffic signal and control. In multimodal intelligent control, BangBang, PI control, adaptive fuzzy PID control, and expert monitoring control under special circumstances can be used, respectively, according to the error and the rate of change of the error, which can achieve the best control effect under safe conditions. Take the allowable speed of ATP as the target speed of the control system, and combine the operation process, operation requirements, traction characteristics, braking characteristics of high-speed trains, and meet the two conditions for improving the operating efficiency of high-speed trains. According to the dynamic expected speed value of high-speed trains, dynamically adjust the switching threshold. This study uses a pulse signal generator to simulate the speed data of the vehicle speed sensor (all pulse data), and then read the speed (pulse) signal data through the pulse signal acquisition card, and display the simulated speed data under the Kingview software. The monitoring computer is used to collect train speed information, display speed information, manage speed information, and output speed information. Then, through OPC technology, the simulation speed data is transmitted to MATLAB software for multidata fusion filtering processing and multimodal control simulation. In the simulation process, the train adopts a multimodal intelligent control response scheme, with a total time of 2183.7 s, which is shortened by 214.5 s and improved by nearly 10%. The multimode intelligent control scheme of multidata fusion filtering proposed in this study can better meet the control of high-speed train traffic signals.

1. Introduction

The twenty-first century is an excellent period for the development of high-speed railways in the world. It is a new era characterized by high speed in the history of world transportation, especially in China. In recent years, the construction of high-speed railways has made brilliant achievements. At the same time, China also has its own train operation control system CTCS (Chinese Train Control System). In addition, ATO technology has been successfully applied in urban rail and intercity rail transit, but it is rarely used in high-speed railways.

In order to realize the full utilization and efficient transmission of multimodal data, this paper will study a fusion transmission scheme for multimodal data, that is, adopt the method of fusing multimodal data first and then transmitting the fused information to effectively reduce network energy. At the same time, it is ensured that the fusion information can contain important expressions hidden in the original multimodal data, so that even if the amount of transmitted data is reduced, the key information contained in the original multimodal data will not be lost.

The fusion filtering algorithm increases the reliability of location information. F Caron simulates the algorithm by fusing GPS and IMU data from actual tests on land vehicles. Bad data transmitted by GPS sensors can be detected and rejected using contextual information, thereby improving reliability. In addition, the current GPS/INS correlation is not satisfactory [1]. Although the filter he developed makes it possible to easily add other sensors to achieve the desired

performance, the research lacks simulation data [2]. Zhu H believes that accurate measurement of dynamic displacement is very important for structural health monitoring and safety assessment of super high-rise structures. It is difficult for him to accurately measure the displacements of super high-rise structures using traditional methods because they are inaccurate or inconvenient to set in practice. His research provides an accurate and economical method to accurately measure the dynamic displacement of super high-rise structures by fusing acceleration and strain data, which are usually available in structural health monitoring systems. The dynamic displacement is first derived from the measured longitudinal strain based on the geometric deformation and does not require a modal shape. He uses an optimization technique to optimize the deployment of strain sensors to achieve more accurate strain-derived displacements. Although his research has been applied to numerical super high-rise structures and laboratory cantilever beams to verify the displacement of the high-frequency component and pseudostatic component of the method, the research lacks logic [3]. Amamra A proposed a new method; his method can accurately track the driving vehicle by using the multiview setting of the red-green-blue depth (RGBD) camera. He first proposed a correction method to eliminate the offset that occurs when the depth sensor is worn. Otherwise, using conventional calibration procedures cannot solve this problem. Next, he introduces a sensor-based filtering system to correct unknown vehicle movement. The data fusion algorithm is then used to best merge the estimated trajectories of the sensor orientation. He implemented most of the solution in the graphics processor. Although the accuracy obtained by his research and the robustness of the solution in overcoming the uncertainty of measurement and modeling, the research lacks contrast [4]. Balakrishnan S N proposed a modular method to solve the multisensor multitarget problem in space. His method combines clustering techniques developed in the field of pattern recognition with filtering techniques developed to estimate multiple target states in space. He introduced the results of cluster analysis and used two scenes with multiple targets and used an orbital platform as a sensor. Although his research gave the estimation error history of position and velocity, it did not describe their relevance to target recognition and data fusion [5].

This research mainly discusses the application of multimode intelligent control of multidata fusion filtering in high-speed train traffic signal and control. In multimodal intelligent control, BangBang, PI control, adaptive fuzzy PID control, and expert monitoring control under special circumstances can be used, respectively, according to the error and the rate of change of the error, which can achieve the best control effect under safe conditions. Take the allowable speed of ATP as the target speed of the control system and combine the operation process, operation requirements, traction characteristics, and braking characteristics of high-speed trains, and meet the two conditions for improving the operating efficiency of high-speed trains. According to the dynamic expected speed value of high-speed trains, dynamically adjust the switching threshold. This study uses a pulse signal generator to simulate the speed data of the vehicle speed sensor (all pulse data), and then read the speed (pulse) signal data through the pulse signal acquisition card, and display the simulated speed data under the Kingview software. The monitoring computer is used to collect train speed information, display speed information, manage speed information, and output speed information. Then, through OPC technology, the simulation speed data is transmitted to MATLAB software for multidata fusion filtering processing and multimodal control simulation.

2. High-Speed Train Traffic Signal and Control

2.1. Traffic Signal Control. Using multimodal control based on feature identification, it follows the speed control target well. In addition, there are control methods such as two-level fuzzy neural network control, fuzzy PID control, adaptive fuzzy PID control, and fault-tolerant control. These control methods and algorithms include classic PID control and improved PID control. Some of these control methods theoretically verify the feasibility of the method, and some first conduct theoretical research and analysis and then apply the theoretical research results to actual train control. These studies have achieved good results to a large extent, solved certain practical problems, and obtained a series of research results [6, 7]. Most of the above research methods and control algorithms ignore an important issue, that is, assuming that the real-time detection value of the control system (strictly speaking, it should be the real-time speed detection value or the detection processing value) is very accurate, and the quality of the control method is measured. The control effect is to make the output value of the control system follow the expected value of the control system well and/or to improve the robustness, rapidity, and stability of the system. However, the real-time speed detection value of the actual running train is sometimes inaccurate. For a control system with inaccurate detection value itself, the control algorithm, control method, and control effect cannot fully reflect the true effect, and if the speed measurement error or speed processing error is too large, there may be a rear-end collision safety risk [8].

At present, the actual control of high-speed trains has not reached the level of theoretical research. Most high-speed train control only implements functions such as ATP, and the ATO function needs to be introduced into the high-speed train operation control system. In recent years, a small number of high-speed trains have realized the ATO function, but the control algorithm still adopts the traditional PID control, and the control system design does not consider the accuracy of the detection and processing. In the actual operation of high-speed trains, in order to avoid safety problems caused by speed measurement errors (or speed processing errors), the maximum speed of multiple speed sensors is often used when calculating speed, and the speed control setting value is lower than the allowable speed of ATP, resulting in speed of high-speed trains is reduced or the interval between train departures becomes longer, which affects the operating efficiency of high-speed trains, which in turn affects the utilization rate of the entire high-speed railway network, and cannot give full play to the transportation

capacity of the entire high-speed railway network, resulting in a waste of resources [9].

There is usually a certain delay in road network traffic [10].

$$\begin{cases} W_{i,j} = \exp\left(\dfrac{\alpha_i D_{\mathrm{HOL},i} - x}{1+\sqrt{x}}\right) \times \dfrac{r_{i,j}}{R_i}, \\ x = \dfrac{1}{N}\sum_{1}^{N} \alpha_i D_{\mathrm{HOL},i}, \end{cases}$$

$$P_a\left(s, s'\right) = P\left(s_{t+1} = s' \middle| s_t = s, a_t = a\right) \begin{cases} 1\left(s' = 0, a = a_1\right), \\ P\left(s, s'\right)\left(a = a_2\right), \\ 0(\text{else}). \end{cases} \tag{1}$$

W_{ij} represents the final delayed power. Certain information and data support is required in the loading and transmission of data [11, 12].

$$\Pr\left[E_2\right] = 1 - \frac{q_{\mathrm{sc}}\left(q_{H_2} + q_{H_3}\right)}{2^l}. \tag{2}$$

Among them, $\Pr[E_1]$ represents the intensity of data transmission. The wireless network driver can perform channel tuning, multichannel synchronization, and channel routing, and interact with the upper and lower data protocol $\Pr[E_2]$. In order to request data from above and move down, these are the implementation of the multichannel protocol mechanism $q_{\mathrm{att}}/2$. This is the premise and basis of basic data transmission of signals [13, 14].

Information recognition carried by the Internet of vehicles requires the common realization of the same points of each model [15]

$$\begin{aligned} \Pr[C] = \Pr\left[E_1 \cap E_2 \cap E_3\right] &\geq \left(1 - \frac{q_{\mathrm{ppk}}}{q_{H_1}}\right)\left(1 - \frac{q_{\mathrm{att}}}{2^l}\right) \\ &\cdot \left(1 - \frac{q_{\mathrm{sc}}\left(q_{H_2} + q_{H_3}\right)}{2^l}\right)\mathscr{E}, \\ \Pr[C] &\geq \left(1 - \frac{q_{\mathrm{ppk}}}{q_{H_1}}\right)\left(1 - \frac{q_{\mathrm{sc}}\left(q_{H_2} + q_{H_3}\right)}{2^l}\right)\mathscr{E}. \end{aligned} \tag{3}$$

$P[C]$ represents the final analysis data [16].

2.2. Multimodal Data Fusion. Multimodal data fusion mainly refers to the comprehensive processing of multiple modal information using computers, proposing various theories and algorithms, and comprehensively processing different types of multimodal data to obtain a more accurate state of objective objects, and environmental information is the focus of multimodal data fusion research. The focus of the research is feature recognition methods and fusion algorithms. These algorithms can complete the coordination and complementation of a variety of different sensor information and improve the decision-making process based on uncertain data. What we usually call multimodal data fusion is essentially an imitation of the ability of organisms to comprehensively process a variety of information. In a multimodal fusion system, the data measured by various sensors will have different characteristics and be expressed in different formats. The multimodal data fusion system will make full use of the resources provided by a variety of sensors, and through the reasonable analysis and utilization of various data, the data will be coordinated according to the pregiven optimization principles to obtain the final fusion result. Observe the state or activity law of the target to make judgments and interpretations. Compared with a single sensor system, a multimodal sensor system has the following advantages:

(i) System stability is strong. When there are several sensors due to their own reasons or strong interference from the environment, there will always be several sensors that cannot work normally, and the range of target activities is often not covered by all sensors. Through the various sensors provided by various sensors. The analysis of redundant information in the form can ensure that the system works normally under any conditions

(ii) Wide coverage. In a system composed of multiple sensors, the range of the area detected by each sensor is also different. It is possible for a certain sensor to detect places that other sensors cannot detect. Therefore, the coverage of the system is greatly improved

(iii) Information is provided at all times. Due to the different working hours and detection cycles of various sensors, the synergy of multiple sensors can greatly improve the time coverage of the system and ensure the continuity of information supply

(iv) High credibility. The redundant information provided by a variety of sensors can ensure that the system finds its own errors in time, which greatly improves the reliability of the system [17]

In order to accurately analyze the characteristics of the original data sequence, after the network training prediction is completed, we need to denormalize the predicted value. The calculation formulas are

$$\begin{aligned} X(i) &= X_{gvh}(\max(X) - \min(X)) + \min(X), \\ X(i) &= X_{gvh}(i)\sigma_x + \bar{X}. \end{aligned} \tag{4}$$

The denormalized data is in the same dimension as the original data, and analyzing it can more accurately extract the features and laws contained in the relevant data [18, 19].

2.3. Fusion Model. High-speed train operation automatic control systems such as ETCS and CTCS can realize functions such as the high-speed train operation automatic

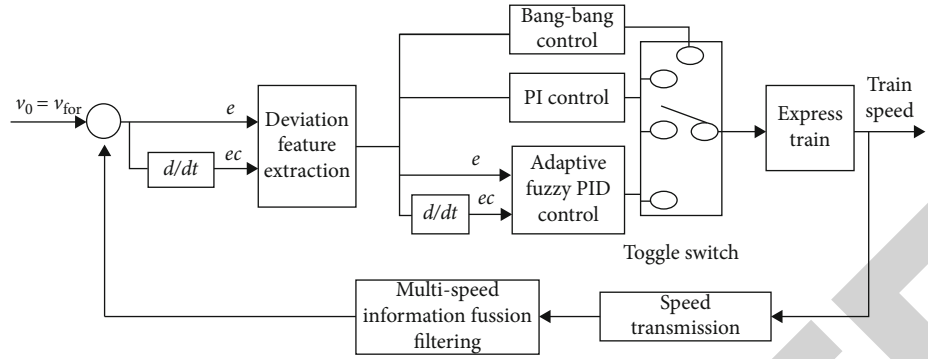

Figure 1: High-speed train speed control based on multi-information fusion filtering and multimodal intelligent control.

protection system ATP (Automatic Train Protection). As for the high-speed train automatic driving technology ATO (Automatic Train Operation) based on the high-speed train operation automatic protection system, it is still more theoretical studies and fewer practical applications. When designing the multimodal fusion method for ranging, this article considers the following application objectives and scenarios: a variety of ranging sensors are used to simultaneously measure a target to cope with the environment where noise factors such as climate and environment change rapidly, ground configuration, and synchronous sampling. The distance dynamic model of the target is

$$\begin{aligned} R_x E\left[X(t)X^H(t)\right] &= AE\left[SS^H\right]A^H + AE\left[SN^H\right] \\ &= E\left[NS^H\right]A^H + E\left[NN^H\right]. \end{aligned} \tag{5}$$

There are a variety of ranging sensors such as radar and infrared, and their measurement models are [19]

$$Z = Hx + v. \tag{6}$$

Among them, Z is the measured value and H is the state transition matrix. Assuming that the signal and noise are independent, and the noise is Gaussian white noise with zero mean and variance of σ^2, namely,

$$E\left[NN^H\right] = \sigma^2 I. \tag{7}$$

Then, the above formula can be simplified to [20]

$$R_x = AR_sA^H + \sigma^2 I, \tag{8}$$

where R_s is the covariance matrix of the incident signal. TDOA is a technology derived from TOA. Its main advantage is to overcome the problem of electronic clock time synchronization, that is, it does not require a strictly synchronized electronic clock [21, 22]. Assuming there are two signals with different propagation speeds, the calculation formula of distance R is as follows:

$$R = \left|(T_4 - T_3) - (T_2 - T_1)\right| \times \frac{V_2 - V_1}{V_2 \times V_1}. \tag{9}$$

In the formula, V1 and V2 are the propagation speeds of the two signals, respectively. Data fusion can be expressed as

$$Y = \frac{C_{1j} \times Z1 + C_{21j} \times Z2 + C_{3j} \times Z3 + \cdots + C_{nj} \times Zn}{N}. \tag{10}$$

2.4. Multimodal Intelligent Control of High-Speed Train Speed Signal. The speed signal control of high-speed trains needs to consider many factors, such as line speed, train speed limit, ramps, curves, and target points. There have been many studies on the speed control of high-speed trains, but in practical applications, advanced control algorithms and control methods are still relatively few, and the control algorithm is mainly based on classic PID control [23]. Therefore, in this paper, a specific multimodal control method is designed in combination with the operation goals of high-speed train safety, efficiency, and comfort.

In the multimodal intelligent control in Figure 1, Bang-Bang, PI control, adaptive fuzzy PID control, and expert monitoring control under special circumstances can be used according to the error and the rate of change of the error, which can achieve the best under safe conditions. The multi-speed information fusion filtering module in the high-speed train speed control system mainly performs fusion filtering processing on the information of the four speed sensors to improve the detection processing accuracy [24, 25].

This design idea is not essentially different from the general multimodal control, but the given value of the high-speed train speed control system is optimized, that is, the allowable speed of the ATP is taken as the target speed of the control system, and combined with the operation process of the high-speed train, operation requirements, traction characteristics, braking characteristics, and satisfying the two conditions for improving the operating efficiency of high-speed trains, the switching threshold of the multimodal intelligent control algorithm is optimized [26]. The specific content of the optimization design is to dynamically adjust the switching threshold according to the dynamic expected speed value of the high-speed train [27, 28].

$$\begin{aligned} E_{\max} &= \mathrm{V0} - 1, \\ E &= \mathrm{V0} - \mathrm{V}. \end{aligned} \tag{11}$$

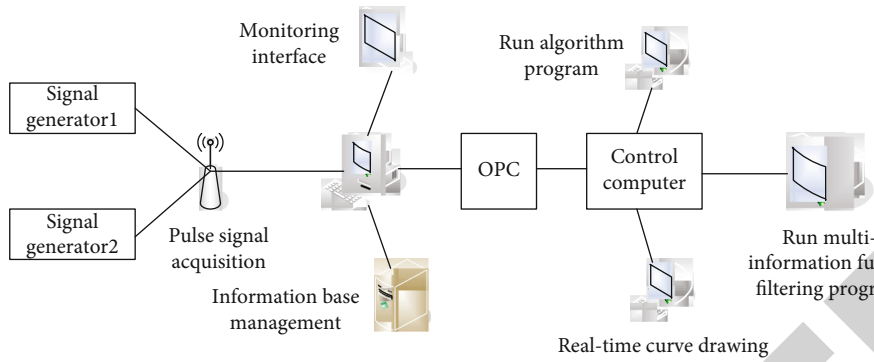

Figure 2: Real-time control of multimodal intelligent control system.

That is, when the expected speed is higher, the switching thresholds E_{max} and E are set to be smaller to ensure that the maximum acceleration and deceleration time are longer, and the speed and efficiency are improved; when the expected speed is lower, the switching thresholds E_{max} and E are set to be larger. One point is to improve the control accuracy without affecting the operating efficiency [29].

3. High-Speed Train Traffic Signal and Control Experiment

3.1. Simulation Test Platform. There are on-board speed and distance measurement unit SDU (Speed & Distance Unit) and SDP (Speed & Distance Processing Unit) in the on-board equipment of high-speed trains, which are used to provide real-time speed value and positioning information. However, the real-time speed data of the study cannot be obtained from actual high-speed trains, and it is inconvenient to use real test benches to simulate high-speed train speed measurement [30]. Therefore, this study uses a pulse signal generator to simulate the speed data of the on-board speed sensor (all pulse data). Then, read the speed (pulse) data through the pulse signal acquisition card, display, store, and manage the simulated speed data under the Kingview software, and then, transfer the simulated speed data to the MATLAB software for multidata fusion filtering processing through OPC technology control simulation with multimodal control. The advantage of this design method is to make full use of the advantages of configuration software to read hardware data and the advantages of MATLAB software data processing.

3.2. Overall Structure Principle of the Simulation Test Platform

(1) Signal detection

The signal detection part completes the detection and conditioning of the speed sensor information. The speed sensor is used to detect the real-time speed information of the train running process, and the signal conditioning circuit is to perform standardized processing such as filtering and pulse shaping on the detected speed sensor information.

(2) Monitoring computer

The monitoring computer is used to collect train speed information, display speed information, manage speed information, and output speed information.

(3) OPC technology

OPC (Object Linking and Embedding for Process Control) technology is a software interface standard for the transmission and exchange of train speed information, which realizes the communication between the monitoring computer and the control computer.

(4) Control computer

The control computer is used to receive the simulation speed information transmitted by OPC (Object Linking and Embedding for Process Control), realize multispeed information fusion filtering and simulation research, and use the fusion filtering result as the feedback value of the multimodal intelligent control system to realize the simulation real-time closed-loop control of the same speed of high-speed trains, complete the drawing, and display of related simulation curves. The real-time control of the multimodal intelligent control system is shown in Figure 2.

3.3. Hardware Design of Simulation Test Platform. The hardware design of the simulation test platform adopts pulse data acquisition card and related accessories to realize multichannel speed information detection. The pulse data acquisition card is a counter/timer and digital input/output card for IBM PC/AT. The card provides six 16-bit counter channels, and it also has 16 digital inputs and 16 digital outputs. The two 8254 chips on the card provide various counter/timer function modes, which can be used in experimental equipment and actual industrial products.

The pulse data acquisition card is equipped with a special digital filter, which can eliminate the noise in the input pulse signal, and its frequency can be adjusted to provide a more stable output reading during use. The main function of the pulse signal data acquisition card is six counters or timers. The board also has 16 switching output and 16 switching input functions. The output and input levels of the board are both standard TTL levels. In this research, the pulse

Table 1: RH3 model train size parameters.

Project	The main parameters
Chief of EMU	200.67 m
Length of head car	25.52 m
Maximum width of car body	3.265 m
Maximum height of car body	3.890 m
Gauge	1.435 m

Table 2: Traction and braking parameters of CRH3 EMU.

Project	The main parameters
Total traction power	8800 (kW)
Start acceleration	0.38 (m/s) (0-200 km/h)
Weight of empty car marshalling	479.36 (t)
Capacity of capacity	536 (t)
Speed class	300 (km/h)

Table 3: Braking distance requirements.

Braking speed	Distance requirement
Initial braking speed 300 km/h	≤3700 m
Initial braking speed 200 km/h	≤2000 m
Initial braking speed 160 km/h	≤1400 m

counting function is mainly used to realize the output pulse counting of analog speed sensors (wheel Hall speed sensor and Doppler radar speed sensor) to calculate the real-time running speed and running distance of high-speed trains.

3.4. Configuration Software Design

(1) Monitoring interface design

Use pulse signal generator, pulse signal acquisition card, and related accessories; connect to industrial control computer; and realize real-time simulation speed data acquisition and display through Kingview software.

The simulation test platform designed in this study uses OPC technology to connect KingView configuration software and MATLAB software and utilizes the advantages of MATLAB software's strong data processing ability and good simulation to realize multi-information fusion filtering and multimodal intelligent control algorithms. KingView configuration software realizes real-time simulation speed data acquisition and real-time monitoring of the main parameters of the system. Taking full advantage of the strong human-machine interface of KingView configuration software, it is easier to realize the collection of peripheral hardware data. At the same time, it showed the friendly man-machine interface of KingView configuration software, which well completed the real-time monitoring of simulation speed information.

To design real-time data variables, you must first define the data variables. Specifically, click the data dictionary in the menu bar on the left side of the configuration software to create 4 sets of I/O integer data variables, namely, display, display 1, display 2, and display 3. The connected device is selected as the new I/O device, the register is selected as the RADOM type, and the data type is the SHORT type.

After completing the "data dictionary" design, you can start various other interface designs. The design content mainly includes simulation test system monitoring main interface, simulation speed information acquisition and display interface, and simulation real-time speed curve generation interface. The high-speed train analog signal detection interface is shown in Figure 2.

(2) OPCTOOL design under MATLAB software

The specific design process is to first open the MATLAB software, enter the OPCTOOL command at the MATLAB command window command prompt, and then, press the Enter key to open the OPCTOOL toolbox. After understanding the function of OPCTOOL, familiar with and mastering the connection method of OPCTOOL, you can design the OPC communication system. The OPCTOOL toolbox is mainly divided into three parts for the OPC communication connection: first, the computer DCOM setting, the second is the establishment and setting of the OPC server of the configuration software, and the third is the debugging of the MATLAB software, and the final communication of the OPC is successful. Computer DCOM settings, click the start menu, enter dcomcnfg in the run box, and click Enter; the configuration window will pop up and click Component Services, Computer, My Computer, DCOM Configuration in turn. Find OPCEnum in the DCOM configuration, right-click to enter the properties interface, click Security, select all three items as custom, and click OK, DCOM configuration is complete. To establish and set up the configuration software OPC server, click the OPC server in the project browser, double-click the new icon, enter \localhost in the network node name field, select KingView-View1 for the server, and click OK. Then, select the board and click new to use the default new IO device, make corresponding settings, and complete the configuration software configuration.

3.5. Simulation Platform Software Joint Debugging and Simulation. After completing the Kingview interface design, Kingview software OPC design, and MATLAB software OPCTOOL setting design, the system software will be debugged. After the system is running, the Kingview software detects the pulse generated by the pulse signal generator in real time through the pulse signal acquisition card information (i.e., simulated speed information), and then, realize the real-time display of the simulation speed, the storage of the simulation speed data, and the generation of the curve of the simulation real-time speed value in the configuration software environment. From these results, we can basically understand the real-time speed information of the external simulation. Later, Kingview software transfers the collected simulation real-time speed information to the OPC of MATLAB software through OPC technology. OPC receives the simulation speed information through OPCTOOL and then processes the simulation speed information. On the

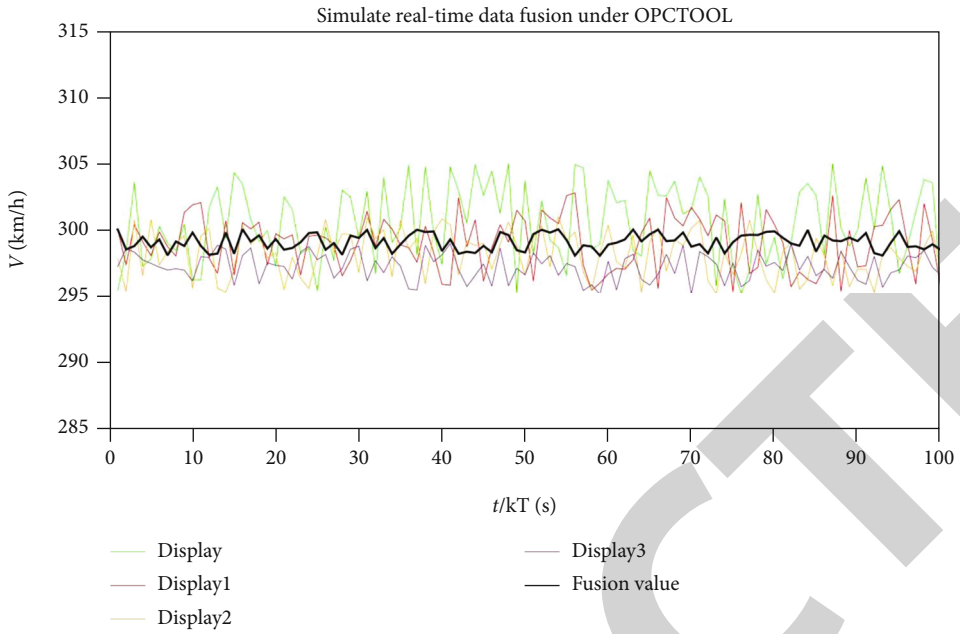

Figure 3: Multi-information fusion filtering processing of the simulated real-time speed value received by MATLAB.

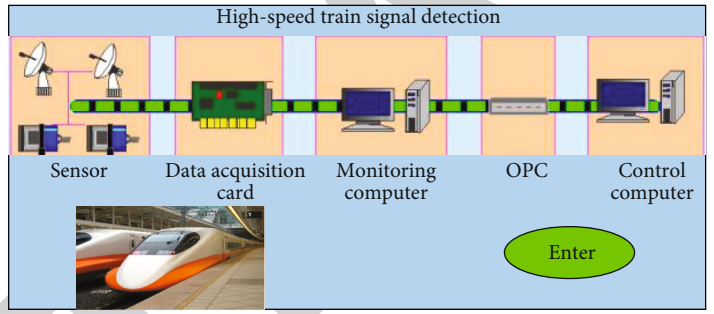

Figure 4: High-speed train analog signal detection interface.

one hand, it performs real-time display and storage. On the one hand, the received simulation real-time speed value is drawn into a curve. In this way, the consistency and synchronization of the simulation speed data under the Kingview software and the simulation speed data under the MATLAB software can be observed intuitively.

4. Results and Discussion

4.1. Joint Debugging of Software System. The CRH3 high-speed train was selected for the simulation. This model is a 4-motion +4 drag train, single-phase power supply, and the standard voltage is AC25kV, 50 Hz. The axle load is about 17 t when the capacity is fixed, and the number of people: 600 people, 72 people for the first-class seats, 528 people for the second-class seats, and the capacity $M = 536$ t. The minimum radius of train passing requirements: rotation quality coefficient $r = 0.08$, $R = 250$ m in continuous operation, and $R = 150$ m in single-vehicle shunting. CRH3 model train size parameters are shown in Table 1.

CRH3 EMU traction and braking parameters are shown in Table 2.

On a straight track, the braking distance for emergency braking of high-speed trains of EMUs needs to meet the requirements. The specific braking distance requirements are shown in Table 3.

Multi-information fusion filtering is performed on the simulated real-time speed value received by MATLAB, and the result after processing is shown in Figure 3. In Figure 4, the real-time curves of the 4 channels of speed information simulation values all have certain fluctuations (a random disturbance signal is added when reading the pulse of the pulse signal generator to simulate the actual speed error), so the use is based on the self. It adapts to the federated Kalman data fusion method for processing, and the processed speed value fluctuates little, which improves the accuracy of simulated speed measurement.

The previous research based on the simulation test platform verified the correctness and rationality of the multi-information fusion filtering method. Let us continue to use the simulation test platform to verify the multimodal intelligent control algorithm. The 4-channel simulation speed information has large errors and unevenness, and good results have been obtained after multi-information fusion

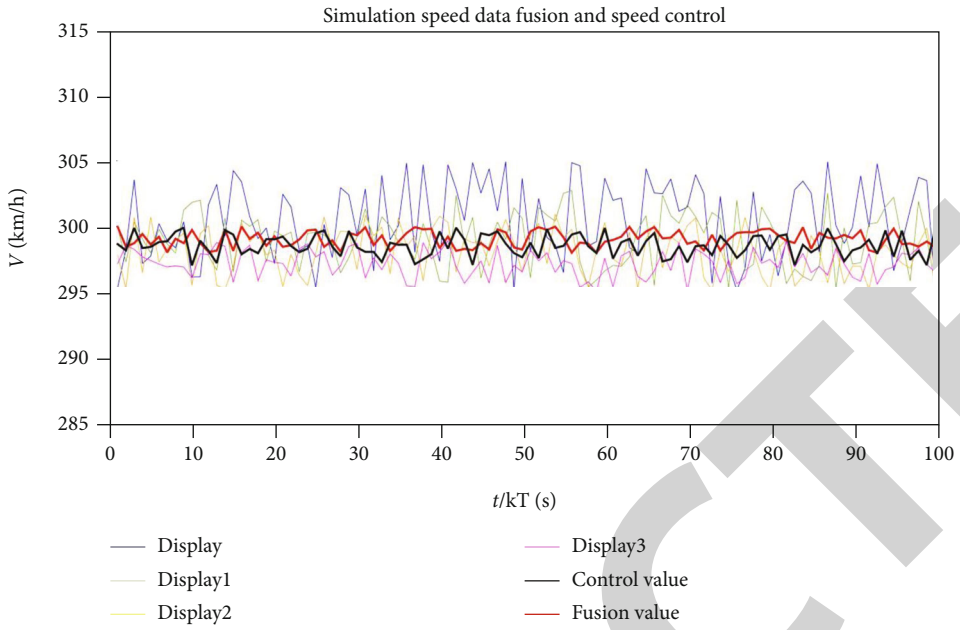

Figure 5: Simulation speed data fusion and speed control.

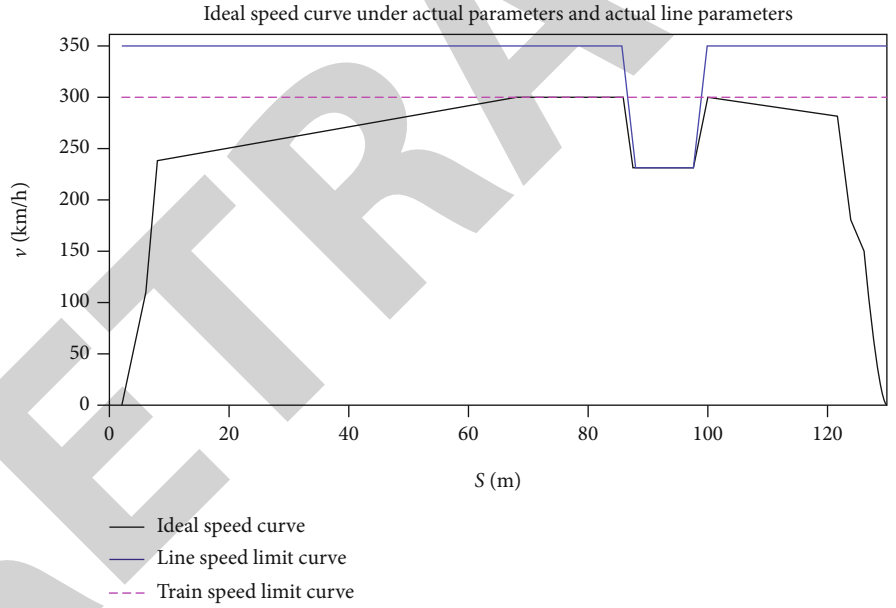

Figure 6: Specific ideal speed curve and speed limit curve.

filtering processing. At the same time, the multimodal intelligent control simulation using the result of multispeed information fusion filtering as the speed feedback value of speed control has also achieved good results. Simulation speed data fusion and speed control are shown in Figure 5.

4.2. Simulation Analysis of High-Speed Train Speed Signal. On the ideal speed curve, the line speed limit and the high-speed train speed limit are added to obtain the specific ideal speed curve and speed limit curve (as shown in Figure 6). In order to ensure the safety of train operation, the current speed control of high-speed trains mostly adopts reduced speed operation, that is, the maximum positive error value is used for control. This result can ensure safety, but affects the efficiency of train operation. The ideal speed curve after speed reduction is simulated based on the average value of 3 km/h-5 km/h reduced by the ATP allowable speed curve of the CTCS-3 grade control system. In the actual programming process, the ideal value is also derived from theory according to the line parameters, high-speed train parameters, and control requirements. Figure 6 does not show a big difference. It can only reflect that the ideal speed value

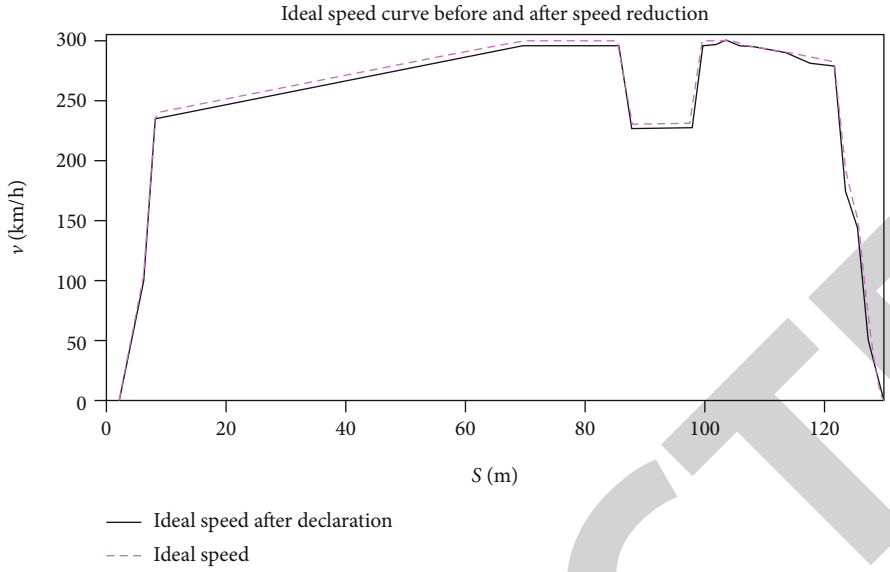

Figure 7: Multimodal intelligent control of multidata fusion filtering and ideal train speed.

of the high-speed train after speed reduction is always lower than the ideal speed value during the operation of the high-speed train in the simulation section.

The multimodal intelligent control of multidata fusion filtering and the ideal train speed are shown in Figure 7. It can be seen that the ideal speed curve before deceleration takes less time, the total time is 2183.7 s, which is shortened by 214.5 s, and the time is shortened by nearly 10%. That is to say, the use of tracking the ideal speed curve control can increase the efficiency by about 10%. The multimodal intelligent control response curve has small fluctuations and can better follow the ideal speed curve; although the PID control response curve can also better track the ideal speed curve after speed reduction, the curve fluctuations are large, which affects the high speed to a certain extent. The smoothness of the train running process affects comfort. Therefore, multimodal intelligent control can achieve better results when used for speed control of high-speed trains.

5. Conclusion

This research mainly discusses the application of multimode intelligent control of multidata fusion filtering in high-speed train traffic signal and control. In multimodal intelligent control, BangBang, PI control, adaptive fuzzy PID control, and expert monitoring control under special circumstances can be used, respectively, according to the error and the rate of change of the error, which can achieve the best control effect under safe conditions. Take the allowable speed of ATP as the target speed of the control system and combine the operation process, operation requirements, traction characteristics, and braking characteristics of high-speed trains, and meet the two conditions for improving the operating efficiency of high-speed trains. According to the dynamic expected speed value of high-speed trains, dynamically adjust the switching threshold. Then, through OPC technology, the simulation speed data is transmitted to MATLAB software for multidata fusion filtering processing and multimodal control simulation. In future research, when there are many data modalities involved in the system, the complexity of the model will increase accordingly. How to save computing resources and time overhead to perform model training more efficiently will be a very critical issue. Further research can reduce the difficulty of multimodal data fusion, expand the scope of application of multimodal data fusion, and enhance its practical application value.

Data Availability

No data were used to support this study.

Conflicts of Interest

There are no potential competing interests in our paper.

Authors' Contributions

All authors have seen the manuscript and approved to submit to your journal.

Acknowledgments

This work was supported by the Guangxi University Innovation Team and Excellence Scholar Program. Also, the paper is supported by the Basic Research Ability Improvement Project of Young and Middle-aged Teachers in Guangxi Universities in 2021 (No. 2021KY1398).

References

[1] M. Zhou, Y. Wang, Y. Liu, and Z. Tian, "An information-theoretic view of WLAN localization error bound in GPS-denied environment," *IEEE Transactions on Vehicular Technology*, vol. 68, no. 4, pp. 4089–4093, 2019.

Hindawi
Journal of Sensors
Volume 2021, Article ID 9916339, 19 pages
https://doi.org/10.1155/2021/9916339

Research Article

Improved Particle Filter Using Clustering Similarity of the State Trajectory with Application to Nonlinear Estimation: Theory, Modeling, and Applications

Ziquan Jiao,[1,2] **Zhiqiang Feng**,[2] **Na Lv**,[3] **Wenjing Liu**,[4] **and Haijian Qin**[2]

[1]*School of Mechanical and Electrical Engineering, Guilin University of Electronic Technology, Guilin 541004, China*
[2]*Guangxi Engineering Technology Research Center of Ship Digital Design and Advanced Manufacturing, Beibu Gulf University, Qinzhou 535011, China*
[3]*Department of Instrument Science and Engineering, Shanghai Jiao Tong University, Shanghai 200240, China*
[4]*Faculty of Education, Saitama University, Saitama City 338-8570, Japan*

Correspondence should be addressed to Zhiqiang Feng; bbgufjzq@126.com

Received 8 March 2021; Revised 13 April 2021; Accepted 10 May 2021; Published 26 May 2021

Academic Editor: Ying-Ren Chien

A clustering similarity particle filter based on state trajectory consistency is presented for the mathematical modeling, performance estimation, and smart sensing of nonlinear systems. Starting from an information fusion model based on the consistency principle of the spatial state trajectory, the predicted observation information of the current particle filter (original trajectory) and future multistage Gaussian particle filter (modified trajectory) are selected as the state trajectories of the sampling particles. Clustering similarity methods are used to measure the state trajectories of the sampling particles and the actual system (reference trajectory). The importance weight of a first-order Markov model is updated with the measurement results. By integrating the targeted compensation scheme of the latest measurement information into the sequential importance sampling process, the adverse effects of the particle degradation phenomenon are effectively reduced. The convergence theorems of the improved particle filter are proposed and proved. The improved filter is applied to practical cases of nonlinear process estimation, economic statistical prediction, and battery health assessment, and the simulation results show that the improved particle filter is superior to traditional filters in estimation accuracy, efficiency, and robustness.

1. Introduction

Nonlinear phenomena are common in natural engineering technology. As a popular research topic with important theoretical and practical value in solving nonlinear problems, state estimation has been applied to problems such as target tracking and navigation, fault diagnosis and detection, process feedback and control, biochemical reaction and extraction, and economic prediction and control. Nonlinear state estimation applies to a wide range of fields, especially the industrial field. Applications include longitudinal vehicle speed estimation [1], fault detection of piezoceramic actuators [2], battery health assessment [3], state detection of impending rollover [4], and state estimation of dynamic systems with hysteresis [5]. Many solutions have been proposed, such as the Luenberger observer [6], robust observer [7], Gaussian process regression, Kalman filter [8], proportional integral observer [9], unknown input observer [10], high-gain observer [11], and nonsmooth observer [12]. For example, on the premise of satisfying the Gaussian noise distribution, the Kalman filter (KF) calculates the conditional probability density of random variables using a recursive formula and iteratively updates the linear minimum variance estimate. From this come extended KF, unscented KF, invariant extended KF [13], and adaptive extended KF [14]. The above methods have many advantages and wide applications for nonlinear system state estimation, but there is still much room for optimization and improvement in terms of nonlinear complexity and environmental noise uncertainty of different practical applications.

With the rapid development of computer technology, the particle filter (PF) algorithm based on Bayesian and Monte Carlo theories has shown many advantages and considerable potential to solve estimation problems involving nonlinear and non-Gaussian systems. The prototype algorithm, sequential importance sampling (SIS), was formed in the middle of the last century and is mainly applied to physics and automatic control applications. Due to inherent sample degradation and computer hardware limitations, the study of the PF algorithm slowed until 1993, when Gordon et al. [15, 16] introduced a resampling strategy to SIS and developed sequential importance resampling (SIR), which improved the method and laid the theoretical foundation for the PF. With the development of stochastic probability theory and Monte Carlo methods, the auxiliary particle filter (APF) [17] and Gaussian (sum) particle filter (GPF) [18, 19] were proposed. Introduced by Guarniero et al. [20], APF is based on the idea that the latest observation will approach the optimal proposed distribution if an auxiliary variable is imported to represent the prior probability of the current state. When the system noise is strong, the filtering accuracy is difficult to guarantee due to the lack of information. The GPF algorithm of Sun et al. [21] uses a Gaussian distribution to estimate the posterior probability density function (PDF) of a system state under the basic SIS framework, and the mean and variance are recursively obtained. The filtering effect depends heavily on the problem's degree of nonlinearity and is limited to the dimension of the system variables [22]. With the high complexity of current natural engineering structures, the degree of nonlinearity of systems is growing. Although these algorithms somewhat improve the performance of PFs, issues remain, such as low accuracy of filter estimation and poor stability due to particle degradation and depletion, which do not meet the needs of modern engineering. Moreover, as a probabilistic method, the nonlinear estimation of PF leads to uncertainty in the result [23].

For this reason, a clustering similarity particle filter (CSPF) based on the consistency principle of the spatial state trajectory is presented. The clustering similarity method is used to measure the state distance between the actual system and the sampling particles, including the observation information of the current state filtering and future multistage state prediction, to guide the generation and improvement of new distributions and update the weight calculation of the importance sampling process. This makes up for using the prior PDF instead of the importance function in the standard PF algorithm, which can prevent the occurrence of particle degradation and significantly improve the accuracy and robustness of estimation. The resampling strategy in the traditional PF algorithm is abandoned to eliminate particle depletion, which improves the quantization accuracy of uncertainty and efficiency of the algorithm. The above methods adopt the idea of simply modifying the proposed distribution. The designed method uses clustering theory to measure the similarity of observation information corresponding to multistage (from k to $k + L + l$) state trajectories so as to guide the generation and updating of the latest proposal distribution, which significantly improves the computational complexity of the designed method. To ensure the efficiency of the improved method for different nonlinear state estimation applications, the following two aspects can be improved. (a) The order of the state trajectory should be selected reasonably. Theoretically, the higher the order of trajectory selection, the more accurate the corresponding observation information can express the actual state, and the more accurate the estimation result, but the computational efficiency is greatly decreased. (b) The number of sampling particles N should be reduced appropriately. With the increase of the number of particles, the sampling probability density function will gradually approach the probability distribution of the actual state. While improving the accuracy of state estimation, the computational effort will increase. For these reasons, it is necessary to coordinate the contradiction between estimation accuracy and computational efficiency. The nonlinear state estimation results are largely affected by the signal information, which involves the quality and scale of the research object dataset, appropriate parameter identification, and state tracking training methods. In different research and application objects, increasing the quality and scale of experimental datasets containing more physical model information can improve the state estimation performance of data mining; an appropriate parameter training method can ensure that the model can obtain as much useful information as possible from the dataset and help to establish an appropriate state space model. Based on the above measures, compared to traditional estimation methods under the premise of consistent preconditions, the designed method can greatly improve the accuracy of state results, and it also improves computational efficiency.

The remainder of this paper is structured as follows. Section 2 discusses nonlinear system theory. In Section 3, an improved CSPF algorithm is proposed based on the analysis of the defects of the PF. Section 4 provides a theoretical explanation of the improved algorithm and proves the relevant theorems. Section 5 compares the simulation results of the proposed algorithm and the traditional improved PF algorithm. We discuss our conclusions in Section 6.

2. Theory Statement

We summarize the basic definitions and properties of the state space and optimal Bayesian recursion theory of nonlinear systems.

2.1. State Space Model. We set (Ω, P, F) as a random probability space and define two actual vector stochastic processes: $X = \{X_k, k \in N\}$ and $Y = \{Y_k, k \in N \setminus \{0\}\}$, where sample space Ω is the set of all possible outcomes, event space F is a set of outcomes in the sample space, probability function P assigns a probability to each event in the event space, X is the state process, and Y is the observation information. Let n_x and n_y be the dimensions of the state X and observation information Y, respectively, corresponding to the state space, and define $B(\mathfrak{R}^n)$ as the Borel σ-algebra set on n-dimensional Euclidean space $\mathfrak{R}^n$. Most nonlinear systems can take

the form of a dynamic state space (DSS) [24]:

$$\begin{aligned} X_k &= F(X_{k-1}, \omega_k)\ (\text{state model}), \\ Y_k &= H(X_k, \upsilon_k)\ (\text{observation equation}), \end{aligned} \tag{1}$$

where k is the discrete-time (stage) index, $X_k \in \mathfrak{R}^n$ is the set of system states at time k, and $Y_k \in \mathfrak{R}^n$ is the observation information corresponding to state X_k. $F(*)$ and $H(*)$ are known state transition and observation functions, respectively, corresponding to the state transition kernel PDF $K(X_k \mid X_{k-1})$ and observation likelihood PDF $g(Y_k \mid X_k)$ in the statistical description. The system shift noise $\{\omega_k \in \mathfrak{R}^n\}$ and measurement noise $\{\upsilon_k \in \mathfrak{R}^m\}$ are independent and identically distributed (i.i.d.) sequences that obey any PDF form.

The state space X follows the first-order Markov process; i.e., the state X_k of the current moment is only related to the state X_{k-1} of the previous moment. Assuming an initial distribution $X_0 \sim \mu(dX_0)$, the probability density functions of the state transition kernel PDF $K(X_k \mid X_{k-1})$ and observation likelihood PDF $g(Y_k \mid X_k)$ are Lebesgue measures:

$$\begin{aligned} K(X_k \mid X_{k-1}) &= P_\omega(X_k - F(X_{k-1})), \\ g(Y_k \mid X_k) &= P_\upsilon(Y_k - H(X_k)), \end{aligned} \tag{2}$$

where P_ω and P_υ are the probability functions under the influence of shift noise ω_k and measurement noise υ_k, respectively.

2.2. Optimal Bayesian Recursion Theory. In Bayesian theory [15], the state X_k of a nonlinear system at time k is updated based on the observation information $Y_{1:k}$ to obtain a minimum mean squared error (MSE) estimate. The optimal state estimation of the system is the conditional expected value $E(X_k \mid Y_{1:k})$ of the posterior PDF $P(X_k \mid Y_{1:k})$. Based on the premise that the state variable and observation function follow a first-order Markov process, the posterior PDF $P(X_k \mid Y_{1:k})$ is obtained by two steps of recursive iterations: prediction and updating. $X_{k:l} \triangleq (X_k, X_{k+1}, \cdots, X_l)$ and $Y_{k:l} \triangleq (Y_k, Y_{k+1}, \cdots, Y_l)$ are defined as the space path information of the state process and observation likelihood from time k to l, respectively.

2.2.1. Prediction. Combined with the transition kernel PDF $K(X_k \mid X_{k-1})$ calculated by the state space equation, the prior PDF $P(X_k \mid Y_{1:k-1})$ is predicted using the Chapman–Kolmogorov equation and the posterior PDF $P(X_{k-1} \mid Y_{1:k-1})$ at time $k-1$:

$$\begin{aligned} P(X_k \mid Y_{1:k-1}) &= \int P(X_k, X_{k-1} \mid Y_{1:k-1}) dX_{k-1} \\ &= \int P(X_k \mid X_{k-1}, Y_{1:k-1}) P(X_{k-1} \mid Y_{1:k-1}) dX_{k-1} \\ &= \int K(X_k \mid X_{k-1}) P(X_{k-1} \mid Y_{1:k-1}) dX_{k-1}, \end{aligned} \tag{3}$$

where the state PDF $P(X_k, X_{k-1} \mid Y_{1:k-1})$ specifies the conditional probability of $X_k \cap X_{k-1}$ given $Y_{1:k-1}$, and $P(X_k \mid X_{k-1}, Y_{1:k-1})$ specifies the conditional probability of X_k given $X_{k-1} \cap Y_{1:k-1}$.

2.2.2. Updating. The prior PDF $P(X_k \mid Y_{1:k-1})$ is updated using the observation likelihood PDF $g(Y_k \mid X_k)$ at time k, and the posterior PDF $P(X_k \mid Y_{1:k})$ of state X_k is obtained as

$$\begin{aligned} P(X_k \mid Y_{1:k}) &= \frac{P(Y_k \mid X_k, Y_{1:k-1}) P(X_k \mid Y_{1:k-1})}{P(Y_k \mid Y_{1:k-1})} \\ &= \frac{g(Y_k \mid X_k) P(X_k \mid Y_{1:k-1})}{\int g(Y_k \mid X_k) P(X_k \mid Y_{1:k-1}) dX_k}, \end{aligned} \tag{4}$$

where the observation PDF $P(Y_k \mid X_k, Y_{1:k-1})$ specifies the conditional probability of Y_k given $X_k \cap Y_{1:k-1}$, and $P(Y_k \mid Y_{1:k-1})$ specifies the conditional probability of Y_k given $Y_{1:k-1}$.

The system state PDF measure $\pi_{k:l|m}(dX_{k:l})$ is defined as

$$\pi_{k:l|m}(dX_{k:l}) \triangleq P(X_{k:l} \mid Y_{1:m}). \tag{5}$$

The joint posterior PDF measure $\pi_{0:k|k}(dX_{0:k})$ can be obtained by Bayes' theorem (Equations (3) and (4)):

$$\pi_{0:k|k-1}(dX_{0:k}) = \int_{\mathfrak{R}^{n_x}} K(dX_k \mid X_{k-1}) \pi_{0:k-1|k-1}(dX_{0:k-1})\ (\text{prediction}), \tag{6}$$

$$\pi_{0:k|k}(dX_{0:k}) = \frac{g(Y_k \mid X_k) \pi_{0:k|k-1}(dX_{0:k})}{\int_{\mathfrak{R}^{n_x}} g(Y_k \mid X_k) \pi_{0:k|k-1}(dX_{0:k})}\ (\text{updating}). \tag{7}$$

The marginal posterior PDF measure $\pi_{k|k-1}(dX_k)$ is obtained by

$$\pi_{k|k-1}(dX_k) = \int_{\mathfrak{R}^{n_x}} K(dX_k \mid X_{k-1}) \pi_{k-1|k-1}(dX_{k-1})\ (\text{prediction}), \tag{8}$$

$$\pi_{k|k}(dX_k) = \frac{g(Y_k \mid X_k) \pi_{k|k-1}(dX_k)}{\int_{\mathfrak{R}^{n_x}} g(Y_k \mid X_k) \pi_{k|k-1}(dX_k)}\ (\text{updating}). \tag{9}$$

Similarly, $x_{k:l} \triangleq (x_k, x_{k+1}, \cdots, x_l)$ and $y_{k:l} \triangleq (y_k, y_{k+1}, \cdots, y_l)$ are, respectively, defined as the sampling particle path information of the state process and observation likelihood from time k to l.

Definition 1. Suppose that ν is a probability measure and φ represents an arbitrary function, Θ and Ψ are arbitrary function variables, K is the PDF of the transfer kernel satisfying the Markov process, and the following calculation method

is defined:

$$(\nu, \varphi) \triangleq \int \varphi \nu,$$
$$\nu K(\Theta) \triangleq \int \nu(dx) K(\Theta \mid x), \tag{10}$$
$$K\varphi(x) \triangleq \int K(d\Psi \mid x)\varphi(\Psi).$$

According to the above symbols, for any function φ, Bayesian theory (prediction and updating processes) can be redefined, using Equation (8), as

$$\begin{aligned}(\pi_{k|k-1}, \varphi) &= \int_{\mathfrak{R}^{n_x}} p(x_k \mid y_{1:k-1})\varphi(x_k)dx_k \\ &= \int_{\mathfrak{R}^{n_x}} \left[\int_{\mathfrak{R}^{n_x}} K(x_k \mid x_{k-1}) p(x_{k-1} \mid y_{1:k-1})dx_{k-1}\right]\varphi(x_k)dx_k \\ &= \int_{\mathfrak{R}^{n_x}} p(x_{k-1} \mid y_{1:k-1}) \left[\int_{\mathfrak{R}^{n_x}} K(x_k \mid x_{k-1})\varphi(x_k)dx_k\right]dx_{k-1} \\ &= (\pi_{k-1|k-1}, K\varphi) \text{ (prediction)}.\end{aligned} \tag{11}$$

From Equation (9), it is concluded that

$$\begin{aligned}(\pi_{k|k}, \varphi) &= \int_{\mathfrak{R}^{n_x}} p(x_k \mid y_{1:k})\varphi(x_k)dx_k \\ &= \frac{\int_{\mathfrak{R}^{n_x}} g(y_k \mid x_k) p(x_k \mid y_{1:k-1})\varphi(x_k)dx_k}{\int_{\mathfrak{R}^{n_x}} g(y_k \mid x_k) p(x_k \mid y_{1:k-1})dx_k} \\ &= \frac{(\pi_{k|k-1}, g\varphi)}{(\pi_{k|k-1}, g)} \text{ (updating)}.\end{aligned} \tag{12}$$

Except for a small number of dynamic models, it is difficult to obtain an analytic solution in Bayesian theory (Equations (6)–(9), (11), and (12)) and the exact solution of the posterior probability for general nonlinear and non-Gaussian systems.

3. Particle Filter

To solve the complex problem in the above optimal Bayesian filtering algorithm, Monte Carlo sampling is used instead of an integral operation [25]. The idea is to use a discrete distribution with a series of random samples and their corresponding weights to approximate the posterior PDF measure $\pi_{k|k}$ and calculate the expected value of the samples to estimate the actual system state X_k. The importance PDF $q(x_k \mid y_{1:k})$ is generally used to represent the discrete distribution to obtain the sampling particle set $\{x_{0:k}^i : i = 1, 2, \cdots, N\}$ to calculate the posterior empirical measure distribution $\pi_{k|k}^N$:

$$\pi_{k|k}^N(dx_k) \triangleq \frac{1}{N}\sum_{i=1}^{N} \delta_{x_k^i}(dx_k), \tag{13}$$

where $\delta_{x_k^i}(*)$ is the Dirac delta function. With the sampling number $N \to \infty$, the empirical measure $\pi_{k|k}^N$ is infinitely close to the actual posterior PDF measure $\pi_{k|k}$.

3.1. Sequential Importance Resampling (SIR) Filter. Since the posterior PDF distribution $p(x_k \mid y_{1:k})$ is unknown, it is necessary to construct the importance PDF $q(x_k \mid x_{k-1}, y_{1:k})$ to satisfy the requirements of the Monte Carlo sampling method and make up for the shortcoming that sampling cannot be carried out in the target distribution, and

$$q(x_k|x_{k-1}, y_{1:k}) = K(x_k|x_{k-1}), \tag{14}$$

is typically selected during the SIR process.

Assuming that the posterior PDF measure $\pi_{k-1|k-1}^N(dx_{k-1})$ at time $k-1$ is known and the particle set is $\{x_k^i\}_{i=1}^N \sim \pi_{k-1|k-1}^N(dx_{k-1})K(dx_k|x_{k-1})$ at time k, the prediction measure $\pi_{k|k-1}^N$ of the prediction stage can be obtained as

$$\pi_{k|k-1}^N(dx_k) \triangleq \frac{1}{N}\sum_{i=1}^{N} \delta(x_k - x_k^i). \tag{15}$$

When the number of sample particles N is large enough, the prediction measure $\pi_{k|k-1}^N$ is infinitely close to the actual state $\pi_{k|k-1}$. The Monte Carlo approximate posterior measure $\pi_{k|k}^N$ is obtained by substituting the prediction measure $\pi_{k|k-1}^N$ into Equation (9):

$$\pi_{k|k}^N(dx_k) \triangleq \frac{g(y_k|x_k)\pi_{k|k-1}^N(dx_k)}{\int_{R^{n_x}} g(y_k|x_k)\pi_{k|k-1}^N(dx_k)} = \frac{\sum_{i=1}^N g(y_k|x_k^i)\delta_{x_k^i}(dx_k)}{\sum_{i=1}^N g(y_k|x_k^i)}. \tag{16}$$

The above formula is equivalent to

$$\pi_{k|k}^N(dx_k) = \sum_{i=1}^{N} \omega_k^i \delta_{x_k^i}(dx_k), \quad \sum_{i=1}^{N} \omega_k^i = 1, \tag{17}$$

where $\omega_k^i \propto g(y_k|x_k^i)$ is the weight of the importance PDF $q(x_k \mid y_{1:k})$ after normalization of all sampling particles $\{x_{0:k}^i\}_{i=1}^N$, and the posterior measure $\pi_{k|k}^N$ is the weighted sum of the Dirac delta function. The above process is called SIS filtering.

After several updating iterations, the weights of some particles in the SIS process may be small enough to ignore, which cannot be avoided due to the shortcomings of the algorithm. To overcome this, resampling is usually used to solve the degradation problem of the standard PF algorithm. By duplicating particles with higher weights and discarding those with smaller weights, the particle set $\{\tilde{x}_{0:k}^i : i = 1, 2, \cdots, N\}$ is gathered in the high-probability posterior region to obtain the approximate value of the unweighted empirical

Step 1. Particle initialization
At time $k = 0$, for $i = 1, 2, \cdots, N$
Sample $x_0^i \sim \pi_{0|0}(dx_0)$
At time $k \geq 1$, for $i = 1, 2, \cdots, N$
Step 2. Sequential importance sampling
Predict $\pi_{k|k-1}^N$, sample $x_k^i \sim \pi_{k-1|k-1}^N K(dx_k)$
Evaluate the normalized importance weights ω_k^i
$\omega_k^i \propto g(y_k|x_k^i)$, and $\sum_{i=1}^N \omega_k^i = 1$
Step 3. Resampling strategy
Calculate effective samples $N_{\text{eff}} = \left(\sum_{i=1}^N (\omega_k^i)^2\right)^{-1}$
Compare resampling threshold N_{th}
if $N_{\text{eff}} < N_{\text{th}}$
$[\tilde{x}_k^i, \tilde{\omega}_k^i] = \text{RESAMPLE}[x_k^i, \omega_k^i]$, and $\tilde{\omega}_k^i = 1/N$
else $[\tilde{x}_k^i, \tilde{\omega}_k^i] = [x_k^i, \omega_k^i]$
Step 4. State estimation
$x_k = \sum_{i=1}^N \tilde{\omega}_k^i \tilde{x}_k^i$

Algorithm 1: Standard particle filter.

distribution measure $\tilde{\pi}_{k|k}^N$:

$$\tilde{\pi}_{k|k}^N = \frac{1}{N} \sum_{i=1}^N \delta_{\tilde{x}_k^i}(d\tilde{x}_k). \tag{18}$$

It can be inferred that the essence of resampling is realized using N sampling iterations in the empirical distribution measure $\pi_{k|k}^N$, and the new particle set obtained by this method approximates the actual posterior measure $\pi_{k|k}$. Common resampling methods are random, system, polynomial, and residual resampling. The process of the standard PF algorithm is shown as Algorithm 1.

3.2. Clustering Similarity Particle Filter (CSPF). The standard PF algorithm is simple in structure and easy to execute. Under the optimal estimation, the approximate estimated value of the algorithm converges to the actual state value. However, there are some issues in practical engineering applications.

3.2.1. Particle Degradation Phenomenon. The standard PF introduces the importance PDF distribution in the SIS process, which causes the variance of the particle weight to accumulate with each iteration. The importance weights corresponding to most particles tend to zero, resulting in a particle degradation phenomenon [26]. The above effects lead to a significant waste of computing resources, with the result that the approximate estimation cannot accurately describe the posterior distribution of the actual state. This degradation phenomenon cannot be avoided due to defects of the algorithm.

3.2.2. Particle Depletion Problem. A resampling strategy is an effective and important method to improve particle degradation. By resampling the discrete approximate posterior PDF distribution obtained by the importance sampling process, samples with larger weights are duplicated many times under the guidance of the particle motion and the distribution of the state at the previous moment so that the number of effective particles increases and degradation is suppressed. However, resampling is likely to cause the abandonment or loss of some low-weight particles, which causes the resampled particles to prematurely move away from the actual state posterior region. This results in sample dilution [27] and eventually in the increase of state estimation variance, which greatly diminishes filtering performance.

In view of the above problems, our improved PF algorithm relies on the consistency principle of the spatial state trajectory [28]; i.e., the closer the state trajectory of a particle is to the actual state trajectory, the more likely the particle state represents the actual state. By using clustering similarity theory to measure the degree of trajectory consistency, the higher the degree of consistency similarity, the closer it is to the actual state, and the particle weights of the SIS process are updated to improve particle degradation. The improved algorithm abandons the resampling strategy, which can fundamentally eliminate the particle depletion problem.

The particle set $\{X_k^\bullet(i)\}_{i=1}^N = \{x_j^\circ(i)\colon j = k, \cdots, k+L\,; x_j'(i)\colon j = k+L+1, \cdots, k+L+l\}_{i=1}^N$ from time k to time $k+L+l$ is selected as the state trajectory at time k, where L and l are predefined constants. The original trajectory set $x_j^\circ(i)$ follows the SIS filtering process [15], and the modified trajectory set $x_j'(i)$ complies with the GPF prediction algorithm [18]. Because the actual state is unknown, the observation likelihood information is used to represent the consistency parameter of the state trajectory. Depending on the particle state trajectory, the corresponding observed likelihood trajectory set $\{Y_k^\bullet(i)\}_{i=1}^N = \{y_j^\circ(i)\colon j = k, \cdots, k+L\,; y_j'(i)\colon j = k+L+1, \cdots, k+L+l\}_{i=1}^N$ is determined as

$$Y_k^\bullet(i) = H(X_k^\bullet(i), \upsilon_k), \tag{19}$$

where the measurement noise is $\upsilon_k = 0$; i.e., the observation equation $H(*)$ is a known function determined by the specific research objects without noise interference. The observed likelihood trajectory corresponding to the actual state (reference trajectory) is $\{Y_k\} = \{y_j : j = k, \cdots, k+L+l\}$. In this work, a clustering method using distance-based similarity is selected to analyze the trajectory consistency, and the distance similarity measurement $d_k^\bullet(i)$ [29] of the observed likelihood trajectories of the actual state and sampling particles is calculated as

$$\begin{aligned} d_k^\bullet(i) &= \text{dis}\left(\{Y_k\}, \{Y_k^\bullet(i)\}_{i=1}^N\right) \\ &= \sqrt[s]{\sum_{j=k}^{k+L} \left|y_j - y_j^\circ(i)\right|^s + \sum_{j=k+L+1}^{k+L+l} \left|y_j - y_j'(i)\right|^s}, \end{aligned} \tag{20}$$

where $\text{dis}(*)$ is the distance similarity function, $\text{dis}(*) \geq 0$, and s is the measurement type parameter. To increase the

reliability of the algorithm, the distance similarity function is transformed to an exponential similarity function:

$$d_k(i) = e^{\lambda \times d_k^{\bullet}(i)}, \quad i = 1, \cdots, N, \tag{21}$$

where λ is the gradient factor. The importance weights $w_k^{\bullet}(i)$ and $w_{k+L+l}^{\bullet}(i)$ corresponding to times k and $k+L+l$ can be calculated as

$$w_k^{\bullet}(i) = d_k^{-1}(i) \times p_v(Y_k - H(X_k^{\bullet}, v_k)), \quad i = 1, \cdots, N, \tag{22}$$

$$w_{k+L+l}^{\bullet}(i) = d_k^{-1}(i) \times p_v(Y_{k+L+l} - H(X_{k+L+l}^{\bullet}, v_{k+L+l})), \quad i = 1, \cdots, N, \tag{23}$$

where $p_v(*)$ is the PDF of the observed likelihood noise. Using the above algorithm, the original trajectory set $\{x_k^{\circ}(i)\}_{i=1}^N$ of the SIS process and the corresponding importance weights $\{w_k^{\bullet}(i)\}_{i=1}^N$ at time k represent the posterior PDF $\pi_{k|k}^N$ of the system state, modified trajectory set $\{x'_{k+L+l}(i)\}_{i=1}^N$ of the GPF-predicted distribution, and corresponding importance weights $\{w_{k+L+l}^{\bullet}(i)\}_{i=1}^N$ at time $k+L+l$, which can approximately represent the predicted PDF $\pi_{k+L+l|k}$. Therefore, the state estimate value x_k can be obtained by the filtering operation, and the state estimate x_{k+L+l} can be calculated by the prediction step. The implementation of the improved PF algorithm is as follows.

(1) Estimation. This step is consistent with the SIS(GPF) estimation process used to extract the particle distribution set $\{X_k^{\bullet}(i)\}_{i=1}^N$.

(2) Updating. The weights $\{w_k^{\bullet}(i)\}_{i=1}^N$ and $\{w_{k+L+l}^{\bullet}(i)\}_{i=1}^N$ are determined and normalized to $\{w_k(i)\}_{i=1}^N$ and $\{w_{k+L+l}(i)\}_{i=1}^N$, respectively, to estimate and predict system states x_k and x_{k+L+l}:

$$\begin{aligned} x_k &\approx \tilde{x}_k = \sum_{i=1}^{N} w_k(i) x_k^{\circ}(i) \text{ (filtering)}, \\ x_{k+L+l} &\approx \tilde{x}_{k+L+l} = \sum_{i=1}^{N} w_{k+L+l}(i) x'_{k+L+l}(i) \text{ (prediction)}. \end{aligned} \tag{24}$$

The above steps constitute an iterative process of the improved algorithm. Unlike the standard PF, this method uses an estimate-update-filter (prediction) process without resampling. The improved PF algorithm (CSPF) is shown as Algorithm 2.

Step 1. Particle initialization
At time $k = 0$, for $i = 1, 2, \cdots, N$
Sample $x_0^i \sim \pi_{0|0}(dx_0)$
At time $k \geq 1$, for $i = 1, 2, \cdots, N$
Step 2. Importance sampling
Predict $\pi_{k|k-1}^N$, sample $x_k^i \sim K(x_k|x_{k-1}^i)$
Step 3. Similarity measurement
Particle state trajectories $\{X_k^{\bullet}(i)\}$
  Draw $x_j^{\circ}(i) \sim$ SIS, $j = k, k+1, \cdots, k+L$
    $x_j'(i) \sim$ GPF, $j = k+L+1, \cdots, k+L+l$
      Calculate $d_k^{\bullet}(i) = \text{dis}(\{Y_k\}, \{Y_k^{\bullet}(i)\}_{i=1}^N)$
  Exponential transformation $d_k(i) = e^{\lambda \times d_k^{\bullet}(i)}$
Step 4. Recursive importance weights
Revised proposal distribution
  $q(x_k|x_{k-1}, y_k) = d_k(i) K(x_k|x_{k-1}^i)$
Update weights $w_k^{\bullet}(i) \propto d_k^{-1}(i) g(y_k|x_k^i)$
    Normalize $w_k(i) = w_k^{\bullet}(i) / \sum_{i=1}^N w_k^{\bullet}(i)$
Step 5. State estimation
  $x_k = \sum_{i=1}^N w_k(i) x_k^i$

Algorithm 2: Clustering similarity particle filter.

4. Convergence Proof

The proposed algorithm is based on bootstrap filtering theory, and Bayesian state estimation can be realized by a weighted bootstrap method [15, 30]. It is assumed that the sampling particle set $\{X_k^{\bullet}(i)\}_{i=1}^N$ is derived from a continuous PDF, $R(x)$. The posterior PDF $\pi_{k|k}$ and $R(x)S(x)$ are proportional, and $S(x)$ is a known function. If the sample number $N \to \infty$, then the discrete distribution of particles composed of $\{X_k^{\bullet}(i)\}_{i=1}^N$ and its corresponding weights $\{S(X_k^{\bullet}(i)) / \sum_{i=1}^N S(X_k^{\bullet}(i))\}_{i=1}^N$ can be regarded as approaching the actual posterior PDF $\pi_{k|k}$. Referring to Equation (16), the posterior PDF $\pi_{k|k}$ of system state x_k is proportional to the product of the observation likelihood function and prior PDF $\pi_{k|k-1}$, which can be equivalent to $R(x)$, and the weight $w_k^{\bullet}(i)$ in Equation (22) can be regarded as the observation likelihood function equivalent to $S(x)$, which follows bootstrap filtering theory and is reasonable and effective.

4.1. Convergence of the Improved Algorithm. Suppose that the probability density measure space on set $E = \Gamma(\mathfrak{R}^{n_x})$ is the probability measure set on the largest-dimensional Euclidean space $\mathfrak{R}^{n_x}$ with convergence topology and set (E, d) is the measure space. $(a_k)_{k=1}^{\infty}$ and $(b_k)_{k=1}^{\infty}$ are two continuous function sequences: $E \to E$. In the stochastic filtering setup, space E will be all probability measure spaces on n-dimensional Euclidean space $\mathfrak{R}^{n_x}$.

Definition 2. a_k and b_k, respectively, represent the mapping relationships of measure $\pi_{k-1|k-1} \to \pi_{k|k-1}$ and of measure $\pi_{k|k-1} \to \pi_{k|k}$. We define a_k as the mapping relation (prediction) satisfied on measure set $\Gamma(\mathfrak{R}^{n_x}) \to \Gamma(\mathfrak{R}^{n_x})$:

$$a_k(\nu)(dx_k) \triangleq \nu K(dx_k) = \int_{R^{n_x}} \nu K(dx_k|x_{k-1})(dx_{k-1}). \tag{25}$$

This holds for any measure ν. Therefore, substituting the continuous function $\varphi \in \mathbb{C}_b(R^{n_x})$ in the prediction Equation

(11), we obtain

$$(a_k(\nu), \varphi) = \iint_{R^{n_x}} \nu K(dx_k|x_{k-1})\varphi(x_k)(dx_{k-1}) = (\nu, K\varphi). \tag{26}$$

The prediction measure expression can be obtained as

$$\pi_{k|k-1} = a_k\left(\pi_{k-1|k-1}\right). \tag{27}$$

Definition 3. Referring to Equation (12), we define b_k as the mapping relation (updating) satisfied on measure set $\Gamma(\Re^{n_x}) \to \Gamma(\Re^{n_x})$:

$$(b_k(\nu), \varphi) = \frac{(\nu, g\varphi)}{(\nu, g)}. \tag{28}$$

The Bayesian filtering process can be expressed as

$$\pi_{k|k} = b_k\left(\pi_{k|k-1}\right) \triangleq b_k \odot a_k\left(\pi_{k-1|k-1}\right), \tag{29}$$

where the operator "$\odot$" represents the composite mapping function.

Definition 4. Setting h_k and $h_{1:k}$ as the conversion functions of measure $\pi_{k-1|k-1} \to \pi_{k|k}$ and of measure $\pi_{0|0} \to \pi_{k|k}$, respectively, the Bayesian filtering process can be expressed as

$$\begin{aligned} h_k &\triangleq b_k \odot a_k, \\ h_{1:k} &\triangleq h_k \odot h_{k-1} \odot \cdots \odot h_1. \end{aligned} \tag{30}$$

In an abstract environment, the PF algorithm uses the Monte Carlo method to solve a problem for which it is difficult to obtain the exact analytical integral solution in Bayesian theory. The principle is to generate a series of samples from the target distribution to approximately estimate the partial characteristics of the actual state, and the estimation result is only the expectation of a "good performance" function, which can be approximated as the average value:

$$E_\pi(\varphi(x)) \approx \frac{\varphi(x_1) + \varphi(x_2) + \cdots + \varphi(x_N)}{N} = \bar{E}_{\varphi,N}. \tag{31}$$

When $N \to \infty$, the estimated value $\bar{E}_{\varphi,N}$ converges to the expected value $E_\pi(\varphi(x))$. It can be assumed that

$$\begin{aligned} E_\pi(\varphi(x)) &= \mu \text{ (expectation)}, \\ \operatorname{Var}(\varphi(x)) &= \sigma^2 \text{ (variance)}, \end{aligned} \tag{32}$$

where μ is the most basic digital feature to measure the centralized position or average level of a random variable x, and σ^2 is a numeric characteristic of the dispersion of the random variable x.

Based on the law of large numbers and the central limit theorem [31], it can be concluded that

$$\bar{E}_{\varphi,N} \to \mu, \tag{33}$$

$$\Pr\left\{\lim_{N\to\infty} \left|\mu - \bar{E}_{\varphi,N}\right| = 0\right\} = 1, \tag{34}$$

where $\Pr\{*\}$ is the probability function.

Therefore, for the analytical solution of the integral operation, the disturbance caused by the Monte Carlo sampling method is inevitable, mainly because the estimated value is based on a random and limited sample set. However, under the guarantee of the law of large numbers and the central limit theorem, when the number of particles tends to infinity, the disturbance is minimal and satisfies the following Gaussian distribution $N(*|*)$:

$$\bar{E}_{\varphi,N} \sim N\left(\bar{E}_{\varphi,N}\middle|\mu, \sigma^2/N\right). \tag{35}$$

When $N \to \infty$, the state estimate $\bar{E}_{\varphi,N}$ converges to the real expected value μ, and the estimation variance decreases with the increase of the number of sample particles.

From the above analysis, it can be concluded that the particle filter is based on Bayesian filtering and can be combined with the Monte Carlo sampling method to generate a sampling disturbance function c^N [32]. The perturbation Equations (33) and (34) can be expressed as

$$\lim_{N\to\infty} c^N\left(\bar{E}_{\varphi,N}\right) = \mu. \tag{36}$$

The process formulas (29) and (30) of the particle filter algorithm can be expressed as

$$\pi^N_{k|k} = b_k \odot c^N \odot a_k\left(\pi^N_{k-1|k-1}\right) = h^N_k\left(\pi^N_{k-1|k-1}\right) = h^N_{1:k}(\kappa), \tag{37}$$

where κ is the initial value $\pi_{0|0}$. Our improved algorithm uses clustering analysis to measure the similarity of multistage measurement information [33] as the proposed distribution $q(x_k|x_{k-1}, y_k)$ to replace the prior PDF $p(x_k \mid x_{k-1})$ in the SIS process:

$$q(x_k|x_{k-1}, y_k) = d_k(i)K(dx_k|x_{k-1}). \tag{38}$$

The importance weight calculation is updated and modified as follows:

$$w_k(i) \propto g(y_k|x_k)d_k^{-1}(i) = \widehat{g}(y_k|x_k). \tag{39}$$

Substituting this in Equation (28), the updating formula of

the improved algorithm becomes

$$\left(\widehat{b}_k(\nu_N), \varphi\right) = \frac{\left(\nu_N, \widehat{g}\varphi\right)}{\left(\nu_N, \widehat{g}\right)}, \tag{40}$$

where $\widehat{b}_k$ represents the mapping relationship of the improved algorithm measure $\pi^N_{k|k-1} \to \pi^N_{k|k}$ and Monte Carlo measure $\lim_{N\to\infty} \nu_N = \nu$. Referring to Equations (37) and (30), the improved PF can be expressed as

$$\widehat{\pi}^N_{k|k} = \widehat{b}_k \odot c^N \odot a_k\left(\pi^N_{k-1|k-1}\right) = \widehat{h}^N_k\left(\pi^N_{k-1|k-1}\right) = \widehat{h}^N_{1:k}(\kappa). \tag{41}$$

Theorem 5. *It is assumed that the state transition kernel function K satisfies the first-order Markov process, and the observation likelihood function g is continuous, bounded, and strictly positive in $x_k \in \mathfrak{R}^{n_x}$. Under the condition of the Monte Carlo sampling disturbance c^N, the improved PF algorithm measure $\widehat{\pi}^N_{k|k}$ converges to the theoretical value (actual state value) $\pi_{k|k}$ of Bayesian optimal filtering:*

$$\lim_{N\to\infty} \widehat{\pi}^N_{k|k} = \pi_{k|k}. \tag{42}$$

Proof. In the PF algorithm, the Monte Carlo sampling disturbance is random and uncertain. $c^{N,\vartheta}$ is set as a random disturbance, the sample number $N > 0$, and the independent variable $\vartheta \in \Omega$. For all measures $\nu \in \Gamma(\mathfrak{R}^{n_x})$,

$$c^{N,\vartheta}(\nu) = \frac{1}{N}\sum_{j=1}^{N} \delta\left\{V_j(\vartheta)\right\}, \tag{43}$$

where $V_j : \Omega \to \mathfrak{R}^d$ is an i.i.d. random variable with measure ν. According to the algorithm and the simplification of Equations (29) and (41), we can obtain

$$\pi_{k|k} = b_k\left(\pi_{k|k-1}\right) = b_k \odot a_k\left(\pi_{k-1|k-1}\right), \tag{44}$$

$$\widehat{\pi}^N_{k|k} = \widehat{b}_k\left(\widehat{\pi}^N_{k|k-1}\right) = \widehat{b}_k \odot c^N \odot a_k\left(\widehat{\pi}^N_{k-1|k-1}\right) = \widehat{b}_k \odot c^N(a_k). \tag{45}$$

At time k, the measure of the Bayesian prediction stage is a_k, and the sampling disturbance measure of the PF prediction stage is $c^N(a_k)$. Using the i.i.d. random variables V_j, $\forall\varphi \in \Lambda$, and $\Lambda = \{\varphi_i\}_{i>0} \in C_b(\mathfrak{R}^{n_x})$, we can obtain

$$\begin{aligned} E\left[\left(\left(c^N(a_k), \varphi_i\right) - \left(a_k, \varphi_i\right)\right)^4\right] &= \frac{1}{N^4} E\left[\left(\sum_{j=1}^{N}\left(\varphi_i(V_j) - \left(a_k, \varphi_i\right)\right)\right)^4\right] \\ &= \frac{1}{N^4}\sum_{j=1}^{N} E\left[\left(\varphi_i(V_j) - \left(a_k, \varphi_i\right)\right)^4\right] \\ &= \frac{4}{N^4}\sum_{j_1,j_2=1,j_1\neq j_2}^{N} E\left[\left(\varphi_i\left(V_{j_1}\right)\right.\right. \\ &\quad \left.\left. - \left(a_k, \varphi_i\right)\right)^2\left(\varphi_i\left(V_{j_2}\right) - \left(a_k, \varphi_i\right)\right)^2\right] \\ &\le \frac{N\|2\varphi_i\|^4 + 3N(N-1)\|2\varphi_i\|^4}{N^4} \le \frac{48\|\varphi_i\|^4}{N^2}, \end{aligned} \tag{46}$$

where $E[*]$ is the solution function of set expectation, $\|*\|$ represents the supremum norm in the domain $C_b(\mathfrak{R}^{n_x})$, and $\|\varphi\| \triangleq \sup_{x\in\mathfrak{R}^{n_x}}|\varphi(x)|$. The summed expectation of the number of sampled particles from 1 to ∞ is

$$E\left[\sum_{N=1}^{\infty}\left(\left(c^N(a_k), \varphi_i\right) - \left(a_k, \varphi_i\right)\right)^4\right] \le 48\|\varphi_i\|^4 \sum_{N=1}^{\infty}\frac{1}{N^2} < \infty. \tag{47}$$

Hence,

$$\sum_{N=1}^{\infty}\left(\left(c^N(a_k), \varphi_i\right) - \left(a_k, \varphi_i\right)\right)^4 < \infty. \tag{48}$$

This implies that for the prediction stage, the measure at a certain time can be expressed as

$$\lim_{N\to\infty}\left(\left(c^N(a_k), \varphi_i\right) - \left(a_k, \varphi_i\right)\right) = 0. \tag{49}$$

Referring to Equation (40), for $\nu \in \Gamma(\mathfrak{R}^{n_x})$ and any function φ, the updating stage measure can be obtained as

$$\begin{aligned} \lim_{N\to\infty}\left(\widehat{b}_k(\nu_N), \varphi\right) &= \frac{\lim_{N\to\infty}\left(\nu_N, \widehat{g}\varphi\right)}{\lim_{N\to\infty}\left(\nu_N, \widehat{g}\right)} \\ &= \frac{\lim_{N\to\infty} d_k^{-1}(i)(\nu_N, g\varphi)}{\lim_{N\to\infty} d_k^{-1}(i)(\nu_N, g)} \\ &= \frac{(\nu, g\varphi)}{(\nu, g)} = (b_k(\nu), \varphi). \end{aligned} \tag{50}$$

This result is compared with Equations (28) and (50), and it is concluded that the improved algorithm has the same measures as the Bayesian filter in the updating stage, i.e.,

$$\lim_{N\to\infty}\widehat{b}_k(\nu_N) = b_k(\nu). \tag{51}$$

Combining Equations (44), (45), (49), and (51), we can

obtain

$$\lim_{N\to\infty} \widehat{\pi}_{k|k}^{N} = \pi_{k|k}^{N}. \tag{52}$$

Therefore, the improved PF algorithm (CSPF) based on the clustering similarity of the state trajectories still converges to the actual state under the interference of Monte Carlo sampling disturbances. Theorem 5 is proved.□

4.2. Convergence of the Mean Squared Error of Results. Combined with the conditions and conclusions of Section 4.1, we analyze the convergence of the results by calculating the boundary of the MSE of the improved algorithm [34]. We demonstrate that the convergence of the reasoning process is related to the number of sample particles at each stage of the algorithm. Suppose that in the neighborhood of $E = \Gamma(\mathfrak{R}^{n_x})$, $(\nu_N^w)_{N=1}^{\infty}$ represents a measure sequence of random probability and satisfies $\lim_{N\to\infty} \nu_N = \nu$. For any function $\varphi \in C_b(\mathfrak{R}^{n_x})$, it can be obtained from Theorem 5 that

$$\lim_{N\to\infty} E\left[((\nu_N, \varphi) - (\nu, \varphi))^2\right] = 0. \tag{53}$$

Theorem 6. *It is assumed that the state transition kernel function K satisfies the first-order Markov process, and the observation likelihood function g is continuous, bounded, and strictly positive in $x_k \in \mathfrak{R}^{n_x}$. For any function φ, there must be a real constant $C_{k|k}$ satisfying*

$$E\left[\left(\left(\widehat{\pi}_{k|k}^{N}, \varphi\right) - \left(\pi_{k|k}, \varphi\right)\right)^2\right] \le C_{k|k} \frac{\|\varphi\|^2}{N}, \tag{54}$$

where $\|\varphi\| \triangleq \sup_{x\in\mathfrak{R}^{n_x}} |\varphi(x)|$.

Proof. According to the improved PF algorithm, the proof is divided into prediction and updating parts.□

Lemma 7. *Refer to the prediction stage in Algorithm 2 (steps 1 and 2) and assume that the conditions set by Theorem 6 are met. When $k \ge 0$, there must be a real constant $C_{k|k-1}$, and the prediction measure $\pi_{k|k-1}^{N}$ satisfies*

$$E\left[\left(\left(\pi_{k|k-1}^{N}, \varphi\right) - \left(\pi_{k|k-1}, \varphi\right)\right)^2\right] \le C_{k|k-1} \frac{\|\varphi\|^2}{N}. \tag{55}$$

We use induction to complete the proof. When time $k = 0$, for any function φ, there must be a real constant $C_{0|0}$ satisfying

$$E\left[\left(\left(\pi_{0|0}^{N}, \varphi\right) - \left(\pi_{0|0}, \varphi\right)\right)^2\right] \le C_{0|0} \frac{\|\varphi\|^2}{N}. \tag{56}$$

From step 1 in Algorithm 2, when $k = 0$, N i.i.d. particles are sampled from the prior PDF measure $\pi_{0|0}$, $x_0^i \sim \pi_{0|0}(dx_0)$. Using the Marcinkiewicz–Zygmund inequality [35], we obtain

$$\begin{aligned} E\left[\left(\left(\pi_{0|0}^{N}, \varphi\right) - \left(\pi_{0|0}, \varphi\right)\right)^2\right] &= E\left[\left(\frac{1}{N}\sum_{i=1}^{N}\varphi(x_i) - \left(\pi_{0|0}, \varphi\right)\right)^2\right] \\ &= \frac{1}{N^2} E\left[\left(\sum_{i=1}^{N}\varphi(x_i) - N\left(\pi_{0|0}, \varphi\right)\right)^2\right] \\ &\le C_{0|0} \frac{\|\varphi\|^2}{N}. \end{aligned} \tag{57}$$

Thus, when $k = 0$, Equation (55) is proved, and $\pi_{0|0}^{N}$ converges to $\pi_{0|0}$.

At time $k-1$, for any function φ, there must be a real constant $C_{k-1|k-1}$ satisfying

$$E\left[\left(\left(\pi_{k-1|k-1}^{N}, \varphi\right) - \left(\pi_{k-1|k-1}, \varphi\right)\right)^2\right] \le C_{k-1|k-1} \frac{\|\varphi\|^2}{N}. \tag{58}$$

At time k, step 2 in Algorithm 2 can be derived:

$$E\left[\left(\left(\pi_{k|k-1}^{N}, \varphi\right) - \left(\pi_{k|k-1}, \varphi\right)\right)^2\right] \le C_{k|k-1} \frac{\|\varphi\|^2}{N}. \tag{59}$$

By substituting the prediction stage formula (11) in the above formula, we obtain

$$\begin{aligned} \left|\left(\pi_{k|k-1}^{N}, \varphi\right) - \left(\pi_{k|k-1}, \varphi\right)\right| &= \left|\left(\pi_{k|k-1}^{N}, \varphi\right) - \left(\pi_{k-1|k-1}^{N}, K\varphi\right) \right. \\ &\quad \left. + \left(\pi_{k-1|k-1}^{N}, K\varphi\right) - \left(\pi_{k-1|k-1}, K\varphi\right)\right| \\ &\le \left|\left(\pi_{k|k-1}^{N}, \varphi\right) - \left(\pi_{k-1|k-1}^{N}, K\varphi\right)\right| \\ &\quad + \left|\left(\pi_{k-1|k-1}^{N}, K\varphi\right) - \left(\pi_{k-1|k-1}, K\varphi\right)\right|. \end{aligned} \tag{60}$$

Setting ζ_{k-1} as the σ-field generated by particle set $\{x_k^i\}_{i=1}^{N}$ and combining this with the Monte Carlo method, we obtain

$$E\left[\left(\pi_{k|k-1}^{N}, \varphi\right)|\zeta_{k-1}\right] = \left(\pi_{k-1|k-1}^{N}, K\varphi\right). \tag{61}$$

Substituting $\|k\varphi\| \le \|\varphi\|$ in the above formula,

$$\begin{aligned} E\left[\left(\left(\pi_{k|k-1}^{N}, \varphi\right) - \left(\pi_{k-1|k-1}^{N}, K\varphi\right)\right)^2\right] &= E\left[\left(\left(\pi_{k|k-1}^{N}, \varphi\right) - E\left[\left(\pi_{k|k-1}^{N}, \varphi\right)|\zeta_{k-1}\right]\right)^2|\zeta_{k-1}\right] \\ &= E\left[\left(\pi_{k|k-1}^{N}, \varphi\right)^2|\zeta_{k-1}\right] - 2E^2\left[\left(\pi_{k|k-1}^{N}, \varphi\right)|\zeta_{k-1}\right] \\ &\quad + E^2\left[\left(\pi_{k|k-1}^{N}, \varphi\right)|\zeta_{k-1}\right] = E\left[\left(\pi_{k|k-1}^{N}, \varphi\right)^2|\zeta_{k-1}\right] \\ &\quad - E^2\left[\left(\pi_{k|k-1}^{N}, \varphi\right)|\zeta_{k-1}\right] \le \frac{\|\varphi\|^2}{N}. \end{aligned} \tag{62}$$

Referring to Equation (58), there must be a real constant:

$$E\left[\left(\left(\pi^N_{k-1|k-1}, K\varphi\right) - \left(\pi_{k-1|k-1}, K\varphi\right)\right)^2\right] \le C_{k-1|k-1}\frac{\|K\varphi\|^2}{N} \le C_{k-1|k-1}\frac{\|\varphi\|^2}{N}. \tag{63}$$

Using the Minkowski inequality, we obtain

$$\begin{aligned} E\left[\left(\left(\pi^N_{k|k-1}, \varphi\right) - \left(\pi_{k|k-1}, \varphi\right)\right)^2\right]^{1/2} &\le E\left[\left(\left(\pi^N_{k|k-1}, \varphi\right) - \left(\pi^N_{k-1|k-1}, K\varphi\right)\right)^2\right]^{1/2} \\ &\quad + E\left[\left(\left(\pi^N_{k-1|k-1}, K\varphi\right) - \left(\pi_{k-1|k-1}, K\varphi\right)\right)^2\right]^{1/2} \\ &\le \sqrt{C_{k|k-1}}\frac{\|\varphi\|}{\sqrt{N}}, \end{aligned} \tag{64}$$

where $C_{k|k-1} = (1 + \sqrt{C_{k-1|k-1}})^2$. *Lemma 7 is proved.*

Lemma 8. *Refer to the updating stage in Algorithm 2 (steps 3–5) and assume that the conditions set by Theorem 6 and Lemma 7 are met. When* $k \ge 0$, *for any function* φ, *there must be a real constant* $C_{k|k}$, *and the prediction measure* $\widehat{\pi}^N_{k|k}$ *satisfies*

$$E\left[\left(\pi^N_{k|k-1}, \varphi\right)|\zeta_{k-1}\right] = \left(\pi^N_{k-1|k-1}, K\varphi\right), \tag{65}$$

where $\|\varphi\| \triangleq \sup_{x\in\Re^{n_x}}|\varphi(x)|$, *setting* ζ_{k-1} *as the* σ*-field generated by particle set* $\{x^i_k\}^N_{i=1}$.

Combined with the updating stage, we can obtain the following using Equation (12):

$$\begin{aligned} \left(\widehat{\pi}^N_{k|k}, \varphi\right) - \left(\pi_{k|k}, \varphi\right) &= \frac{\left(\pi^N_{k|k-1}, \widehat{g}\varphi\right)}{\left(\pi^N_{k|k-1}, \widehat{g}\right)} - \frac{\left(\pi_{k|k-1}, g\varphi\right)}{\left(\pi_{k|k-1}, g\right)} \\ &= \frac{\left(\pi^N_{k|k-1}, \widehat{g}\varphi\right)}{\left(\pi^N_{k|k-1}, \widehat{g}\right)} - \frac{\left(\pi^N_{k|k-1}, g\varphi\right)}{\left(\pi_{k|k-1}, g\right)} \\ &\quad + \frac{\left(\pi^N_{k|k-1}, g\varphi\right)}{\left(\pi_{k|k-1}, g\right)} - \frac{\left(\pi_{k|k-1}, g\varphi\right)}{\left(\pi_{k|k-1}, g\right)}. \end{aligned} \tag{66}$$

Substituting Equation (39) in this result yields

$$\begin{aligned} \left|\frac{\left(\pi^N_{k|k-1}, \widehat{g}\varphi\right)}{\left(\pi^N_{k|k-1}, \widehat{g}\right)} - \frac{\left(\pi^N_{k|k-1}, g\varphi\right)}{\left(\pi_{k|k-1}, g\right)}\right| &= \left|\frac{\left(\pi^N_{k|k-1}, \widehat{g}\varphi\right)\left(\pi_{k|k-1}, g\right) - \left(\pi^N_{k|k-1}, g\varphi\right)\left(\pi^N_{k|k-1}, \widehat{g}\right)}{\left(\pi^N_{k|k-1}, \widehat{g}\right)\left(\pi_{k|k-1}, g\right)}\right| \\ &= \left|\frac{\left(\pi^N_{k|k-1}, d_k^{-1}g\varphi\right)\left(\pi_{k|k-1}, g\right) - \left(\pi^N_{k|k-1}, g\varphi\right)\left(\pi^N_{k|k-1}, d_k^{-1}g\right)}{\left(\pi^N_{k|k-1}, d_k^{-1}g\right)\left(\pi_{k|k-1}, g\right)}\right| \\ &= \frac{\left(\pi^N_{k|k-1}, g\varphi\right)}{\left(\pi^N_{k|k-1}, g\right)\left(\pi_{k|k-1}, g\right)}\left|\left(\pi_{k|k-1}, g\right) - \left(\pi^N_{k|k-1}, g\right)\right| \\ &\le \frac{\|\varphi\|}{\left(\pi_{k|k-1}, g\right)}\left|\left(\pi_{k|k-1}, g\right) - \left(\pi^N_{k|k-1}, g\right)\right|. \end{aligned} \tag{67}$$

Similarly, using the Minkowski inequality and Equation (64), we obtain
where $(2\|g\|/(\pi_{k|k-1}, g))\sqrt{C_{k|k-1}} = \sqrt{C_{k|k}}$. *Lemma 8 is proved, and the MSE of the improved PF algorithm is convergent.*

5. Practical Applications

The factors that affect the performance of the state estimation method based on the PF are mainly determined by the construction of the spatial state model and the quality of the algorithm. The accurate architecture of the spatial state model is mainly realized by the reasonable selection of prior knowledge of the physical mechanism, as reflected in empirical physical equations, scientific parameter identification and training, multifeature search, and optimization of noise distribution. The method's advantages and disadvantages are limited by the particle degradation caused by an unreasonable proposed distribution and particle depletion caused by the resampling strategy. Therefore, to improve and obtain the best performance of state estimation methods for a fair comparison depends on the following. (a) The architecture of the spatial state model is

consistent. The same empirical physical equation and noise distribution are used in the application cases. The state tracking

$$
\begin{aligned}
E\left[\left(\left(\widehat{\pi}_{k|k}^{N},\varphi\right)-\left(\pi_{k|k},\varphi\right)\right)^{2}\right]^{1/2} &\le E\left[\left(\frac{\left(\pi_{k|k-1}^{N},\widehat{g}\varphi\right)}{\left(\pi_{k|k-1}^{N},\widehat{g}\right)}-\frac{\left(\pi_{k|k-1}^{N},g\varphi\right)}{\left(\pi_{k|k-1},g\right)}\right)^{2}\right]^{1/2}+E\left[\left(\frac{\left(\pi_{k|k-1}^{N},g\varphi\right)}{\left(\pi_{k|k-1},g\right)}-\frac{\left(\pi_{k|k-1},g\varphi\right)}{\left(\pi_{k|k-1},g\right)}\right)^{2}\right]^{1/2}\\
&\le E\left[\left(\frac{\left(\pi_{k|k-1}^{N},\widehat{g}\varphi\right)}{\left(\pi_{k|k-1}^{N},\widehat{g}\right)}-\frac{\left(\pi_{k|k-1}^{N},g\varphi\right)}{\left(\pi_{k|k-1},g\right)}\right)^{2}\right]^{1/2}+E\left[\left(\frac{\left(\pi_{k|k-1}^{N},g\varphi\right)}{\left(\pi_{k|k-1},g\right)}-\frac{\left(\pi_{k|k-1},g\varphi\right)}{\left(\pi_{k|k-1},g\right)}\right)^{2}\right]^{1/2}\\
&\le \frac{\|\varphi\|}{\left(\pi_{k|k-1},g\right)}E\left[\left(\left(\pi_{k|k-1},g\right)-\left(\pi_{k|k-1}^{N},g\right)\right)^{2}\right]^{1/2}+\frac{1}{\left(\pi_{k|k-1},g\right)}E\left[\left(\left(\pi_{k|k-1}^{N},g\varphi\right)-\left(\pi_{k|k-1},g\varphi\right)\right)^{2}\right]^{1/2}\\
&\le \frac{2\|g\|}{\left(\pi_{k|k-1},g\right)}\sqrt{C_{k|k-1}}\frac{\|\varphi\|}{\sqrt{N}}\le\sqrt{C_{k|k}}\frac{\|\varphi\|}{\sqrt{N}},
\end{aligned}
\tag{68}
$$

ability of each method is fully used, and the model parameter identification is trained. (b) The advantages of different methods are fully exploited. Commonly used and effective strategies are random, polynomial, system, and residual resampling. The applicability and accuracy of resampling strategies vary for different complex nonlinear systems. Considering the advantages of the above state estimation methods, according to the application case studied in this paper, through the analysis of simulation test results, it is concluded that the system resampling strategy performs best.

Therefore, based on the performance improvements of the method, the improved method can be flexibly applied to practical application fields to solve engineering problems on the premise of application scenario guarantees, such as the accurate architecture of the state space model for the research object, scientific identification and training of physical parameters, multifeature search, and optimization of noise distribution. We compared the clustering similarity particle filter (CSPF) to several traditional filtering algorithms on two examples. All methods were implemented in MATLAB, and the root mean squared error (RMSE) was used to evaluate accuracy.

Example 1. The advantages of the improved algorithm can be seen in both the Gaussian and non-Gaussian nonlinear systems. A typical univariate nonstationary growth model (UNGM) [36] with highly nonlinear and bimodal characteristics of the state distribution is selected, which is widely used in social and economic fields such as the evaluation of urban development and short-term predictions of insurance stocks and bank interest. The following model was selected to verify the effectiveness of the CSPF algorithm:

$$
\begin{aligned}
x_k &= \alpha x_{k-1}+\beta\frac{x_{k-1}}{1+x_{k-1}^2}+\gamma\cos\left(\delta*(k-1)\right)+\omega_k,\\
y_k &= \frac{x_k^2}{\varepsilon}+\upsilon_k,
\end{aligned}
\tag{69}
$$

where the measurement noise $\upsilon_k \sim N(0, R_k)$, and $R_k = 1$. The initial state was $x_0 = 0.1$, $\alpha = 0.5$, $\beta = 25$, $\gamma = 8$, $\delta = 1.2$, and $\varepsilon = 20$. The number of particles was $N = 100$. The simulation steps were $k = 1, 2, \cdots, T$, where $T = 5000$. The correlation coefficients were $L = 2$ and $l = 1$, and the gradient factor was $\lambda = 1.3$. SIR, APF, GPF, and the proposed algorithm were implemented in MATLAB, and 100 trials were conducted. The computer processor speed was 2.7 GHz, and the memory capacity was 8 GB. The RMSE,

$$
\mathrm{RMSE} = \sqrt{\frac{1}{T}\sum_{k=1}^{T}\left(x_k^{\mathrm{tur}}-x_k^{\mathrm{est}}\right)},
\tag{70}
$$

was used to evaluate the performance of the algorithms, where x_k^{tur} and x_k^{est} are, respectively, the real and state estimation values of the system.

The basic framework of the particle filter has state estimation and update parts. State estimation realizes state prediction of the current time based on the state prediction value of the previous time and the system state shift equation (including shift noise). Because the state variables are inevitably disturbed by various noises in the working environment, it is necessary to modify the estimated values based on actual observations to be as close to the real state values as possible so as to realize the update process of state estimation according to the observation values and measurement noise. Furthermore, the purpose of constructing the probability density function of the unknown system state using prior knowledge and actual observation data is realized. It can be seen that the shift and measurement noise will directly and greatly affect the nonlinear estimation method. This paper takes this case as an example, setting different kinds of shift noise to analyze the performance level of the nonlinear estimation methods. The two types of shift noise were Gaussian noise $\omega_{k\_G} \sim N(\omega_k; 0, 1)$ and non-Gaussian noise $\omega_{k\_NG} \sim \xi N(\omega_k; 0, \sigma_{\omega 1}^2) + (1-\xi)N(\omega_k; 0, \sigma_{\omega 2}^2)$, where $\xi = 0.8$, $\sigma_{\omega 1}^2 = 1$, and $\sigma_{\omega 2}^2 = 10$. The non-Gaussian noise ω_{k_NG} was a heavy-

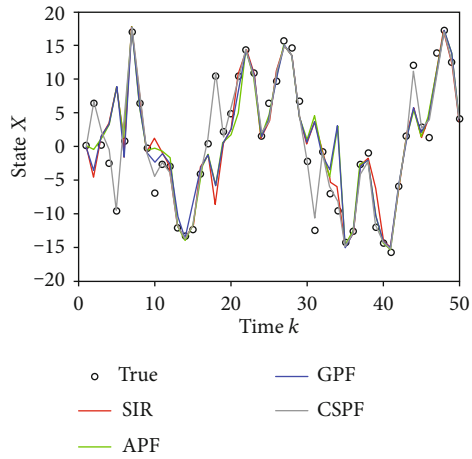

Figure 1: Comparison of state estimation based on different algorithms in the Gaussian noise environment. Note: SIR = sequential importance resampling; APF = auxiliary particle filter; GPF = Gaussian particle filter; CSPF = clustering similarity particle filter.

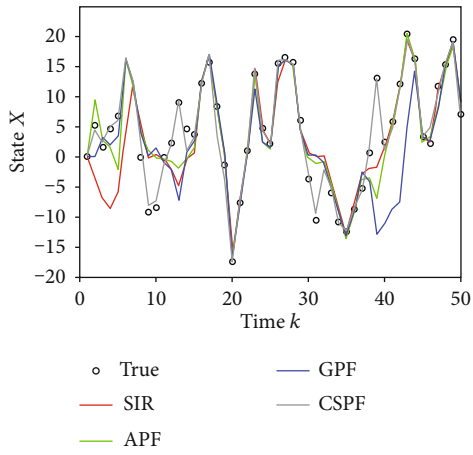

Figure 2: Comparison of state estimation based on different algorithms in the non-Gaussian noise environment. Note: SIR = sequential importance resampling; APF = auxiliary particle filter; GPF = Gaussian particle filter; CSPF = clustering similarity particle filter.

tailed distribution, and the acceptance-rejection sampling procedure used in Monte Carlo simulations [25] was adopted to achieve noise sampling with a confidence level of 97.5%. The simulation results are shown in Figures 1–3 and Tables 1 and 2.

The consistency of the state trajectory of the improved PF algorithm (clustering similarity particle filter (CSPF)) was measured by the Euclidean spatial distance (ECSPF), $s = 2$, and Chebyshev spatial distance (CCSPF), $s \to \infty$. Figures 1 and 2 compare various PF algorithms for a single operation of the nonlinear system in Gaussian and non-Gaussian noise environments (the improved algorithm is represented by ECSPF), which can directly evaluate the effect of state estimation. Figure 3 compares the RMSE of the simulation results

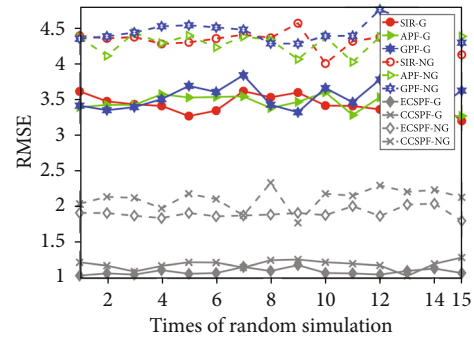

Figure 3: RMSE of SIR, APF, GPF, ECSPF, and CCSPF for 15 random simulation runs. Note: SIR = sequential importance resampling; APF = auxiliary particle filter; GPF = Gaussian particle filter; ECSPF = Euclidean distance clustering similarity particle filter; CCSPF = Chebyshev distance clustering similarity particle filter.

after 15 simulation runs. Algorithm labels ending in the letter G are denoted by solid curves and correspond to Gaussian system noise ω_{k_G}, and those ending in the letters NG are denoted by dotted curves and correspond to non-Gaussian system noise ω_{k_NG}. Tables 1 and 2 show the RMSE mean and variance of state estimation results after 100 simulation runs to compare the accuracy of the improved algorithm and other algorithms.

Figures 1 and 2 show that the state estimation accuracy of CSPF was significantly better than that of the other algorithms in the two noise environments, and the fluctuation trends of the CSPF estimated curve at any time continued moving and approaching the fluctuation trends of the actual state curve. By contrast, the other algorithms were not consistent at each time point. As shown in Figure 3 and Tables 1 and 2, the RMSE means and variances of the two improved algorithms were lower than those of SIR, APF, and GPF. For example, the prediction accuracy (variance) of CSPF was improved by 65%–69% (67%–89%) in the Gaussian noise environment and by 52%–57% (14%–54%) in the non-Gaussian noise environment. Therefore, the improved algorithm had greater accuracy and more stability, and the performance of ECSPF was particularly significant.

Under the same running time, the accuracy of the state estimation of the different algorithms was determined by adjusting the number of sampling particles N and the order of the state trajectory. From this, the efficiency of the improved algorithm was verified by comparing the corresponding operational cost (see Table 3 for details). In Gaussian and non-Gaussian noise environments, the improved algorithm with Euclidean and Chebyshev distance similarity measures was compared with SIR, APF, and GPF. For the same operational cost, i.e., for the same computing and simulation times, the improved algorithm not only used the fewest sampling particles but also had significantly better accuracy than the other three algorithms. The RMSE was reduced by factors of about 3 and 2 in Gaussian and non-Gaussian noise environments, respectively. This verified that

Table 1: Mean and variance of RMSE for five nonlinear algorithms running 100 times under both the Gaussian and non-Gaussian noise models.

Filter estimation	SIR	APF	GPF	ECSPF	CCSPF
RMSE mean (Gaussian)	3.4771	3.4368	3.5677	1.1003	1.2027
RMSE variance (Gaussian)	0.0171	0.0135	0.0221	0.0025	0.0045
RMSE mean (non-Gaussian)	4.3332	4.3939	4.4726	1.9273	2.0941
RMSE variance (non-Gaussian)	0.0222	0.0155	0.0235	0.0108	0.0133

Note: SIR = sequential importance resampling; APF = auxiliary particle filter; GPF = Gaussian particle filter; ECSPF = Euclidean distance clustering similarity particle filter; CCSPF = Chebyshev distance clustering similarity particle filter; RMSE = root mean squared error.

Table 2: Accuracy improvement percentage of mean and variance of RMSE for five nonlinear algorithms running 100 times under both the Gaussian and non-Gaussian noise models.

Filter	RMSE	Gaussian noise			Non-Gaussian noise		
		SIR	APF	GPF	SIR	APF	GPF
ECSPF	Mean	68.4%	68.0%	69.2%	55.5%	56.1%	56.9%
	Variance	85.4%	81.5%	88.7%	51.4%	30.3%	54.0%
CCSPF	Mean	65.4%	65.0%	66.3%	51.7%	52.3%	53.2%
	Variance	73.7%	66.7%	79.6%	40.1%	14.2%	43.4%

Note: SIR = sequential importance resampling; APF = auxiliary particle filter; GPF = Gaussian particle filter; ECSPF = Euclidean distance clustering similarity particle filter; CCSPF = Chebyshev distance clustering similarity particle filter; RMSE = root mean squared error.

Table 3: Computation time analysis for five nonlinear algorithms running 100 times under Gaussian and non-Gaussian noise models.

Filter	Gaussian noise ($T = 5000$)			Filter	Non-Gaussian noise ($T = 1000$)		
	N	RMSE mean	AVG time (s)		N	RMSE mean	AVG time (s)
SIR	500	3.2556	1.5	SIR	320	4.0904	2.3
APF	250	3.3211	1.5	APF	160	4.2697	2.3
GPF	800	3.3093	1.5	GPF	340	4.1536	2.3
ECSPF	100	1.1003	1.5	CCSPF	100	2.1215	2.3

Note: AVG = average; RMSE = root mean squared error; SIR = sequential importance resampling; APF = auxiliary particle filter; GPF = Gaussian particle filter; ECSPF = Euclidean distance clustering similarity particle filter; CCSPF = Chebyshev distance clustering similarity particle filter.

the improved algorithm had higher operational efficiency and substantial advantages in computation time.

Example 2. We assessed the health status of a lithium-ion battery. Through the state tracking and capacity training of historical samples, the physical model parameters of the empirical degradation and distribution information of the noise were identified and optimized [3]. Different nonlinear methods were used to establish state tracking and remaining useful life (RUL) prediction models for the battery. The performances of various algorithms were evaluated based on the state tracking effect and prediction accuracy.

In order to solve the problem regarding battery health assessment, it is particularly important to ensure the accurate structure of the decay physical model (state space model) and scientific parameter identification; this is done under the premise of the reasonable selection of the state tracking training set (noise distribution) and initial parameters. In this paper, parameter identification is carried out based on the attenuation information of state tracking historical samples to construct the RUL prediction model [37]. Since the accuracy of state tracking and RUL prediction largely depends on the physical model of the battery capacity degradation, the development of the model requires physical knowledge of the system [38]. This is usually represented by information collected by sensors, including battery parameters (e.g., charge-discharge voltage and current, power, electrochemical impedance spectroscopy, frequency, and temperature), to build an equivalent circuit model [39] to characterize the degradation trend of battery capacity, as shown in Figure 4, which includes the open-circuit voltage (OCV), electrolyte resistance R_E, polarization current I_R, double-layer voltage

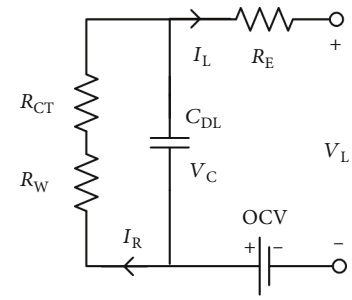

Figure 4: Battery equivalent circuit model.

V_C, capacitance C_{DL}, charge transfer resistance R_{CT}, Warburg impedance R_W, load current I_L, and terminal voltage V_L.

Relying on the attenuation mechanism of the electrochemical characteristics, the relationship between capacity degradation and internal impedance of the battery was determined using statistical regression. The simulated attenuation characteristic of the impedance increased with the number of charge-discharge cycles to obtain a double-exponential empirical degradation model [40, 41],

$$C_{ap} = a * \exp(b * k) + c * \exp(d * k), \tag{71}$$

where C_{ap} is the battery capacity $(A \cdot h)$ and k is the number of charge-discharge cycles. The unknown model parameters a and c are related to the battery impedance, b and d are related to the rate of capacity degradation, and $\exp(*)$ is the exponential function.

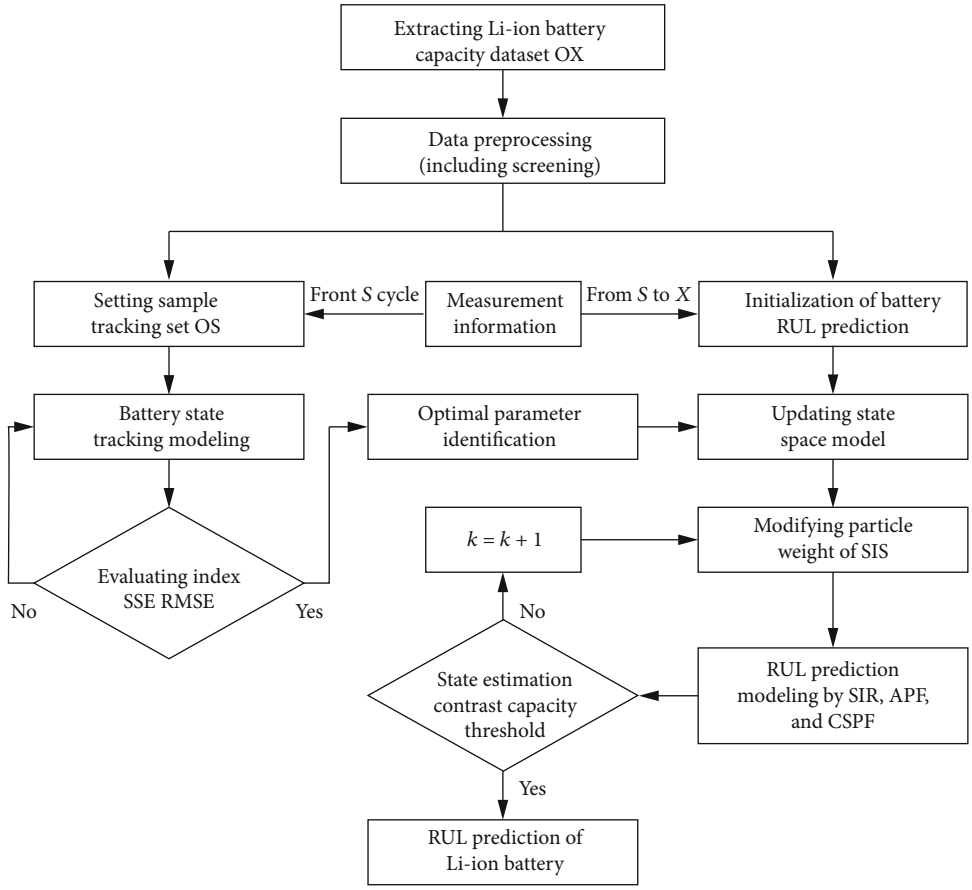

Figure 5: Battery state tracking and remaining useful life (RUL) prediction method for the Li-ion battery based on different algorithms.

Table 4: Experimental test conditions of CALCE dataset M8.

Battery ID	Experimental platform	Temperature	Charging	End condition	Discharge	End condition
M8	Arbin BT2000	20-25°C	Constant current/voltage	4.2 V/0.05 A	Constant current	2.7 V

A tracking and training model was constructed using historical samples of the battery capacity to estimate the model parameters of the empirical degradation in real time and optimize the multicharacteristic noise [42]. The identified physical model effectively converged to the gradual trend of actual battery degradation, which provided reasonable identification parameters and effective initial values to establish an RUL prediction model. This enabled the updating of the state space model composed of the state transition equation (physical model of the battery system), which can represent the recursion law of the system, and the observation equation (data characteristic measurement relationship), which can transform the implicit information of the system to visible output. The state estimation of the current time is obtained by the state transfer process and the prediction results of the previous time. Using the error between the actual measurement (noise interference) and the estimated observation information at the current moment, a weighted correction term is generated to realize the updating process. This allows the state estimation and prediction system model to be obtained with high reliability, and the process of battery state tracking and RUL predictive evaluation can be realized. A flowchart is shown in Figure 5.

Using the state tracking process to identify the model parameters and battery RUL prediction, the SIR, APF, and CSPF algorithms were compared (since the application of the algorithm is limited by the dimension of the system variables, the GPF is not suitable for this example). State tracking parameters were identified before the charge-discharge cycle S; i.e., we estimated the optimal model parameters that can minimize the error between the predicted value of the algorithm and the actual value of the experiment. After the charge-discharge cycle S, the battery capacity was predicted to determine whether the failure threshold was exceeded. The original data of the capacity degradation of the lithium-ion battery were from the open-source experimental data of the Center for Advanced Life Cycle Engineering (CALCE) of the University of Maryland. An Arbin BT2000 battery system was the experimental platform, and the test data were stored in Excel format. A data sample with a

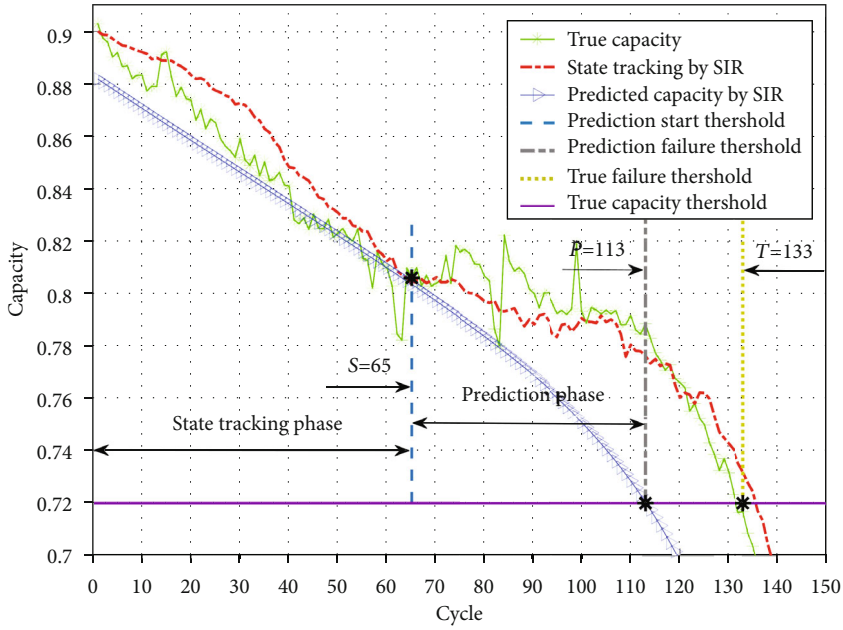

(a) SIR

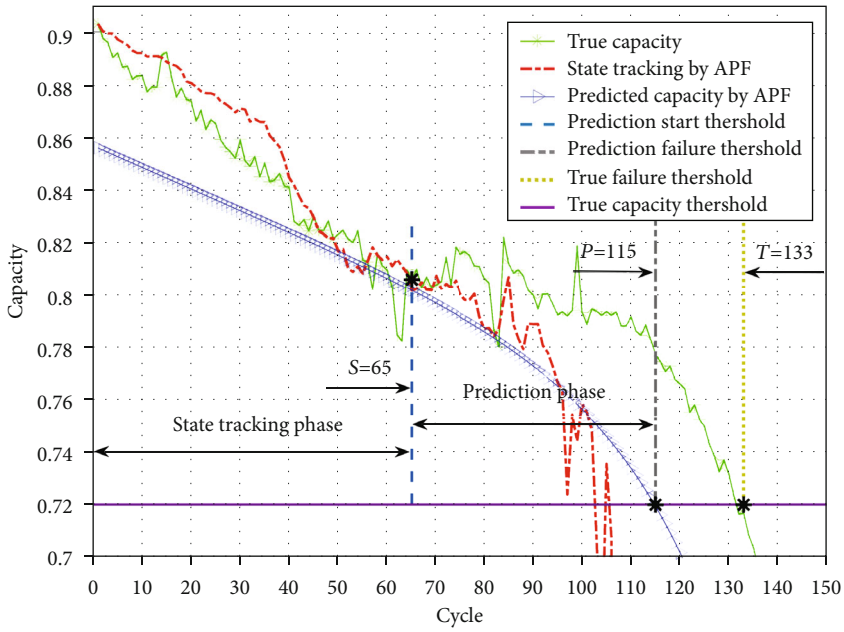

(b) APF

Figure 6: Continued.

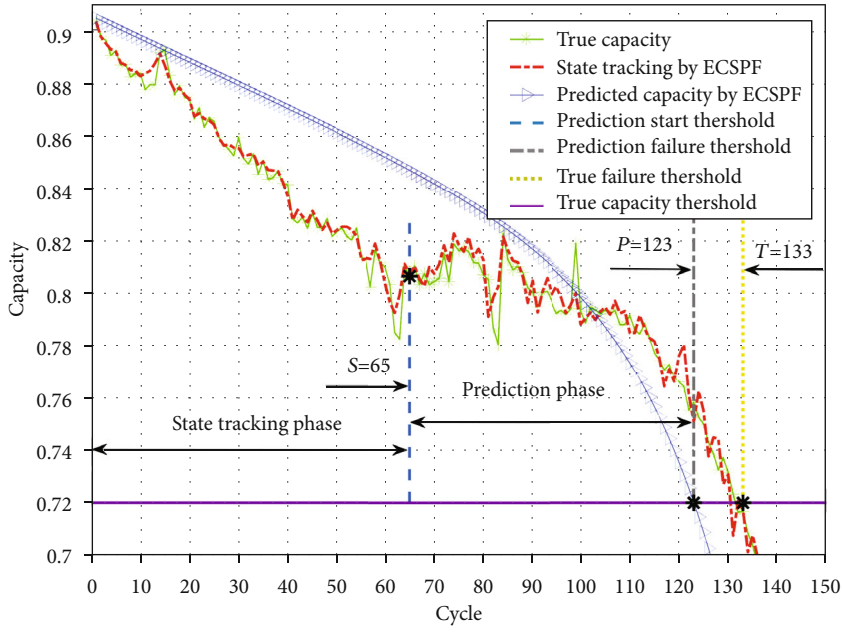

(c) ECSPF

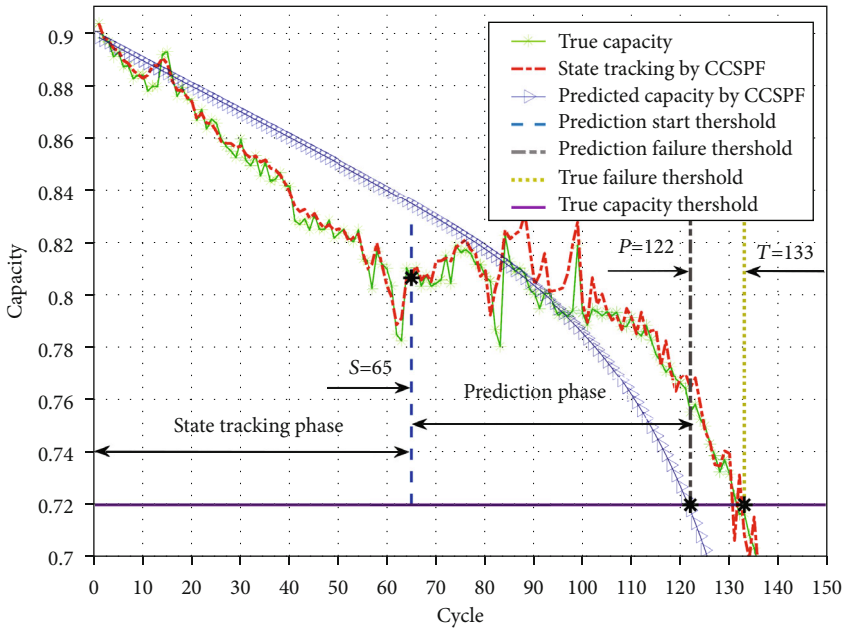

(d) CCSPF

FIGURE 6: State tracking and RUL prediction results for the battery based on SIR, APF, ECSPF, and CCSPF. Note: SIR = sequential importance resampling; APF = auxiliary particle filter; ECSPF = Euclidean distance clustering similarity particle filter; CCSPF = Chebyshev distance clustering similarity particle filter.

normalized capacity of 0.90 Ah, M8, was selected as the test set for comparison of the state assessment methods. The battery was charged at the standard constant current of 0.5 C until it reached 4.2 V and was switched to constant voltage charging until the current decayed to 0.05 A, and the discharge was considered complete when the voltage dropped to 2.7 V during the charge-discharge cycle [43], as shown in Table 4. While collecting experimental data, due to the error from the accuracy of measuring equipment and human misoperation, a small amount of abnormal data was extracted from the battery dataset, as it would have affected the quality of the history dataset. The size of the dataset would also affect the operational cost, and simplifying the data (e.g., taking one point from each n point) would reduce this cost. Therefore, the original data were preprocessed, filtered, and simplified.

Generally, 80% of the rated capacity was taken as the end-of-life threshold T, and the actual failure threshold was 133 cycles according to open-source data, where the state tracking set was $S = 65$ and the number of particles was $N = 100$. The simulation results are shown in Figure 6 and Tables 5

Table 5: Comparison of the average state tracking effect for four nonlinear algorithms running 1000 times.

Filter	SSE	MSE	RMSE	R^2
SIR	1.3526×10^{-5}	2.0810×10^{-7}	1.4328×10^{-5}	7.8318×10^{-1}
APF	1.8923×10^{-5}	2.9112×10^{-7}	1.6408×10^{-5}	6.4347×10^{-1}
ECSPF	8.7368×10^{-7}	1.3441×10^{-8}	3.6547×10^{-6}	9.8419×10^{-1}
CCSPF	1.0425×10^{-6}	1.6038×10^{-8}	3.9975×10^{-6}	9.8281×10^{-1}

Note: SIR = sequential importance resampling; APF = auxiliary particle filter; ECSPF = Euclidean distance clustering similarity particle filter; CCSPF = Chebyshev distance clustering similarity particle filter; SSE = sum of squared error; MSE = mean squared error; RMSE = root mean squared error; R^2 = coefficient of determination.

Table 6: Comparison of RUL prediction results based on four nonlinear algorithms running 100 times.

Comparison items	SIR	APF	CSPF	
			ECSPF	CCSPF
Mean	113	115	123	122
Variance	156.3	476.6	5.9	6.2
Error	15.0%	13.5%	7.5%	8.3%
RMSE	23.5%	26.8%	10.6%	11.1%

Note: SIR = sequential importance resampling; APF = auxiliary particle filter; ECSPF = Euclidean distance clustering similarity particle filter; CCSPF = Chebyshev distance clustering similarity particle filter; RMSE = root mean squared error.

and 6. Figure 6 can be used to compare the effect of state tracking and the accuracy of capacity prediction of different algorithms. Tables 5 and 6 compare the state tracking and prediction results obtained by multiple simulation calculations. The evaluation indicators of the state tracking effect are the sum of squared error (SSE), MSE, RMSE, and coefficient of determination (R^2). The closer SSE, MSE, and RMSE were to 0, the closer R^2 was to 1, and the better was the effect of state tracking. The evaluation indicators of the prediction accuracy were the mean, variance, relative error, and RMSE of the prediction failure threshold.

Figure 6 and Table 5 show that compared with the SIR and APF algorithms, the state tracking indicators and effect of the proposed CSPF algorithm were superior, and the Euclidean distance measure yielded the best results. The excellent state tracking effect of the CSPF method also guarantees that the attenuation mechanism of state tracking in the early period is the same as in later-stage predictions over the whole life cycle of the battery. As shown in Figure 6 and Table 6, after 100 simulations using SIR, APF, ECSPF, and CCSPF, the average failure thresholds of RUL prediction were 113, 115, 123, and 122 cycles, respectively, and the relative error was within 15.0%. Taking ECSPF as an example, the variance, relative error, and RMSE of the RUL prediction failure threshold were significantly lower than those of SIR and APF, and the prediction trend was relatively closer to the actual capacity degradation curve. The relative error of ECSPF was better than those of SIR and APF by about 50% and 45%, respectively, and the threshold variances were lower by factors of about 26 and 80, respectively. RMSE was about 55% and 60% greater, respectively. The results show that the prediction accuracy of CSPF was relatively higher than those of the other algorithms, the discrete degree of the state particle set of prediction results was the minimum, the degree of uncertainty expression was the lowest, and the algorithm was more robust.

6. Conclusions

Facing the difficulties of the standard PF algorithm in nonlinear system state estimation, such as low precision, instability, and low computational efficiency, we proposed an improved PF algorithm (CSPF) based on the consistency principle of the spatial state trajectory. Relying on the model construction of spatial trajectories between sampled particles and actual states, current and future multistage measurement information was predicted by SIS and GPF to form trajectories combining the original and modified trajectories. The similarity of the combined trajectories was measured by clustering analysis to guide the generation of new distributions and update the particle importance weights to mitigate the particle degradation phenomenon. Because resampling is not adopted in the improved algorithm, the problem of particle depletion is fundamentally eliminated. The convergence theorem of the improved algorithm of the CSPF and MSE of the results was proved. The effectiveness of CSPF was verified by comparison with current methods in cases of socioeconomic prediction and battery health assessment. The application experiments showed that, compared to SIR, APF, and GPF, CSPF had higher accuracy and better robustness for the state estimation of nonlinear systems under the influence of Gaussian or non-Gaussian noise. Primary conclusions are summarized as follows:

(1) In Gaussian and non-Gaussian noise environments, the prediction accuracy of CSPF was improved significantly, more than 50% in typical cases

(2) The latest measurement information was used to update the new proposal distribution, and the computational cost of CSPF was reduced by adjusting the number of sampling particles and the order of the state trajectory. In a typical case, the RMSE of CSPF was reduced by a factor of more than 2 in the same computing time

(3) The first-order Markov model was modified by the clustering similarity of state trajectories so that the indicators of state tracking effects were relatively

higher, which provided an accuracy guarantee for the prediction model. In the battery application, the prediction accuracy of CSPF was the best, and the relative error of the RUL failure threshold was maintained within 8%

Data Availability

The data used to support the findings of this study are available from the corresponding author upon request.

Conflicts of Interest

The authors declare that there are no conflicts of interest regarding the publication of this paper.

Acknowledgments

The authors sincerely thank the Guangxi Engineering Technology Research Center of Ship Digital Design and Advanced Manufacturing and the Intelligentized Robotic Welding Technology Laboratory of Shanghai Jiao Tong University for their intelligence support and valuable comments in performing this research. We appreciate the generous financial support of the National Natural Science Foundation of China (Nos. 51969001 and 61763006), the Guangxi Natural Science Foundation of China (Nos. 2018GXNSFAA138080 and 2021GXNSFBA075023), the Guangxi Science and Technology Plan Project of China (No. GuikeAD18281007), and the Innovation Project of Guangxi Graduate Education (YCBZ2019050).

References

[1] X. Ding, Z. Wang, L. Zhang, and C. Wang, "Longitudinal vehicle speed estimation for four-wheel-independently-actuated electric vehicles based on multi-sensor fusion," *IEEE Transactions on Vehicular Technology*, vol. 69, no. 11, pp. 12797–12806, 2020.

[2] Z. Zhou, Y. Tan, and R. Dong, "Fault detection of piezoceramic actuator using non-smooth observer," *International Journal of Applied Electromagnetics and Mechanics*, vol. 47, no. 4, pp. 975–991, 2015.

[3] Q. Wang, Z. Wang, L. Zhang, P. Liu, and Z. Zhang, "A novel consistency evaluation method for series-connected battery systems based on real-world operation data," *IEEE Transactions on Transportation Electrification*, vol. 7, no. 2, pp. 437–451, 2021.

[4] C. Wang, Z. Wang, L. Zhang, D. Cao, and D. G. Dorrell, "A vehicle rollover evaluation system based on enabling state and parameter estimation," *IEEE Transactions on Industrial Informatics*, vol. 17, no. 6, pp. 4003–4013, 2021.

[5] Z. Zhou, Y. Tan, and X. Liu, "State estimation of dynamic systems with sandwich structure and hysteresis," *Mechanical Systems and Signal Processing*, vol. 126, pp. 82–97, 2019.

[6] D. Luenberger, "An introduction to observers," *IEEE Transactions on Automatic Control*, vol. 16, no. 6, pp. 596–602, 1971.

[7] Z. Zhou, Y. Tan, R. Dong, and L. Zhang, "Fault detection for sandwich systems with hysteresis based on robust observer," *International Journal of Applied Electromagnetics and Mechanics*, vol. 49, no. 4, pp. 577–595, 2015.

[8] R. E. Kalman, "A new approach to linear filtering and prediction problems," *Journal of Basic Engineering*, vol. 82, no. 1, pp. 35–45, 1960.

[9] Z. Zhou and X. Liu, "State and fault estimation of sandwich systems with hysteresis," *International Journal of Robust and Nonlinear Control*, vol. 28, no. 13, pp. 3974–3986, 2018.

[10] Y. Guan and M. Saif, "A novel approach to the design of unknown input observers," *IEEE Transactions on Automatic Control*, vol. 36, no. 5, pp. 632–635, 1991.

[11] H. K. Khalil and L. Praly, "High-gain observers in nonlinear feedback control," *International Journal of Robust and Nonlinear Control*, vol. 24, no. 6, pp. 991-992, 2014.

[12] Z. Zhou, Y. Tan, Y. Xie, and R. Dong, "State estimation of a compound non-smooth sandwich system with backlash and dead zone," *Mechanical Systems and Signal Processing*, vol. 83, pp. 439–449, 2017.

[13] K. S. Phogat and D. E. Chang, "Discrete-time invariant extended Kalman filter on matrix Lie groups," *International Journal of Robust and Nonlinear Control*, vol. 30, no. 12, pp. 4449–4462, 2020.

[14] Q. Meng, Y. Sun, and Z. Cao, "Adaptive extended Kalman filter (AEKF)-based mobile robot localization using sonar," *Robotica*, vol. 18, no. 5, pp. 459–473, 2000.

[15] N. J. Gordon, D. J. Salmond, and A. F. M. Smith, "Novel approach to nonlinear/non-Gaussian Bayesian state estimation," *IEEE Proceedings F Radar and Signal Processing*, vol. 140, no. 2, pp. 107–113, 1993.

[16] M. S. Arulampalam, S. Maskell, N. Gordon, and T. Clapp, "A tutorial on particle filters for online nonlinear/non-Gaussian Bayesian tracking," *IEEE Transactions on Signal Processing*, vol. 50, no. 2, pp. 174–188, 2002.

[17] M. K. Pitt and N. Shephard, "Filtering via simulation: auxiliary particle filters," *Journal of the American Statistical Association*, vol. 94, no. 446, pp. 590–599, 1999.

[18] J. H. Kotecha and P. M. Djuric, "Gaussian particle filtering," *IEEE Transactions on Signal Processing*, vol. 51, no. 10, pp. 2592–2601, 2003.

[19] J. H. Kotecha and P. M. Djuric, "Gaussian sum particle filtering," *IEEE Transactions on Signal Processing*, vol. 51, no. 10, pp. 2602–2612, 2003.

[20] P. Guarniero, A. M. Johansen, and A. Lee, "The iterated auxiliary particle filter," *Journal of the American Statistical Association*, vol. 112, no. 520, pp. 1636–1647, 2017.

[21] Y. Sun, X. Ran, Y. Li, G. Zhang, and Y. Zhang, "Thruster fault diagnosis method based on Gaussian particle filter for autonomous underwater vehicles," *International Journal of Naval Architecture and Ocean Engineering*, vol. 8, no. 3, pp. 243–251, 2016.

[22] M. L. Psiaki, J. R. Schoenberg, and I. T. Miller, "Gaussian sum reapproximation for use in a nonlinear filter," *Journal of Guidance, Control, and Dynamics*, vol. 38, no. 2, pp. 292–303, 2015.

[23] X. Tang, K. Liu, X. Wang, B. Liu, F. Gao, and W. D. Widanage, "Real-time aging trajectory prediction using a base model-oriented gradient-correction particle filter for lithium-ion batteries," *Journal of Power Sources*, vol. 440, pp. 227118.1–227118.11, 2019.

[24] X. Fu and Y. Jia, "An improvement on resampling algorithm of particle filters," *IEEE Transactions on Signal Processing*, vol. 58, no. 10, pp. 5414–5420, 2010.

[25] A. T. Cemgil, "A tutorial introduction to Monte Carlo methods, Markov Chain Monte Carlo and particle filtering,"

Academic Press Library in Signal Processing, vol. 1, pp. 1065–1114, 2014.

[26] M. Ahwiadi and W. Wang, "An adaptive particle filter technique for system state estimation and prognosis," *IEEE Transactions on Instrumentation and Measurement*, vol. 69, no. 9, pp. 6756–6765, 2020.

[27] R. Havangi, "Robust evolutionary particle filter," *ISA Transactions*, vol. 57, pp. 179–188, 2015.

[28] A. Salarpour and H. Khotanlou, "Direction-based similarity measure to trajectory clustering," *IET Signal Processing*, vol. 13, no. 1, pp. 70–76, 2019.

[29] H. He and Y. Tan, "Unsupervised classification of multivariate time series using VPCA and fuzzy clustering with spatial weighted matrix distance," *IEEE Transactions on Cybernetics*, vol. 50, no. 3, pp. 1096–1105, 2020.

[30] J. Candy, "Bootstrap particle filtering," *IEEE Signal Processing Magazine*, vol. 24, no. 4, pp. 73–85, 2007.

[31] L. Zhang, Y. Zhu, P. Shi, and Y. Zhao, "Resilient asynchronous H∞ filtering for Markov jump neural networks with unideal measurements and multiplicative noises," *IEEE Transactions on Cybernetics*, vol. 45, no. 12, pp. 2840–2852, 2015.

[32] Z. Zhou, Y. Tan, and P. Shi, "Fault detection of a sandwich system with dead-zone based on robust observer," *Systems & Control Letters*, vol. 96, pp. 132–140, 2016.

[33] H. He, Y. Tan, and J. Xing, "Unsupervised classification of 12-lead ECG signals using wavelet tensor decomposition and two-dimensional Gaussian spectral clustering," *Knowledge-Based Systems*, vol. 163, pp. 392–403, 2019.

[34] Z. Zhou, Y. Tan, Y. Xie, and R. Dong, "Soft measurement of states of sandwich system with dead zone and its application," *Measurement*, vol. 87, no. 1, pp. 219–234, 2016.

[35] H. Zhou, Z. Deng, Y. Xia, and M. Fu, "A new sampling method in particle filter based on Pearson correlation coefficient," *Neurocomputing*, vol. 216, pp. 208–215, 2016.

[36] M. Rhif, A. B. Abbes, I. Farah, B. Martínez, and Y. Sang, "Wavelet transform application for/in non-stationary time-series analysis: a review," *Applied Sciences*, vol. 9, no. 7, 2019.

[37] K. Liu, Y. Shang, Q. Ouyang, and W. D. Widanage, "A data-driven approach with uncertainty quantification for predicting future capacities and remaining useful life of lithium-ion battery," *IEEE Transactions on Industrial Electronics*, vol. 68, no. 4, pp. 3170–3180, 2021.

[38] A. Wen, J. Meng, J. Peng, L. Cai, and Q. Xiao, "Online parameter identification of the lithium-ion battery with refined instrumental variable estimation," *Complexity*, vol. 2020, Article ID 8854618, 12 pages, 2020.

[39] B. Saha, K. Goebel, and J. Christophersen, "Comparison of prognostic algorithms for estimating remaining useful life of batteries," *Transactions of the Institute of Measurement and Control*, vol. 31, no. 3-4, pp. 293–308, 2009.

[40] R. B. Wright, C. G. Motloch, J. R. Belt et al., "Calendar- and cycle-life studies of advanced technology development program generation 1 lithium-ion batteries," *Journal of Power Sources*, vol. 110, no. 2, pp. 445–470, 2002.

[41] W. He, N. Williard, M. Osterman, and M. Pecht, "Prognostics of lithium-ion batteries based on Dempster-Shafer theory and the Bayesian Monte Carlo method," *Journal of Power Sources*, vol. 196, no. 23, pp. 10314–10321, 2011.

[42] Z. Wei, J. Zhao, D. Ji, and K. J. Tseng, "A multi-timescale estimator for battery state of charge and capacity dual estimation based on an online identified model," *Applied Energy*, vol. 204, pp. 1264–1274, 2017.

[43] Z. Jiao, X. Fan, X. Zhang, Y. Luo, and Y. Liu, "State tracking and remaining useful life predictive method of Li-ion battery based on improved particle filter algorithm," *Transaction of China Electrotechnical Society*, vol. 35, no. 18, pp. 3979–3993, 2020.

Hindawi
Journal of Sensors
Volume 2021, Article ID 5577852, 11 pages
https://doi.org/10.1155/2021/5577852

Research Article

Financial Time Series Image Algorithm Based on Wavelet Analysis and Data Fusion

Wuwei Liu and Jingdong Yan

School of Management, Wuhan University of Technology, Wuhan, 430070 Hubei, China

Correspondence should be addressed to Wuwei Liu; liuww02@whut.edu.cn

Received 3 March 2021; Revised 26 March 2021; Accepted 2 April 2021; Published 27 April 2021

Academic Editor: Mu Zhou

In recent years, people are more and more interested in time series modeling and its application in prediction. This paper mainly discusses a financial time series image algorithm based on wavelet analysis and data fusion. In this research, we conducted an in-depth study on the scale decomposition sequence and wavelet transform sequence in different scale domains of wavelet transform according to the scale change rule based on wavelet transform. We use wavelet neural network with different input neurons and hidden neurons to predict, respectively. Finally, the prediction results are integrated into the final prediction results based on the original time series by using wavelet reconstruction technology. Using RBF algorithm in neural network and SPSS Clementine, the wavelet transform sequences on five scales are modeled. Each network model has three layers: one input layer, one hidden layer, and one output layer, and each output layer has only one output element. In order to compare the prediction effect of the model proposed in this study, the ordinary RBF network is used to model and predict the log yield itself. When the input sample is 5, the minimum mean square error is obtained when the hidden layer is 6, and the mean square error is 1.6349. The mean square error of the training phase is 0.0209, and the validation error is 1.6141. The results show that the prediction results of the wavelet prediction method combined with the RBF network prediction method are better than those of wavelet prediction or RBF network prediction.

1. Introduction

As a new research achievement in recent years, wavelet analysis has been widely used because of its local amplification and multiresolution analysis characteristics. However, due to the superficial understanding of wavelet analysis method, it has not made full use of its powerful function. However, in the future, the wavelet toolkit can only be used to improve the results of MATLAB.

For stock price trend prediction, the commonly used techniques are moving average method and index smoothing method or other conventional technical index analysis methods. However, the stock price financial data is a typical nonstationary time series, with a peak thick tail; the traditional forecasting method is obviously not suitable. Moreover, due to the influence of various accidental factors, the data of stock market are often random. Moreover, it is difficult to analyze the long-term trend of China's stock market due to its short-term establishment and imperfect aspects. With the introduction of wavelet analysis theory into the financial field, it is found that wavelet transform is effective in extracting useful information from noisy data.

For lossless coding, a novel method based on wavelet is proposed to improve the coefficient independence of hyperspectral images. The regression wavelet analysis (RWA) proposed by Amrani et al. use multiple regressions to exploit the relationship between wavelet transform components. It is based on the previous nonlinear scheme, and their scheme estimates each coefficient from neighbor coefficients. Specifically, RWA performs pyramid estimation in the wavelet domain, thereby reducing the residual

and the statistical relationship representing energy compared with the existing wavelet-based scheme. They proposed three regression models to solve problems related to estimation accuracy, component scalability, and computational complexity. Other suitable regression models can be designed for other goals. Their research process lacks data [1]. Arneodo et al. use continuous wavelet transform to formalize multifractals into fractal functions. They reported on the latest application results of the so-called Wavelet Transform Modulus Maximum (WTMM) method to fully developed turbulence data and DNA sequences. As a summary, they briefly introduced some ongoing work that may become a guide for future research. Their research has no practical significance [2]. Bousefsaf et al. use a low-cost webcam to record and analyze pulse wave signals to extract amplitude information and evaluate participants' vasomotor activity. They used continuous wavelet transform to analyze the photoplethysmographic signal obtained from the webcam. After a brief but intense physical exercise, they used an approved contact probe to evaluate a group of 12 healthy subjects to evaluate the performance of the proposed filtration technology. During rest, skin vasodilation can be observed. Their research lacks comparative experiments [3]. Alcala et al. believe that because the Fourier method assumes that the energy is distributed in the entire given window. They used wavelet analysis techniques to divide the rocket data set collected during the polar midlevel summer echo event, which was characterized by the Norwegian sounding system radar. They found that edges can be isolated in space or juxtaposed with turbulence, and similarly, turbulence areas without steep edges can be found. Their research method lacks innovation [4]. Chen uses continuous wavelet analysis to study the dynamic relationship between American health development and economic growth. His discovery reconciled the long-term anticyclicality of longevity with the procyclicality of longevity related to the business cycle in the long run. In addition, he also identified four causal relationships between health progress and economic growth: income view, health view, feedback view, and neutrality assumption. His research sample is too small [5, 6].

In this study, wavelet transform depends on the law of scale changes. The different scale domains of wavelet transform correspond to the scale decomposition sequence and wavelet transform sequence. The wavelet neural network containing different input neurons and hidden neurons is used to make predictions. Finally, the separately predicted results are then combined with wavelet reconstruction technology into the final prediction results based on the original time series. Using the RBF algorithm in the neural network and using SPSS Clementine to model wavelet transform sequences on 5 scales, each network model has three layers, namely, an input layer, a hidden layer, and an output layer, and each output layer has only one output element. In order to compare the forecasting effect of the model proposed in this study, at the same time, the ordinary RBF network is used to model and predict the logarithmic return itself.

2. Financial Time Series Image Algorithm

2.1. RBF Neural Network Algorithm. The i neuron in the hidden layer of the RBF neural network algorithm is

$$k_i^q = \sqrt{\sum_j \left(w1_{ji} - x_j^q\right) \times b1_i},$$
$$o_j = f\left(\text{net}_j\right) = \frac{1}{1 + \exp\left(\sum_i \omega_{ij} o_i + \theta_j\right)}. \tag{1}$$

Among them, θ is the threshold of the neural network [7, 8]. The output is

$$r_i^q = \exp\left(-\left(k_i^q\right)^2\right) = \exp\left(-\left(\sqrt{\sum_j \left(w1_{ji} - x_j^q\right)^2} \times \text{b1}_i\right)^2\right),$$
$$E = \frac{1}{2}\sum_k (t_k - 0_k)^2. \tag{2}$$

The relationship between b1 and C is b1 = 0.8326/C, and the output of the hidden layer neuron becomes

$$g_i^q = \exp\left(-0.8326^2 \times \frac{\|w1_1 - X^q\|}{C_i}\right),$$
$$\Delta\omega = -\eta\frac{\partial E}{\partial \omega_k} = -\eta(t_k - o_k)o_k(1 - o_k)o_j. \tag{3}$$

$\Delta\omega$ is the corresponding weight; the output is

$$y^q = \sum_{i=1}^{n} r_i \times w2_i. \tag{4}$$

The complete process structure is shown in Figure 1.

2.2. Wavelet Analysis. In order to avoid excessive network data from affecting the convergence speed of the network and to improve the generalization ability of wavelet neural networks, the original data is normalized so that the corresponding mapping of the processed data is in the range of [0,1] [9]. The normalized data can not only eliminate the dimension but also simplify the calculation, while the processed data still retain the characteristics of the original data [10, 11]. There are two main normalization methods:

The max-min normalization method [12]: this kind of wavelet is similar to the RBF network, but the scale parameter and displacement parameter of the wavelet network can be set according to the time-frequency localization characteristics of the wavelet [13, 14].

$$X_{\text{gvh}}(i) = \frac{X(i) - \min(X)}{\max(X) - \min(X)}, \tag{5}$$

where $X_{\text{gvh}}(i)$ is the ith value after normalization [1].

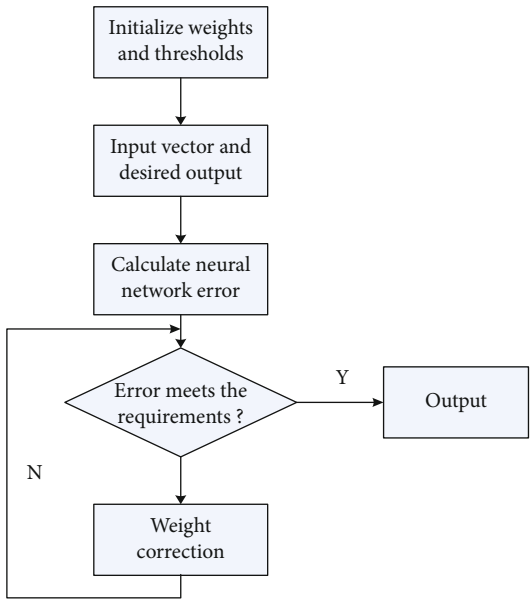

Figure 1: Complete process structure.

0-1 mean normalization method:

$$X_{\text{gvh}} = \frac{X(i) - \widehat{X}}{\sigma_x}. \tag{6}$$

$X(i)$ is the ith value in the original data X [2, 5].

The input vector of wavelet neural network is standardized by the maximum-minimum normalization method, and then, the model is fitted [15, 16]. In order to accurately analyze the characteristics of the original data sequence, after the network training prediction is completed, we need to reverse-normalize the predicted value [17, 18]. The calculation formulas are

$$\begin{aligned} X(i) &= X_{\text{gvh}}(\max(X) - \min(X)) + \min(X), \\ X(i) &= X_{\text{gvh}}(i)\sigma_x + \bar{X}. \end{aligned} \tag{7}$$

The denormalized data is in the same dimension as the original data, and analyzing it can more accurately extract the features and laws contained in the relevant data [19]. Data normalization and denormalization are realized using the MATLAB command map min-max [20, 21].

2.3. Wavelet-RBF Network Prediction. There are many decomposition methods for wavelet decomposition, as long as the direct sum of the set of subspaces can cover the V space without overlapping each other. Wavelet decomposition is actually just a special case of wavelet packet decomposition [22]. The diverse and flexible decomposition characteristics of wavelet provide the possibility to select the optimal decomposition according to different purposes [23, 24]. For the convenience of discussion, here, we no longer use V and W to denote subspaces but unify them as U_{nj}, where j is the scale and n is the number of the subspace in a certain scale, then

$$U_{n,j-1} = U_{2n,j} \oplus U_{2n+1,j}. \tag{8}$$

The corresponding sequence satisfies:

$$x_{n,j-1}(k) = x_{2n,j}(k) + x_{2n+1,j}(k). \tag{9}$$

The traditional method is based on some additivity cost functions that can measure concentration, such as maximum entropy. However, these cost functions are of great significance in data compression and other research fields, and they are useless for the decomposition of this research for the purpose of prediction. What this research needs is a wavelet packet decomposition method that can achieve the highest prediction accuracy. For this reason, we must first consider the judgment method of prediction accuracy [25]. There are many indicators to judge the prediction accuracy. This paper selects the mean square error (MSE), which reflects the deviation variance of the predicted value from the actual value, which is more suitable for the application of this article. Its definition is shown in the following formula:

$$\text{MSE} = \frac{1}{N}\sum_{k=1}^{N}[x(k) - x\wedge(k)]^2. \tag{10}$$

Among them, $\widehat{x}(k)$ is the predicted value. This research creates a relatively fast optimal decomposition search algorithm, which uses neural networks to predict $x_{n,j-1}(k)$, $x_{2n,j}(k)$, and $x_{2n+1,j}(k)$, respectively.

In this case,

$$\text{MSE} > \text{MSE}'. \tag{11}$$

Among them, MSE is the actual error.

It shows that decomposition can improve the prediction accuracy and the decomposition is effective, and further considers the decomposition of $x_{2n,j}(k)$ and $x_{2n+1,j}(k)$ in the same way; on the contrary, it shows that the neural network has been able to directly grasp the fluctuation law of the sequence $x_{n,j-1}(k)$, and its prediction accuracy is no longer sensitive to the decomposition. Further decomposition can only make the prediction accuracy fluctuate within a small range. Therefore, once the decomposition cannot further improve the prediction accuracy, the decomposition can be stopped, and this sequence can be directly retained as one of the optimal decomposition sequences of the wavelet packet. Therefore, by using this top-down search algorithm to compare the magnitude of MSE and MSE′, the optimal wavelet decomposition with the highest prediction accuracy, that is, the smallest MSE, can be gradually obtained [26, 27].

3. Financial Time Series Image Algorithm Experiment

3.1. Neural Network Learning

Step 1. First, use the function prestd to normalize the input data.

Step 2. Establish a network net = new ff (min max (input), [1, 7], tansig, purelin, traingdx); the learning algorithm used for weight update is tradingdx.

Step 3. Determine the number of training of the network which is 1000; the training target is 0001.

Step 4. Train the network net = train (net, input, output).

Step 5. Network training is completed when the number of network training or training target reaches the preset value.

Use the trained neural network to simulate and predict the data for a total of 18 days, num − = sim (net, input test); yuce = poststd (num, meant_test, stdt_test); input test is the preprocessed test set data network input; yuce is the final output prediction result.

Neural networks are used for time series modeling, and time needs to be embedded in the network structure. The commonly used method is time delay, which can be implemented in the input layer of the network. The nonlinear system model $f : R'' \rightarrow RP$ is used for prediction. When p is 1, it is a single-step prediction. The normalized RBF network can be used as this nonlinear system model, and its parameters can be learned through input samples with the ability to predict.

3.2. Establishment of RBF Model. The parameters related to the prediction effect in the actual application of the RBF network are the size of the training set, the number of input nodes, the number of output nodes, the number of hidden nodes, the center of the hidden layer, the weight w, the width parameter, etc., among which the number and center of the hidden layer have a greater impact on the performance of the network; the following describes the selection of parameters. The data is divided into a training sample set and a validation sample set. The 138 days before the closing price of the 50th Shanghai Stock Exchange and 198 hours before the time-sharing closing price are used as the training sample set, and the next 35 days and 50 hours are, respectively, used as the validation sample set. The error of the training sample is called the fitting error, and the error of the validation sample is called the prediction error. For the daily chart considering input nodes 5 and 3, the actual closing price training samples should be 133 and 135 groups, respectively. For the time-sharing chart considering input nodes 8 and 5, the actual training samples are 190 and 193, respectively. At the same time, the classical technical analysis wave theory of stocks points out that a complete upcycle consists of 5 waves and a downcycle consists of 3 waves. The 5-3 rule exists in large numbers. Therefore, when the RBF model is established, there are 5 daily charts. The RBF model with 8 input points or 5 input points and one output point on the input point and 3 input points and the hour chart examine its performance.

Too many or too few hidden nodes will lead to the weakening of the RBF generalization ability. Similarly, choosing different hidden layer centers will also cause the same problem. This study will use the RBF optimization algorithm for the number of hidden nodes and the selection of hidden layer centers.

3.3. Modeling of Wavelet Transform Sequence. The basic method of this research is to use the law that wavelet transform depends on the scale change, and the different scale domains of wavelet transform correspond to the scale decomposition sequence and the wavelet transform sequence, and the wavelet neural network containing different input neurons and hidden neurons is used to perform, respectively. Forecast and finally combine the results of the respective predictions using wavelet reconstruction technology into the final prediction results based on the original time series. Using the RBF algorithm in the neural network and using SPSS Clementine to model the wavelet transform sequence on 5 scales, each network model has three layers, namely, an input layer, a hidden layer, and an output layer, and each output layer has only one output element. In order to compare the forecasting effects of the models proposed in this article, we also use ordinary RBF networks to model and predict the logarithmic rate of return itself. The specific modeling steps are as follows:

(1) Setting input and output fields: each model has 10 input fields; that is, the lag 1 to 10 periods of each wavelet transform sequence are taken as the input fields of the model, and the current value of the wavelet transform is used as the output field

(2) Use the maximum minimum specification method to normalize the input variables

(3) Set the training set

(4) Set modeling parameters

(a) Modeling method: the method of modeling is rapid modeling; in SPSS Climentine12, the method of rapid modeling is BP algorithm

(b) Number of training: since the training samples in this article are only 2030, the amount of data is limited, but the prevention of overtraining of the amount of data must be considered, so the setting of the prevention of overtraining parameters is relatively high, 80%. That is, every time you model, 20% of the data is not added to the neural network learning process

(5) Validate the model with the data of the CSI 300 Index closing price return rate for a total of 18 trading days. Combine the predicted value of each wavelet transformation sequence with the predicted value of the scale transformation sequence obtained using the ARMA model, and construct the prediction of the original sequence through wavelet reconstruction

(6) Input the data of the verification set into the neural network model of the return rate sequence to obtain the predicted value using the ordinary RBF neural network modeling. Evaluate the degree of fit and compare it with the degree of fit of the unobtained prediction in (5)

Since the logarithmic return rate of the daily closing price of the Shanghai and Shenzhen 300 Index has great volatility, we choose wavelets with orthogonal and symmetric characteristics to eliminate redundancy and deviation; in order to separate periodicity and trend, the decomposition layer is now the number which is relatively high. Based on the above considerations, this research selects sym4 wavelet for 5-layer decomposition.

3.4. Wavelet Analysis Combined with Neural Network Prediction. The learning process consists of forward propagation of information and back propagation of errors. In the process of forward propagation, the input information is processed from the input layer through the hidden layer and then transmitted to the output layer. The state of neurons in the first layer only affects the state of neurons in the next layer. If the desired output result is not obtained in the output layer, it will switch to back propagation and return the error signal along the original connection channel. By modifying the weights of neurons in each layer, the error mean square is minimized. The three-layer network can realize any nonlinear mapping between input and output.

The wavelet decomposition divides the frequency space V occupied by the original sequence. Assuming that a wavelet is used to decompose the original index sequence into three scales, the principle of the wavelet-RBF neural network prediction method is shown in Figure 2.

Among them, d1, d2, and d3 are the high-frequency part (i.e., the detail part) of the sequence at each scale, respectively, and a3 is the low-frequency part (i.e., the approximate part) of the sequence. However, since the Mallat decomposition algorithm of wavelet requires two extractions, the length of the subsequence obtained from each decomposition will be halved relative to the parent sequence of the previous layer. Therefore, it is necessary to reconstruct the subsequence to have the same length as the original sequence for our forecast needs. In this way, the wavelet-RBF neural network prediction method can be divided into 4 steps:

(i) Perform wavelet decomposition on the original index sequence

(ii) Using wavelet coefficients to reconstruct the decomposed subsequences to make them the same length as the original sequence

(iii) Using the RBF neural network to model and predict wavelet subsequences

(iv) Reconstruct the predicted value of each subsequence to generate the final predicted value of the Shanghai Stock Exchange Composite Index sequence.

4. Financial Time Series Image Algorithm Analysis

4.1. Prediction of Each Subsequence Wavelet Decomposition. The selected 18-day data and time-sharing data are normalized after wavelet filtering is performed to remove the noise data. Considering that the stock market pays more attention to the trend transformation of the index, it is then input into the RBF network for training and testing. After denormalization, 40 predicted values of each subsequence are obtained. The predicted value results are shown in Table 1 below. It should be noted that the optimal value of spread of each subsequence is obtained through repeated tests of the MATLAB program based on the mean square error (MSE) and the smoothness of the curve. The wavelet decomposition of the predicted value of each subsequence is reconstructed to obtain a total of 40 Shanghai Composite Index predicted by the wavelet-RBF network model. The actual value and the predicted value are shown in Figure 3.

4.2. RBF Network Model Analysis. Use sym4 wavelet to decompose the original data signal (256 data at the daily closing price of the Shanghai Composite Index) into 3 scales, and use wavelet coefficients to reconstruct a single branch to obtain a low-frequency subsequence a and the same length as the original sequence The wavelet decomposition results of high-frequency subsequences d1, d2, d3 and signals are shown in Figure 4. The number of input nodes and hidden nodes is shown in Table 2. Generally speaking, using wavelet network of the RBF algorithm to predict stock price, the result is quite satisfactory. Through the above results, it is found that the increase of embedding dimension does not cause the decrease of network prediction error. No matter how many times the network is iterated, from the error evaluation index, when the embedding dimension $D = 2$, the network prediction result is the most ideal. It shows that when using history to predict the future, it is not that the more historical data, the more accurate the prediction of the future; that is, the current stock price is only closely related to the daily closing price of the last two days. It may also be a problem with the algorithm itself. When the embedding dimension is increased, it is prone to poor convergence performance when the quantum wavelet analysis is training high-dimensional problems, and the convergence to the best point cannot be guaranteed. When the input sample is 3, the mean square error is the lowest when the hidden layer is 6, and the network generalization performance is the best when the hidden layer nodes are 131, 92, 29, 13, 117, and 68, and the mean square error is 0.2028. The mean square error in the training phase is 0.0198, and the validity error is 0.2028.

According to the predicted values obtained by the three models, the respective prediction accuracy MSEs are calculated, and the results are shown in Table 3. It can be seen that wavelet decomposition and wavelet packet decomposition have significantly improved the prediction accuracy of the Shanghai Composite Index series. Therefore, the RBF network model based on wavelet decomposition and the RBF network model based on wavelet packet decomposition are both suitable for short-term stock price time series. For

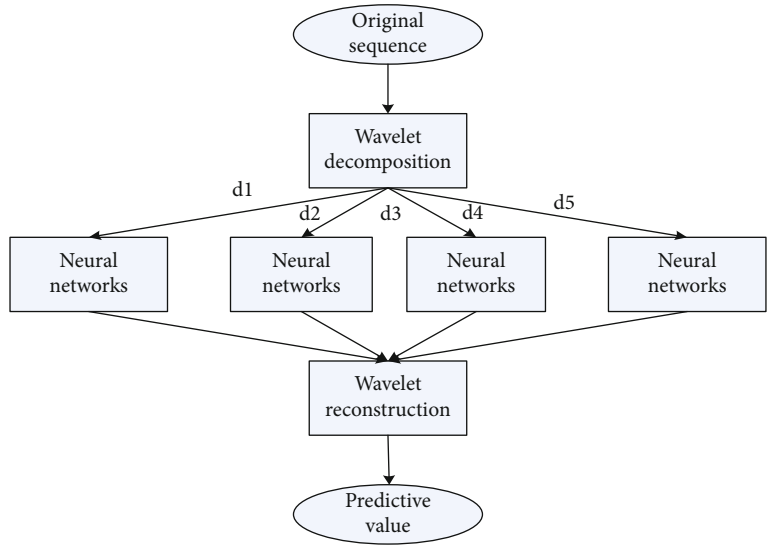

Figure 2: Complete process structure.

Table 1: Predicted value results.

a3 (spread = 8)		d3 (spread = 13)		d2 (spread = 6)		d1 (spread = 12)	
Actual value	Predictive value	Actual value	Predictive value	Actual value	Predictive value	Actual value	Predictive value
4998.9660	4980.2382	22.620	14.4011	-8.2090	-15.6493	18.7530	-3.0045
4,939.3525	4929.1337	9.327	3.2568	-25.6261	-10.1909	35.7956	36.3852
4887.0065	4860.9668	-3.915	-7.9799	-47.3708	-19.194	25.3911	61.6584
4877.4518	4819.6352	-11.913	-16.5212	5.0004	-1 1.636	-67.1442	-67.2613
4888.6199	4872.4904	-15.445	-17.0293	77.1446	66.4869	52.8915	41.7159

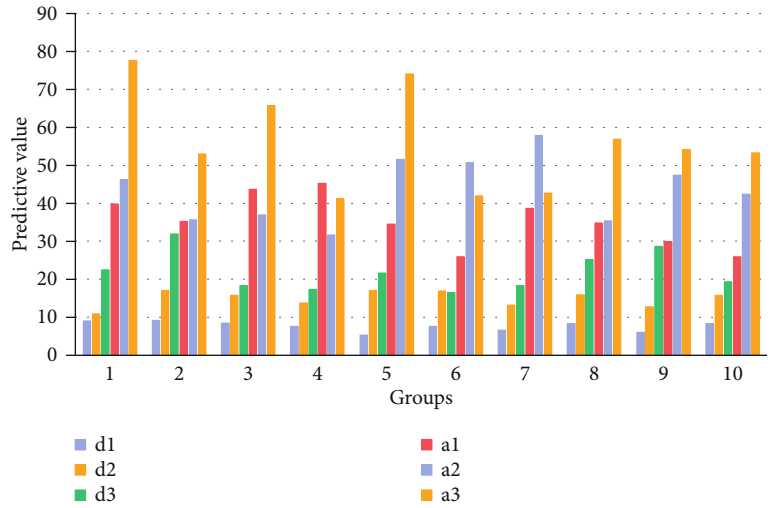

Figure 3: Actual and predicted values.

prediction, especially for wavelet packet decomposition, because the optimal decomposition subsequence set that minimizes MSE is selected, the MSE of the original sequence is also significantly reduced, and the prediction effect is very good. In addition, since there are many points with large fluctuations in the data we selected, comparing Table 2 can see that the RBF network model is not very effective in predicting these skyrocketing points. However, the wavelet-BF network model and wavelet packet-RBF the network model still gives a better fit to them. However, in the process of using RBF algorithm and wavelet analysis to optimize wavelet parameters for security forecasting, when reaching an almost equivalent error target, wavelet analysis has an advantage in time. Of course, the results obtained here are based on all the

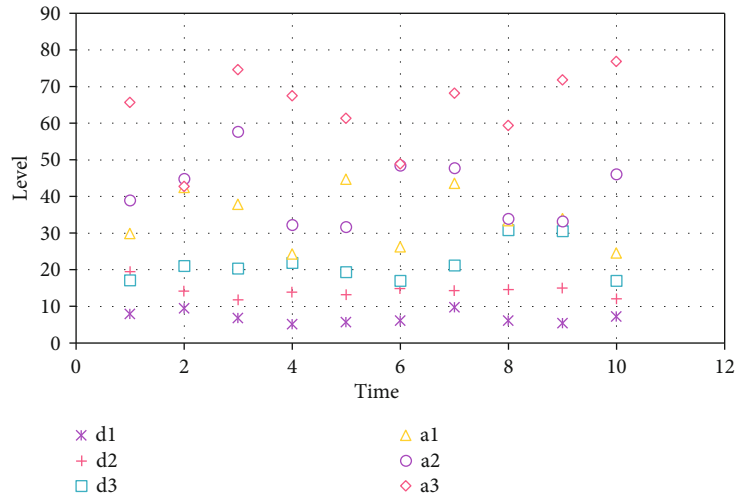

Figure 4: Wavelet decomposition result of signal.

Table 2: Number of input nodes and hidden nodes.

Parameter	First wavelet neural network	Second wavelet neural network	Third wavelet neural network	Fourth wavelet neural network	Fifth wavelet neural network	Sixth wavelet neural network
Input node	9	9	8	4	7	8
Hidden node	7	6	7	7	9	8

Table 3: Calculate the respective prediction accuracy MSE results.

Model	MSE
RBF network	4675.43
Wavelet-RBF network	1062.17
Wavelet packet-RBP network	398.00

algorithms are iteratively run 1000 times. Perhaps, for wavelet analysis, premature phenomena appear in the iterative process, and the possibility of falling into local extremes is relatively high.

4.3. Wavelet-RBF Network Analysis. Combining wavelet analysis with the RBF network for financial data forecasting, here, we take the Shanghai and Shenzhen 300 Index return rate as an example for detailed calculation research and combine the calculation results of the Shanghai and Shenzhen 300 Index return rate for research and discussion. Using the db7 wavelet with a decomposition level of 6 layers, the CSI 300 Index return data s from July 10 to November 23 is decomposed and reconstructed into approximate part a6 and detailed parts d6, d5, d4, d3, d2, and d1. Use a quadratic polynomial to fit and predict the approximate part a6, and use the cosine wave approximation method to fit and predict the detail parts d6, d4, and d3. For d5, we use the symmetric method to predict according to its graphical characteristics. d2 and d1 were fitted and predicted with the AR model, respectively. We use the normalization formula to approximate the data s to part a6 and detail parts d6, d5, d4, d3, d2, and d1 and their corresponding predicted values a. Take d6, d5, d4, d3, d2, and d1 as the input vectors and SI as the output vector, and use the RBF network for training. For this reason, we take spread = 10. After the RBF network is trained, enter the predicted value and get the predicted value of S1. At this time, the predicted value of the original time series s we need is obtained through the inverse operation of the normalization formula. The results of wavelet analysis combined with the RBF neural network to predict the return value of the Shanghai and Shenzhen 300 Index are shown in Table 4. The daily closing price of the CSI 300 Index is shown in Figure 5.

The use of wavelet analysis and RBF neural network to predict the average relative error of Shanghai and Shenzhen and Shanghai Stock Exchange, respectively, is shown in Table 5. The daily closing price of the CSI 300 Index is shown in Figure 6. It can be found from Figure 6 that the logarithmic return of the daily closing price of the Shanghai and Shenzhen 300 Index has obvious volatility and aggregation; the kurtosis of the sample is $K > 3$, the peak of the distribution; and the sample skewness $S < 0$; the distribution is left skewed; therefore, the logarithmic rate of return has a sharp peak and thick tail. The Jarque-Bera test of the sample sequence shows that the associated probability P value is 0, and the assumption of normal E distribution is rejected. Also, according to the comparison chart of the sample and the standard normal score, it can be seen that the logarithmic return of the Shanghai and Shenzhen 300 Index is not a normal distribution. Similarly, in the construction of the RBP network model of the SSE 50 Index time-sharing graph, the normalized data

Table 4: Wavelet analysis combined with the RBF neural network to predict the return value of the Shanghai and Shenzhen 300 Index.

Date	11.24	11.27	11.28	11.29	11.3	12.1	12.4
Actual data	7150	7090	7000	6980	7065	7020	7000
Forecast data	7125.2	7183.3	7168.4	7157.5	7103.4	7078.7	7025
Date	12.5	12.6	12.7	12.8	12.11	12.12	12.13
Actual data	7150	6965	6840	6865	6930	6830	6705
Forecast data	7011.6	6985.2	6994.4	7018.3	7060.5	7061.9	7086.9

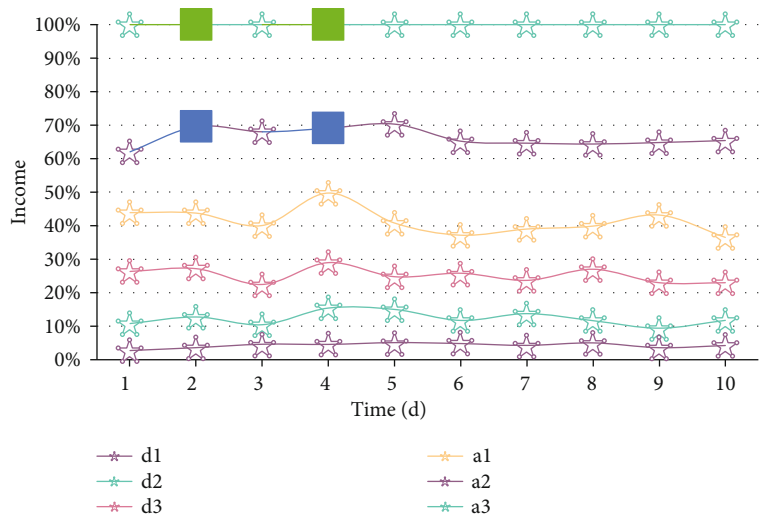

Figure 5: Daily closing price of CSI 300 Index logarithmic return.

Table 5: Using wavelet analysis combined with the RBF neural network to predict the average relative error of Shanghai and Shenzhen and Shanghai Stock Exchange, respectively.

Data	Shanghai and Shenzhen Index	Shanghai Composite Index
Average relative error	1.85%	3.71%

is also used, and the data is divided into a training sample set and a validation sample set as described above. Due to the short data interval represented by the time-sharing for the time-sharing graph, considering the input nodes 8 and 5, the actual input samples are 190 and 193, respectively. The network parameters are also genetically evolved according to 500 generations of the genetic algorithm. When the input sample is 5, the mean square error is the smallest when the hidden layer is 6, and the network generalization performance is the best when the hidden layer nodes are 116, 12, 4, 33, 179, and 165, and the mean square error is 1.6349, where the training stage mean square error is 0.0209, and the validity error is 1.6141. When the input sample is 8, the mean square error is the smallest when the hidden layer is 4, and the network generalization performance is the best when the hidden layer nodes are 146, 159, 11, and 150, and the mean square error is 1.4161, where the mean square error in the training phase is 0.0234, the validation error is 1.3926, and the network performance is better than the network performance of the sample 5 when the input sample is 8. From

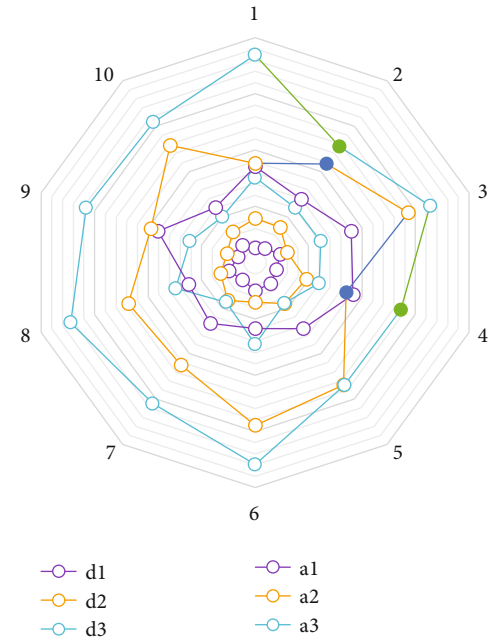

Figure 6: Daily closing price of Shanghai and Shenzhen 300 Index.

the hourly forecast and simulation, an interesting problem is also found; that is, the network performance tends to be better when the number of hidden layer nodes is small.

For the convenience of research, we take the average relative error obtained by using wavelet analysis for prediction,

Table 6: The average relative error obtained by using wavelet analysis combined with the RBF neural network to predict.

Data	Shanghai and Shenzhen Index	Shanghai Composite Index
Wavelet prediction average relative error	1.91%	3.77%
RBF neural network predicts relative error	7.12%	8.67%
Wavelet-RBF neural network prediction relative error	1.85%	3.71%

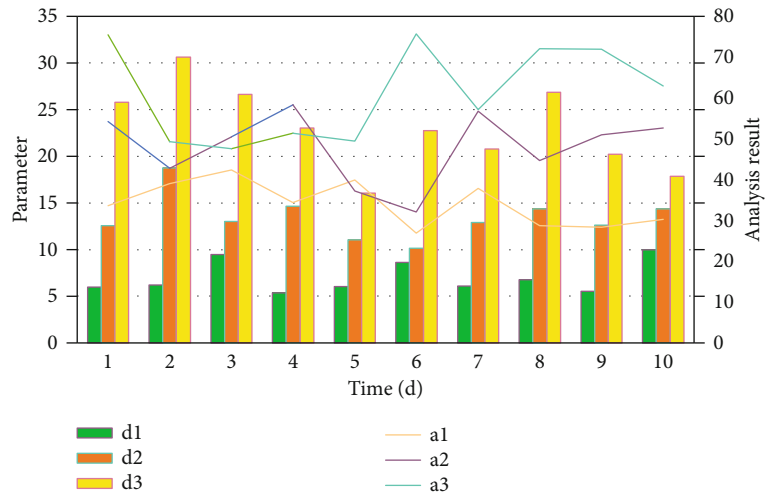

Figure 7: The average relative error analysis result of wavelet analysis combined with the RBF neural network for prediction.

the average relative error obtained by directly using RBF neural network for prediction, and the average relative error obtained by using wavelet analysis combined with RBF neural network for prediction, as shown in Table 6. The average relative error analysis result obtained by combining wavelet analysis and RBF neural network for prediction is shown in Figure 7. It can be found from Table 6 that the average relative error of prediction using wavelet analysis is much smaller than that of directly using neural network. This is because the wavelet analysis method is used to predict, it can extract the main trend part and detail part of the data, so the average relative error of the fitting prediction will not be very large. Using neural networks for prediction, of course, as mentioned earlier, it has many advantages, but in general, this method is not particularly mature. For example, here is the use of RBF neural network for prediction, and spread is a key role in the prediction results. When spread takes different values, different predicted values will be obtained. Therefore, it is necessary to train the network through a large number of experiments and past experience to select a more appropriate spread value. Training the network in different groups on the data can also affect the predicted value of the neural network. It can be seen that there are various factors that can have a direct impact on the predicted value of the neural network. Therefore, the average relative error of directly using the neural network to predict is slightly larger than that of using the wavelet analysis method to predict. When the average relative error of the prediction by the neural network and the average relative error of the prediction with the wavelet analysis method are both within a reasonable range, the prediction of the neural network can be directly used for calculation by MATLAB programming, and the program is simple and easy to understand. For the prediction with wavelet analysis method, it is necessary to decompose layer by layer and calculate layer by layer; the calculation is more complicated. In this case, the neural network can be given priority for prediction. At the same time, it can be seen that the prediction results obtained by the wavelet prediction method combined with the RBF network prediction method are better than those obtained by pure wavelet prediction or pure RBF network prediction.

Table 7: Comparison results of RBF, WNN, and WWNN network prediction and evaluation indicators.

Model	Evaluation index			
	MAE	MSE	MAPE	MSPE
BP	1.6956	0.7702	26. 0566	8.9771
WNN	1.1130	0.4823	11.2030	7.5455
WWNN	0.0938	0.0420	0.1735	0.0944

Table 7 shows the comparison results of RBF, WNN, and WWNN network prediction evaluation indicators. RBF, WNN, and WWNN network predictive analysis results are shown in Figure 8. Based on Figure 8 and Table 7, the prediction accuracy of the wavelet neural network is better than that of the traditional RBF network. The wavelet neural network based on wavelet decomposition and reconstruction has better results than the prediction of pure wavelet neural network. The sum of squares of network prediction, the evaluation indicators of error, average absolute error, mean square error, average absolute percentage error, and square percentage error are better than those of the RBF neural

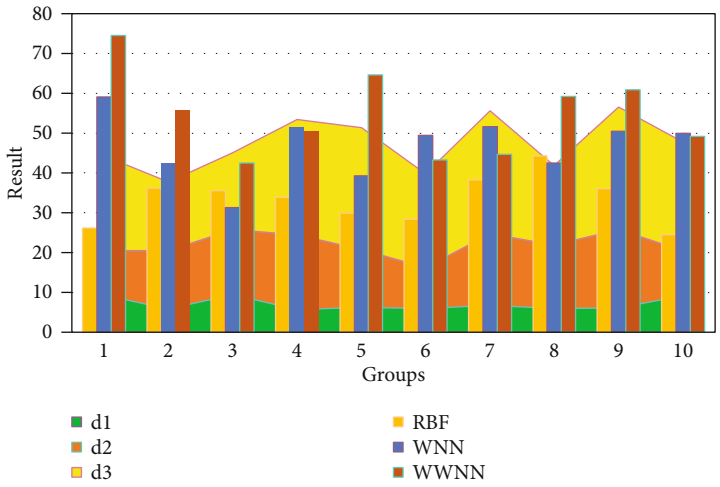

Figure 8: RBF, WNN, and WWNN network prediction analysis results.

network and pure wavelet neural network. It can be seen that the WWNN network has good approximation and generalization ability, although the two kinds of wavelet networks are inferior to the BP neural network in predictive power in some cases. But starting from the time dimension, the training time of the wavelet network model, especially the WNN model, is 1/2 of the BP neural network model, indicating that the wavelet transform and neural network and the wavelet network formed by the combination of networks still have a good development prospect in time series forecasting. The WNN model is based on multiscale wavelet basis functions. It has more adjustable scale parameters and translation parameters and has stronger learning ability. However, based on the comparison of the effects of the WNN model and the WNN model in the time series prediction, the WNN model performs better, because the homogeneous (single variable) model is mainly used to predict the future exchange rate through historical exchange rates, without taking into account other key factors such as national interest rate, inflation rate, original price, and gold price, which have an impact on the exchange rate. Therefore, the performance of the WNN model in time series forecasting cannot be determined. It is not as powerful as the WNN model, and multifactor consideration and analysis are needed in the later stage.

5. Conclusion

This research mainly discusses the financial time series image algorithm based on wavelet analysis and neural network. The parameters related to the prediction effect in the actual application of the RBF network are the size of the training set, the number of input nodes, the number of output nodes, the number of hidden nodes, the center of the hidden layer, the weight w, the width parameter, etc., among which the number and center of the hidden layer have a greater impact on the performance of the network. Neural networks are used for time series modeling, and time needs to be embedded in the network structure. The commonly used method is time delay, which can be implemented in the input layer of the network.

The basic method of this research is to use the law that wavelet transform depends on the scale change, and the different scale domains of wavelet transform correspond to the scale decomposition sequence and the wavelet transform sequence, and the wavelet neural network containing different input neurons and hidden neurons is used to perform, respectively. Forecast and finally combine the results of the respective predictions using wavelet reconstruction technology into the final prediction results based on the original time series. Using the RBF algorithm in the neural network and using SPSS Clementine to model wavelet transform sequences on 5 scales, each network model has three layers, namely, an input layer, a hidden layer, and an output layer, and each output layer has only one output element. In order to compare the forecasting effects of the models proposed in this article, we also use ordinary RBF networks to model and predict the logarithmic rate of return itself.

The wavelet-RBF neural network prediction method can be divided into four steps: wavelet decomposition of the original exponential sequence; use of wavelet coefficients to reconstruct the decomposed subsequences to make them the same length as the original sequence; use RBF neural network to separate the wavelet subsequences carry out modeling and prediction; and reconstruct the predicted value of each subsequence to generate the final predicted value of the Shanghai Composite Index sequence. The learning process consists of forward propagation of information and back propagation of errors. In the process of forward propagation, the input information is processed from the input layer through the hidden layer and then transmitted to the output layer. The state of neurons in the first layer only affects the state of neurons in the next layer. If the desired output result is not obtained in the output layer, it will switch to back propagation and return the error signal along the original connection channel. By modifying the weights of neurons in each layer, the error mean square is minimized. The three-layer network can realize any nonlinear mapping between input and output.

Data Availability

The data that support the findings of this study are available from the corresponding author upon reasonable request.

Conflicts of Interest

The authors declare that they have no conflicts of interest.

References

[1] N. Amrani, J. Serra-Sagrista, V. Laparra, M. W. Marcellin, and J. Malo, "Regression wavelet analysis for lossless coding of remote-sensing data," *IEEE Transactions on Geoscience and Remote Sensing*, vol. 54, no. 9, pp. 5616–5627, 2016.

[2] A. Arneodo, B. Audit, E. Bacry, S. Manneville, J. F. Muzy, and S. G. Roux, "Thermodynamics of fractal signals based on wavelet analysis: application to fully developed turbulence data and DNA sequences," *Physica A: Statistical Mechanics and its Applications*, vol. 254, no. 1-2, pp. 24–45, 1998.

[3] F. Bousefsaf, C. Maaoui, and A. Pruski, "Peripheral vasomotor activity assessment using a continuous wavelet analysis on webcam photoplethysmographic signals," *Bio-medical Materials and Engineering*, vol. 27, no. 5, pp. 527–538, 2016.

[4] C. M. Alcala, M. C. Kelley, and J. C. Ulwick, "Nonturbulent layers in polar summer mesosphere: 1. Detection of sharp gradients using wavelet analysis," *Radio Science*, vol. 36, no. 5, pp. 875–890, 2001.

[5] W. Y. Chen, "Health progress and economic growth in the USA: the continuous wavelet analysis," *Empirical Economics*, vol. 50, no. 3, pp. 831–855, 2016.

[6] M. Zhou, Y. Wang, Y. Liu, and Z. Tian, "An information-theoretic view of WLAN localization error bound in GPS-denied environment," *IEEE Transactions on Vehicular Technology*, vol. 68, no. 4, pp. 4089–4093, 2019.

[7] G. R. J. Cooper, "Locating thin dykes using wavelet analysis of their magnetic anomalies," *Exploration Geophysics*, vol. 50, no. 5, pp. 554–560, 2019.

[8] L. Li, P. Liu, Y. Xing, and H. Guo, "Wavelet analysis of the far-field sound pressure signals generated from a high-lift configuration," *AIAA Journal*, vol. 56, no. 1, pp. 432–437, 2018.

[9] X. Wen, Q. Feng, R. C. Deo, M. Wu, and J. Si, "Wavelet analysis-artificial neural network conjunction models for multi-scale monthly groundwater level predicting in an arid inland river basin, northwestern China," *Nordic Hydrology*, vol. 48, no. 6, pp. 1710–1729, 2017.

[10] A. Banskota, M. J. Falkowski, A. M. S. Smith et al., "Continuous wavelet analysis for spectroscopic determination of subsurface moisture and water-table height in northern peatland ecosystems," *IEEE Transactions on Geoscience and Remote Sensing*, vol. 55, no. 3, pp. 1526–1536, 2017.

[11] M. Durocher, T. S. Lee, T. B. M. J. Ouarda, and F. Chebana, "Hybrid signal detection approach for hydro-meteorological variables combining EMD and cross-wavelet analysis," *International Journal of Climatology: A Journal of the Royal Meteorological Society*, vol. 36, no. 4, pp. 1600–1613, 2016.

[12] A. Osipov, "Wavelet analysis on symbolic sequences and two-fold de Bruijn sequences," *Journal of Statistical Physics*, vol. 164, no. 1, pp. 142–165, 2016.

[13] G. I. Donskikh, M. I. Ryabov, A. L. Sukharev, and M. Aller, "Singular-spectrum analysis and wavelet analysis of the variability of the extragalactic radio sources 3C 120 and CTA 102," *Astrophysics*, vol. 59, no. 2, pp. 199–212, 2016.

[14] P. Gupta and R. N. Mahanty, "An approach for detection and classification of transmission line faults by wavelet analysis," *Energy Education Science and Technology*, vol. 34, no. 1, pp. 109–122, 2016.

[15] M. R. Kaloop and D. Kim, "De-noising of GPS structural monitoring observation error using wavelet analysis," *Geomatics, Natural Hazards and Risk*, vol. 7, no. 2, pp. 804–825, 2016.

[16] M. Zhou, X. Li, Y. Wang, S. Li, Y. Ding, and W. Nie, "6G multi-source information fusion based indoor positioning via Gaussian kernel density estimation," *IEEE Internet of Things Journal*, 2020.

[17] C. Ma, S. Song, Z. Gao et al., "Electrochemical noise monitoring of the atmospheric corrosion of steels: identifying corrosion form using wavelet analysis," *Corrosion Engineering, Science and Technology*, vol. 52, no. 6, pp. 432–440, 2017.

[18] G. J. Wang, C. Xie, and S. Chen, "Multiscale correlation networks analysis of the US stock market: a wavelet analysis," *Journal of Economic Interaction and Coordination*, vol. 12, no. 3, pp. 561–594, 2017.

[19] M. Gallegati, M. Gallegati, J. B. Ramsey, and W. Semmler, "Long waves in prices: new evidence from wavelet analysis," *Cliometrica*, vol. 11, no. 1, pp. 127–151, 2017.

[20] J. J. Yang, Z. B. He, W. J. Zhao, J. Du, L. F. Chen, and X. Xi, "Assessing artificial neural networks coupled with wavelet analysis for multi-layer soil moisture dynamics prediction," *Sciences in Cold and Arid Regions*, vol. 8, no. 2, pp. 116–124, 2016.

[21] M. R. Mosavi and A. Tabatabaei, "Traveling-wave fault location techniques in power system based on wavelet analysis and neural network using GPS timing," *Wireless Personal Communications*, vol. 86, no. 2, pp. 835–850, 2016.

[22] A. Singh, S. Maiti, and R. K. Tiwari, "Modelling discontinuous well log signal to identify lithological boundaries via wavelet analysis: an example from KTB borehole data," *Journal of Earth System Science*, vol. 125, no. 4, pp. 761–776, 2016.

[23] D. Das, M. Kannadhasan, A. K. Tiwari, and K. H. al-Yahyaee, "Has co-movement dynamics in emerging stock markets changed after global financial crisis? New evidence from wavelet analysis," *Applied Economics Letters*, vol. 25, no. 20, pp. 1447–1453, 2018.

[24] B. Das, S. Pal, and S. Bag, "Weld quality prediction in friction stir welding using wavelet analysis," *International Journal of Advanced Manufacturing Technology*, vol. 89, no. 1-4, pp. 711–725, 2017.

[25] G. Pugliano, U. Robustelli, F. Rossi, and R. Santamaria, "A new method for specular and diffuse pseudorange multipath error extraction using wavelet analysis," *GPS Solutions*, vol. 20, no. 3, pp. 499–508, 2016.

[26] W. Huang and Y. Yang, "Water quality sensor model based on an optimization method of RBF neural network," *Computational Water, Energy, and Environmental Engineering*, vol. 9, no. 1, pp. 1–11, 2020.

[27] L. Yue, L. Yu-Nan, L. Bing, and W. Chuan-Biao, "Research on the correlation between physical examination indexes and TCM constitutions using the RBF neural network," *Digital Chinese Medicine*, vol. 3, no. 1, pp. 11–19, 2020.